Proceedings of the Advanced Coal-Fired Power Systems'96 Review Meeting

July 16-18, 1996

METC

Host and Sponsor:
U.S. Department of Energy, Office of Fossil Energy
Morgantown Energy Technology Center
P.O. Box 880, Morgantown, West Virginia 26505-0880
http://www.metc.doe.gov

Report Numbers:
DOE/METC-96/1037
(DE96011356)
(CONF-960757)

Contents

This Contents page has been set up with each section title linked to the corresponding section. To use this feature, move your cursor to the section you wish to view. (You will note that your cursor arrow changes to a pointing finger.) Click your left mouse button to jump to the beginning of that section. To return to the previously viewed page, click the Go Back button (the double left-pointing arrow) from the tool bar at the top of the screen, or choose Go Back from the view menu.

Disclaimer

Foreword

Papers and Presentations

- Opening Session
- Session 1: Advanced Power Systems
- Session 2: Hot Gas Particle Control
- Session 3: Hot Gas Desulfurization
- Session 4A: Sorbent and Process Development
- Session 4B: Hazardous Air Pollutants (HAPs)
- Session 4C: Hot Gas Filter Development
- Poster Session A: METC CRADA Opportunities
- Poster Session B: Filters, Desulfurization, and Related Environmental Issues

Meeting Participants

Proceedings of the Advanced Coal-Fired Power Systems '96 Review Meeting

Opening Session

This Contents page has been set up with each paper title linked to the corresponding paper. To use this feature, move your cursor to the paper you wish to view. (You will note that your cursor arrow changes to a pointing finger.) Click your left mouse button to jump to the beginning of that paper.

Fossil Energy R&D for a Competitive Power Industry
Rita A. Bajura — Morgantown Energy Technology Center

To return to the Proceedings *Contents* page or the *Cover*, click the **Go Back** button (the double left-pointing arrow) from the tool bar at the top of the screen, or choose **Go Back** from the view menu.

Proceedings of the Advanced Coal-Fired Power Systems '96 Review Meeting

Session 1: Advanced Power Systems

This Contents page has been set up with each paper title linked to the corresponding paper. To use this feature, move your cursor to the paper you wish to view. (You will note that your cursor arrow changes to a pointing finger.) Click your left mouse button to jump to the beginning of that paper.

PFBC and IGCC Power Generation Technologies - Status and Opportunities
R. Daniel Brdar and Robert B. Reuther — Morgantown Energy Technology Center

Medical Waste Co-Firing Comes of Age
Karl Smith-Bernston and James M. Stuart — DONLEE Technologies, Inc.

Power Systems Development Facility: Design, Construction, and Commissioning Status
Charles A. Powell, Pannalal Vimalchand, Howard L. Hendrix, and Peter M. Honeycut — Southern Company Services, Inc.

METC's Pilot-Scale Hot-Gas Desulfurization Process Development Unit
Michael H. McMillian and Larry A. Bissett — Morgantown Energy Technology Center

Pulsed Atmospheric Fluidized Bed Combustion
William G. Steedman — ThermoChem, Inc.

Design and Performance of a Low Btu Fuel Rich-Quench-Lean Gas Turbine Combustor
Alan S. Feitelberg, Melvin R. Jackson, Michael A. Lacey, Kenneth S. Manning, and Ann M. Ritter — GE Corporate Research and Development

Assessment of PFBC and Gasification Repowering
Donald L. Bonk and Mark D. Freier — Morgantown Energy Technology Center; and Thomas L. Buchanan, Michael R. DeLallo, Harvey N. Goldstein and Jay S. White — Parsons Power Group, Inc.

Optimizing Advanced Power System Designs Under Uncertainty

E.S. Rubin and U.M. Diwekar — Carnegie Mellon University; and H.C. Frey — North Carolina State University

To return to the Proceedings *Contents* page or the *Cover*, click the **Go Back** button (the double left-pointing arrow) from the tool bar at the top of the screen, or choose **Go Back** from the view menu.

Proceedings of the Advanced Coal-Fired Power Systems '96 Review Meeting

Session 2: Hot Gas Particle Control

This Contents page has been set up with each paper title linked to the corresponding paper. To use this feature, move your cursor to the paper you wish to view. (You will note that your cursor arrow changes to a pointing finger.) Click your left mouse button to jump to the beginning of that paper.

Westinghouse Advanced Particle Filter System
Thomas E. Lippert, Gerald J. Bruck, Zal N. Sanjana, Richard A. Newby, and Dennis M. Bachovchin — Westinghouse Science & Technology Center

Filter Component Assessment
Mary Anne Alvin, Thomas E. Lippert, Edward S. Diaz, and Eugene E. Smeltzer — Westinghouse Science & Technology Center

Properties of Ceramic Filters
Jack D. Spain — Southern Research Institute

Simultaneous Hot Gas Desulfurization and Improved Filtration
Paul M. Eggerstedt, James F. Zievers, and Parul C. Patel — Industrial Filter & Pump Manufacturing Co., Inc.; and Elizabeth C. Zievers — Universal Porosics, Inc.

Moving Granular Bed Filter Development Program
Keith B. Wilson and John C. Haas — Combustion Power Company; and Raghubir P. Gupta and Brian S. Turk — Research Triangle Institute

Filter Systems for IGCC and PFBC Applications
John W. Sawyer — Pall Corporation, Inc.

Application of CFCC Technology to Hot Gas Filtration Applications
Merrill Smith — U.S. Department of Energy, Office of Industrial Technologies

Hot-Gas Filter Testing with a Transport Reactor Development Unit
Michael L. Swanson and Robert O. Ness, Jr. — Energy & Environmental Research Center, UND

CeraMem Filter Development Program

Bruce Bishop — CeraMem Separations, Inc.; and Neil Raskin — CeraFilter L.P.

To return to the Proceedings *Contents* page or the *Cover*, click the **Go Back** button (the double left-pointing arrow) from the tool bar at the top of the screen, or choose **Go Back** from the view menu.

Proceedings of the Advanced Coal-Fired Power Systems '96 Review Meeting

Session 3: Hot Gas Desulfurization

This Contents page has been set up with each paper title linked to the corresponding paper. To use this feature, move your cursor to the paper you wish to view. (You will note that your cursor arrow changes to a pointing finger.) Click your left mouse button to jump to the beginning of that paper.

Operation of a Pressurized Gasifier, Hot Gas Cleanup System and Turbine Simulator
Stephen Bevan, Raul E. Ayala, Anthony H. Furman, and David J. Najewicz — GE Environmental Services

Hot Gas Desulfurization Using Transport Reactors
Eric L. Moorehead and Gunnar B. Henningsen — The M.W. Kellogg Company

Phillips Sorbent Development for Tampa Electric Company and Sierra Pacific Power Company
Gyanesh P. Khare, Gary A. Delzer, Gil J. Greenwood, and Donald H. Kubicek — Phillips Petroleum Company

Bench-Scale Development of Fluidized-Bed Spray-Dried Sorbents
Raghubir P. Gupta, Brian S. Turk, and Santosh K. Gangwal — Research Triangle Institute

Sorbent Development for Low-Temperature Moving-Bed Desulfurization
Rául E. Ayala, Venkat S. Venkataramani, and Timothy L. Chuck — GE Corporate Research and Development; and Raghubir P. Gupta — Research Triangle Institute

Bench-Scale Testing of Attrition Resistant Moving Bed Sorbents
James H. Swisher — E&A Associates; and Raghubir P. Gupta — Research Triangle Institute

Durability Testing of the Direct Sulfur Recovery Process
Jeffrey W. Portzer, Brian S. Turk, and Santosh K. Gangwal — Research Triangle Institute

To return to the Proceedings *Contents* page or the *Cover*, click the **Go Back** button (the double left-pointing arrow) from the tool bar at the top of the screen, or choose **Go Back** from the view menu.

Proceedings of the Advanced Coal-Fired Power Systems '96 Review Meeting

Session 4a: Sorbent and Process Development

This Contents page has been set up with each paper title linked to the corresponding paper. To use this feature, move your cursor to the paper you wish to view. (You will note that your cursor arrow changes to a pointing finger.) Click your left mouse button to jump to the beginning of that paper.

Testing and Analysis of METC10 Sorbent
Ranjani V. Siriwardane — Morgantown Energy Technology Center

Advanced Hot-Gas Desulfurization Sorbents
K. Jothimurugesan and Adeyinka A. Adeyiga — Hampton University; and Santosh K. Gangwal — Research Triangle Institute

Advanced Low-Temperature Fluid Bed Sorbents
Javad Abbasian, Rachid B. Slimane, and James R. Wangerow — Institute of Gas Technology

Advanced Sulfur Control Processing
Wu-Ning Huang, Alejandro Lopez-Ortiz, Julie D. White, Frank R. Groves, Jr., and Douglas P. Harrison — Louisiana State University

Advanced Sulfur Control Processing
Santosh K. Gangwal, Jeffrey W. Portzer, Brian S. Turk, and Raghubir Gupta — Research Triangle Institute

Hot Coal Gas Desulfurization With Manganese-Based Sorbents
Berns and Hepworth — University of Minnesota

Catalytic Ammonia Decomposition for Coal-Derived Fuel Gases
Santosh K. Gangwal, Raghubir P. Gupta, Jeffrey W. Portzer, and Brian S. Turk — Research Triangle Institute; Gopala N. Krishnan — SRI International; and Stephen L. Hung and Raul E. Ayala — GE Corporate Research & Development

Decomposition of Ammonia in IGCC Fuel Gas Streams
Shaik A. Qader and Qusro A. Qadar — Energy and Environmental Technology Corporation; and Lawrence J. Muzio — Fossil Energy Research Corporation

Assessment of Hot Gas Contaminant Control

Michael D. Rutkowski, Michael G. Klett, and Roman Zaharchuk — Parsons Power Group, Inc.

To return to the Proceedings *Contents* page or the *Cover*, click the **Go Back** button (the double left-pointing arrow) from the tool bar at the top of the screen, or choose **Go Back** from the view menu.

Proceedings of the Advanced Coal-Fired Power Systems '96 Review Meeting

Session 4B: Hazardous Air Pollutants (HAPs)

This Contents page has been set up with each paper title linked to the corresponding paper. To use this feature, move your cursor to the paper you wish to view. (You will note that your cursor arrow changes to a pointing finger.) Click your left mouse button to jump to the beginning of that paper.

Assessment of HAPs Emissions from Advanced Power Systems
T.A. Erickson and D.W. Brekke — Energy & Environmental Research Center, UND; and P.E. Botros — Morgantown Energy Technology Center

Trace Metal Transformation in Gasification
Steven A. Benson, Thomas A. Erickson, Christopher J. Zygarlicke, Cathy A. O'Keefe, Karen A. Katrinak, Sean E. Allan, David J. Hassett, and William B. Hauserman — Energy & Environmental Research Center, UND; and Norman T. Holcombe — Morgantown Energy Technology Center

To return to the Proceedings *Contents* page or the *Cover*, click the **Go Back** button (the double left-pointing arrow) from the tool bar at the top of the screen, or choose **Go Back** from the view menu.

Proceedings of the Advanced Coal-Fired Power Systems '96 Review Meeting

Session 4C: Hot Gas Filter Development

This Contents page has been set up with each paper title linked to the corresponding paper. To use this feature, move your cursor to the paper you wish to view. (You will note that your cursor arrow changes to a pointing finger.) Click your left mouse button to jump to the beginning of that paper.

Development and Testing of PRD-66 Hot Gas Filters
Jeffrey A. Chambers and John S. Garnier — DuPont Lanxide Composites, Inc.

Novel Oxide-Oxide Fiber Reinforced Hot Gas Filter Development
Richard A. Wagner — Babcock & Wilcox

3D Oxide/Oxide Composite Filter
Jay E. Lane — Westinghouse Electric Corporation; Jean-Francois LeCostaouec — Techniweave, Inc.; and Carol J. Painter, We-Fang A. Su, and Ken C. Radford — Northrop Grumman Corporation

Iron Aluminide Hot Gas Filters
J. Hurley, S. Brosious, and M. Johnson — Pall Corporation

Metal Filter Materials in Combustion Environments
Roddie R. Judkins, Peter F. Tortorelli, and Ian G. Wright — Oak Ridge National Laboratory

Characterization and Testing of CFCC Hot Gas Filters Made Via Gas Phase Reaction Synthesis -- A Synopsis of the Textron/METC Advanced Hot Gas Filter Program
Stephen DiPietro — Textron Systems Divisions

To return to the Proceedings *Contents* page or the *Cover*, click the **Go Back** button (the double left-pointing arrow) from the tool bar at the top of the screen, or choose **Go Back** from the view menu.

Proceedings of the Advanced Coal-Fired Power Systems '96 Review Meeting

Poster Session A: METC CRADA Opportunities

This Contents page has been set up with each paper title linked to the corresponding paper. To use this feature, move your cursor to the paper you wish to view. (You will note that your cursor arrow changes to a pointing finger.) Click your left mouse button to jump to the beginning of that paper.

CRADA Opportunities

Cooperative Research and Development Agreements at METC
J. Christopher Ludlow — Morgantown Energy Technology Center

Combustion

Low Emissions Combustor Test and Research Facility
Kent H. Casleton, Daniel J. Maloney, and Thomas S. Norton — Morgantown Energy Technology Center

Combustion Oscillation Control
George A. Richards and Michael C. Janus — Morgantown Energy Technology Center

High-Pressure Optical Combustion Probe
Steven D. Woodruff — Morgantown Energy Technology Center

FLUENT Simulations of the Westinghouse Multi-Annular Swirl Burner for Design Optimization
Thomas S. Norton and Darren J. Mollot — Morgantown Energy Technology Center

Filtration

High-Temperature Gas-Stream Cleanup Test Facility
Doug Straub, Ta-Kuan Chiang, and John Shultz — Morgantown Energy Technology Center

Granular Filtration in a Fluidized Bed
Joseph S. Mei and Paul C. Yue — Morgantown Energy Technology Center

High-Temperature, High-Pressure Probe for Hazardous Air Pollutants Sampling in Advanced Power Systems
William P. Chisholm — Morgantown Energy Technology Center

Measurements of Filter-Cake Properties
Duane H. Smith, Ulrich Grimm, and George J. Haddad — Morgantown Energy Technology Center

A New Hot Gas Cleanup Filter Design Methodology
John G. VanOsdol, Richard A. Dennis, and Franklin D. Shaffer — Morgantown Energy Technology Center

Gas Stream Cleanup

Hot Gas Desulfurization PDU Project
Larry A. Bissett — Morgantown Energy Technology Center

Fluidized-Bed Reactor and Hot Gas Cleanup Facility
John M. Rockey — Morgantown Energy Technology Center

Transport Reactor Facility
David A. Berry and Susan R. Shoemaker — Morgantown Energy Technology Center

Cold Flow Verification Test Facility
Abolghasem Shamsi and Lawrence J. Shadle — Morgantown Energy Technology Center

To return to the Proceedings *Contents* page or the *Cover*, click the **Go Back** button (the double left-pointing arrow) from the tool bar at the top of the screen, or choose **Go Back** from the view menu.

Proceedings of the Advanced Coal-Fired Power Systems '96 Review Meeting

Poster Session B: Filters, Desulfurization, and Related Environmental Issues

This Contents page has been set up with each paper title linked to the corresponding paper. To use this feature, move your cursor to the paper you wish to view. (You will note that your cursor arrow changes to a pointing finger.) Click your left mouse button to jump to the beginning of that paper.

Filters

Particulate Hot Gas Stream Cleanup Technical Issues
Duane H. Pontius and Todd R. Snyder — Southern Research Institute

Hot-Gas Filter Ash Characterization Project
Bruce A. Dockter, John P. Hurley, Tina A. Watne, Karen A. Katrinak, and Catherine A. O'Keefe — Energy & Environmental Research Center, UND

Nondestructive Degradation Evaluation of Ceramic Candle Filters Using Vibration Signatures
Roger H.L. Chen and Balaji Parthasarathy — West Virginia University

Determination of Filter-Cake Thicknesses from On-Line Flow Measurements and Gas/Particle Transport Modeling
Duane H. Smith, Victor Powell, and Essam Ibrahim — Morgantown Energy Technology Center; Martin Ferer — West Virginia University; and Goodarz Ahmadi — National Research Council

Development of a Monolithic Ceramic Cross-Flow Filter: Part 2
David A. Larsen, Blasch Precision Ceramics, Inc.

Initial Failure Analysis of Ceramic Filters
Ziaul Huque, Daniel Mei, and Jianren Zhou — Prairie View A&M University

Ceramic Component Development Process Analysis
D. Boss, S. Sambasivan, C. Kuehmann, and K. Faber — BIRL/Northwestern University

Performance of Ceramic Membrane Filters
Rajesh K. Ahluwalia, Kwan H. Im, and Howard K. Geyer — Argonne National Laboratory; and David L. Shelleman and Richard E. Tressler — The Pennsylvania State University

Preliminary Strength Measurements of High Temperature Ash Filter Deposits
B.S. Kang, E.K. Johnson, R. Mallela, and J.F. Barberio — West Virginia University

Desulfurization

Long Life ZnO-TiO_2 and Novel Sorbents
Robert J. Copeland, Mike Cesario, Dan Feinberg, Brent MacQueen, Jack Sibold, Brian Windecker, and Jing Yang — TDA Research, Inc.

Manganese-Based Sorbents for Coal Gas Desulfurization
Lee D. Gasper-Galvin and Edward P. Fisher —Morgantown Energy Technology Center; and William J. Goyette — Chemetals

Reactivity of Metal Oxide Sorbents for Removal of H_2S
Kyung C. Kwon and Edward R. Crowe — Tuskegee University

Development of Disposable Sorbents for Chloride Removal from High-Temperature Coal-Derived Gases
Gopala N. Krishnan and Anastasia Canizales — SRI International; Raghubir Gupta — Research Triangle Institute; and Raul Ayala — GE Corporate Research & Development

A Membrane Reactor for H_2S Decomposition
D. Edlund — Bend Research, Inc.

Separation of Hydrogen Using an Electroless Deposited Thin-Film Palladium-Ceramic Composite Membrane
Shamsuddin Ilias, Franklin G. King, Ting-Fang Fan, and Sabita Roy — North Carolina A&T State University

Related Environmental Issues

Advances in Ammonia Removal from Hot Coal Gas
K. Jothimurugesan — Hampton University; and Santosh K. Gangwal — Research Triangle Institute

Market Assessment and Technical Feasibility Study of Pressurized Fluidized Bed Combustion Ash Use
Alan E. Bland and Terry H. Brown — Western Research Institute

The Impact of Leachate From Clean Coal Technology Waste on the Stability of Clay and Synthetic Liners
Terry H. Brown — Western Research Institute

Utilization of Lightweight Materials Made from Coal Gasification Slags
Vas Choudhry and Steve Hadley — Praxis Engineers, Inc.

Continuous Mercury and Chloride Monitors for Coal Gasifiers
G. Norton, D. Eckels, and C. Criswell — Iowa State University

Dynamic Analysis of Process Reactors
Lawrence J. Shadle, Larry O. Lawson, and Stephen D. Noel — Morgantown Energy Technology Center

To return to the Proceedings *Contents* page or the *Cover*, click the **Go Back** button (the double left-pointing arrow) from the tool bar at the top of the screen, or choose **Go Back** from the view menu.

Disclaimer

This report was prepared as an account of work sponsored by an agency of the United States Government. Neither the United States Government nor any agency thereof, nor any of their employees, makes any warranty, express or implied, or assumes any legal liability or responsibility for the accuracy, completeness, or usefulness of any information, apparatus, product, or process disclosed, or represents that its use would not infringe privately owned rights. Reference herein to any specific commercial product, process, or service by trade name, trademark, manufacturer, or otherwise does not necessarily constitute or imply its endorsement, recommendation, or favoring by the United States Government or any agency thereof. The views and opinions of authors expressed herein do not necessarily state or reflect those of the United States Government or any agency thereof.

Available to DOE and DOE contractors from the Office of Scientific and Technical Information, 175 Oak Ridge Turnpike, Oak Ridge, TN 37831; prices available at (615) 576-8401.

Available to the public from the National Technical Information Service, U.S. Department of Commerce, 5285 Port Royal Road, Springfield, VA 22161; phone orders accepted at (703) 487-4650.

Foreword

The Advanced Coal-Fired Power Systems ’96 Review Meeting was held July 16-18, 1996, at the Morgantown Energy Technology Center (METC) in Morgantown, West Virginia. This meeting was sponsored and hosted by METC, the Office of Fossil Energy, and the U.S. Department of Energy (DOE).

METC annually sponsors this conference for energy executives, engineers, scientists, and other interested parties to review the results of research and development projects; to discuss the status of advanced coal-fired power systems and future plans with the industrial contractors; and to discuss cooperative industrial-government research opportunities with METC’s in-house engineers and scientists. Presentations included contractor and METC in-house technology developments related to (1) the production of power by coal-fired Integrated Gasification Combined Cycle (IGCC) and Pressurized Fluidized Bed Combustion (PFBC) systems; and (2) developments and advancements in advanced technology subsystems, such as hot gas cleanup. Activities at the Power System Development Facility in Wilsonville and plans for the Desulfurization Process Development Unit at METC were highlighted. The keynote speaker, a representative from a leading international power producer, gave his assessment of international markets and challenges for Advanced Power systems. A theme of the conference was planning fossil energy research and development for a competitive power industry.

This meeting contained seven formal sessions and two poster sessions, and included 43 formal papers and 34 poster presentations. The papers and presentations in this document were produced in large measure from electronic files provided by the authors. They have been neither refereed nor extensively edited. The meeting Proceedings was provided to participants on a CD-ROM, and the papers and presentations are available worldwide on the METC Homepage over the internet (URL: http://www.metc.doe.gov).

Conference Technical Coordinators:
Thomas P. Dorchak
Charles A. Komar

Conference Technical Assistance:
Richard A. Dennis
Darren J. Mollot

METC

FOSSIL ENERGY R&D FOR A COMPETITIVE POWER INDUSTRY[1]

Rita A. Bajura

Thank you. I am pleased to be here today to discuss a vision for the Morgantown Energy Technology Center's (METC's) advanced power generation program. I will cover four topics:

- The status of the electric industry as it deregulates, particularly those aspects of deregulation that impact advanced power generation technologies;
- A snapshot of the environmental trends that influence the program;
- How we're structuring our research, development, and demonstration (RD&D) program in response to these trends; and
- The status of METC's merger with our sister center, the Pittsburgh Energy Technology Center.

Starting with deregulation, in April of this year, the Federal Energy Regulatory Commission issued the final version of Order Number 888. This Order requires electric utilities to open their transmission lines to competitors on a nondiscriminatory basis. Order 888 will effectively deregulate electric power generation in the U.S. In a deregulated world, electric utilities can sell electricity to any customer--whether that customer is inside or outside their traditional service area.

I do not have to be a visionary to predict the impact of deregulation on the electric industry. We know what happened when the Government deregulated the natural gas, telephone, trucking, and airline industries. Cutthroat price competition is the most visible sign of deregulation--and it has started. Some utilities are selling their excess electricity on the wholesale market for 2 cents/kWhr. This is the incremental price to produce the electricity, with virtually no capital recovery in the price.

Deregulated utilities will aggressively market their products. Utilities in Argentina carried this to the extreme recently. There, the electric industry is further down the deregulation path. Argentina had a month-long electricity "price war." In an attempt to attract new customers, utilities were giving away their electricity free. In the U.S., when deregulation is extended to retail customers, expect to see more advertisements for electricity--the equivalent of Sprint, MCI, and AT&T ads--but for electric products. These products will be anything we, the customers, want and are willing to pay for, be that total energy supply (electric, gas, steam), energy management services, coupled energy/telecommunications services, or tree-pruning services by the utilities' line crew.

To reduce cost, electric companies are cutting staff and are merging. Some are friendly mergers; some hostile. They are also getting more out of their existing equipment by shipping more electrons through existing transmission systems and generating more kWhr of electricity in existing plants. To achieve higher utilization rates, equipment has to be available to dispatch. This makes reliability and ease of maintenance important parameters for the electric industry.

---

[1] Presented at the Advanced Coal-Fired Power Systems '96 Review Meeting, July 16-18, 1996, Morgantown, WV.

To increase demand during off-peak times of the day, many utilities are exploring time-of-day pricing. Cheaper electricity at midnight may encourage us to stay up to midnight to do our laundry--thereby filling a valley in the daily demand profile. This greater use of existing plants means there is much more excess capacity than anyone thought!

Reducing fuel cost is another cost reduction strategy. Deregulation is the death knoll for pass-through-fuel-costs. Without past-through-fuel-cost, efficiency becomes an important parameter in the cost of electricity equation. Utilities are looking for low-cost upgrades for their existing plants to improve efficiency. The industry is negotiating lower-cost fuel supply contracts. They are also exploring the use of low-cost opportunity fuels such as orimulsion and petroleum coke.

The electric industry will cut societal benefit programs way back in a competitive market. These programs range from wind farms, to demand side management, to helping the poor pay their electric bills. In the past, the industry paid for these programs through a hidden subsidy in the rate structure. In a competitive market, there will be no more hidden subsidies.

The outlook for natural gas in a deregulated environment is less clear. Electronic bulletin boards and open access will let utilities transmit low-cost coal or nuclear power over long distances. This suggests a downward trending in gas use. However, gas prices are projected to stay low for at least the next 2 decades. The Department of Energy's Energy Information Agency (DOE/EIA) projects that wellhead gas prices will rise a modest 1.5 percent per year between now and the year 2015.

Low gas prices coupled with low prices for gas turbine equipment means that the total cost of electricity from new, state-of-the-art combined cycles is very low, in the range of 2.5 to 3.0 cents per kWhr. Clearly, in the near term, natural gas will be the fuel of choice for new capacity additions. New gas-fired combined cycles can also be used in the near term for economic replacements. These are replacement and/or repowering of nuclear or old coal plants that have high operating and maintenance (O&M) costs.

RD&D will suffer in a deregulated, competitive industry, particularly long-range R&D. For the utility industry, RD&D is a back burner issue. Issues like deregulation and mergers are more important. Utilities are spending their limited RD&D funds to reduce O&M costs or to improve reliability. There is little incentive to invest in advanced power generation technologies. The technology will still produce electrons, and customers cannot distinguish one electron from another.

Utilities also have little incentive to invest in collaborative RD&D projects, particularly if the project helps their competitors. The Electric Power Research Institute and the Gas Research Institute are seeing this dynamic play out in real time as they lose their supporting members.

Utilities also have limited incentive to cost share in Government RD&D projects. This is a difficult trend for the Government to deal with. Congress is demanding that we shift our RD&D projects toward longer-term research. Yet they are defining success as increased levels of industry cost sharing.

A major remaining uncertainty is how fast deregulation will occur. It could occur quickly, over a 2- to 3-year period, or it

could drag out for a decade or more. Further, each state Public Utility commission could establish their own version of deregulation and their own timetable for it. These uncertainties coupled with the low domestic demand growth mean that the industry is reluctant to invest in new plants in the U.S. With excess capacity available at 2 cents per kWhr (at least in some parts of the country), it is difficult to find sites where new units make economic sense. And with deregulation, the electric industry does not have captive customers to foot the bill for imprudent investments.

Switching from deregulation to the environment, the U.S. public is clearly committed to the goal of clean water, blue skies, and a healthy environment for our children and our children's children. For the electric industry, the uncertainty in the environmental arena is what is reality and what is fear-mongering. The Integrated Gasification Combined Cycle (IGCC) and Pressurized Fluidized-Bed Combustion (PFBC) technologies that are the subjects of this conference will meet the Phase I and Phase II requirements of the Clean Air Act amendments for SO_x and NO_x emissions. I see three remaining environmental uncertainties for these advanced power generation technologies.

The first uncertainty relates to both air toxics and fine particulate matter--particles less than 10 microns or less than 2.5 microns. We need, and we plan to obtain, quality data from our Clean Coal Technology (CCT) demonstration projects to learn the real emission levels and if we need mitigation strategies. However, we are confident that emissions will be not higher than those from conventional coal-fired power plants; we have good reason for believing the emissions will be much lower. Whatever the outcome of the measurements, the air toxic and fine particulate issue is common to other coal-fired technologies.

The second environmental issue is the Not in My Backyard (NIMBY) syndrome. NIMBY can apply to the siting of both new transmission and new generation facilities. This syndrome manifests itself in concerns over electromagnetic fields which makes it nearly impossible to obtain new right-of-ways for high-voltage transmission systems.

A partial answer to the transmission system dilemma may be distributed power generation technologies--fuel cells, small gas turbines, and gas-fired reciprocating engines. These can be installed close to the end-user of the electricity. Thus, no new transmission system is needed but an adequate gas supply pipeline is required.

The last environmental issue is global warming. There are strong opinions on both sides of this debate. On one end of the spectrum, a few months ago, an editorial in Wall Street Journal suggested that publicity on global warming was a political strategy "to keep the populace alarmed and hence clamorous to be led to safety by menacing it with an endless series of hobgoblins, all of them imaginary." At the other end of the spectrum, the banking and insurance industry are becoming vocal on the topic. They want to limit fossil fuel that they feel is causing global warming, which is triggering giant storms, which are costing them billions of dollars.

Given these environmental trends and deregulation in the electric industry, how is DOE structuring its coal power systems RD&D program? The first issue we need to address is, should the Government fund an RD&D program at all? Is it corporate welfare? Why should the Government support

electric sector R&D when it does not fund R&D in other industries?

I believe the Government's unique role in assuring that regulatory requirements do not choke our economy. We, the Federal Government, originate most of these requirements, and, therefore, we should help industry in developing cost-effective technologies to meet these requirements. Electric power generation has a major impact on the economy. We spend nearly $200 billion per year for electricity in the U.S. The ripple effect to the industrial, commercial, and residential sectors is several times that amount.

The issue then becomes--why do R&D on power generation technologies when our demand growth rate will continue to be low for the next 20 years? DOE/EIA projects a growth rate of 1.4 percent per year. The reality is despite the low demand growth rate, the U.S. is applying this growth rate to a large and aging fleet of power plants. Thus, there are lots of opportunities to build new plants to meet both new capacity and retirement needs. DOE/EIA projects more than 230 gigawatts (GW) of new capacity will be needed between 1996 and 2015 to meet these needs. While much of this will be peaking capacity, we will need 27 GW of new coal capacity. We will need the new coal base-load capacity primarily after 2005 to replace nuclear plants that are being retired at the end of their 40-year licensing period. Thus, in the next 20 years, the domestic investment in new plants will be more than $100 billion. If nuclear plants are retired early, then the new capacity needs will shoot up dramatically. Some believe this will happen because of nuclear's high O&M costs.

The offshore need for new plants is many times larger than our domestic needs. I am sure the next speaker will enlighten us on this topic. The large offshore demand will provide U.S. jobs through the export of generation equipment (particularly high power density equipment such as gas turbines and fuel cells) and engineering and project development services.

The debate continues. Some advocate abandoning fossil-based power generation. But fossil energy currently provides 68 percent of our electricity. DOE/EIA projects this will grow to 79 percent by 2015. The growth is primarily due to increased use of natural gas and coal. The fact is we cannot say <u>no</u> to coal and to gas-fired power generation and still keep electric prices low and the economy healthy. We believe it is vital that cleaner, less expensive advanced technology for producing electricity be available. The goal of our R&D program is to produce these technologies--technologies that are responsive to the need of the deregulated electric industry and to environmental drivers.

Thus, our R&D program responds to eight issues that I want to cover:

1. <u>Repowering</u>. Advanced technologies like IGCC and PFBC are ideal technologies to repower existing permitted sites. These sites are irreplaceable assets. Repowering means using the existing steam turbine-generator and any other usable equipment at an existing site, including coal-handling equipment. You do not need to obtain new transmission right-of-ways with repowering. It is relatively free of NIMBYism since it generally reduces net emissions from the existing site. The market opportunities for repowering are large. More than 280 GW of existing fossil/steam

capacity will be >40 years old by 2015, with about one-half of that capacity the 65 to 250 MW range of interest for repowering.

2. Use of opportunity fuels--petroleum coke and other low-cost fuels. We are starting to address the use of opportunity fuels in the program. Low-cost, opportunity fuels may offer the best approach to move advanced technologies along the path toward commercialization.

3. Capital cost reduction. The program is emphasizing reducing capital cost of our technologies--without compromising either efficiency or reliability. For example, tight integration of the gasifiers and the turbine can improve efficiency but devastate cost and/or reliability. Advanced technologies must be much cheaper, more reliable, and more efficient than conventional technologies to offset any perceived increased technical risk.

4. Right-sized technologies. The program is committed to targeting the "right-sized" technologies for the deregulated market. New power plants will need to be small enough to reduce capital exposure, large enough to capture the benefits of economy of scale. Thus, new units are likely to be 100- to 400-megawatt (MW) size range. This is a much more modest size than the 800- and 1000-MW units that utilities built in the 1970's.

5. Global warming. We are convinced we need to take the global warming challenge head-on. Thus, we set a long-term goal of zero emissions--including CO_2 emissions--from our advanced technologies. In the nearer term, we intend to push on improving efficiency as an approach to reducing CO_2 emission. Fuel/cell turbine systems on natural gas will have efficiencies of more than 70 percent--nearly twice that of today's average fossil steam plant. On coal, these systems will be more than 60 percent efficient. In the longer term, at a minimum, we will develop better estimates of the real cost of zero emission systems, including CO_2 mitigation strategies such as tree planting.

6. R&D partnerships. We will work to develop more R&D partnerships with industry and with other parts of DOE. These partnerships may be outside our traditional menu of power generation technologies. We are exploring the formation of joint research programs with DOE/Energy efficiency and DOE/Energy Research to leverage funding.

7. Grand challenges. We intend to seek out some grand challenges and explore how we can integrate them into our R&D program, at least on a small scale. In the late 1970's and early 1980's, the Government sponsored two massive systems studies to develop conceptual designs for a whole boatload of advanced power generation concepts. For students of history, these were the ECAS and the DAFFS studies. We have dropped the losing technologies from the program: magneto hydrodynamics, air-cooled PFBC, and metal vapor Rankine topping cycles. The winners, as you will hear today, are in the demonstration stage in the CCT program. There are not many new fossil energy technologies in the pipeline.

The grand challenge is to envision what power generation technology the U.S. will be using 100 or 200 years from now--and then do the enabling research to bring them into existence. It could be the fossil equivalent of cold fusion coupled with room temperature superconductivity. We believe that an appropriate role for the Government is to lead the charge with "paradigm shifters" that could remake the electric industry. This is fertile for the university community to contribute to understanding--what could be. We must focus on forging the future, not preserving the past.

8. Working smarter. The reality is that Government funding for R&D is being reduced. We need to work smarter to structure programs that offer taxpayers the best value for their investment in the context of lower budgets. Part of working smarter is merging METC and PETC--my last topic.

Discussions on a METC and PETC merger have been underway since 1993. It takes a long time to make things happen in the Government! At last year's Contractor's meeting we thought the merger would happen soon. My hope is that it is really much closer now! After several on-again/ off-again over the past few weeks, I believe the merger is back on track and will be completed this fiscal year. The language in the report accompanying the Senate subcommittee markup of the Fiscal Year 1997 Appropriation bill conditionally approved the merger--subject to several conditions--none of which appear to be showstoppers. The merger will be a complete integration of METC and PETC. The consolidated center will have one Director and a joint management team operating both sites as if they were co-located. With modern communications systems, we believe this is eminently doable. We will lose the "lead center" designation for R&D programs. Thus, personnel at either center can carry out R&D programs.

I see two primary benefits of the merger for you, our customers. First, it will reduce our overhead costs, leaving more funds available for the R&D program. Second, joint planning and budgeting will enable us to make better strategic decisions on the direction of the program.

In conclusion, we cannot ignore the role that low-cost electrical power plays in keeping the U.S. economy globally competitive. Advanced power systems will help keep electric costs low while still meeting our environmental imperatives. The combination of improved environmental performance and lower cost is critical if U.S. companies are to compete and win in the domestic and burgeoning global markets. We need your leadership in making sure that we are working on the right technologies, addressing the right R&D issues, and providing you the information you need to do your job--be that university researcher, equipment developer, or utility participant.

The "new DOE" is more than open to your opinions; we will assertively seek it and we commit to reflect it in our actions. Unless our customers succeed, we have no reason for being.

Thank you for your attention and hopefully your comments and questions during this conference.

RBAJUR\961269.w61

Advanced Coal-Fired Power Systems '96

Dan Brdar IGCC Product Manager
Bob Reuther PFBC Product Manager

Morgantown Energy Technology Center
July 16, 1996

M96001844C

Overview

- *Product Lines*
- *Product Goals*
- *Product Development Strategy*
- *This Year's Successes*
- *Barrier Issues*
- *Key Plans For Next Year*
- *Technical Status*
- *Market Opportunities*

Vision

Worldwide, Most New And Repowered Electric Generating Capability Will Use IGCC And PFBC Technologies Due To Their Superior Environmental Performance, Cost And Efficiency

M96001867C

Product Lines

"The Future of Coal Based Power Generation"

IGCC

PFBC

M96001846C

Integration Gasification Combined Cycle (IGCC)

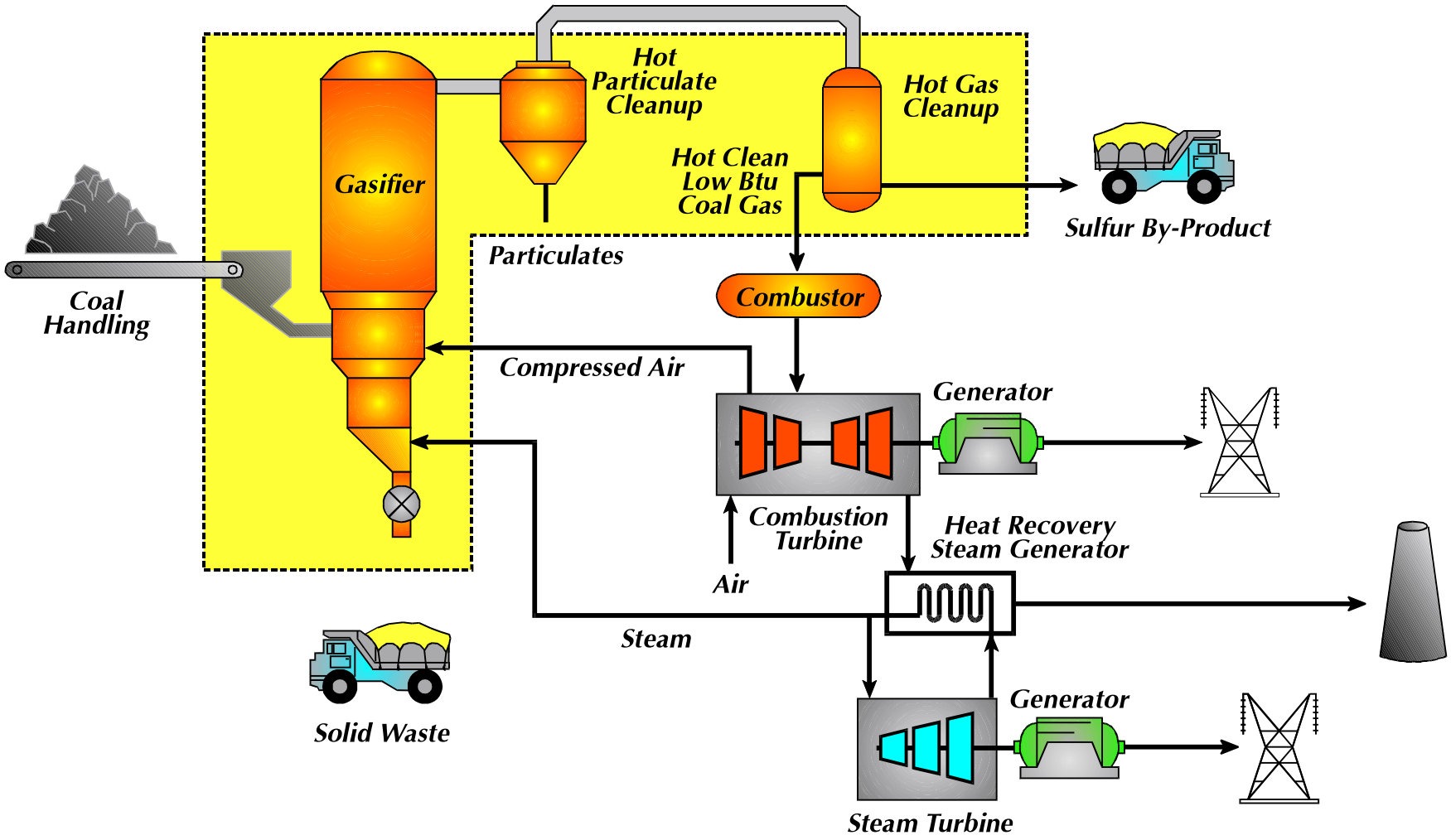

M96001814C

Pressurized Fluidized Bed Combustion (PFBC)

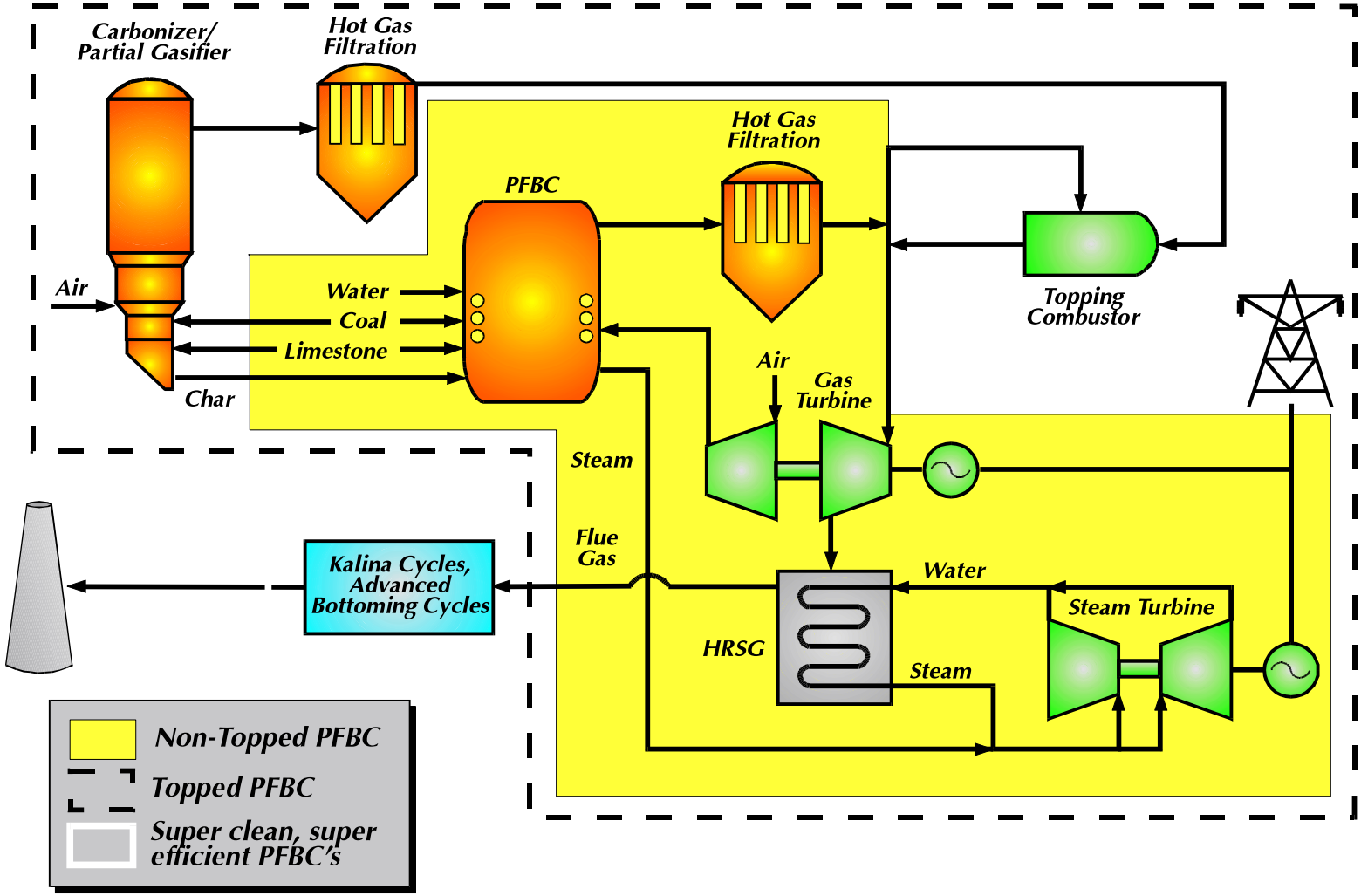

M96001851C

Goals

- *Coal Based Power Systems*
  - *Environmental Performance*
  - *Efficiency*
  - *Cost*

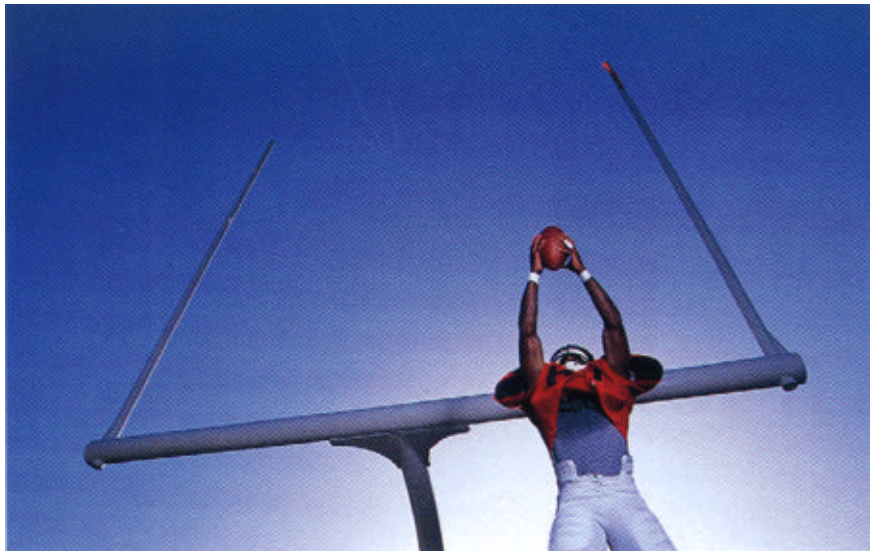

M96001850C

IGCC Goals

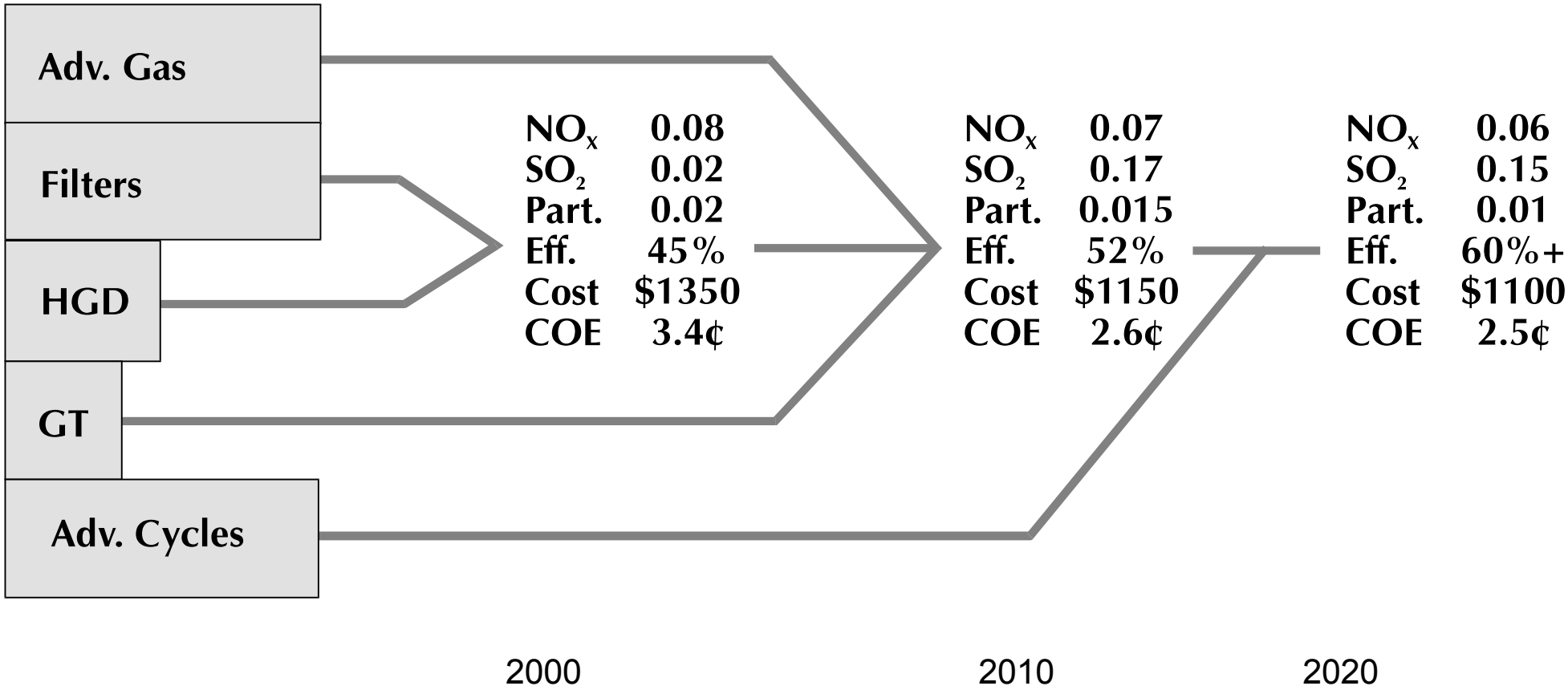

M96001859C

PFBC Goals

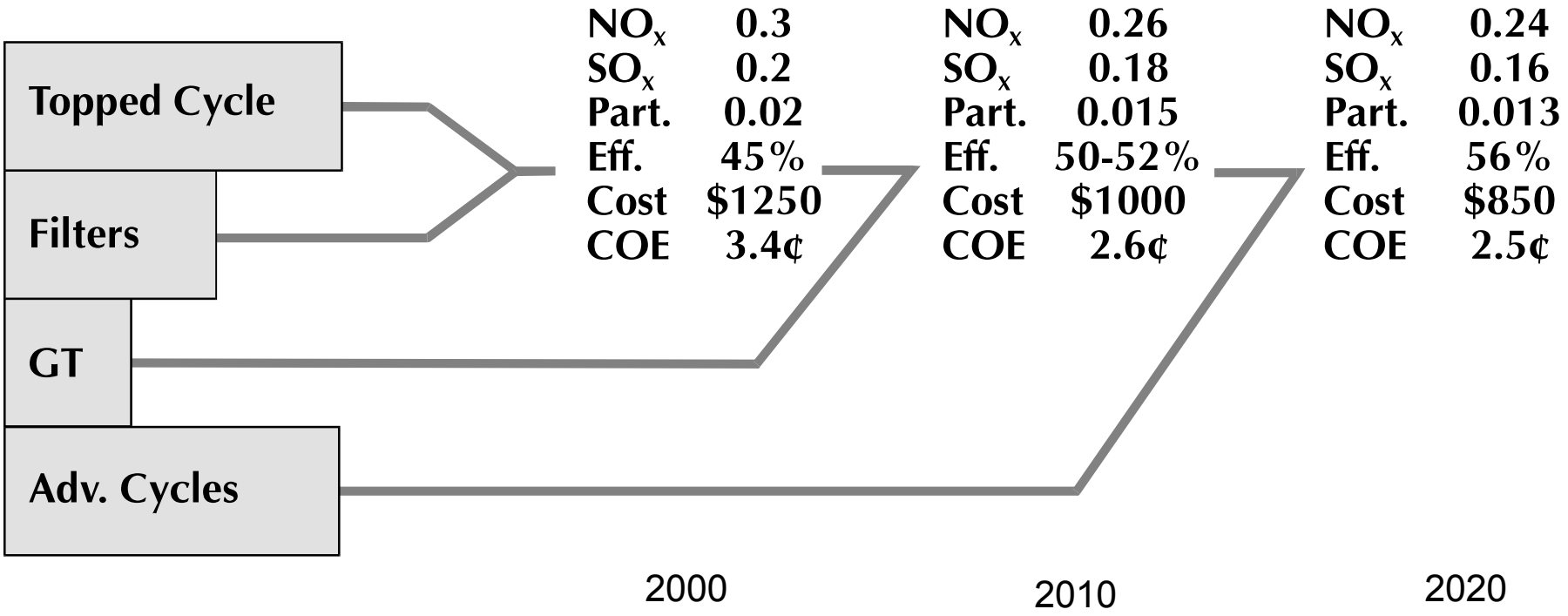

M96001860C

Product Development Cycle

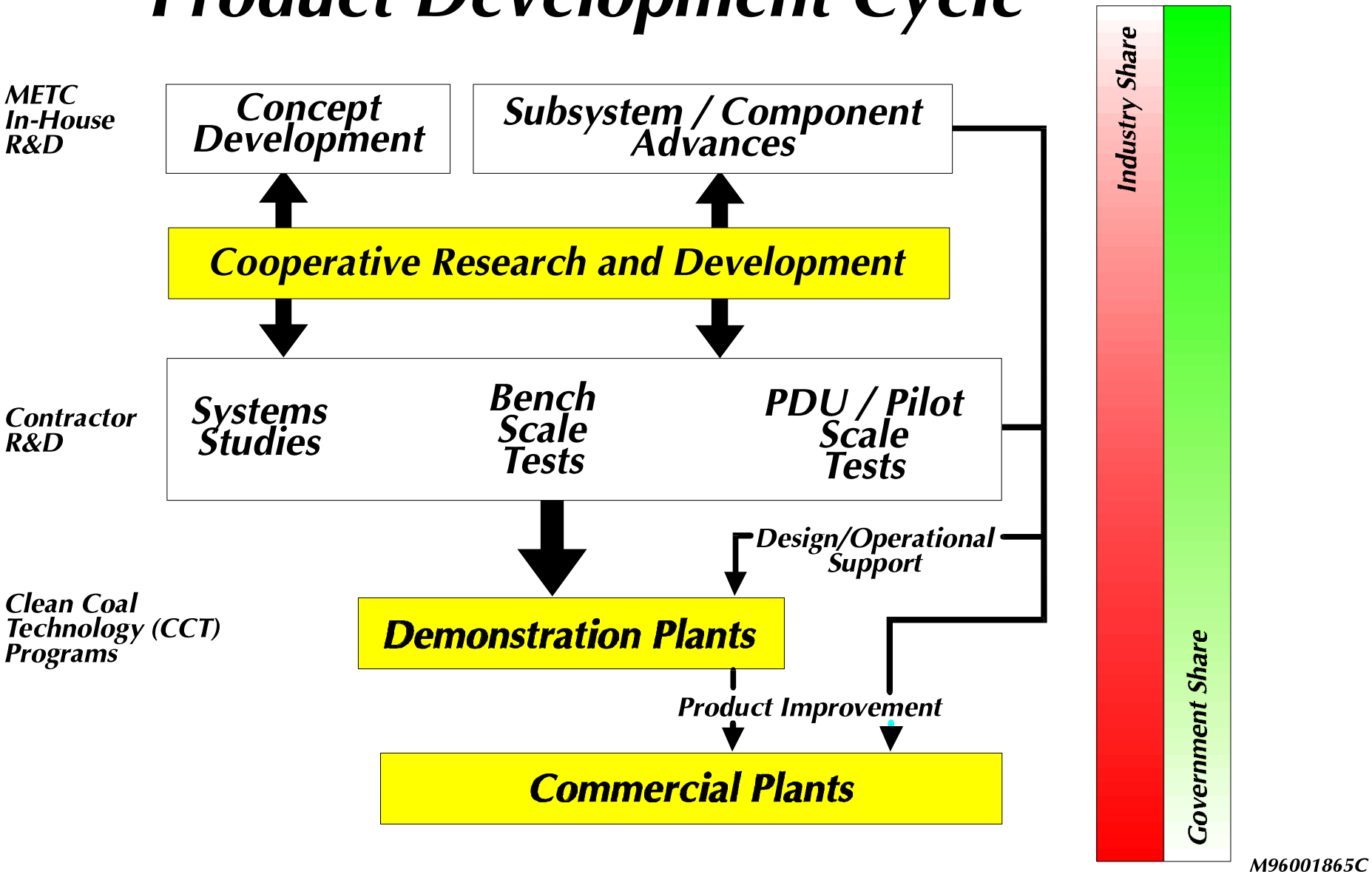

Product Development Cycle

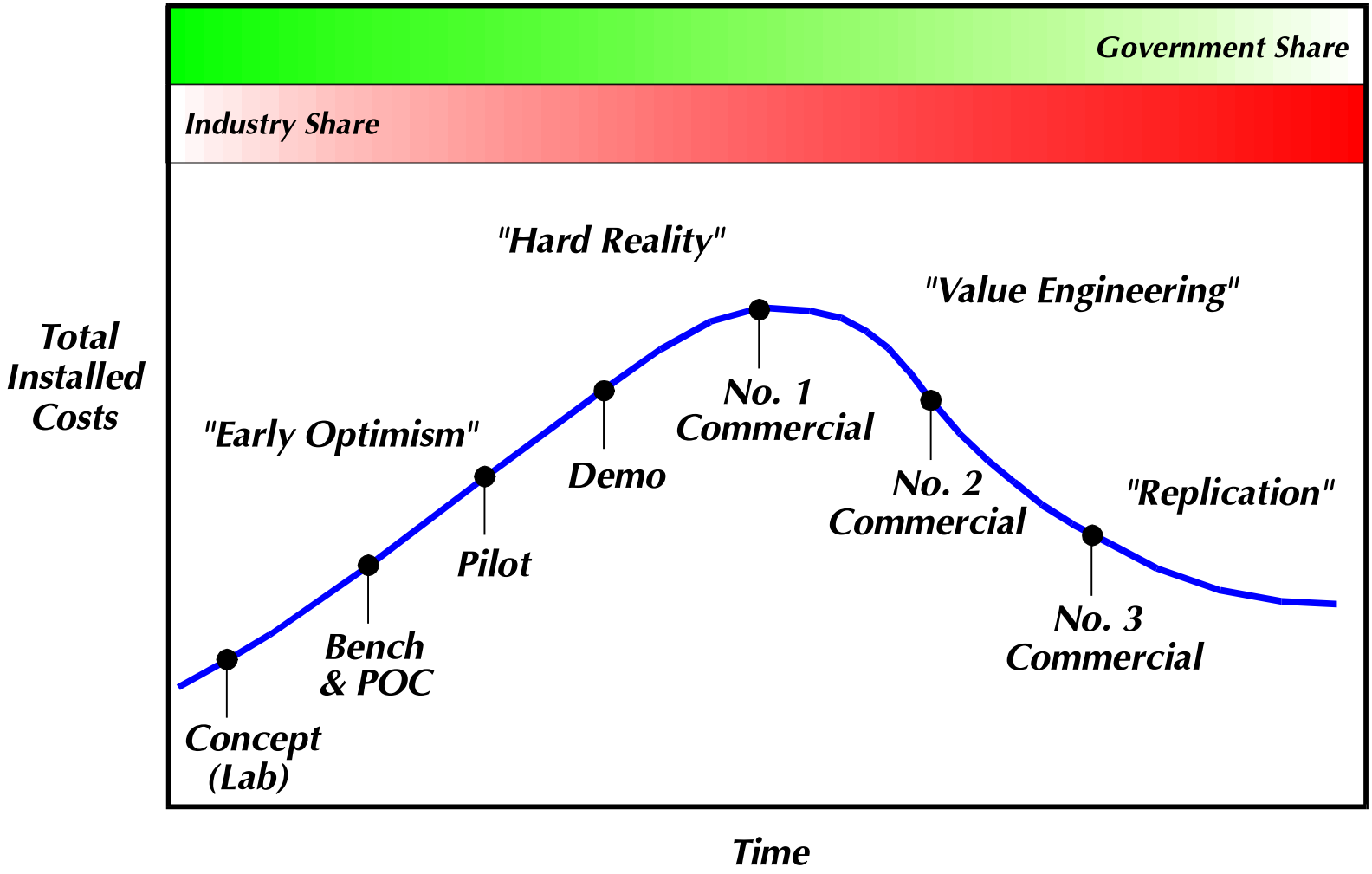

M96001864c

Technical Status

- ***Key R&D Activities***
- ***Product Development***
- ***Demos and R&D***

M96001855C

Key R&D Activities

Filters

EERC
MGCR
KARHULA
METC

Sorbents

ICCI
GEESI
METC
RTI

Air Toxics

LGTI
AMES

M96001858C

IGCC Projects, Major R&D, Support

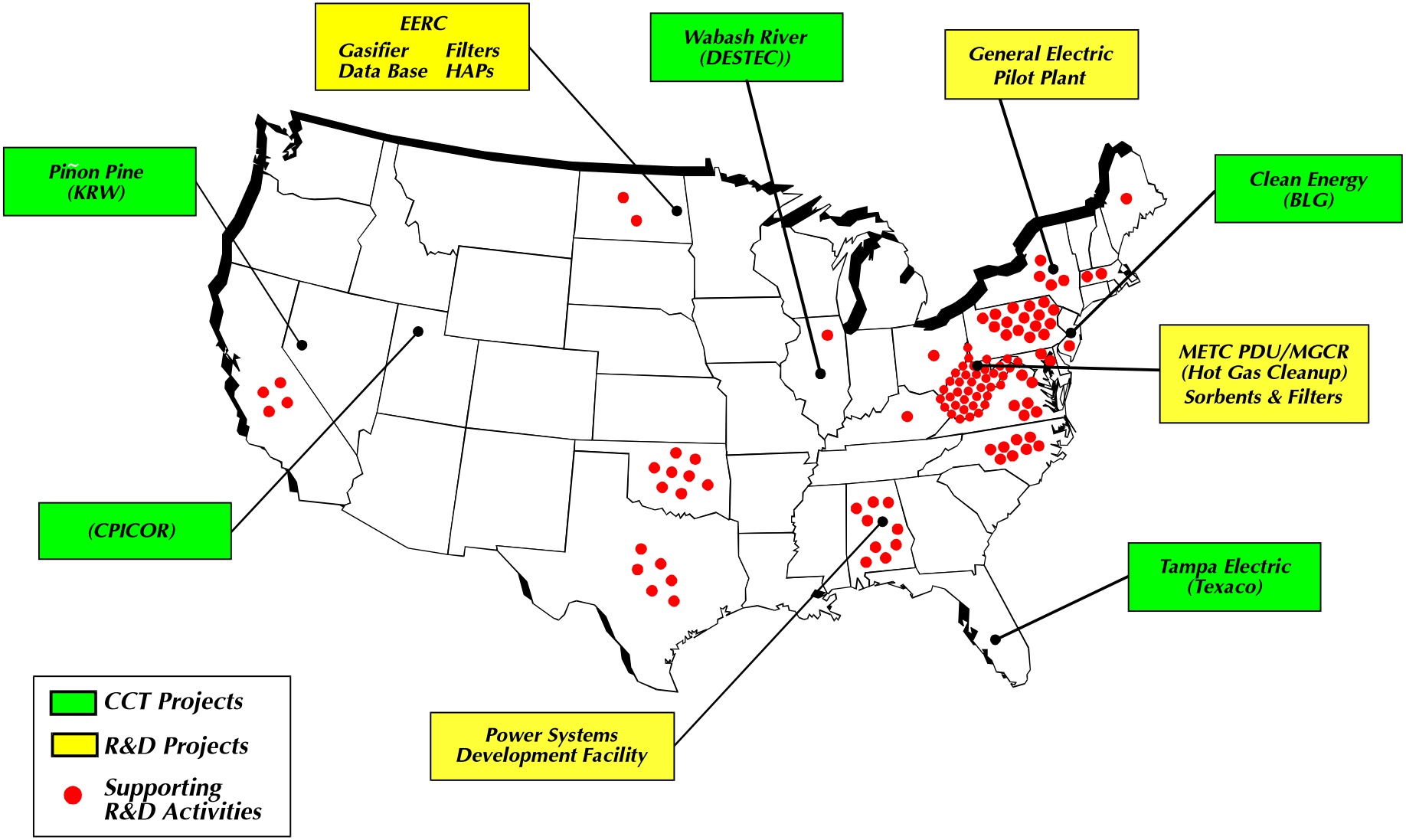

PFBC Projects, Major R&D, Support

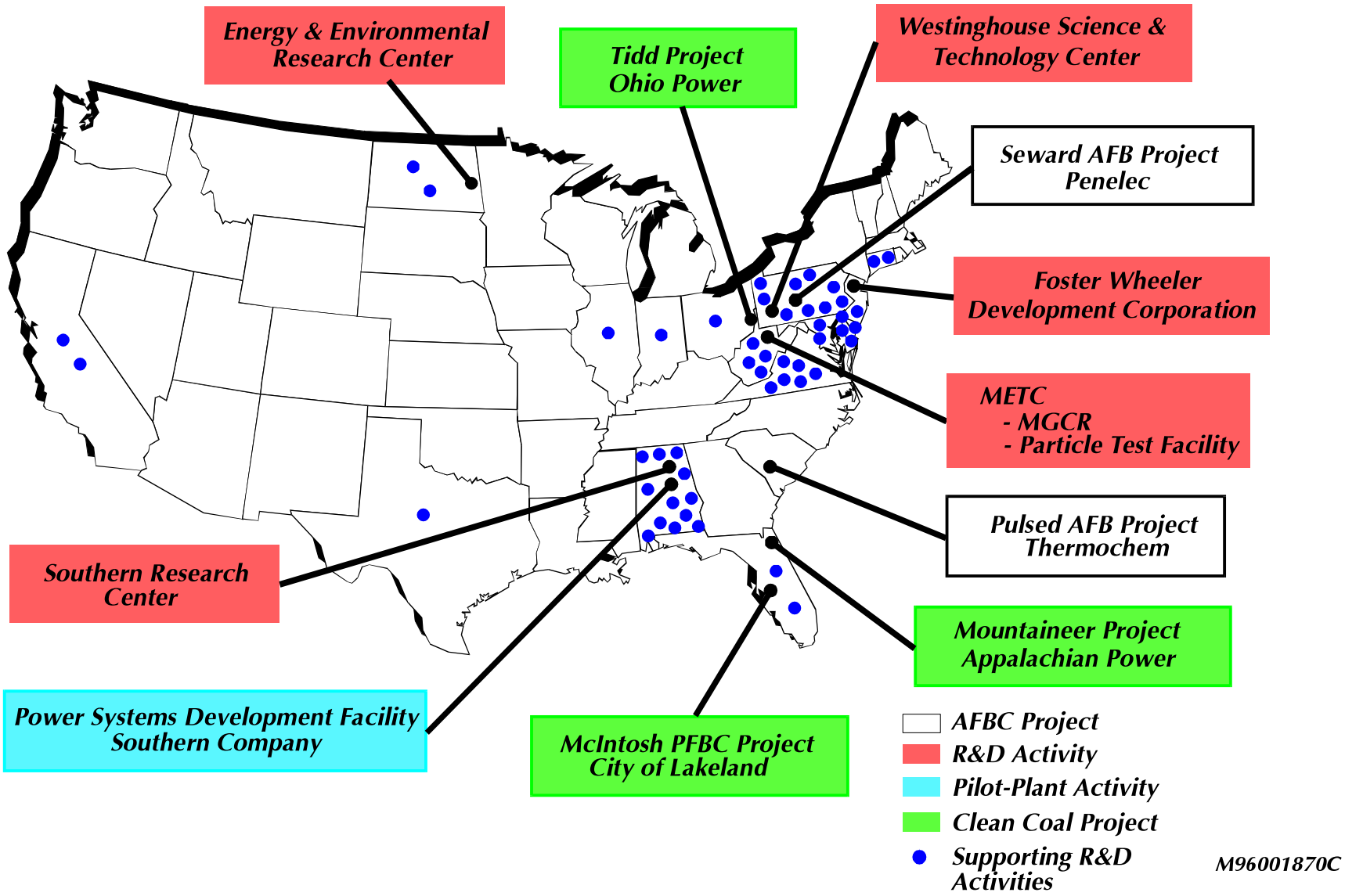

Power Systems Development Facility Consists of Two Separate Reactor Systems

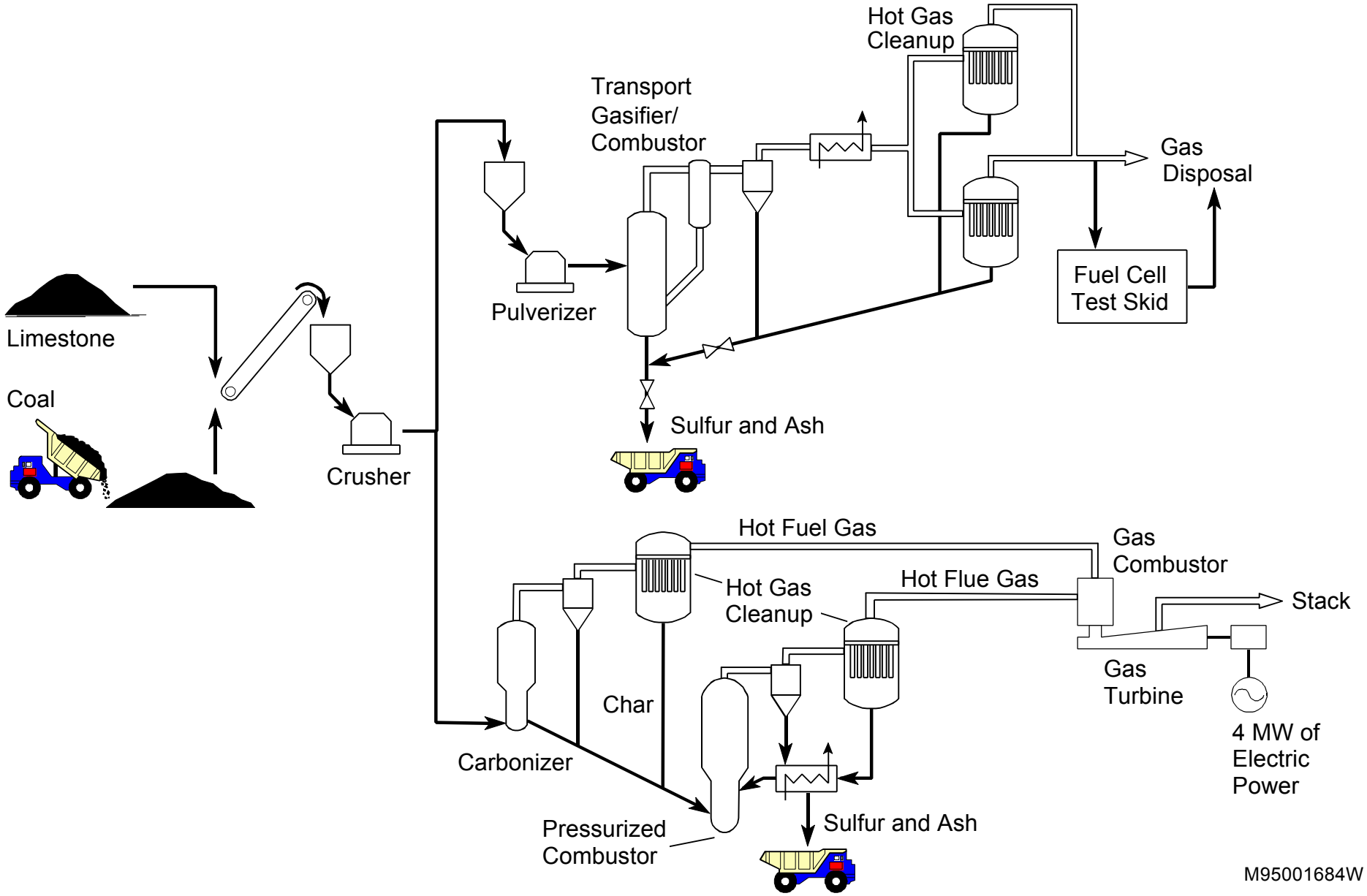

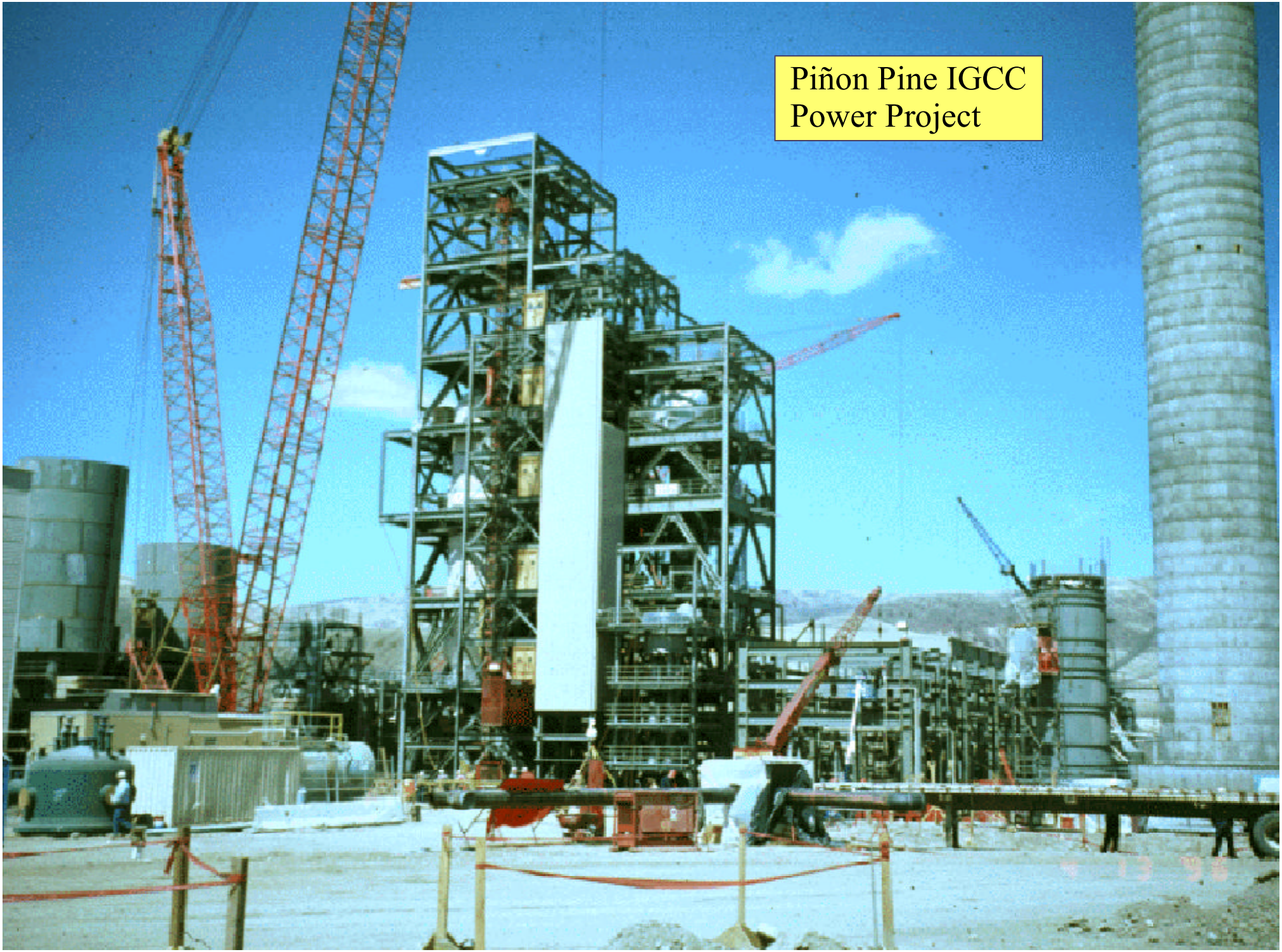
Piñon Pine IGCC
Power Project

GEESI Moving Bed Desulfurizer

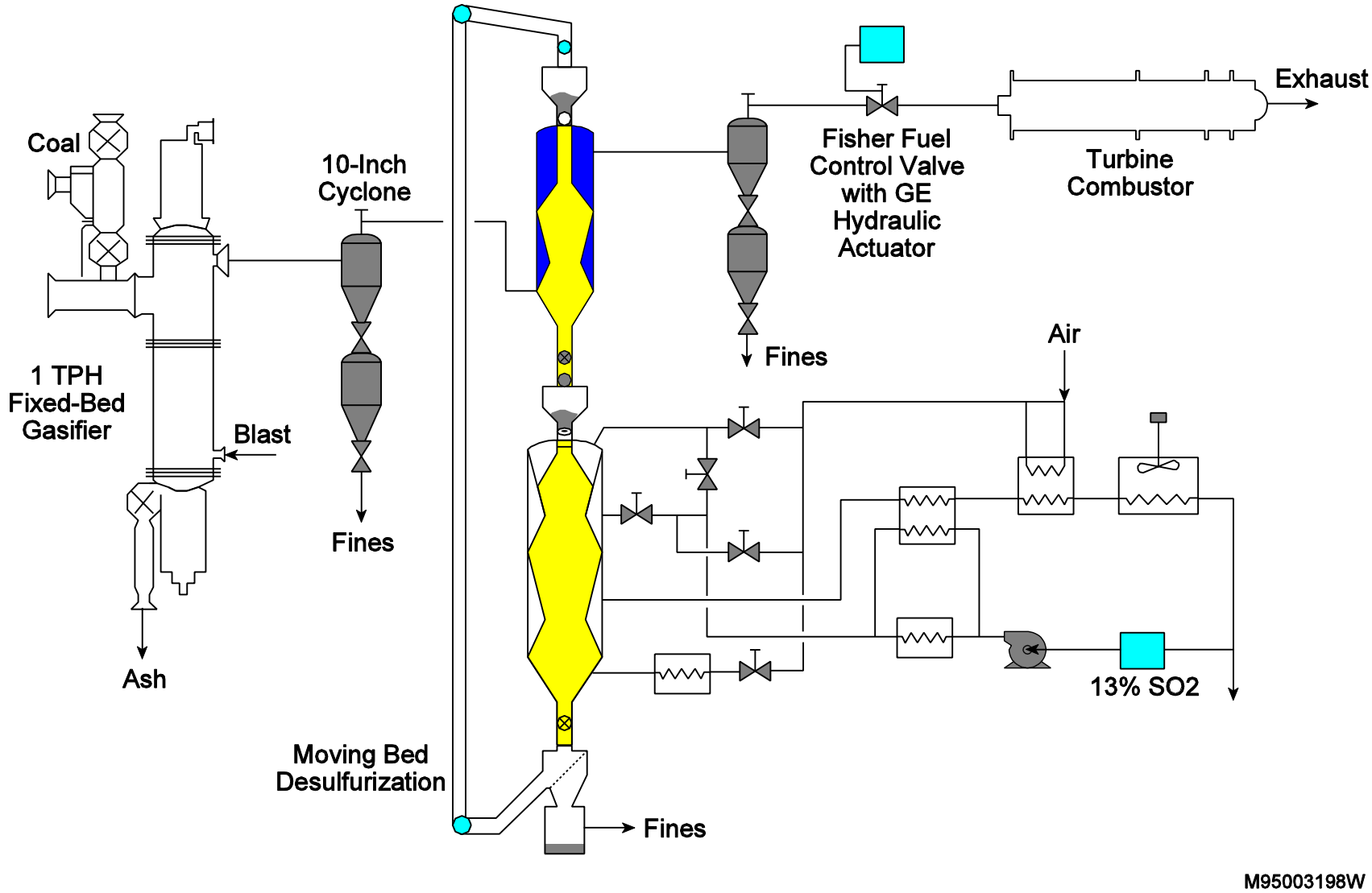

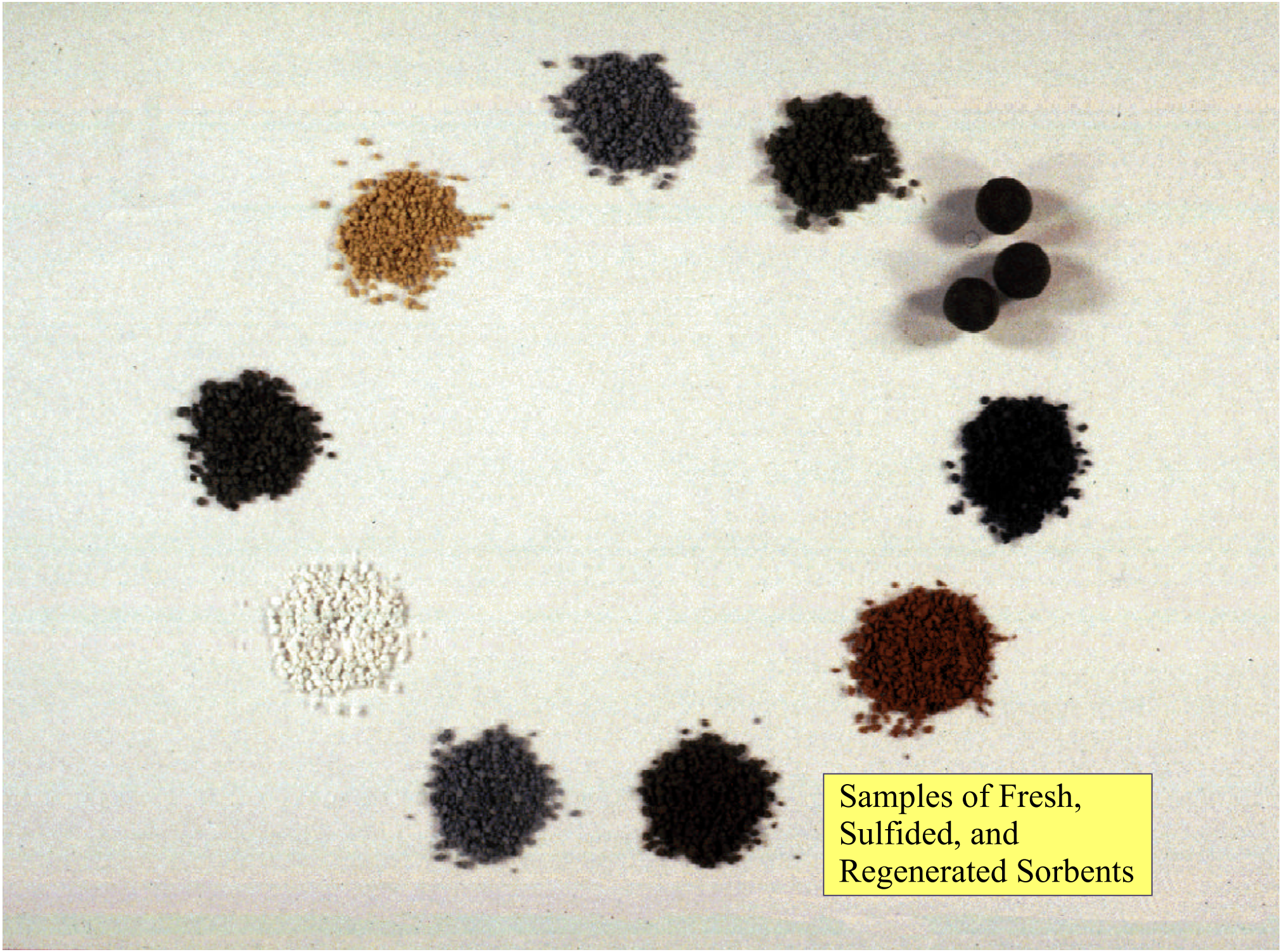

Samples of Fresh, Sulfided, and Regenerated Sorbents

PDU Reactor Schematic

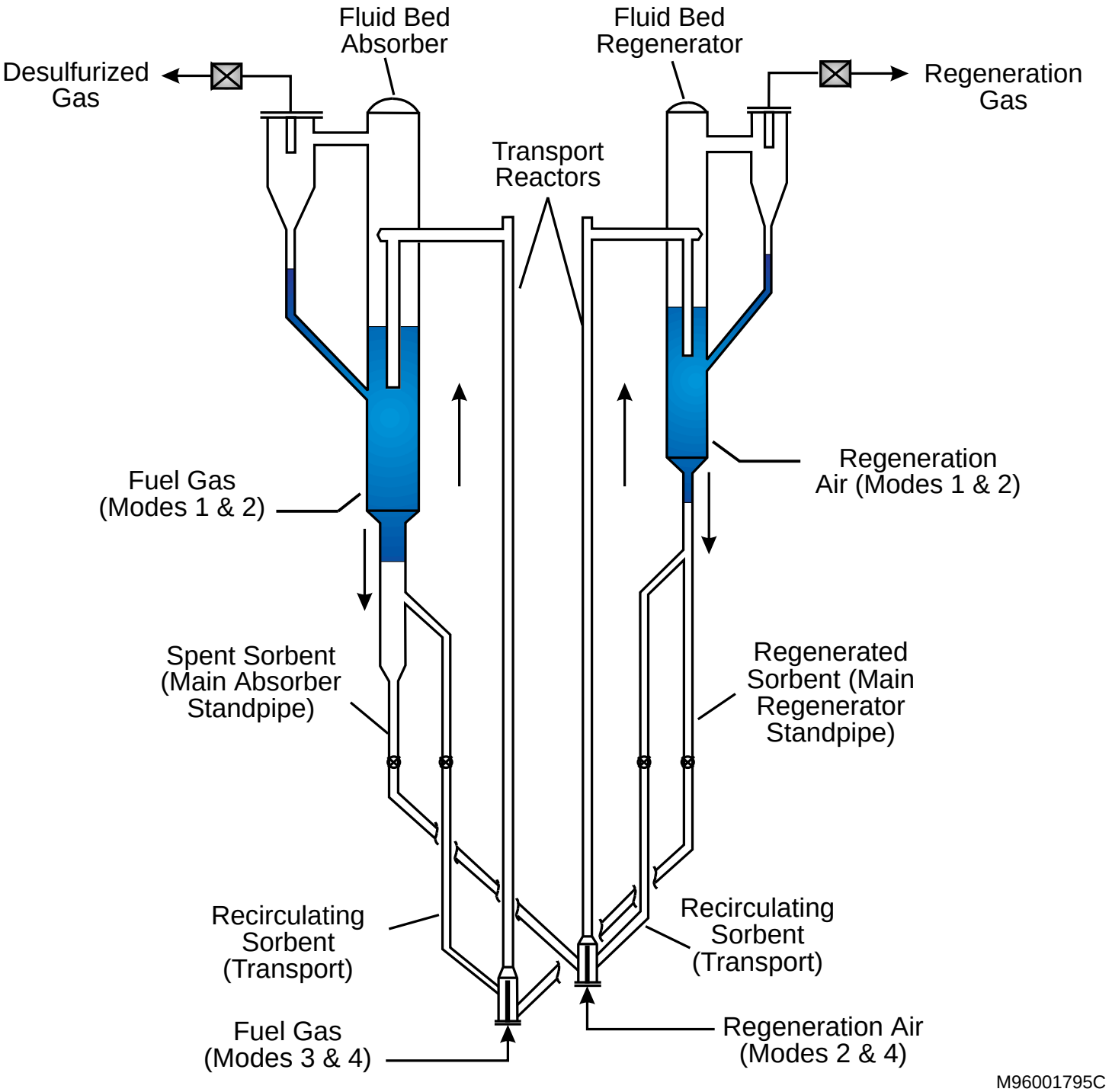

METC
Desulfurization PDU

Transport Reactor with Hot-Gas Filter System

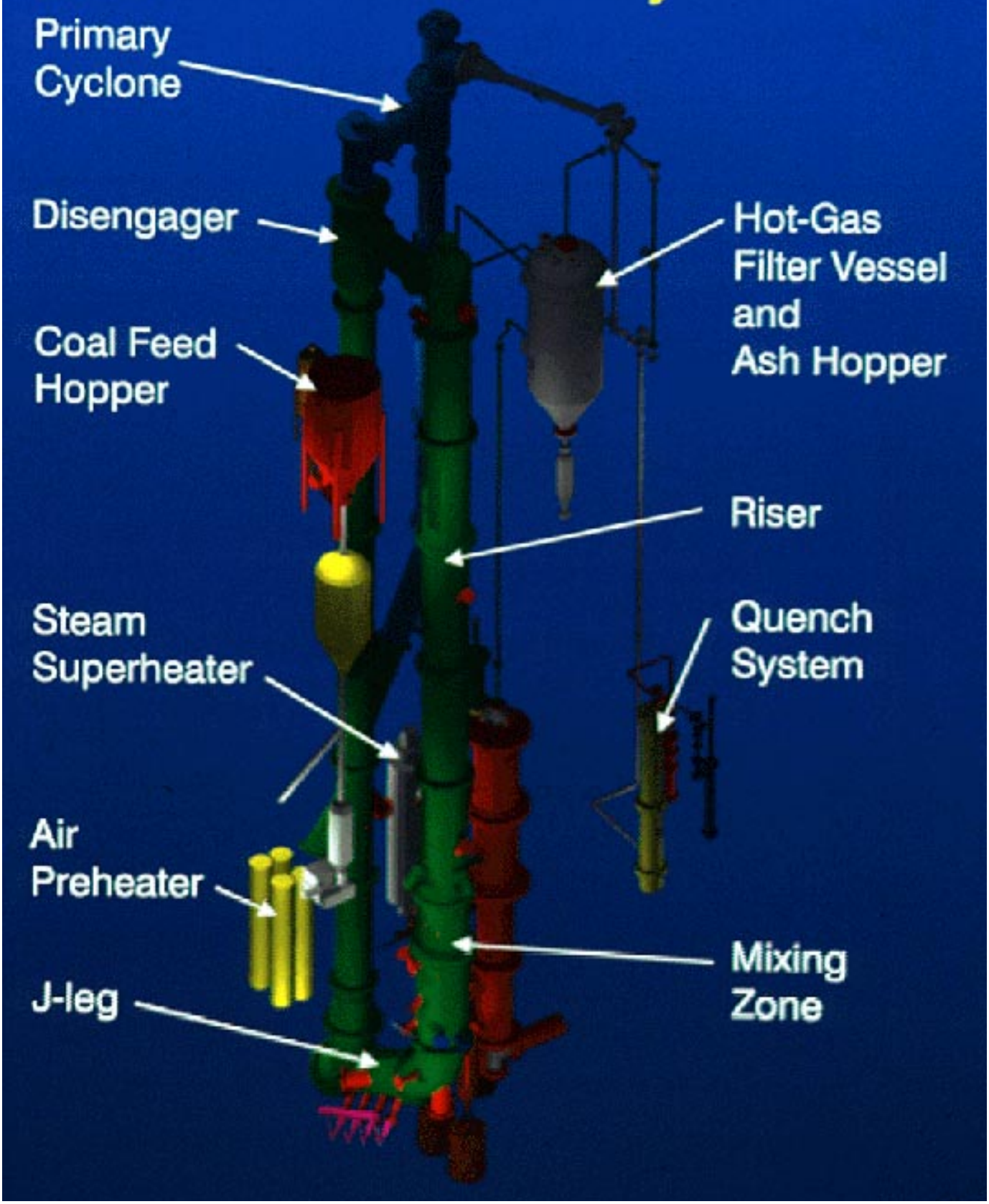

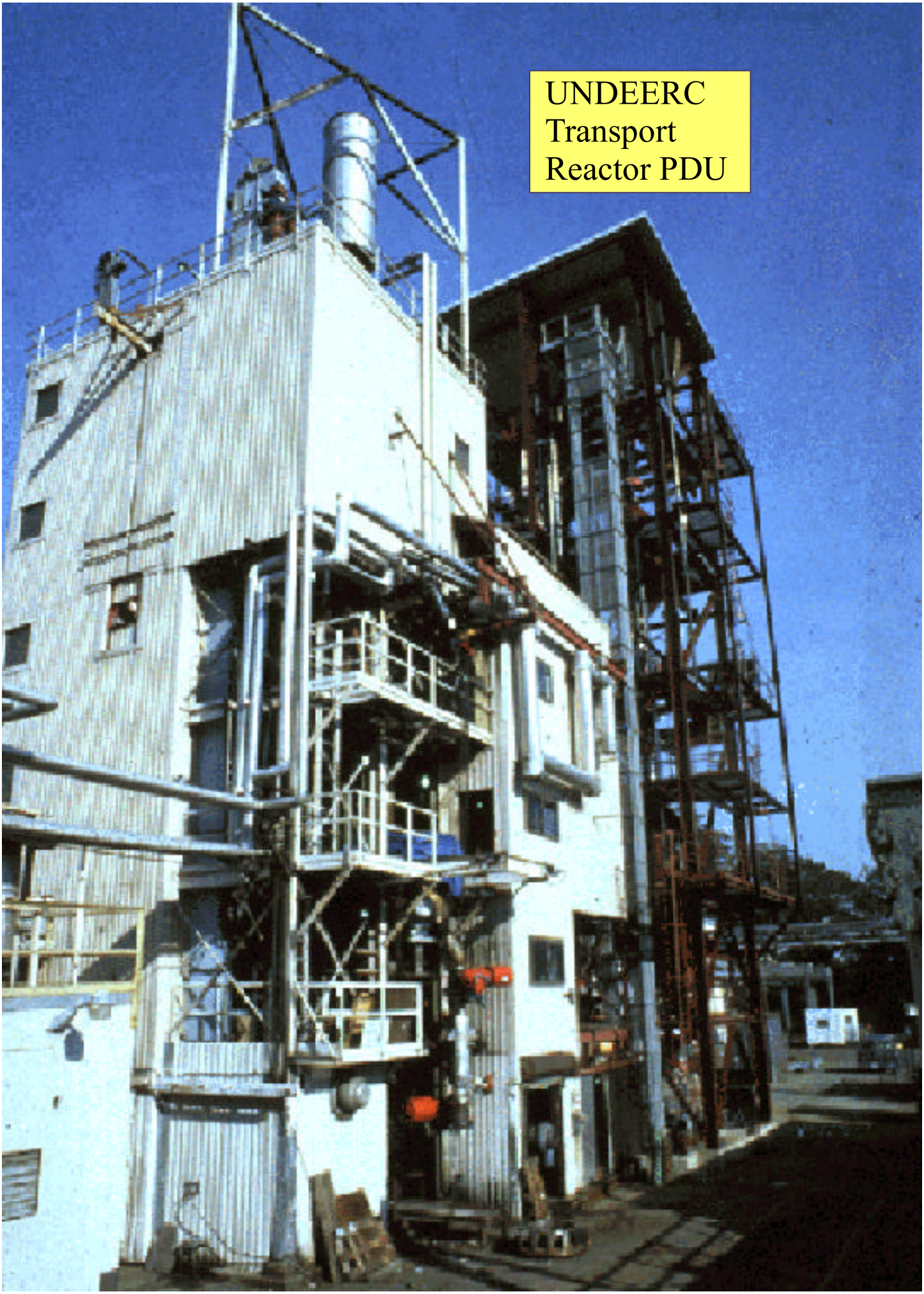
UNDEERC
Transport
Reactor PDU

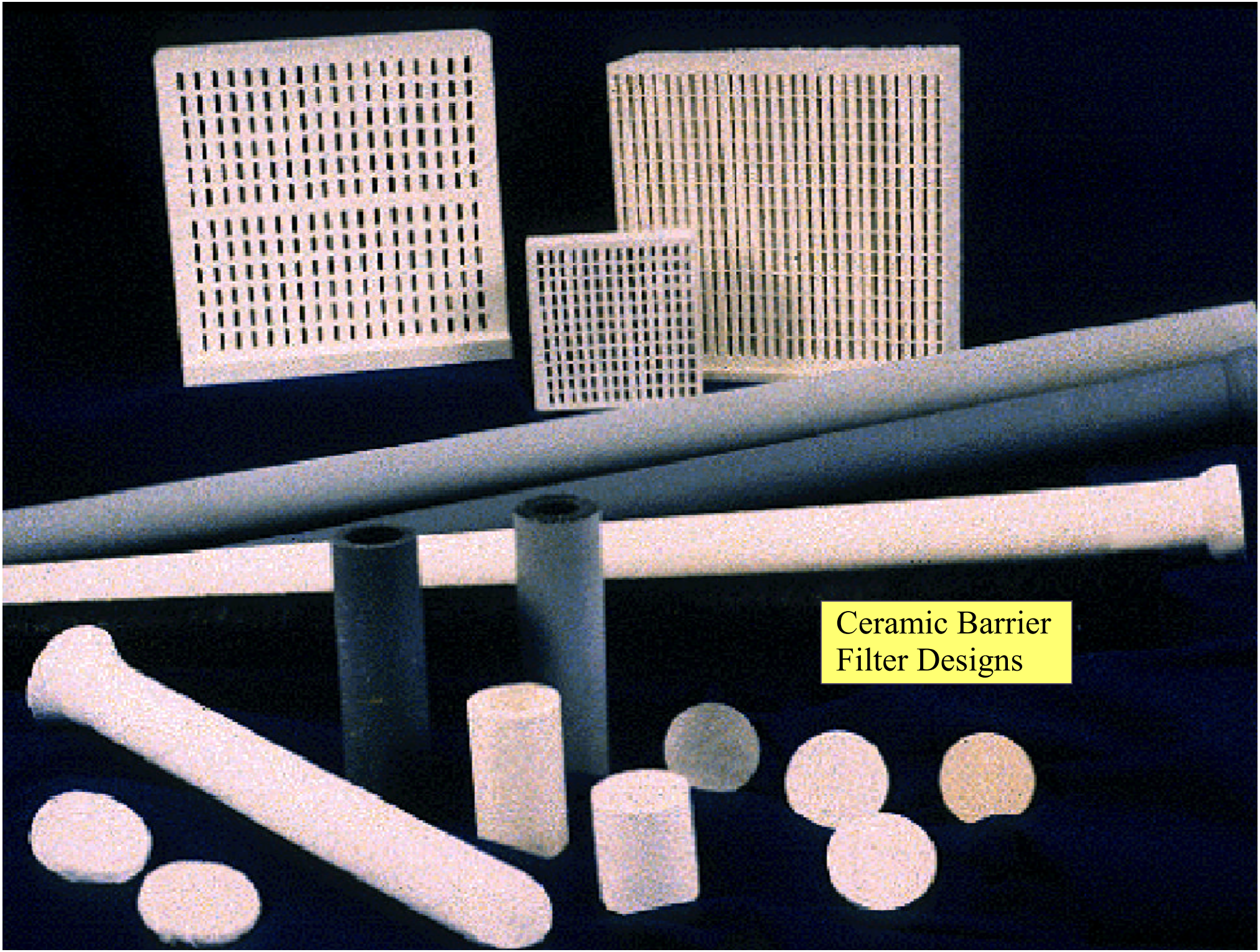
Ceramic Barrier
Filter Designs

Westinghouse Cold
Flow Filter Module

TIDD PFBC Ceramic Filter Test Slipstream

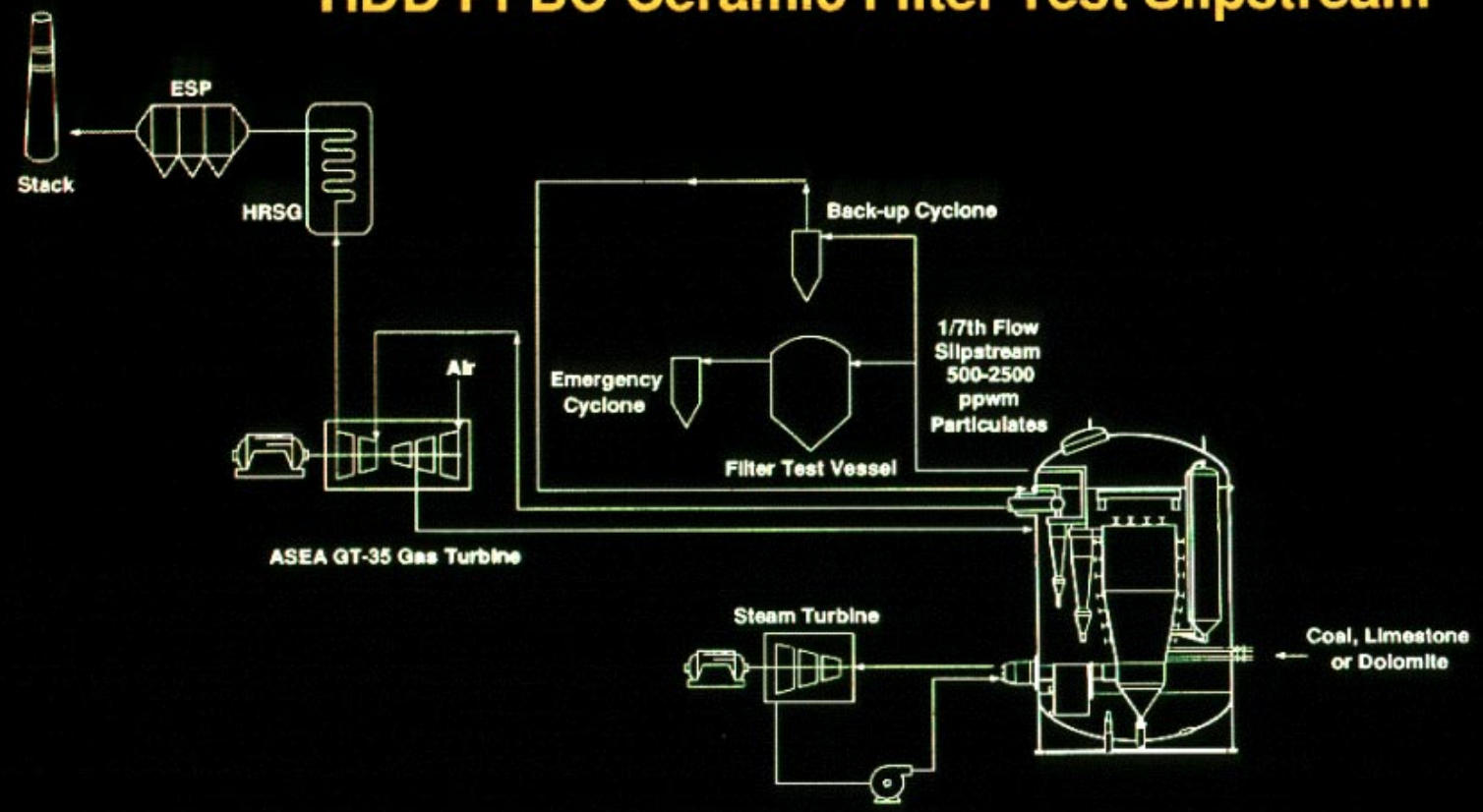

- Conduct large-scale engineering tests of ceramic filter systems for commercial 1st & 2nd Generation PFBC
  - Demonstrate 5,000 hours of operation
- $20 million program separate from Clean Coal
- Test filters on 2nd & 3rd years of operation
- Westinghouse ceramic candle filters first system to be tested
- Potential for a different filter in 2nd test period

M91001904

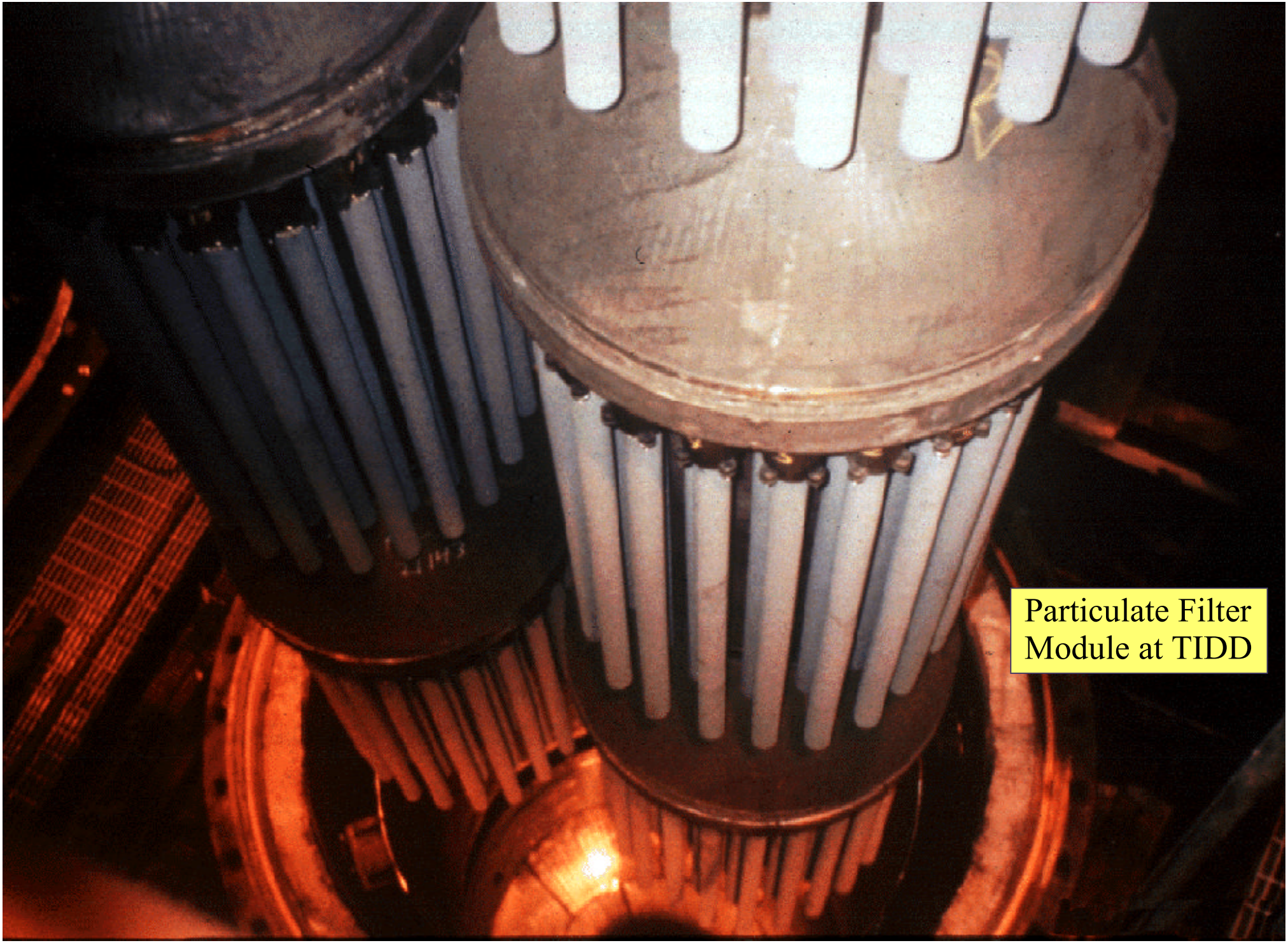
Particulate Filter
Module at TIDD

KARHULA

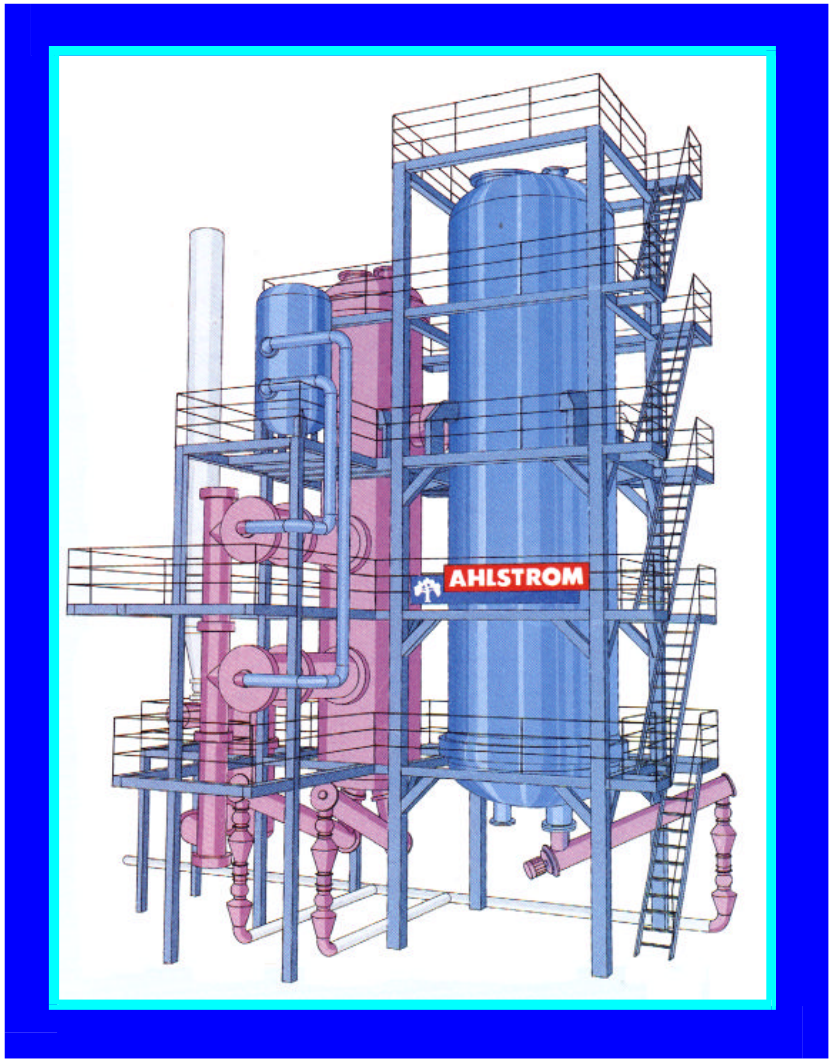

M96001848C

Barrier Issues

- ***Technical***
  - ***Filters***
  - ***CO_2***
  - ***S and other gases***
  - ***Materials***

- ***Market***
  - ***Domestic capacity growth***
  - ***Capital cost***
  - ***Incentive for risk***

M96001853C

IGCC R&D Issues

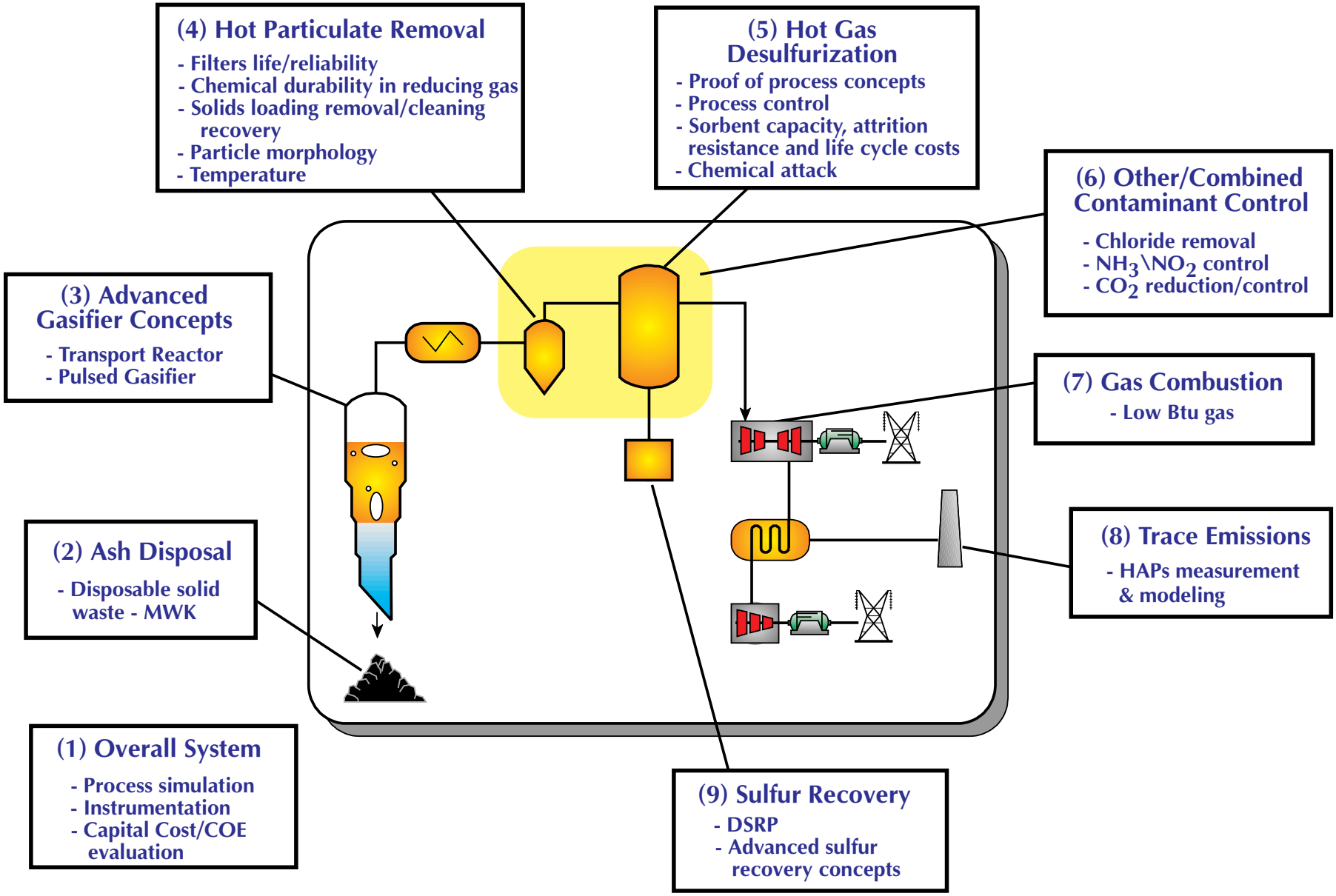

M96001815W

PFBC R&D Issues

Hot Particulate Removal
- Filters life/reliability
- Solids loading removal/cleaning recovery
- Particle morphology
- Temperature

Other/Combined Contaminant Control
- Chloride
- Alkali

Gas Combustion
Low Btu gas
- Stability
- NO_x issues

Advanced Carbonizer Concepts/ Sulfur Removal
- Transport Reactor
- Pulsed Gasifier

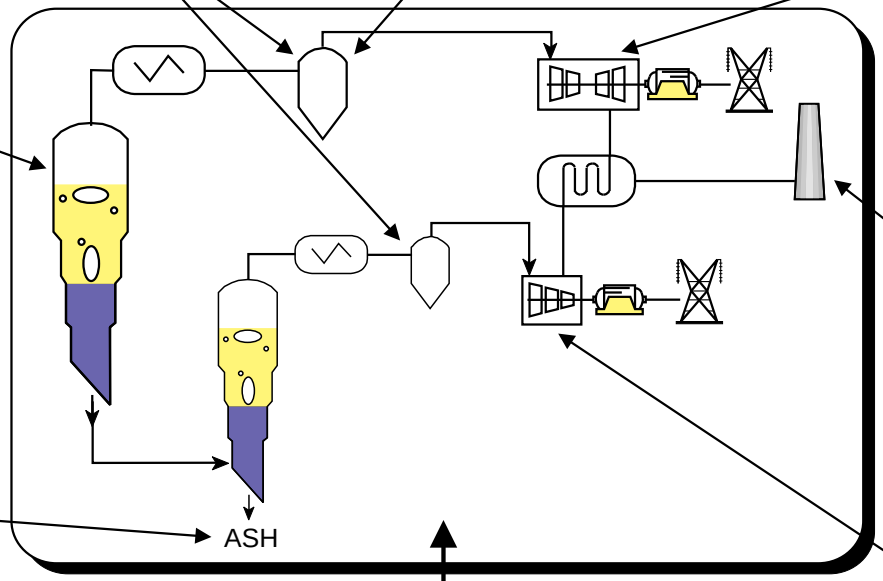

Trace Emissions
- HAPs measurement and modeling

Ash Disposal/ Reuse

Advanced Steam Cycles
- Kalina Cycle
- Materials Issues

Overall System
- System studies
- Components
- Instrumention & control

M96001812C

Key Plans

- ***Startups***
  - ***Tampa***
  - ***Piñon***
  - ***PSDF***

- ***Construction***
  - ***Lakeland***
  - ***Seward***

- ***Testing***
  - ***Filter Materials***

M96001854C

Wabash River Coal Gasification
Repowering Project

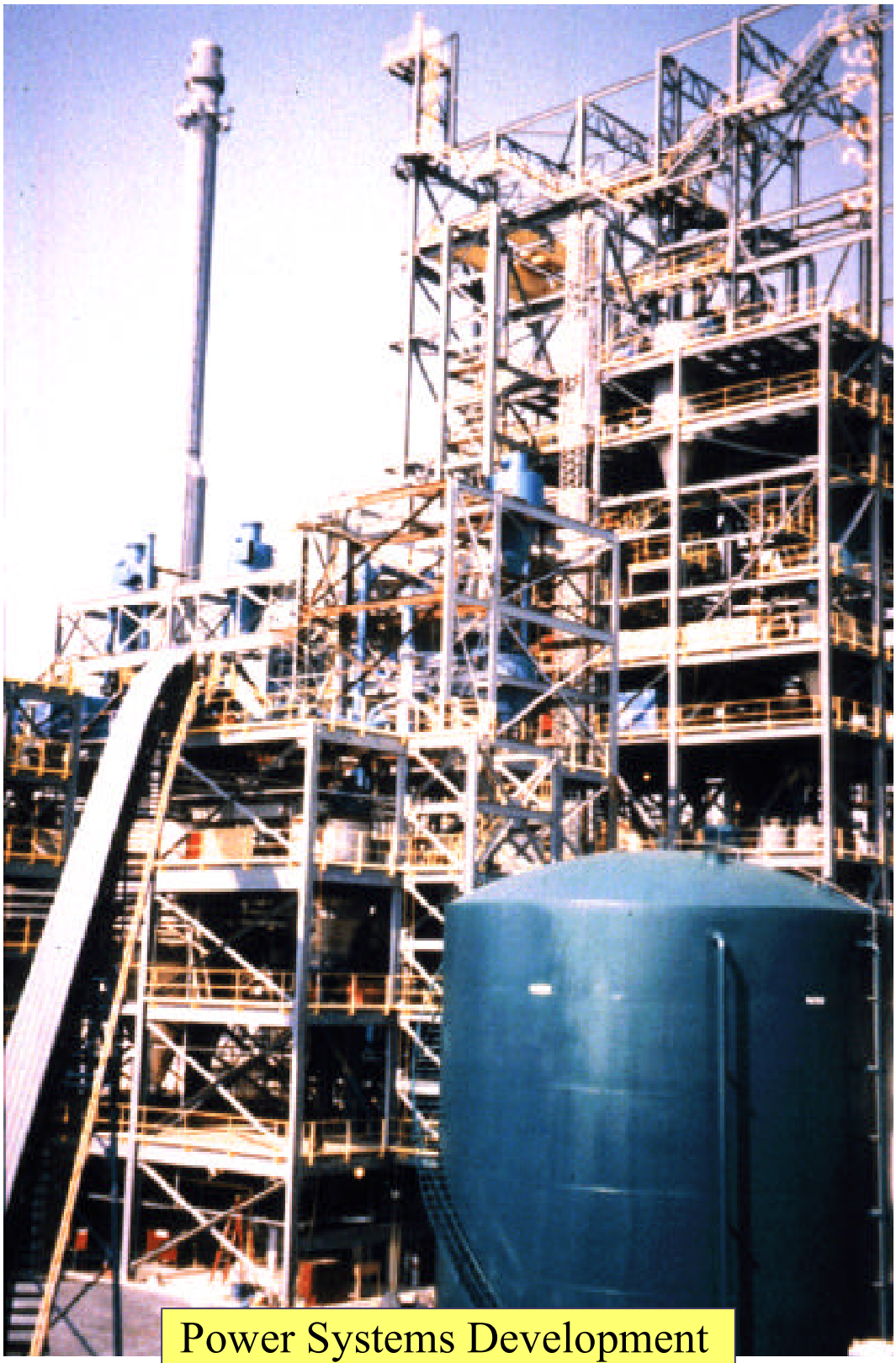

Power Systems Development Facility at Wilsonville, AL

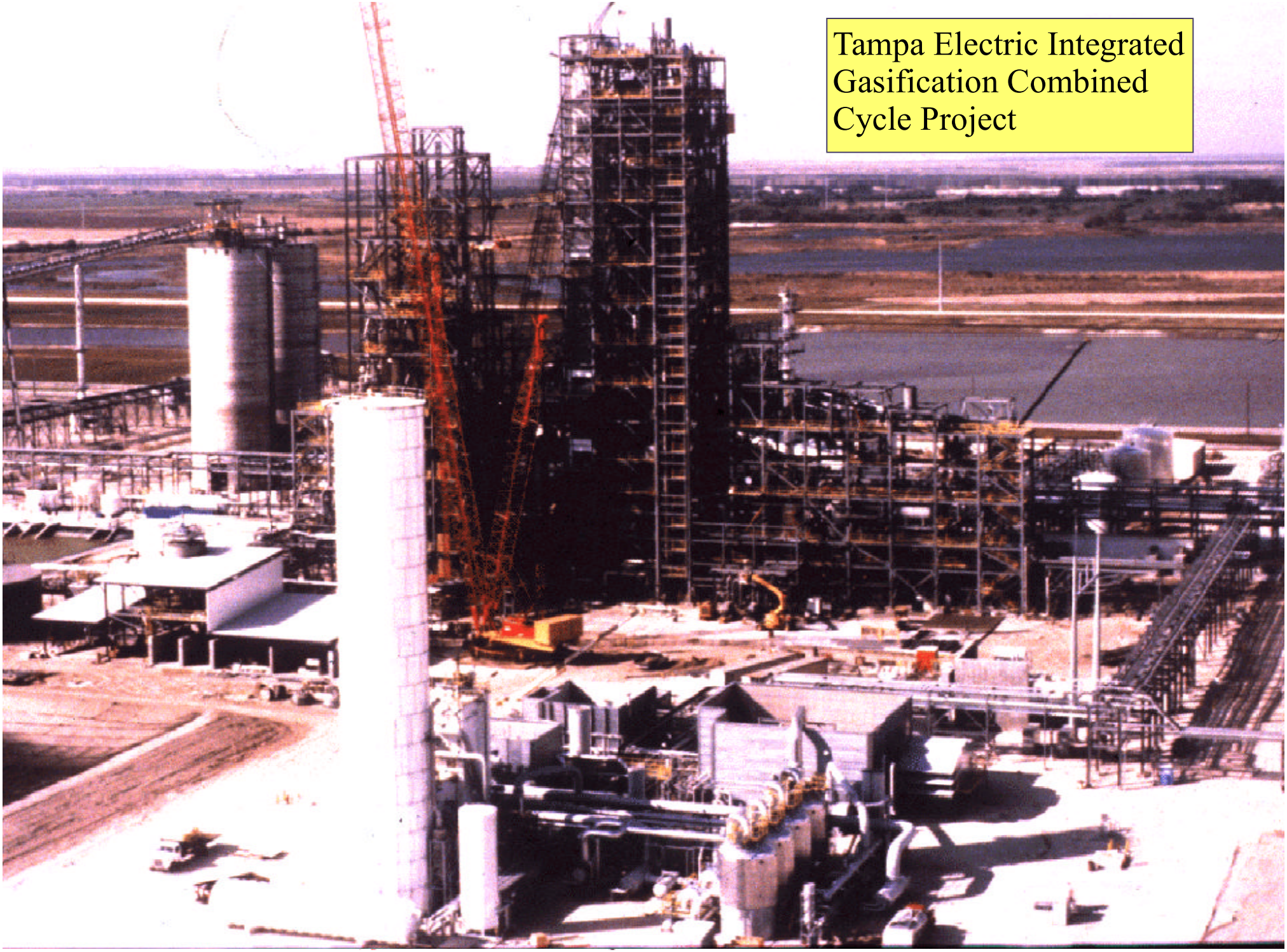
Tampa Electric Integrated
Gasification Combined
Cycle Project

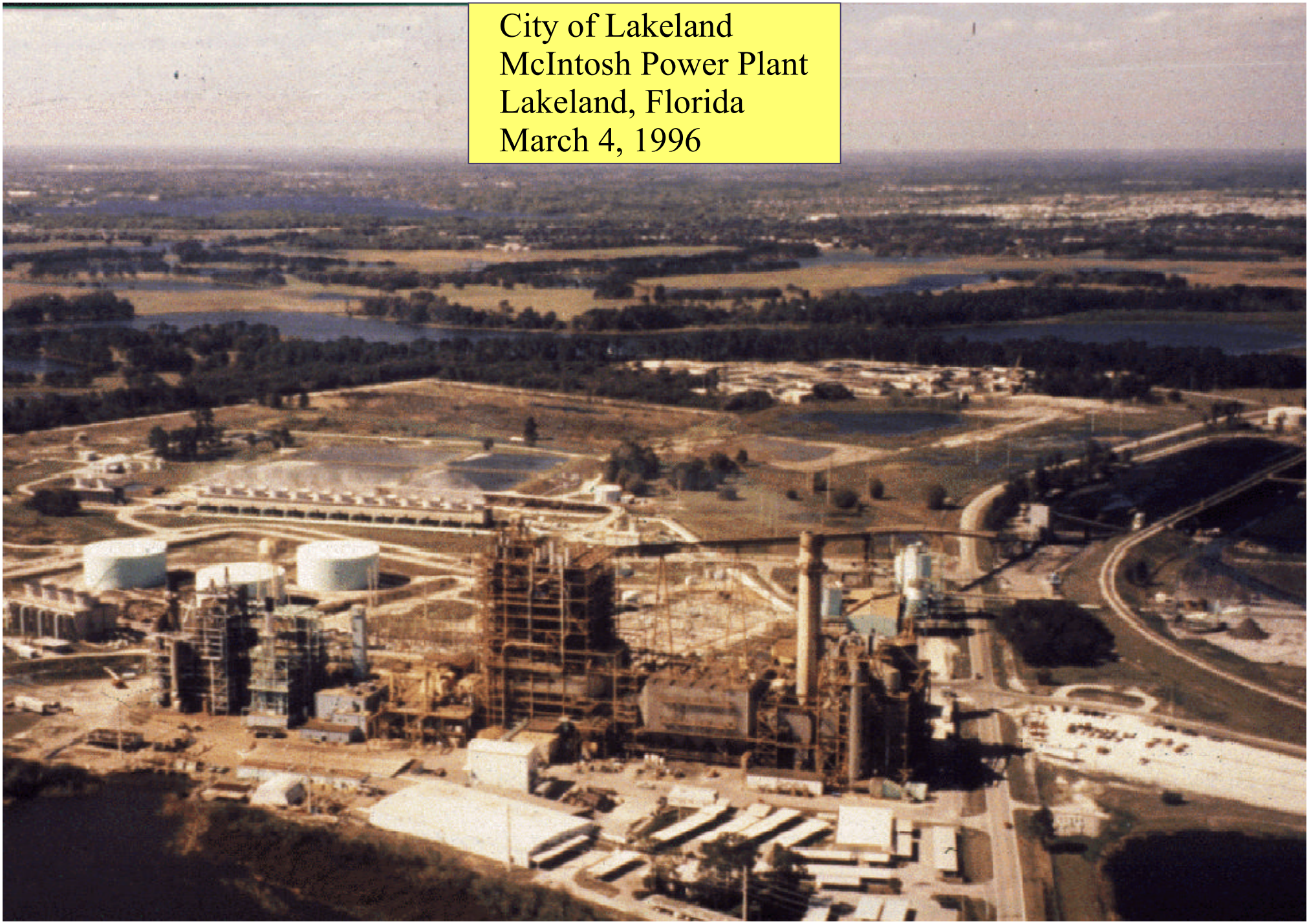
City of Lakeland
McIntosh Power Plant
Lakeland, Florida
March 4, 1996

List of IGCC Projects in the World

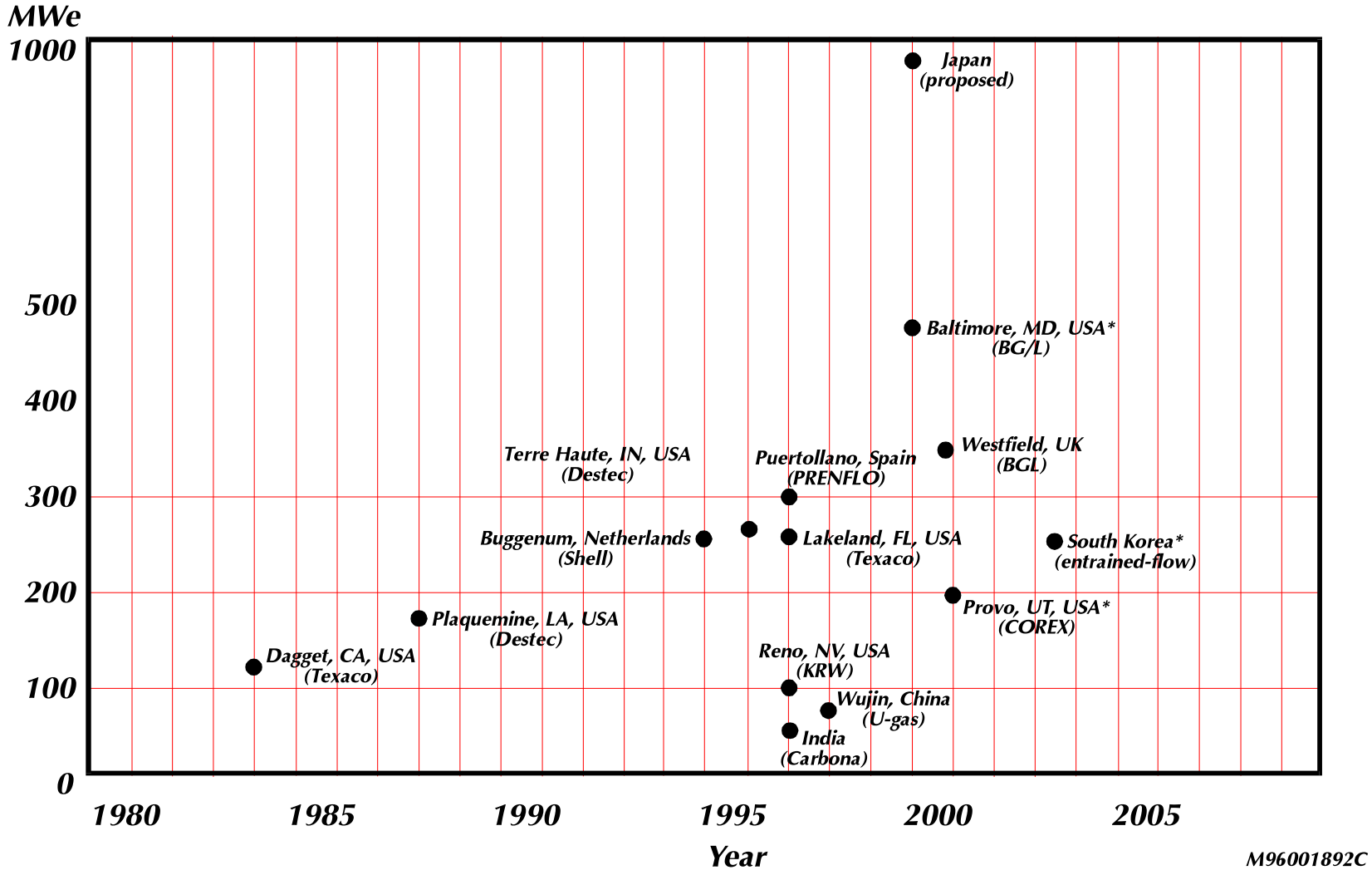

M96001892C

IGCC Plants and Projects

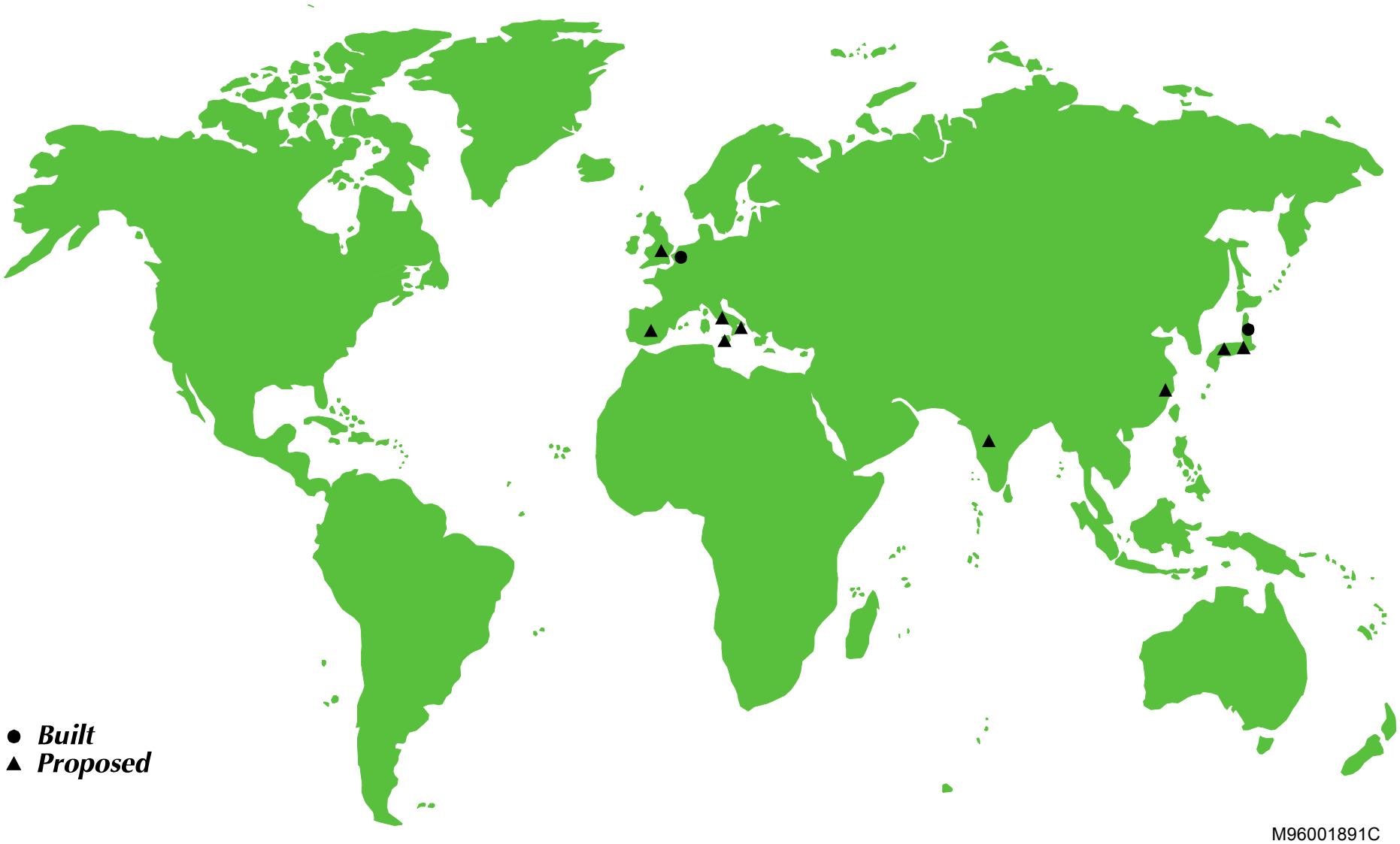

List of PFBC Projects in the World

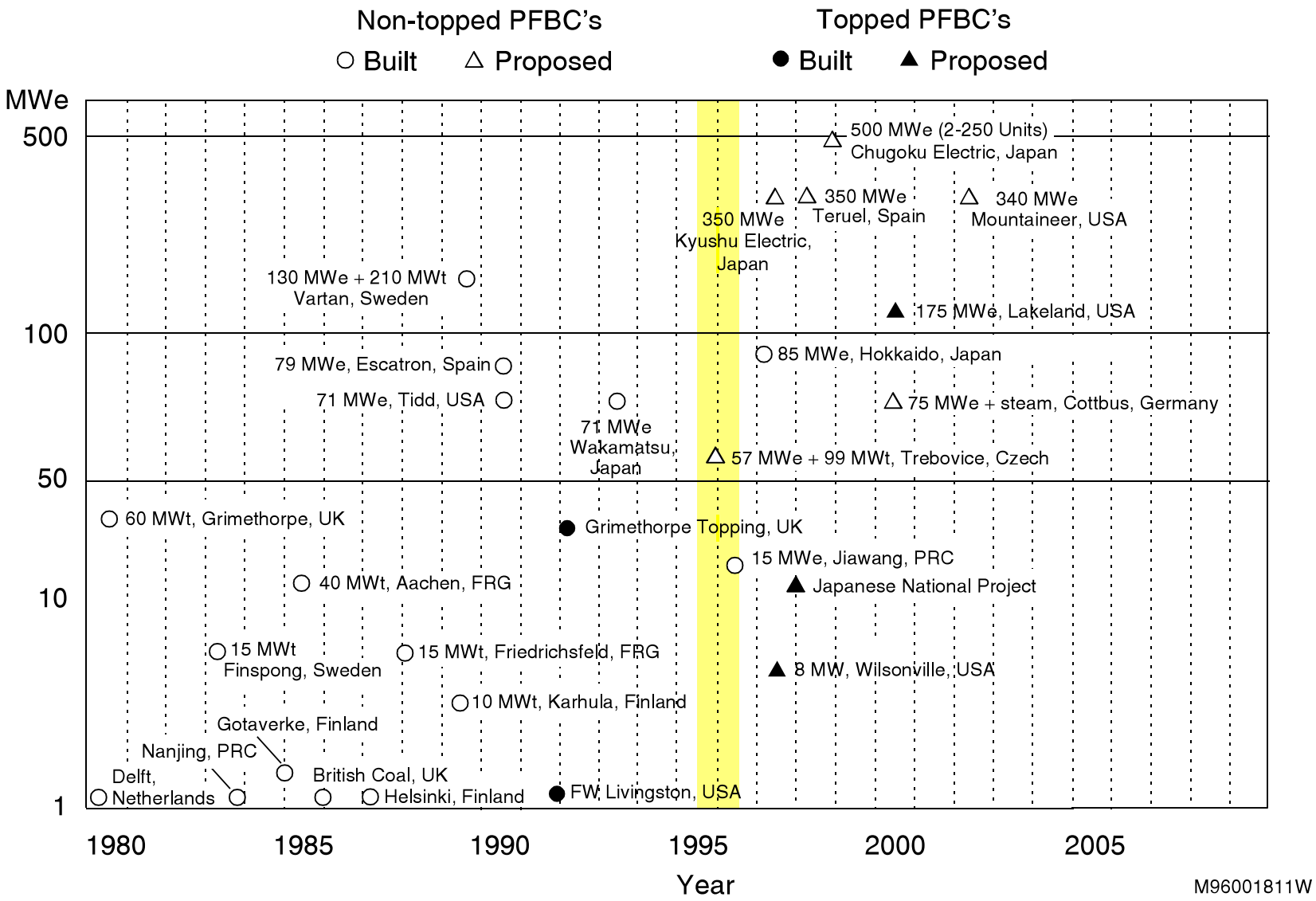

PFBC Plants and Projects

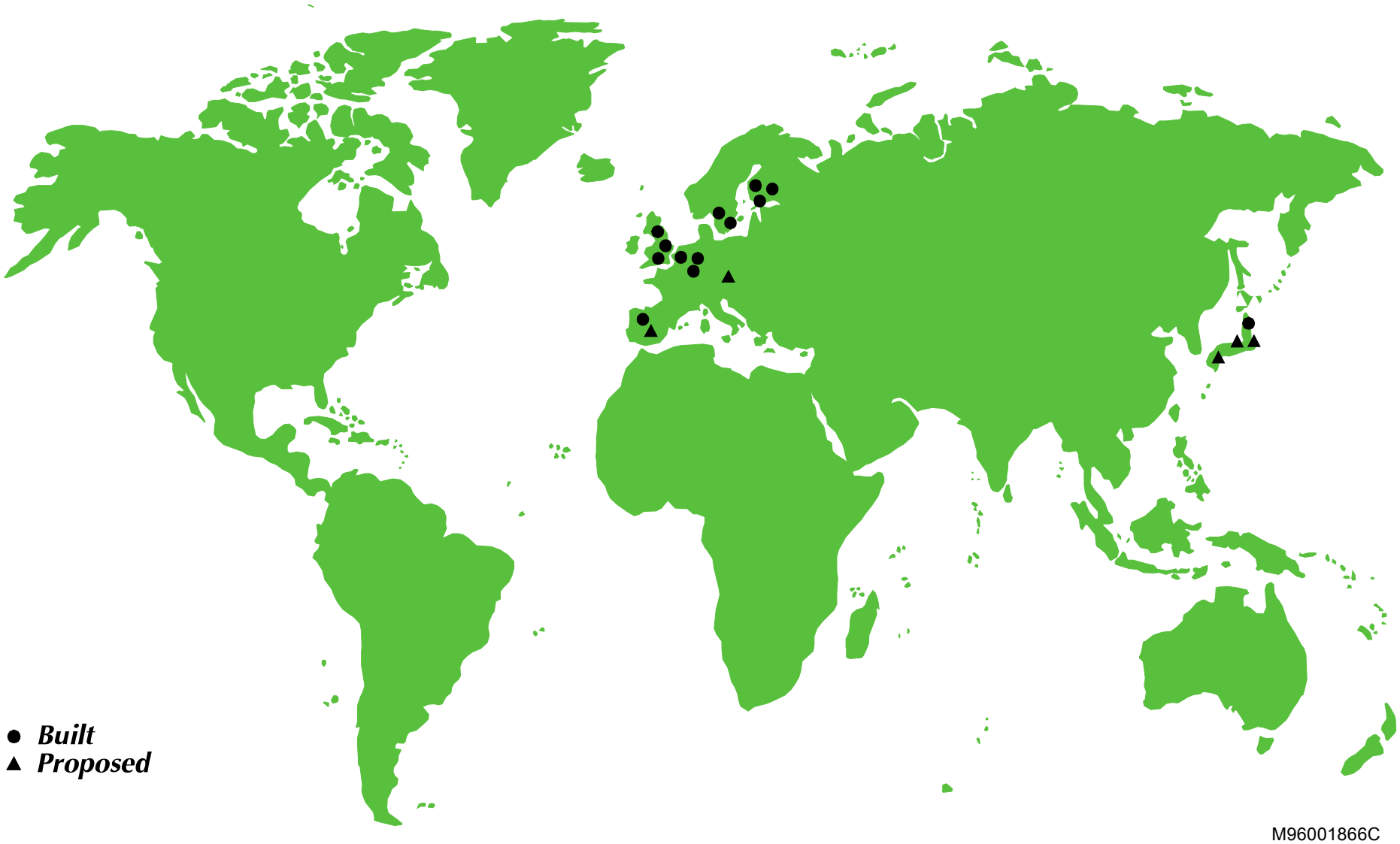

Marketplace Opportunities

- *U.S. repowering*
- *Global demand*
- *Co-production*
- *Opportunity fuels*
- *Environmental drivers*
- *Advanced systems*

M96001856C

Global Demand

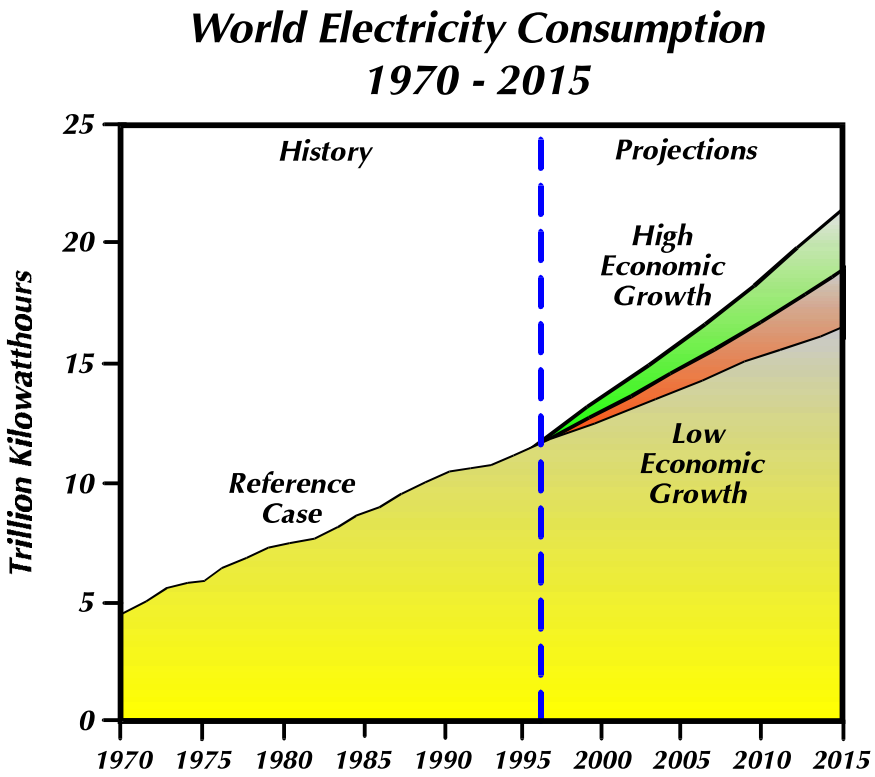

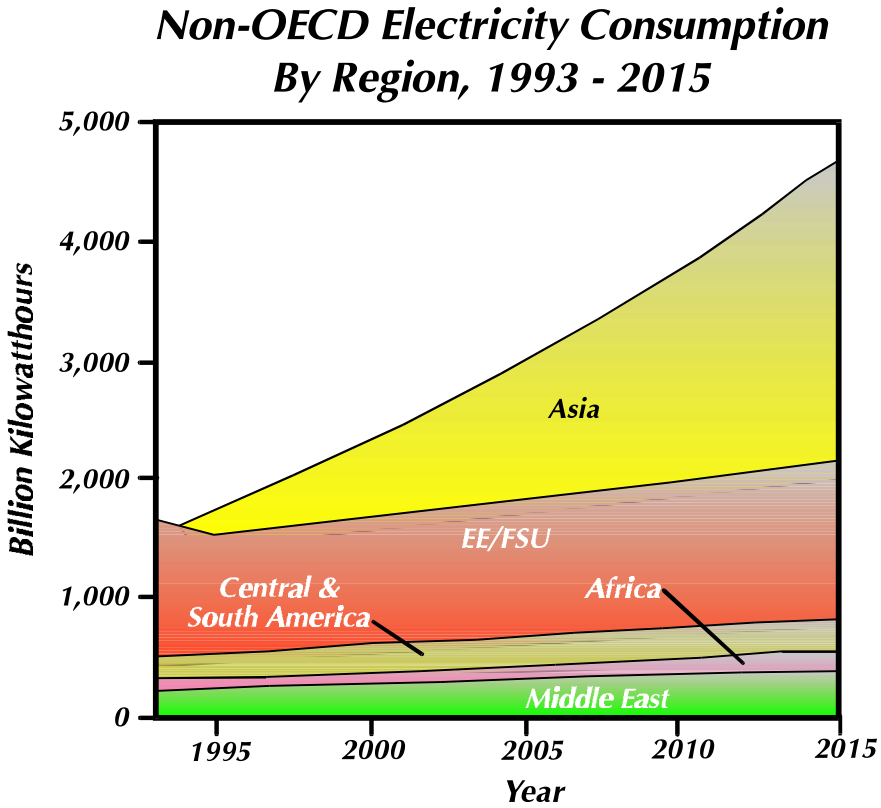

Source: History: Energy Information Administration (EIA) International Energy Annual 1993, DOE/EIA-0219(93) (Washington, D.C., May 1995). Projections: EIA, World Energy Projection Stystem (1996).

M96001862C

U.S. Repowering

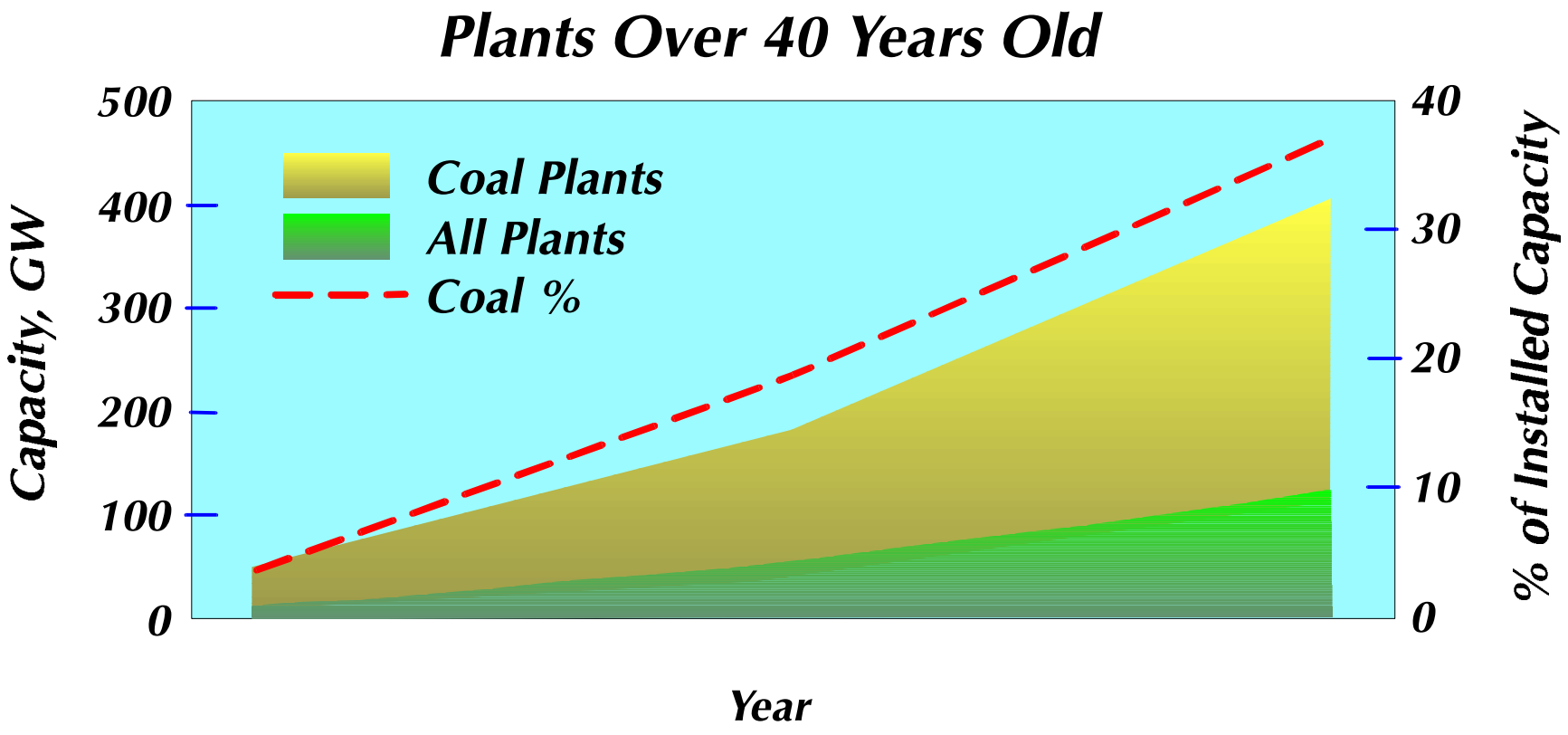

M96001861C

Co-Production

COAL

Electricity

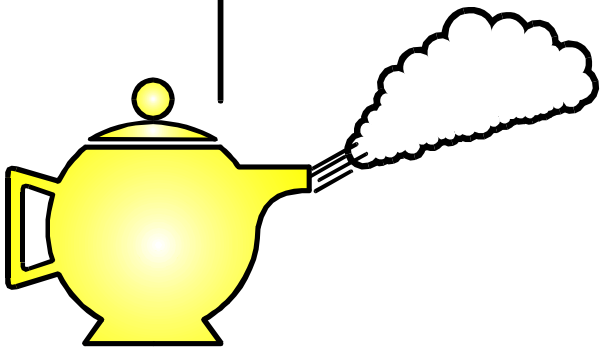

Steam

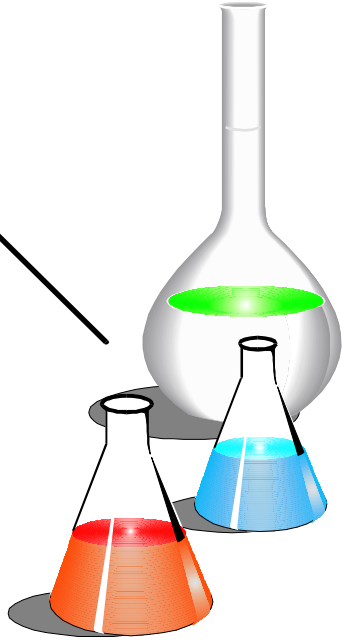

Chemicals

M96001874C

Opportunity Fuels

- Plastic
- Biomass
- Sewage
- RDF
- Petcoke
- Waste Fuel

M96001842C

Environmental Drivers

- SO_2
- NO_x
- CO_2
- Particulates
- HAPs

M96001843C

Advanced Systems

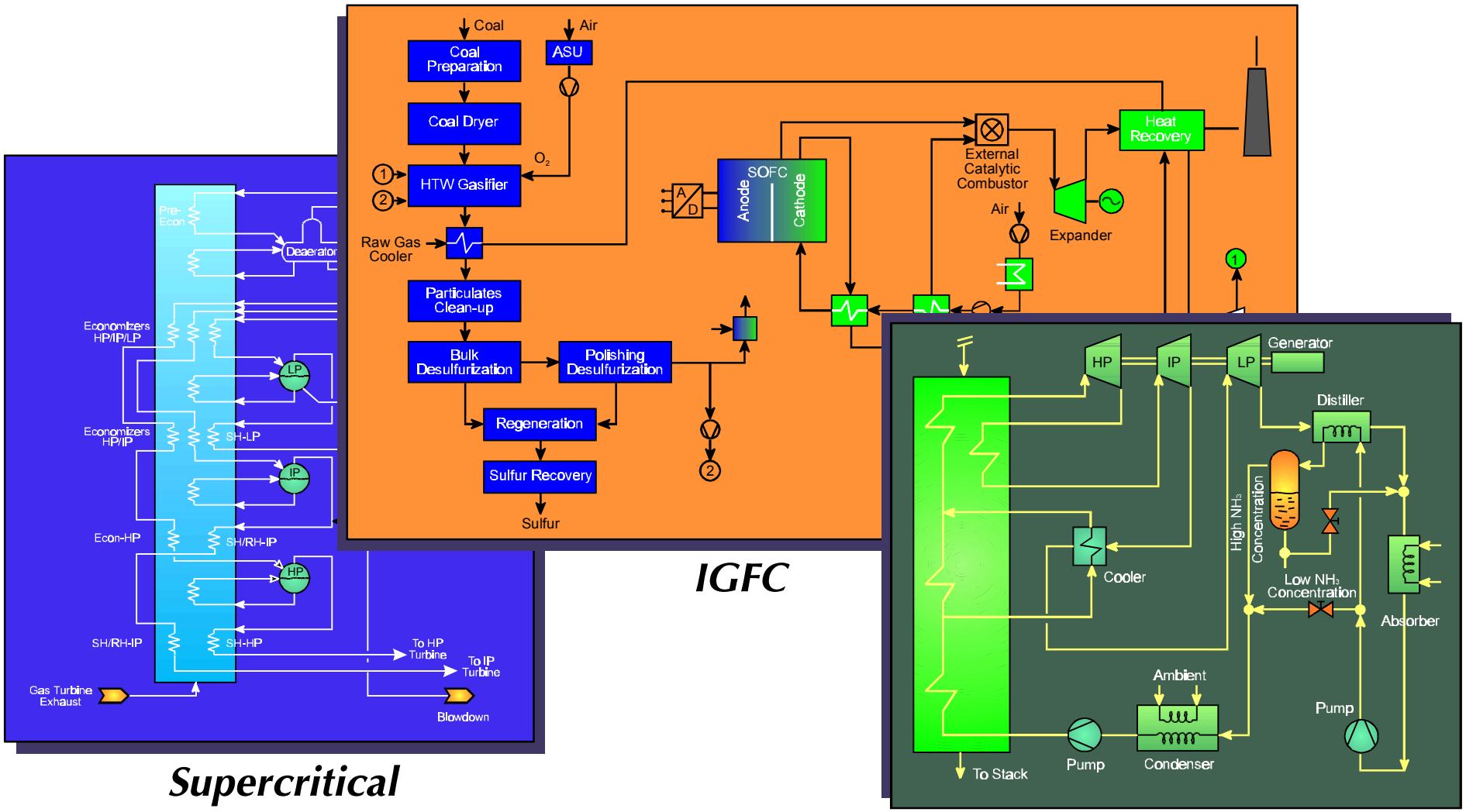

Supercritical

IGFC

Kalina and Other Advanced Cycles

M96001857C

Medical Waste Co-Firing Comes of Age

Karl Smith-Berntson (71370.146@compuserve.com; 717-755-1081)
James M. Stuart (717-755-1081)
DONLEE Technologies, Inc.
693 North Hills Road
York, PA 17402-2211

Abstract

The United States Environmental Protection Agency has estimated that about 4.3 million metric tons of medical/hospital wastes are generated annually in the United States, of this approximately 60% comes directly from hospitals. The other 40% are generated by such facilities as laboratories, physicians offices, dental offices, veterinarian clinics, funeral homes and care facilities, just to name a few. There are approximately 6,700 Medical Waste Incinerators (MWIs) in the United States. The dioxin emissions from these incinerators is a major public health hazard and therefore other means of medical waste disposal must be found.

In early 1992 DONLEE Technologies, Inc., in cooperation with the Department of Energy Fossil Energy Program, completed pilot testing of simulated non-infectious waste combustion, co-fired with coal, at its test facility in York, Pennsylvania. The goal of this testing was to demonstrate the ability of fluidized bed combustion to completely destruct medical waste with minimized dioxin emissions. The test facility is a full scale circulating fluidized bed unit with a maximum heat input capability of ten million BTU per hour. The tests showed that the circulating fluidized bed system is ideally suited to meet the medical/ infectious waste destruction needs of the health care industry. The dioxin emission levels proved to be significantly lower than those from presently operating MWIs.

Based on the successful test results, a cooperative agreement with the Department of Energy Fossil Energy Power Systems, DONLEE Technologies, and the Veterans Administration was reached to design, construct, and test a demonstration unit at the Veterans Administration Medical Center in Lebanon, Pennsylvania. Plant design and construction was started in 1993, with DONLEE Technologies functioning as both the technology supplier and the plant EPC contractor.

After some delay the construction of the demonstration unit finally reached completion in the spring of 1996. The unit is currently undergoing initial shakedown and testing to

---

Research sponsored by the U.S. Department of Energy's Morgantown Energy Technology Center, under contract DE-FG21-91MC27205 with DONLEE Technologies, Inc., 693 N. Hills Rd., York, PA 17402-2211; telefax: 717-755-0020.

verify the base operating parameters. The unit will first be fired with coal only, followed by the introduction of non-infectious waste and finally total waste, including the "red bag" material.

The program calls for an extended testing period of up to one year. While the unit is being operated as part of the stream supply system at the VA Hospital, the hospital's waste is destroyed via combustion in the Fluidized Bed Unit.

It is anticipated that after successful demonstration at the Lebanon facility, several other VA or private hospitals will be interested in utilization of this technology for disposal of their infectious and non-infectious waste.

1.4 Power Systems Development Facility: Design, Construction, and Commissioning Status

Charles A. Powell (charles.a.powell@scsnet.com; 205-669-5869)
Pannalal Vimalchand (p.vimalchand@scsnet.com; 205-669-5852)
Howard L. Hendrix (howard.1.hendrix@scsnet.tom; 205-669-5876)
Peter M. Honeycutt (peter.m.honeycuttfj!scsnet.tom; 205-669-5875)
Southern Company Services
P.O. Box 1069
Wilsonville,AL35186

Abstract

This paper will provide an introduction to the Power Systems Development Facility, a Department of Energy sponsored, engineering scale demonstration of two advanced coal-fired power technologies; and discuss current status of design, construction and commissioning of this facility.

The Power Systems Development Facility (PSDF) will test and demonstrate a second generation combined cycle pressurized circulating fluidized bed combustion system with a syn-gas fired topping cycle (APFBC); an advanced circulating fluidized bed transport reactor acting as either a combustor or as a gasifier; (presently) three different Hot Gas Clean-Up technologies (Particulate Control Devices or PCDs); and (in later years) fuel cells and desulfurization technologies.

Design and construction of the Transport Reactor and required associated equipment will be completed in early summer 1996, Design of the APFBC is over 95% complete, and construction has begun. Commissioning of the Transport reactor is presently underway, with the separate components and sub-systems being fully operational and work focused on integration issues for the entire reactor system. Commissioning of APFBC components should begin in early 1997. The first ceramic candle filter vessel has been loaded and is undergoing testing at temperatures over 1000°F. Initial operation of the transport reactor will be as a combustor, with plans to test operation as a gasifier scheduled for this Fall.

Construction of the Granular Bed Filter is presently underway, with plans for sub-system commissioning to begin this Fall. The first ceramic candle filter system will be tested on the transport reactor before being relocated mid-next year to the APFBC train; at which time it will be replaced by another candle filter system on the transport reactor.

Research sponsored by the U.S. Department of Energy's Morgantown Energy Technology Center, under contract DE-FC21 -90MC25 140 with Southern Company Services, Inc., P.O. Box 1069, Wilsonville, AL 35186; telefax: 205-669-5843

Construction of the APFBC system, with the installation of the combustor vessels, heat exchangers and refractory lined piping is underway. The electrical design is being completed this summer; as is the assembly of the major components of this system: The Combustion Turbine, The Topping Combustor, and the inlet/outlet piping for both, By using common Balance of Plant facilities, the condensate, cooling, control air, purge and auxiliary fuel systems are installed to support operation of the transport reactor and require only minimal work to support the APFBC operation.

Construction of the PSDF has presented several problems different from those encountered in constructing a traditional pulverized coal plant: Pneumatic pressure boundaries, fuel (and sorbent) injection under pressure, gas sampling under temperature and pressure, exotic material procurement and fabrication, and complex piping due to the large number of fluidizing gas connections to the pressurized reactor.

POWER SYSTEMS DEVELOPMENT FACILITY

Design, Construction, and Commissioning Status

DOE Cooperative Agreement No. DE-FC21-90MC25140

Southern Company Services, Inc.
Wilsonville, Alabama

PSDF Program Objective

Develop advanced coal-based power generation technologies that can produce electricity at competitive cost and meet all environmental standards.

PSDF Program Goal

The PSDF is a site where new process configurations and components for advanced power systems can be tested in an integrated process environment at sufficient size to provide data for scale-up toward commercialization. DOE's intent is that:

- The **PSDF** be recognized by equipment vendors, process developers, and generators of electric power as the **best place to test** new components and integrated process configurations for **advanced power systems**.

- **Data** from the PSDF be recognized as a clear indicator of the usefulness of new components and integrated process configurations for advanced power systems and be **sufficient to support commercial scale-up**.

- Public and private funding agencies recognize the **PSDF** as a readily accessible, politically neutral, **cost effective testing location** for advanced power system components and integrated process configurations.

- The **staff** at the **PSDF** be recognized as **experts** in their respective technologies by all their customers.

Project Overview

- METC sponsored project to demonstrate two Advanced Coal-fired Power Generation Technologies, three Hot Gas Clean-Up Technologies, and Fuel Cells (future)
- Southern Company Services is acting as Prime Contractor and is responsible for Operation of the facility as well as Design of Balance of Plant (BOP) Equipment, Design Integration, Construction and Start-Up
- M.W. Kellogg (Kellogg), Foster Wheeler (FW), Westinghouse (W), Combustion Power Corp. (CPC) and Industrial Filter and Pump (IF&P) are major participants.

Project Overview

- Increased integration of process components
- All possible components were commercially available to minimize scale up concerns and allow use of existing technologies if possible.
- Kellogg is supplying a pressurized transport reactor that can be configured as either a combustor or a gasifier.
- Foster Wheeler is supplying an integrated, Advanced Pressurized Fluidized Bed Combustion (APFBC) system, including a gas turbine equipped with a topping combustor supplied by Westinghouse.

Project Overview

- Particulate Control Devices (or PCD's) are supplied by Westinghouse, CPC, and IF&P.
- Two are using ceramic candle filters (Westinghouse and IF&P).
- CPC is supplying a Granular Bed Filter.
- The ceramic candles are being supplied by several vendors.

PARTICIPANT RESPONSIBILITIES

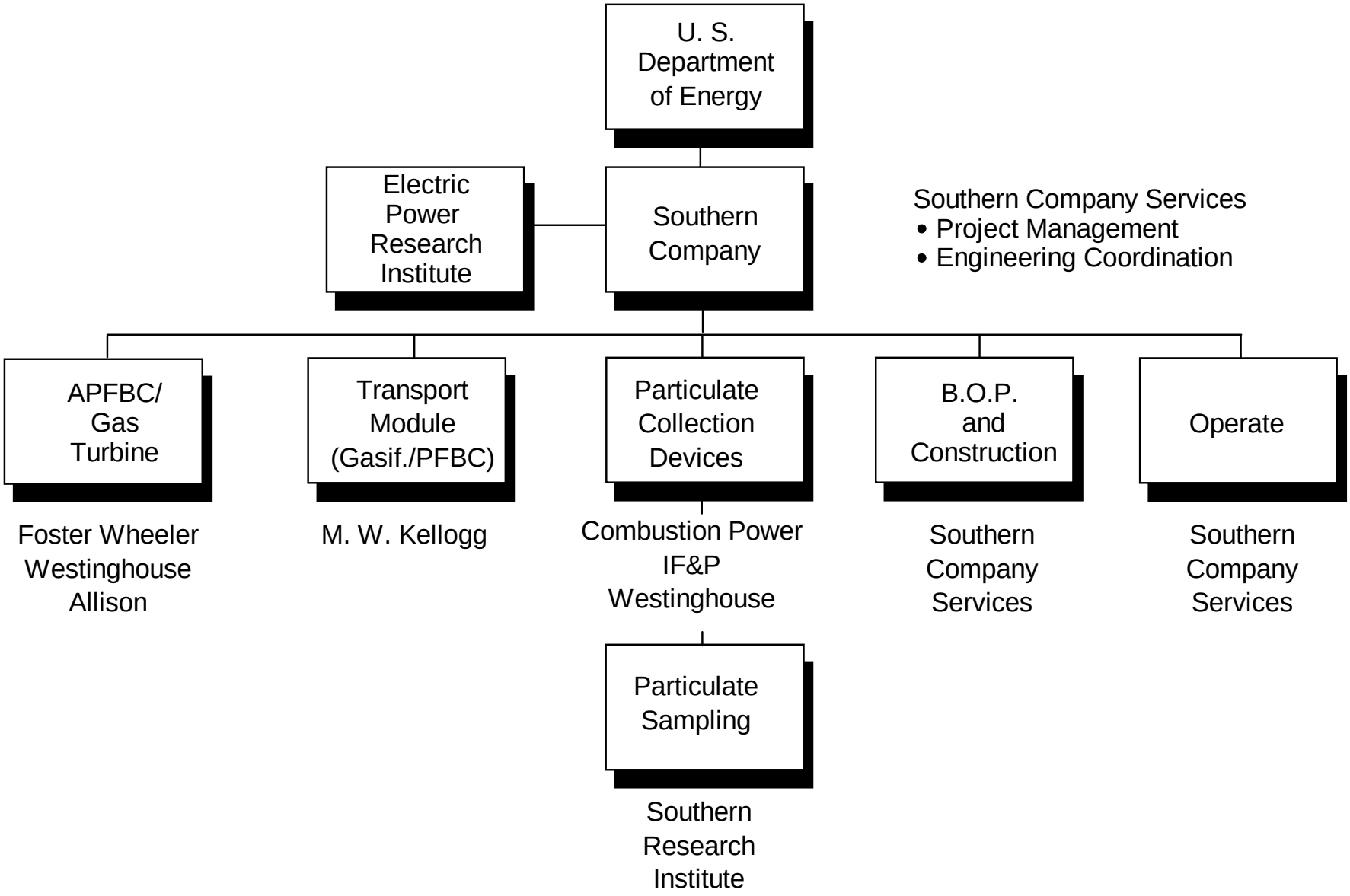

PSDF SITE ORGANIZATION

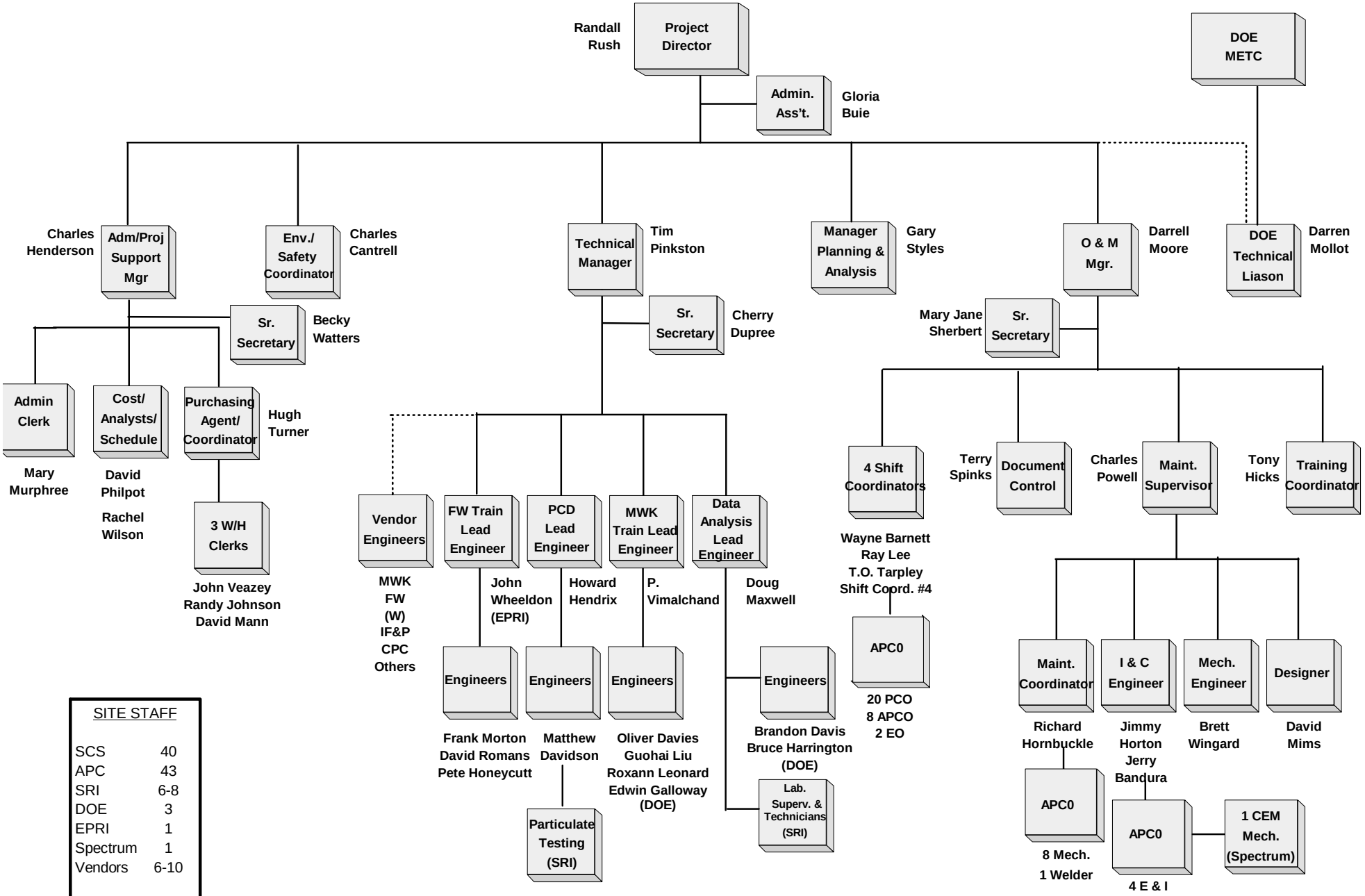

SITE STAFF	
SCS	40
APC	43
SRI	6-8
DOE	3
EPRI	1
Spectrum	1
Vendors	6-10
TOTAL	100-106

S:\PAPRPRES\DUPREE.PRE

Project Status

- Design and Engineering are complete, except for electrical integration of Foster Wheeler equipment, which will be complete this fall.
- Construction of Kellogg and Kellogg required BOP equipment is complete.
- Start-up of BOP equipment began last September with the electrical station service.
- Start-up of Kellogg's transport reactor as a combustor is in the final stages.
- Several design enhancements have been incorporated during construction to improve operability during system malfunctions.

Design Enhancements

- Start-Up Bed Material Injection Spools
- Propane Supply Option Spools
- Steam Supply Piping Modifications
- PCD Warm-Up Modifications
- Using Primary Gas Cooler as a Condensation Heater
- Using Sulfator Start-Up Heater
- Using a Screw Cooler to Cool Pulverized Coal
- Using Process Air to Fluidize the Combustion Heat Exchanger
- Nitrogen Purge Connections

Systems Operational

- Electrical Station Service
- Distributed Control and Data Collection
- Cooling Water Systems
- Instrument, Control, and Service Air
- Feedstock (Coal and Sorbent) Storage, Reclaim and Preparation
- Condensate and Steam Generation
- Kellogg Process and Transport Air
- Reactor Aeration, Instrument Purge, Spoiling and Fluidization
- Dense Phase Transport of Feedstock and Ash

Systems Operational

- Burners on Thermal Oxidizer, Sulfator Start-up Heater and Transport Reactor Start-up Heater
- Ash Cooler Heat Transfer Fluid and Screw Coolers
- Recycle Gas Compressor
- Westinghouse PCD Backpulse
- Baghouse and Thermal Dilution Fan
- Liquid Nitrogen Storage and Delivery
- Propane Storage and Delivery
- Backpulse Air

Issues Encountered

- Piping and electrical conduit density in the process structure
- First of a kind specification requirements
- Aggressive schedule forcing design decisions
- Exotic material requirements due to temperature, pressure and chemical activity
- Designs for single case, limiting range of operation
- Pneumatic pressure boundaries
- Gas sampling at pressure and temperature
- Feedstock injection into pressurized reactor
- Suitable start-up bed materials for reactors

Design Issues
Piping Density in the Process Structure

- Due to cost constraints, the structure was reduced in size by 20’ in both directions.
- Every pressure tap must be supplied with a purge gas (Nitrogen) that must be metered and flow controlled to minimize biasing.
- Fluidization requires many aeration nozzles to prevent layout of solids.
- Staged combustion and controlled gasification require fine control of location and flow of combustion (oxidizing) air.
- PSDF transport reactor has as many connections as a 150 MW unit would.

Design Issues
First of a Kind Specification Requirements

- Specifications for coal and limestone size require additional equipment and feedstock wastage to achieve design requirements.
- Conservativism in inclusion of alkalai getters, cyclones, baghouses, and sulfator into process designs
- High Nitrogen usage, especially during start-ups and shut-downs
- Requirements for specialized alloys of limited availability and high price
- Incomplete or untried control configuration

Design Issues
Aggressive Schedule

- Aggressive schedule forcing design decisions
- Coal (feedstock) prep building started before the pulverizers were purchased, requiring modification before installation could be completed.
- Cooling water system redesign caused by increased requirements of Foster Wheeler, and other vendors' equipment
- Station service equipment being modified in response to increasing electrical loads
- This aggressive schedule did force project to progress.

Design Issues
Specialized Material Requirements Due to Temperature, Pressure and Chemical Activity

- Gas Analyzers
- Recycle Gas Compressor Piping
- Foster Wheeler's Carbonizer Gas Valves and Piping
- Reactor Emergency Pressure Let-down Piping
- Gas Cooler Bypass Orifices

Design/Operation Issues
Designs for Single Case, Limits Range of Operation

- Several instances of design short-comings
  - *Transport reactor start-up burner*
  - *Transport reactor pressure control valve*
  - *Recycle gas compressor control logic*
  - *Dense phase transport control logic*
  - *Transport reactor process air compressor control logic*
- Kellogg Process Control is not yet integrated, unable to link process variables of different systems to allow smooth parametric changes

Design/Operation Issues
Pneumatic Pressure Boundaries

- Reactors using piping lined with two layers of refractory totaling 9 inches thick
- Refractory lined piping 36" in diameter weigh several hundred pounds per running foot
- Due to weight and size, the piping is difficult to assemble in place, requiring each joint to be caulked and sealed with flexatalic gaskets.
- Flexatalic gaskets are fragile during storage and installation and are single use only.

Design/Operation Issues
Pneumatic Pressure Boundaries

- Refractory is hydroscopic and requires specialized curing procedures after thirty days at ambient air conditions.
- Problems with long term storage of un-cured refractory required minor repairs.
- Vessels and piping have rate of change restrictions on temperature and pressure to prevent cracking and failures
- A pressure test is required after every inspection or maintenance.

Design/Operation Issues
Gas Sampling at Pressure and Temperature

- First of a kind engineering to extract dust- laden samples at temperature and pressure
- Several gas components have dew points over 700F, and the liquid phase is highly corrosive.
- Requires exotic alloys for strength and corrosion protection
- Concentrations and compounds require specialized analyzers.

Design/Operation Issues
Feedstock Injection into Pressurized Reactor

- Tidd and Other PFBC Plants Use Hybrid Slurry Pumps to Inject Feedstock
  - *Add water to process*
  - *High maintenance items*
- PSDF Using Dense Phase Feed Technology
  - *Dry conveying using Nitrogen or air as transport media*
  - *Metering feedstock and transport media*
  - *Using pressures less than 20 psi higher than reactor*

Operation Issues
Suitable Start-Up Bed Materials for Transport Reactor

- Friable Alumina Initially Procured and used
  - *Fluidizes well, and temperature resistant*
  - *Twice as dense as other feedstocks, causing problems with dense phase equipment*
  - *Very hard and abrasive, causing failure of control valve*
- Spherical Alumina
  - *Nonabrasive, fluidizes well*
  - *Hard to procure, very dense*

Operation Issues
Suitable Start-Up Bed Materials for Reactors

- River Sand
  - *Used at Tidd*
  - *High Silica will not withstand heat*
- Furnace Ash
  - *Difficulty in finding adequate source*
- Conclusion: Use Alumina Until Enough Transport Reactor Ash is Generated.
  - *Pre-sized, dry, inert, temperature resistant*

Progress to Report

- Passed reactor pressure test with no welds failing and few minor flange leaks
- Candled Westinghouse PCD with no candle breakage
- Thermal oxidizer refractory was cured to 1600F, and thermal oxidizer was nearly 1000 hours of operation
- Sulfator/PCD warm-up heater refractory cured in 4 days of operation
- Successfully balanced purge flows to zero differential pressure transmitters at three reactor pressure settings

Progress to Report

- Successfully fired reactor start-up burner to cure reactor refractory lining to 1000F
- Successfully fluidized reactor with alumina as start-up bed material; circulating bed material through the reactor, riser, and heat exchanger at circulation rates of up to 90,000 lbs/hr and velocities to 45 ft/sec
- Demonstrated operation of feeders under pressure with alumina
- Preparing for the Foster Wheeler combustor refractory cure
- Currently firing with coal at 165 PSI

Future Plans

- July - Aug: Operate transport reactor as combustor for shake-down trials
- Sept - Oct: Operate transport reactor as combustor for parametric testing
- Oct - Nov: Operate transport reactor as gasifier for shake-down trials
- Nov - Mar ’97: Operate transport reactor as gasifier for parametric testing
- Apr - May ’97: Operate transport reactor as combustor for shake-down trials of Combustion Power’s granular bed filter

Future Plans

- Apr - May ’97: Foster Wheeler Combustion Turbine Start-Up
- Sept - Oct ’97: PFBC Start-Up of Foster Wheeler
- Jan - Feb ’98: APFBC Start-Up of Foster Wheeler

METC's Pilot-Scale Hot-Gas Desulfurization Process Development Unit

Michael H. McMillian (mmcmil@metc.doe.gov; 304-285-4669)
Larry A. Bissett (lbisse@metc.doe.gov; 304-285-4266)
Morgantown Energy Technology Center

Introduction

The Morgantown Energy Technology Center (METC) has designed and is currently constructing an on-site, hot gas desulfurization (HGD) Process Development Unit (PDU). The PDU is designed to use regenerable solid metal oxide sorbents that absorb hydrogen sulfide from high-temperature, high-pressure simulated coal-gasification fuel gas that is generated by a METC-designed syngas generator. The simulated coal gas is a mixture of partially combusted natural gas, water, carbon dioxide and hydrogen sulfide. PDU process conditions will be representative of anticipated commercial applications in terms of temperatures, pressures, compositions, velocities, and sorbent cycling. The PDU supports the Integrated Gasification Combined Cycle (IGCC) mission at METC by providing a test bed for development of IGCC cleanup systems that offer low capital cost, operating costs, and costs of electricity. METC intends to develop additional industrial involvement opportunities as the project progresses towards operations.

Objectives

The primary objectives of the PDU are to: (1) fill the gap between small-scale testing and large-scale demonstration projects by providing a cost effective test site for transport and fluid-bed desulfurization reactor and sorbent development, (2) demonstrate sorbent suitability over a wide range of parameters and (3) generate significant information on process control for transport and fluidized bed based desulfurization. PDU data is expected to be used to optimize process performance by expanding the experience for larger-scale demonstration projects, such as Sierra Pacific Power Company's Clean Coal Technology project.

Background

During the PDU's early conception (1,2), an IGCC-system economic study showed minimal cost and performance differences when using low velocity HGD fluid beds versus fixed or moving beds. However, costs could be lowered by using higher fluidizing velocities (3). The study also revealed economic advantages for a system that uses a minimal amount of undiluted regeneration air. Given this information and the encouraging results from small-scale transport reactor testing, METC designed the PDU to explore the advantages of higher velocity regimes and alternate contacting modes. Transport reactor provisions were then incorporated into the conceptual design on both the sulfidation and regeneration sides of the

PDU (4). Because the PDU does not require a coal feed or gasifier system, it should cost 25 to 75 percent less per test-hour than would otherwise be required.

Then METC decided to draw upon existing gas-solid processing technology. In particular, the similarity between the continuous, integrated cracking and catalyst regeneration operations used in fluid and transport catalytic cracking (FCC) units and the PDU concept was viewed as a potential link to success. METC took advantage of much of the existing industry expertise by teaming with the M.W. Kellogg Co. (MWK) for preliminary and detailed design activities. MWK designed the PDU reactor system, and METC designed the balance of plant facilities.

METC acted as the general construction contractor, and activities were split between several contractors for underground and above-ground utilities, civil construction and vessel fabrication. METC personnel are doing instrumentation and control, piping field fits and similar activities. In addition, METC will conduct all operations and maintenance.

PDU Description

Design Features

The PDU operates at 400 psia (2,750 kPa) pressure and at temperatures up to 1,200° F (650 ° C) on the sulfidation (fuel gas) side and up to 1,400° F (760° C) on the regeneration (air) side. The unit continuously circulates sorbent material between the sulfidation and regeneration sides of the desulfurization system. The PDU has provisions for fluid bed and transport contacting. When operating in the fluid bed contacting mode, fuel gas is fed into an 18 inch (.457 meters) inside diameter (i.d.) reactor and sorbent is circulated with steam or nitrogen to the 10 inch (.254 meters) i.d. regenerator reactor. When operating in the transport mode, a 5.2 inch (.132 meters) i.d. absorber riser reactor is used along with a 1.7 inch (.043 meters) i.d. regenerator reactor. Density difference is the primary driving potential for circulation. The following are a few of the primary design features of the METC PDU.

- Fuel gas flow: 60,000 to 120,000 scfh typical
- H_2S concentration: 0.5 to 1 volume % typical
- Absorption temperature: 1,000 to 1,200° F design
- Regeneration temperature: 1,100 to 1,400° F design
- Absorber-regenerator differential temp.: 400° F maximum
- Operating pressure: 400 psia maximum
- Fluid-bed absorber: 18-inch i.d., 10-ft bed maximum
- Transport absorber: 5.2-inch i.d., 50-ft length
- Fluid-bed regenerator: 10-inch i.d., 12-ft bed maximum
- Transport regenerator: 1.7-inch i.d., 50-ft length
- Underflow standpipes: 1.7 to 6.8 inch i.d., 20-ft length (approx.)
- Fluid-bed superficial velocities: 1 to 3 ft/s typical
- Riser superficial velocities: 15 to 20 ft/s typical

• Sorbent inventory:	1,000 to 2,000 lb typical
• Sorbent cycles per day:	50 to 100 typical
• Circulation rate:	2,000 to 5,000 lb/hr typical
• Transport absorber recirculation rate:	5,000 to 55,000 lb/hr typical
• Transport regenerator recirculation rate:	0 to 2,000 lb/hr typical
• Riser bulk densities:	2 to 12 lb/ft^3 design
• Sorbent size:	50 to 300 micrometers typical
• Sorbent flux:	100 lb/sec-ft^2 design
• Reactor Vessels	Refractory lined, carbon steel
• Major Piping	Hot-walled, Inconel 800H alloy

PDU Operation

Overview

Simulated low-Btu coal gasification gas will be supplied to the PDU by a natural gas-fired fuel-gas (syngas) generator. This precludes the ability to test the effects of trace contaminants on sorbent performance. This approach is more cost-effective and presents fewer site environmental issues. A previous description of the fuel gas generator remains generally accurate (5). Notable changes include the decision to use sulfuric acid rather than sulfur dioxide as the source of hydrogen sulfide for the fuel gas, and the use of a direct water quench instead of an indirect heat exchanger for final fuel gas temperature trim. A simple block flow diagram of the PDU is shown in Figure 1. In the absorber, a sorbent, such as zinc oxide, becomes sulfided by absorbing sulfur species from the fuel gas stream. In the regenerator, the captured sulfur in the sulfided sorbent is reacted with air, which restores or "regenerates" the activity of the sorbent. The sorbent is then recirculated back to the absorber, thus providing continuous operation. Inert gases (steam and/or nitrogen) are used to fluidize the sorbent in the standpipes above the valves and to prevent fuel gas and air intermixing.

The project also has two natural gas-fired indirect heaters to preheat inert gases and regenerant gases up to 1,400°F (760 ^{o} C), and filter lockhopper arrangements downstream of the cyclones, (as shown in Figure 2) to collect sorbent fines that carry over from the cyclones. Since process gases are cooled to around 600° F (315 ^{o} C) prior to entering the filter vessel, the filter elements will be porous metal with a 2-micron pore size. The off-gas from the regenerator, which contains sulfur as SO_2, will be captured in a packed tower absorber using sodium hydroxide and will be disposed of by METC rather than by being recovered as a useful product (such as sulfuric acid) or being recycled to the gasifier as in a commercial system. Similarly, the relatively sulfur free exit gas from the absorber will be burned in the incinerator, to convert any combustible gases prior to venting to the atmosphere. In a commercial unit, the absorber exit gas would be burned in a gas turbine to produce power.

The METC PDU is designed for operation in four distinct modes, which are combinations of fluid bed and transport contacting on both the absorber and regenerator sides. The four distinct modes are shown in Figure 3. Initial METC efforts will focus on transport

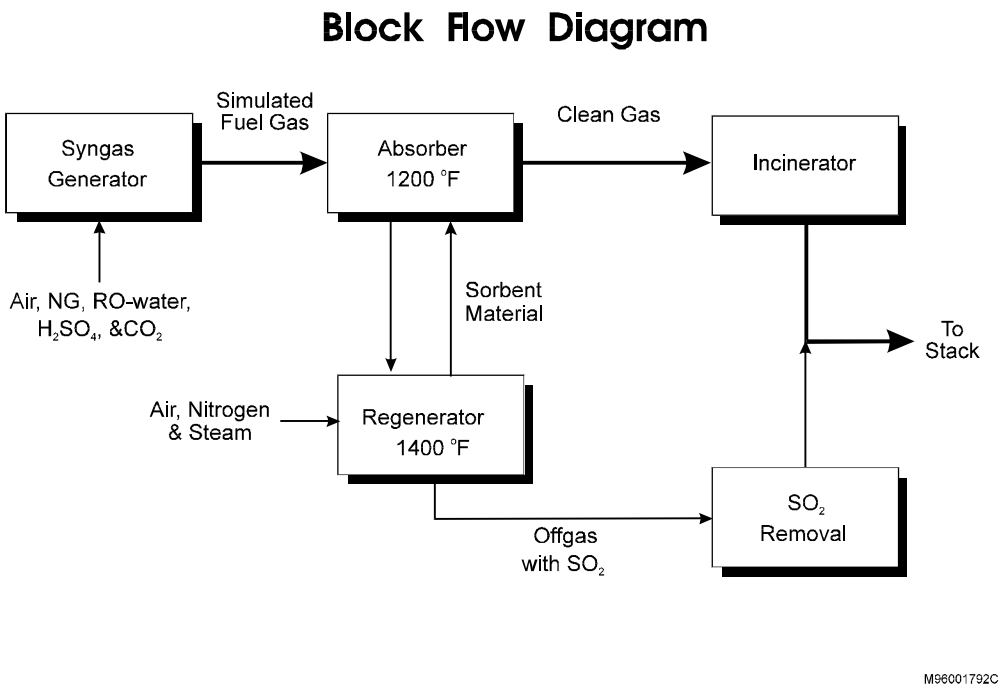

Figure 1

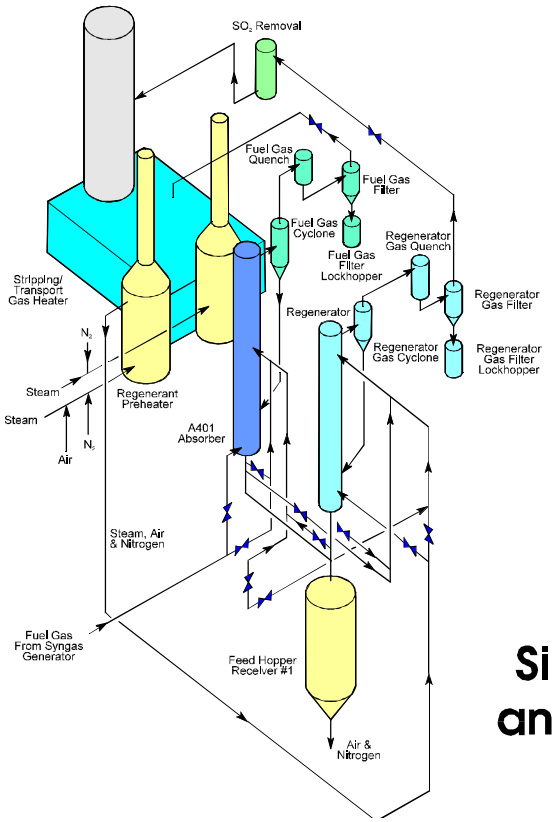

HGD/PDU Simplified Vessel and Piping Layout

Figure 2

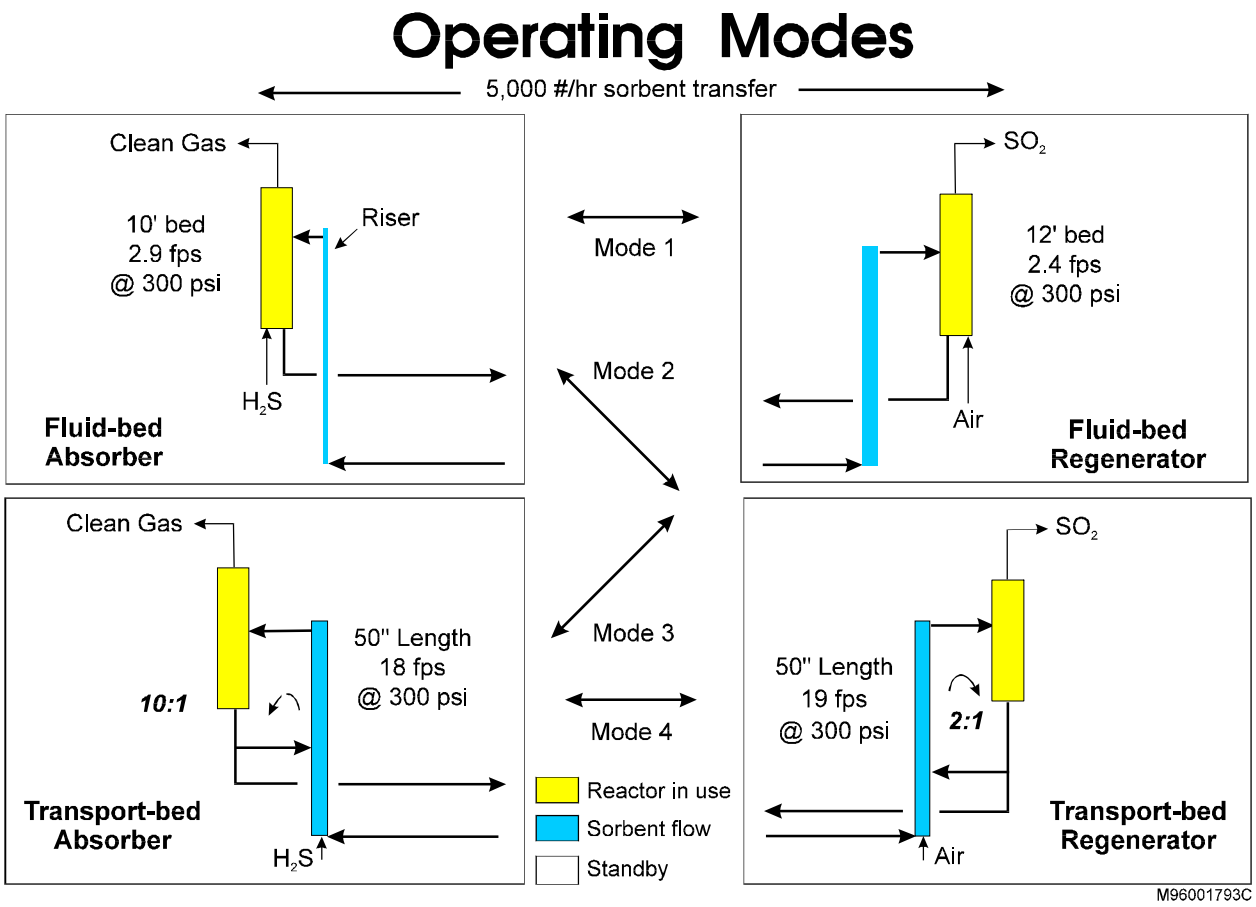

Figure 3

absorption and regeneration (Mode 4) due to the similarities to the Sierra Pacific Power Company's Clean Coal Technology project and because transport-based contacting offers potential economic benefits in both capital investment and operating simplicity.

General Operation

Some of the more important independent process variables to be studied regardless of the configurational mode include: H_2S concentration, sorbent type and particle size, sorbent sulfur loading, regenerant composition, and process temperatures. For fluid-bed modes, additional variables are bed level and fluidization regime (i.e., bubbling or turbulent); and for transport reactor modes, riser velocity and density are important added factors. The dependent variables include: sorbent circulation rate, absorber-regenerator differential pressure, pressure drop across circulation slide valves, amount and type of inert gases, and feed temperatures of the input gas streams.

The general operating strategy for the PDU will be to maintain constant flow rates, temperatures, pressures, and compositions during a specific test run. Values for independent

variables will be specified prior to a run, and dependent variables will then be calculated to provide initial control setpoints. In order not to exceed design temperatures, operations will start with both the absorption and regeneration temperatures below the targeted values, and then feed temperatures will be increased. Process changes will be made gradually and the unit will be allowed to stabilize. As a general rule, the sorbent inventory will be cycled a minimum of three times between process state changes.

A stable pressure balance must be maintained for smooth, uninterrupted sorbent circulation. The absorber-regenerator differential pressure will be set to a constant value to balance the hydrostatic pressure buildups in the fluid beds and standpipes versus the pressure drops across the circulation slide valves and the risers. The normal differential pressure between the absorber and regenerator freeboards is expected to be in the range of +/-2 psi (13.8 kPa), depending upon the operating mode. The pressure drop across the circulation control slide valves should generally be about 5 to 10 psi (35 to 70 kPa). The absorber-regenerator differential pressure will be maintained by modulating the regenerator backpressure valve in response to the differential pressure. To keep the differential pressure as constant as possible, this controller will be tuned for a fast response relative the controller for the absorber backpressure valve.

Sorbent flow rates can not be measured directly. They will be inferred from pressure drops across the standpipe slide valves, which must be calibrated during startup activities. During operation, the circulation rate will be set at a targeted test value by positioning the slide valve in the absorber circulation standpipe (see Figure 4). This will establish a constant flow rate of sorbent from the absorber to the regenerator. The return flow rate of sorbent from the regenerator to the absorber will be automatically controlled by modulating the slide valve in the regenerator circulation standpipe to maintain a preset sorbent bed level in the absorber. The regenerator bed level "floats” in this scheme, but a constant sorbent feed rate is maintained to the regeneration side of the process where temperature concerns are greatest and the need for uniform sorbent flow is therefore more critical. Recirculation rates to the transport reactors will be set by positioning the slide valves in the recirculation standpipes.

Bed levels will be determined from bed differential pressures. Initial bed levels will be established by the amount of sorbent charged to the system. A drop in regenerator bed level during a test will indicate that sorbent inventory is declining because of attrition and carryover from the cyclones into the downstream filters. If necessary, makeup sorbent from the feed hopper can be added to the regeneration side of the process without interrupting the test run.

The entire output of the syngas generator will be fed to the PDU during normal operations. A slipstream approach is not possible due to air permit restrictions. Delivery pressure is set by a backpressure valve on the feed line to the PDU. The fuel-gas flow rate is established and controlled by input rates to the gas generator. The major composition will be established by firing stoichiometry and the proportional amounts of injected water and carbon dioxide. The hydrogen sulfide content will be controlled by the injection rate of sulfuric acid.

PDU Reactor Schematic

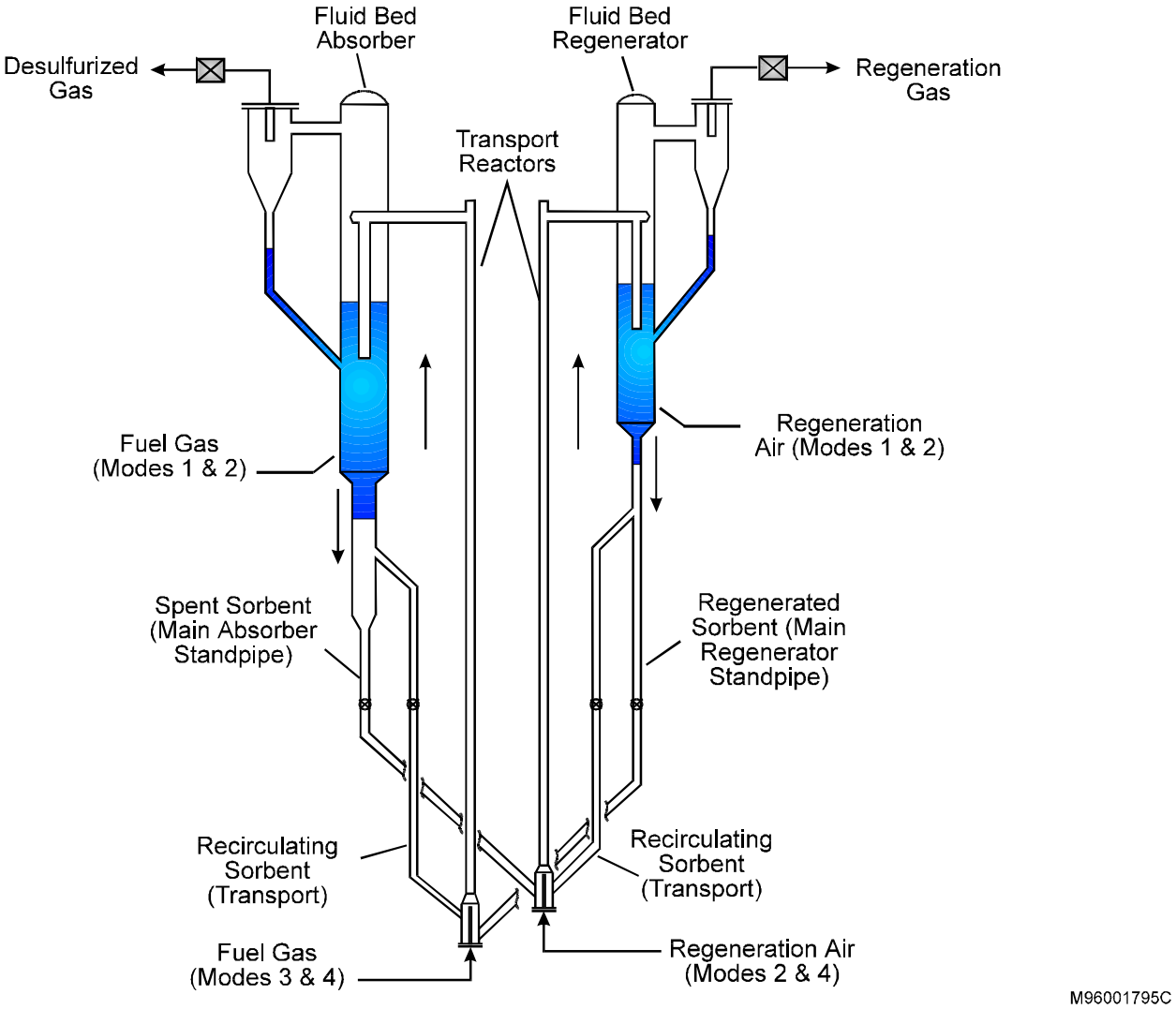

Figure 4

Nearly complete conversion of the sulfuric acid to hydrogen sulfide is expected. This air-blown, partial combustion process is projected to produce a nominal 100 to 130 Btu/scf (3,726 to 4,844 kJ/m^3) gas. Although the unit will be monitored for soot generation, any soot remaining in the gas that is fed to the PDU is not expected to be a significant problem due to the relatively high moisture content of the gas (minimum about 15 mole %), the hot refractory wall temperatures (minimum 1,250° F or 677 ^{o} C), and the long piping length from the syngas unit to the PDU absorber (approximately 200 feet or 61 meters). These three features combined are expected to promote the conversion of soot to gaseous compounds.

Regenerant gas will be pure air, or mixtures of air with steam and/or nitrogen. To avoid condensation in the preheater coils, any steam used will be blended in downstream of the regenerant preheater. Required regenerant preheat temperatures can range from about 500° to 1400° F (260 ° C to 760 ° C) to maintain heat balance. Regenerant flow rates will vary depending upon test objectives. For a regeneration scheme using minimum air, the molar input rate of oxygen (in air) will be set stoichiometrically to be 1.5 times the molar sulfur removal rate of the absorber.

Inert gas will be used for stripping/aeration of standpipes, aeration of cyclone diplegs, and aeration of the mixing chambers at the bases of the transport reactors. Inert gas will also be a transport gas in fluid-bed modes, a fluidizing gas in transport modes, and a regenerant diluent if desired. To minimize operating costs, steam will be used as an inert gas as much as possible; however, pure nitrogen or steam-nitrogen blends can be used in some configurations.

Temperature Control

Temperature control is one of the more important areas of overall process control since temperature has a major impact on process and sorbent performance. Higher temperatures tend to give faster reaction rates and thus potentially better process performance, but can also damage sorbents and equipment. In addition, temperature control strategies must cope with heat of reaction effects. In HGD technology, the reaction effects range from relatively minor on the absorption side (about 926 Btu released per pound of hydrogen sulfide removed) to rather significant on the regeneration side (about 2993 Btu released per pound of sulfur dioxide formed). Therefore, we have outlined the temperature control strategies that will be used initially in the PDU. All of the following strategies take into account the relatively high heat losses that will occur due to the high surface-to-volume ratio of the PDU equipment compared to commercial equipment size.

Fluid-bed Absorber. Absorption temperature primarily depends upon the temperature of the entering fuel gas and, to a much lesser extent, on the temperature of the transport, aeration, and stripping gases. The temperature of regenerated sorbent and the circulation rate also affects absorption temperature but cannot be used as control parameters since these are set by test conditions. Therefore, the fuel-gas feed temperature was selected as the control parameter and the absorber vessel freeboard temperature was selected as the control point. The temperature of the fuel gas exiting the syngas generator will be established by syngas generator operating conditions and will be set higher than that required by the PDU. A temperature controller in the PDU fuel-gas inlet line will provide the final temperature trim by controlling the direct injection of water into the fuel gas transfer pipeline leading to the PDU. The PDU freeboard and fuel-gas inlet temperature controllers will be initially cascaded to provide a faster, smoother response to process upsets. Preliminary runs may indicate that cascading is not required, in which case the final absorption temperature control will come directly from the freeboard controller.

Transport Absorber. For this mode, the temperature control point will be switched from the absorber vessel freeboard to the transport reactor outlet. The control strategy will remain the same as that for the fluid-bed mode, except for additional solids recirculation considerations. The temperature of the recirculated solids will be set by the flow rate and temperature of the inert gas used to fluidize sorbent in the absorber vessel. A fluidizing flow rate will generally be set at a low value to minimize solids entrainment out of the vessel. Once the flow rate is set, it will generally be held constant and the fluidizing gas inlet temperature will then be adjusted so that the sorbent leaving the absorber vessel will be within about 5° F (3.5 °C) of the desired absorption temperature. The heat balance around the transport absorber establishes the necessary temperature of the entering fuel gas with this approach.

Fluid-Bed Regenerator. The temperature of sulfided sorbent, the circulation rate, the regeneration heat release, and the regenerant air rate and composition all affect the regeneration temperature, but these will be set by test conditions and cannot be used as control parameters. Although heat losses from the regenerator vessel/cyclone are significant and are estimated to be about 30 percent of the regeneration heat release for the fluid-bed design case, these losses will remain nearly constant for a given test. Thus, they cannot be incorporated into a control scheme. The regeneration temperature will also be affected by the temperature of the transport, aeration, and stripping gases, but the effect will be too minor for control purposes. Therefore, only the regenerant feed temperature can be used as a control parameter, which is analogous to the fuel-gas feed temperature on the absorption side. Analogously, the regenerator freeboard temperature was selected as the control point. The regenerant feed temperature will be controlled by adjusting the natural gas firing rate of the regenerant gas preheater.

Transport Regenerator. Transport regeneration control is more complicated than fluid-bed mode control due to solids recirculation and other constraints. Consequently, it is likely to change as experience is gained during initial operations. The constraints include the need to maintain a minimum reaction initiation temperature (thought to be around 1,100° F (593 °C) at the bottom of the transport reactor, the need to limit the maximum regeneration temperature (thought to be around 1,400° F (760 °C)), and the need to complete the desired extent of regeneration within the transport reactor length. The location of maximum temperature in the transport reactor is unknown, since this will depend upon sorbent characteristics and process conditions. For example, it is currently believed that increasing sorbent recirculation will spread the riser temperature profile and decreasing recirculation will compress the profile.

The list of variables identified in the fluid-bed mode as being available or unavailable for use as control parameters still applies. However, in the transport mode, the recirculation of sorbent will have a major impact on the regeneration temperature. Therefore, the flow rate and temperature of the recirculated sorbent were selected as the primary control parameters, demoting the regenerant feed temperature to a secondary status. Skin temperature measurements will be made at multiple points along the transport reactor length, and the maximum temperature in this profile will be selected as the control point. To make this selection,

sorbent recirculation will be established and set at a sufficiently high flow rate (up to the hydrodynamic limit) to achieve the desired extent of regeneration within the reactor length. Then, with the recirculation rate held constant, the selected control point will be used to adjust the temperature of the recirculated sorbent, thereby controlling the regeneration temperature. Ideally, the selected control point will still correspond to the maximum regeneration temperature along the reactor length. If not, it may be necessary to change the control point at this time and repeat the procedure. The temperature of the recirculated sorbent will be adjusted by controlling the flow rate and the temperature of the inert gas that fluidizes the sorbent in the regenerator vessel. Thus, the temperature rise of the fluidizing gas closes the heat balance around the regenerator/cyclone circuit. Once the desired regeneration temperature profile is obtained, it can be fine-tuned by adjusting the regenerant feed temperature. If sorbent recirculation is not employed, then the regenerant feed temperature becomes the primary control parameter just as in the fluid-bed regeneration mode.

PDU Project Status and Schedule

Structural steel fabrication and steel erection was 100 percent complete in June 1996. The incinerator, barrier filter vessels, fines lock hoppers, sorbent feed vessel, filter blowback accumulator, and air and inert gas preheaters were mounted in the structure. As of June 1, 1996, project construction was 60 percent complete, up from 32% a year ago and progressing according to plan.

The project is on schedule to desulfurize coal-gas by October 1997. The project schedule is given in Figure 5.

Future Activities

In addition to demonstrating fully integrated operations, process and control scale-up data, performance data, and addressing other actual engineering challenges, future tests will concentrate on key operational and sorbent durability issues such as the following. (1) Which is more optimum from a sorbent as well as an overall process economic viewpoint; operating with small changes in sulfur loading on the circulating sorbent and thus at high circulation rate, versus running "deep" cycles with larger changes in sulfur loading but at comparatively lower circulation rates? (2) Which flow regime is best for chemical reaction and/or sorbent life, bubbling, turbulent, or transport?

These data will be generated at METC during six nominal 5-day test periods per year beginning after PDU shakedown in the fall of 1997. Initial testing will involve more numerous but shorter duration test periods. Test planning, operations, data reduction and reporting will be performed by DOE/METC personnel in partnership with industry.

Schedule

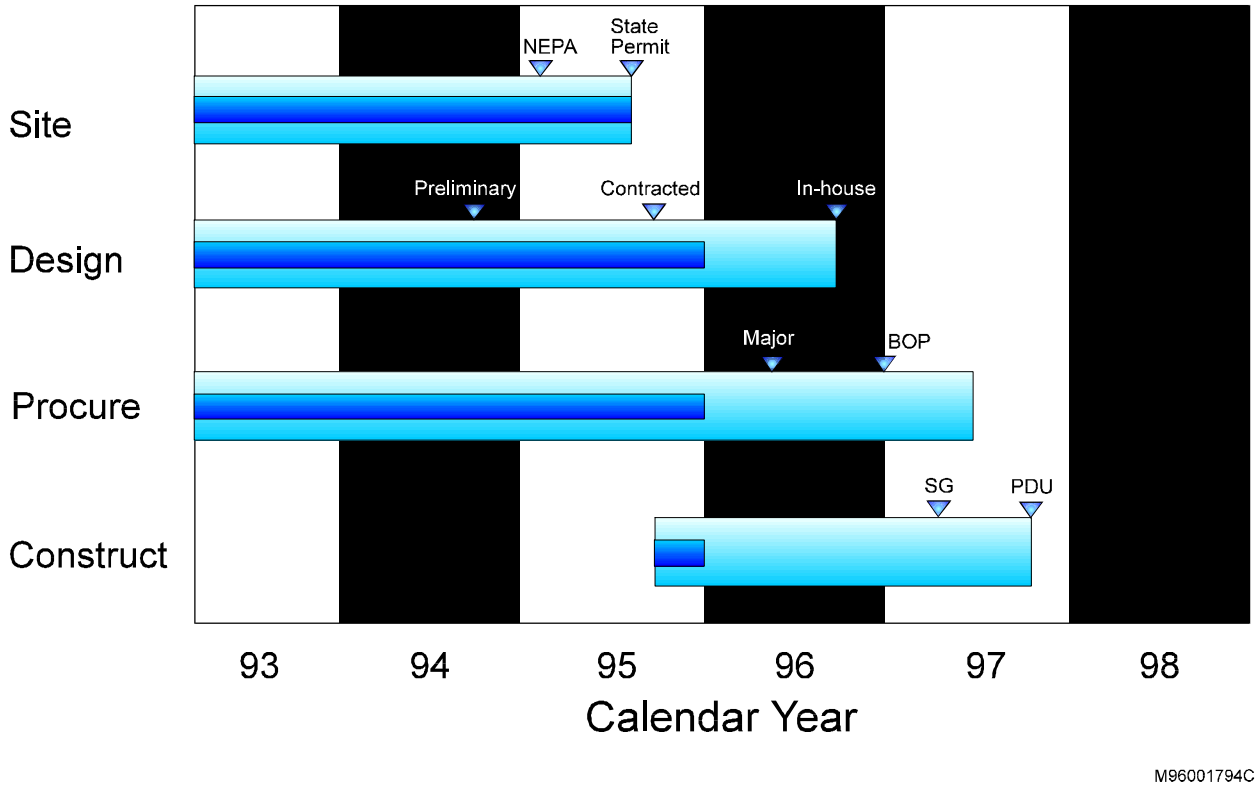

Figure 5

Summary

The PDU offers coupled system operation of various reactor configurations to optimize gas/solids contacting and to prove system safety and control aspects. The operating flexibility, and high degree of instrumentation mean that the PDU will provide design data on this complex HGD process over a broad operating window for about a dozen major operating variables.

At this point the PDU is not linked to a single developer. Therefore, intellectual property provided by the PDU will be available for application to other IGCC systems, including those using oxygen-blown gasifiers. The expected cost savings can thereby be realized by a much broader market than if the technology were limited in use to only one gasifier supplier. METC is interested in pursuing industrial cost sharing of PDU activities through arrangements such as cooperative research and development agreements, whereby intellectual property rights can be obtained by the industrial partner.

References

1. Bissett, L.A., J.M.Rockey, and S.C.Walczak. 1991. Preliminary Conceptualization of METC's Fluid-Bed, Hot-Gas Desulfurization PDU. In *Proceedings of the Eleventh Annual Gasification and Gas Stream Cleanup Systems Contractors Review Meeting*, 556-565, DOE/METC-91/6123, Vol. 2. NTIS/DE92001102. Springfield, VA.: National Technical Information Service.

2. Bissett, L.A. 1993. Fluid-Bed HGD PDU. In *Proceedings of the Coal-Fired Power Systems 93 -- Advances in IGCC and PFBC Review Meeting*, 302-306. DOE/METC-93/6131, NTIS/DE93000289. Springfield, VA.: National Technical Information Service.

3. Rutkowski, M.D., H.T. Chen, and M.G. Klett. 1993. Sensitivity of Hot-Gas Desulfurization on IGCC Cost of Electricity. *Proceedings of the 12th Annual Gasification and Gas Stream Cleanup Systems Contractors Review Meeting,* 263 -279. DOE/METC-92/6128, Vol. 1, NTIS/DE93000228. Springfield, VA: National Technical Information Service.

4. Bissett, L.A., 1994. METC Fluid-Bed Hot-Gas Desulfurization PD. *Proceedings of the Coal-Fired Power Systems 94 -- Advances in IGCC and PFBC Review Meeting Vol. I,* 256 -262. DOE/METC-94/1008, Vol.1, NTIS/DE94012252. Springfield, VA. National Technical Information Service.

5. Monahan, M.J., 1992. METC's Synthetic Gas Generator Project. *Proceedings of the Eleventh Annual Gasification and Gas Stream Cleanup Systems Contractors Review Meeting.* 533-540. DOE/METC-91/6123, NTIS/DE92001102. Springfield, VA. National Technical Information Service.

MMCMIL\961232

Pulsed Atmospheric Fluidized Bed Combustion

William G. Steedman
ThermoChem, Inc.

Abstract

The scale-down of conventional fluidized bed combustion (FBC) technology for application to the commercial, institutional, and light industrial market sectors has been hampered by unfavorable cost, performance, start-up, and load following characteristics in comparison to oil- and gas-fired boilers. ThermoChem and Manufacturing and Technology Conversion International, Inc. (MTCI), have developed an advanced FBC concept known as Pulsed Atmospheric Fluidized Bed Combustion (PAFBC) that addresses this market sector.

The PAFBC integrates a pulse combustor with a bubbling atmospheric fluidized bed combustor. Fine coal is burned in the pulse combustor upstream of the fluidized bed of sorbent, reducing NO_x and sulfur emissions relative to conventional FBC technology. Furthermore, the acoustic effect of the pulse combustor enhances combustion efficiency and heat transfer in the bed; resulting in modestly sized units with high throughput rates and lower costs compared with conventional FBC units.

A commercial-scale boiler (50,000 lb./hr. stream generation) has been installed at Clemson University as part of the Department of Energy funded development program. This facility and the results of its initial operation are described.

Design and Performance of a Low Btu Fuel Rich-Quench-Lean Gas Turbine Combustor

Alan S. Feitelberg (feitelberg@crd.ge.com; 518-387-5737)
Melvin R. Jackson (jacksmr@crd.ge.com; 518-387-6362)
Michael A. Lacey (lacey@crd.ge.com; 518-387-7989)
Kenneth S. Manning (manning@crd.ge.com; 518-387-5143)
Ann M. Ritter (ritter@crd.ge.com; 518-387-7621)
GE Corporate Research & Development
P.O. Box 8
Schenectady, NY 12301

Introduction

General Electric Company is developing gas turbines and a high temperature desulfurization system for use in integrated gasification combined cycle (IGCC) power plants. High temperature desulfurization, or hot gas cleanup (HGCU), offers many advantages over conventional low temperature desulfurization processes, but does not reduce the relatively high concentrations of fuel bound nitrogen (FBN) that are typically found in low Btu fuel. When fuels containing bound nitrogen are burned in conventional gas turbine combustors, a significant portion of the FBN is converted to NO_x. Methods of reducing the NO_x emissions from IGCC power plants equipped with HGCU are needed.

Rich-quench-lean (RQL) combustion can decrease the conversion of FBN to NO_x because a large fraction of the FBN is converted into non-reactive N_2 in a fuel rich stage. Additional air, required for complete combustion, is added in a quench stage. A lean stage provides sufficient residence time for complete combustion.

Objectives

General Electric has developed and tested a rich-quench-lean gas turbine combustor for use with low Btu fuels containing FBN. The objective of this work has been to design an RQL combustor that has a lower conversion of FBN to NO_x than a conventional low Btu combustor and is suitable for use in a GE heavy duty gas turbine. Such a combustor must be of appropriate size and scale, configuration (can-annular), and capable of reaching "F" class firing conditions (combustor exit temperature = 2550°F).

Approach

The development of RQL2, a full scale (14" diameter, 10 lb/s total flow), rich-quench-lean gas turbine combustor is the culmination of a five year research and development effort. This effort began with testing of a small (2" diameter) perforated plate burner, using natural gas and natural gas/ammonia mixtures for fuel (Goebel and Feitelberg, 1992). The promising perforated plate burner tests were followed by the development of RQL1, a reduced scale (6" diameter, 0.75 lb/s total flow), rich-quench-lean combustor. RQL1 was tested using high temperature low Btu fuel produced by the pilot scale coal gasification and HGCU facility located at GE Corporate Research

and Development in Schenectady, NY (Bowen *et al*., 1995). At the optimum operating conditions, the conversion of NH_3 to NO_x in RQL1 was about 15%, or about a factor of 2 lower than expected from a conventional gas turbine combustor burning the same fuel. A detailed discussion of the RQL1 design and test results can be found in Bowen *et al*. (1995).

The approach taken to design RQL2 combustor was to build upon the prior RQL and low Btu combustor designs that were developed and tested at GE Corporate Research and Development (Bowen *et al*., 1995). Several design features from the RQL1 combustor such as a converging rich stage geometry, a radially stratified quench section, and a backward facing step, were incorporated into the RQL2 design. Design features from conventional low Btu combustors were also used in the RQL2 design. The RQL2 combustor uses a fuel nozzle that was developed for conventional swirl stabilized diffusion flame low Btu combustors (Battista *et al*., 1996) and the RQL2 combustor uses a filmed cooled lean stage liner which is similar to the liners used in conventional low Btu combustors. Additionally, the RQL2 combustor takes advantage of new gas turbine technology; for example, the RQL2 rich stage liner uses a new cooling scheme developed at GE Corporate Research and Development (Jackson *et al*., 1996).

The general methodology used to design RQL2 is shown in Figure 1. The overall fuel/air ratio was determined by selecting the maximum combustor exit temperature, and by the decision to use pilot plant low Btu gas as the fuel (see Table 1). The goal of designing a combustor suitable for use in GE heavy duty gas turbines, which use multi-can combustors, dictated the overall dimensions of the RQL2 combustor. The distribution of the total available volume between the rich, quench, and lean stages was determined by combining: (1) a computational fluid dynamics (CFD) analysis, which predicted the overall flow field and the size and shape of the recirculation zones, and (2) chemical kinetic models, which related the rich stage residence time and temperature to the conversion of NH_3 to NO_x.

The separation of the the air supplies for the rich stage and quench/lean stage is a design feature carried over from RQL1. Dividing the total combustion air into two separate, independent-

Table 1: Typical Pilot Plant Low Btu Fuel Composition

Species	Mole Percent
CO	8.6
H_2	17.3
CH_4	2.7
N_2	30.1
CO_2	12.6
H_2O	28.0
Ar	0.3
NH_3	0.4
TOTAL	100.0

ly controlled streams is important from a research perspective, because this capability allows us to search for the optimum rich stage operating conditions. In addition, overall air management (e.g., air pressure drop) is simplified, because the rich stage cooling scheme can be designed almost independently of the quench/lean stage cooling scheme. This allowed much of the detailed design and modeling work for the rich stage to proceed independently of the quench/lean stage design.

Project Description

A schematic of the RQL2 combustor and test stand can be found in Figure 2. The 24" diameter pressure vessel containing the RQL2 combustor is divided into two separate chambers that are fed by independently controlled air supplies. The hot combustion gases flow through the RQL2 combustor, an impingement cooled transition piece, a sector from the film cooled first stage nozzle of a GE LM6000 gas turbine, and then exit into a water cooled exhaust duct. The burned gas is sampled with a water cooled probe located downstream of the LM6000 nozzle sector. The transition piece and all downstream components were used previously in tests of low Btu gas fuel nozzles (Bowen *et al.*, 1995).

A single low Btu gas fuel nozzle produces the swirl stabilized rich stage diffusion flame. This fuel nozzle, referred to as the N7B fuel nozzle, was originally designed for use in conventional low Btu fuel gas turbine combustors. Details of the development and testing of this fuel nozzle may be found elsewhere (Battista *et al.*, 1996; Bowen *et al.*, 1995).

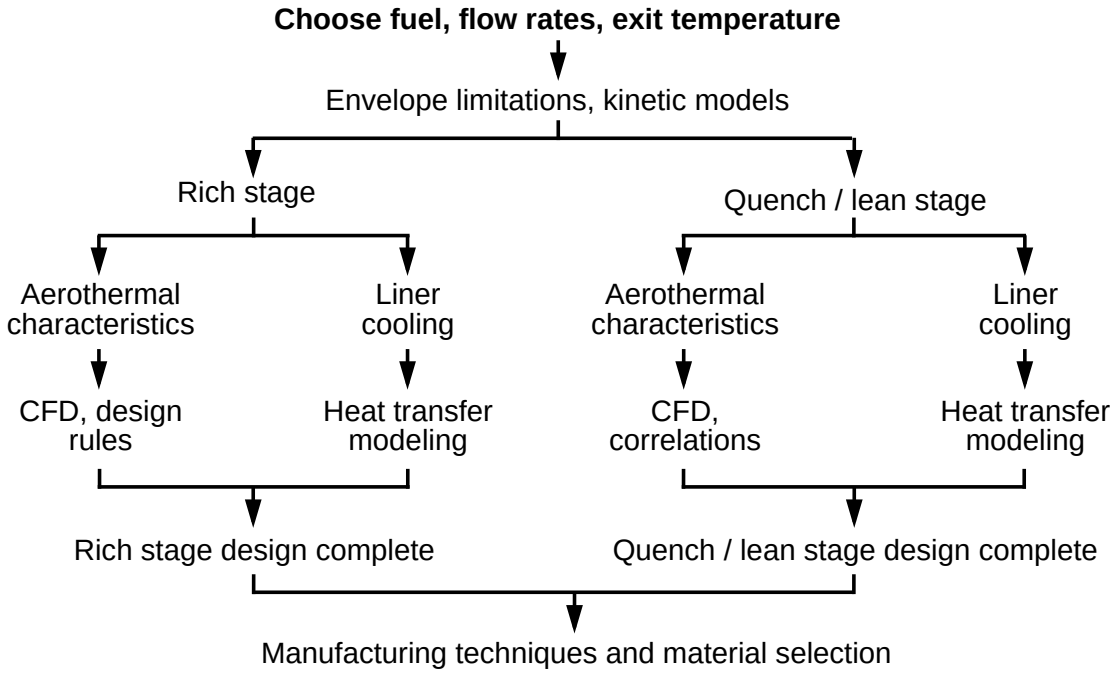

Figure 1: RQL2 design methodology.

The rich stage combustor liner consists of a 14" diameter cylindrical section followed by a conical section which reduces the diameter of the flow path from 14" to 7". Both the cylindrical and conical sections are approximately 13.5" long. Flow visualization tests and computational fluid dynamics (CFD) analysis have shown that the converging section is necessary to prevent the low pressure core of the swirling flow from drawing lean stage gases back upstream into the rich section. The converging section also provides a convenient method of reducing the flow area to a reasonable size for proper quenching.

Developing an adequate cooling scheme for the rich stage liner presented special challenges. The rich stage liner is relatively large, but relatively little air is available for cooling. Film cooling, one of the most effective methods of combustor liner cooling, is not desirable on the rich stage if NO_x emissions are to be minimized. For these reasons, the RQL2 rich stage combustor liner was fabricated with a novel double-walled structure developed at GE Corporate Research and Development. Internal cooling passages with narrow dimensions conduct cooling air circumferentially around the liner (see Figure 3). Air enters each rectangular cooling channel through an inlet hole and exits each channel through a slot which discharges into one of eight longitudinal collection tubes. The collection tubes, in turn, discharge into a plenum which supplies the air for the fuel nozzle and cap/cowl. The final design shown in Figure 3 was selected only after a detailed heat transfer analysis which used literature correlations for convective heat transfer, a finite element analysis code, and custom software tools. Haynes 230 was selected as the material for construction because of its superior properties at high temperatures.

The rich stage cooling structure was formed by first rolling the conical and cylindrical inner shells and then machining the shallow cooling channels into these shells. Bosses were welded longitudinally along the shells to provide enough material to weld the collection tubes and outer

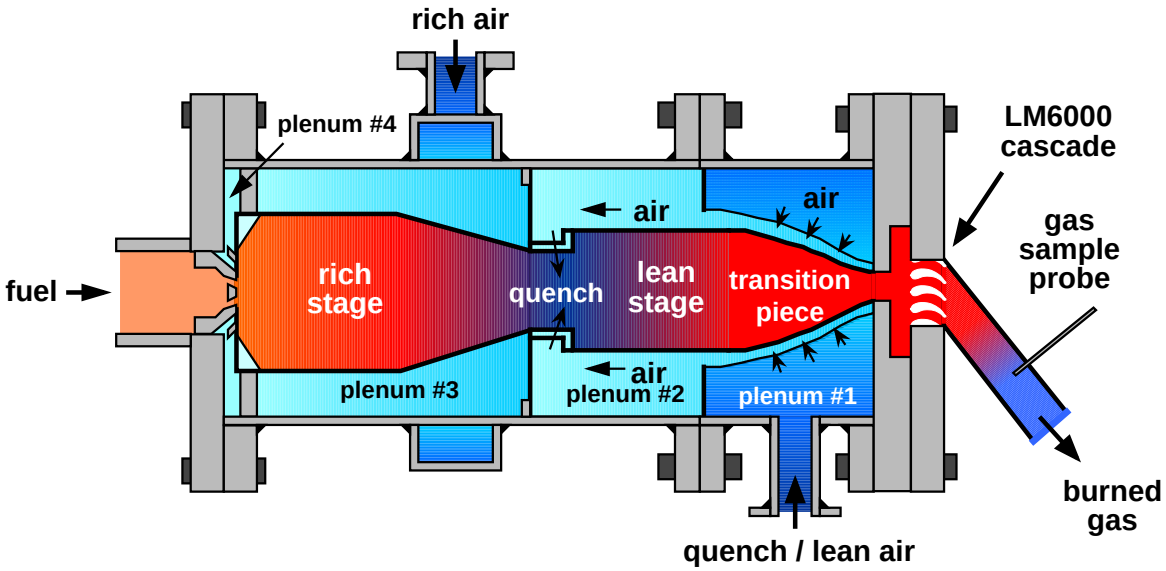

Figure 2: RQL2 combustor and test stand.

skin segments to the inner shell. The skin segments, with pre-drilled inlet air holes, were then welded to the bosses. The outer skin segments were bonded to the ribs of the inner shell using a laser spot welding technique. Finally, the cylindrical and conical sections were welded together and the collection tubes were welded in place using manual gas tungsten arc welds. Additional details of the manufacturing methods can be found in Jackson *et al*. (1996).

The quench section consists of a 7" diameter cylindrical section, approximately 4.3" long, and a backward facing step at the entrance to the lean section. The quench/lean stage air enters the combustor through quench air holes located at the downstream end of the cylindrical section. Rapid quenching is achieved with quench air holes of different sizes, referred to here as a "radially stratified quench". Larger holes create larger jets with greater momentum and which penetrate fur-

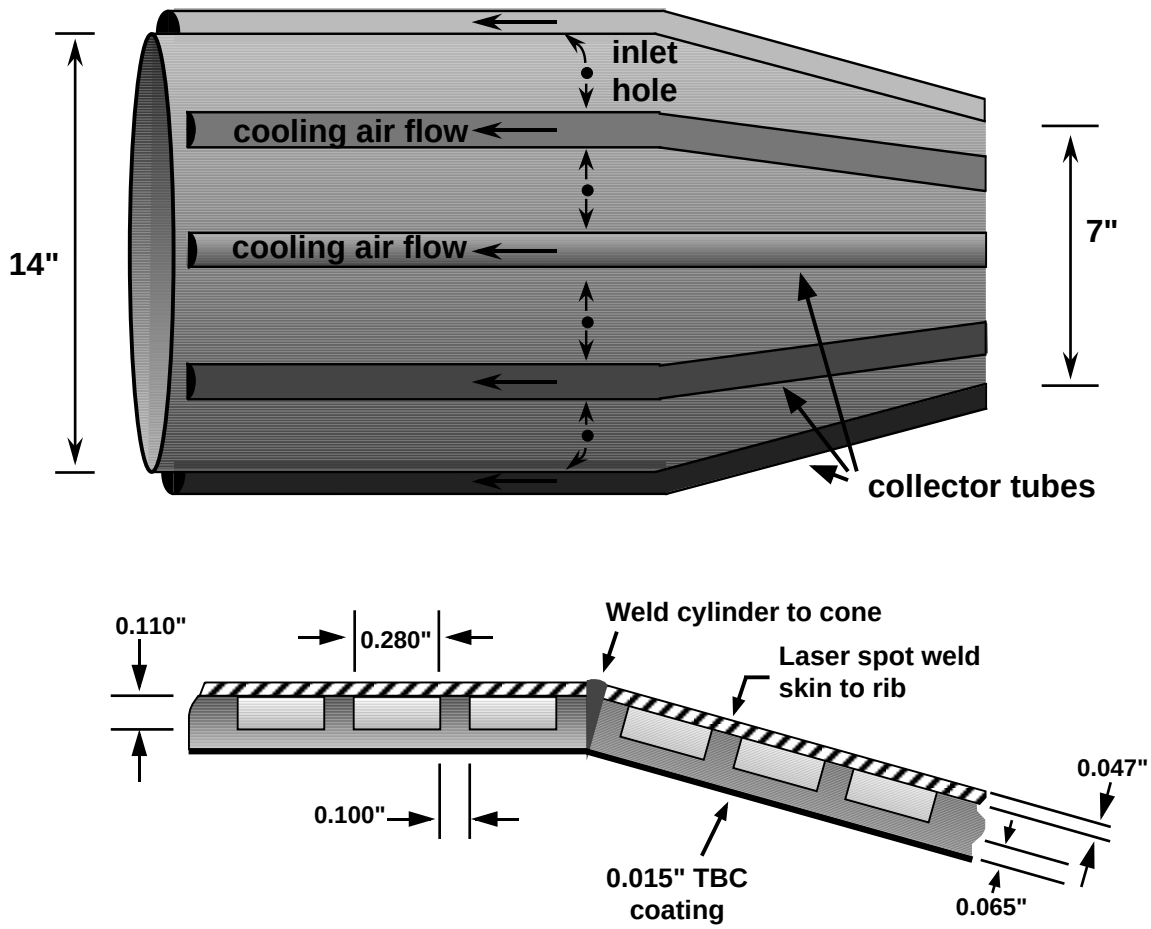

Figure 3: Double-walled rich stage combustor liner. **Top:** General arrangement of inlet cooling holes and collector tubes, with direction of air flow indicated. For clarity, the inlet holes are shown for only one circumferential cooling channel. **Bottom:** Liner wall cross-section in the region of the junction between the cylindrical and conical sections, showing the dimensions of the internal cooling channels.

ther into the hot gas flow. Smaller holes create smaller jets which do not penetrate to the centerline of the combustor. The quench/lean air entering through the smaller holes mixes with the flow closest to the wall, while the quench/lean air entering through the larger holes mixes primarily with the flow near the centerline of the combustor. The quench holes were sized using standard correlations for jets penetrating into a cross flow (Lefebvre, 1983). Both the cylindrical section and backward facing step are impingement cooled.

The lean section was fabricated from the aft portion of a modified MS6000 liner, and is approximately 10.5" in diameter and 14.5" long. The MS6000 film cooling holes were reduced in diameter and all of the mixing and dilution air holes were eliminated. The design goal was for 70% of the quench/lean air to enter the combustor through the quench holes, with the remaining 30% entering through the lean stage film cooling holes. To reduce cooling air leakage, a modified MS6000 combustor hula seal is used to seal the interface between the lean section and the transition piece.

Using flow sleeves, baffles, and seals, the region inside of the pressure vessels was divided up into four plenums (see Figure 2). The quench/lean stage air is fed into plenum #1, and from this plenum the air flows through an impingement sleeve to cool the transition piece. After cooling the transition piece all of the air from this plenum flows into plenum #2, which feeds the quench holes and the lean stage liner film cooling holes. Similarly, the air for the rich stage is feed into plenum #3, flows through the double-walled rich stage combustor liner and into plenum #4, which supplies air to the fuel nozzle and cap/cowl.

Results

The first pilot plant test of RQL2 (designated as Test 9 for programmatic reasons) was conducted during March 1996. RQL2 test conditions are listed in Table 2. Due to limitations of the HGCU system, the low Btu fuel flow rate was limited to 1.5 lb/s, rather than the gasifier capacity

	Rich Stage/Lean Stage Air Flow Rate Ratio		
	20/80	30/70	40/60
Low Btu Fuel Temperature	680 °F	680°F	640°F
Low Btu Fuel Flow Rate	0.8 – 1.5 lb/s	0.7 – 1.3 lb/s	0.5 – 1.3 lb/s
Rich Stage Air Temperature	680°F	690°F	700°F
Rich Stage Air Flow Rate	0.85 lb/s	1.1 lb/s	1.4 lb/s
Lean Stage Air Temperature	740°F	740°F	710°F
Lean Stage Air Flow Rate	3.3 lb/s	2.6 lb/s	2.1 lb/s

Table 2: RQL2 test conditions. Combustor chamber pressure = 10 atm ±10% for all air splits.

of 2.2 lb/s. Although the HGCU system accepts low Btu gas at about 1000°F, the relatively low fuel flow rates and heat losses from the piping combined to produce relatively low fuel temperatures at the combustor inlet (see Table 2). The reduction in fuel flow rate and temperature necessitated corresponding reductions in the air flow rate to achieve the target combustor exit temperature.

RQL2 was fired for more than 96 hours during Test 9. During this time several series of tests were conducted with the total combustion air divided into varying fractions between the rich and quench/lean stages. In a typical series, both the total air flow rate and the fractional distribution of the combustion air between the rich and quench/lean stages were held constant. The fuel flow rate was then adjusted in steps to vary the combustor exit temperature from about 1600°F to more than 2550°F. During this process, which typically required several hours to complete, continuous measurements were made of NO_x, CO, CO_2, and O_2 concentrations in the exhaust gas. An analyzer failure early in Test 9 prevented measurements of unburned hydrocarbon emissions.

Figure 4 shows NO_x emissions measured during Test 9 with 20% of the combustion air sent to the rich stage and 80% of the combustion air sent to the lean stage. Figures 5 and 6 show measured NO_x emissions with air splits of 30% rich/70% lean and 40% rich/60% lean, respectively. The conversion of NH_3 to NO_x is also shown in Figures 4 through 6. Conversion was calcu-

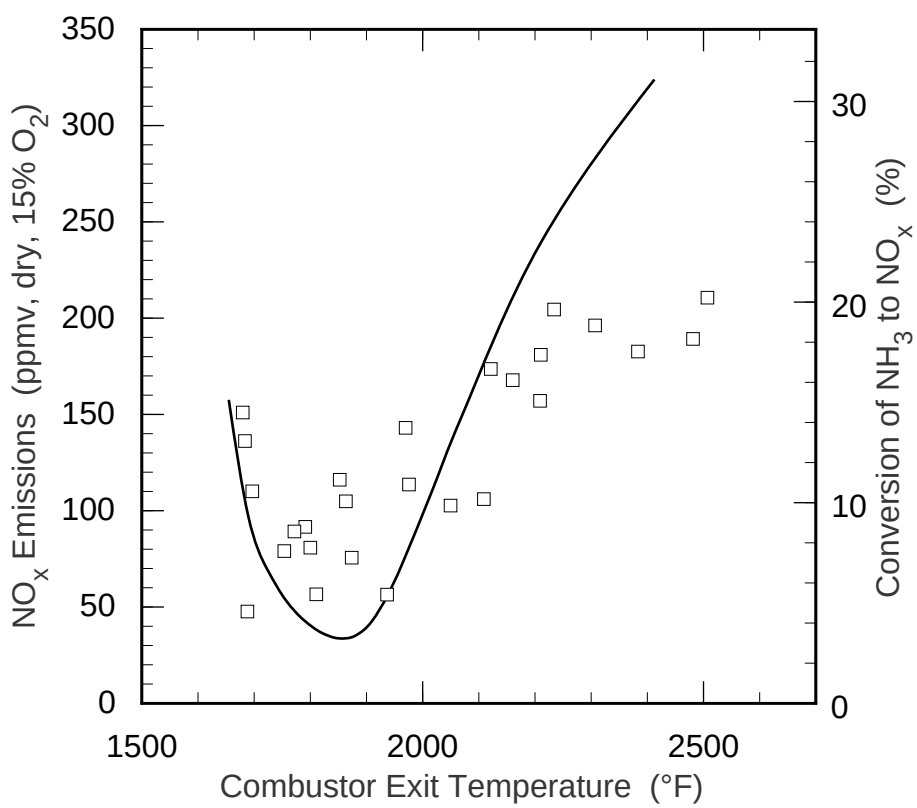

Figure 4: RQL2 NO_x emissions at a 20/80 rich/lean air split. The solid line represents the SLICER model predictions.

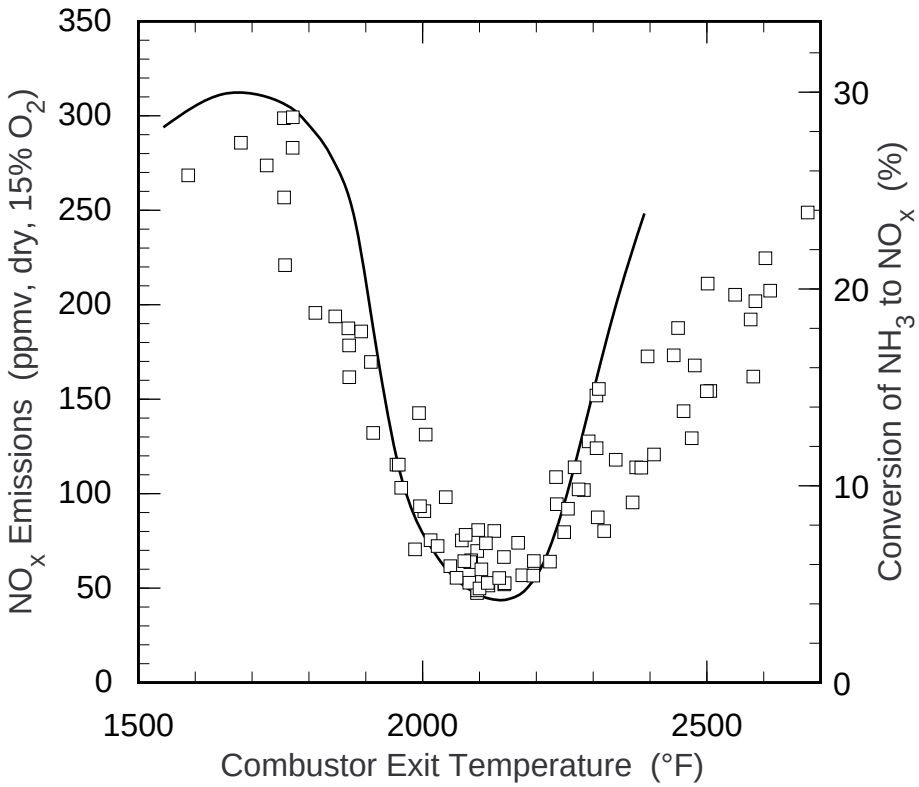

Figure 5: RQL2 NO_x emissions at a 30/70 rich/lean air split. The solid line represents the SLICER model predictions.

lated using the measured fuel NH_3 concentration of 4600 ppmv, and by assuming non-FBN NO_x formation (e.g., thermal NO_x) was negligible. This is a reasonable assumption for the very low heating value pilot plant fuel (higher heating value = 110 Btu/SCF).

As expected from models and previous RQL1 results, NO_x emissions were a strong function of the air split between the rich and lean stages, as well as the rich stage equivalence ratio (i.e., the combustor exit temperature). With the air split held constant, a distinct minimum in NO_x emissions was observed at the optimum rich stage equivalence ratio. With an air split of 40% rich/60% lean, the minimum in NO_x emissions occurred at a combustor exit temperature of about 2400°F. With a 30/70 rich/lean air split, the minimum in NO_x occurred at a combustor exit temperature of about 2100°F. With a 20/80 air split, the minimum in NO_x occurred at about 1800°F. For all three air splits, the minimum occurred at a rich stage equivalence ratio of about $\varphi_{rich} = 1.25$.

At the optimum rich stage equivalence ratio, NO_x emissions were about 50 ppmv (on a dry, 15% O_2 basis). With 4600 ppmv NH_3 in the fuel, this corresponds to a conversion of NH_3 to NO_x of about 5%. At the optimum conditions, RQL2 NO_x emissions were more than a factor of 3 lower than expected from a conventional diffusion flame combustor burning the same fuel. For example, in previous pilot plant tests using a GE MS6001B combustor, the conversion of

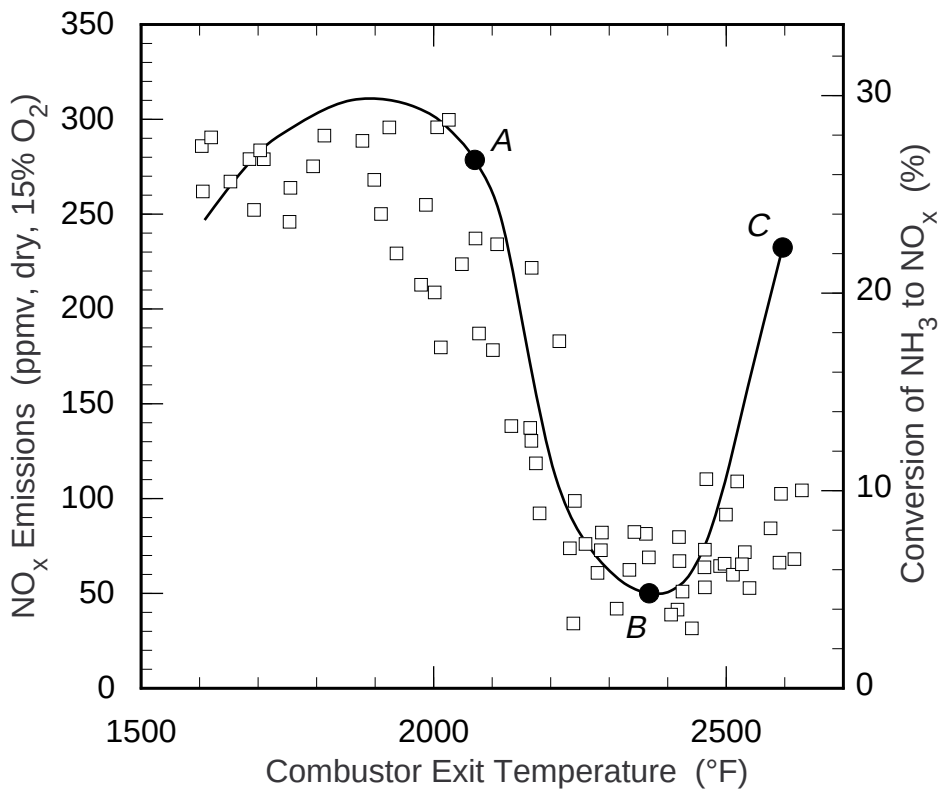

Figure 6: RQL2 NO_x emissions at a 40/60 rich/lean air split. The solid line represents the SLICER model predictions. Model points labeled "*A*", "*B*", and "*C*" correspond to rich stage equivalence ratios of 0.9, 1.25, and 1.6, respectively.

NH_3 to NO_x ranged from 20 to 80%, depending upon the combustor exit temperature (Battista *et al*., 1996). As conditions were shifted away from the optimum, RQL2 NO_x emissions gradually increased until they were comparable to a standard combustor.

RQL2 NO_x emissions measured during Test 9 were modeled with SLICER, a set of custom software modules for modeling sequentially linked ideal chemical reactor networks. SLICER models are assembled from these custom software modules and the Chemkin II package of programs and subroutines (Glarborg *et al*., 1986; Lutz *et al*., 1988; Kee *et al*., 1989). In the SLICER model of RQL2, the rich stage was represented as an equivolume perfectly stirred reactor (PSR) and a plug flow reactor (PFR) in series. The SLICER model combines the flow exiting the rich stage PFR with the quench/lean stage air in a second PSR, which feeds a second PFR. Inputs to the SLICER model include the measured combustion chamber pressure, rich and quench/lean air flow rates, air temperature, fuel composition, fuel flow rate, and fuel temperature. The chemical kinetic mechanism included more than 50 species and 250 elementary reaction steps (Michaud *et al*., 1992).

Results from the SLICER modeling are indicated by the solid lines in Figures 4, 5, and 6. The SLICER representation of RQL2 both qualitatively and quantitatively matches the NO_x emissions measurements. The SLICER predictions are insensitive to the relative sizes of the rich stage PSR and PFR. At high rich stage equivalence ratios the SLICER NO_x emissions are slightly sensitive to the relative size of the quench/lean PSR and PFR. Increasing the quench PSR volume tends to decrease model NO_x emissions at high φ_{rich}.

The key chemical reactions that govern NH_3 destruction and NO_x formation in RQL2 can be identified using the SLICER model and by performing a reaction path analysis (RPA) on individual reactors. For example, consider the chemical reactions within the rich stage PSR at a 40/60 air split. Near the optimal rich stage equivalence ratio (designated by point "*B*" in Figure 6), a major route for NH_3 destruction is

$$NH_3 \rightarrow NH_2 \rightarrow NH \rightarrow N \rightarrow N_2$$

where reaction partners have been omitted for brevity. Key reactions in this NH_3 destruction pathway are

$$NH + H \rightarrow N + H_2 \qquad \text{(R1)}$$

and

$$N + NO \rightarrow N_2 + O \qquad \text{(R2)}$$

R1 is a simple abstraction reaction, while R2 is the reverse of one of the well-known thermal NO_x formation reactions. Comparing reaction rates at point "*A*" ($\varphi_{rich} = 0.9$) to point "*B*" ($\varphi_{rich} = 1.25$) shows that when the rich stage PSR is too lean, the molar flux of N atoms through the forward direction of R1 slows down by a factor of four, mainly due to a nine fold reduction in the H atom concentration. This reduces N atom concentrations by a factor of twelve. As a consequence, N_2 formation (and NO destruction) through R2 slows down at point *A* relative to point *B*. The gas leaving the rich stage PSR at point *B* contains only 55 ppmv NO_x (on a dry, 15% O_2 basis), and some of this NO_x will be destroyed in the rich stage PFR. In contrast, the gas leaving the rich stage PSR at point *A* contains 278 ppm NO_x (on a dry, 15% O_2 basis), and none of this NO_x will be destroyed in the rich stage PFR.

When the rich stage PSR is too fuel rich (point "*C*" in Figure 6, $\varphi_{rich} = 1.6$), a different reaction becomes important. Reaction R3

$$NH_3 + H \rightarrow NH_2 + H_2 \qquad \text{(R3)}$$

is a **source** of NH_2 at point *B*, but is an NH_2 **sink** at point *C*. The rich stage PSR NH_2 concentration at point *C* is more than 5 times the NH_2 concentration at point *B*, causing R3 to proceed in the reverse direction and **make** NH_3 rather than **destroy** NH_3. The NH_3 concentration in the rich stage PSR at point *C* is 39 times greater than at point *B*. With NH_3 destruction dramatically slowed in the rich stage, a relatively large amount of NH_3 survives until the quench stage, where a significant fraction is converted into NO_x. Overall, the reaction path analysis of the RQL2 SLICER model yields similar insights and conclusions as the RPA of the RQL1 kinetic model.

Measured CO emissions are shown in Figures 7, 8, and 9 for the same air splits shown in Figures 4, 5, and 6, respectively. CO emissions were between 5 and 30 ppmv (dry, 15% O_2) under all conditions, indicating the quench stage design provided adequate mixing, and the short lean stage provided sufficient residence time to complete combustion. Overall, CO emissions were lowest when the air split was closest to the design value (the 40/60 air split) and tended to increase as the air split was adjusted away from the design value (the 30/70 and 20/80 air splits).

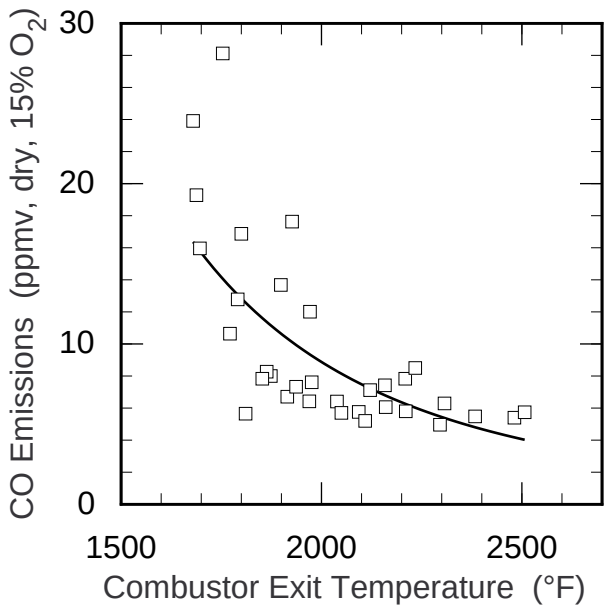

Figure 7: RQL2 CO emissions at a 20/80 rich/lean air split. The solid line shown in Figures 7 through 9 is a best-fit through the measurements, not a model prediction.

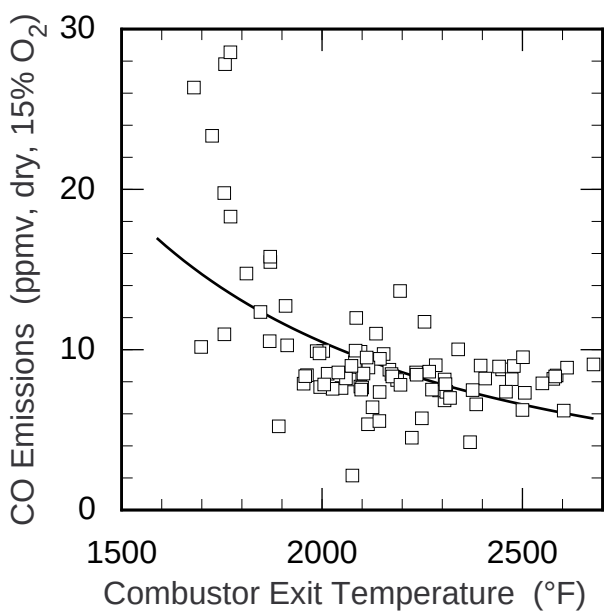

Figure 8: RQL2 CO emissions at a 30/70 rich/lean air split.

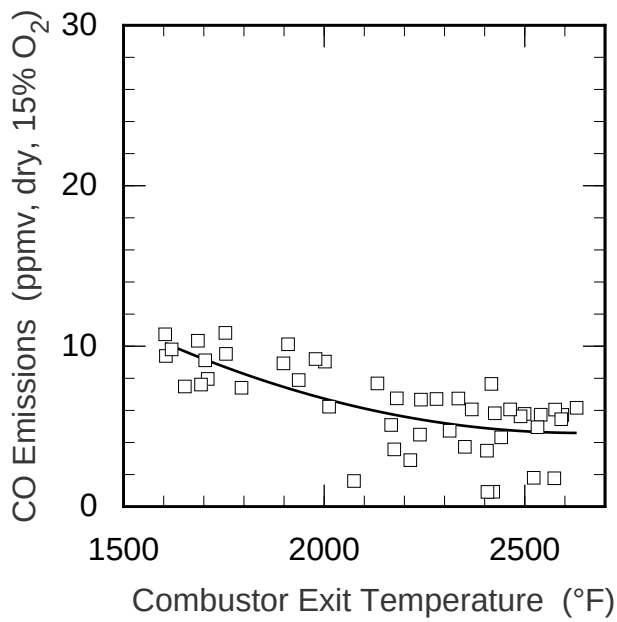

Figure 9: RQL2 CO emissions at a 40/60 rich/lean air split.

Applications

The RQL2 combustor has demonstrated the potential for low NO_x emissions from IGCC power plants equipped with HGCU. Combustor modifications (such as RQL2) are almost always a less expensive method of NO_x reduction than flue gas treatment. The concepts generated in the design and development of RQL2, as well as the improved understanding of rich-lean combustion, may be applied in future low Btu fueled gas turbines. RQL2 concepts may also be incorporated into low NO_x combustors for natural gas and liquid fuel turbines.

Future Activities

The SLICER model and reaction path analysis described above serve several useful purposes. First, RPA identifies the elementary chemical reactions which are most important in the conversion of NH_3 to NO_x in a rich-quench-lean combustor. Research aimed at improving chemical kinetic models of RQL combustion should focus on these key chemical reactions. Second, the RPA indicates that HCN does not play a significant role in the NH_3 destruction chemistry, as has been proposed in the literature. This further suggests that the fuel methane concentration should have little impact on the overall conversion of NH_3 to NO_x. Finally, the excellent agreement between the SLICER model and the Test 9 measurements over a wide range of combustor exit temperatures and air splits suggests that the model can be used to perform "what-if" calculations. Because the model has been validated against experimental data, variations in the fuel composition (including NH_3 content), fuel temperature, and rich stage residence time can all be considered computationally. This type of numerical study may be the part of future work.

Acknowledgements

This research was sponsored by the U.S. Department of Energy's Morgantown Energy Technology Center, under contract DE-AC21-87MC23170, with GE Environmental Systems, 200 North Seventh Street, Lebanon, PA 17046; telephone 717-274-7000, telefax 717-274-7103. The support of METC project managers Abbie Weigand-Layne and Edward L. Parsons, Jr. is gratefully acknowledged.

References

Battista, R. A., A. S. Feitelberg, and M. A. Lacey, "Design and Performance of Low Heating Value Fuel Gas Turbine Combustors," 41st ASME Gas Turbine and Aeroengine Congress, Exposition, and Users Symposium, June 10-13, 1996, Birmingham, UK (in press).

Bowen, J. H., A. S. Feitelberg, S. L. Hung, M. A. Lacey, and K. S. Manning, "Performance of Low Btu Fuel Gas Turbine Combustors," in *Proceedings of the Advanced Coal-Fired Power Systems '95 Review Meeting*, DOE/METC-95/1018, pp. 250-262 (1995).

Glarborg, P., Kee, R. J., Grcar, J. F., and Miller, J. A.: PSR: A FORTRAN Program for Modeling Well-Stirred Reactors, Sandia National Laboratories Report SAND86-8209 (1986).

Goebel, S. G. and A. S. Feitelberg, "Experimental and Theoretical Study of Low Emissions Rich-Quench-Lean Combustion," a poster paper presented at the 24th Symposium (International) on Combustion, July 5 – 10, Sydney, Australia (1992).

Jackson, M. R., A. M. Ritter, N. Abuaf, M. A. Lacey, A. S. Feitelberg, and P. Lang, "Joining of Wrought Ni-Base Combustor Alloys," ASME paper no. 96-GT-219 (1996).

Kee, R. J., Rupley, F. M. and Miller, J. A.: Chemkin-II: A Fortran Chemical Kinetics Package for the Analysis of Gas-Phase Chemical Kinetics, Sandia National Laboratories Report SAND89-8009 (1989).

Lefebvre, A. H.: *Gas Turbine Combustion*, Hemisphere, New York (1983).

Lutz, A. E., Kee, R. J. and Miller, J. A.: SENKIN: A Fortran Program for Predicting Homogeneous Gas Phase Chemical Kinetics With Sensitivity Analysis, Sandia National Laboratories Report SAND87-8248 (1988).

Michaud, M. G., Westmoreland, P. R., and Feitelberg, A. S.: *Twenty-Fourth Symposium (International) on Combustion*, The Combustion Institute, Pittsburgh, pp. 879-887 (1992).

Assessment of PFBC and Gasification Repowering

Donald L. Bonk (dbonk@metc.doe.gov; (304) 285-4889)
Mark D. Freier (mfreie@metc.doe.gov; (304) 285-4759)
U.S. Department of Energy
Morgantown Energy Technology Center
3610 Collins Ferry Road
Morgantown, WV 26507-0880

Thomas L. Buchanan (gc!ghmail02!a1074@gilcom.attmail.com; 610-855-2677)
Michael R. DeLallo (gc!ghmail02!a1569@gilcom.attmail.com; 610-855-2675)
Harvey N. Goldstein (gc!ghmail01!a2912@gilcom.attmail.com; 610-855-3281)
Jay S. White (gc!ghmail02!a9446@gilcom.attmail.com; 610-855-2693)
Parsons Power Group Inc.
2675 Morgantown Road
Reading, PA 19607

Introduction

One of the first implications of full competition in the utility industry is the reluctance to risk capital intensive investments in new plant construction. As the Department of Energy's Clean Coal Technology program readies a suite of technologies for commercial application, and as deregulation unfolds, the electric utility industry begins to look at the potential for repowering existing sites. This approach to power plant investment involves applications of repowering technologies, upratings, and refurbishing older stations. The decision to repower is influenced by factors that include market demand, power station characteristics, and technology choices. This paper describes the results of a comparative technical and economic evaluation of several clean coal technologies in a repowering application.

Objectives

The objectives of the study were to compare thermal and economic performance of a suite of clean coal technologies in a repowering application under a consistent set of guidelines.

Approach

The approach taken in this comparative evaluation of Advanced Technologies in a repowering application was to define a reference pulverized coal (PC) fired power station, and then apply each candidate technology in succession. Each case was modeled in a modified version of the ASPEN/SP flow sheet simulation program, along with a suitable combustion turbine, where applicable, and the host plant steam cycle. Pittsburgh No. 8 coal is used for most of the cases evaluated, except for one case involving a natural gas fired combustion turbine, another case where the technology variable is the use of a Process Derived Fuel (ENCOAL Corp. PDF) in place of coal, and a third case where coal is the primary fuel, but some natural gas is used for topping combustion.

The reference station configuration was based on an evaluation of a UDI data base containing the complete domestic U. S. generating fleet. In a series of queries of the data base, a set of bar graphs were generated showing the numbers of units in various discrete size categories, ages, and steam conditions. This exercise revealed that a large number of units existed that were between 100 and 200 MWe in size, were commissioned in the 1950's, and had main steam pressures between 1450 and 2400 psig. Main and reheat steam temperatures of 1000F were by far the most prevalent value.

Based on these findings, a Reference PC host plant was defined, consisting of a site containing twin 150 MWe, net, PC units, with steam conditions of 1800 psig/1000F/1000F. The units each utilize a steam turbine with a triple flow LP turbine section, with 23 inch dia. last stage buckets exhausting to a single pressure condenser at 1.0 in. Hga.

In this study, the original steam turbines are refurbished and reused, along with much of the steam cycle equipment. This is an important consideration, as it constrains the configuration of the power conversion cycle, whereas in a greenfield plant the designer can select optimal steam cycle design parameters and equipment. However, certain advantages accrue from this approach, such as the ability to retain the original once through cooling system, which provides low condensing pressure and auxiliary power requirements. Refurbishment of the original turbine includes replacement of selected steam path components, improving adiabatic efficiency by about 1-1/2% relative to the original machine, when new.

As each advanced technology was evaluated, a combustion turbine was selected for the topping cycle portion of the power conversion system. Based on a time frame for application in the years 2000 to 2010, the Westinghouse 501G machine was selected for use where feasible. This large, efficient combustion turbine provides sufficient exhaust heat for the bottoming cycle to match effectively with most of the cases evaluated, while only requiring a single machine to be installed. In the cases involving the first and 1-1/2 generation Circulating Pressurized Fluid Bed Combustors, the W501D5 machine was used, as it provided a more suitable match for the overall system. The bubbling bed Pressurized Fluid Bed case relies on the ASEA GT-140 machine.

Description of Technologies

1. Reference Pulverized Coal Plant. See Reference Plant Definition, above.

2. Atmospheric Fluid Bed Combustor. This is based on a Foster Wheeler design available for commercial service at this time. Existing coal handling equipment and other infrastructure are refurbished and reused. Plant performance is relatively unchanged except for emissions, which are significantly reduced. Solid waste production is increased.

3. Refueling with Process Derived Fuel (Encoal Corp.). This case represents a refueling rather than a repowering. The original boilers are refurbished along with the steam turbines and other site equipment, and are fired with 100% Encoal Corp. PDF, which is a dried and mildly pyrolised Powder River Basin coal. The fuel is specified to contain low sulfur as delivered, (0.3% sulfur, by weight). For the purposes of this study, the original boiler

capacity is maintained, with some enhancement of soot blowing capacity, and other modifications to compensate for the somewhat different combustion characteristics of the process derived fuel. This refueling results in a slight reduction in net output to 293 MWe, and a slight reduction in net heat rate to 8890 Btu/kWh.

4. Pressurized Fluid Bed Combustor (Bubbling Bed). This technology is represented by the ABB P-800 commercial module, incorporating an ASEA Stahl GT-140 gas turbine. In the current repowering study, the combustor is located inside a pressure vessel that is 57 feet in diameter and 160 feet high, operating at a nominal pressure of 245 psig. The new equipment, comprising the PFBC package and the gas turbine and its associated equipment, is arranged adjacent to the original powerhouse. Net plant output is increased to 348 MWe, while net plant heat rate is reduced to 8729 Btu/kWh.

5. Pressurized Fluid Bed Combustor (Circulating Bed, First Generation), based on Foster Wheeler technology. This concept utilizes a circulating pressurized bed for complete combustion of the coal. Hot air/gas leaving the bed is cleaned in a series of cyclone and ceramic candle filters, and is then ducted to a gas turbine for expansion. Most of the gas turbine compressor discharge air is used in the circulating bed; the hot gases returning to the turbine for expansion are limited in temperature to 1600F. A machine based on the W501D5 is used in this arrangement, with a single drum HRSG in the exhaust to supplement the steam production in the circulating bed heat exchanger. Plant net output is increased to 314 MWe, while net heat rate is reduced to 8506 Btu/kWh.

6. Pressurized Fluid Bed Combustor (Circulating Bed, One and One-Half Generation). This version of CPFBC technology is similar to the first generation scheme mentioned above. However, in this case, natural gas is fired in the combustion turbine to reach the original design turbine inlet temperature of the machine. An external, motor-driven boost compressor is used to compensate for the unrecovered pressure drop in the CPFBC circuit external to the gas turbine. The W501D5 is again selected, exhausting through economizer coils for condensate and feedwater heating. Steam is produced in the CPFBC heat exchanger to drive both of the existing steam turbines. Plant net output is increased to 368 MWe, while net heat rate is reduced to 8087 Btu/kWh.

7. Pressurized Fluid Bed Combustor (Circulating Bed, Second Generation). In this CPFBC case, a pyrolizer is added to the process upstream of the circulating bed combustor. Low Btu fuel gas produced by the pyrolizer is conveyed to the gas turbine where it is mixed with the returning vitiated air from the CPFBC and combusted to produce the design basis firing temperature of the turbine. This configuration is based on the use of a modified W501G machine, with an external, motor-driven boost compressor as in the previous case. Steam is produced in a HRSG and in the CPFBC heat exchanger to drive both of the steam turbines in the existing station. Net output is increased to 433 MWe, while net heat rate is reduced to 7043 Btu/kWh.

8. Integrated Gasification Combined Cycle (IGCC) (Air Blown KRW Gasifier). This case utilizes the air blown, fluidized bed, KRW type gasification process, including hot gas cleanup and a transport type gas polisher (desulfurizer) to supplement the sulfur removal that occurs in the gasifier bed. The clean hot low Btu gas that is produced is fired in a

modified W501G gas turbine, which is coupled to a HRSG for steam production. Both existing steam turbines are repowered in this example, providing a net station power increase to 407 MWe, and a reduction in net heat rate to 7355 Btu/kWh.

9. Integrated Gasification Combined Cycle (Oxygen Blown Entrained Bed Gasifier). In this example, a two-stage, entrained flow gasifier is supplied with 95% pure oxygen from a dedicated air separation plant located on-site. A single gasifier module produces medium Btu fuel gas which is desulfurized in a GE moving bed cleanup system, and is then fired in a modified W501G machine. The turbine exhausts through a HRSG to produce steam to drive one of the two existing steam turbines. A Monsanto type (H_2S burning, catalytic conversion) sulfur recovery process produces commercial grade sulfuric acid for sale as a byproduct. The net station output is increased to 353 MWe, while net heat rate is reduced to 7379 Btu/kWh, (including the air separation plant and other auxiliary loads).

10. Integrated Gasification Combined Cycle (British Gas/Lurgi Oxygen Blown Gasifier). This fixed bed gasifier is supplied with 95% pure oxygen from an on-site air separation unit. The gasifier produces a cold medium Btu gas, which is desulfurized in a Purisol cleanup train. Tail gas from the Purisol unit is converted to commercial grade sulfuric acid for sale, in a Monsanto type H_2S burning and catalytic conversion unit. The fuel gas is fired in a modified W501G machine, which exhausts through a HRSG to produce steam to drive one of the existing steam turbines. A portion of the compressor discharge air is supplied to the high pressure air separation plant, eliminating the need for a separate air compressor. This repowering example produces a net power increase to 313 MWe, and a heat rate reduction to 7669 Btu/kWh.

11. Integrated Gasification Combined Cycle (Air Blown Transport Reactor). This IGCC concept is based on the air blown transport reactor. The hot low Btu gas is desulfurized in the reactor, followed by a polishing step in a transport desulfurizer, chloride removal in a chloride guard bed, and filtration in a ceramic candle filter array. The fuel gas is fired in a modified W501G machine and exhausted through a HRSG to produce steam for one of the existing steam turbines. The transport gasifier concept evaluated in this study is based on concepts being evaluated at the DOE Power Systems Development Facility in Wilsonville, AL. This concept may not be commercially available at the beginning of the reference time frame, but can be expected to be ready for service at the end of this time period. The transport reactor in this repowering application results in an increase in net output to 368 MWe, and a reduction in heat rate to 6854 Btu/kWh.

12. Combustion Turbine/Combined Cycle. A natural gas fired, state-of-the-art combustion turbine is used in conjunction with a HRSG to repower one of the two existing steam turbines in this case. The W501G machine is coupled to a multi-pressure HRSG to provide a net station output that is 312 MWe, with a net heat rate of 7080 Btu/kWh. Two gas turbines repowering both existing steam turbines were not used, since the resulting net power would be more than double the original output, and in excess of study guidelines. The second of the two original steam turbines is placed in reserve status.

Results

The completed study provides thermal performance for each repowering application, as well as a conceptual cost estimate and economic projections. The study results should be interpreted with caution, since changes in site conditions, financial ground rules and inputs, or other factors could impact the relative performance of the technologies. Based on the inputs adopted for this study, stated in the report, the following comparisons are presented:

The first two graphs illustrate net electric output and heat rate for the various repowering configurations. In several instances, only one of the two existing steam turbines is reused. For these cases (CT/HRSG, Transport Gasifier, Destec, and BG/L Gasifiers), utilization of the second steam turbine would have required additional combustion turbine capacity, and would have yielded about twice the net power output. This large increment of power was considered to be beyond the site transmission capacity, and therefore was not attempted.

TOTAL NET PLANT GENERATION

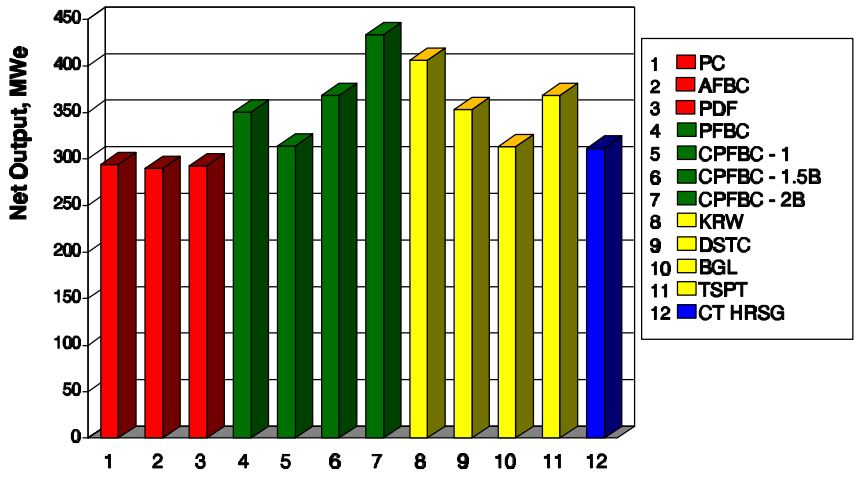

HEAT RATE COMPARISON

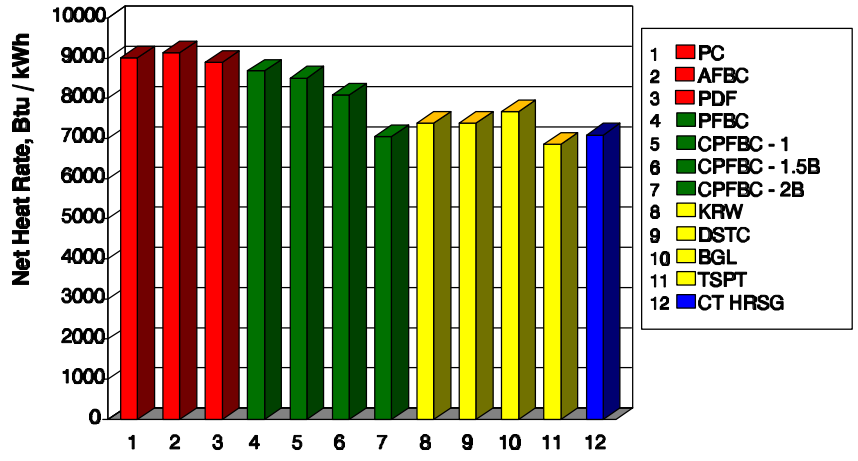

The second set of graphs presents plant capital costs on a Total Plant Cost (TPC) basis, both in absolute and in per kWe terms. As a group, the advanced technologies range from about $700 to $1000 per kWe, in this repowering application.

TOTAL PLANT COST

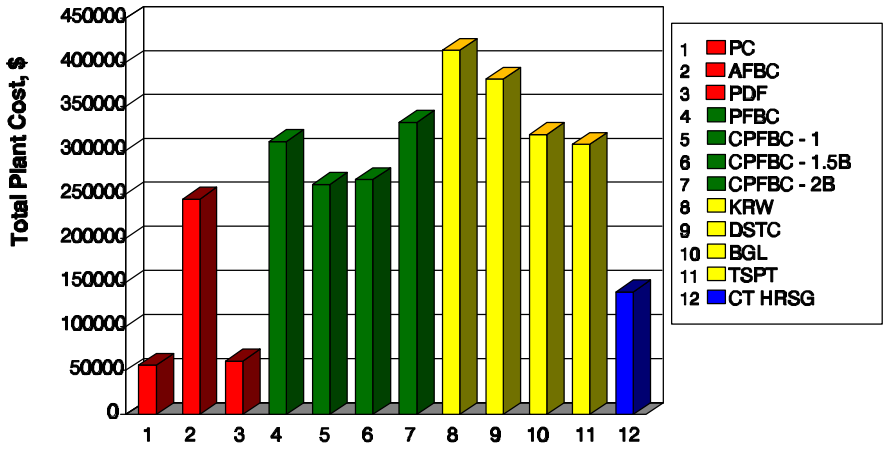

TOTAL PLANT COST/kW

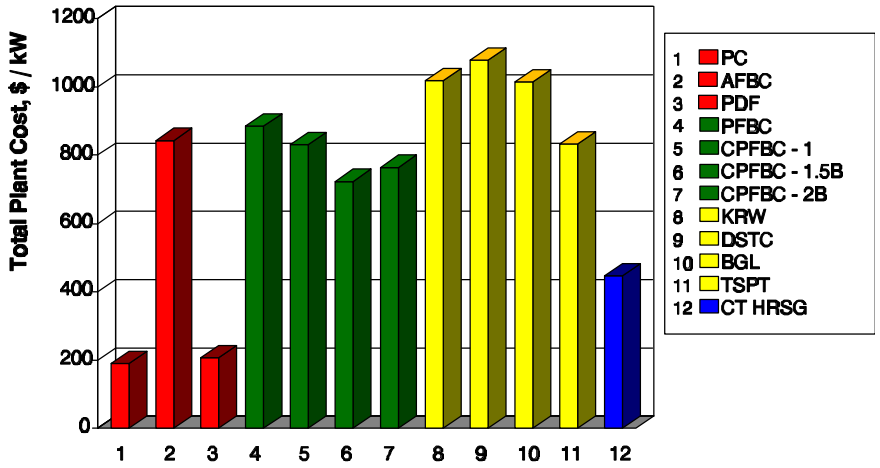

The next charts compare variable and fixed costs for the technologies evaluated. The first chart compares variable costs, which are comprised of the following components: fuel, sorbent, consumables, emissions credits or charges, byproduct credits or charges, and the variable portion of operation & maintenance. The second chart shows the effects of capacity factor on levelized carrying charges for a range of values (45, 65, and 85%).

VARIABLE PRODUCTION COSTS

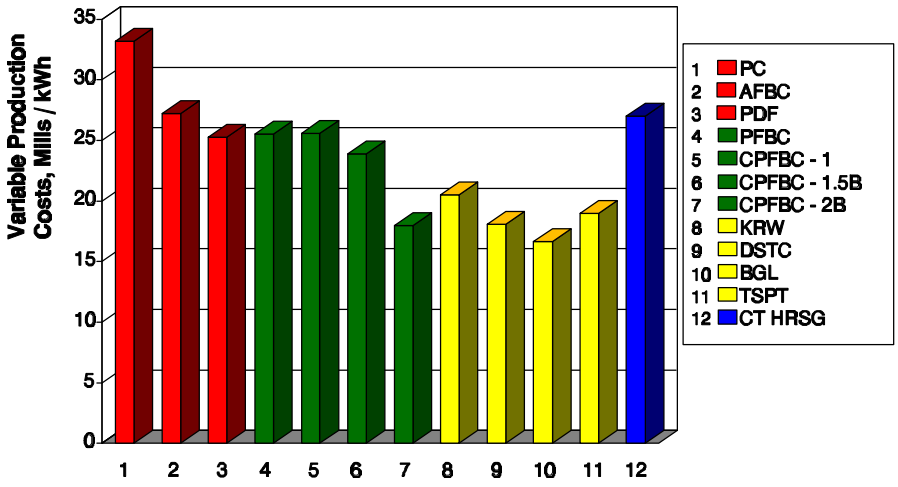

LEVELIZED CARRYING CHARGES

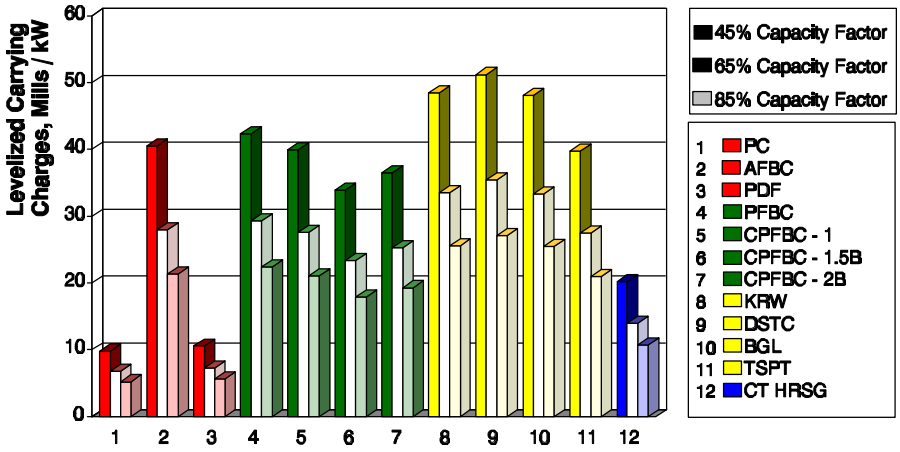

In general, cases involving relatively large capital investment should (and do) result in plants that offer better operating efficiencies and costs. Cases that only require minimal capital investment may offer little or no change in variable operating costs. The combination of levelized capital carrying charges and variable production costs provides insight into the ultimate economic benefits of the repowerings. The most valid appraisal of each case may be obtained by evaluating it in a specific production costing simulation representing an actual application. The relative ranking of the repowering alternatives may vary from one actual application to another, depending on how all of the cost, financial, and economic parameters resolve into final data.

Contract Information

Investigation sponsored by the U. S. Department of Energy's Morgantown Energy Technology Center, under Contract DE-AC21-94MC31166 with Gilbert/Commonwealth, Inc., dba Parsons Power Group Inc., 2675 Morgantown Road, Reading, PA 19606.

Acknowledgement Information

Work reported on herein was carried out as Task 1 of the above noted contract. Period of performance was from October 1994 to July, 1996. The METC COTR is Donald Bonk.

OPTIMIZING ADVANCED POWER SYSTEM DESIGNS UNDER UNCERTAINTY

E.S. Rubin and U.M. Diwekar
Carnegie Mellon University
Pittsburgh, PA 15213

H.C. Frey
North Carolina State University
Raleigh, NC

ABSTRACT

This paper describes recent developments in ongoing research to develop and demonstrate advanced computer -based methods for dealing with uncertainties that are critical to the design of advanced coal-based power systems. Recent developments include new deterministic and stochastic methods for simulation, optimization, and synthesis of advanced process designs. Results are presented illustrating the use of these new modeling tools for the design and analysis of several advanced systems of current interest to the U.S. Department of Energy, including the technologies of integrated gasification combined cycle (IGCC), advanced pressurized fluid combustion (PFBC), and the externally fired combined cycle (EFCC) process. The new methods developed in this research can be applied generally to any chemical or energy conversion process to reduce the technological risks associated with uncertainties in process performance and cost.

INTRODUCTION

Increasing environmental awareness and regulations have placed new requirements on process design for advanced power systems, and increased the need for more sophisticated simulation and design tools to examine pollution prevention options. Conventional process models now in use are largely based on a deterministic framework for simulation of a specified flowsheet. An important shortcoming of these models is their inability to analyze uncertainties rigorously. Uncertainty analysis capability is especially important in the context of advanced energy systems, since available performance data typically are scant, accurate predictive models do not exist, and many technical as well as economic parameters are not well established.

In essence, the current project is focused on developing better ways to minimize technological risk by seeking process designs that minimize the likelihood of performance shortfalls, high emissions and high costs. A related goal is to help focus research and development in areas that offer the greatest potential payoffs in terms of process efficiency, emissions and cost. Our thesis is that advanced design and analysis methods are needed in light of the increasing complexity of advanced processes, involving multiple options for component design and selection; strong interactions among system components (which often can be overlooked by traditional design methods); and significant performance and cost uncertainties, particularly for processes at an early stage of development.

The approach adopted in this research has been one that employs a systems analysis framework that combines engineering models of process performance with companion models of process costs, and which utilizes advanced software capabilities for design and analysis. In this project, we have specifically focused on advanced technologies of interest to the U.S. Depart-

ment of Energy's Morgantown Energy Technology Center (DOE/METC). Thus, the technologies modeled and evaluated in this research include various types of integrated coal gasification combined cycle (IGCC) system, including both air-blown and oxygen blown gasifiers; fixed-bed and fluidized bed gasifiers; hot gas and cold gas clean up systems; and a variety of by-product recovery options, including sulfur and sulfuric acid recovery by conventional (e.g., Claus plant) and advanced (e.g., direct sulfur reduction process) methods. Other advanced systems analyzed include advanced pressurized fluidized bed combustion (PFBC) systems and externally fired combined cycle (EFCC) systems.

In all of these areas, we have utilized existing DOE/METC computer models of process thermal performance, and have enhanced these models in a number of areas, including the characterization of emissions, and the coupling of process performance and economics via models of capital cost, operating costs, and overall cost of electricity. Details of these models are summarized in a series of topical reports dealing with specific technologies (CMU, 1990; 1995).

In this project, we also have developed a set of new analytical modeling capabilities built around the public version of the Aspen process simulator used by DOE/METC for advanced process modeling. These new capabilities include both deterministic and stochastic methods for process simulation, process optimization, and process synthesis. The stochastic methods, which explicitly incorporate uncertainties into the design and analysis stage, represent an especially important capability which has not heretofore been available. The remainder of this paper briefly describes these new modeling tools and their applications to advanced coal-based technologies.

SIMULATION CAPABILITIES

Conventional process modeling involves deterministic simulation in which parameter values are input to a process model, yielding results for the quantities of interest (e.g., thermal efficiency, emissions, cost). In many cases, the process models used for deterministic simulations may be quite detailed, as is the case with several of the Aspen models developed by DOE for advanced energy conversion processes. Nonetheless, a characteristic of deterministic models is that each of the input parameters specified for given model run has only a single value, and similarly all of the results are single-valued.

However, many model parameters may in fact have significant uncertainty or variability that can lead to significant uncertainties in the results, particularly for processes at an early stage of development. In stochastic simulation, these uncertainties are incorporated explicitly. Input parameters are described as uncertainty distributions which are sampled by the stochastic modeling software and developed for the Aspen simulator (Diwekar and Rubin, 1991). The results can then be displayed as a cumulative distribution function showing the likelihood of different outcomes for a given simulation. Information on input uncertainties may come from a variety of sources, including data analysis and expert judgments. Previous papers and reports have elaborated on this methodology, and displayed results from case studies of IGCC systems which often showed significant probability of performance shortfalls and cost overruns relative to nominal or deterministic analyses (Frey and Rubin, 1992a).

In our more recent work, we have extended stochastic simulations to include two new process flowsheets, the EFCC system and the second generation PFBC system. Figure 1 illustrates one result from an analysis of the EFCC plant efficiency. Though this technology is expected to achieve net thermal efficiencies significantly higher than those of conventional pulverized coal power plants, the magnitude of efficiency revealed by the probabilistic analysis is generally

lower than the result from conventional deterministic simulation. In this case, the performance shortfall is attributed primarily to uncertainties in the process combustor and ceramic heat exchanger, which were characterized by experts at DOE/METC. Figure 1 indicates over a 95 percent probability of a performance shortfall.

In Figure 2, results are presented for the total capital cost of a second generation PFBC system. This technology appears to have a lower cost than most of the IGCC systems previously analyzed. However, a stochastic simulation indicates a very high probability that the total capital cost will exceed the deterministic estimate developed for DOE in a detailed 1989 study. In this case, the potential for higher cost is attributed primarily to uncertainties in various indirect cost factors, particularly the process and project contingency costs.

In previous papers (Frey and Rubin, 1992a; 1992b; Frey et al., 1994), we have shown how stochastic simulation methods can help identify and reduce technological risks such as costs overruns and performance shortfalls by identifying the factors that contribute most to overall uncertainty, and targeting R&D in these critical areas. Quantitative measures of the value of additional research can be developed in conjunction with these methods.

OPTIMIZATION CAPABILITIES

In the current research project we have extended the set of modeling capabilities to include both deterministic and stochastic optimization of process flowsheets. Deterministic optimization is well established in the technical literature, and some commercial simulators have such capabilities. The problem typically is formulated in terms of an objective function to be achieved (e.g., cost minimization) subject to specified constraints. The optimizations software begins with a set of initial values for process parameters and iterates until the objective function is achieved. Details of this problem formulation are presented elsewhere (Diwekar et al., 1993).

We have added a deterministic optimization capability to the public version of the Aspen simulator, and also have combined this feature with the stochastic sampling capability described earlier, yielding new capabilities for stochastic optimization and stochastic programming. In stochastic optimization, depicted in Figure 3, the objective function can be specified probabilistically, as can the constraints. An objective function might be specified in terms of minimizing an expected value, or use chance constraints to minimize a given technological risk (e.g., no more than a 5 percent chance of a performance shortfall). By inverting the sampling and optimization loops, various stochastic programming problems also can be addressed. Such problem formulations reveal the effects of uncertainty on optimal designs. The mathematical formulation of stochastic optimization and programming problems is described in Diwekar et al., 1993.

These new capabilities allow a broad range of questions to be addressed. For example:

- Is there a better choice of parameter values for this process to improve its performance? To lower its cost?
- What levels of performance and cost can we expect from an optimized design?
- How do uncertainties in process performance and cost variables affect the optimal design?
- What design choices will minimize the risk of a performance shortfall? Or the risk of a cost overrun?

Applications

We illustrate the new optimization capabilities with a case study of the environmental control system design for an advanced IGCC system employing hot gas cleanup (HGCU). Systems with HGCU promise higher thermal efficiency than conventional systems with cold gas cleanup. However, one potential drawback is that NO_x emissions can be high because ammonia in the fuel gas is not removed by the HGCU unit, and thus can be converted to NO_x in the combustor. For current process design, this may result in NO_x emissions that are two to four times higher than the Federal New Source Performance Standard for coal-fired power plants. NO_x control methods employing advanced stage combustion are currently under development in an attempt to address this problem. In this case study, we examine the use of selective catalytic reduction (SCR) systems to reduce NO_x emissions. A detailed model of an SCR process has been developed (CMU, 1995) and incorporated into the Aspen flowsheet for a 650 MW IGCC system employing an air-blown moving bed gasifier. The plant uses an Illinois No. 6 coal and operates at an annual capacity factor of 80 percent. Uncertainties have been assigned to 20 key parameters identified in screening studies as having the greatest impact on process performance, emissions and costs. Table 1 summarizes these input assumptions.

Figures 4 to 6 show the results of different stochastic optimization and stochastic programming problems applied to the IGCC flowsheet. Figure 4 first shows results of a stochastic optimization problem in which the expected cost of electricity (COE) is minimized for different levels of NO_x control. As the expected (mean) value of NO_x emissions is decreased, the expected value of NO_x removal efficiency in the SCR unit increases proportionally. The expected cost of the optimal design also increases, as seen in Figure 4. A key finding is that the optimal design reduces the expected COE by about 0.3 mills/kWh relative to the base case design achieving 0.44 lbs NO_x /10^6 Btu. For the 650 MW plant modeled in this example, this is equivalent to a total savings of approximately $2 million per year. This savings is a measure of the benefit resulting from use of the new stochastic method to optimize the design parameters of the zinc ferrite and SCR units.

Figure 5 shows another example in which NO_x emissions are minimized subject to a cost constraint. For a cost constraint of 60 mills/kWh, emissions between 0.15 and 0.3 lbs/10^6 Btu can be achieved. However, for a tighter constraint of 54 mills/kWh, only 80% of the optimal designs are within the cost constraint, and some will exceed 0.6 lbs/10^6 Btu of NO_x, the Federal New Source Performance Standard for coal-fired power plants. For these cases, there is a significant risk that the process may not be viable under the economic constraints imposed in this example, since the plant might not comply with applicable emission limits.

To illustrate results for a stochastic programming formulation, Figure 6 shows the effect of uncertainties on the cost of an optimal design. Here, for each sample the cost is minimized and NO_x emissions are constrained to 0.6 lbs/10^6 Btu or less, and SO_2 emissions 0.06 lbs/10^6 Btu or less (the DOE design goal of one tenth the current U.S. federal standard). The cost of electricity for the optimal design configuration is seen to vary by more than a factor of four due to the performance and cost uncertainties in the variables shown in Table 1. An 80% confidence interval gives expected costs between 45 and 60 mills/kWh.

These results are intended only to be illustrative of the new modeling capabilities now possible with stochastic optimization and stochastic programming. Additional case studies for other advanced power systems, including other IGCC designs, pressurized fluid bed combustion (PFBC) systems, and externally fired combined cycle (EFCC) systems will be the subject of other reports.

SYNTHESIS CAPABILITY

In process simulation and optimization, the flowsheet being analyzed already has been specified by a knowledgeable process designer. In process synthesis, we employ computer-aided design tools to ask what the flowsheet should look like in the first place in order to achieve process goals and reduce technological risks.

We have previously described the formulation of a deterministic process synthesis problem involving mixed integer non-linear programming (MINLP) (Diwekar et al., 1991). This capability now has been implemented around the public version of the Aspen simulator, yielding a new capability that does not currently exist in most commercial simulators.

Figure 7 shows this capability schematically. The synthesis loop begins with a superstructure of all possible alternatives for combining unit operations into a process flowsheet. The mixed integer linear programming (MILP) master program selects a given flowsheet topology, which is then passed to the non-linear programming (NLP) optimization loop described earlier. The optimizer then selects values of continuous variables to meet specified objective functions and constraints. The overall process is then repeated in the synthesis loop until a flowsheet topology and design parameter that best meets desired objectives are found.

An initial case study to demonstrate this capability involved choosing a desulfurization system to minimize the total cost of an IGCC system employing an air-blown KRW gasifier with hot gas cleanup, subject to an SO_2 emission constraint of less than 0.015 lbs/million Btu. In this case, there were three possible flowsheet options: in-bed sulfur removal only; gastream cleanup only; and combined in-bed plus gas stream cleanup. Each option yielded a different waste or byproduct stream which also was considered in the design.

Details of this case study are reported in Diwekar et al., 1992. The MINLP selected the combination of in-bed plus gas stream desulfurization as the optimal configuration, and optimized the design parameters of the zinc ferrite desulfurization system to achieve minimum cost. The total cost of the optimized configuration was approximately 20 percent less than the next best alternative, illustrating the power of this new analytical method.

Recently, we have extended the process synthesis capability to include more complex design alternatives, such as the synthesis problem depicted in Figure 8. Because the MINLP approach is not well suited to some types of synthesis problems, we have applied the method of simulated annealing to handle complex problems more efficiently. We also have developed a new variant of simulating annealing, called stochastic annealing, which offers far greater computational speed, and is well suited to handling problems of process synthesis under uncertainty. For example, for the twelve design choices represented in Figure 8 by the choice of coals and air or oxygen-blown gasification, the stochastic synthesis problem was solved in nearly one fifth the time required to solve the twelve problems individually. These new methods thus appear to offer substantial benefits in addressing complex design problems that have heretofore not been amenable to computer-aided approaches.

CONCLUSIONS

The key message stemming from the work described in this paper is that we now have a power new set of computer-based design tools that can be generally applied to any chemical or energy conversion process. These tools include both deterministic and stochastic capabilities for process simulation, process optimization, and process synthesis. Applications of these new tools can help minimize technological risks and maximize research productivity by considering

uncertainties in the early stage of design and analysis.

Future work will continue to focus on methodological improvements to enhance the speed and versatility of the new analytical techniques described in this paper. At the same time, new case studies will be undertaken to enhance process flowsheets and demonstrate the power and applicability of advanced analysis methods to real engineering and process design problems of interest to DOE and its contractors. Key areas for application of these models will include process design, risk analysis, cost estimation, R&D management, technology evaluation, environmental compliance, marketing studies, and strategic planning.

ACKNOWLEDGEMENTS
The authors happily acknowledge the important contributions to this project made by graduate students Prosenjit Chaudhuri and Donna Riley at Carnegie Mellon University, and Pankaj Agarwal at North Carolina State University. This work was supported under Contract No. DE-AC21-92MC29094

REFERENCES

Diwekar U. M. and E. S. Rubin, 1991, Stochastic Modeling of Chemical Processes, *Comput. Chem. Engng*., **15**, 105.

Diwekar U. M., I. E. Grossmann, and E. S. Rubin, 1991, An MINLP process synthesizer for a sequential modular simulator, *I&EC Res*., **31**, 313.

Diwekar U. M., H. C. Frey, and E. S. Rubin, 1992, Synthesizing optimal flowsheets: applications to IGCC system environmental control, *I&EC Res*., **31**, 1927.

Diwekar U. M., E. S. Rubin and H.C. Frey, Optimization of Advanced Energy Systems Under Uncertainty, *Proceedings of METC Contractors Meeting* , U.S. Department of Energy, Morgantown, WV.

CMU 1990, "Stochastic Modeling of Coal Gasification Combined Cycle Systems: Cost Models for Selected Integrated Gasification Combined Cycle (IGCC) Systems," Task 2 Topical Report, Morgantown Energy Technology Center, Morgantown, WV.

CMU, 1995, Development and Application of Optimal Design Capability for Coal Gasification Systems, Task 1 Topical Report, Volumes 1-4: Vol. 1: "Development and Application of Performance and Cost Models for Gas Turbine Based Selective Catalytic Reduction NOx Control." Vol. 2: Development and Application of Performance and Cost Models for The Externally Fired Combined Cycle." Vol. 3: "Performance and Cost Models for the Direct Sulfur Recovery Process," Vol. 4: "Performance and Cost Models for a Second Generation Pressurized Fluidized Bed Combustion System," Morgantown Energy Technology Center, Morgantown, WV.

Frey H. C. and E. S. Rubin, 1992a, Evaluation of Advanced Coal Gasification Combined-Cycle Systems under Uncertainty, *I&EC Res*., **31**, 1299.

Frey H. C. and E. S. Rubin, 1992b, Integration of Coal Utilization and Environmental Control in Integrated Gasification Combined Cycle System, *Env. Sci. Tech*., **26**, 1982.

Frey H. C., E. S. Rubin, and U. M. Diwekar, 1994, Process Modeling of Advanced Technologies Under Uncertainty, *Energy*, **19** (4), 449.

Table 1. Uncertain Model Parameters for Illustrative Case Studies

DESCRIPTION AND UNITS (a)	Val (b)	Type	Min	Max	Prob.
Gasifier Fines Carryover,	5.0	F	0.0	1.0	5%
wt-% of Coal Feed			1.0	3.5	20%
			3.5	5.0	25%
			5.0	8.0	25%
			8.0	15.0	15%
			15.0	20.0	5%
			20.0	30.0	5%
Fines Capture in Recycle Cyclone,	95	F	50	90	25%
wt-% of Fines Carryover			90	95	25%
			95	97	25%
			97	98	25%
Carbon Retention in the Bottom Ash, wt-%	2.5	T	0.75	10.0	2.5
Gasifier Coal Throughout, lb DAF coal/(h-ft2)	305	T	1.52	381	305
Gasifier NH3 Yield, % of coal-N converted	0.9	T	0.5	1.0	0.9
Gasifier Air/Coal Ratio, lb air/lb DAF coal	3.1	T	2.7	3.4	3.1
Steam/Coal Ratio, lb steam/lb DAF coal					
air/coal = 2.7	0.81	U	0.54	1.08	
air/coal = 3.1	1.55	U	1.24	1.86	
air/coal = 3.4	2.38	U	2.04	2.72	
Zinc Ferrite Sorbent Sulfur Loading, wt-% sulfur in sorbent	17.0	N	2.16	31.84	17.0
Zinc Ferrite Sorbent Attrition Rate, wt-% sorbent loss per absorption cycle	1.0	F	0.17	0.34	5%
			0.34	0.50	20%
			0.50	1.10	25%
			1.10	1.50	25%
			1.50	5.00	20%
			5.00	25.00	5%
Fuel NOx, % conversion of NH3 to NOx	90	T	50	100	90
Gasifier Direct Cost Uncertainty, % of estimated direct capital cost	20	U	10	30	
Sulfuric Acid Direct Cost Uncertainty, % of estimated direct capital cost	10	U	0	20	
Gas Turbine Direct Cost Uncertainty, % of estimated direct capital cost	25	U	0	50	
SCR Unit Catalyst Cost, $/ft3	840	U	250	840	
Standard Error of HRSG Direct Cost Model, $Million	0	N	-17.3	17.3	
Maintenance Cost Factor, Gasification, % of process area total cost	3	T	2	12	3
Maintenance Cost Factor, Combined Cycle, % of process area total cost	2	T	1.5	6	2
Unit Cost of IC Ferrite Sorbent, $/lb	3.00	T	0.75	5.00	3.00
Indirect Construction Cost Factor, %	20	T	15	25	20
Project Contingency Factor, %	17.5	U	10	25	

(a) DAF = dry, ash free; SCR = selective catalytic reduction; HRSG = heat recovery steam generator (b) DET. VAL. = deterministic (point-estimate) value. The next column indicates the type of distribution, where F = fractile, T = triangular, N = normal, and U = uniform. The remaining columns provide the parameters of the distribution.

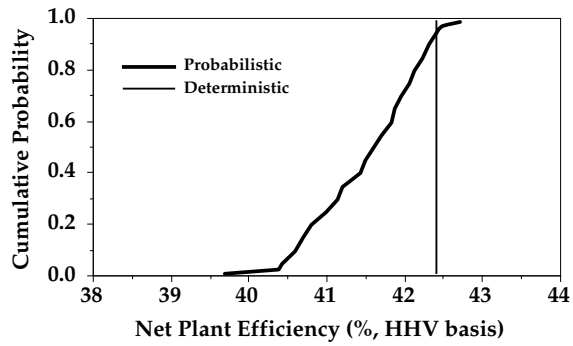

Figure 1. EFCC Plant Efficiency

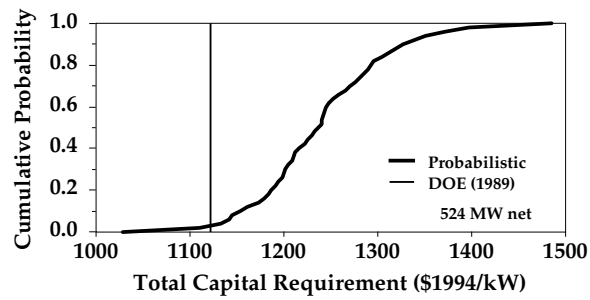

Figure 2. Second Generation PFBC System Total Capital Cost

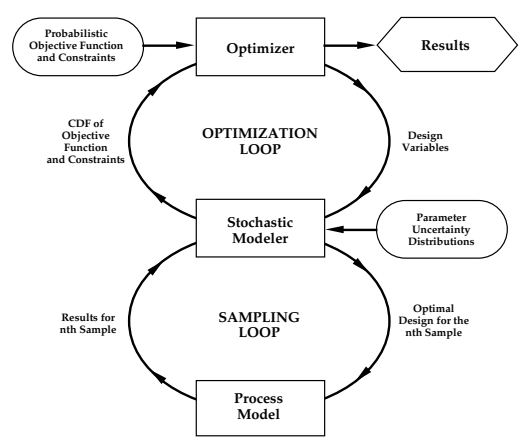

Figure 3. Schematic of the Stochastic Optimization Framework

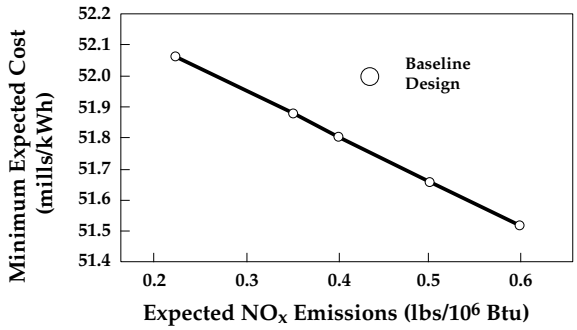

Figure 4. Minimize Total Cost Subject to NO_x Emission Constraint

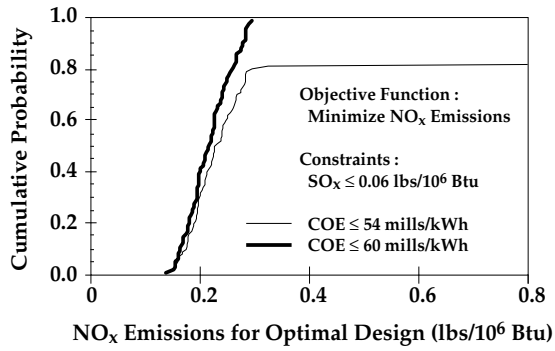

Figure 5. Minimize NO_x Subject to a Cost Constraint

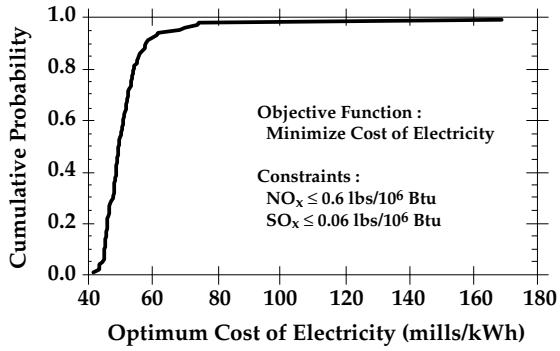

Figure 6. Effect Of Uncertainties on Cost of Optimal Design

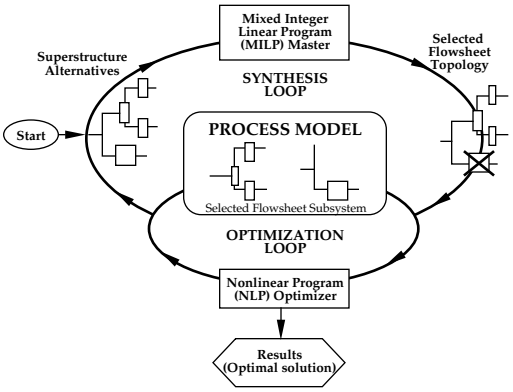

Figure 7. Schematic of the MINLP Synthesizer Framework

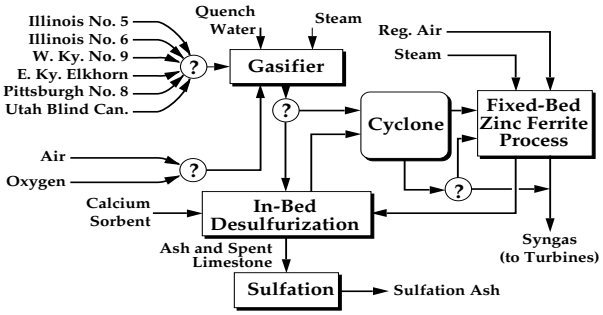

Figure 8. Synthesis of IGCC System

Westinghouse Advanced Particle Filter System

Thomas E. Lippert (412-256-2440)
Gerald J. Bruck (412-256-2102)
Zal N. Sanjana (412-256-2231)
Richard A. Newby (412-256-2210)
Dennis M. Bachovchin (412-256-2250)

Westinghouse Electric Corporation
Science and Technology Center
1310 Beulah Road
Pittsburgh, PA 15235

Abstract

Integrated Gasification Combined Cycles (IGCC) and Pressurized Fluidized Bed Combustion (PFBC) are being developed and demonstrated for commercial, power generation application. Hot gas particulate filters are key components for the successful implementation of IGCC and PFBC in power generation gas turbine cycles. The objective of this work is to develop and qualify through analysis and testing a practical hot gas ceramic barrier filter system that meets the performance and operational requirements of PFBC and IGCC systems.

This paper reports on the development and status of testing of the Westinghouse Advanced Hot Gas Particle Filter (W-APF) including:

- W-APF integrated operation with the American Electric Power, 70 MW_t PFBC clean coal facility. Approximately 6000 test hours completed.
- Approximately 2500 hours of testing at the Hans Ahlstrom 10 MW PCFB facility located in Karhula, Finland.
- Over 700 hours of operation at the Foster Wheeler 2 MW 2nd generation PFBC facility located in Livingston, New Jersey.
- Status of Westinghouse HGF supply for the DOE Southern Company Services Power System Development Facility (PSDF) located in Wilsonville, Alabama.
- The status of the Westinghouse development and testing of HGF's for Biomass Power Generation.
- The status of the design and supply of the HGF unit for the 95 MW Pinon Pine IGCC Clean Coal Demonstration.

Research sponsored by the U.S. Department of Energy's Morgantown Energy Technology Center, under contract DE-AC21-94MC31147 with Westinghouse Electric Corporation, Science & Technology Center, 1310 Beulah Road, Pittsburgh, PA 15235-5098; telefax: 412-256-2121.

Results reported include operating history, operating characteristics and filter performance. Schedules and objectives for future testing are summarized.

Introduction

High temperature particulate filters are a key component in advanced, coal based gas turbine cycles (IGCC, Integrated Gasification Combined Cycle and PFBC, Pressurized Fluidized Bed Combustion) that are currently under development by DOE/METC for clean coal demonstration. In these applications the hot gas particulate filter protects the downstream heat exchanger and gas turbine components from particle fouling and erosion effects and cleans the gas to meet particulate emission requirements. Both PFBC and IGCC plants benefit because of lower cost downstream components, improved energy efficiency, lower maintenance and the elimination of additional and expensive flue gas treatment systems.

IGCC Systems

In IGCC systems, the hot gas particulate filter must operate in reducing gas conditions (i.e., presence of H_2, CH_4, CO), high system pressure (150 psi to 350 psi) and at operating temperatures usually determined by the method of sulfur removal, i.e., in bed, external or by cold gas scrubbing, Figure 1. Typically, these temperatures range around 1650°F (in bed), 900 to 1200°F (external) and 1000°F to 500°F (cold scrubbing).

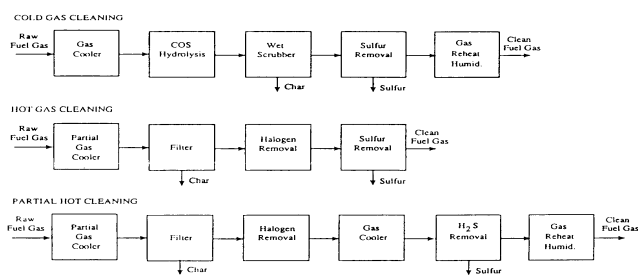

Figure 1. IGCC - Fuel Gas Cleaning Options

In gasification applications, cold scrubbing of the fuel gas has been demonstrated as effective in cleaning the fuel gas to meet turbine and environmental requirements. However, with this process, plant energy efficiency is reduced, and higher capital costs are incurred. Incorporating a hot particulate filter upstream of the scrubbing unit reduces heat exchanger costs and provides for dry ash handling (partial hot gas cleaning).

Hot fuel gas cleaning concepts (in bed and external) have also been proposed that utilize reactive solid sorbents to remove gas phase sulfur and hot gas filters to collect the ash and sorbent particles. This approach in IGCC provides for highest energy efficiency and lowest cost of electricity.

IGCC systems may utilize air or oxygen blown entrained or fluid bed gasifiers. Specific operating conditions of the hot gas particulate filter will vary depending on these choices. In general, hot gas filter pilot plant test experience suggests that gasifier ash/char is noncohesive with relatively high flow resistance. Thus, the potential for fines re-entrainment and high filter pressure drop are reduced by selecting a relatively low design filter operating face velocity (<5 ft/min). Since the filter treats only the fuel gas component of the total gas flow, the choice of a low filter face velocity does not adversely impact economics. Typically, for a 100 MW_e IGCC system, the filter is required to treat only 6000 to 12,000 acfm, depending if the gasifier is oxygen or air blown. Inlet dust loadings may also vary widely, ranging from <1000 ppmw to 10,000 ppmw.

PFBC Systems

Bubbling bed PFBC technology is currently being demonstrated at commercial scale. Two PFBC units are located in Sweden (Stockholm Energi, Vartan Plant), another one at the Endesa's Escatron Plant in Spain and one in the United States at the American Electric Power's (AEP Tidd Plant located in Brilliant, Ohio. The Tidd PFBC is a 70 MW_e demonstration plant awarded through the Round 1 of U.S. DOE Clean Coal Technology Demonstration Program. Currently, all four plants utilize high efficiency cyclones to remove greater than 95% of the ash and a ruggedized gas turbine to tolerate ash carried over from the upstream cyclones. Economic and performance improvements in these first generation type PFBC plants can be realized with the application of hot gas particulate filters. Both the secondary cyclone(s) and stack gas ESP(s) could be eliminated saving costs and providing lower system pressure losses. The cleaner gas (basically ash free) provided with the hot gas filter, also permits a wider selection of gas turbines with potentially higher performance.

For these bubbling bed PFBC applications, the hot gas filter must operate at temperatures of 1580°F and system pressures of 175 psia (conditions typical of the Tidd PFBC plant). Inlet dust loadings to the filter are estimated to be about 500 to 1000 ppm with mass mean particle diameters ranging from 1.5 to 3 μm. For commercial applications typical of the 70 MW_e Tidd PFBC demonstration unit, the filter must treat up to 56,600 acfm of gas flow. Scaleup to about 310 MW_e would require filtering over 160,000 acfm gas flow. For these commercial scale systems, multiple filter vessels are required. Thus, the filter design should be modular for scaling.

An alternative to the bubbling bed PFBC is the circulating bed concept. In this process the hot gas filter will in general be exposed to higher operating temperatures (1650°F) and higher (factor of 10 or

more) particle loading. Although the inlet particle loading is high, it contains a significantly coarser fraction (mass mean generally >15 μm) which helps mitigate the effect of the higher mass loading. For a 75 MW_e commercial scale circulating bed PFBC plant, gas flow to the filter is approximately 70,000 acfm. At this scale, multiple vessels with modular filter subassemblies are required.

Second generation or topping PFBC is being developed and planned for demonstration and commercialization. In this plant, higher (than first generation PFBC) turbine inlet temperatures are achieved by partially devolatilizing the coal in a carbonizer unit producing a fuel gas. The char produced is transferred and burned in a circulating PFBC unit with high excess air. The hot (1600°F) vitiated air produced is used to combust the hot fuel gas to raise the combustion gas temperature to as high as 2350°F (Robertson, et al., 1989). With second generation PFBC, two hot gas filters are required. One filter is used to collect the ash and char material carried over from the carbonizer unit with the hot fuel gas. The second filter is used to remove ash and sorbent particles carried over with the hot vitiated air leaving the circulating pressurized fluidized bed combustor (CPFBC). Both filter units are required to operate at high temperatures (1200 to 1600°F) and high particle loading. The fuel gas filter will operate in reducing gas while the CPFBC filter operates in oxidizing conditions. A 95 MW_e second generation PFBC demonstration plant requires a hot fuel gas flow to its filter of about 8000 acfm and hot vitiated air flow to its filter of approximately 64,000 acfm.

Objectives

The objective of this work is to develop and qualify through analysis and testing a practical hot gas ceramic barrier filter system that meets the performance and operational requirements of Advanced, Solid Fuel Power Generation Cycles, Table 1.

Table 1 Hot Gas Filter Application Requirements

- Effective Filter
  - Meet NSPS
  - Protect Downstream Equipment
- Operate Reliably
  - Cleanable
  - Stable Pressure Drop Characteristics
- Robust
  - Oxidizing/Reducing Environments
  - Alkali/Acid Gas
  - Thermal Cycling

The hot gas filter must remove sufficient particulate to protect the gas turbine from erosion damage, corrosion and particle deposition and meet power plant environmental standards (NSPS). Turbine tolerance estimates and current NSPS requirements are shown in Figure 2. Also shown are ceramic barrier filter outlet particle loading data from subpilot and pilot plant test facilities. This data shows the high performance potential of the hot gas ceramic filter device relative to power generation application.

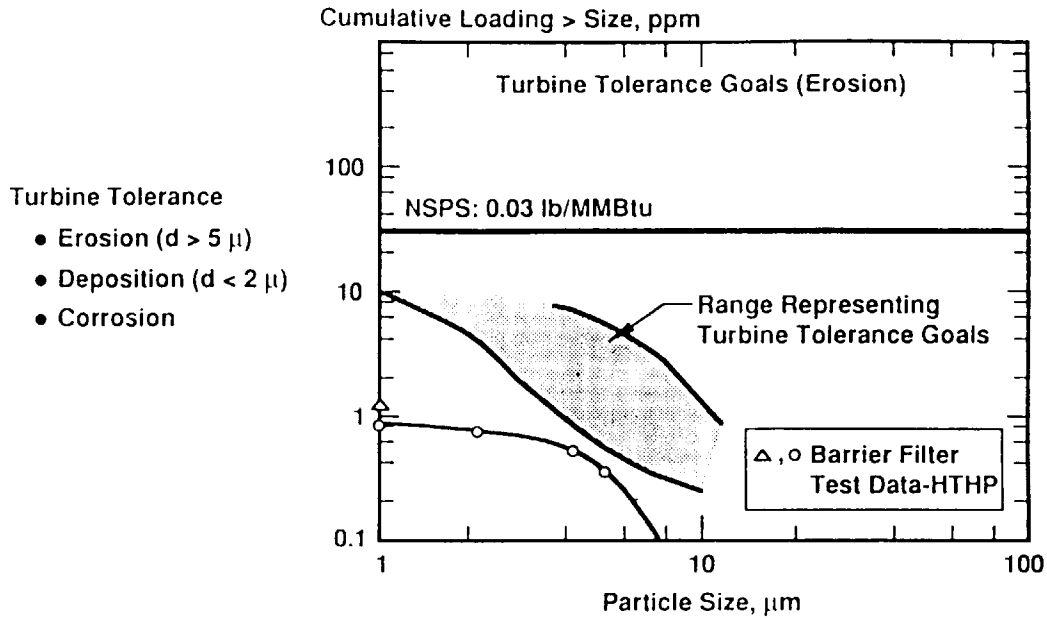

Figure 2. Turbine Tolerance and Particulate Emission Requirements in Coal Fueled Gas Turbine Applications

Candle, crossflow and tube filters are examples of ceramic barrier filter devices being developed for high temperature particle filtration. These filter devices are basically absolute filters on ash materials, can be operated at high throughput and can be cleaned by simple pulse jet methods.

Project Description

Background

The Westinghouse hot gas filter system is being supported through key sub-pilot, pilot and demonstration programs, Table 2. This testing has included approximately 3150 hours of operation in reducing gas environments (gasification) and 9460 hours in combustion (oxidizing) conditions. In addition to this field experience, over 25,000 hours of test experience has been compiled in the Westinghouse HGF, high temperature, high pressure simulators.

Hot Gas Filter System

The Westinghouse hot gas filter design, schematically shown in Figure 3, consists of stacked arrays of filter elements supported from a common tubesheet structure. In this design, the arrays are formed by attaching individual candle elements (Item 1) to a common plenum section (Item 2). All the dirty gas filtered through the candles comprising this single array is collected in the common plenum section and discharged through a pipe to the clean side of the tubesheet structure. Each array of filterelements is cleaned from a single pulse nozzle source. The individual plenum assemblies (or

Table 2. Westinghouse IGCC and PFBC Hot Gas Cleaning Testing Experience

Application	Facility	Pressure (psi)	Temperature Range (°F)	Flow (ACFM)	Dust Load (ppmw)	Test Hours
Gasification (IGCC)	Fluid bed (KRW)	131-231	1050	50-300	1,000 - 25,000	1300
	Texaco Gasifier	350	1000-1400	50-110	300-25,000	700
	Biomass (NREL) IGT/WHBGP	195-260	1000-1650	125	1,000-2,500	500-IGT (*Continuing)*
	SCS Wilsonville (MWK)	200-350	1200-1900	1000-1700	4,000-40,000	Startup 1996
	SPPC, Pinon Pine IGCC	260	1000	13,391	18,000	Startup 1996
Combustion (PFBC)	AEP Tidd, PFBC	135	1200-1550	7,500	600-10,000	5,800
	Ahlstrom Karhula, PCFB	160	1550-1650	3,070	4,000-18,000	2,056 (*Continuing)*
Advanced PFBC	FWDC/Livingston • Carbonizer • Combustor	150-200	1100-1500	100-400	5,000-35,000	 400 (700)* 900 (700)*
	SCS/PSDF (FW-7MW$_t$)	200-350	1200-1650	2,000	11,000	Startup 1996/97

**Integrated Operation,1995*

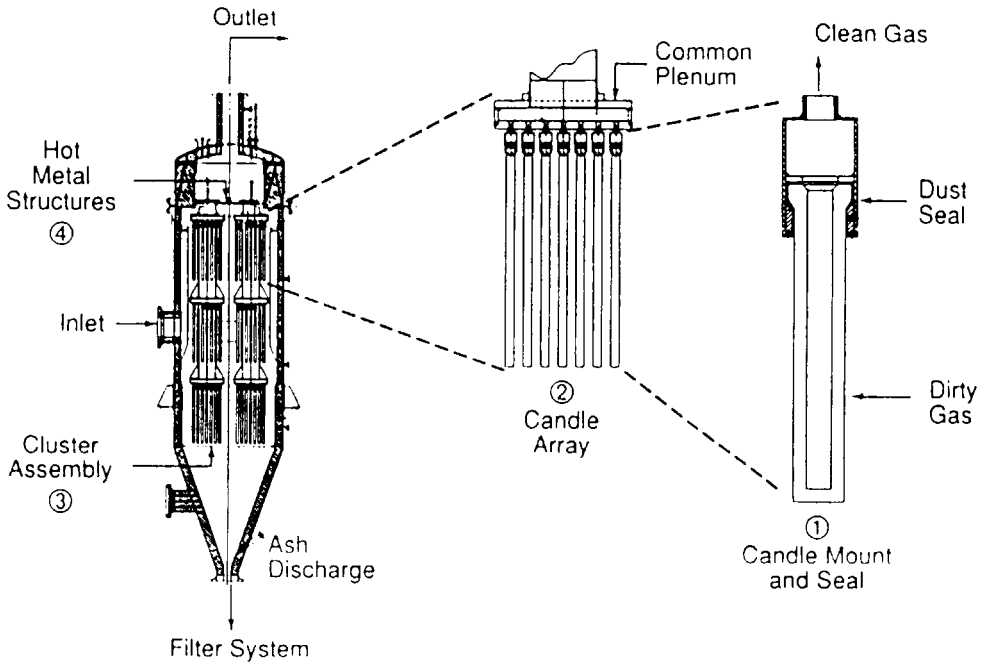

Figure 3. Hot Gas Cleaning Systems - Westinghouse Candle Filter System

arrays) are stacked vertically from a common support structure (pipe), forming a filter cluster (Item 3). The individual clusters are supported from a common, high alloy tubesheet structure and expansion assembly (Item 4) that spans the pressure vessel and divides the vessel into its “clean” and “dirty” gas sides. Each cluster attaches to the tubesheet structure by a specially designed split ring assembly. The cluster is free to grow down at temperatures. The plenum discharge pipes ducting the filtered gas to the clean gas side of the tubesheet structure are contained within the cluster support pipe and terminate at the tubesheet. Each discharge pipe contains an eductor section. Separate pulse nozzles are positioned over each eductor section. The eductors assist pulse cleaning. During cleaning, the pulse gas is contained within and ducted down the discharge pipe and pressurizes the respective plenum section.

The plenum assembly and cluster (stacked plenums) form the basic modules needed for constructing large filter systems indicative of PFBC requirements. The scaleup approach is:

- Increasing plenum diameter (more filter elements per array)
- Increasing the number of plenums per cluster
- Increasing the vessel diameter to hold more clusters

In general, vessel diameter will be limited by the tubesheet structure and desire to shop fabricate the vessel. Larger PFBC plants would utilize multiple vessels.

Filter Element Technology

Ceramic barrier filter devices, such as candles and cross flow filters, are under development for hot gas filter application. These devices have been shown to be basically absolute filters on ash material, can be operated at relatively high gas throughput with acceptable pressure drop and cleanable by simple reverse pulse jet methods. Clay bonded silicon carbide (SiC) candle filters are commercially available. The structure of these elements is mainly a coarse-grained SiC bonded by a clay-based binder. Each element is provided with a fine grained SiC or aluminosilicate fiber outer skin that serves as the filtration surface. Alternate, oxide-based ceramic materials are also being developed for ceramic barrier filter application. Both first generation, full-scale cross flow and candle filter elements have been constructed using a homogeneous structure that is an alumina/mullite (A/M) matrix containing a small percentage of amorphous (glass) phase. Laboratory and field evaluation of these and other materials are being conducted to identify, characterize and compare their respective chemical and thermal stability for IGCC and PFBC applications. The status of this work is presented in a companion paper entitled “Filter Component Assessment.”

This paper updates the assessment of the Westinghouse hot gas filter design based on ongoing testing and analysis.

Approach

The development and qualification of the Westinghouse hot gas filter is being supported through key sub-pilot, pilot and demonstration projects. Test sites include government furnished and industrial facilities.

Results

Entrained Gasification

In this program, a sub-pilot scale hot gas filter was integrated with a 15 tpd Texaco entrained gasifier. The facility is located in Montebello California. The filter test program was conducted from April 1989 through August 1992 and reported (Lippert et al., 1993). Filter testing was in support of a base program that was focused on evaluating hot desulfurization technologies. In this testing, the filter was used to protect the external sulfur sorbent beds from ash plugging. This work showed that in the entrained gasification application, stable pressure drop operation can be achieved but the ceramic barrier filter system must be sized and designed for relatively low face velocity (<4 ft/min) and high operating pressure drop (>3 or 4 psi).

Biomass IGCC/HGF Testing

A 14 candle-element HGF unit was integrated and operated with the Institute of Gas Technology's (IGT) RENUGAS biomass gasification process. The RENUGAS process is a pressurized fluidized bed, air or oxygen blown gasifier. The development and operation of the IGT's 10 ton per day process development unit (PDU) is described by Wiant, et al., 1993 and Lau, et al., 1993. The testing program at IGT utilized bagasse and alfalfa feed and was conducted in support of the DOE Biomass Power Program, and specifically the Biomass Gasification Facility Demonstration in Paia, Hawaii.

The IGT/PDU included a tar cracker that was first operated and characterized. It was concluded from this work that the majority of the oil and tar from the RENUGAS process would not crack within the pores of the filter elements if the filter temperature is maintained below 1500°F (815°C), but above the condensation temperature of the highest boiling-point components (approximately 950°F (510°C)).

The hot gas filter testing was conducted in two, one week test campaigns resulting in about 50 operational hours at conditions. The testing was sufficient to establish initial performance evaluations and to identify potential longer term issues. A summary of the testing conditions is given in Table 3. Test Series 1 was conducted with the full 14-element complement of candle elements. In this test series, the upstream cyclone was disabled to increase particle size and solid loading to the filter unit. Particle analysis showed a 10.8 micron mass mean. This short duration test showed no operational issues, with stable baseline pressure drop. Visual inspection, following testing confirmed filter integrity and high performance level (high collection efficiency). The filter elements were observed to have a hard reddish pottery-like crusty coating. This coating was apparently a permanent porous coat of iron-rich material deposited during the highest temperature portion of the first test segment. The source of the reddish coating was determined to be dirt in the feedstock.

Table 3. Biomass/IGT Hot Gas Filter Testing Summary

	Test 1	Test 2
Feed Stock	Bagasse	Bagasse
Filter Pressure	1.8 Mpa (260 psig)	1.3 to 1.7 Mpa (195 to 245 psig)
Filter Gas Temperature	860 to 900°C (1580 to 1650°F)	540 to 665°C (1000 to 1230°F)
No. of Candle Elements	14	10
Face Velocity	1.4 cm/s (2.8 ft/min)	0.6 to 2.1 cm/s (1.2 to 4.2 ft/min)
Dust Loading	2900 ppm	980 to 2500 ppm
Operating Hours	21	30
Outlet Dust Loading	Not Detectable	Not Detectable
Alkali	--	0.7 to 1.0 ppm

Test series 2 was conducted utilizing ten candle element and with the upstream cyclone fully operational. Again, particle analysis showed that the mass mean size, 3.8 microns, now entering the filter decreased significantly compared to Test Series 1. Initially, in the Test Series 2 testing, steady filter pressure drop characteristics were observed but in the latter portion of Segment 3, a steady rise in the baseline pressure drop was observed, likely reflecting re-entrainment because of the smaller particle mean size. Post test inspection confirmed the filter integrity and no dust was found on the clean gas side. These test results show that better performance will be achieved with larger particle size, thus eliminating the need for the upstream cyclone.

Sierra Pacific, Pinon Pine IGCC/HGF Project

Westinghouse has designed and supplied the HGF unit for the Department of Energy's Clean Coal Technology Demonstration, Pinon Pine IGCC project. The coal gasification process uses the KRW fluid bed technology owned by The M.W. Kellogg Co. who specified and purchased the filter. The final filter design evolved to satisfy the project requirements of both The M.W. Kellogg Co. and the Sierra Pacific Power Co. The plant is located at the Sierra Pacific Power Company's Tracy station near Reno, Nevada. The plant will gassy approximately 880 tons/day of coal using the KRW air blown gasification process to produce about 95 Mwe. The plant is scheduled to begin commercial operation in late 1996.

Table 4 summarizes the design basis for the HGF unit. The unit is schematically shown in Figure 4. The filter consists of 784 candle elements, arrayed on four clusters. Each cluster contains four plenums each with 187 candle elements. The internals are designed using a high silicon stainless Alloy, RA85H, to resist metal dusting, a catastrophic form of carburization.

The filter unit is designed for Seismic Zone 4. To protect the internals from damage due to lateral displacement in the event of a seismic event, the clusters are contained by a set of radially

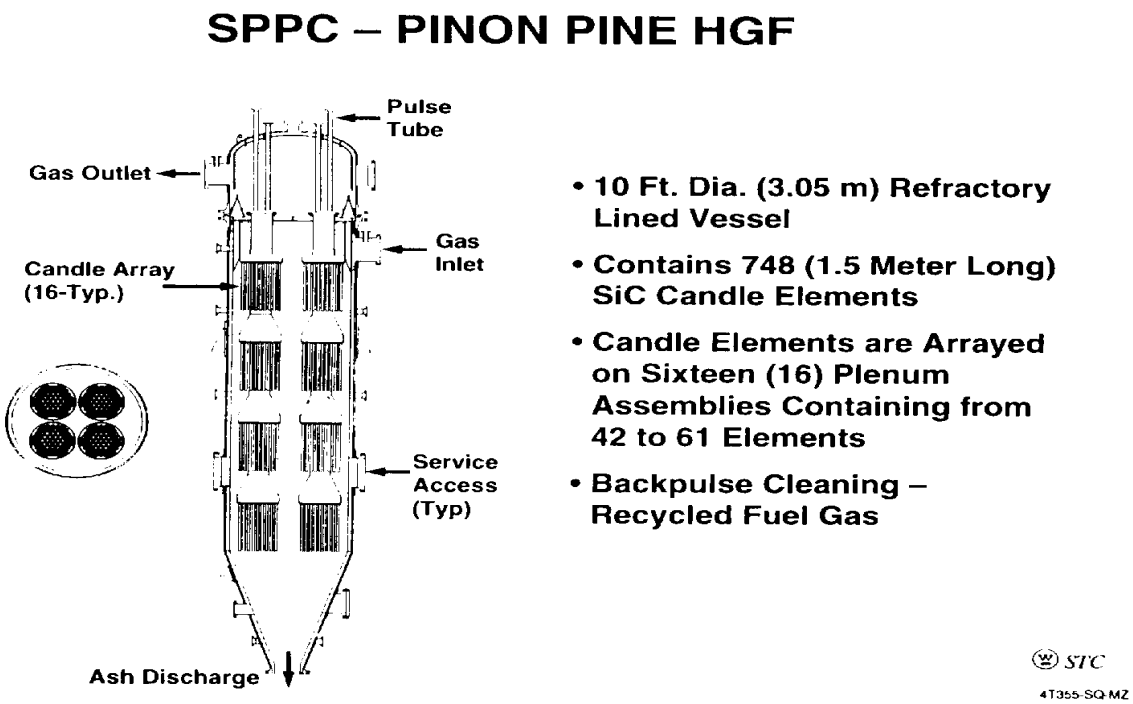

Figure 4. SPPC - Pinon Pine HGF

Table 4. SPPC -Pinon Pine HGF Design Basis

Gas Environment:	Reducing
Gas Flow:	307,800 lb/hr/ 139,600 kg/hr
Pressure:	260 psi/18 Bar
Gas Temperature:	1011°F/554°C
Inlet Dust Loading:	18,400 ppm/22 gm/NM^3
Max. Pressure Drop:	9 psi/0.62 Bar
Operating Face Velocity:	5.8 ft/min/2.9 cm/s
No. of Candle Elements:	748 (1.5m)

oriented shoes that fit against the refractory lining. Relative motion between clusters is further restricted by tabs attached at the tangent points between adjoining plenums.

For commercial operation, the Filter is designed for maintainability. Access into the filter body is provided by four, 36 inch diameter manways. Two diametrically opposite manways are positioned between clusters to access the top level of plenums. Similarly, two diametrically opposite manways are positioned between clusters to access the lower middle level of plenums. Platforms were designed to

bolt to the manway flanges to provide staging for personnel to stand inside the vessel for in-situ service work. Below each manway a set of vertically oriented rails are provided. Ladders treads are strung between the rails to provide access to the lower plenum service area. Personnel climb down the ladder and work off a second platform. The arrangement is illustrated in Figure 5. At any given platform location, all filters for two adjacent plenums are accessible by rotating the associated cluster. Such rotation is accomplished by entering the vessel head above the tubesheet, disengaging the cluster top flange from the tubesheet and with standard manual rigging attached between the vessel head and cluster top flange, lifting and rotating the cluster.

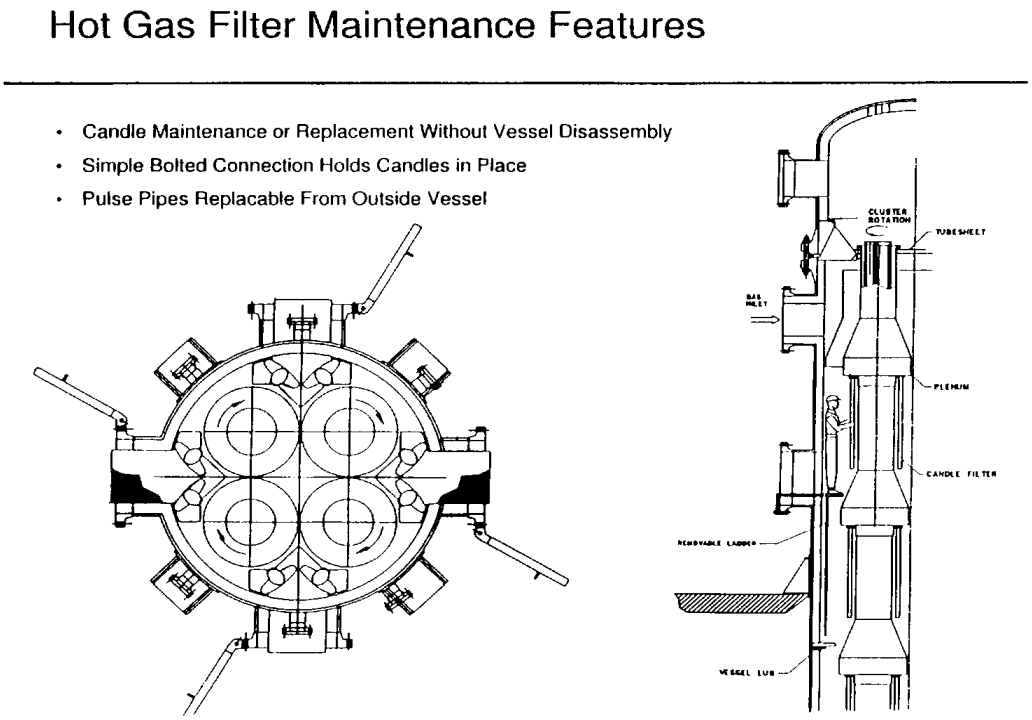

Figure 5. Hot Gas Filter Maintenance Features

The first application of the maintenance hardware was demonstrated at the initial filter installation. Four teams of boilmakers were trained. They worked simultaneously inside the filter vessel and accomplished assembly of all the 748 candle elements, demonstrating the overall approach to maintainability.

Pressurized Fluidized Bed Combustion

Westinghouse is conducting hot gas filter testing at two different PFBC facilities: at the American Electric Power (AEP) 70Mwe Tidd-PFBC demonstration plant located in Brilliant Ohio, and at the Foster Wheeler (formally Ahlstrom) 10 MWt circulating PCFB facility located in Karhula Finland.

Testing at the AEP/Tidd has been completed and reported (Lippert, et.al., 1995). In addition, an initial series of HGF tests were conducted at the Karhula PCFB from November 1992 through June, 1994. A description of this facility and discussion of results of this testing has been reported (Lippert et. al., 1995). In November 1995, a second series of tests were initiated utilizing the same Westinghouse candle cluster that was in place for the earlier test programs. The purpose of the current testing is to evaluate several advanced candle materials at operating temperatures between 1550°F to 1650°F. To date, approximately 500 test hours have been accomplished. Materials evaluations are ongoing and reported in a companion paper, "Filter Component Assessment."

Topping PFBC

Development of the Topping PFBC (second generation PFBC) is taking place at the Foster Wheeler Development Corporation (FWDC) pilot plant facility located at the John Blizard Research Center in Livingston, New Jersey. The program is in three phases. Phase 1, already completed, developed a conceptual design of the commercial scale plant and identified R&D needs (Robertson et al., 1989). The second phase, also completed, involved separate subscale pilot tests of the carbonizer/filter and combustor/filter. Carbonizer/filter testing occurred in 1992. Combustor/filter testing was completed in 1993. In 1994 the facility was converted for integrated operation, Phase III.

During the carbonizer/filter testing in 1992, the carbonizer was operated as a jetting fluidized bed unit. Approximately 150 hours of filter operation was achieved. This testing used cross flow filter elements for about 400 hours. Stable filter operation was demonstrated. The carbonizer char showed relatively high flow permeability compared to earlier entrained gasification experience and was free flowing.

Following carbonizer testing, the facility was modified to operate in the pressurized circulating fluidized bed combustion mode. The filter unit was configured to a 22-element candle array. Approximately 900 operating hours were accumulated in this testing.

The final Phase II PCFB test run following shakedown included a 180 hour continuous test period in which the PCFB and filter operated under char and coal fired conditions. In this test, the filter was configured with 14 candle elements to operate at a face velocity of about 8 ft/min. The PCFB operated smoothly and without major upset. Filter operating pressure drop was stable throughout the test run. Inspection of the filter following completion of the test run showed no indication of dust leaks to the clean side.

Phase III operation was completed in 1995. In this testing, the carbonizer and combustor were integrated. The carbonizer filter is the 22-element candle array previously utilized in the Phase II testing. A second candle filter unit was designed and supplied for the combustor leg. This filter contained 45 candle elements in a two plenum array. Approximately 700 hours of operation was achieved in the Phase III testing.

Development of the topping PFBC will be continued at larger scale at the Southern Company Services, Power Systems Development Facility (PSDF) located in Wilsonville, Alabama. Westinghouse is providing two HGPFs for this facility.

Application

The successful development and demonstration of hot gas particulate filters will enable achieving higher energy efficiencies and lower costs in Advanced Power Generation cycles such as IGCC, PFBC and Advanced PFBC. The technology has application for a wide range of solid fuels, including coal and biomass. In addition, many industrial applications could benefit from HGF technology application.

Future Activities

FWDC/Karhula PCFB

Test operations continue at the FWDC, 10Mwt PCFB facility at Karhula Finland that utilize the Westinghouse HGF candle unit containing up to 128 elements. HGF testing is focused on evaluating alternative candle materials to temperatures above 830°C.

Power Systems Development Facility

Westinghouse has designed and supplied two HGF units (PCD-301 & PCD-352) for installation and operation at the SCS/PSDF. The PCD-301 unit has been installed into the MWK entrained reactor test loop. Operation is expected to begin in the July/August 1996 time frame. Initial operation will be in the combustion mode. The PDC-301 is a two-plenum, single cluster unit containing 92 candle elements. For initial MWK Transport Reactor shakedown operations, the PCD-301 has been fitted with used (from Tidd testing) clay-bonded, SiC elements.

PCD-352 unit has been completely fabricated and delivered to site. This unit will serve as the HGF for the Combustion Leg of the FWDC/APFB test loop. Installation is ongoing, with operation expected early in 1997. The PCD-352 is a 3-Cluster, 2-Plenum unit that can hold up to 273 candle elements. Clusters from the PCD-301 are interchangeable with clusters from the PCD-352 unit. Candles for the PCD-352 have not been selected.

Sierra, Pinon Pine 95 Mwe IGCC

Plant start-up is expected late 1996. The Westinghouse HGF unit is installed and ready for operation.

Acknowledgments

We wish to acknowledge the DOE/METC CTO's involved in the various programs related to the hot gas particulate filter development for their technical guidance and support during the conduct of these programs; Mr. Richard Dennis, Mr. James Longanbach, Mr. Donald Bank and Mr. Theodore McMachon. Also, the following organizations are recognized: Foster Wheeler Development Company; American Electric Power; Southern Company Services; Electric Power Research Institute; M. W. Kellogg Company.

References

Lau, F. S., et al, 1993, "Development of the IGT RENUGAS® Process." In Proceedings of Strategic Benefits of Biomass and Waste Fuels Conference, Washington, DC: Electric Power Research Institute.

Lippert, T. E., et al, 1995, "Westinghouse Advanced Particle Filter System," Proceedings of the Advanced Coal-Fired Power Systems '95 Review Meeting, DOE/METC-95/1018.

Lippert, T.E., M.A. Alvin, E. E. Smeltzer, D. M. Bachovchin, and J. H. Meyer, 1993, "Subpilot Scale Gasifier Evaluation of Ceramic Cross Flow Filter -Final Report," DOE/METC Contract no. DE-AC21-88MC24021, August.

Robertson, A., et al., 1989, "Second-Generation Pressurized Fluidized Bed Combustion Plant: Research and Development Needs," Foster Wheeler Development Corporation, Livingston, NJ. Phase 1, Task 2 Report FWC/FWDC-TR-89/06 to the U.S. DOE under contract DE-AC21-86MC21023.

Wiant, B. C., et al, 1993, "Biomass Gasification Hot Gas Cleanup for Power Generation," In Proceedings of First Biomass Conference of the Americas, Burlington, VT.

Filter Component Assessment

Mary Anne Alvin (412-256-2066)
Thomas E. Lippert (412-256-2440)
Edward S. Diaz (412-256-1822)
Eugene E. Smeltzer (412-256-2240)

Westinghouse Electric Corporation
Science & Technology Center
1310 Beulah Road
Pittsburgh, PA 15235-5098

Abstract

Advanced particulate filtration systems are currently being developed at Westinghouse for use in both coal-fired Integrated Gasification Combined Cycle (IGCC) and Pressurized Fluidized Bed Combustion (PFBC) systems. To date, Westinghouse has demonstrated 5855 hours of successful operation of first generation monolithic filter elements in PFBC applications when ash bridging or process thermal transient excursions are avoided.

Alternate advanced monolithic and second generation fiber reinforced, filament wound, and vacuum infiltrated filters are also being developed which are considered to have enhanced high temperature creep resistance, improved fracture toughness, or enhanced thermal shock characteristics, respectively. Mechanical and component fabrication improvements, as well as degradation mechanisms for each filter element have been identified by Westinghouse during exposure to simulated PFBC operating conditions and alkali-containing steam/air environments.

Additional effort is currently being focused on determining the stability of the advanced monolithic high temperature creep resistant clay bonded silicon carbide (SiC) materials, alumina/mullite, and chemically vapor infiltrated (CVI) SiC materials during operation in the Westinghouse Advanced Particulate Filtration (W-APF) system at Foster Wheeler's pressurized circulating fluidized-bed combustion (PCFBC) test facility in Karhula, Finland. Select advanced filter materials are being defined for additional long-term exposure in integrated gasification combined cycle (IGCC) gas streams. The results of these efforts are summarized in this paper.[†]

Introduction

Westinghouse in conjunction with DOE/METC has developed and established filter qualification and material surveillance programs related to the operation of hot gas filter systems in pilot plant and demonstration test units. This protocol has been a valuable aid in identifying and resolving filter performance and material stability issues. Recent experience has been focused primarily on the operation of hot gas filtration systems in oxidizing gas environments,

[†] Research sponsored by the U.S. Department of Energy's Morgantown Energy Technology Center, under contract DE-AC21-94MC31147 with the Westinghouse Electric Corporation, Science & Technology Center, 1310 Beulah Road, Pittsburgh, PA. 15235-5098; Telefax: 412-256-2121.

with limited experience in reducing gas environments (Table 1). General findings from previous material surveillance programs have shown that:

- During operation under PFBC conditions, first-generation clay bonded silicon carbide candle filters experienced creep, while the oxide-based alumina/mullite filters exhibited limited resistance to thermal fatigue and/or shock during exposure to severe process thermal transient events.
- During process operation in the oxidizing PFBC environment, both clay bonded silicon carbide and alumina/mullite candles exhibited a loss of strength until a conditioned or stabilized matrix strength was achieved. Similarly, these materials experienced numerous phase and microstructural changes as a function of process operating time.
- A reduction in the strength of an as-manufactured, clay bonded silicon carbide candle filter from 1400-1800 psi to 650-770 psi after 5855 hours of operation in the American Electric Power (AEP) PFBC gas environment occurred without catastrophic damage being suffered by the filter elements.

In addition to characterization of field-tested filter elements, information obtained from coupon samples exposed to process gases at temperature for periods of ~3000 to ~10,000 hours has provided significant insight into the stability and/or changes which resulted in both the first-generation monolithic, and advanced, fiber-reinforced, second-generation filter materials.

In conjunction with field testing, development of the as-manufactured material properties, and identification of the mechanical, thermal, and chemical response of the filter materials during simulated PFBC and high temperature corrosion testing have demonstrated the possible long-term, life-limiting degradation mechanisms of the commercially available monolithic and recently developed second generation filter elements which are likely to occur during field service operation (Tables 2 and 3). For the advanced second generation materials which are the focus of this program, critical issues related to the stability of the 3M CVI-SiC and DuPont SiC-SiC matrices include oxidation along both surfaces of the deposited SiC, viability of the interface coating, stability of the fibers, and bonding of the fibers to the SiC encasement during process operation. Alternately retention of the DuPont PRD-66 membrane, mitigation of divot formations, strengthening of the flange, and production of a barrier vs bulk filter remain to be addressed. Similarly successful operation of the IF&P Fibrosic™ candles in Westinghouse's filter arrays during pulse cycling remains to be demonstrated.

Objectives

The objectives of the Base Program are to:

- Provide a more "ruggedized" filter system that utilizes porous ceramic filters which have improved resistance to damage resulting from crack propagation, thermal fatigue and/or thermal excursions during plant or process transient conditions, and/or mechanical ash bridging events within the candle filter array (Task 1).

Table 1

Westinghouse APF Field Experience

Process	Temperature °C	Operating Conditions	Operating Hours	Candle Filter Type	Test Facility
AEP PFBC	620 - 845	Oxidizing	5855 2815 2815 1705 1705 1705	SiC (a) Alumina/Mullite SiC (b) SiC Composite Filament Wound SiC (c)	Demonstration Plant
Karhula PCFBC	850 - 900 690 - 850 850 850	Oxidizing Oxidizing Oxidizing Oxidizing	716 1341 540 387	Alumina/Mullite SiC (b) SiC (c,d) Alumina/Mullite (e) SiC Composite	Pilot Plant
FW PFBC	700 - 870 700 - 870	Oxidizing Oxidizing	58 ~ 900	Alumina/Mullite SiC (a)	Pilot Plant
FW Carbonizer	<760	Reducing	63 ~ 400	Alumina/Mullite SiC (a)	Pilot Plant
Texaco Gasifier	700	Reducing	~ 400	SiC (a) Alumina/Mullite	Pilot Plant
IGT Biomass	760 - 915 675	Reducing Reducing	21 30	SiC (a) SiC (a)	Pilot Plant

(a) Schumacher Dia Schumalith F40
(b) Pall Vitropore 442T
(c) Schumacher Dia Schumalith FT20
(d) Pall 326
(e) Alumina/Mullite (1110 Hr PFBC-Exposed).

- Assess the effects of long-term (i.e., 1000-1500 hours) pilot-scale exposure under actual pressurized circulating fluidized-bed combustion (PCFBC) conditions on advanced candle filter failure modes and degradation mechanisms (Task 2).
- Assess the stability of select advanced filter materials when subjected to long-term exposure in actual integrated gasification combined cycle (IGCC) gas streams (Task 3).

Table 2

Hot Gas Filter Materials

Commercial or Near Commercial Filters	As-Manufactured Permeability	Membrane	Dust Cake Removal	Load Bearing Capacity	Creep Resistance (>600°C)	Thermal Fatigue/ Shock Resistance	Volatile Alkali Sorption (T>600-800°C)	Volatile Alkali Impact
Schumacher/Pall Clay Bonded SiC*	High	Present	High	High	Low	High/High	High	High; Silicate Eutectic Formation
Coors Alumina/Mullite	Moderate-High	Typically Not Present	High	High	High	High/ Susceptible	Moderate	Negligible; Crystallization and Strength Increase
3M CVI-SiC Composite	High	Open Woven Outer Structure	Moderate	Low	High	High/High	Negligible Initial Uptake; Accelerated Oxidation	Embrittlement; Eutectic Formation
DuPont PRD-66	High	Present	High	Low	High (TBD)	High/High	(TBD)	Membrane Cracking and Spalling
DuPont SiC-SiC	Moderate-High	Present	High	Low	High (TBD)	High/Low	Negligible Initial Uptake; Accelerated Oxidation	Embrittlement; Eutectic Formation
IF&P Fibrosic™	High	Present	High	Very Low	High	Low/High	Moderate-High	Phase Changes; Rigidization Spalling

* Original Matrices: Schumacher Dia Schumalith F40; Pall Vitropore 442T.
TBD: To Be Determined.

Table 3

High Temperature Filter Material Stability

Filter Matrix	Thermal Fatigue	Thermal Shock	Flow-Through Oxidation/Corrosion	
	Accelerated Pulse Cycling	Thermal Transient Testing	Steam/Air	Alkali/Steam/Air
Coors Alumina/Mullite	Intact	Susceptible	Conversion Of Amorphous Phase To Anorthite; Strength Increase	Conversion Of Amorphous Phase To Albite; Anorthite; Strength Increase
Schumacher F40	Intact	Intact	NT	Eutectic Formation; Plastic Deformation
Pall Vitropore 442T	Intact	Intact	NT	Eutectic Formation; Plastic Deformation Expected
3M CVI-SiC Composite	Intact	Intact	Strength Loss; Surface Oxidation	Strength Loss; Accelerated Oxidation; Eutectic Formation; Embrittlement
DuPont PRD-66	Flange Failure; Matrix Strengthening; Holder Redesign	Intact	Strength Increase	Strength Loss; Membrane Cracking and Spalling
DuPont SiC-SiC	Intact	Lapped Seam Rupture	Strength Loss; Surface Oxidation	Strength Loss; Accelerated Oxidation; Eutectic Formation; Embrittlement
IF&P Fibrosic™	Mid-Body Fracture; Hole Formations	Intact	Tearing; Rupture	Rigidization

NT: Not Tested.

Approach

In order to provide a more "ruggedized" filter system that utilizes porous ceramic filters, Westinghouse subjects full-body filter elements to qualification testing in its PFBC simulator test facility in Pittsburgh, PA, prior to considering any filter element for use in field operation. During filter qualification testing, filter elements are subjected to

- Simulated steady state PFBC operating conditions
- Accelerated pulse cycling to determine the impact of thermal fatigue primarily along the inner surface of the filter element
- Simulated thermal transient conditions which reflect possible rapid system start-up and shut-down cycles.

In addition to determining the response of the filter material to the simulated PFBC environment, qualification testing demonstrates

- Filtration efficiency during steady state operation
- Dust cake removal capability
- Conditioned filter pressure drop
- Sealing and mounting capability of the element(s) within the metal housing.

Post-test non-destructive evaluation of filter elements is generally conducted to assess the

- Retention of fines along the outer surface of the elements
- Integrity of the flange
- Overall integrity of the filter body.

Alternately post-test destructive characterization of the filter elements identifies the

- Integrity of the cross-sectioned filter matrix (i.e., crack formations)
- Microstructure of the resulting filter matrix
- Semi-quantitative elemental composition throughout the element
- Residual room and process temperature bulk strength
- Residual room temperature hoop strength
- Resulting elastic modulus and Poisson's ratio
- Thermal coefficient of expansion
- High temperature creep strain
- Affinity of ash or char fines to the membrane
- Penetration of fines through the filter wall
- Composition of the ash fines.

In order to demonstrate the long-term thermal/chemical stability of the various filter materials, high temperature corrosion testing is conducted utilizing either discs or mini-candles. These materials are exposed generally for a period of 400 hours at temperatures of 870ºC to a flow-through environment which contains either 5-7% steam/air or 20 ppm NaCl/5-7% steam/air.

The materials are also subjected to simulated pulse cycling at every 20 minute intervals throughout the course of flow-through testing. Post-test characterization of the material includes:

- Inspection for cracks
- Determining the residual bulk strength of the matrix along both gas stream and pulse cycled surfaces
- Identifying whether microstructural and/or compositional changes have occurred within the material.

Project Description

The focus of the Filter Component Assessment program in Task 1 has been to evaluate the filtration characteristics, mechanical integrity, and corrosion resistance of the following advanced or second generation candle filters for use in advanced coal-fired applications:

- 3M CVI-SiC composite — Chemical vapor infiltration of silicon carbide on an aluminosilicate Nextel™ 312 fiber preform
- DuPont PRD-66 — Filament wound candle containing corundum, cordierite, cristobalite, and mullite
- DuPont SiC-SiC composite — Chemical vapor infiltration of silicon carbide on a Nicalon™ felt or mesh screen support layer
- IF&P Fibrosic™ — Vacuum infiltrated oxide-based chopped fibrous matrix.

In order to assess the effects of long-term (i.e., 1000-1500 hours) pilot-scale exposure on advanced candle filter failure modes and degradation mechanisms in Task 2,

- Advanced monolithic, high temperature, creep resistant Schumacher Dia Schumalith FT20 candles
- Advanced monolithic, high temperature, creep resistant Pall 326 candles
- Coors P-100A-1 alumina/mullite candles, and
- 3M CVI-SiC composite candles

were installed in the Westinghouse Advanced Particulate Filtration (W-APF) system that was operated at Foster Wheeler's PCFBC test facility in Karhula, Finland. To date, two test campaigns have been completed in which 112 candles were operated for a period of 540 hours at temperatures of ~850ºC using Illinois No. 6, Sparta coal, as the feed material and Linwood limestone as the sulfur sorbent (Table 4).

Post-test characterization of PCFBC surveillance candles which has recently been completed included determining the resulting gas flow resistance of the filter elements, residual process temperature bulk strength, high temperature creep and thermal expansion properties, and residual microstructure and phase composition. In addition, characterization of ash samples that were removed from various locations within the three filter arrays was also conducted. These analyses included determining the bulk density, moisture content, bulk strength, thermal expansion, and identification of the morphology and composition of the ash materials. Continued testing at Karhula is planned to begin in August 1996, tentatively for an additional ~1000 hours

Table 4 Summary of PCFBC Filter Operation		
	Test Segment No. 1	**Test Segment No. 2**
Number of Candles	112	112
Filter Operating Temperature, ºC	826-853	818-860
Filter Operating Pressure, bar	10.7-11.1	10.6-11.3
Nominal Face Velocity, cm/s	3.5-4.1	3.1-4.2
Inlet Dust Load, ppmw	11,400-15,000	11700
Coal Feed	Illinois No. 6 (Sparta)	Illinois No. 6 (Sparta)
Sulfur Sorbent	Linwood Limestone	Linwood Limestone
Operating Hours (Coal)	153	387

of service operation in Test Segment No. 3. The information obtained from the filter material and ash analyses will serve as the basis for determining continued use of the various filter elements in selected Clean Coal Technology Demonstration projects.

Additional effort is being initiated in Task 3, to assess the stability of select advanced filter materials when subjected to long-term exposure in actual IGCC gas streams. A pressurized mini-vessel will tentatively be installed downstream of the W-APF at the Sierra Pacific Piñon Pine IGCC Demonstration Plant in Reno, NV. There either mini-candles or coupons will be exposed at temperature to the process fuel gas for extended periods of time in the absence of char fines. Post-test characterization of either the mini-candles or coupon materials will be conducted as previously described.

Results

First generation monolithic porous ceramic filter materials have been shown by Westinghouse to experience thermal fatigue, high temperature creep, and loss of material strength when operated for extended periods of time in advanced coal-fired process applications.[1,2] In order to mitigate high temperature creep and/or creep crack growth, both Schumacher and Pall developed a creep resistant binder for use in the manufacture of the clay bonded silicon carbide candle filters. High temperature creep testing conducted at Westinghouse using the Schumacher Dia Schumalith FT20 and Pall 326 filter materials demonstrated the absence of creep when either material was subjected for ~500 hours to a 500 psi, 4-point bending load at ~845°C.

Additional effort at Westinghouse was conducted to assess the impact of thermal fatigue and/or thermal shock on the stability of the clay bonded silicon carbide and alumina/mullite filter materials. During simulated PFBC testing at Westinghouse, both the clay bonded silicon carbide and Coors P-100A-1 alumina/mullite candles were instrumented with high speed thermocouples in order to measure the axial and radial temperature profiles through the filter wall during pulse cleaning (i.e., thermal fatigue), and during exposure to simulated thermal transient conditions (i.e., thermal shock). As described in Appendix A, the resulting temperature profiles were

utilized to establish the stress intensity within the filter elements.[3] Clearly the use of the fail-safe/regenerator above the Coors P-100A-1 alumina/mullite candle filters significantly reduced the stress intensity experienced along the inner surface of the filter element during pulse cycling. In contrast, however, depending on the magnitude of the thermal transient event, stresses which exceeded the rupture strength of the Coors P-100A-1 alumina/mullite filter matrix were established along the outer surface of the candle. Under similar thermal transient conditions, stresses established within the clay bonded silicon carbide candles were calculated to be equal to, or below the rupture modulus of the filter matrix. As a result, the clay bonded silicon carbide filter elements were considered to have a greater likelihood for survival in process systems that experience rapid shut-down or start-up cycles in comparison to the Coors P-100A-1 alumina/mullite filter elements.

In order to develop a more "ruggedized" filter system, identifying the stability and life of candidate filter materials during operation in advanced coal-fired applications is essential. In the following sections, discussions are provided which summarize Westinghouse's material characterization and filter surveillance efforts that were conducted during the past year.

HTHP PFBC Filter Qualification Testing

Prior to selection, installation, and operation in the field, candle filter qualification testing is conducted at Westinghouse to assure that developmental, prototypic, or commercial filter elements demonstrate a >99.99% particle collection efficiency during steady state, simulated PFBC operation. Similarly the initial pressure drop across the elements at process temperature, dust cake removal efficiency, and the as-manufactured strength of the flange and mechanical sealing/mounting of the element within the filter holder are assessed. In addition, Westinghouse qualifies the performance of the various filters under extreme conditions as accelerated pulse cycling which monitors the performance of the matrix with respect to thermal fatigue, as well as exposure to thermal transient events which simulate rapid start-up or shut-down ramps experienced during process upset conditions.

In order to evaluate the performance of the advanced second generation filter elements, an array which included a DuPont PRD-66, a 3M CVI-SiC composite, and a DuPont SiC-SiC composite filter was installed in the Westinghouse high temperature, high pressure (HTHP) PFBC simulator test facility in Pittsburgh, PA.[2] Initially the filter array was heated to temperatures of ~845°C prior to initiating thermal transient testing. A series of seven increasing severity thermal transients were delivered to the array which reduced the outer surface temperature of the filter elements by 6-110°C and 20-240°C within the first five and sixty seconds, respectively, after transient initiation. Nine maximum severity thermal transients followed. Subsequently the array was subjected to ten accelerated pulse cleaning cycles, and a final maximum severity thermal transient.

After 42 hours of thermal transient testing, the filter array was slow cooled, and the elements were removed for destructive characterization. Characterization of the resulting morphology and phase composition via scanning electron microscopy/energy dispersive x-ray analysis (SEM/EDAX) and x-ray diffraction (XRD) analysis has not been completed for the thermal transient-tested DuPont PRD-66 and 3M CVI-SiC filter matrices. However, when the

DuPont SiC-SiC composite was subjected to SEM/EDAX analyses, several interesting changes were observed as a result of simulated PFBC thermal transient testing.[4] These included:

- Evidence of oxidation of the CVI-SiC outer surface
- Removal of the interface layer that was originally deposited around the Nicalon™ fibers in the single-ply felt layer of the DuPont SiC-SiC composite
- Removal of the interface layer particularly along the outer fiber bundle or tow, directly beneath the CVI-SiC encapsulating layer in the mesh support screen
- Melting or "sintering" of adjacent Nicalon™ fibers with the enhanced oxidation phase that was added during the manufacture of the mesh screen support layer.

Retention of the interface layer along the interior of the fiber bundle or tow in the mesh screen support layer remains to be determined.

Based on the resulting load versus deflection curves that were generated during compressive and tensile strength testing, the fracture toughness of the DuPont SiC-SiC composite appeared to be reduced after 42 hours of thermal transient testing.[2] Loss of fracture toughness was primarily attributed to removal of the interface layer in the single-ply felt and mesh screen support layers, and to the "sintering" of the Nicalon™ fibers in the mesh screen support layer.

In order to identify the thermal fatigue resistance of the advanced second generation filters, a second set of DuPont PRD-66, 3M CVI-SiC composite, and DuPont SiC-SiC composite candles were installed in the Westinghouse PFBC simulator and subjected to 3514 accelerated pulse cleaning cycles during a period of 197 hours. The temperature of the filter array was maintained at ~845°C while accelerated pulse cycling was conducted.

The interface layer that initially surrounded the Nicalon™ fibers in the single-ply felt layer of the DuPont SiC-SiC filter matrix was again seen to be removed after 197 hours of accelerated pulse cycle testing. Similarly crack formations were evident along the outer periphery of the Nicalon™ fibers.[4] Typically the cracks had rounded tips, as well as segmented "step-like" characteristics.

"Halo-like" areas were readily evident along the periphery of the Nicalon™ fibers in the single-ply felt. These areas were generally enriched with oxygen, and effectively demarcated the location to where the cracks penetrated. Bonding of the Nicalon™ fiber to the inner surface of the CVI-SiC encapsulating shell often resulted near the crack formations.

Within the mesh screen support layer, thin CVI-SiC bands which followed the contour of the Nicalon™ fibers, the enhanced oxidation phase, and perhaps the interface layer were evident. Near the periphery of the fiber bundle or tow (i.e., adjacent to the CVI-SiC encapsulating layer), as well as within the bundle, irregularly shaped Nicalon™ fibers were evident. Melting of the fibers was frequently observed, as well as mottling of the fiber surface. These were considered to result as a response or reaction of the Nicalon™ fibers with the enhanced oxidation phase that was included in the mesh screen support layer. Adjacent to the CVI-SiC encapsulating layer, the melted fibers formed an interconnected network which readily formed cracks during fast fracture. Void formations that were observed in the fractured mesh screen support layer may have resulted from fiber pull-out during sample preparation, or

alternately reflected removal of the interface phase during exposure to simulated PFBC process operating conditions. The Nicalon™ fibers in the mesh screen support layer of the DuPont SiC-SiC composite filter matrix did not exhibit crack formations along their periphery.

Oxidation of the outer surface of the CVI-SiC encapsulting layer was again evident after 197 hours of accelerated pulse cycling in the Westinghouse PFBC simulator test facility.

As previously discussed, the reduced fracture toughness of the DuPont SiC-SiC filter matrix after 197 hours of accelerated pulse cycling was primarily attributed to removal of the interface layer in the single-ply felt and mesh screen support layers, and to the "sintering" of the Nicalon™ fibers in the mesh screen support layer.

After ~800 hours of steady state, thermal transient, and accelerated pulsing of DuPont SiC-SiC candles in the simulated PFBC process environment which contained ash and 2 ppm gas phase sodium chloride (i.e., equivalent to 20 NaCl at 1 atm), further changes were evident within the filter matrix.[5] These included an apparent swelling of the Nicalon™ fibers within the single-ply felt layer. As a result, the fibers completely, or nearly completely filled the void in the CVI-SiC encapsulating shell. Bonding of the Nicalon™ fibers to the inner wall of the CVI-SiC shell was also apparent in the single-ply felt layer.

Efforts are required to conduct similar post-test characterization of the accelerated pulse cycled and thermal transient-tested 3M CVI-SiC composite and DuPont PRD-66 filter materials.

Characterization of Long-Term PFBC-Exposed Filter Coupons

Monolithic Filter Materials[3]

Porous ceramic monolithic filter material coupons (i.e., flat discs) were installed in an open metal structure and placed above the combustor freeboard area at the AEP Tidd Demonstration Plant in Brilliant, OH. These coupons were exposed to the PFBC process gases and fines in a flow-over fashion for ~10,000 hours (i.e., May 1992-January 1995). Both the ceramic filter coupons and metal structure remained intact during the prolonged exposure in the 815-843°C PFBC environment.

As shown in Table 5, numerous phase changes occurred within the porous ceramic monolithic filter materials after extended exposure to the high temperature PFBC environment. Although the filter materials were exposed as coupons in a flow-over fashion, the phase changes appeared to result throughout the entire matrix (i.e., not simply along the surface that was contacted with the process gas and/or particulate fines). The impact of phase changes on the residual bulk strength was not determined for the small coupons since insufficient material was available for evaluation.

Table 5

Stability of the Porous Ceramic Monolithic Filter Materials after ~10,000 Hours of Flow-Over Exposure at AEP

Filter Material	Microstructural Changes
Coors P-100A Alumina/Mullite	• Matrix remained intact • Extensive mullitization • Composition of the ligaments included oxygen, aluminum, and silicon, with secondary contributions of calcium • Composition of the pore cavity wall included oxygen, aluminum, and silicon, with secondary contributions of magnesium, calcium, and potassium • Migration of magnesium, calcium, etc., from the interior of the matrix to the pore cavity wall typically results during exposure to high temperature oxidizing environments
Coors P-100A-1 Alumina/Mullite	• Matrix remained intact • Extensive crystallization/mullitization • Migration of magnesium to the pore cavity wall
Coors Mullite	• Matrix remained intact • As-manufactured matrix contained ~50-100 µm agglomerates that were enriched with oxygen, silicon, and aluminum • "Melt-like" features were evident along the pore cavity walls which encapsulated a subsurface crystalline phase after exposure to the PFBC environment
GTE Cordierite	• Matrix remained intact • Crystallization along the pore cavity walls
GTE Cordierite-Silicon Nitride	• Matrix remained intact • Numerous sintered submicron particles were present throughout the PFBC-exposed matrix • Open porosity retained • Ligaments contained additional porosity, particularly near the pore cavity surface
AiResearch Sintered Silicon Nitride	• Matrix remained intact • Retention of extensive formation of the "whisker-like" α-Si_3N_4 mat formation along the pore cavity walls

In addition to the flat coupons discs, O-rings or cylindrical sections removed from alumina/mullite and clay bonded silicon carbide candle filters were exposed for ~10,000 hours to the 815-843°C PFBC environment above the combustor freeboard at AEP. The residual bulk strengths of the ~10,000 hour exposed Coors P-100A alumina/mullite, Refractron 505, and Schumacher Dia Schumalith F40 (production lot from 1991) materials were determined at temperatures of 732ºC.[a]

The residual high temperature, bulk strengths of the ~10,000 hour exposed filter coupons are shown in Table 6. Unfortunately, neither the as-manufactured Coors P-100A nor Refractron 505 matrices were available for characterization at nominal filter operating temperatures of 732°C. From preliminary data that were generated at Westinghouse for the as-manufactured Coors P-100A alumina/mullite candles that were used at the Texaco reentrained gasification plant in Montebello, CA, the alumina/mullite filter matrix was determined to have an initial C-ring compressive strength of 2203±215 psi at 870°C. The as-manufactured strength for the P-100A alumina/mullite filter matrix would be expected to be close to, or possibly slightly greater than 2203 psi at 732°C. The strength of the P-100A filter matrix appeared to be reduced after ~10,000 hours of exposure above the combustor freeboard area at AEP (i.e., 1655±149 psi).

Table 6

C-Ring Compressive Strength of the ~10,000 Hour Combustor Freeboard-Exposed Porous Ceramic Monolithic Filter Materials

Filter Matrix	Strength, psi (732°C)
Coors P-100A	1577.0 1694.8 1845.1 1503.1 Average ± 1σ: 1655 ± 149
Refractron 505	2041.9 2343.7 2173.2 2567.0 Average ± 1σ: 2282 ± 227
Schumacher Dia Schumalith F40	1103.3 1050.2 967.4 976.0 Average ± 1σ: 1002 ± 38

[a] Typical operating temperature of the W-APF throughout the five test campaigns at AEP. The Coors P-100A alumina/mullite and Refractron 505 matrices are no longer utilized to produce full body candle filters for use in field applications. These materials have been replaced by the Coors P-100A-1 alumina/mullite and Pall Vitropore 442T filter matrices, respectively.

Since the filter materials were not pulse cycled during flow-over exposure above the combustor freeboard, the reduction in strength is considered to result from microstructural changes within the P-100A alumina/mullite material as a result of exposure to the PFBC operating temperatures and flue gas chemistry.

Similar to the Coors P-100A alumina/mullite filter matrix, strength measurements for the Refractron 505 filter matrix were previously generated at Westinghouse at temperatures of 870°C. The high temperature C-ring compressive strength of the as-manufactured Refractron 505 filter matrix was 2507±229 psi. The as-manufactured strength of the Refractron 505 filter matrix would be expected to be close to, or possibly slightly greater than 2507 psi at 732°C. After ~10,000 hours of exposure above the combustor freeboard area at AEP, the residual bulk strength of the Refractron 505 matrix was determined to be 2282±227 psi. Once again the strength of the Refractron 505 filter sample which had not been subjected to pulse cycling, was reduced primarily as a result of exposure to the process gas environment (i.e., gas chemistry and process operating temperature).

Based on the information generated in Westinghouse's surveillance program with AEP,[1] the Schumacher Dia Schumalith F40 filter matrix which had been produced in 1991, had an as-manufactured C-ring compressive strength of 1416±127 psi at 732°C. After ~10,000 hours of exposure at AEP, the residual strength of the Schumacher Dia Schumalith F40 filter matrix was 1002±38 psi. These data also imply that exposure to the process gas environment (i.e., gas chemistry and process operating temperature) had an impact on the residual strength of the filter matrix. As with the Coors P-100A and Refractron 505 filter samples, the Schumacher Dia Schumalith F40 filter samples did not experience pulse cleaning.

Since only four C-rings of each PFBC-exposed material were subjected to compressive strength testing at the elevated process operating temperatures, the question of statistical significance of the residual bulk material strength data arises. Obviously only general material response trends can be identified.

Second Generation Porous Ceramic Filter Materials

Sections removed from 3M CVI-SiC, DuPont PRD-66, DuPont SiC-SiC (double-ply felt), and IF&P Fibrosic™ candles were exposed above the W-APF tubesheet at the AEP Tidd Demonstration Plant in Brilliant, OH. These materials were placed on a material surveillance coupon tree, and exposed to PFBC conditions during Test Segments 3, 4, and 5. Post-exposure characterization of each material was conducted in order to determine whether microstructural changes had occurred after extended static exposure to the PFBC environment. Highlights of this effort follow:

3M CVI-SiC Composite

- Oxidation resulted along the exterior and interior of the CVI-SiC encapsulating structure of the 3M CVI-SiC composite filter matrix.
- The thin ~2 μm CVI-SiC infiltrated layer that was originally formed within the interior of the triaxial support braid consisted of ~1 μm SiC and ~1 μm SiO_2. Cracks were evident which penetrated through the SiO_2-enriched encapsulating layer.

- The oxygen-enriched layer along the interior of the CVI-SiC encapsulating shell appeared to bond to the Nextel™ 312 fibers in the 3M composite filter matrix.
- Oxidation of the ~2 μm CVI-SiC layer along the outer confinement and filtration mat layers of the 3M composite filter matrix occurred after exposure to the PFBC environment, again leading to the formation of SiO_2. Spalling of the SiO_2-enriched layer may occur during thermal cycling of the filter, subsequently causing loss of material.
- After 2815 hours of exposure to static PFBC process operating conditions, ~21% of the initial strength of the triaxial support braid remained (Table 7). Neither the filtration mat nor outer confinement layers were expected to significantly contribute to the overall strength of the 3M CVI-SiC composite filter matrix.

DuPont PRD-66

- Crystallization of the fibers in the filament wound PRD-66 filter matrix was evident after exposure to flow-over PFBC conditions. Crystallization and grain growth were expected to lead to the lowered high temperature strength of the matrix after 4094 hours of exposure in the PFBC environment. Approximately 67% of the as-manufactured strength of the PRD-66 filter matrix remained after 4094 hours of exposure to static PFBC operating conditions.

DuPont SiC-SiC Composite

- Removal of the interface layer within the DuPont SiC-SiC double-ply felt filter matrix resulted during exposure to flow-over PFBC conditions.
- Longitudinal crack formations resulted along the Nicalon™ fibers in the DuPont SiC-SiC double-ply felt filter matrix after 4094 hours of exposure to flow-over PFBC conditions.
- Oxidation along the inner surface of the CVI-SiC shell resulted during exposure to flow-over PFBC operating conditions.
- In addition to crack formations, the Nicalon™ fibers experienced a volume increase due to oxidation. As a result of oxidation along the inner surface of the CVI-SiC shell and the Nicalon™ fibers, the void space between the fibers and shell decreased. The fibers ultimately become bonded to the encapsulating shell through contact with the oxygen-enriched (i.e., silica) “melt-like” phase. As a result, fracture toughness of the material was reduced.
- The strength of the DuPont double-ply SiC-SiC matrix appeared to slightly increase during flow-over exposure to PFBC operating conditions. This was considered to result from bonding of the residual fibers to the inner surface of the oxidized CVI-SiC encapsulating shell.

Table 7

Summary of the Strength and Morphology of the Second Generation Filter Materials after Exposure to PFBC Test Conditions above the W-APF Tubesheet at AEP

Filter Matrix	Exposure Time, Hrs	Initial Process Strength, psi	PFBC-Exposed Process Strength, psi	SEM/EDAX Characterization
3M CVI-SiC	2815	10652± 2184[a,b] (Composite Fracture)	2187[b] (0.4 lbs[c] Composite Failure)	Oxidation of CVI-SiC Outer and Inner Surfaces; Bonding of Nextel™ 312 Fibers to CVI-SiC-SiO_x
DuPont PRD-66	4094	988±86[a] (Brittle Fracture)	666 (6.8 lbs Brittle Fracture)	Crystallization and Grain Growth of the Polycrystalline Fibers; Limited Slurry Infiltration into Interior of Filament Bundles; Voids within Individual Fibers
DuPont SiC-SiC	4094	4703[d] (Brittle Fracture)	5867[d] (10.4 lbs; Brittle Fracture)	Removal of the Interface Layer; Oxidation of CVI-SiC Outer and Inner Surfaces; Oxidation of Nicalon™ Fibers; Bonding of Fibers to CVI-SiC
IF&P Fibrosic™	2815	ND	ND	Morphology Similar to As-Manufactured Filter Matrix

(a) Previously Reported Strengths From An Alternate Filter Production Lot.
(b) Triaxial Braid Wall Thickness Used To Calculated Resulting Bulk Strength.
(c) Ultimate Load To Failure.
(d) Double Ply Felt.
As-Manufactured and PFBC-Exposed Process Strengths Determined at 843°C.
ND: Not Determined.

IF&P Fibrosic™

- Virtually little change in the morphology of the IF&P Fibrosic™ fibers was observed after 2815 hours of exposure to the flow-over PFBC gas environment.

Characterization of the PCFBC-Exposed Candle Filter Materials

In order to assess the effects of long-term, pilot-scale exposure on the stability of the advanced monolithic and second generation fiber reinforced filter elements (Task 2), 112 candles were installed in the Westinghouse APF system at Foster Wheeler's test facility in Karhula, Finland (Table 4). An assessment of the performance and characterization of the material properties of the Schumacher Dia Schumalith FT20, Pall 326, Coors P-100A-1 alumina/mullite, and 3M CVI-SiC composite surveillance candles were conducted at the conclusion of Test Segments 1 and 2. Post-test filter element characterization included:

- Room temperature gas flow resistance measurements
- Scanning electron microscopy/energy dispersive x-ray analysis (SEM/EDAX)
- Compressive and tensile bulk strength testing at room and process temperature
- Hoop stress, elastic modulus, and Poisson's ratio
- Thermal expansion
- High temperature creep testing.

The results of these analyses follow.

Room Temperature Gas Flow Resistance

PCFBC surveillance candle filters were shipped to Westinghouse at the conclusion of Test Segment No. 2, and were initially subjected to room temperature gas flow resistance measurements. A partial dust cake remained along the outer surface of each filter element after shipment. Each candle was then brushed in order to remove the residual dust cake layer, and resubjected to room temperature gas flow resistance measurements. The as-received and brushed gas flow resistance measurements were generally comparable for each filter element type (Figure 1).

Scanning Electron Microscopy/Energy Dispersive X-Ray Analysis

Sections of material were removed from each filter element at the conclusion of Test Segment No. 2. Each section was fresh fractured and subjected to SEM/EDAX analyses in order to determine whether microstructural changes had occurred along either the outer (i.e., membrane surface) or pulse cycled surfaces, or throughout the cross-sectioned wall of the PCFBC-exposed filter elements.

Extensive crystallization of the high temperature creep resistant Schumacher Dia Schumalith FT20 filter matrix occurred after 540 hours of operation in the 850°C PCFBC environment. Negligible changes were detected within the fibrous outer membrane.

Similar extensive crystallization of the high temperature creep resistant binder resulted within the Pall 326 filter matrix after 540 hours of operation in the 850°C PCFBC environment. Changes within the fine silicon carbide grit membrane tended to indicate the presence of silica, implying oxidation of the grit, or localized (i.e., nondispersed) areas of the binder phase.

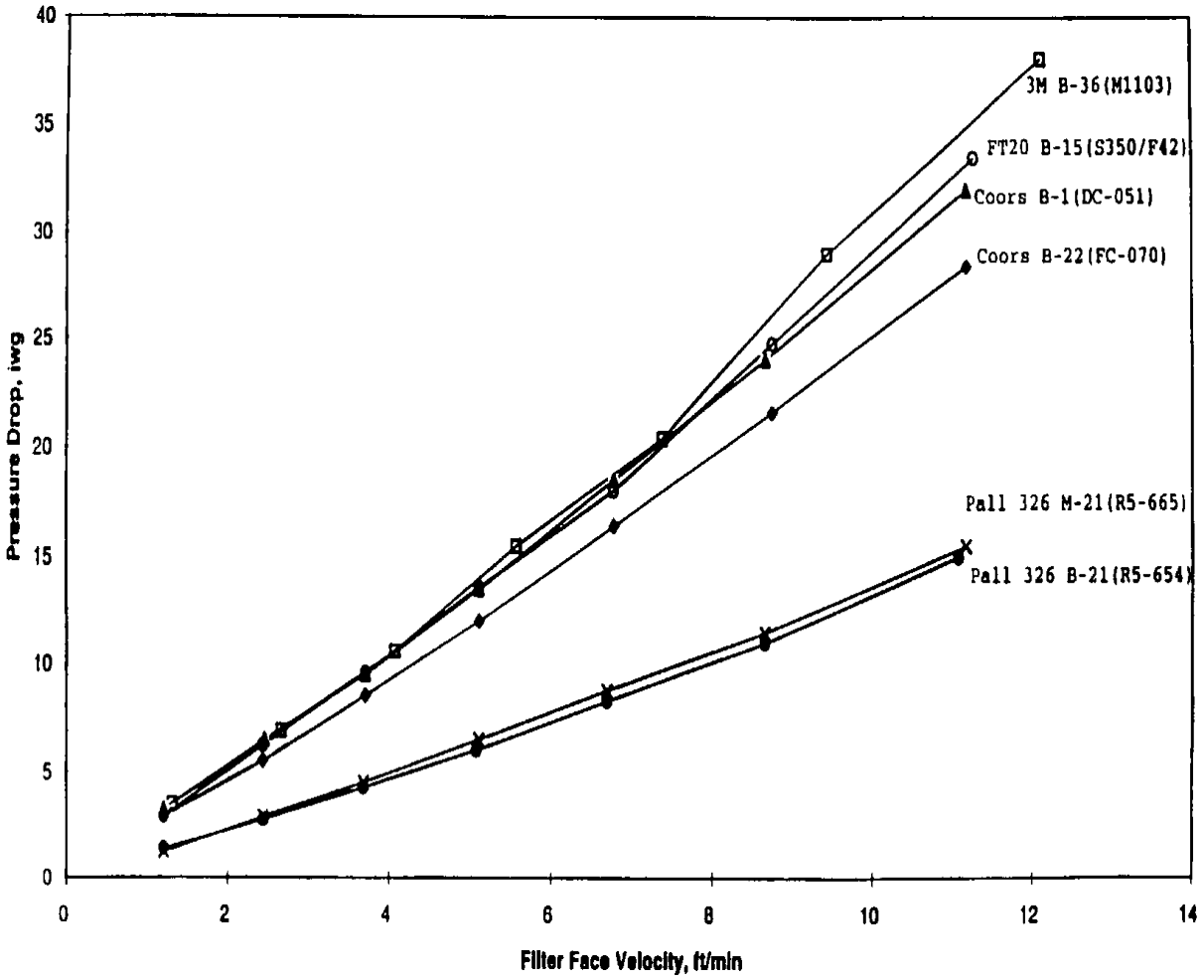

Figure 1 — Room Temperature Gas Flow Resistance of the PCFBC Surveillance Candle Filters (Test Segment No. 2)

Both newly manufactured Coors P-100A-1 alumina/mullite candles, as well as candles that had been operated in the W-APF system at AEP were installed prior to initiating PCFBC testing in Test Segment No. 1. Post-test SEM/EDAX characterization of the 505 hour PCFBC-exposed, and 1650 hour PFBC/PCFBC-exposed Coors P-100A-1 alumina/mullite filters indicated that crystallization resulted along the pore cavity walls, and throughout the structural ligaments.

When removed from the filter array after 387 hours of operation at 850°C in the PCFBC environment, a color change was readily evident along the outer confinement and possibly filtration mat layers of the 3M CVI-SiC composite candle filters. The original dark black color of the 2 µm CVI-SiC coating that encapsulated either the Nextel™ 312 fibers in the outer confinement layer, or the alumina-based fibers in the filtration mat layer was not retained along the majority of the filter body. Instead after 387 hours of operation, the outer confinement layer appeared to be white (i.e., excluding the presence of ash fines), while the filtration mat layer was generally a light to medium grey. A similar change in the color of the 3M CVI-SiC composite candle filters had been experienced at Westinghouse during qualification testing under simulated PFBC conditions. Initial consideration was that the "strand-like" appearance of the confinement layer exposed "bare" fibers as a result of removal of the CVI-SiC encapsulating shell during exposure in the high temperature oxidizing environment. Generally the triaxial support braid which consisted of an ~100 µm CVI-SiC layer that encapsulated twisted Nextel™ 312 filaments or fiber bundles, retained its as-manufactured dark black appearance.

SEM/EDAX characterization of the PCFBC-exposed 3M CVI-SiC composite filter matrix confirmed removal of the 2 µm SiC layer that initially encapsulated the Nextel™ 312 fibers in the outer confinement layer. Characterization of the lapped filtration mat indicated that oxidation of the 2 µm CVI-SiC shell had also occurred. As a result, an ~1 µm oxygen-enriched layer formed along the outer surface of the as-manufactured CVI-SiC coating. An oxygen-enriched region also formed along the inner surface of the CVI-SiC shell, bonding the shell to the filtration mat fibers. Bonding of the oxygen-enriched CVI-SiC shell to the fibers ultimately reduces fracture toughness and possibly increases strength within this layer of the composite filter matrix.

Characterization of the triaxial support braid identified oxidation and pitting along the outer surface of the CVI-SiC shell that encapsulated underlying Nextel™ 312 filaments. Within the filament or fiber bundles, a thin layer of CVI-SiC generally coated individual fibers. Frequently gaps were evident between the thin CVI-SiC layers and the fibers, as well as areas which clearly showed bonding of the shell to the surface of the contained fiber.

Compressive and Tensile Strength Testing

Strength characterization of the as-manufactured Schumacher Dia Schumalith FT20, Pall 326, Coors P-100A-1 alumina/mullite, and 3M CVI-SiC composite candle filters was conducted via compressive and tensile testing of C-rings at room temperature, 850°C, 870°C, and 900°C. In addition, Coors P-100A-1 alumina/mullite and 3M CVI-SiC composite candles removed after

completion of Test Segments 1 and 2, and Schumacher Dia Schumalith FT20 and Pall 326 filters removed after completion of Test Segment No. 2 were subjected to C-ring compressive and tensile strength testing at room temperature, 850°C, and 900°C. Process temperature strengths (i.e., 850°C) of sections from broken filter elements that were removed from the ash hopper at the conclusion of Test Segment No. 2 were also identified. The results of these analyses are presented in Table 8 and Figure 2.

In summary, the as-manufactured

- Schumacher FT20 filter matrix retained its brittle fracture characteristics during C-ring compressive and tensile testing up to temperatures of 900°C.
- Pall 326 filter matrix exhibited brittle fracture characteristics during C-ring compressive and tensile testing at room temperature and 850°C, but underwent plastic deformation at temperatures of 870-900°C.
- Coors P-100A-1 matrix exhibited brittle fracture characteristics during C-ring compressive and tensile testing up to temperatures of 900°C.
- 3M CVI-SiC composite matrix similarly retained its composite characteristics (i.e., room temperature to 900° C).
- Testing of the as-manufactured Schumacher FT20 and Pall 326 filter matrices at high temperature (i.e., 850°C, 870°C, and 900°C) resulted in higher compressive/tensile strengths in comparison to the calculated room temperature strengths. Although these materials were manufactured at substantially higher temperatures, the apparent enhanced strength was considered to reflect the response of the clay bonded silicon carbide filter matrix to the higher test temperatures. Flaws generated during cooldown from process operating conditions, or edge cracks/flaws created during sample preparation (i.e., cutting) may have “self-healed” when the clay bonded silicon carbide filter materials were re-exposed to high temperature (850-900°C).
- The resulting load bearing capability of each filter material at 850°C follows:
    - Schumacher Dia Schumalith FT20: 58.8±2.5 lb (compression); 36.4±0.2 lb (tension)
    - Pall 326: 95.7±1.2 lb (compression); 53.9±8.0 lb (tension)
    - Coors P-100A-1 alumina/mullite: 54.3±1.8 lb (compression); 39.5±2.1 lb (tension)
    - 3M CVI-SiC composite: 3.2±0.8 lb (compression); 2.1±0.4 lb (tension).

After exposure to PCFBC conditions,

- The Schumacher Dia Schumalith FT20, Pall 326, and Coors P-100A-1 alumina/mullite materials (i.e., intact, as well as broken filter elements) exhibited brittle fracture characteristics during C-ring compressive and tensile strength testing at room temperature, 850°C, and 900°C.

Table 8

As-Manufactured and Residual Process Strength of the PCFBC-Exposed Porous Ceramic Filter Materials

		C-Ring Compressive Strength, psi				C-Ring Tensile Strength, psi			
Candle ID No.	**Time, Hrs.**	**25°C**	**850°C**	**870°C**	**900°C**	**25°C**	**850°C**	**870°C**	**900°C**
Schumacher FT20									
S350F/108	---	2135±155 (8)	3147± 85 (2)	3409±205 (8)	3549±127 (4)	1727± 74 (6)	3070± 52 (2)	3023± 72 (6)	2937±141 (4)
S350F/8 (T12)	540	2140± 88 (8)	3716±426 (8)	ND	3602± 38 (5)	1957±146 (8)	2927±169 (8)	ND	3076±251 (6)
S350F/42 (B15)	505	2014± 72 (8)	3711±240 (8)	ND	3758± 93 (6)	1837±96 (8)	3185±187 (8)	ND	3343±212 (6)
Test Segment No. 2 Broken Section	540	ND	3242±454 (9)	ND	ND	ND	3001±205 (9)	ND	ND
Pall 326									
R3-676	---	2961±186 (8)	4713±133 (2)	4953±270 (8)	3942±345 (4)	2480±124 (6)	4019±576 (2)	4498±262 (6)	4057±203 (4)
R5-654 (B21)	505	2001±167 (8)	2998±215 (8)	ND	3078±236 (6)	1807±92 (8)	2816±361 (8)	ND	2848±243 (6)
R5-665 (M21)	540	1784±159 (8)	3126±221 (8)	ND	3342±237 (6)	1792±170 (8)	3309±426 (8)	ND	3088±313 (6)
Test Segment No. 2 Broken Section	540	ND	2979±210 (9)	ND	ND	ND	2824±329 (8)	ND	ND

Table 8 (Continued)

As-Manufactured and Residual Process Strength of the PCFBC-Exposed Porous Ceramic Filter Materials

		C-Ring Compressive Strength, psi				C-Ring Tensile Strength, psi			
Candle ID No.	**Time, Hrs.**	**25°C**	**850°C**	**870°C**	**900°C**	**25°C**	**850°C**	**870°C**	**900°C**
Coors P-100A-1									
FC-030	---	2587±268 (8)	2843± 76 (2)	2966±222 (8)	2668±345 (4)	2751±248 (6)	2927±851 (2)	2928± 69 (6)	3019±223 (4)
FC-043 (B17)	118	2166±127 (8)	2759±126 (2)	2658±253 (8)	2710±290 (4)	2344± 77 (6)	2325±232 (2)	2588±124 (6)	2367±171 (4)
FC-070 (B22)	505	1900±106 (8)	2540±188 (8)	ND	2338±119 (6)	2406±152 (8)	2516±203 (8)	ND	2560±111 (6)
DC-051 (B1)	1650[(a)]	1611±199 (8)	1921±112 (8)	ND	1950±117 (6)	2065±185 (8)	2161±197 (8)	ND	2321±70 (6)
Test Segment No. 2 Broken Section	505 or 540	ND	2236±105 (9)	ND	ND	ND	2382±117 (9)	ND	ND
3M CVI-SiC Composite									
M-51076	---	1903±362 (8) 12448±2620 (8)	2472±414 (2) 11194±4509 (2)	1823±532 (8) 12286±4014 (8)	2173±725 (4) 13987±4105 (4)	1715±281 (6) 10718±2035 (6)	1754±266 (2) 10816±1771 (2)	1781±124 (6) 10632±538 (6)	1119±238 (4) 6800±1335 (4)
M-51093 (B47)	35	1092±262 (8) 8799±1844 (8)	1296±518 (2) 9858±3321 (2)	1151±461 (8) 9303±3335 (8)	1575±322 (4) 11328±1489 (4)	1197±332 (6) 8397±2340 (6)	1095±134 (2) 7737±1273 (2)	911±227 (6) 6808±1038 (6)	1049±297 (4) 7182±1529 (4)
M-51103 (B36)	387	667±193 (8) 5880±1733 (8)	1491±292 (8) 12701±2561 (8)	ND	1185±639 (6) 9845±4545 (6)	657±198 (8) 5044±1582 (8)	878±156 (8) 6520±659 (8)	ND	979±255 (6) 7471±1478 (6)
Test Segment No. 2 Broken Section	387	ND	1841±308 (9) 11724±1598 (9)	ND	ND	ND	1277±436 (9) 7192±2045 (9)	ND	ND

(a) Element Was Exposed For 1110 Hrs To PFBC Test Conditions In Test Segment No. 5 At AEP (Location AB-32).

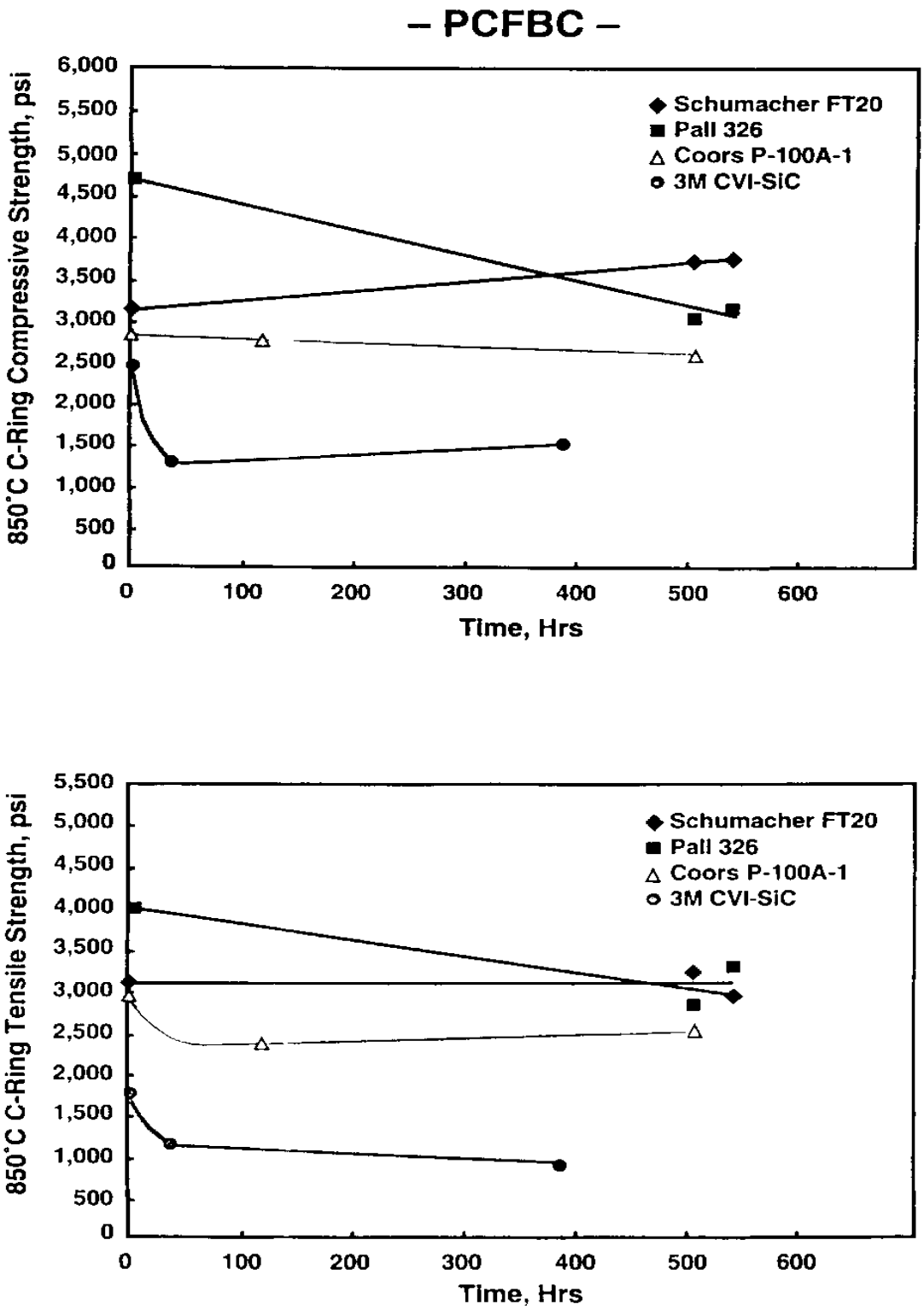

Figure 2 — Residual High Temperature Strength of the PCFBC-Exposed Candle Filters

- The 3M CVI-SiC composite filter matrix (i.e., intact, as well as broken filter elements) retained its composite failure characteristics during C-ring compressive and tensile strength testing at room temperature, 850°C, and 900°C.
- In general, either virtually no change, or an increase in strength of the Schumacher Dia Schumalith FT20 filters resulted along the OD and ID surfaces of the material after 505-540 hours of operation in the 850°C, PCFBC environment (i.e., elements located in the top and bottom arrays).[b]
- In contrast to the Schumacher Dia Schumalith FT20 filter material, the Pall 326 filters that were located in the middle and bottom arrays exhibited a loss of strength along both OD and ID surfaces after 505-540 hours of operation in the 850°C, PCFBC environment (i.e., 34-36% compressive strength reduction at 850°C; 18-30% tensile strength reduction at 850°C).
- Within the first 505 hours of PCFBC operation, the Coors P-100A-1 alumina/mullite filter elements that were located in the bottom array tended to experience a loss of strength along their OD surface (i.e., 3% compressive strength loss after 118 hours at 850°C; 11% compressive strength loss after 505 hours at 850°C). An initial reduction in strength was also apparent along the ID surface of the Coors P-100A-1 alumina/mullite filter elements during exposure to PCFBC operating conditions. A slight increase in strength may have resulted along the ID wall between 118 and 505 hours of operation (i.e., 21% tensile strength loss after 118 hours at 850°C; 14% tensile strength loss after 505 hours at 850°C). Continued operation of the Coors P-100A-1 alumina/mullite filters is required to demonstrate whether strengthening of the matrix is indeed occurring with time.
- The Coors P-100A-1 alumina/mullite filter elements that experienced 1110 hours of PFBC operation at the AEP Tidd Demonstration Plant in Brilliant, Ohio, remained intact after an additional 540 hours of operation in the Foster Wheeler PCFBC test facility in Karhula, Finland. As shown in Table 8, the compressive and tensile strength of the PFBC/PCFBC-exposed Coors P-100A-1 alumina/mullite matrix was lower than that of the PCFBC-exposed Coors P-100A-1 alumina/mullite elements.[c]
- When compared with the residual process temperature strengths of the clay bonded silicon carbide filter elements, a lower residual process temperature strength was evident for the Coors P-100A-1 alumina/mullite candle filters.
- In order to determine the strength of the 3M CVI-SiC composite filters, 15 mm C-rings were cut from intact filter elements or broken sections, and were tested in a similar fashion as the Schumacher, Pall, or Coors filter materials. In calculating the

---

[b] Compressive strength testing evaluates the residual strength along the OD surface of the candle filter that was in direct contact with the process gas. Tensile strength testing evaluates the residual strength along the ID surface of the candle filter that was in direct contact with the pulse cycled gas. If the porous ceramic filter matrix is susceptible to thermal fatigue, generally due to repetitive pulse cycling, a reduction in strength of the matrix would be evident along the ID or tensile-tested surface of the filter element.

[c] Comparison of the as-manufactured room temperature C-ring compressive and tensile strengths of the Coors P-100A-1 alumina/mullite filters with the reported PFBC/PCFBC-exposed filters indicates a 37% reduction in strength along the OD surface of the matrix, while a 24% loss of strength results along the ID surface of the material. Strength testing at 850°C, 870°C, and 900°C of the Tidd manufactured alumina/mullite P-100A-1 filters (i.e., "DC" series) was not conducted, and therefore comparison of the high temperature PFBC/PCFBC strengths can not be made.

residual strength, the wall thickness of the triaxial support braid was utilized, as well as the entire thickness of the three layer composite structure.[d] Depending on which wall thickness was used, strengths exceeding 5000 psi can be estimated (i.e., triaxial braid thickness only), or strengths ranging between ~600 and ~2500 psi can be determined (i.e., entire wall thickness).

- Using the entire wall thickness to calculate strength, the strength of the as-manufactured and PCFBC-exposed 3M CVI-SiC composite filter matrices was lower than either the Schumacher, Pall, or Coors as-manufactured or PCFBC-exposed filter materials.
- In general, the 3M CVI-SiC composite filter matrix exhibited a loss of strength after operation in the PCFBC environment (i.e., 48% and 40% compressive strength loss at 850°C after 35 and 387 hours, respectively; 38% and 50% tensile strength loss at 850°C after 35 and 387 hours, respectively).
- The load bearing capability of each PCFBC-tested filter material at 850°C follows:
    - Schumacher Dia Schumalith FT20: 61-73 lb (compression); 38-41 lb (tension)
    - Pall 326: 57-61 lb (compression); 35-42 lb (tension)
    - Coors P-100A-1 alumina/mullite: 34-43 lb (compression); 25-29 lb (tension)
    - 3M CVI-SiC composite: 2-2.5 lb (compression); 1.2-1.5 lb (tension).

Hoop Stress, Elastic Modulus, and Poisson's Ratio

A 254 mm (10 inch) section was removed from the Test Segment No. 2, PCFBC-exposed candle filters. Two 90° strain gage rosettes were installed along both inside and outside surfaces of the filter sections, at approximately the center of the test sample. A water filled bladder was inserted into the ID bore of each filter section, and was subsequently pressurized to determine the ultimate hoop strength of the filter matrix. The outer strain gage measurements for the 3M CVI-SiC composite filter matrix were somewhat in question, since delamination and shear were expected to have resulted between the layers of the composite structure during burst testing.

The pressure required to fail each filter section, as well as the ultimate hoop stress, elastic modulus, and Poisson's ratio for each of the Test Segment No. 2, PCFBC-exposed filter sections are presented in Table 9. Also included in Table 9 are similar material properties for the as-manufactured filter matrices.

Thermal Expansion

Sections of the PCFBC-exposed Schumacher Dia Schumalith FT20 and Pall 326 filter materials were subjected to thermal expansion testing. As shown Figure 3, the thermal expansion of the PCFBC-exposed Schumacher and Pall filter materials is nearly identical. Similarly the thermal expansion of the PCFBC-exposed clay bonded silicon carbide filter materials is nearly identical to that of the as-manufactured Coors P-100A-1 alumina/mullite and Schumacher Dia Schumalith F40 filter matrices.

[d] Entire wall thickness of the 3M CVI-SiC composite filter includes the thickness of the outer confinement layer, the middle filtration mat, and the structural support or triaxial braid.

Table 9

Material Properties of the PCFBC-Exposed Porous Ceramic Candle Filters —-Test Segment No. 2 —

Candle ID No.	Operating Time, Hrs	Burst Pressure, psi	Ultimate Hoop Stress, psi	Modulus, psi x 10^6	Poisson's Ratio
Schumacher Dia Schumalith FT20					
As-Manufactured	--	665	1703	7.3	0.17
S350F/108 (T12)	540	555	1496	7.44	0.208
S350F/42 (B15)	505	590	1584	7.39	0.152
Pall 326					
As-Manufactured	--	NE	NE	NE	NE
R5-655 (M21)	540	525	1369	5.00	0.162
R5-654 (B21)	505	520	1344	5.15	0.160
Coors P-100A-1 Alumina/Mullite					
As-Manufactured	--	860	2317	5.7	0.23
FC-070 (B22)	505	540	1503	4.84	0.205
DC-051 (B1)	1650[(a)]	505	1373	5.18	0.196
3M CVI-SiC Composite					
As-Manufactured	--	NE	1.01 ksi	2.96-3.38	0.14-0.27
M-51103 (B36)	387	133	1179	3.35	0.224

NE: Not Evaluated.
(a) PFBC/PCFBC-Exposed Candle Filter.

The thermal expansion of the porous ceramic filter materials is lower than the thermal expansion of the PCFBC or PFBC ash materials. The PCFBC ash sample that was used in the thermal expansion testing was representative of the dust cake layer that remained along the outer surface of the candle filters at the conclusion of Test Segment No. 2 at the Foster Wheeler test facility in Karhula, Finland. The PFBC ash sample was taken from a densely packed ash plug that formed within the inner bore of the filter elements during Test Segment No. 5 at the AEP Tidd Demonstration Plant in Brilliant, OH. The relatively wide range in the percent expansion of the ash materials as a function of temperature is expected to reflect the difference in the density, as well as the variation in the composition of the ash deposits.

High Temperature Creep

High temperature creep testing was conducted on 115 mm x 8.5 mm x 12 mm bars removed from PCFBC-exposed Schumacher Dia Schumalith FT20 and Pall 326 candle filters. As shown in Figure 4, these materials, unlike the Schumacher Dia Schumalith F40 and Pall

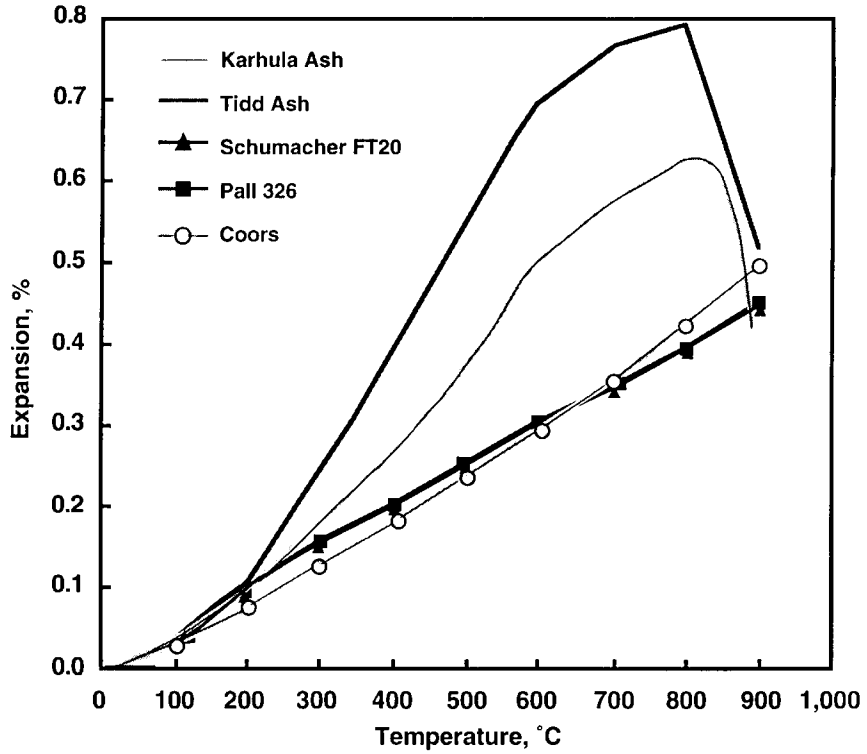

Figure 3 — Thermal Expansion of the Porous Ceramic Filter and Ash Materials

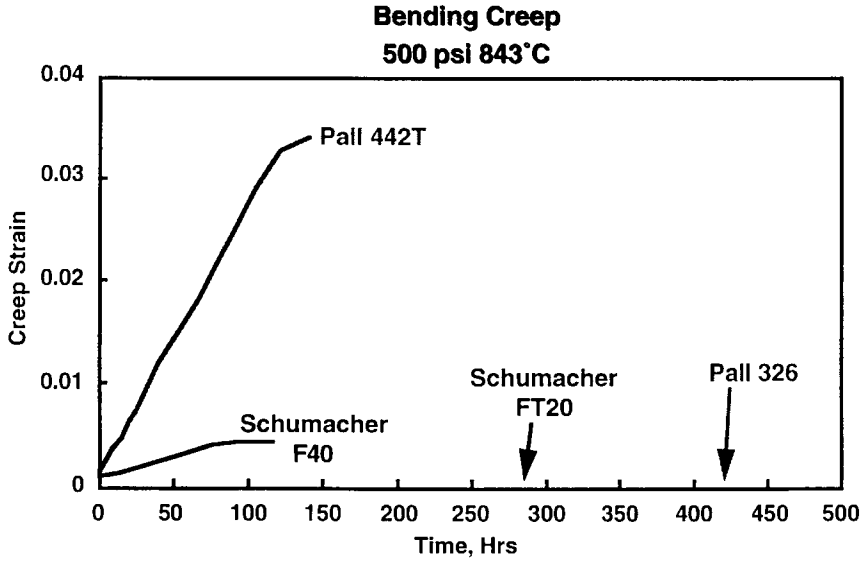

Schumacher Dia Schumalith F40 (S418/312B): 3038 Hrs, 732°C PFBC
Schumacher Dia Schumalith FT20 (S350F/106): 540 Hrs, 850°C PCFBC
Pall Vitropore 442T (R3-86): 1341 Hrs, 830°C PCFBC
Pall 326 (R5-665): 540 Hrs, 850°C PCFBC

Figure 4 — High Temperature Creep Strain as a Function of Time

Vitropore 442T materials, did not exhibit high temperature creep when a 500 psi, 4-point bend, flexural load was applied for ~300-500 hours at temperatures of 843°C (1550°F).

Similar high temperature creep testing was conducted using the 3M CVI-SiC composite filter matrix. Although delamination of the triaxial braid from the filtration and outer confinement layers resulted, testing indicated that the 3M CVI-SiC composite matrix did not exhibit creep strain after ~300-500 hours when a 500 psi, 4-point bend flexural load was applied to the material at temperatures of 843°C (1550°F).

Summary

With the exception of oxidation and removal of silicon carbide from the outer confinement and filtration mat layers of the 3M CVI-SiC composite filter matrix, degradation of the porous ceramic filter materials after operation in the PCFBC environment appeared to be limited. Additional operation in the PCFBC environment will be required to determine whether the advanced monolithic and fiber reinforced filter materials have achieved a conditioned residual bulk strength.

In addition to oxidation and removal of silicon carbide, the low load bearing capability of the 3M CVI-SiC composite filter elements, generally increases the potential for failure during ash bridging events, as well as crushing during handling and installation within the filter array, and maintaining adequate sealing around the filter flange.

Characterization of the PCFBC Ash (Test Segment No. 2)

Samples of the ash cake deposits were removed from various locations of the W-APF at the conclusion of Test Segment No. 2, and subjected to the following analyses:

- Scanning electron microscopy/energy dispersive x-ray analysis (SEM/EDAX)
- X-ray diffraction analysis (XRD)
- Moisture content
- Room temperature compression strength
- Density
- Thermal expansion.

Typically two types of particles were present within the ash cake layer that deposited along the outer surface of the candle filters in the top array. These include:

- Submicron and micron particulates that were enriched with aluminum and silicon. These particles were considered to be entrained fly ash fines that were released during the combustion of coal. “Melt-like” features were evident along the ash fines.
- Larger sulfated or partially sulfated calcium-based limestone or sorbent fines.

The aluminum and silicon-enriched coal ash fines were generally seen to adhere to the larger sulfated or partially sulfated sorbent fines. Extensive crystalline features were evident along the outer surface of the sulfated or partially sulfated sorbent fines. Agglomeration of crystalline

formations and/or “melt-like” features were detected, particularly along the surface of coal ash fines. In addition, spherical, ~10 µm particles enriched with silicon and calcium were also present within the deposited ash cake layer.

Dense packing of fines resulted within the ash cake layer that formed along the outer surface of the candle filters in the top array. Based on the analyses conducted, the cross-sectioned ash cake did not show evidence of fracturing of bonds or “melt-like” phases that may have originally been present between adjacent particles. This implies close packing of fines, with limited point contact between particles prior to fresh fracturing of the deposited ash cake layer.

Ash deposits that collected along the metal filter holders were also characterized. SEM/EDAX analysis indicated that porosity existed within the interconnective network of ash and sorbent particles that deposited around the metal filter holders. Within the deposit, a “melt-like” phase formed, sintering adjacent particles together. The sintered bond frequently formed point contact, necks, and channels between particles within the PCFBC deposit. The bond was identified by EDAX to be silicon and/or silicon-aluminum-enriched.

Sorbent particles were also present within the ash cake deposit that formed around the metal filter holders. Based on EDAX analyses, the limestone sorbent was considered to be completely or nearly completely sulfated. As in the filter cake deposit, the metal holder deposit contained discrete sorbent fines which were larger than the retained ash fines or agglomerates.

Similar analyses were conducted on ash removed from the filter hopper. A greater quantity of the larger calcium-containing sorbent and possibly the iron-enriched particles was detected in the ash hopper deposit in comparison to the quantity of these particles found within either the filter ash cake layer or metal holder deposits. When viewed at high magnification, the filter hopper ash was seen to contain extensive porosity. Porosity resulted from the interconnective network of fines that were held together through a silicon and/or aluminum-silicon-enriched “melt-like point contact, neck or channel phase.

X-ray diffraction (XRD) analysis was conducted to identify bulk composition of the PCFBC ash cake deposits. As shown in Table 10, the PCFBC ash consisted primarily of anhydrite and quartz, with secondary contributions of hematite, aluminosilicate phases, as well as an amorphous phase. Characteristically the PCFBC ash had a higher concentration of α-SiO_2 in comparison to the PFBC ash which formed within the W-APF at the AEP Tidd Demonstration Plant.[6] Although small, the concentration of the amorphous phase present in the PCFBC fines was greater than in the PFBC fines.

Comparison of the PFBC and PCFBC candle filter ash cake deposits indicated that

- The concentration of anhydrite was generally comparable in both materials.
- A higher concentration of hematite (Fe_2O_3) and quartz (α-SiO_2) resulted in the PCFBC ash cake layer.

Table 10 PCFBC Ash Composition — Test Segment No. 2 —	
X-Ray Diffraction Analysis, wt%	
Anhydrite ($CaSO_4$)	46-60%
Quartz (α-SiO_2)	21-40%
Hematite (Fe_2O_3)	9-11%
Aluminosilicate	3-8%
Anorthite ($CaAl_2Si_2O_8$)	
Margarite ($CaAl_2(Si_2OAl_2)O_{10}(OH)_2$_	
Kyanite (Al_2SiO_5)	
Amorphous	0-3%
* Additional Phases Present	

- Magnesium sulfate hydrates ($MgSO_4 \bullet xH_2O$), periclase (MgO), calcite ($CaCO_3$), and monticellite ($CaMgSiO_4$) were present in the PFBC ash which resulted from the utilization of a dolomitic limestone sorbent at Tidd vs limestone at Karhula.

With respect to the composition of the ash cake deposits that formed around the W-APF filter holders,

- The ash deposit that formed around the holders in the top filter arrays at Tidd was extremely hard and tenaciously bonded. This material had a substantially higher concentration of anhydrite (i.e., sulfated sorbent; $CaSO_4$) in comparison to either the deposits formed around middle and bottom holders at Tidd, or around the holders in the top array at Karhula. The tenacious nature of the ash cake deposit formed at Tidd decreased as the concentration of anhydrite and magnesium sulfate hydrate decreased, and the concentration of periclase (MgO), calcium carbonate ($CaCO_3$), monticellite ($CaMgSiO_4$), and calcium sulfate ($CaSO_4$) increased.[e]
- Hematite (Fe_2O_3) and quartz (α-SiO_2) were present at a higher concentration in the PCFBC fines that deposited around the holder in the top array at Karhula, in comparison to the fines that collected along the top array filter holders at Tidd.

PCFBC ash deposits that were removed from the W-APF cluster at the conclusion of Test Segment No. 2 were subjected to density, compressive strength, and moisture analyses. The resulting averaged density of the PCFBC ash samples was determined to be 0.587±0.062 gm/cm^3.

[e] The filter holder ash deposit formed at Karhula was less tenaciously bonded in comparison to the ash that formed along the filter holders in the top arrays at Tidd. The consistency of the Karhula filter holder deposit along the top array was similar to the middle and bottom array filter holders at Tidd in Test Segment No. 5, as well as throughout all arrays in prior test segments at Tidd.

The compressive strength of the various ash deposits ranged between 0.7 and 18.8 psi (i.e., average compressive strength: 11.01±7.3 psi; 4.7±3.1 lbs to failure). Typically the ash deposits had an 0.02-0.07% moisture content.

Application

As a key component in advanced coal- or biomass-based power applications, hot gas filtration systems protect the downstream heat exchanger and gas turbine components from particle fouling and erosion, cleaning the process gas to meet emission requirements. When installed in either PFBC or IGCC plants, lower downstream component costs are projected, in addition to improved energy efficiency, lower maintenance, and elimination of additional and expensive fuel or flue gas treatment systems. As a critical component, long-term performance, durability, and life of the porous ceramic filter elements are essential to the successful operation of the hot gas filtration system in advanced combustion and gasification applications.

Future Activities

Efforts will be focused on continuing testing of the advanced monolithic and second generation fiber reinforced candle filters in the W-APF system at Foster Wheeler's PCFBC test facility in Karhula, Finland (Task 2).

Effort is being initiated in Task 3, to assess the stability of select advanced filter materials (Table 11) when subjected to long-term exposure in actual IGCC gas streams. A pressurized mini-vessel will tentatively be installed downstream of the W-APF system at the Sierra Pacific Piñon Pine IGCC Demonstration Plant in Reno, NV. There either mini-candles or coupons will be exposed to the process fuel gas at temperature for extended periods of time in the absence of char fines. Post-test characterization of either the mini-candles or coupons will be conducted .

Based on the information obtained during PCFBC and IGCC testing, additional component or material improvements will be identified and discussed with the various candle filter suppliers. If available, modified elements will be resubjected to qualification testing in Westinghouse's PFBC simulator (Task 1), or included within the Piñon Pine mini-vessel (Task 3).

Acknowledgment

We wish to acknowledge Mr. Richard Dennis at DOE/METC for his guidance and technical support during conduct of this program which was initiated on September 15, 1994. In addition we wish to acknowledge Mr. Theodore McMahon, DOE/METC, Dr. Richard Tressler, The Pennsylvania State University, Dr. Jeffrey Chambers, Mr. George Forsythe, Mrs. Elizabeth Connolly, Dr. Al Fresco, and Dr. Paul Gray at the DuPont Lanxide Corporation, Mr. Edward Fischer and Mr. Joseph Eaton at 3M, and Mr. Paul Eggerstedt and Mr. Jim Zievers at IF&P for their involvement in the numerous candid discussions which have occurred since initiating effort

Table 11

Candidate Porous Ceramic Candle Filters and Material Coupons for Testing under IGCC Conditions

Mini-Filters	Coupons
Schumacher Dia Schumalith F40	DuPont SiC-SiC
Schumacher Dia Schumalith FT20	Ultramet CVI-SiC Reticulated Foam
Pall Vitropore 442T	Kaiser Carbon-Based Matrix
Pall 326	Kaiser Pyrolyzed Carbon-Nicalon
Coors P-100A-1 Alumina/Mullite	INEX Siliconized Silicon Carbide
3M CVI-SiC Composite	Textron Nitride Bonded Silicon Carbide
DuPont PRD-66	Textron Nitride Bonded Silicon Nitride
Pall Iron Aluminide	Triad Corporation Calcium Aluminosilicate
Blasch Alumina	Phoenix Oxide-Based Zirconate
Blasch Alumina/SiC	Corning Cordierite
3M Oxide-Based CFRCC	Scapa Aluminosilicate-Based Fibers
Techniweave Oxide-Based CFRCC	
B&W Oxide-Based CFRCC	

on this program. Finally we wish to acknowledge Mr. Reijo Kuivalainen, Mr. Juhani Isaksson, Mr. Timo Eriksson, and Mr. Pekka Lehtonen for conduct of the hot gas filtration testing at the Foster Wheeler PCFBC test facility in Karhula, Finland, and Mr. Richard Kunkle, Mr. Robert Walko, Mr. Thomas Mullen, Ms. Paula Freyer, Mr. George Schneider, Mr. Art Fellers, Mr. Joseph Condle, Mr. Anthony Gasparovic, and Mr. John Meyer for their participation in materials characterization, and corrosion and filter qualification testing at Westinghouse.

References

1. M. A. Alvin, T. E. Lippert, E. S. Diaz, and E. E. Smeltzer, “Thermal and Chemical Stability of Ceramic Candle Filter,” *Proceedings of the Advanced Coal-Fired Power Systems ‘95 Review Meeting*, 485-509, DOE/METC-95/1018.

2. M. A. Alvin, T. E. Lippert, E. S. Diaz, and E. E. Smeltzer, “Filter Component Assessment,” *Proceedings of the Advanced Coal-Fired Power Systems ‘95 Review Meeting*, 160-182, DOE/METC-95/1018.

3. M. A. Alvin, “Thermal/Chemical Degradation of Ceramic Cross Flow Filter Materials,” Final Report, Westinghouse Electric Corporation, DOE/METC Contract No. DE-AC-88M25034, to be issued.

4. M. A. Alvin, “Advanced Ceramic Materials for Use in High Temperature Particulate Removal Systems,” American Institute of Chemical Engineers Annual Meeting, Miami

Beach, FL, November 13, 1995. Paper to be issued in *Industrial and Engineering Chemistry Research.*

5. M. A. Alvin, E. E. Smeltzer, Z. N. Sanjana, J. P. Oberst, and T. E. Lippert, "Assessment of the DuPont Composite Matrix for Use in Hot Gas Filter Applications," Westinghouse Electric Corporation, DOE Cooperative Agreement No. DE-FC02-92CE40994, January 19, 1996.

6. M. A. Alvin, "Advanced Coal-Fired and Biomass Ash and Char Formations," 12th International Pittsburgh Coal Conference, Pittsburgh, PA, September 11-15, 1995.

Appendix A

Thermal Stress Modeling

Under simulated PFBC process conditions, Westinghouse monitored the temperature profile through various porous ceramic filter elements to determine the axial and radial temperature gradients that resulted along the entire length of the candle filter during pulse cleaning, or when a thermal transient event occurred. During pulse cycling, a maximum temperature drop of ~420°C (750°F) was shown to result along the inner surface of the filter body, near the mid-section of the element, 0.35 sec after delivery of the pulse. The extent of cooling of the filter matrix was limited to ~2 mm from the inner surface, similar to the area where circumferential cracking was observed after PCFBC and accelerated pulse cycle testing of the alumina/mullite candle filters. Within 5 sec after delivery of the pulse, the inner surface of the element returned to within ~30ºC (50°F) of the initial operating temperature (Figure A-1).

In order to reduce the impact of thermal stress induced along the inner surface of the filter elements, Westinghouse installs a fail-safe/regenerator device above each candle. During pulse cycling with the inclusion of the fail-safe/regenerator device, a maximum temperature drop of ~170°C (300°F) was shown to result along the mid-section of the filter element, 0.35 sec after delivery of the pulse.

The axial and radial temperature measurements generated along and through the P-100A-1 filter wall during pulse cycling were utilized to identify a corresponding stress intensity profile throughout the matrix via finite element modeling. Along the mid-section of the candle filter, the stress intensity was calculated to be ~10,000 psi, primarily within the first 0.5 mm from the inner surface of the candle, at 0.35 sec after delivery of the pulse. The stress intensity resulting from pulse cleaning exceeded the rupture modulus of the as-manufactured P-100A-1 alumina/mullite filter matrix (i.e., 2500-3000 psi). As a result of high stress in this area of the filter element, microcrack formations are likely to occur. With the inclusion of the fail-safe/regenerator device, stress intensities as high as 3600 psi were calculated within the first 1 mm along the inner surface of the candle, at 0.35 sec after initiation of the pulse cycle. Clearly the use of the fail-safe/regenerator device sufficiently heats the incoming pulse gas to the extent that thermal stress within the matrix approaches or is below the rupture modulus of the as-manufactured P-100A-1 alumina/mullite filter matrix. As a result, the formation of circumferential and/or radial microcracks along the inner surface of the filter element is expected to be mitigated.

Temperature gradients were also measured along the outer surface of the P-100A-1 alumina/mullite and clay bonded silicon carbide filter elements during simulated thermal transient testing. These measurements were utilized to project the temperature profile, hoop stress, and hoop strain through each filter wall. Using a simple axisymetric heat transfer model, the projected temperature through the wall as a function of time after transient initiation was shown to closely correspond to the temperature measurements from high-speed thermocouples that were embedded within the filter wall.

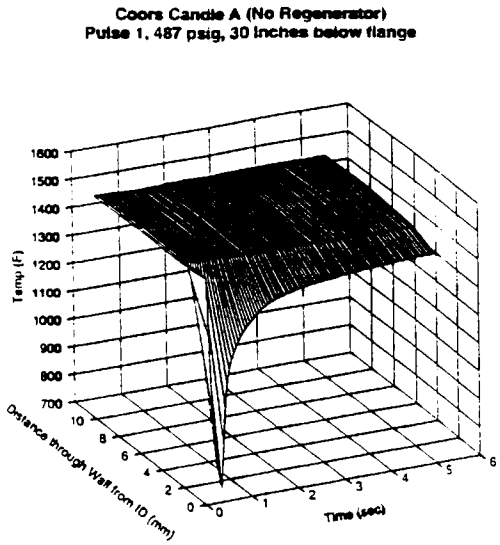

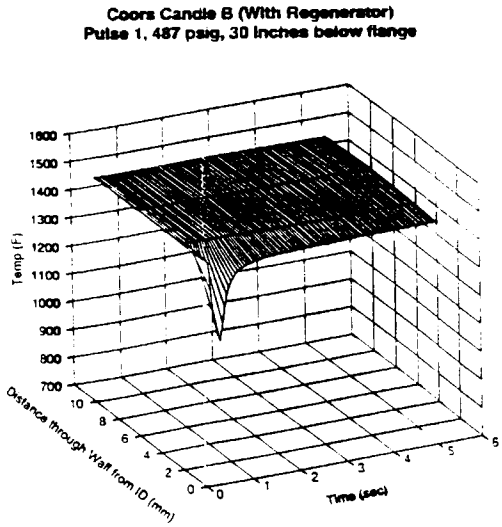

Figure A-1 — Axial and Radial Temperature Profile During Pulse Cycling of Porous Ceramic Candle Filters

During exposure to simulated maximum thermal transient conditions, the P-100A-1 alumina/mullite filter matrix maintained the original operating temperature along the inner surface of the filter element while the outer surface rapidly cooled (Figure A-2). Between 10 and 60 sec after initiation of the event, the projected maximum hoop stress along the outer surface of the candle approached the rupture modulus of the filter matrix. For process-aged materials which have reduced bulk strengths, the stresses resulting during transient testing would be sufficient to induce microcrack formations along the outer surface of the filter element. In

conjunction with thermal fatigue along the inner surface of the alumina/mullite filter matrix which results from pulse cycling without the inclusion of the fail-safe/regenerator, the matrix is expected to be highly susceptible to slow crack growth, particularly in the presence of steam. As a result subcritical crack extension may occur during thermal excursions, leading to failure of the filter element.

As shown in Figure A-3, a more suppressed temperature gradient resulted through the wall of the clay bonded silicon carbide filter elements in comparison to the P-100A-1 alumina/mullite candle filters during exposure to thermal transient conditions. A maximum stress of ~450 psi was projected along the outer surface of the clay bonded silicon carbide filter during exposure to a maximum severity thermal transient event. This is substantially lower than the 2500-3000 psi bulk strength of the as-manufactured clay bonded silicon carbide filter matrix.

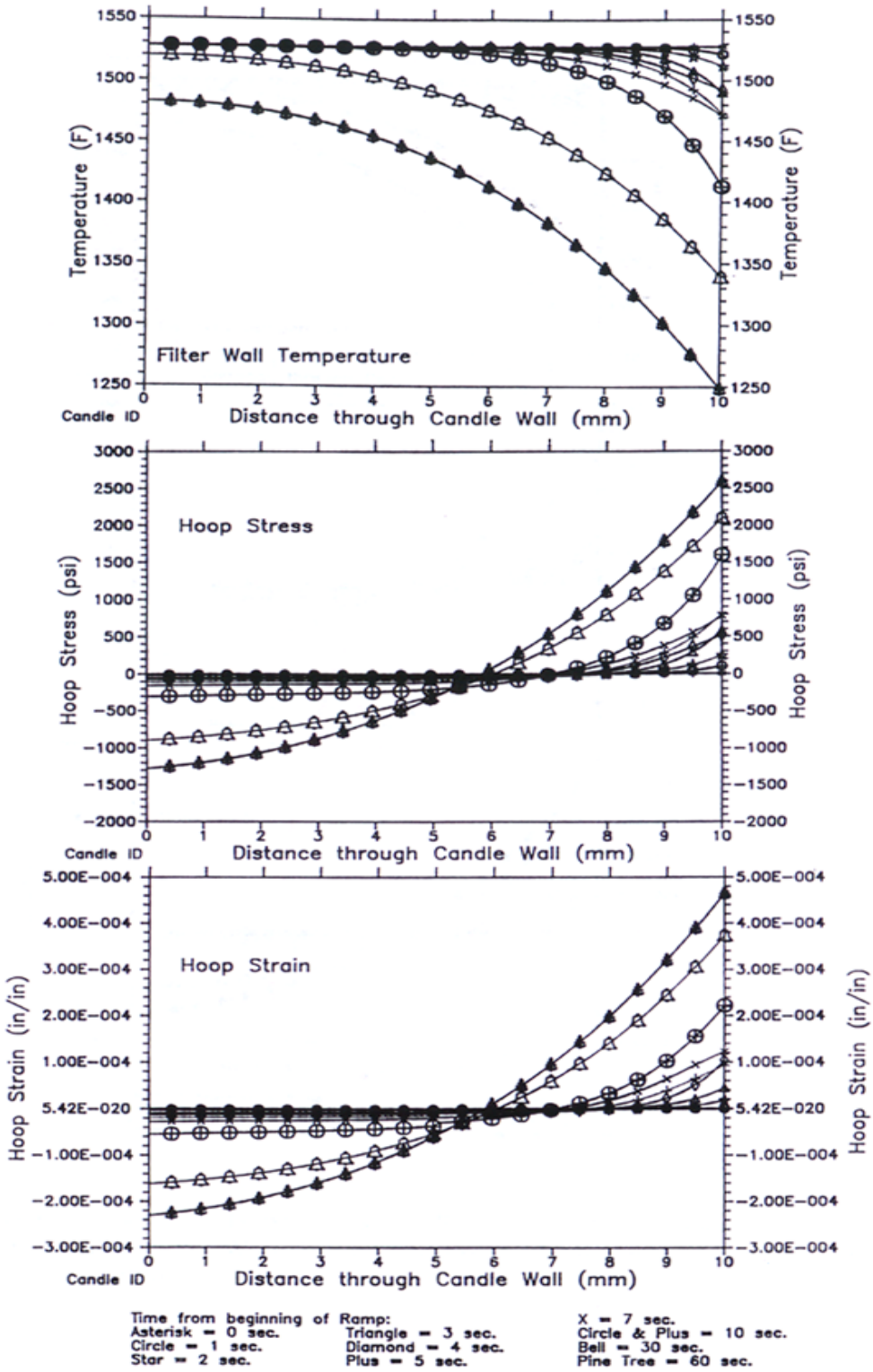

Figure A-2 — Projected Temperature, Hoop Stress, and Strain through the Coors P-100A-1 Alumina/Mullite Filter Wall during Exposure to Maximum Severity Thermal Transient Conditions

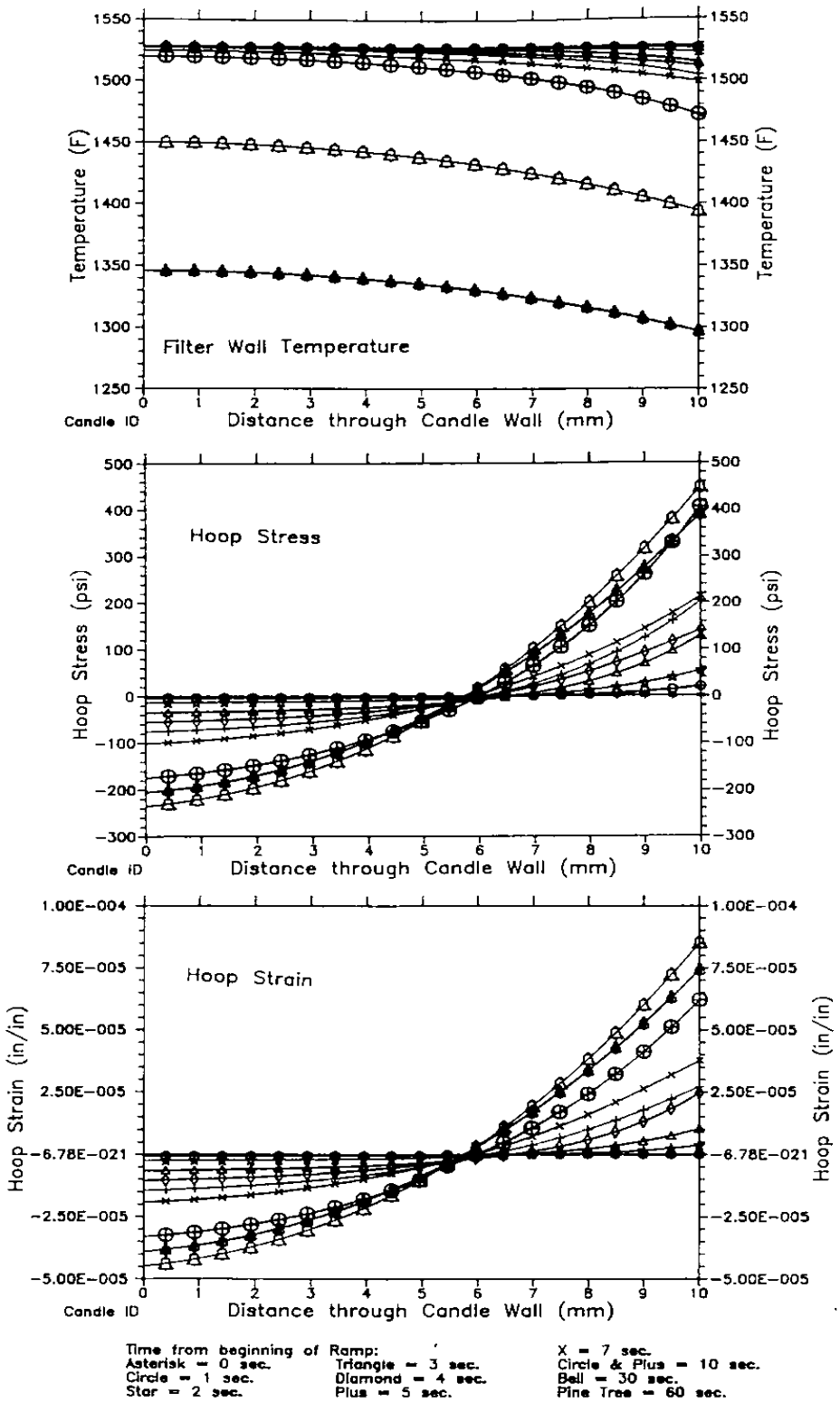

Figure A-3 — Projected Temperature, Hoop Stress, and Strain through the Pall Vitropore 442T Filter Wall during Exposure to Maximum Severity Thermal Transient Conditions

Properties of Ceramic Filters

Jack D. Spain (205-581-2323)
Southern Research Institute
P. O. Box 55305
Birmingham, Alabama 35255-5305

Introduction

The mechanical integrity of ceramic filter elements is a key issue for hot gas cleanup systems. To meet the demands of advanced power systems, the filter components sustain thermal stresses of normal operations (pulse cleaning), of start-up and shut-down, and of process upsets such as excessive ash accumulation without catastrophic failure. They must also survive various mechanical loads associated with handling and assembly, normal operation, and process upsets. For near-term filter systems, the elements must survive operating temperatures of 1650 °F for three years.

Schumacher F40, Refractron 442T, and Coors alumina mullite candle filters tested at American Electric Power's PFBC at the Tidd plant and the Ahlstrom-Pyropower PFBC in Karhula, Finland resulted in failure of some candles. Coors monolithic ceramic filters were susceptible to thermal stresses. Refractron 442T and Schumacher F40 filters showed substantial creep and degradation of the binder material. Test results obtained at SRI showed that microcracking due to thermal stresses generated during pulse cleaning could occur when the temperature drop on the I.D. of the candle is 100 °F to 200 °F. Tensile creep tests indicated that the clay-bonded materials began to creep at ~1400 °F. Degradation of mechanical properties was measured in clay-bonded materials after exposure in Tidd and Karhula.

New Schumacher and Refractron candle filters - Schumacher FT20 and Refractron 326 - have been tested at SRI. These materials have a different binder intended to decrease the creep rate. Axial tensile, hoop tensile, tensile creep, and thermal expansion properties of these materials are presented here. One Refractron 326, one Schumacher FT20, and one Coors alumina mullite candle filter were sent to SRI after ~540 hours in service at Karhula. Hoop tensile strength was measured on several rings taken from various axial locations on each used candle filter. Hoop tensile strengths of the used and as-manufactured candle filters were compared to evaluate strength degradation after 540 hours in service.

Research sponsored by the U.S. Department of Energy's Morgantown Energy Technology Center, under contract DE-AC-21-94MC31160 with Southern Research Institute, P.O.Box 55305, Birmingham, Alabama 35255-5305

Objectives

Objectives of the testing conducted at SRI were as follows:

1. Measure basic physical, mechanical, and thermal properties of candle filter materials and relate these properties to in-service performance.

2. Perform post-exposure testing of candle filter materials after service at Tidd and Karhula and compare post-exposure results to as-manufactured results to evaluate property degradation.

3. Based on measured properties and in-service performance, develop an understanding of material requirements for candle filter materials and help establish property goals.

4. Establish a test protocol for evaluation of candle filter materials.

Approach

Based on the hot gas cleanup conditions and the in-service performance of candle filters to date, several issues have been identified as critical issues for hot gas filter materials. Candle filters must posses sufficient mechanical strength to withstand handling and assembly and to withstand the weight and side loading due to pulse cleaning, start-up, and shut-down. Creep is an issue because ash accumulation has generated side loads leading to excessive creep in Schumacher FT20 and Refractron 326 materials. The materials must operate in the hot gas cleanup environment without excessive property degradation, and the candles must filter effectively. Some of these issues are not applicable to all materials. The materials received and tested to date at SRI and the critical issues for each material are summarized in Table 1.

Southern's approach is to measure basic material properties of candle filter materials and predict in-service performance based on the measured material properties. The properties measured address the critical issues discussed. For example, mechanical strength is addressed by the tensile and compressive strength while thermal stress susceptibility is addressed by measuring tensile stress-strain response and thermal expansion. A summary of critical material issues and Southern's methods for evaluation of each issue is given in Table 2.

Table 1

Summary of Critical Issues for Hot Gas Cleanup Filter Materials

Material	Mechanical Strength	Thermal Stress	Creep	Property Degradation	Filtration/ Pressure Drop
Clay-Bonded (Schumacher, Refractron)	X	X	X	X	X
Monolithic Ceramics (Coors)	X	X	X [1]	X	X
3M Composite	X	X	X		
Dupont/Lanxide PRD-66	X	X		X	X
Dupont/Lanxide Composite	X	X		X	X
Industrial Filter and Pump	X			X	X
Blasch	X	X		X	X

[1]Slow crack growth

Table 2

Critical Material Issues and Methods of Evaluation

Material Issue	Methods for Evaluation
Mechanical Strength, "Toughness"	Tensile Strength Compressive Strength Fracture Toughness
Thermal Stress Susceptibility	Tensile Stress-Strain Curve Thermal Expansion
Creep	Tensile Creep/Heat Deflection
Property Degradation	Tensile Stress-Strain After Exposure Ring Tensile After Exposure Microstructure
Filtration/Pressure Drop	Permeability

Test results presented in this paper are for Schumacher FT20 and Refractron 326 materials. The test matrix used to evaluate these two materials is given in Table 3.

Table 3

Test Matrix for Refractron 326 and Schumacher FT20 Candle Filter Materials

Test Type	Orientation	RT	1600 °F	1700 °F	1800 °F
Tensile	Hoop	9			
	Axial	4	4	4	4
Tensile Creep	Axial		4	4	
Thermal Expansion	Hoop	2	---------->		
	Axial	2	---------->		

Results

Schumacher FT20

Tensile results measured for Schumacher FT20 are plotted versus temperature in Figures 1 - 3. Tensile properties previously reported for Schumacher F40 are included in these figures for comparison. Figure 1 shows an average axial tensile strength for Schumacher FT20 of ~600 psi at room temperature increasing to a maximum value of ~1340 psi at 1600 °F. Schumacher F40 had an average axial tensile strength of ~1120 psi at room temperature increasing to a maximum value of ~1360 psi at 1500 °F. These results indicate that Schumacher FT20 has a reduced room temperature tensile strength; however, in the operating range the strength is near the same for FT20 and F40 materials. Schumacher FT20 had an average room temperature hoop tensile strength of ~1690 psi. Figure 2 shows that the average value of Young's modulus of FT20 decreased with temperature from ~4.0×10^{6} psi at room temperature to ~2.2×10^{6} psi at 1600°F. Figure 3 shows that the tensile strain-to-failure of FT20 increased with temperature from ~0.00016 in/in at room temperature to ~0.00073 in/in at 1600 °F and ~0.0013 in/in at 1700 °F. Only one value of strain-to-failure was obtained at 1600 °F and 1700 °F. Additional results are needed at these test temperatures to confirm that these results are typical. Strain-to-failure results were near the same for FT20 and F40.

Unit thermal expansion of Schumacher FT20 and F40 are plotted in Figure 4. The thermal expansion curve of FT20 had a "kink" at ~400 °F which was not seen for F40. This kink in thermal expansion has been seen in other ceramics tested at SRI in the past and is probably due to the new binder used. From ~500 °F up, the shape of the

thermal expansion curves for FT20 and F40 was the same. Therefore, the coefficient of thermal expansion (CTE) in the operating range is the same. Figure 4 shows graphically the relationship between strain-to-failure and thermal expansion. The strain-to-failure measured at 1600 °F for FT20 is shown along with the temperature drop on the I.D. of a candle filter operating at this temperature which would cause this strain. This temperature drop does not take the cylindrical geometry into account. Based on the measured properties and the dimensions of Schumacher candle filters, a temperature drop of ~250 °F was calculated to cause microcracking in FT20 filters. For F40 filters, a temperature drop on the I.D. of the candle of ~180 °F was calculated to cause microcracking.

Room temperature hoop tensile strength was measured on nine Schumacher FT20 specimens after ~540 hours in-service at Karhula. Hoop tensile strength values of as-manufactured and post-exposure FT20 specimens are compared in Figure 5. This graph compared both the tensile strengths and the strength distributions. After ~540 hours in-service at Karhula, the average hoop tensile strength was decreased by ~9% from 1690 psi to 1530 psi. Post-exposure testing of previous clay-bonded SiC materials indicated that most of the strength degradation occurred rapidly and then the strength leveled off. Testing of the FT20 material after different exposure durations is needed to determine if the tensile strength would degrade further with longer exposure.

Creep testing of Schumacher FT20 is summarized in Figure 6. At 1600 °F and an axial tensile stress of 500 psi, the secondary creep rate was ~6.4×10^{-9} in/in/sec. Figure 6 shows the initial creep rates of specimens Creep-ax-2 and Creep-ax-7 were different; however, the secondary creep rates appear near the same. After ~117 hours at 1600 °F, specimen Creep-ax-7 was heated to 1700 °F with the same 500 psi tensile stress applied. The specimen then broke after ~17 hours. Creep rates of FT20 and F40 are compared graphically, along with creep rates for the Refractron materials, in Figure 7. Creep rates are compared by comparing glass/binder viscosity. Glass/binder viscosity is calculated from

$$\mu = \sigma_{binder} / 3\varepsilon_{binder}$$

where, μ = glass/binder viscosity
σ_{binder} = stress in glass/binder
ε_{binder} = strain rate in glass/binder

From microstructural models developed for Schumacher F40, stress and strain in the glass are related to average body stress and strain by

$$\sigma_{binder} = 17\sigma_{avg.}$$

and $$\varepsilon_{binder} = 50\varepsilon_{avg.}$$

Microstructural models have not yet been developed for FT20 so the models for F40 were applied to this material also. Although this calculation does not give an accurate value for binder viscosity in Schumacher FT20, it does serve to provide a comparison of creep rates for FT20 and F40 materials. Figure 7 indicates that the creep rate of Schumacher FT20 is 1 to 2 orders of magnitude less than the creep rate of F40.

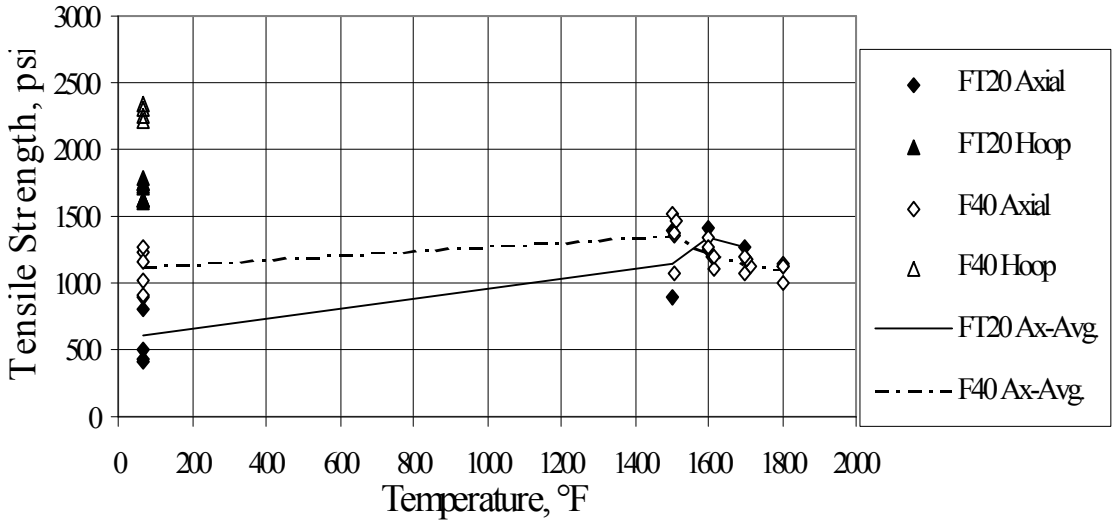

Figure 1. Ultimate Tensile Strength Versus Temperature for Schumacher FT20 and F40 Materials

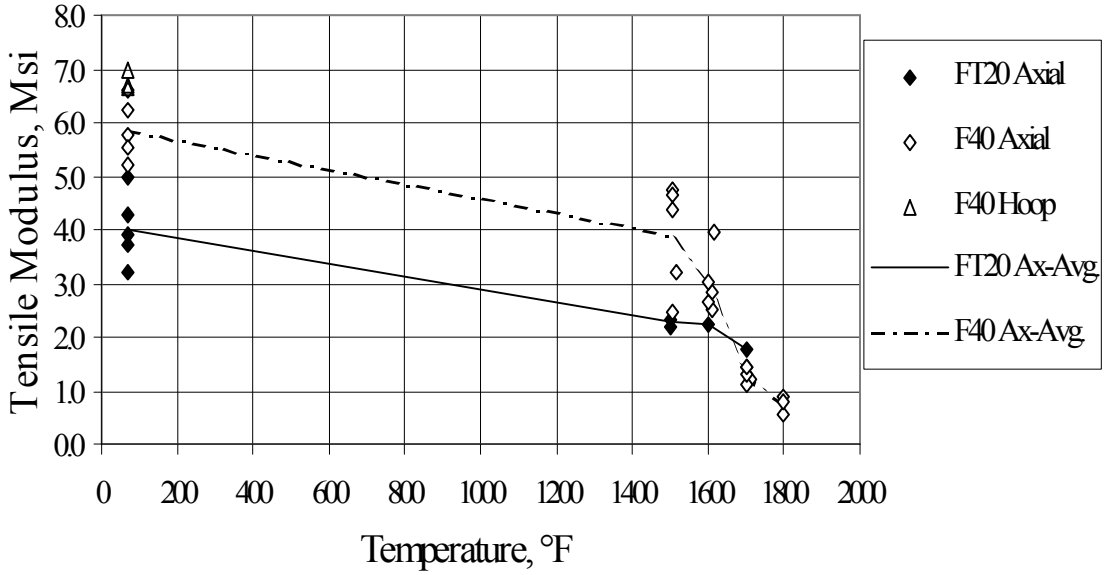

Figure 2. Young's Modulus Versus Temperature for Schumacher FT20 and F40 Materials

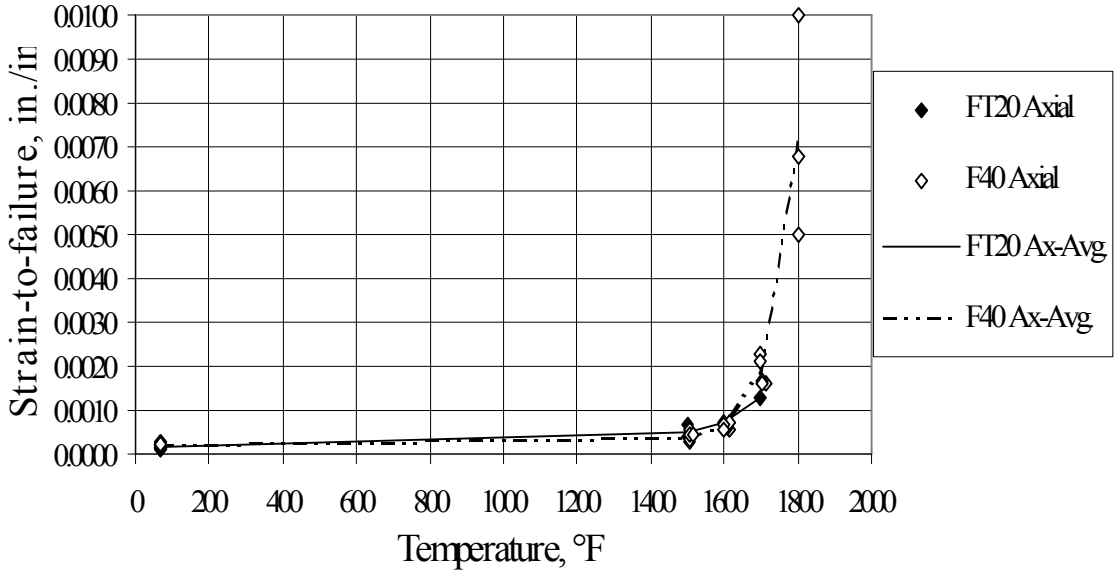

Figure 3. Tensile Strain-to-Failure Versus Temperature for Schumacher FT20 and F40 Materials

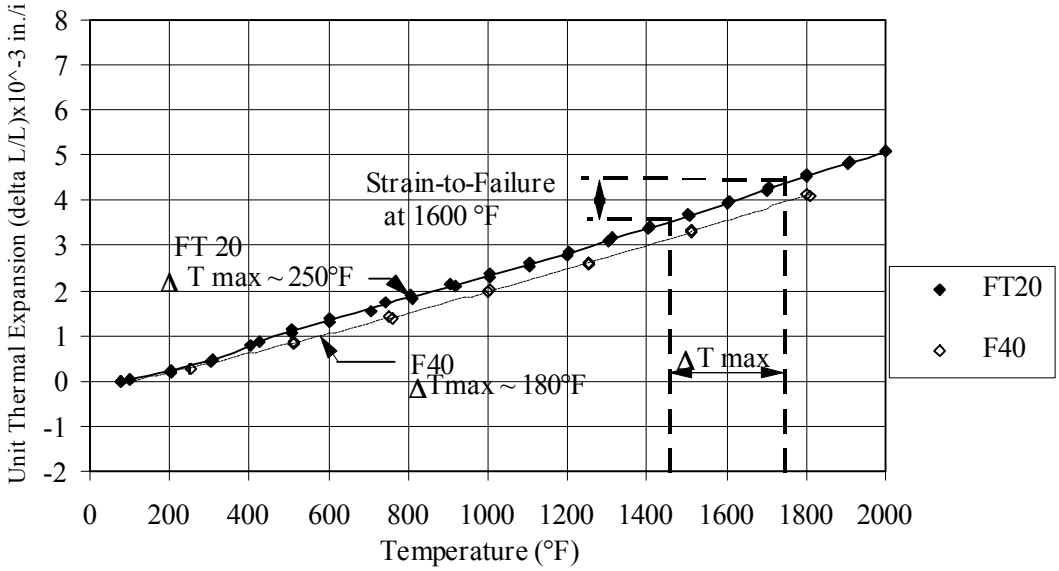

Figure 4. Unit Thermal Expansion of Schumacher FT20 and F40 Materials

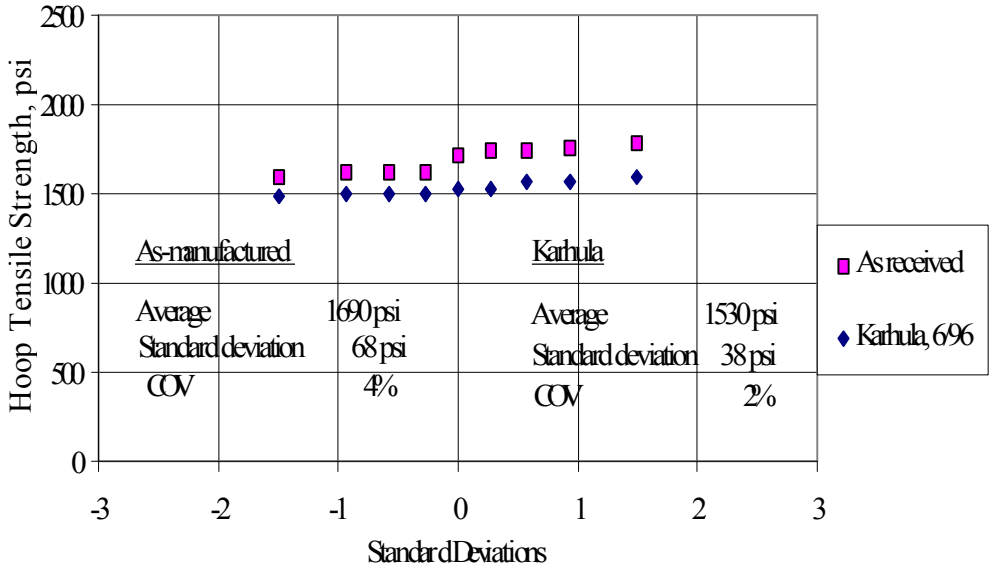

Figure 5. Hoop Tensile Strength Distribution for As-Manufactured and Used Schumacher FT20

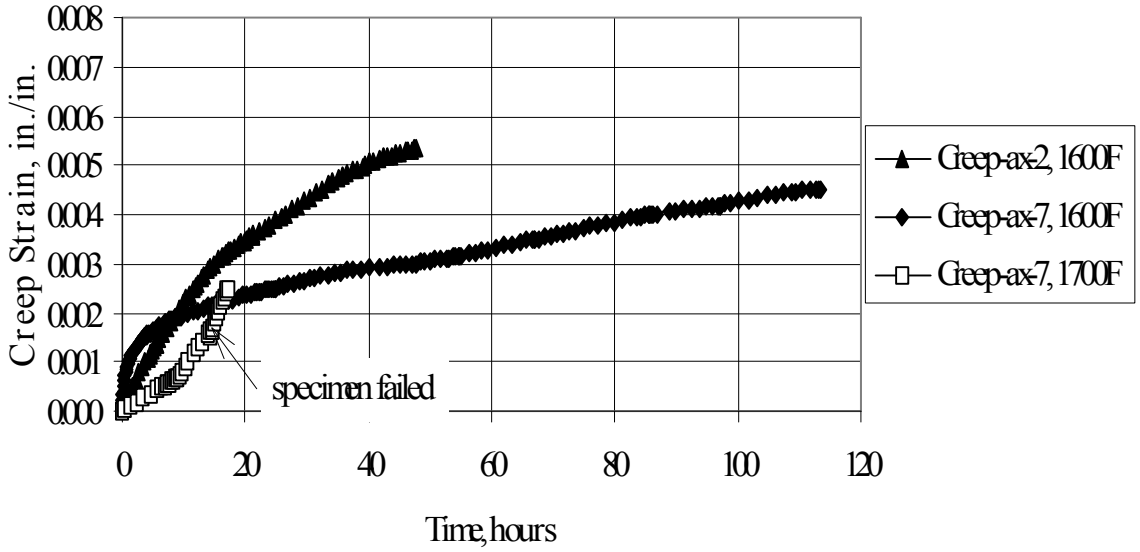

Figure 6. Creep Strain Versus Time for Schumacher FT20 at 1600 °F and 1700 °F, 500 psi

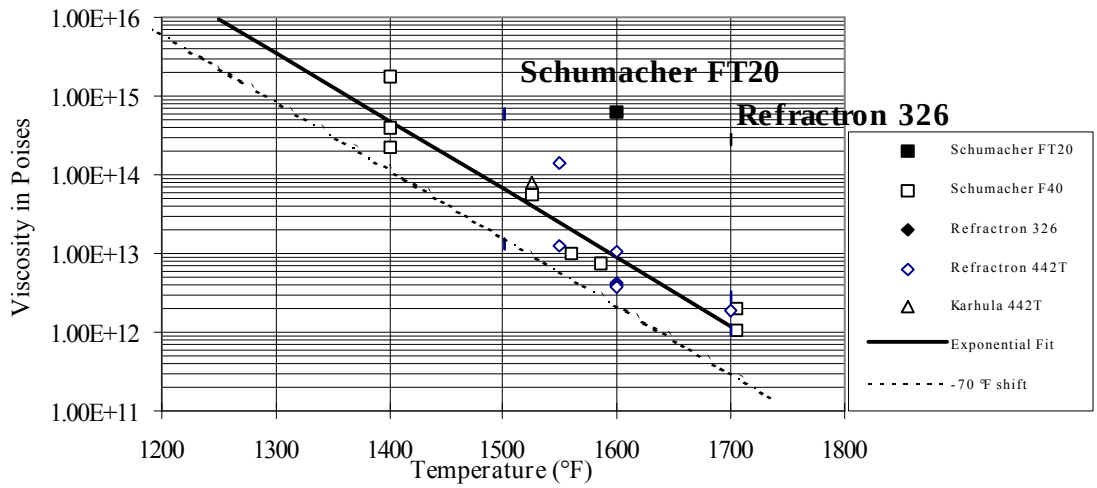

Figure 7. Glass Viscosity Versus Temperature for Schumacher and Refractron Candle Filter Materials

Refractron 326

Tensile results measured for Refractron 326 are plotted versus temperature in Figures 8 - 10. Tensile properties previously for Refractron 442T are included in these figures for comparison. Figure 8 shows an average axial tensile strength for Refractron 326 of ~1200 psi at room temperature increasing to a maximum value of ~1600 psi at 1600 °F. Additional testing at 1400 °F or 1500 °F is needed to determine whether the strength values obtained at 1600 °F represent the maximum strength of this material or if the maximum strength is at some lower temperature. Refractron 442T had an average axial tensile strength of ~2000 psi at room temperature decreasing to ~1430 psi at 1600 °F. These results indicate that Refractron 326 has a reduced room temperature tensile strength; however, in the operating range the strength is near the same for 326 and 442T materials. Refractron 326 had an average room temperature hoop tensile strength of ~2130 psi. Figure 9 shows that the average value of Young's modulus of Refractron 326 decreased with temperature from ~5.6 x 10^{6} psi at room temperature to ~2.4 x 10^{6} psi at 1600 °F. Figure 10 shows that the tensile strain-to-failure of Refractron 326 increased with temperature from ~0.00020 in/in at room temperature to ~0.00165 in/in at 1600 °F and then decreased to ~0.00050 in/in at 1800 °F. The decrease in strain-to-failure from 1600 °F to 1800 °F is different from any other clay-bonded SiC materials tested thus far. No reason for this decrease has been determined. This figure again shows the need for tensile measurements at ~1400 °F or 1500 °F to determine whether the strain-to-failure of 0.00165 in/in at 1600 °F is the maximum value or if the maximum value occurs at some lower temperature.

Unit thermal expansion of Refractron 326 and 442T are plotted in Figure 11. The thermal expansion curve of 326 had a "kink" at ~400 °F, similar to Schumacher FT20. This kink is probably due to the new binder used. From ~500 °F up, the shape of the thermal expansion curves for 326 and 442T was the same. Therefore, the CTE of

Refractron 326 and 442T at the operating temperature are near the same. Figure 4 shows graphically the relationship between strain-to-failure and thermal expansion. The strain-to-failure measured at 1600 °F for 326 is shown along with the temperature drop on the I.D. of a candle filter operating at this temperature which would cause this strain. This temperature drop does not take the cylindrical geometry into account. Based on the measured properties and the dimensions of Refractron candle filters, a temperature drop of ~320 °F was calculated to cause microcracking in 326 filters. For 442T filters, a temperature drop on the I.D. of the candle of ~180 °F was calculated to cause microcracking. Note that the temperature drop to cause microcracking was calculated based on the measured thermal expansion at 1600 °F. Because strain-to-failure is changing rapidly with temperature in this range, the temperature drop to cause microcracking is also changing rapidly. When strain-to-failure is measured at some intermediate temperature, probably 1500 °F, the temperature drop calculated to cause microcracking may be more than or less than 320 °F.

Room temperature hoop tensile strength was measured on nine Refractron 326 specimens after ~540 hours in-service at Karhula. Hoop tensile strength values of as-manufactured and post-exposure 326 specimens are compared in Figure 12. This graph compares both the tensile strengths and the strength distributions. After ~540 hours in-service at Karhula, the average hoop tensile strength decreased by ~33% from 2130 psi to 1430 psi. Testing of the 326 material after different exposure durations is needed to determine if the tensile strength would degrade further with longer exposure.

Creep testing of Refractron 326 is summarized in Figure 13. One specimen tested at 1600 °F and an axial tensile stress of 500 psi had a secondary creep rate was ~8.6 x 10^{-9} in/in/sec. Testing of a second specimen at 1700 °F and 500 psi was stopped after ~17 hours because of heater failure. Creep strain measured over 17 hours for this specimen is plotted in Figure 12 and is similar to the initial creep strain rate measured at 1600 °F. Re-testing of this specimen has begun and is still in progress. Creep rates measured for Refractron 326 and 442T are compared graphically, along with creep rates for the Schumacher materials, in Figure 7. As discussed previously, creep rates are compared by comparing glass/binder viscosity where binder viscosity is calculated from

$$\mu = \sigma_{binder}/3\varepsilon_{binder}$$

From microstructural models developed for Refractron 442T, stress and strain in the glass/binder are related to average body stress and strain by

$$\sigma_{binder} = 14\sigma_{avg.}$$

and

$$\varepsilon_{binder} = 65\varepsilon_{avg.}$$

Microstructural models have not yet been developed for 326 so the models for 442T were applied to this material also. Although this calculation does not give an accurate

value for binder viscosity in Refractron 326, it does serve to provide a comparison of creep rates for 326 and 442T materials. Figure 7 indicates that the creep rate of Refractron 326 is ~2 orders of magnitude less than the creep rate of 442T.

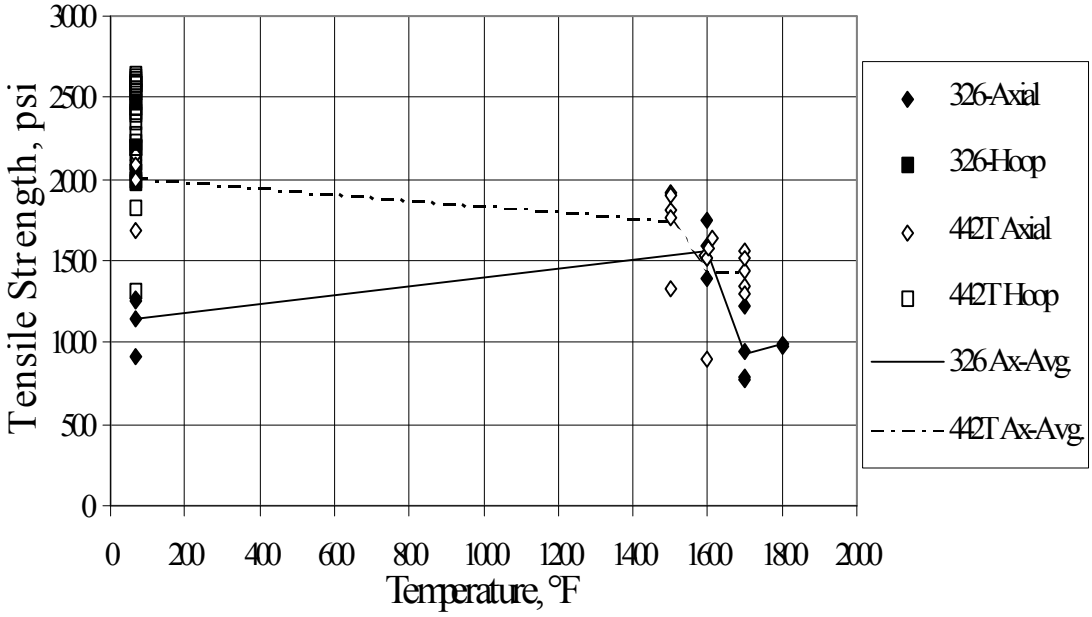

Figure 8. Ultimate Tensile Strength Versus Temperature for Refractron 326 and 442T Materials

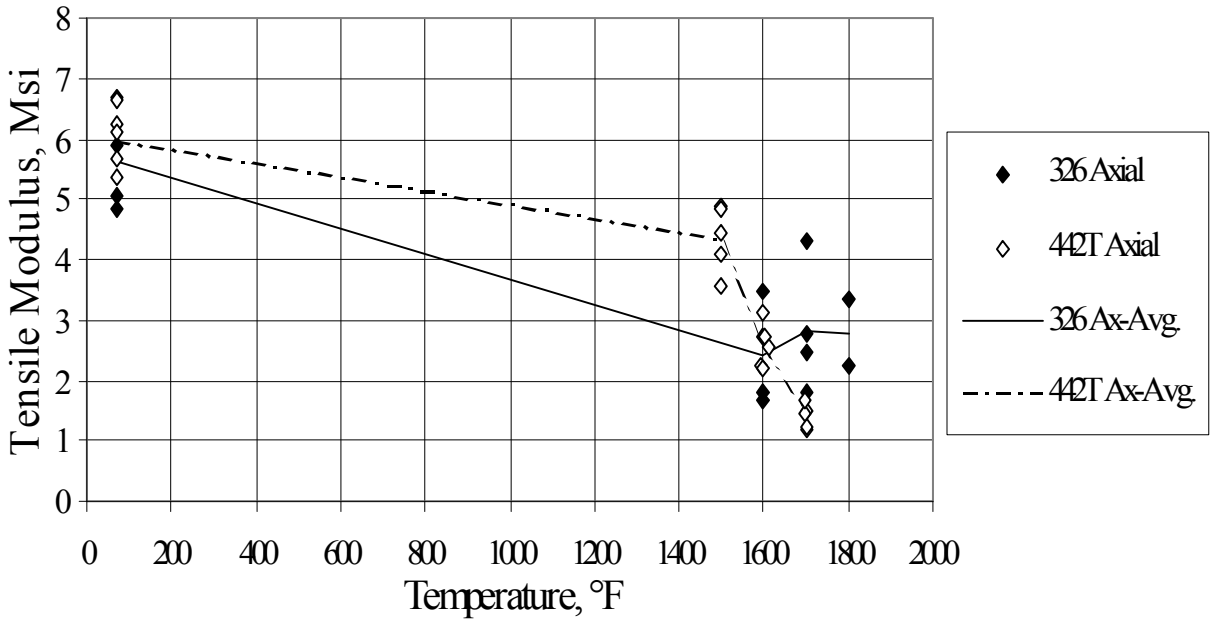

Figure 9. Young's Modulus Versus Temperature for Refractron 326 and 442T Materials

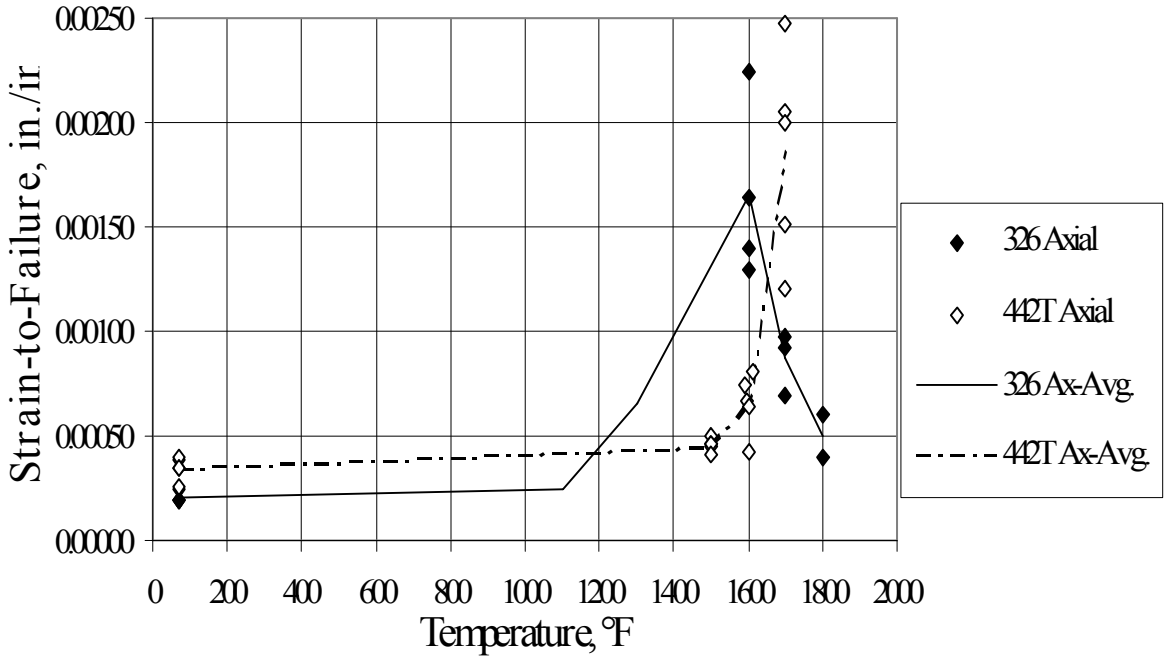

Figure 10. Strain-to-Failure Versus Temperature for Refractron 326 and 442T Materials

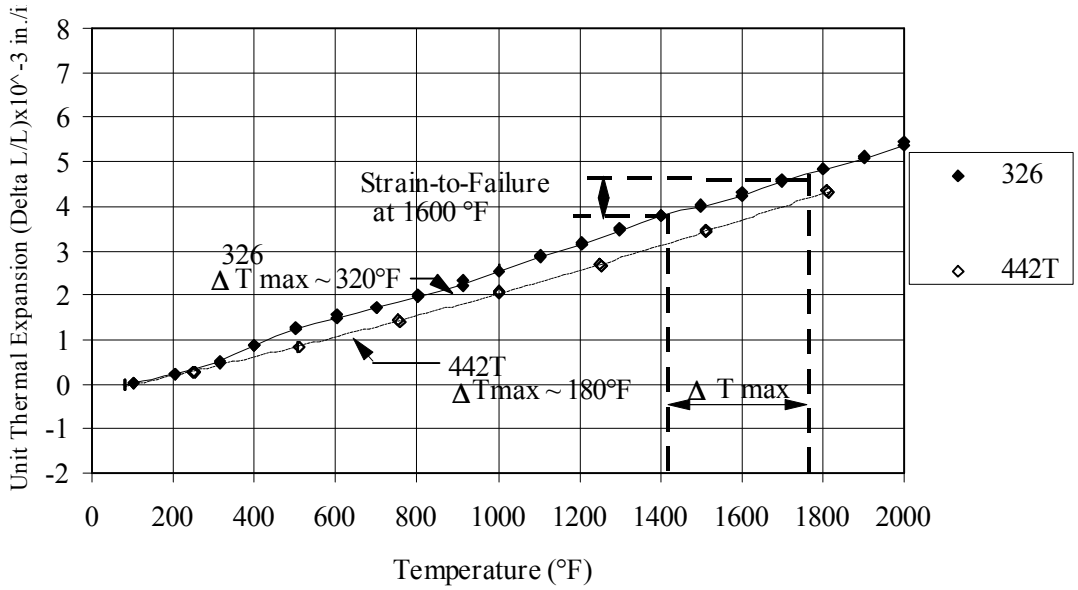

Figure 11. Unit Thermal Expansion of Refractron 326 and 442T Materials

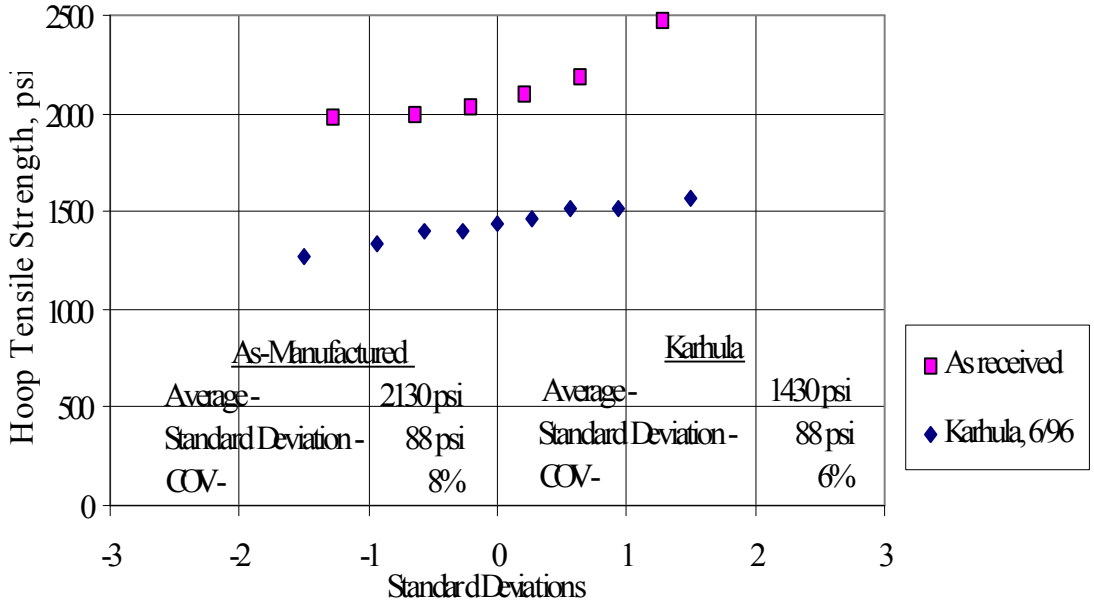

Figure 12. Room Temperature Hoop Tensile Strength Distribution for As-Manufactured and Post-Exposure Refractron 326 Material

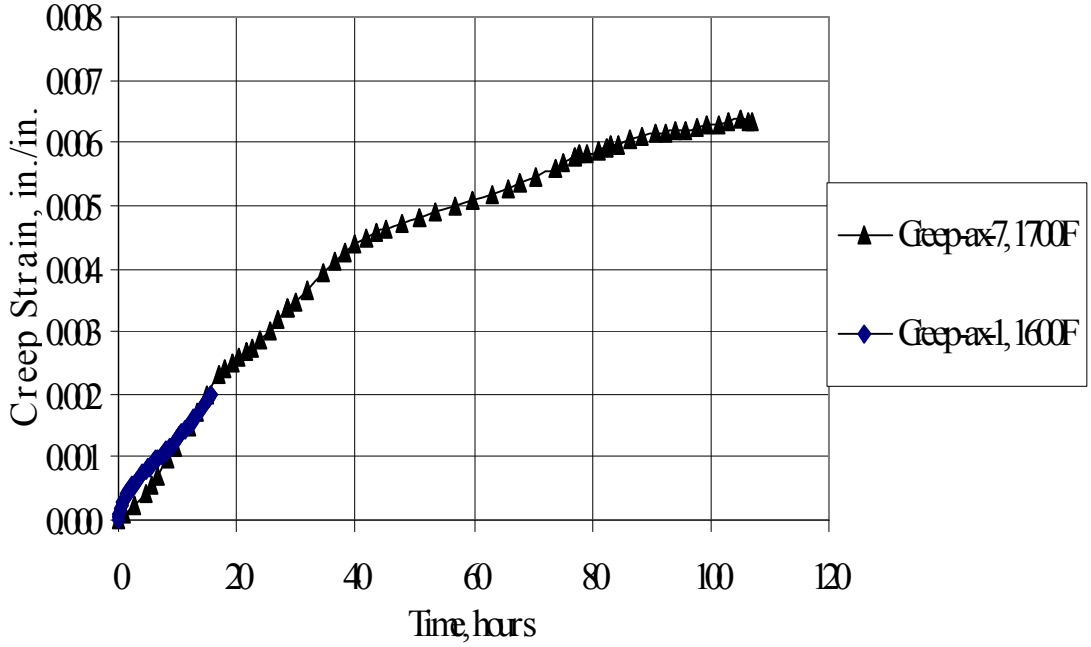

Figure 13. Creep Strain Versus Time for Refractron 326 at 1600 °F and 1700 °F, 500 psi

Based on the properties measured, the following conclusions were obtained :

1. Schumacher FT20 and Refractron 326 materials have lower room temperature strengths than Schumacher F40 and Refractron 442T. In the operating range, the strength difference is small.

2. For Schumacher FT20 at an operating temperature of 1600 °F, thermal stress microcracking is likely to occur for $\Delta T \cong 250$ °F. For Schumacher F40, $\Delta T \cong 180$ °F would likely cause microcracking.

3. For Refractron 326 at an operating temperature of 1600 °F, thermal stress microcracking is likely to occur for $\Delta T \cong 320$ °F. For Refractron 442T, $\Delta T \cong 180$ °F would likely cause microcracking.

4. The average room temperature hoop tensile strength of Schumacher FT20 decreased ~9% from 1690 psi to 1530 psi after ~540 hours in-service at Karhula.

5. The average room temperature hoop tensile strength of Refractron 326 decreased ~33% from 2130 psi to 1430 psi after ~540 hours in-service at Karhula.

Future Activities

Microstructural evaluations of Schumacher FT20 and Refractron 326 are needed to model the creep response of these materials. Microstructural evaluations of Schumacher F40 and Refractron 442T provided the models of creep in these materials as flow of the binder and allowed calculations of glass viscosities and prediction of creep rates for various temperature and stress levels. Similar studies of FT20 and 442T materials are in progress. Microstructures of as-manufactured material and post-exposure material will be compared to determine the mechanisms and degree of degradation suffered in-service.

Post-exposure hoop tensile testing after some service times other than 540 hours are needed to determine whether the degradation suffered at Karhula would continue with longer service durations. For Schumacher F40 and Refractron 442T, most of the property degradation occurred in the first few hours. The properties of Schumacher F40 and Refractron may or may not degrade further with service durations greater than 540 hours.

Axial tensile testing of Refractron 326 is needed at ~1500 °F because the properties are changing rapidly with temperature in this range. The maximum tensile strength and strain-to-failure measured were at 1600 °F; however, the maximum values for may occur at a lower temperature. Testing at ~1500 °F is needed to define the properties within the operating range.

Acknowledgments -

We wish to acknowledge Mr. Theodore J. McMahon, METC Contracting Officer Representative for this project, and Mr. Richard Dennis of METC for technical support during this program. The contract period of performance is October 1, 1994 to September 30, 1998.

Simultaneous Hot Gas Desulfurization and Improved Filtration

Paul M. Eggerstedt (ifpco@interaccess.com; 708-656-7800)
James F. Zievers (ifpco@interaccess.com; 708-656-7800)
Parul C. Patel (ifpco@interaccess.com; 708-656-7800)
Industrial Filter & Pump Mfg. Co.
5900 Ogden Avenue
Cicero, IL 60650

Elizabeth C. Zievers (708-354-5757)
Universal Porosics, Inc.
1240 Carriage Lane
La Grange, IL 60525

Introduction

Although the United States has some of the greatest coal reserves in the world, much of it will remain unusable until technology is developed to meet both Clean Air Act mandates and New Source Performance Standards (NSPS) for particulate, SO_2, and NO_x emissions effectively and economically. Recent breakthroughs in particulate control, specifically ceramic filtration technology, have shown that NSPS limits on particulates can be achieved at high process temperatures, thereby minimizing thermal losses and system complexity. While both calcium based and regenerable metal oxide sorbents are currently utilized for sulfur mitigation, problems such as sintering, temperature limitations, physical attrition, and cost have limited their success.

This research suggests the use of waste metal oxide materials for the removal of sulfur in hot gas streams as an alternative to either traditional calcium based sorbents, or regenerable metal oxide sorbents. When classified to a desired particle size and injected into a high temperature coal utilization process, such a "once-through" sorbent can effectively remove sulfur and simultaneously increase the permeability of dust collected at a downstream ceramic filter station in a highly cost effective manner.

There is considerable technical and economic promise in the use of waste metal oxides for the removal of sulfur dioxide (SO_2) and hydrogen sulfide (H_2S) from coal gas streams containing these components, based upon results from tests under controlled laboratory conditions. Several waste metal oxides, including the oxides of iron, tin, and zinc, have been evaluated both individually and in combination to assess their capacity for sulfur capture in both oxidizing and reducing atmospheres. Additionally, inert materials such as silica sand as well as more traditional materials such as dolomite and limestone, were evaluated as sorbents under identical test conditions to serve as reference data. Efforts also explored the overall domestic availability

---

Research sponsored by the U.S. Department of Energy's Morgantown Energy Technology Center, under contract DE-FG02-94ER81786 with Industrial Filter & Pump Mfg. Co., 5900 Ogden Avenue, Cicero, IL 60650; telefax: 708-656-7806.

of the best performing waste metal oxide sorbents, taking into account their geographic distributions, intrinsic value, etc. to provide the groundwork for commercial implementation of a low cost, highly effective sulfur sorbent for eventual use in both coal combustion and coal gasification processes. Recent elevated temperature thermogravimetric analysis (TGA) testing of these samples, performed at the Institute of Gas Technology (IGT), has further confirmed the trends in sulfur affinity which were observed in the preliminary testing. In that all of the sorbent samples tested were of an identical, carefully selected particle size, the data collected will serve as the basis for future research efforts which will additionally evaluate these waste metal sorbents as a means of increasing or maintaining the permeability of the dust collected on downstream particulate control devices, such as ceramic filters.

Objectives

The primary goal associated with this research is to promote the dual use of waste metal oxides as sorbents and filter aid additives in gas streams requiring both desulfurization and enhanced particle removal efficiency at elevated temperatures.

Specific goals related to this project include the following:

- Determination of the most prevalent types of domestically available waste metal oxides and evaluate their current and future availability, geographic distribution, purity, and intrinsic value;

- Assessment of the potential reactivity of several waste metal oxides with sulfur in both oxidizing and reducing atmospheres;

- Performance of a series of ambient laboratory screening tests to ascertain the affinity for sulfur, by way of chemisorption, of the waste metal oxides in both oxidizing and mildly reducing atmospheres, and compare these data with similar tests involving non-reactive materials and calcium-based sorbents;

- Performance of a series of TGA tests on the more promising waste metal oxides, in both oxidizing and reducing atmospheres, to determine their activities and capacities in comparative sulfation and sulfidation tests at several elevated temperatures;

- Performance of a series of packed bed reactor tests on the most promising waste metal oxides, in both oxidizing and reducing atmospheres, to further validate their desulfurization capacity in simulated fuel and flue gas conditions;

- Assessment of the most promising waste metal oxide materials as high temperature additives for improved filtration in a ceramic candle filter station at elevated temperature.

Upon completion of the above objectives, efforts will be made for implementation of this technology within the private sector.

Approach

In recent years, ceramic filtration devices have shown that particle removal levels well within New Source Performance Standards (NSPS) limitations can be achieved at high temperature, thereby improving the efficiency and overall performance of processes such as Integrated Gasification Combined Cycle (IGCC) and Pressurized Fluidized Bed Combustion (PFBC). Unfortunately, removal of the high levels of sulfur indigenous to much of America's coal reserves has been problematic, requiring exotic (and expensive) sorbents, substantial coal feed pretreatment, or a reduction in off-gas temperature to obtain acceptable sulfur emissions.

Many researchers are aware that metal oxide sorbents can be used to effectively reduce sulfur emissions in such processes. However, because of the high cost of most metal oxides, especially such materials as zinc titanate and zinc ferrite, economic studies have shown that for such materials to be cost effective they must be used, regenerated, and reused as many as several hundred times[1] before a return on investment is realized. Additionally, preliminary testing of such sorbents in a pelletized bed configuration, which lends itself to such a regenerative process, has shown that the strength of the pelletized metal sorbent can significantly decrease in as few as five six regenerative cycles. In view of this, it is apparent that a "once through", non-regenerable metal oxide sorbent can be a much more attractive solution from the standpoints of capacity, overall sulfur removal efficiency, and process economics, particularly if a low cost (or no cost) source of sorbent is readily available. Moreover, in combination with ceramic filtration technology, the use of such a sorbent becomes even more practical in that the sorbent can be introduced well upstream of a ceramic filter station, have sufficient residence time for sulfur removal to take place, and then be easily collected on the surface of the filter, along with the ash and other particulate. By properly classifying and sizing the waste metal oxide sorbent particles, the permeability of the dust accumulating on the filter surface can be enhanced, resulting in lower pressure differentials, better pulse cleaning efficiency, and less susceptibility to filter pore "blinding".

The test results reported herein show that significant sulfur removal capacities can be achieved using classified, spent metal oxides. Such materials are generated in tremendous volume as a result of metal processing, smelting, and refining operations, and are generally available for little if any cost.

Project Description

Preliminary Tests

Preliminary tests involved the assessment of the sulfur affinity of waste metal oxides under controlled laboratory conditions by exposing a prepared bed of each material to sulfur dioxide (SO_2) and hydrogen sulfide (H_2S), in separate trials. The testing was performed at the Research & Development Department of Industrial Filter & Pump Mfg. Co., Inc. The waste metal oxides tested are listed in Table 1 which follows:

Table 1. Waste Metal Oxides Evaluated in Preliminary Test Series

Sorbent	Source
Iron oxide	Basic Oxygen Furnace (BOF)
Zinc oxide	Chicago area zinc smelter
Zinc oxide	2nd Chicago area zinc smelter
Tin oxide	Chicago area tin refiner
Zinc/iron/lead oxide mixture	Chicago area smelter

Although waste copper oxide was readily available and considered as yet another material suitable for testing, it was decided that since many waste copper oxide sources contain significant amounts of arsenic, no testing of this material would be undertaken for safety reasons.

In addition to the testing of the above waste metal oxides, test trials were performed without any sorbents, with commercially available dolomite and limestone, and with inert or moderately inert sorbents, such as silica sand and diatomaceous earth, for reference purposes.

In all of the above test scenarios, the flowrate of the SO_2 or H_2S gas and nitrogen carrier gas, which was used as a diluent to the SO_2 or H_2S, was held constant. Likewise, the sample volume and temperature for each test were maintained constant. By bubbling the effluent gas through analyzed collection water, the elapsed time required to depress the pH of the collection water was recorded and indicated the end point of sulfur removal for each sample being tested. Table 2 below shows the preliminary test series conditions; Figure 1 schematically depicts the test apparatus used in the research effort. By plotting the reduction in collection water pH as a function of time for each sample tested, a series of "break through" curves were generated and proved useful in directly comparing the sulfur affinity of each material.

Table 2. Preliminary Test Series: Test Conditions

Test Temperature:	Ambient
Test Pressure:	3 psig
Sample Size:	50 cm^3
SO_2 or H_2S Gas Flowrate:	38 cm^3/min
N_2 Carrier Gas Flowrate:	82 cm^3/min
Sample Particle Size:	75-106 micron; 90 micron average
pH Endpoint:	5.00 (SO_2); 6.5 (H_2S)

Initial "shakedown" trials involving nitrogen carrier gas and either SO_2 or H_2S, without a test sample bed, were conducted to determine the time delay (due to piping lengths and volumes) from the onset of the test until pH depression in the collection beaker.

Both the effect on pH of the nitrogen carrier gas as well as the "time delay" associated with the internal volume of the test apparatus were used in the final data analysis. All tests involving sample test beds were conducted in an identical fashion. Test samples were prepared by drying in an air-circulated oven, after which the weight of the sample stabilized, indicating the removal of any moisture present. The samples then underwent particle size classification using a

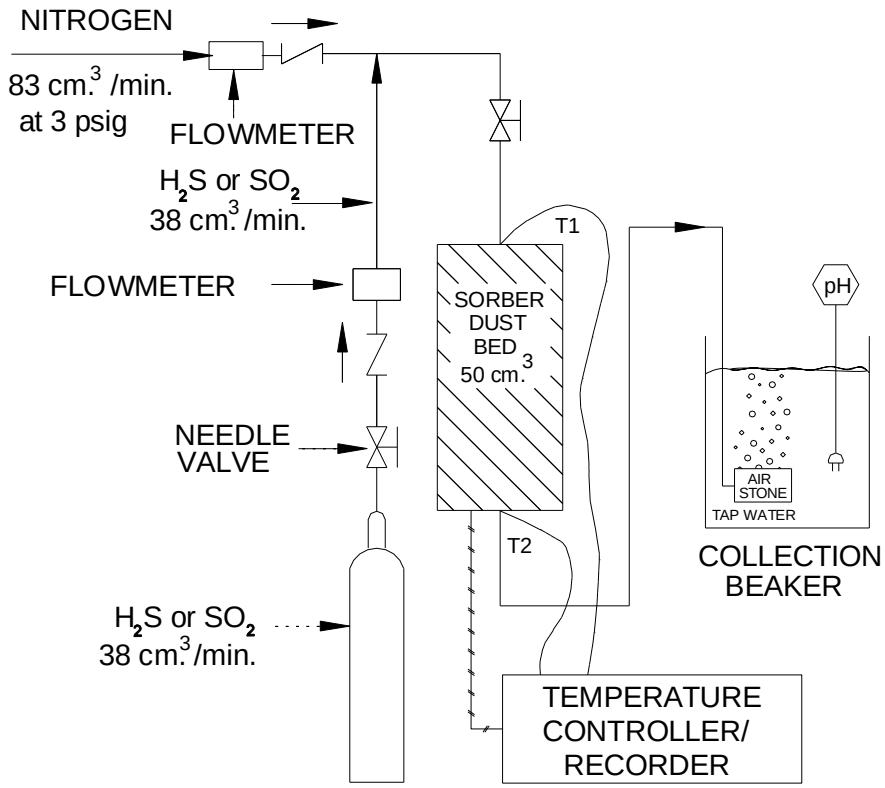

Figure 1. Preliminary Test Series Apparatus

CE Tyler Sieve Products, Inc. portable sieve shaker. Each sample material was classified and the particle fraction passing through a 140 mesh (106 micron opening) screen which was retained on a 200 mesh (75 micron opening) screen was utilized for each test specimen. This particle size is representative of that which would be used to enhance filter cake porosity in the eventual and effective use of IF&P U. S. Patent #4,865,629, which is the focus of future research efforts. By using an identical particle size fraction for each sample tested, it was hoped that the bed permeability in each sample trial would be essentially constant at constant gas flowrate conditions; also, the total available surface area exposed to the sulfur laden gas would be similar from one test to the next. Just prior to each test, the sample material was again dried in an air circulated oven to insure no moisture was retained, after which the classified sample was extracted and weighed for test purposes.

Thermogravimetric (TGA) Testing

Selected waste sorbents for TGA testing included tin oxide, zinc oxide, iron oxide, and a mixture of metal oxide and iron oxide, and was conducted by the Institute of Gas Technology in Des Plaines, IL. These sorbents were evaluated for their reactivities and absorption capacities with respect to H_2S and SO_2 using a high pressure, high temperature thermogravimetric analyzer (HPTGA) unit. The comparative sulfidation tests were conducted at 538ºC (1000ºF) using fuel gas containing H_2S, H_2 and N_2; sulfation tests were conducted at 650ºC (1200ºF) using flue gas containing SO_2, O_2, and N_2.

During a typical TGA test, the sample weight, the rate of weight change, and the temperature of the furnace are recorded. The sample is contained in a platinum basket, suspended from a recording balance by a platinum wire chain, while a metered gas flow is introduced at the bottom of the reactor chamber. The desired composition of the reactant gas is obtained by mixing different streams of gases at pre-determined ratios. Any movement of the balance arm, because of a change in sample weight, is sensed by a linear differential transformer on the sample arm of the balance. A restoring force that is proportional to the change in weight is supplied to the opposite arm with an electromagnet. The recording balance control unit senses the force required to maintain a null and converts this into a signal proportional to the weight of the sample. The procedure for these tests includes heating the sorbent in a nitrogen atmosphere to a pre-determined temperature. At this point the reactant gas mixture containing H_2S or SO_2 is allowed to flow past the sorbent while the change in the sample weight is continuously monitored. The sample is exposed to the reactant gas until the sorbent is converted to its peak value. The weight gain-versus-time curve produced in these tests is used as a measure of reactivity and capacity of the sorbent tested. The TGA test apparatus employed in this phase of testing is depicted schematically in Figure 2.

Results

Preliminary Tests: SO_2 Trials

In the preliminary tests, an end-point pH of 5.00 was chosen for the SO_2 test series. Of the various materials tested using SO_2 gas, waste iron oxide and especially tin oxide appeared to have a significant potential for sulfur removal, as shown in Table 3 which follows.

Preliminary Tests: H_2S Trials

Because H_2S is a weaker acid than SO_2 when dissolved in water, and because tap water (which was purposely selected in favor of distilled or demineralized water) was used in the collection beaker, the pH depression observed upon exhaustion of the sample bed in the H_2S test series would not be nearly as notable as that observed in the SO_2 test series. Consequently, for the preliminary tests, an end-point of 6.50 was selected for all tests involving H_2S. In addition to pH depression, the total suspended solids (TSS) and total sulfites were periodically monitored and recorded in the H_2S test series to serve as two other means of validating the data.

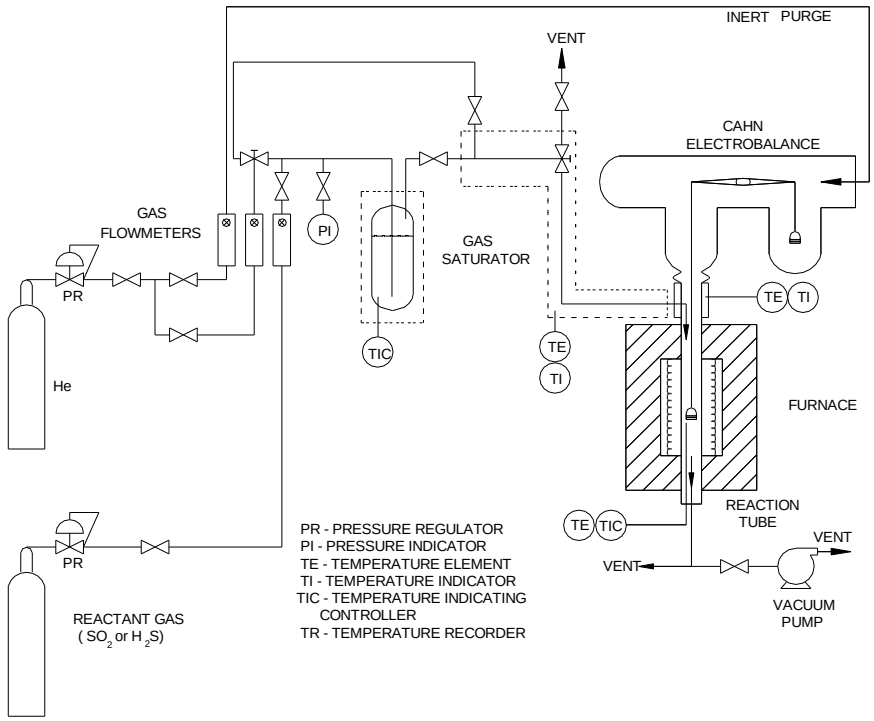

Figure 2. Thermogravimetric (TGA) Test Apparatus

Of the materials tested in an H_2S laden atmosphere, iron and zinc oxides appeared to exhibit high affinity for sulfur. Table 3 shows the various sorbent capacities for H_2S; Figure 3 shows the actual breakthrough plots for both SO_2 and H_2S.

Table 3. Preliminary Test Trials: Sulfur Removal Capacity
(grams of sulfur/kilogram of sorbent)

Sorbent*	SO_2 Capacity	H_2S Capacity
Tin oxide	66.02	19.13
Iron oxide	21.22	59.86
Zinc oxide	14.92	70.22
Iron & zinc oxide	20.99	82.70
Dolomite & limestone mix	16.09	4.23

(*) normalized to 85% purity (typical)

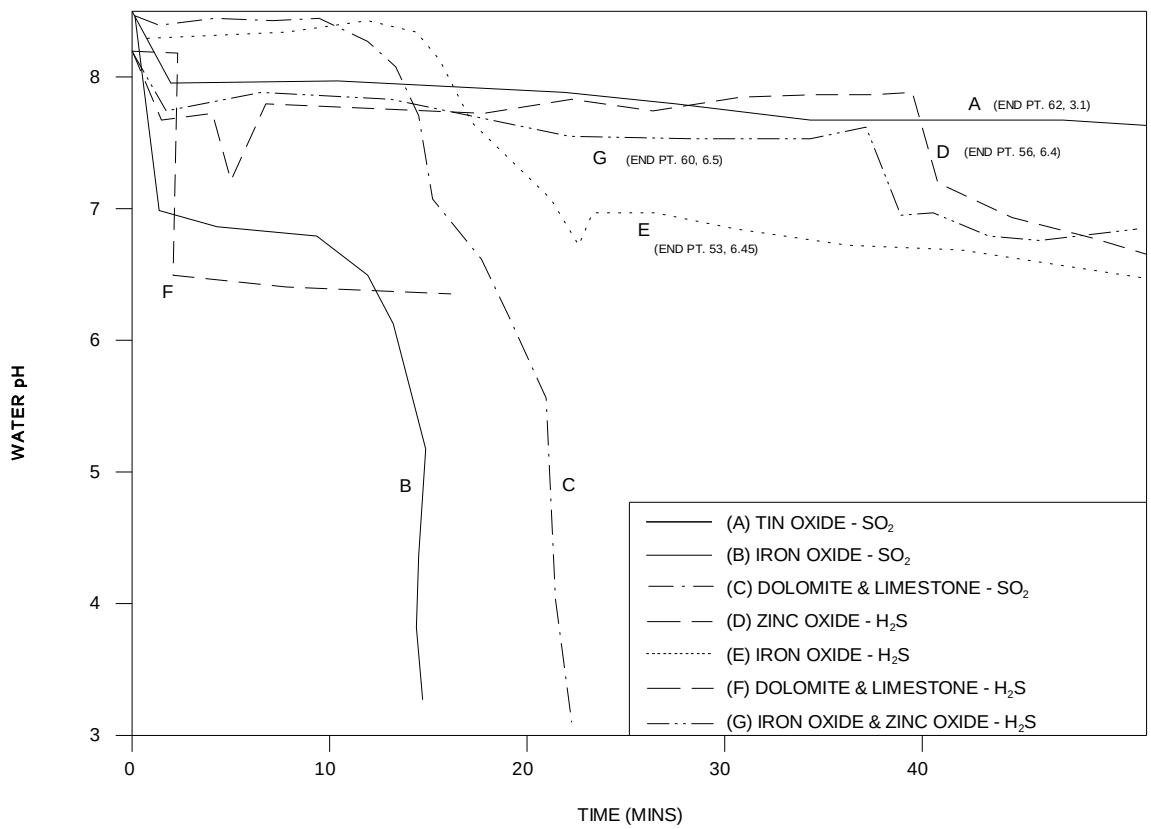

Figure 3. Preliminary Test Series Breakthrough Plots

TGA Tests: Sulfation Conditions

In the case of sulfation, the reaction may be represented by the following equation:

$$Me_xO_y + z\ SO_2 + (z\text{-}y/2)\ O_2 = Me_x(SO_4)_z$$

Initial sulfation tests at high temperature (1600ºF) indicated no significant sulfation reaction with the zinc oxide waste at such a high temperature. This is consistent with the theoretical thermodynamic limitation of the metal oxide sorbents tested. Comparative sulfation tests were carried out at 650ºC (1200ºF). Since each mole of oxygen is replaced by 1 mole of sulfur and 4 moles of oxygen, the weight gains during the sulfation reaction are much more significant than during sulfidation. The results indicate that in terms of the overall sulfur capacity, zinc oxide waste is the best sorbent, followed by tin oxide waste and iron oxide. As in the sulfidation tests, both the reaction kinetics and final weight gain of the ZnFe mixed oxide waste are intermediate between those obtained with each of the iron oxide waste and the zinc oxide waste, further indicating the consistency of the results.

TGA Tests: Sulfidation Conditions

For a metal oxide Me_xO_y, the sulfidation reaction may be represented by the following equation:

$$Me_xO_y + z\ H_2S + (y-z)\ H_2 = Me_xS_z + y\ H_2O$$

The weight gain is therefore due to the exchange of sulfur (M.W.=32 g/mole) and for oxygen (M.W.= 16 g/mole) during the sulfidation reaction. The results from comparative sulfidation tests at 538ºC (1000ºF) using all four metal oxide waste materials indicate that in terms of overall sulfur capacity, iron oxide waste is the best sorbent, followed by zinc oxide waste and tin oxide waste. Both the reaction kinetics and final weight gain of the ZnFe mixed oxide waste are intermediate between those obtained with each of the iron oxide waste and the zinc oxide waste, further indicating the consistency of the results.

Waste Metal Oxides: Availability

As mentioned earlier, an additional task involved the compilation of information related to the availability, geographical location, and processes which generate the various waste materials tested in this research effort. Among the waste materials tested, namely the oxides of tin, zinc, and iron, waste iron oxide appears to be the most promising because of its tremendous availability and very low cost. Highlights of the availability for each of these materials are given below[2].

<u>Iron</u>

Iron is the most widely used of all the metals. In 1990, the iron and steel shipments in the United States consisted of steel mill products (90%), iron castings (9%), and steel castings (1%). Iron and steel products make up about 75% of the weight of an automobile. Steel is widely used in building, highway, industrial and all other forms of construction, and industrial machinery.

Consumption of steel mill products in the United States amounts to about 100 Mmt/yr. Steel production generates a number of wastes that contain ferrous and nonferrous metal residues. Junked automobiles are the largest source of obsolete or post consumer scrap.

<u>Tin</u>

Tin is one of the earliest metals known to humankind, and is commonly used as a protective coating or as an alloying metal with other metals. The major uses for tin are: cans and containers, 32%; electrical, 22%; construction, 10%; transportation, 11%; and other, 25%.

Waste tin oxides are available from new and old tin scrap by recycling and recovering. In 1991, about 50,000 metric tons of tin was consumed; 98% of the new tin scrap and 96% of the old tin scrap generated was recovered.

Zinc

Zinc is the fourth most widely used metal after iron, aluminum, and copper. More than 90% of the metal is used for galvanizing steel and for alloys; the remainder is used to produce dust, oxide, and various chemicals. In 1991, about 354,000 mt of secondary zinc valued at about $412 million, was recovered in basic forms--refined metal, alloys, dusts, and chemicals. Scrap, containing about 96,000 mt of zinc and valued at $62 million, was exported in 1991, whereas 38,000 mt of zinc in scrap, valued at $19 million, was imported into the United States.

Application

As a result of the preceding discussions on tin, zinc, and iron oxide, it becomes apparent that extremely large quantities of these materials are and will continue to be readily available in America. In instances where such classified particles are not available, the use of "off-the-shelf" bulk handling, particle size reduction, and classification equipment can be easily used to achieve the desired particle size fraction, and to optimize sorbent capacity and filtration performance. In view of the availability of these three waste materials, one further remaining aspect from an economic standpoint (assuming handling costs, permits, and particle size reduction and classification are similar) is the intrinsic value of each material.

As of June 1996, the intrinsic value of the three base metal materials was as follows:

Tin (composite)	$4.16/lb.
Zinc (high grade)	$0.49/lb.
Iron (steel)	$0.07/lb.

In contrast, pelletized zinc ferrite or zinc titanate is significantly higher in cost. Even the most novel, fluidized zinc titanate formulations, such as "ZT-4", were reported to be $7.91/lb, as of June, 1994.[3] It should be emphasized that the intrinsic values shown above are commodity prices for the base metals of each material, and do not represent the cost of the corresponding waste metal oxides, which are much less. The prices do, however, provide an idea of the value of each material after it has been recycled and recovered for sale as pure metal, and are indicative of the relative value of the three metal oxides which showed the most significant affinity for sulfur. By using the sulfur removal capacity recorded in Table 3 and the intrinsic value noted above, a relative cost comparision for sulfur removal, in grams of sulfur removed per dollar value, is shown in Table 4 as follows:

Table 4. Waste Metal Oxide Sorbents: Cost Comparison

Sorbent	SO_2*	H_2S*
Iron oxide	137.79	388.70
Zinc oxide	13.84	65.14
Tin oxide	7.21	2.09

(*) in grams of 'S' removed/dollar value of pure metal

Future Activities

Future efforts will focus on conducting packed bed testing at IGT with the most promising waste metal oxide sorbents, followed by a series of tests at IFP to determine their additional capability as a high temperature filter aid. Given their high affinity for sulfur, overall availability, and low cost in relation to other metal oxide sorbents, the select use of waste metal oxides as a "once-through" sorbent in combination with ceramic filtration technology will provide effective sulfur removal and enhanced filter performance in a cost-effective manner.

References

1) Robin, Allen *"Integration and Testing of Hot Desulfurization and Entrained Flow Gasification for Power Generation Systems"*; U.S.D.O.E. Cooperative Agreement DE-FC21-87MC23277; from the "Proceedings of the Twelfth Annual Gasification and Gas Stream Clean-Up Systems Contractors Review Meeting", Morgantown, WV DOE/METC - 92/6128, Vol. 1, pg. 95.

2) U.S. Dept. of Interior Bur. of Mines Annual Reports for Tin, Zinc, Iron (1992).

3) Gupta, R. P. and Gangwal, S. K. "*Fluidized-Bed Sorbents"*; (D.O.E. Contract No. DE-AC21- 88MC25006) excerpted from the "Proceedings of the Coal-Fired Power Systems 94 -Advances in IGCC and PFBC Review Meeting", Morgantown, WV. DOE/METC - 94/1008 Vol. 2, pg. 646.

Acknowledgments

The authors wish to acknowledge Mr. Theodore J. McMahon, METC's Contracting Officer Representative for this project, as well as Dr. Javad Abbasian of the Institute of Gas Technology for their involvement in this research effort, the period of performance of which is August 15, 1994 through June 20, 1997.

Moving Granular Bed Filter Development Program

Keith B. Wilson (cpc@hooked.net; 415-372-1155)
John C. Haas (cpc@hooked.net; 415-372-1155)
Combustion Power Company
150 West 20th Avenue
San Mateo, CA 94403

Raghubir P. Gupta (gupta@rti.org; 919-541-8023)
Brian S. Turk (bst@rti.org; 919-541-8024)
Research Triangle Institute
P.O. Box 12194
Research Triangle Park, NC 27709-2194

Introduction

For coal-fired power plants utilizing a gas turbine, the removal of ash particles is necessary to protect the turbine and to meet emission standards. Advantages are also evident for a filter system that can remove other coal-derived contaminants such as alkali, halogens, and ammonia. With most particulates and other contaminants removed, erosion and corrosion of turbine materials, as well as deposition of particles within the turbine, are reduced to acceptable levels. The granular bed filter is suitable for this task in a pressurized gasification or combustion environment.

Objectives

The objective of the base contract was to develop conceptual designs of moving granular bed filter (GBF) and ceramic candle filter technologies for control of particles from integrated gasification combined cycle (IGCC), pressurized fluidized-bed combustion (PFBC), and direct coal-fueled turbine (DCFT) systems. The results of this study showed that the GBF design compared favorably with the candle filter.

Three program options followed the base contract. The objective of *Option I, Component Testing*, was to identify and resolve technical issues regarding GBF development for IGCC and PFBC environments. This program was recently completed. The objective of *Option II, Filter Proof Tests*, is to test and evaluate the moving GBF system at a government-furnished hot-gas cleanup test facility. This facility is located at Southern Company Services (SCS), Inc., Wilsonville, Alabama. The objective of *Option III, Multicontaminant Control Using a GBF*, is to develop a chemically reactive filter material that will remove particulates plus one or more of the following coal-derived contaminants: alkali, halogens, and ammonia.

Research sponsered by the U.S. Department of Energy's Morgantown Energy Technology Center, under contract DE-AC21-90MC27423 with Combustion Power Company, 150 West 20th Avenue, San Mateo, CA 94403; telefax: 415-372-1145.

Approach

The GBF was developed through low-pressure, high-temperature (1,600 °F) testing in the late 1970s and early 1980s. Collection efficiencies over 99 percent were obtained. In 1988, high-temperature, high-pressure (HTHP) testing was completed at New York University (NYU), Westbury, New York, using a coal-fired pressurized fluidized-bed combustor. High particulate removal efficiencies were confirmed by the fact that both New Source Performance Standards (NSPS) and turbine tolerance limits could be met (Wilson, 1989).

The early scale-up work of the GBF indicated potential limitations due to size, cost, and mechanical complexity. These limitations were addressed in the current program by using the information gained from the filter development up through the NYU test program to reassess the commercial approach (Wilson et al., 1992). Figure 1 shows a GBF designed for a 100-MWe Kellogg-Rust-Westinghouse (KRW) air-blown fluidized-bed gasifier. The filter has an inside diameter of 14 ft with a nominal bed depth of 5 ft.

Dust-laden gas enters the filter through an inlet duct, which brings the gas and dust to the gas filter medium interface. The gas flows downward initially, turns and flows across the filter medium, and then turns upward to flow counter-current to the downward moving filter medium. As the gas and dust pass through the filter medium, dust is removed. Dust and filter media are removed at the bottom cone of the filter. A pressurized pneumatic lift pipe moves the filter medium for return to the filter. After separation of the filter medium, the transport gas and dust are cooled in a recuperative heat exchanger and pass through a pressurized baghouse, which removes the collected dust. The cleaned transport gas pressure is boosted 15 psi through a blower, reheated in the recuperative heat exchanger, and returned to the bottom of the lift pipe. The cleaned filter medium from the disengagement vessel at the top of the lift pipe flows by gravity back into the top of the filter.

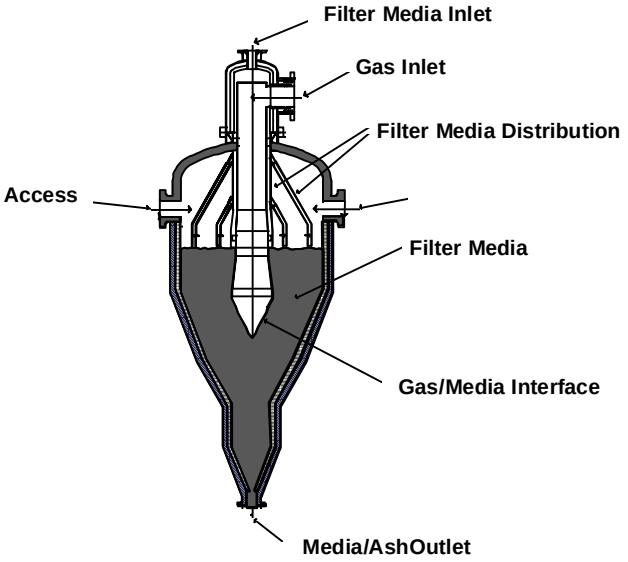

Figure 1. Granular Bed Filter for 100-MWe KRW (Air) Gasifier

Project Description

The status of three GBF projects is reported in this paper: (1) the recently completed GBF component development program (Option I), (2) the development of multicontaminant control filter material (Option III), and (3) impending filter proof tests (Option II).

GBF Component Development Program

Technical issues that are associated with the development of a GBF for the control of particulate in IGCC and PFBC environments were addressed. Some of the technical issues are due to problems encountered during testing of a GBF at NYU. Other issues are a result of the redesign of the GBF to make it more commercially competitive. The issues are prioritized based on the seriousness of the issues and the difficulty in resolving them. Some issues are amenable to being settled in a component test facility, while others will have to be dealt with in the U.S. Department of Energy's (DOE's) Power Systems Development Facility (PSDF) located at an SCS facility in Wilsonville, Alabama.

A test plan defined a component test program to address the following issues:

- Effect of filter cone angle and sidewall materials on medium flow and ash segregation
- Maximum gas filtration rate
- GBF media issues
- Filter pressure drop.

A 3.5-ft-diameter split filter was used with a transparent cross section that allowed visual examination of filter media characteristics. Two different-sized filter arrangements were used for the evaluation, with different sets of internals and different cone configurations. Data on differences in movement of filter material, air, and ash provided insight into the optimum GBF design.

Multicontaminant Control

Besides particulate removal, a GBF may be able to capture other coal contaminants through the use of chemically reactive filter media. Combustion Power Company (CPC) proposed to develop a reactive filter medium composed of limestone and clay for the removal of sulfur and alkali species, repectively. This approach was changed because of the well-evolved alternative methods of sulfur removal, the thermodynamic limitations of limestone for H_2S removal, and the problems associated with the oxidation of calcium sulfide to sulfate. CPC entered into a subcontract agreement with Research Triangle Institute (RTI) to investigate alternative reactive filter materials. The program is divided into four phases. In the first phase, RTI is investigating clay-based sorbents for control of alkali, primarily sodium vapors, under IGCC and PFBC conditions. Option I will focus on clay-based sorbents for the additional sorption of lead, cadmium, barium, beryllium, and chromium. Under Option II, the sodium-based sorbents will be investigated for the sorption of halogen and metalloid species, and Option III will involve investigation of Ni-based catalysts for ammonia decomposition.

GBF Testing at Power Systems Development Facility

SCS has entered into a cooperative agreement with DOE/Morgantown Energy Technology Center (METC) for the design, construction, and operation of a hot-gas cleanup test facility for gasification and pressurized combustion. This facility is being commissioned in Wilsonville, Alabama. Shakedown and testing of the GBF at SCS are scheduled for early 1997.

The basic filter design is patterned after successful test units developed at CPC in the 1970s and tested at NYU during the 1980s. Anticipated filter design changes necessary for scaleup for commercial testing are based on computational fluid dynamics simulations. Dimensions of the filter are adjustable. The filter diameter can be changed by altering the refractory lining to allow operation at different capacities. The depth of the filter can be changed from 10 to 5 ft, if it is determined that a shallower filtration bed is suitable for ash collection efficiency. System design of the GBF is the same as for a commercial unit.

Results/Accomplishments

GBF Component Development Program

In the cold flow tests in the component test facility (Wilson et al., 1995), basically all configurations yielded such similar characteristics that it was not possible to conclude that one configuration was superior. More elaborate, or longer-running, tests would be needed to yield conclusions.

A full-circumference, 3.5-ft-diameter filter with simulated refractory lining was built that closely duplicated the commercial arrangement. Difficulty with ash collection with the 6-mm filter material was encountered. This issue was not anticipated. As a result, testing concluded prematurely.

Findings from the cold-flow tests are as follows:

- Airflow measurements at the filter top surface were influenced by the surface topography due to the media angle of repose between the media fill pipes. The air velocity would consistently increase in the valleys. The lowest valley occurs at the wall, and the air velocity was highest at that location. When the surface was leveled, the top surface flow measurements were much more consistent.

- The media velocity across the top surface of the filter was constant except for lower velocity at the filter vessel wall. This velocity profile existed for all media and airflow combinations.

- When commercial operation near maximum filter capacity was simulated, an air bubble at the end of the filter inlet tube grew with the gas flow. When the airflow reached about 80 to 90 percent of minimum fluidization, the bubble bulged around the sides of the inlet and released, rising up about 12 in. before dissipating into the filter. This observation gives insight into the operation of the filter near maximum capacity.

- The filter pressure drop was examined as a function of superficial velocity. When the airflow reached minimum fluidization, the media began bubbling in regions of the filter. Instead of large bubbles forming at the top surface and splashing over the vessel side walls as the media started to fluidize, more material entered the vessel from the supply reservoir above the filter and the filter level continued rising.

Multicontaminant Control

The multicontaminant control work is being done at RTI. Some recent results on the development of a clay-based filter material for alkali removal are reported here.

Sorbent Screening

Identification of Target Clay Materials. Emathlite, kaolin, bauxitic kaolin, attapulgite, and calcium montmorillonite were selected as potential candidates for GBF media capable of alkali removal. In addition to previous documentation as alkali getters, these materials were found to be readily available in quantities sufficient for production of large amounts of GBF media in the southeastern part of the United States. Alpha-alumina, a known sodium nongetter, was also added to this list to provide a zero-reactivity baseline for alkali sorption. Loss on ignition (LOI), chemical composition based on LOI, and bulk price per LOI weight for these materials are listed in Table 1.

Alkali Sorption Screening Procedure. Problems generating and monitoring alkali vapor complicate effective screening efforts. A simple screening procedure for alkali sorption was

Table 1. Chemical Composition and Bulk Cost of Various Clays[a]

	Emathlite 3000	Emathlite 600	Kaolin	Bauxitic Kaolin	IGB[b]	Attapulgite	Alumina
P_2O_5	3.48	3.75	0.30	0.09	0.12	0.99	0.00
SiO_2	68.97	68.79	51.15	35.77	53.78	61.76	0.00
Na_2O	0.3	0.40	0.10	0.06	1.47	0.07	0.00
K_2O	0.95	1.04	0.15	0.12	0.53	0.85	0.00
SO_3	0.14	0.18	0.12	0.26	1.45	0.30	0.00
MgO	2.95	2.73	0.10	0.04	5.32	10.38	0.00
CaO	5.43	5.83	0.10	0.06	12.59	4.81	0.00
Al_2O_3	8.33	7.75	44.17	57.59	17.68	10.41	100.00
TiO_2	0.38	0.39	1.73	2.41	0.10	0.46	0.00
Fe_2O_3	0.37	2.98	0.62	1.18	1.43	3.90	0.00
Loss on ignition (LOI)	9.81	8.87	13.78	23.94	20.87	21.61	0.00
Bulk cost ($/ton)	74.50	60.35	68.25	231.40	106.25	141.60	

[a] Mineral analysis and bulk cost reported as weight percent on LOI-free basis.
[b] Trade name for calcium montmorillonite.

developed by Dr. Schulz's group at the University of Surrey, U.K. (McLaughlin, 1990). Reagent-grade NaCl is added to the material being tested, producing a mixture with 10 wt% NaCl. Thermogravimetric analysis (TGA) records the weight loss of this sample as it is heated from room temperature to 1,000 °C. As the NaCl is heated, it begins to evaporate, releasing sodium vapor. An alkali nongetter will release the vapor products and experience a weight loss equivalent to the amount of salt in the sample. An alkali getter absorbs the sodium vapor and experiences a weight loss that is related to its alkali sorption activity.

Thermal Analysis. A DuPont 1090 thermal analysis system (Gupta and Gangwal, 1992) was used to screen the clay materials for alkali sorption activity in nitrogen, a simulated IGCC gas containing 87 vol% CO_2, 10 vol% H_2, and 3 vol% H_2O and a simulated PFBC gas with 6.9 vol% CO_2, 13 vol% O_2, 3 vol% H_2O, and the balance nitrogen. During these screening tests, a 20-mg sample was heated at 15 °C/min from room temperature to 1,000 °C in 50 mL/min of test gas.

The TGA screening results are summarized in Table 2 , which lists ultimate percent weight loss for all seven samples as a function of gas composition. As expected, α-alumina, a known non-getter, showed 10 percent weight loss for all three test gases, indicating no alkali sorption. Based on an average weight loss for the three test conditions, a list of the clay materials from most effective alkali getter to the known alkali nongetter is emathlite 600 > kaolin > emathlite 3000 > bauxitic kaolin > calcium montmorillonite (IGB) > attapulgite > α-alumina.

Table 2. TGA Reactivity of Various Clays

	Percent Weight Loss			
Clay Sample	**N_2**	**IGCC**	**PFBC**	**Average**
Emathlite 3000	8.40	5.65	6.09	6.71
Emathlite 600	5.75	5.50	6.23	5.83
Kaolin	7.04	5.37	7.03	6.48
Bauxitic kaolin	7.43	7.44	8.57	7.81
Calcium montmorillonite	8.60	7.86	7.68	8.05
Attapulgite	8.49	7.60	8.13	8.07
α-Alumina	10.24	10.39	10.32	10.32

Sorption Activity for Various Heavy Metals. A series of TGA runs were performed to evaluate kaolin and emathlite 600 as potential high-temperature sorbents for Pb, Ba, Be, Cd, and Cr. Samples for these TGA runs were prepared by mixing 90 wt% of either kaolin or emathlite 600 and 10 wt% of a trace metal chloride. The samples were heated in the TGA at 15 °C/min to 1,000 °C in 50 mL/min of helium using the same procedure as described previously. The TGA results are summarized in Table 3, as final weight losses for both emathlite and kaolin

Table 3. Summary of TGA Results

	Percent Weight Loss	
Trace Metal	**Kaolin**	**Emathlite 600**
$PbCl_2$	10.1	8.4
$CrCl_3$	9.8	7.2
$BaCl_2$	2.1	3.1
$BeCl_2$	4.5	6.1
$CdCl_2$	8.1	9.4

samples with each of the metal chlorides. Arranging the trace metals in lists of decreasing sorption capability produces Ba > Be > Cr > Pb > Cd for emathlite 600 and Ba > Be > Cd > Cr > Pb for kaolin.

GBF Media Development

Based on the TGA screening tests, emathlite and kaolin were identified as effective alkali sorbents. The next step was to identify a simple and inexpensive production process for converting the raw clays into GBF media. A GBF medium must possess mechanical strength and attrition resistance to survive the mechanical demands of a moving-bed process. For alkali removal, the GBF medium must also maintain a high level of reactivity with alkali vapor. Economic constraints for the preparation process require the ability to produce large quantities of material at minimal costs.

Figure 2 illustrates that high mechanical strength and chemical reactivity are a direct consequence of the binders, additive, and the pelletization method used. Identification of the correct combination for optimal strength and reactivity proceeded in iterative steps. Extrusion with spheronization and disk pelletization were selected as pelletization techniques based on economic and production capacity constraints. Pure emathlite and kaolin pellets were produced by each pelletization technique and tested for mechanical strength and reactivity. Binders and additives were used to improve pellet properties and achieve pellet design requirements.

Figure 3 shows crush strength and attrition loss for calcined kaolin and emathlite pellets prepared by both extrusion/spheronization and disk pelletization. From data reported in Figure 3, crush strength values for calcined kaolin and emathlite pellets produced by extrusion/ spheronization are almost an order of magnitude higher than those produced by disk pelletization. A similar trend is observed for attrition resistance. Because pellet production by disk pelletization is much less expensive than extrusion/spheronization, extensive binder and additive testing was performed in

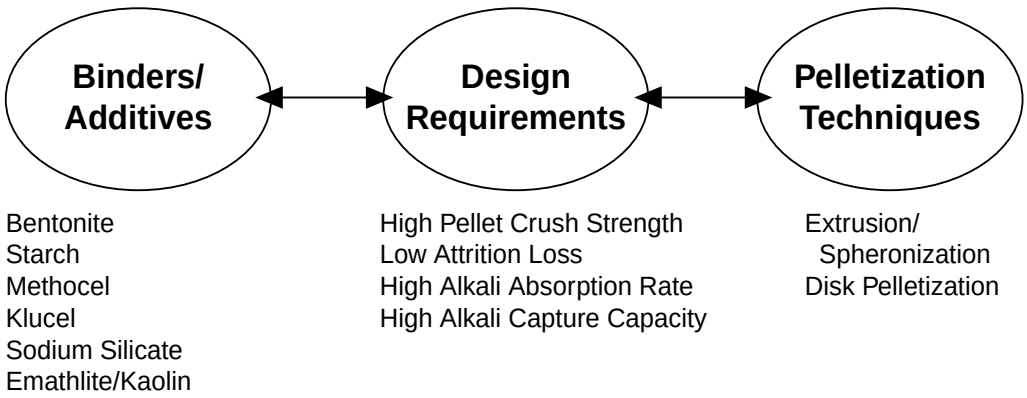

Figure 2. Approach to GBF Media Development

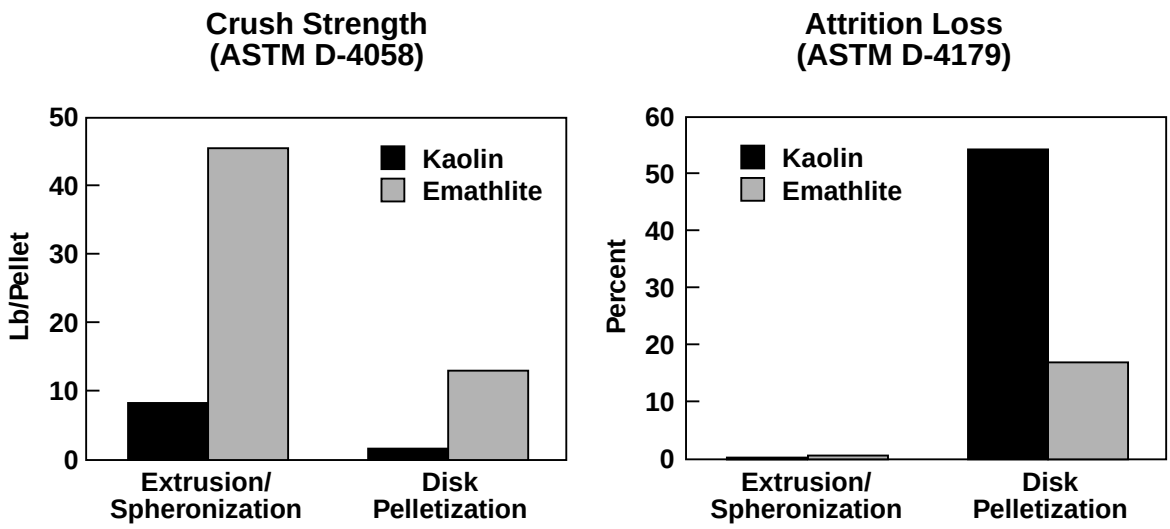

Figure 3. Mechanical Properties of Kaolin at Emathlite Pellets Produced By Extrusion and Disk Pelletization

an attempt to improve the strength characteristics of pellets produced by disk pelletization. Unfortunately, the strength of pellets produced by disk pelletization could not be increased and testing of pellets produced by disk pelletization was discontinued.

Unlike disk pelletization, extrusion/spheronization produced strong attrition-resistant pellets with both kaolin and emathlite. Comparison of the strength characteristics of these extruded pellets indicates emathlite pellets possess significantly more strength than kaolin pellets. The TGA reactivity of these pellets, shown in Figure 4, clearly demonstrates kaolin pellets are more reactive. As binders and additives are more likely to affect mechanical strength than reactivity, research efforts were focused on increasing the mechanical strength of extruded kaolin pellets with binders and additives. As extruded emathlite pellets are very strong, emathlite was tested as a potential strengthening additive for extruded kaolin pellets.

Effects of binders and additives on mechanical strength of extruded kaolin pellets are summarized in Figure 5. A kaolin sorbent with 2 wt% sodium silicate binder (designated as KOS-1) emerged a winner in terms of crush strength and attrition resistance based on the data shown in Figure 5. Another promising candidate was a kaolin and emathlite mixture containing 35 wt% emathlite and 65 wt% kaolin (designated KE-35).

Alkali sorption activity for extruded pellets of kaolin (KO-2), emathlite (ET-1), kaolin with 2 wt% sodium silicate (KOS-1), and 35 wt% emathlite in kaolin (KE-35) is compared in Figure 6. From this figure, the weight increase associated with alkali absorption is 7.5×10^{-4} mg/min for KO-2, 3.7×10^{-4} mg/min for KOS-1, 3.0×10^{-4} mg/min for KE-35, and 2.3×10^{-4} mg/min for ET-1.

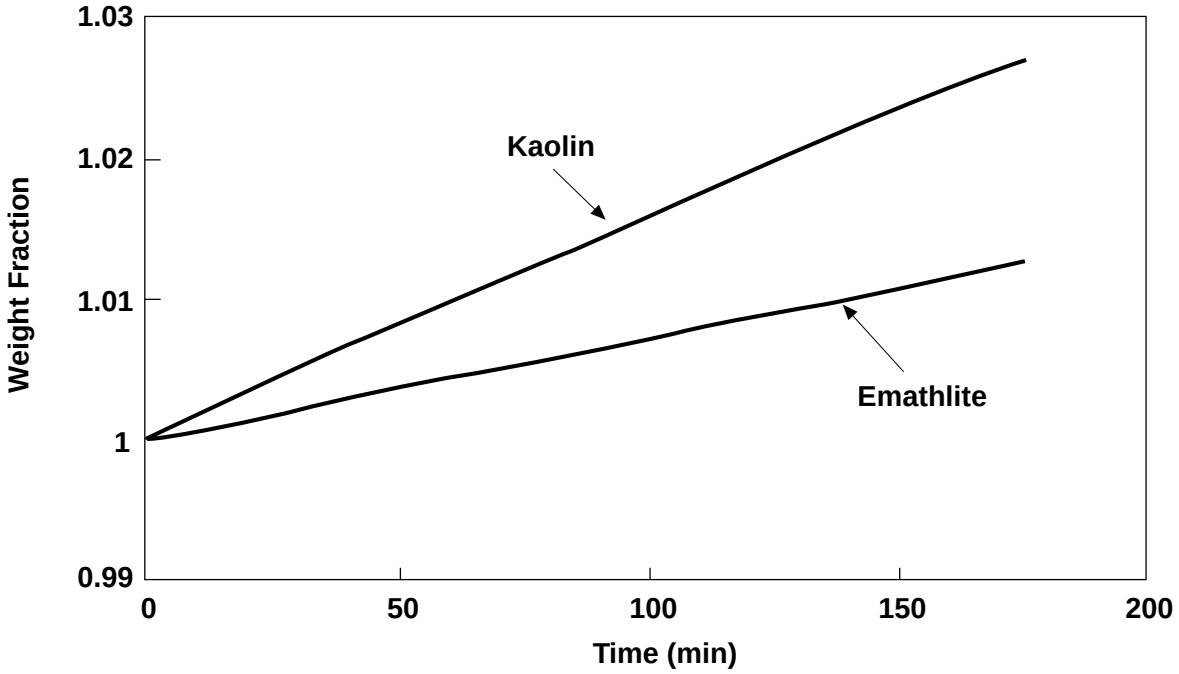

Figure 4. Comparison to TGA Reactivity of Kaolin and Emathlite Extruded Pellets With 40 ppm of Na Vapor at 870 °C

Based on the chemical reactivity and mechanical strength measurements, KOS-1 was selected as the optimum formulation for bench-scale testing as well as lift-tube attrition testing. A 40-lb batch of this sorbent was prepared.

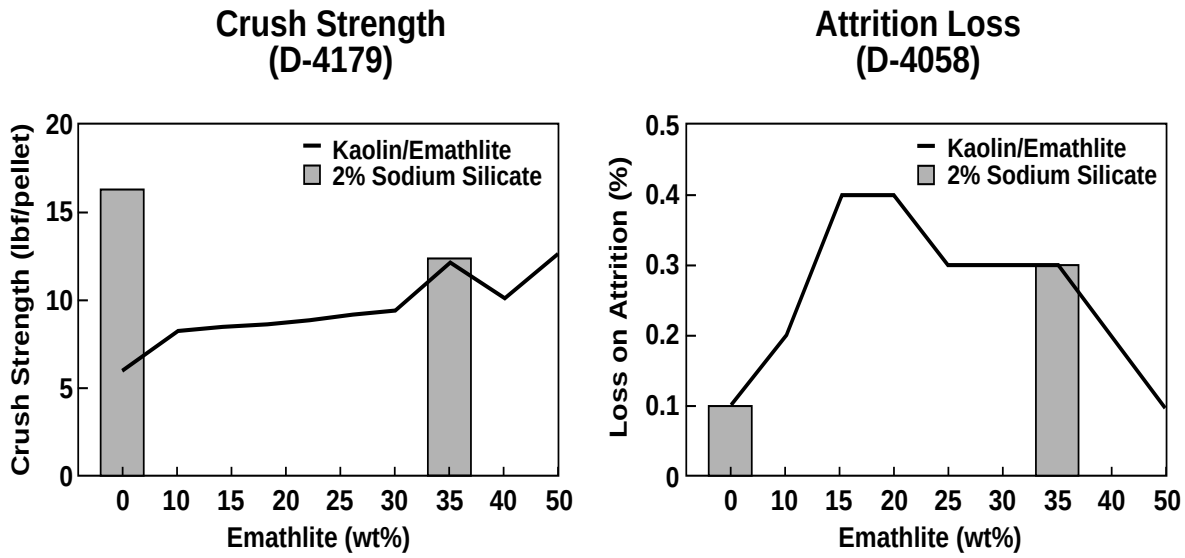

Figure 5. Mechanical Strength of Kaolin Pellets as a Function of Emathlite Content

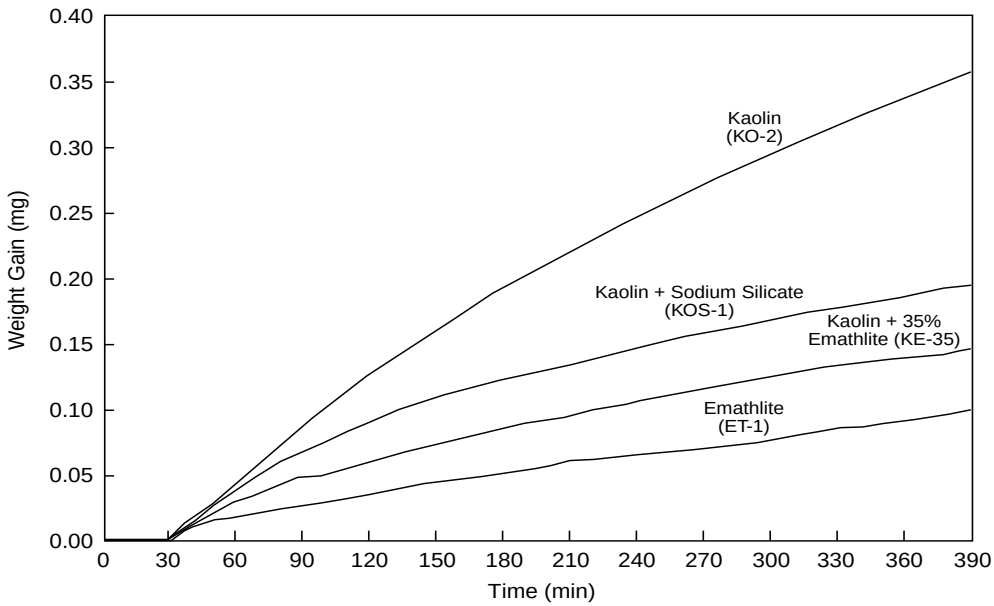

Figure 6. TGA Reactivity of Various Formulations At 870 °C With 40 ppmv of Na Vapor in Nitrogen

Bench-Scale Reactor Results. A schematic diagram of the bench-scale test system is shown in Figure 7. This reactor system is composed of a gas generation system, preheating section, and a quartz reactor. The gas delivery system can simulate a gas stream generated from coal combustion in either a PFBC or an IGCC system. Steam is generated from a metered water flow, which is mixed with a gas stream in the preheater section. The gas generation system can also provide a stream containing HCl to achieve a concentration of 100 ppmv in gas entering the reactor. This HCl stream is mixed into the gas after the preheating section to minimize system corrosion resulting from an HCl and steam mixture. Rather than having one main gas supply stream, the main gas supply has been split into two separate streams to generate 40 ppmv of sodium vapor in the reactor by salt vaporization.

The preheater section serves to vaporize the water generating steam, to reduce heating demands in the furnace, and to maximize salt vaporization during sodium vapor generation.

Problems with sodium vapor corrosion and condensation were minimized by generating the sodium vapor in the reactor near the sorbent bed. Sodium vapor is generated by passing a fraction of the gas supply through a bed of approximately 10 to 15 g of coarse salt crystals between 700 and 800 °C. The amount of sodium vaporized is controlled by the fraction of gas supply forced through the salt bed and the temperature of the salt bed. Furnace heating zones and set points have been optimized to minimize the temperature gradient in the sorbent bed. The temperature gradient in the top half of the bed, where a majority of the reaction is expected to

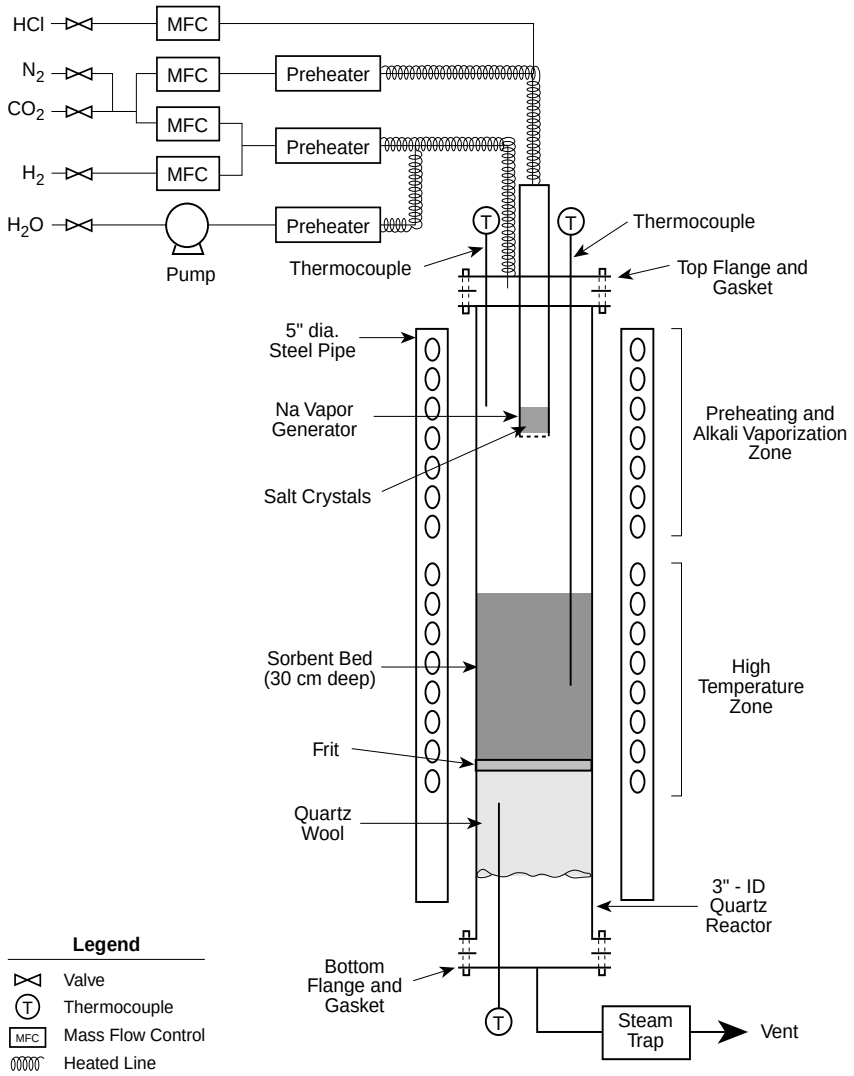

Figure 7. Schematic Diagram of Bench Unit

take place, is less than 5 °C. Any sodium vapor managing to escape the sorbent bed is trapped in a cold section of the reactor filled with quartz wool. Effluent from the reactor is vented through a steam trap to collect any condensed steam.

Because removing sequential layers in a precise and systematic fashion is important to modeling the alkali absorption profile in the sorbent bed, a specialized vacuum sampling system was designed and constructed. This sampling system has just enough vacuum to remove and collect a known depth of sorbent. Successive layers of the sorbent bed are removed by lowering the sampling system.

Sorbent tests of 150 hours of continuous operation are scheduled to begin with the KOS-1 sorbent in the near future. Results from these tests will be used to develop a kinetic model for alkali absorption of the most promising sorbent formulation.

GBF Testing at Power Systems Development Facility

The filter is currently under construction in Wilsonville, Alabama. Checkout and shakedown are scheduled in the first quarter of 1997 followed by combustion and gasification tests. The test objectives are to establish a filter material size suitable for particulate collection, determine filter capacity, and optimize filter efficiency.

Application

It is technically advantageous to capture coal-derived contaminants as well as particulate matter in a single vessel. The gas stream cleanup process in advanced power system would be simpler with a single vessel, and capital and operating costs would be lower. A GBF is a perfect candidate for multicontaminant control. The test program to develop chemically reactive filter material is showing good results with alkali control utilizing kaolin and emathlite clays.

Future Activities

Other options for chemically reactive filter material include a sodium-based filter material for the control of halogens and metalloids in reducing gas environments, and a nickel catalyst for the destruction of ammonia and hydrogen cyanide in a reducing gas environment. A single filter that can accomplish control of particulate and one or more of these other contaminants has an advantage in advanced power plant applications.

Combustion and gasification tests are planned at the PSDF to determine filter capacity, optimize filter efficiency, and compare different filter materials. These tests are scheduled to begin during the first quarter of 1997. Testing is scheduled to continue until late 1999. Filter material developed for contaminant control could be made available for testing at the PSDF.

Acknowledgements

The METC Contracting Officer's Representative (COR) is Mr. Thomas P. Dorchak. The period of performance is from October 1992 to November 1996 for the work being done for METC. Multicontaminant control filter material is being developed under subcontract to RTI. The testing at SCS is scheduled from 1997 to 1999.

References

Gupta R.P., and S.K. Gangwal, 1992. “Enhanced Durability of Desulfurization Sorbents for Fluidized-Bed Applications,” Topical Report No.: DOE/MC/25006-3271 (DE 93000247), November.

McLaughlin, J. 1990. “The Removal of Volatile Alkali Salt Vapors from Hot Coal-Derived Gases.” Ph.D. Thesis, Guilford, UK, Dept. of Chemical and Process Engineering, University of Surrey, 214 pp.

Wilson, K.B. 1989. Performance Evaluation of a Screenless (Counter-Current) Granular Bed Filter on a Subpilot-Scale PFBC. In *Proceedings of the Sixth Annual Coal-Fueled Heat Engines and Gas Stream Cleanup Systems Contractors’ Review Meeting,* ed. R.C. Bedick, T.P. Dorchak, N.F. Rekos, H.A. Webb, pp. 293-303. DOE/METC-89/6101 (DE89000952), Morgantown, West Virginia, March.

Wilson, K.B., J.C. Haas, and M.B. Eschelman. 1992. Moving Granular Bed Filter Development Program. In *Proceedings of the Twelfth Annual Gasification and Gas Stream Cleanup Systems Contractors’ Review Meeting Vol 1,* ed. R.A. Johnson and S.C. Jain, pp. 289-296. DOE/METC-92/6128 (DE93000228), Morgantown, West Virginia.

Wilson, K.B., J.C. Haas, and J.W. Prudhomme. 1995. Status of Granular Bed Filter Development Program. In *Proceedings of the Advanced Coal-Fired Power Systems '95 Review Meeting Vol 1,* ed. H.M. McDaniel, D.J. Mollot, pp. 150-157. DOE/METC-95/1018 (DE95009732), Morgantown, West Virginia.

Filter Systems for IGCC and PFBC Applications

John W. Sawyer (John_Sawyer@Pall.com)
Pall Advanced Separation Systems
Pall Corporation
2200 Northern Boulevard
East Hills, NY 11548

Abstract

Pall Corporation through the Pall Advanced Separation Systems group is involved in filter systems for advanced coal-fired processes such as IGCC and PFBC. This paper provides information on the approach taken by Pall in selecting filter media from the available media, and designing the filter system to meet the process needs as well as meet the requirements for the filter media.

IGCC

For IGCC systems, Pall currently offers both metal and ceramic filter elements. Currently, metal filter elements are only suitable for application in low-sulfur (0 to 100 ppmv) environments. In applications with higher sulfur levels (H2S, COS, etc.), we currently apply ceramic filters. However, we are developing an intermetallic filter media (iron aluminide) which will be available for use in high sulfur atmospheres. This media should be commercially available in the near future.

PFBC

For PFBC systems, Pall offers two ceramic media. Both media are silicon carbide based, but have different binder compositions. The Vitropore™ ceramic media is commercially available and has been widely used in demonstration projects. We are also developing a ceramic media with a new binder specifically formulated to enhance high temperature properties. This media is currently undergoing testing.

This paper presents information about the filter media mentioned here and the filter system designs for these two applications.

Application of CFCC Technology to Hot Gas Filtration Applications

Merrill Smith (merrill.smith@hq.doe.gov; 202-586-3646)
Office of Industrial Technologies
U. S. Department of Energy
1000 Independence Ave., SW
Washington, DC 20585-0121

Introduction

U.S. industry has a critical need for materials that are light, strong, corrosion resistant, and capable of performing in high temperature environments. Although many ceramics perform well at considerably higher temperatures than conventional metal alloys, they are generally brittle, and as a result can undergo catastrophic failure in service. The goal of the Continuous Fiber Ceramic Composite Program is to develop materials that will overcome these limitations,

The CFCC Program is a collaborative effort between industry, national laboratories, universities, and the government to develop advanced composite materials to a point at which industry will assume the full risk of further development. There are currently eight industry teams comprised of 50 members (led by AlliedSignal, Amercom, Babcock & Wilcox, Dow Corning, Dupont Lanxide, General Electric, and Textron) developing more than 20 applications for continuous fiber ceramic composite materials. Oak Ridge National Laboratories leads a team of other laboratories and universities in conducting performance evaluations and developing supporting technologies (e.g., material design, processing methods, manufacturing techniques, and codes and standards),

CFCC Hot Gas Filters

The CFCC program is working on a number of applications including the hot gas filters, Three of the industry teams are developing hot gas filters, and another will be demonstrating filters in an industrial application, The use of CFCC filters will be in the form of tubular sheets and/or plenums. For example, ceramic components are being developed for hot gas filters to be installed ahead of the turbines in industrial systems to protect the turbines from impingement of particulate. The cleaning system would help industries and utilities meet stringent emission control regulations, and increase the efficiency of processing and power generating facilities. Candle filters will be used in advanced coal combustion combined cycle plants.

Babcock & Wilcox--Sol Gel Impregnation

The objective of B&W's CFCC effort is to develop advanced ceramic composite materials which should be ideal for the oxide-based composite system and allow scaling to cost-effective manufacturing operations, The focus is on a liquid-to-solid-based processing

method, referred to as sol-gel impregnation. B&W is working with Westinghouse on a candle filter configuration, which is a porous closed end tube that will be fabricated at B&W using filament winding. The candidate CFCC is alumina fibers in an alumina matrix. Prototype components will be tested, and models developed to demonstrate the properties and reliability of CFCCs to manufacturers and end-users.

Near-term emphasis will be on the development and testing of hot gas filters, intended for application in advanced fossil energy systems. The project focuses on (1) improving properties, (2) reducing cost by decreasing infiltration cycles and developing filament winding, (3) generating a property data base suitable for design modeling, and (4) evaluating and selecting viable applications and fabrication/test initial representative components.

Du Pent Lanxide Composites--CVI

The objective of Du Pent Lanxide's CFCC effort is to develop Chemical Vapor Infiltration (CVI) of silicon carbide (SiC) CFCC components and incorporate them into a variety of high-temperature, heat-management, and power generation equipment including hot gas filters.

The team is now fabricating, exposing, and testing CVI SiC/SiC CFCC materials in simulated application conditions to prove their suitability for the selected applications, Du Pent Lanxide produces CFCCS by first fabricating ceramic fiber preforms in the shape of final parts. These preforms are infiltrated with chemical vapors that react to form a dense SiC matrix between the fibers. Du Pent operates commercial-scale CVI facilities capable of producing parts 1.2m in diameter and 2m high. Du Pent Lanxide's hot gas filters were successfully tested for 800 hours in the high-pressure, high-temperature rig by Westinghouse.

Amercom--Chemical Vapor Infiltration

Amercom/Atlantic Research and Industrial Filter and Pump Manufacturing are collaborating on development of a CFCC candle filter for hot gas filtration to support DOE's clean coal technology needs. The CFCC candle filter potentially will allow direct removal of particulate pollutants from 1500-1800° F gas streams in advanced pressurized fluidized bed and coal gasification systems. This will enable efficient direct use of the cleaned high temperature gas streams to power a gas turbine.

Amercom is using silicon carbide as the base matrix material and reinforcing it with carbide, nitride, or oxide fibers. This effort involves the Chemical Vapor Infiltration (CVI) of ceramic matrices into net or near-net-shape preforms of continuous, multifilament ceramic fibers. Potential solutions are being investigated to overcome key technical problems so that the CVI silicon carbide fiber reinforced silicon carbide matrix (SIC/SIC) composites can be commercialized.

Hot-Gas Filter Testing with a Transport Reactor Development Unit

Michael L. Swanson (mswanson@eerc.und.nodak.edu; 701-777-5239)
Robert O. Ness, Jr. (rness@eerc.und.nodak.edu; 701-777-5209)
University of North Dakota
Energy & Environmental Research Center
PO Box 9018
Grand Forks, ND 58202-9018

Introduction

The U.S. Department of Energy's Morgantown Energy Technology Center (DOE METC) has a hot-gas cleanup (HGC) program intended to develop and demonstrate gas stream cleanup options for use in combustion- or gasification-based advanced power systems. One objective of the METC HGC program is to support the development and demonstration of barrier filters to control particulate matter. The goal is not simply to meet current New Source Performance Standards (NSPS) with respect to particulate emissions, but also to protect high-efficiency gas turbines and control particulate emissions to levels low enough to meet the more stringent regulatory requirements anticipated in the future. DOE METC is investing significant resources in the Power Systems Development Facility (PSDF) under a cooperative agreement with Southern Company Services, Inc. (SCS). The PSDF will comprise five modules, including an advanced gasifier module and a HGC module. The gasifier module involves the M.W. Kellogg transport reactor technology for both gasification and combustion (1, 2). Several other demonstration-scale advanced power systems that will also utilize hot-gas particulate cleanup technology will benefit indirectly from this research. These systems include the Clean Coal IV Piñon Pine IGCC Power Project located at the Sierra Pacific Power Company's Tracy Station near Reno, Nevada.

The transport reactor demonstration unit (TRDU) was built and operated at the Energy & Environmental Research Center (EERC) under Contract No. C-92-000276 with Southern Company Services, Inc. The M.W. Kellogg Company designed and procured the reactor and provided valuable on-site personnel for start-up and operation. The Electric Power Research Institute (EPRI) was involved in establishing the program and operating objectives with the EERC project team.

The purpose of the previous program was to build a reactor system larger than the Transport Reactor Test Unit (TRTU) located in Houston, Texas, in support of the Wilsonville PSDF transport reactor train. The program was to address design and operation issues for the Wilsonville unit and also help develop information on the operation of the unit to decrease start-up costs.

Research sponsored by the U.S. Department of Energy (DOE) Morgantown Energy Technology Center (METC), under contract DE-FC21-93MC30097 with the Energy & Environmental Research Center, University of North Dakota, PO Box 9018, Grand Forks, ND 58202-9018; telefax: 701-777-5181.

The TRDU (91–136-kg/hr coal–limestone feed rate) now provides an intermediate scale to the TRTU (4.5 kg/hr coal–limestone feed rate) and the Wilsonville transport reactor (1540 kg/hr feed rate). Some of the design, construction, start-up, and operational issues for the Wilsonville transport train were addressed during this project (3, 4).

Objectives

The objective of the HGC work on the TRDU located at the EERC is to demonstrate acceptable performance of hot-gas filter elements in a pilot-scale system prior to long-term demonstration tests. The primary focus of the experimental effort in the 2-year project will be the testing of hot-gas filter elements as a function of particulate collection efficiency, filter pressure differential, filter cleanability, and durability during relatively short-term operation (100–200 hours). A filter vessel will be used in combination with the TRDU to evaluate the performance of selected hot-gas filter elements under gasification operating conditions. This work will directly support the PSDF utilizing the M.W. Kellogg transport reactor located at Wilsonville, Alabama (5) and indirectly the Foster Wheeler advanced pressurized fluid-bed combustor, also located at Wilsonville (6, 7) and the Clean Coal IV Piñon Pine IGCC Power Project.

Approach

This program has a phased approach involving modification and upgrades to the TRDU and the fabrication, assembly, and operation of a hot-gas filter vessel (HGFV) capable of operating at the outlet design conditions of the TRDU. Phase I upgraded the TRDU based upon past operating experiences. Additions included a nitrogen supply system upgrade, upgraded LASH auger and coal feed lines, the addition of a second pressurized coal feed hopper and a dipleg ash hopper, and modifications to spoil the performance of the primary cyclone. Phase II included the HGFV design, procurement, and installation. Phases III through V consist of 200-hour hot-gas filter tests under gasification conditions using the TRDU at temperatures of 540 °–650 °C (1000–1200 °F), 9.3 bar, and face velocities of 1.4, 2.3, and 3.8 cm/s, respectively. The increased face velocities are achieved by removing candles between each test.

Project Description

The TRDU is a 91–136-kg/hr (200–300-lb/hr) pressurized circulating fluid-bed gasifier similar to the gasifier being tested at the Wilsonville facility. The TRDU has an exit gas temperature of up to 980 °C (1800 °F), a gas flow rate of 590 m^3/hr (340 scfm), and an operating pressure of 9.3 bar (120 psig). The TRDU system can be divided into three sections: the coal feed section, the TRDU, and the product recovery section. The TRDU proper, as shown in Figure 1, consists of a riser reactor with an expanded mixing zone at the bottom, a disengager, and a primary cyclone and standpipe. The standpipe is connected to the mixing section of the riser by a J-leg transfer line. All of the components in the system are refractory-lined and designed mechanically for 11.4 bar (150 psig) and an internal temperature of 1090 °C (2000 °F). A detailed description of the TRDU and HGFV design has been given in other reports (4, 8).

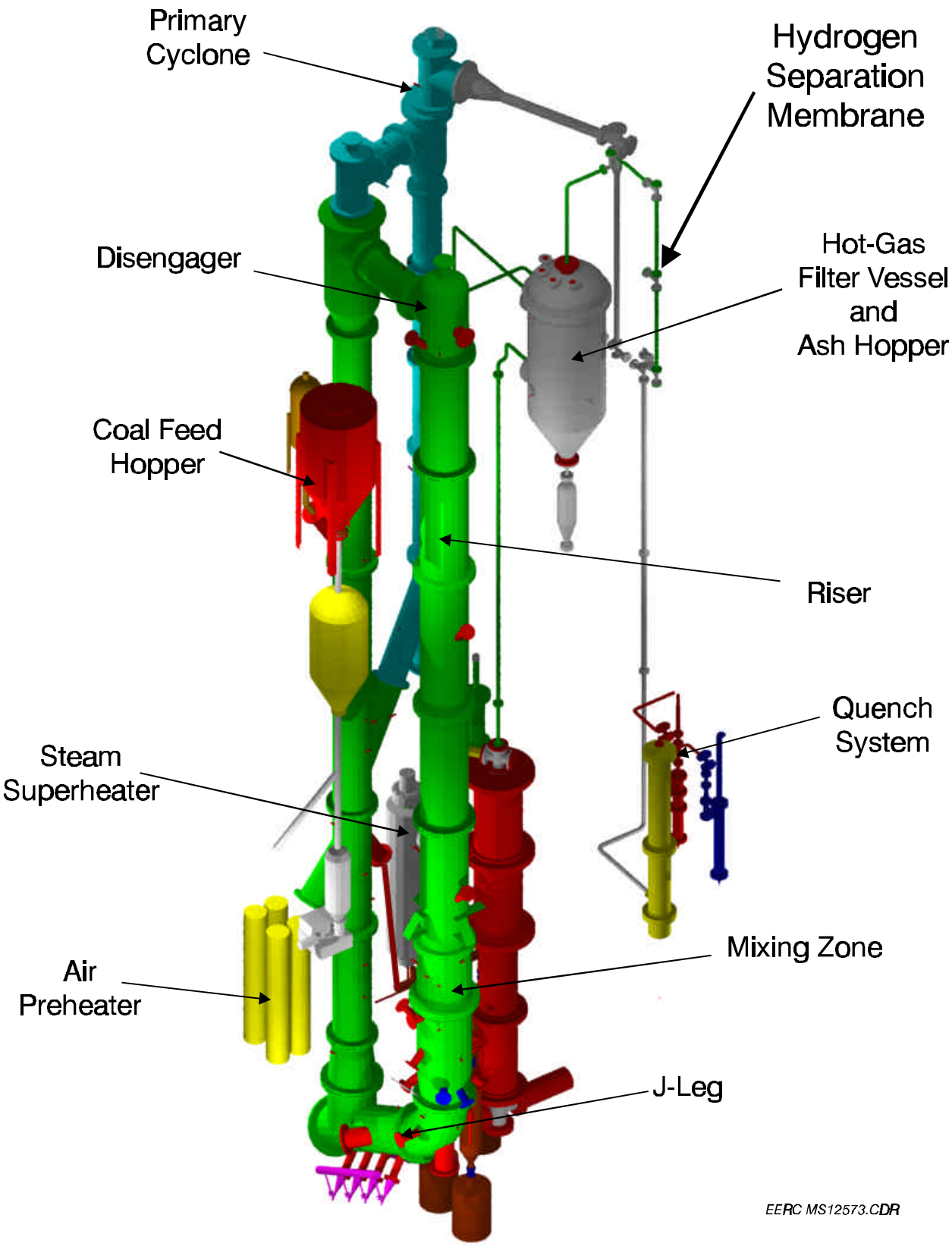

Figure 1. TRDU with HGFV in EERC gasification tower.

The HGFV is designed to handle all of the gas flow from the TRDU at its nominal operating conditions. This vessel has a 1.22-m inner diameter and is 4.7 m long with a refractory inside diameter of 71 cm (28 in.) and a shroud diameter of 61 cm (24 in.). The filter design criteria are summarized in Table 1. Filter vessel design capabilities include operation at elevated temperatures (to 950 °C) and pressures (up to 11.4 bar), with the initial test program operating in the 540°–650°C range. The HGFV can operate with filter face velocities in the range of 1.25 to 5.1 cm/s. Nineteen 1-meter candles were used in the initial tests, but 1.5-meter candles can be installed in the filter vessel. An existing heat exchanger has been modified to allow for the reduction of the gas stream temperature at the inlet to the filter vessel. An unheated nitrogen backpulse system was constructed to test the effects of backpulsing parameters on candle performance and cleanability. The nitrogen back-pulse system was constructed to backpulse up to four sets of four- or five-candle filters in a time-controlled or differential pressure-controlled sequence. During this test, the candles were typically pulsed at 87 mbar (35 in. H_2O) pressure drop across the candles. Sample ports for obtaining particulate and hazardous air pollutant samples were added to the piping system. A high-pressure and high-temperature sampling system (HPHTSS) was used to extract dust-laden flue gas isokinetically from the TRDU's reducing environment. Details of the HPHTSS are given elsewhere (8). A Fibroplate™ ceramic tube sheet and seven Fibrosic™ candle filters from Industrial Filter & Pump Mfg. Co., six silicon carbide fiber ceramic candle filters from the 3M Corporation, and six (one iron aluminide and five Vitropore™ silicon carbide) candle filters from Pall Advanced Separations Systems were tested in the filter vessel. A schematic of the internal design of the filter vessel is presented in Figure 2.

TABLE 1

Design Criteria and Operating Conditions for the Pilot-Scale Hot-Gas Filter Vessel

Operating Conditions	Design	Actual
Inlet Gas Temperature	540°–980°C	460°–475°C
Operating Pressure	8.6–11.4 bar	8.3 bar
Volumetric Gas Flow	550 m^3/hr	590 m^3/hr
Number of Candles	19 (1- or 1.5-meter)	19 (1-meter)
Candle Spacing	10.2 cm ℄ to ℄	10.2 cm ℄ to ℄
Filter Face Velocity	1.25–5.1 cm/s	1.4 cm/s
Particulate Loading	<10,000 ppm	6700 ppm
Temperature Drop Across HGFV	< 30°C	25°–30°C
Nitrogen Backpulse System Pressure	up to 56 bar	11.4 bar
Backpulse Valve Open Duration	up to 1-s duration	¼-s duration

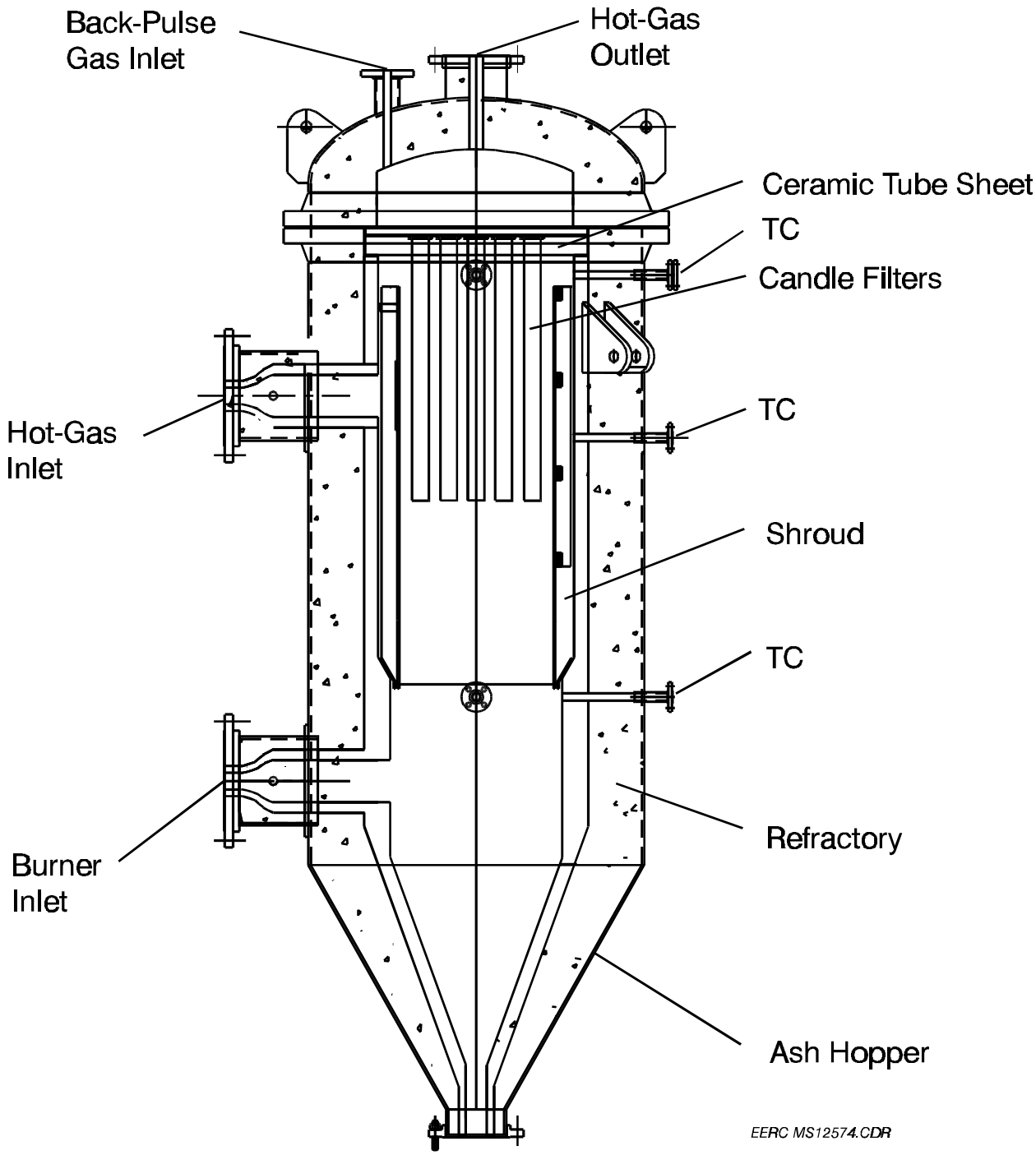

Figure 2. Schematic of the internal design of the HGFV.

Results

Two test campaigns were conducted during the weeks of March 25–31, 1996, and April 15–21, 1996. During these weeks, 138.5 hours of coal feed and 107 hours of gasification were achieved, with the system gases and fly ash passing through the filter vessel during the whole test campaign.

The TRDU was operated at three different average temperatures of 925 °, 900 °, and 860 °C to alleviate some deposition problems seen in the disengager. Analysis of the deposits indicated that a low melting eutectic between the calcium in the coal ash and the aluminosilicate in the fluid catalytic cracking (FCC) starting bed material resulted in the disengager deposits. Table 2 summarizes the operational performance for the TRDU during these test periods. Coal feed rates ranged from 100 to 109 kg/hr, and the gasifier pressure ranged from 8.3 to 8.6 bar. The dry product gas produced was 4%–6% CO and H_2, 10%–12% CO_2, 0.1%–1% CH_4, with the balance being N_2 and other trace constituents. The moisture in the fuel gas averaged 14%. The H_2S concentration averaged 400 to 600 ppm. Calculated recirculation rates ranged from 3630 to 8200 kg/hr.

TABLE 2

TRDU Actual Operating Conditions

Parameter	P046B	P047A	P047B
Conditions	Gasification	Gasification	Gasification
Coal	Wyodak	Wyodak	Wyodak
Moisture Content, %	23.3	23.3	23.3
Pressure, bar	8.3	8.3	8.3
Steam:Coal Ratio	0.28	0.28	0.30
Air:Coal Ratio	3.49	3.33	3.25
Ca:S Ratio, mole	4.7	4.7	4.7
Coal Feed Rate, kg/hr	100	100	100
TC411, °C , average (min.) (max.)	816 (733) (872)	857 (690) (902)	800 (606) (838)
Conversion, %	98	93	89
Carbon in Bed, %, Standpipe (dipleg)	ND[1]	0.5 (1.0)	1.0 (3.0)
Riser Velocity, m/s	8.5 (12.8)	9.8 (12.2)	9.1 (12.2)
Standpipe Velocity, m/s	0.061	0.12	0.12
Circulation Rate, kg/hr	ND	4000	6804
Duration, hr	28.5	41.5	56
Time	12:00–14:00	22:00–13:00	21:00–10:00
Date	3-29 to 3-30	4-15 to 4-17	4-18 to 4-21

[1] Not determined.

The HGFV was operated at ~460° to 475°C, with an average temperature drop across the filter vessel of 25° to 30°C. The candles were backpulsed 70 times, with no major candle failures. Backpulse operating parameters were an 11.4-bar reservoir pressure with a ¼-second full open time. The N_2 backpulse system and the filter vessel ash letdown system presented no operational problems. The only observed problems were a leak around the ceramic tube sheet and three of the candles that did not seal in the tube sheet correctly. In addition, the gas inlet temperature was approximately 80°C lower than the desired inlet temperature of 540°C. The average particulate loading going into the HGFV was 6700 ppm, with a d_{50} of 11.3 μm, while the outlet loading was 300 ppm with a d_{50} of 2.3 μm. A small increase in the "cleaned" filter baseline (from ~12.5 to 35.0 mbar) was observed over the course of the testing.

The leakage around the candles is the result of mixing four different candle types in a tube sheet with a common holddown plate. The tube sheet and holddown plate were specifically designed for the square-flanged IF&P Fibrosic™ candles. Pall's metal iron aluminide candle had its flange machined to match that of the IF&P candles; however, the Pall Vitopore and the 3M candles were installed using specially machined stainless steel adaptors to convert their hemispherical flange design to match that of the square-flanged tube sheet, resulting in slightly uneven candle flange heights. The tube sheet seal leak was probably due to the lower-than-expected temperature of the HGFV not expanding the intumescent sealing gaskets properly.

One bridge was observed between two adjacent candles. The bridge was very soft and fell off during removal of the tube sheet from the filter vessel; however, samples from the bridge were obtained before the bridge fell. It appeared that the bridge was the result of a slightly bowed candle coming close enough to the adjacent candle that a bridge was able to be formed and sustained during operation of the TRDU HGFV. Chemical analysis of the bridge material indicates that the bridge formed at the bottom (smallest distance between the candles) and built upward. Chemical analysis of the particulate samples indicates that mostly the finest size fraction was comprised by the coal ash and very little of the aluminosilicate FCC start-up material. Chemical analysis of the TRDU standpipe, dipleg, and filter vessel samples indicates that the standpipe material was approximately 50% coal ash, while the dipleg and filter vessel samples were approximately 75% coal ash. Sodium also seemed to be preferentially remaining in the larger particle sizes, indicating a possible interaction with the standpipe material.

Applications

In addition to direct support for the PSDF at Wilsonville, TRDU operation and filter element testing will benefit other ongoing projects at the EERC. The first sampling and analysis activities were conducted to generate HAPs data concerning trace metal transformations, speciation of mercury, and metal concentrations at selected points within the TRDU and HGC in support of a project entitled "Trace Element Emissions" funded by METC. In addition, materials and ash data concerning the high-temperature filter media and ash interactions were collected and analyzed in support of a project entitled "Hot-Gas Filter Ash Characterization" jointly funded by METC and EPRI. Testing of a hydrogen separation membrane by Bend Research, Inc., was also conducted on a slipstream of product gas from the TRDU. While the cost of this specific data collection was covered by the individual projects, the synergy that results from the integration of these projects minimizes the cost for collecting this information for all projects involved.

Future Activities

Future plans are to perform two HGFV tests at slightly higher temperatures and much higher filter face velocities to evaluate filter operation at these conditions and to ensure the ceramic tube sheet seal integrity and durability. Other future plans could include piping modifications to allow higher- temperature filter tests (at temperatures up to 900°C).

Acknowledgements

The EERC acknowledges the contributions of Rich Dennis, the METC Contracting Officer's Representative (COR) and the contributions of all three filter vendors (Industrial Filter & Pump Mfg. Company, 3M Corporation, and Pall Advanced Separations Corporation). The contributions from Southern Company Services and the M.W. Kellogg Company are also greatly appreciated. The contract period of performance is January 1, 1995, through December 31, 1996.

References

1. Sears, R.E., Griswald, G.H., Kastner, C.E., and Pontius, D.H., "Hot Gas Cleanup Test Facility for Gasification and Pressurized Combustion," Proc. Twelfth Annual Gasification and Gas Stream Cleanup Systems Contractors Review Meeting, Vol. 1, DOE/METC-92/6128, (DE93000228), Sept. 1992, pp. 53–63.

2. Dahlin, R.S., Pontius, D.H., Haq, Z.U., Vimalchand, P., Brown, R. and Wheeldon, J., "Plans for Hot Gas Cleanup Testing at the Power Systems Development Facility," Proc. Thirteenth Inter. Conf. on Fluidized Bed Combustion, Vol. 1, May 1995, pp. 449–459.

3. Rush, R.E., Fankhanel, M.O., and Campbell, W.M., "Transport Reactor Development Status," Proc. Coal-Fired Power Systems 94—Advances in IGCC and PFBC Review Meeting, Vol. 1, DOE/METC-94/1008 (DE94012252), June 1994, pp. 73–82.

4. Ness, R.O., "Transport Reactor Demonstration Unit, Volume 1 – Final Report," EERC Publication No. 95-EERC-02-06, May 1995, 150 p.

5. Ness, R.O., "Transport Reactor Demonstration Unit," Proc. Coal-Fired Power Systems '93—Advances in IGCC and PFBC Review Meeting, DOE/METC-93/6131 (DE93000289), June 1993, pp. 357–358.

6. Sears, R.E., Griswald, G.H., Boyd, T.J., Fankhanel, M.O., Crumm, C.J., and Pontius, D.H., "Power Systems Development Facility, PFBC System Perspectives," Proc. Coal-Fired Power Systems '93—Advances in IGCC and PFBC Review Meeting, DOE/METC-93/6131 (DE93000289), June 1993, pp. 121–128.

7. Rush, R.E., Moore, D.L., Hag, Z., Pinkston, T.E., Vimalchand, P., McClung, J.D., and Quandt, M.T., "Status of the Advanced PFBC at the Power Systems Development Facility," Proc. Coal-Fired Power Systems '94—Advances in IGCC and PFBC Review Meeting Vol. 1, DOE/METC-94/1008 (DE94012252), June 1994, pp. 127–137.

8. Swanson, M.L., Ness, R.O., Mann, M.D., and Haley, J.S., "Hot-Gas Filter Testing with the Transport Reactor Demonstration Unit," Proc. Adv. Coal-Fired Power Systems '95 Review Meeting, Vol. I, DOE/METC-95/1018 (DE95009732), June 1995, pp. 87–97.

CeraMem Filter Development Program

Bruce Bishop (617-899-0467)
CeraMem Corporation
12 Clematis Avenue
Waltham, MA 02154

Neil Raskin (619-452-3301)
CeraFilter L. P.
8925 Rehco Road
San Diego, CA 92121

Introduction

Advanced fossil energy power systems such as PFBC'S and IGCC's require high temperature barrier filters in order to operate effectively. In high temperature, high pressure combustors, ash must be removed from the combustion flue gas stream before it can enter a gas turbine. Ash particles will erode the turbine blades if the concentration and size of the particles is large enough, Even relatively small concentrations of particles can be very damaging, therefore, small numbers of seal or filter failures that allow bypass of the flue gas stream can not be tolerated for long periods of time. In addition, the filters must perform at very high temperatures or the power generation system will not operate at its optimum efficiency.

In gasification systems, the ash and char that is suspended in the syngas stream must be removed prior to the gas stream's introduction to other downstream air pollution control systems (e.g., hydrogen sulfide removal). The char, once captured, can be reinfected into the gasification reactors to increase the overall system efficiency. If the ash and char are not captured before the other downstream equipment, these solids can foul process piping or columns and cause downtime for the entire system.

The following paper describes, in general, a development program between CeraMem Separations and Foster Wheeler for a high temperature ceramic filtration system to be sold by their partnership, CeraFilter L.P. In addition, detailed test results of ceramic filters operating at conditions approaching those of high temperature combustors will be discussed. The successful development of this hot gas filtration system based upon the CeraMem ceramic-membrane-coated, monolithic filter will help address the critical challenges of particulate removal under the severe conditions imposed by advanced fossil energy power systems.

Research sponsored, in part, by the U.S. Department of Energy's Morgantown Energy Technology Center, under Grant Number DE-FG2-90ER80896 with CeraMem Corporation, 12 Clematis Avenue, Waltham, MA 02154; 617-899-0467

Objectives

To date, limited success has been achieved using various high temperature barrier filters under severe advanced combustion system conditions. Areas in which filters have had limited success include 1) mechanical and thermal stability of the filters, 2) high temperature sealing of the filters to the system, and 3) detrimental effects of system operation on the filters.

Mechanical and thermal stability of barrier filters has been a problem restricting the long term use of these filters at high temperatures. The present day leading technology, ceramic candle filters, has had a tendency to mechanically fail under PFBC conditions, These failures allow the bypass of flue gas and considerable amounts of damaging fly/ash particles. In addition, some candle materials have been susceptible to thermal shock and material degradation at high temperature.

Sealing of barrier filters into high temperature systems has been a challenge. A large number of seal designs have been developed to hold filters in place that are being exposed to relatively high differential pressures. Seals which fail allow particulate-laden flue gas to bypass the filter and thus lead to downstream system problems or failures,

The dynamics of filtration system operation are very complex. Two aspects that have been of concern are dust reentrainment and ash bridging. Reentrainment occurs if the ash pulsed from the filter is not allowed to settle into the ash hopper at the bottom of the filtration vessel and is reentrained back into the gas flow entering the filter. A considerable amount of cold modeling and vessel configuration testing has been performed to understand gas flows within filtration vessels in an effort to minimize fly/ash reentrainment. Bridging of ash between candle filters has been observed to occur in filtration systems operating for long periods of time. The bridging phenomena has caused mechanical failures of the candle filters.

The above issues have been considered in the preparation of the joint Product Development Program presently being undertaken by CeraFilter L.P. Therefore, the program is attempting to develop filtration systems with the following attributes:

- High particulate removal efficiency
- Refractory filter materials
- Resistance to oxidizing and reducing conditions
- Thermal shock resistance
- Mechanically rugged configuration
- Robust seal design
- Compact, modular design
- Optimum gas flow within the vessel to prevent ash retainment
- Minimum bridging potential between filters

Approach

As a solution to the above filter system problems, CeraMem has developed a compact, high temperature barrier filter that is resistant to catastrophic mechanical failure. This filter was developed under a US DOE Small Business Innovation Research grant (Grant Number DE-FG02-90ER80896) to clean hot flue gas from advanced coal conversion power processes.

The ceramic filter is based on a honeycomb ceramic monolith. This low cost ceramic material is widely used as a catalyst support for automotive catalytic converters. The monoliths are extruded in a variety of configurations and are commercially available from Coming, Inc. The monoliths have a multiplicity of "cells" or passageways which extend from an inlet end face to an opposing outlet end face. The cell structure is usually square and the cell "density" can vary from 4 to 16 cells per square centimeter,

The most commonly available monolith ceramic material is cordierite. The mean pore size of this material in the monoliths can range from about 4 to 50 microns with a porosity of 30% to 50%. The properties of these ceramic monoliths make them ideally suited for applications requiring high thermal stability, mechanical strength, and corrosion resistance. These rigid ceramics have been used for years as automotive catalyst supports where conditions of high vibration and thermal cycling are encountered in a combustion gas environment.

CeraMem modifies the honeycomb monoliths to produce high efficiency, dead-ended hot gas filters. First, a ceramic microfiltration membrane is cast onto the monolith passageway surfaces. The flow path through the monolith is then modified by plugging every other cell at the upstream face of the device with a high temperature inorganic cement. Cells which are open at the upstream face of the monolith are plugged at the downstream face. Gas is thereby constrained to flow from the inlet cells, through the porous ceramic membrane and cell walls, and then out the cells open at the downstream end. Any particles that flow into the filter with the gas stream are filtered out by the membrane. When the pressure drop across the filter rises to a predetermined level, compressed gas is pulsed back through the filter to dislodge the solids from the filter and they are collected in a hopper situated below the filter elements. A schematic of the filter is shown in Figure 1 and a photograph of an 18 cm diameter by 38 cm long filter is located in Figure 2.

This filter construction results in a number of advantages. First, the cordierite material results in a filter that is thermally stable in both oxidizing and reducing conditions, and is thermal shock resistant. The membrane coating produces a filter with high filtration efficiency, The monolith honeycomb structure, in conjunction with the housing which is similar to that of a catalytic converter, results in a mounted filter that is mechanically rugged and resistant to catastrophic failure. The honeycomb monolith also creates a filter with a large surface area to volume ratio which minimizes the size, and therefore the cost, of the filtration system. Consequently, the filters using this concept are capable of withstanding the severe environments of advanced power systems, have high filtration efficiency, and result in compact, cost efficient systems.

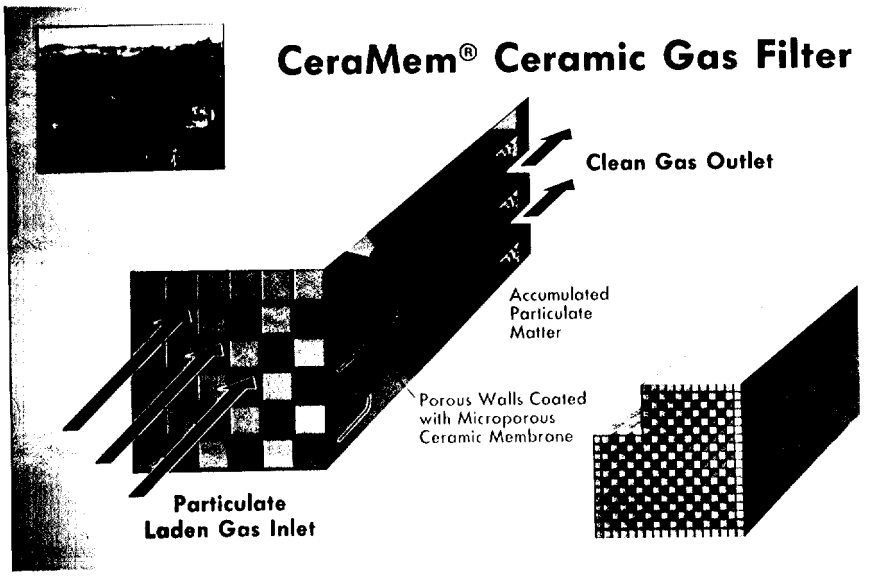

Figure 1. CeraMem® Gas Particulate Filter Schematic

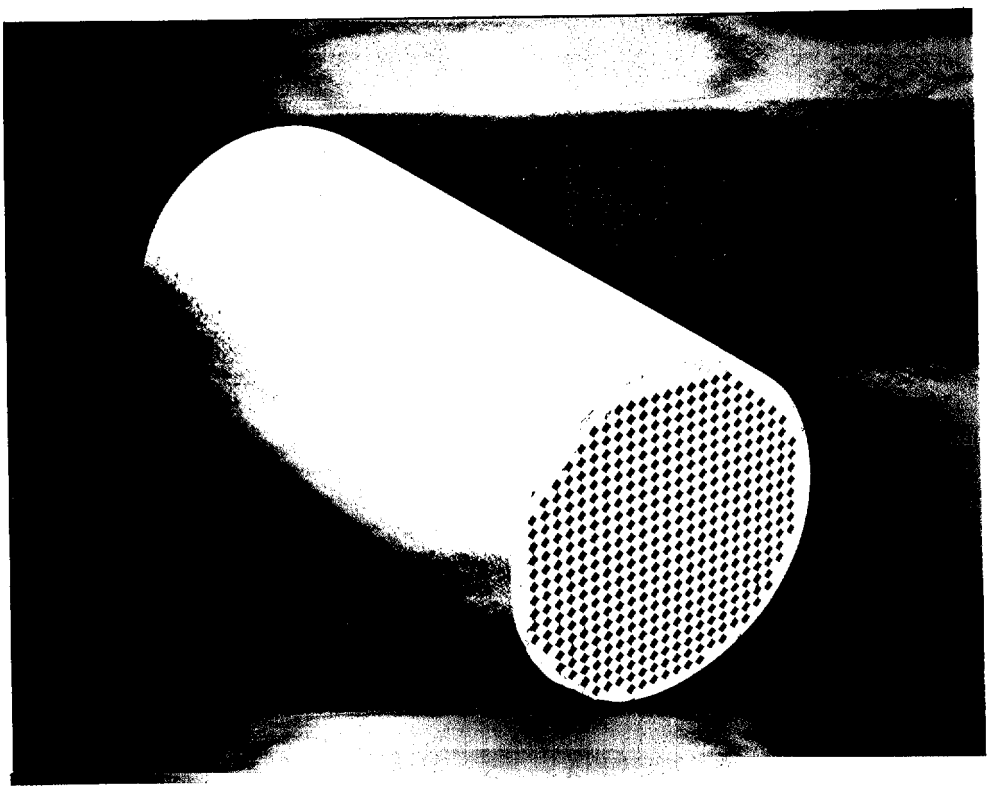

Figure 2. Photograph of 18 cm Diameter by 38 cm Long CeraMem® Gas Particulate Filter

CeraMem has entered into a partnership (CeraFilter L. P.) with Foster Wheeler to further develop the CeraMem filters and engineering systems for hot gas cleanup applications. In this partnership, CeraMem brings the filter technology while Foster Wheeler brings the system engineering capabilities and an indepth knowledge of the advanced power systems market. CeraFilter has put together a Product Development Plan through which CeraMem and Foster Wheeler have worked to bring high temperature filtration systems to commercialization.

Project Description

There are four sections of the Product Development Program. These are 1) Engineering Analysis, 2) Filter Development, 3) Filter Testing, and 4) System Design and Testing. There are a total of 16 tasks in the program, of which 14 have been completed. As part of the program, the intent is to conduct a pilot scale demonstration test. Upon successful completion of the demonstration test, the system will be ready for commercialization.

Engineering Analysis

In the engineering analysis section, several aspects of filtration systems were evaluated in paper studies. First, the conditions for design and testing were researched, The conditions selected for PFBC (non-topping) applications were a process temperature of 850 - 900°C, a process pressure of 12-17 atmospheres, and a dust loading of 50-180 g/m^3 while those for IGCC applications were 370- 540°C, 14-21 atmospheres, and 100-1500 g/m^3. It should be noted that the filtration temperature for gasification could increase depending on availability of materials, Second, the importance of backpulse gas consumption and filter pressure drop were investigated. It appears that these parameters will be more sensitive in PFBC applications than IGCC applications. Third, the effect of a pre-cyclone before a filtration system was evaluated. Fourth, the types of materials for various components throughout the system were selected. Using a variety of materials to meet the various operating conditions throughout filtration systems for both PFBC and IGCC applications is necessary in order to minimize material costs yet provide a reliable system.

Filter Development

The filter and filter mounting development tasks have been completed. First, the specifications and processes required to manufacture commercial scale filters (12” diameter x 15” length) have been developed. Prototype production runs have been completed at commercial yields to prove the manufacturing process. Second, the mountings used to connect the filter to the filtration system have been developed, The mountings have several subcomponents which have been evaluated to withstand the various operating conditions.

Filter Testing

Various aspects of the filters have been tested. First, a filter in its mounting has been tested successfully for its ability to hold differential pressure over many temperature cycles simulating actual operating conditions. Second, test scale filters have been evaluated for filtration performance during a 300 hour test on "live" flue gas at 870°C. This task will be described in detail in the results section. Third, filter performance was also tested in a cold model test in order to better understand the filtration process and formulate guidelines for successful gas filter regeneration. Fourth, a production scale filter was successfully tested in a simulated particulate-laden gas stream for 1,000 hours at temperature to determine if the mounted filter would regenerate over a long period of time. Last, a mounted filter was exposed to thermal cycling to determine if this configuration would be rugged enough to withstand actual filtration conditions. An examination following the tests indicated that no degradation of the filter or mounting construction occurred.

System Design and Testing

The last section of the develop plan called for the design of the commercial system and pilot testing. First, different subsections of the system were modeled to determine the proper designs. These included thermal gradient modeling of the filter mounted assemblies, gas flow modeling of the backpulse system, and gas flow modeling of the dirty side of the filtration system (reentrainment). Then, the entire commercial system design was put together and analyzed from the perspective of manufacturing, transportation, operation, reliability, maintenance, and capital and operating cost. The results of the Product Development Program to date indicate that the technology is now ready to be pilot tested using production scale filters in a system that represents the commercial system design.

Results

CRADA Objectives

As an example of the type of work that was performed in the Product Development Plan, the 300 hour filtration evaluation will be described. This test was sponsored, in part, by a CRADA between CeraMem and DOE METC, No. 93-012. Aspects of the project were subcontracted to the University of North Dakota's Energy and Environmental Research Center, Foster Wheeler (formerly Ahlstrom Pyropower), and The Pennsylvania State University.

The purpose of this test was to evaluate the filtration performance of CeraMem filters on "live" flue gas at temperatures similar to those in PFBC'S. The objectives of the test to be discussed in this paper areas follows:

- To demonstrate that the CeraMem filters could be cleaned effectively for 300 hours while operating on "live" particulate-laden flue gas.
- To evaluate filter operating parameters such as filter cleaning frequency.
- To investigate ash-to-filter chemical interactions.

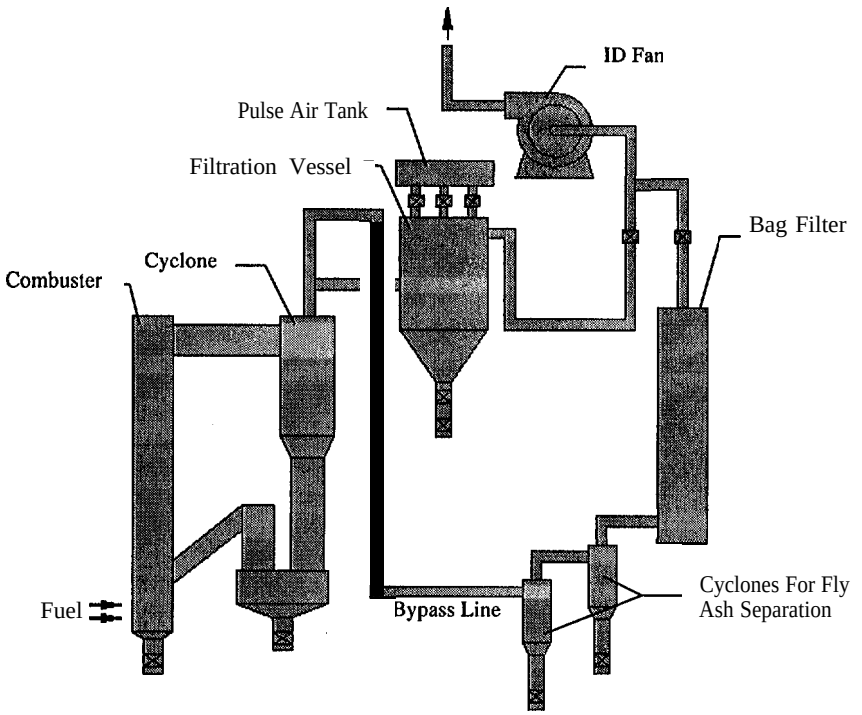

Figure 3. CRADA Filtration Vessel

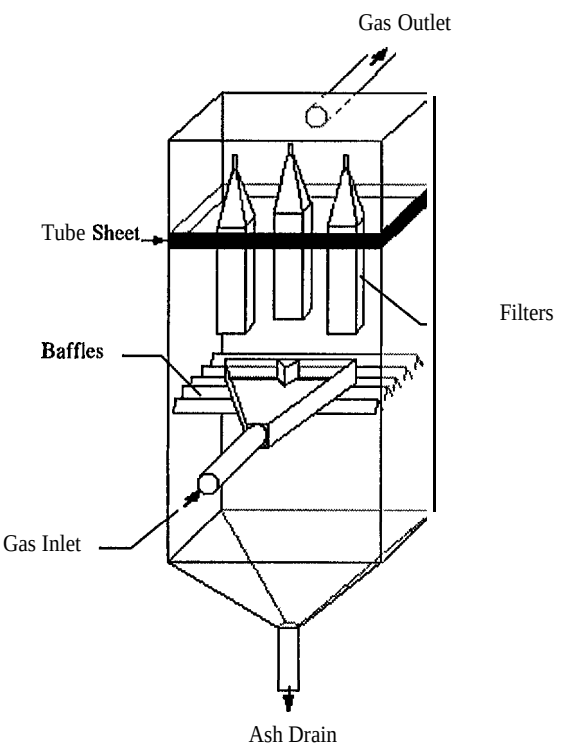

Figure 4. Circulating Fluidized Bed Combustor System Used in CRADA Testing

CRADA Materials and Equipment

The filters in this test were identical to commercial filters except that the cross section was reduced to fit the quantity of gas flow through the test facility. The filters had an 84 mm square cross section and 381 mm length with a filtration surface area of 0.62 m^2. The filters were sealed into housings using a similar approach to the design used in the commercial housing design. One end of the housing was flanged in order to attach the housed filter to the filtration system tubesheet.

Filters were tested three at a time in a single filter vessel (Figure 3) which was attached to a bench scale atmospheric circulating fluid bed combustor (CFBC; Figure 4). The test vessel was comprised of three sections. The upper section above the tube sheet contained the venturis, pulse equipment, and clean gas outlet. The middle section held the tubesheet to which the filters were attached. The lower section located below the filter inlets contained the flue gas inlet, baffles, and ash hopper.

The filtration vessel design and resulting flue gas flow was the result of modeling conducted at DOE METC. The approach to the design was to ensure uniform gas flow to the filters while minimizing any chance of ash reentrainment back into the gas flow entering the filters. The flue gas flow entered the side of the vessel from the CFBC. The gas was allowed to expand to reduce its velocity and promote drop out of large particles from the flue gas stream. After entering the vessel, the flue gas turned ninety degrees upward to enter into the bottom of each of the three filters, The flue gas was filtered as it proceeded up through the filters and then exited the vessel by flowing through the venturis and then out the clean gas outlet. During backpulsing, jets of gas and particles were sent through the arrow baffles located just below the flue gas inlet. The intent of the baffles was to minimize ash reentrainment into the inlet flue gas flow. Once below the baffles, the backpulse gas velocity was reduced due to the volume of the vessel and the particles were allowed the settle out of the gas stream. Ash was removed from the hopper via a slide gate valve.

The backpulse system was fabricated to allow individual pulsing of each filter. Compressed air at 6.5 bar was pulsed by fast acting valves through dedicated nozzles into venturis located over each filter. The combination of the gas pulsed into the venturi and gas flow induced by the venturi design resulted in a pressure differential across the filter large enough the dislodge the ash from the filter.

The entire vessel was instrumented with fast response pressure transducers and thermocouples to allow for evaluation of pressures and temperatures during the testing, All data was acquired through two independent data acquisition systems. One system was used to record the combustion and emission data at slow rates. The second system acquired filter vessel data (temperature or pressure readings) at either slow rates during normal operation or at high rates during backpulsing. This second system also triggered the backpulsing sequence.

The test facility fired a mixture of high sulfur bituminous coal (Illinois No. 6; 9.7% ash) and industrial grade limestone (Iowa Industrial Lime No. 1) that had been premixed prior to

being introduced into the combustor. The resultant fuel and limestone mixture gave a Ca/S molar ratio of 2.

CRADA Operating and Test Procedures

The filter testing was conducted in two 150 hour tests. During the first test, three filters were tested. After completing the first test, one filter was removed and a fourth new filter was installed, After completing the change out, a second 150 hour test was conducted. At the end of the 300 hour test period, two filters had been exposed to 150 hours of operation while two others had been exposed to 300 hours of operation.

The test facility operated very well during the two 150 hour tests. The fuel feed rate was approximately 5,5 kg/hr resulting in an average bed temperature of 870°C. The combustion efficiency was about 99,8% for each run. The resulting flue gas (dry basis) had about 17% CO_2 and 4% O_2.

The filter operating conditions for the two 150 hour tests were very similar. The filters were operated at a temperature of approximately 863°C and a total gas flow of about 39.7 Nm^3/hr which resulted in a face velocity of about 2.24 cm/s. The baseline pressure drop across the filters at the start of the tests was about 25 mbar. The filters were automatically regenerated at 40 mbar differential pressure in each test. The number of pulses per cleaning cycle was one pulse per filter per cleaning cycle for the first test and two pulses per filter per cleaning cycle for the second test.

During each 150 hour test, ash samples were taken at the filter vessel inlet and outlet by personnel from the University of North Dakota's Energy and Environmental Research Center, Samples were obtained using EPA Method 5 taking approximately 1% of the total flow.

In order to measure the thermal shock that the clean side of the filters experienced during the very rapid backpulse process, optical pyrometers were used. Three high-speed, two-color, fiber optic pyrometer systems were used to measure the filter surface temperature at the center, edge, and corner of one filter during backpulsing. These tests were performed at approximately 600°C due to system limitations prior to the systems being completely debugged, However, these measurements gave an indication of the type of thermal shocks that the filter materials were exposed to without the effects of instrument lag experienced by other thermal sensors.

After the tests were completed, the midsections of the two filters that were exposed to 300 hours of operation were sent to The Pennsylvania State University for mechanical property characterization, Flexural strength specimens about 5 cm in length were machined from the filter samples, Two different types of specimens were prepared for mechanical testing. A "clean-side" specimen was prepared where the maximum tensile stress during the flexural strength test was generated along a surface which was not exposed to particulate. A "dirty-side" specimen was prepared where the maximum tensile stress during the flexural strength test was generated along

a surface which was exposed to particulate. Four point bend tests were performed on approximately 10 specimens at each of three different temperatures.

CRADA Results

Figure 5 shows a plot of filter pressure drop versus time for a selected 50 hour section of the first 150 hour test. As indicated above, the backpulse was triggered at 40 mbar after an increase in filter pressure drop from the initial 25 mbar. Overall, the backpulse cleaning resulted in cleaned filter pressure drops of about 28.6 mbar and 29.9 mbar for the two tests respectively after 150 hours of operation, In both cases, the initial duration between pulse cleanings was about 45-50 minutes at the start of the test and decreased to 30 minutes at the end of the test, The slight increase in filter pressure drop and decrease in filtration cycle time are due to filter conditioning under the test conditions. In this test, the use of double pulses was not more effective than a single pulse in maintaining a lower clean out filter pressure drop.

Figures 6 and 7 show plots of filter permeance versus time for both 150 hour tests, Permeance is defined as follows:

$$k_{20^\circ C} = \frac{v \times \mu}{dP \times \mu_{20^\circ C}}$$

where

$k_{20^\circ C}$	= permeance, cm/s-mbar at 20"C
v	= filtration face velocity, cm/s
μ	= dynamic viscosity at test conditions
dP	= pressure drop, mbar
$\mu_{20^\circ C}$	= dynamic viscosity at 20"C

The use of permeance normalizes the gas filter pressure drop to face velocity and temperature which may vary during an actual test.

In both Figures 6 and 7, the permeance is approaching a constant value. This indicates that the filters are going through an initial conditioning which may be the result of various ash-to-filter interactions. Over a long filtration run, the backpulse cleaning mechanism would continue to clean the filters and maintain the permeance at a value slightly less than that indicated after each 150 hour run,

Table 1 shows the particulate sampling information obtained by the University of North Dakota. For both tests, the dust loading entering the filter vessel was between 1.8 and 1.9 g/Nm^3. The dust loading exiting the filter vessel was much smaller at 0.0025 g/Nm^3 and 0,0011 g/Nm^3 for the two tests respectively. While the outlet dust loading is well below the target maximum concentration for gas turbine operation, the effective particulate capture efficiencies do not appear to be overly high. Analysis of the outlet ash collected during the tests indicated that a significant percentage of the outlet materials was from system contamination. As a result, the actual filtration efficiencies of the filters should be much higher than those reported.

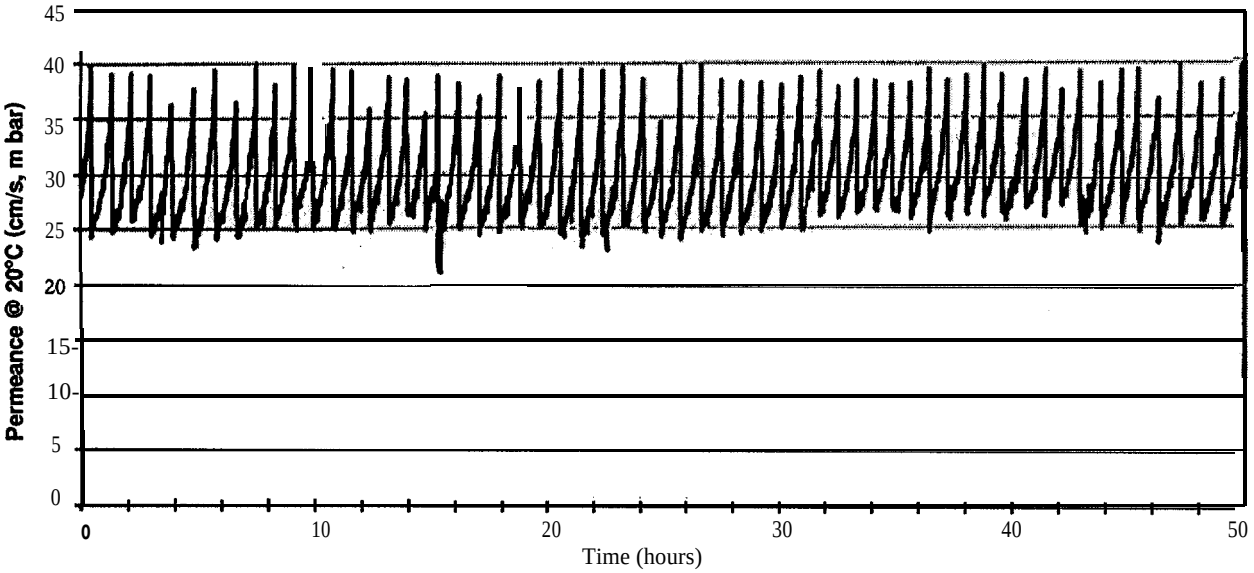

Figure 5. Selected 50 Hours Interval of Filter Pressure Drop Versus Time from First Test

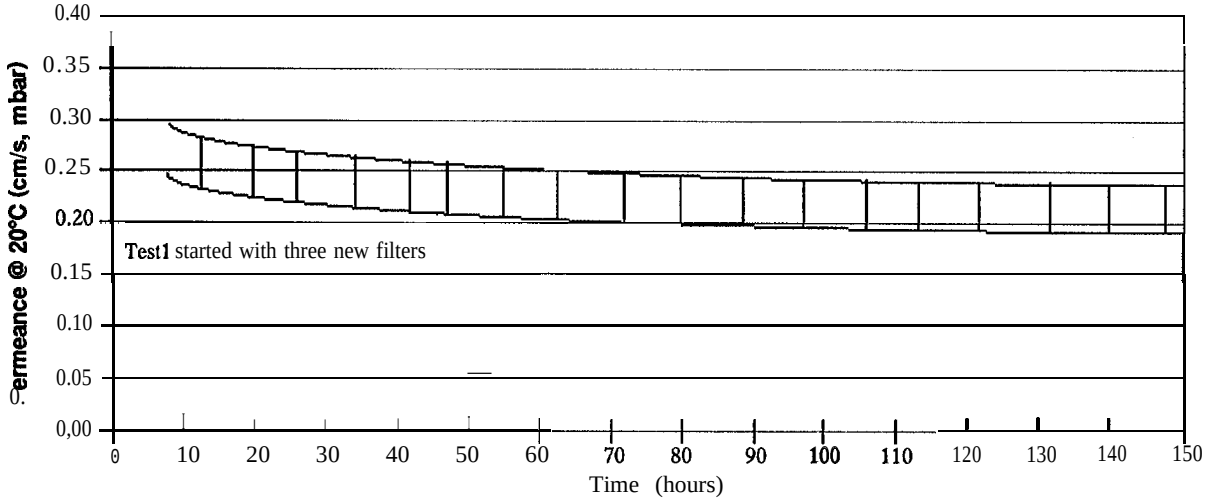

Figure 6. Permeance Versus Time for First 150 Hour Test

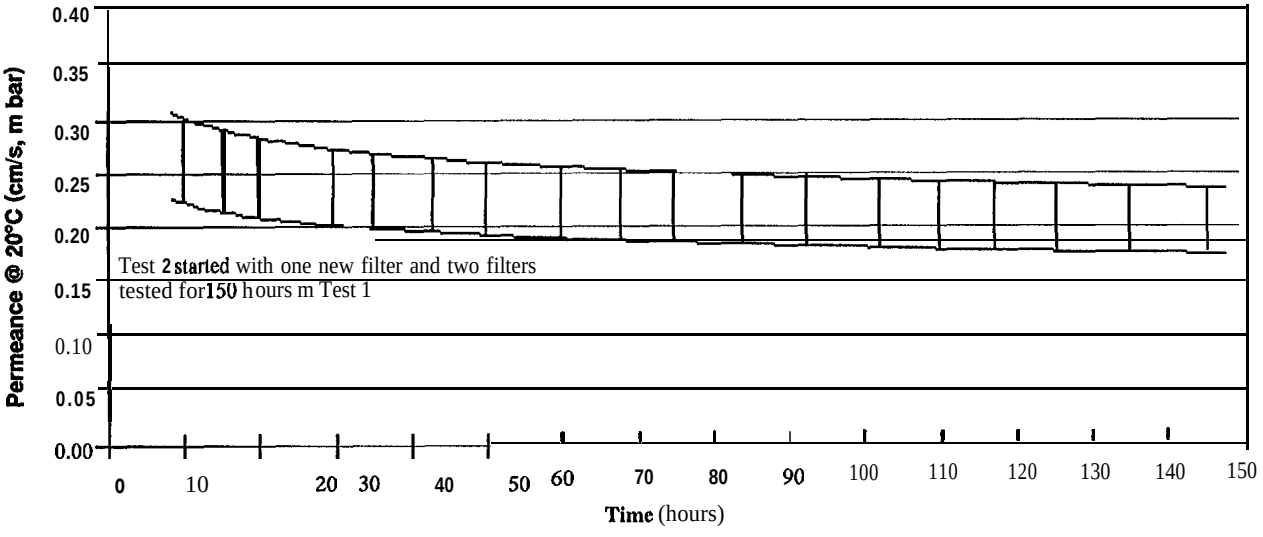

Figure 7. Permeance Versus Time for Second 150 Hour Test

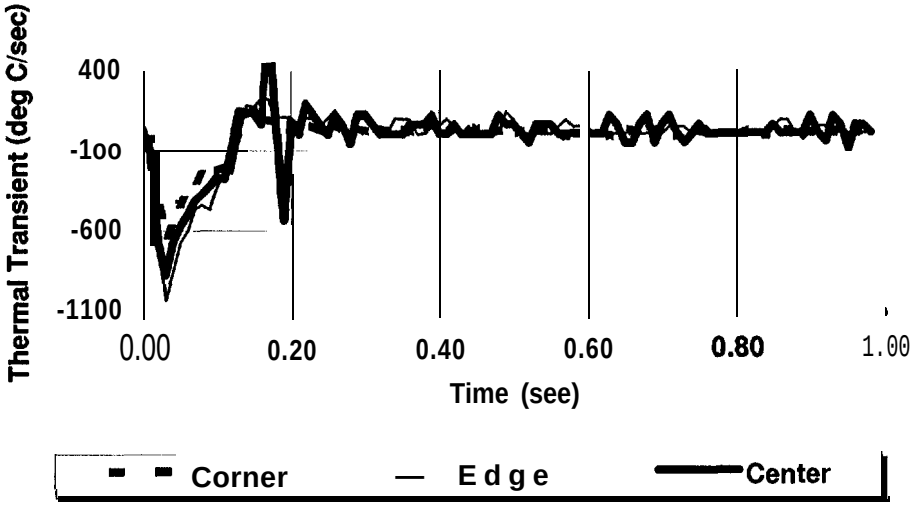

Figure 8. Gas Filter Termal Shock During Backpulse at 600°C

Table 1. Particulate Removal Efficiency as Measured in Tests 1 and 2

Parameter	Test Number 1	Test Number 2
Inlet Loading	1.88 g/Nm^3	1.83 g/Nm^3
Outlet Loading	0.0025 g/Nm^3	0,0011 g/Nm^3
Efficiency	99.87%	99.94%

Figure 8 shows the type of thermal shock the clean face of the filter is exposed to during operation, Thermal shocks approaching 1000”C per second were measured using the optical pyrometry equipment. It should be noted that these thermal shocks had no effect on the cordierite monolith support material due to its very low thermal expansion coefficient,

Table 2 shows the results of the flexural strength tests as a function of temperature. It is clear that the filter materials were as strong after 300 hours as they were at the start of the test, In addition, it makes no difference whether the surface of maximum tensile stress during the flexural strength test was exposed directly to the particulate-laden flue gas or not. As a result, it can be concluded that ash and alkali contaminants which impinged on the filter surfaces had not interacted with the filter materials so as to change their inherent strength. In addition, the thermal shocks that were experienced by the filter during each backpulse sequence had no effect on filter strength.

Table 2. Filter Flexural Strength as a Function of Temperature After Testing for 300 Hours

Temperature	Average Flexural Strength (MPa)		
	Unexposed	Clean Side	Dirty Side
20°c	10,1 +/- 0.4	10.9 +/- 0.7	10.4 +/- 0.7
800°C	10,2 +/- 1.3	11.3 +/- 1.8	12.3 +/- 2.2
870°C	No Data	10.7 +/- 1.5	12,5 +/- 1.0

CRADA Conclusions

Four filters were successfully tested over the course of a 300 hour test using “live” flue gas at 870°C that was produced by an atmospheric circulating fluidized bed combustor. Specifically, the filters were able to be cleaned over the time period with a small increase in filter resistance attributed to filter conditioning. Particulate removal was considered to be high (> 99.94%) since a significant amount of material seen downstream was concluded to have been contamination. Thermal shock evaluations indicated that the filters were exposed to gradients approaching 1000°C/s based on optical measurements, However, even with exposure to this thermal shock and ash and alkali at high temperature, there was no indication that the filter material degraded. Furthermore, it was concluded that long term testing under process conditions of commercial interest was a necessary next step in the development of the technology.

Benefits

Based on the Product Development Program tasks completed to date, several benefits can be seen in this technology as compared to candle filter technology. These are described as follows.

1, The honeycomb monolith structure is less prone to catastrophic failure, The combination of advanced monolith support material microstructure, relatively equiaxed honeycomb structure, and rugged mounting design make it very unlikely that the filters will catastrophically fail and leave a gapping hole through which particulate-laden flue gas can pass.
2. Compared to some candle filter materials, the strength of the CeraMem filter does not change as a function of temperature. Also, due to the high temperature corrosion resistance of the materials, the filters can withstand high temperature oxidizing conditions better than some candle filter materials.
3. The thermal shock resistance of the cordierite monolith is excellent due to its phase composition and advanced microstructure.
4. The present CeraFilter commercial filtration system design has a higher packing density (surface area per unit volume of vessel and surface area per vessel) than candle filter systems by a minimum of 25%. As a result, not only are there fewer vessels required to process a particular gas stream, but the quantity of auxiliary equipment (e.g., compressors), structural steel, and plan area are significantly reduced.
5. Once demonstrated, the present CeraFilter commercial filtration system design will be a minimum of 25% less costly over a 20 year life cycle as compared to candle filter systems.

Future Activities

The status of the overall development program is that the technology is ready for pilot testing. CeraFilter is presently pursuing opportunities to conduct pilot testing over long periods of time (2,000 to 10,000 hours) on advanced combustion power systems of reasonable size so as to make them representative of the full size commercial system.

Acknowledgements

The authors would like to acknowledge the support of DOE METC under SBIR Grant Number DE-FG02-90ER80896 and Mr. Norman Holcombe who was the Contracting Officer's Representative, The period of performance for this grant was May 1991 to March 1996. The authors would also like to thank DOE METC for the CRADA support (Number 93-012) and DOE's project manager, Mr. Douglas Straub. In addition, the authors would like to acknowledge the subcontractors who worked on the CRADA project: Dr. K. Katrinak and Ms. T. Watne of the University of North Dakota's Energy and Environmental Research Center, Mr. J. Tuncay of the Foster Wheeler Development Corporation, and Prof. Richard Tressler at The Pennsylvania State University.

Operation of a Pressurized Gasifier, Hot Gas Cleanup System and Turbine Simulator

Stephen Bevan - GE Environmental Services
Raul E. Ayala GE-CRD
Anthony H. Furman GE-CRD
David J. Najewicz GE-CRD
200N. Seventh Ave.
Lebanon, PA 17046

Abstract

GE Environmental Systems, supported by the GE Corporate Research and Development (GE-CRD) center is developing a high temperature (1000 *F) moving bed desulphurization system for use in advanced IGCC systems. The hot gas cleanup system is based on the use of palletized mixed metal oxide sulfur sorbents to remove H_2, and COS from coal gas, followed by controlled regeneration of the sorbent to produce an SO_2 rich tail gas for final conversion to sulfuric acid or elemental sulfur. Testing of a pilot scale system at the CE-CRD has been underway since 1990, Previous system testing has resulted in numerous process improvements and hardware modifications to improve the performance of the system. Initial testing utilized Zinc Ferrite as the sorbent material, with subsequent testing of Zinc Titanate and other proprietary sorbents, as previously reported. The hot gas cleanup system also contains a circulating fluidized bed chloride removal system to remove Chlorine from the coal gas using sodium bicarbonate as a sorbent.

Efforts during 1995/96 have focused on identifying and testing sorbents for use in the DOE sponsored Clean-Coal IGCC/hot gas cleanup demonstration project under construction by Tampa Electric in Polk County Florida. Two long duration, 200 hour tests were completed since the last Contractor's Report. Test 8 based on a modified Zinc Titanate sorbent was conducted in September 1995. Test 9 based on METC-10 sorbent was performed in March 1996. In addition, during Test 8 the turbine simulator was operated using an improved low-BTU combustor. Test 9 included the first operation of an advanced Rich-Quench-Lean (RQL) combustor designed to minimize the conversion of ammonia (present in the coal gas) to NO_x during the combustion process, The RQL testing was very successful resulting in ammonia to NO_x conversion of So/O.

Research sponsored by the U.S. Department of Energy's Morgantown Energy Technology Center, under contract DE-AC21-87MC23 170, with GE Environmental Systems, 200 North Seventh Street, Lebanon, PA; telefax 717-274-7103.

Hot Gas Desulfurization Using Transport Reactors

Eric L. Moorehead (moorehead@mwk.com, 713-492-5713)
The M.W. Kellogg Technology Company
16200 Park Row
Houston, TX 77084

Gunnar B. Henningsen, Satyan Katta, and James J. O'Donnell
The M.W. Kellogg Company
601 Jefferson Avenue
Houston, TX 77210

Abstract

Sierra Pacific Power Company is building a 100 MW_e IGCC power plant based on KRW fluid bed gasifier technology that utilizes transport reactors for hot gas desulfurization and sorbent regeneration. Use of a transport absorber avoids the need for pre-filtration of dust-laden gasifier effluent, while a transport regenerator allows for the use of 100% air without the need for heat exchange equipment.

Selection of transport reactors for hot gas desulfurization using a proprietary sorbent, based on testing performed in a transport reactor test unit (TRTU) at the M. W. Kellogg Technology Development Center and in a fixed bed reactor at Morgantown Energy Technology Center (METC), is outlined in the paper. The results obtained in these two test facilities and reasons for selecting transport reactors for the above IGCC power plant in preference to either fixed bed reactors or fluidized bed reactors are discussed. This paper reviews the evolution of the hot gas desulfurization system designs and includes selected results on H_2S absorption and regeneration of sulfided sorbent over several absorption/regeneration cycles conducted in the TRTU and the METC fixed bed reactor.

The original design for the Sierra Pacific Project was based on fixed bed reactors with zinc ferrite as the sorbent. Owing to high steam requirements of this sorbent, zinc titanate was selected and tested in a fixed bed reactor and was found unacceptable due to loss of strength on cyclic absorption/regeneration) operation. Another sorbent evaluated was Z-Sorb® sorbent, a proprietary sorbent developed by Phillips Petroleum Company. This sorbent was found to have excellent sulfur capacity, structural strength and regenerability. Steam was found unsuitable as fixed bed regenerator diluent, this results in a requirement for a large amount of inert gas, whereas a transport regenerator requires no diluent. The final Sierra design features transport reactors for both desulfurization and regeneration steps using neat air.

Research sponsored by the U.S. Department of Energy's METC, under cooperative Agreement No. DE-FC21-92MC29309 with Sierra Pacific Power Company, 6100 Neil Road, P.O. Box

10100, Reno, Nevada-89520.

INTRODUCTION

The Hot Gas Desulfurization (HGD) Unit for the Sierra Pacific Power Company (SPPCo) Piñon Pine Project has evolved almost continually since the start of the project. Originally, the design was based on a fixed bed cyclic reactor unit, using zinc ferrite as the sorbent. Although this sorbent is very effective in capturing H_2S, it has the undesirable characteristic of promoting carbon formation unless a large quantity of steam is added to the process gas. This requirement of process steam was not practical for the specific application at Sierra Pacific. To satisfy the specific requirements at Piñon Pine, a program was initiated to evaluate and identify an alternative HGD sorbent.

The first alternative sorbent selected for evaluation was a zinc titanate formulation reputed to have both good absorption capacity and durability. However, tests on this material showed that it was unable to withstand the repeated cycling between absorption and regeneration, experiencing both physical and chemical deterioration (1).

The second sorbent evaluated was a proprietary material developed by the Phillips Petroleum Company, Z-Sorb® sorbent (2). Extended fixed bed testing conducted at METC demonstrated that the sorbent has outstanding physical durability, but its initial high capacity decreased significantly with repeated cycling. Steam, used as a diluent during regeneration, was identified as a major cause of this deterioration. Although this sorbent is satisfactory for the proposed fixed bed commercial system, its use requires the addition of a large and expensive nitrogen system for supplying the diluent required during regeneration.

In order to reduce the cost of the desulfurization system, The M. W. Kellogg Company proposed the use of a transport reactor design, using Z-Sorb® sorbent. This concept was demonstrated in Kellogg's pilot plant in mid-1993 and appeared to be a viable alternative to the fixed bed design. A transport reactor system has the advantage of not requiring dilution gas for regeneration, and has the additional advantage of limiting the exposure of the sorbent to high temperatures. The latter is also suspected of contributing to loss in sorbent capacity in a fixed bed reactor system..

OBJECTIVE

The objective of the project to be discussed was to obtain the necessary design data for the transport system, and to answer some of the technical questions which arose from the fixed bed test results, a comprehensive test program was developed and carried out at Kellogg's Technology Development Center (KTDC).

APPROACH

I. METC Testing of Z-Sorb® Sorbent

In order to evaluate and qualify Z-Sorb® sorbent for application in original fixed bed cyclic reactor design of the Piñon Pine desulfurization reactor system, METC conducted a total of forty absorption tests (3). The test apparatus used in this study was a 2" ID fixed bed reactor. These tests investigated sorbent performance in terms of sulfur capacity and durability under a variety of absorption conditions. Parametric tests were done to determine optimum operating conditions for the commercial reactor and included evaluation of superficial gas velocity, absorption temperature, HCl in the feed gas, diluents for use in sorbent regeneration, and various regeneration techniques.

The key conclusions from the testing at METC were:

1. The sulfur absorption capacity for Z-Sorb® sorbent averaged about 11-15 wt.% sulfur, with good reproducibility. The sorbent also showed excellent physical stability, with no loss of physical integrity.

2. At absorption temperatures of 900-1100°F the absorption rate is essentially independent of temperature. Superficial gas velocity was varied between 0.5 fps and 2.0 fps, and results indicate that the reaction wave front is quite short, approximately the depth of the experimental bed (16 cm) at velocities of 1.0-1.5 ft/s.

3. At temperatures of 900-1100 °F, sulfur sorbent capacity declined as a function of the number of regeneration cycles. In these tests the capacity reached a final lower level of 4-6 wt.% sulfur. During regeneration, the use of either steam or nitrogen is required for minimizing sorbent bed exotherms.

4. At regenerator temperatures below 1100 °F, the sorbent is partially sulfated, leading to lower sulfur absorption capacities.

5. Regeneration at temperatures around 1350°F results in complete regeneration of the sorbent. No metal sulfates were observed using these higher regeneration temperatures.

6. The physical stability of the sorbent is affected by the use of high regeneration temperatures.

On the basis of these test data, a process design was proposed for the Piñon Pine HGD unit. This proposed HGD unit for Piñon Pine, required a large amount of diluent nitrogen to be available during regeneration. The production of this nitrogen required the installation of an air separation unit at Piñon Pine. The capital cost for the air separation unit was found to be too high for inclusion in this project.

The need to identify an alternative process for using Z-Sorb® sorbent at Piñon Pine that will meet the technical and financial objectives of this project led to the application of a transport

reactor for this service. The major advantage that the transport reactor was believed to offer was that the heat balance of the absorption (riser) and regeneration could be established such that there was no need for a large volume of a diluent nitrogen stream. By limiting the sulfur regeneration per cycle to a level such that the heat liberated during regeneration does not lead to excessive exotherms, the need for the diluent nitrogen stream is eliminated.

Simplified Transport Reactor System

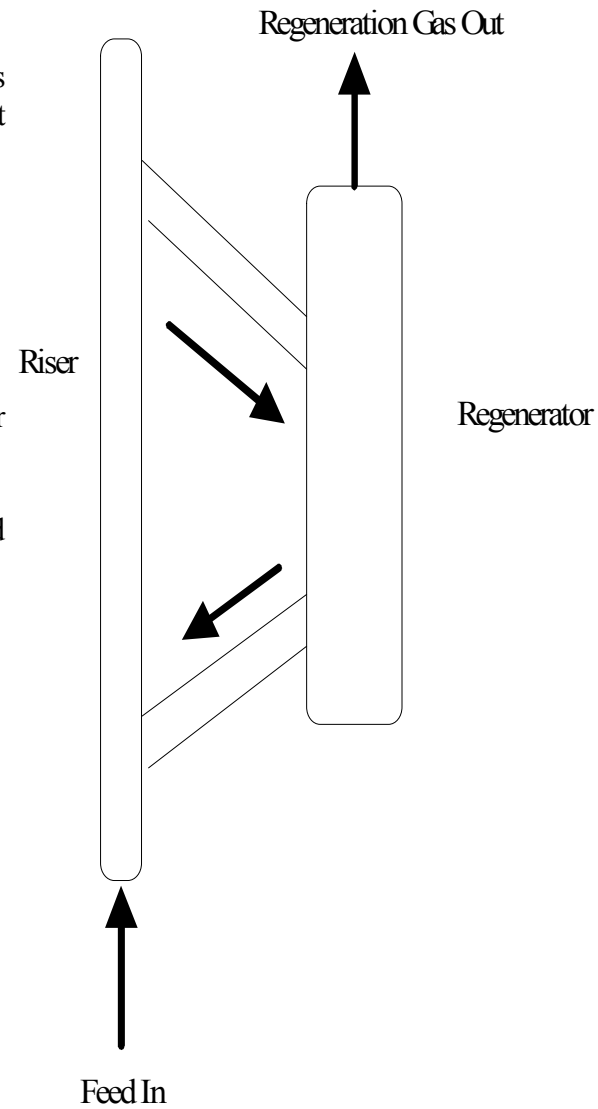

II. Features of the Transport Reactor

For the purposes of this discussion, a transport reactor is defined as a dilute phase, fluid bed reactor. In its simplest form, the transport reactor is analogous to a modern day riser reactor commonly used in the fluid catalytic cracking unit of a modern day refinery. Figure 1 presents a simplified process flow diagram of a generic transport reactor system.

In this system, there is a riser absorber and a regenerator that are coupled such that circulating solids continually pass from the riser standpipe to the regenerator back to the riser absorber.
For hot gas desulfurization applications, the riser absorber is used for the absorption of H_2S, and the regenerator is used for oxidation of the metal sulfide to generate SO_2.

The simplified stoichiometry for these two basic reactions are presented below:

Riser Reactor

$$ZnO + H_2S \longrightarrow ZnS + H_2O \qquad (1)$$

Regenerator Reactor

$$ZnS + 3/2\ O_2 \longrightarrow ZnO + SO_2 \qquad (2)$$

Overall Reaction

$$H_2S + 3/2\ O_2 \longrightarrow + SO_2 + H_2O \qquad (3)$$

In general, the residence times for the riser reactors are significantly shorter then the residence times for regeneration. In addition, the linear velocities of the solids being transported in the riser are significantly higher than those for the regenerator. Table 1 summarizes typical ranges for residence times and solids velocities commonly used in a typical transport reactor system.

Table 1: Characteristics of Riser and Regenerator Reactors		
	Residence Time	Linear Velocity
Riser	1-10 seconds	10-30 ft/sec
Regenerator	1-10 minutes	< 15 ft/sec

The successful application of a transport reactor in the place of fixed bed reactors for hot gas desulfurization at Piñon Pine demands that the following requirements be addressed:

- The rate of H_2S absorption must be significantly fast such that no sulfur breakthrough from the riser to the regenerator is observed.
- Regenerator must be capable of operating using neat air as oxidant. Sorbent must be capable of initiating regeneration at 1000 ^{o}F, temperature at which sulfided sorbent enters the regenerator.
- Sorbent must be operated at partial loading, as regeneration requires only a small amount of the sulfide is oxidized per pass to reach maximum operating temperature.
- The successful sorbent must be able to retain its activity over multiple cycles.
- Attrition rate of the sorbent must be low, preferably in line with chemical deactivation rate.
- Fines emissions from absorber require that the transport absorber be located ahead of the absolute filter, this in turn means that char fines from the gasifier must pass through the absorber without interfering with the operation of the absorber and/or regenerator.

As discussed further in this paper, the transport reactor system designed by The M. W. Kellogg Company in combination with the proprietary sorbent developed by Phillips Petroleum Company, meets all of these requirements.

Heat Balance Considerations

A key feature of the transport reactor for HGD, is the coupling of the sulfur absorption and sorbent regeneration. Circulation of sulfided sorbent from absorber standpipe to regenerator is such only a small amount of the sulfide is oxidized per pass. This oxidation heat is absorbed by the sorbent and given up in the riser absorber.

III. Transport Reactor Development at Kellogg

The results from the fixed bed testing at METC clearly demonstrated that Z-Sorb® sorbent was an effective sorbent for HGD application using a cyclic fixed bed reactor system. To use a transport reactor for this service however, requires that the absorption rate of H_2S be exceedingly high. Given the short residence times of transport reactors (Table 1), the absorption of H_2S must occur within a few seconds.

In 1993, Kellogg modified its pilot plant sized transport reactor test unit (TRTU) that was supporting gasification studies, in order to demonstrate the application of this reactor technology for HGD (3). The results from this study, summarized in Table 2, clearly demonstrated that the rates of H_2S absorption were very high. On the basis of these results, the development of the transport reactor HGD unit for Piñon Pine was formally initiated.

In support of this development activity, three different reactor systems were used.

Reactor 1: A small fluidized bed quartz reactor was used to determine sorbent capacity.

Reactor 2: A larger fluidized bed unit (BRU) was used for a long term multi-cycle test.

Reactor 3: Transport reactor conditions required for adequate absorption and regeneration were evaluated in the TRTU. This unit, as well as a plastic cold flow model corresponding in design to the TRTU, were used to investigate the capture and interaction of fines with circulating sorbent.

Sulfur capacity tests were conducted with fresh sorbent as well as samples exposed to steam and an inert environment (N_2) at temperatures of 1000-1400°F. In all tests, the physical form of Z-Sorb® sorbent was consistent with that required for use in a transport reactor. In particular, the particle size was in the range of 40-300 microns.

RESULTS

I. Sulfur Capacity

Using Reactor 1, the sulfur absorption capacity of fresh Z-Sorb® sorbent was measured at 12.0-12.3 wt.%. This sulfur capacity is consistent with the results reported by METC for the pelleted form of Z-Sorb® sorbent. (Table 2)

Table 2: Summary of Z-Sorb® Sorbent Sulfur Capacities		
Temperature, °F	Atmosphere	Sulfur capacity, wt.%
1000	nitrogen	12.8
1400	nitrogen	12.0
1000	steam	12.1
1400	steam	3.2

Exposure to steam at temperatures above 1000°F reduced the sorbent capacity significantly, with the capacity falling to about 3 wt.% after a 1400°F steam soak. Exposure to N_2 at temperatures as high as 1400°F had no apparent effect.

II. Multi-Cycle Tests

The multi-cycle test in the BRU (Reactor 2) consisted of 20 absorption and regeneration cycles, with H_2 pretreatment, before the absorption cycle, being included in about half of the runs. The absorption cycles, primarily done at 1000°F, loaded the sorbent to nominally 1 wt.% sulfur using a feed gas containing 1 mole% H_2S. Regenerations were done with N_2-diluted air (1.5, 3.5 mole% O_2), with the key variable being the regeneration temperature. The following observations were made based on the results from 20 cycles of testing in the BRU:

Absorption

- Absorption of H_2S was very good with no H_2S in the outlet gas during the absorption cycles.
- When no pretreatment step was used prior to absorption, SO_2 evolution exceeded conc. of 1000 ppm during absorption. This indicated that the sulfate formed during regeneration was reduced to ZnO with SO_2 evolution.
- With pretreatment in 5 to 15% H_2, SO_2 is evolved, but does not react with H_2 to form H_2S. Subsequent absorption gives off no SO_2.

Regeneration

- In all the tests done in the quartz reactor and the BRU, sulfate was formed during regeneration. The amount varied depending upon the temperature.

- Heating the sorbent to 1370 °F prior to regeneration and a peak temperature of 1400 °F yielded the least amount of SO_2 during pretreatment.

- For the initial and peak temperatures of 1370 and 1400 °F during regeneration, the amount of sulfur (present on the sorbent) converted to sulfate during regeneration is about 0.43%.

These tests showed complete absorption of H_2S over the entire multi-cycle period. Sulfur capacity dropped slightly, to 11 wt.% after 17 cycles and to 10 wt.% after the final cycle. During the initial absorption cycles, as well as the hydrogen pre treatment periods, SO_2 (not H_2S) evolved due to the reduction of sulfate formed during the prior regeneration per reaction (4). The SO_2 leakage observed during the absorption cycles may be attributed either to the stripping of SO_2 from the reactor wall/piping or to the following reaction of sulfate formed during regeneration:

$$ZnSO_4 + H_2 \text{ ---> } ZnO + SO_2 + H_2O \qquad (4)$$

The concentration of SO_2 was minimized by running the regenerations at nominally 1400°F. At this temperature, residual sulfate on the regenerated sorbent was less than 0.5 wt.%.

III. Transport Reactor Pilot Plant Testing

Description of Transport Reactor Test Unit

The TRTU at Kellogg's Technology Development Center (KTDC) was originally built for developing a new coal gasification technology. A simplified schematic of the TRTU is presented in Figure 2.

The general features of the TRTU include a mixing zone, a riser, a cyclone and a standpipe. The mixing zone of the reactor, which can be operated either as a dense phase fluid bed or as an entrained reactor. Solids from the standpipe are returned to the bottom of this zone. Fluidization gas which can be N_2, air, steam, O_2, or any combination of these, is fed to the bottom of the mixing zone through a specially designed gas distributor.

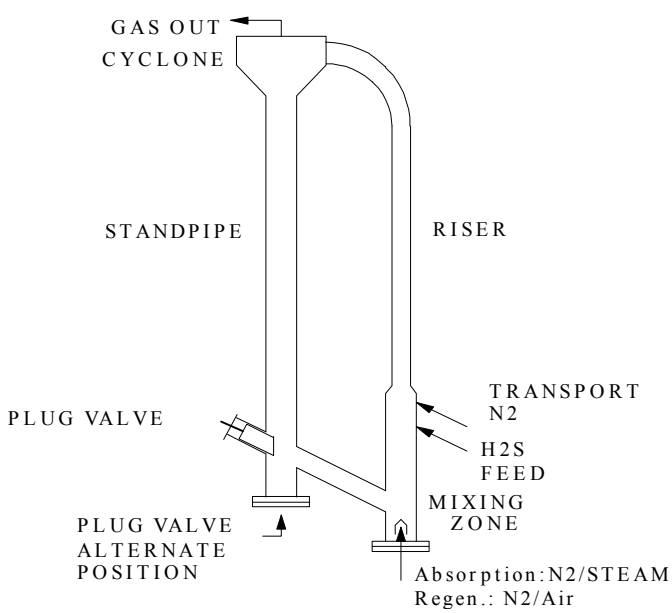

Figure 2 Simplified Process Flow Diagram of Kellogg's TRTU

Above the mixing zone is a 32-foot tall, 1" riser. At the base of the riser is an injection nozzle that is used for introducing feed gases, which include H_2 and H_2S/N_2 blend. Dilution of the this feed gas with the mixing zone fluidization gas resulted in actual H_2S concentration of 1-2 mole %. At the velocity of 12.8 ft/s used during many of the runs, the gas residence time was about 2.5 seconds in the riser section.

Gas and solids (sorbent) leave the top of the riser and flow directly to a high efficiency cyclone. Gas leaving the cyclone is cooled and the volume and composition are measured.

Solids from the cyclone enter the top of the standpipe. The standpipe consists of a 33-foot tall, 1.5" pipe. Solid samples may be withdrawn at any time from the bottom section of the standpipe. Makeup solids are added to the top of the standpipe as needed. Solids flow from the bottom of the standpipe to the mixing zone of the riser via a lateral transfer line.

The testing with the TRTU focused primarily on sulfur absorption and sorbent regeneration studies.

Sulfur Absorption Tests

The sulfur absorption tests in the TRTU included 5 complete cycles, with multiple regenerations being done during 2 of the cycles. Absorptions were done typically at 1000°F with a nominally 1 mole % H_2S feed gas. Regenerations were done using air, with the regeneration temperature being varied from 1000°F to 1200°F to study its effect.

The following observations were made based on the TRTU testing:

- Z-Sorb® sorbent was loaded to as high as 8.3 wt.% sulfur. H_2S was not detected in the outlet gas throughout the absorption cycles.
- Hydrogen pretreatment resulted in very low SO_2 release in subsequent absorption cycles.
- During regeneration, oxygen breakthrough resulted below 1200°F temperature.
- Residual sulfate existed and was highest at lowest regeneration initiation temperature. Chemical analyses of samples after regeneration showed sulfate contents of 0.1-0.2 wt.%.

Regeneration Studies

The effect of oxygen partial pressure and temperature on the regeneration of pre-sulfided Z-Sorb® sorbent was studied in the TRTU. This test was run to determine the most favorable regeneration conditions for the multi-cycle Z-Sorb® sorbent test runs. The Z-Sorb® sorbent was

pre-sulfided in the absence of steam to a nominal 6 wt.% and regenerated to a nominal 4 wt.%. The reactor was operated at 85 psig pressure and at three riser temperatures namely, 1000, 1100 and 1200°F. Two oxygen partial pressures equivalent to 40% and 60% by volume of oxygen in the oxidant stream were used. The oxidant stream was injected into the riser for a sufficient time to reduce the sulfide sulfur consistent with the heat balance requirements of the commercial unit.

The most favorable regeneration temperature for oxidant partial pressures of 40 to 60 psi was found to be 1200 °F. The sulfate sulfur content in the Z-Sorb® sorbent at the end of the five regeneration runs was 0.09 wt.%. The maximum capacity of the sorbent for sulfur absorption decreased from 14 wt.% for the virgin sorbent to 13 wt.% at the end of the last regeneration run.

Subsequent Z-Sorb® sorbent formulations have resulted in the manufacture of an improved sorbent capable of initiating regeneration at 950 °F to 1000 °F. This is the formulation that will be used at SPPCo.

CONCLUSIONS

The results of the bench scale and pilot plant testing conducted at KTDC confirmed that a transport reactor, using a proprietary sulfur sorbent from Phillips Petroleum (Z-Sorb® sorbent), could be used for HGD application at Sierra Pacific. The basic design of the Transport Reactor for this service provides a very efficient, low cost option that will meet the technical and financial requirements of this facility. Figure 3 provides a simplified process flow diagram of the HGD Unit for Sierra Pacific.

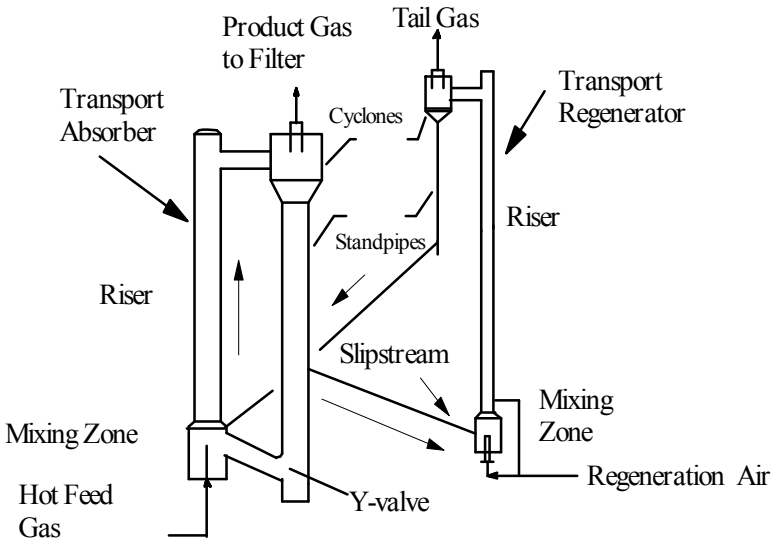

Figure 3 Simplified Process Flow Diagram of the HGD Unit for Sierra Pacific

The causes of sorbent capacity deterioration, observed during these tests, are not specifically known. Since regeneration with steam diluent is suspected as a potential problem, it should be avoided in the commercial design unless additional test data prove it satisfactory.

The major conclusions from this study can be summarized as follows:

- Complete absorption of H_2S was obtained under all conditions tested. No problems are expected with H_2S leakage in the commercial reactor, even at low riser density.

- BRU tests show a decline in Z-Sorb ® sorbent sulfur capacity with repeated cycling, but the final capacity at the end of the multi-cycle test was still well above the intended sulfur loadings for the commercial absorber.

- Exposure of the Z-Sorb® sorbent to steam at temperatures above 1100-1200°F results in an unacceptably high loss in sulfur capacity.

- Exposure of the Z-Sorb® sorbent to nitrogen (inert atmosphere) at temperatures up to 1400°F had no apparent effect on sulfur capacity.

- Testing in the TRTU, performed to determine the effect of char fines on sorbent absorption/regeneration, showed that the HGD unit could be located ahead of the current absolute filter and does not require additional filters.

REFERENCES

1) J. S. Mei, C. E., Everitt, and S. Katta, "Fixed Bed Tesing of a Molybdenum-Promoted Zinc Titantate Sorbent for Hot Gas Desulfurization", D.O.E. Contractors Review Meeting, Morgantown W.V., June 1993.

2) F. M. Brinkmeyer and G. A. Delzer, "Z-Sorb-A new Sulfur Removal Process", National Meeting of the AIChE, session 28. Tail Gas Treatment, Paper 28d, San Diego, August 1990.

3) W. M. Campbell, J.J. O'Donnell, S. Katta, T. Grindley, G. Delzer and G. Khare, "Desulfurization of Hot Fuel Gas with Z-Sorb III Sorbent." Proceedings of the Coal Fired Power Systems 93--Advances in IGCC and PFBC Review Meeting, pg. 179. DOE/METC-93/6131, NTIS/DE 93000289, Springfield, VA: National Technical Information Service.

PHILLIPS SORBENT DEVELOPMENT FOR TAMPA ELECTRIC COMPANY AND SIERRA PACIFIC POWER COMPANY

Gyanesh P. Khare (gpkhare@bvemx.ppco.com; 918-661-9435)
Gary A. Delzer (gad@bvemx.ppco.com; 918-661-7995)
Gil J. Greenwood (gjgreen@bvemx.ppco.com; 918-661-3693)
Donald H. Kubicek (918-661-3148)
Phillips Petroleum Company
Corporate Technology
Bartlesville, OK 74004

ABSTRACT

Phillips Z-Sorb® sorbent will be used for startup at both Tampa Electric Company and Sierra Pacific Power Company Integrated Gasification Combined Cycle (IGCC) demonstration projects. Commercial preparations for these two applications required additional development to meet specific client needs. Tampa Electric required a presulfiding of the sorbent to facilitate startup. Sierra Pacific desired emphasis on operational flexibility and attrition. Procedures and test results from these commercial developments will be discussed.

PHILLIPS SORBENT DEVELOPMENT FOR TAMPA ELECTRIC COMPANY AND SIERRA PACIFIC POWER COMPANY

CONTRACT INFORMATION

Contract Number	N/A
Contractor	N/A
Other Funding Sources	N/A
Contractor Project Manager	N/A
Principal Investigators	G. P. Khare G. A. Delzer G. J. Greenwood D. H. Kubicek
METC Project Manager	N/A
Period of Performance	N/A

INTRODUCTION

Research and Development in IGCC technology will come to fruition in 1996 as two commercial demonstration projects undertake their startup operations. Tampa Electric Company has its Polk Power Station in Tampa, Florida, scheduled for August; Sierra Pacific Power Company's Piñon Pine station near Reno, Nevada, will begin in November. Phillips Z-Sorb® sorbent has been selected as the first load for each of these units. In the first case, a moving-bed sorbent Z-Sorb® III-M will be used in the TECO plant. This material is designed as a sphere with an average pellet diameter of about 4 mm. In the second case, the Piñon Pine site will use a fluid-bed sorbent with an average particle size of 175 μm.

APPROACH

Previous publications from us have disclosed the efforts in preparing and testing these two formulations of sorbent (1). The goal of the present paper is to discuss final development of each of these sorbents as commercially manufactured materials for use in the respective demonstration projects. From this scenario, it will be clear that commercial quantities of Phillips sorbent for hot gas cleanup systems are available in whatever forms are required. There are numerous options available to the end-user, depending on the particular need to remove hydrogen sulfide from a

coal gasification stream. A conclusion we have reached from our experience is that no single sorbent will suffice for every situation, and it is our goal to have a suite of sorbents available.

TECHNOLOGY

Phillips Petroleum Company has been engaged in testing its proprietary Z-Sorb® sorbent for a number of applications in which the removal of hydrogen sulfide is important. A new class of regenerable zinc based sorbents has been developed for the removal of hydrogen sulfide in the fuel gas that is produced in a clean coal technology power plant at moderate pressure (5-20 atm) and a broad range of operating temperatures (600-1000°F). Tests have been carried out in fixed-, moving-, and fluid-bed applications. All formulations have been successfully produced by commercial vendors.

ACCOMPLISHMENTS

Z-Sorb® Sorbent for Tampa Electric Company Polk Station

Sulfur capacity and mechanical strength were important parameters in the design of the moving-bed sorbent for the TECO Polk Station. Z-Sorb® III-M sorbent was tested by Phillips in a fixed bed unit under the guidelines of a protocol established by General Electric. Table 1 shows the relevant parameters for the test.

Table 1

Fixed Bed Testing of Z-Sorb® III-M Sorbent

Absorption	
Bed Temp. (°F)	900
Absolute Pressure (atm)	20
Space Velocity (h^{-1})	1000 to 2000
Inlet H_2S (%)	3.3 to 3.6
Regeneration	
Initial Bed Temp. (°F)	1050
Absolute Pressure (atm)	7
Oxygen Concentration (%)	2.2 to 3.3

Figure 1 depicts the loading curve that was measured during this test of fifteen cycles. There is a slight fall-off of sulfur capacity with cycle number, but the loading stayed above the design limit of 6 lb/ft^3 at the top of the bed. The low level at cycle 2 was attributed to incomplete regeneration after cycle 1. Once the regeneration scheme was adjusted, the loading recovered.

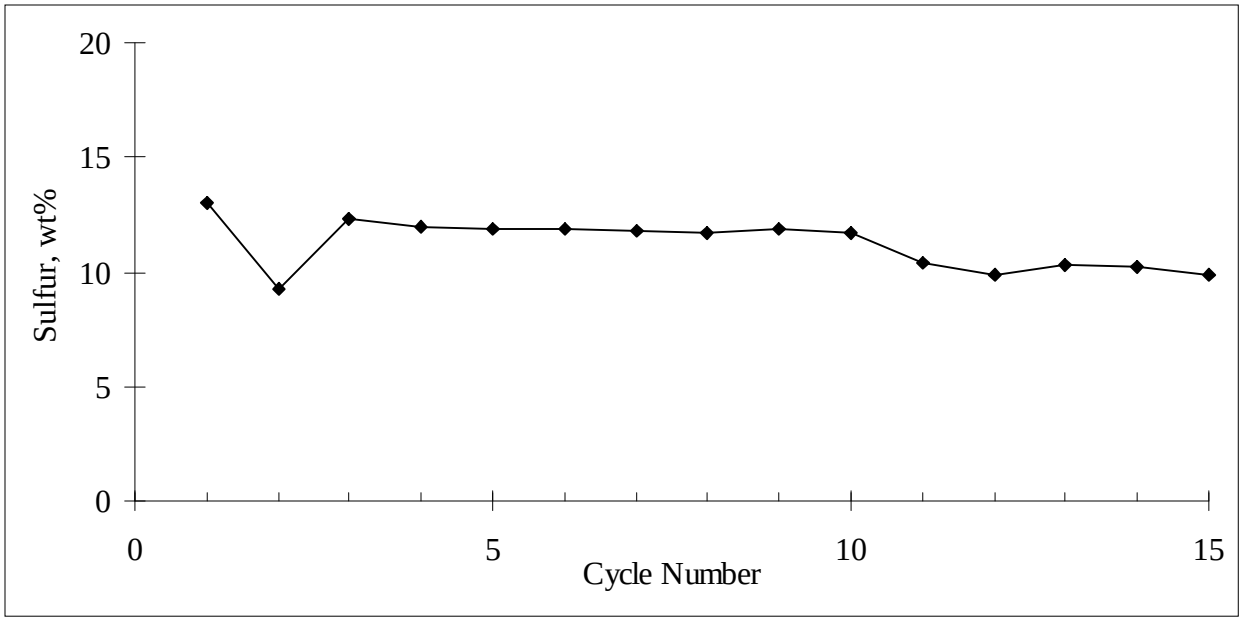

Figure 1. Loading curve of Z-Sorb® III-M Sorbent in Fixed-Bed Testing under GE Protocol.

The excellent performance of the sorbent is shown in Figure 2, which shows the breakthrough curves of hydrogen sulfide. Loadings are based on a 200 ppm breakthrough. Even after fifteen cycles, hydrogen sulfide stays low until just before breakthrough.

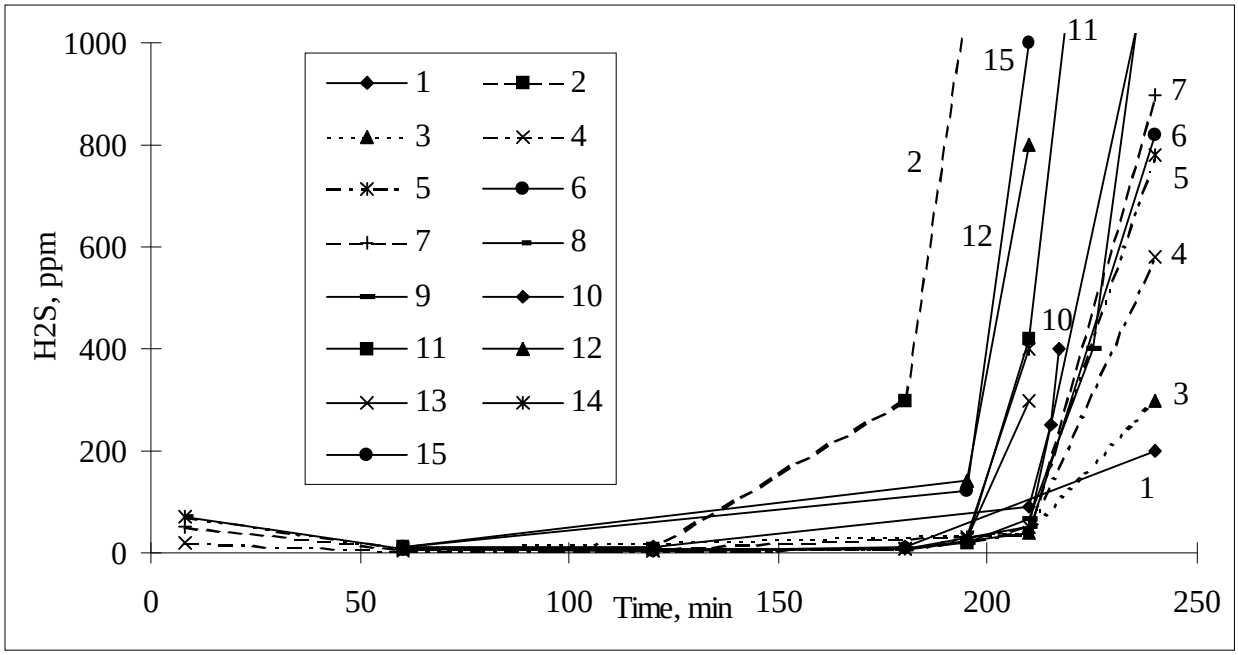

Figure 2. Breakthrough curves of Z-Sorb® III-M Sorbent in Fixed-Bed Testing under GE Protocol.

An additional critical feature of the sorbent was the attention given to dealing with the methanation reaction that may occur on the nickel-promoted Z-Sorb® sorbent when synthesis gas passes over it the first time. An exotherm approaching 200°F can take place (2). However, testing in the moving-bed pilot plant at the General Electric Corporate Research and Development site in Schenectady, New York, (3) did not show such an exotherm, but it was deemed desirable to make sure that such a heat release would not be a problem in the commercial plant. Initial pilot plant and lab tests at Phillips showed that using a low absorption temperature would keep this exotherm under control. An example of such a case is illustrated in the study mentioned above in which Z-Sorb® III-M sorbent was tested by Phillips in a fixed-bed unit. The sorbent was sulfided in-situ at 500°F in the first cycle, and there was no temperature rise in that cycle and only minor temperature increases in subsequent cycles at 900°F. Note, too, that at 500°F, the sulfur loading was 14 wt%. Secondly, since sulfur is a poison for the methanation reaction, we also verified that presulfiding the sorbent would minimize the methanation reaction. Table 2 illustrates the results that were found for controlling the methanation reaction and, hence, the exotherm. We examined cases in which the sorbent was presulfided ex-situ by treating with hydrogen sulfide at room temperature, incorporating a sulfur containing poison in the preparation procedure, and presulfiding using two different proprietary commercial techniques. The off-gas from a lab reactor was sampled and analyzed using mass spectrometry during the first cycle absorption run at 900°F using a simulated fuel gas.

Table 2

Control of Methanation Reaction in Z-Sorb® III-M Sorbent

Method	Methane, ppm	Sulfur Capacity, wt%
No pretreatment	1100	>10
Sulfiding with H_2S at room temperature	20	>10
Incorporation of sulfur poison during preparation	5	>10
Commercial method A	10	>10
Commercial method B	15	>10

It was judged not to be possible to sulfide the sorbent in-situ at ambient conditions while it was in the TECO reactor, so an ex-situ presulfiding route was chosen. In the final commercial preparation, we let the manufacturers develop their proprietary procedure to presulfide the sorbent, hence poisoning the methanation reaction. The reduced methane level translates into a lower exotherm for the large quantities of sorbent used in a commercial reactor. From the time of our initial discussions of the need to presulfide the sorbent until the time of delivery to TECO of the commercially presulfided material, only seven months had elapsed.

Z-Sorb® Sorbent for Sierra Pacific Power Company Piñon Pine Plant

Development of a fluid-bed sorbent for the Sierra Pacific Power Company plant initially centered on the issue of flexible operation, that is, ease of transporting the sorbent in the reactor. Once that matter had been settled, two additional characteristics evolved, namely attrition and low regeneration temperature. The attrition had to be fine-tuned so that proper transport control and

minimum make-up rate could be achieved. Regeneration temperature was an issue because it was desired to initiate the regeneration without requiring additional heat input to raise the sorbent temperature. By comparison, a moving-bed sorbent is heated at least 100°F in going from the absorption zone to the regeneration zone. Because of the nature of the work that was required, all testing was done at the Kellogg Technical Development Center. However, we tested several formulations of the fluid-bed sorbent in a bench scale reactor, and the sulfur capacities of two of these are given in Table 3. Formulation B is the one chosen for loading at the Piñon Pine plant, which provides an obvious advantage over the first fluid-bed formulation.

Table 3

Sulfur Capacities and Attrition Resistance of Fluid-bed Z-Sorb® Sorbent

Fluid-bed Sorbent	Sulfur Capacity[a], wt%	Attrition Resistance[b], %
Formulation A	12.8	91
Formulation B	18.0	99

[a]Average sulfur capacity over 20 cycles
[b]Measured in a 3-hole attrition tester (4)

FUTURE ACTIVITIES

We have earlier noted the adverse effect of steam regenerations at high temperatures (1400°F) on Z-Sorb® III sorbent (2). Phillips has undertaken an R&D program to develop enhanced steam resistant sorbents. The bench scale test results of one new fluid-bed formulation at atmospheric pressure and 1000°F temperature are shown in Figure 3. The activity of the new sorbent and Z-Sorb® III sorbent are compared. It is evident from this data that the new sorbent does not show any sulfur loading capacity loss when regenerated in air diluted with 42 vol% steam at 1200°F. At 1400°F, however, there is a 30% loss in capacity, but the residual capacity is still very high, estimated to be 16-17 wt% sulfur, in contrast to the Z-Sorb® III sorbent where a similar treatment resulted in a capacity of only about 6 wt%.

Figure 3. Sulfur Loading of Fluid-Bed New Generation Sorbent; Regeneration: 7.6% O_2/42.4% H_2O/50% N_2.

Figure 4 shows the reactivity of a 4 mm spherical sorbent at 900°F and 4 atm pressure. The sulfidation feed contained 3.4% H_2S, 20% water and the balance CO_2/N_2. Regenerations were conducted with a gas containing 4.6, 42.8, 52.4 vol% O_2, N_2 and H_2O, respectively and at 4 atm pressure. The new sorbent again exhibited superior resistance to steam and suffered no sulfur capacity loss in 1200°F steam regenerations while Z-Sorb® III sorbent lost a major portion of its capacity under the same conditions.

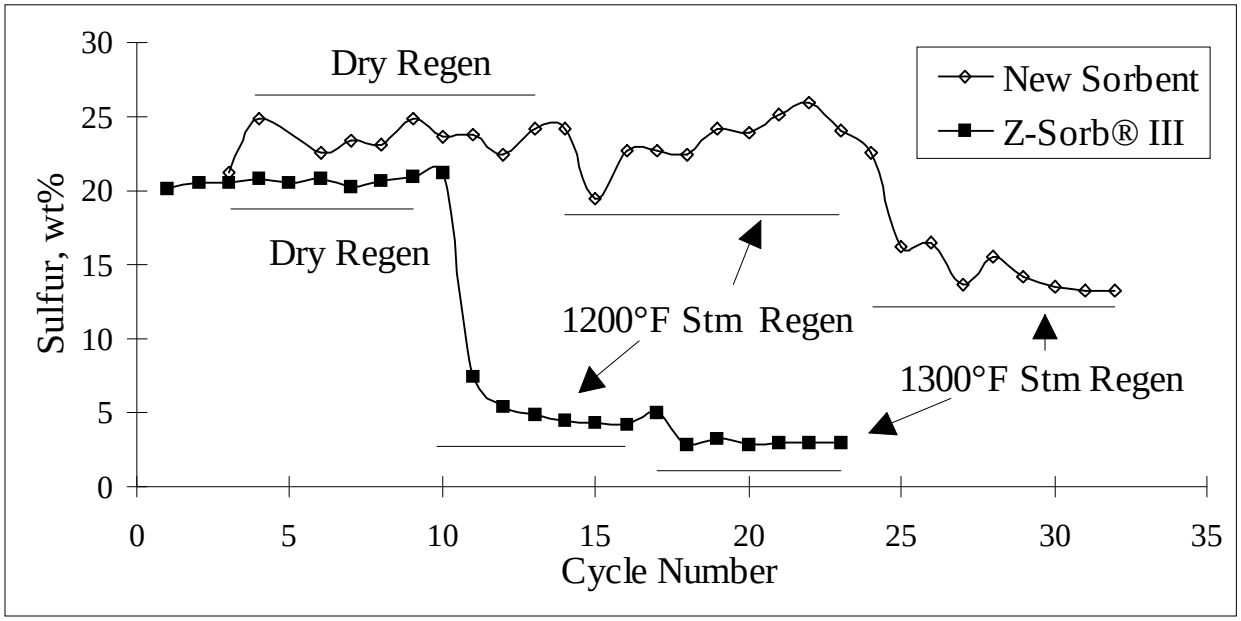

Figure 4. Effect of Steam Regeneration on Sorbents; Absorption: 900°F, 4 atm, 3.4% H_2S/20% H_2O/bal. CO_2-N_2; Regeneration: dry - 4.6% O_2; stm - 4.6% O_2/52.4% H_2O.

ACKNOWLEDGMENTS
The authors would like to acknowledge the cooperation they have received from colleagues at United Catalysts Incorporated, Calsicat, and The M.W. Kellogg Company.

REFERENCES

1. G.P. Khare, G.A. Delzer, D.H. Kubicek and G.J. Greenwood. 1995. Hot Gas Desulfurization with Phillips Sorbent in Moving Bed and Fluidized Bed Reactors, Environmental Progress, 14(3), p. 146-150.

2. G.A. Delzer, G.P. Khare, and G.J. Greenwood. 1993. Z-Sorb® Absorbent for Hot Gas Desulfurization, AIChE Annual Meeting, Symposium on Gas Purification, No. 130f, St. Louis, MO, November 7-12.

3. S. Bevan, D. Najewicz, E. Gal, A.H. Furman, R. Ayala and A. Feitelberg, 1994. Integrated Operation of a Pressurized Gasifier, Hot Gas Desulfurization System and Turbine Simulator. Proceedings of the Coal-Fired Power Systems 94--Advances in IGCC and PFBC Review Meeting. p. 222, DOE/METC 94/1008. NTIS/DE 94012252. Springfield, VA, National Technical Service.

4. Attrition resistance measured using a procedure similar to that described in USP 4,010,116.

Bench-Scale Development of Fluidized-Bed Spray-Dried Sorbents

Raghubir P. Gupta (gupta@rti.org; 919-541-8023)
Brian S. Turk (bst@rti.org; 919-541-8024)
Santosh K. Gangwal (skg@rti.org; 919-541-8033)
Research Triangle Institute
3040 Cornwallis Road
Research Triangle Park, NC 27709

Introduction

Successful development of regenerable mixed-metal oxide sorbents for removal of reduced sulfur species (such as H_2S and COS) from coal-derived fuel gas streams at high-temperature, high-pressure (HTHP) conditions is a key to commercialization of the integrated-gasification-combined-cycle (IGCC) power systems. Among various available coal-to-electricity pathways, IGCC power plants have the most potential with high thermal efficiency, simple system configuration, low emissions of SO_2, NO_x and other contaminants, modular design, and low capital cost. Due to these advantages, the power plants of the 21st century are projected to utilize IGCC technology worldwide. Sorbents developed for sulfur removal are primarily zinc oxide-based inorganic materials, because of their ability to reduce fuel gas sulfur level to a few parts-per-million (ppm).

Although desulfurization and regeneration reactions can be carried out using fixed-, moving-, or fluidized-bed reactors, fluidized-bed reactors offer several potential advantages including excellent gas-solid contact, ability to add or remove sorbent continuously, excellent temperature control of the highly exothermic regeneration reaction, faster overall kinetics associated with using smaller particles, and continuous steady-state operation. However, highly attrition-resistant sorbents with high reactivity capable of withstanding the stresses induced by rapid temperature swings, chemical transformations, and fluidization and transport are required before fluidized-bed hot-gas desulfurization systems can be commercialized.

Pure zinc oxide sorbents are not suitable because they are prone to undergo reduction in coal gas resulting in zinc vaporization. Similarly, zinc ferrite sorbents have limited applicability due to excessive attrition, iron carbide formation, and carbon deposition (Gupta and Gangwal, 1992). Zinc titanate sorbents do not suffer from these problems and therefore have emerged as alternatives to zinc ferrite sorbents.

Earlier in this study, efforts focused on development and testing of highly reactive and durable zinc titanate sorbents with a 100- to 300-μm particle size range for bubbling fluidized-bed reactors. These efforts led to the development of ZT-4 prepared using a granulation technique (Gupta et al., 1993). A number of life-cycle tests were performed on the ZT-4 sorbent to demonstrate its long-term chemical reactivity and attrition resistance using simulated coal gas

---

Research was sponsored by the U.S. Department of Energy's Morgantown Energy Technology Center, under Contract No. DE-AC2C-88MC25006 with Research Triangle Institute, 3040 Cornwallis Road, Research Triangle Park, NC 27709, telefax: 919-541-8000.

mixtures (Gupta and Gangwal, 1995b). Tests were also conducted using fuel gas produced directly from coal gasifiers at three pilot plant sites: Enviropower in Finland, U.S. Department of Energy/Morgantown Energy Technology Center (DOE/METC) at Morgantown, West Virginia, and Coal Technology Development Division (CTDD) in England. The superior performance exhibited by the ZT-4 sorbent in all three tests is reported elsewhere (Gupta and Gangwal, 1995b).

As an alternative to granulation, a spray-drying process to prepare zinc titanate sorbent is being investigated. Spray drying is extensively employed in the production of various catalysts, particularly fluid catalytic cracking (FCC) catalysts, for use in fluidized-bed reactors. Spray drying offers a number of advantages over a granulation process. For example, spray drying is a commercial process that can be readily scaled to industrial production using existing technology to produce large quantities of a product. Spray drying facilitates the addition of other additives and reagents to the composition since additional reagents can be simply added to a slurry prior to spray drying. Furthermore, spray drying provides particles of uniform spheroidal shape in the desired size range.

Objectives

This project extends the prior work on the development of fluidizable zinc titanate particles using a spray-drying technique to impart high reactivity and attrition resistance. Specific objectives are:

- Develop highly reactive and attrition-resistant zinc titanate sorbents in 40- to 150-μm particle size range for transport reactor applications using semicommercial- to full commercial-scale spray driers;

- Transfer sorbent production technology to private sector; and

- Provide technical support for Sierra Pacific's Clean Coal Technology Demonstration plant and METC's hot-gas desulfurization process development unit (PDU), both employing a transport reactor system.

Project Description

This study is a collaborative effort with Contract Materials Processing (CMP), Inc., a small speciality catalyst manufacturing company in Baltimore, Maryland, the M.W. Kellogg Company of Houston, Texas, that developed the transport reactor technology for hot-gas desulfurization, and Intercat, Inc., another catalyst manufacturing company located in Savannah, Georgia. Both CMP and Kellogg are subcontractors to the Research Triangle Institute (RTI) on this project. RTI and Intercat have entered into a teaming agreement to jointly develop and commercialize spray-dried zinc titanate sorbents.

Development and Testing of CMP-5 Sorbent

In FY 1994-95, CMP made a series of spray-dried zinc titanate sorbents in the 40- to 150-µm particle size range (average particle size [APS] = 80 µm). Screening of these spray-dried sorbents led to the development of CMP-5 sorbent which had excellent chemical reactivity and good initial attrition resistance as measured using a three-hole airjet attrition apparatus (13.4% 5-h loss). Twenty cycles of HTHP testing were performed on this sorbent at RTI. Results of this testing indicated that, unlike the ZT-4 sorbent, this sorbent did not undergo capacity reduction; however, it lost its attrition resistance. Attrition resistance of the sorbent after testing was 53 wt% 5-h loss compared to 13.4 wt% loss for the fresh sorbent (Gupta and Gangwal, 1995a).

Development and Testing of CMP-107 Sorbent

In preparation for operation of the transport hot-gas desulfurization reactor at Sierra Pacific's Clean Coal Technology Demonstration plant, Kellogg had investigated Z-Sorb III sorbent in a particle size range of 100- to 300-μm with an APS of about 180 μm (Campbell et al., 1995). Z-Sorb III is a proprietary ZnO-based sorbent developed by the Phillips Petroleum Company and contains Ni and additional activators and promoters. Kellogg recommended production of CMP-107 in comparable particle size range as Z-Sorb III to obtain a direct comparison of the performance of these two sorbents.

RTI and CMP worked jointly to produce a spray-dried zinc titanate sorbent with the appropriate particle size distribution. In the summer of 1995, a CMP-107 sorbent with an APS of 165 µm was developed. Table 1 shows a comparison of physical and chemical properties of CMP-5 and CMP-107 sorbents. Chemical composition of both formulations was similar in terms of relative amounts of ZnO and TiO_2. The primary difference between these two was in the APS, as noted above.

Table 1. Properties of CMP-5 and CMP-107 Sorbents

	CMP-5	CMP-107
Particle size range (μm)	40-150	80-250
APS (μm)	80	160
Surface area (m^2/g)	2.83	14.2
Bulk density (lb/ft^3)	38.3	34.4
Thermogravimetric analyzer (TGA) sulfur capacity (wt%)	22.5	16.6
Attrition loss (wt%)		
5-h	13.4	5.8
20-h	14.2	12.0

TRTU Testing of CMP-107 Sorbent

In order to qualify a sorbent as a potential candidate for the Sierra system, Kellogg designed and built a bench-scale transport reactor test unit (TRTU). This facility is located at the M.W. Kellogg Technology Development Center in Houston. Figure 1 shows a simplified sketch of the TRTU system.

Description of TRTU

As shown in Figure 1, Kellogg's TRTU system consists of a mixing zone, a riser, a cyclone, and a standpipe. The lower mixing zone of the reactor, which can be operated either as a dense phase fluidized-bed or as an entrained-bed reactor, consists of a 10-ft tall section of 1.5-in. Schedule 160 stainless steel (SS) pipe. Solids from the standpipe are returned to the bottom of this zone. Fluidization gas, which can be air, oxygen, steam, nitrogen, or any combination of these, is fed to the bottom of the zone through a specially designed gas distributor.

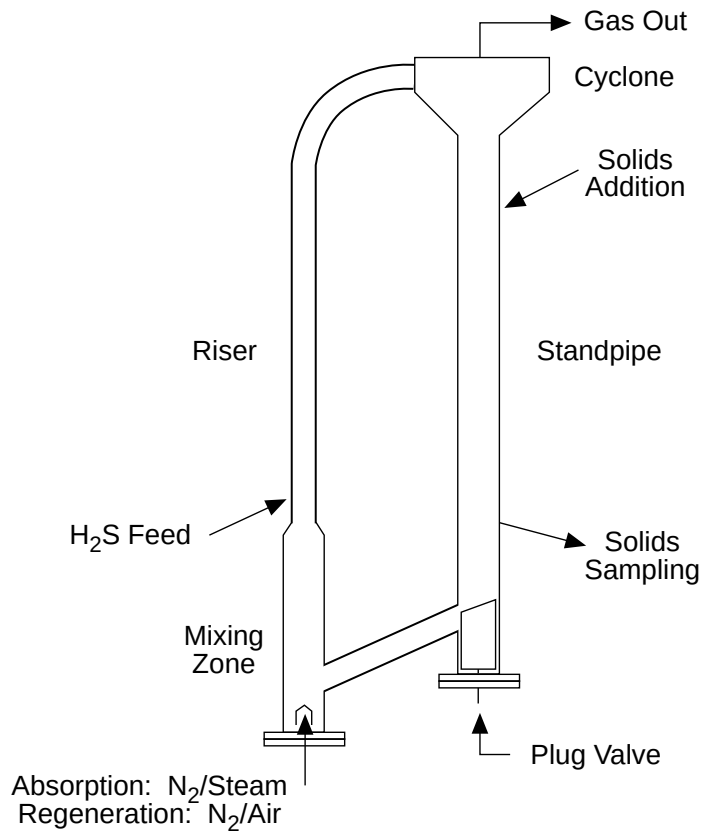

Figure 1. Schematic Sketch of Kellogg's TRTU System.

Above the mixing zone is a 32-ft tall riser made of 1 in. Schedule 160 SS pipe. Gas and solids leaving the top of the riser flow to a high-efficiency cyclone, which separates the solids from the gas and returns them, via a standpipe, to the reactor. The standpipe is a 33-ft tall 1.5-in. Schedule 160 SS pipe. Use of a relatively small diameter standpipe results in a low solids inventory requirement and minimal solids holdup time. Make-up solids are added, if necessary, at the top of the standpipe to compensate for attrition losses. Solid samples may be withdrawn at any time from the bottom section of the standpipe. Solids are returned to the bottom of the mixing zone via a lateral return leg, with solids flow rate controlled by means of a plug valve located at the base of the standpipe. This system is a prototype of the hot-gas desulfurization system being built at Sierra Pacific.

Experimental Procedure

Both sulfidation and regeneration were carried out at nominally 1,200 °F and at a system pressure of 100 psia.

During sulfidation, outlet H_2S concentration was measured every 5 min with a Varian 3300 gas chromatograph (GC) that employs a flame photometric detector (FPD). The H_2S concentration measured by this GC was verified by Dräeger tubes. SO_2 concentration during regeneration was monitored continuously using a Bovar 721-M ultraviolet (UV) photometric analyzer. The O_2 concentration in the regeneration outlet gas was continuously measured with an MSA model 4000 O_2 analyzer. This instrument uses an electrogalvanic cell to detect and quantify O_2. All

thermocouple readings and pressure drop measurements were continuously recorded by a computer data logging system. Table 2 shows the sulfidation gas composition used during the TRTU testing.

Table 2. Gas Composition Used During Sulfidation

Gas Component	Vol%
H_2S	1.2
H_2	4.1
H_2O	7.8
N_2	86.9
Total	100.0

Before starting either sulfidation or regeneration, N_2 flow to the unit was divided between the mixing zone and the riser to match the velocities intended for the individual steps. During sulfidation, the mixing zone was maintained at a velocity of 1.6 ft/s, and the riser velocity was maintained at about 12.8 ft/s. During regeneration, these velocities were slightly lower as given in Table 3.

Table 3. Operating Conditions for the Multicycle TRTU Test

Sorbent	RTI/CMP-107 ZnTi
Operating pressure (psia)	100
Operating temperature (°F)	1,160 to 1,225
Sulfidation time (min)	26 to 98
Regeneration time (min)	7 to 30
Mixing zone density (lb/ft^3)	13 to 24
Mixing zone velocity (ft/s)	1.1 to 1.6
Riser density (lb/ft^3)	0.6 to 0.9
Riser velocity (ft/s)	11.5 to 12.8
Gas residence time for sulfidation (s)	2.5
H_2S concentration at riser inlet (%)	1.2
Solid inventory (lb)	8.0
Solid circulation rate (lb/h)	90 to 150

At the beginning of sulfidation, steam was introduced into the mixing zone. A small amount of H_2 was then added to the riser to ensure a reducing atmosphere in the sulfidation zone. An H_2S/N_2 mixture was then added to the riser, giving an H_2S inlet concentration of 1.2 mol%. As the H_2 and H_2S streams were added, N_2 flow was reduced accordingly to maintain constant riser velocity. After sulfidation was complete, these steps were reversed to bring the unit back to purge conditions.

Air was introduced to replace the N_2 feed into the mixing zone to begin regeneration. At the end of regeneration, air was replaced with N_2 to return to purge conditions. Gas flow rates were monitored and carefully controlled during the test. An adequate purge period was maintained between sulfidation and regeneration steps of each cycle.

Prior to the multicycle test, several cold flow tests were conducted with the CMP-107 sorbent in the TRTU to determine optimum operating conditions required in the mixing zone and riser, and the solids plug valve position in order to achieve reliable operation at extremely low riser densities. The initial test plan called for a riser density of about 2 lb/ft^3, but, due to problems encountered with the solids plug valve, a riser density of 0.6 to 0.9 lb/ft^3 was found to provide a steady circulation of sorbent.

Results

TRTU Testing

Sulfidation. For the first two cycles, the sorbent was sulfided until the H_2S leakage was >1,000 ppmv to determine sulfur loading of the fresh sorbent at breakthrough. During Cycles 3 to 48, the sorbent was sulfided for a predetermined period of 26 min to obtain a sulfur loading of about 2 wt%. Figure 2 shows the maximum H_2S leakage as a function of cycle number during the 50-cycle test. Except for seven cycles, the maximum H_2S leakage was below the detection limit of GC, indicating excellent chemical reactivity of the CMP-107 even with extremely low riser density.

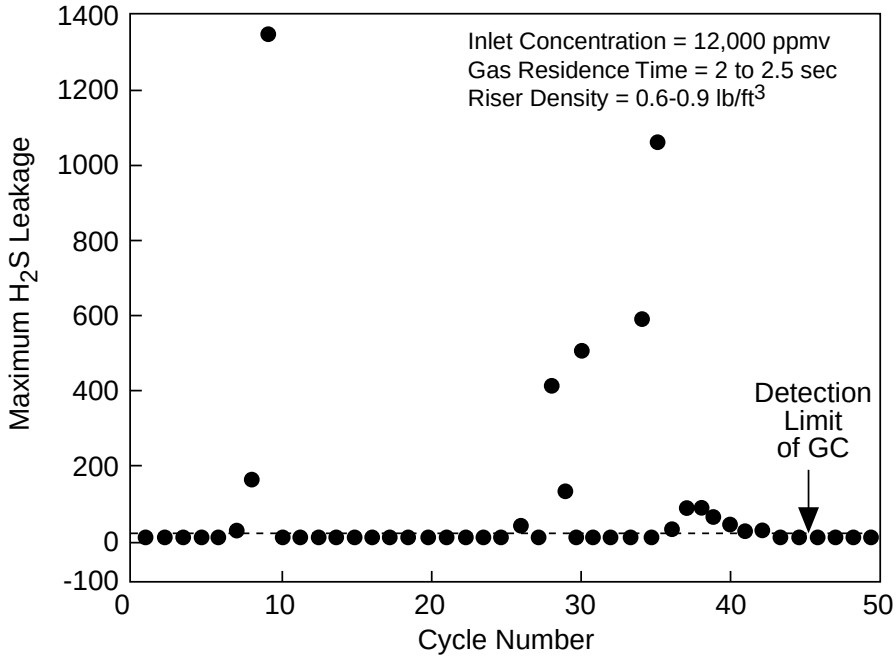

Figure 2. Maximum H_2S Leakage During the 50-Cycle TRTU Test.

During the 9th and 35th sulfidation cycles, H_2S concentration exceeded 1,000 ppmv. This was primarily attributed to flow maldistributions resulting from system upsets (unstable solids circulation). Similarly, small H_2S leakage during the other five cycles was also associated with flow problems in the TRTU.

Regeneration. Sorbent performance during regeneration, as represented by SO_2 and O_2 concentration profiles and temperature exotherms recorded by two thermocouples, namely TE201 (temperature of the upper portion of the mixing zone) and TE200 (temperature of lower portion of the mixing zone) from Cycle 8 to Cycle 27 (selected randomly for illustration purposes), is shown in Figure 3. Peak SO_2 concentration measured in various cycles compared well with the theoretical value of 3.6 percent, based on gas flow rates used, as shown in Figure 3. This figure clearly shows that the sorbent regenerated very well in all the cycles as shown by the relatively constant peak SO_2 concentration and temperature exotherm. Absence of O_2 breakthrough and stoichiometric SO_2 formation demonstrated that no sulfate was formed during regeneration.

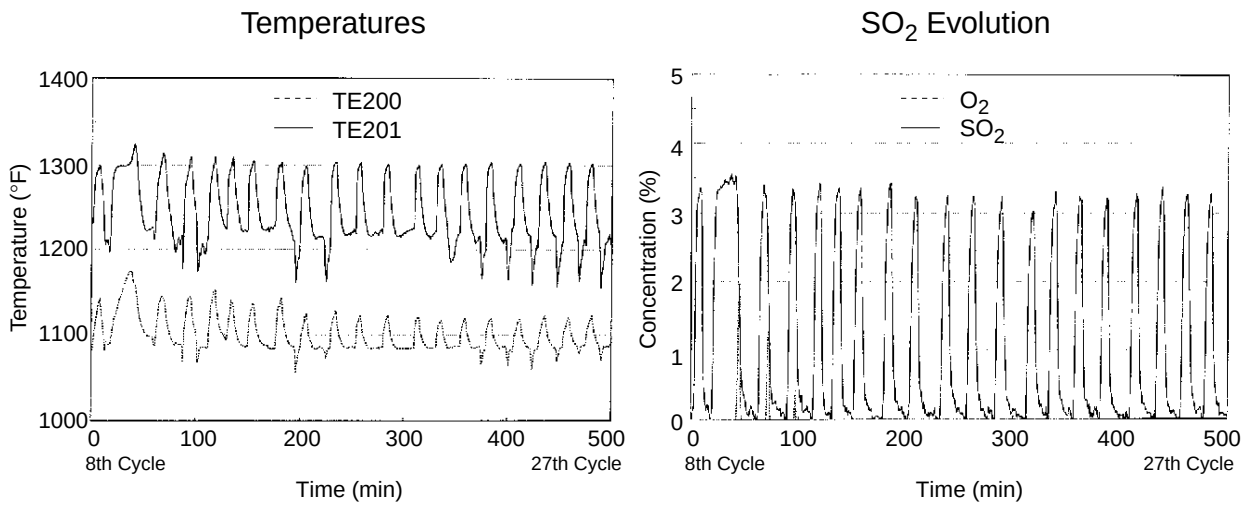

Figure 3. Regeneration of CMP-107 in the TRTU.

Sorbent Attrition. As mentioned previously, in addition to possessing high chemical reactivity required to remove H_2S below detection limits in 2 to 3 sec, the sorbent must be physically strong to withstand the mechanical stresses generated in a transport reactor. To determine sorbent attrition during the 50-cycle TRTU testing, a material balance was used to estimate the amount of fines lost as a percentage of the feed. Defining fines as particles <11 μm (as <11 μm particles were not found in the feed or the bed drain), 5.13 percent of the feed was lost as fines.

The particle size distributions of the feed, bed drain, and filter fines obtained at the end of the test were measured by means of a Microtrac (laser-based particle size analyzer) and sieve analysis. Results are presented in Figure 4. It is quite evident from Figure 4 that particle size distribution has shifted toward finer size during testing. Based on the cumulative distribution shown in Figure 4, the APS (determined as d_{50}) changed from 160 μm for the feed to about 70

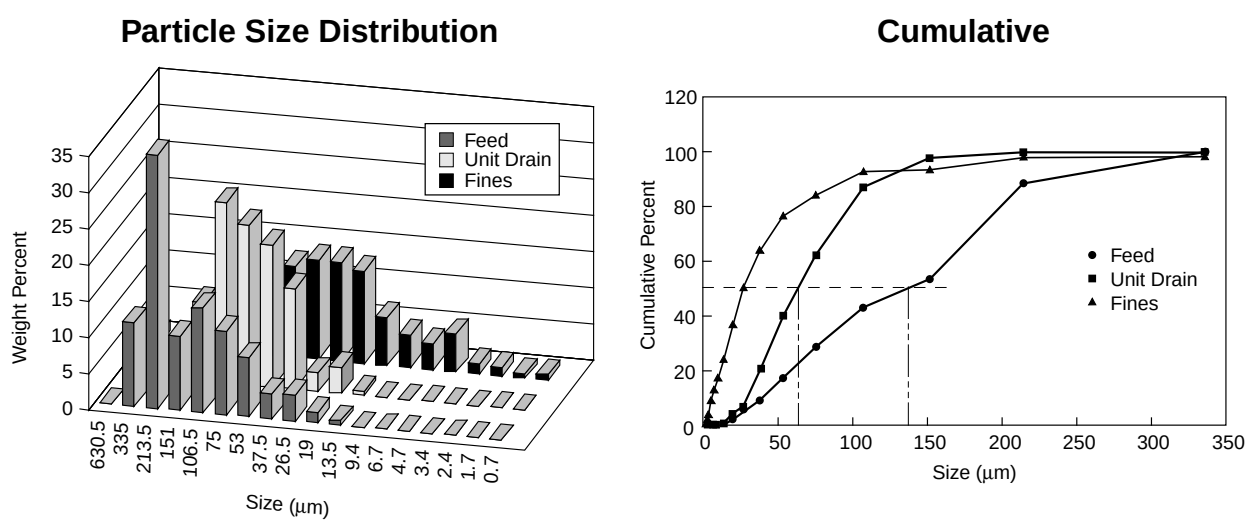

Figure 4. Change in Particle Size Distribution During TRTU Testing.

μm for the unit drain. Based on additional data taken at RTI and Kellogg, it was determined that most of the particle size reduction occurred during the first cycle.

From the particle size and fines generation data, Kellogg estimated that the attrition rate was about 7×10^{-5} lb sorbent attrited per lb of sorbent circulated. The design value for the sorbent attrition rate for the Sierra plant is 3×10^{-5} based on the assumption of 15 lb of sorbent lost per hour for a circulation rate of approximately 500,000 lb/h using a commercially available Z-Sorb III sorbent from the Phillips Petroleum Company. Despite this ambitiously low attrition rate target, the attrition rate of spray-dried CMP-107 zinc titanate sorbent was sufficiently close to the design target to suggest this target could be readily met with minor improvements in the sorbent.

Post-test Characterization

Table 4 shows physical and chemical properties of fresh sorbent and sorbent removed after the 50th regeneration in the TRTU. As noted previously, during testing, the APS decreased from 160 μm to 73.4 μm. BET surface area increased by 50 percent while the bulk density increased by 30 percent. The increase in bulk density can be attributed to reduction in APS. Attrition resistance of sorbent removed after testing measured in a three-hole airjet attrition tester was quite poor compared with fresh sorbent.

Table 4. Comparison of Physical and Chemical Properties of Fresh and 50-Cycle Regenerated CMP-107 Sorbent

	Fresh	After 50th Regeneration
APS (μm)	160	73.4
Surface area (m^2g)	14.2	21.4
Bulk density (lb/ft^3)	34.4	44.9
TGA sulfur capacity (wt%)	16.6	15.0
Attrition loss (wt%)		
5-h	5.8	63.0
20-h	12.0	69.0
Chemical analyses		
Carbon (wt%)	0.23	0.10
Total sulfur (wt%)	<0.05	1.15
Sulfate sulfur (ppmw)	223	402

Although the sorbent lost its attrition resistance during the 50-cycle TRTU testing, its chemical reactivity remained unchanged as confirmed by TGA and TRTU testing. As listed in Table 4, TGA sulfur capacity of reacted sorbent was > 90 percent that of fresh sorbent. These results were confirmed by running a sulfidation in the TRTU on the 50-cycle regenerated sorbent. Sulfur capacity at breakthrough for 50-cycle regenerated sorbent was 93.3 percent that of fresh material, corroborating the TGA results. Therefore, the sorbent did not undergo any decline in either chemical reactivity (indicated by H_2S removal) or sulfur capacity.

MGCR Testing of CMP-107 Sorbent

In addition to testing in Kellogg's TRTU, CMP-107 sorbent was also tested in DOE/METC's modular gas cleanup rig (MGCR) during August 1995. This test was conducted using a slipstream of real coal gas generated in METC's fluidized-bed gasifier. Conditions during MGCR

testing are shown in Table 5.

Figure 5 shows H_2S breakthrough behavior of CMP-107 in the MGCR. As can be seen, CMP-107 reduced H_2S concentration to a few ppm before breakthrough. Sulfur capacity of the sorbent at breakthrough was 17.6 percent. These results indicated other impurities present in real coal gas did not affect the desulfurization performance of the sorbent.

Table 5. Test Conditions for MGCR Testing of CMP-107

Gas flow rate	1,000 scfh
Average H_2S content	1,300 ppmv
Temperature	1,000 °F (538 °C)
Pressure	20 atm (280 psig)
Gas composition (vol%)	
CH_4	2.87
H_2S	0.13
H_2	14.14
Ar	0.48
CO_2	11.21
CO	11.87
N_2	48.50
H_2O	10.47
NH_3	0.33
Total	100.00

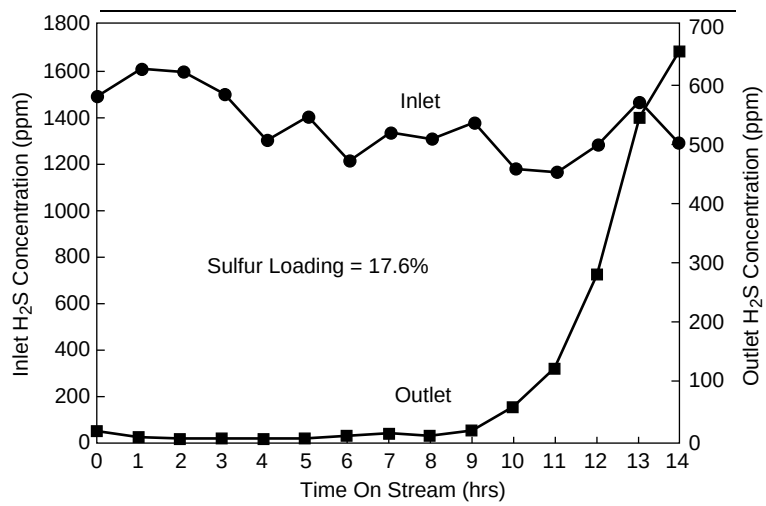

Figure 5. Testing of CMP-107 in METC's MGCR with Real Coal Gas.

Criteria for Commercial Sorbent Selection

Comprehensive analysis of results obtained during bench-scale testing at RTI, TRTU testing at Kellogg, and MGCR testing at DOE/METC with CMP-107 sorbent indicated that a proper combination of reactivity and attrition properties is required to minimize the impact of sorbent costs on operation of the hot gas desulfurization system at Sierra. Figure 6 depicts the interrelationship of various process parameters involved in the sorbent selection process. Every candidate sorbent should be subjected to the screening process of Figure 6 to estimate costs of operation of a hot-gas desulfurization system.

Based on the screening process of Figure 6, analysis of CMP-107 sorbent test results led to the following recommendations by Kellogg:

- Sulfidation activity of the sorbent is quite adequate.
- Bulk density should be increased to ≥50 lb/ft^3.
- The APS should be between 80 and 90 μm with <5 percent below 40 μm and <1 percent

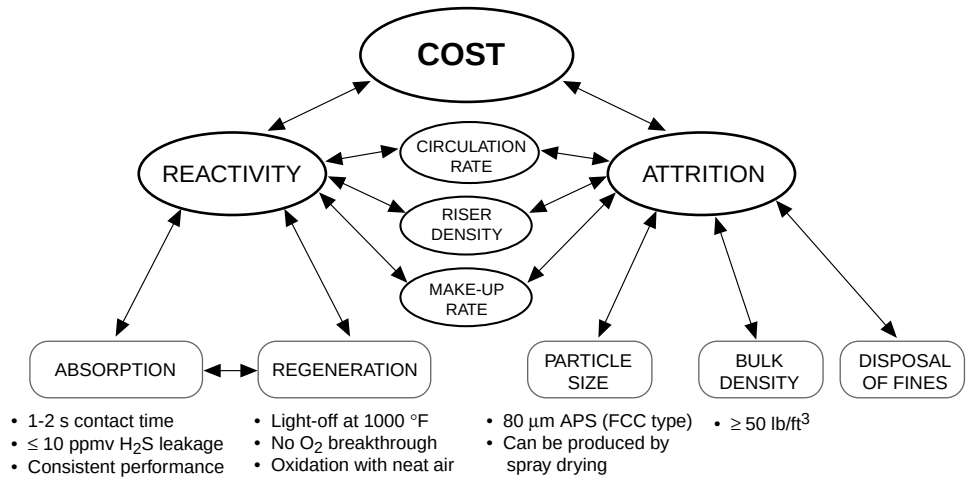

Figure 6. Criteria for Commercial Sorbent Selection.

below 20 μm.

- During regeneration, the sorbent should light off at a temperature ≤1050 °F (565 °C) with neat air to operate the transport reactor system is an isothermal mode with minimal sulfate formation.

- Attrition resistance of the sorbent should be improved by a factor of three to meet the 15 lb/h design target.

Regeneration Light-off Study

Of the recommendations made by Kellogg, lowering regeneration light-off temperature was the most challenging to achieve. Currently, a proprietary additive is being tested, which lowers the temperature required for regeneration light-off of zinc titanate sorbents. Figure 7 shows two temperature profiles taken during regeneration of CMP-107 sorbent in RTI's HTHP bench-scale reactor. Without additive, the minimum light-off temperature for regeneration of CMP-107 was about 1,130 °F; however, with a small amount of the additive, regeneration of CMP-107 was initiated at 925 °F. Details about this additive are proprietary and a patent application is being prepared.

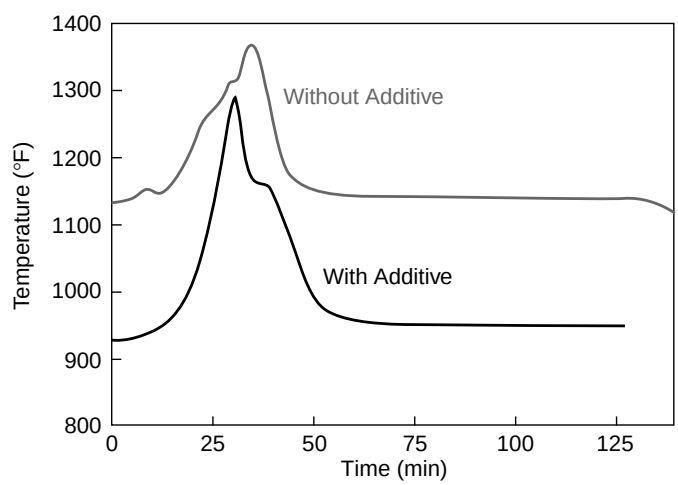

Figure 7. Regeneration Light-off Additive for the CMP-107 Sorbent.

Additional Sorbent Improvements

In parallel to lowering regeneration light-off temperature, work has commenced with Intercat, Inc., to improve the attrition resistance of spray-dried zinc titanate sorbent. RTI and Intercat have entered into a teaming agreement to develop and commercialize this sorbent technology. After preparing a number of trial batches, Intercat has developed a formulation (designated as IX-SO1) that appears promising.

Figure 8 shows a comparison of properties (that were found critical for the transport reactor applications) of CMP-107 and IX-SO1 sorbents along with target values recommended by Kellogg. In this figure, K_s and K_r are kinetic constants for sulfidation and regeneration, respectively. These target values were determined by extensive experimentation in a TGA and correlation with bench-scale and TRTU testing results. IX-SO1 sorbent meets the target property values except for the APS and bulk density, which can be increased when sorbent production is scaled up from laboratory-scale to pilot or semicommercial scale.

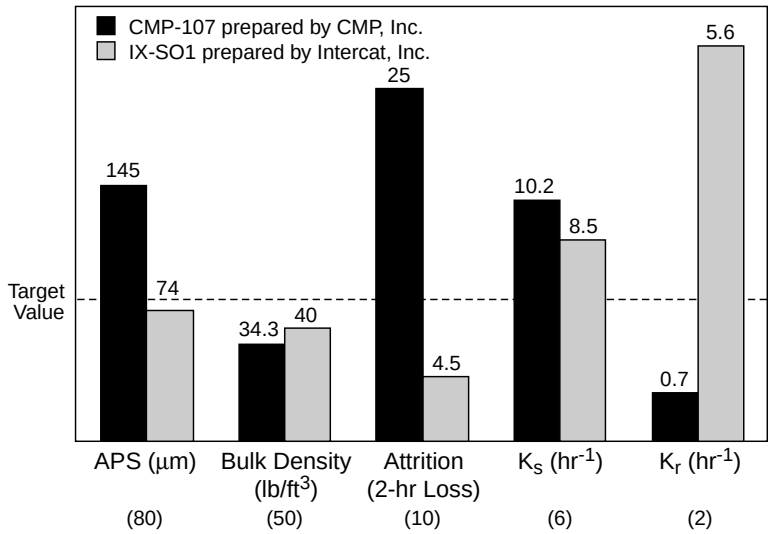

Figure 8. Properties of Current Spray-Dried Zinc Titanate Sorbents.

Applications

Near-term application of the spray-dried zinc titanate sorbents is contemplated in the transport reactor hot-gas desulfurization system in the Sierra Pacific Clean Coal Technology Demonstration plant. This 100 MWe (net) IGCC system, which will involve the KRW gasifier and transport reactor hot-gas desulfurization system developed by M.W. Kellogg, is expected to be online in early 1997. It is estimated that a 30,000 lb charge of sorbent will be needed in this system. This charge is expected to last for 2,000 h provided a sorbent with an attrition rate of $\leq$15 lb/h used.

With the successful demonstration of transport reactor technology at Sierra, the projected long-term IGCC market appears enormous with IGCC plants producing as much as 130 GW of electricity in the year 2040.

Future Activities

Future activities involve demonstration of zinc titanate sorbent production in a commercial-scale spray drier. A batch of the sorbent produced in the commercial-scale spray drier will be tested at M.W. Kellogg in their TRTU system to evaluate its performance, particularly chemical reactivity, attrition resistance, and regenerability.

Acknowledgments

The authors gratefully acknowledge the guidance and assistance of Mr. Daniel C. Cicero, the METC Contracting Officer's Representative. Subcontract support is provided by Contract Materials Processing (CMP), Inc., the M.W. Kellogg Company and Intercat, Inc. The contract period of performance is from September 21, 1988, to April 30, 1997.

References

Campbell, W.M., et al. 1995. Hot-Gas Desulfurization Using Transport Reactors. In *12th International Pittsburgh Coal Conference Proceedings*. pp. 1059-1064. September.

Gupta, R., et al. 1993. "Fluidizable Zinc Titanate Materials with High Chemical Reactivity and Attrition Resistance." U.S. Patent No. 5,254,516. October 19.

Gupta, R., and S.K. Gangwal. 1992. "Enhanced Durability of Desulfurization Sorbents for Fluidized-Bed Applications—Development and Testing of Zinc Titanate Sorbents." Topical Report to DOE/METC. Report No. DOE/MC/25006-3271. Morgantown Energy Technology Center, U.S. Department of Energy, Morgantown, WV. NTIS/DE93000247. November.

Gupta, R., and S.K. Gangwal. 1995a. Spray-Dried Fluid-Bed Sorbent Tests—CMP-5. In *Proceedings of Advanced Coal-Fired Systems '95 DOE/METC Review Meeting*. DOE No. DE95009732. Morgantown Energy Technology Center, U.S. Department of Energy, Morgantown, WV. pp. 601-608. June.

Gupta, R., and S.K. Gangwal. 1995b. Bench-Scale Testing of Fluidized-Bed Sorbents—ZT-4. In *Proceedings of Advanced Coal-Fired Systems '95 DOE/METC Review Meeting*. DOE No. DE95009732. Morgantown Energy Technology Center, U.S. Department of Energy, Morgantown, WV. pp. 229-240.

Sorbent Development for Low-Temperature Moving-Bed Desulfurization

Raúl E. Ayala (ayala@crd.ge.com; 518-387-5850)
Venkat S. Venkataramani (venkata@crd.ge.com; 518-387-5322)
Timothy L. Chuck (chucktl@crd.ge.com; 518-387-6523)
GE Corporate Research and Development
One Research Circle, Bldg. K-1
Niskayuna, NY 12309

Raghubir P. Gupta (gupta@rti.org; 919-541-8023)
Research Triangle Institute
P.O. Box 12194
Research Triangle Park, NC 27709

Introduction

Coal gas desulfurization at elevated temperatures is now recognized as crucial for efficient and economic coal utilization in Integrated Gasification Combined-Cycle (IGCC) systems. Recent system studies of IGCC technology have suggested the temperature range of 350 °C to 550 °C (662 °F and 1022 °F), instead of temperatures above 1200 °F (648 °C), as a desirable range to remove coal gas contaminants, particularly sulfur species [Droog et al., 1993; Schreurs, 1994]. In general, the benefit to be gained at these "lower" temperatures (e.g., lower plant costs, hardware reliability, and engineering feasibility) outweighs the slight loss in desulfurization efficiency and still result in a lower overall cost of electricity. The U.S. Department of Energy/Morgantown Energy Technology Center (DOE/METC) has sponsored development of various configurations of high-temperature desulfurization systems using mixed metal oxide sorbents over the last decade [McDaniel et al., 1995], and a need exists for the development of more efficient sorbents for the lower end of the high temperature range of operation, i.e., the so-called "low" temperature sorbents.

GE is developing a moving-bed, high-temperature desulfurization system for integrated gasification combined-cycle (IGCC) power systems in which zinc-based regenerable sorbents are currently being used as desulfurization sorbents [Bevan et al., 1995; Bevan et al., 1994]. Zinc titanate and other zinc-based oxides are being considered as sorbents for use in the Clean Coal Technology Demonstration Program at Tampa Electric Co.'s (TECO) Polk Power Station I. A key to success in the development of high-temperature desulfurization systems is the matching of sorbent properties, namely sustainable desulfurization kinetics, sulfur capacity, and mechanical durability over multiple cycles, to operate at the selected plant process operating conditions. Integrating desulfurization with gasifier and turbine components in the IGCC system results in a more efficient overall system [Rath et al., 1994; Buchanan, 1994; Corman, 1986].

Research sponsored by the U.S. Department of Energy's Morgantown Energy Technology Center, under contract DE-AC21-94MC31089 with GE Corporate Research and Development, P.O. Box 8, Schenectady, NY 12301; telefax: 518-387-7258

Several other reasons related to sorbent operability favor desulfurization below 650 °C. Although the reaction rates for hot gas desulfurization using metal oxides increase with increasing temperatures and making it desirable to operate above 500 °C, the lower thermal stresses and propensity to sintering experienced by the sorbent at lower temperatures can lead to better sorbent reactivity and mechanical durability over a large number of cycles. The net effect is a reduction in the sorbent replacement cost. In turn, the benefit to be gained by lower temperature operation results in lower overall cost of electricity. However, no extensive study has been done on the development of advanced sorbents for the lower temperature application.

Objectives

In this program, the effort is geared towards developing advanced mixed-metal oxide sorbents for desulfurization in moving-bed systems in the temperature range 343-538 °C (650-1000 °F), where technical viability and process efficiency result in lower overall process costs. In addition, a cost assessment and a market plan for large-scale fabrication of sorbents will be developed. As an optional task, a long-term bench-scale testing of the best moving-bed sorbent formulation will be conducted.

The sorbents must have chemical characteristics that permit cyclic desulfurization and regeneration over many cycles without a drastic loss of activity. The sorbents must be capable of reducing the hydrogen sulfide level in the fuel gas to less than 20 ppmv in the specified temperature range and pressures in the range of 1 to 20 atmospheres. In addition, they must also have physical characteristics that are compatible with the selected reactor, e.g., pellet size/shape for sorbent flowability in moving beds, and maintain these properties over repetitive cycles. This paper will discuss in more detail recent developments in the fabrication and use of molybdenum-doped zinc titanate sorbents for moving-bed configurations at temperatures below 538 °C (1000 °F).

Project Description

This project is being pursued as part of DOE/METC Program “Advanced Sorbent Development” which includes development of sorbents for both moving-bed and fluidized-bed applications. GE Corporate Research and Development (GE-CRD) is acting as the main contractor to DOE and is also in charge of the development of moving-bed sorbents described in this paper. The Institute of Gas Technology (IGT) is acting as a subcontractor to GE-CRD in the development of sorbents for fluidized-bed applications. IGT’s work is presented under a separate paper at this conference.

The near-term thrust of moving-bed sorbent development is to support the commercialization of the GE hot gas cleanup demonstration system at Tampa Electric Co.’s Polk Station I, where desulfurization will take place near 430-500 °C (~800-930 °F). The long-term thrust is to develop moving-bed sorbents for use in future IGCC systems optimized to operate at temperatures as low as 343 °C (650 °F).

Three classes of sorbent materials are being considered for moving-beds: zinc-based materials (including zinc titanates), advanced (non-zinc) metal oxide materials, and proprietary materials

developed by independent vendors. Work on zinc titanate sorbent materials has been published under various DOE contracts [Ayala et al., 1995a; Gangwal and Gupta, 1993; Ayala 1993]. A study of non-zinc metal oxides suitable for desulfurization in the 343-538 °C range was performed last year and reported in the literature [Ayala et al., 1995b].

The implementation of hot coal gas desulfurization heavily relies on the development of regenerable sorbent materials that have high sulfur capacity and can efficiently remove H_2S (from several thousand ppmv levels down to a few ppmv) over many cycles of sulfidation/regeneration. Structural stability and good mechanical strength are also desirable features in a sorbent. Not surprisingly, only a few metal oxides can meet these stringent requirements.

Results

The effort in this project has concentrated in two aspects during the past year:

1. Screening of (non-zinc) metal oxides for applicability in the lower end of high temperature desulfurization (i.e., towards 343 °C, or 650 °F), and
2. Optimization of performance of molybdenum-doped zinc titanates for use in pilot- and demonstration-scale systems at temperatures near 430-500 °C (~800-930 °F)

Screening of metal oxides

The selection of metal oxides was presented last year [Ayala et al., 1995b] and it described the following metals as being potentially useful for our study: Zn, Cu, Co, Fe, Ce, Mo, Sn, W, and Ni. Many of these metals have weaknesses when considered as pure metal oxides for desulfurization, but become useful when considered in combination with others (e.g., Zn-Fe, Cu-Cr, Zn-Mo). In addition, inert binders and pore formers may be required for stable desulfurization and physical integrity of the formed (pelletized or agglomerated) particles.

The main criteria for selection was based on:

1. High desulfurization capability: thermodynamic equilibria and reasonable oxidation kinetics in the temperature range of 343-538 °C (650-1000 °F).

2. Minimization of undesired reactions under reducing gas conditions (e.g., interactions with HCl, CO, and H_2, and catalysis of gas phase reactions).

3. Ease of regeneration capability: thermodynamic stability and fast reaction kinetics compatible with the desulfurization temperature range.

4. Minimization of undesired reactions under oxidizing gas conditions (e.g., sulfate formation, hydrothermal stability).

It is important to emphasize that the selection of useful metals was made keeping in mind both i) short term goals (such as providing for support in the selection of the TECO sorbents within the next year), and ii) long-term goals (such as providing for laboratory evaluation of the next generation sorbents for use in future large-scale systems).

The cost of purchasing raw materials was also considered (Table 1). These costs will be kept in mind when developing formulations, but it was considered that it is too early to make decisions whether or not to use to use an oxide just because of its price, since the relative amounts of secondary components may be too small (e.g.,<1%) to have a significant impact on the cost of the sorbent and yet have a tremendous impact on the durability of the material. As seen in Table 1, most cost fall in three ranges: low cost ($0.5-1/lb), medium cost ($2-5/lb), and high cost ($8-10/lb). These costs have been estimated assuming purchases in large quantities (i.e., tons) and relatively good purity materials. Testing of mixed-metal oxides sorbents continues in the laboratory and results will be presented in the future. In this paper, the work on the Zn-Mo system (i.e., Mo-doped zinc titanates) will be presented, emphasizing the characterization and testing sequence from small laboratory samples to pilot-plant scale quantities.

Table 1.- Relative Cost of Sorbent Metal Oxide Raw Materials

Oxide	Cost, $/lb
TiO_2	0.5-1
ZnO	0.5-1
CuO	2-5
MnO_2	2-5
ZrO_2	2-8
NiO	3-5
CoO	7-10
CeO_2	8-10
Cr_2O_3	8-10
MoO_3	8-10

Screening tests of Mo-containing zinc titanate

Zinc titanate has been under study for several years, and there is a significant amount of information on its performance characteristics in reducing (coal) and oxidizing (regeneration) gases. With respect to desulfurization ability, its performance has been excellent, and there is little doubt on its suitability for desulfurization at temperatures below 600 °C. However, as with any other sorbent, there is always a desire to improve its mechanical durability in order to reduce the sorbent replacement cost to minimize overall operating costs. The purpose of the screening tests at GE-CRD was to improve the mechanical durability of zinc titanate sorbent formulations by adjusting the additives concentration (e.g., molybdenum) and calcination conditions (i.e., enduration at various time/temperatures) that would result in improved performance in pilot plant tests. The improved formulation was targetted for testing at the GE-CRD pilot plant during Run 8 in September 1995.

Several formulations of zinc titanate sorbents were extruded, rounded, and calcined by United Catalysts Inc., (UCI). From attrition tests, the four most promising formulations were selected for bench-scale screening for twenty cycles at GE-CRD. The screening of four molybdenum-doped zinc titanate formulations was performed using a 7-cm (2.75 in.) ID fixed-bed bench reactor at

GE-CRD. Details of the bench reactor system and its operation have been given before [Ayala et al., 1994]. The cross sectional area of the reactor was divided into four quadrants, and each quadrant was filled with a different zinc titanate formulation.

The four formulations tested ranged in molybdenum content from zero percent (Formulation A) to 1.5% (Formulation B) to 2.0% (Formulations C and D). Formulations C and D differed in the calcination history (i.e., calcination temperature and/or time). For screening purposes, both absorption and regeneration were performed at 5 atm each, since GE-CRD's reactor does not have the capability to operate at 20 atm in its present configuration. Absorption was performed at 482 °C using a simplified coal gas composition similar to that of an oxygen-blown gasifier with high H_2S (39% CO, 10% CO_2, 30% H_2, 20% H_2O, 1% H_2S). Regeneration was performed between 482 °C and 760 °C using 1-4% O_2 in nitrogen. At the end of the twenty cycles, the sorbent bed was unloaded for chemical and reactivity analyses of the pellets. Figure 1 shows the outlet H_2S concentration (i.e., the H_2S breakthrough curve) of the composite four-formulation test. Figure 2 shows the comparison of envelope of breakthrough curves (at the 200 ppm outlet H_2S) taking the highest breakthrough time (~ 2 hr.) as 100% of initial sorbent performance. These resulting breakthrough measurements are the composite of the four formulations being tested in parallel in the same reactor (to make exposure conditions comparable). All absorptions had H_2S levels below 25 ppm prior to breakthrough. The results were very promising, with about 80% capacity maintained from cycles ten to twenty. In addition, the convergence of the envelope of breakthrough curves from 10 to 20 cycles suggests that the level of regeneration improved as we learned from each of the previous cycle results. The four sorbents were unloaded, and pellet quality (absence of hairline cracks) was better when molybdenum was present.

Figure 3 Figure 5 show the properties of the fresh and cycled samples. Some of the conclusions that can be drawn from those figures are:

- All formulations A, B, C, and D met the ASTM attrition criterion for fresh pellets (i.e., <4% ASTM attrition loss), but formulations B and D did not meet the ASTM attrition criterion for long-term operation (i.e., <5% ASTM attrition) (Figure 3). Formulation C had the lowest ASTM attrition for both the fresh (0.7%) and after 20 cycles (2.2%).

- The distribution of broken pellets and whole pellets after the ASTM attrition tests in the 20th regeneration samples is shown in Figure 4. Formulation C again fares better than the other three formulations tested.

- Sulfur capacity of the pellets was compared as fresh and after 20 cycles (Figure 5). Formulation C comfortably exceeded the minimum sulfur capacity required for TECO (i.e., 6 to 7 lb Sulfur/ft^3, or approximately 3.2% wt. gain on TGA sulfidation for a bulk density of 100 lb/ft^3). Weight gain for formulation C was more than twice the minimum.

Overall, formulation C (containing 2% equivalent molybdenum oxide) exhibited the best combination of desired properties for long-term operation and was recommended for subsequent preparation and testing for long-term (50 cycles) at RTI's bench-scale reactor system.

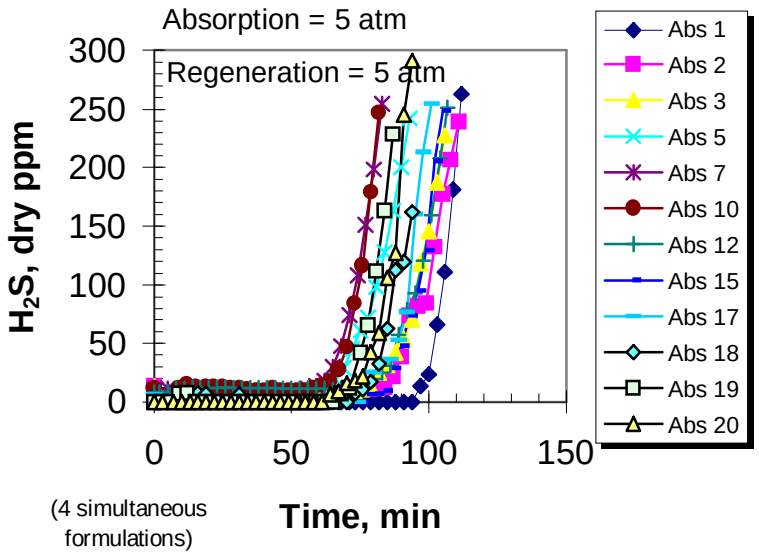

Figure 1.- H2S breakthrough curve for the simultaneous bench reactor testing of four formulations at GE-CRD

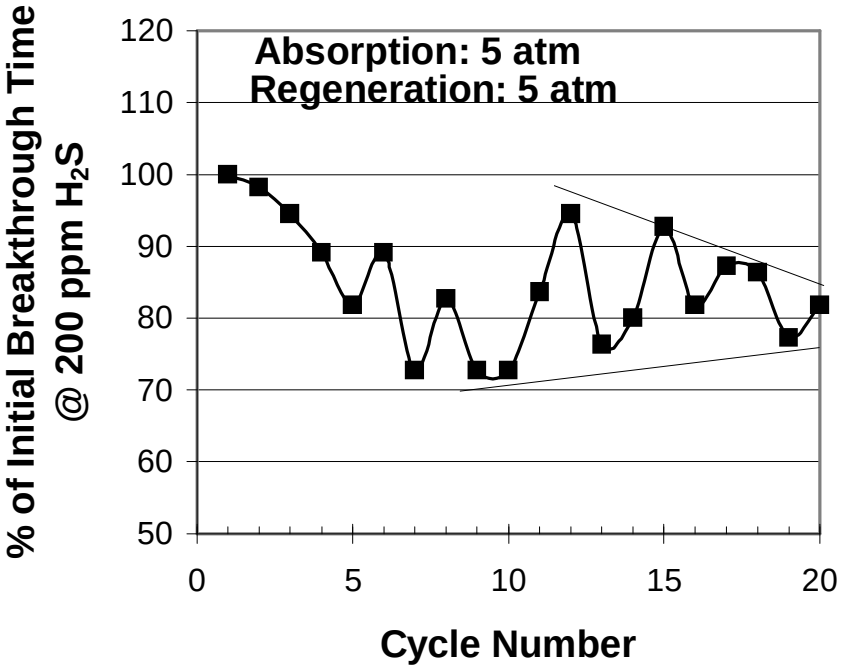

Figure 2.- Envelope of breakthrough curves for zinc titanate screening at GE-CRD

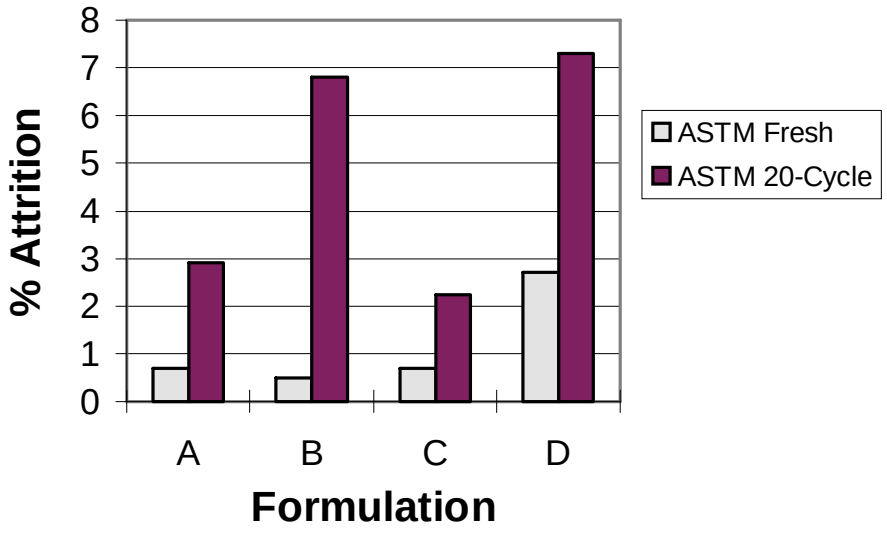

Figure 3.- ASTM attrition results on sorbents after the 20th regeneration in bench screening at GE-CRD

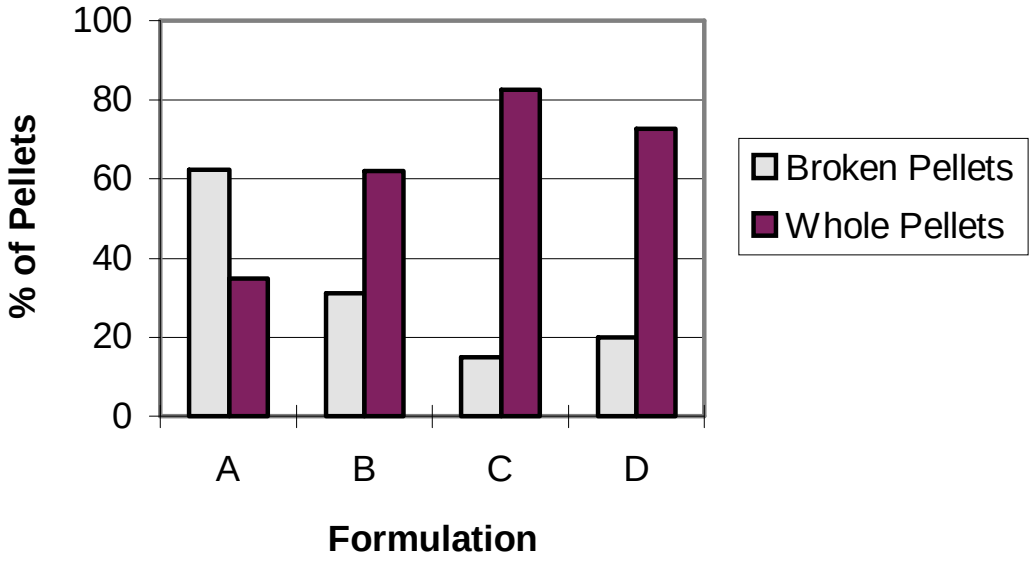

Figure 4.- Pellet Distribution after ASTM Attrition Test (20th. regeneration)

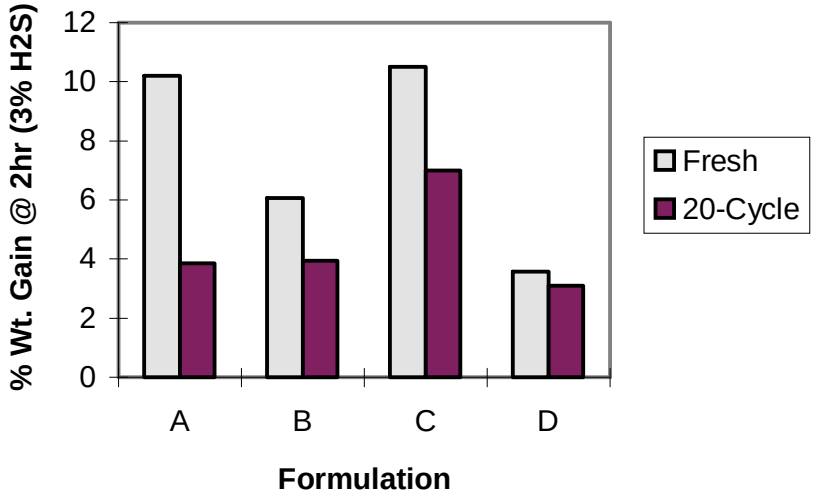

Figure 5.- TGA capacity of sorbents after 20-cycles at GE-CRD

50-cycle of Bench Test at Research Triangle Institute

In support of the effort for the selection of sorbent for the Tampa Electric Co's Polk Station, a subcontract was issued by GE-CRD to Research Triangle Institute to conduct an independent 50-cycle bench-scale test on one selected zinc titanate formulation. The test would provide information on the long-term chemical reactivity and mechanical durability of the pelletized sorbent for moving-bed applications. The selected sorbent for 50-cycle testing was Formulation C, previously shown in Figure 3 to Figure 5, which exhibited low ASTM attrition and high sulfur loading in the GE-CRD screening tests. The sorbent was fabricated again by UCI under similar calcinations conditions and designated as formulation PP3121. The testing at RTI proceeded according to the test protocol written at GE-CRD to provide uniformity in test procedures for the development of moving-bed sorbents. Conditions for the testing are shown in Table 2 and. Table 3.

Table 2.- Gas compositions for 50-cycle test

	Absorption	*Regeneration*
CO	Balance	
CO_2	10	
H_2	20	
H_2O	20	
N_2	16.3	Balance
H_2S	2.0	
O_2		0-4

Table 3.- Target test conditions during absorption

Parameter	*Operating Condition*
Desired Sorbent Sulfur Loading	6-7 lb S/ft^3 of bed (96.2 g S/liter of bed) at the gas inlet location
H_2S Breakthrough point	200 ppm
Gas space velocity	≥2000 hr^{-1} (STP)*
Pressure	20 atm
Temperature	900 °F

* STP (standard temperature and pressure is defined at 20 °C and 1 atm).

The bed volume was adjusted to obtain the desired gas space velocity, meet the requirement of sulfur loading at the gas inlet location, meet the 200 ppmv breakthrough in a reasonable time (<5 hr.), and meet the test schedule for completion of the 50 cycles. Test conditions during absorption (Table 2) follow the TECO conditions, except for the reduced pressure (20 atm vs. 30 atm) and definition of breakthrough (200 ppmv vs. less than 50 ppmv). The reduced pressure is a result of limitations in the existing hardware; the definition of breakthrough was selected for ease of measurement and for historical comparisons. Regeneration was conducted at 7 atm and between 482 °C and 760 °C.

Figure 6 shows the raw data of the breakthrough curves for PP3121 zinc titanate. Pre-breakthrough H_2S concentrations were below the detection limit (<5 ppm H_2S) suggesting good desulfurization kinetics and thermodynamics. Target desulfurization is less than 50 ppmv for the Polk Station hot gas cleanup system.

Figure 7 shows the corresponding envelope of the breakthrough curves at the 200 ppm level. The bed performance stabilizes to a constant level as the number of cycles increases. This result suggests that steady state operation can be achieved, and loss in bed capacity is not a linear process with number of cycles. Hence, extrapolation of bed performance to longer number of cycles is possible.

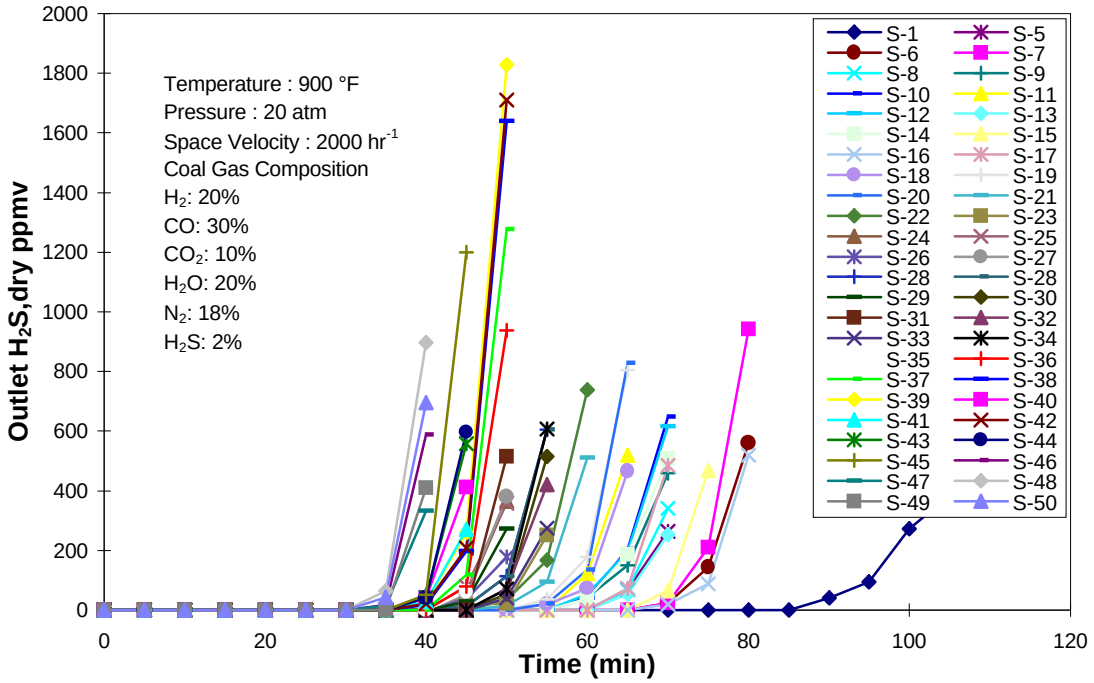

Figure 6.- H2S Breakthrough Curves for 50-Cycle Test of Zinc Titanate at RTI

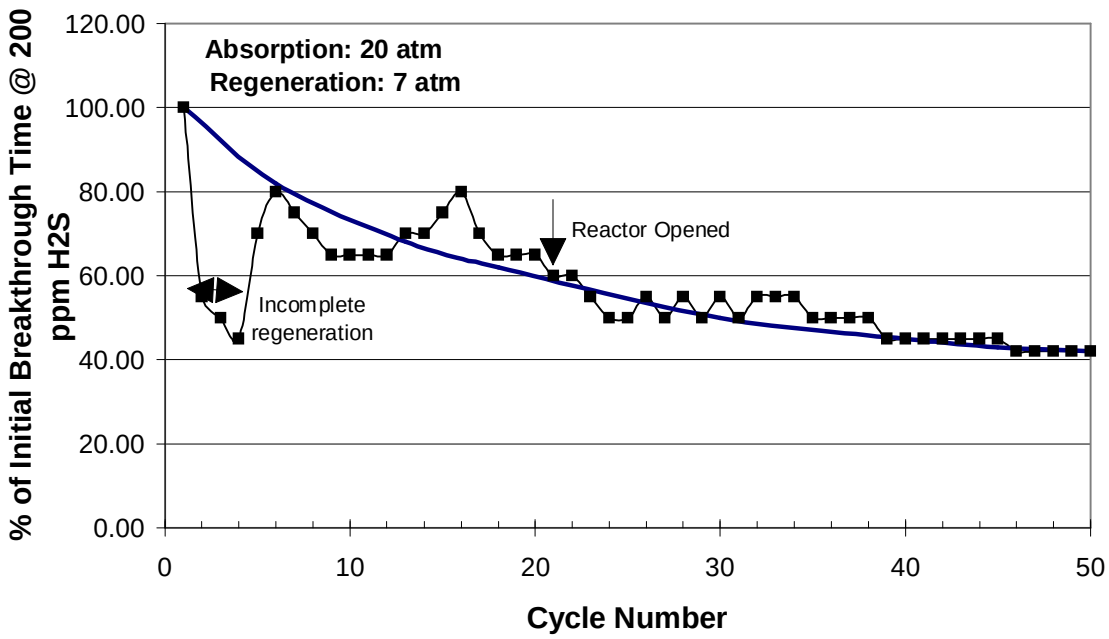

Figure 7.- Envelope of breakthrough curves for zinc titanate testing at RTI

Table 4 shows the comparison of sulfur loading for the fresh and cycled sorbents. The target sulfur loading depends on current bulk density as the sorbent densifies upon cycling. Sulfur loadings were measured by a thermogravimetric analyzer (TGA) as regenerable sulfide on gas inlet location samples. Sulfur analysis by the induction furnace (LECO) method were performed for reference and agreed with the TGA measurements.

Table 4 .- Sulfur Loading of Zinc Titanate Sorbent

Sulfur Loading	*Sulfur Loading as % Sulfur in sulfided pellet*
Target: 7 lb sulfur/ft^3 of bed	6.0-7.0 % (depending on bed bulk density)
Sulfur loading @ 21 cycle (60-min sulfidation)	5.5%
Sulfur loading @ 50th cycle (90-minute sulfidation)	6.1%

Given that the 60-minute absorption at cycle 21 resulted in below target sulfur loading, the absorption time was increased to keep loading within target range. Overall, the target sulfur loading at the gas inlet location was maintained over the 50 cycle test.

In addition to the current sulfur loadings on the pelletized sorbent at the end of selected sulfidations, the measurement of total sulfur capacity available in the powder was also made by TGA and shown in Table 5 and in Figure 8. Samples were in powder form to determine the intrinsic reactivity of the oxide while minimizing pore diffusion mass transfer resistances across the pellets. A sorbent is considered acceptable for long-term operation if its sulfur capacity is retained at 50% or higher of its initial (i.e., theoretical) capacity. In other words, if the sorbent decreases its capacity by no more than a factor of two at the end of fifty cycles.

Table 5.- Sorbent Sulfur Capacity

Bed Capacity	*% Sulfur Capacity by GE TGA Test (At 2-hr exposure)*
Target: as % of theoretical after 50 cycles	50%
Fresh	95%
After 21 cycles	60%
After 50 cycles	55%
After 50 cycles (at 3-hr exposure)	62%

The rate of sulfur loading on the sorbents as a function of time is given by the TGA curves presented in Figure 8. Standard GE TGA test was performed at 1 atm/538 °C/3% H_2S for 2 hours.

After the standard 2-hr TGA test, the 50-cycle powder sample was allowed to sulfide for 1 additional hour to determine if sorbent was saturated at that point. The measured the sulfur capacity was higher (62%) after one additional hour of sulfidation, confirming that the target sulfur loading requirement was exceeded comfortably and that further capacity was still available

in the sorbent. All samples exceeded the acceptance requirement for sulfur capacity, as shown in Table 5.

In addition to measuring the chemical reactivity of the cycled sorbent, the mechanical durability was also measured by ASTM D4058-81 attrition tests (Table 6).

Table 6.- Attrition Results of Zinc Titanate Bench Tests at RTI

Sample Source	*ASTM (D4058-81) Attrition Loss, %*
Target: Fresh sorbent	<4
Fresh	0.7
After 50 cycles: Target	<5
After 50 cycles: gas inlet location	8.0
After 50 cycles: gas outlet location	6.9
After 50 cycles: average	7.4

The attrition loss for the fresh sorbent were well below the initial target of 4% by the ASTM method. The target for the fresh sorbent is as defined in the performance specifications for pilot plant sorbent procurement. The attrition loss for the 50-cycle sorbent was above the target value. Given the fact that the chemical reactivity was satisfactory and exceeded the minimum requirements but the attrition was above target, the performance suggests that the calcination process should be differed to further increase pellet strength at the expense of lower reactivity. As we have stated in the past, calcination conditions determine a balance of reactivity and strength: generally speaking, the higher the reactivity (because of higher pellet porosity) the lower the pellet strength and the higher the ASTM attrition.

Overall, the PP3121 zinc titanate sorbent formulation exceeded minimum specifications of reactivity, sulfur capacity, H_2S equilibrium removal levels, and initial attrition losses. An improvement in the attrition resistance at the 50th cycle (i.e., 50th regeneration) is still desirable. In order to correlate any laboratory data with actual plant operation during evaluation of future sorbent formulations, a batch of this same zinc titanate composition was recommended for fabrication and testing at the GE-CRD pilot plant.

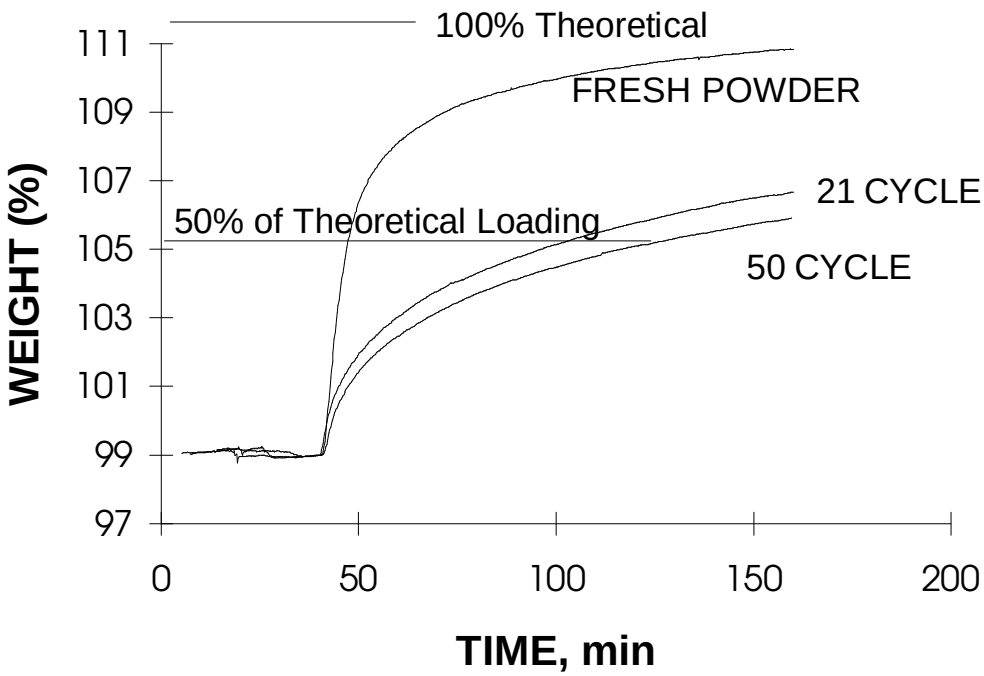

Figure 8.- TGA sulfur capacity of powdered samples after 50 cycles of testing at RTI

Pilot Plant Test Results

Formulation PP3121, and tested at RTI for fifty cycles, was again fabricated by UCI as a 6,400 Kg batch (~14,000 lb) (designation T-2594M) for testing in the GE-CRD pilot plant during Run 8 in September 1995. From the point of view of sorbent development, the purpose of the pilot plant testing was to collect data on the scaling factors of chemical reactivity and sorbent mechanical durability between laboratory tests and larger-scale systems. A second objective was to measure the manufacturability of large sorbent batches given larboratory target specifications.

Figure 9 shows the absorber outlet H_2S during operation of the GE-CRD pilot plant (Test 8) using the zinc titanate sorbent developed in the current sorbent program. Complete results of the pilot plant Test 8 are presented in a separate GE paper in this conference [Furman et al., 1996]. Absorption is carried out at 20 atm and close to 480 °C (~900 °F). After some initial excursions in the desulfurization performance during the first 100 hours, the sorbent and hardware were made to operate in integrated fashion, with close to 99% H_2S removal (from 3500 ppmv dry to 30-40 ppmv dry), achieving desired sorbent reactivity, while simultaneously accomplishing target SO_2 production in the regeneration loop (results not shown here). The attrition loss in the pilot plant test was measured at 1.7% under one set of conditions (i.e., a V-Wire screen in the regenerator fines separator) and 0.3% loss under another set of conditions after the test (i.e., a 1 mm x 1 mm square mesh screen at the same location). These measured pilot plant attrition losses compare favorably with the ASTM attrition losses of approximately 7% ASTM attrition loss measured in the laboratory, indicating that the large scale operation is less severe and cost of sorbent

replenishment is less than predicted from ASTM tests. No corresponding scaling factors are available for the TECO Demonstration plant, and these will be obtained when the demonstration system is placed in operation for the first time in the Fall of 1996.

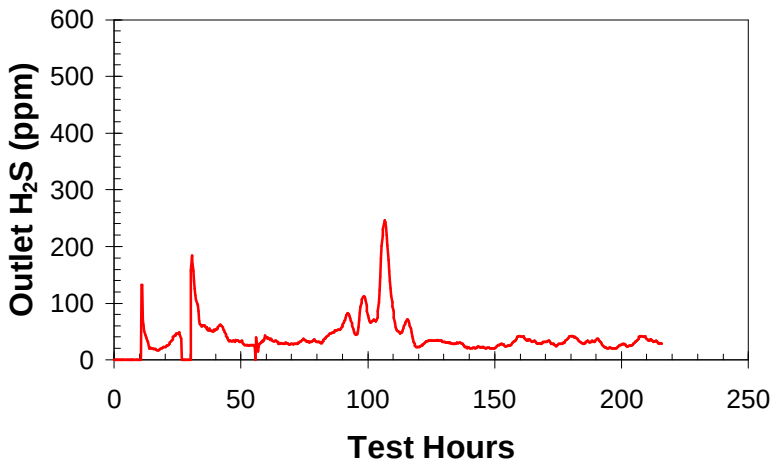

Figure 9.- Absorber outlet H_2S during pilot plant test 8

In conclusion, three levels of testing were performed on molybdenum-doped zinc titanate: laboratory screening at GE-CRD, long-term (50-cycle) bench-scale testing at RTI, and pilot plant testing (200-hr, Test 8) at the GE-CRD pilot plant. The results indicate that the flow of information and technology transfer from laboratory to pilot plant is consistent and prediction of large scale system operation is possible from laboratory and bench test results. Prediction of sorbent replenishment costs due to attrition at the Tampa Electric demonstration-scale plant cannot be made yet, but will be available after plant startup.

Benefits

Coal gas desulfurization to sufficiently low levels at elevated temperatures is now recognized as crucial to efficient and economic coal utilization in Integrated Gasification-Combined Cycle (IGCC) systems. As mentioned before, sensitivity studies of IGCC systems in The Netherlands [Schreurs, 1994; Droog et al., 1993] outlined the economic advantages of desulfurization at 350 °C or above over commercial low-temperature cleanup systems below 100 °C, while in the U.S. [Buchanan et al., 1994] an independent study compared different configurations of gasifiers, hot gas desulfurization (including moving-bed systems), particulate cleanup, and process integration to compare the performance of several system configurations. In both cases, the assumptions for successful implementation of hot coal gas desulfurization relied on the successful development of regenerable sorbent materials.

These sorbents must meet a minimum set of chemical reactivity and mechanical durability criteria to reduce operating costs in large systems. The present sorbent development program is aimed at

minimizing the risks (technical and cost) associated with scaling up of the moving-bed hot gas desulfurization process.

The early thermodynamic analysis by Westmoreland and Harrison in 1976 [Westmoreland and Harrison, 1976] set the stage for desulfurization candidates in the range 400 to 1200 °C (752-2182 °F). With the new requirements of lower temperatures (343-538 °C), an update of the thermodynamic analysis was needed to redefine the temperature regime of interest and the suitable metal oxide candidates for hot gas desulfurization. This resulting information, which we obtained and published last year [Ayala et al., 1995b], defines potential candidates worth pursuing for the next generation of suitable hot gas cleanup sorbents.

Over the past year, testing of zinc titanate sorbent in laboratory screening, long-term bench scale testing, and pilot plant scale operation, has proven that zinc titanate is a suitable sorbent for desulfurization in the target temperature range of 343-538 °C, and consistent with relatively easy regeneration requirements and minimal undesired side reactions. In this sense, the advanced sorbent development program is providing support to the development of more efficient and economically viable large-scale IGCC systems for power generation.

Future Activities

Previous laboratory data have indicated that desulfurization reactivity and mechanical strength of sorbent pellets are inversely proportional. Having demonstrated at the pilot plant that integrated operation of hot gas desulfurization using zinc titanate sorbent achieved 99% desulfurization simultaneously with good sorbent regeneration, the next step is to further increase the mechanical durability of the sorbent for lowering further plant operating costs. Additives/promoters for stabilization of pellet internal morphology will impart strength to the pellets. An alternate approach is to decrease the ratio of inert to active species for desulfurization. Several sorbent manufacturers and research laboratories are being contacted for implementation of these fabrication enhancements to the family of zinc-based sorbents.

Work will continue in the laboratory on the screening of (non-zinc) mixed-metal oxides. Formulations that exhibit good desulfurization/regeneration characteristics will be pelletized and calcined under suitable conditions for further testing in the laboratory and, eventually, under pilot plant operation.

Acknowledgments

The authors gratefully acknowledge the technical assistance of Daniel Cicero, P.E., the METC Contracting Officer's Representative. United Catalysts, Inc.'s cooperation is also appreciated for providing free of charge several sorbent formulations for testing. The contract period of performance is from September 30, 1994 to February 29, 1997.

References

Ayala, T. Chuck, E. Gal, and R.P. Gupta. 1994. Development of High Temperature Desulfurization Sorbents for Moving-Bed Systems. In Proceedings of the *Coal-Fired Power Systems 94 – Advances in IGCC and PFBC Review Meeting*, p. 637. DOE/METC-94/1008. NTIS/DE94012252. Springfield, Va.: National Technical Information Service.

Ayala, R.E. T.L. Chuck, and R.P. Gupta. 1995a. . Moving-Bed Sorbents. In *Proceedings of the Advanced Coal-Fired Power Systems '95 Review Meeting*, Vol II , pp 591-600. DOE/METC-95/1018 Vol 2. NTIS/DE95009733. Springfield, Va.: National Technical Information Service.

Ayala, R.E., V.S. Venkataramani, J. Abbasian, and A.H. Hill. 1995b. Advanced Low-Temperature Sorbents. In *Proceedings of the Advanced Coal-Fired Power Systems '95 Review Meeting*, Vol I , pp 407-416. DOE/METC-95/1018 Vol. 1. NTIS/DE95009732. Springfield, Va.: National Technical Information Service.

Bevan, D.J. Najewicz, R.E. Ayala, A. Feitelberg, and A. Furman. 1995. Integrated Operation of a Pressurized Gasifier, Hot Gas Desulfurization System and Turbine Simulator. In *Proceedings of the Advanced Coal-Fired Power Systems '95 Review Meeting,* Vol I , pp. 187-201. DOE/METC-95/1018. NTIS/DE95009732. Springfield, Va.: National Technical Information Service.

Bevan, S., D.J. Najewicz, E. Gal, A.H. Furman, R. Ayala, and A. Feitelberg. 1994. Integrated Operation of a Pressurized Gasifier, Hot Gas Desulfurization System and Turbine Simulator. In Proceedings of the Coal-Fired Power Systems 94 – Advances in IGCC and PFBC Review Meeting, p. 222. DOE/METC-94/1008. NTIS/DE94012252. Springfield, Va.: National Technical Information Service.

Buchanan, T.L., H.T. Chen, M.G. Klett, M.D. Rutkowski, and R. Zaharchuk. Optimization of Stream Cleanup in Three IGCC Systems. Final Report to U.S. DOE/Fossil Energy by Gilbert/Commonwealth, Inc., Reading, PA, USA under Contracct DE-AC01-88FE61660.

Corman, J.C. 1986. *System Analysis of Simplified IGCC Plants,* Topical Report. U.S. Dept of Energy, DOE/ET/14928-2233.

Droog, H.A., A. Delwel, and R. Assink. 1993. Comparison of High-Temperature Gas Treatment Options with Low-Temperature Gas Treatment in IGCC's following Entrained Flow Gasification. In *Proceedings 12th EPRI Conference on Gasification Power Plants.*San Francisco, CA, Oct 27-29, 1993

Furman, A.H., R. Ayala, A. Feitelberg, D. Najewicz. 1996. Integrated Operation of a Pressurized Fixed Bed Gasifier, Hot Gas Desulfurization System and Turbine Simulator. Paper 3.1. *Advanced Coal-Fired Power Systems '96 Review Meeting*. Morgantown, WV, July 16-18, 1996.

Gangwal, S.K., and R.P. Gupta, 1993. Enhanced Durability of Desulfurization Sorbents for Fluidized-Bed Applications. In *Proceedings of the Coal-Fired Power Systems 93 – Advances in IGCC and PFBC Review Meeting*, p. 146-157. DOE/METC-93/6131. NTIS/DE93000289. Springfield, Va.: National Technical Information Service.

McDaniel, M.H., D.J. Mollot, and V.K. Venkataraman. 1995. Editors. *Proceedings of the Advanced Coal-Fired Power Systems '95 Review Meeting*, Vol I and II ,. DOE/METC-95/1018. NTIS/DE95009732. Springfield, Va.: National Technical Information Service.

Rath, L.K., G.T. Lee, and P.H. Le. 1994. IGCC System Studies. In *Proceedings of the Coal-Fired Power Systems 94 – Advances in IGCC and PFBC Review Meeting*, p. 66. DOE/METC-94/1008. NTIS/DE94012252. Springfield, Va.: National Technical Information Service.

Schreurs, H. 1994. Hot Clean Up of coal Gas. An Overview of Applicability. Netherlands Agency for Energy and the Environment Novem. August 31, 1994. Report No. 94/E0705/229100.

Westmoreland, P.W., and D. P. Harrison. 1976. Evaluation of Candidate Solids for High-Temperature Desulfurization of Low-Btu Gases. Env. Sci. Tech., 10, 659 (1976).

Bench-Scale Testing of Attrition Resistant Moving Bed Sorbents

James H. Swisher (jims@siu.edu; 618 453-7324)
E&A Associates
126 Misty Lake Drive
Murphysboro, IL 62966

Raghubir P. Gupta (gupta@rti.org; 919 541-8023)
Research Triangle Institute
P.O. Box 12194
Research Triangle Park, NC 27709-2194

Introduction

Integrated Gasification Combined Cycle (IGCC) systems with cold-gas cleanup have now reached the early stages of commercialization. The foundation for this was successful completion of the Cool Water Coal Gasification Program several years ago.[1] Destec Energy, Inc., a subsidiary of Dow Chemical Company, has a plant in operation in Louisiana, and the Wabash River Plant in Indiana is now starting up.[2] A similar plant based on the Shell gasification technology is operating in the Netherlands.

In two new plants now under construction, the Tampa Electric Plant in Florida and the Sierra Pacific Power Plant in Nevada, incorporating hot-gas cleanup technology is desirable. Unfortunately, some nagging problems remain with both sulfur sorbent and particle filter technology that may result in the use of cold-gas, rather than hot-gas, cleanup in these plants. With sulfur sorbents, the main problems are with mechanical property degradation and/or loss of sulfur capacity over many sulfidation-regeneration cycles. The sorbents receiving the most attention are all zinc based. They include various zinc titanate formulations and proprietary materials developed by the U.S. Department of Energy/Morgantown Energy Technology Center (DOE/METC) staff and the Phillips Petroleum Company.

The investigators on this project are now completing their third year of effort on a superstrong zinc titanate sorbent. Prior to this year, various formulations were prepared and evaluated for their potential use in fixed- and fluidized-bed hot-gas desulfurization systems.[3,4] A unique feature, the reason for the high strength, is that the zinc titanate is contained in a matrix of titanium dioxide. The formulation with the best combination of properties has a starting composition of 33.5 wt% ZnO and 66.5 wt% TiO_2. It was prepared from 2 µm oxide powders and calcined at 1,000 °C (1,832 °F) . Its crush strength is compared to values obtained by prior

---

Research co-sponsored by the U.S. Department of Energy's Morgantown Energy Technology Center and the Illinois Dept. of Commerce and Community Affairs under Cooperative Agreement No. DE-FC22-92PC92521 (Year 4) with E&A Associates, 126 Misty Lake Drive, Murphysboro, IL 62966; telefax (618)-985-2919.

investigators listed in Table 1. It can be seen that a crush strength of more than six times that of prior investigators was achieved.

A scanning electron micrograph of the sorbent after a 10-cycle fluidized-bed test is shown in Figure 1. The relatively coarse oxide powders in the starting material produce an initial network of large pores in the sorbent. During repeated sulfidation-regeneration cycles, a network of finer pores develops. The consequence of this structural change is that the chemical reactivity of the sorbent increases with cycle number. This year, the R&D has focused on General Electric (GE) Company's moving bed application for the sorbent,[8] and the pellets have been made with commercial equipment in the pilot plant of United Catalysts, Inc. (UCI). Details of the chemical compositions and manufacturing procedures will not be discussed because a patent application is being prepared. It should be noted, however, that modifications had to be made to the sorbent to achieve the desired properties when pellet making was shifted from the laboratory to the pilot plant, and minor modifications are still in progress.

Table 1. Crush Strength Comparisons for Zinc Titanate Sorbents

Investigators/ References	Crush Strength (lb/in.)
Swisher, Yang, and Gupta[3]	1,279
Mei, Gasper-Galvin, Everett, and Katta[5]	97
Ayala, Gal, Gupta[6]	69-183
Grindley[7]	206

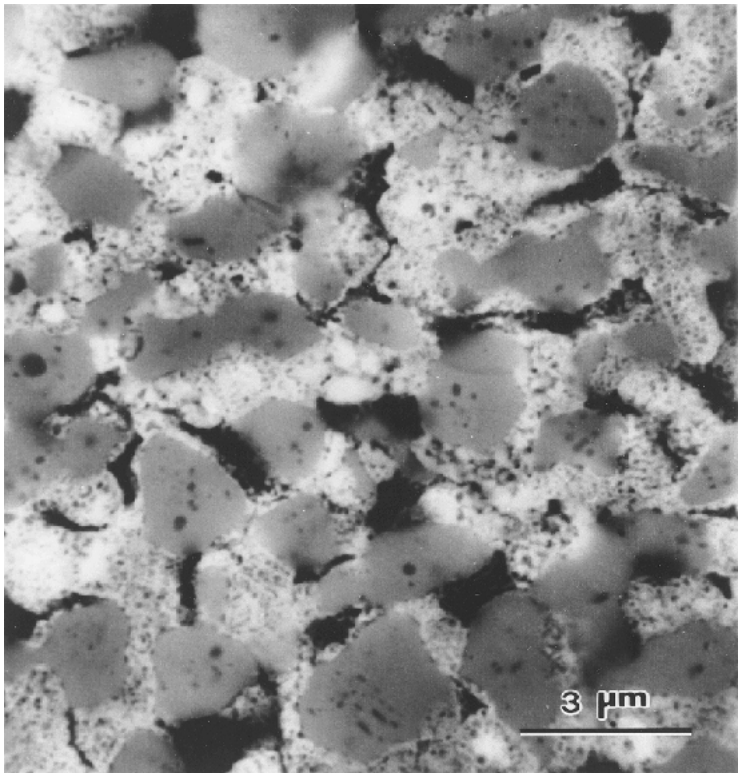

Figure 1. Scanning electron micrograph (backscatter image) of a specimen after a ten-cycle fluidized-bed test. The dark phase is TiO_2, and the light phase is Zn_2TiO_4.

Objectives

The project is designed to extend prior work on the development of a zinc titanate sorbent containing excess titania for high strength and decrepitation resistance. The specific objectives are:

- Specify properties and procure 3- to 5-mm diameter pellets from a catalyst manufacturing company.
- Carry out a 50-cycle test with a reduction-oxidation pretreatment and related sorbent characterization.

- Initiate technology transfer activities to acquaint potential manufacturers and users of the sorbent with its properties and potential.

Project Description

The prime contractor in the project this year is E&A Associates. Contractual arrangements were made for sorbent manufacturing with UCI, and for sorbent characterization and testing with the Research Triangle Institute (RTI). Several 5-lb batches of pellets were produced by a proprietary extrusion and rolling process. The starting materials, calcining temperature, and chemical composition of the sorbent were varied with the goal of matching or improving on the properties of hand-made pellets studied previously.[3] It is important to mention that the sorbent was originally developed for desulfurization temperatures in the range of 550 to 650 °C (1,022 to 1,202 °F). For the moving-bed application, desulfurizing the coal gas at 482 °C (900 °F), which could require a minor change in the formulation to impart needed reactivity at lower temperatures, is desirable.

In March, a formulation designated as ICCI-1 was selected for a multicycle test. The selection was made on the basis of physical property data and thermogravimetric analysis (TGA) measurements of chemical reactivity. A schematic drawing of the apparatus used by RTI for the fixed-bed tests is shown in Figure 2. This test rig has been used extensively for long-term tests on various sorbents including zinc ferrite, zinc titanate, and Z-Sorb. A simulated Texaco coal gas representing the GE moving-bed system for the TECO demonstration plant is generated by mixing and preheating metered quantities of individual gases. The composition of the mixture is listed in Table 2. The H_2S concentration was made artificially high at 2 vol% (20,000 ppmv) to

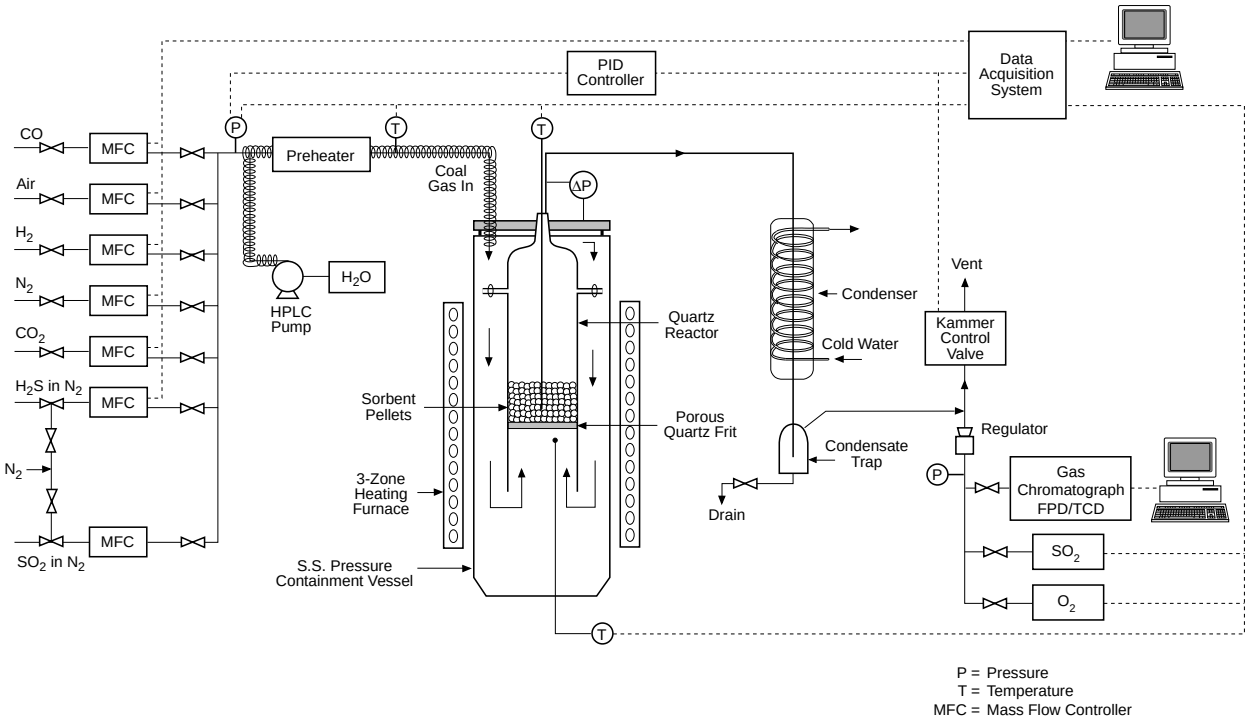

Figure 2. Apparatus used at RTI for multicycle qualification tests.

obtain breakthrough in a reasonable amount of time. Sulfidations were carried out at a total pressure of 20 atm (280 psig) and a space velocity of 2,000 h^{-1} (STP). Regenerations were carried out in a mixture of 3 vol% O_2 and 97 vol% N_2 at a pressure of 7 atm (88 psig).

Table 2. Gas Composition for Fixed-Bed Tests

Component	Concentration (vol%)
CO	30
CO_2	10
H_2	30
N_2	18
H_2O (steam)	20
H_2S	2

The test on formulation ICCI-1 consisted of 20 sulfidation-regeneration cycles. The results led to a development iteration to strengthen the material. In April, another multicycle test was started on the improved formulation, ICCI-2. After 20 cycles, the test was interrupted so that the reactor could be opened to inspect the pellets. An additional 30 cycles were carried out in June. This test duration of 50 cycles is preferred by GE in the qualification of sorbent materials for testing in its moving-bed pilot-plant system.

A considerable effort in the project is being made on technology transfer. Emphasis in this task is on networking with potential raw materials suppliers, manufacturers, and users of the sorbent being developed. Numerous organizations have been contacted so far as a part of this effort.

Results

Because the results for the two formulations subjected to multicycle fixed-bed tests should be discussed in detail, only brief mention will be made of the materials prepared initially. In the exploratory work, variations were made with raw materials, binder additions, and calcining temperatures to try to achieve the physical properties and TGA reactivity desired. One of the reasons that several attempts were needed was that a transition had to be made from the use of reagent-grade oxide powders to raw materials that could be purchased in large quantities at a reasonable price. The outcome of the exploratory work was the selection of a formulation called ICCI-1 for in-depth evaluation.

Properties of ICCI-1

Results are shown in Figure 3 for the TGA reactivities of ICCI-1, ICCI-2 (to be discussed later), and hand-made material evaluated previously.[3] The TGA tests were carried out at 538 °C (1,000 °F) at 1 atm pressure. The gas composition for sulfidation was essentially the same as that given in Table 2, the only difference being that the H_2S concentration was 1.2 vol% instead of 2 vol%. Note that ICCI-1 was more reactive than the hand-made material. While this result is good per se, it raises the question of whether or not mechanical properties were compromised too much in obtaining the high reactivity.

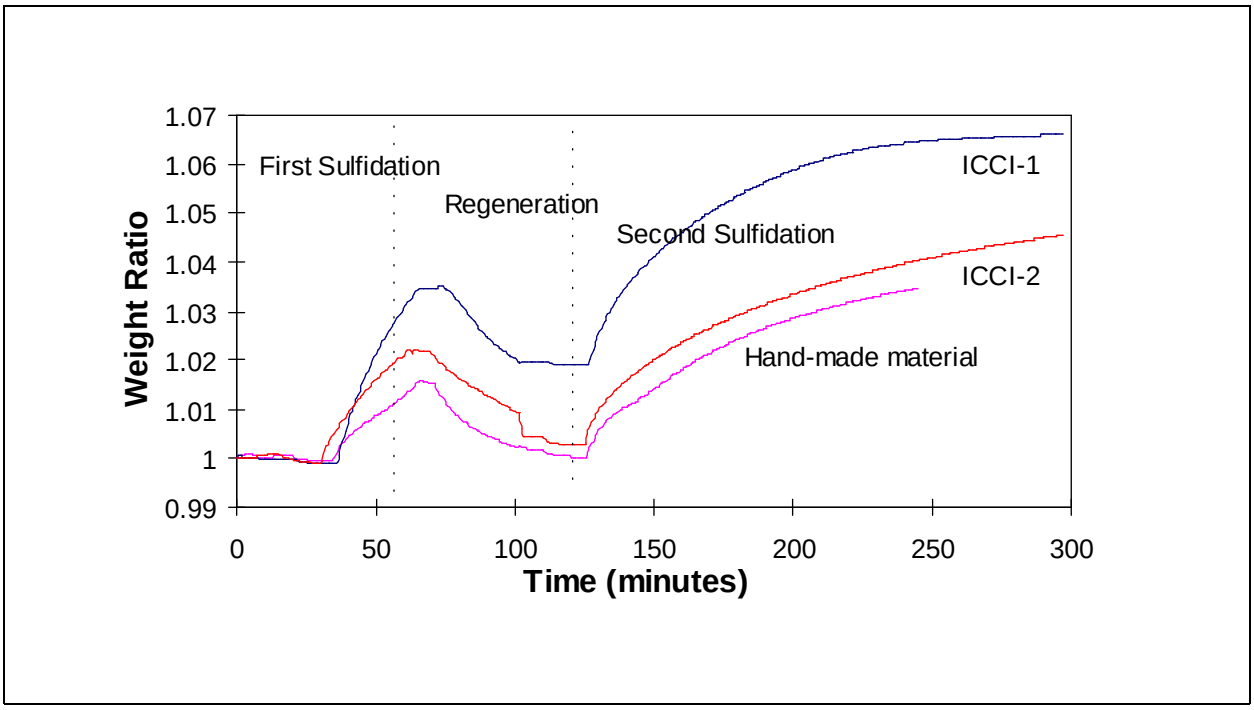

Figure 3. TGA reactivities of ICCI-1, ICCI-2, and hand-made material from prior investigation.[3]

H_2S breakthrough data for ICCI-1 are plotted in Figure 4. With breakthrough defined as 200 ppmv H_2S in the exit gas, the breakthrough times ranged from 105 to 144 min with no trend up or down as the number of cycles increased. It is not understood why breakthrough occurred sooner in Cycles 5, 6, and 7 than in the others. The average sulfur capacity of the sorbent calculated from the breakthrough data ranged from about 7 to 9 lb S/100 lb fresh sorbent. The important conclusion to be drawn from the results is that the sorbent did not degrade in reactivity. When the reactor was opened to inspect the pellets after 20 cycles of testing, some of the pellets near the inlet end of the reactor contained surface cracks. Pellets near the outlet end showed no signs of degradation. Because this was the first time cracking had ever been observed in 3 years of research, it was decided to prepare a stronger formulation and restart the 50-cycle test. Before doing that, however, extensive physical property measurements were made on pellets from both the inlet and outlet ends of the reactor. The results are summarized in Table 3, along with property data for the fresh material. The bulk density of the fresh material was 96.8 lb/ft^3.

A comparison of the physical property data shows that the fresh sorbent and the sample taken near the gas exit have nearly the same properties. The reason for this is that the material near the gas exit did not absorb much sulfur at breakthrough. The sample taken near the gas inlet had poorer crush strength and attrition resistance, which correlates with the surface cracking that was observed. The changes in pore characteristics are similar to those observed before,[3] except that the decreases in percent porosity and pore volume are larger than expected. Perhaps regeneration of the sample was incomplete, leaving the pores constricted by residual zinc sulfide.

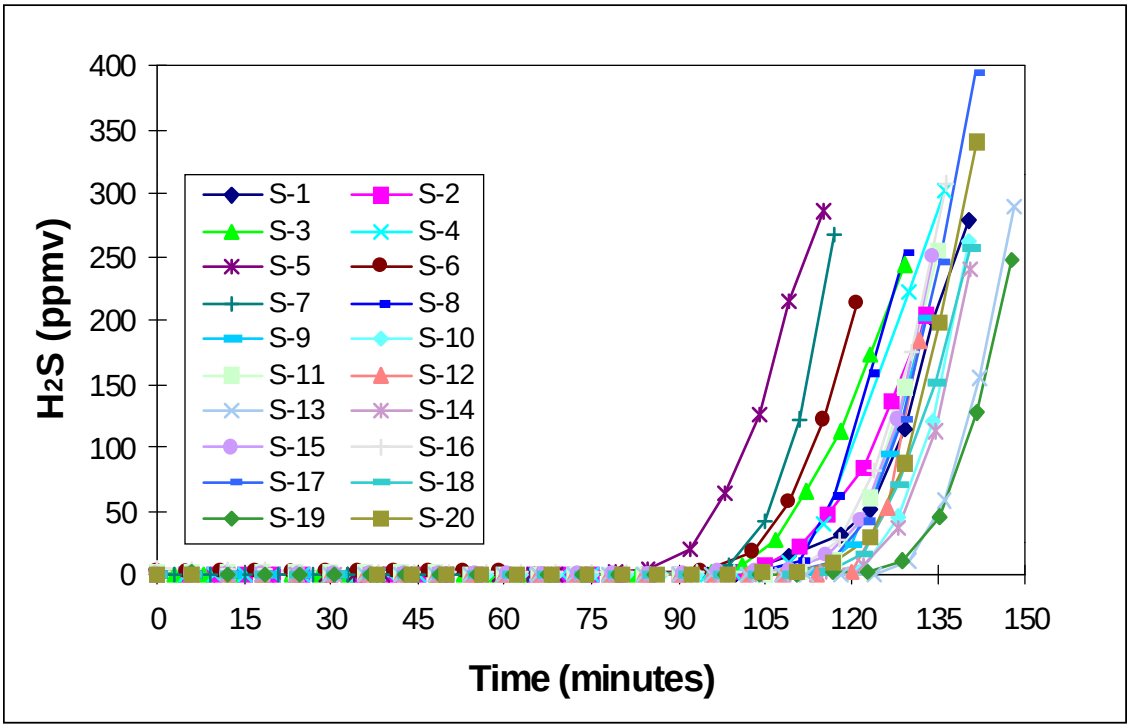

Figure 4. H_2S breakthrough results for ICCI-1 sorbent.

Table 3. Physical Property Data on ICCI-1 Sorbent Before and After Testing[a]

		20-cycle Regenerated	
Property	**Fresh**	**Near gas inlet**	**Near gas outlet**
Average pellet size (mm)	4.45	4.78	4.45
Crush strength (lb/pellet)	27.3	11.3	32.0
ASTM attrition (%)	1.25	6.7	3.1
BET surface area (m^2/g)	1.84	3.40	1.84
Mercury pore volume (cm^3/g)	0.174	0.112	0.172
Median pore diameter (Å)	4419	2983	4556
Porosity (%)	44.5	30.4	44.4

[a] Sorbent in oxidized state.

The physical property results on ICCI-1 highlight an important difference between the fixed-bed test simulation and actual conditions present in a moving-bed reactor. In the latter, sulfur uptake is more uniform in the sorbent material. Thus, in the fixed-bed simulation, the sorbent near the inlet to the bed is subjected to an overtest. To partially correct for this problem, it was decided, with GE staff approval, to adjust the procedure for future tests. With this change, sulfidation would be continued to breakthrough in some but not all of the cycles.

ICCI-2

Referring back to Figure 3, the TGA reactivity of ICCI-2 is lower than that of ICCI-1. This decrease was expected and is a consequence of the higher strength of ICCI-2. A fixed-bed test on ICCI-2 was started in April. Prior to starting the 20-cycle test, a 2-cycle oxidation-reduction pretreatment with hydrogen at 500 °C followed by oxidation in diluted air was used to modify the pore structure and improve initial reactivity.[3] The cycling procedure for sulfidation and regeneration was modified slighty, as mentioned above. Sulfidation to breakthrough was carried out for cycles 1 to 5, 10, 15, and 20. In other cycles, sulfidation was carried out for 75 min, which was about 20 min less than the time required for breakthrough. This procedure corrected, in part, for the oversulfiding of the pellets at the inlet end of the reactor during the testing of the ICCI-1 sorbent.

H_2S breakthrough data for the ICCI-2 sorbent are shown in Figure 5. The breakthrough time can be seen to improve during the first three cycles as the secondary pore structure developed

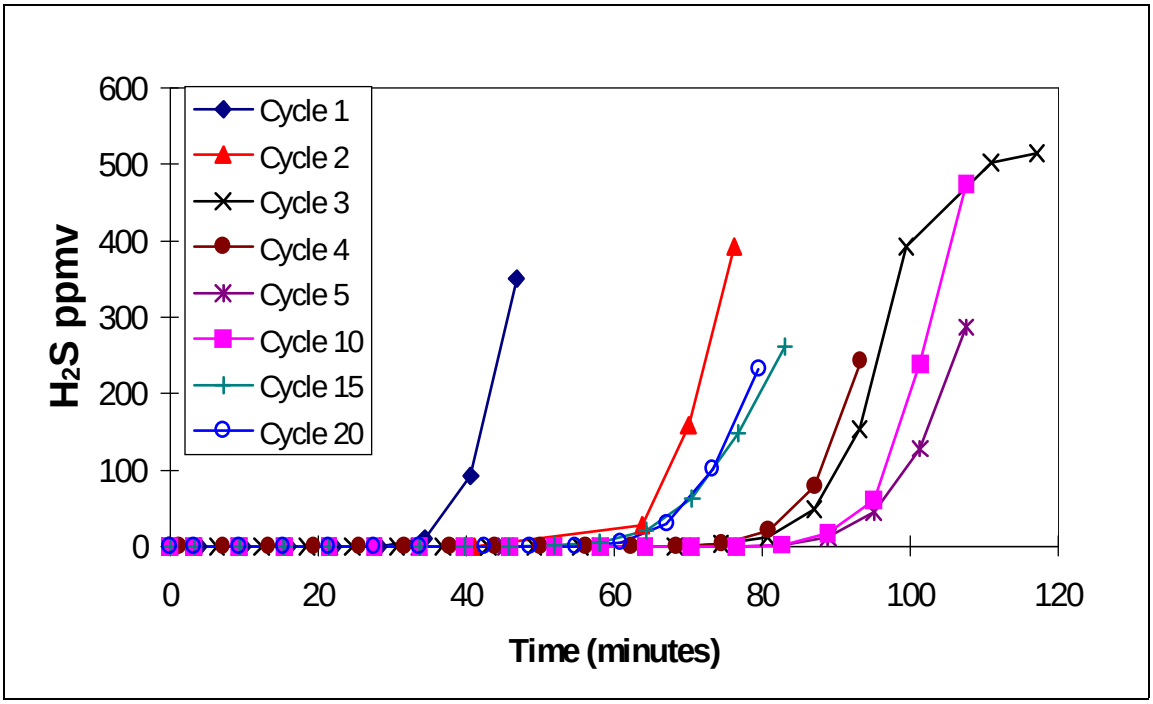

Figure 5. H_2S breakthrough results for ICCI-2 sorbent.

beyond that which occurred during the activation pretreatment. Some loss in breakthrough time occurred during cycles 10 to 15, an effect that is not presently understood. The same effects can be seen in Figure 6, where the calculated sulfur pickup at breakthrough is plotted versus cycle number. When the pellets were inspected after the twentieth sulfidation, the surface cracking of pellets near the inlet end of the reactor was barely noticeable and was much less than with the ICCI-1 sorbent. A summary of the sorbent's physical properties before and after the test is provided in Table 4. The fresh material is in the oxidized state and the tested material is in two different states of sulfidation, so direct comparisons should be made with caution. Probably the only important conclusion that can be drawn from Table 4 is that mechanical property degradation was much less with the ICCI-2 sorbent than with the ICCI-1 material. If one extrapolates the attrition loss data to 50 cycles, assuming a linear change through the bed and a linear change with cycle number, the result is an average attrition loss of 4.15% over 50 cycles. The goal set by GE is 5%, so the data appear promising. Thus, the effort to strengthen the pellets produced the desired result, and a better compromise was reached between mechanical properties and chemical reactivity. While this progress is encouraging, the investigators feel that further improvements are possible because the properties of the ICCI-2 sorbent are still not quite as good as those obtained with hand-made pellets. In view of promising performance of the ICCI-2 test during the 20-cycle test, authorization was given to continue the test for another 30 cycles. This effort is funded by a budget supplement provided by DOE/METC.

Because of the progress being made, a special task was included in this year's contract on technology transfer. A list of many of the organizations contacted is given in Table 5. Of the

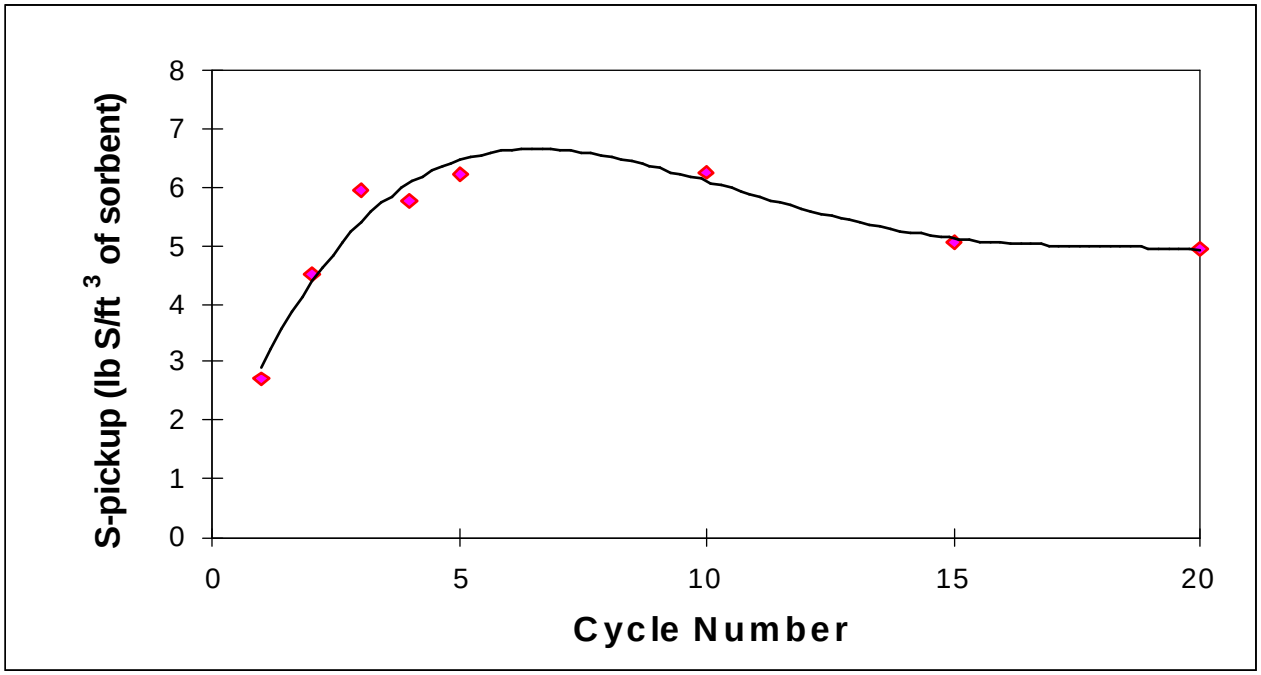

Figure 6. Calculated sulfur capacity of ICCI-2 sorbent.

Table 4. Physical Property Data on the ICCI-2 Sorbent Before and After Testing

		After 20th sulfidation	
Method	**Fresh**	**Near gas inlet**	**Near gas outlet**
Average pellet size (mm)	4.05	3.75	3.69
Bulk density (lb/ft^3)	93.2	102.0	98.1
Crush strength (lb/pellet)	30.4	22.1	18.5
ASTM attrition (%)	1.9	4.0	2.8
BET surface area (m^2/g)	1.11	2.52	1.63
Mercury pore volume (cm^3/g)	0.159	0.102	0.139
Median pore diameter (Å)	6458	4829	6116
Porosity (%)	42.0	29.0	38.0
Sulfur (wt%)[a]	0.0	8.5	3.8

[a] TGA measurement

potential sorbent manufacturers, only UCI showed an interest in making material for evaluation tests, presumably because there is no assured market for IGCC sorbents as yet. The response from potential users and other organizations was more enthusiastic. They realize that all the technology problems are not solved and that cold-gas cleanup may continue to be used. However, there appears to be a consensus that hot-gas cleanup has sufficient promise that additional R&D is justifed.

Table 5. Technology Transfer Contacts

Catalyst manufacturers	United Catalysts, Norton, Degussa
Potential user	General Electric, Kellogg, Destec, Public Service of Colorado
Raw materials suppliers	Total of 12 potential suppliers of ZnO, TiO_2, and binders
Others	EPRI, Parsons Power Group, TDA Research, Phillips Petroleum

The part of the technology transfer task on materials suppliers proved to be critically important because the properties of the sorbent depend on the choice of raw materials. Therefore, the identity of any information obtained from these companies will not be published at

this time. Samples from several companies were evaluated, and one of them prepared a new grade of powder for our possible use.

Benefits

The market potential for IGCC systems in the long term is enormous. In 1993, DOE projected that IGCC plants may produce as much as 130 GW of electricity in the year 2040.[9] This power estimate corresponds to 1.2 million tons/day of coal consumption, much of which would be high-sulfur bituminous coal. A clear description of expected benefits of IGCC systems was expressed by Feibus et al.[10] In their words,

> One of the most fundamental and important advantages exhibited by the IGCC power plant over direct combustion systems is the ability of the plant to control sulfur emissions to any extent necessary at a reasonable cost. The penalties imposed by the IGCC system, as a result of increasing the level of sulfur removal from 90 to 99.5, are a loss in efficiency of 1.3%, an increase in the capital cost of 3.5%, an increase in the heat rate of 1.5%, and an increase in the levelized cost of electricity of 2.6%.

These values were calculated for early plant designs with cold-gas rather than hot-gas desulfurization. The implication is that high-sulfur bituminous coal can be used in IGCC systems at an affordable cost.

With successful development of hot-gas desulfurization (HGD) technology, the efficiency of IGCC systems can be increased by 2% to 3%. There is an ongoing debate on the optimum temperature for desulfurization. The undesirable effects of desulfurizing at temperatures above 500 or 600 °C lie mainly in the affordability and technology readiness of valves, particle filters, and materials of construction. In a recent report by Buchanan et al., the effect of desulfurization temperature on the total cost of producing power from IGCC plants was analyzed.[11] While there did not seem to be a significant direct effect, there may be indirect benefits of using a high temperature related to lower emissions, less solid waste, etc.

There are three IGCC plants in the United States in operation or in the final stages of construction–the Wabash River, Tampa Electric, and Sierra Pacific Plants.[12] Now in operation, the Wabash River Plant, with cold-gas cleanup, repowers an old facility with an efficiency gain from about 31% to 38% and an increase in power output of 150%. When the Tampa Electric Plant goes online later this year, it will use 1,900 tons/day of bituminous coal. If the sorbent being developed here were to be used in the three plants mentioned above, approximately 150,000 tons/year of the sorbent would be needed.

Future Activities

Under a separate contract from the Illinois Clean Coal Institute, a 14,000 lb lot of sorbent will be produced. Small but important changes in preparation procedures are being made to further

improve properties. It is hoped that the material will be tested in GE's moving-bed pilot plant later this year.

Acknowledgments

The authors wish to acknowledge the contibutions to the project of David Wolfe and his staff at UCI; Daniel Banerjee and Herman Feldman, ICCI; and Daniel Cicero and Thomas Dorchak, DOE/METC.

References

1. L. Lamarre, "Worldwide Activity in IGCC," *EPRI Journal*, Vol. 19, No. 5, 1994, pp. 6-15.

2. T. Moore, "Repowering as a Competitive Strategy," *EPRI Journal*, Vol 20, No.5, 1995, pp. 6-13.

3. J. H. Swisher, J. Yang, and R.P. Gupta, "Attrition-Resistant Zinc Titanate Sorbent for Sulfur," *Ind. & Eng. Chem. Research*, Vol. 34, 1995, pp. 4463-4471.

4. J. Yang, "Improving the Properties of Zinc Titanate-Based Sorbents for Sulfur Removal," Ph.D. Dissertation, Southern Illinois University, Carbondale, IL, 1995.

5. J. S. Mei, L. Gasper-Galvin, C.E. Everett, and S. Katta, "Fixed-Bed Testing of a Molybdenum-Promoted Zinc Titanate Sorbent for Hot Gas Desulfurization," in D.L Bonk, Ed., *Proceedings of Coal-Fired Power Systems 93–Advances in IGCC and PFBC Review Meeting*, Report No. DOE/METC-93/61131, U.S Department of Energy/Morgantown Energy Technology Center, Morgantown, WV, 1993, pp. 315-325.

6. R.E. Ayala, E. Gal, and R.P. Gupta, "Testing of Zinc Titanate Desulfurization Sorbents for Moving Bed Applications," in D.L Bonk, Ed., *Proceedings of Coal-Fired Power Systems 93–Advances in IGCC and PFBC Review Meeting*, Report No. DOE/METC-93/61131, U.S. Department of Energy/Morgantown Energy Technology Center, Morgantown, WV, 1993, pp. 136-145.

7. T. Grindley, "Effect of Chlorine on Hot Gas Desulfurization Sorbents," In V.P. Kothari and J.L. Beeson, Eds., *Proceedings of the Tenth Annual Gasification and Gas Stream Cleanup Systems Contractors' Review Meeting*, Vol. 1, Report No. DOE/METC 90/6115, U.S. Department of Energy/Morgantown Energy Technology Center, Morgantown, WV, 1990, pp. 215-226.

8. R.E. Ayala, A.H. Furman, and D.J. Najewicz, "Integrated Operation of a Pressurized Fixed Bed Gasifier, Hot Gas Desulfurization System and Turbine Simulator," in *Proceedings Advanced Coal-Fired Power Systems '95 Review Meeting*, U.S. Department of Energy/Morgantown Energy Technology Center, Morgantown, WV, 1995, pp. 187-201.

9. "IGCC Product Plan," U.S. Department of Energy, Washington, DC, April 1993.

10. H. Feibus, G. Voelker, and S. Spadone, "The Role of Advanced Coal Cleaning Technology in the Reduction of Sulfur Dioxide Emissions," In D.S. Gilleland and J.H. Swisher, Eds., *Acid Rain Control II. The Promise of New Technology*, Southern Illinois University Press, Carbondale, IL, 1986, pp. 51-84.

11. T.L. Buchanan, H.T. Chen, M.G. Klett, and M.D. Rutkowski, "Extended Parametric Sensitivity Studies on IGCC Systems," Final Report on Contract No. DE-ACO1-88 FE 61660, U.S. Department. of Energy, Washington, DC, March 1994.

12. "Clean Coal Technology Demonstration Program: Program Update 1995," Report No. DOE/FE-0346, U.S. Department of Energy, Washington DC, April 1996.

Durability Testing of the Direct Sulfur Recovery Process

Jeffrey W. Portzer (jwp@rti.org; 919-541-8025)
Brian S. Turk (bst@rti.org; 919-541-8024)
Santosh K. Gangwal (skg@rti.org; 919-541-8033)
Research Triangle Institute
P.O. Box 12194
Research Triangle Park, NC 27709-2194

Introduction

Designs for advanced integrated gasification combined cycle (IGCC) power systems call for desulfurization of coal gasifier gas at high-temperature, high-pressure (HTHP) conditions using highly efficient, regenerable metal oxides such as zinc titanate. Regeneration of the sulfided sorbent using an oxygen-containing gas stream results in a sulfur dioxide (SO_2)-containing off-gas at HTHP conditions. The patented Direct Sulfur Recovery Process (DSRP) developed by the Research Triangle Institute (RTI) with Morgantown Energy Technology Center (METC) support is an attractive option for treatment of this regeneration off-gas. Using a slipstream of coal gas as a reducing agent, it efficiently converts the SO_2 to elemental sulfur, an essential industrial commodity that is easily stored and transported.

In the DSRP (Dorchak et al., 1991), the SO_2 tail gas is reacted with a slipstream of coal gas over a fixed bed of a selective catalyst to directly produce elemental sulfur at the HTHP conditions of the tail gas and coal gas. Overall reactions involved are shown below:

$$2\ H_2 + SO_2 \rightarrow (1/n)\ S_n + 2\ H_2O$$

$$2\ CO + SO_2 \rightarrow (1/n)\ S_n + 2\ CO_2$$

$$H_2 + (1/n)\ S_n \rightarrow H_2S$$

$$2\ H_2S + SO_2 \rightarrow (3/n)\ S_n + 2\ H_2O\ .$$

The DSRP was initially developed as a two-stage process using simulated coal gas in the laboratory. The original process concept employed two catalytic reactors in series, each followed by a sulfur condenser. Hot regeneration tail gas was mixed with a hot coal gas slipstream (to act as the reducing gas) and fed to the first DSRP reactor. Approximately 95 percent of the combined sulfur in the inlet stream to the first reactor was converted to elemental sulfur. The outlet gas of the first reactor was then cooled, condensing out the sulfur. The cooled gas stream was reheated and sent to the second DSRP reactor where 80 to 90 percent of the remaining

---

Research sponsored by the U.S. Department of Energy's Morgantown Energy Technology Center, under contract DE-AC21-93MC30010, with Research Triangle Institute; telefax: 919-541-8000.

sulfur compounds were converted to elemental sulfur via the modified Claus reaction at high pressure. The total efficiency of the two reactors for the conversion of sulfur compounds to elemental sulfur was projected to be 99 percent.

However, based on the initial results from the slipstream tests with actual coal gas (Portzer and Gangwal, 1995) and additional data presented here, the second stage does not appear necessary. A sulfur recovery of 98 percent can be consistently achieved in a single stage with careful control of the stoichiometric ratio of the gas input. The single-stage process, as it would be proposed to be integrated with a metal oxide sorbent regenerator, is shown in Figure 1. There is a potential for "zero" sulfur emissions if the DSRP tail gas is recycled.

Objectives

Prior to the current project, the development of the DSRP was done in a laboratory setting, using synthetic gas mixtures to simulate the regeneration off-gas and coal gas feeds. The objective of the current work is to further the development of zinc titanate fluidized-bed desulfurization (ZTFBD), and the DSRP for hot-gas cleanup by testing with actual coal gas. There are three main goals of this project:

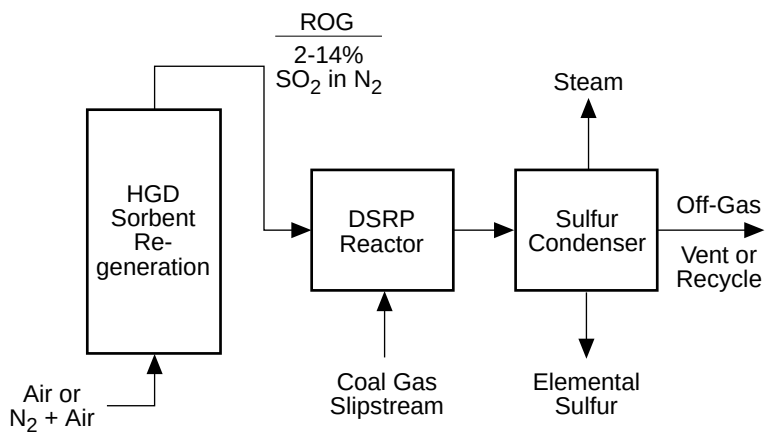

Figure 1. Sorbent Regeneration - DSRP Integration

- Develop and test an integrated, skid-mounted, bench-scale ZTFBD/DSRP reactor system with a slipstream of actual coal gas;

- Test the DSRP over an extended period with a slipstream of actual coal gas to quantify the degradation in performance, if any, caused by the trace contaminants present in coal gas (including heavy metals, chlorides, fluorides, and ammonia); and

- Design and fabricate a six-fold larger-scale DSRP reactor system for future slipstream testing.

Accomplishment of the first objective, testing of the DSRP with actual coal gas and integrated with hot-gas desulfurization, was described previously (Portzer and Gangwal, 1994, 1995). This paper describes the accomplishment of the second objective — an extended test period (durability testing) of the DSRP. One of the main reasons for testing the DSRP for an extended period with actual coal gas from an operating gasifier was to quantify the degradative effect, if any, of the trace contaminants present in coal gas.

Approach

Since coal gas is not available at RTI's laboratories in Research Triangle Park, North Carolina, other approaches were used to accomplish the desired DSRP testing. The first strategy — slipstream testing — moved the existing bench-scale DSRP apparatus to the coal gas source (METC 10-in. gasifier) using a mobile laboratory. At METC, the process equipment was operated to produce elemental sulfur using a small slipstream of the total gasifier output.

The second strategy — canister testing — moved only the catalyst to the source of the coal gas (General Electric [GE] pilot-plant gasifier) and exposed it for an extended period. The exposure was followed by testing in a second bench-scale DSRP unit at RTI that used simulated coal gas to verify the catalyst's efficacy.

Project Description

Figure 2 shows the equipment, consisting of RTI's ZTFBD/DSRP mobile laboratory (trailer), used for the slipstream testing at METC. It was described previously (Portzer and Gangwal, 1994). Following the 1994 slipstream test, a number of modifications were made to the bench-scale DSRP unit contained in the trailer. The second stage reactor and sulfur condenser were removed to convert the unit into a single-stage process. An improved-design sulfur separator pot was added to the steam-heated sulfur condenser. A temperature- and pressure-corrected orifice flow meter was added to the coal gas line feeding the DSRP. A PC-based flow controller was installed that compared the coal gas composition (continuous analyzer data from METC data network) with the regeneration off-gas SO_2 content and adjusted the mass flow of the coal gas in order to maintain the desired 2:1 stoichiometric ratio of the reducing components (H_2 and CO).

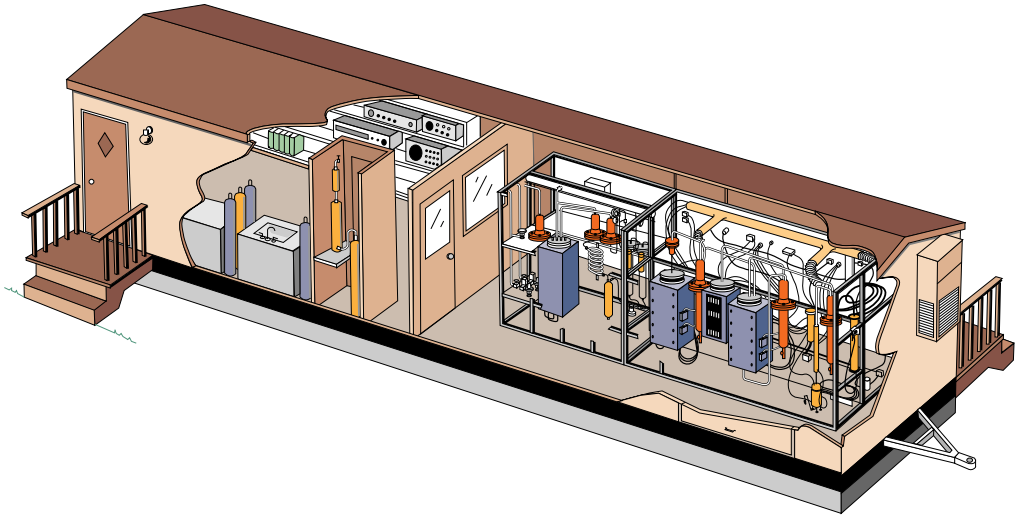

Figure 2. DSRP Mobile Laboratory.

The 1995 long duration slipstream test used simulated regeneration off-gas (ROG) to react with the actual coal gas. The ROG was prepared by evaporating liquid SO_2 from a pressurized transfer cylinder into a heated nitrogen stream. The cylinder was mounted on an electronic balance to monitor weight change. Flow was controlled by a rotameter with a manual needle valve. The mixed gas composition was analyzed continuously for input to the coal gas stoichiometric flow control.

The METC coal gasifier is a fluidized-bed gasifier providing approximately 4,750 std ft^3/h of low-Btu coal gas from a nominal charge rate of 80 lb/h of coal. A heated slipstream, approximately 170 std ft^3/h (80 std L/min), was directed to the RTI trailer. Of this, approximately 32 std ft^3/h (15 std L/min) were used to operate the DSRP.

The DSRP was operated in conjunction with a 2-week gasifier campaign at METC in July 1995. During this period coal gas was flowing through the DSRP catalyst bed for 160 h. The simulated regeneration off-gas was fed to the catalyst bed for a total of 44 h, divided into nine separate periods of multihour operation. The duration of the runs with SO_2 flowing were limited by problems associated with solid sulfur plugging of the downstream vent lines. The METC coal gas was sampled several times for trace contaminants (volatile heavy metals) using a modified EPA "Method 29" protocol.

Several months following completion of the 160-h slipstream run, the DSRP catalyst was removed from the reactor, placed in a canister, and installed in a coal gas line at the GE pilot gasifier in Schenectady, New York. The canister was a simple fabrication of perforated stainless steel with a capacity of approximately 850 mL. Thus, the entire charge of 1 L of catalyst could not be subjected to this additional exposure. The canister was placed in the piping prior to the start of a 200-h gasifier campaign and was removed following completion of the campaign. No trace contaminant sampling of the GE gasifier gas was performed. Table 1 summarizes the exposure conditions. The canister and catalyst were shipped in tightly closed bottles that had been purged with dry nitrogen prior to filling; however, the bottles were not hermetically sealed.

Table 1. GE Exposure Test Conditions

- 20 atm (294 psia)
- 482 to 538 °C (900 to 1,000 °F)
- Illinois #6 Coal Gas
- 200 h
- Downstream of absorber

The idea of the canister exposure test was that the DSRP catalyst would have 200 h of additional exposure to actual coal gas (beyond what was achieved during the METC 160-h campaign) so that the effect, if any, of the trace contaminants could be determined. In normal DSRP operation, the catalyst is exposed to a mixture of gases containing about 15 percent coal gas. Assuming that concentration and exposure time are directly related, 200 h of pure coal gas would be equivalent to 1,330 h of diluted (15%) coal gas.

The most effective way to demonstrate the continued activity of the DSRP catalyst is to install it in an HTHP reactor and actually conduct the SO_2 reduction reaction using a reducing gas mixture. Thus, to determine if additional coal gas exposure of the catalyst had any deleterious effects, the doubly exposed catalyst was tested in a bench-scale DSRP unit set up in a laboratory

in RTI's main campus in Research Triangle Park. The reactor design was essentially identical to that of the trailer-mounted unit; the sulfur condenser design was identical. The coal gas was simulated by using a purchased custom gas mixture, and the regeneration off-gas was generated similarly to the method used in the trailer: vaporization of liquid SO_2 under pressure. The continuous H_2S/SO_2 tail gas analyzer used in the Mobile Laboratory was moved to RTI for the duration of the bench-scale testing.

Results

Table 2 summarizes the operating conditions of the DSRP reactor in the Mobile Laboratory (1995 slipstream test) and compares them to the conditions used for the followup testing of the exposed catalyst (1996 testing) in the RTI laboratory. The conditions are very similar, with the exception that less catalyst was available for the lab tests (due to a limitation of canister volume, as described). However, the gas flow rate was reduced to maintain the same space velocity.

Table 2. Reactor Test Conditions

	1995 Field Test	**1996 Lab Test**
Temperature (°C)	590-630	575-640
Pressure (psig)	210-265	275
Space velocity (std cm^3/cm^3-h)	5,100	2,700-8,200
Reactor diameter (in.)	3.0	3.0
Catalyst volume (cm^3)	1,000	600
Inlet SO_2 (%)	2.4-4.9%	2.1-5.4%

Table 3 presents some of the results of the 1995 slipstream testing. Single-stage conversion to elemental sulfur of 98% was achieved at the beginning of the run and at the end. Thus, there was no detrimental effect of 160 h of exposure of the catalyst to coal gas. These calculations are based on measurements of the inlet and outlet gas compositions by continuous analyzers and by gas chromatograph (GC), and they include the H_2S in the coal gas feed. The "percent conversion to elemental sulfur" is the difference of the molar flow rates of sulfur compounds in the reactor inlet and outlet, divided by the molar flow rate of the inlet sulfur compounds. The SO_2 conversion to elemental sulfur and other sulfur compounds is essentially 100 percent (as evidenced by low concentrations of SO_2 in the DSRP tail gas). Some of the elemental sulfur produced is apparently further reduced, however, as Table 3 shows. The "percent conversion [of SO_2] to H_2S and COS" is the difference in the molar flow rates of the outlet and inlet reduced sulfur compounds, divided by the inlet SO_2 molar flow. Thus, even though total conversion of the SO_2 in the ROG was achieved, the ultimate value of total overall conversion to elemental sulfur was limited by the presence of reduced sulfur compounds (in the outlet) to less than 100 percent.

Table 3. One Stage DSRP Results During Lined-out Operation (1995)

Run Time (min)	SO_2 Conversion (%)	SO_2 Conversion to H_2S and COS	SO_2 Conversion to Sulfur (%)
Run No. 1 (0-4 h exposure time)			
200	100.0	5.8	93.2
220	100.0	1.1	98.0
240	9.6	0.2	98.6
260	96.4	-2.1	96.4
Run No. 9 (155 h exposure time)			
91	100.0	0.7	97.8
117	100.0	1.0	97.7
134	100.0	0.8	98.1
151	99.7	0.8	97.9

Following 200 h additional coal gas exposure in early 1996, the catalyst charge was tested in the RTI laboratory DSRP bench unit using simulated ROG and simulated coal gas. Table 2 summarizes the operating conditions; Table 4 summarizes the results of the best runs. Several test runs were made, with a total operating time (with SO_2 feed) of 22 h. Known optimum conditions, as well as less-than-optimum conditions were used. Only 86 percent conversion was obtained initially; by the end of the series the conversion was up to 96 percent, with the runs that Table 4 reports. This value compares to the 98 percent that was achieved using the same catalyst during the July 1995 METC campaign. Examining the data, it was difficult to determine the effect of any of the process variables because of the overwhelming effect of an uncontrolled variable: operating time.

Table 4. Performance of Exposed Catalyst (1995 + 1996 exposure)

Run No.	Space velocity	SO_2 (%)	Conversion to elemental sulfur (%)
5B	4,000	3.5	94.5
6A	2,800	5.4	94.9
6B	2,700	5.4	95.9

Figure 3 shows that, as the trials proceeded, the conversion gradually improved. This suggests that some sort of "induction period," not previously observed with the DSRP, was involved with the doubly exposed DSRP catalyst. It was planned that the coal gas would be relatively particulate-free, and to that end the canister was installed downstream of the desulfurizer at the GE pilot plant. Nevertheless, when the catalyst was received back from GE, it was covered with soot and tar (a possible experimental artifact that is also related to the specifics of the fixed-bed gasifier used at GE). It is possible that the tar has had an effect on conversion, as noted below.

Table 5 reports the results of carbon analysis of the DSRP catalyst. Normally, carbon is not a factor with the DSRP process, as the fresh catalyst and that used at METC are both essentially carbon free. However, the catalyst exposed at METC had over 30 wt% carbon clinging to the pellets, and even after testing in the reactor in the RTI lab it still had nearly 6 percent carbon. The carbon presence is believed to be the reason for the conversion shortfall experienced by the doubly exposed catalyst. It is interesting to note that even with 5.7 percent carbon contamination, the DSRP performance is nearly as good as that obtained with fresh catalyst.

A major goal of the long duration testing of the DSRP is to determine if the presence of trace contaminants (principally volatile heavy metals) affects performance over time. Table 6 reports the results of sampling of the METC coal gas for trace metals. It is apparent that the heavy metals of concern — As, Hg, Pb and Se — are present, although at low levels, in the coal gas

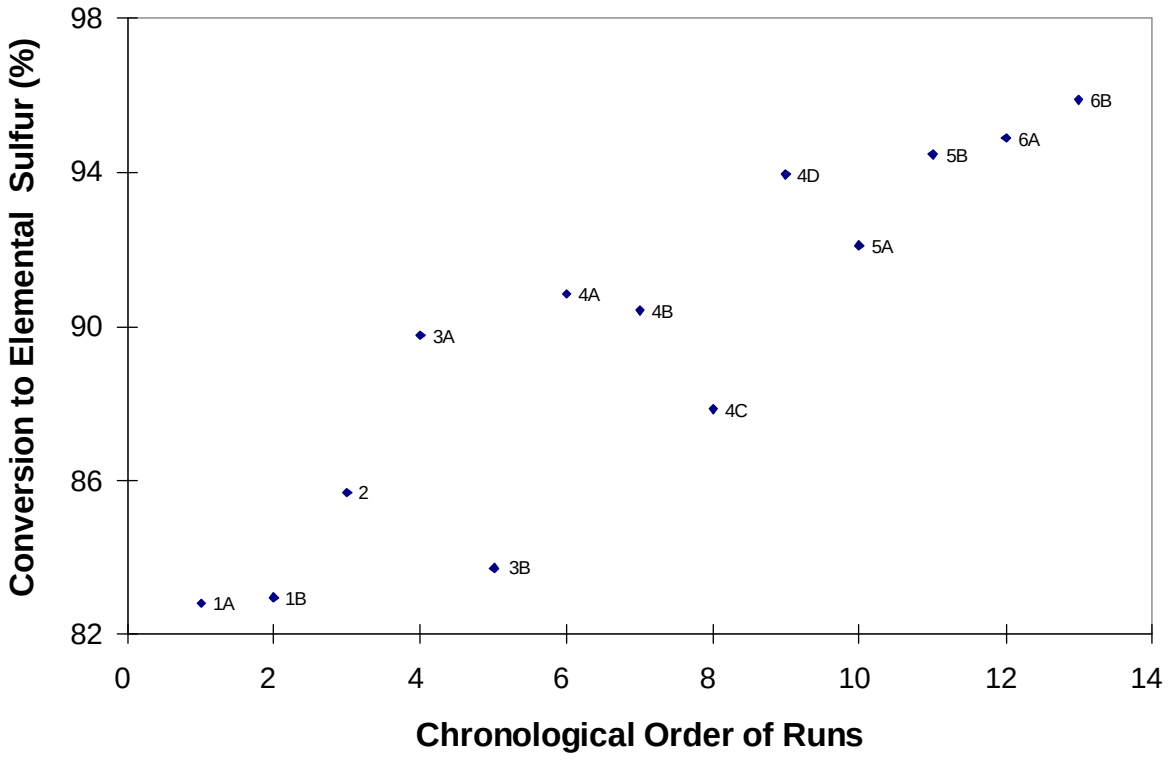

Figure 3. Conversion Improvement with Operating Time.

Table 5. Results of Carbon Testing

	Percent
Fresh DSRP catalyst	0.036
After 160+ h at METC	0.037
After 200 additional h at GE	31.32
After testing in RTI bench unit	5.70

Table 6. Trace Metal Content of METC Coal Gas (1995 Test)

Trace Metal	Concentration (μg/L)
As	0.0015
Hg	0.0075
Pb	0.0075
Se	0.0015

being fed to the DSRP. The fact that performance of the process did not seem to deteriorate with 160 h of exposure at METC suggests that trace metals are not a factor. However, some additional analysis was undertaken to determine if the DSRP catalysts act to sequester trace contaminants.

Table 7 reports the results of the analysis of the DSRP catalyst; this analysis is ongoing. No sequestering of mercury was detected. The arsenic and selenium analyses were confounded by the background signals from the matrix of the catalyst components — and require additional analytical work. Lead was not found after exposure at METC, but an appreciable amount was found after the GE exposure.

Applications/Benefits

The results of the development work conducted on this project show that, after a significant exposure time to actual coal gas, the DSRP catalyst continues to function in a highly efficient manner to convert SO_2 in a simulated regeneration off-gas to elemental sulfur. This

Table 7. Results of Trace Metal Testing

	Concentration on Catalyst (μg/g)			
	Fresh	After 160 h @ METC	After 200 h additional @ GE	After testing in DSRP
As	Additional analysis required			
Hg	<0.005	<0.005	<0.005	<0.005
Pb	2.5	3.0	167	144
Se	Additional testing required			

demonstration of a rugged, single-stage catalytic process resulted in additional on-line experience and the assembling of more process engineering data. The development of the DSRP continues to look favorable as a feasible commercial process for the production of elemental sulfur from hot gas desulfurizer regeneration off-gas.

Future Activities

The future work on this project will consist of completion of the third objective, design and fabrication of a six-fold larger DSRP test unit, to make it available for slipstream testing on a larger pilot gasifier or commercialized desulfurizer. Discussions about such a future test are under way.

Acknowledgments

RTI gratefully acknowledges the assistance and guidance of the current and former METC contracting officer's representatives on this project — Mr. Daniel C. Cicero and Mr. Thomas P. Dorchak. RTI also wishes to thank the METC in-house staff for their enthusiastic support during the slipstream test campaign, and GE Corporate Research and Development, Schenectady, New York, for conducting the operations to expose the DSRP catalyst to the pilot plant coal gas. The period of performance is July 1993 to September 1996.

References

Portzer, J.W., and S.K. Gangwal. 1994. "Slipstream Testing of the Direct Sulfur Recovery Process." in *Proceedings of the Coal-Fired Power System 94—Advances in IGCC and PFBC Review Meeting*, 246-255. DOE/METC-94/1008, Vol. 1. NTIS/DE94012252. Springfield, VA: National Technical Information Service.

Portzer, J.W., and S.K. Gangwal. 1995. "Slipstream Testing of Hot-Gas Desulfurization with Sulfur Recovery." In *Proceedings of the Advanced Coal-Fired Power Systems '95 Review Meeting*, 220-228. DOE/METC-95/1018, Vol. 1. NTIS/DE95009732. Springfield, VA: National Technical Information Service.

Dorchak, T.P., S.K. Gangwal, and W.J. McMichael. 1991. "The Direct Sulfur Recovery Process." *Environmental Progress* 10(2):68.

Testing and Analysis of METC10 Sorbent

Ranjani V. Siriwardane Ph.D.
(RSiriw@METC.DOE.GOV; 304-285-4513)

Morgantown Energy Technology Center

ABSTRACT:

Development of a suitable regenerable sorbent is a major barrier issue in the Hot Gas Cleanup program for Integrated Gasification Combined Cycle systems. This has been a challenging problem for the last 20 years. Many of the sorbents developed in prior work did not retain their reactivity and physical integrity during repeated sulfidation/regeneration cycles. This paper is a report on a promising sorbent (METC10) developed at the Morgantown Energy Technology Center (METC) which has demonstrated sustained reactivity and physical integrity during repeated sulfidation and regeneration cycles.

METC10 sorbent was tested in a low pressure (260 kPa/23 psig) fixed-bed reactor at 538^{0}C (1,000^{0}F) with simulated air blown Kellogg Rust Westinghouse (KRW) coal gas. The sorbent was subjected to 3.5 sulfidation/regeneration cycles using steam as the regeneration diluent. There were no appreciable changes in reactivity during the 3.5 cycles and spalling or other physical deterioration was not observed.

Sorbent pellets, which were prepared by a commercial vendor (United Catalysts, Inc.) to METC specifications, were exposed to fifty sulfidation/regeneration cycles using conditions typical of the Tampa Electric Company (TECO) Clean Coal Technology (CCT) demonstration project. After the fiftieth sulfidation cycle, both the sulfur loading value (more than 6 lb/ft^3) and the attrition (less than 5 wt%) satisfied the requirements necessary for the TECO/CCT project. These sorbent pellets were also tested with real coal gas for 240 hours in a moving bed reactor at General Electric (GE) company. Sulfur absorption was according to the sorbent movement rate and the attrition rate was very low during 240 hours of the pilot plant operation.

INTRODUCTION

The U.S. Department of Energy (DOE) has funded research, development, and demonstration (RD&D) projects for many years in the field of advanced power generation. The Integrated Gasification Combined Cycle (IGCC) system is one of the most promising advanced power systems. It has been predicted that IGCC systems with hot gas cleanup will offer significant improvements in environmental performance and overall plant efficiency, compared to conventional pulverized coal-fired plants which have efficiencies of 33 to 35 percent. It is expected that IGCC with hot gas cleanup will achieve efficiencies of 52 percent by the year 2010 and will be capable of producing power at a 20 percent lower cost of electricity when compared to conventional coal based systems. Furthermore, this increase in efficiency will reduce CO_2 emissions by 35 percent.

Development of a suitable regenerable sorbent is a major barrier issue in the hot gas cleanup program for IGCC systems. This has been a challenging problem during the last twenty years (Lew et al.,1989, Woods et al., 1989). Various formulations of zinc ferrite and zinc titanate in the form of extrudates and spherical pellets have been studied at METC for removal of sulfurous gases from coal gasification streams (Mei et al., 1993, Siriwardane et al., 1994). Problems of decrepitation and spalling have occurred after sulfidation and regeneration of these sorbents. A series of novel sorbents containing zinc oxide have been developed at METC to address these problems. These METC-developed sorbents showed superior performance during both twenty-cycle high pressure fixed-bed tests with steam regeneration and a fifty-cycle high pressure fixed-bed test with dry regeneration conducted at the METC. One of the METC developed sorbents (METC10) was tested in the moving bed reactor at the General Electric pilot plant. The results of the sorbent testing, in both the bench scale reactors and the GE moving bed reactor, and sorbent analysis data are discussed in this paper.

OBJECTIVES

The overall objective of this project was to develop regenerable sorbents for hot gas desulfurization in IGCC systems. The major criteria for the development of novel sorbents included reasonable chemical reactivity and physical durability during repeated sulfidation/regeneration cycles. The sorbent should be able to withstand reducing gas atmospheres at elevated temperatures and pressures during sulfidation. During regeneration, the sorbent should be able to withstand steam which is added to regeneration air to maintain temperature control.

A series of METC sorbents were prepared and tested. Sorbents METC2, METC9, and METC10 have been tested both in the low pressure and the high pressure reactors with steam regeneration (Siriwardane et al., 1994). Sorbent pellets of

METC10, prepared by a commercial vendor to METC specifications, were tested under conditions typical of UCI the TECO/CCT demonstration project.

Results of the both low pressure and high pressure fixed-bed reactor testing of METC10 will be discussed in this paper. Fifty cycles of sulfidation reactions were completed for commercially (UCI) prepared METC10 under conditions typical of the TECO/CCT demonstration project. METC10 was also tested in the moving bed reactor at the GE pilot plant.

EXPERIMENTAL

METC10 sorbent was prepared at METC by a solid state mixing method (physical mixing of sorbent constituents with water) utilizing a mixer pelletizer. The sorbents contained about 50 wt% of zinc oxide. The solid materials were thoroughly mixed in the mixer pelletizer and a sufficient amount of water was added to the mixture to form pellets. Sorbent pellets in the size ranges of both -5+8 mesh and -4+5 mesh were utilized for low pressure reactor testing.

All of the sulfidations in the low pressure reactor were performed at 538 °C (1000 °F) and 260 kPa (38 psia), utilizing a feed gas containing 2000 ppmv H_2S. The superficial velocity for all sulfidations in the low pressure reactor was maintained at 0.09 m/s (0.30 ft/s) and the space velocity was 2000 h^{-1}. The outlet H_2S concentration was monitored using detector tubes and gas chromatography. All regenerations in the low pressure reactor were done at 272 kPa (39.7 psia) and the gas velocity was maintained constant during each stage at 0.04 - 0.05 m/s (0.13 - 0.15 ft/s) . The steam regenerations were conducted in three stages. The temperatures of the stages were 538, 593, and 649 °C (1000, 1100, and 1200 °F). The steam concentration in all three stages was 50% wt, with a varying concentration of oxygen and nitrogen. The oxygen concentrations during the three stages were 1.0, 2.5, and 3.5 %, respectively.

METC10 (3 mm pellets) prepared by a commercial vendor, UCI, was also tested in the high pressure reactor which contained a 5.5 cm (2.2-inch) inside diameter reactor. The reactor was constructed of Incoloy 800HT alloy steel pipe. A gas distributor was fixed at the bottom of the cage to support the sorbent. The inside of the sorbent cage was Alon-processed to prevent corrosion of stainless steel by sulfurous gases in the presence of steam. The reactor was housed inside a three-zone furnace equipped with separate temperature controllers for each zone. The details of this system are reported by Mei et al., 1993. The reactor bed height was 15 cm (6 in), the pressure was 2,026.5 kPa (293.2 psia), and the temperature of the bed was 482^{0}C (900^{0}F). The gas composition utilized during the sulfidation was 20,000 ppmv H_2S, 18 percent nitrogen, 20 percent steam, 10 percent carbon dioxide, 30 percent carbon monoxide, and

20 percent hydrogen which simulated the TECO coal gas. Regeneration was performed with 2 percent oxygen and nitrogen at 594^0 to 705^{0}C (1,100^0 to 1,300^{0}F). After the regeneration with air, 100 percent nitrogen was introduced at 732^{0}C (1,350^{0}F). The pressure during the regeneration was 793 kPa (102.8 psia). Both sulfidation and regeneration were performed in the upflow direction, and the space velocities during the sulfidation and regeneration were 2000 hr^{-1}.

METC10 was tested in the moving bed reactor at the GE pilot plant. Sorbent movement rate was between 400 - 600 lbs/hr. Typical coal gas composition in the GE gasifier was 10% nitrogen, 16% steam, 13.7% CO_2, 30.1% CO, 30% H_2, and 0.25-0.40 % H_2S. Absorber in the moving bed reactor was at a temperature of 482 ^{0}C (900^{0}F) and a pressure of 2,026.5 kPa (293.2 psia). Coal gas was introduced at the bottom of the absorber and the outlet H_2S was monitored at both the top of the reactor bed and a location one third below the top of the reactor bed in the absorber. Air, recycled SO_2, and H_2O were present in the regeneration gas stream.

RESULTS

Results of the METC10 Testing in the Low Pressure Unit

The sulfidation breakthrough curves of METC10 in the low pressure unit are shown in Figure 1. There was an increase in sulfur capacity from sulfidation 1 to 2, but the sulfur capacity decreased in the third sulfidation. The sulfidation breakthrough curves overlapped after the third sulfidation, indicating sorbent stabilization at that point. As shown in Figure 1, the outlet hydrogen sulfide concentration was zero for about twenty-eight hours indicating that the efficiency of the sorbent was excellent. It is clear that the sulfur capacity of METC10 is excellent, and regeneration can be performed utilizing steam.

Results of the Commercially Prepared METC10 Testing in the High Pressure Unit

Results of the two and half cycle test of METC10 is shown in Figure 2. During the first sulfidation cycle, the breakthrough time (200 ppmv outlet H2S) was 1 hour and 15 minutes and it increased to 4 hours at the third sulfidation as shown in Figure 2. The solid analysis of the sorbent indicated 18-19 weight percent sulfur per 100g of the fresh sorbent after the third sulfidation cycle. The packing density of the fresh sorbent was 106 lb/ft^3 (in the 2"x6" bed). The required sulfur loading is about 6 weight percent for the TECO/CCT demonstration project. Thus, the sulfur absorption capacity of METC10 far exceeds the required sulfur loading.

The results of the fifty-cycle testing of METC10 are shown in Table 1. The sulfur loading value measured by the LECO sulfur analyzer at the gas inlet location after the fiftieth sulfidation cycle was more than the required sulfur loading of 6 weight percent. The crush strength of the sorbent was higher than that of the fresh sample. Scanning electron photomicrographs of the sorbent, after the fifty-cycle testing, indicated that there was no cracking or spalling of the pellets. The attrition loss (ASTM D 4058-92) was less than the value of 5 percent required for the moving bed operation TECO/CCT demonstration project. The commercial METC10 showed a superior level of performance during the fifty-cycle testing and met all the criteria as a possible sorbent for the Tampa Electric CCT project.

TABLE 1

Characteristics of the Fresh and Sulfided METC10

Measurement	Fresh	Third Sulfidation	Twentieth Sulfidation	Fiftieth Sulfidation
1. Crush Strength	31 N	71 N	85 N	80 N
2. Sulfur loading at the gas inlet	----	18 wt%	18 wt%	14 wt%
3. Attrition	<1%	1.5%	3.5%	4.5%

Results of the Testing of METC10 in the Moving Bed Reactor at the GE Pilot Plant

The attrition loss of the sorbent after 240 hours of moving bed reactor operation at GE was 0.45%, and this indicated that the attrition resistance of the sorbent was excellent. During the moving bed testing at GE, the outlet H_2S (at the top of the absorber) was maintained at 100 ppm when proper oxygen concentrations and temperatures were utilized during the regeneration. The H_2S outlet concentration detected at a location one third below the top of the sorbent bed in the absorber was below 50 ppm. Thus, the 100 ppm H_2S detected at the top of the reactor bed in the absorber was mainly due to the decomposition of residual sulfate formed during the regeneration. Solid analysis of the sorbent from the absorber indicated that the sulfur absorption was in agreement with the sorbent movement rate. After 168 hours of operation the temperatures in the regenerator dropped below 538 C^0 (1000 F^0) due to mechanical problems and proper regeneration could not be achieved. The sorbent pellets collected at various times during the moving bed operation were analyzed for reactivity utilizing both the bench scale reactor and the thermogravimetric analyzer (TGA). Mercury

pore volume analysis and atomic absorption analysis were also conducted to determine the changes in the pore structure and the elemental composition of these sorbent pellets. Both bench scale reactor studies and the TGA reactivity studies indicated that there was sufficient reactivity in the sorbent pellets collected after 240 hours of moving bed operation. Elemental analysis indicated that there was a minimal loss of some elements in the sorbent pellets. The concentration of the HCl released during the first 72 hours of moving bed operation was in the range of 50-250 ppm. The elemental loss in the sorbent pellets occurred during that time period. Analysis of pore volume and average pore diameter indicated that the pore structure of the sorbent pellets collected after 240 hours of moving bed operation was similar to that of the activated METC10 sorbent pellets.

CONCLUSIONS

METC10 sorbent showed a superior level of performance during 3.5 cycles of low pressure fixed bed testing. The METC10 sorbent also performed extremely well during the high pressure fifty-cycle fixed bed reactor test. This sorbent functioned well in the reducing gas environment at high temperatures which will be present in the coal gasification process. This sorbent was prepared with readily available materials utilizing solid state mixing which is very inexpensive.

Steam regeneration did not adversely affect the performance of METC10 during the 3.5 cycles of low pressure testing. Crush strengths of the sorbents after the fourth sulfidation cycle were greater than those of the original sorbents. This sorbent was spalling resistant and had excellent chemical and physical durability during the three and half cycle test. Overall performance of these sorbents were superior to other zinc-based sorbents tested previously at METC.

Commercially prepared METC10 sorbent performed well during the fifty-cycle high pressure testing under conditions suitable for the TECO/CCT demonstration project. During the fifty-cycle test, this sorbent retained sufficient reactivity, and physical durability (as measured by crush strength and attrition resistance) was also excellent.

METC10 sorbent performed well during the GE moving bed operation when proper temperatures and oxygen concentrations were utilized during the regeneration. Sufficient reactivity was retained in the sorbent pellets after 240 hours of operation of the moving bed reactor. Attrition loss, after 240 hours of moving bed operation, was 0.45% and this indicated that the attrition resistance of the sorbent was excellent.

REFERENCES

Lew, S.; Jothimurugesan, K.; Flytzani-Stephanopoulos, M. "High Temperature Regenerative H_2S Removal from Fuel Gases by Regenerable Zinc Oxide - Titanium Dioxide Sorbents" Ind. Eng. Chem. Res. 1989, 28, 535-541.

Mei, J.S.; Gasper-Galvin, L.D.; Everitt, C.E.; and Katta, S. "Fixed Bed Testing of a Molybdenum-Promoted Zinc Titanate Sorbent for Hot Gas Desulfurization" DOE Contractors Review Meeting, Morgantown, WV, June 1993

Siriwardane, R.V.; Grimm, U.; Poston, J.; Monaco, S.J. "Fixed Bed Testing of Durable, Steam Resistant Zinc Oxide Containing Sorbents" AIChE Annual Meeting, San Francisco, California, 1994, Symposium on Gas Purification, Paper No. 247g

Siriwardane, R.V.; Poston, J.A.; Evans Jr, G. "Spectroscopic Characterization of Molybdenum-Containing Zinc Titanate Desulfurization Sorbents" Industrial and Engineering Chemistry Research, Vol.33, No.11, 1994

Woods, M.C.; Leese, K.E.; Gangwal, S.K.; Harrison, D.P.; Jothimurugesan, K.; "Reaction Kinetics and Simulation Models for Novel High-Temperature Desulfurization Sorbents" Final Report, DE-AC21-87MC24160, DOE/METC, WV, February, 1989.

Advanced Hot-Gas Desulfurization Sorbents

Kandaswamy Jothimurugesan (jothi@et.hamptonu.edu; 804-727-5817)
Adeyinka A. Adeyiga (yinka@et.hamptonu.edu; 804-727-5288)
Department of Chemical Engineering
Hampton University, Hampton, VA 23668.

Santosh K. Gangwal (skg@rti.org; 919-541-8033)
Research Triangle Institute
3040 Cornwallis Road
Research Triangle Park, NC 27709.

Introduction

Advanced high-efficiency integrated gasification combined cycle (IGCC) power systems are being developed to produce power from coal under the U.S. Department of Energy's (DOE's) multibillion dollar Clean Coal Technology (CCT) Program (Gangwal et al., 1993). In these advanced systems, coal is gasified to produce a gas at high-temperature and high-pressure (HTHP) conditions. The hot gas is cleaned of contaminants, primarily particulates and sulfur gases such as hydrogen sulfide (H_2S) and burned in a combustion turbine. IGCC systems are capable of lower gaseous, liquid, and solid discharges than conventional pulverized-coal-fired power plants. Hot gas cleanup offers the potential for higher plant thermal efficiencies and lower costs due to the elimination of fuel gas cooling and associated heat exchangers.

Sulfur sorbents based on zinc oxide are currently the leading candidates and are being developed for moving- and fludized-bed reactor applications. Zinc oxide sorbents can effectively reduce the H_2S in coal gas to around 10 ppmv and can be regenerated for multicycle operation. However, all of the current first-generation leading sorbents undergo significant loss of reactivity with cycling, as much as 50% or greater loss in only 25 to 50 cycles. Stability of the hot-gas desulfurization step over hundreds of cycles is essential for improved IGCC economics over conventional power plants.

Most hot-gas desulfurization sorbents in the past have been developed for hot-gas cleanup at temperatures greater than 538 °C (1,000 °F). Recent economic evaluations (NOVEM, 1991; Leininger et al., 1992; Rutkowski et al., 1993) have indicated that the thermal efficiency of IGCC systems increases rapidly with the temperature of hot-gas cleanup up to 350 °C and then very slowly as the temperature is increased further. This suggests that the temperature severity of the hot-gas cleanup devices can be reduced without significant loss of thermal efficiency. For this reason, this project aims to develop hot-gas cleanup sorbents for relatively low-temperature applications, 343 to 538 °C, with emphasis on the temperature range from 400 to 500 °C.

Research sponsored by the U.S. Department of Energy's Morgantown Energy Technology Center, under contact DE-FG21-94MC31393 with Hampton University, Department of Chemical Engineering, Hampton, VA 23668. Telefax: 804-727-5189.

Objectives

The objective of this project is to develop advanced hot-gas desulfurization sorbents for relatively low-temperature application that show stable and high sulfidation reactivity at 343 to 538 °C.

Approach

A number of zinc-based formulations will be prepared and screened for testing in a fixed-bed reactor at high pressure (1 to 20 atm) and high temperatures using simulated coal-derived fuel gases. One of the superior formulations will be tested for long-term durability and chemical reactivity in the reactor. To prevent sulfation, catalyst additives will be investigated, which would promote a lower regeneration temperature.

Project Description

Sorbent Preparation

A highly promising method was recently developed under this project in coopearation with a commercial sorbent manufacturer for preparing suitable sorbents. Various sorbents were prepared using this proprietary technique. The role of the commercial manufacturer was to ensure scalability of the manufacturing process and to keep the cost competitive. The following analytical techniques were used to characterize the fresh, sulfided, and regenerated sorbents: (1) X-ray Diffraction (XRD) for the crystalline phase; (2) the standard BET method for surface area measurement; (3) Hg-porosimetry for determination of pore volume, bulk density, average pore diameter, and pore size distribution; and (4) Atomic Absorption (AA) Spectrometry for elemental composition analysis.

Experimental Setup

The materials prepared were tested in a laboratory-scale, high-pressure and high-temperature fixed-bed reactor. Briefly, the experimental setup consisted of a gas delivery system, a fixed-bed reactor, and a gas analysis system. In the gas delivery system, a simulated fuel gas of any desired composition could be generated using bottled gases, a set of mass flow controllers, and high-pressure syringe pumps. Steam was added to the mixed dry gas by vaporizing liquid water and injecting it into the gas stream at a controlled rate by a high-pressure syringe pump. The reactor was constructed of stainless steel pipe. Inside the pipe there was a removable 316 stainless steel 1.0 cm I.D. tube with a porous alumina plate in the bottom that acts as a gas distributor. The inside of the pipe was Alon-processed to prevent corrosion of stainless steel by sulfurous gases in the presence of steam. The pressure inside the reactor was controlled by a back pressure regulator and measured by an electronic pressure sensor. The thermocouples were positioned to measure the temperatures of the preheated feed gas, the reactor bed, and the product gas. The tests were conducted with a simulated gas containing 10% H_2, 15% CO, 5 mol% CO_2, 1 mol% H_2S, 15 mol% H_2O, and balance N_2. The outlet H_2S and SO_2 concentrations were monitored using detector tubes and gas chromatography.

A typical run consisted of loading approximately 1 g of the sorbent in a particle size range of -32+ 64 mesh and heating the reactor to a desired temperature of 300 to 500 °C with continuous flow of nitrogen. Once the desired temperature was attained, the flow of fuel gas to the reactor was started and the concentration of H_2S was measured continuously in the effluent gas. When the H_2S concentration in the effluent gas reached 300 ppmv, indicating breakthrough, the sulfidation was stopped and the system was prepared for regeneration. The regeneration of sulfided material was carried out at the desired temperature ranging between 400 and 650 °C with 2 to 4% oxygen in nitrogen. In all runs, the space velocity used was in the range of 2,000 to 3,000 h^{-1}. The regeneration of the sulfided material was carried out until the SO_2 concentration in the reactor effluent chopped below 50 ppmv. These sulfidation-regeneration cycles were repeated as many times as desired. Typically each material was tested for 5 to 10 cycles to obtain meaningful data on material durability. At the end of a 5- to 10-cycle run, the material was removed from the reactor and all physical and chemical characterizations, as listed above, were carried out on the reacted material to determine changes due to the reaction.

Results

The ZnO-based sorbent (MCRH-1) was evaluated in a sulfidation gas mixture containing (in mole%): H_2=10%, CO=15%, CO_2=5%, H_2S=1%, H_2O=15%, and balance N_2. Figure 1 shows the H_2S breakthrough profiles as a function of normalized time. In tests with the MCRH-1 sorbent conducted at 427 °C, the sorbent conversion at breakthrough was 80 percent. In fact, the H_2S

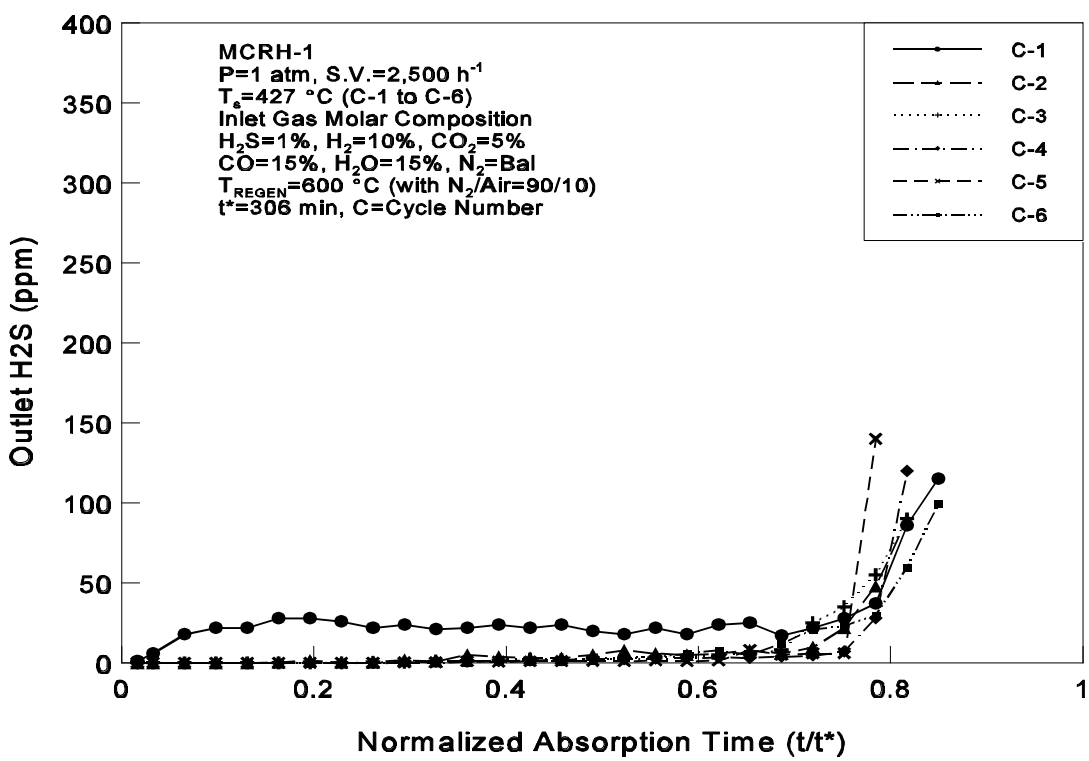

Figure 1. H_2S Breakthrough Curves in Successive Sulfidation Cycles of Sorbent MCRH-1

level remained at 0 ppm until 17 percent sorbent conversion and then gradually increased to ~5 ppm when conversion reached 80%. The sorbent conversions at 343 and 538 °C were 60 and 100%, respectively.

Figure 2 shows the H_2S breakthrough profiles for a another ZnO-based sorbent (MCRH-10) as a function of normalized time. Complete (>95%) sorbent conversion was observed at breakthrough at 800 °F, and the pre-breakthrough H_2S level was below 50 ppm.

Figure 3 shows the breakthrough profiles for a superior zinc-based sorbent (MCRH-25). This sorbent was modified to regenerate at temperataures as low as 475 to 525 °C. It was tested for 100 cycles of sulfidation in the laboratory-scale reactor. Regeneration between cycles was conducted with 10 mol% air-90 mol% with N_2 at 579 °C. However, in independent tests at Research Triangle Insititute, the sorbent was found to be fully regenerable at temperatures as low as 475 °C with 2% O_2. The gas hourly space velocity for the 100-cycle test was about 2,500 h^{-1} (STP) both in sulfidation and in regeneration. Sulfidation tests were carried out with a sulfidation gas containing 10 mol% H_2, 15 mol% CO, 5 mol% CO_2, 1 mol% H_2S, 15 mol% H_2O, and balance N_2. At 427 °C sulfidation, for cycles 1 to 20 the pre-breakthrough conversion was between 80 and 90%. For cycles 21 to 30 the conversion increased from 90 to 100% and remained constant at 100% conversion up to the 100 cycles.

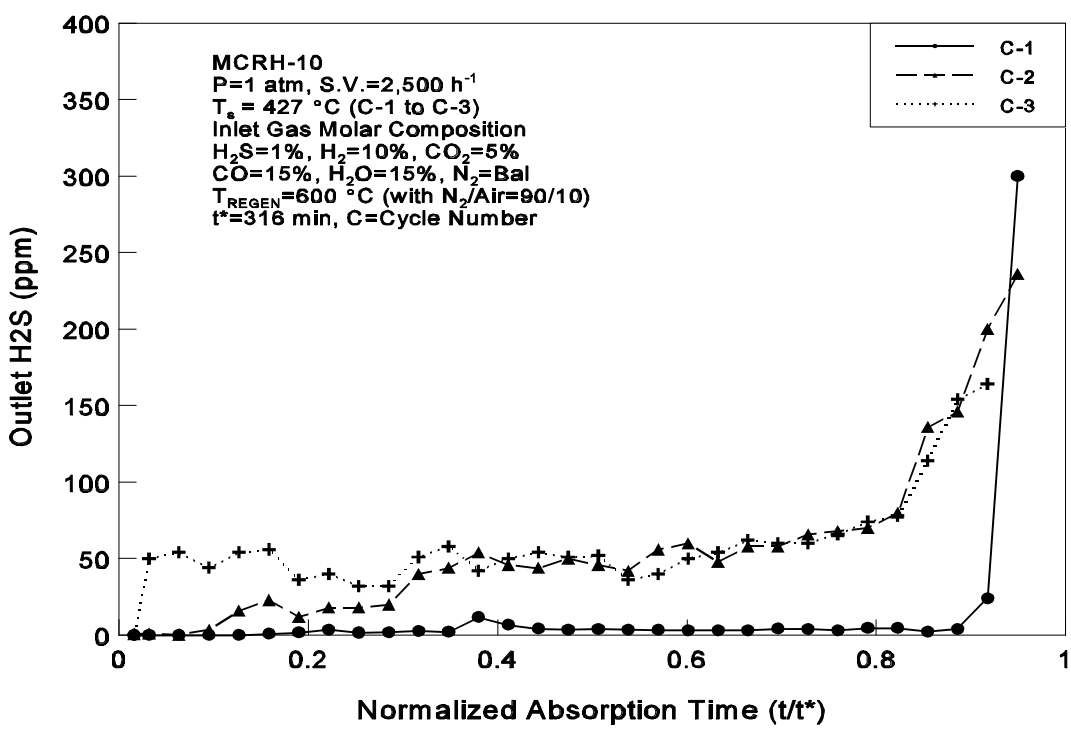

Figure 2. H_2S Breakthrough Curves in Successive Sulfidation Cycles of Sorbent MCRH-10

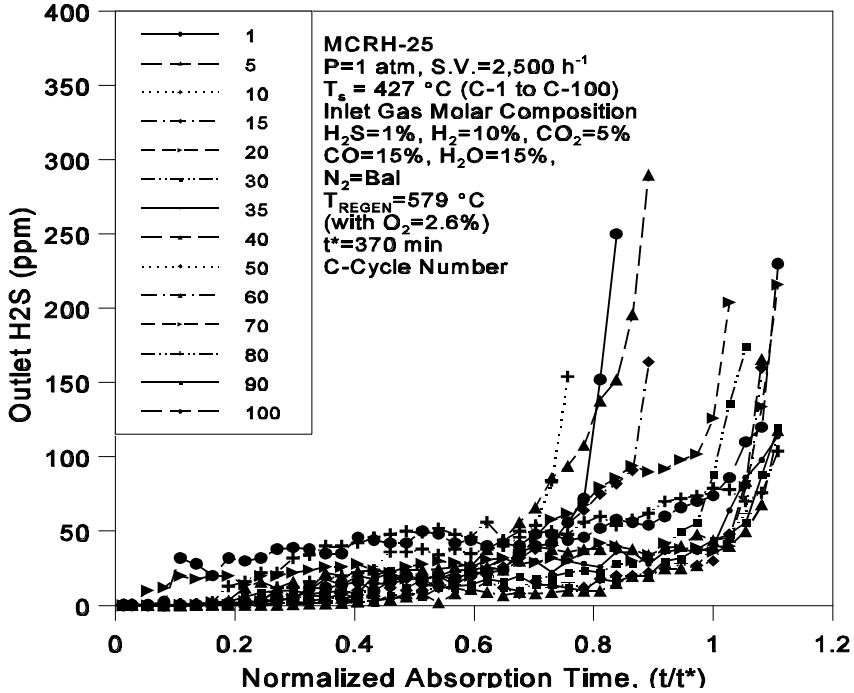

Figure 3. H_2S Breakthrough Curves in Successive Sulfidation Cycles of Sorbent MCRH-25

There was no deactivation in 100 cycles in this fixed-bed study. The sulfur capacities of the MCRH-25 sorbent during cycles 1, 25, 50, 75, and 100 were 22.5, 27.7, 27.7, 27.7, and 27.7 gS/100 g of sorbent, respectively, again indicating a 100 percent capacity utilization even after 100 cycles. Sulfur capacity was calculated using the concentration of hydrogen sulfide in the feed, the breakthrough time, and the amount of sorbent used. The chemical reactivity was measured by using TGA for fresh, and 100-cycle used sorbent. The TGA results indicated that the rate of sulfur pickup for the fresh and the 100-cycle used sorbent remained relatively constant. An interesting observation was that the reactivity of the 100-cycle used sorbent was higher than that of the fresh sorbent in the TGA results. This result agreed with the observed increase in breakthrough time in the 100-cycle fixed-bed study.

Application

The 100-cycle test clearly demonstrated that the MCRH-25 sorbent does not chemically deactivate. This is in contrast to existing leading sorbents such as Z-sorb and ZT-4 that deactiviated significantly, as much as 50% in 50 to 100 cycles. Furethermore, the sorbent regenerated at temperatures as low as 475 °C, in conrast to current zinc-based sorbents taht require 600 °C or higher. As the current scale of tests is with powders only, the sorbent needs to

be made attrition resistant for moving-bed and fluidized-bed reactors. This research is currently ongoing.

Future Activities

The future activity will include development and testing of attrition resistant zinc-oxide-based sorbents for fluidized bed applications suitable for the Sierra-Pacific plant.

Acknowledgments

The authors would like to gratefully acknowledge the guidance and assistance of Dr. Kamalendu Das, the METC Contracting Officer's Representative. Mr. Daniel C. Cicero of METC provided significant suggestions leading to investigation of methods to reduce the regenration temperatures. Research Triangle Institute provided subcontract support to the project. The period of performance is from September 30, 1994 to August 29, 1997.

References

Gangwal, S.K., R. Gupta, and W. J. McMichael, "Sulfur Control Options For IGCC Systems," Proceedings of UNDEERC Low-Rank Fuels Symposium, St.Louis, MO, 1993.

Leininger, T., et al., "Integration and Testing of Hot Desulfurization and Entrained Flow Gasification for Power Generation Systems," Proceedings of the 12th Annual Gasification and Gas Stream Cleanup Contractor's Review Meeting, Vol.1, DE93000228, p. 95, 1992.

NOVEM. System Study high temperature gas cleaning at IGCC systems. Netherlands Agency for Energy and the Environment, 1991.

Rutkowski,M., et al., "IGCC Database and Hot Gas Cleanup Systems Studies," Proceedings of the Coal-Fired Power Systems 93-Advances in IGCC and PFBC Review Meeting, DOE/METC-93/6131(DE93000289), p. 359, 1993.

Advanced Low-Temperature Fluid Bed Sorbents

Javad Abbasian (abbasian@igt.erg; 847-768-0611)
Rachid B. Slimane (slimane@igt.erg; 847-768-0606)
James R. Wangerow (wangerow@igt.erg; 847-768-0610)
Institute of Gas Technology
1700 S. Mt. Prospect Rd.
Des Plaines, IL 60018

Abstract

The Integrated Gasification Combined Cycle (IGCC) process is emerging as the most promising technology for advanced electric power generation from coal that is likely to replace conventional coal combustion. The commercialization of this technology and realization of its full potential, however, depend to a great extent on the development of regenerable sorbents capable of reducing the H_2S content of gasifier fuel gas from several thousand ppmv levels down to a few ppmv at elevated temperatures (i.e., >3500C), over hundreds or even thousands of sulfidation/regeneration cycles.

Over the last two decades, development of high temperature regenerable desulfurization sorbents has been pursued, primarily using various combinations of transition metal oxides. The primary focus has been directed toward application above 550°C, limiting the choice of metal oxides to those which possess favorable thermodynamic equilibria. These efforts led to the emergence of zinc-based sorbents, such as zinc titanates, as the leading candidates. However, because of problems with sorbent deterioration, further improvement is needed to minimize the overall cost of desulfurization in the IGCC process.

Recent studies on total IGCC system integration have indicated that system components become prohibitively expensive with increasing operating temperature and that the overall process efficiency gains of conducting desulfurization at above 550°C may not be sufficient to justify operation at such high temperatures. The optimum desulfurization temperature appears to be in the range of 350 °-550°C, where technical viability and process efficiency result in lower overall process costs. In addition, because of the more favorable thermodynamic equilibria at the lower temperature range, a large number of metal oxides can be considered for coal gas desulfurization, increasing the likelihood of developing suitable sorbents.

Research sponsored by U.S. Department of Energy, under contractDE-AC21-94MC3 1089 "Advanced Sorbent Development Program ."

The three most advanced reactor configurations for hot gas desulfurization include fixed-bed, moving-bed, and fluidized-bed systems. The fluidized-bed approach offers advantages over the moving-bed and fixed-bed reactors because of its ability to control temperature particularly during the highl y exothermic regeneration step; however, a more durable, attrition-resistant sorbent is required.

This paper discusses the results obtained in an ongoing study geared towards developing advanced mixed-metal oxide sorbents for desulfurization of coal-derived fuel gases in the temperature range of 350° to 550°C. The paper focuses on the study related to the development of durable sorbents suitable for fluidized-bed application and addresses thermodynamic considerations, sulfidation kinetics, regenerability, and the physical and chemical characteristics of a number of novel sorbents.

Acknowledgments

The authors would like to express their appreciation to the Department of Energy, Morgantown Energy Technology Center and General Electric Corporate Research and Development for financial support under Contract DE-AC21-94MC3 1089 "Advanced Sorbent Development Program." The period of performance for this project is from September 30, 1994 to February 27, 1997. The authors would also like to thank METC Project Manager, Mr. Daniel C. Cicero, for providing technical support and guidance during the course of this project

4A.3 Advanced Low-Temperature Fluid Bed Sorbents

Javad Abbasian
Rachid B. Slimane
James R. Wangerow

Institute of Gas Technology
Des **Plaines,** Illinois

Overall Objective

Develop **regenerable sorbents** for removal of hydrogen sulfide from **coal-**derived fuel gases in **fluidized** bed reactor in the temperature range of **343-538°C (650-1000 "F)**

Why Lower Temperature?

- Alkali condensation and removal
- More favorable H_2S Equilibria
- Greater number of suitable metal oxides
- Lower stress on sorbent
- Higher sorbent stability in long run
- Less expensive system components

Specific Objectives

- Selection of potential candidate sorbents
- Screening of potential candidate sorbents
- Laboratory evaluation of selected sorbents
- Bench scale testing of superior sorbent formulations
- Development of cost assessment/Market Plan
- Long-term testing of most promising sorbent

Thermodynamic Calculations

- H_2S equilibria calculations
  - Pure metal oxides
  - Sorbent/H_2S =2
  - 350-5500C, 20 bar
  - Texaco & U-Gas

- Phase stability diagrams

SULFIDATION FEED GAS COMPOSITION

Component	Mel%
H_2S	0.5-2
H_2	10
CO	20
CO_2	10
H_2O	10
N_2	48.49.5

METAL OXIDE SCREENING

Function	Metals Chosen
Primary Desulfurization	Cu, Fe, Zn, Mn, Ce
Secondary Additives	Cu, Fe, Mn, Cr, Ce, Co, Mo
Support/Stabilizers	TiO_2, ZrO_2, Al_2O_3, Binders

H_2S Equilibrium Concentration: U-GAS

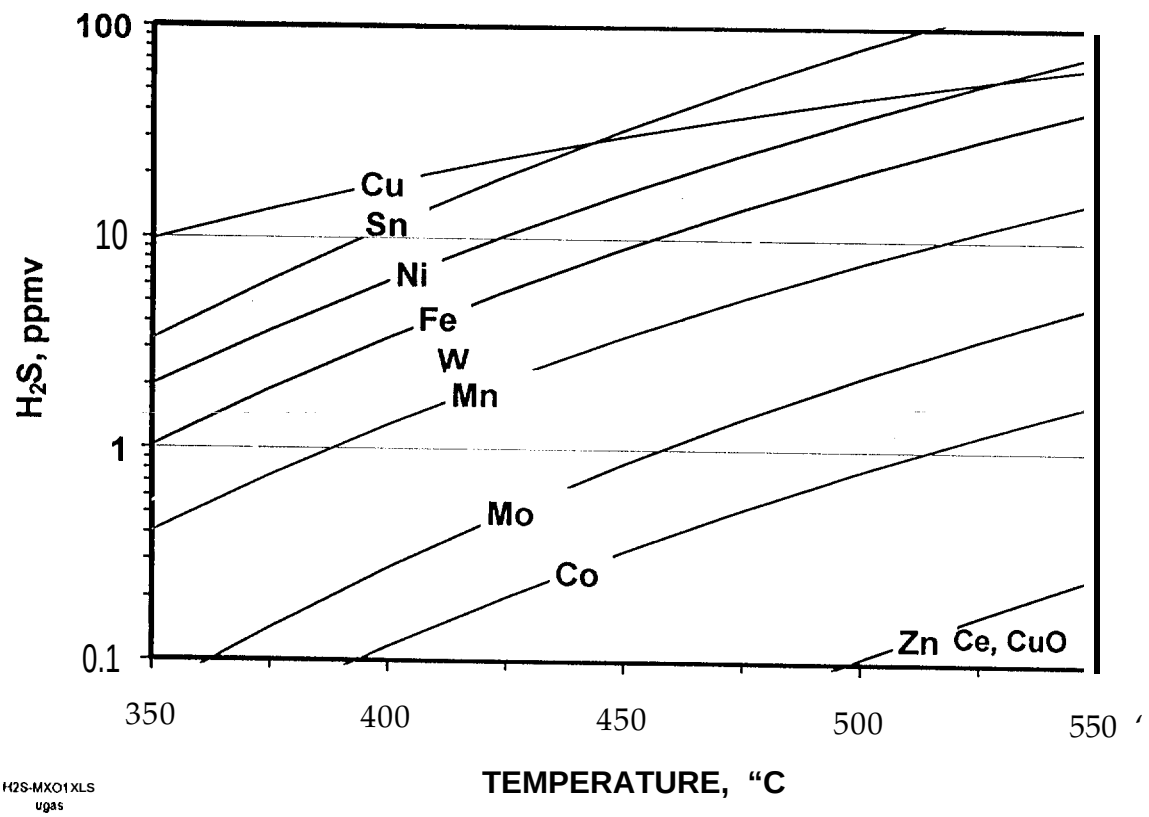

H2S-MXO1XLS
ugas

H_2S Equilibrium Concentration: TEXACO

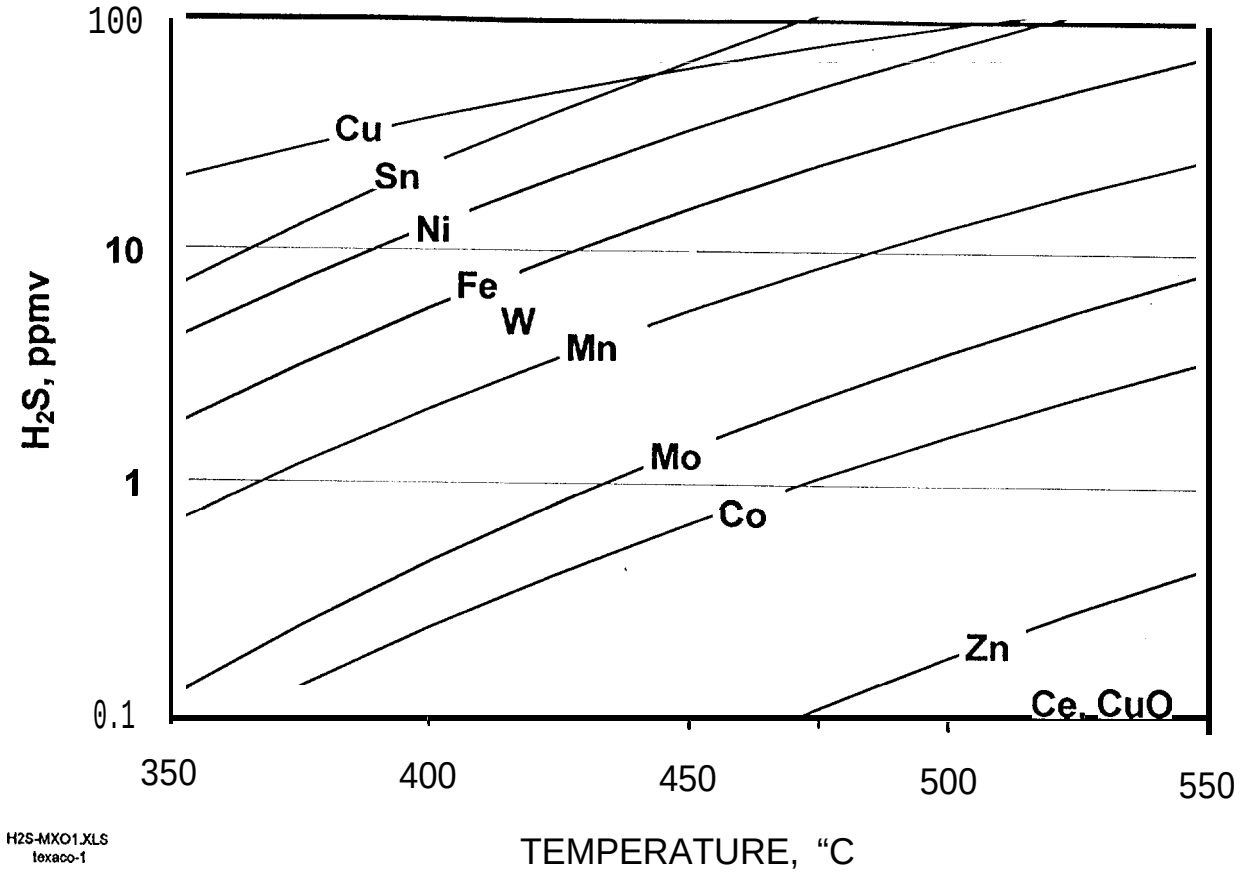

Comparison of effective conversion

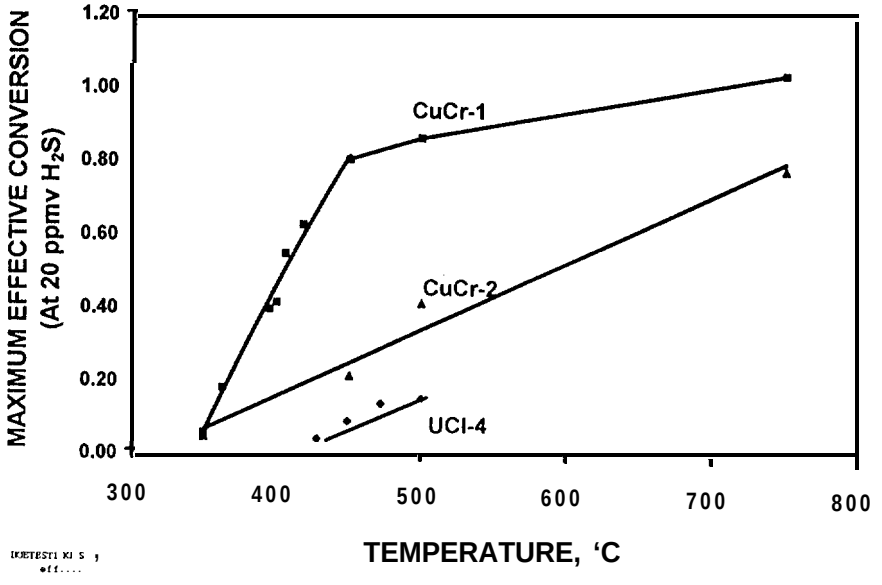

Comparison of Sulfur Loading

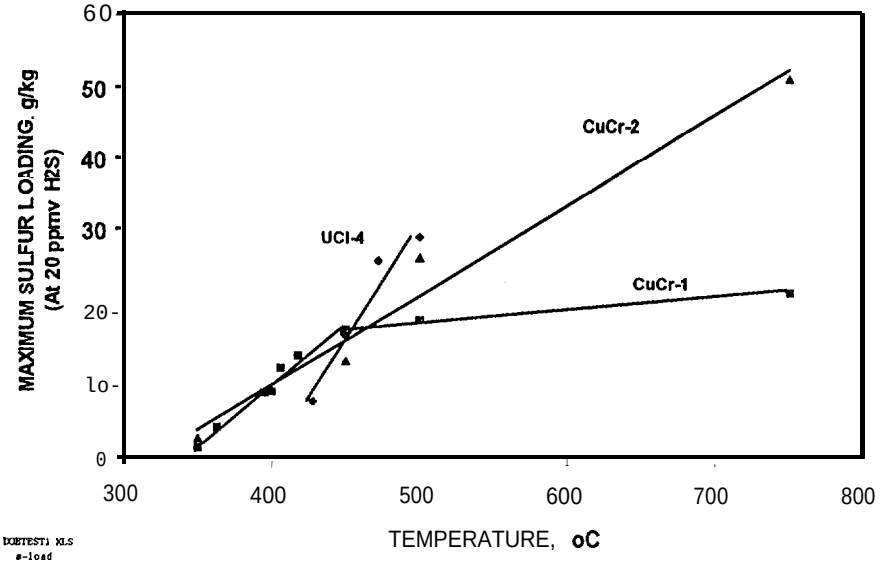

Sorbent Performance at different Space Velocity

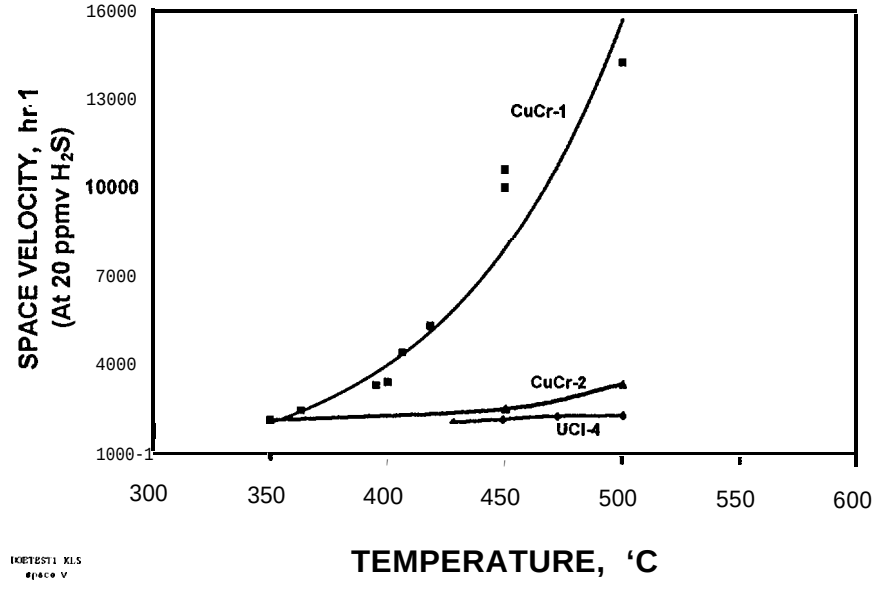

Performance of CuCr-1 at Different

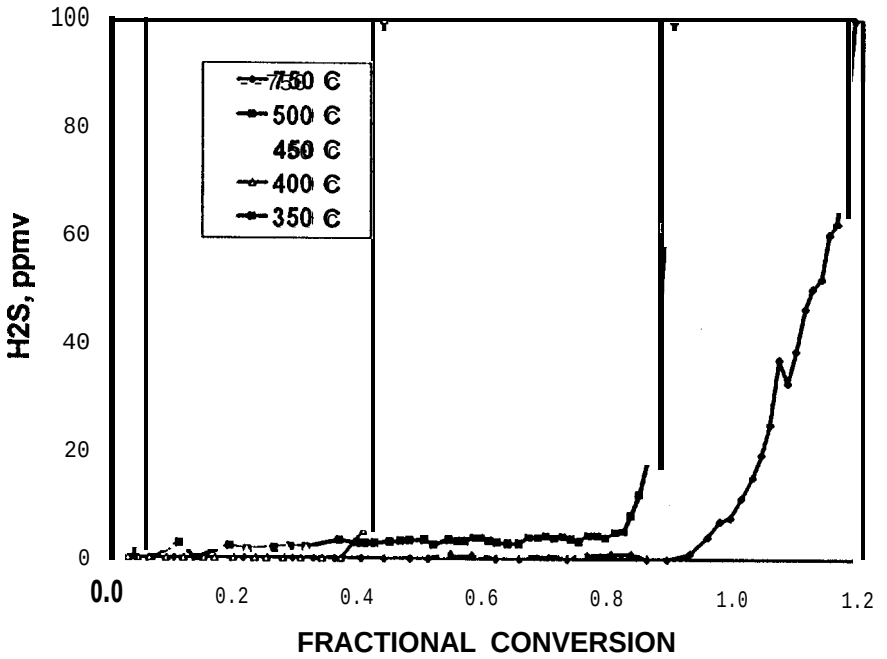

DOETEST1 XLS

Performance of Zinc Titanate at Different Temperatures

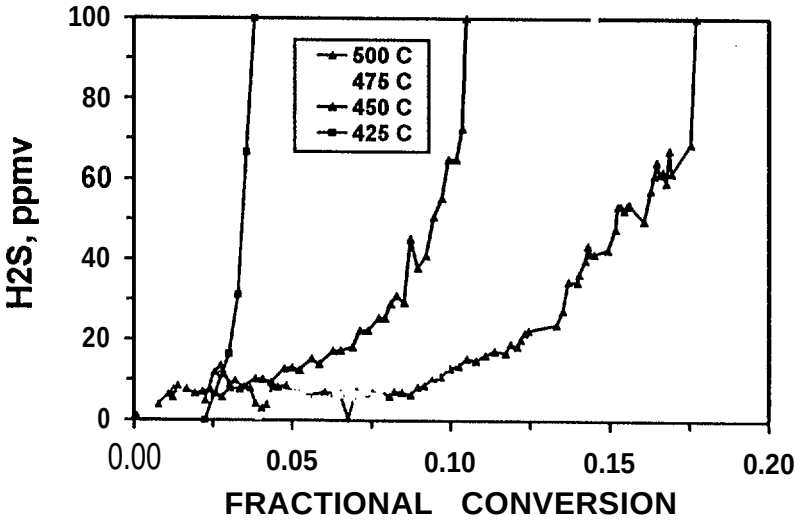

Performance of IGTSS-1 at 350“C

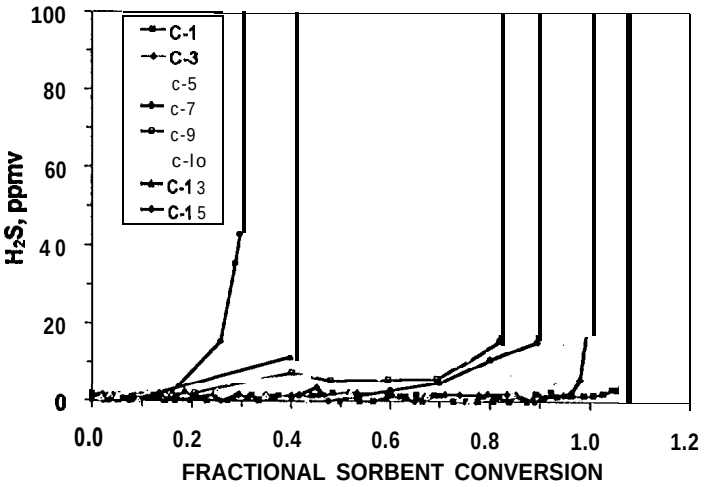

Performance of IGTSS-6 at 350“C

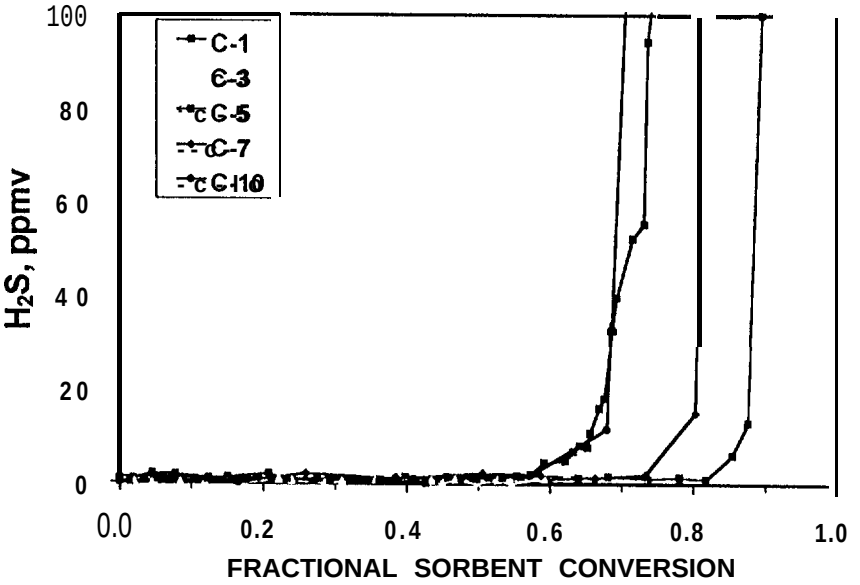

566p

Performance of IGTSS-11 at 450“C

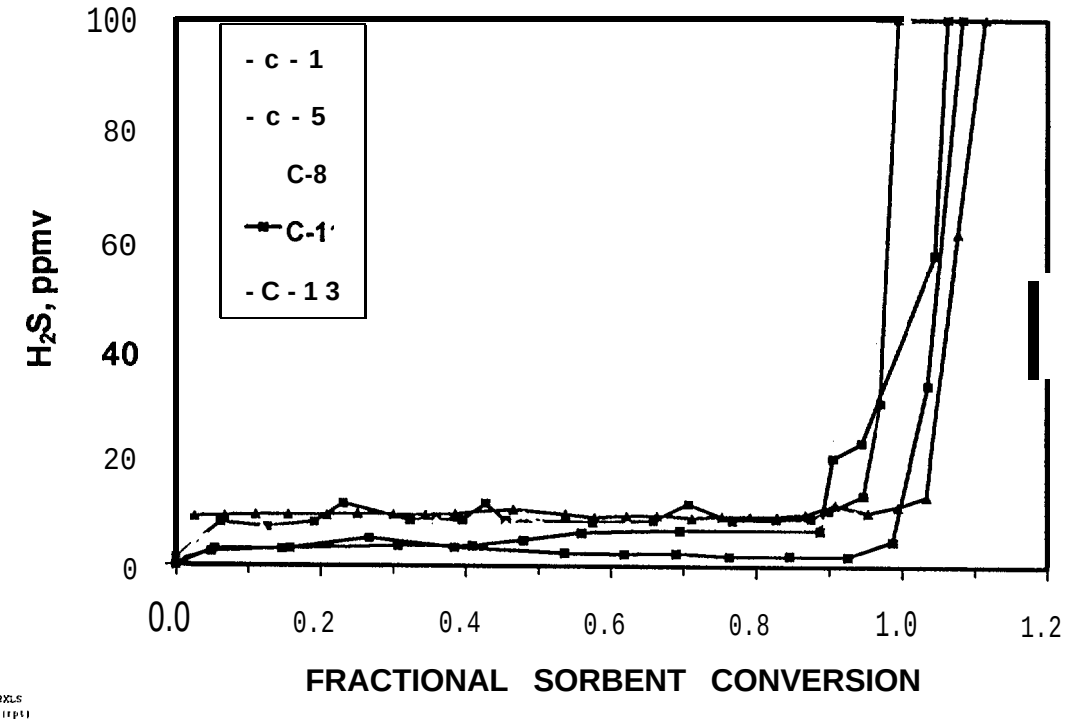

SERIES 2.XLS
#8-11 (rpt)

Breakthrough Conversion of IGTSS-6 at 350 “C

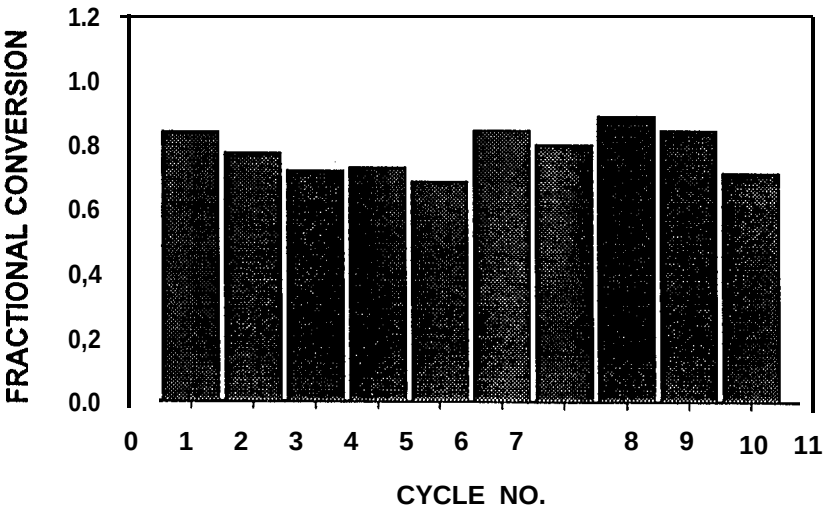

RUN-LOG1.XLS
K-V-CV #6

Breakthrough Conversion of IGTSS-11 at 450 *C

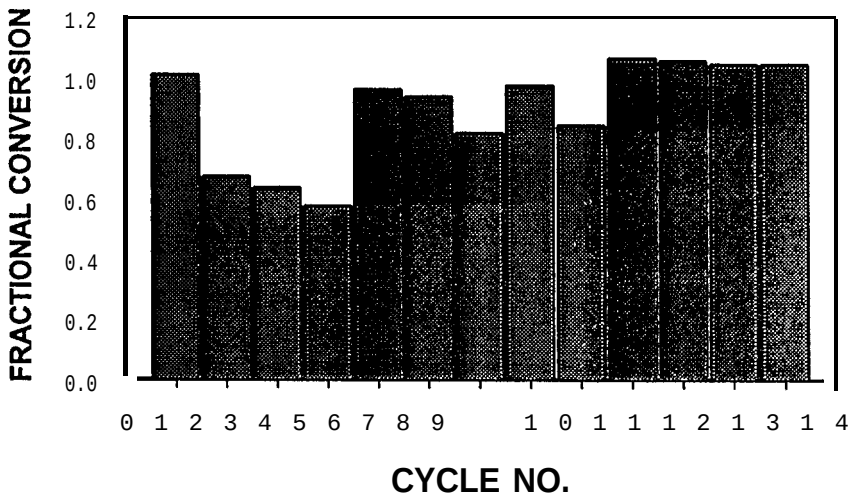

RUN-LOG1.XLS
x-y-cy ss11

Comparison of Sorbent Conversion at 350 *C

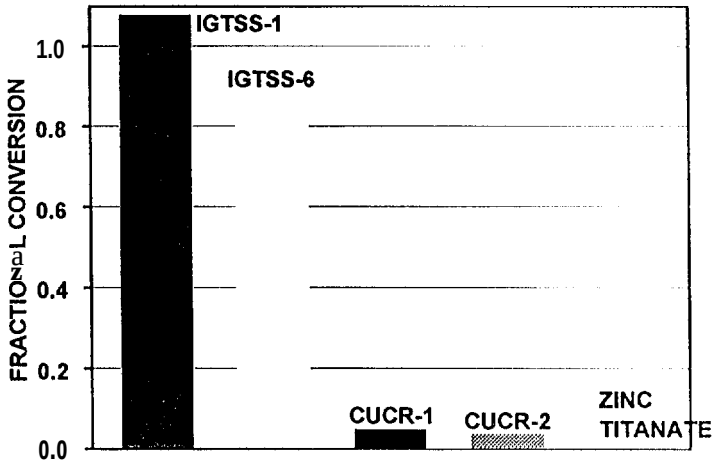

Comparison of Sorbent Conversion at 450“C

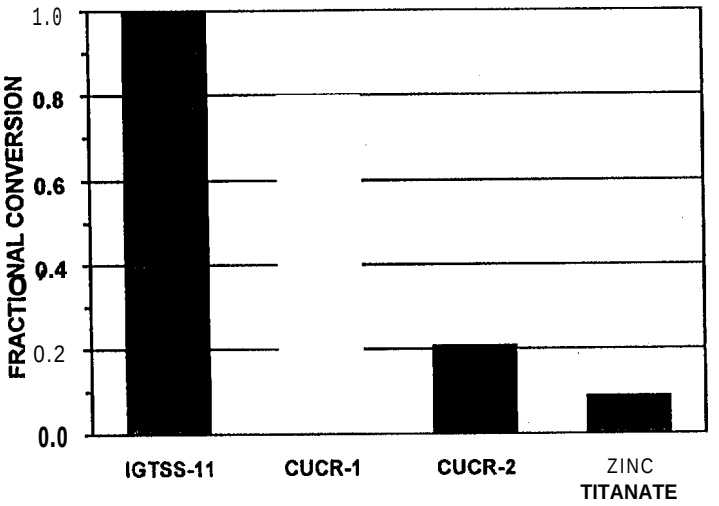

DOETEST1.XLS
sorb-450

Performance ofIGTSS-57at450“C

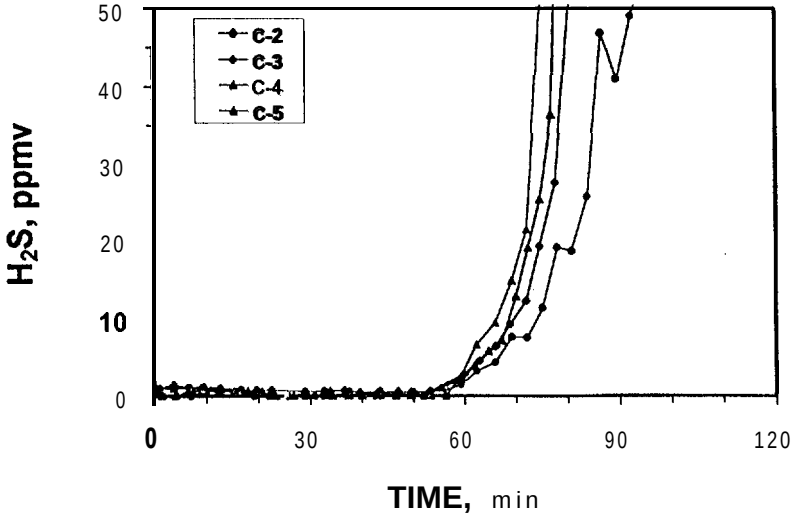

SS-57B.XLS
ss57bs2-45

Performance ofIGTSS-68at550“C

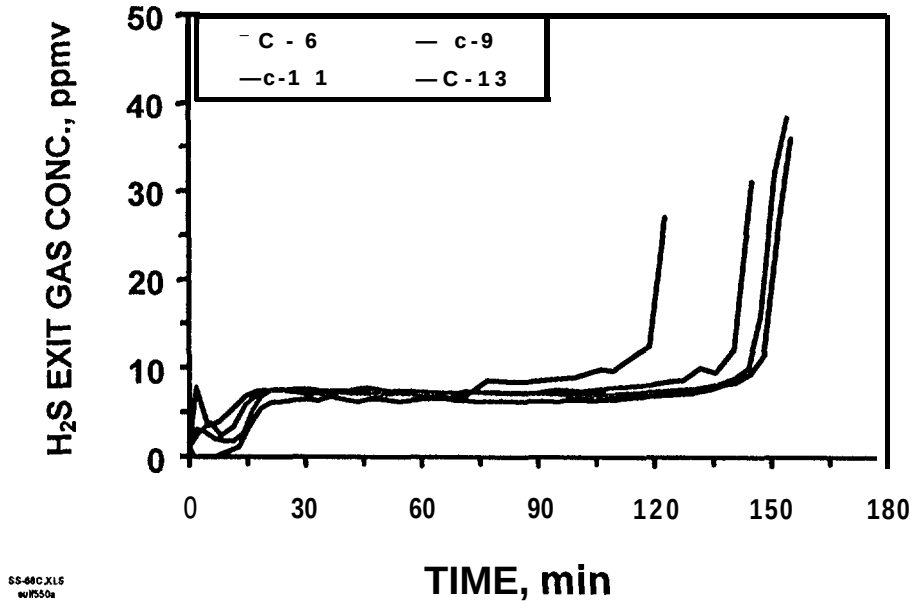

Conclusions

- Three promising sorbents have been developed for temperature range of 350°-550°C

- The sorbents reactivities and sulfur capacity appear to be stable or improving during the first 10 to 15 cycles

- The attrition resistance of the sorbent are better than UCI-4169 Zinc Titanate sorbent.

Advanced Sulfur Control Processing

Wu-Ning Huang (cmhuang@lsuvm.sncc.lsu.edu; 504-388-1426)
Alejandro Lopez-Ortiz (cmlopeo@lsuvm.sncc.lsu.edu; 504-388-1426)
Julie D. White (cmwhit@lsuvm.sncc.lsu.edu; 504-388-1426)
Frank R. Groves, Jr. (cmgrov@lsuvm.sncc.lsu.edu; 504-388-3060)
Douglas P. Harrison (cmharr@lsuvm.sncc.lsu.edu; 504-388-3066)
Louisiana State University
Department of Chemical Engineering
Baton Rouge, LA 70803-7303

Abstract

The primary objective of this project is to determine the feasibility of an alternate concept for the regeneration of high temperature desulfurization sorbents in which elemental sulfur, instead of SO_2, is produced. If successful, this concept will eliminate or alleviate problems caused by the highly exothermic nature of the regeneration reaction, the tendency for metal sulfate formation, and the need to treat the regeneration off-gas to prevent atmospheric SO_2 emissions.

Iron and cerium-based sorbents were chosen on the basis of thermodynamic analysis to determine the feasibility of elemental sulfur production. The ability of both to remove H_2S during the sulfidation phase is less than that of zinc-based sorbents, and a two-stage desulfurization process will likely be required.

Preliminary experimental work used electrobalance reactors to compare the relative rates of reaction of O_2 and H_2O with FeS. More detailed studies of the regeneration of FeS as well as the sulfidation of CeO_2 and regeneration of Ce_2O_2S are being carried out in a laboratory-scale fixed-bed reactor equipped with a unique analytical system which permits semi-continuous analysis of the distribution of elemental sulfur, H_2S, and SO_2 in the reaction product gas.

Introduction

High temperature desulfurization of coal-derived gas is an important component in the development of the integrated gasification combined cycle (IGCC) process for electric power generation. A number of metal oxide sorbents are capable of reacting with H_2S . The generic desulfurization reaction may be represented as follows:

$$MeO(s) + H_2S(g) \leftrightarrow MeS(s) + H_2O(g) \quad \textbf{(1)}$$

Research sponsored by the U.S. Department of Energy's Morgantown Energy Technology Center, under contract DE-RP21-94MC30012 with Louisiana State University, Baton Rouge, LA 70803.

The sorbent must be regenerable and must maintain activity and structural integrity through many sulfidation-regeneration cycles. The standard reaction used for regeneration is as follows:

$$MeS(s) + \frac{3}{2}O_2(g) \leftrightarrow MeO(s) + SO_2(g) \qquad \textbf{(2)}$$

In addition to the obvious problem of SO_2 control in the product gas, the highly exothermic nature of the reaction creates temperature control problems which may accelerate the deterioration of the high surface area, porous sorbent. Decreasing the O_2 content of the regeneration feed gas to assist in temperature control will also reduce the SO_2 content of the product gas and complicate the SO_2 control problem. Finally, the combination of SO_2 and O_2 favors the formation of stable metal sulfates which, particularly in zinc-based sorbent systems, are believed to be a major contributor to sorbent pellet fragmentation and spalling.

The direct production of elemental sulfur during sorbent regeneration would eliminate or alleviate all of these problems. In addition, elemental sulfur is a marketable by-product which can be safely and economically stored and transported.

Project Description

The project began with a literature search to identify possible concepts for the direct production of elemental sulfur during sorbent regeneration. The literature search was followed by a detailed thermodynamic analysis to determine the feasibility of sulfur formation using a number of metal oxides known to have high temperature desulfurization capability. Results of the literature search and thermodynamic analysis have been reported (Harrison et al., 1995), and only a brief summary is presented here.

Three possible concepts for elemental sulfur formation were identified: (1) partial oxidation in a steam-oxygen atmosphere under oxygen-starved conditions, (2) reaction with SO_2, and (3) reaction with steam to produce H_2S concentrations suitable for conversion to elemental sulfur in a Claus unit. The thermodynamic analysis showed that metal oxides having the strongest affinity for H_2S in the sulfidation phase (e.g., ZnO) were least conducive to elemental sulfur production during regeneration. The thermodynamic properties of CeO_2, SnO_2 and, to a lesser degree, Fe_2O_3 provide a unique combination of H_2S removal capability and the potential for elemental sulfur production.

The regeneration of FeS using the partial oxidation concept, and the sulfidation of CeO_2 followed by regeneration of Ce_2O_2S using all three of the regeneration concepts are being studied in the experimental phase of the program. The experimental studies are designed to determine reaction conditions -- temperature, pressure, regeneration gas composition and flow rate -- which maximize the production of elemental sulfur.

Preliminary FeS regeneration experiments used an electrobalance reactor to compare the relative rates of reaction of O_2 and H_2O with FeS. More detailed studies of FeS regeneration

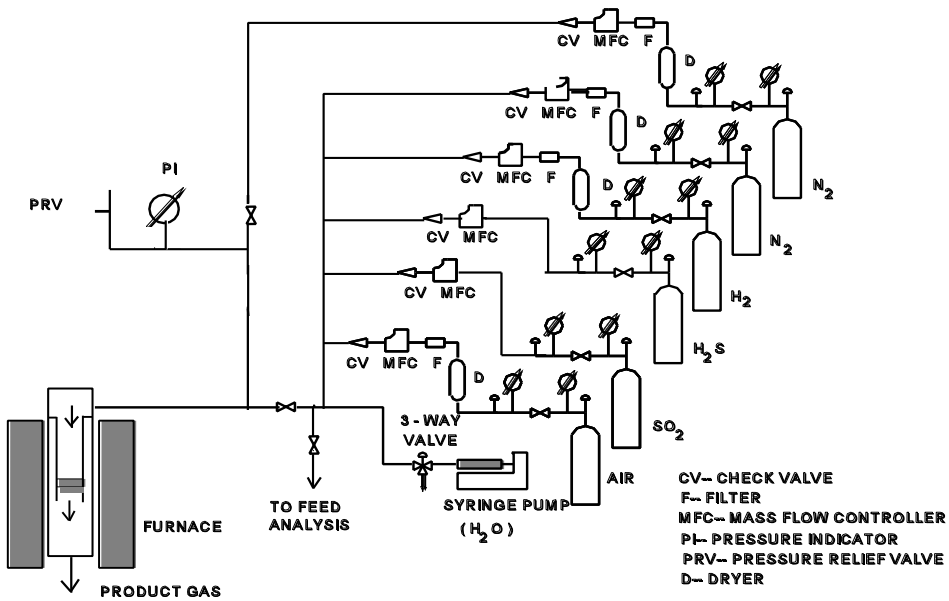

Figure 1. Schematic Diagram of the Fixed-Bed Reactor System

as well as CeO_2 sulfidation and CeO_2S regeneration are being carried out in a laboratory-scale fixed-bed reactor. Conversion of $2CeO_2$ to Ce_2O_2S does not involve a change in solid mass so that all cerium studies are limited to the fixed-bed reactor.

A schematic diagram of the fixed-bed reactor system is shown in Figure 1. Inert and reactive gases are obtained from high purity cylinders and their flow rates are controlled by high pressure mass flow controllers. Water is fed as a liquid using a high-pressure syringe pump, and gas feed lines are preheated to insure that the water is completely vaporized and mixed with other gases before entering the reactor. Combined gases enter near the top of the pressure vessel and flow downward over the sorbent which is contained in the reactor insert tube. The reactor is capable of operating at temperatures and pressures to about 800°C and 15 atm.

The unique gas analytical train, which provides semi-continuous analysis of the sulfur species in the product gas, is shown in Figure 2. The reactor product, which must be maintained above the condensation temperature of elemental sulfur, is split into two streams, with one portion flowing through a capillary flow restrictor into an oxidation chamber where all sulfur compounds are converted to SO_2. From the oxidation chamber, the gases flow through a UV-fluorescence detector where the total sulfur content of the reactor product is measured. The sample flow rate through this leg of the analytical train is determined by the resistance of the capillary restrictor and the reactor pressure. Frequent recalibration of the flow through the capillary restrictor and the UV-fluorescence detector response are required.

The remainder of the reactor product flows through a condenser and series of filters for removal of water and elemental sulfur, through a back pressure regulator which establishes the reactor pressure, and to a gas chromatograph where the SO_2 and H_2S concentrations of the

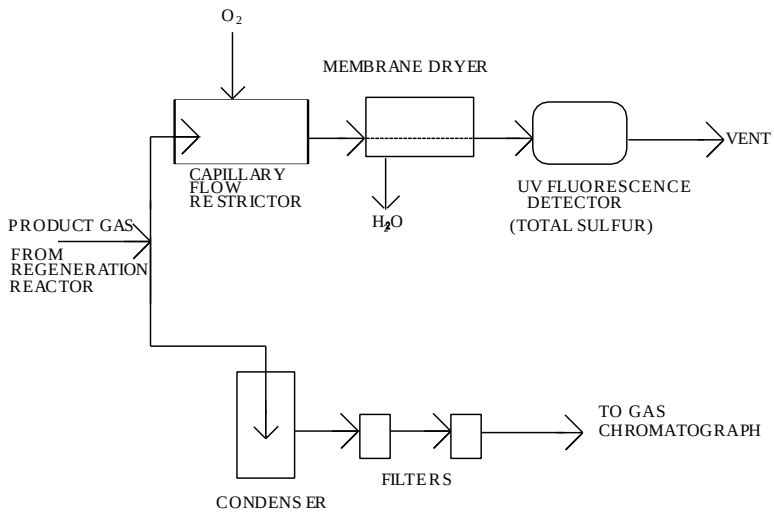

Figure 2. Product Gas Analysis Train

product gas are determined. Although this analytical method involves the determination of elemental sulfur by difference (total sulfur - H_2S - SO_2), it provides acceptable accuracy when sufficiently large quantities of elemental sulfur are present.

The gas and water feed systems for the electrobalance reactor are analogous to those of the fixed-bed reactor. The operating temperature and pressure limits are also the same. The difference is that the progress of the reaction in the electrobalance is followed by monitoring the change in mass of the solid reactant. Product gas composition is not monitored, and for this reason, the use of the electrobalance is largely limited to systems in which a single gas-solid reaction having known stoichiometry occurs.

Experimental Results

Electrobalance Studies

The electrobalance reactor was used in preliminary studies to compare the rates of reaction between O_2-FeS and H_2O-FeS as a function of temperature (600-800°C), pressure (1-15 atm), and reactive gas composition (0.5 to 3.0% O_2 in N_2 and 10 to 50% H_2O in N_2). Complete regeneration of FeS to Fe_2O_3 in O_2 runs and to Fe_3O_4 in H_2O runs was achieved except in certain low temperature-high pressure runs where some $Fe_2(SO_4)_3$ was formed. Much of the data analysis was based upon the initial global reaction rate which was found to be first order in either O_2 or H_2O, only weakly dependent on temperature, and to decrease at high pressure. The rate of the reaction of FeS with O_2 was much faster than with H_2O as shown by the dimensionless mass versus time results in Figure 3. In spite of the fact that the H_2O concentration was 3.3 times greater than the O_2 concentration, the reaction required about 10 times as long to approach completion in H_2O.

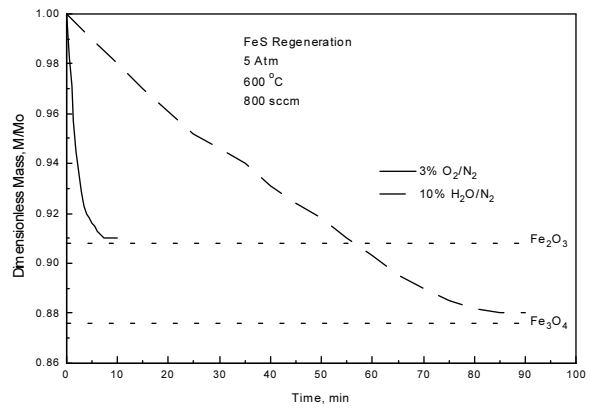

Figure 3. Comparison of the Reaction Rates of O_2 and H_2O with FeS

Initial reaction rates were correlated as a function of temperature and mol fraction of reactive gas to produce a rate equation of the form

$$r_i = k_{oi} \exp(-E_i/RT)\, y_i \qquad \textbf{(3)}$$

r_i is the initial time rate of change of dimensionless mass, k_o is the frequency factor, E the activation energy, R the gas constant, T the absolute temperature, and y the mol fraction of reactive gas. The subscript i represents the reactive gas, either O_2 or H_2O. Table 1 presents the frequency factors and activation energies for both reactions at 15 atm, and compares the initial rates of the two reactions at equal reactive gas mol fractions as a function of temperature. In spite of the higher activation energy for the FeS-H_2O reaction, the initial rate was still more than two orders of magnitude larger in O_2 at the maximum temperature of 800°C.

When O_2 and H_2O were both present in the feed gas, the initial regeneration rate was equal to the sum of the individual rates. This is illustrated in Figure 4 for a series of tests at 700°C in which y_{H2O} was held constant at 0.30, while y_{O2} and pressure were varied between 0.0005 and 0.005 and 1 and 15 atm, respectively. The discrete points represent the measured initial reaction rates while the straight lines were calculated by summing the pure component initial rates using eqn.(3) and the appropriate values of k_{oi}, E_i, and y_i. This figure also shows the unexpected effect of pressure with an increase in initial rate from 1 to 5 atm, and then a decrease between 5 and 15 atm.

Fixed-Bed Reactor Studies

FeS Regeneration.

The regeneration of FeS is being studied using the partial oxidation concept, with key reaction parameters of temperature, pressure, and gas flow rate and composition.

Table 1. Parameters in the Initial Rate Equation for the Regeneration of FeS in O_2 and H_2O (P=15 atm)

$$r_i = k_{oi} \exp(-E_i/RT)\, y_i$$

Reacting Gas	k_{oi} (min^{-1})	E_i (cal/mol)
O_2	4.65	1440
H_2O	1.52	9700

Ratios of Initial Rates at Equal y_i	r_{O2}/r_{H2O}
600	366
700	219
800	147

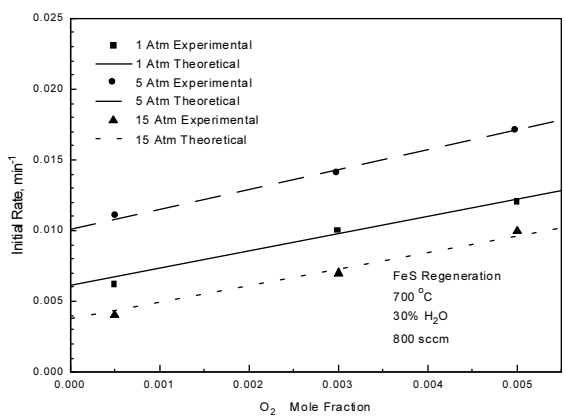

Figure 4. Initial Rate of Regeneration of FeS in O_2-H_2O-N_2

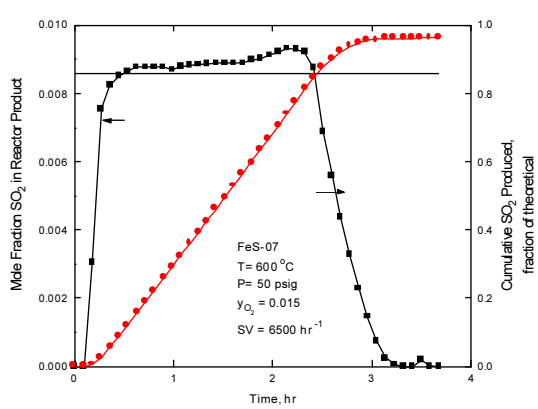

Figure 5. Fixed-Bed Reactor Response for the Regeneration of FeS With O_2

The results of an FeS regeneration run at 600°C and 4.4 atm with the feed gas containing 1.5% O_2/balance N_2 are shown in Figure 5. The mol fraction SO_2 in the reactor product and the cumulative amount of sulfur produced, expressed as a fraction of stoichiometric sulfur, are plotted versus time. SO_2 is the only sulfur compound which should be formed at these regeneration conditions, and product gas analysis was determined by gas chromatography. The horizontal line at y_{SO2}= 0.0086 represents the stoichiometric maximum SO_2 mol fraction associated with complete conversion of the 1.5% O_2 according to the equation

$$2FeS(s) + 3.5\ O_2(g) \rightarrow Fe_2O_3(s) + 2SO_2(g) \qquad \textbf{(4)}$$

After a brief time delay, the SO_2 content of the product gas increased to a value slightly above theoretical, remained relatively constant for about 2 hours, and then decreased to zero after about 3 hours. The cumulative production of SO_2 increased linearly during the time that the SO_2 content of the product gas was constant, and reached 96% of theoretical by the end of the run.

In contrast, the rate of the reaction between steam and FeS is much smaller, and the H_2S content of the product gas during a steam regeneration experiment is much less than the stoichiometric value. This is shown in Figure 6 where the mol fraction of H_2S in the regeneration product gas as well as the cumulative amount of sulfur produced, again expressed as a fraction of the stoichiometric sulfur, is plotted versus time. Again, gas chromatography was used for product gas analysis as H_2S was the only sulfur compound expected. In this test the H_2S content gradually increased for the first hour, and reached a steady-state value of about 0.0015 mol fraction after that time. The steady-state mol fraction is only about 2% of the stoichiometric value associated with 0.10 mol fraction steam in the feed gas. Only about 16% of the sulfur originally present as FeS was accounted for in the H_2S product when the run was terminated after 2.5 hours.

The production of elemental sulfur from FeS using the partial oxidation regeneration concept requires that the feed gas contain both O_2 and steam. Results from a partial oxidation regeneration test in which the feed gas contained 10% H_2O, 1.5% O_2 in N_2 are shown in Figure 7. H_2S and SO_2 were detected by the chromatograph at about the same time that total sulfur was detected by the UV analyzer. H_2S mol fraction increased quickly to about 0.0011, remained near that level for about 1.5 hours, and then slowly decreased to zero after about 2.25 hours. SO_2 mol fraction increased quickly to about 0.006, slowly increased to about 0.0077 over the next two hours, then decreased steadily to zero after about 3.25 hours. The gradual increase in SO_2 mol fraction corresponded quite well with the gradual decrease in H_2S. The mol fraction of total sulfur was approximately constant near 0.008 between 0.5 and 2.25 hours, after which the decrease in total sulfur closely matched the decrease in SO_2. The cumulative production of total sulfur was approximately equal to the sum of the SO_2 and H_2S production, indicating good closure of the sulfur material balance, and also that little elemental sulfur was formed at these conditions. The absence of elemental sulfur was not unexpected because a much higher ratio of steam-to-oxygen should be required for significant elemental sulfur formation.

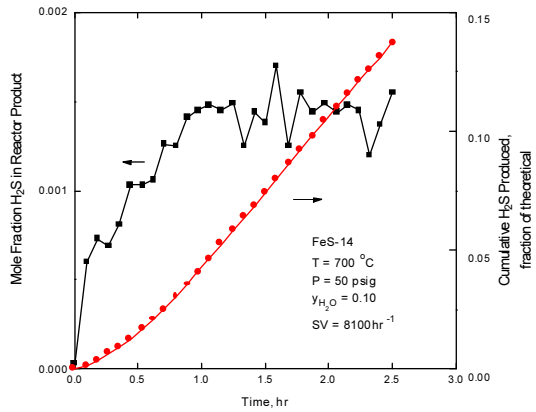

Figure 6. Fixed-Bed Reactor Response for the Regeneration of FeS With H_2O

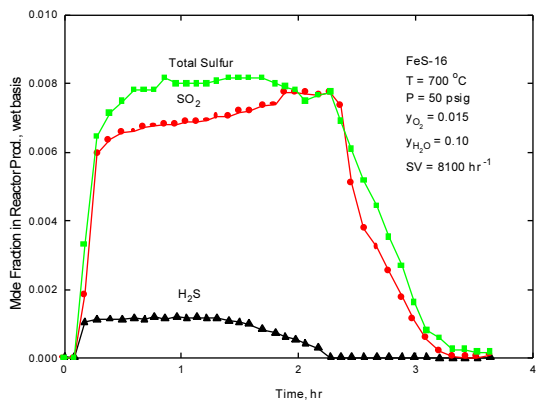

Figure 7. Fixed-Bed Reactor Response for the Partial Oxidation Regeneration of FeS (H_2O:O_2 = 3.3:1)

Increasing the H_2O to O_2 ratio in the regeneration feed gas results in the production of significant quantities of elemental sulfur as shown in Figure 8. FeS was reacted at 600°C and 4.4 atm with a feed gas containing 20% H_2O, 0.25% O_2, and balance N_2 (a H_2O to O_2 ratio of 80 to 1). The H_2S concentration peaked at about .0006 mol fraction after about 1.5 hours and gradually decreased to near zero after 5.2 hours. The SO_2 mol fraction remained near zero for 1 hour, gradually increased to a maximum of 0.0007 at 5.5 hours, and was about 0.0001 when the run was terminated. It is significant that the maximum SO_2 mol fraction was only about 50% of the stoichiometric maximum associated with 0.0025 mol fraction O_2 in the feed gas. In other runs such as shown in Figure 5 in which the reactor feed gas contained only O_2, the SO_2 concentration in the product gas was always near the stoichiometric maximum. Similarly, the maximum H_2O mol fraction was only about 0.4% of the stiochiometric maximum, compared to typical values of about 2% of the stoichiometric maximum when H_2O was the only reactive gas in the reactor feed.

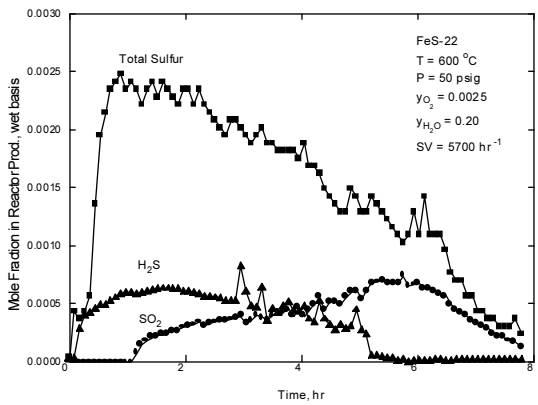

Figure 8. Fixed-Bed Reactor Response for the Partial Oxidation Regeneration of FeS (H_2O:O_2 = 80:1)

The areas under the respective curves are proportional to the quantities of H_2S, SO_2 and total sulfur produced. Of the sulfur originally present as FeS, approximately 22% was produced as H_2S and 24% as SO_2. The area under the total sulfur curve represented 99% of the original sulfur charge so that about 50% of the sulfur produced was in elemental form.

We expect to be able to increase the proportion of elemental sulfur by further increasing the H_2O to O_2 ratio, decreasing the space velocity, and decreasing the reaction temperature.

CeO_2 Sulfidation and Ce_2O_2S Regeneration.

Both the sulfidation and regeneration cycles must be carried out experimentally because Ce_2O_2S is not commercially available. Sulfidation tests have been plagued by "over-sulfidation" in that the total quantity of H_2S removed from the feed gas exceeded the stoichiometric maximum associated with conversion of CeO_2 to Ce_2O_2S. The problem was attributed initially to further sulfidation of Ce_2O_2S to Ce_2S_3 which was thermodynamically feasible in the feed gas containing only N_2, H_2, and H_2S. However, the addition of steam, which according to thermodynamics should prevent Ce_2S_3 formation, did not solve the problem. It soon became clear that the "over-sulfidation" was caused by reaction between H_2S and the walls of the reactor vessel. Apparently, the aluminized coating on the stainless steel was either ineffective at the reaction conditions or had deteriorated to the point that it no longer offered protection. A new quartz reactor insert has been designed, and, at the time of this writing, is being fabricated.

Although no quantitive information on elemental sulfur production during regeneration is available, limited qualitative results are encouraging. In run CeO_2-06r, a mixture of CeO_2 and Ce_2O_2S (unknown proportions) was regenerated at 750°C and 5 atm with the feed gas containing 1% O_2 in N_2. The regeneration lasted for about 1 hour and had to be terminated due elemental sulfur plugging the product line. Effectively all of the sulfur produced prior to plugging was in elemental form as

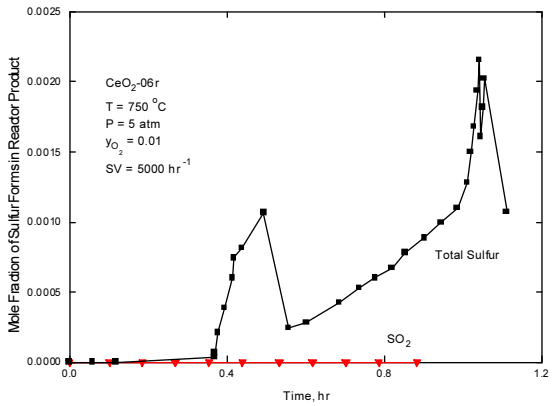

Figure 9. Fixed-Bed Reactor Response for the Regeneration of Ce_2O_2S

shown in Figure 9. No SO_2 or H_2S was detected using the GC while the mol fraction of total sulfur (= elemental sulfur) reached 0.002 just prior to the end of the run.

The formation of elemental sulfur at these conditions can be explained on the basis of the following pair of reactions

$$Ce_2O_sS + 2O_2 \rightarrow 2CeO_2 + SO_2 \quad \textbf{(1)}$$

$$Ce_2O_2S + SO_2 \rightarrow 2CeO_2 + S_2 \quad \textbf{(2)}$$

The first reaction should dominate near the entrance to the reactor where oxygen is plentiful. In downstream sections of the reactor, the oxygen will be depleted leaving SO_2 to react with Ce_2O_2S and produce elemental sulfur.

Improvements have been made in the condenser and filters since this time so that plugging problems have been greatly reduced. Additional cerium tests are now awaiting the quartz reactor insert.

Applications

One of the major problems facing hot gas desulfurization processes is the proper control and disposal of sulfur compounds in the regenerator off-gas. The G.E. moving-bed process is designed to produce an off-gas containing SO_2 at concentrations suitable for conversion to sulfuric acid (Bevan et al., 1995). However, in many instances the location of the power plant will not correspond to the location of existing H_2SO_4 plants or markets. Long distance transportation of H_2SO_4 is both hazardous and expensive. When a fluidized-bed gasifier is used, in-bed bulk sulfur removal may be accomplished by limestone or dolomite injection. The off-gases from the regeneration phase of the polishing desulfurization step may be recycled to the gasifier for ultimate conversion to $CaSO_4$ (Ghazanfari et al., 1995). However, this option is not applicable to all gasification processes, and creates immense land disposal problems. Successful development of the

direct sulfur recovery process (DSRP) (Gangwal and Portzer, 1995) for reducing the SO_2 in dilute gases to elemental sulfur will solve the disposal problem, but with the penalty of adding an additional chemical processing step to the power plant and reducing the flow of clean coal gas by the amount required to reduce the SO_2. Clearly the direct production of elemental sulfur during sorbent regenerator is the preferred option.

References

Bevan, S., et al., 1995, Integrated Operation of a Pressurized Fixed Bed Gasifier, Hot Gas Desulfurization System and Turbine Simulator, in Proceedings of the Advanced Coal-Fired Power Systems '95 Review Meeting, Vol. I, p. 187, DOE/METC-95/1018, NTIS/DE95009732, Springfield, VA, National Technical Information Service.

Gangwal, S.K., and Portzer, J.W., 1995, Slipstream Testing of Hot-Gas Desulfurization With Sulfur Recovery, in Proceedings of the Advanced Coal-Fired Power Systems '95 Review Meeting, Vol. I, p. 220, DOE/METC-95/1018, NTIS/DE95009732, Springfield, VA, National Technical Information Service.

Ghazanfari, R., et al., 1995, Pilot Scale Experience on IGCC Hot Gas Cleanup, in Proceedings of the Advanced Coal-Fired Power Systems '95 Review Meeting, Vol. I, p. 202, DOE/METC-95/1018, NTIS/DE95009732, Springfield, VA, National Technical Information Service.

Harrison, D.P., et al., 1995, Advanced Sulfur Control Concepts, in Proceedings of the Advanced Coal-Fired Power Systems '95 Review Meeting, Vol. I, p. 610, DOE/METC-95/1018, NTIS/DE95009732, Springfield, VA, National Technical Information Service.

Acknowledgements

The authors are grateful to Mr. Thomas Dorchak, the METC Contracting Officer's Representative (COR) for his patience, encouragement, and assistance on this research project.

Advanced Sulfur Control Processing

Santosh K. Gangwal (skg@rti.org; 919-541-8033)
Jeffrey W. Portzer (jwp@rti.org; 919-541-8025)
Brian S. Turk (bst@rti.org; 919-541-8024)
Raghubir Gupta (gupta@rti.org; 919-541-8023)
Research Triangle Institute
P.O. Box 12194
Research Triangle Park, NC 27709-2194

Introduction

Advanced integrated gasification combined cycle (IGCC) power plants call for hot particulate removal and hot-gas desulfurization (HGD) following gasification in order to achieve high thermal efficiency. The Morgantown Energy Technology Center's (METC's) HGD research program has focused on the development of regenerable metal oxide sorbents to remove hydrogen sulfide (H_2S) from coal gas. Leading sorbents such as zinc titanate can reduce the H_2S in coal gas to low parts-per-million levels and can be regenerated using air for multicycle operation. The sulfidation-regeneration cycle for a generic metal oxide (MO) is as follows:

$$MO + H_2S \rightarrow MS + H_2O \qquad \text{(sulfidation)}$$
$$MS + {}^{3}/_{2}O_2 \rightarrow MO + SO_2 \ . \qquad \text{(regeneration)}$$

Because the regeneration reaction is highly exothermic, temperature control is required to prevent overheating and sorbent sintering. One way to control the temperature is to use a highly dilute air stream, typically containing up to 3 vol% oxygen. This would result in a tail gas containing up to 2 vol% sulfur dioxide (SO_2). More elegant methods to control exothermicity of air regeneration that could potentially produce up to 14 vol% SO_2 are being developed (Cook et al., 1992; Campbell et al. 1995). In any event, a problematic tail gas containing 2 to 14 vol% SO_2 is produced that must be disposed of. The most desirable treatment option for the tail gas is to convert the SO_2 to elemental sulfur. METC is sponsoring the development of the Direct Sulfur Recovery Process (DSRP) (Gangwal and Portzer, 1995) that uses the reducing components (H_2, CO) of coal gas to directly and efficiently reduce the SO_2 to elemental sulfur in the presence of a catalyst in one step:

$$SO_2 + 2H_2 \text{ (or } 2CO) \rightarrow 2H_2O \text{ (or } 2CO_2) + \tfrac{1}{2}S_2 \ .$$

In the DSRP, for every mole of SO_2, 2 mol of reducing components are used. DSRP is a leading first generation technology and is undergoing field testing at gasifier sites. This study seeks to develop more advanced HGD approaches leading to elemental sulfur recovery in IGCC systems.

Research sponsored by the U.S. Department of Energy's Morgantown Energy Technology Center, under Contract DE-AC21-93MC31258, with Research Triangle Institute, 3040 Cornwallis Road, Research Triangle Park, NC 27709, telefax: 919-541-8000.

Objectives

The objective of this study is to develop a second generation HGD process that produces elemental sulfur without or with minimal use of coal gas and has better overall economics than DSRP when integrated with the overall IGCC system.

Approach

Direct production of elemental sulfur during sorbent regeneration was chosen as the approach for development of the required second generation HGD process. Concepts that were evaluated to produce elemental sulfur from sulfided sorbent included:

1. SO_2 regeneration

$$2MS + SO_2 \rightarrow 2MO + {}^{3}/_{2}S_2$$

2. Substoichiometric oxidation

$$2MS + O_2 \rightarrow 2MO + S_2$$

3. Steam regeneration followed by H_2S oxidation

$$MS + H_2O \rightarrow MO + H_2S$$
$$H_2S + ½O_2 \rightarrow H_2O + ½S_2$$

4. Steam-air regeneration followed by Claus reaction

$$MS + H_2O \rightarrow MO + H_2S$$
$$MS + {}^{3}/_{2}O_2 \rightarrow MO + SO_2$$
$$2H_2S + SO_2 \rightarrow 2H_2O + {}^{3}/_{2}S_2 \quad .$$

Preliminary assessment of these concepts indicated that Concept 1, SO_2 regeneration faced the fewest technical and economic problems among the four options (Gangwal et al., 1995). Elemental sulfur is the only likely product of SO_2 regeneration and the SO_2 required for the regeneration can be obtained by burning a portion of the sulfur produced. With SO_2 regeneration, sulfate formation, a major cause of sorbent decrepitation, does not occur. This should result in longer sorbent life. At high pressure, dry SO_2 is also simpler to separate from elemental sulfur than steam. Thus, recycle of unused SO_2 to the regenerator would be possible and this would be much less energy intensive than the use of steam. Efforts have thus concentrated on SO_2 regeneration.

Based on a theoretical evaluation of a number of potential sorbent candidates, iron- and zinc-based regenerable sorbents were chosen for experimental evaluation in this study (Gangwal et al., 1995). The selection criteria included desulfurization efficiency, SO_2 regenerability, cost, and knowledge base. Iron was considered to be the most promising candidate among numerous metals based on the above selection criteria. Also zinc remained a candidate for consideration (primarily in combination with iron) due to its excellent desulfurization efficiency, its extensive knowledge base, and its low cost, even though ZnS showed essentially no SO_2 regenerability at temperatures of interest. In combination with iron, zinc can act as a polishing agent to remove

H_2S down to very low levels and can be regenerated using air to produce SO_2 needed for regeneration of the iron sulfide. Thermogravimetric analyzer (TGA) and lab-scale reactor testing of a number of iron-zinc sorbents demonstrated the feasibility of direct regeneration of these sorbents using SO_2 to produce elemental sulfur (Gangwal et al., 1995). This year the experimental work has progressed to the bench-scale. A number of sorbents were prepared and tested at the bench-scale over multiple cycles. Work on development and multicycle testing of attrition-resistant zinc and iron sorbents is continuing. Based on results of bench-scale testing of promising sorbents, an economic evaluation for a 300 MWe plant is to be conducted next year.

Project Description

Summary of Previous Experiments

Laboratory experiments to test the SO_2 regeneration concept were carried out using a high-pressure TGA and a high-pressure lab-scale reactor (Gangwal et al., 1995). The reactor was made of a ½-in. stainless steel tube capable of operation at 750 °C and 200 psig. Provision was made for sulfiding up to 10 g of sorbent with simulated coal gas and regenerating the sulfided sorbent with up to 15 vol% SO_2. The gas exiting the reactor passed through heated tubing into a 130 °C convective oven where a 0.1-μm filter was used to collect sulfur. The gas finally vented through a back pressure regulator.

A number of proprietary sorbents based on iron and zinc oxides were prepared and tested for SO_2 regeneration. The benchmark zinc titanate and zinc ferrite sorbents were ZT-4 and L-7. These sorbents have been developed for fluidized-bed desulfurization incorporating air regeneration under a previous DOE contract. The sulfided ZT-4 sorbent which was based purely on ZnO as the active sorbent showed essentially no regeneration with 3.3 percent SO_2 in N_2 at up to 800 °C and 10 atm. However, sulfided iron- and zinc-iron-based sorbents showed good regeneration with SO_2. TGA rates of SO_2 regeneration ranged from 2.2×10^{-4} to 5.8×10^{-4} g sulfur/g sorbent/min with 3.3 vol% SO_2 at 700 °C and 10 atm.

A zinc-iron sorbent designated R-5 showed promising results and was tested further using the high-pressure lab-scale reactor. About 5 g of the sorbent was loaded in the reactor and fully sulfided using simulated coal gas. SO_2 regeneration was then started at 7.8 atm and 700 °C with 15 vol% SO_2 in N_2. Samples were withdrawn after 5.5 h and 10 h of regeneration for TGA analysis. As expected, the TGA analysis showed that the zinc portion of the sorbent was not regenerated but the iron portion of the sorbent regenerated at a rate of 2.1×10^{-4} g sulfur/g sorbent/min. This result is similar to rates with the high-pressure TGA. At the end of 10-h, sulfur plugging occurred and solid yellow sulfur was recovered downstream of the reactor.

The R-5 sorbent was also tested for SO_2 regeneration as a function of SO_2 concentration and for air regeneration. The SO_2 regeneration rate, as measured by the high pressure TGA, increased from 2.2×10^{-5} to 3.7×10^{-4} g sulfur/g sorbent/min at 650 °C and 10 atm when SO_2 concentration was increased from 3.3 to 15 vol%. The air regeneration rate at 10 atm and 700 °C was around 5×10^{-4} g sulfur/g sorbent/min with 2 vol% O_2 in N_2.

Process Concept

Based on the results presented above, the concept of SO_2 regeneration with iron- and zinc-based sorbents showed significant promise for development as an effective HGD system resulting in sulfur recovery with limited use of coal gas. A number of HGD processes could be conceptualized using alternative combinations of SO_2 and air regeneration. The similarity of air and SO_2 regeneration rates and the significant increase in SO_2 regeneration rate with SO_2 concentration were highly encouraging. It suggested that, with further increase in SO_2 concentration to 90 to 100 vol%, rates could be increased sufficiently to allow the use of even lower regeneration temperatures around 600 °C. This temperature is closer to the expected sulfidation temperature of iron sorbents which is around 450 °C. A conceptual three-reactor process based on sulfidation of iron-zinc sorbents followed by SO_2 regeneration followed by air regeneration is shown is Figure 1. The SO_2 regeneration produces sulfur from the iron portion of the sorbent and the air regeneration regenerates the zinc portion of the sorbent.

In this process concept, the sorbent from the sulfider at around 450 °C would have to be heated to around 600 °C for SO_2 regeneration. The required heat could be obtained using indirect heat exchange with coal gas which is being cooled to 450 °C, by injecting a small amount of O_2 along with SO_2 in the SO_2 regenerator, by indirect heat exchange with the sorbent being returned from the air regenerator to the sulfider, or using a convenient combination of these approaches. An alternative process concept with partial air (or O_2) regeneration of the sorbent to effect the required temperature increase and some zinc regeneration prior to SO_2 regeneration can also be visualized. A number of other process combinations are also possible but are not presented here in the interest of space.

Bench-Scale Testing

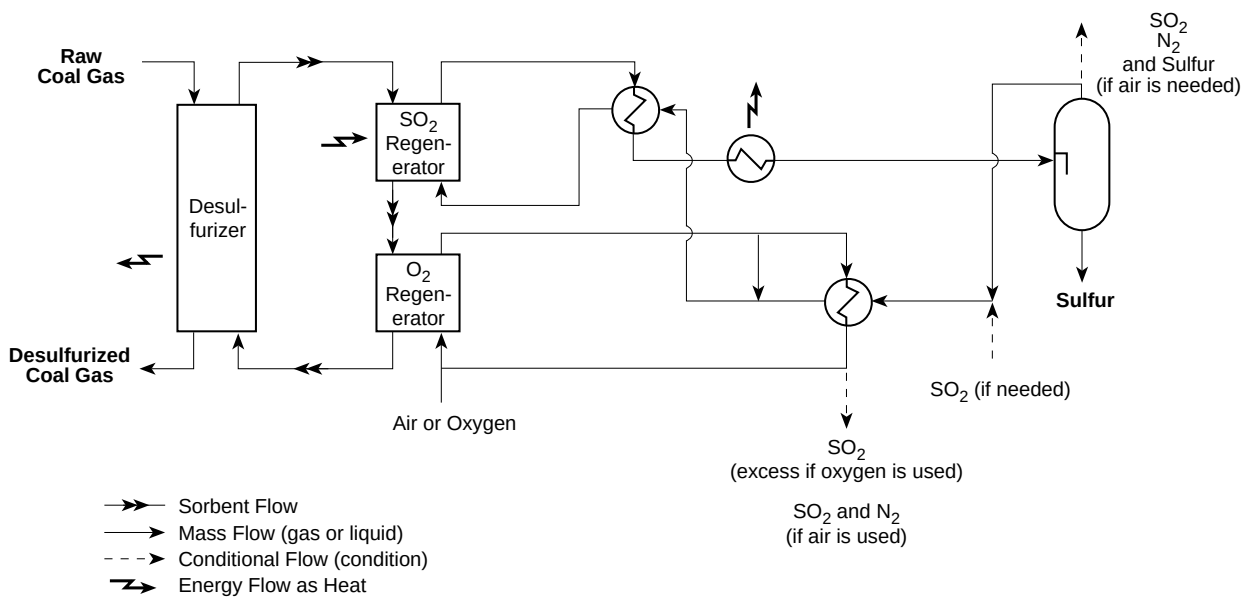

Figure 1. Three-Reactor System for SO_2 Regeneration Followed by O_2 Regeneration

Efforts this year have concentrated on scale-up of the R-5 sorbent preparation to

attrition-resistant fluidizable form, construction and commissioning of a high-temperature, high-pressure (HTHP) bench-scale unit and multicycle HTHP testing of the iron-zinc sorbents simulating the conceptualized three-reactor process of Figure 1.

The bench-scale reactor system which was built by modifying an existing unit is shown in Figure 2. The system has the capability of simulating a complex coal gas mixture using a set of mass flow controllers for gaseous components and a positive displacement pump for water to generate steam. The reactor can operate either as a fluidized-bed or as a fixed-bed with up to a 3-in. inside diameter sorbent cage. The pressure and temperature rating of the reactor is 400 psig at 750 °C and it is Alon-processed to reduce corrosion of the stainless steel. Reactor throughput up to 400 slpm of gas can be processed and sorbent up to 1.0 liter can be tested.

For SO_2 regeneration, pure SO_2 or SO_2 mixed with N_2 can be fed to the reactor by displacement of liquid SO_2 from a tank using a head pressure of nitrogen. Air regeneration (air line not shown in the figure) can also be carried out. Two separate reactor exits and downstream vent systems are utilized. SO_2 regeneration is conducted through a hot exit line with a sulfur condenser, catch pot, and a hot pressure control valve. This line is maintained hot to prevent sulfur plugging. Sulfidation and air regeneration are conducted through the other exit line. Gas samples are analyzed continuously for H_2S during sulfidation and SO_2 during air regeneration using Ametek continuous analyzers. Oxygen during air regeneration is measured continuously using a fuel cell-based analyzer and H_2S, COS, and SO_2 are measured intermittently during

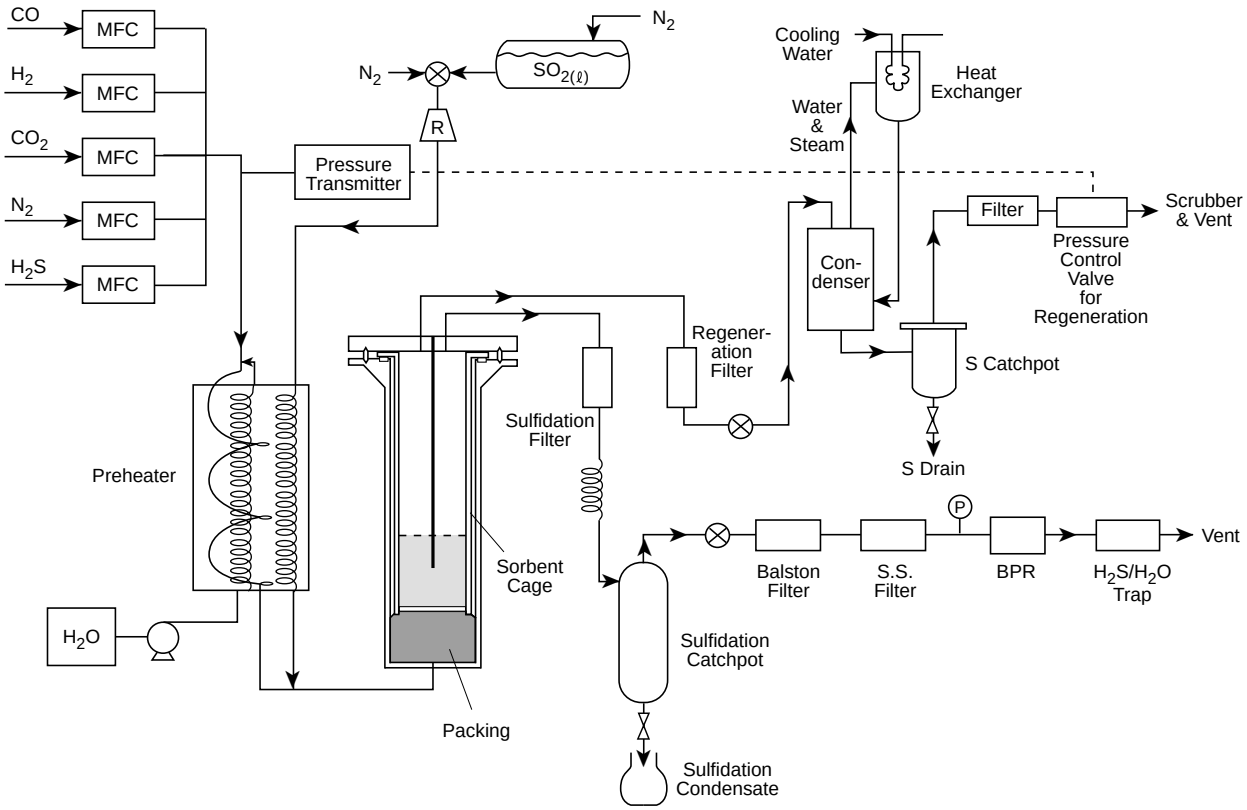

Figure 2. Bench-Scale Reactor System

sulfidation using a gas chromatograph with a flame photometric detector.

Results

Iron- and zinc-based sorbents were tested at HTHP conditions for multiple cycles. The sorbent preparation is proprietary and a patent application is pending, thus any information that could result in revealing the chemical composition and structure of the sorbents such as breakthrough curves and physical properties will not be presented. The R-5 sorbent recipe was scaled up to kilogram quantities of fluidizable attrition-resistant form with the help of a catalyst manufacturer. Two separate scale-up procedures were attempted. Using the first procedure, sorbents R-5-AWB, R-5-B, and R-5-C were produced in kilogram quantities. Using the second procedure, sorbents R-5-52, R-5-57, and R-5-58 were prepared in kilogram quantities.

R-5-B had poor attrition resistance and was immediately rejected. R-5-AWB, R-5-C, R-5-52, and R-5-58 were tested over multicycles simulating the three-reactor process of Figure 1 (R-5-57 is yet to be tested). The nominal test conditions for these multicycle tests are shown in Table 1.

The cycles typically consisted of sulfidation until breakthrough, followed by two types of regeneration. The first type of regeneration was a full air regeneration (up to 60 min) whereas the second type consisted of SO_2 regeneration (for 30 to 120 min followed by air regeneration for up to 60 min. Since a procedure for directly measuring elemental sulfur in a gas stream containing large amounts of SO_2 is yet to be developed, the amount of elemental sulfur produced during SO_2 regeneration was determined by actual measurement of the elemental sulfur that was collected or by the difference between the SO_2 produced by the two types of regeneration.

A total of 40 cycles have been run. The number of cycles completed with the various sorbents is shown in Table 2.

Table 1. Bench-Scale Test Conditions

Pressure:	275 psig	Coal gas composition (vol%)	
Flow rate:	18-75 slpm	CO:	15
Sorbent amount:	270-350 g	H_2:	10
Temperature (°C)		N_2:	Balance
Sulfidation:	420-460	CO_2:	10
SO_2 regeneration:	625	H_2O:	10-15
Dilute air regeneration:	600-650	H_2S:	0.3
SO_2 gas (vol%)		Oxidizing gas (vol%)	
SO_2:	50-65	O_2:	1-2
N_2:	Balance	N_2:	Balance

Because of the proprietary nature of the sorbents, the results presented here are of a general nature while patent protection is being sought. Generally each of the sorbents was able to reduce the H_2S to below 100 ppmv and was regenerable over multiple cycles. Also, measurable (several grams) quantities of elemental sulfur were produced during SO_2 regeneration of each of the sorbents. As much as 60 to 80 percent of the sulfur adsorbed by the sorbents has been recovered as elemental sulfur. However, the sorbents produced by the first procedure, namely R-5-AWB and R-5-C, underwent excessive loss in reactivity with cycles. In addition, they underwent significant attrition, as measured by a three-hole attrition tester, following cyclic testing. On the other hand, the sorbents prepared by the second procedure, namely R-5-52 and R-5-58, showed no loss in reactivity over the cyclic operation and also very low attrition, comparable to FCC catalysts, as measured both before and after cyclic testing by the three-hole attrition tester. In fact, the reactivity of both R-5-52 and R-5-58 improved with cycling.

Table 2. No. of Cycles Completed

Sorbent	Active metal	No. of cycles
R-5-AWB	Zn, Fe	5
R-5-C	Zn, Fe	17
R-5-52	Fe	10
R-5-58	Zn, Fe	8

Applications

As briefly discussed, the HGD process envisioned in Figure 1 or other similar processes that could result in direct production of elemental sulfur during regeneration have potential advantages over existing process options if they can be economically integrated with IGCC. The other options are production of undesirable calcium waste, production of sulfuric acid, or production of elemental sulfur using DSRP. Production of sulfuric acid is attractive if a market is readily available nearby. It may be difficult to find several such sites for IGCC plants. Elemental sulfur is the preferred option and DSRP is a highly efficient process but, as discussed earlier, requires the use of a small portion of the coal gas that results in an energy penalty to the power plant. Application of reactive and attrition-resistant sorbent such as R-5-58 to an IGCC with the capability to undergo direct SO_2 regeneration to elemental sulfur, where the SO_2 can be obtained by burning a portion of the elemental sulfur product, is a process option that needs to be developed further.

Future Activities

Approximately 15 cycles will be completed with sorbents R-5-58 and R-5-57 each. Then one of these sorbents will be tested for up to 50 cycles to demonstrate sorbent and process durability. Based on the results of testing, an economic evaluation for a 300 MWe plant will be conducted.

Acknowledgments

The authors would like to gratefully acknowledge the assistance and guidance of the METC Contracting Officer's Representative, Mr. Thomas P. Dorchak. The contract period of performance is from March 21, 1994, to March 20, 1997. United Catalyst, Inc., is assisting with preparation of zinc- and iron-based sorbents. Texaco is following the work on the project and will provide their existing nonproprietary data to assist in the economic evaluation.

References

Cook, C.S., et al. 1992. Integrated Operation of a Pressurized Fixed-Bed Gasifier and Hot Gas Desulfurization System. In *Proceedings of the 12th Annual Gasification and Gas Stream Cleanup System Contractors' Review Meeting.* Vol. 1, DE93000228, p. 84.

Campbell, W.M. et al. 1995. Hot-Gas Desulfurization Using Transplant Reactors. In *12th International Pittsburgh Coal Conference Proceedings,* pp. 1059-1064. September

Gangwal, S.K., and J.W. Portzer. 1995. Slipstream Testing of Hot-Gas Desulfurization with Sulfur Recovery. In *Proceedings Advanced Coal-Fired Power Systems' 95 Review Meeting,* pp. 220-228, DOE/METC-95/1018 Vol. 1. NTIS/DE 95009732. Springfield, VA.

Gangwal, S.K., B.S. Turk, and R. Gupta. 1995. Advanced Sulfur Control Concepts. In *Proceedings Advance Coal-Fired Systems' 95 Review Meeting,* pp. 622-630, DOE/METC-95/1018, Vol. 2, NTIS/DE 95009733. Springfield, VA.

Hot coal gas desulfurization with manganese-based sorbents[1]

Berns (Bern0010@maroon.tc.umn.edu; (612) 624-7587)
Hepworth (Hepwo001@maroon.tc.umn.edu; (612) 625-6354)
University of Minnesota
Department of Civil Eng.
500 Pillsbury Dr., S. E.
Minneapolis, MN 55435-0220

Abstract

The objective of this project is to develop a pellet formulation which is capable of achieving low sulfur partial pressures and a high capacity for sulfur, loaded from a hot fuel gas and which is readily regenerable. Furthermore the pellet must be strong for potential use in a fluidized bed and regenerable over many cycles of loading and regeneration. Regeneration should be in air or oxygen-depleted air to produce a high-concentration sulfur dioxide.

Fixed-bed tests were conducted with several formulations of manganese sesquioxide and titania, and alumina. They were subject to a simplified fuel gas of the oxygen-blown Shell type spiked with a 30,000ppmv concentration of H_2S. Pellet crush strengths for 4 and 2mm diameter pellets was typically 12 lbs per pellet and 4 lbs per pellet, respectively.

For the most favorable of the formulations tested and under the criteria of break-through at less than 100ppmv H_2S and loading temperatures of 500°C and an empty-bed space velocity of 4,000 per hour, breakthrough occurred an effective loading of sulfur of 27 to 29% over 5 loading and regeneration cycles. At 90% of this saturation condition, the observed level of H_2S was below 10ppmv.

For regeneration, a temperature of 900°C is required to dissociate the sulfide into sulfur dioxide using air at atmospheric pressure. The mean sulfur dioxide concentration which is achieved during regeneration is 8% with empty-bed space velocities of 700/hr.

TGA tests on individual pellets indicate that bentonite is not desirable as a bonding material and that Mn/Ti ratios higher than 7:1 produce relatively non-porous pellets. Whereas the reactivity is rapid below 12% conversion, the kinetics of conversion decreases significantly above this level. This observation may be the result of plugging of the pellet pores with sulfided product creating inaccessible pore volumes or alternately an increase in diffusional resistance by formation of MnS.

[1]Research sponsored by the U. S. Department of Energy's: University Coal Research Program, under contract DE-FG-2294PC94212.

Introduction

Department of Energy is actively investigating hot fuel gas desulfurization sorbents for application to the Integrated Gasification Combined Cycle Power Generation (IGCC). A sorbent must be highly active towards sulfur at high temperatures and pressures, under varying degrees of reducing atmospheres. High conversion of the metal oxide and low hydrogen sulfide exit partial pressures are required. Also, it must regenerate nearly ideally to maintain activity over numerous cycles. Furthermore, regeneration must yield a sulfur product which is economically recoverable directly or indirectly.

In response to stability difficulties to formulate single and binary metal oxide sorbents, effort is increasingly being directed towards incorporation of an inert component into sorbent formulation as witnessed by the various Zn-titanates. The role of the inert component is primarily to increase pore structure integrity while stabilizing the active metal oxide against reduction. The inert solid may also be used as a porous monolith for impregnated active metals. Mn-based sorbents are resistant to reduction to the metal in most coal gas atmospheres. However, their pore structure requires further investigation, as this may determine desulfurization kinetics due to intra-particle transport resistances.

Objective

The objective of this project is to develop a pellet formulation which is capable of achieving low sulfur partial pressures and a high capacity for sulfur, of being loaded from a hot fuel gas and which is readily regenerable. Furthermore the pellet must be strong for potential use in a fluidized bed and regenerable over many cycles of loading and regeneration. Regeneration should be in air or oxygen-depleted air to produce a high-concentration of sulfur dioxide.

Approach

Pellet Composition

Exploratory investigation of Mn-based sorbents began with the consideration of the following parameters of feed materials and preparation techniques. Composition variables were;

- Manganese source,
- Substrate composition,
- Mn to substrate molar ratio,
- Non-volatile binder wt %,
- Porosity enhancer composition,
- Porosity enhancement wt%.

The manganese sources were chosen from a commercially available $MnCO_3$ and a pyrolusite ore. Substrate were chosen based on thermodynamic equilibrium between the mixed metal oxide sorbent ($MnO.Me_xO_y$) and hydrogen sulfide (H_2S).

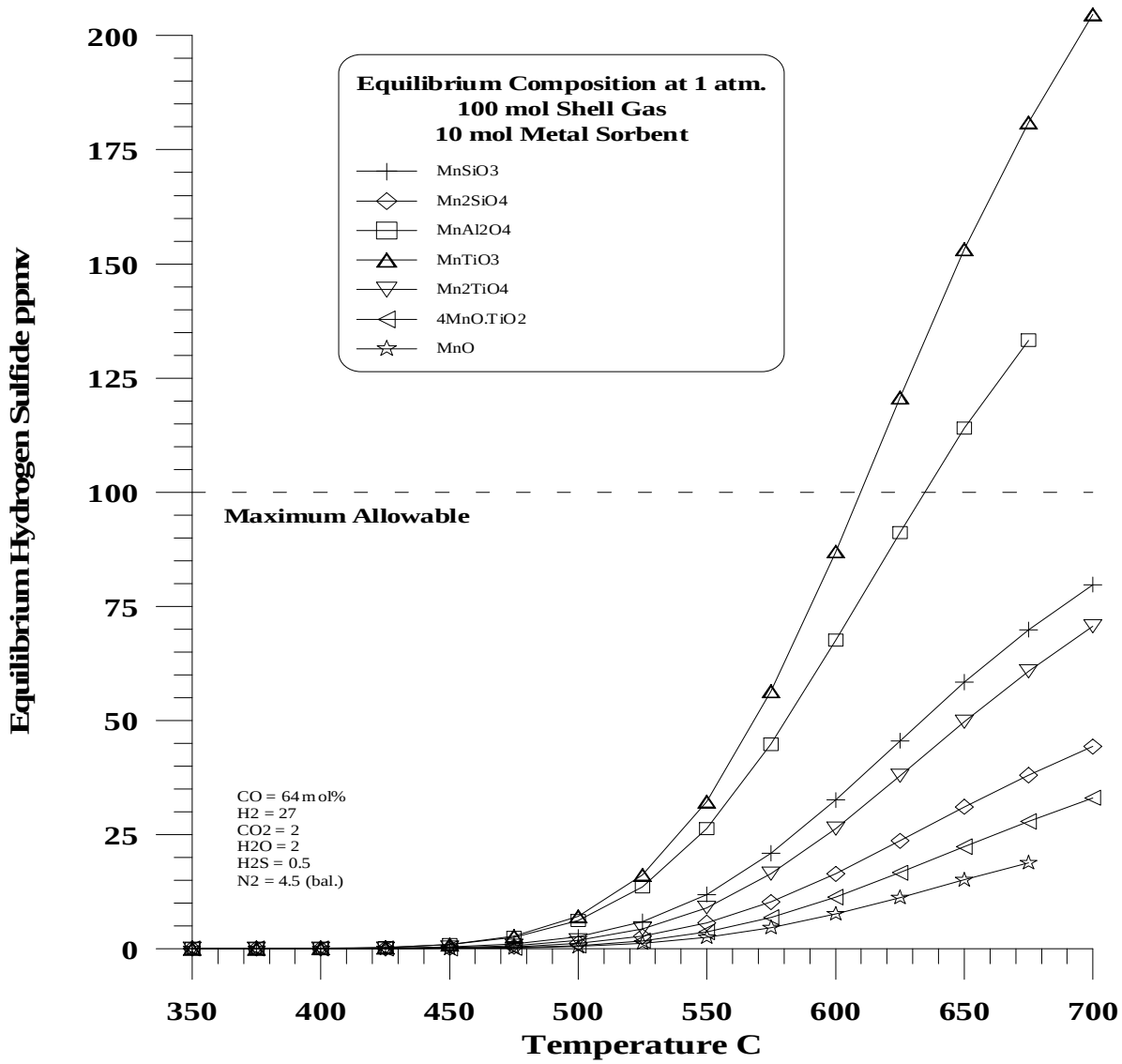

Figure 1. Equilibrium composition for Mn-based sorbents with various substrates in a simplified Shell type fuel gas.

Figure 1. is a thermodynamic analysis of the hydrogen sulfide levels which can theoretically be produced for a series of manganese oxide phases.

The molar ratio of Mn to substrate was varied in an attempt to optimize this parameter. Only bentonite was used as a non-volatile binder with 0,2, or 5% by weight added to various formulations. In an effort to increase the pore volume and surface area of the indurated pellet, volatile components were added to initial pellet mixtures. Finally, the amount of porosity enhancer was varied for a selected number of formulations.

Pellet Preparation

Feed powders were hand mixed and pelletized in a balling wheel forming "green" pellets. Green pellets were air dried for one day than dried to a constant weight at 100 ^{o}C. Dry pellets

were calcined for four hours at 350°C. Immediately after calcination, pellets were placed in a high-temperature furnace (preheated to 500°C), where the temperature was ramped up for two hours until final induration temperature was achieved. Due to the variety of pellet compositions, it was decided to restrict the induration length to two hours, at the designated temperature, for all formulations.

To date over 50 induration campaigns have been conducted for the fifteen present formulations (approximately four campaigns per formulation). The indurated pellet size was formulated in the range of 1-3 mm.

Characterization

Several methods of physical and chemical characterization were employed. Crush strength was the first parameter measured for all freshly indurated sorbent. Sorbent with requisite strength was then reduced and sulfided in a thermogravimetric analyzer to determine reaction evolution and fractional conversion. The test conditions for reduction/sulfidation are reported in Table 1.

Sample mass	200-800 mg
Reduction duration: T > 550°C T < 550 ^{o}C	30 min 60 min
Sulfidation duration	120 min
Average pellet diameter	1-3 mm
Gas composition and flow rate	1 L/min H_2
H_2S concentration	30,000 ppmv
Pressure	1 atm

Table 1. Conditions of TGA reduction/sulfidation experiments for all formulations.

Each TGA test sample consisted of three pellets. The sulfided pellets were also regenerated in the TGA. Regeneration conditions are described in Table 2.

Sample mass	200-800 mg
Regeneration Temperature	900 ^{o}C
Regeneration duration	60 min
Average pellet diameter	1-3 mm
Gas composition and flow rate	1 L/min Air
Pressure	1 atm

Table 2. Conditions of TGA regeneration experiments for all formulations.

A limited number of formulations were subjected to mercury porosimetry for pore structure characterization. This testing is currently limited to freshly indurated sorbent. Also, chemical analysis of unreacted and reacted sorbent was conducted to corroborate TGA data. Sorbent S capacities' (based upon initial formulation and chemical analysis) are listed in Table 3.

Formula	Sulfur Capacity Sg / 100g sorbent	Formula	Sulfur Capacity Sg / 100g sorbent
A1-0	28.8 (29.1)	C4-5	28.2 (27.9)
A1-2	28.1 (27.8)	C5-2	31.4 (33.4)
A2-2	29.8 (29.1)	C5-5	30.1 (30.7)
C4-2	29.3 (27.3)	C6-2	25.5 (31.7)
C4-2A	29.3 (27.5)	C7-2	23.0 (21.6)
C4-2D	29.3 (27.8)	C8-0	25.9 (28.3)
C4-2M	29.3 (*)	C9-2	32.6 (34.1)
C10-2	29.3 (27.6)		

Table 3. Formula designations and sulfur capacities based on; initial formulation and chemical analysis ( ).*Chemical analysis not available.

Formulation designations are described by listing sequentially; a letter, a number, a dash, a second number, a second dash, and finally a third number (ex. C6-2-1100). The first letter corresponds to the manganese source (C for $MnCO_3$, and A for MnO_2-ore). The first number refers to the molar ratio of Mn to substrate and the substrate composition (1,2,4,5,7 for alundum, 6,8, 9 for titania, and 10 for bauxite). The second number is the weight percent of bentonite binder. Note, some C4-2 formulations have letters following the weight percent bentonite. These letters refers to porosity promoters added, i.e., C4-2x (A for activated, D for dextrin, and M for MoO_3).

The most promising sorbents are to be further tested in an ambient pressure fixed-bed reactor. This will allow operational parameters of; space velocity, temperature, and gas composition, to be varied to determine sorbent performance during sulfidation and regeneration. Primarily, steady-state H_2S concentrations and breakthrough times are being measured. Also, regeneration SO_2 concentrations and breakthrough times are measured.

Characterization of fixed-bed pellets includes crush strength, sulfur analysis, porosimetry, and scanning electron microscopy.

The reactor consists of a 1" inner diameter tube and bed outlet thermocouple. Figure 2. is a schematic of the reactor system.

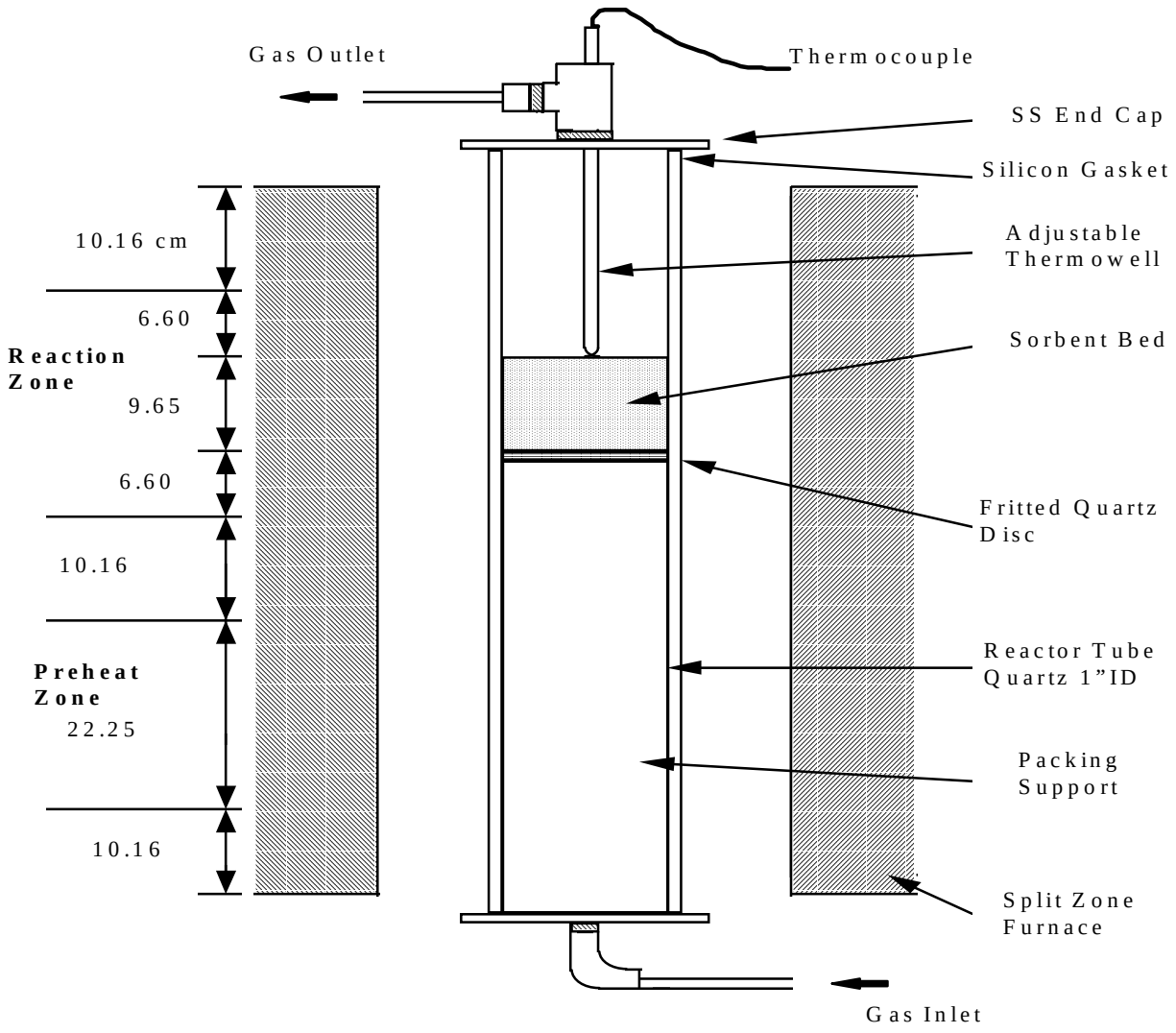

Figure 2. Desulfurization Reactor

Screening Protocol

The composition and preparation technique for sorbent formulation was based upon the fundamental requirement of desulfurization steady-state H_2S concentrations less than 50 ppmv. Further central requirements are; fully regenerable providing a sulfur product stream of at least 6 % SO_2, and activity retention for at least 50 cycles. The screening procedure is given in Figure 3.

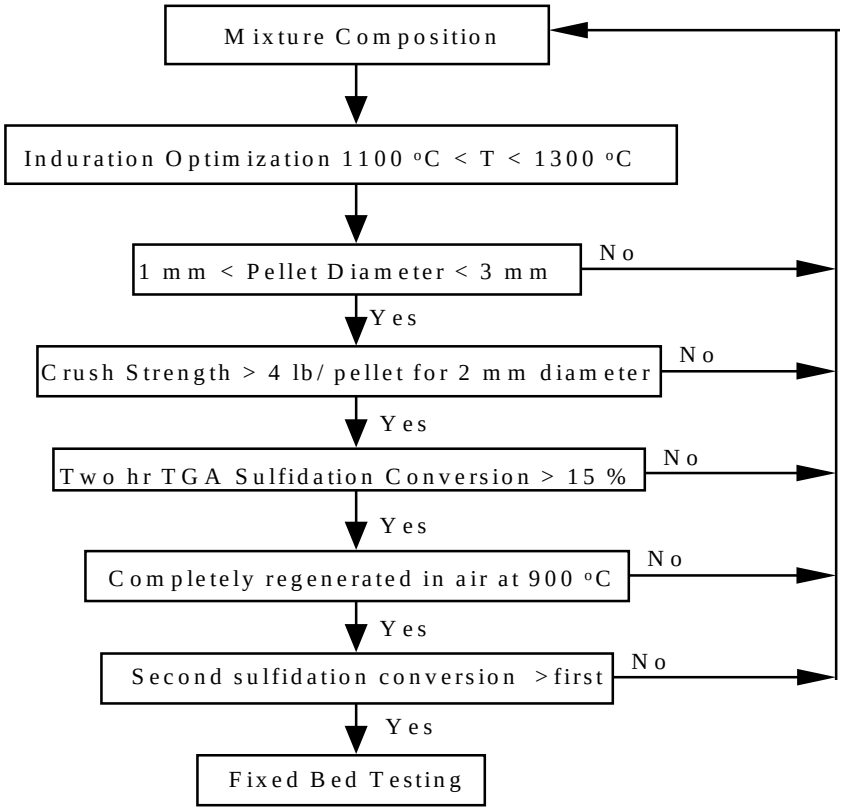

Figure 3. Strength and thermogravimetric screening protocol.

Substrate metal oxides were previously determined to quantitatively increase sorbent strength and porosity. Therefore, candidate substrates were evaluated according to their thermodynamic equilibrium between the Mn-substrate mixture and H_2S for typical operating desulfurization conditions. Sorbent formulations were then prepared as previously described.

A lower limit of 1100 ^{o}C was placed on sorbent induration temperature to preclude sintering during regeneration which is currently set at 900 ^{o}C. An induration upper temperature limit of 1300 ^{o}C was set due to furnace limitations. Therefore, all potential sorbents were required to be indurated in this temperature range for further consideration. Crush strength tests of freshly indurated sorbent was then conducted with the requirement of 1 lb / pellet / mm of diameter.

This was determined assuming the crush strength increased proportionally with the pellet cross-sectional area; thus, providing a basis for comparing different diameter pellets. Minimization of the induration temperature was conducted for all formulations. Following the preparation and strength screening the kinetic screening for sulfidation and regeneration was conducted.

Sulfidation screening was primarily conducted at 500 ^{o}C. Sorbents showing sufficient sulfur absorption were regenerated according to the previously described. Finally, the superior performing sorbents are to be tested in the fixed-bed reactor to determine their effectiveness when subject to recycle testing.

Results

Over fifty induration campaigns have been conducted among the fifteen Mn-based sorbent formulations. All indurated sorbents has been tested for crush strength and chemical analysis. Also, fifteen sorbent formulations have been tested in a TGA for at least one induration condition.

There are three main groups of formulations tested. They are the $MnCO_3$ supported with TiO_2 (with or without bentonite), $MnCO_3$ supported with Al_2O_3 (with or without porosity enhancers), and MnO_2 ore supported with alundum (with and without bentonite).

$MnCO_3$-TiO_2 Formulations

The results of the crush strength tests are given in Figures 4-6 for manganese carbonate/Titania; Manganese carbonate/Alumina; and Manganese ore/Alumina formulations, respectively.

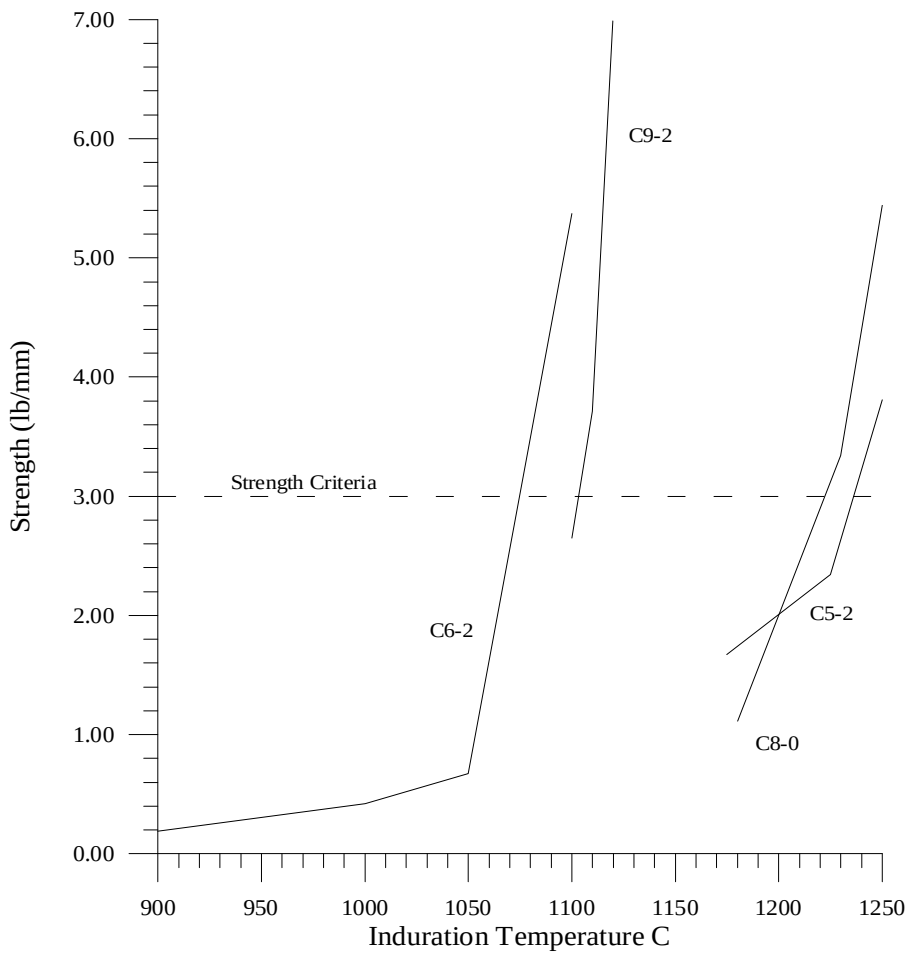

Figure 4. Crush strength of Manganese carbonate/ Titania formulations.

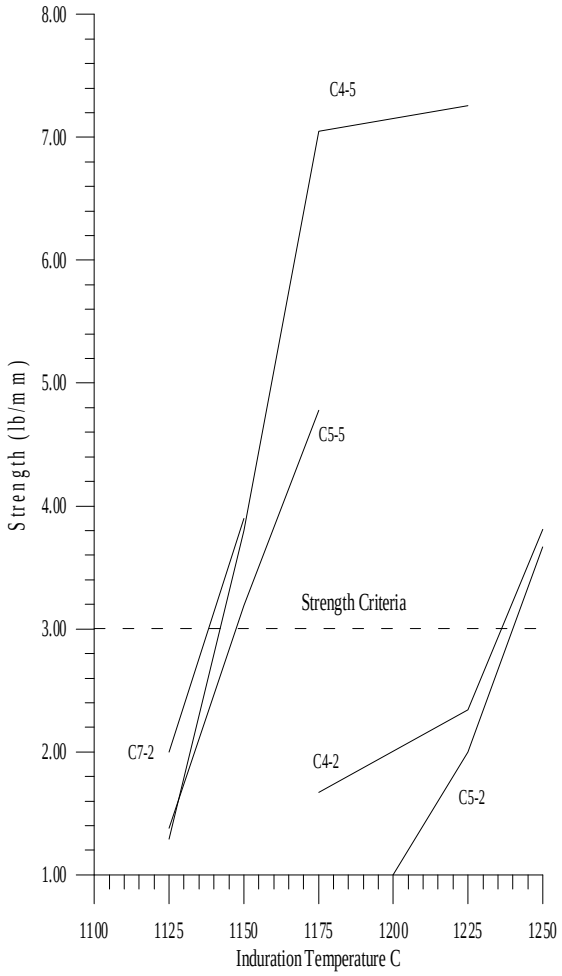

Figure 5. Crush strength of Manganese carbonate/ Alumina formulations.

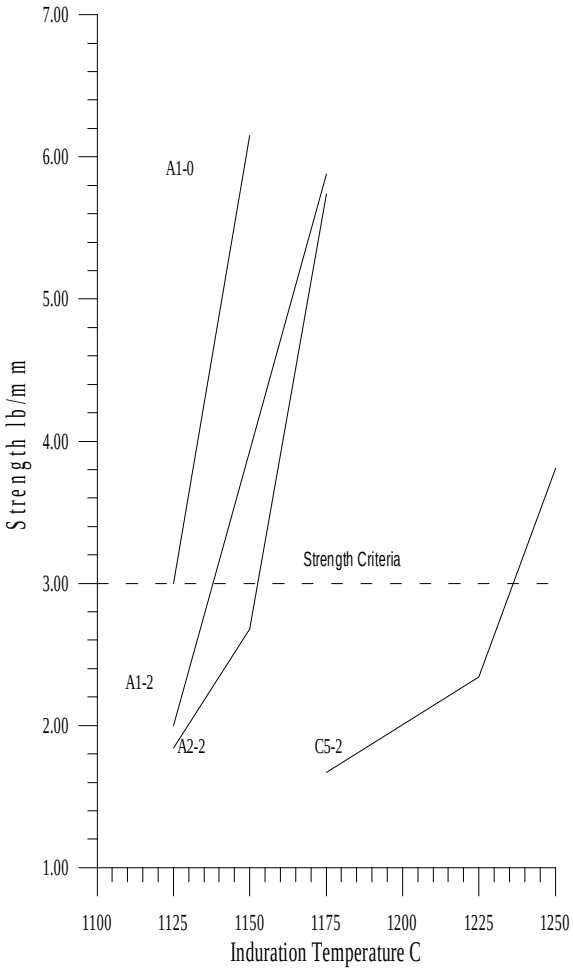

Figure 6. Crush strength of Manganese ore/ Alumina formulations.

Limited porosimetry analysis is summarized in Table 4. Comparing C6-2-1100 and C9-2-1110, the former has a larger intrusion volume while having a similar mean pore diameter. This points to more surface area in C6-2-1100 pellets than in C9-2-1110. Further porosimetry data is required, especially of C8-0-1230.

Pellet Properties	A1-2-1125	C6-2-1100	C9-2-1110	C5-2-1250
Total Intrusion Volume, Ml/g	0.2220	0.2328	0.1618	0.2901
Total Pore Area, m^2/g	0.490	---	0.199	0.103
Median Pore Diameter (volume), mm	4.7579	4.1741	4.1157	10.9701
Median Pore Diameter (area), mm	0.0142	---	2.9058	10.0270
Average Pore Diameter (4V/A), mm	1.8116	---	3.2474	11.3167
Bulk Density, g/ml	---	2.1073	2.4126	1.8807
Apparent Density (skeletal), g/ml	---	4.1357	3.9580	4.1390
Porosity, %	---	49.05	39.05	54.56

Table 4. Results of Mercury porosimetry of freshly indurated pellets.

TGA results on sulfidation tests are shown in Figure 7. and Figure 8. for $MnCO_3/TiO_2$ and other selected formulations.

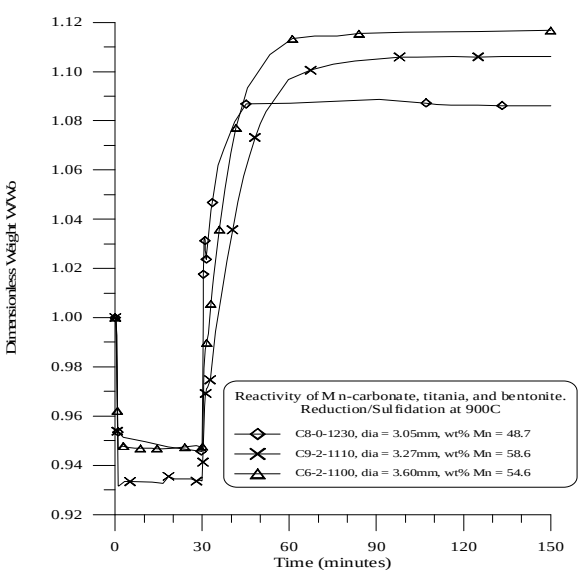

Figure 7. $MnCO_3/TiO_2$ reactivity evolution.

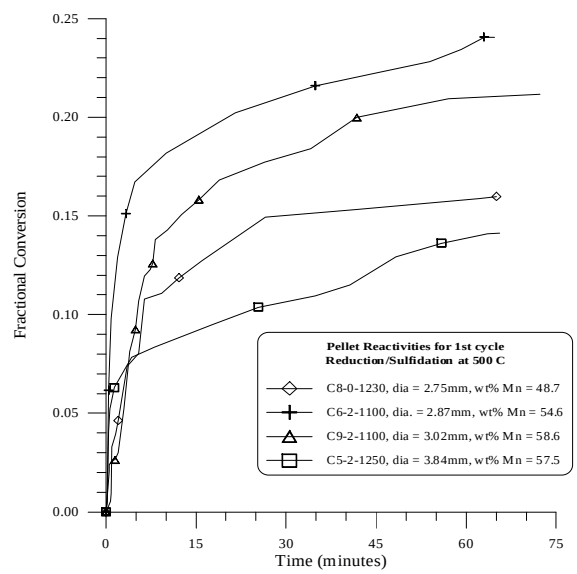

Figure 8. Mn-based formulation reactivity at 500°C.

All Mn-Ti formulations react rapidly initially at 500°C, with C6-2-1100 obtaining the highest fractional conversion. Formulation C9-2, which has a higher Mn:Ti molar ratio than C6-2-1100, did not produce greater sulfidation kinetics or sulfur capacity.

With bentonite as a bonding agent, it is believed that higher Mn:Ti ratios greater than 7:1 produced less reactive pellets. This may be explained by porosimetry data which suggest C6-2-1100 has higher surface area than C9-2-1110. All rates on the $MnCO_3$-TiO_2 formulations decrease rapidly between 12-20% conversion. This kinetic deceleration may be due to plugging of the pellet pores with sulfur creating inaccessible pore volume or a large increase in diffusional resistance from MnO to MnS.

Sintering during the first reduction and sulfidation cycle is believed to be negligible. Further testing of C6-2-1100 was conducted to determine the strong dependence of preparation temperature on strength and sulfidation fractional conversion, given in Figure 9.The effect of pellet diameter on sulfidation kinetics as is shown in Figure 10. suggests intra-particle rate limitation. The effect of temperature is given in Figure 11. for C6-2-1100.

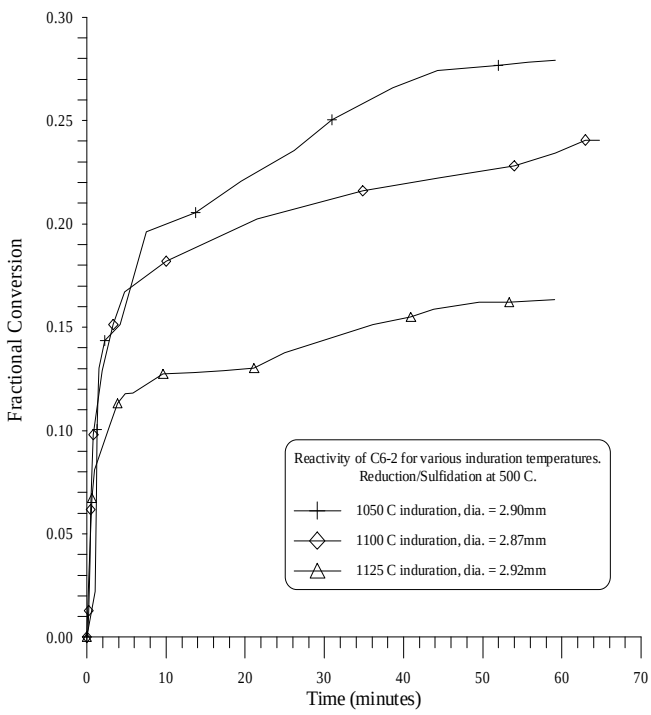

Figure 9. Effect of preparation temperature on reactivity for C6-2-1100.

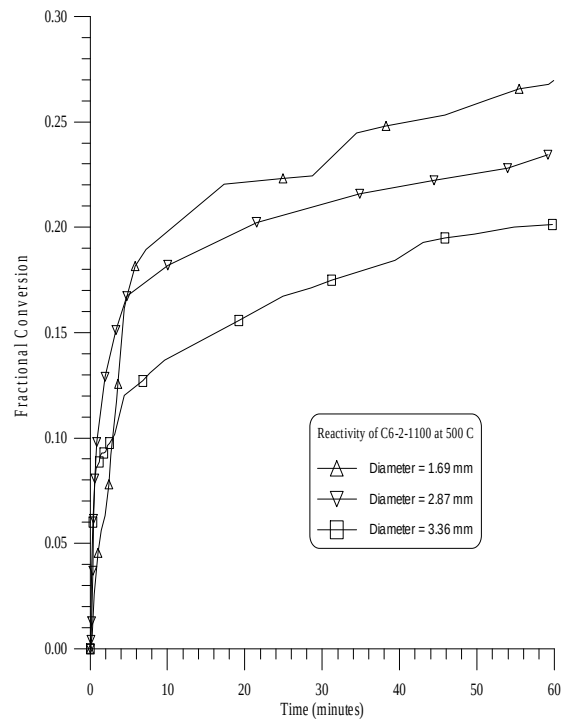

Figure 10. Effect of pellet diameter on reactivity for C6-2-1100.

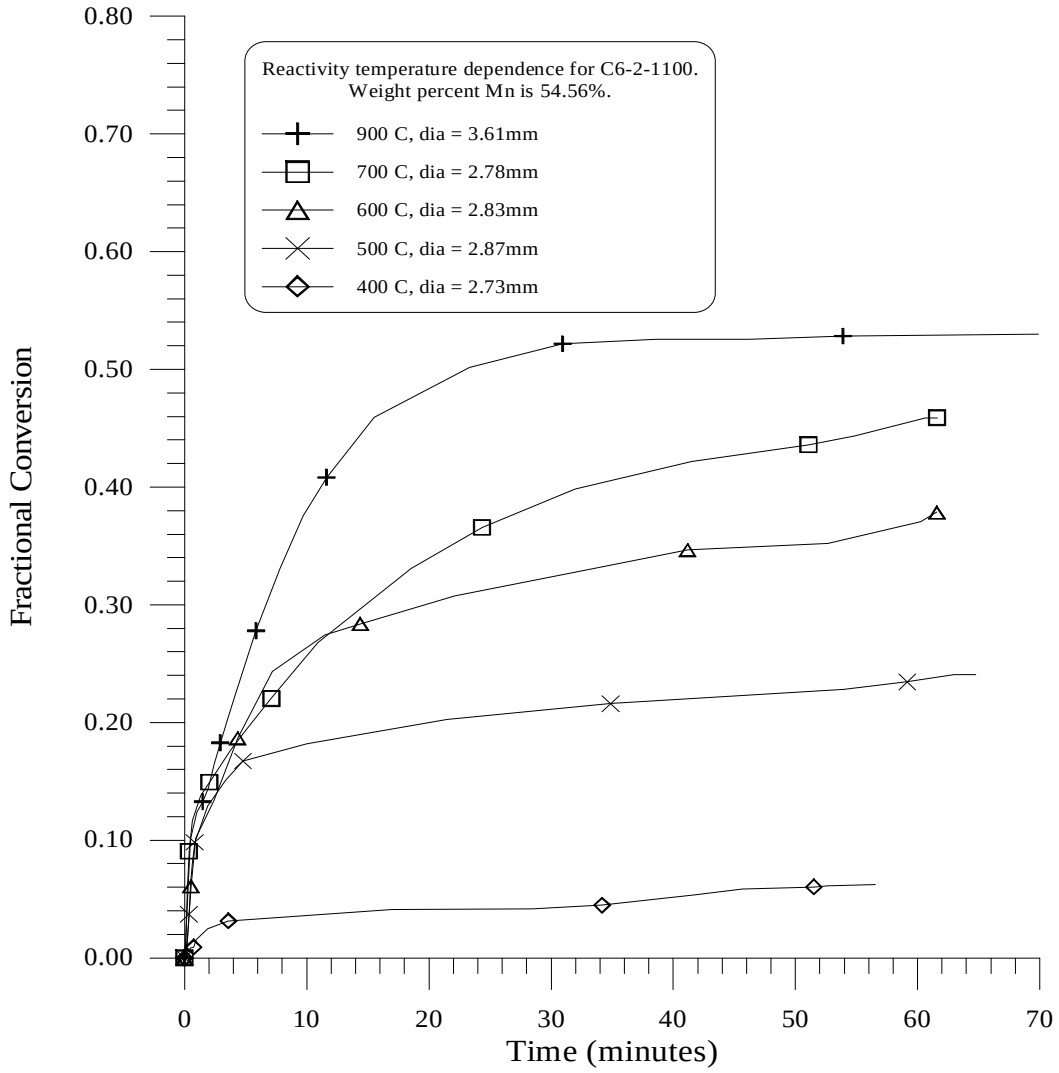

Figure 11. Effect of sulfidation temperature on reactivity for C6-2-1100.

Formulation C9-2-1110 was eliminated from regeneration testing while C8-0-1230 was included. Both $MnCO_3$-TiO_2 sorbents are completed regenerated as shown in Figures 12, and 13 for formulations C6-2-1100, and C8-0-1230, respectively.

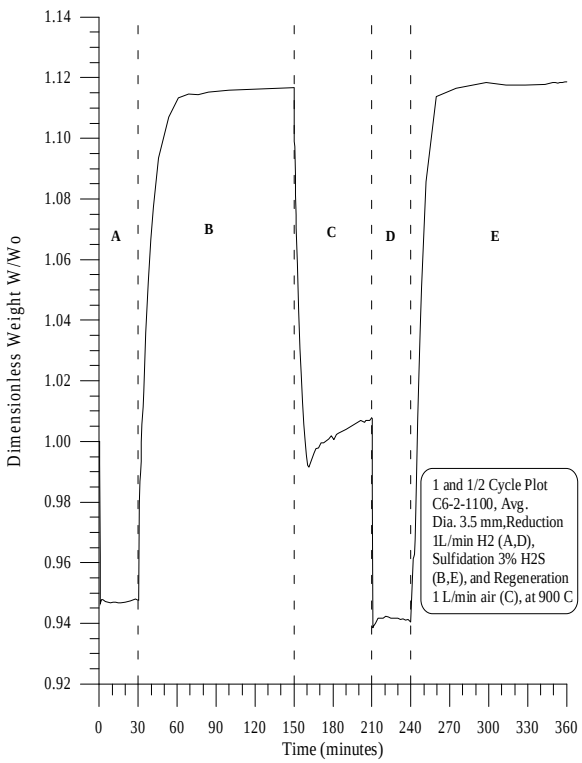

Figure 12. 1 and 1/2 cycle plot for C6-2-1100.

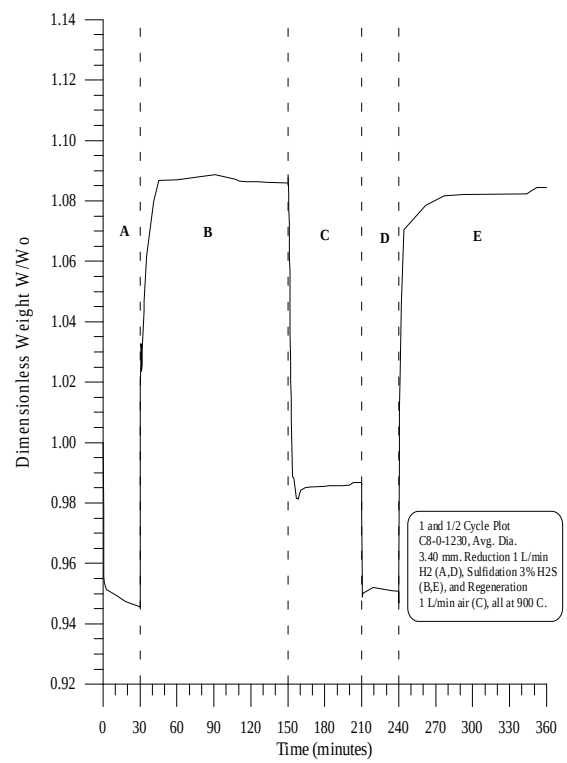

Figure 13. 1 and 1/2 cycle plot for C8-0-1230.

$MnCO_3$-Al_2O_3 Formulations

The $MnCO_3$-Al_2O_3 group contains the majority of formulations investigated to date. As the weight percentage of bentonite is increased, the required induration temperature for a given strength criteria is markedly decreased. To reduce the induration temperature, formulations high in Al_2O_3 and bentonite were produced. This proved unsuccessful as presumably the bentonite reduces capacity and $MnO.Al_2O_3$ equilibrium with H_2S in unfavorable. Reduction/sulfidation tests for $MnCO_3$-Al_2O_3 formulations is presented in Figure 14.

MnO_2 ore-Al_2O_3 Formulations

The required induration temperature for these formulations is generally much less than for $MnCO_3$-Al_2O_3 formulations as the gangue constituents (primarily silicates) have a relatively low sintering temperature. The reactivities for all ore-based pellets is given in Figure 15.

Formulations A2-2-1175 and A1-0-1150 have identical weight fractions of Mn; yet, A2-2-1175 has 2% bentonite and relatively less alundum then A1-0-1150. Interestingly, their reduction and sulfidation curves look qualitatively identical at 900°C. The exception is that A1-0-1150 reduces more completely as expected from lack of bentonite. Use of bentonite is probably a poor method of increasing strength since it diminishes absorption capacity and rate.

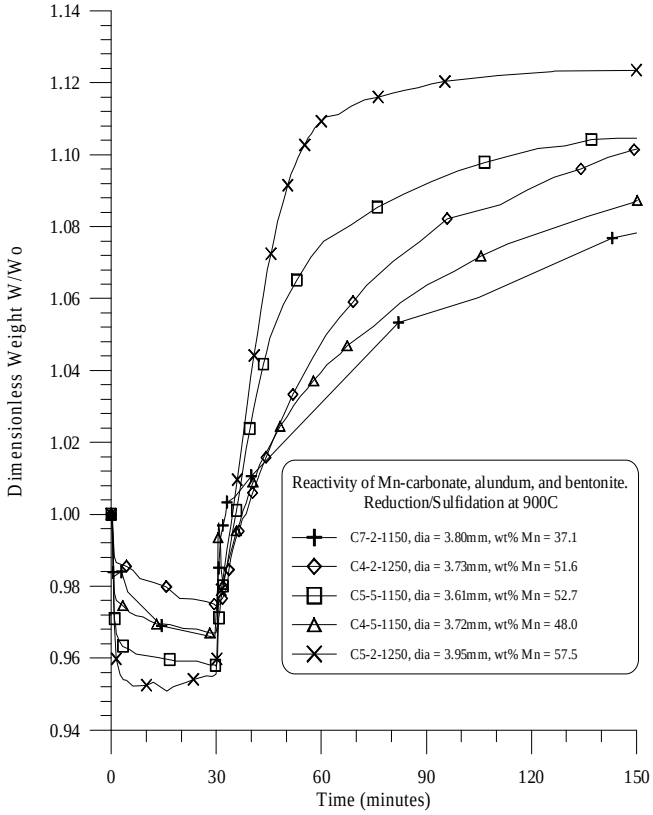

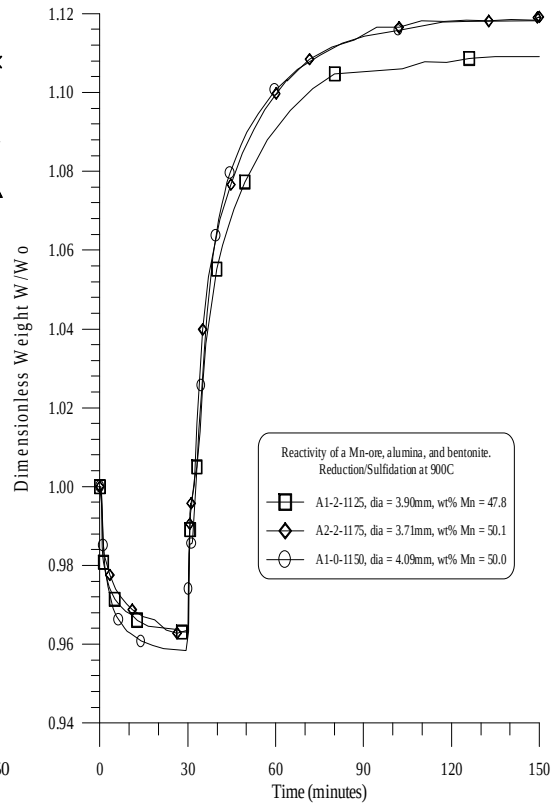

Conclusions

• Pellet strength is primarily determined by induration temperature. All formulations made to date have met the crush strength required. The sensitivity of this parameter requires further optimization.

• Preliminary work appears to indicate titania is a superior substrate than alumina probably because the manganese/titania bond is chemically weaker than the manganese/alumina bond. This means the manganese which is tied up in forming a spinel has a higher activity in the titania form than the alumina form and is more effective in reacting with sulfur.
• Bentonite addition increases the strength of the pellet, however; it reduces the pellet absorption capacity for a given induration condition. Furthermore, it seems as bentonite addition can be avoided by increasing the substrate fraction.

• Current pellet formulations are limited by intra-particle transport resistances. Pore structure design and characterization are to be the direction of additional research through higher substrate fractions and with no bentonite addition.

Future Activities

The last year of this three year program will be devoted to optimizing the most favorable formulations which have been developed with respect to increasing the rate of loading and reducing the loading and the regeneration temperatures.

Acknowledgement

The assistance of Dr. V. Venkataraman, the Contracting Officer's Representative at METC is gratefully acknowledged. The period of performance is from September 1994 to June, 1996.

Catalytic Ammonia Decomposition for Coal-Derived Fuel Gases

Santosh K. Gangwal (skg@rti.org; 919-541-8033)
Raghubir P. Gupta (gupta@rti.org; 919-541-8023)
Jeffrey W. Portzer (jwp@rti.org; 919-541-8025)
Brian S. Turk (bst@rti.org; 919-541-8024)
Research Triangle Institute
3040 Cornwallis Road
Research Triangle Park, NC 27709

Gopala N. Krishnan (gopala_krishnan@qm.sri.com; 415-859-2627)
SRI International
333 Ravenswood Avenue
Menlo Park, CA 94025

Stephen L. Hung (hung@crd.ge.com; 518-387-6895)
Raul E. Ayala (ayala@crd.ge.com; 518-387-5850)
General Electric Corporate Research & Development
Building K-1, P.O. Box 8
Schenectady, NY 12301

Introduction

Advanced coal gasification-based electric power plants such as integrated gasification combined cycle (IGCC) and molten carbonate fuel cell (MCFC) call for hot-gas cleanup following gasification in order to achieve high thermal efficiency. The Morgantown Energy Technology Center (METC) hot-gas cleanup research program has focused on the development of high-temperature removal methods for particulates and chemical contaminants. Chemical contaminants that have received the most attention are sulfur gases, particularly hydrogen sulfide (H_2S). However, other chemical contaminants such as nitrogen compounds, must also be considered in the design of the hot-gas cleanup train.

During gasification, fuel-bound nitrogen in coal is principally released into the coal gas as ammonia (NH_3). When this coal gas is combusted in a gas turbine, NH_3 has the propensity to form oxides of nitrogen (NO_x) which are difficult to remove hazardous pollutants and precursors to "acid rain." In MCFC applications, when the anode exhaust gas is burned with air to supply CO_2 for the regeneration of the carbonate electrolyte, NO_x formed can react with the electrolyte to form relatively volatile nitrates that evaporate resulting in loss of electrolyte. Thus, it is desirable to remove NH_3 from the coal gas before use in IGCC or MCFC applications.

Research sponsored by the U.S. Department of Energy's Morgantown Energy Technology Center, under Contract No. DE-AC21-92MC29011, with Research Triangle Institute, 3040 Cornwallis Road, Research Triangle Park, NC 27709; telefax: 919-541-8000.

According to published data, the NH_3 concentration in coal gas can vary from 200 to 5,000 ppmv depending on the nitrogen content of coal and the configuration and operation of the gasifier. For example, the coal gas from a Texaco entrained-bed coal gasifier gasifying Illinois coal typically contains 1,800 to 2,000 ppmv NH_3. In contrast, a fixed-bed coal gasifier (e.g., Lurgi) typically produces about 5,000 ppmv NH_3 whereas a fluidized-bed coal gasifier (e.g., U-Gas, Kellogg) produces about 1,000 ppmv or less NH_3.

The NH_3 concentration in the exit coal gas appears to depend on the time-temperature history of the gas in the gasifier, with longer residence time at high temperature (~1,000 °C or higher) favoring removal of NH_3 by thermal decomposition [$NH_3 \rightarrow (½)\ N_2 + (3/2)\ H_2$]. However, the NH_3 concentration does not reduce further via thermal decomposition once the fuel gas exits the gasifier because of the low temperature and short residence time in downstream process piping.

One potential approach for enhancing NH_3 decomposition would be to use a heterogenous catalyst in the hot-gas cleanup train to increase the decomposition rate. To be effective, the catalyst must be active in the harsh coal gas environment and resistant to poisoning by H_2S, steam, and other gases.

SRI International identified Ni- and MoS_2-based catalysts capable of decomposing NH_3 in hot coal-derived gas streams (Krishnan et al., 1988). The SRI study showed that, in the absence of H_2S, decomposition of NH_3 can be carried out readily in the temperature range of 550 to 800 °C using Ni-based catalysts. The SRI study demonstrated that HTSR-1, a proprietary Ni-based catalyst on a refractory support from Haldor-Topsoe, exhibited excellent activity and high-temperature stability. However, its tolerance to H_2S was found to be a function of temperature. Above 800 °C, no catalyst deactivation was observed even in gas streams containing 2,000 ppmv of H_2S. At lower temperatures, HTSR-1 deactivated rapidly when significant levels of H_2S were present in the fuel gas. Molybdenum-based catalysts were also investigated as potential NH_3 decomposition catalysts. Both General Electric (Ayala, 1993) and SRI International (Krishnan et al., 1988) have reported on the catalytic role of molybdenum sulfide (MoS_2) in ammonia decomposition.

Objectives

The objective of this study is to develop and demonstrate catalytic approaches for decomposing a significant percentage (up to 90 percent) of the NH_3 present in fuel gas to N_2 and H_2, at elevated temperatures (550 to 900 °C).

Approach

The NH_3 concentration considered in this study was ~1,800 to 2,000 ppmv, which is typical of oxygen-blown, entrained-flow gasifiers such as the Texaco coal gasifier being employed at the TECO Clean Coal Technology Demonstration plant. Catalysts containing Ni, Co, Mo, and W were candidates for the study. Before undertaking any experiments, a detailed thermodynamic evaluation was conducted to determine the concentration of NH_3 in equilibrium with the Texaco gasifier coal gas. Thermodynamic evaluations were also performed to evaluate the stability of the

catalytic phases (for the various catalysts under consideration) under NH_3 decomposition conditions to be used in this study. Two catalytic approaches for decomposing NH_3 have been experimentally evaluated. The first approach evaluated during the early phases of this project involved the screening of catalysts that could be combined with the hot-gas desulfurization sorbents (e.g., zinc titanate) for simultaneous NH_3 and H_2S removal. In a commercial system, this approach would reduce capital costs by eliminating a process step. The second approach evaluated was high-temperature catalytic decomposition at 800 to 900 °C. In a commercial hot-gas cleanup system this could be carried out after radiative cooling of the gas to 800 to 900 °C but up stream of the convective cooler, the hot particulate filter, and the hot-gas desulfurization reactor. Both approaches were tested in the presence of up to 7,500 ppmv H_2S in simulated fuel gas or actual fuel gas from a coal gasifier.

Project Description

Thermodynamic Evaluation

Thermodynamic calculations were performed to determine the concentration of NH_3 in equilibrium with a coal gas stream typical of the Texaco entrained-bed coal gasifier. The range of Texaco gas compositions selected for thermodynamic evaluation and experimental study is shown in Table 1.

The equilibrium concentration of NH_3 in a Texaco coal gas as a function of temperature (500 to 900 °C) and pressure (1 to 20 atm) is shown in Figure 1. As expected, since the ammonia decomposition reaction is endothermic, the concentration of NH_3 decreases with increasing temperature. However, at elevated pressures, the equilibrium levels of NH_3 may be at a maximum at about 600 °C. This characteristic is attributed to a greater level of CH_4 formation at lower temperatures that reduce H_2 concentration. For example, at 500 °C and 20 atm, the calculated equilibrium compositions of CH_4 and H_2 are 28.1 and 2.6 vol%, respectively. In contrast, at 900 °C, the equilibrium compositions of CH_4 and H_2 are 2.31 and 28.7 vol%, respectively. Hence, at temperatures below 600 °C, NH_3 decomposition is favored by the removal of H_2 due to CH_4 formation, and at higher temperatures the equilibrium of the NH_3 decomposition reaction ($NH_3 \rightarrow (½)\ N_2 + (3/2)\ H_2$) begins to determine the equilibrium NH_3 levels. Equilibrium values in Figure 1 indicate that the extent of NH_3 decomposition is thermodynamically limited, but NH_3 decomposition >90 percent is possible in the temperature range of 500 to 900 °C in Texaco gas.

Table 1. Texaco Gasifier Simulated Gas Composition (vol%)

H_2	28.5-31.1
CO	38.0-45.7
CO_2	10.0-12.9
H_2O	12.5-18.1
H_2S	0.5-0.75
NH_3	0.18-0.20
N_2	0.0-1.62

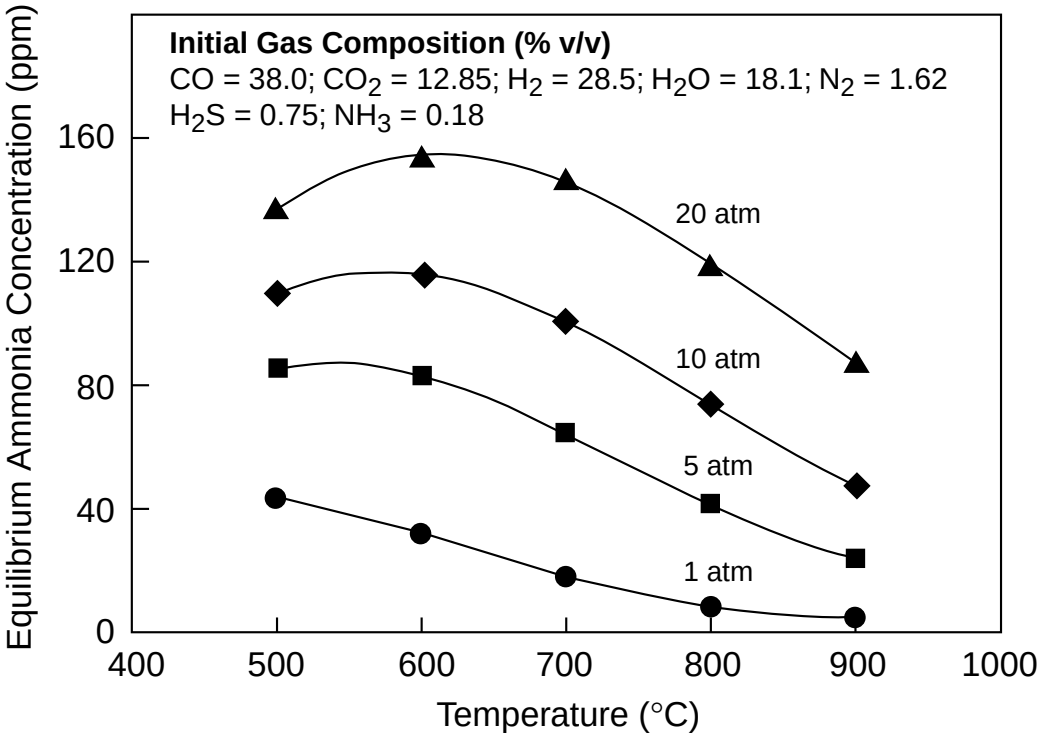

Figure 1. Equilibrium concentration of ammonia as a function of temperature and pressure in a Texaco coal gasifier gas stream.

Thermodynamic calculations were also performed to evaluate the stability of the catalysts and their desirable phases under NH_3 decomposition conditions of interest in this study. For the simultaneous NH_3 and H_2S removal approach, state of the catalyst in reducing, sulfiding, and oxidizing environment was considered. For the high-temperature catalytic decomposition approach, state of the catalyst in reducing and sulfiding environment at high temperature was considered.

The activity of the sulfide-based catalysts (MoS_2, WS_2) for NH_3 decomposition could depend on whether the catalyst can be kept in the sulfided state. Thermodynamic calculations show that MoS_2 will be stable at 723 °C (1,000 K) at an H_2S to H_2 mole ratio of 0.0005 or higher. At the same temperature WS_2 will be stable at ratios higher than 0.001. The product gas stream from the Texaco gasifier contains sufficient H_2S to keep these sulfides stable for the high-temperature catalytic decomposition approach. However, in the simultaneous NH_3 and H_2S removal approach, the zinc titanate sorbent could reduce the H_2S concentration in the bed dramatically. In this environment, the sulfides may reduce to metal as the stable phase which may resulfide once the H_2S concentration increases. Thermodynamic calculations indicate that vapor pressures of the sulfided and metallic states of the catalytic species of interest are insignificant in reducing environment.

In the simultaneous NH_3 and H_2S removal approach, a combined desulfurization sorbent and NH_3 decomposition catalyst need to survive oxidative regeneration. This implies that whatever state they exist in during regeneration, they should not disappear by vaporization. During regeneration, all the catalytic and active sorbent species are likely to be converted to oxide or sulfate.

Based on thermodynamic calculations, the only species among all of the catalytic species with considerable volatility during regeneration was found to be molybdenum oxide. Thermodynamic calculations indicate that Mo_3O_9, Mo_4O_{12}, and Mo_5O_{15} are the dominant vapor species in equilibrium with solid MoO_3 in the temperature range 525 to 825 °C. Equilibrium partial pressures at 625 °C, for example, of Mo_3O_9 and Mo_4O_{12} vapor in the presence of 2 vol% O_2 are 4.4×10^{-6} and 4.1×10^{-6} atm, respectively, which may lead to significant loss of Mo during regeneration. One possible mechanism by which Mo vaporization could be reduced or rendered insignificant is by formation of a bimetallic species involving Mo such as molybdates. Among the five metals (Cu, Co, Fe, Ni, and Zn) considered as possibly capable of forming molybdates, thermodynamic calculations indicated that Cu was the only metal that formed a molybdate above 527 °C (800 K). It effectively reduced the total vapor pressure of Mo-containing species by four orders of magnitude.

Simultaneous NH_3 and H_2S Removal

Several catalysts containing Ni, Co, Mo, and W (with Al_2O_3, TiO_2, and other oxides as supports) were prepared and tested by themselves or in combination with a zinc titanate sorbent. To rank the activities of the new materials prepared, a number of baseline materials were designated. These included HTSR-1 and molybdenum sulfide catalysts (CRC-653 and CRC-530) tested by SRI International (Krishnan et al., 1988), L-3787M, molybdenum-doped zinc titanate developed for the General Electric (GE) moving-bed desulfurization system (Ayala, 1993), and ZT-4, a granulated zinc titanate sorbent prepared by the Research Triangle Institute (RTI) for fluidized beds (Gupta and Gangwal, 1992). The tests were conducted using fixed-bed microreactors at SRI and GE and a 2.0-in. high-temperature, high pressure (HTHP) bench-scale fluidized-bed reactor system at RTI. These systems have been described in detail in a previous paper (Gangwal et al., 1993) and a topical report (Gupta and Gangwal, 1992). Identical analytical systems including a photoionization detector for NH_3 measurement were installed with each reactor system for cross-checking of results.

Unfortunately, none of the catalysts and sorbent-catalysts prepared exhibited significant NH_3 decomposition activity at temperatures up to 725 °C in Texaco coal gas containing up to 7,500 ppmv H_2S. In contrast, the HTSR-1 exhibited significant ammonia decomposition activity at 800 °C or higher in the presence of H_2S. Thus the simultaneous NH_3 and H_2S removal approach was deemphasized in favor of the high-temperature catalytic decomposition approach. Selected highlights of results for the simultaneous NH_3 and H_2S removal approach are presented in the Results section.

High-Temperature Catalytic Decomposition

A number of commercial catalysts, including HTSR-1, were tested for this approach. All tests were conducted using a simulated Texaco gas (Table 1) except for a 100-h test described below at METC using a mobile skid-mounted reactor system. Nonproprietary information about the catalysts tested is presented in Table 2.

Four separate reactor systems have been used for testing these catalysts. Initial screening of these catalysts at atmospheric pressure was conducted using a 1.0-in. quartz reactor system (Gupta and Gangwal, 1992) modified for operation with NH_3 up to 850 °C. Further screening of selected catalysts at high pressure was conducted using a HTHP 2.0-in. quartz reactor system (Krishnan et al., 1995) at RTI. This special reactor system consisted of a quartz insert within a HTHP 316-stainless steel reactor housing so that NH_3 and H_2S came in contact only with the quartz at high temperature.

Finally, two 100-h tests of a selected catalyst were conducted by RTI and GE, respectively. The RTI test was conducted using a mobile skid-mounted reactor facility with a hot slip stream of actual coal gas from the METC 10-in. dia fluidized-bed coal gasifier. This facility is described in detail elsewhere (Gangwal et al., 1994). The schematic of the skid-mounted NH_3 decomposition reactor system used at METC is shown in Figure 2. As seen, the hot coal gas entered a 3.0-in. dia catalytic reactor surrounded by a 3-zone furnace. The nominal composition of the hot-coal gas is shown in Table 3. Reactor pressure was controlled using two back pressure regulators in series with an electronic mass flow meter (MFM) in between. This configuration maintained the reactor pressure at 150 psig and limited the pressure drop across the MFM to within specified limits. The MFM signal was sent to a proportional controller to control coal gas flow rate with a Badger high-temperature flow control valve. The system was designed to run at space velocities up to 5,000 scc/(cc·h) with one liter of catalyst. The inlet and outlet coal gas were sampled for NH_3

Table 2. Catalysts Tested for High-Temperature Catalytic Decomposition Approach

Catalyst Designation	Vendor	Composition/ Support	Bulk Density	Shape/Size
HTSR-1	Haldor-Topsoe	Ni on refractory support	1.6	Cylinder (1/8" × 1/8")
G-47	UCI	3% Fe_2O_3 on SiO_2/Al_2O_3	1.1	Sphere (1/4")
C11-9-02	UCI	12% Ni on ceramic	1.1	Rings (5/16" × 5/16" × 1/8")
C-100 N	CMP	10% Ni on stabilized Al_2O_3	0.5	Powder (90 to 150 μm)

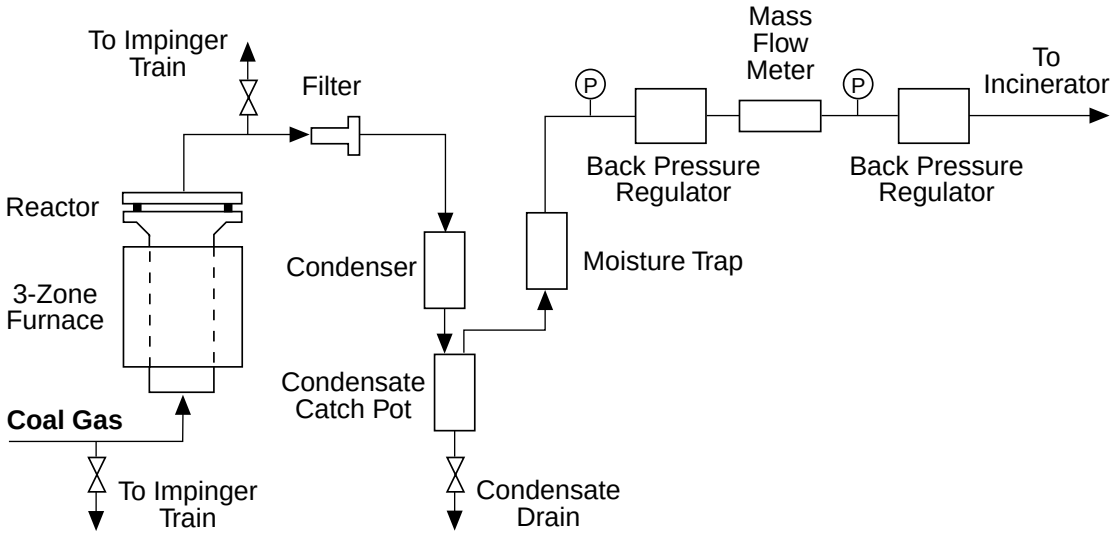

Figure 2. Schematic of skid-mounted reactor system.

measurement (by ion chromatography) using an acidic impinger. Also, condensate samples were periodically collected upstream and downstream to provide an integrated measure of NH_3 and its decomposition.

Table 3. METC Gasifier Coal Gas Composition

	Vol%
CH_4	2.87
H_2S	0.13
H_2	14.14
Ar	0.48
CO_2	11.21
CO	11.87
N_2	48.50
H_2O	10.47
NH_3	0.33

The GE 100-h test was conducted using a bench-scale reactor system shown in Figure 3, with simulated coal gas at 900 °C and 8.5 atm. Due to high operating temperature and high H_2S levels to be used (7,500 ppmv), the reactor was made from a 3/4-in. nominal pipe using a HR-160 material (a highly sulfur resistant material from Haynes International). The reactor had an inside diameter of 2.15 cm and the system was designed to operate continuously at 900 °C with space velocities of up to 10,000 scc/(cc·h). The analytical system was similar to that for the RTI system described above.

Results

Simultaneous NH_3 and H_2S Removal

Numerous catalysts were prepared and tested for this approach. These catalysts are summarized in Table 4. Nearly all the tests were performed at 725 °C, which was initially the target test temperature.

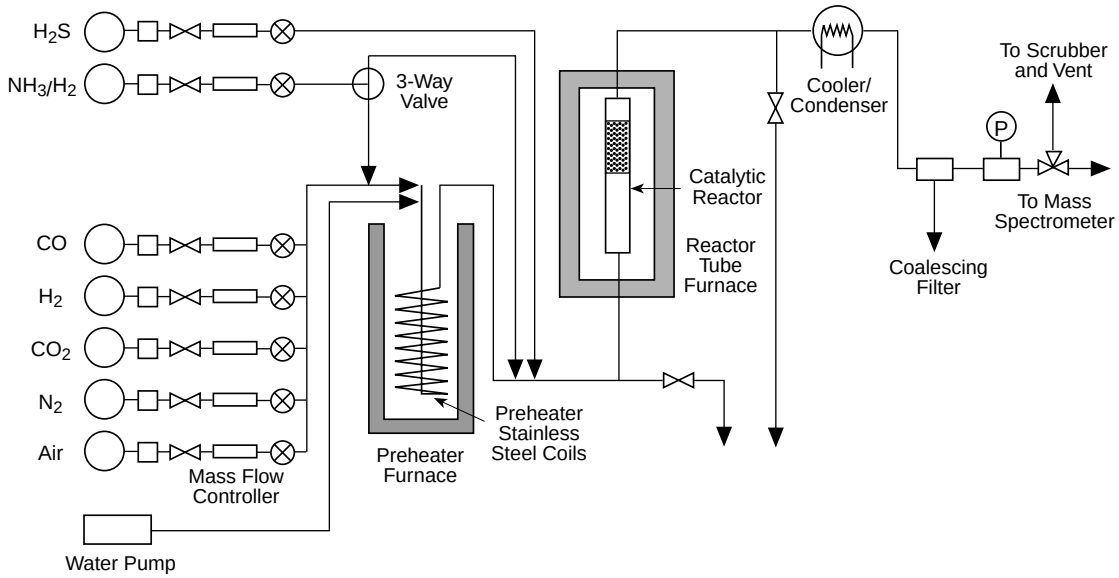

Figure 3. GE-CRD bench-scale ammonia decomposition reactor system.

Table 4. Catalysts Tested for Simultaneous NH_3 and H_2S Removal

HTSR-1 + ZT-4 (zinc titante)	Co/TiO_2
MoS_2 (CRC-653)	Mo/TiO_2
MoS_2 (CRC-530)	$Co\text{-}Mo/TiO_2$ + ZT-4
ZT-4	W/TiO_2
Ni/TiO_2 - ZrO_2	$W\text{-}Mo/TiO_2$
$Ni\text{-}Mo/TiO_2$ - ZrO_2	ZnO - WO_3
Co-Mo-L-3787M (zinc titanate)	$Co\text{-}ZnO\text{-}WO_3\text{-}ZrO_2$

Highlights of the results are as follows:

- HTSR-1 exhibited excellent activity for NH_3 decomposition in simulated Texaco gas without H_2S, at 725 °C. With H_2S the catalyst was poisoned but the activity could be restored at 800 °C even in the presence of H_2S.

- MoS_2-based catalysts show low activity for NH_3 decomposition. Surface area stabilization with ZrO_2 was necessary for these catalysts to have any activity at all.

- The catalysts containing Ni, Co, Mo, and W on a high surface area TiO_2 support showed moderate activity (typically 10 to 20 percent decomposition) for NH_3 decomposition at 725 °C. The TiO_2 support sintered extensively at 725 °C and required stabilization with ZrO_2.

- Mixing the Ni, Co, Mo, and W catalysts with zinc titanate sorbent allowed the catalysts to function longer. As the sorbent got loaded with H_2S, the exit H_2S level increased, thereby decreasing the activity for NH_3 decomposition.

High-Temperature Catalytic Decomposition

Screening Tests. Results are presented for catalyst screening and the two 100-h tests described earlier. Figure 4, which shows an activity comparison for the three fixed-bed catalysts in Table 2, clearly indicates the superiority of HTSR-1. In a separate experiment with C11-9-02 at 850 °C and atmospheric pressure, the inhibiting effect of H_2S-containing coal gas components was evaluated. It was found that replacing coal gas with N_2 increased the activity of C11-9-02 from about 40 percent decomposition to >90 percent decomposition. This phenomenon was reversible, i.e., when coal gas was restored, the activity fell back to around 40 percent decomposition. The number of catalysts to be tested further was narrowed at this point to HTSR-1 (for fixed beds) and C-100N (for fluidized beds).

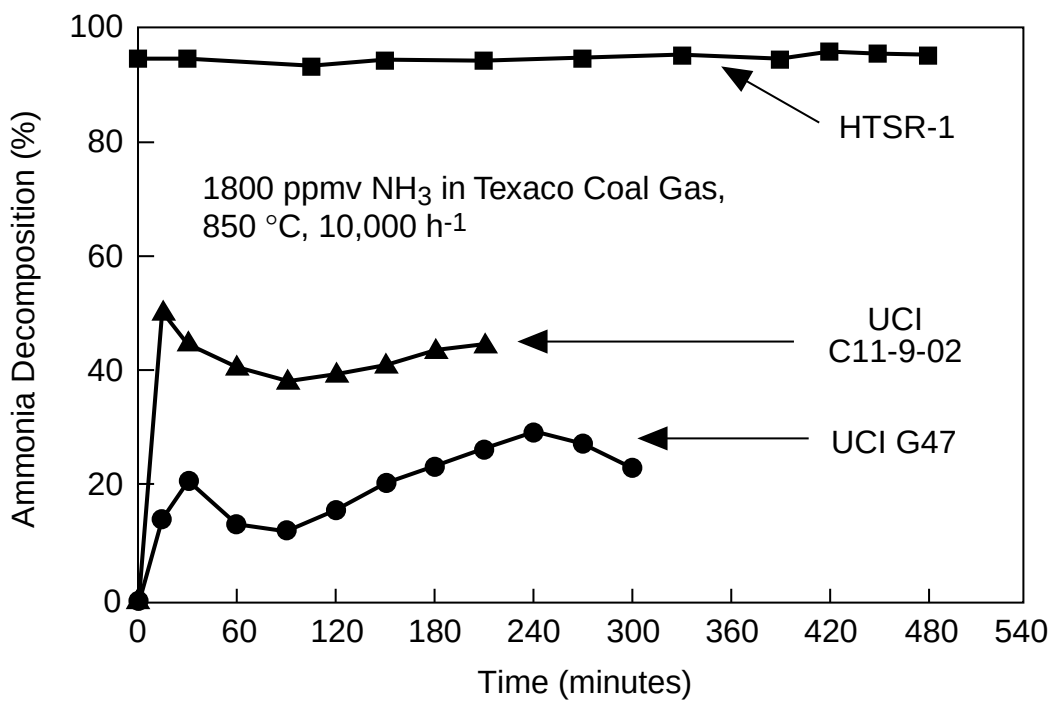

Figure 4. Activity comparison for HTSR-1, UCI C11-9-02, and UCI G47.

The ability of HTSR-1 to increase throughput was evaluated by testing it in Texaco gas at a space velocity of 20,000 scc/(cc·h), 1 atm, and 850 °C. Under these conditions, the conversion ranged between 54 and 70 percent over a 50-h test. Screening tests at high pressure were then initiated for HTSR-1 and C100-N.

The results of screening tests at 11.2 atm are shown in Figures 5 and 6. Figure 5 showed that under identical conditions, the HTSR-1 was better than C-100N. The decomposition over HTSR-1 was initially about 75 percent and stabilized at around 50 to 60 percent. But, the decomposition on C-100N decayed exponentially, indicating that under these conditions the catalyst was continuing to deactivate. Another interesting experiment to evaluate the effect of H_2S was conducted in the steady-state regime for HTSR-1 as shown in Figure 6. For a period of time, H_2S was removed from the coal gas. This increased the activity to around 90 percent decomposition. When H_2S was restored, the activity very quickly fell back to its earlier steady-state value. This result clearly indicates partial but reversible poisoning of NH_3 decomposition sites at 850 °C by H_2S.

100-h Tests

The results of the RTI 100-h test at METC with actual coal gas (Table 3) is shown in Figure 7. The conditions used for this test were 146 psig (10.8 atm), 780 °C, and 4,975 scc/(cc·h) space velocity. During the test period, ammonia decomposition averaged 91.7 percent based on impinger sampling and 87.4 percent based on condensate sampling. No catalyst deactivation was

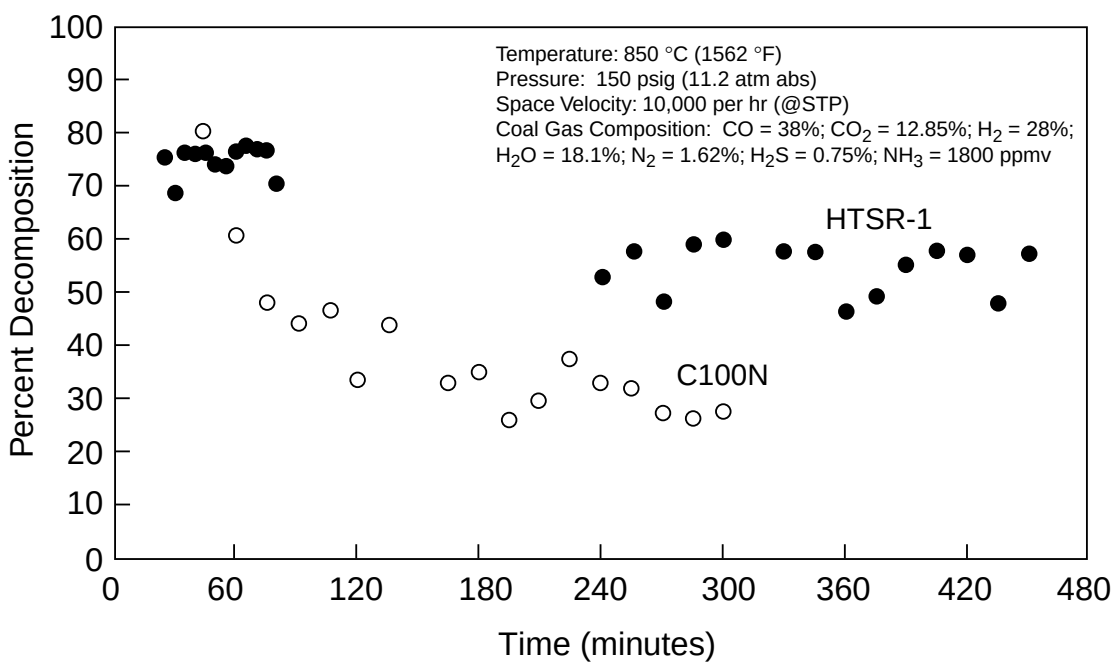

Figure 5. Comparison of high-temperature ammonia decomposition on HTSR-1 and C-100N catalysts.

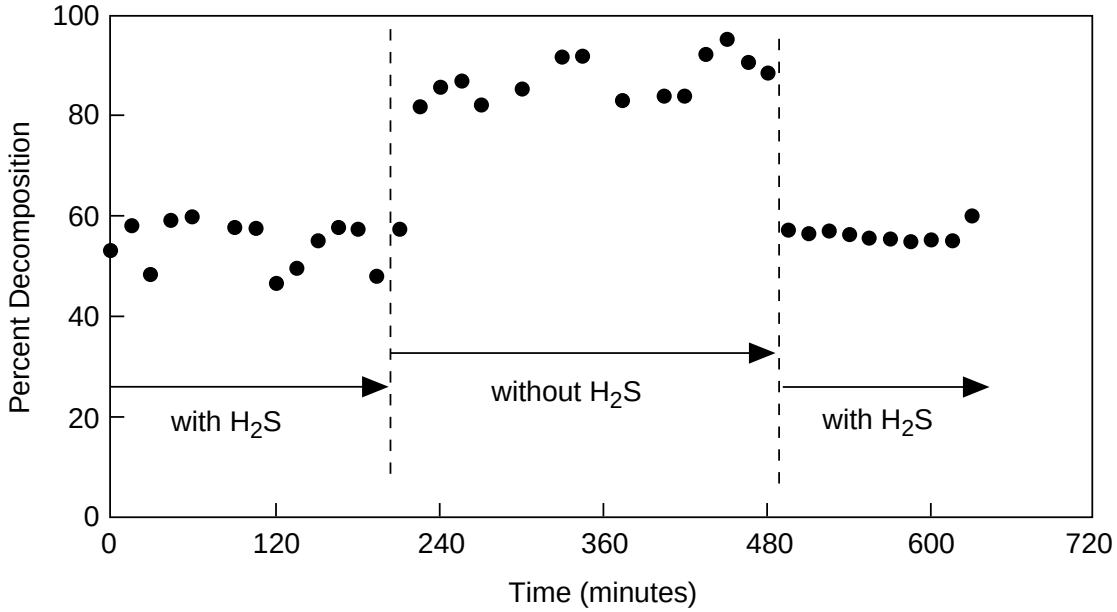

Figure 6. Effect of H_2S on ammonia decomposition by HTSR-1 catalyst.

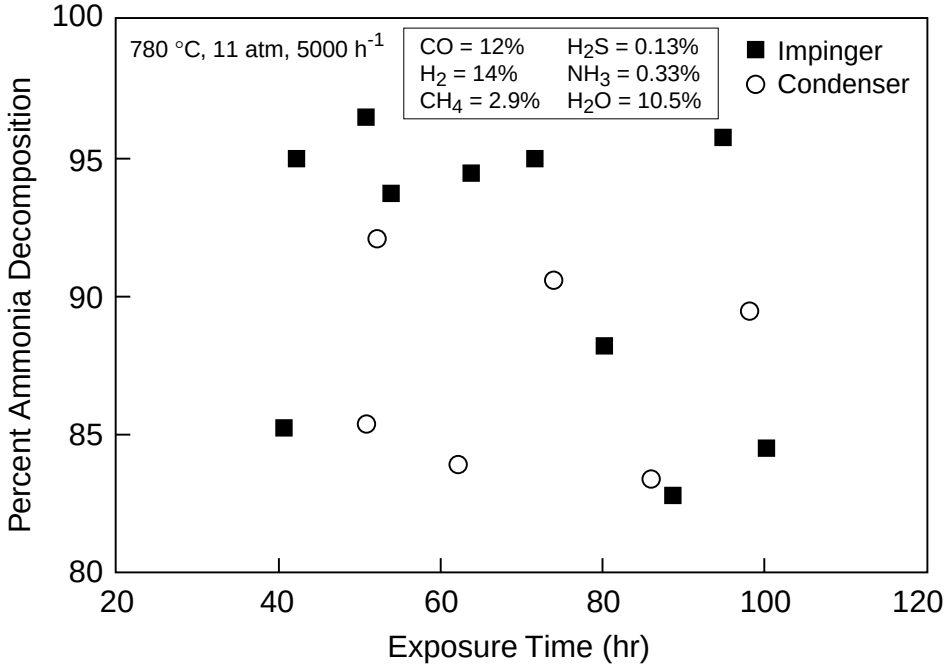

Figure 7. RTI 100-h test-ammonia decomposition on HTSR-1 catalyst.

observed over the test. One interesting observation was made during the test. The reactor inlet coal gas preheated to 850 °C dropped in temperature to 780 °C in the bed. N_2 under identical preheat and flow conditions remained at 850 °C in the bed. This suggests that an endothermic reaction may be occurring to absorb heat.

The results of the GE 100-h test carried out using a simulated Texaco gas (containing 7,500 ppmv H_2S) at 8.5 atm, and 900 °C are shown in Figure 8. The average inlet NH_3 on a dry basis was 1,950 ppmv (or ~1,550 ppmv on a wet basis). During operation at a space velocity of 10,000 h^{-1}, the average outlet NH_3 concentration was reduced to 310 ± 100 ppm (wet) over the course of the run to give an NH_3 conversion of 80 percent. At a reduced space velocity of 5,000 h^{-1}, outlet NH_3 concentration was further reduced to 200 ± 40 ppm to give an NH_3 conversion of 88 percent. Under the test conditions, equilibrium limitations were not present since the equilibrium NH_3 was estimated to be 10 to 11 ppm.

During the first 40 hours of the test, some catalyst deactivation was seen, but the activity stabilized thereafter. When the reactor was sawed apart at the end of the test, it was found that a single layer of catalyst pellets had fused against the reactor walls. This layer closed off a fraction of the flow area in the tube and may have contributed to the decrease in activity over the first 40 hours. Although no further analyses were made, other factors, such as catalyst sintering may have also contributed to the initial loss of activity.

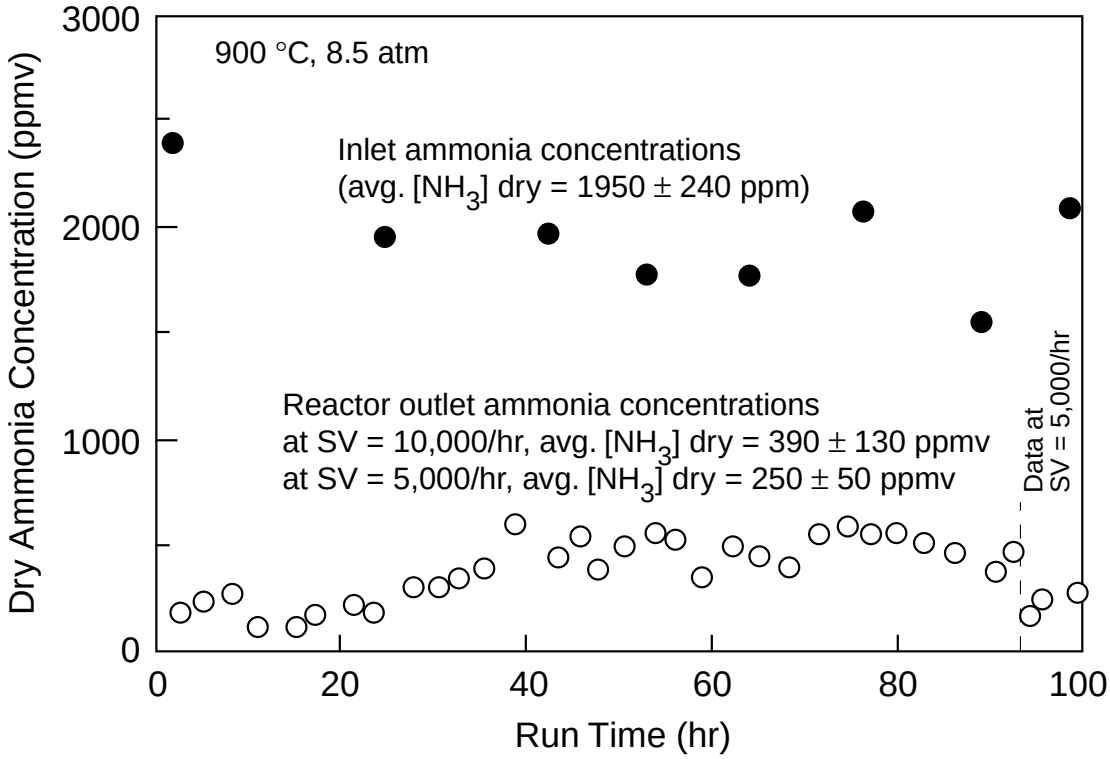

Figure 8. GE 100-h test-ammonia decomposition on HTSR-1 catalyst.

Applications

The two 100-h tests demonstrate that HTSR-1, a nickel-based catalyst on a refractory support, is capable of decomposing up to 90 percent of the NH_3 in typical coal gasifier gases. Further work is needed to reduce the cost of the catalyst and develop it in a form, such as monolith, that could operate in the presence of particles. Also continued research is needed for development of catalysts that would work at relatively lower temperatures down to 500 °C. Alternative technologies to catalytic decomposition include the use of conventional selective catalytic reduction (SCR) past the turbine at low pressure or using modified advanced turbines that could reduce NO_x emissions. Because of the low pressure, high volumetric flow rates, and low NO_x concentrations, the SCR approach is likely to be very expensive. While work is ongoing on the turbine modifications approach, it will be difficult to achieve a very high level, i.e., > 90 percent, NO_x reduction in large-scale applications using this approach because of difficulties in scaleup.

Future Activities

Discussions are under way for development of an H_2S-resistant material that could be effective at temperatures as low as 500 °C for simultaneous H_2S removal and NH_3 decomposition. A topical report will be submitted to METC summarizing the work to date.

Acknowledgments

The authors gratefully acknowledge the guidance and assistance of Mr.. Ron K. Staubly, the METC Contracting Officer's Representative. Subcontract support is provided by SRI International and General Electric Corporate Research and Development. Haldor Topsoe and UCI provided catalysts free of cost for testing. The contract period of performance is from September 29, 1992 to January 31, 1997.

References

Ayala, R.E. 1993. "Molybdenum-Based Additives to Mixed-Metal Oxides for Use in Hot-Gas Cleanup Sorbents for the Catalytic Decomposition of Ammonia in Coal Gas." U.S. Patent 5,188,811.

Gangwal, S.K., R. Gupta, G.N. Krishnan, and S.L. Hung. 1993. "NH_3/H_2S Advances." *Proceedings of the Coal-Fired Power Systems '93—Advances in IGCC and PFBC Review Meeting*, p. 399, DOE/METC - 93/6131 (DE93000289).

Gangwal, S.K., J.W. Portzer, G.B. Howe, D.H. Chen, and M.H. McMillan. 1994. "Slip-Stream Testing of the Direct Sulfur Recovery Process." In *Proceedings of the Coal-Fired Power Systems '94—Advances in IGCC and PFBC Review Meeting*, p. 246, DOE/METC - 94/1008, Vol. 1 (DE94012252).

Gupta, R.P., and S.K. Gangwal. 1992. “Enhanced Durability of Desulfurization Sorbents for Fluidized-Bed Applications—Development and Testing of Zinc Titanate Sorbents.” Topical Report to DOE/METC. Report No. DOE/MC/25006-3271. November.

Krishnan, G.N., B.J. Wood, A. Canizales, R.P. Gupta, S.D. Shelukar, and R.E. Ayala. 1995. “Development of Disposable Sorbents for Chloride Removal from High-Temperature Coal Derived Gases.” In *Proceedings of the Advanced Coal-Fired Power Systems ‘95 Review Meeting*, p. 631, DOE/METC–95/1018. Vol. 2. (DE95009733).

Krishnan, G.N., B.J. Wood, G.T. Tong, and J.G. McCarty. 1988. “Study of Ammonia Removal in Coal Gasification Processes.” Final Report to U.S. DOE/METC. Contract No. DE-AC21-86MC23087. September.

Decomposition of Ammonia in IGCC Fuel Gas Streams

Shaik A. Qader (909) 466-6266
Qusro A. Qader (9o9) 466-6266
Energy and Environmental Technology Corporation
11609 Treviso Way
Rancho Cucamonga, California 91701

Lawrence J. Muzio (714) 859-4466
Fossil Energy Research Corporation
22342C South Pointe
Laguna Hills, California 92653

Introduction

Integrated Coal Gasification Combined Cycle (IGCC) technology has the potential to emerge as an efficient and environmentally clean technology for generation of power from coal. Development of processes to clean coal gas at high temperatures prior to its combustion in gas turbines improves efficiency and economics of IGCC technology. Particulate, NH_3, and H_2S comprise the main impurities of coal gas.

During combustion, NH_3 present in coal gas is oxidized to NO_X which necessitates NO_X removal from gas turbine exhaust using the expensive Selective Catalytic Reduction (SCR) process (Refs. 1-3). Decomposition of NH_3 present in coal gas at high temperatures prior to combustion results in higher IGCC efficiency and lower costs.

Ammonia can be removed from coal gas by scrubbing the gas with water or H_2SO_4 at a low temperature of 1500F (Ref. 4). Ammonia present in the flue gas of a large incinerator operating in Switzerland was reduced by injection of methanol at high temperatures in the range 1300-20000F (Ref. 5). Research on catalytic decomposition of NH_3 at high temperatures is also being carried out at Research Triangle Institute under DOE sponsorship (Ref. 6).

The Energy and Environmental Technology Corporation (EETC) is developing processes to decompose NH_3 at high temperatures, Bench-scale tubular flow reactors operating isothermally have been used to test two new approaches,

Objective

The main objective of the research work is to develop technically feasible and potentially low cost processes to decompose NH_3 present in coal gases at high temperatures upstream of the gas turbine. Specific objectives of the work include development of NH_3 decomposition processes applicable to both air-blown and oxygen-blown coal gasification-based combined cycle power plants,

Technical Approach

Ammonia decomposition tests were carried out in a bench-scale tubular flow reactor shown in Figure 1. The flow system includes feed gas supply with flow control and pressure regulation, preheater and reactor, heaters, monitoring and control of system temperature and pressure, and feed and product anal ysis instrumentation. Non-catal ytic NH_3 decomposition tests were carried out in both Alloy RA-330 and quartz reactors. Catalytic tests were conducted only in the quartz reactor.

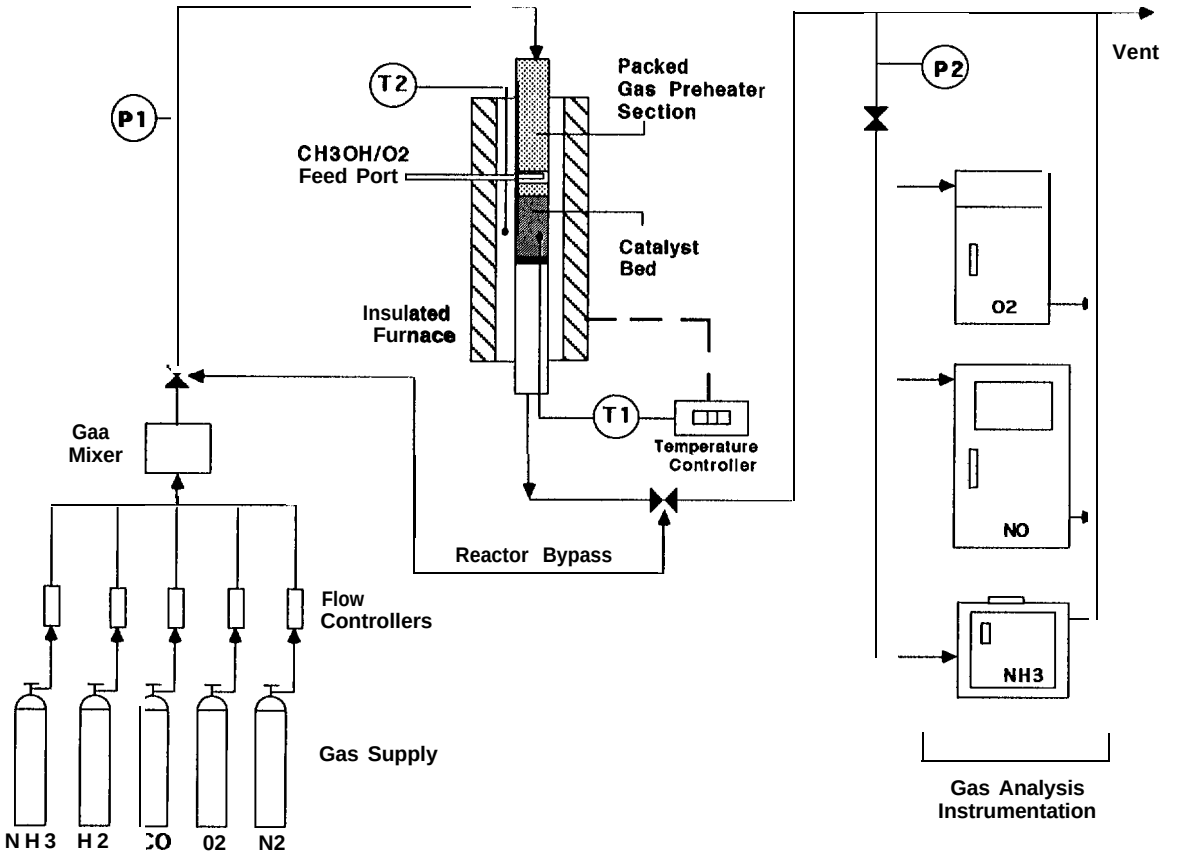

Figure 1. Schematic of Bench-Scale Flow System

Alloy RA-330 and quartz reactors of 0.25 in, -0.35 in. I.D. and 24 in. -36 in. length were used. The alloy and quartz reactors employed for non-catalytic NH_3 decomposition tests were packed with alloy and quartz packing, respectively, having an average diameter of 3 mm. For the catalytic tests, the quartz reactor was packed with alumino-silicate catalyst particles of 3-4 mm diameter.

Tests were carried out in three temperature ranges: 800- 10OOOF, 1200- 13000F, 1600”-18000F. The non-catalytic tests were performed in the two higher temperature ranges, and the catalytic tests were carried out in the lower temperature range. Ammonia decomposition tests were also carried out in the presence of H_2 and CO. Oxygen was used in the catalytic decomposition tests. Tests were designed to obtain data applicable to air-blown as well as oxygen-blown coal gasification-based IGCC systems. Gas analyses were done by standard methods.

Project Description

Two processes have been developed for decomposition of ammonia present in coal gases. In the first process, NH_3 undergoes decomposition on the surface of Alloy RA-330 in the temperature ranges of 1200- 13000F and 1500- 16000F. In the second process, NH_3 undergoes decomposition on the surface of an alumino-silicate catalyst in the temperature range of 800-10000F.

RA-330 Promoted Decomposition (RAPD) Process

Figure 2 shows the basic RAPD process concept. In this concept, coal gas containing NH_3 enters a reactor packed with RA-330 honeycombs in the temperature ranges of 1200- 13000F and 1500- 16000F. Ammonia is decomposed on the surface of RA-330 honeycomb. Some NH_3 may decompose in the gas phase. The technical feasibility of the concept was established by tests performed in the flow system using a RA-330 tubular reactor packed with RA-330 packing of 3-4 mm diameter pieces. The packing was used to provide surface for NH_3 decomposition, Tests were carried out in the presence and absence of methanol.

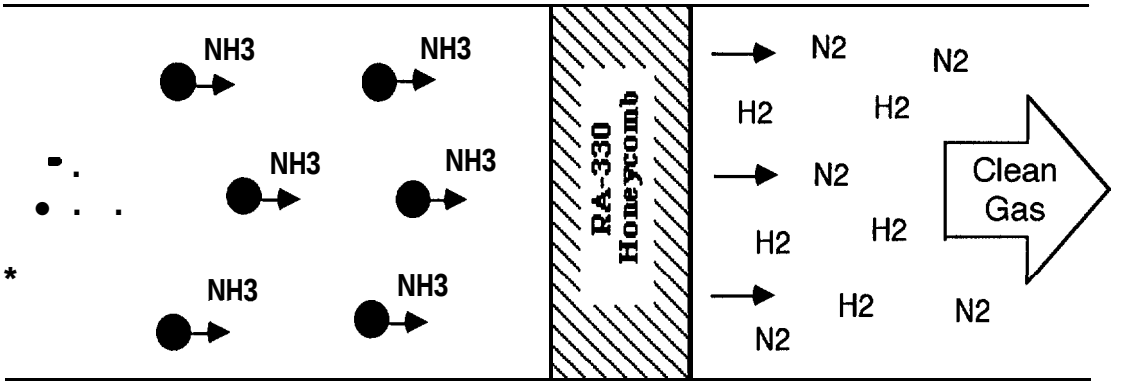

Figure 2. Basic RAPD Process Concept

Table 1 contains data which were obtained with methanol injection in the RA-330 reactor. The data show that total NH_3 conversion increases from 95% at 10OOOF to greater than 99% at 13000F and above. However, 76% and 65% of the NH_3 was converted to amine as an intermediate product at 10000 and 12000F respectively. But at 13000F and above, all the NH_3 was ultimately decomposed to N_2 and H_2. If any amine was formed as an intermediate product, it may have decomposed at the higher temperatures. The data of Table 1 led to the conclusion that most of the NH_3 is converted to amine at temperatures in the range 1000- 12000F. At temperatures of 13000F and higher, NH_3 and any possible amine undergoes decomposition to nearly 10OO/O.

Table 1: Effect of Temperature on Ammonia Decomposition in RA-330 Reactor

CH_3OH/NH_3 moles = 1.0
Residence Time = 0.6- 0.8 sec.

Temperature (o)F	Total NH_3 Conversion (%)	NH_3 Conversion to Amine (%)
1000	**95**	**76**
1200	97	65
1300	>99	Trace
1600	>99	--
1800	>99	--

Table 2 contains data which were obtained with methanol injection in the quartz reactor. The total NH_3 conversions obtained at 1300 and 16000F are lower than the corresponding conversions obtained in the RA-330 reactor. Even at these high temperatures, most of the NH_3 is converted to amine which did not undergo decomposition.

Table 2: Effect of Temperature on Ammonia Decomposition in Quartz Reactor

CH_3OH/NH_3 moles = 1.0
Residence Time = 0.5- 0.6 sec.

Temperature (oF)	Total NH_3 Conversion (%)	NH_3 Conversion to Amine (%)
1300	80	70
1600	91	82
1800	>99	41

Table 3 contains data which were obtained in the RA-330 reactor without methanol injection. NH_3 decomposition of close to 100% was obtained at 13000F, 16000F and 18000F, which indicates that NH_3 decomposes directly to N_2 and H_2 on the surface of RA-330 which promotes the decomposition reaction.

Table 3: Effect of Temperature on NH_3 Decomposition

Reactor = RA-330 Alloy **Residence Time = 0.8 -1.0 sec.**

Temperature (oF)	NH_3 Decomposition (%)
1000	27
1200	44
1300	>99
1600	>99
1800	>99

The data of Tables 1-3 led to the conclusion that NH_3 decomposition by reaction with CH_3OH is not technically feasible due to the formation of amine as an intermediate product. The data also led to the conclusion that NH_3 can be completely decomposed on the surface of RA-330 without addition of CH_3OH.

Table 4 contains data which were obtained in the RA-330 alloy reactor at 1300 and 16000F in the presence of H_2 and CO. Hydrogen present in the gas reduces NH_3 decomposition. At 13000F, NH_3 decomposition decreases from greater than 99% at 0% H_2 to 85% at 19% H_2 and to 76% at 34% H_2. At 1600oF, NH_3 decomposition decreases from >99% at O% H_2 to 92% at 20!% H_2 and to 84% at 3 5°/0 H_2. Carbon monoxide does not seem to have any significant effect on NH_3 decomposition.

Table 4: Effect of H_2 and CO on Ammonia Decomposition

Reactor = RA-330 Alloy
Residence Time = 0.8 -0.9 sec.

Temperature (oF)	H_2 Concentration (%)	CO Concentration (%)	NH_3 Decomposition (%)
1300	19	0.0	85
1300	34	0.0	76
1600	20	0.0	92
1600	35	0.0	84
1300	20	30	86
1600	30	32	88

Application of RAPD Ammonia Decomposition Process

The test data of Tables 1-4 were evaluated to determine applicability of the RAPD concept for decomposition of NH_3 present in coal gas at high temperatures before the gas is fed to the gas turbine. The evaluation showed that the RAPD process is technically feasible and is applicable for decomposition of NH_3 present in coal gas at high temperatures upstream of the gas turbine. Figures 3 and 4 contain conceptualized schematics of the RAPD process.

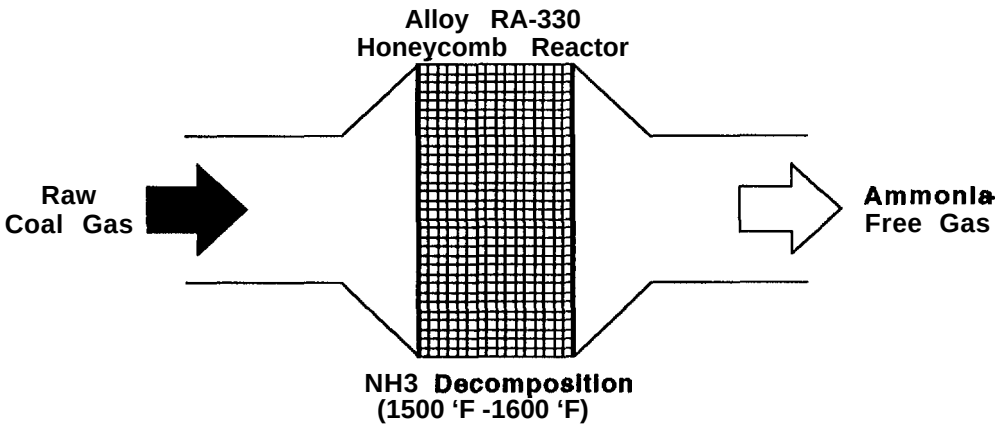

Figure 3. Schematic of High Temperature RAPD Process for NH3 Decomposition

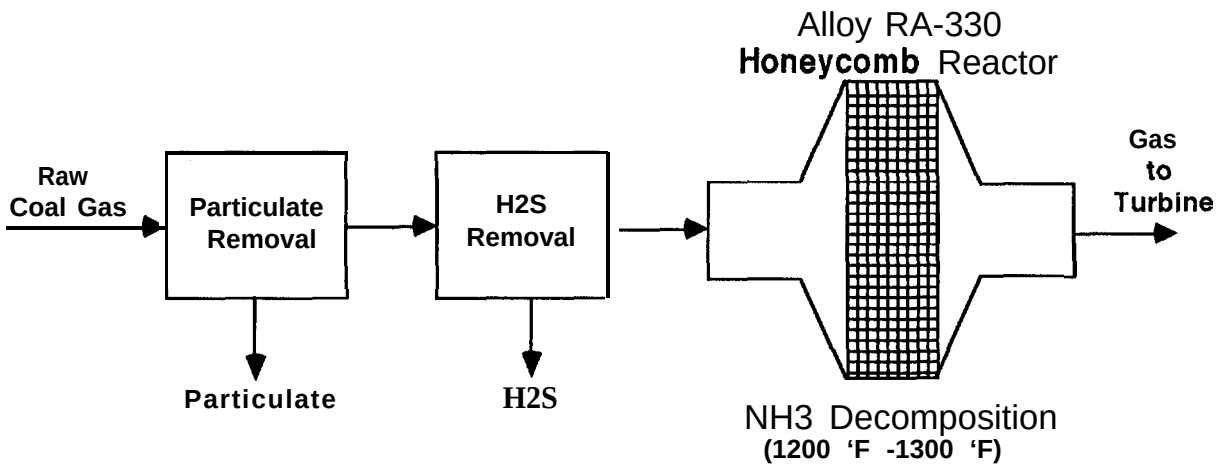

Figure 4. Schematic of Low Temperature RAPD Process for NH3 Decomposition

In the process scheme of Figure 3, coal gas enters the NH_3 decomposition reactor which contains a packed bed of RA-330 honeycombs at a temperature of 1500 - 16000F. Ammonia decomposes to N_2 and H_2 on RA-330 surface which promotes decomposition. In the process scheme of Figure 4, coal gas, after removal of particulate and H_2S, enters the NH_3 decomposition reactor which contains a packed bed of M-330 honeycombs at a temperature of 1200-13 00°F. Ammonia decomposes to N_2 and H_2 on RA-330 surface which promotes decomposition,

Table 5 contains NH_3 decomposition data applicable to IGCC technology. Ammonia decomposition depends upon temperature and H_2 concentration in the coal gas. At H_2 concentration of 19-20°/0, which is characteristic of air-blown coal gasification processes, NH_3 decomposition of 80-85% can be obtained at 1200- 13000F. At H_2 concentration of 30-35%, which is characteristic of oxygen-blown coal gasification processes, NH_3 decomposition of 85-90% can be obtained at 1500 - 16000F.

Table 5: RAPD Ammonia Decomposition Process - Application to IGCC Technology

Temperature (oF)	H_2 Concentration (%)	NH_3 Decomposition (%)	Potential Application
1200-1300	19-20	80-85	Air-blown gasification based IGCC technology
1500-1600	30-35	85-90	Oxygen-blown gasification based IGCC technology

These NH_3 decomposition percentages are calculated from raw experimental data. There is potential to improve NH_3 decomposition rates by providing more surface for decomposition and by optimizing process conditions,

Catalytic Ammonia Removal (CAR) Process

Figure 5 contains a schematic of the CAR process for removal of NH_3 from coal gas. In this process, coal gas free of particulate and H_2S enters the reactor in the temperature range of 800-1000°F. Air or oxygen is injected into the gas stream before it enters the catalyst bed. The process uses commercially available honeycomb catalysts, The technical feasibility of the process was established by performing tests in the flow system (Figure 1) using a quartz tube packed with an alumino-silicate catalyst of 3-4 mm pieces cut from a honeycomb. Tests were carried out in the temperature range of 850- 10000F in the presence of H_2 and O_2.

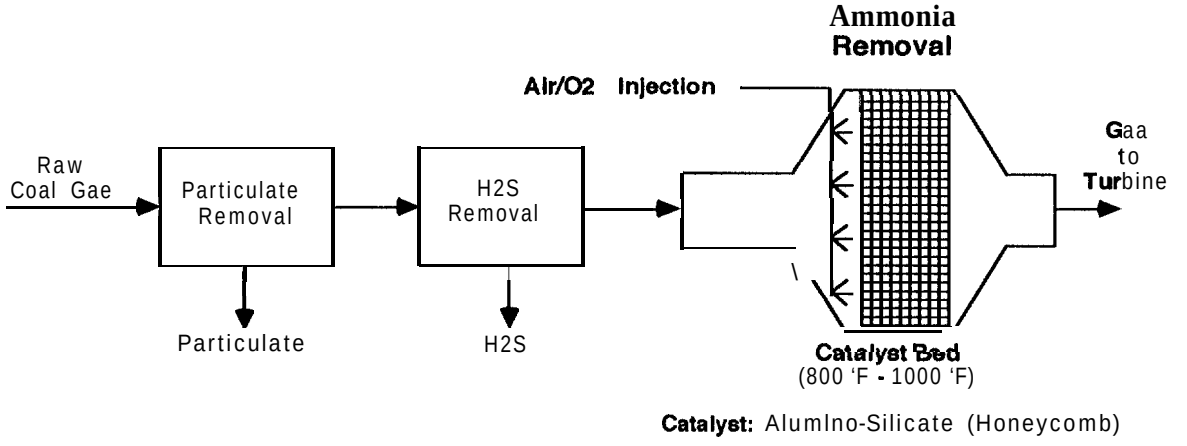

Figure 5. Schematic of Catalytic Process for NH3 Removal

Figure **6** contains process data obtained at 8500F and residence time of 0.5 -0.6 seconds. The data show that NH_3 conversion decreases with increase in hydrogen concentration but increases with increase in O_2 concentration. At H_2 concentration of 10-20°/0, 85-90°/0 of NH_3 can be removed by maintaining O_2 concentration of 2.0- 2.5%. At H_2 concentration of 30-35%, NH_3 conversion of only 50-70°/0 was obtained in the same O_2 concentration range. More O_2 is required to get higher ammonia conversion at higher H_2 concentration.

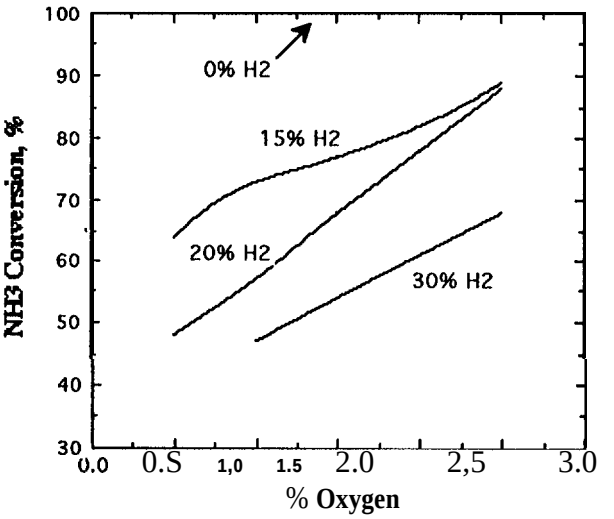

Figure 6. Effect of H2 and 02 on NH3 Removal at 850 F

Figure 7 contains process data obtained at 9000F and residence time of 0.5 -0.6 seconds, The data show similar effects of H_2 and 0_2 on NH_3 removal as the data of 8500F showed. Ammonia removal decreases with H_2 concentration but increases with O_2 concentration, However, higher NH_3 conversions were obtained at 9000F when compared to conversions obtained at 850°F. At H_2 concentration of 10-20°)6, 85-95°A of NH_3 can be removed by maintaining O_2 concentration of 2.0-2.5%. At H_2 concentration of 30-35%, 65-70% of NH_3 can only be removed at O_2 concentration of 2.0- 2.50/o.

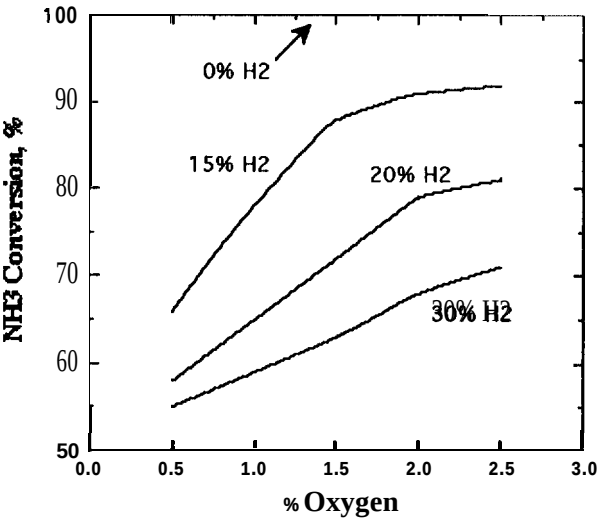

Figure 7. Effect of H2 and 02 on NH3 Removal at 900 F

Figure 8 contains process data obtained at 950 and 1000oF at H_2 concentration of 35%. At 9500F, NH_3 removal of 70-80% was obtained at 0_2 concentration of 2.0- 2.5%. Ammonia removal has increased at 10000F. At O_2 concentration of 2.0- 2.5%, NH_3 removal of 85-95% was obtained.

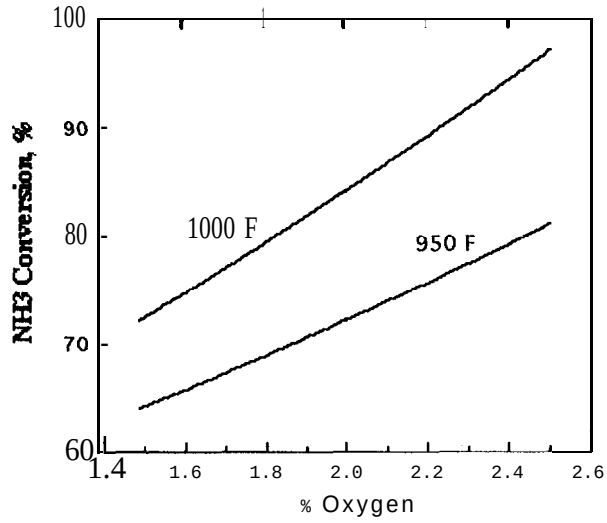

Figure 8. Effect of Temperature and 02 on NH3 Removal with 35% HZ

Application of Catalytic Ammonia Removal Process

The catalytic conversion data presented in Figures 6-8 and Table 6 show that the process has potential applications for NH_3 removal from both air-blown and oxygen-blown gasification based IGCC technologies. For air-blown gasification based application, 80-90% of NH_3 can be removed in the temperature range of 850- 9000F. For oxygen-blown gasification application, 85-95°/0 of NH_3 can be removed in the temperature range of 950- 10000F. In both cases, O_2 concentration of 2.0-2.5% **is** required.

Table 6: Catalytic Ammonia Removal Process - Application to IGCC Technology

Hydrogen Concentration (%)	Temperature (oF)	Oxygen Concentration (%)	Ammonia Removal (%)	Potential Application
15-20	**850-900**	**2.0- 2.5**	**80-90**	Air-blown gasification based IGCC technology
30-35	**950-1000**	2.0- 2.5	85-95	Oxygen-blown gasification based IGCC technology

There is potential to further improve NH_3 conversion by increasing residence time and optimizing process conditions.

Accomplishments

The Energy and Environmental Technology Corporation developed two new process concepts for decomposition/removal of ammonia present in IGCC fuel gas streams. Bench-scale test data showed that the process concepts are technically feasible and are applicable to both air-blown and oxygen-blown coal gasification based IGCC technologies. The processes have potential for decomposing/removing ammonia by more than 90%.

Future Activities

More work needs to be done to determine the full potential of the NH_3 decomposition/removal processes. More bench-scale tests and scale-up of the processes are required to determine viability for practical applications. Cost estimates of the processes have to be made to determine cost saving potential when compared to removal of NO_X from gas turbine exhausts of IGCC plants.

Acknowledgement

Research sponsored by the U. S. Department of Energy's SBIR Program under grant FG03-95ER8 1964 with Energy and Environmental Technology Corporation.

References

1. Schonbucher, B., *Reduction of Nitrogen Oxides from Coal-Fired Power Plants by Using the SCR Process. Experience in the Federal Republic of Germany with Pilot and Commercial Scale DeNO$_X$ Plants,* Proceedings of 1989 Symposium on Stationary Combustion Nitrogen Oxide Control, EPRI GS-6423, Vol. 2, 1989, p. 6A-1 to 6A-17.

2. Mori, T., and Shimizu, N., *Operating Experience of SCR Systems at EPDC's Coal-Fired Power Station,* Proceedings of 1989 Symposium on Stationary Combustion Nitrogen Oxide Control, EPRI GS-6423, Vol. 2, 1989, p. 6A-85 to 6A-104.

3. Roble, C. P., and Ireland, P. A., *Technical Feasibility and Cost of Selective Catalytic Reduction (SCR) NO$_X$ Control,* EPRI GS-7266, 1991.

4. Kohl, A., and Riesenfeld, F., *Gas Purification,* 4th Edition, Gulf Publishing Company, Houston, 1985.

5. Jones, D. G., et al., *Two Stage DeNO$_X$, Process Test Data from Switzerland's Largest Incineration Plant,* EPRI Report GS-6423, Vol. 2, 1989.

6. Stanby, R. K., *High Temperature Catalytic Ammonia Decomposition for Reducing Fuel Bound NO$_X$ in Integrated Gasification Combined Cycle Plants,* METC Internal Document, April 21, 1994.

Assessment of Hot Gas Contaminant Control

Michael D. Rutkowski (GC!GHMAIL02!A6575@gilcom.attmail.com; 610.855.2698)
Michael G. Klett (GC!GHMAIL02!A4712@gilcom.attmail.com; 610.855.2854)
Roman Zaharchuk (GC!GHMAIL01!A9975@gilcom.attmail.com; 610.855.2689)
Parsons Power Group Inc.
2675 Morgantown Road
Reading, PA 19607

Introduction

The National Research Council's (NRC) Committee on the Strategic Assessment of the DOE's Coal Program was asked to recommend the emphasis that DOE ought to consider in updating its coal program to respond to the Energy policy Act of 1992. The advanced coal-based Integrated Gasification Combined Cycle (IGCC)and Pressurized Fluidized Bed Combustion (PFBC) power generation systems under development with DOE and commercial funding were divided into three groups by the National Research Council committee based on projected efficiency:

Group 1 approximately 40 percent efficiency - includes PFBC with a low temperature gas turbine; and IGCC with cold gas cleanup;

Group 2 approximately 45 percent efficiency - includes PFBC with a carbonizer and a commercial gas turbine; and IGCC with hot gas cleanup, by 2000;

Group 3 50 percent or greater efficiency - includes PFBC with carbonizer and advanced gas turbine; and IGCC with hot gas cleanup and advanced gas turbine, by 2010.

Hot gas cleanup is necessary to obtain the highest system efficiencies. Hot gas cleanup systems comply with environmental requirements, protect advanced gas turbines from corrosive impurities such as volatile alkali metals and from erosive particles. The NRC committee concluded that the components for the advanced IGCC and PFBC power plant systems needing the most development are the hot gas cleanup sections.

A key recommendation in the NRC report to DOE was that an assessment of hot gas cleanup systems for advanced IGCC and PFBC should be undertaken to determine the ability to meet, within the next 3 to 5 years, all requirements for future high temperature (>1260 °C [2300 °F]) turbine operation and environmental acceptability.

Objective

The objective of this work is to gather data and information to assist DOE in responding to the NRC recommendation on hot gas cleanup by performing a comprehensive assessment of hot gas cleanup systems for advanced IGCC and PFBC including the status of development of the components of the hot gas cleanup systems, and the probable cost and performance impacts. The scope and time frame of information gathering is generally responsive to the boundaries set by the NRC, but includes a broad range of interests and programs which cover hot gas cleanup through the year 2010. As the status of hot gas cleanup is continually changing, additional current data and information are being obtained for this effort from this 1996 METC Contractors' Review Meeting as well as from the 1996 Pittsburgh Coal Conference, and the University of Karlsruhe Symposium.

Approach

The technical approach to completing this work consists of:

1. Determination of the status of hot gas cleanup technologies: particulate collection systems, hot gas desulfurization systems, and trace contaminant removal systems.
2. Determination of hot gas cleanup systems cost and performance sensitivities. Analysis of conceptual IGCC and PFBC plant designs with hot gas cleanup have been performed. The impact of variations in hot gas cleanup technologies on cost and performance was evaluated using parametric analysis of the baseline plant designs and performance sensitivity.

Status of Particulate Collection Systems

Particulate removal devices are required at the operating temperature of the IGCC gas stream and at the exit temperatures of the carbonizer and PFBC of the PFBC system. The IGCC operating temperature ranges from 340 to 600 ^{o}C (650 to 1100 ^{o}F), while the PFBC temperatures may be as high as 870°C (1600°F). High-temperature particulate collection has been accomplished using several types of equipment, ranging from modified traditional devices, such as upgraded electrostatic precipitators, to new devices such as candle filters developed specifically for this service. Most of the results of testing and development work has been published, discussed at meetings or distributed by vendors. The primary sources of particulate test results are through the DOE-supported meetings, such as the METC Contractor's Meetings. What is generally lacking, is long term operation under actual commercial scale conditions. Presently, a coordinated program is in place to commercialize hot gas particulate collection technology. This program includes Research & Development, slipstream/pilot plant testing, and CCT demonstration plants. There are two pilot facilities which will have a great impact on the development of PFBC filters: Wilsonville and Karhula. At the demonstration level only Wakamatsu is active and the only filter being tested there is the Asahi tube filter. The testing of various filters at Wilsonville and Karhula will be very important since the Clean Coal Technology demonstration plants, Four Rivers and DMEC, are still in the negotiating process.

Ceramic Monolithic Candle filters have the most extensive testing of any high-pressure, high-temperature particulate filtration device. Candle filters have been formulated from either clay bonded silicon carbide (SiC) or aluminum oxide, or, more recently, ceramic fiber filters using a variety of fibers embedded in either an organic or inorganic binder. New filter designs using different clay binders are being tested. Modified candle filters made of clay bonded silicon carbide and alumina mullite have been developed to minimize problems encountered in previous testing. These are presently undergoing testing.

Ceramic Candle Filters Modified with Ceramic Fibers have been developed to solve the problems that were experienced with ceramic filters, such as creep and brittle failure. METC is sponsoring a program to design, build and test a group of these advanced filters. The program is focused on providing a diversity of approaches at obtaining a stronger more durable candle filter by building on work done elsewhere in government programs, such as the Energy Efficiency and Renewal (EE) Program in DOE and the Air Force Materials Program.

Ceramic tube filters, manufactured by Asahi Glass Co., Japan, are typically made of porous cordierite. The tube differs from a candle filter in that it is generally of much larger diameter and is mounted to tube sheets at the top and bottom of the butted tubes. Asahi ceramic tube filters were tested at Karhula with mixed results and are now being tested at the Wakamatsu PFBC facility in Japan. Preliminary results have indicated some tube failures.

Sintered Metal Candle Filters are being developed by Pall Corporation for high temperature applications. They have recently received a patent for a high-temperature, high-pressure filter vessel design for any type of filter that uses an inner filter in each candle for protection when a ceramic candle breaks. Pall will provide a filter having 56 sintered stainless candles for testing at the Tampa Electric Company CCT demonstration plant on a 25 MWe slipstream in 1996.

Granular bed filters have been used to filter hot particulate at temperatures above 425 ^{o}C [800°F] for over 80 years. Fluidized, packed or moving bed granular bed filters are an option for both PFBC and IGCC conditions. Testing was done by the Coal Mining Research Center at Yubari, Japan in the 4 MWe IGCC pilot plant. In addition to the work done in Japan, Combustion Power Company (CPC) and Westinghouse have been developing versions of a granular bed filter in the United States, sponsored by DOE. Proof testing of a large CPC granular bed filter is scheduled to be performed at the 4 MWe Wilsonville Test Facility, at both oxidizing and reducing conditions, and these tests should provide data on which commercial offerings can be based.

Advanced Materials: There are several advanced materials now under development that appear promising for ceramic tube filters: Dupont Lanxide PRD-66, 3M CVI silicon carbide/Nextel, Dupont Lanxide silicon carbide, Westinghouse/Techniweave continuous fiber ceramic composite, and Pall iron aluminide and stainless steel sintered metal candles. The development of ceramic composites is sponsored by DOE's Office of Industrial Technology's Continuous Fiber Ceramic Composite (CFCC) Program. The Oak Ridge National Laboratory is conducting a program for DOE which is focused on increasing knowledge of operational degradation, measurement of mechanical properties, long term performance, thermal shock and cycling, creep and fatigue, and non-destructive characterization.

Status of Hot Gas Desulfurization Systems

The major issue associated with hot gas desulfurization (HGD) is the need for the technology to be demonstrated for an extended period at a scale equivalent to commercial operation. Sorbent capacity and physical attrition of hot gas desulfurization sorbents are the key issues in sorbent development. A third issue for HGD sorbents is the formation of sulfates during regeneration. Research objectives are aimed at developing sorbents to resolve these issues.

Desulfurization Sorbents

In the mid-1970's, work at METC resulted in development of iron oxide sorbent, but the need for a regenerable sorbent that could lower the sulfur levels to 10 ppm or less led to zinc ferrite as a likely candidate for testing as a regenerable sorbent in 1980. There has been no further METC development on iron oxide, but the Japanese continue to utilize iron oxide in a fluid bed reactor.

Zinc-based sorbents such as zinc ferrite and zinc titanate are capable of reducing the COS and H_2S level in syngas to about 10 ppm in both air blown and oxygen-blown syngas. Z-Sorb III, another zinc-based sorbent is being developed by Phillips Petroleum Company. It is about to be used in two of the Clean Coal Technology projects. Table 1 lists the sorbents under development and their status.

TABLE 1
STATUS OF SORBENT DEVELOPMENT

SORBENT	DEVELOPER	MOLAR RATIO COMPOSITION	APPLICATION	LEVEL OF TESTING	TEST RESULTS	ADDITIONAL TESTING	MANUFACTURER
METC-9	METC	50% ZINC OXIDE	MOVING BED	50 CYCLE HP BENCH SCALE	ACCEPTABLE	NONE PLANNED	UCI
METC-10	METC	50% ZINC OXIDE	MOVING BED	50 CYCLE BENCH SCALE	ACCEPTABLE	200 HR AT GE PDU 3/96	UCI
ZT-4, 180 MICRON	RTI	1.5 ZnO/TiO2	FLUIDIZED BED	100 CYCLE AT RTI BENCH SCALE	POSITIVE	CIEMAT-SPAIN; COAL TECHNOLOGY DEVELOPMENT DIVISION, BRITISH COAL	CMP
ZT-4L UCI-5	RTI	1.5 ZnO/TiO2	FLUIDIZED BED	5-6 DAYS ENVIROPOWER 15 MWe	POSITIVE	NONE PLANNED	CMP/UCI
CMP-5, 80 MICRON RTI/CMP-107	RTI/CMP	1.5 ZnO/TiO2	FLUIDIZED BED	50 CYCLE AT MW KELLOGG TRTU, 1995	ATTRITION LEVEL TOO HIGH	NONE PLANNED	CMP
ICCI-2	E&A ASSOCIATES/RTI	EXCESS TiO2 $ZnO{\cdot}2TiO_2$	FIXED BED/ MOVING BED	BENCH SCALE	PRELIMINARY	50 CYCLE AT RTI WAITING FOR MANUFACTURE	UNITED CATALYSTS
Z-SORB III	PHILLIPS PETROLEUM COMPANY	ZINC-BASE PROPRIETARY	FIXED BED/MOVING BED/FLUIDIZED BED/TRANSPORT REACTOR	200 HR TESTING AT GE PDU, 1994 MW KELLOGG TRTU	GE DETERIORATION WITH STEAM REGENERATION ATTRITION RESISTANT /TRTU POSITIVE	FIRST FILL AT TAMPA ELECTRIC CCT SLIPSTREAM FIRST FILL AT SIERRA PACIFIC CCT	CALSICAT AND UNITED CATALYSTS
Z-SORB IV	PHILLIPS PETROLEUM COMPANY	ZINC-BASE PROPRIETARY	FIXED BED/FLUIDIZED BED/MOVING BED	50 CYCLE TEST TO BE SCHEDULED	N/A	ONGOING	TBD

N/A: NOT AVAILABLE

HGD Test Facilities

METC is conducting high -pressure test at 20 bar (300 psia) in a bench scale fixed bed hot gas desulfurization unit with a 5.6 -cm (2.2-inch) I. D. reactor. METC is also currently in the process of constructing a Fluidized Bed/Transport Reactor Process Development Unit (PDU) to support METC strategic plans for IGCC. METC also has available for testing a 9 -mm (0.334-inch) I. D. riser tube reactor which operates as a transport reactor.

General Electric, with support from DOE, has been developing the moving bed hot gas desulfurization process which consists of a moving bed absorber and regenerator with a recycle regeneration gas system to produce a consistent level of SO_2 product. The moving bed PDU, integrated with a fixed-bed gasifier and a turbine combustion test rig is located at GE CR&D in Schenectady, New York.

Research Triangle Institute (RTI) is conducting testing with a 10 -cm (4-inch) bench-scale fluidized bed sorbent test facility capable of operation up to 870 ^{o}C (1600°F) at 20 bar (300 psia). Sorbent tested in the test rig varies in particle size range from 100 to 300 microns and pellets to 5 millimeters.

M. W. Kellogg completed their Transport Reactor Test Unit (TRTU) pilot plant in May 1995 to operate either as a dense-phase fluid bed or as an entrained reactor, and either as an absorber or as a regenerator.

Table 2 lists the prominent HGD processes and their test status.

Sulfur Fixation

Hot gas desulfurization (HGD) results in sulfur being produced from the regeneration of sorbent as SO_2, or as CaS from the bottom of the gasifier. In order for the sulfur to be acceptable for landfill or commercial use, the IGCC products must pass through a fixation process which produces elemental sulfur, $CaSO_4$, or sulfuric acid.

There are several approaches to sulfur fixation once the HGD sorbent is regenerated. If the HGD is utilized as a sulfur polisher when the gasifier uses a limestone or dolomite sorbent for in-situ sulfur capture, the SO_2-rich regeneration gas and the gasifier solids are fed to a sulfator where sulfides are oxidized to sulfates for disposal. Also, METC has sponsored the development of the Direct Sulfur Recovery Process (DSRP), in which SO_2 with stoichiometric fuel gas is converted directly to elemental sulfur over a catalyst. Other approaches to sulfur fixation include commercially available contact acid plants and the Wet Sulfuric Acid Process.

The potential commercialization of the KRW gasifier with in-situ desulfurization is dependent upon successful integration with a sulfator to convert CaS to $CaSO_4$ by roasting in air at a temperature high enough for rapid conversion without excessive emissions of SO_2. Significantly higher oxidation levels were obtained in air at 900 ^{o}C (1,700^{o}F) with DASH (dolomite and ash) rather than LASH (limestone and ash).

This reinforced the recommendation that dolomite be used as an in-situ sorbent. Pinon Pine utilizes circulating bed heavy oil cracking technology for the sulfator.

A 160-hour DSRP test at the METC RTI Trailer in 1994 has shown that sulfur recovery in excess of 99% can be achieved in a single stage. Because of the high conversion with a single stage, the DSRP design will be changed from a two stage to a single stage system, with improved economics.

TABLE 2
HGD PROCESS DEVELOPMENT STATUS

PROCESS/ DEVELOPER/ CONTRACTOR	DATES OF DEVELOPMENT FOR HGD	OTHER APPLICATIONS	OPERATIONAL ISSUES	LEVEL OF TESTING	FACILITIES AVAILABLE FOR TESTING	PLANNED DEMONSTRATION
FIXED BED/ METC	1985-1990	CPI CATALYST BEDS	HIGH TEMPERATURE VALVING IN-BED TEMPERATURE CONTROL PLUGGING FROM FINES RETENTION	BENCH-SCALE AT METC WALTZ MILL PDU	BENCH-SCALE AT RTI, IGT, GE, METC	NONE
MOVING BED/ GEESI/METC	1990-PRESENT	PETC CuO PROCESS	HIGH TEMPERATURE VALVING IN-BED TEMPERATURE CONTROL PLUGGING FROM FINES RETENTION SORBENT ATTRITION	3 MWe PDU AT GE CR&D 1990 TO PRESENT	GE 10 CYCLE TEST FOR BENCH-SCALE TEST GE 3 MWe PDU AT GE CR&D FOR 200 HR TESTING	10 PERCENT SLIPSTREAM (25 MWe) SCHEDULED AT TAMPA ELECTRIC POWER CCT
FLUIDIZED BED METC/ REGENERABLE	1988-PRESENT	PROCESS REACTORS REQUIRING PRECISE TEMPERATURE CONTROL	SORBENT ATTRITION FLUIDIZING VELOCITY CONVERSION EFFICIENCY	BENCH SCALE AT METC AND RTI ENVIROPOWER CRADA	BENCH SCALE AT RTI METC PDU IGT	NONE
FLUIDIZED BED/IHI/ REGENERABLE	1981-PRESENT	NONE IDENTIFIED	OPERATES ON IRON OXIDE AT 427-482C (800-900F)	4 MWe PILOT PLANT 20 MWe NEDO DEMO.	4 MWe PILOT PLANT	20 MWe NEDO DEMO.
TRANSPORT REACTOR/ M. W. KELLOGG	1992-PRESENT	TECHNOLOGY BASED ON MANY YEARS OF COMMERCIAL OPERATION WITH FLUIDIZED CATALYTIC CRACKER BY MWK	SORBENT ATTRITION DUE TO FAST BED CIRCULATION LOW TEMP REGENERATION	BENCH-SCALE TESTING AT METC AND M. W. KELLOGG TRTU	METC PDU METC RISER KELLOGG TRTU	95 MWe FULL SCALE DEMONSTRATION PLANNED AT PINON PINE

HGD Demonstrations

Pinon Pine will be the initial demonstration of the integrated hot gas cleanup system at a full scale of 100 MWe. Hot gas cleanup will consist of; desulfurization in-situ by dolomite feed with the coal; sulfur polishing by Z-Sorb III sorbent in a transport reactor desulfurizer; regeneration with neat air initiated at 550 ^{o}C (1000 ^{o}F); regeneration stream and DASH sulfated in a fluid bed heavy oil cracker; and particulate cleanup with a ceramic candle filter. Plant startup is projected for 1997.

Tampa Electric Power will use a 10 -percent slip stream at the 250 MWe Tampa Electric Company CCT plant to demonstrate hot gas desulfurization utilizing the GE Moving Bed Process. This demonstration is for physical checkout only and, as such, the Z-Sorb III sorbent is being supplied by METC.

Status of Trace Contaminant Removal Systems

A number of trace and minor species including alkali metals, chlorides, nitrogen compounds and hazardous air pollutants (HAPs) may require control either for process reasons or to ensure that environmental standards are met. Interest in the formation and control of HAPs in IGCC and PFBC systems is just beginning. Research to date has been aimed at defining a HAPs emission data base and documenting the effectiveness of present control technologies in reducing HAPs emissions. At present, mercury is the HAP emission of greatest concern, and is the only HAP likely to be recommended for control from power plant emissions.

Trace contaminants that form compounds that condense at operating temperatures [370 to 595 °C (700 to 1100 °F) for IGCC and 760 to 870 °C (1400 to 1600 °F)] for PFBC can be captured by efficient particulate removal devices. At the lower temperatures of IGCC, it is possible that these contaminants can be controlled by simply filtering the gases. In addition to condensation and filtration mechanisms being investigated, other methods including the use of sorbents and catalytic decomposition are also being studied and tested. Table 3 lists the trace contaminants of interest and the sorbents planned to control them.

Alkali Control Using Sorbents

Several research organizations are conducting programs to evaluate alkali removal using sorbents. In addition, testing of an alkali control device is planned at the Power System Development Facility in Wilsonville, Alabama. The alkali problem in IGCC systems is not as severe as in PFBC systems because of the lower gas temperature in IGCC systems. At IGCC temperatures, alkali should be controlled by condensation and efficient particulate filtration. At higher PFBC temperatures, a method to reduce these vapors may be necessary. Additional work may be needed to demonstrate techniques to reduce alkali efficiently upstream of the particulate filters.

Chloride Control

A primary concern for IGCC power plants is the formation of chloride compounds. If they build up in recycle loops (such as in the GE moving bed process), they can subsequently deposit on syngas coolers and heat exchangers. Bench-scale experiments have demonstrated that nahcolite pellets and granules are capable of reducing HCl levels to less than 1 ppm in high temperature coal gas streams at the temperatures between 400 and 650 °C (750 to 1200 °F). The GE Hot Gas Cleanup (HGCU) Program focuses on an enhanced circulating fluidized bed (CFB) chloride removal system.

TABLE 3
STATUS OF TRACE CONTAMINANT CONTROL SYSTEMS

TRACE CONTAMINANT	SORBENTS	INVESTIGATORS
Alkali	Emathlite, Activated bauxite kaolinite, fullers earth	Surrey University EERC, Westinghouse CPC
Chloride	nahcolite sodium bicarbonate	SRI International RTI GE Corporate R&D
Ammonia	NH_3 decomposition catalysts Co-Mo-zinc titanate Ni and Ru-based catalysts	Krishnan and others (1988) SRI International RTI GE Corporate R&D Hampton University Enviropower

Ammonia Control

The approaches to NH_3 removal being developed involve rich-quench-lean (RQL) combustion and catalytic decomposition. RQL combustion techniques are being developed to meet present NO_x emission limits for fuels that contain fuel-bound nitrogen. Development of another ammonia removal system may be necessary to meet stringent NOx limits for certain gasifiers that produce higher levels of NH_3.

Nickel-based catalysts have been tested which can reduce NH_3 by greater than 90 percent at high temperature [800-1000 ^oC (1470-1830 ^oF)] in the presence of high levels of H_2S, a known catalyst poison. Combined sorbent-catalysts to simultaneously remove H_2S and NH_3 are actively being pursued. Recent test results on Hart-49, a Hampton University/RTI material, demonstrated that this is a viable concept.

Hazardous Air Pollutants

Title III of the CAAA of 1990 requires that EPA study HAP emissions from utility boilers. The field sampling efforts are primarily being concluded by DOE and EPRI, with a few utility companies generating data for their specific systems.

The testing results demonstrate that the plants studied have fairly low emission factors for total CAAA trace elements on average. While HCl is the largest HAP emission from coal-fired power plants, it has not been determined to be a health hazard and thus is not likely to be controlled. Mercury is the only HAP likely to be controlled.

Impact of Hot Gas Cleanup on Advanced Power Systems Costs and Performance

The sensitivity of the capital cost, operating cost, and cost of electricity to variations in hot gas cleanup system parameters was determined by adjusting the parameters, and assessing the changes to baseline plant design and cost figures. Sensitivities were determined for IGCC and PFBC applications.

HGCU Impact on IGCC Plant Costs

Two 400-MWe IGCC plants were selected as baselines to encompass the wide range of gasifier products and the utilization of desulfurization as either a polisher or as a bulk sulfur remover. The first plant is based on the KRW air-blown gasifier with in-situ desulfurization and a hot gas desulfurizer. The second plant is based on the Destec oxygen-blown entrained flow gasifier with a hot gas desulfurizer to remove the bulk of the sulfur. Both IGCC plant designs utilize ceramic candle filters as final particulate control devices before combustion in the gas turbine.

As a general observation, the gas cleanup portion of the capital cost has a relatively minor impact on COE, as does the cost of consumables. The capital cost of hot gas cleanup systems are between 10 and 15 percent the IGCC total plant cost (TPC). Desulfurizer and particulate filter costs are 8 to 11 percent and 2 to 4 percent, respectively, of the TPC of an IGCC plant. The changes in IGCC COE resulting from 10-percent increases in selected hot gas cleanup parameters are shown in Table 4.

Table 4
HGCU Influences on IGCC COE with 10% Increase in Parameter

Parameter	Destec Percent COE change	KRW Percent COE change
Desulfurization Cost	+.4%	+.7%
Sorbent cost	+1%	+.4%
Sorbent attrition rate	+1%	+.4%
Candle filter face velocity	-.2%	-.3%
Candle filter cost	+.1%	+.1%
Candle filter life	-.05%	-.1%

PFBC Plants

The 535 MWe PFBC baseline plant was based on a Foster-Wheeler design with a coal pyrolyzer and a circulating PFBC. The hot gas cleanup systems associated with the PFBC power plants include only ceramic candle filter particulate control at 871 ^{o}C (1,600^{o}F). Sulfur control is achieved by dolomite injection into the carbonizer and FBC. Changes in the capital and consumables have less impact on the PFBC COE than on the IGCC.

The capital cost of hot gas particulate filter is about 10 percent the total plant cost of a PFBC plant. Changes in the PFBC COE due to 10 -percent increases in selected hot gas cleanup parameters are shown in Table 5.

TABLE 5
HGCU Influences on PFBC COE with 10% Increase in Parameter

Parameter	Carbonizer Percent COE change	PFBC Percent COE Change
Candle filter face velocity (FBC)	-.2%	-.5%
Candle filter cost (FBC)	+.1%	+.3%
Candle filter life (FBC)	-.1%	-.2%

Findings

- Hot gas cleanup is necessary to obtain higher system efficiencies, comply with environmental requirements, and protect advanced gas turbines from corrosive and erosive impurities. Several development programs for hot gas desulfurization systems and the more critical hot gas particulate removal systems are underway. Results to date have verified the technical ability to clean hot gases, and longer duration tests would establish the long term durability record required for commercial acceptance.
- A coordinated program is in place for the development of hot gas cleanup systems and to resolve critical issues. This program consists of research and development, proof of concept tests and technology demonstrations. A timetable is in place to implement this program.
- Successful completion of these plans will demonstrate the ability to meet, within the next 3 to 5 years for IGCC and 4 to 6 years for PFBC, all requirements for future high temperature turbine operation and environmental acceptability.
- Key tests planned for 1996 and 1997 are critical to the demonstration of both IGCC and PFBC cleanup systems. IGCC tests include filter tests at Wilsonville; slipstream tests of a filter and desulfurization system at Tampa; and hot gas cleanup demonstration at Pinon Pine. PFBC tests include filter tests at Karhula, Finland; Wilsonville Alabama.; and Wakamatsu, Japan.
- Hot gas cleanup systems costs are about 10 to 15 percent of the total plant costs. While significant, this is a much smaller portion than any other major system. The most critical parameters impacting costs include the face velocity for particulate control and sorbent attrition and costs for desulfurization.
- The rapid progress in the development of advanced gas turbines coupled with the successful development of reliable hot gas cleanup systems will assure that the IGCC and PFBC program goals are achieved in the proposed time frame.

Contract Information

Research sponsored by the U. S. Department of Energy, (FE-231) under contract No. DE-ACO1-94FE62647, Task 18 with Parsons Power Group Inc., 2675 Morgantown Road, Reading, PA 19607. Telefax: 610.855.2384

Acknowledgments

This work is conducted under the direction of DOE/Fossil Energy, Gerald F. Wheeler, Program Manager and Suresh C. Jain, Technical Monitor. The providing of detailed information regarding hot gas clean up activity by DOE's Morgantown Energy Research Center is gratefully acknowledged.

Assessment of HAPs Emissions from Advanced Power Systems

T. A. Erickson (terickson@eerc.und.nodak.edu; 701-777-5153)
D.W. Brekke (tbrekke@eerc.und.nodak.edu; 701-777-5154)

Energy & Environmental Research Center
University of North Dakota
PO Box 9018
Grand Forks, ND 58202-9018

P.E. Botros (pbotro@metc.doe.gov; 304-285-4162)
Morgantown Energy Technology Center, U.S. Department of Energy
PO Box 880
Morgantown, WV 26507-0880

Introduction

The 1990 Clean Air Act Amendments (CAAA) identified 189 substances as air toxics or hazardous air pollutants (HAPs). Under the CAAA, the U.S. Environmental Protection Agency (EPA) must regulate emissions of these HAPs at their sources, including advanced power systems used for the production of electricity. Eleven trace elements are included in the CAAA list of HAPs, as shown in Table 1. The EPA will define those sources that require regulation and limit their emissions according to regulatory directives. This project focused on evaluating and manipulating the advanced power systems HAPs data currently available for presentation to the U.S. Department of Energy (DOE)[1].

TABLE 1

Trace Components Included in the 189 HAPs of the 1990 CAAA

Antimony Compounds	Arsenic Compounds	Beryllium Compounds
Cadmium Compounds	Chromium Compounds	Cobalt Compounds
Lead Compounds	Manganese Compounds	Mercury Compounds
Nickel Compounds	Selenium Compounds	

The review of trace element emissions from advanced power systems and hot-gas cleanup systems included data from Tidd Station [2], General Electric hot-gas cleanup (GE HGCU)[3], Louisiana Gasification Technology Incorporated (LGTI)[4], and the Cool Water plant [5]. Very few other sources of information were located, and those that were contained significantly flawed information that was not of value to this project. To offset the shortage of information, thermochemical equilibrium predictions were used in evaluating advanced control systems. An outline of the systems reviewed is given in Table 2. In addition to the four demonstration and

full-scale systems reviewed, nine conventional systems were also reviewed for comparison with the advanced systems [6–14].

TABLE 2

Advanced Power Systems and Cleanup Technologies

Plant Name	System Type	System Description	Particulate Control	Sulfur Control
Tidd	PFBC[1]	Bubbling-bed PFBC	Two-stage cyclone/ ESP[2]	Dolomite bed
Tidd	APF[3]	Barrier filter	Cyclone/ceramic barrier APF	None
LGTI	IGCC[4]	Entrained-flow, oxygen-blown, two-stage, slagging gasifier	Venturi scrubber	Selectamine® absorber
GE HGCU	IGCC, turbine simulator	Pressurized, air-blown, fixed-bed gasifier	Cyclones	Zn titanate sorbent with regenerator
Cool Water	IGCC	Entrained-flow, oxygen-blown, slagging gasifier	Water scrubber	Selexol absorber

[1] Pressurized fluidized-bed combustor.
[2] Electrostatic precipitator.
[3] Advanced particle filter.
[4] Integrated gasification combined cycle.

Methods

Sample Collection, Characterization, and Manipulation. The sample collection and characterization techniques used at Tidd and at the conventional sampling-sites can be found in the individual sampling reports [1–10]. In general, all sampling teams followed accepted EPA sampling and analysis techniques and most teams utilized American Society for Testing and Materials (ASTM) or American Society of Mechanical Engineers (ASME) data manipulation routines. Since significant differences in methodology among contractors was noted, the 95% confidence limit was calculated from raw data in the individual reports. The confidence limits include only the precision of the data and contain no information related to the bias of the measurements. Comments are offered to help qualify any potentially incorrect data.

Modeling. To aid in the interpretation of the advanced power systems emission data, a thermochemical equilibrium software package was used. FLUENT was used to generate predicted partitioning between vapors and solids at various locations within the system. The FLUENT code predicts this partitioning through the minimization of Gibbs free energy, over a given set of inouts and potential output phases.

Results

Review of Sampling and Analysis Procedures. The sampling procedures used at all of the plant sites generally conformed to established sampling methods. At all four of the sites, the contractor for sampling and testing was Radian Corporation. Sampling strategy at the sites was normally consistent with the U.S. Department of Energy (DOE) programs under which these plants were studied. Since each plant has a unique system and configuration, however, the methods were slightly different for each plant. Modifications or adaptations were necessary in some instances because of product gas compositions, temperatures, and trace metal content in the apparatus disposables.

The primary methods used to obtain samples from flue gas streams were EPA Methods 5 and 29. Particulate emissions were normally measured using Method 5. The major modification to this method was the use of a quartz filter, which reduced the amount of trace metals in the collection medium. The multimetals sampling train technique, Method 29, was used to collect trace metal samples in the flue and product gases. This technique involves a filter and a series of impingers. However, the procedure is designed for oxidizing conditions and has not been validated for use in reducing environments. Gases such as H_2S, CO, and H_2 rapidly deplete the oxidizing capacity of the impingers, and the train fails to retain the vapor-phase metals. None of the vapor-phase trace element samples taken in any of the systems from reduced gas streams are believed to be accurate.

Effect of Conversion Technology. The type of coal conversion technology can affect the total plant emissions by reducing the amount of emissions that the hot-gas cleanup system must encounter. The Tidd pressurized fluidized-bed combustor (PFBC) showed a lower release of most trace elements to the cleanup device than did the neighboring Cardinal station, a pulverized coal (pc)-fired system. The lower operating temperatures of the PFBC and the primary cyclone are the principal causes of this. Figure 1 displays the partitioning of species as the ratio of the element mass in the flue gas to that leaving the system in the slag. Mercury emission was about the same for both systems, as expected.

The emission of trace elements from the gasifier section of gasification systems was not adequately measured in the studies reviewed. The commonly held view, that everything is forced into the slag within a gasification system, is readily apparent upon inspection of the gasification data. However, samples taken exiting gasifiers were subject to very low closure because of inappropriate sampling techniques. It is more likely that a significant amount of trace elements do indeed exit the gasifier, but these elements are removed during the cooling and sulfur removal stages, processes that were not investigated in this project. Since these particular sulfur removal processes will not be used in the newer technologies, trace metal emission may still present a problem, although sufficient data were not available to support this assessment.

Total Plant Emissions. Figure 2a summarizes the emissions data for the 11 elements listed in the CAAA for both advanced and conventional systems. Also shown are the two most commonly volatile elements, mercury and selenium. The CAAA trace element emissions for the GE HGCU and the Cool Water plant are significantly higher than for the other systems. The GE

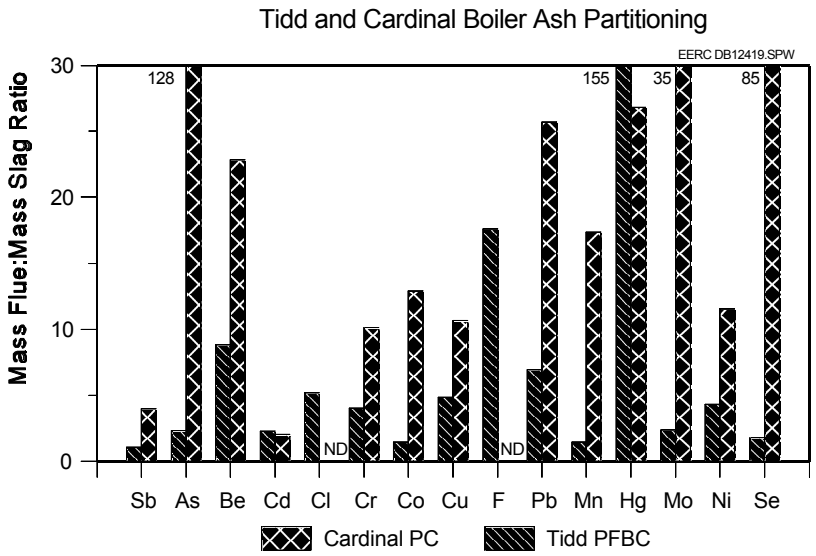

Figure 1. Partitioning of trace elements in ash within the "boiler" for the Tidd PFBC and the Cardinal pc-fired units. The partitioning factor is equal to the ratio of the mass of the element leaving the system in the flue gas to the mass in the slag/bottom ash. ND = Not detected.

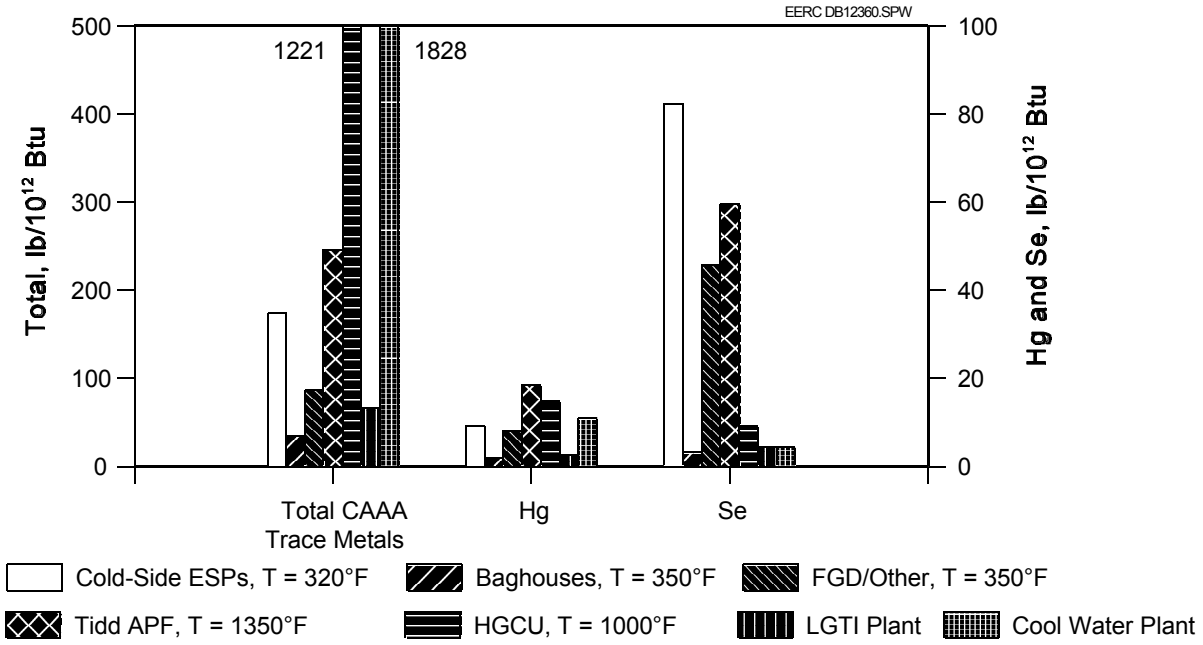

Figure 2a. Summarized emission factors of total CAAA trace elements, Hg, and Se. Note that contamination of Cr and Ni in the Tidd APF outlet samples is suspected. Results from both GE HGCU and Cool Water were subject to sampling error.

HGCU and Cool Water data are highly suspect and should not be considered valid for these comparisons. The Tidd advanced particle filter (APF) data indicate that it is the third highest emitter. However, most of these emissions are chromium and nickel, which are believed to be contamination from the sampling probe. Thermochemical equilibrium calculations also suggest that this is contamination. By assuming that the chromium and nickel values are from contamination and that they are present in the system primarily as particulate, a new estimate for the CAAA emissions can be calculated. Removing 99% of their values (which allows 1% for breakthrough, a high estimate) gives the new results shown in Figure 2b. Considering this assumption, both the Tidd APF and the LGTI systems show emission as low or lower than conventional systems.

The emissions of mercury and selenium appear to be elevated in the Tidd APF, likely because of the high operation temperature of the system. Since the mercury mass balance around the APF is very close to 100 with only a small deviation, it is assumed that the elevated mercury emissions are real and warrant future attention. The GE HGCU and Cool Water systems also show slightly elevated mercury emission values. However, since sampling errors occurred, the true extent of the emissions is not clear.

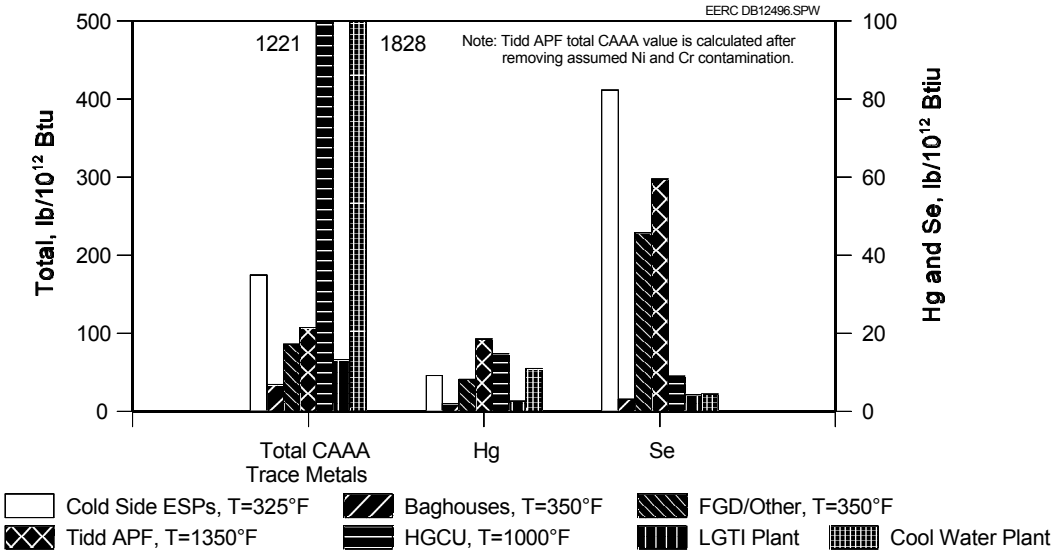

Figure 2b. Summarized emission factors for all 11 CAAA trace elements, Hg, and Se with the Tidd APF total CAAA value corrected for contamination of Cr and Ni.

Evaluation of Control Technologies. The average control efficiency for total particulate, total CAAA trace elements, and mercury and selenium are shown in Figure 3. The LGTI and Cool Water plants are included as a total plant efficiency value, not as a control technology efficiency. The poor performance of the GE HGCU system was expected because of sampling errors, and the poor performance of the APF is due to chromium and nickel contamination in the APF data.

Thermochemical Equilibrium Predictions. The efficiency and environmental friendliness of emerging advanced power systems largely depends upon the effective removal of particulates from the gas stream at temperatures higher than those in conventional systems. These higher temperatures result in a change in the equilibrium abundances of inorganics present in the solid and vapor state, as compared to conventional systems. The ability to physically collect inorganic species depends largely upon their existence as particulate. Thermochemical equilibrium programs are an effective tool to aid in the determination of trace metal partitioning between vapor and solid species.

In using the thermochemical equilibrium programs to aid in the design and operation of higher-temperature cleanup systems, predictions must be made using exact parameters. However, to generalize, the lower the pressure, the lower the temperature needed for effective collection. At atmospheric pressure, systems should be run below approximately 900°F, while under higher pressures, temperatures can be extended to 1100°F (at 20 atm), as shown in Figures 4 and 5. The presence of vapor-phase lead at lower temperatures is an unresolved problem in predicting lead species; it is assumed that the lead is primarily particulate up to 1000°F.

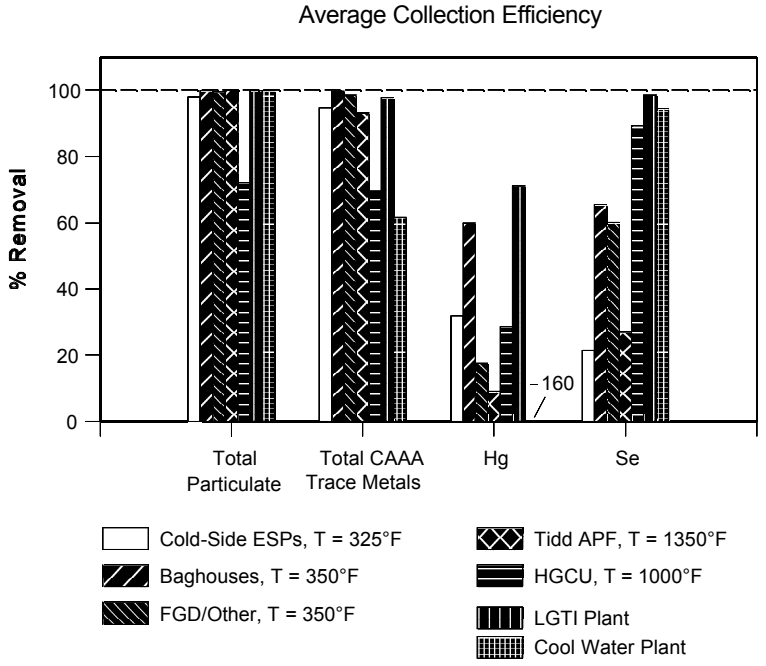

Figure 3. Average collection efficiency for all 11 CAAA trace elements, Hg, and Se for both conventional and advanced control systems.

Potential Regulatory Impact. The potential for the regulation of advanced power systems is currently being driven by the 1990 CAAA. The CAAA list 189 compounds considered HAPs that must be minimized. The current form of the regulations would allow only 10 tons/year of any single HAP and 25 tons/year of all HAPs combined. Any major source exceeding these limits will be required to apply the maximum achievable control technology to their system to meet the regulations. It is assumed that advanced systems will be governed under regulations derived from the results of conventional system testing.

Assuming that only the Tidd APF and LGTI data sets are valid, the overall emission of trace elements from advanced power systems appears to be equal to or lower than that of conventional systems, on average. All systems fall below 1 ton of emission per year. The only area of concern is likely the emission of mercury from the advanced power systems. Regulation of mercury is to be expected because of its environmental and health risks. Informal reports indicate that the EPA believes there is significant mercury contamination of lakes from air deposition and that coal-burning power plants are one of the major sources. Since the Tidd APF and other future advanced technologies will operate at temperatures exceeding conventional technologies, it is anticipated that mercury emissions will be an issue.

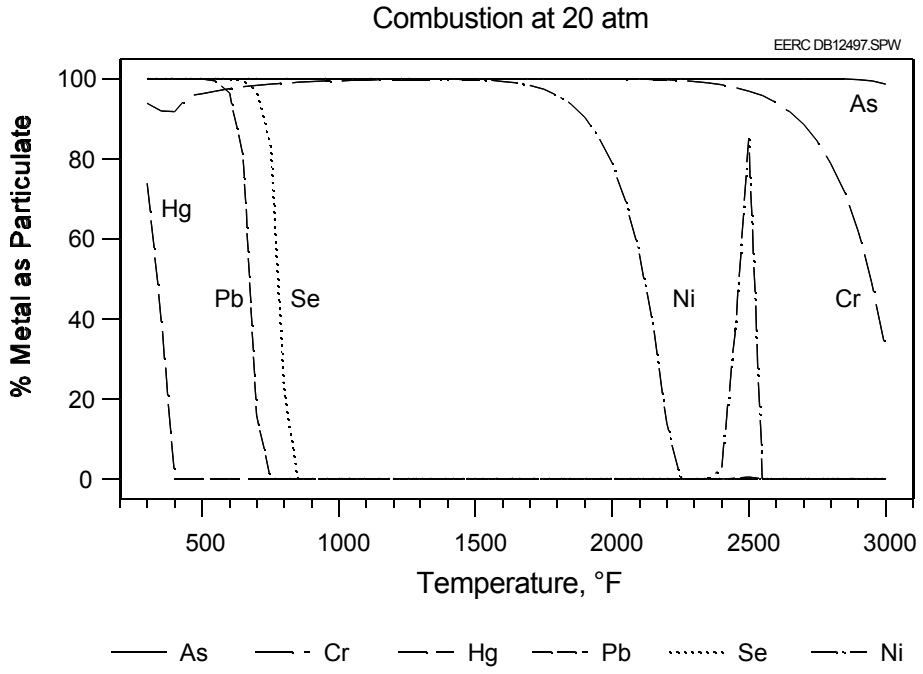

Figure 4. Amount of each element present as particulate as a function of temperature under typical combustion conditions as simulated for the Tidd PFBC system at 20 atm.

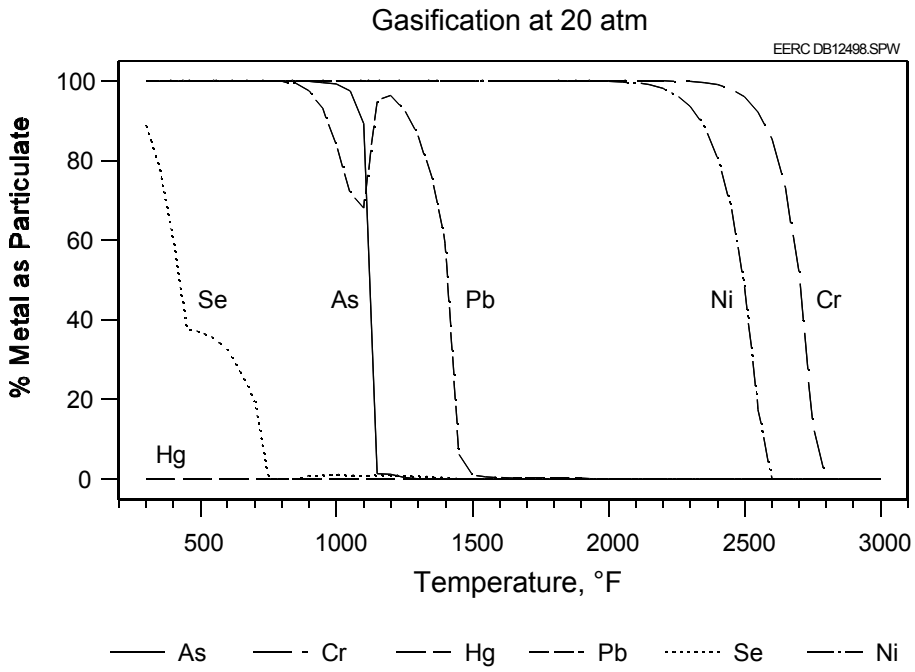

Figure 5. Amount of each element present as particulate as a function of temperature under typical combustion conditions as simulated for an entrained-flow gasifier at 20 atm.

Recommendations for Future Work

The following is a list of recommendations for future work involving the evolution of advanced power systems into proven, environmentally safe coal conversion systems. These recommendations are given in order of importance as determined by the authors of this report, starting with the most important.

- Control of Mercury in Advanced Combustion Systems. Since mercury is likely to be regulated, notwithstanding its low concentration, a suitable method of control must be identified for advanced power systems. For the current gasification systems using low-temperature cleanup devices, this does not appear to be a problem. As systems switch to high-temperature cleanup technologies, this will become a problem. In PFBC systems, this problem is evident from the sampling around the APF. Research should focus on the use of high-temperature mercury sorbents (possibly scrap metals) in both oxidizing and reducing environments and on the economics of placing low-temperature mercury cleaning systems prior to stack emission (now being developed for conventional combustion systems).

- Development of Sampling Techniques for Use in Reducing Environments. To fully research the impacts of cleanup technologies on trace elements, an effective technique to quantitatively sample trace elements is needed. The technique may be either a

modification to the existing EPA Method 29 technique or a completely new one. Until such a technique is found, all gasification system sampling for trace metals should be limited to the fully oxidized gas streams (flue gas exiting turbines and incinerators). The most near-term solution to this sampling problem may be to oxidize the gas stream after particulate removal and prior to impinger sampling. A second filter should be located just prior to the impingers to capture any metals that condense during the oxidation. The overall gas-phase concentration can then be calculated from the second filter and the impingers. Optional methods of oxidizing the gas stream include installing a burner or passing the gas over/through an oxidizing catalyst (platinum) with excess oxygen.

- Need for More Data. Much of the information presented within this report is based on a limited amount of data, of which a large part is significantly flawed. Considering the imminent arrival of clean coal technologies, it is recommended that an initiative be undertaken to sample emissions from numerous advanced power systems. Internal process measurements should also be mandated, but only if the appropriate sampling techniques exist. The use of ceramic filters should be monitored closely for mercury control as noted in the first recommendation. All sampling projects should be highly structured, including validation of sampling and analysis prior to initiation.

- Use of Modeling to Aid in Research. In cases where data do not exist or sampling methods are not yet appropriate, thermochemical equilibrium modeling can be performed to aid in research. Thermochemical equilibrium predictions can support the development of sampling techniques by identifying species present and can assist in the design of hot-gas cleanup systems where it can be used to predict points of condensation and particulate capture. Models do not replace advanced research, but rather help focus the research to provide answers at a lower cost.

Contract Information

The work reported here was performed under U.S. Department of Energy Contract No. DE-AC21-92MC28016.

References

1. "Assessment of Hazardous Air Pollutants for Advanced Power Systems," topical report for U.S. Department of Energy Contract No-DE-AC21-92MC28016; Energy & Environmental Research Center publication, Dec. 1995.

2. Radian Corporation. "A Study of Hazardous Air Pollutants at the Tidd PFBC Demonstration Plant," draft report for U.S. Department of Energy Contract No. 94-633-021-02; Sept. 9, 1994.

3. Radian Corporation. "Trace Element Determinations During Integrated Operation of a Pressurized Fixed Bed Gasifier, Hot Gas Desulfurization System, and Gas Turbine Simulator," final report DCN 94-643-011-01 for General Electric Company; July 1994.

4. Radian Corporation. "A Study of Toxic Emissions from a Coal-Fired Gasification Plant," draft final report DCN 95-643-004-06 for U.S. Department of Energy, Electric Power Research Institute, and Louisiana Gasification Technology, Inc.; August 1995.

5. Electric Power Research Institute. "Cool Water Coal Gasification Program: Final Report," Report No. GS-6806; December 1990.

6. Radian Corporation, "A Study of Toxic Emissions from a Coal-fired Power Plant Utilizing an ESP While Demonstrating the ICCT CT-121 FGD Project," final report for U.S. Department of Energy Contract No. DE-AC22-93PC93252; June 16, 1994.

7. Energy & Environmental Research Corporation. "Assessment of Toxic Emissions from a Coal-Fired Power Plant Utilizing an ESP," final report for U.S. Department of Energy Contract No. DE-AC22-93PC93252; Dec. 15, 1994.

8. WESTON. "Toxics Assessment Report, Minnesota Power Company, Boswell Energy Center – Unit 2," final report for U.S. Department of Energy Contract No. DE-AC22-93PC93255; July, 1994.

9. WESTON. "Toxic Assessment Report, Illinois Power Company, Baldwin Power Station – Unit 2," final report for U.S. Department of Energy Contract No. DE-AC22-93PC93255; July, 1994.

10. Battelle. "A Study of Toxic Emissions from a Coal-fired Power Plant Utilizing an ESP/Wet FGD System," final report for U.S. Department of Energy Contract No. DE-AC22-93PC93251; July 1994.

11. Battelle. "A Study of Toxic Emissions from a Coal-fired Power Plant – Niles Station Boiler No. 2," final report for U.S. Department of Energy Contract No. DE-AC22-93PC93251; June 1994.

12. Battelle. "A Study of Toxic Emissions from a Coal-fired Power Plant Utilizing the SNOX Innovative Clean Coal Technology Demonstration," final report for U.S. Department of Energy Contract No. DE-AC22-93PC93251; July, 1994.

13. Southern Research Institute. "Springerville Generating Station Unit No. 2," final report for U.S. Department of Energy Contract No. DE-AC22-93PC93254; June 21, 1994.

14. Southern Research Institute. "Bailly Station Units 7 and 8 and AFGD ICCT Project," final report for U.S. Department of Energy Contract No. DE-AC22-93PC93254; Aug. 11, 1994.

Trace Metal Transformations in Gasification

Steven A. Benson (sbenson@eerc.und.nodak.edu, 701-777-5177)
Thomas A. Erickson (terickson@eerc.und.nodak.edu, 701-777-5153)
Christopher J. Zygarlicke (czygarlicke@eerc.und.nodak.edu, 701-777-5123)
Cathy A. O'Keefe (cokeefe@eerc.und.nodak.edu, 701-777-5238)
Karen A. Katrinak (kkatrinak@eerc.und.nodak.edu, 701-777-5283)
Sean E. Allan (sallan@eerc.und.nodak.edu, 701-777-5166)
David J. Hassett (dhassett@eerc.und.nodak.edu, 701-777-5261)
William B. Hauserman (bhauserman@eerc.und.nodak.edu, 701-777-5169)
Energy & Environmental Research Center
University of North Dakota
PO Box 9018
Grand Forks, ND 58202-9018

Dr. Norman T. Holcombe (nholco@metc.doe.gov, 304-285-4829)
Morgantown Energy Technology Center, U.S. Department of Energy
PO Box 880
Morgantown, WV 26507-0880

Objectives

The Energy & Environmental Research Center (EERC) is carrying out an investigation that will provide methods to predict the fate of selected trace elements in integrated gasification combined cycle (IGCC) and integrated gasification fuel cell (IGFC) systems to aid in the development of methods to control the emission of trace elements determined to be air toxics. The goal of this project is to identify the effects of critical chemical and physical transformations associated with trace element behavior in IGCC and IGFC systems. The trace elements included in this project are arsenic, chromium, cadmium, mercury, nickel, selenium, and lead. The research seeks to identify and fill, experimentally and/or theoretically, data gaps that currently exist on the fate and composition of trace elements. The specific objectives are to 1) review the existing literature to identify the type and quantity of trace elements from coal gasification systems, 2) perform laboratory-scale experimentation and computer modeling to enable prediction of trace element emissions, and 3) identify methods to control trace element emissions.

Background Information

Trace element emissions pose a potential problem to two emerging coal gasification electric power-generating systems: IGCC and IGFC. The potential problems associated with trace elements are the release of substances that are considered air toxics and the degradation of fuel cell efficiency due to contamination with minor elements. In order to develop effective technologies to control trace element emissions within anticipated regulatory requirements and to ensure the efficient operation of fuel cells, the type and quantity of trace elements emitted from coal gasification-based systems must be determined as a function of system, system conditions, and coal composition.

The fate of trace elements in coals used in IGCC and IGFC systems is closely tied to how the trace elements are associated in the coal and the gasification conditions. Trace elements in coals are associated in several forms, including organic associations, such as salts of carboxylic acid groups and organic coordination complexes, and mineral associations, such as sulfides, sulfates, silicates, phosphates, and carbonates. During gasification, these inorganic elements are partitioned into gases, liquids, and solids. The transformation of these trace elements into the various states and phases depends upon the fundamental characteristics of the elements and their association with minerals and coal particles. Minerals that are not directly associated with coal particles experience a different process environment than minerals that are intimately associated with coal particles during gasification.

In order to predict the form of the inorganic species during gasification, it is essential that detailed information on the distribution of major mineral phases and organically associated inorganic elements be determined. This information is critical since the transformations and interactions during utilization impact the partitioning of trace elements. The primary transformations that occur to major and minor trace species during coal conversion are illustrated in Figure 1. Modeling the transformations using thermochemical equilibrium calculations combined with various chemical and physical constraints to reach equilibrium can be effectively used to estimate the distribution of gas, liquid, and solid components as a function of gasification conditions.

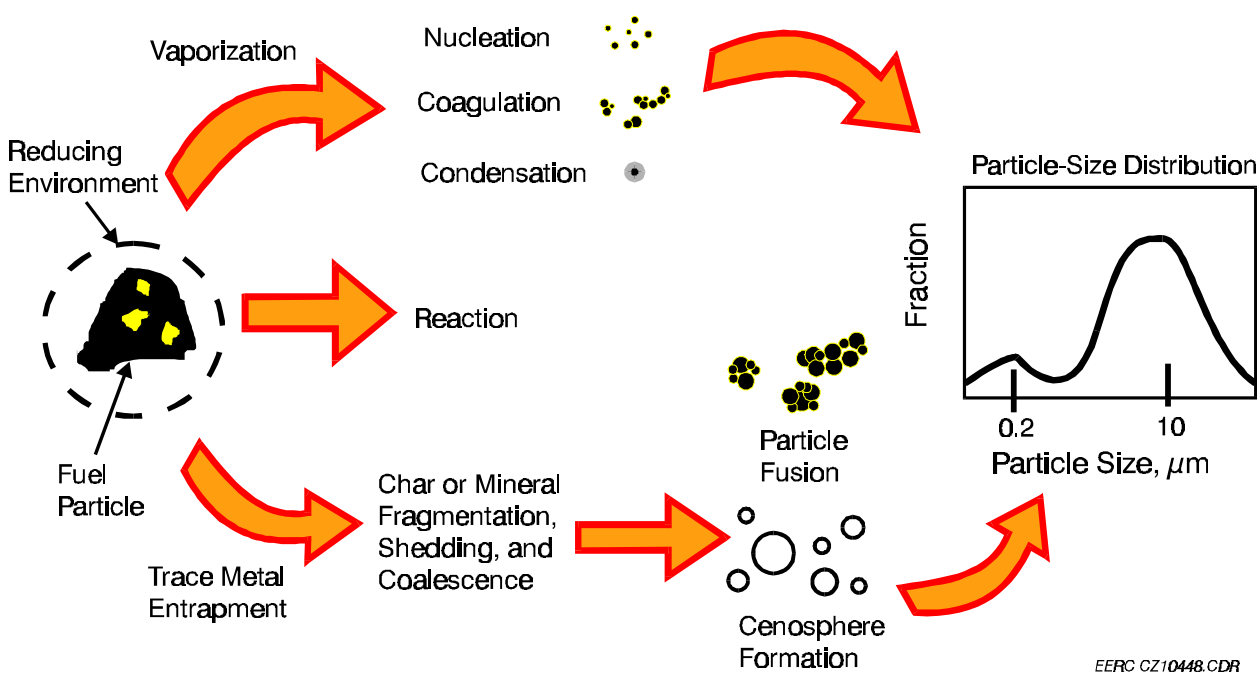

Figure 1. Trace metal transformations and partitioning.

Project Description

The approach of this project is to identify and model important physical and chemical transformation mechanisms of the trace elements during gasification as a function of coal compositions (trace element abundance and association) and gasification conditions. Identification of the reactions and transformations, coupled with accurate modeling of trace element behavior, is providing essential information for the identification of the form of the inorganic species. Gasification conditions—such as reducing and oxidizing atmospheres, gas-phase composition, pressure, and temperature—influence the partitioning of the air toxics between various gases, liquids, and solid inorganic components as a function of location in the gasifier. This information will be used to identify the most effective control technology by predicting the form of the trace element as a function of operational conditions. The model will be used to predict the initial partitioning of the metals in the gasifier and their form downstream of the gasifier in the gas cleanup systems.

This project has four work categories: partitioning experiments and analysis, modeling, identification of control technologies, and model testing and verification. The partitioning experiments and analysis have concentrated on the operation of closely controlled experimental equipment to produce the appropriate samples and the analysis/characterization of those samples by state-of-the-art analytical techniques.

A pressurized drop-tube furnace (PDTF) was utilized for the experiments. Testing has been conducted for three coals under the following conditions: 1000°–1500°C, 50–200 psi, and 0.5–2.0 O/C ratio. The samples produced in the PDTF have been analyzed using inductively coupled plasma spectroscopy, atomic absorption, x-ray fluorescence (XRF), scanning electron microscopy (SEM), and various other techniques.

The modeling work has concentrated on the modification of two existing codes at the EERC: ash transformations (ATRAN) and thermochemical equilibrium analysis of coals and ashes (TEACH). Both codes are being modified to include specific algorithms associated with trace element behavior. The resultant model is a consolidation of the aforementioned codes into a single program capable of predicting the size, composition, and phase of the inorganic species at a given temperature and pressure. An operational shell is being developed to incorporate the two codes.

The identification of control technologies will be incorporated into the project after most of the testing and modeling are complete, at which time multiple scenarios can be addressed using the data and models. The model testing and verification will consist of testing the model and assumptions on the transport reactor scaleup facility located at the EERC.

Results

The levels of the metals found in the coals are summarized in Table 1. The associations of the metals with minerals and organic portions of the coal were described in detail at the last conference (Benson and others, 1994). Table 2 summarizes the generalized associations found for the metals.

Partitioning of Trace Metals. The partitioning of trace metals was ascertained by determining the fraction in which the different trace metal species were collected. Metals that are not vaporized during gasification remain in the residual ash and are collected in the size fraction greater than 1 µm. Metals that are vaporized but condense in the system are collected in the submicron fraction. Metals such as Se and Hg, which may not condense in the system but remain in a vapor state, will escape the multicyclone system and will be collected in the impinger train. Several runs were made in the PDTF varying pressure, gas temperature, and O/C ratio.

Comparison of the average percentages of each element in the collection devices shows that a substantial portion, 40% or more, of the total amount of the trace elements is recovered in the coarse ash of the first cyclone (Figures 2 and 3). The trace elements have remained with the larger ash particles, have recondensed, or have been captured on the ash. Cr, Ni (Figure 3) and, surprisingly, Hg (Figure 2) partition with the coarse ash, with an average of more than 65% remaining in the >3-µm fraction of collected sample, with the balance appearing in the

TABLE 1

Abundance of Trace Metals in Coals Tested (µg/g, dry coal basis)

	Illinois No. 6	Sufco Utah	Pittsburgh No. 8
Arsenic	1.5	0.66	7.80
Cadmium	0.33	0.048	0.10
Chromium	26.0	26.9	18.8
Lead	2.84	0.86	3.87
Mercury	0.067	0.033	0.082
Nickel	15.1	8.35	14.9
Selenium	3.03	1.05	1.41

TABLE 2

Trace Metal Associations

Element	Associations
As	Pyrite, other sulfides, arsenates
Cd	Sulfides, clays
Cr	Clays, organic compounds
Hg	Pyrite, other sulfides
Ni	Pyrite, clays, organic compounds
Pb	Pyrite, other sulfides, clays
Se	Pyrite, other sulfides, organic compounds, sulfate

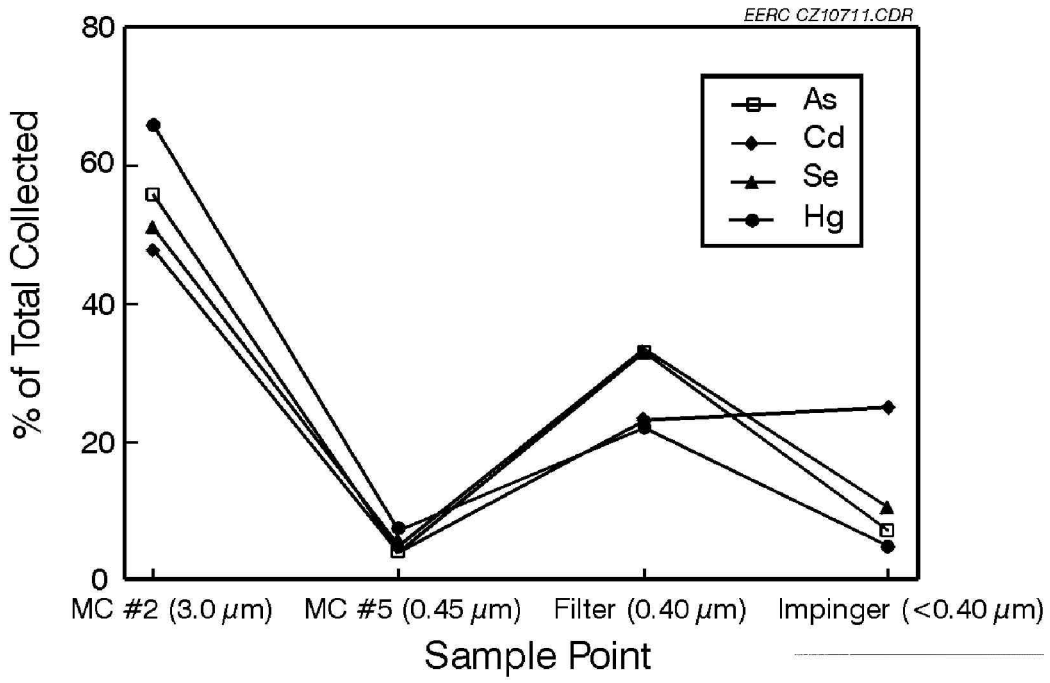

Figure 2. Average percentages of As, Cd, Se, and Hg collected in size fractions of the sampling train.

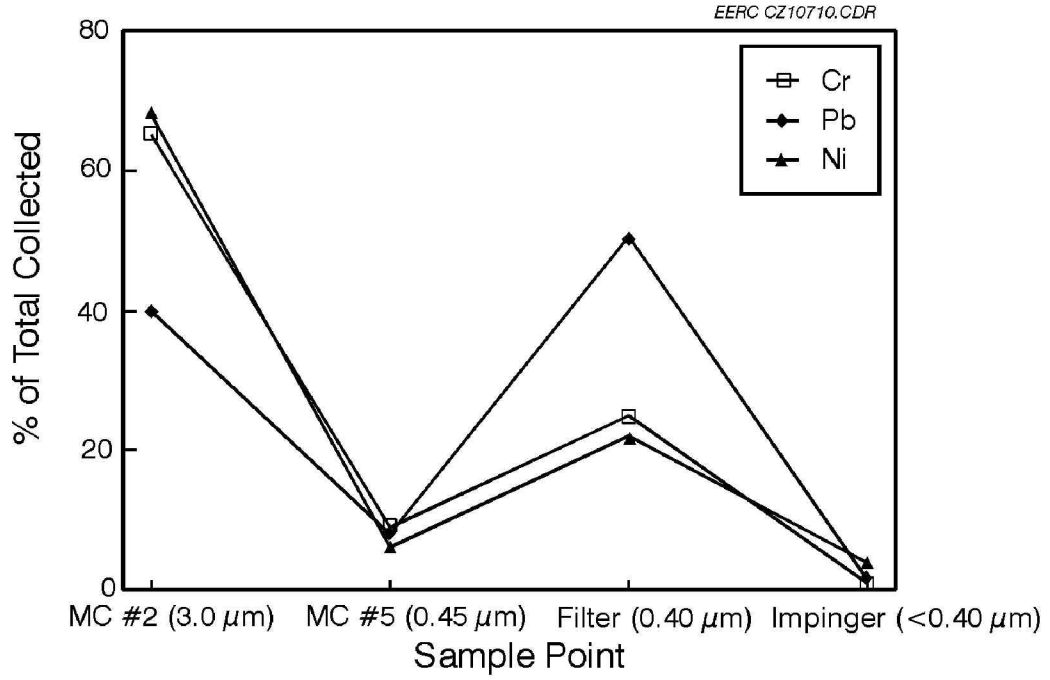

Figure 3. Average percentages of Ni, Cr, and Pb collected in size fractions of the sampling train.

1–3-µm fraction or the <0.4-µm filter fraction. Very little Cr and Ni pass through the filter into the impingers (Figure 3), which is probably an indication that they are nonvolatile species, such as refractory oxides. The behavior of Hg is more complex. Although much of the Hg is collected in the cyclones and filter, under certain test conditions up to 30% of the Hg is in a volatile form passing through the filter into the impingers. Pb partitions primarily in the 1–3-µm ash fraction and the <0.4-µm filter, probably as a very fine oxide fume (Figure 3). Generally, little Pb passes through the filter into the impingers. Along with Hg, the trace elements As, Cd, and Se showed appreciable quantities in the impingers. Cd in particular appears to be exceptionally volatile or in the form of a very fine fume, with approximately 25% of that recovered present in the impingers (Figure 2).

In general, it can be summarized that Hg, As, Cd, and Se appear to be the most volatile, simply because a greater portion of the mass of these elements is in what would be considered condensed volatile size fractions. Here we are assuming that the trace metals in these fractions, since they are associated with particulate that is essentially less than 0.45 µm, were in a vapor phase until capture. In contrast, Ni and Cr, along with Pb to a certain degree, concentrate primarily with the larger-sized particulate and are classified more as nonvolatile or vaporized species, with Pb showing consistently more mass in the 1–3-µm range than Ni and Cr. Caution must be taken in making these types of assumptions, because some of these trace metal species may be condensing onto the particulate already trapped in the multicyclones or on the filter. For example, elemental Hg and mercury chloride are known to be captured on activated carbon, coal char, and fly ash. Of special concern in these results is the amount of unburned carbon present in the ash samples. Because the PDTF tests were all run under reducing conditions, unburned carbon was found to varying degrees in nearly every size fraction of product ash collected. It is possible that some of the trace metals have not been released from their original coal host minerals or particles. Several ash grains from the largest cyclone were analyzed using wavelength-dispersive spectrometry (WDS) and yielded only Ni and Hg in iron–sulfur-rich particles and Cr in aluminosilicate particles. When this information is compared with Table 2, it could be inferred that trace metal-bearing pyrite and clay mineral aluminosilicates may not have yielded the trace metals contained within them to a vapor or fine aerosol form before they were quenched in the multicyclone. Ideally, the PDTF test runs should have 100% carbon conversion, which would ensure a minimum of carbon carryover and would maximize the release of trace metals into true postflame forms.

The effects of pressure were not clear from the data collected; however, some trends were noted for O/C and temperature effects. Figures 4 and 5 illustrate the effect of O/C ratio on the abundance of As, Cd, Se, and Hg in the assumed vapor phase at 1500° and 1000°C initial gasification temperatures, respectively. The results indicate a general decrease in As, Cd, and Hg with increasing O/C ratio and a slight increase in Se with increasing O/C ratio. A possible explanation for these results is that more oxidized forms of As, Cd, and Hg are less volatile, whereas the oxidized form or species of Se is more volatile. The lower volatility of reduced Se relative to the oxide form has been discussed by Dismukes (1994).

The effect of initial gasification temperature on the abundance of trace metals in the gas phase is depicted in Figure 6. At a constant pressure of 50 psi and an O/C ratio of 2.0, increasing the gas

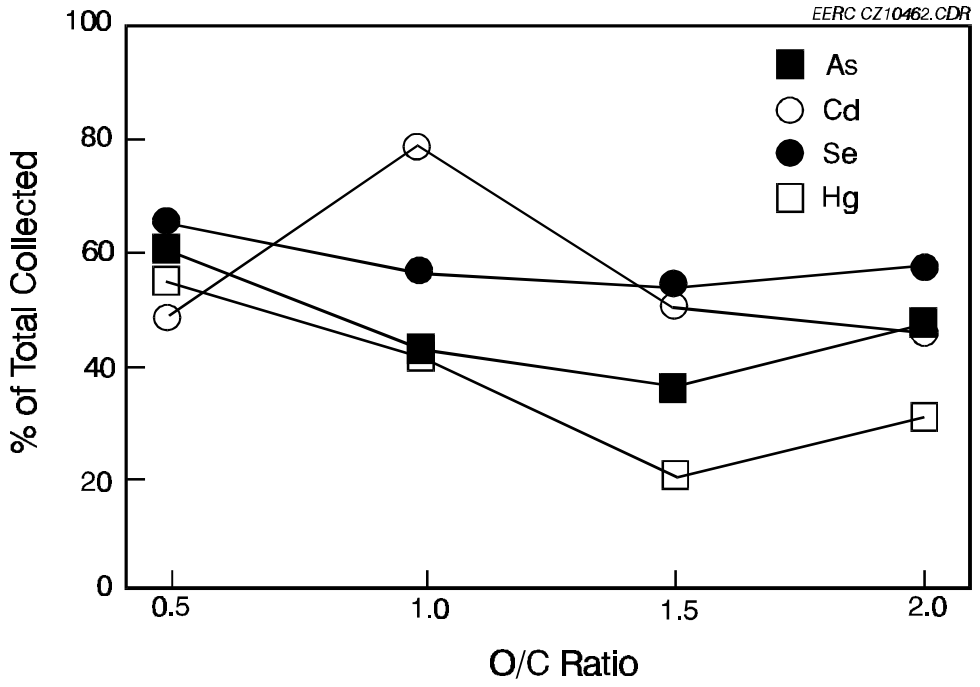

Figure 4. Trace metal distribution vs. O/C ratio for Illinois No. 6.

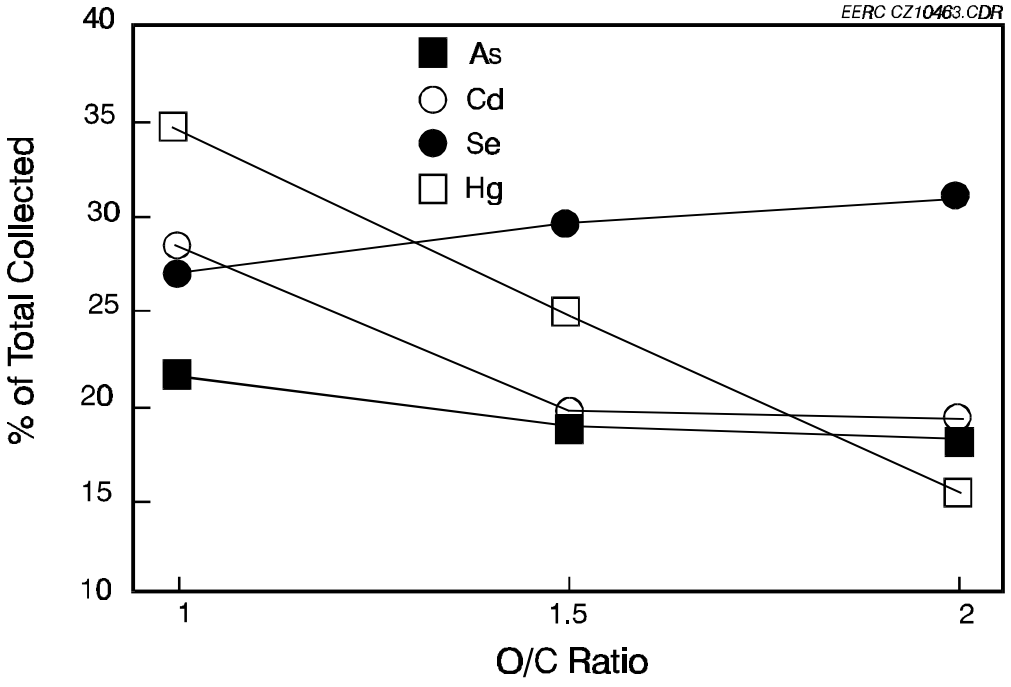

Figure 5. Trace metal distribution vs. O/C ratio at 1500°C.

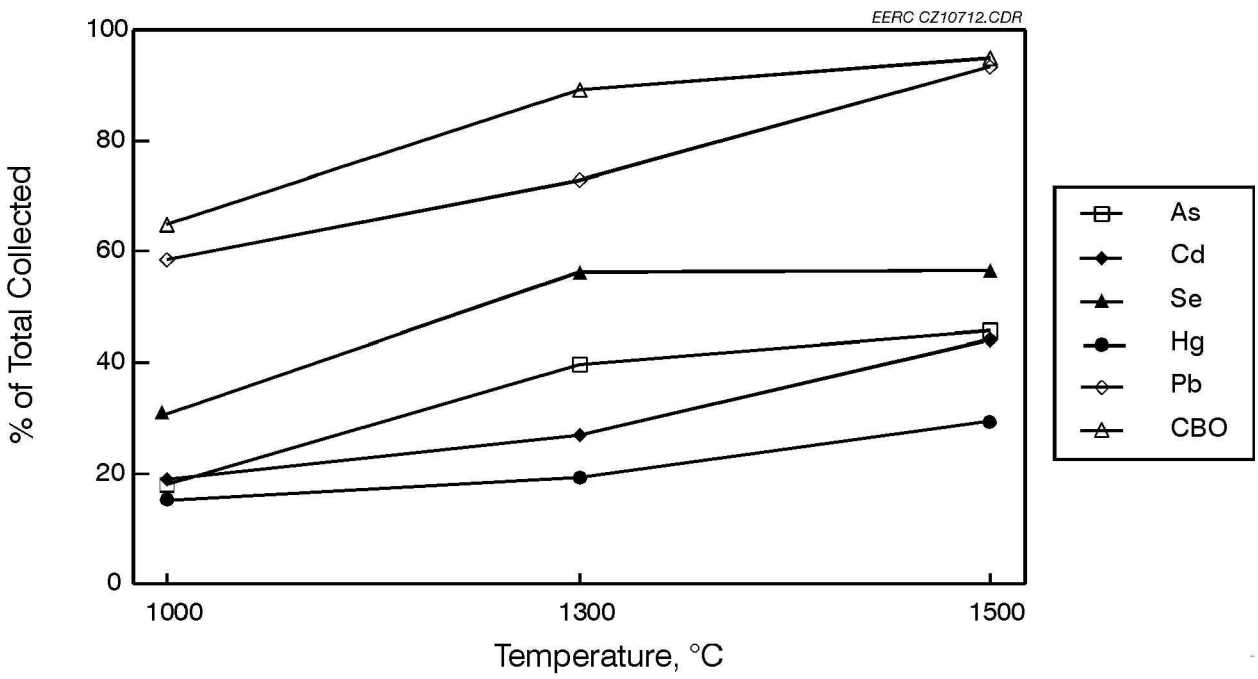

Figure 6. Trace metal distribution vs. O/C ratio at 1000°C.

temperature causes the abundance of As, Cd, Se, Hg, and Pb to increase. The effects of carbon burnout, which also tends toward greater values with increasing temperature, may be overshadowing the temperature effect somewhat. Figure 7 illustrates a temperature effect by showing that the concentrations in the vapor phase of two of the more volatile elements, Hg and Se, increase with increasing temperature at constant carbon burnout.

Predicting Trace Metals Behavior

Model Design. A computer model, TraceTran, to predict the evolution of major, minor, and trace elements during coal combustion and gasification has been created (Erickson and Benson, 1993), based on the algorithm shown in Figure 8.

The first task of the model is to determine the associations of the major, minor, and trace elements in the coal prior to utilization. The association of the elements prior to utilization will affect their phase, size, and composition distribution in the residual ash and gas streams. The three primary inorganic associations are water, organic, and mineral. Water-associated constituents are generally in the form of sulfates or chlorides present in the moisture of a coal particle. The organically associated constituents are generally found as the salts of carboxylic acid groups attached to the carbon matrix and as oxygen replacement (such as organic sulfur).

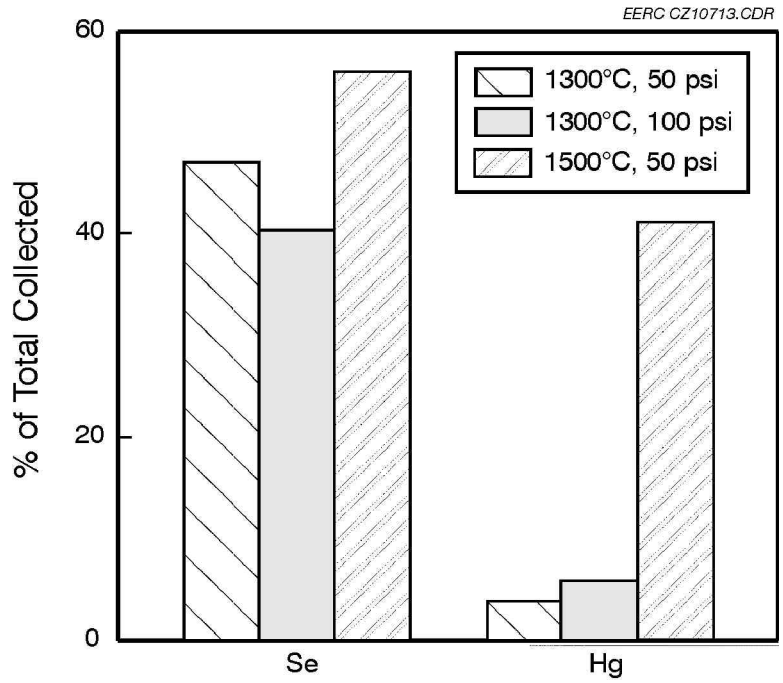

Figure 7. Concentrations in the vapor phase of Hg and Se with increasing temperature at constant pressure and carbon burnout.

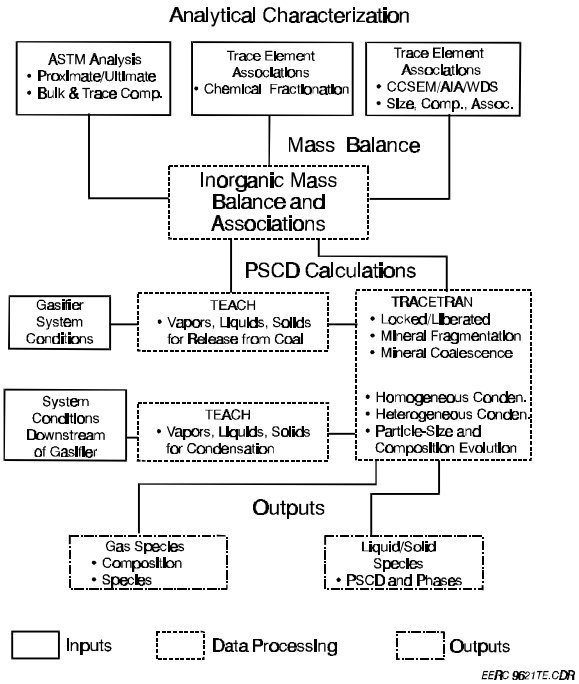

Figure 8. Model algorithm for trace element emissions.

The mineral associations are elements that comprise discrete minerals in the coal (such as clays, carbonates, and sulfides).

Because of the complexity of the interaction of inorganics during coal gasification, the mineral associations are further divided into mineral type, trace, minor, and major element content, size, and juxtaposition. Juxtaposition refers to the association of the minerals with the coal matrix and with other minerals. A locked mineral is intimately associated in the coal particle, while a liberated mineral is external to the carbon matrix. The detailed mineral classification is very important because different minerals behave differently. For instance, carbonates will commonly release CO_2, resulting in a greater potential for mineral fragmentation, depending on the system conditions. Clays that contain high levels of moisture may fragment initially because of the release of H_2O from their porous structures. Silicates are much less prone to fragmentation because they lack any of the previously discussed components.

Many of the mineral particles encountered in coal utilization contain trace and minor components. To predict the transformations of the trace and minor elements effectively, their distribution among the minerals is required. Whether a mineral is locked within the coal matrix or external to the coal can also have a large impact on its transformations. Locked minerals will be much more likely to coalesce with other minerals and organically associated constituents than are the liberated minerals. The liberated particles will also experience a slightly different gas environment during coal gasification, since they are not in intimate contact with the highly reducing, exothermic reaction of the carbon matrix.

Once a mass balance is performed around the coal input data, it is necessary to determine which of the inorganic components will be vaporized during the initial conversion process. These calculations are performed with the use of a thermochemical equilibrium program created at the EERC. This code has been upgraded to include some of the appropriate trace element phases, and the ability to include more phases is being considered through the use of additional thermochemical equilibrium programs. With the exclusion of the vaporized species, the remaining constituents are processed through algorithms for mineral fragmentation, coalescence of both minerals and organically associated species, and the shedding of resulting particles. Examples of data obtained from the thermochemical equilibrium portion of the code are illustrated in Figures 9–11.

The fragmentation, coalescence, and shedding algorithms have been developed with the aid of data from full-scale systems and data generated in pilot- and laboratory-scale facilities. These algorithms are designed using data on various frequency distributions for each of the minerals and physical processes. The organically associated species that do not readily volatilize will also undergo coalescence with mineral particles as a function of the surface area of the minerals during coalescence. A portion of the organically associated species also homogeneously coalesces. The liberated minerals undergo fragmentation, but do not appreciably coalesce with other minerals because of their lack of intimate contact with the coal.

The state of the volatile species at the desired downstream conditions will then be determined. The quantity of species that will condense prior to the given conditions is calculated from the

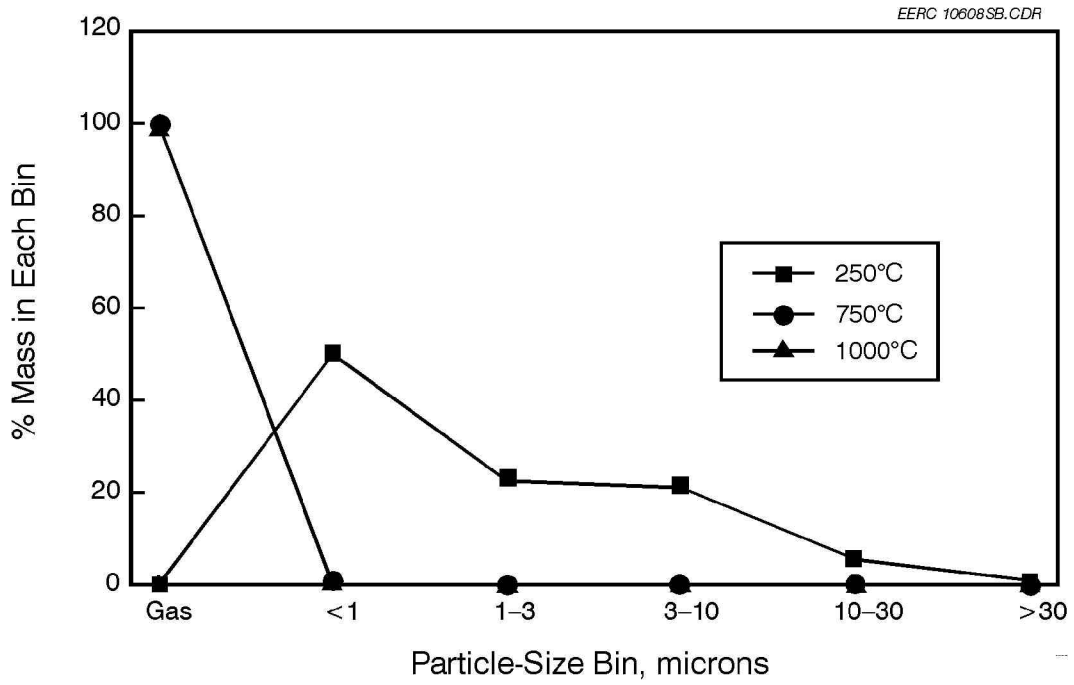

Figure 9. Illinois No. 6: TraceTran predictions – arsenic particle-size distribution.

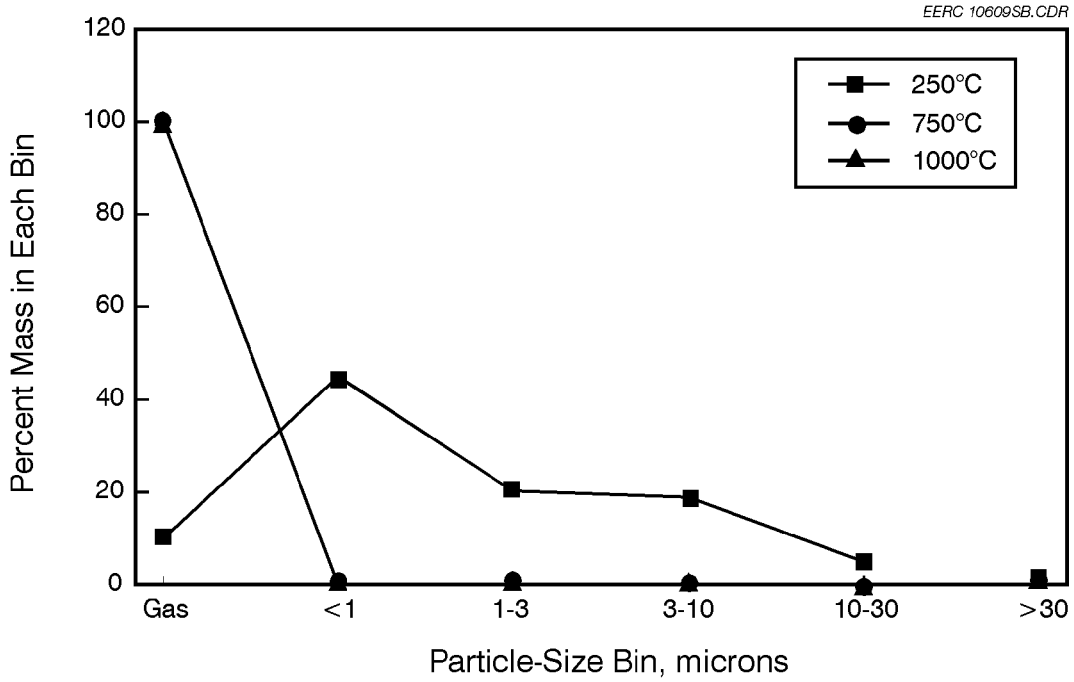

Figure 10. Illinois No. 6: TraceTran predictions – cadmium particle-size distribution.

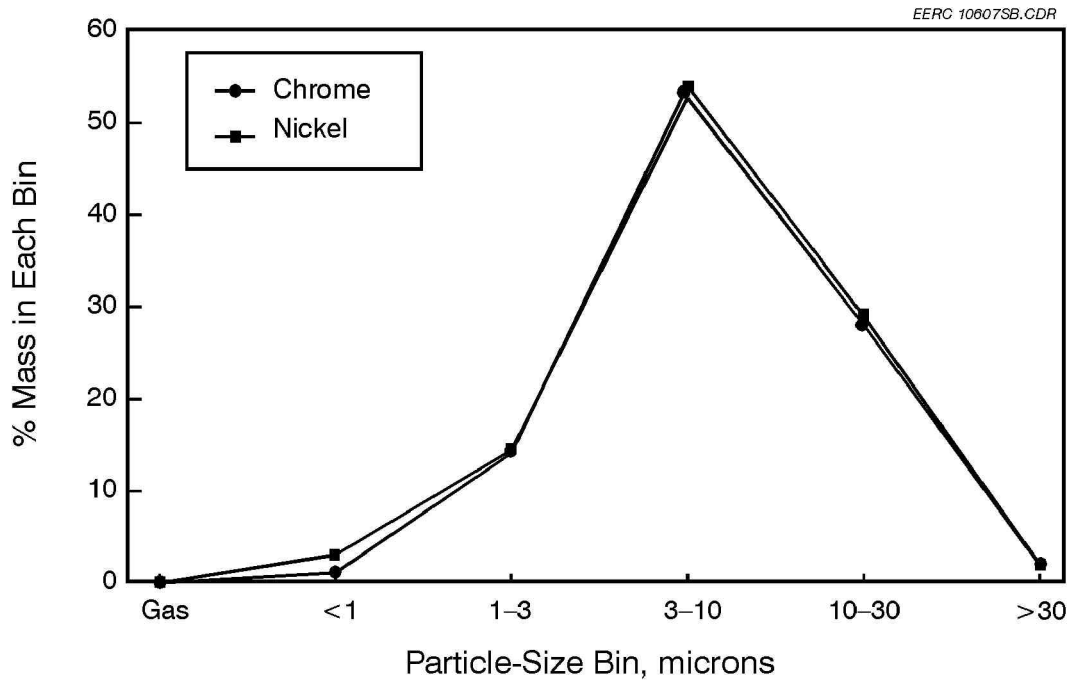

Figure 11. Illinois No. 6 TraceTran predictions – particle-size distribution, 750°C.

thermochemical equilibrium predictions. The species will then be both homogeneously and heterogeneously condensed. Heterogeneous condensation is based on the surface area of the existing particles. The resultant particulate and vapor-phase species will be compiled and manipulated into various composition and size distributions at the user's discretion. These distributions can be used to determine effective control technologies for a specific coal or to locate a coal compatible to a specific control technology.

Although the emphasis of this model is to aid in the control of trace element emissions, only minor attention has been given at this time to the engineering mechanisms of the control technologies within a system. Once this model has been fully tested and verified, the next logical step will be to incorporate engineering models that mimic the control technologies. Figure 12 shows an example of the overall model applied to a pressurized fluid-bed combustor for selected elements and the measured element distributions from full-scale sampling. A series of "crude" engineering algorithms were used for bed fluidization, cyclone efficiency, and filter performance. As expected, the model predicts well for Hg and Na, which are found largely in the vapor state, but performs only marginally for the mostly particulate lead (primarily because of the lack of robust engineering models).

Similarly, Figure 13 shows the predictions of partitioning for the seven trace elements in an air-blown entrained-flow gasifier at three different locations. In this case, no partitioning was performed to remove some materials in the gasifier slag, ash filter, or gas cleanup device. The

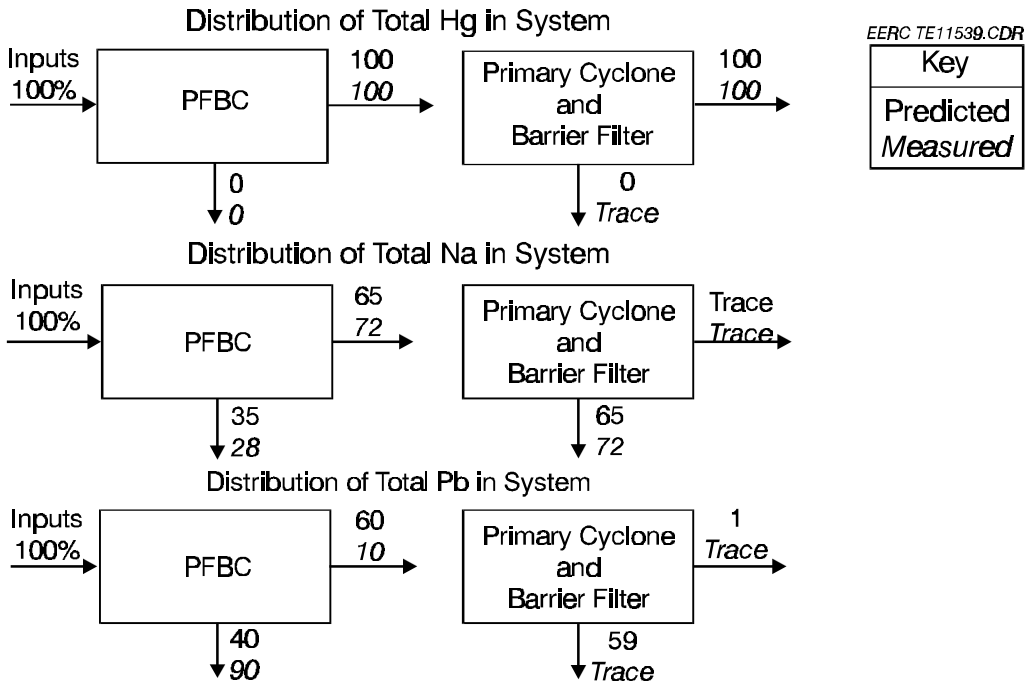

Figure 12. Trace metal distributions predicted and measured for a pressurized fluid-bed combustor.

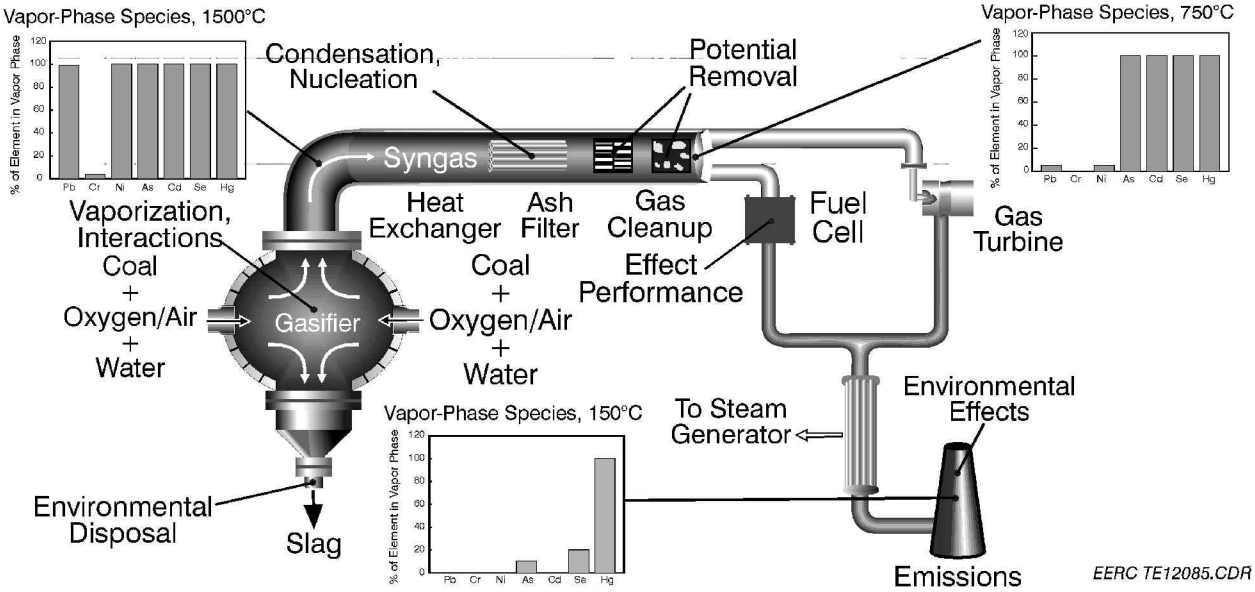

Figure 13. Trace metal vapor-phase distributions in an air-blown gasification system at various locations. No partitioning of the solids has been performed.

calculations were performed assuming all of the inorganics passed throughout the entire system. This is shown as an example of how the different conditions affect the overall vapor-phase distributions. In actual application, only the vapor phase and a limited amount of the very fine particulate would pass throughout the system.

Model Verification and Scaleup

To ensure the overall model is applicable to larger systems, a verification task is under way. The transport reactor demonstration unit (TRDU) was sampled, and the results will be compared to model predictions. Gas samples were pulled from the TRDU before and after the hot-gas filter; solid samples were also collected from the filter vessel and from the coal. The trace element concentrations from the two gas samples (collected in duplicate) are shown in Table 3. Upon full integration of the model, the predicted concentrations of trace elements will be compared to those that were measured.

TABLE 3

TRDU Trace Element Sampling at Hot-Gas Filtration Unit Runs

	Run No. 5	Run No. 6	Run No. 7	Run No.8
Date	4/17/96	4/19/96	4/19/96	4/19/96
Time	11:14	08:39	12:09	15:46
Port	Inlet	Inlet	Outlet	Outlet
Conc.	$\mu g/m^3$	$\mu g/m^3$	$\mu g/m^3$	$\mu g/m^3$
As	–*	–*	–*	–*
Cd	–*	–*	–*	–*
Cr	10.37	13.22	8.16	4.76
Pb	2.01	–	–	–
Ni	50.53	46.87	31.48	9.05
Se	43.83	36.62	31.37	29.28
Hg	3.30	4.99	4.78	4.79

* Denotes below detection limit.

Future Work

Future work will involve the following:

- Completing the integration of the TraceTran computer code. The thermochemical equilibrium data set will be interfaced into the remainder of the code using a series of look-up tables. In addition, the code will be interfaced with a graphical user interface developed under separate funding.

- Verifying the predictive capability of TraceTran using data obtained from larger-scale systems. Data manipulation from the TRDU sampling will be completed and compared with model predictions. In addition, future TRDU testing in the fall of 1996 is planned. Similar samples will be collected and the results compared.

References

Benson, S.A.; Erickson, T.A.; Steadman, E.N.; Zygarlicke, C.J.; Hauserman, W.B.; Hassett, D.J. 1994. Presented at Coal-Fired Power Systems 93—Advances in IGCC and PFBC Contractors' Review Meeting, DE-AC21-92MC28016.

Dismukes, E.B. 1994. Trace Element Control in Electrostatic Precipitators and Fabric Filters, In Trace Element Transformations in Coal-Fired Power Systems, Special Issue of Fuel Processing Technology; Benson, S.A.; Steadman, E.N.; Mehta, A.K.; and Schmidt, C.E.; Eds.; Vol. 39, Nos. 1–3, pp 403–416, August 1994.

Erickson, T.A.; Benson, S.A., 1993. Trace Element Emissions from Gasification Systems. Presented at the 205th American Chemical Society Meeting, Denver, CO, March 28–April 2, 1993.

Development and Testing of PRD-66 Hot Gas Filters

Contract Information

Contract Number	DE-AC21-94MC31214
Contractor	DuPont Lanxide Composites Inc. 1300 Marrows Road PO Box 6077 Newark, DE 19714-6077 (302) 456-6235 (telephone) (302) 456-6480 (FAX)
Other Funding Sources	
Contract Project Manager	Jeffrey A. Chambers, Ph.D.
Principal Investigator	Jeffrey A. Chambers, Ph.D.
Presenting Author	John E. Garnier, Ph.D.
METC Project Manager	Theodore J. McMahon
Period of Performance	September 29, 1994 to August 31, 1996

Abstract

The overall objective of this program is to develop and commercialize PRD-66 hot gas filters for application in pressurized fluidized bed combustors (PFBC) and Integrated Gas Combined Cycle (IGCC) power generation systems. The work is being carried out in phases with the following specific objectives:

1. Demonstrate acceptable mechanical, chemical, and filtration properties in exposure tests.
2. Produce and qualify selected prototype design filter elements in high temperature high pressure (HTHP) simulated PFBC exposure tests.
3. (Option) Generate a manufacturing plan to support commercial scale-up.
4. (Option) Recommend process equipment upgrades and produce 50 candle filters.

Since the beginning of this program, a parallel evaluation of DuPont Lanxide Composites Inc. (DLC) PRD-66 hot gas candle filters took place using AEP's TIDD PFBC facility. Several PRD-66 filters experienced damage during the final testing phase at TIDD, after highly successful testing in earlier runs. During the past year, DLC has undertaken a study under this contract to understand the mechanism of damage sustained in TIDD Test Segment 5. DLC has formulated a hypothesis for the damage mechanism based on the available evidence, and verified that the damage mechanism is possible given the conditions known to exist in TIDD. Improvements to the filter design to eliminate the root cause of the failure have been undertaken. This report details DLC's conclusions regarding the failure mechanism, the evidence supporting the conclusions, and steps being taken to eliminate the root cause.

FY 1996 Program Schedule

O N D J F M A M J J A S

Analysis of Field Exposed Filters

Corrosion Testing

During the performance of this contract, DuPont Lanxide Composites Inc. (DLC) has been involved in a series of tests at American Electric Power's TIDD pressurized fluidized bed combustor system, exposing PRD-66 hot gas candle filters to pilot scale testing in Westinghouse's filter vessel. After a completely successful test of three candles in Test Segment 4, numerous failures occured in Test Segment 5. In TIDD Test Segment 4, PRD-66 candle filters had a 100% survival rate, with no noticeable damage or decrease in mechanical properties after a run which lasted 1700 hours and operated at temperatures up to 760_C. However, in Test Segment 5, filters essentially identical to those which survived Test Segment 4 had a <10% survival rate, with all filters showing some damage after only 1100 hours and peak temperatures of 845_C. There were many other significant differences between these two runs. For instance, ash loadings were more than five times higher in Test Segment 5 than in previous runs, due to inactivation of the primary cyclone. While Test Segment 4 suffered significant bridging events (though none was observed involving PRD-66 filters) Test Segment 5 was essentially free of bridging. Many other differences will be discussed below.

To understand the cause of the discrepancy between the results of TIDD Test Segments 4 and 5, DLC undertook Task 3.4 of this program, titled Analysis of Field Exposed Filters. This task was carried out in five phases. They were Consultation, Elimination of Known Faults, Hypothesis Formulation, Hypothesis Verification, and Correction.

Phase 1 - Consultation

In the Consultation phase, DLC held discussions with numerous experts in the field of hot gas filtration. They included Ted McMahon, Rich Dennis and Dwayne Smith of METC, Mary Anne Alvin and Rich Newby of Westinghouse Science and Technology Center, Tina Watne and John Holmes of UND's Energy and Environmental Research Center, and Dick Tressler of Penn State. Valuable evidence and insight was gained from these discussions.

Phase 2 - Elimination of Known Faults

In Phase 2, DLC undertook detailed evaluations of all the manufacturing records for filters supplied to TIDD Test Segment 5 to seek any anomalies in manufacturing which might explain the differences in performance. While some minor changes in the process were found, no process variations correlated with performance. X-ray diffraction tests on the filters fired in the same run with Test Segment 5 filters showed no difference with those in Test Segment 4.

Phase 3 - Hypothesis Formulation

Unable to find any significant differences in the filters, Phase 3 focused on physical

evidence found in filters which survived Test Segment 5 in whole or in part, and documented differences in run conditions between Test Segments 4 and 5.

As shown in Table 1, there were significant differences between Test Segments 4 and 5. Ash loading increased

Test Segment	TIDD 4	TIDD 5
Test Duration	1700 hr.	1100 hr.
Survival Rate	100%	10%
Ash Cake	Thin, uniform	Thin patchy
Damage	None	Divots Mid-body Flange
Bridging	None	None
Operating Temperature, °C	660-760	760-845
Ash Loading, ppmw	3,200	18,000
Primary Cyclone	Detuned	Inactive

Table 1. Comparison of test conditions in TIDD Test Segments 4 and 5.

from 3,200 ppmw to 18,000 ppmw because of the inactivation of the primary cyclone before the filter vessel. The mean particle size of the ash increased significantly. The highest run temperature increased from 760 to 845_C. Different adsorbents and coals were used. In Test Segment 4, the PRD-66 candle filters were placed in the middle array, while in Test Segment 5, they were in the top array. Two failure modes were observed. One was a classic flange failure, with the fracture locus high up in the holder. These filters, in order to remain identical to the ones tested in Test Segment 4, did not use the selective reinforcement technique developed by DLC under this contract, and described ion our paper last year. This reinforcement technique increased the strength of PRD-66 materials by about 50%. DLC is confident the the reinforcement will ameliorate this problem. A second, more puzzling failure mechanism is found in mid-body failures, as well as filters which survived the full duration of the test. The physical evidence seen on the filters included 'divots,' as shown in Figure 1.

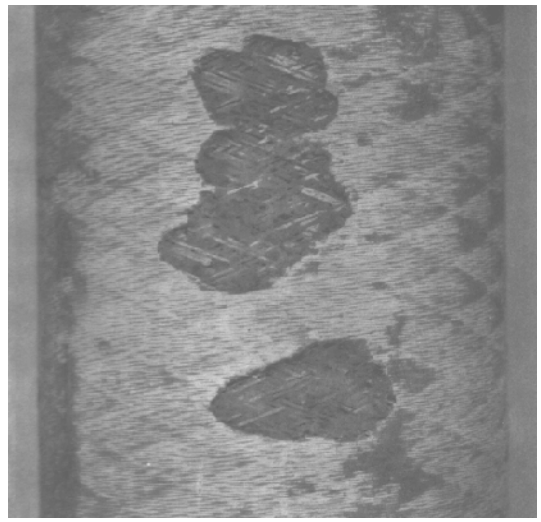

Figure 1. Divots in a PRD-66 filter segment.

Divots are pieces of the candle filter membrane and body, avulsed from the filter. Such divots were found aligned along the filter body on roughly opposite sides. A divot was also found under the sock and holder, which eliminates mechanical impact as a cause of the damage. There was no visible evidence of corrosion. The filter body walls were filled with ash, as they had been in Test Segment 4. The body of the filter was covered with a thin layer of loose ash, roughly 2mm thick in most regions. There were also denser ash deposits, aligned with the divots described above. All divots were packed with dense ash, though some ash-packed divots were covered with loose ash. Finally, in Test Segment 5, all filters of all types in the top array were somehow 'glued' in place, i.e., they were strongly adhered to their holders. This was not observed in the middle or bottom arrays. Filter segments tested by Westinghouse showed no decrease in mechanical properties after exposure. Finally, micrographs taken at EERC by Tina Watne showed inclusions of a white material, identified by EDX as containing magnesium, calcium, sulfur, and oxygen, well inside the filter body.(See Figure 2) This white deposit was of a physical size far too large to have penetrated the undamaged

filter above it intact. Undamaged filter areas showed no such deposits.

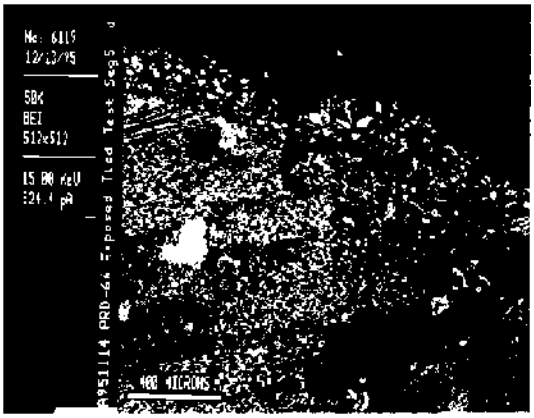

Figure 2. White deposit (middle left) in vicinity of divot (upper right.)

Based on this evidence, DLC formulated a hypothesis of the failure mechanism of PRD-66 candle filters in Test Segment 5.
DLC hypothesized that despite earlier results of room temperature and high temperature tests to the contrary, ash containing adsorbent penetrated the surface filtration membrane of PRD-66 filters. This ash then became trapped in the bulk filtering body of the candle. Once trapped there, it was subjected to long term exposure to hot SO_2 gas, causing *in situ* sulfation of the ash to calcium and/or magnesium sulfates in the pores and microcracks of the filters. Once lodged in a microcrack at high temperature, these deposits could change in size by several mechanisms. One possible damage mechanism is by thermal expansion and contraction of the sulfate deposit during process interruptions, of which there were several in Test Segment 5. A second possible mechanism is by crystal growth by successive hydration of the sulfates during cooling in moisture containing atmosphere, which also would occur on process interruptions. Figure 3 shows how the unit cell volume of anhydrous magnesium sulfate increases as it picks up waters of hydration.

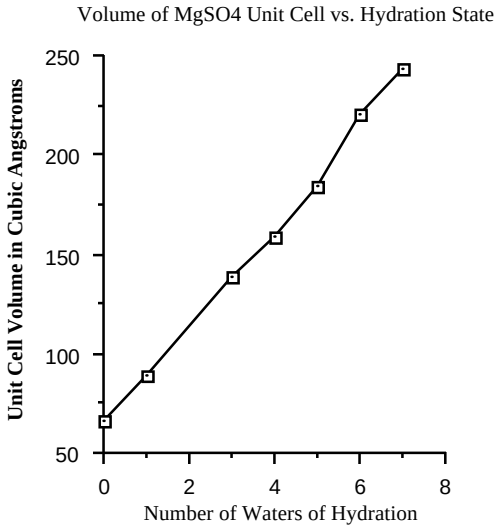

Figure 3. Unit cell size of magnesium sulfate vs. state of hydration.

The roughly four-fold volume increase associated with formation of the hexahydrate salt would induce a linear strain in a microcrack of over 150%, far larger than the strain tolerance of most ceramics. By either of these mechanisms, severe internal stresses could be placed on the filter body, causing localized failure in the vicinity of a sulfate deposit. In areas where multiple deposits formed, a 'divot in a divot' could occur, either fracturing the wall or weakening the wall enough to cause mechanical failure in a backpulse. (See Figure 4)

Phase 4 - Hypothesis Verification

In Phase 4, DLC set out to verify that 1) this hypothesis is in keeping with the known conditions of Test Segment 5, and 2) the possibility of penetration of ash through the surface membrane, contrary to previous test results. DLC found that all conditions necessary for the hypothesis to be true existed in the TIDD test conditions. All that was required was the presence of trapped ash in the filter, the presence of gas phase

SO_2, and possibly moisture, plus

Figure 4. Wall thickness reduced by divot at fracture surface, lower left.

excursions of temperature. All these circumstances can be verified from knowledge of the system, the run history, and physical examination of the field exposed filters. To verify that it was possible that ash leaked through what was thought to be 'leak proof' surface membrane, DLC devised a room temperature test of surface filtration characteristics more rigorous than the ones it had previously passed. In the previous tests, filter segments were exposed to gas flows containing ash. Once a smooth filter cake built up, it was supposed that the ash cake would strongly adhere and then take over filtration. A sample passes the test if after one exposure, no ash penetrates to the inner diameter. Since physical evidence from TIDD test segments 4 and 5 showed that the ash cake was thin and only loosely adhered, DLC worked under the assumption that the crystalline alumina surface of our filter released the ash essentially completely on each backpulse. Therefore, after exposing filter segments to ash by applying a vacuum to the inner diameter, the resulting ash cake was physically removed with light brushing. This ash exposure/cleaning cycle was repeated 25 times. The intent was to simulate the effect of complete ash cake release after a series of cleaning backpulses. This more stringent test showed that ash consistently penetrated into the filter body and was trapped in the wall using the filter design tested in TIDD. Figure 5 shows the results of a non-destructive test which images where ash penetrates the membrane surface.

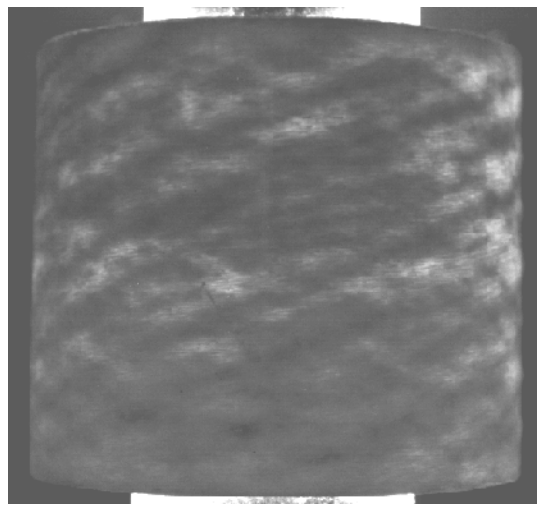

Figure 5. Non-destructive evaluation of ash penetration. Dark areas show ash penetration, light areas show no penetration.

Even after the extensive penetration shown in the figure, ash still does not penetrate to the inner diameter after 25 cycles. This shows the bulk filtering body does trap ash in the wall. Because of the expense associated with recreating the *in situ* sulfation of the penetrated ash, no such experiments were conducted.

Further verification of this hypothesis was found by Westinghouse's independent investigation of the failure mechanism. Westinghouse discovered differences in the ash adhered to the filters and uncleaned surfaces in the top array, versus the ash in the two lower arrays. They verified that the filters of the top array were 'glued' in place. Westinghouse also reported the presence of magnesium sulfate hexahydrate in the ash, as found by X-ray diffraction, on uncleaned, stagnant surfaces of the top array, such as the holders and tubesheet. As described

above, DLC hypothesized the formation of magnesium sulfate hexahydrate in the filter body as a potential cause of damage, without formally verifying the existence of the compound by XRD. Westinghouse's proof of the formation of the hexahydrate salt verifies that actual system conditions present in Test Segment 5 could cause its formation, and therefore supports the likelihood of DLC's hypothesis. The fact that no such compound was found in the middle array could explain why ash-filled PRD-66 candles in the middle array of Test Segment 4 showed no damage.

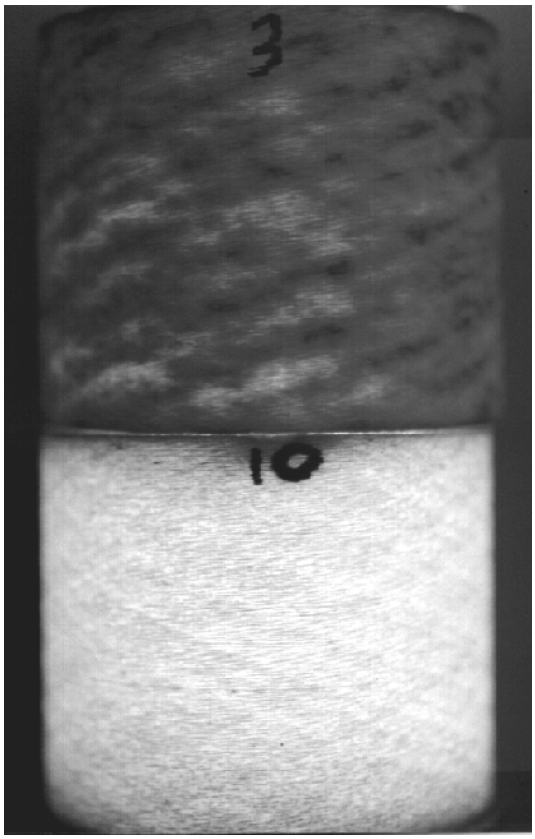

Figure 6. NDE test showing: ash penetration in TIDD filter design (top) no penetration in improved design (bottom).

Phase 5 - Correction

The task for Phase 5 is therefore obvious; to stop the penetration of ash through the membrane into the body of the filter. Without ash in the body of the filter, the damage caused by the hypothesized failure mechanism could not occur. To this end, DLC is designing improved surface filtration membranes. We have already designed several membranes which pass our ash infiltration test, and offer acceptable pressure drops. Figure 6 shows a filter segment of the type tested in TIDD, which shows significant penetration, and one of the new membranes which show no ash penetration. DLC will fabricate full scale filters incorporating the new membrane for corrosion and high temperature, high pressure testing at Westinghouse's test facilities, which will fit us back into the original program design for this contract.

Conclusion

After an investigation of filter failures in TIDD Test Segment 5, DLC formulated a hypothesis that *in situ* sulfation of ash trapped in the filter wall caused deposits which damaged the filter material on thermal excursions. DLC has verfied that necessary and sufficient conditions to bring about that failure condition existed in TIDD. To correct the problem, DLC has invented new surface filtration membranes to prevent the problem in the future.

Acknowledgements

The authors and DuPont Lanxide Composites Inc. gratefully acknowledge conversations with Ted McMahon, Rich Dennis and Dwayne Smith of METC, Mary Anne Alvin and Rich Newby of Westinghouse Science and Technology Center, Tina Watne and John Holmes of UND's Energy and Environmental Research Center, and Dick Tressler of Penn State. Their knowledge, experience and creativity provided an excellent foundation for the work in this task. DLC gratefully acknowledges financial support from METC under contract DE-AC21-94MC31214.

Novel Oxide-Oxide Fiber Reinforced Hot Gas Filter Development

Richard A. Wagner (rich.a.wagner@mcdermott.com; 804-522-5697 telephone)
Babcock & Wilcox
P. O. Box 11165
Lynchburg, VA 24506-1165

Research sponsored by the U.S. Department of Energy's Morgantown Energy Technology Center, under contract DE-AC21-94MC31212 with Babcock & Wilcox, P.O. Box 11165, Lynchburg, VA 24506-1165; telefax 804-522-6980.

1.0 INTRODUCTION

This report describes the fabrication and testing of continuous fiber ceramic composites (CFCC) based hot gas filters. The work was divided into two primary tasks. In the first task, a preliminary set of compositions was fabricated in the form of open end tubes and characterized. The results of the first task were then used to identify the most promising compositions for sub-scale fabrication and testing. In addition to laboratory measurements of permeability and strength, exposure testing in a coal combustion environment was performed to assess the thermo-chemical stability of the CFCC materials. The results of this testing were then used to down-select the filter composition for full-scale filter fabrication and testing in the optional Phase II of the program.

2.0 BACKGROUND INFORMATION

Pressurized fluid bed combustion (PFBC) and integrated gasification combined cycle (IGCC) systems are among the advanced coal-based energy cycles being considered for low cost, clean power generation. Hot gas filters are required to remove particulates from the high temperature inlet stream to the turbine in order to protect turbine components from excessive erosive wear and to meet clean air requirements.

The level of mechanical durability exhibited by the currently available filters in field tests indicates that more rugged filters are required to meet the demands of large power generation systems. Furthermore, long term corrosion resistance of currently available filters has yet to be demonstrated in PFBC systems.

The essential requirements of a composite material designed to meet the program objective for a toughened hot gas filter include the following:

- stable continuous fiber
- rigid porous matrix
- engineered fiber-matrix interface
- cost effectiveness

3.0 PROGRAM OBJECTIVES

The objectives of this program are to develop toughened ceramic hot gas filters and evaluate these filters for application in Pressurized Fluidized Bed Combustor (PFBC) and Integrated Gasification Combined Cycle (IGCC) power generation systems.

4.0 APPROACH

Composite preforms were fabricated by a modified filament winding process. The preforms were then bonded and heat treated and machined to produce the test samples. Laboratory testing was used to refine the initial compositions which were then evaluated through additional laboratory and field tests.

Filament winding technology developed under the CFCC program was transferred to the B&W ERI-Lynchburg manufacturing division. Particular attention was given to the development of a consistent macro/micro-structure over the length of the test specimen in terms of the relative amounts and distributions of the chopped and continuous fiber. Controlling this distribution is considered to be essential to achieving the desired properties. Four candidate compositions were included in this task. These compositions, included variations in the type and amount of continuous fiber as well as alternate bond systems and fiber coatings. The compositions were evaluated in terms of permeability, corrosion resistance, and mechanical properties. The characterization results were then used to refine the test compositions used in the full-scale fabrication task.

Based on CFCC results, Mitsui's Almax alumina fiber and 3M's Nextel 610 fibers were used as the reinforcements in the candidate composites. The Almax fiber consists of 1000 filament tows of polycrystalline fibers. The Nextel 610 fibers are comprised of 400 filament tows. The unit weights of the fibers are 2250 denier and 1500 denier for the Almax and Nextel 610 respectively. Saffil chopped fiber was used for all test compositions. Ten samples of each of the compositions given in Table 1 were fabricated in the form of sub-scale filter elements (2.4" diameter by 12" long).

Fiber coatings are generally required to control the fiber/matrix interface and to protect the continuous fibers from degradation during processing and/or service. While the fiber architecture used in this work does not actually have a continuous matrix phase it is important that the fiber to fiber bond does not degrade the continuous fibers. Fugitive carbon coatings have been shown to be effective means of protecting the fibers in many composite systems. The fact that the coating disappears in service is expected to have less of an affect on the long term properties of an oxide composite system than for non-oxide systems. For the oxide fibers utilized in this program, the primary requirement was to protect the fibers during processing with the acid stabilized bonding solutions.

An improved fiber coating process based on the work of Hay [1] was implemented under the CFCC program for the sub-scale fabrication task because the high temperature mechanical properties of samples containing pyrolyzed fiber sizings exhibited brittle failure . This process utilized the surface tension differences in immiscible liquids to minimize the coating bridges that normally occur within the fiber tow.

Sample filter elements were characterized in terms of their microstructure, permeability, corrosion resistance, and mechanical properties. The permeability of test specimens was determined from the

face velocity and the associated pressure drop across the specimen. Compressive C-ring tests were performed on a computer controlled mechanical test machine using calibrated load and deflection sensors. All C-ring testing was performed at 1600 °F. Five one inch wide C-rings were tested from each sub-scale filter element. .

The distribution and relative amounts of continuous fiber, chopped fiber, and bond phase was determined by examination of polished sections in an Etech scanning electron microscope (SEM) equipped with energy dispersive spectroscopy (EDS). The samples were vacuum impregnated with low viscosity resin in order to minimize open porosity in the mount.

The corrosion resistance of the candidate filter compositions was determined by an exposure test in a coal combustion environment. The original plan was to perform the test in the Tidd PFBC. Because the Tidd operation ended in March, 1995, an alternate test site was investigated. The 55 MWe circulating fluid bed (CFB) combustion unit located at Ebensburg, PA was selected because it provided a good simulation of the atmosphere and ash characteristics of a PFBC. The disadvantage of the CFB concerned the much higher ash loading in the gas stream which would require careful erosion protection of the samples.

Since the Ebensburg CFB is a commercial utility boiler, it was obviously not possible to shut the unit down to install and retrieve samples. A sample probe was therefore designed to be installed through standard 3" observation ports in the side wall of the CFB while the boiler was on-line. The outer assembly was fabricated from solid and perforated 304 stainless and was intended to protect the sample from excessive erosion by the heavily ash loaded gas stream of the circulating fluid bed combustor. Prior to sample probe insertion, low pressure seal air was injected into the port to prevent the escape of the combustion gas stream. During the 250 hour exposure period, the ash/sorbent was expected to penetrate through the perforated tube and accumulate around the sample. Two samples of each composition received static exposures at temperatures of 1500 °F and 1625 °F.

The exposure test was originally intended to be a static exposure test; however, one additional sample probe of each composition was modified to provide periodic back pulsing with ambient air as part of the CFCC program to add a thermal fatigue component to the test. Plant air at about 90 psi was plumbed to the center of the probe and triggered by a timer controlled pneumatic valve (COAX model VMK20). A single timer/pilot valve was used to control the pulse duration and cycle time of the four coax valves. A pulse duration of about 0.4 seconds was applied to the samples at 15 minute intervals for a total of approximately 1000 cycles.

5.0 RESULTS AND DISCUSSION

The properties of the sub-scale filter elements are summarized in Table 2. Typical high temperature C-ring results for each of the sub-scale compositions in the "as fabricated" condition are given in Figure 1. Composition C1 exhibited relatively low strength but with an extended strain at near maximum load. Composition C2 produced a very brittle fracture behavior in the as-fabricated condition. Composition C3 exhibited high strength and good fracture behavior. The contrast in failure behavior between composition C3 and C2 is not understood since both compositions use the same bond system and carbon coated fiber. The compressive C-ring results for composition C4 are very similar to C1 in terms of maximum strength and failure behavior. As discussed above for

composition C1, the distribution of the bond phase in composition C4 appears to account for the lower observed strength.

Figure 2 summarizes the C-ring results for the samples taken from the 1500 °F region of the CFB. Composition C1 increased strength by approximately 16 percent compared to the as-fabricated condition and maintained good failure behavior. Composition C2 retained approximately 80 percent of the as-fabricated strength and exhibited non-brittle failure behavior following the CFB exposure. Composition C3 retained 69 percent of the as-fabricated strength and exhibited non-brittle failure behavior. The compressive C-ring strength of composition C4 increased by about 47 percent and displayed a non-brittle failure behavior.

The high temperature C-ring results for the samples located in the 1625 °F region of the CFB are shown in Figure 3. These results are very similar to 1500 °F CFB samples. Composition C1 increased in strength by about 21 percent with a non-brittle type of failure. Composition C2 retained approximately 74 percent of its as-fabricated strength and also exhibited non-brittle failure behavior. Composition C3 exhibited a strength retention of about 70 percent with a non-brittle failure. Composition C4 produced a 73% increase in strength with a non-brittle failure.

The post-test high temperature C-ring results for CFB thermal fatigue samples are shown in Figure 4. These samples received approximately 1000 back pulses and were located in the 1500 °F region of the CFB. The composition C1 sample showed a 25 percent increase in strength with a relatively non-brittle failure. The composition C2 sample retained 80 percent of the as-fabricated strength and exhibited non-brittle failure. Composition C3 exhibited a retained strength of 72 percent with a non-brittle failure behavior. Composition C4 increased in strength by about 18 percent and also exhibited non-brittle failure.

In general, the SEM examination revealed very little evidence of ash or sorbent penetration into the samples following the thermal fatigue test exposure in the CFB. In composition C1, the distribution of the Almax fiber tows appeared relatively uniform but widely spaced due to the large number of filaments in each tow. The bond phase in this sample was more concentrated near the outside of the sample. This concentration gradient from the OD to the ID most likely caused the low strength and low permeability of these samples.

The microstructure of composition C2 revealed a much more uniform distribution of bond phase compared to composition C1 described above. In composition C3, the increased concentration of Nextel 610 was apparent. The distribution of continuous fibers appears more uniform at the 2:1 Nextel to Saffil ratio. The microstructure is otherwise similar to C2 in terms of there being no evidence of bond phase concentration gradients.

The cross-section of sample C4-4 following the CFB thermal fatigue exposure test also exhibited a bond phase concentration gradient from OD to ID is very similar to that observed in composition C1. There appears to be good potential to improve the properties of this composition if the bond phase can be distributed more uniformly.

Based on the mechanical properties, permeability, and the microstructure results described above, composition C3 was selected for Phase II, the full scale fabrication and simulated PFBC testing and

characterization. The overall status of the project is summarized in Table 3 which compares the filter requirements to the current status of the B&W filter manufacturing process.

6.0 BENEFITS

This program has demonstrated a hot gas filter concept and fabrication method that resulted in an oxide-oxide composite based filter with improved strength and toughness compared to monolithic filter materials. In addition, the low density of these filter elements results in substantial weight savings in the filter system (approximately 10 lb. per filter element or 60,000 lb. in a 350 MWe plant).

7.0 FUTURE ACTIVITIES

Four near full size filter elements have been fabricated and will be tested in the Westinghouse High Temperature High Pressure filter test facility during July. These samples along with two baseline samples will be characterized to guide future filter improvements. In addition, an optimization/cost reduction effort is underway to reduce the amount of continuous fiber and/or eliminate the need for a fiber coating. The results of the filter optimization task will be utilized in the production of 50 filter elements for testing in a DOE demonstration facility. In order to guide future filter development activities, a better definition of the mechanical loads imposed by the mounting method as well as in service is required to establish the wall thickness and flange configuration. The method used in this program can accommodate thicker walls but this has a predictable effect on cost.

8.0 ACKNOWLEDGEMENTS

The assistance of T. J. McMahon, METC COR, is gratefully acknowledged. In addition, the U.S. Department of Energy Continuous Ceramic Fiber Composite program has provided valuable material development support for this project. Finally, the cooperation of Ebensburg Power for the 55 MWe Circulating Fluid Bed sample exposure testing is gratefully acknowledged.

9.0 REFERENCE

1. R. S. Hay, "Sol-Gel Coating of Fiber Tow", Ceram. Eng. Sci. Proc. 12[7-8] pp. 1064-1074 (1991).

Table 1. Candidate sub-scale filter compositions.

	C1	C2	C3	C4
continuous fiber	Almax	Nextel 610	Nextel 610	Nextel 610
chopped fiber	Saffil	Saffil	Saffil	Saffil
continuous to chopped ratio	1:1	1:1	2:1	1:1
continuous fiber coating	none	carbon	carbon	none
bond type	B1	B2	B2	B1
continuous fiber architecture	45° helical	45° helical	45° helical	45° helical

Table 2. Properties of sub-scale hot gas filter elements

sample comp.	comments	% fiber	% saffil	% bond	delta P @ 10ft/min (inches H_2O)		C-ring 1600 F (psi)
					pre test	post test	
C1	as fabricated	38.2	41.0	20.8	6.3	na	825
C1	CFB	36.5	40.4	23.1	5.6	10.3	995
C2	as fabricated	31.4	38.0	30.6	6.2	na	1704
C2	CFB	35.5	40.4	24.2	3.8	9.0	1330
C3	as fabricated	52.6	28.1	19.3	11.9	na	1752
C3	CFB	52.3	28.5	19.2	5.9	10.2	1228
C4	as fabricated	37.4	42.8	19.8	5.3	na	856
C4	CFB	34.1	40.4	25.5	9.6	13.5	1249

Table 3. Hot Gas Filter Summary

Property	Req't.	Status	Challenge
size	2.4 x 60"	2.4 x 43"	minor
shape	flanged, closed end tube	flanged, closed end tube	complete
pressure drop @10ft/min	10	10-15	moderate
strength	1 - 4 ksi	0.8 - 1.7 ksi	moderate
toughness	non-brittle failure	non-brittle failure	moderate
thermal shock	ambient air back pulse	72 - 125% retained strength after 1000 back pulses	moderate
corrosion resistance	3 year life	70 - 146% retained strength after 250 hrs in CFB	moderate

Figure 1

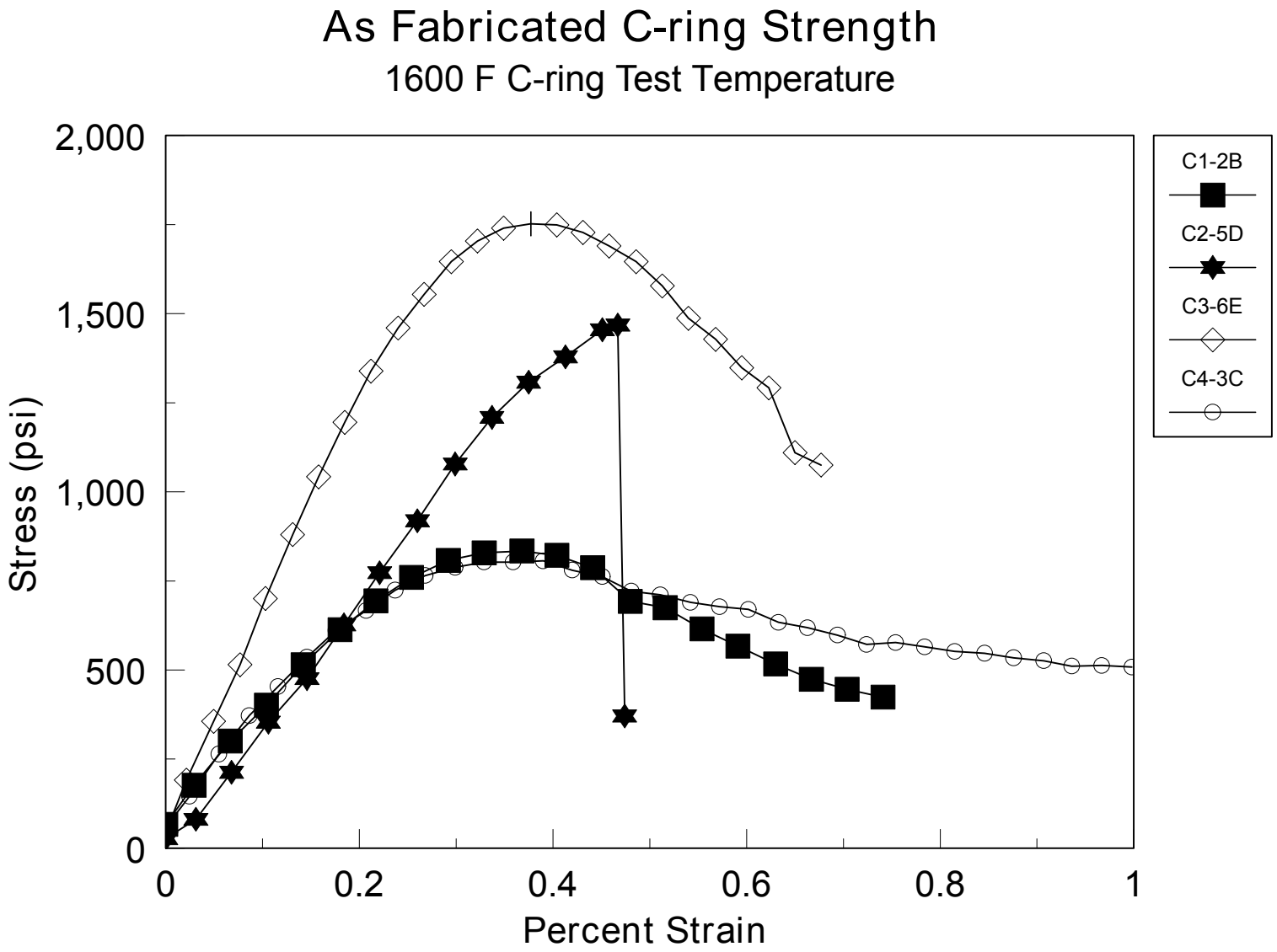
As Fabricated C-ring Strength
1600 F C-ring Test Temperature
2,000
1,500
1,000
500
0
Stress (psi)
0
0.2
0.4
0.6
0.8
1
Percent Strain
C1-2B
C2-5D
C3-6E
C4-3C

Figure 2

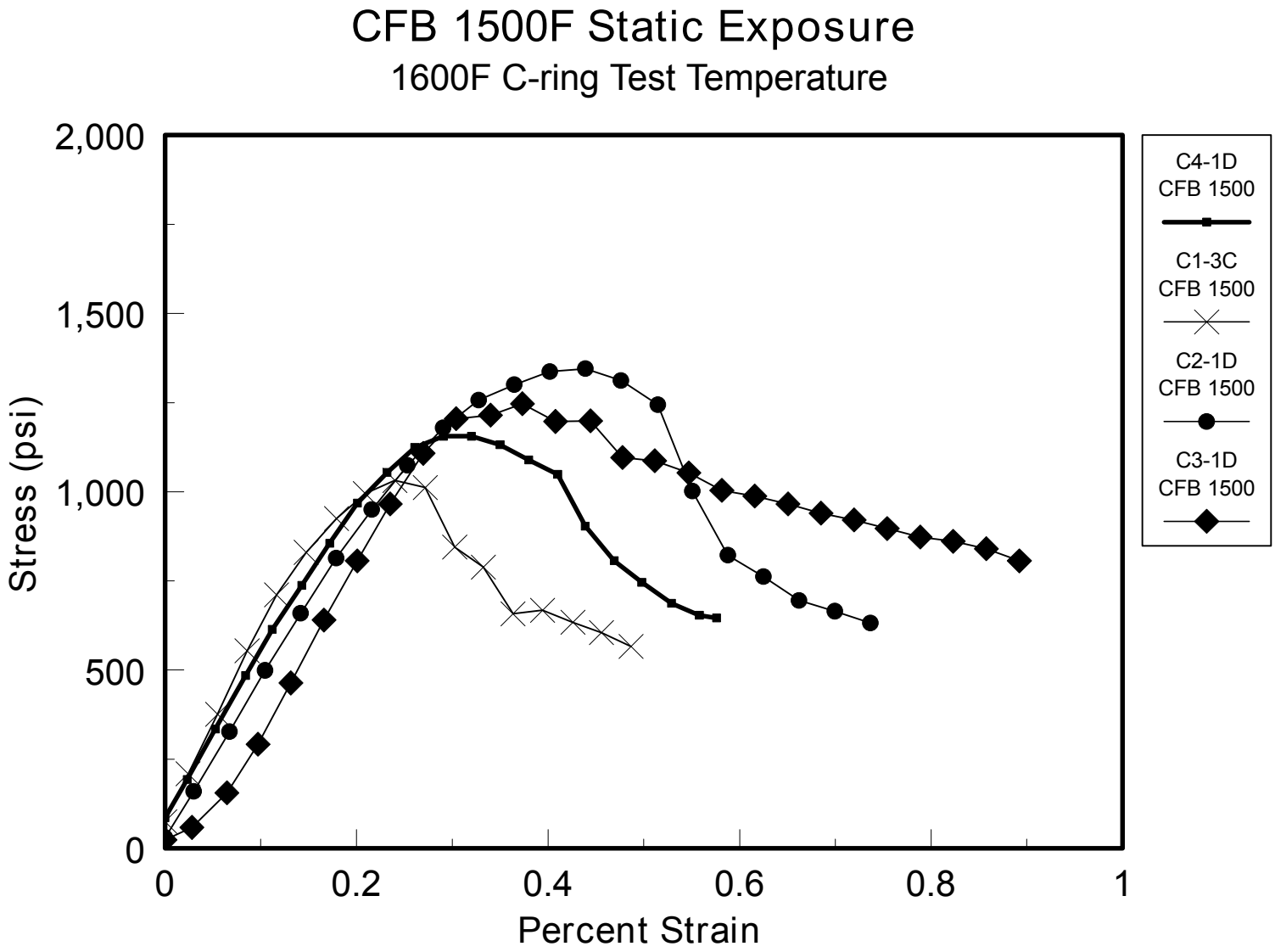
CFB 1500F Static Exposure
1600F C-ring Test Temperature
2,000
1,500
1,000
500
0
Stress (psi)
0
0.2
0.4
0.6
0.8
1
Percent Strain
C4-1D
CFB 1500
C1-3C
CFB 1500
C2-1D
CFB 1500
C3-1D
CFB 1500

Figure 3

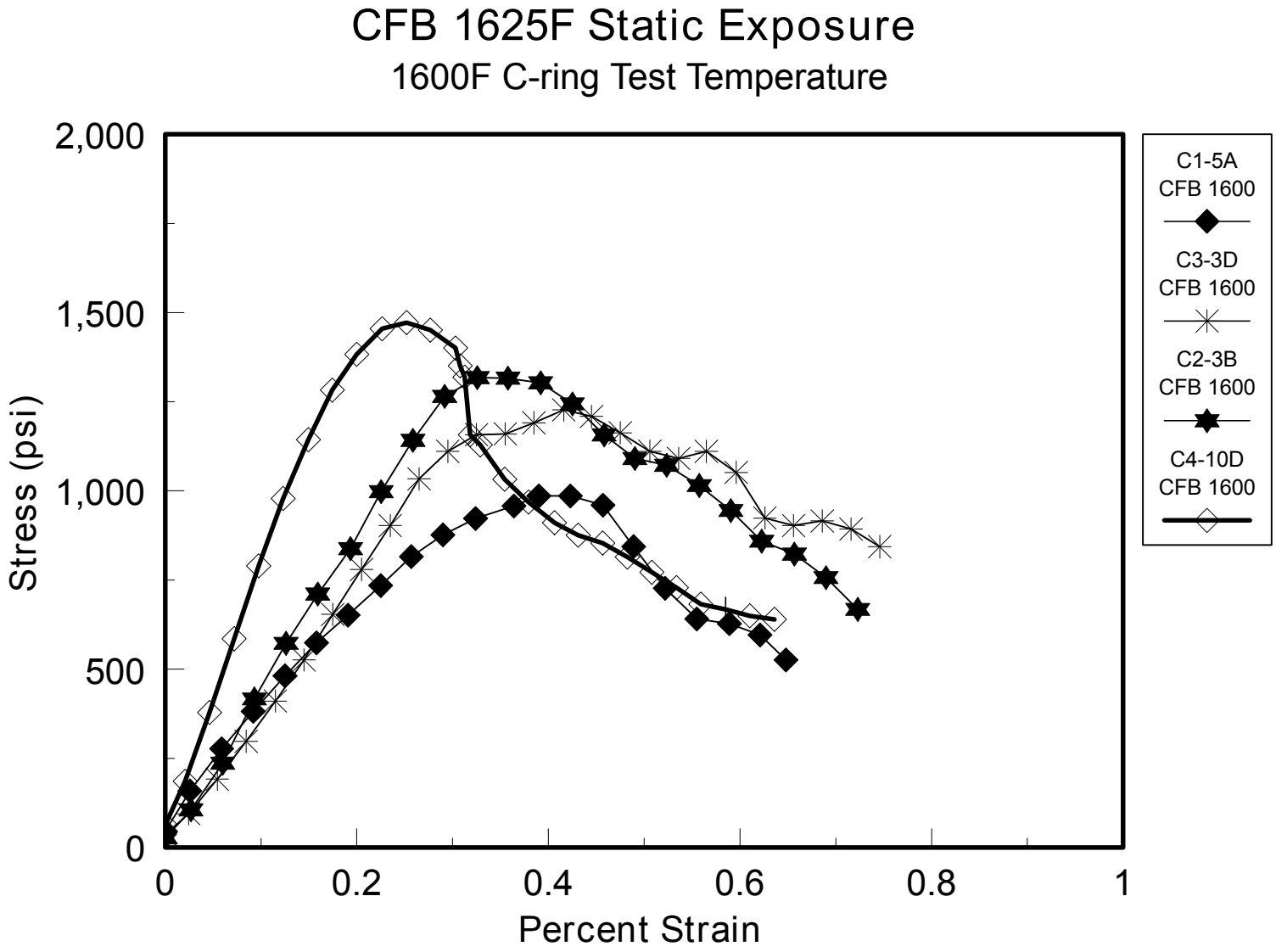
CFB 1625F Static Exposure
1600F C-ring Test Temperature
Stress (psi)
2,000
1,500
1,000
500
0
0
0.2
0.4
0.6
0.8
1
Percent Strain
C1-5A
CFB 1600
C3-3D
CFB 1600
C2-3B
CFB 1600
C4-10D
CFB 1600

Figure 4

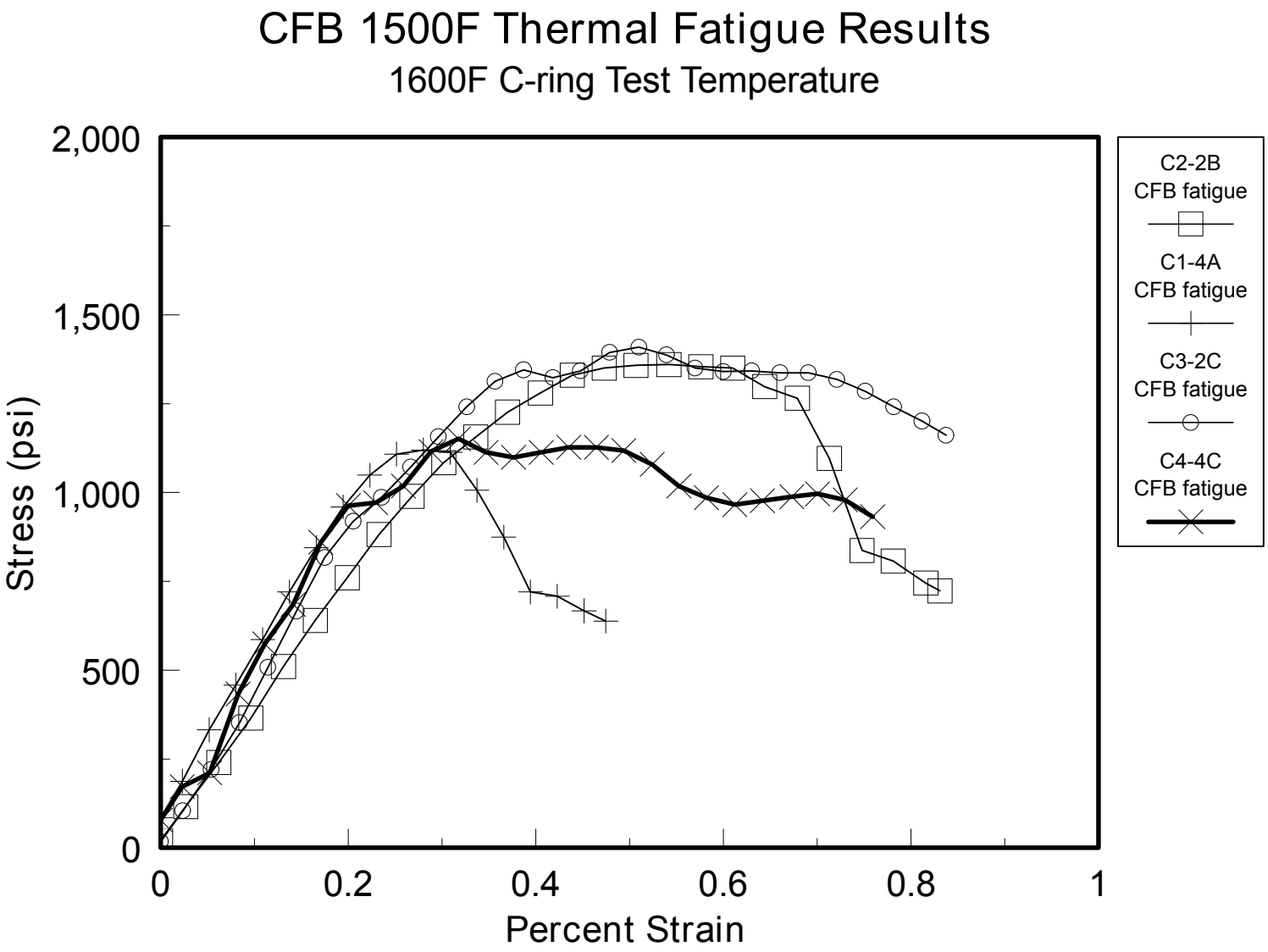
CFB 1500F Thermal Fatigue Results
1600F C-ring Test Temperature
2,000
1,500
1,000
500
0
Stress (psi)
0
0.2
0.4
0.6
0.8
1
Percent Strain
C2-2B
CFB fatigue
C1-4A
CFB fatigue
C3-2C
CFB fatigue
C4-4C
CFB fatigue

3-D Oxide/Oxide Composite Filter

Jay E. Lane (lane.j.e@wec.com, 412-256-2195)
Westinghouse Electric Corporation
Science & Technology Center
1310 Beulah Road
Pittsburgh, PA 15235-5098

Jean-Francois LeCostaouec (603-335-2115)
Techniweave, Inc.
109 Chestnut Hill Road
Rochester, NH 03868

Carol J. Painter [1] (412-256-2202)
Wei-Fang A. Su [1] (412-256-2096)
Ken C. Radford [1] (412-256-1266)
Northrop Grumman Corporation
1310 Beulah Road
Pittsburgh, PA 15235-5098

Introduction

Hot gas particulate filters are key components for the successful commercialization of advanced coal-based power-generation systems such as Pressurized Fluidized-bed Combustion (PFBC), including second-generation PFBC, and Integrated Gasification Combined Cycles (IGCC). Current generation monolithic ceramic filters are subject to catastrophic failure because they have very low resistance to crack propagation. To overcome this problem, a damage-tolerant ceramic filter element is needed.

Objectives

Westinghouse, with Techniweave as a major subcontractor, is conducting a three-phase program aimed at providing advanced candle filters for a 1996 pilot scale demonstration in one of the two hot gas filter systems at Southern Company Service's Wilsonville PSD Facility. The Base Program (Phases I and II) objective is to develop and demonstrate the suitability of the Westinghouse/Techniweave next generation composite candle filter for use PFBC and/or IGCC power generation systems. The Optional Task (Phase III, Task 5) objective is to fabricate, inspect and ship to Wilsonville 50 advanced candle filters for pilot scale testing.

---

[1]Formerly of Westinghouse Electric Corporation

Research sponsored by the U.S. Department of Energy's Morgantown Energy Technology Center, under contract DE-AC21-94MC31167 with Westinghouse Electric Corporation, Science & Technology Center, 1310 Beulah Road, Pittsburgh, PA 15235-5098; FAX (412) 256-1267.

A major objective of the base program is to develop an oxide CMC (ceramic matrix composite) candle filter that is cost competitive with prototype next generation filters. This goal is to be achieved through the use of a low cost sol-gel fabrication process and a 3D fiber architecture optimized for high volume filter manufacturing. During the Base Program, manufacturability for large scale filter production will be assessed in order to meet the needs of commercial scale power generation facilities. The results from this assessment will be implemented during the Optional Task.

Approach

This project plans to develop an advanced filter with damage tolerance, increased durability, increased resistance to crack propagation, and non-catastrophic metal-like failure characteristics through the use of:

- A 3D continuous fiber preform for reinforcement;
- Oxide materials, which are inherently stable in oxidizing environments and have been shown by Westinghouse under DOE Contract #DE-AC21-88MC25034, Thermal/Chemical Degradation of Ceramic Cross-Flow Filter Materials, to be more resistant to corrosive alkali species than nonoxides, such as SiC and Si_3N_4; and,
- Low cost sol-gel processing.

Project Description

Westinghouse and Techniweave have undertaken a three-phase program to develop an advanced ceramic composite oxide-based. Recently completed, Phase I, Filter Material Development and Evaluation, activities included the laboratory-scale development, characterization, and testing of a mullite matrix 3D fiber-reinforced (Nextel 550) ceramic composite filter material. This effort focused on developing the base filter material, minimizing fabrication costs and meeting filter material requirements.

Currently ongoing, Phase II, Prototype Filter Fabrication and Evaluation, activities include additional coupon testing of Nextel 610 (polycrystalline alumina fiber) and Nextel 720 (polycrystalline alumina + mullite fiber) CMC filter materials, the development of a prototype filter, and filter qualification testing in a simulated pressurized-bed combustion environment in the Westinghouse High-Temperature High-Pressure (HTHP) filter test facility.

Phase III, Optional Pilot-Scale Filter Manufacturing, activities include the manufacture of 50 full size candle filters for pilot scale testing at Wilsonville and implementation of quality assurance/quality control and non-destructive evaluation procedures developed in Phase II.

A breakdown of the experimental activity for the recently completed Phase I, Task 3 (Tasks 1 and 2 were the NEPA Report and Test Plan, respectively) and for the ongoing Phase II, remainder of Task 3 and Task 4, follows:

Phase I
Task 3 - Development, Qualification, and Testing of Hot Ga s Filter
3.1 - Coupon Development, Fabrication, and Testing
3.1.1 - Develop 3D Fiber Architecture
3.1.2 - Develop Composite Filter Material Fabrication Process
3.1.3 - Fabricate and Evaluate Best Filter Material

Phase II
Task 3 - Development, Qualification, and Testing of Hot Gas Filter
3.1 - Coupon Development, Fabrication, and Testing
3.1.3 - Fabricate and Evaluate Best Filter Material
3.2 - Develop and Evaluate Prototype Candle Filters
3.2.1 - Weave Filter Preforms
3.2.2 - Make Prototype Ca ndle Filters and Tubes
3.2.3 - Evaluate Prototype Filters
Task 4 - Manufacturing of Hot Gas Filter
4.1 - Filter Manufacturing Plans
4.2 - Filter Materials Test Plan
4.3 - Topical Report

Results

To date, Phase I has been completed. Phase I activities included laboratory-scale development, characterization, and testing of a mullite matrix 3D fiber-reinforced (Nextel 550) ceramic composite filter material. Nine 3D architectures were designed, preforms and CMCs made, tested and evaluated. Permeability, 4-pt bend strength, and microstructural evaluation results were used to downselect to one 3D architecture. High-temperature flow-through corrosion tests up to 400 h and thermal aging tests in static air up to 5000 h were conducted. Based on the above testing, two improvements were made to the filter material. First, modifications were made to the fiber architecture to increase the maximum breaking load. Second, Nextel 550 fiber will be replaced with Nextel 610 or 720 in order to increase corrosion resistance. Additionally, composite test panels made with N610 and N720 showed a significant increase in room temperature bend strength as compared to N550 filter material CMCs. These results are presented in more detail in the remainder of this paper.

3D Fiber Architecture Development

A low cost, three-dimensional (3D) fiber architecture, that is both easy-to-manufacture and automatable, is required to produce an economical 3D preform suitable for candle filter use. Toughness in all directions, good shear properties, homogeneously distributed porosity, and surface smoothness are desirable features for selecting a preform for fabricating a ceramic matrix composite (CMC) candle filter fiber preform. A 3D fiber architecture can be designed to fulfill these requirements. Techniweave's fiber architecture design philosophy has been guided by the selection of automatic net shape weaving techniques, the generation of thin wall

structures, the achievement of fiber continuity through highly stressed regions and the tailoring of the preform to the mode of matrix introduction.

Over the past five years, Techniweave has developed equipment and process technology for weaving seamless, tubular filter preforms with ceramic fibers. During an IRAD program, the use of a multilayer fabric was demonstrated for fabricating a porous mullite/mullite CMC. This technology provides the basis for the fiber architecture variations being evaluated in this program for the economical production of a fiber preform for candle filters. A generic sketch of the multi-layer fabric is presented in Figure 1.

From this baseline weave, Fig. 1, nine fiber architectures were designed to examine the effect of fiber volume, wall thickness, fiber architecture and yarn construction on the CMC filtration characteristics and mechanical properties. The fiber orientation and yarn construction were varied to modify the sizes and distributions of porosity in the preform. The amount of fiber at the preform surface was varied to control the filtering surface smoothness and porosity.

In order to downselect to the best architecture, ceramic composites were fabricated, using the process shown in Figure 2, from each of the nine architectures. Each composite was evaluated for permeability, room temperature 4-point bend strength, toughness, weaving feasibility and potential manufacturing cost. Permeability was measured with a 41 mm diameter disc sample in the Westinghouse permeability rig. Acceptable permeability results from this test rig are gas flow resistance values < 1 in-wg/fpm at room temperature. Bend strength test specimens, 6 mm x 45 mm were machined from both the warp and fill directions of the composite plates and tested according to ASTM C1161-90. The warp and fill directions correspond to the axial and circumferential, or hoop, directions, respectively, of the candle filter geometry. Toughness was determined by a qualitative examination of the load-deflection curves. Weaving feasiblity was evaluated by weaving a closed end section of a filter tube.

The typical macrostructure of the ceramic composite filter materials is shown in Figure 3. The filtering surface has an in-situ deposited membrane layer. As can be seen in the figure, the matrix concentration decreases through the thickness from the dirty gas side to the clean

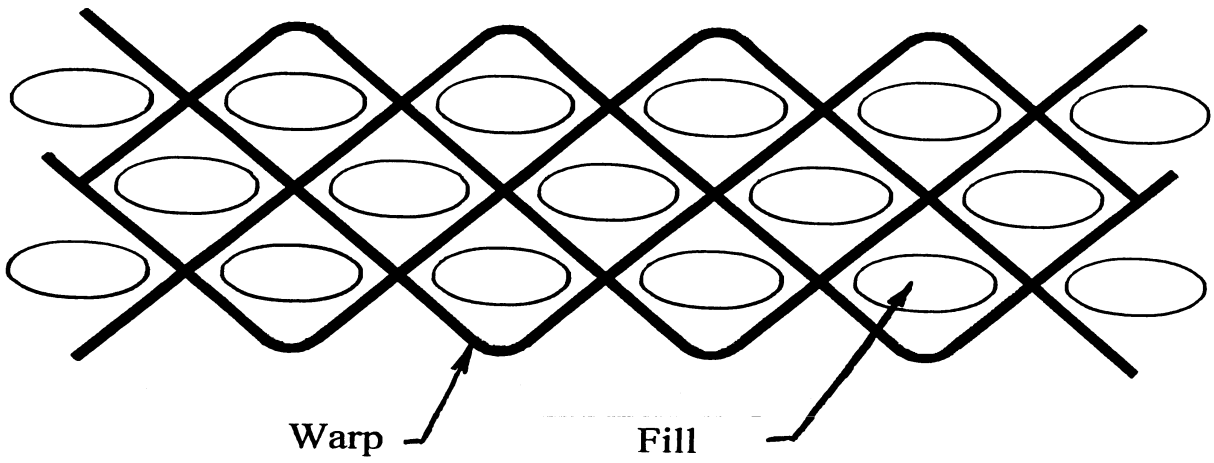

Figure 1. Schematic of multi-layer fabric where the warp yarns provide axial and radial reinforcement while fill yarns provide hoop reinforcement.

gas side. The typical bulk density range for these composites was 1.17 to 1.44 g/cm ^{3}.

Permeability. Gas flow resistance, or permeability, values for all architectures met the gas flow resistance requirement of < 1 in-wg/fpm at room temperature. Permeability was not able to be used as a discriminator in the architecture downselect process.

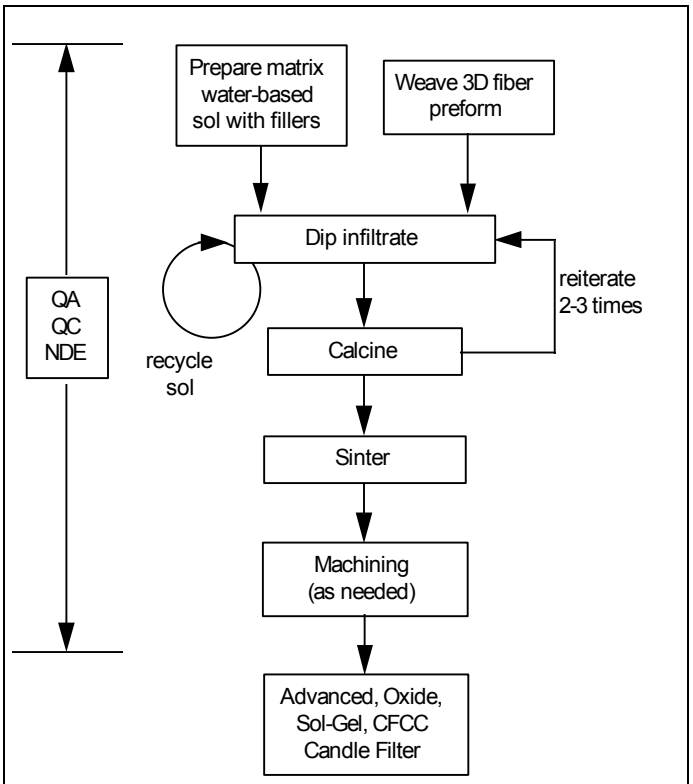

Figure 2 Filter Material Fabrication Process

Mechanical Properties. The downselect process quickly narrowed in on strength and toughness as the primary discriminators between the various architectures. Permeability and cost of fabrication were non-issues as all architectures met the permeability requirements and initial preform weaving trials showed that fabrication costs were expected to be similar. The remainder of this discussion focuses on the differences in strength and toughness as related to the different architectures. The effects of fiber volume, fiber architecture, and matrix content on strength are discussed as is a qualitative analysis of toughness. Table 1 shows the relevant data for this discussion.

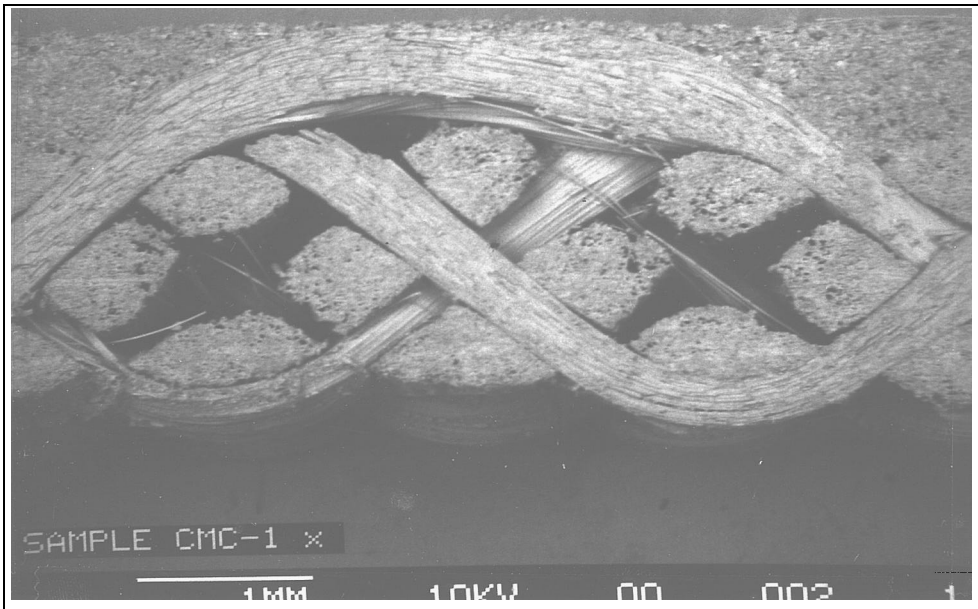

Figure 3 Cross-Sectional View of a Typical Composite Filter Material

Table 1 -- Room Temperature 4-Point Bend Strength Results

CANDIDATE ARCHITECTURES		PREFORM DATA				CMC	CMC BEND STRENGTH	
		Thick.	V_{fw}	V_{ff}	Vf_{tot}	Density	Warp Dir.	Fill Dir.
No.	Description	in.	%	%	%	g/cm³	(psi	(psi)
1	3 surface float	0.080	18	15	33	1.40	1058 ± 224 (5)	1577 ± 455 (6)
2	2 surface float	0.080	17	17	35	1.43	1100 ± 80 (5)	1731 ± 214 (6)
3	2 surface float random	0.080	17	17	34	1.42	1322 ± 289 (5)	1931 ± 328 (5)
4	2 surface float random	0.065	21	12	33	1.25	1104 ± 119 (6)	917 ± 429 (6)
5	baseline warp interlock	0.069	~13	~19	32	1.39	1888 ± 367 (6)	921 ± 122 (6)
6	2 surface float fugitive yarn random	0.064	~14	~11	25	1.79	2076 ± 563 (6)	2061 ± 973 (6)
7	2 surface float random	.0970	19	10	29	1.18	843 ± 255 (12)	625 ± 148 (6)
8	2 surface float random	.0920	16	12	28	1.68	929 ± 148 (10)	1427 ± 328 (6)
9	2 surface float random	.070	20	8	28	1.36	2144 ± 522 (10)	1201 ± 522 (9)

V_{fw}: fiber volume in warp direction; V_{ff}: fiber volume in fill direction; VF_{tot}: total fiber volume
value in parentheses represents number of specimens tested

Effect of Fiber Volume on Strength.

The nine architectures were woven into preforms with total fiber volume ranging from 25 to 35%. Fiber volume in the warp and fill directions was normalized to compare the various architectures. Preforms 5 and 6 were excluded from this analysis as insufficient material was available to accurately measure the fiber volume in the fill (circumferential direction of a filter) and warp (axial or along the length of a filter) directions.

The fiber volume in the fill direction consists of straight fiber tows completely aligned in what would be the circumferential direction of a candle filter. Thus, 100% of the fill fibers are contributing to the strength in the fill direction.

In contrast, the fiber volume in the warp direction, although running in the axial direction of a filter, is not straight but is interwoven around the fill fibers. Thus, the warp fibers have a large proportion of the fiber going through the preform thickness and a lesser quantity of fiber directly aligned in the warp or axial direction. The warp fiber strength is divided to give through thickness strength and integrity to the preform and to give axial strength along the candle filter.

The length of the float (fibers running parallel to the surface in the warp direction) directly contributes to the axial reinforcement with the basic angle interlock architecture #5, which has no fiber parallel at the surface, and the three surface float architecture #1, most fiber parallel at the surface, being the two extremes. The contribution of the warp fibers to the axial reinforcement is, however, more directly dependent on the preform thickness. Thinner wall architectures exhibit through thickness fibers having a smaller angle with the axial direction (i.e., the degree of misalignment with the axial direction is smaller with thinner preforms than thicker ones) which increases their contribution to strength in the axial direction.

Fill Direction Effects. A direct correlation could not be established between strength and the amount of fiber volume in the fill direction. However, composites with fiber volume

greater than 15% in the fill direction, #1, #2, and #3, exhibited greater strength than those with 8-12 % fiber volume.

Examination of the ultimate strength for candidates #4, #7, #8, and #9 indicate that other factors besides fiber volume contribute to the composite strength. Comparison of the #4 to #9 and #8 to #9 would suggest that composite density is also affecting strength, see Table 1. The density of the composite is strongly related to the amount of mullite matrix (from sol + filler powder) in the preform. The penetration of the mullite powder within the preform is affected by the preform architecture (geometrical thickness and yarn construction, or the yarn denier and twist) and the degree of repeatability of the infiltration process.

Warp Direction Effects. Direct comparison of the composite mechanical strength in the warp direction for the different CMCs was only conducted for preforms with equivalent thickness (see prior discussion on fiber volume effects). This comparison was further narrowed to the preforms exhibiting the same double float architecture with the random design: #3, #4, #7, #8, and #9. Normalized fiber volume in the warp direction varied between 16 - 20%. Preform thickness ranged from 0.064 in. to 0.097 in. Given the above constraints, only two sets of architectures were available for direct comparison: #7 to #8 and #4 to #9.

The lowest strengths in the warp direction are observed for #'s 7 and 8, which have thicker preforms, 0.097 in. and 0.092 in., respectively, and intermediate fiber volumes, 18% and 16%, respectively. The strength of these two composites, 843 psi and 929 psi, respectively, is essentially the same.

The other two composites exhibiting similar thickness are #4 and #9, 0.065 in. and 0.070 in., respectively. The normalized warp fiber volume is the same for both composites, about 20%. Analysis of the strength results is complicated because for #4 changes in bend specimen width affected the magnitude of the bend strength; wider specimens were stronger than narrow specimens. The narrow specimen data is given less weight in this analysis because the wider specimens provide a more uniform and representative cross-section of this architecture for bend testing. Composite #9 was tested using wider specimens. The strengths of #4 and #9 are 1908 and 2144, respectively. These strengths are comparative and could be considered relatively the same given the wide standard variations associated with these samples.

The partial conclusions from the review of data in the fill direction were:

- It is possible to achieve reasonable strength level (1200 psi) with only a small amount of fiber in the fill direction (8%).
- Higher strength level (up to 2300 psi) can be achieved with 15% fiber volume.
- The amount of matrix affects the strength level. The respective contributions of the fiber and matrix to the composite strength are not known and their determination is not a trivial issue.

The partial conclusions for the warp direction were:

- Width of the flexure bar specimens can affect the strength data. It is recommended that all future testing be conducted with specimens at least 6 mm (0.24 in.) in width.
- An average bend strength of 2100 psi in the warp direction can be achieved with double float architectures which have low fiber volumes (~11% for #6) and high

densities (1.79 g/cc) or matrix content and which have high fiber volumes (20% for #9) and lower densities (1.36 g/cc) or less matrix content.

Effect of Fiber Architecture on Strength.

Recognizing the complexities in interpreting the test results (limited characterization, sample size effects, etc.) two items, length of the surface float and design repetition, related to the preform architecture were however isolated and are discussed below.

Effect of the Length of Surface Float. Comparison of #1 (3 surface float) and #2 (2 surface float) indicated that the two surface float architecture design provided a narrower spread of strength values than does the three surface float design. The three float design was examined in an attempt to achieve a smoother surface. This approach however does not provide as rigid a preform as does the two surface float. Thus, additional manipulation of the surface float preform would cause variations in the preform which would result in composites with widely varying properties. As noted previously, the use of stuffers in this case would be expected to greatly increase the stability of the preform and result in composite filter materials with more uniform and repeatable properties.

Effect of Design Repetition. Composites #2 and #3 were prepared from preforms exhibiting similar characteristics except for the repetitiveness of the pattern. The #2 architecture has a more oriented fiber pattern than does #3. This preferred orientation of #2 resulted in a rougher surface with aligned ridges and valleys. The random pattern of #3 showed a more uniform surface. Providing a random orientation of the pattern seems to also have a beneficial effect on the mechanical properties of the material; a smoother more uniform surface has less stress concentrations than would the surface of #2. The strength of #3 was slightly higher than that of #2.

Effect of Matrix on Composite Strength.

Architecture #6 was designed with a fugitive yarn to yield a more open composite for improved permeability characteristics. The composite made from #6 had a low fiber volume and a high strength in both directions. The high strength was due to the high density which resulted from a large amount of matrix in the composite. This composite had more matrix because of the fugitive fiber which provided additional surface area to deposit the matrix on during infiltration processing. However, toughness, as discussed below, must also be considered when choosing the right amount of matrix and fiber.

Qualitative Evaluation of Toughness

An appropriate test for toughness is difficult to determine for these composites due to their low thickness. The approach taken here was to compare the shapes of the load-deflection curves (deflection was measured during bend testing with a three probe extensometer) for the various architectures (Note, the load-deflection curves are not shown here because they did not scan very well, but copies of the curves are available for evaluation by contacting the program manager).

A material exhibiting a higher stren gth at the point where the composite loses linearity, i.e. “yields”, (defined in dense composites as the first micro-cracking stress/load) and showing a significant load carrying ability beyond that point can intuitively be qualified as a tougher composite. This point in essence also takes into account the area under the curve. Using this

criteria, #4 (warp direction data only available) was considered the least suitable and #9 was considered the most desirable architecture. Composite #9 exhibits a "yield stress" of 1280 psi in the warp direction and subsequently carried a load to a 2100 psi level and continued to exhibit good strain carrying capability beyond the ultimate load point thus demonstrating a noncatastrophic failure mode.

Architecture Downselect

The architecture downselect process picked #9. The downselect was conducted by direction as follows:

Warp.

- The axial (warp) direction of the candle filter is subjected to bending loads. Candidates with warp strengths less than 1000 psi were first rejected -- #7 and #8.
- Architectures with a nonrandom (oriented design) were rejected (for reasons discussed previously). This left architectures #3, #4, #5, #6, and #9.
- The composites exhibiting the highest warp strengths were then selected. These were #3, #6 and #9.
- Toughness then was considered and #9 had the best qualitatively determined toughness. Architecture #3 might have been further considered if there was additional strength data with wider bend bar specimens for evaluation. Architecture #6 did not have load-deflection data for the warp direction. However, a #6P, the P represents the use of pressure during matrix processing, did have load-deflection curves. From these curves, is was determined that #6 had a low degree of toughness, most likely due to its high matrix content which made it act more like a monolithic.

Fill.

- Using the first two criteria above, minimum strength and randomness of design, the list was narrowed to #3, #6, #8, and #9.
- In general, load-deflection curves in the fill direction showed less load carrying ability after the initial "yield" than those of the warp direction. Again, #6 exhibited poor toughness. This left #3, #8 and #9.
- Combining the results above, #8 was rejected due to its low warp strength. Given the available data, #9 was chosen over #3 due to its higher warp strength and because it had the best toughness characteristics.

In summary, fiber architecture #9, a random double float architecture, was selected because adequate flexure strength was obtained in both the warp and fill directions and because the load-deflection curves exhibited the best toughness.

CMC Evaluations

Two types of tests were conducted to determine the effects of temperature, time, and the environment on the Nextel 550-based filter composite material's mechanical properties and failure characteristics. First thermal aging tests were conducted in which bend specimens were exposed to 150, 300, 800, 2000, and 5000 h at 870°C in static air and then bend tested at

room temperature. Because there was insufficient material from any one architecture to conduct these tests, specimens were used from the first six architectures for the thermal aging experiments. These specimens all had the same matrix composition and were processed identically. The resulting thermal aging bend data was then normalized with respect to the as-received bend data in order to eliminate architecture effects.

Second, four high-temperature, flow-through corrosion tests were conducted in which specimens were exposed to of 400 h at 870°C with simulated pulse cycling in flow-through steam/air with and without alkali. Post-test characterization included high temperature bend testing and microstructural evaluation.

Thermal Aging

Figure 4, shows the normalized bend strength vs. exposure time. From this data, up to 5000 h in static air at 870°C, there appears to be little effect of temperature on strength. Consequently, x-ray diffraction was conducted for each of the thermally aged specimens. X-ray diffraction (XRD) data did not show any change in phase chemistry of the samples. The XRD spectrum for the 5000 h data can be directly overlaid on the 2000 h spectrum and the as-received (unaged) spectrum without any noticeable differences in any of these spectra. (Note, the x-ray diffraction curves are not shown here because they did not scan very well, but copies of the curves are available for evaluation by contacting the program manager).

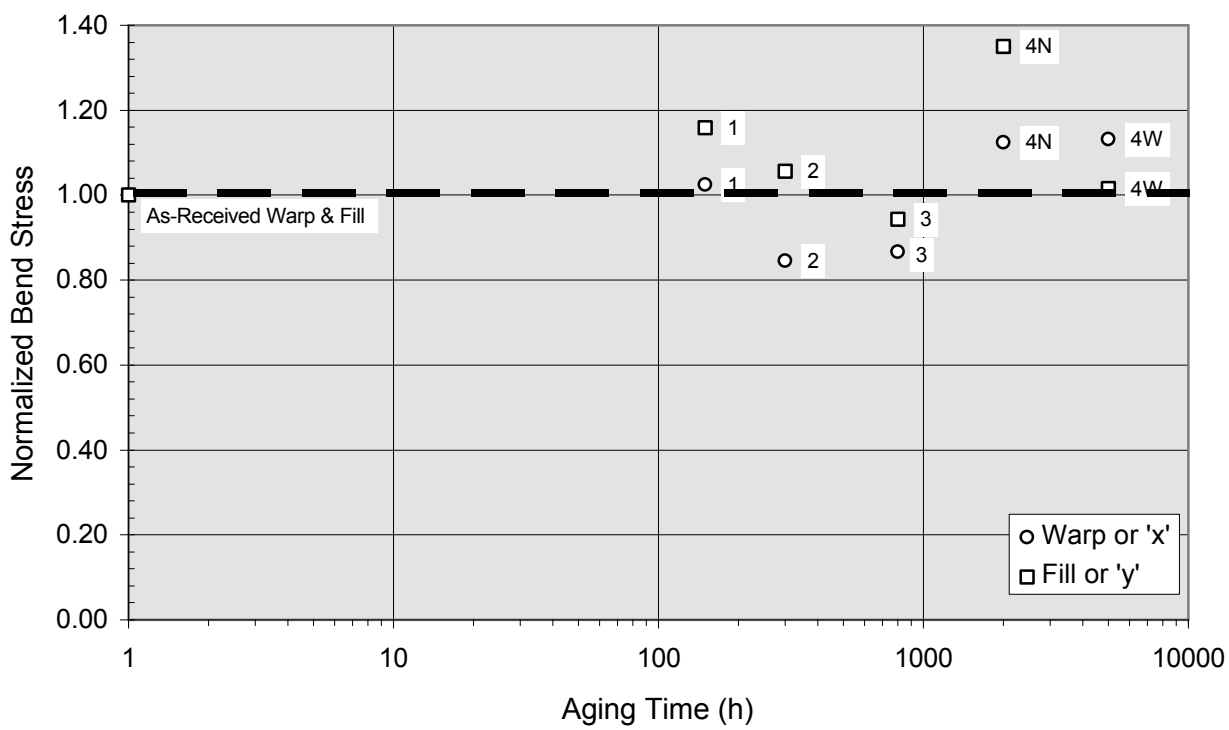

Figure 4 Effect of Thermal Aging at 870°C in Static Air on Room Temperature 4-pt Bend Strength

High Temperature Flow Through Corrosion Testing

Figure 5(a) and (b) clearly demonstrate the results of the flow through corrosion testing. Discs, Fig. 5(a), exposed to steam/air only survived the tested, whereas, discs, Fig. 5(b), exposed to steam/air containing 20 ppm sodium cracked longitudinally in the center, where the stresses would be the highest during backpulsing. Subsequent SEM examinations of the sodium exposed samples showed crystallization along the outer surface of the Nextel 550 fibers. EDAX, energy dispersive x-ray, analyses of these same regions showed the presence of sodium and silicon with a lower concentration of aluminum than expected.

These high-temperature, flow-through tests conducted with Nextel 550 reinforced ceramic composite filter materials showed that this material was susceptible to alkali (Na) attack. The as-produced Nextel 550 fiber is composed of δ- and γ-alumina and amorphous silica. SEM and EDAX analyses indicated that the Nextel 550 fiber, with this amorphous silica phase, was probably attacked by the sodium resulting in devitrification of the amorphous silica which caused embrittlement of the fiber. The test coupons used for the high temperature steam/air/alkali test (870°C, 400 h) broke in two either during testing or immediately upon removal from the test rig; these coupons were highly embrittled. The test coupons subject to steam/air-only were not embrittled and were intact, and remained intact, after removal from the test rig.

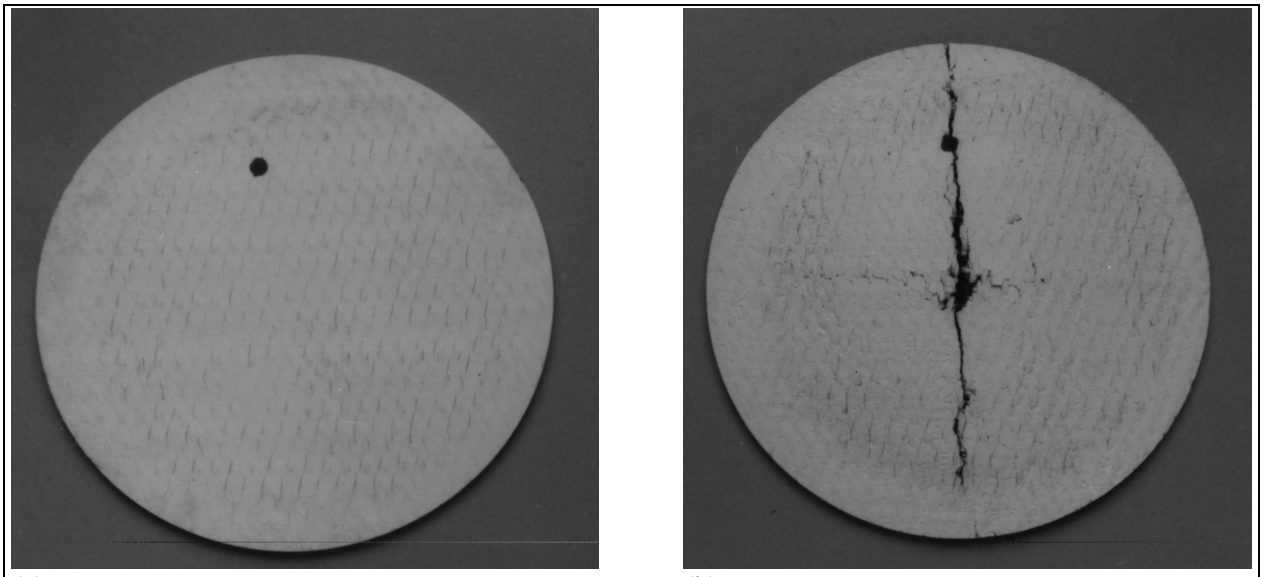

(a) (b)

Figure 5 Optical photographs of flow through test specimens exposed to 870°C for 400 h in (a) 5-7% steam and (b) 20 ppm NaCl/5-7% steam/air

Filter Material Improvements

Bend strength testing and the high temperature, flow-through testing raised the following two technical issues. These issues are discussed in the following paragraphs and the approaches to resolve them are discussed in the following subsections.

First, the ultimate breaking loads, < 1 lb (see Table 1), were considered to be too low, even though the material had sufficient strength, 1000-2000 psi, for filter use. These low breaking loads were primarily due to thin wall structures, 0.100 in., and low fiber volume fractions, < 30 %. Thin wall preforms and minimized fiber volumes were targeted in order to reduce cost. Although, the breaking loads are low for the coupon samples, it is unclear whether or not this would be an issue for full size candle filters. Potential filters made from this material were considered to be susceptible to breakage during handling and installation.

Second, the filter composite material was embrittled during flow-through testing in an alkali environment as discussed in the previous section. Although this test is relatively harsh, it may be considered an accelerated environmental test which could be indicative of long-term material behavior. The embrittlement was due to devitrification of the amorphous phase in the fiber Nextel 550 fiber.

Architecture Modifications

The downselected architecture #9 was modified by adding stuffer yarns which increased the preform thickness. This modification not only raised the breaking load capability of the filter material, as shown in Table 2, but also increased the filter composite material strength as shown in the table. Stuffer architectures #10-#13 represent different combinations of stuffer fiber amount, direction(s) of stuffer fiber, and preform wall thickness. The highest breaking load, warp - 6.6 lb and fill 8.2 lb, was achieved by CMC 13 with a 0.15 in. wall thickness. However, this architecture also uses the most fiber and would result in the highest cost filter of the four stuffer architectures shown in the table.

Architectures 11 and 12 had lower fiber volumes, comparable to the downselected conventional architecture 9, would have comparable filter fabrication costs, and do provide an increased breaking load. These architectures also provide significant strength benefits, without sacrificing cost by increasing fiber volume, as a result of the stuffer modifications the preform architecture, see Figure 6. Based on a qualitative evaluation of the load-deflection curves, toughness for the stuffer modified composites appeared to be better than for architecture 9.

Table 2. Summary of Mechanical Testing Results for CMC 9 and Stuffer Modified CMCs 10-13

Sample ID	Mean Thick (in.)	Warp Direction (X)		Fill Direction (Y)	
		Mean Strength* (psi)	Breaking Load (lb)	Mean Strength* (psi)	Breakin g Load (lb)
9 conventional	0.059	2144 ± 522 (10)	0.64	1201 ± 522 (9)	0.45
10	0.073	3731 ± 160 (4)	3.0	1652 ± 223 (5)	1.6
11	0.069	3745 ± 284 (5)	2.8	2525 ± 245 (3)	2.1
12	0.105	3745 ± 165 (4)	3.3	3044 ± 300 (4)	6.2
13	0.149	2334 ± 280 (5)	6.4	1958 ± 440 (5)	8.2

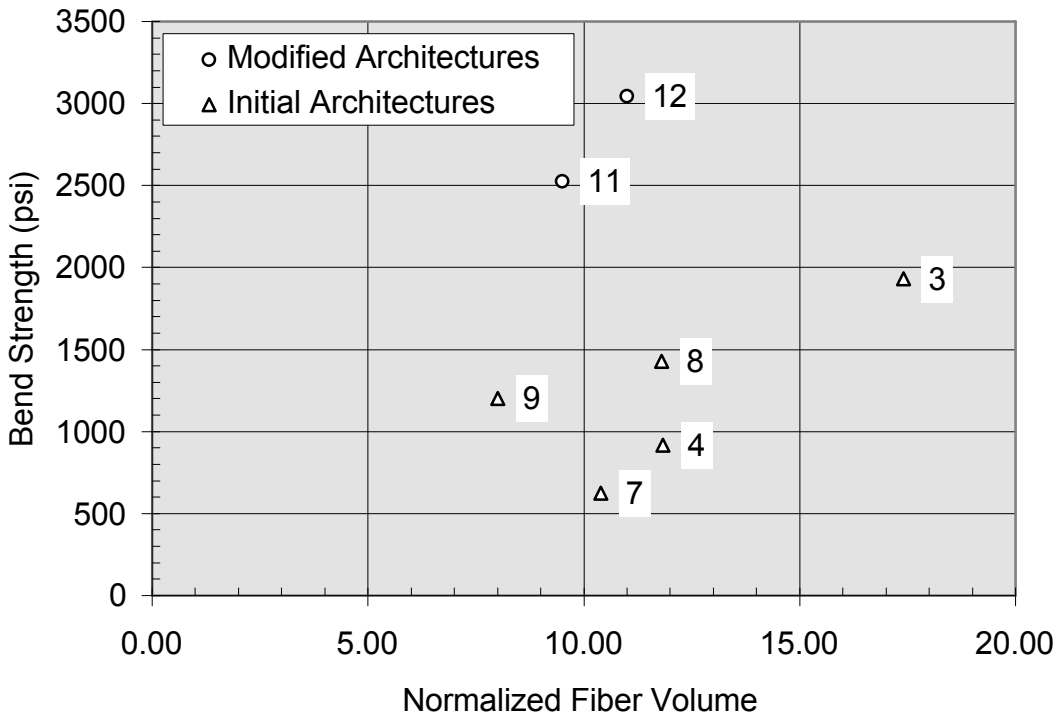

Figure 6 Plot of bend strength vs normalized fiber volume which show the effects of architecture and fiber volume on strength.

*number of samples tested is shown in parentheses

Reinforcement Fiber Selection

Nextel 610 (alumina) and Ne xtel 720 (polycrystalline mullite+alumina) were evaluated as replacements for the Nextel 550 fiber. Preforms were woven using an architecture similar to the stuffer modified architectures 11 and 12. For the Nextel 610 fiber, the precrystallized version was used to weave the preforms. Due to its lower elastic modulus, i.e., reduced stiffness, precrystallized N610 is much easier to weave than crystallized N610. After weaving the precrystallized N610 preform is subjected to a heat treatment cycle which converts the fiber to normal fully crystalline N610. Both preforms were fabricated with stuffers and double floats, based on prior fiber architecture development work discussed earlier. The stuffers increase the breaking load capability and the double floats provide a smoother surface more applicable for ash cleaning during backpulsing. Table 3 provides the relevant measured characteristics of the two preforms.

The preforms were processed in the same manner as the architecture 9 and stuffer modified architectures. Bend bars were machined from each specimen and tested at room temperature. The preform architecture used for both the N610 and N720 samples is most similar to N550 (N550) architectures 11 and 12, which are stuffer modified versions of architecture 9.

Table 3 -- Characteristics of N720 and N610 3D Fiber Preforms

Characteristic	Preform 15	Preform 16
Fiber Type	N720 alumina+mullite	N610 alumina
Thickness (in.)	0.120	0.120
Fiber Volume (%)	30	26.5
Fill (%)	13.9	11.5
Warp Stuffer (%)	6.8	6.0
Warp Interlock (%)	9.3	9.0

Table 4 compares the mean strength and breaking load results of Nextel 550 CMCs 9 and 10-13 (stuffer-modified) to that of Nextel 610 CMC 16-3 and Nextel 720 CMCs 15-3 (warp, or candle axial, direction) and 15-4 (fill, or candle circumferential, direction). These CMCs were all processed using the same standard baseline Techniweave process. The N610 CMCs, in the fill direction, are 42% stronger and have a 42% higher breaking load than the best N550 CMC in the table.

The N720 CMCs are 50% and 94% stronger in the warp and fill directions, respectively, than the best N550 CMCs shown. The greatest improvement is in the breaking load which for the N720 CMCs is 165% and 152% stronger in the warp and fill directions, respectively, than the best N550 CMC shown. Because of the improved breaking loads, the use of either the N610 or N720 fiber greatly increases the handleability of this filter material. Qualitatively both materials also exhibited improved toughness over the Nextel 550 CMCs.

Table 4 -- Bend Strength and Breaking Load Comparison of Filter CMCs made with Nextel 550, 720 and 610 Fibers
(All CMCs were processed the same and fired at the standard baseline processing temperature)

Sample ID	Warp Direction (X)		Fill Direction (Y)	
	Mean Strength* (psi)	Breaking Load (lb)	Mean Strength* (psi)	Breaking Load (lb)
Nextel 550 CMCs				
9 - conventional	2144 ± 522 (10)	0.64	1201 ± 522 (9)	0.45
10 - stuffer	3731 ± 160 (4)	3.0	1652 ± 223 (5)	1.6
11 - stuffer	3745 ± 284 (5)	2.8	2525 ± 245 (3)	2.1
12 - stuffer	3745 ± 165 (4)	3.3	3044 ± 300 (4)	6.2
13 - stuffer	2334 ± 280 (5)	6.4	1958 ± 440 (5)	8.2
Nextel 720 CMCs with preform architecture similar to 11 & 12				
15-3 (warp) and 15-4 (fill)	5507 ± 408 (3)	17.0	5910 ± 628 (3)	20.7
Nextel 610 CMCs with preform architecture similar to 11 & 12				
16-3	not measured	not measured	4334 ± 1168 (3)	11.69

*number of samples tested is shown in parentheses

Future Activities

Future, Phase II, activities consist of conducting high temperature flow-through corrosion tests and short-term (~600 h) thermal aging tests of the above discussed Nextel 610 and Nextel 720 based composite filter materials. The test results will be used to select a fiber to be used for fabricating 1.0 m long candle filters which will be subjected to a series of tests in the Westinghouse High Temperature, High Pressure Filter Test Facility.

Acknowledgments

The authors wish to acknowledge the program support and technical guidance provided by Ted McMahon, the METC/COR, over the course of Phase I, 9/30/94 - 5/31/96. We would also like to thank Mary Ann Alvin for her technical suggestions, the permeability analyses, and with Rich Kunkle, the conduct of the high temperature flow through corrosion tests; Mike Biondi for his diligent work in the laboratory; Tom Mullin for the SEM support; and, Paula Freyer for the XRD analyses.

Iron Aluminide Hot Gas Filters

J. Hurley (John_Hurley@Pall.com;607-753-6041)
S. Brosious (Sandy_Brosious@Pall.com)
M. Johnson (Mark_Johnson@Pall.com)
Pall Corporation
Pall Process Equipment Development Department
3669 State Route 281
Cortland, NY 13045

Period of Performance September 1995 to June 1996

Schedule and Milestones

FY 96 Program Schedule

	M	J	J	A	S	O	N	D	J	F	M	A	M	J	J	A	S
NEPA Info	---	---	---	---													
Test Plan	---	---	---	---	---	---											
Devel., Quali. Testing					---	---	---	---	---	---	---						

Introduction

Currently, high temperature filter systems are in the demonstration phase with the first commercial scale hot filter systems being installed on integrated gasification combined cycle (IGCC) and pressurized fluid bed combustion cycle (PBFC) systems (70 MW). They are dependent on the development of durable and economic high temperature filter systems. These filters are mostly ceramic tubes or candles. Ceramic filter durability has not been high. Failure is usually attributed to mechanical or thermal shock: they can also undergo significant changes due to service conditions.

Research sponsored by the U.S. Department of Energy's Morgantown Energy Technology Center, Theodore J. McMahon METC Project Manager, under Contract DE-AC21-95MC31215 with Pall Aeropower, Kenneth B. Zella Program Manager, 6301 49th Street North, Pinellas Park Florida, 34665-5798; fax (813) 528-0516.

Objectives

The overall objective of this project is to commercialize weldable, crack resistant filters which will provide several years service in advanced power processes.

The specific objectives of this project are to develop corrosion resistant alloys and manufacturing processes to make Iron Aluminide filter media, and to use a "short term" exposure apparatus supported by other tests to identify the most promising candidate (alloy plus sintering cycle). The objectives of the next phases are to demonstrate long term corrosion stability for the best candidate followed by the production of fifty filters (optional).

Approach

Seamless cylinders have over the last several years become widely accepted for the manufacture of stainless steel filters. It follows, therefore, that much of the technology needed to produce seamless cylinders in a different alloy such as Iron Aluminide has already been worked out. For example, experimental Iron Aluminide seamless cylinders are made on the same equipment used for the production of seamless cylinders in stainless steel. Some important changes are obviously needed and they are addressed in this project. Basically three steps must be added or revised. To produce a high strength cylinder in Iron Aluminide it is necessary to first, tailor some processing details during the production of the cylinders, second, add a compaction step for the cylinders and, third, develop an optimized sintering cycle. The manufacture of seamless cylinders is a proprietary process.

There is a wealth of information on solid Iron Aluminide determined and/or compiled by Oak Ridge National Laboratory (ORNL). This provides a valuable resource (1).

Project Description

The project is being carried out in five tasks. Task 1 provided the management plan and the necessary NEPA information. Task 2 provided the test plan. The first two tasks have been completed. Task 3 provides the experimental work to implement the test plan: it is now underway. Figure 1 shows the sequence of steps involved in making a seamless filter. It starts with securing a supply of powder and proceeds to welding the components together to make a filter. Task 3 includes any subsequent steps such as preoxidation that would be carried out before placing the filter in service. The upgrading and operation of a test apparatus for "short term" exposure testing of Iron Aluminide candidates is also covered. Experimental work is authorized to the completion of Task 3. At the end of Task 3 the best composition and processing sequence will be chosen for further development.

In Task 4 the most promising candidate will be subjected to further long term exposure. This will be followed by the manufacture of 50 filters (optional).

FIGURE 1
PRODUCTION OF IRON ALUMINIDE SEAMLESS FILTERS

- POWDER QUALIFICATION
- SPINNING OF SEAMLESS CYLINDERS
- COMPRESSION OF SEAMLESS CYLINDERS
- VACUUM SINTERING
- WELDING END FITTINGS

Candidates

There are four candidates. The first three candidates have different chemical compositions and will be preoxidized (2) before being placed in service:

* Fe_3Al with 2%Cr (Similar to FAS but with 0.19% by weight Zr and without B)
* Fe_3AL with 5%Cr (Similar to FAL with 0.19% by weight Zr but without B)
* FeAl (with 0.19% by weight of Zr plus 0.004 % B).

The fourth candidate is the first composition but without preoxidation.

The preoxidation treatment (800C in air for seven hours) was developed by ORNL (2). The preoxidation treatment favors the formation of a surface enriched in alumina: this is particularly beneficial for resistance to gases containing hydrogen sulfide.

Seamless Cylinders

The preferred product form for Iron Aluminide porous media is as seamless cylinders. The benefits are identified in Figure 2. The uniformity of the pore structure combined with good void volume account for the first four points. The use of seamless cylinders allows the use of advanced alloys such as Iron Aluminide that are tough enough for the intended service but whose ductility may not be sufficient to allow them to be fabricated from flat sheet. The use of a seamless cylinder eliminates the need for a longitudinal seam weld and the resultant heat affected zones (HAZ) on either side of the weld bead. The tensile hoop stresses (during blowback) are twice as high as the stresses at the junction of the endcap with the filter medium. The process produces an intrinsically uniform and inexpensive medium since the key steps are preprogrammed and are under computer control. This removes them from operator variability. Finally, the use of seamless cylinders is economical in that there is almost no powder wastage, the ceramic tubes and the bladders are reusable, etc.

Satisfactory results have been achieved using either water atomized or gas atomized powder. There is a mild preference to use water atomized powder because it promotes high green strength due to its rough surface, as can be seen in Figure 3.

The first step in making a seamless cylinder is to take a ceramic tube and temporarily seal it at one end. Measured quantities of a thickened water based solution and Iron Aluminide powder are mixed together and are poured into the ceramic tube which is again temporarily sealed at the other end. The ceramic tube is then spun in a lathe where the suspended powder deposits uniformly on the interior of the ceramic tube. The remaining liquid is decanted and the assembly is dried. The residual thickener at this point functions as a temporary bonding agent for the powder.

Compression of Preform Seamless Cylinders

With Iron Aluminide the preform assembly is isostatically compressed. Reusable rubber bladders are added to the inside and the outside of the preform assembly and they are sealed to prevent the entry of water during the compression step.

FIGURE 2
BENEFITS OF SEAMLESS TUBE FILTERS

- HIGH VOID VOLUME AND UNIFORM PORE STRUCTURE
- UNIFORM WALL THICKNESS AND TUBE DIAMETER
- BLOWBACK IS UNIFORM DUE TO CONSISTENT PORES
- PRESSURE DROP IS LOWER THAN CONVENTIONAL CONSTRUCTION
- READILY ADAPTS TO HIGH PERFORMANCE ALLOYS SUCH AS Fe_3Al AND FeAl
- FREE FROM WEAKNESS OF LONGITUDINAL WELD HAZ
- CONSISTENT PROGRAMMED MANUFACTURE
- ECONOMIC - LITTLE SCRAP, MOLDS REUSABLE, etc.

FIGURE 3
IRON ALUMINIDE POWDER AS WATER ATOMIZED - SEM AT 300X

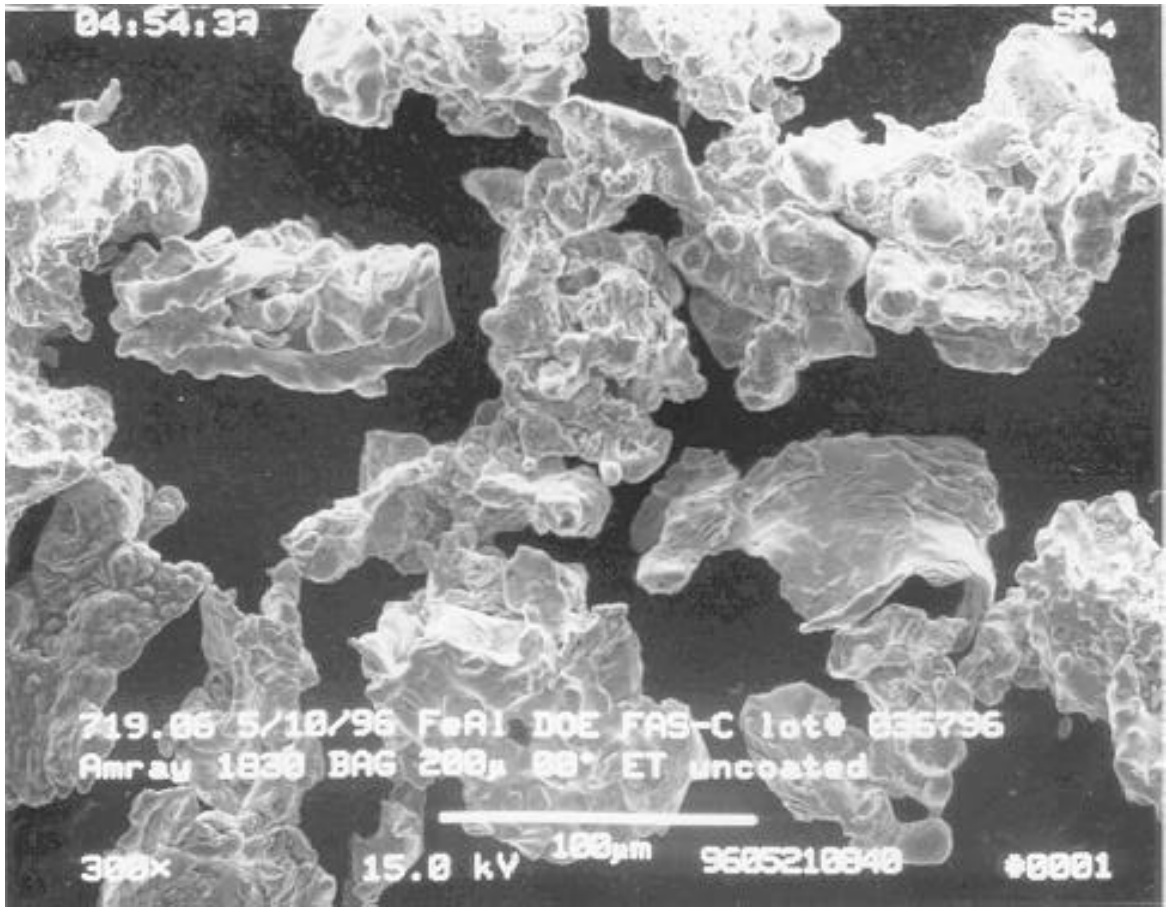

Vacuum Sintering

The tubes are usually sintered in the vertical position. The Iron Aluminide preform is supported by the ceramic tube as the assemblies are heated to the sintering temperature - that is until a point is reached where the Iron Aluminide shrinks markedly as it sinters. There is a straightforward explanation. The Iron Aluminide is held in compression as it is heated since it has a higher coefficient of thermal expansion than the surrounding ceramic. Once the sintering operation is complete the Iron Aluminide seamless cylinders are removed from their protective ceramic tubes. The seamless cylinders are then cut to length.

Welding End Fittings

The end fittings can be 310S (a readily available high temperature stainless steel) or solid Iron Aluminide. Generally speaking, the welding of porous Iron Aluminide to solids is preferably done using a single pass Gas Tungsten Arc (or TIG) weld. The filler can be either 310S or Iron Aluminide. Both fillers have been used successfully but it is distinctly easier to use the 310S. Figure 4 shows that the test specimens are small welded filters.

"Short Term" Exposure Apparatus

As part of this project a "short term" exposure test apparatus has been markedly upgraded. Mixing of the gases that compose the test atmosphere is now done by mass flowmeters. An eight channel programmable controller directs the mass flowmeters.

The test apparatus is composed of two connected tube furnaces. In the first furnace the premixed gases and the injected water are preheated. The preheated atmosphere flows into the second furnace where it contacts the test filters. Figure 5 shows a schematic of this second furnace. The containment tubes for both furnaces are aluminized 310 stainless steel.

Three upgrades have been added in addition to the mass flowmeters. Each was chosen because it allows an important service condition to be studied in greater detail:

* First , the test atmosphere now flows <u>through the wall</u> of the test filter as in actual service,
* Second, an instrumented and programmable<u>blowback</u> capability has been added,
* Third, potential corrosion accelerators such as <u>(HCl + NaCl + KCl)</u> can now be added to the furnace atmosphere.

The upgrades to the test apparatus have been completed and the apparatus is now fully qualified. It is ready for the "short term" testing to begin. At the conclusion of this testing program the results will be analyzed and the best overall composition and processing sequence will be chosen.

Test Results to Date

Powder Supply

A supply of powder for each of the three compositions has been purchased. Air induction melts were made followed by water atomization. Two hundred pounds of each composition have been sieved to the -100 +325 range.

FIGURE 4
IRON ALUMINIDE FILTER MEDIUM IS CIRCUMFERENTIALLY WELDED

GAS TUNGSTEN ARC (TIG) PROCESS USED.

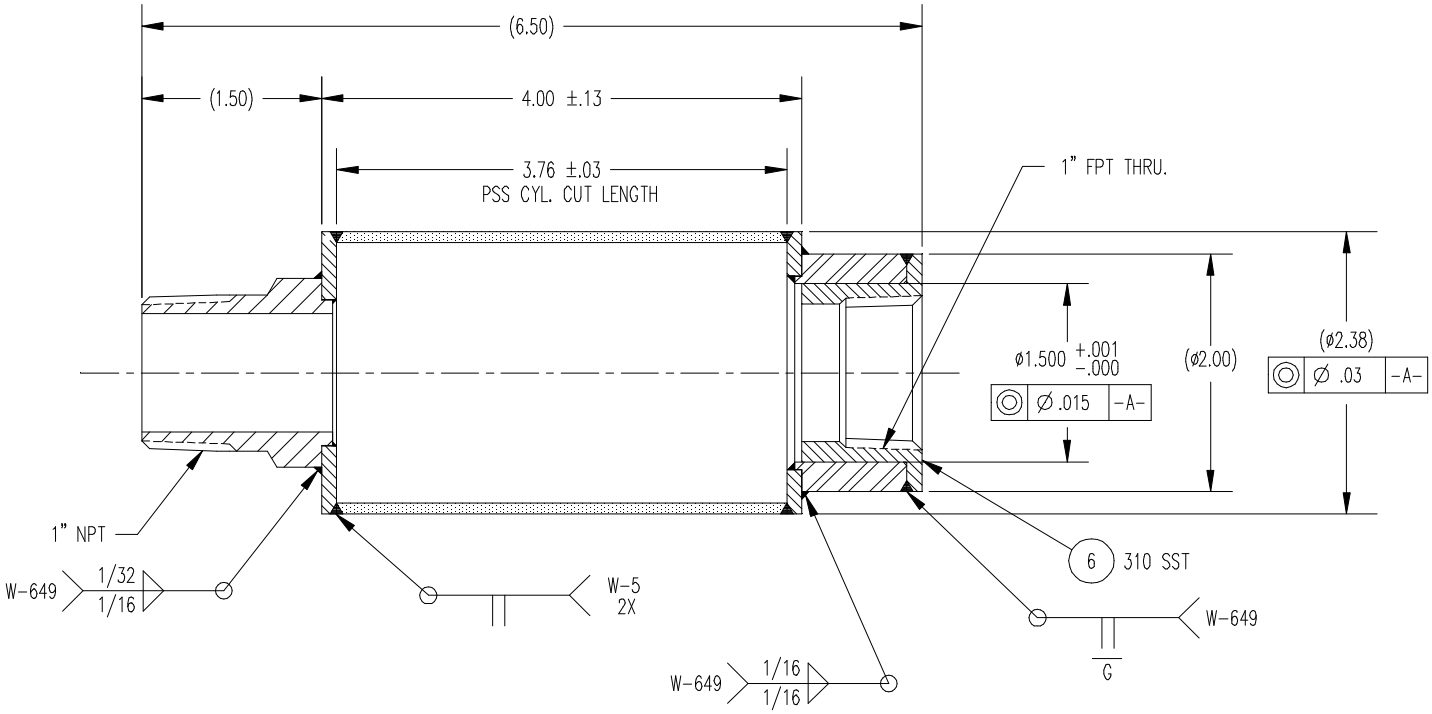

FILTER FOR SHORT TERM TESTING

FIGURE 5
CLOSE-UP SCHEMATIC OF PROCESS TUBE FOR SHORT TERM EXPOSURE

- FLOW THROUGH DESIGN
- PROVISION FOR BLOWING BACK - INTERMITTENT OPERATION
- PROVISION TO ADD HCl+NaCl+KCl TO PREMIXED H_2S CONTAINING ATMOSPHERE

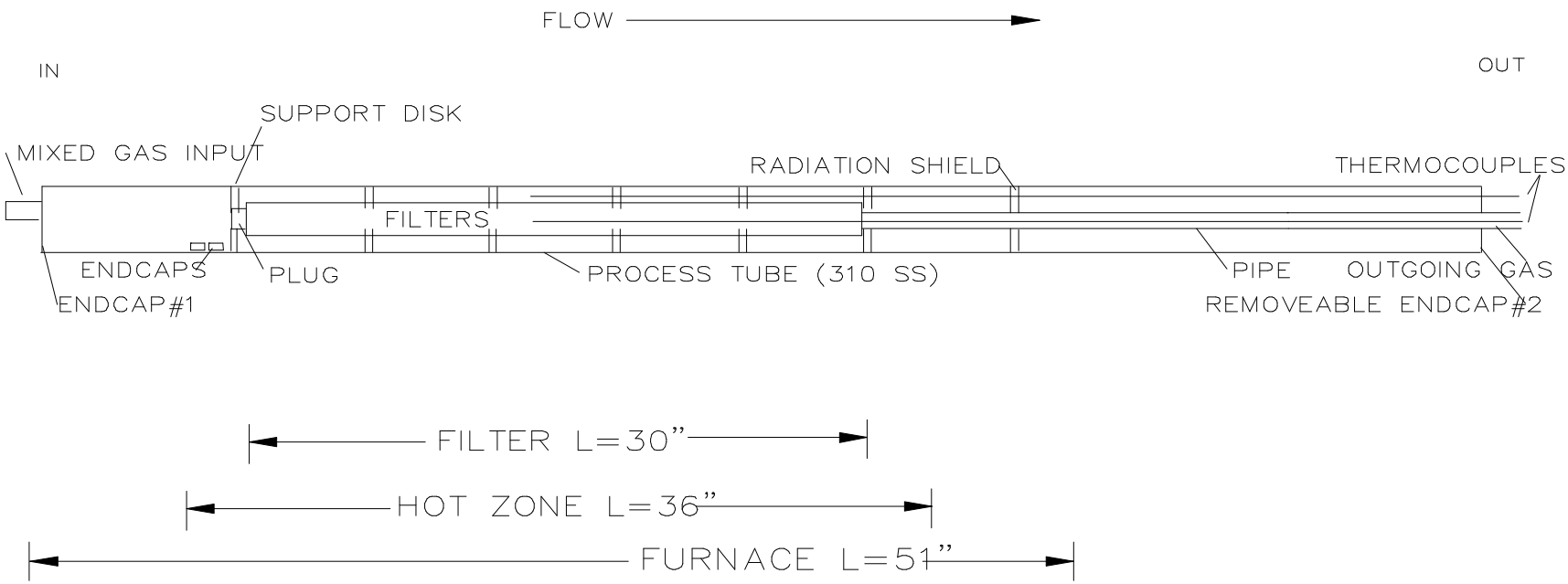

The target and reported analyses for the first three candidates are listed below in weight percent:

		Fe	Al	Cr	O2	C	Zr	B
FAS	T	81.2	16.4	2.2	--	.007	.19	---
	R	BAL	17.1	2.2	.50	.038	.17	---
FAL	T	77.9	16.4	5.5	--	.007	.19	---
	R	BAL	15.8	5.5	.38	.046	.17	---
FeAl	T	76.2	23.6	---	--	.007	.19	.004
	R	BAL	22.8	---	.73	.024	.17	.008

T = Target Comp. R = Reported Comp.

Oxygen contents appear to increase with increasing aluminum content as might be expected. After evaluation it was concluded that powder from all three compositions was satisfactory.

Making Seamless Cylinders and Compressing Them

Procedures for making seamless cylinders in Iron Aluminide are firmly established. Procedures for compressing seamless preforms are well established as well. There is a beneficial major densification in this compression step.

Vacuum Sintering of Seamless Cylinders

Figure 6 shows the Iron Aluminide filter medium after vacuum sintering to 2310F.

The carbon content was higher than expected indicating that some of the carbon from the pyrolyzed (residual) binder had alloyed with the powder. This might add 0.15% carbon over what otherwise would be expected. The carbon, incidentally, is probably improving the high temperature load carrying ability which is a characteristic that is needed (stress rupture, creep strength) with these alloys. In any event, experiments are underway to reduce carbon pickup from this source - by changing processing details, type of binder, etc.

Evaluation of Sintered Seamless Cylinders

Ductility (in an empirical test which measures % contraction in the tube diameter before fracture) was better with all three compositions for the higher sintering temperature. This is seen below:

* Sintering at 2310°F - Gave values of 3.2, 4.9 and 5.9 % ductility before cracking for the FeAl type (0 % Cr), FAL type (5 % Cr) and FAS type (2 % Cr) respectively.

* Sintering at 2345°F - Gave values of 5.3, 5.6, and 7.3 % ductility before cracking for the FeAl type (0 % Cr), FAL type (5 % Cr) and FAS type (2 % Cr) respectively.

FIGURE 6
IRON ALUMINIDE FILTER MEDIUM AS VACUUM SINTERED - SEM AT 300X

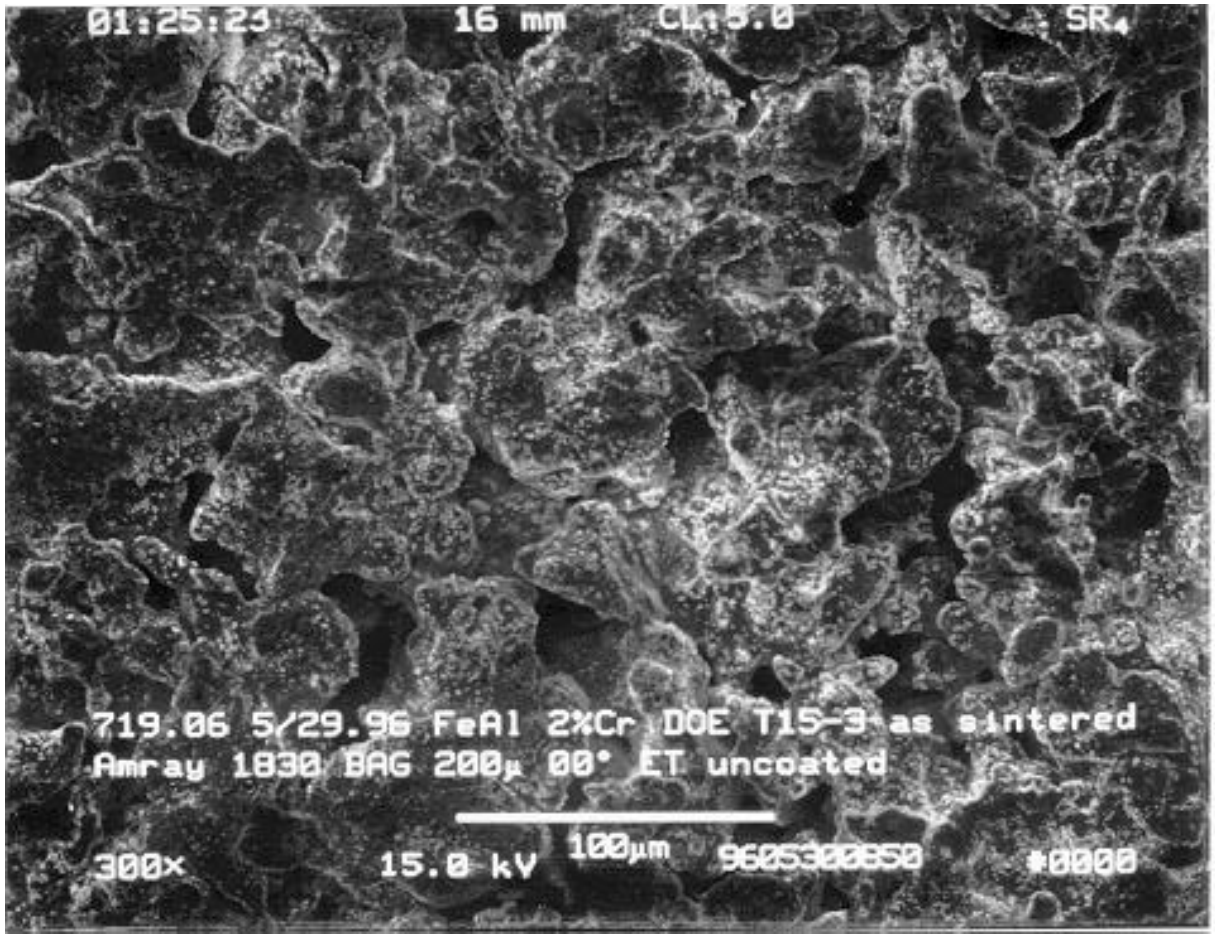

* Sintering at 2385°F - Gave values of 6.6, 5.9, and 6.9% ductility before cracking for the FeAl type (0% Cr), FAL type (5% Cr) and FAS type (2% Cr) respectively.

Experiments are being run to insure that the intrinsic strengths of the tubes are being reported. A new test is being adopted that will be used as a supplement to or perhaps a replacement for "O" ring testing.

Application

Prototype Filters

Three Iron Aluminide candle filters were requested this spring for inclusion in tests that DOE is planning to run at METC. They were needed by the beginning of June. It was decided that the opportunity to develop service experience took precedence over other considerations. A promising alloy and a satisfactory sintering cycle were chosen recognizing that neither had been optimized as yet. Accordingly, it was decided to make the filters from the FAS (2% Cr) type composition, sintered to 2310F, with 310 hardware that was TIG welded. The filters were preoxidized.

Tensile strengths (Av.) for each of three Iron Aluminide cylinders used to make the filters were 9.28, 12.9 and 7.05 ksi.

Preoxidation caused a weight gain of 0.67% most of which appears to be attributable to alumina enrichment of the surface. Preoxidation caused only a 0.7 % average increase in Air /\P (28SCFM) from 27.6 to 27.8 inches of water. First bubble points averaged 21.5 inches of water. The first bubble points were all in the media which is favorable - with none at or immediately adjacent to the welds. The open bubble points of the filters averaged 30.7 inches of water: this corresponds with the "fizz" point for these filters.

Figure 7 shows the Iron Aluminide filter medium after vacuum sintering and preoxidizing in air. There is evidence that the white spots are particles of alumina. Preoxidation of the filters also provided a highly effective stress relief treatment without distortion.

Figure 8 shows the completed filters. Each has a nominal area of one square foot (2 3/8 inch Diameter by 19 1/2 inches long of Fe3Al). The filter media had Void Volumes of 42.5, 41.9 and 45.8% respectively.

In addition to the prototype filters sent to METC, other prototype filters are being prepared for field evaluations.

FIGURE 7
IRON ALUMINIDE FILTER MEDIUM AS VACUUM SINTERED AND PREOXIDIZED (800°C, 7 HOURS) - SEM AT 300X

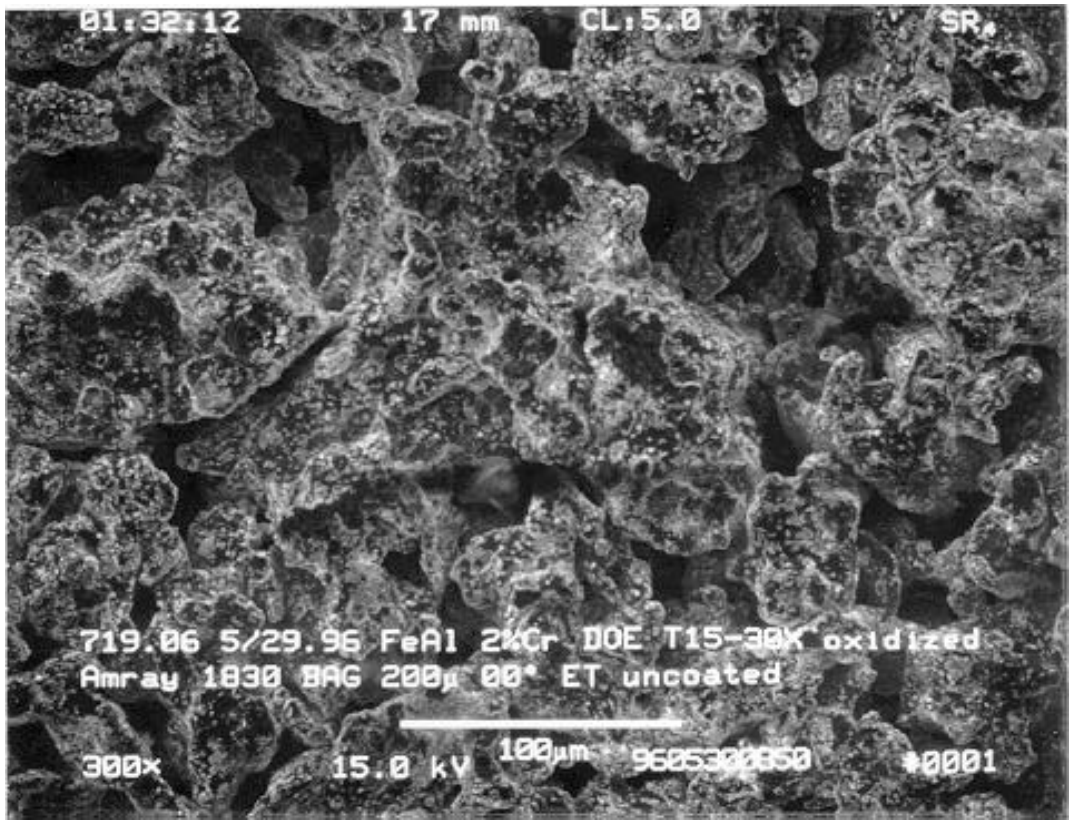

FIGURE 8
THREE IRON ALUMINIDE PROTOTYPE TEST FILTERS

Benefits

To summarize(several observations and points made in this paper), there are four basic advantages offered by this technology:

- First, there is a wealth of information on iron aluminide already available (developed by and/or compiled by ORNL) on the physical properties, mechanical properties and high temperature corrosion resistance - particularly in the presence of hot hydrogen sulfide. While this data was determined for solid materials adjustments can be made to predict performance of porous media.
- Second, an existing manufacturing process is being adopted to produce iron aluminide as seamless cylinders. In fact all the steps for making experimental iron aluminide filters are done on full scale production equipment.
- Third, it is estimated that seventeen thousand square feet of iron aluminide filters could conservatively be produced per year without significant capital expenditures and without interfering with on going production of other grades.
- Fourth, compared to ceramics iron aluminide filters offer crack resistance. Furthermore, fabrication is greatly simplified because iron aluminide can be welded.

Future Activities

In Task 4 the best composition overall will be tested for long term corrosion resistance. This will be followed in Task 5 by the manufacture of 50 filters (optional).

Acknowledgements

Want to acknowledge the advice and encouragement of our METC Project Manager Ted McMahon. Special thanks are due to several individuals at Pall including Steve Geibel (PED) for guidance, to Joe Puzo (MMD) for help in the spinning and vacuum sintering of seamless cylinders and to Keith Rekczis (PED), a team member, for running experiments and for help in upgrading the exposure apparatus. Special thanks are due as well to several staff members at Oak Ridge National Laboratory: this includes Peter Tortorelli and Jack de Van (Ret.) for calculating equilibrium atmospheres.

References

(1). Data Package on Fe3Al-FeAl Based Alloys Developed at ORNL, Compiled by Vinod K. Sikka, January 20, 1993.

(2). J. H. De Van, "Development of Surface Treatments and Alloy Modifications for Corrosion Resistant Oxide Scales", Article InProceedings of the Fourth Annual Conference on Fossil Energy Materials, Compiled by R. R. Judkins and D. N. Braski, August 1990, pgs. 299- 309.

Metal Filter Materials in Combustion Environments*

Roddie R. Judkins (judkinsrr@ornl.gov; 423-574-4572)
Peter F. Tortorelli (tortorellipf@ornl.gov; 423-574-5119)
Ian G. Wright (wrightig@ornl.gov; 423-574-4451)

Oak Ridge National Laboratory
1 Bethel Valley Road
P. O. Box 2008
Oak Ridge, TN 37831

Introduction

Hot gas filtration in pressurized fluidized bed combustion (PFBC) systems is an essentially proven technology at temperatures less than about 750°C (1400°F). Advanced PFBC designs are focused on operational and efficiency improvements and will require filtration at substantially higher temperatures. For example, in first-generation advanced PFBCs, the filters will have to perform at 870°C (1600°F), while second-generation units, which include both carbonizers for fuel-gas production and fluidized-bed combustors, will eventually require filters to operate at temperatures as high as 930 and 870°C (1700 and 1600°F), respectively. Results from the final test campaign at the Tidd PFBC Demonstration Project showed that, at these higher temperatures, ceramic filter technology reliability may be problematical. It is, therefore, of interest to re-examine the possibility of using advanced metal hot-gas filters for these advanced PFBC applications in view of the exceptional corrosion resistance of iron aluminides in high-temperature sulfur-bearing atmospheres.

For the second-generation PFBCs, performance criteria for the carbonizer filters are essentially the same as those for integrated gasification combined cycle (IGCC) systems (reducing environments). For the combustor, the issues are similar to those of advanced first-generation units (oxidizing) except that the fuel (byproduct char from the carbonizer) should be somewhat cleaner and the filter performance requirements less demanding than for PFBC systems such as the Tidd plant. For the carbonizer system, the nearer term (market entry) goals are to develop filter materials that will perform at temperatures of 650-760°C (1200-1400°F), with an increase to 800-930°C (1500-1700°F) for improved cycle efficiency.

---

*Research sponsored by the U.S. Department of Energy's Morgantown Energy Technology Center under Field Work Proposal (FWP) FEAA032 and the Fossil Energy Advanced Research & Technology Development Materials Program under FWP FEAA028 with Oak Ridge National Laboratory, which is managed by Lockheed Martin Energy Research Corporation for the U.S. Department of Energy under contract DE-AC05-96R22464.

Background

Materials used in hot gas filters are required to withstand prolonged exposure to potentially corrosive, high-temperature gaseous environments as well as to condensable vapors and solid species, some of which may have the potential for localized interaction with the filter material after extended times. The gas streams may be oxidizing (in the case of flue gases from PFBCs) or reducing, in which the sulfur species are largely in the form of H_2S (in the case of the product gas from IGCC processes or from carbonizers). The growth of any significant thickness of corrosion product on the filter material cannot be tolerated, since this will lead to rapid pore blockage and failure of the filter. Further, any interaction of the filter material with the deposit or filter cake to form a dense layer, either by sintering or by the formation of low-melting products, also would degrade the functioning of the filter. It is, therefore, necessary to carefully evaluate the environmental compatibility of candidate filter materials with the combination of environmental factors that could potentially cause corrosion to determine the type of corrosion products expected and their rate of formation.

Degradation of metallic filter elements has been observed as an environmental effect under oxidation, sulfidation, and/or carburization conditions and acts as a driving force for the development of ceramic hot-gas filters, particularly for the higher temperatures associated with advanced gasification and combustion designs. However, iron aluminides can also be considered for such applications because of their good to exceptional high-temperature corrosion resistance in a variety of sulfur-bearing environments relevant to coal-derived energy production systems.[1-11] In most cases, the results from these laboratory studies have been directly compared to austenitic stainless steels (particularly type 310). With respect to such alloys, iron aluminides with greater than about 20 at. % Al show exceptional corrosion resistance in coal-gasification environments (high p_{S_2}, low p_{O_2}, and sulfur present as H_2S).[1,4-6,8] While the relative differences in corrosion resistance between these iron aluminides and stainless steels are not as pronounced as in the gasification environment, Fe_3Al and its alloy modifications also show better corrosion behavior under many coal-combustion-gas conditions (high p_{O_2}, low p_{S_2}, and sulfur as SO_2)[2,4,5,8] and in the presence of $CaSO_4$ and circulating-PFBC-type ash deposits[4] up to at least 900°C. Such results, therefore, serve as a basis on which to examine the specific use of selected iron aluminides as materials of construction for hot-gas filters in PFBC systems.

The Oak Ridge National Laboratory (ORNL) is presently working on a project in support of Pall Corporations's development of iron-aluminide filters for coal gasification that can serve as an evaluation of these components for the carbonizer filtration system in second generation PFBCs. Pall Corporation's development of processing techniques for manufacture of the filters is applicable to this project as well. However, some issues associated with the use of iron-aluminide filters for the combustors in the advanced PFBC designs are not being addressed presently. For these environments, iron-aluminide alloys also have potential at both the market entry (650-760°C) and improved

cycle efficiency (870°C) temperatures. However, the efficacy of this material has not been specifically demonstrated in the actual environments that obtain in PFBCs. A need, therefore, exists to examine the corrosion behavior and associated environmental effects on properties relevant to the use of porous iron aluminides as hot-gas filters for the combustion gas stream of advanced PFBC systems.

Approach

This work is structured to examine the corrosion behavior and associated environmental effects on properties relevant to the use of iron-aluminide hot-gas filters for advanced PFBC systems. The project will focus on exposure of porous iron aluminides in mixed gases containing N_2, O_2, H_2O, and CO_2, both with and without the presence of ash. Issues associated with corrosion in gases containing N_2, O_2, H_2O, CO, CO_2, and CH_4 typical of the carbonizer gas stream in second-generation PFBCs will not be addressed, as similar work is being conducted in a project on iron-aluminide filters for coal gasification environments. In this and other ways, the present effort will only focus on the aspects of corrosion that are unique to PFBC applications or are not being examined elsewhere. In so doing, this work complements previous or ongoing research and development associated with the corrosion of iron aluminides in oxidizing/sulfidizing environments related to coal-based energy production. It takes advantage of experience in iron-aluminide alloy development, materials processing, and corrosion testing in appropriate fossil environments at the Argonne and Oak Ridge National Laboratories and will involve the expertise of Pall Corporation in producing porous iron aluminides and evaluation of filter performance.

This project will examine the corrosion behavior of Fe_3Al-type iron aluminides, vis-à-vis other alloys such as stainless steels, that can be used for filter applications. Iron aluminide compositions based on Fe-28Al-2Cr and Fe-28Al-5Cr (at. %) will be used. Although higher chromium levels may be considered for added resistance to corrosion by the alkali metal salts present in the ash, recent results by Foster Wheeler Development Corporation suggest the iron aluminides may possess the necessary resistance to this type corrosion.[11] Both porous and dense iron-aluminide alloys of the compositions cited will be evaluated. Comparison of results for the respective materials will allow evaluation of any effects on corrosion behavior associated with differences in processing and the determination of whether previously generated data for cast iron aluminides can be used to guide material selection for the present hot-gas filter applications.

Bare coupons and ash-coated specimens will be isothermally and cyclically exposed in a simulated combustion gas environment. The ash to be used is that obtained by the University of North Dakota Energy and Environmental Research Center from the Westinghouse Advanced Particle Filter installed at the American Electric Power Company's Tidd PFBC Demonstration Project. Corrosion performance will be evaluated

using gravimetric data, optical metallography, X-ray diffraction, and scanning electron microscopy with associated energy dispersive X-ray analysis. Corrosion exposures will be conducted at 650°C (1200°F), 750°C (1380°F), and 900°C (1650°F) so that the temperature range encompasses both first- and second-generation PFBC hot-gas filtration conditions.

Project Description

This project will begin in the last quarter (July-September) of Fiscal Year (FY) 1996. Specific test environments will be defined on the basis of appropriate thermochemical calculations and in consultation with the University of North Dakota Energy and Environmental Research Center. Procurement of specific iron aluminide compositions (Fe-28Al-2Cr-0.1Zr and Fe-28Al-5Cr-0.1Zr) in porous form will be initiated. While these are being obtained, experimental exposures will be conducted with cast iron aluminides of the same compositions. The first set of experiments will be with uncoated specimens in the simulated combustion gas at 650, 750, and 900°C. Similar exposures of like specimens coated with ash will be initiated.

In FY 1997, the experiments aimed at comparing the corrosion behavior of the two cast iron aluminide compositions in the presence and absence of ash will be completed. Based on those results, a second set of experiments with the porous materials will also be conducted at the specified temperatures. Possible effects of the process used to make the porous iron-aluminide alloys (such as surface conditioning or impurities) on corrosion behavior can then be evaluated. For selected cases, the effects of such exposures on the mechanical behavior can be examined. An assessment of the ability of iron-aluminide alloys to function as the material of construction for the combustion gas stream of PFBCs will be made. If the results for iron-aluminide alloys are promising, testing of actual filter components made from such alloys (in collaboration with Pall Corporation) will be pursued.

References

1. J. H. DeVan, pp. 107-115 in *Oxidation of High-Temperature Intermetallics*, T. Grobstein and J. Doychak (eds.), TMS, 1989.

2. W. H. Lee and R. Y. Lin, "Molten Salt-Induced Hot Corrosion of Iron Aluminides," pp. 475-86 in *Proc. Fourth Annual Conf. Fossil Energy Materials*, R. R. Judkins and D. N. Braski (comp.), ORNL/FMP-90/1, U. S. Department of Energy, August 1990.

3. S. Van Wheele and J. L. Blough, Foster Wheeler Development Corporation report, ORNL/Sub/89-SA187/02, August 1991.

4. K. Natesan, "Corrosion Resistance of Iron Aluminides," pp. 271-82 in *Proc. Sixth Annual Conf. Fossil Energy Materials*, N. C. Cole and R. R. Judkins (comp.), U. S. Department of Energy, July 1992.

5. K. Natesan, "Corrosion Performance of Materials in Coal-Combustion Environments," pp. 353-62 in *Proc. Seventh Annual Conf. Fossil Energy Materials*, N. C. Cole and R. R. Judkins (comp.), U. S. Department of Energy, July 1993.

6. J. H. DeVan and P. F. Tortorelli, "Oxidation/Sulfidation of Iron-Aluminum Alloys," *Mater. at High Temp.* 11 (1993) 30-35.

7. K. Natesan and W. D. Cho, "High Temperature Corrosion of Iron Aluminides," pp. 227-37 in *Proc. Eighth Annual Conf. Fossil Energy Materials*, N. C. Cole and R. R. Judkins (comp.), CONF-9405143, U. S. Department of Energy, August 1994.

8. K. Natesan and R. N. Johnson, "Corrosion Performance of Fe-Cr-Al and Fe Aluminide alloys in Complex Gas Environments," pp. 591-99 in Heat-Resistant Materials II, K. Natesan, P. Ganesan, and G. Lai (eds.), ASM International, August 1995.

9. P. F. Tortorelli et al., "High-Temperature Corrosion Behavior of Iron-Aluminide Alloys and Coatings," pp. 289 - 300 in *Proc. Ninth Annual Conf. Fossil Energy Materials*, N. C. Cole and R. R. Judkins (comp.), U. S. Department of Energy, August 1995.

10. S. R. J. Saunders et al., "Behaviour of Fecralloy and Iron-Aluminide Alloys in Coal Gasification Atmospheres Containing HCl," accepted for publication in *Mater. Sci. Forum,* 1996.

11. J. L. Blough and G. J. Stanko, "Fireside Corrosion Testing of Candidate Superheater Tube Alloys, Coatings, and Claddings - Phase II," to be published in *Proc. Tenth Annual Conf. Fossil Energy Materials*, N. C. Cole and R. R. Judkins (comp.), U. S. Department of Energy, 1996.

Characterization and Testing of CFCC Hot Gas Filters Made Via Gas Phase Reaction Synthesis - A Synopsis of the Textron/METC Advanced Hot Gas Filter Program

Stephen DiPietro (sputboy@aol.com; 508-454-5488)

Textron Systems Division
2 Industrial Avenue
Lowell, MA 01851

Abstract

In 1994, Textron Specialty Materials and their principal subcontractor Westinghouse STC began a collaborative effort with the DOE METC office to engage in the fabrication and testing of continuous fiber ceramic composite (CFCC) hot gas filter materials. Textron's two original candidate CFCC materials systems were SCS-6 monofilament reinforced nitride-bonded silicon carbide (NBSiC) and nitride-bonded silicon nitride (NBSN), to which porosity was introduced via the addition of fugitive and in-situ pore forming agents.

Based upon successes achieved with fabrication of large scale CFCC burner and combustor can components on their DO-funded CFCC Program, Textron initially expected that fabrication of structurally-robust hot gas filter elements with acceptable permeability characteristics would be a straightforward modification of the baseline CFCC process. However, subsequent programmatic activities revealed this assumption not to be the case. While both SCS-6/NBSiC and SCS-6/NBSN ceramic composites could be fabricated in net-shape fashion using modifications of previously-developed processing methods, permeability and corrosion tests at Westinghouse STC revealed that the only CFCC materials which met the targeted gas flow resistance specification of <10 iwg/10 fpm, also exhibited poor mechanical properties and elevated temperature alkali corrosion behavior. Furthermore, CFCC filter materials made at higher matrix densities had good strength characteristics and handleability, but were found to exhibit unacceptably-high gas flow resistance.

The essential conclusion of our program appears to be that considerable work on pore-forming and preform fabrication methods, beyond the scope of this program, would be

---

Research sponsored by the U.S. Department of Energy's Morgantown Energy Technology Center, under contract DE-AC21-94MC31213 with Textron Specialty Materials, 2 Industrial Avenue, Lowell, MA 01851; telefax: 508-454-5632.

required in order to arrive at processing methods and CFCC materials microstructures that would yield the proper combination of gas flow permeability, alkali corrosion resistance, and mechanical durability. Additionally, results from our program seem to raise questions about the thermodynamic stability of high specific surface area silicon carbide and silicon nitride-based materials in the candle filter environment.

CRADA opportunities AT METC

CRADA facts

DEPARTMENT OF ENERGY
OFFICE OF FOSSIL ENERGY

COOPERATIVE RESEARCH AND DEVELOPMENT AGREEMENTS (CRADAS) AT METC

The Morgantown Energy Technology Center (METC) is always interested in discussing partnering opportunities with those in the private sector. One way METC can work with the private sector and academia is through Cooperative Research and Development Agreements (CRADAs). What follows is a short discussion of CRADAs at METC.

What is a CRADA?

The Federal Technology Transfer Act of 1986 (P.L. 99-502) provided a new mechanism for joint research between private parties and METC. Joint projects under this law are called CRADAs. CRADAs are simply agreements between METC and the private sector to work together on a mutually beneficial project. Each partner in the CRADA applies whatever resources are agreed to in the performance of its portion of the project. These resources may include personnel, equipment, or facilities. While partner dollars may be used to fund portions of the Government's effort, METC may not provide federal funds to the private sector partner.

Intellectual property disposition under a METC CRADA is quite flexible. METC can negotiate directly with the partner on issues including the allocation of rights to patents developed during the CRADA, protection of information generated under the CRADA, and the exclusive or non-exclusive licensing of METC inventions.

What Makes a Good CRADA?

From METC's perspective, a good CRADA consists of two elements: a good project and a good CRADA partner. Good CRADA projects address goals that are beneficial to both the private sector participant and METC.

Of primary interest to METC is the development and deployment of clean, efficient power generation technologies and environmental remediation technologies. For power generation, METC's primary focus is on Integrated Gasification Combined Cycle (IGCC) systems, Pressurized Fluidized-Bed Combustion (PFBC) systems, Advanced Turbine Systems (ATS), Externally Fired Combined-Cycle (EFCC) power systems, fuel cell systems, and fuels technology systems. METC's environmental remediation interests focus on the development of high-payoff technologies to clean up the inventory of DOE nuclear component manufacturing sites, and to manage DOE-generated waste faster, safer, and cheaper than environmental cleanup technologies that are currently available.

Regarding CRADA partners, preference is given to small businesses and to business units located in the United States which agree that products resulting from the CRADA will be manufactured substantially in the United States. In the case of foreign-owned companies, METC will take into consideration how U.S.-based companies are dealt with in that country.

Projects will be undertaken based on factors such as those listed above, CRADA partner resources offered, METC resource availability, and the specific contribution of the project to METC's research and development (R&D) program.

CONTACT POINTS

TECHNICAL:

Dr. J. Christopher Ludlow
General Engineer
Office: (304) 285-4608
E-Mail: jludlo@metc.doe.gov

ADMINISTRATIVE:

Dr. Rodney Anderson
Technology Transfer
Program Manager
Office: (304) 285-4709
E-Mail: rander@metc.doe.gov

Ms. Lisa Jarr
Patent Advisor
Office: (304) 285-4555
E-Mail: ljarr@metc.doe.gov

MAIL ADDRESS:

U.S. Department of Energy
P.O. Box 880
3610 Collins Ferry Road
Morgantown, WV 26507-0880

FAX: (304) 285-4469

Cooperative Research and Development Agreements (CRADAs) at METC

How Do I Initiate a CRADA With METC?

Since no funds are transferred from METC to the private sector participant, most of the regulations governing federal procurements do not apply. CRADAs can be implemented relatively quickly and with few complications.

Generally, the first step in formalizing a CRADA is an expression of interest to METC by the potential private sector participant. This expression of interest, while it can be verbal, is most effective when it takes the form of a letter addressed to a METC point of contact listed on the front of this factsheet.

That expression of interest triggers a series of discussions both within METC and with the potential partner to decide whether METC and the private sector party can define a project that will benefit both parties, and whether the needed resources are available to perform the envisioned work. Ultimately, the final decision of whether METC will pursue a particular CRADA opportunity lies with the METC Director.

The CRADA Process

1 Expression of Interest

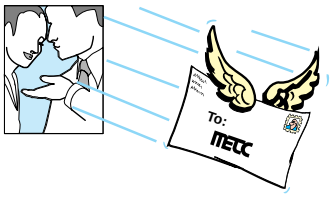

2 Discuss Idea

3 Management Approval

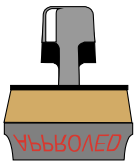

4 Develop CRADA

5 METC Signatures Partners' Signatures

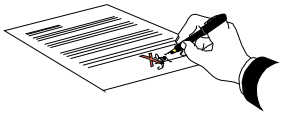

6 Winners' Circle

SIX STEPS TO INITIATE A CRADA

1. Expression of interest is addressed to METC
2. CRADA Team discusses idea and whether the needed resources are available
3. Approval given to develop CRADA
4. CRADA developed
5. CRADA signed
6. Everybody wins

CRADA facts

DEPARTMENT OF ENERGY
OFFICE OF FOSSIL ENERGY

COMBUSTION PROJECT

LOW EMISSIONS COMBUSTOR TEST AND RESEARCH FACILITY

Capabilities

The Morgantown Energy Technology Center (METC) recently built and began operation of a Low Emissions Combustor Test and Research (LECTR) facility with the primary objective of providing test facilities and engineering support to METC customers through programs such as the Advanced Turbine Systems (ATS) University-Industry Consortium and through CRADA participation with industrial partners.

The LECTR is a versatile test facility with capabilities for evaluating a variety of low emissions combustion concepts at temperatures and pressures representative of gas turbine applications. This facility utilizes the full range of high pressure (up to 30 atm), high temperature (800 K/1,000 °F air preheat, 2,100 K/3,300 °F combustor wall), and mass flows (3.4 lb/s combustion air) available in METC's Advanced Combustion Facility. The LECTR design incorporates a set of flanged sections or modules including an inlet plenum, combustor test sections, a gas sampling section, and a quench section. Combustor test sections can be custom designed to meet a specific application by varying the internal refractory dimensions. This modular design approach offers the flexibility to test multiple concepts with rapid turnaround thus maximizing operating time while reducing the time and cost associated with building new inlet, sampling, and quench systems for each application. The high pressure and mass flow capabilities of the LECTR facility make it uniquely suited for evaluation of advanced combustion concepts at combustion scales up to 3 MW_{th} (10 MMBtu/h).

Diagnostic Capabilities

- Multiple optical and probe access ports
- Laser-based diagnostics for flow visualization, velocity, and species measurement
- Video and high-speed imaging capabilities
- Radiation pyrometry
- Extractive gas sampling/analysis

The LECTR has recently been utilized to characterize the operating and emissions characteristics of a small industrial lean premixed gas burner at elevated pressures for potential gas turbine applications. At present, we are in the midst of a test campaign to obtain new experimental data relevant to lean-premixed combustion, and to refine and validate models for lean-premixed combustors with these data.

CONTACT POINTS

TECHNICAL:

Dr. Kent H. Casleton
Chemist
Office: (304) 285-4573
E-Mail: kcasle@metc.doe.gov

Dr. Daniel J. Maloney
Physical Scientist
Office: (304) 285-4629
E-Mail: dmalon@metc.doe.gov

Dr. Thomas S. Norton
Mechanical Engineer
Office: (304) 285-4617
E-Mail: tnorton@metc.doe.gov

ADMINISTRATIVE:

Dr. Rodney Anderson
Technology Transfer
Program Manager
Office: (304) 285-4709
E-Mail: rander@metc.doe.gov

Ms. Lisa Jarr
Patent Advisor
Office: (304) 285-4555
E-Mail: ljarr@metc.doe.gov

MAIL ADDRESS:

U.S. Department of Energy
P.O. Box 880
3610 Collins Ferry Road
Morgantown, WV 26507-0880

FAX: (304) 285-4469

Low Emissions Combustor Test and Research Facility

Construction is under way of a gasification/cleanup Process Development Unit (PDU) and an associated high volume output Syngas Generator. When this Syngas Generator is integrated with the LECTR facility, METC will have a unique test facility capable of evaluating combustion system integration issues associated with utilizing advanced gas turbine systems in Integrated Gasification Combined Cycle (IGCC) and Advanced Pressurized Fluidized-Bed Combustion (APFBC) applications.

Opportunities

- Integration of ATS with IGCC and PFBC Systems (METC Syn-Gas Generator)
- Utilize METC Advanced Combustion Facility capabilities (P, T, Mass Flows)

Test Modules

Refractory-lined test modules with multiple ports for temperature and pressure measurement as well as optical diagnostics

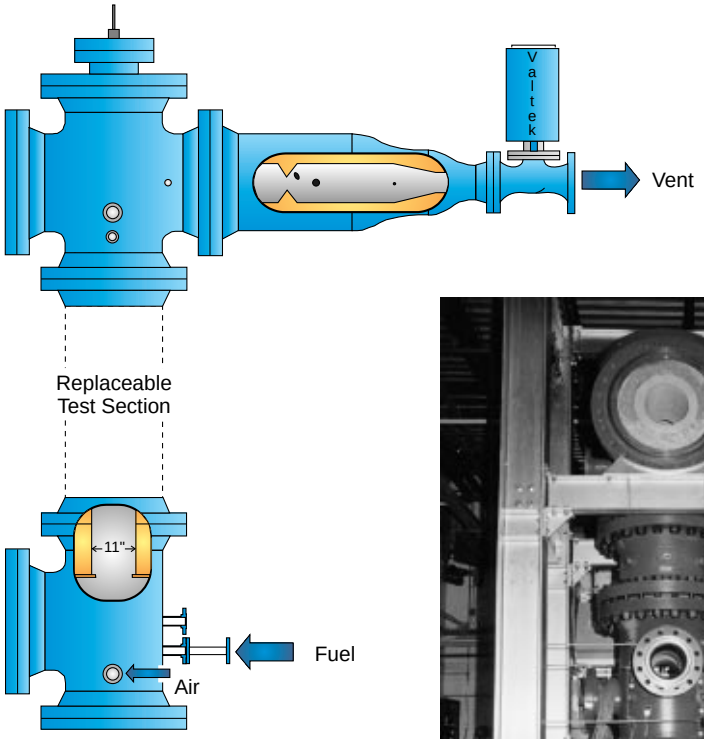

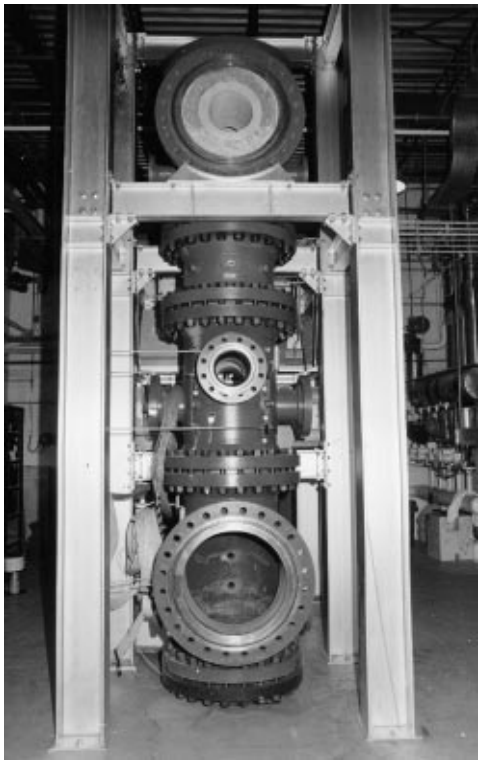

M96001583A

CRADA facts

DEPARTMENT OF ENERGY
OFFICE OF FOSSIL ENERGY

COMBUSTION PROJECT

COMBUSTION OSCILLATION CONTROL

Capabilities

Combustion oscillations have emerged as a significant consideration in the development of low emission gas turbine combustors. In natural gas combustion, very low NOx emissions can be produced by gas turbine fuel nozzles which employ premixing of the fuel and air. Premixing of fuel and air can avoid the high temperatures which produce thermal NOx, but the resulting nozzle configuration is often susceptible to oscillating combustion instability. Oscillating combustion must be eliminated over the entire range of engine operation, because the associated pressure fluctuations and vibration can damage engine hardware.

In Integrated Gasification Combined Cycle (IGCC) applications, premixed combustion may also be used to burn medium or low heating value fuel in the turbine. If premix combustion is used in IGCC turbines, combustion oscillations may occur via the same mechanisms as in premixed natural gas combustion. Methods to control oscillations in natural gas combustion may therefore apply to IGCC systems as well as other power systems.

Techniques to eliminate oscillations include various design modifications to the fuel nozzle, or limiting the operating map to avoid oscillating conditions. Either approach is costly, especially when oscillations are encountered in the final stages of engine testing. As an alternative to design or operating modifications, METC is investigating the use of so-called "active" combustion control to eliminate oscillations. Active control uses repeated adjustment of some combustion parameter to control the variation in heat release that drives oscillations.

Opportunities

- Investigate stability features of proposed nozzle designs
- Sub- and full-scale nozzle testing for combustion stability
- Identify oscillating mechanisms in combustion systems

CONTACT POINTS

TECHNICAL:

Dr. George A. Richards
General Engineer
Office: (304) 285-4458
E-Mail: gricha@metc.doe.gov

Michael C. Janus
Mechanical Engineer
Office: (304) 285-4912
E-Mail: mjanus@metc.doe.gov

ADMINISTRATIVE:

Dr. Rodney Anderson
Technology Transfer
Program Manager
Office: (304) 285-4709
E-Mail: rander@metc.doe.gov

Ms. Lisa Jarr
Patent Advisor
Office: (304) 285-4555
E-Mail: ljarr@metc.doe.gov

MAIL ADDRESS:

U.S. Department of Energy
P.O. Box 880
3610 Collins Ferry Road
Morgantown, WV 26507-0880

FAX: (304) 285-4469

Combustion Oscillation Control

Dynamic Gas Turbine Combustor

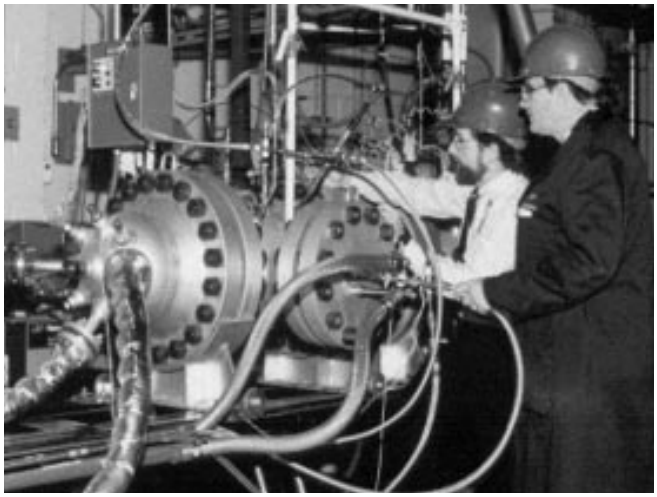

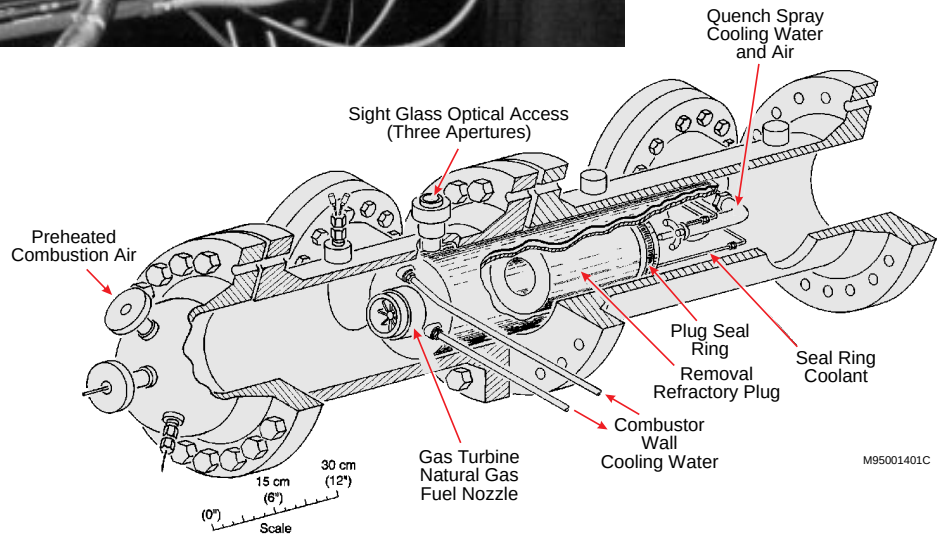

COMBUSTOR DESCRIPTION

- Flow rate: 1.5 pounds per second (4 maximum), 10 atm.
- Preheat air temp: up to 650°F
- Novel features: Hard acoustic boundaries, variable frequency
- Limited optical and diagnostic access

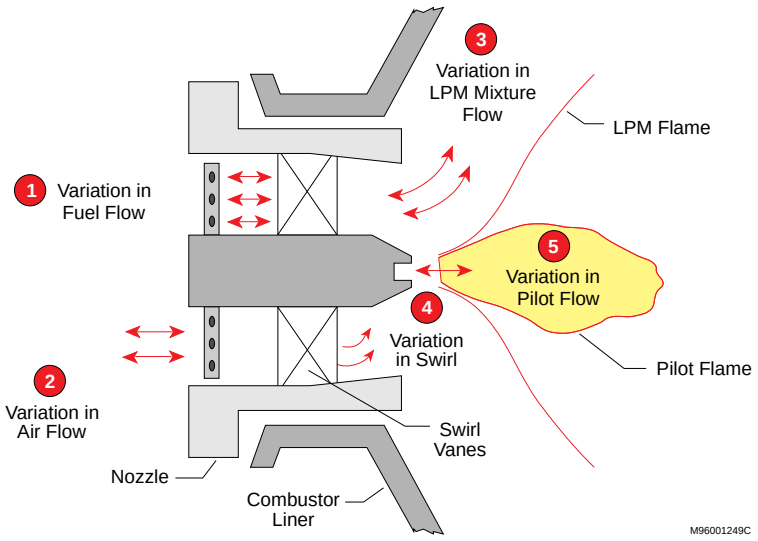

OSCILLATIONS FROM LPM FUEL NOZZLES

- Five oscillation mechanisms identified in METC tests
- Simultaneous occurrence complicates mechanism identification
- Competing design requirements constrain stabilization options

M96001584A

CRADA facts

DEPARTMENT OF ENERGY
OFFICE OF FOSSIL ENERGY

COMBUSTION PROJECT

HIGH-PRESSURE OPTICAL COMBUSTION PROBE

Capabilities

An optical access probe was developed to meet the demands of a gas turbine combustor in a Cooperative Research and Development Agreement (CRADA) with the Westinghouse Science and Technology Center.

The probe is water-cooled, has no external fittings, and is pressure-sealed with a conventional compression fitting. The probe utilizes a 1.0-mm diameter sapphire rod as a lightpipe for optical access and fiber optic coupling to the spectroscopic experiments. This is coupled with a fused silica optical fiber to the optical experiments employed to study the combustion process. The probe has been tested to 10^6 Pa in a test combustor exhibiting 10^5 Pa instability oscillations. To test its spectral range, the probe investigated OH emissions at 310 nm, C_2 and CH emissions from 400 to 500 nm, Near IR emissions from 800 to 1,800 nm, and temperature measurements using an Accufiber detection system.

Opportunities

This probe is designed to meet the needs for optical access in a high-temperature and high-pressure environment. Its construction requires only one welded component with off-the-shelf compression fittings. The experimental data is from light emission collected from a narrow, well-confined cone. The spectral range is from the mid-ultra violet to the near infrared. The probe has no external components to dislodge and damage expensive equipment downstream. The lightpipe may be purged to prevent optical obstruction in a dirty environment.

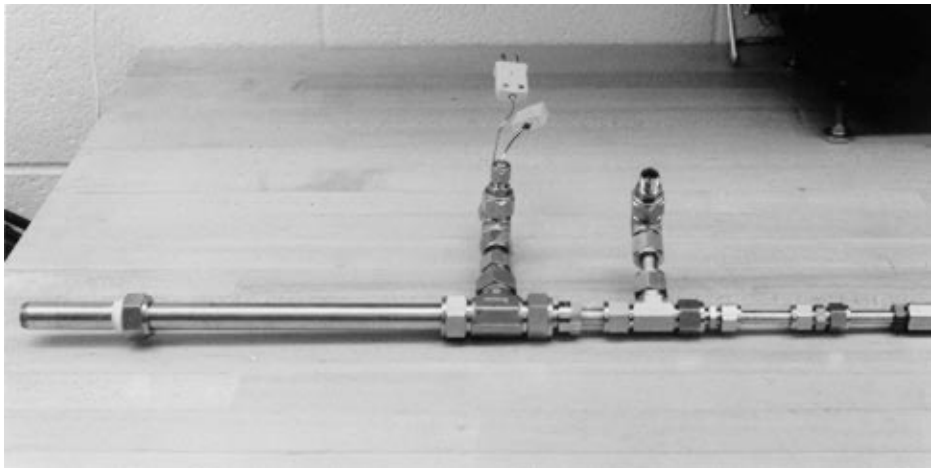

High-Pressure Optical Combustion Probe

CONTACT POINTS

TECHNICAL:

Dr. Steven D. Woodruff
Chemist
Office: (304) 285-4175
E-Mail: swoodr@metc.doe.gov

ADMINISTRATIVE:

Dr. Rodney Anderson
Technology Transfer
Program Manager
Office: (304) 285-4709
E-Mail: rander@metc.doe.gov

Ms. Lisa Jarr
Patent Advisor
Office: (304) 285-4555
E-Mail: ljarr@metc.doe.gov

MAIL ADDRESS:

U.S. Department of Energy
P.O. Box 880
3610 Collins Ferry Road
Morgantown, WV 26507-0880

FAX: (304) 285-4469

Test Modules

CRADA facts

DEPARTMENT OF ENERGY
OFFICE OF FOSSIL ENERGY

COMBUSTION PROJECT

FLUENT SIMULATIONS OF THE WESTINGHOUSE MULTI-ANNULAR SWIRL BURNER FOR DESIGN OPTIMIZATION

Capabilities

The FLUENT computational fluid dynamics code is being used to aid the design of the Westinghouse Multi-Annular Swirl Burner (MASB). The MASB is being designed by Westinghouse for use as a topping combustor in a Pressurized Fluidized-Bed Combustion System as part of the U.S. Department of Energy's Clean Coal Technology Program. The MASB will primarily burn low-energy, coal-derived gaseous fuel (syngas) with vitiated air, at elevated pressure, to supply a gas turbine for power generation. MASB operation will require dual fuel capability, i.e., the ability to burn a high heating value fuel as well as the lower energy syngas. Firing a high heating value gas, such as methane or propane, is required during plant start-up and other off-design conditions.

FLUENT is being used to study the adaptation of the MASB design to the Power Systems Development Facility (PSDF) in Wilsonville, Alabama. Simulations have been performed to investigate the steady, propane-fueled operation of the MASB. These simulations model the complex reacting flow field within the MASB, as influenced by the air-cooled transition piece connecting the burner to the turbine. Various design modifications have been considered in an effort to reduce the simulated radial temperature gradient, or "pattern factor," in the transition piece exit flow. This pattern factor is more of a concern than it would be in a typical commercial installation, because the physical constraints of the PSDF installation require a mildly converging transition duct, which acts to sustain the stratification of the swirling flow that emerges from the MASB. The goal of the current study was to devise a method for introducing dilution air into the MASB to produce an optimum pattern factor without significantly changing the existing design. This design modification must not adversely affect MASB performance when firing syngas.

Opportunities

- Similar FLUENT simulation work is available for any future CRADA partner
- Features of METC modeling resources:
  - Close coupling between lab experiments and computer simulations for model validation
  - State-of-the-art hardware
    - Silicon Graphics workstation network
    - SGI multiprocessor supercomputer
  - Ongoing CRADA with Fluent, Inc., offers unique access to
    - Most current FLUENT code versions
    - Ongoing relationship with FLUENT development and applications groups

CONTACT POINTS

TECHNICAL:

Dr. Thomas S. Norton
Mechanical Engineer
Office: (304) 285-4617
E-Mail: tnorto@metc.doe.gov

Dr. Darren J. Mollot
Mechanical Engineer
Office: (304) 285-5447
E-Mail: dmollo@metc.doe.gov

ADMINISTRATIVE:

Dr. Rodney Anderson
Technology Transfer
Program Manager
Office: (304) 285-4709
E-Mail: rander@metc.doe.gov

Ms. Lisa Jarr
Patent Advisor
Office: (304) 285-4555
E-Mail: ljarr@metc.doe.gov

MAIL ADDRESS:
U.S. Department of Energy
P.O. Box 880
3610 Collins Ferry Road
Morgantown, WV 26507-0880

FAX: (304) 285-4469

FLUENT Simulations of the Westinghouse Multi-Annular Swirl Burner for Design Optimization

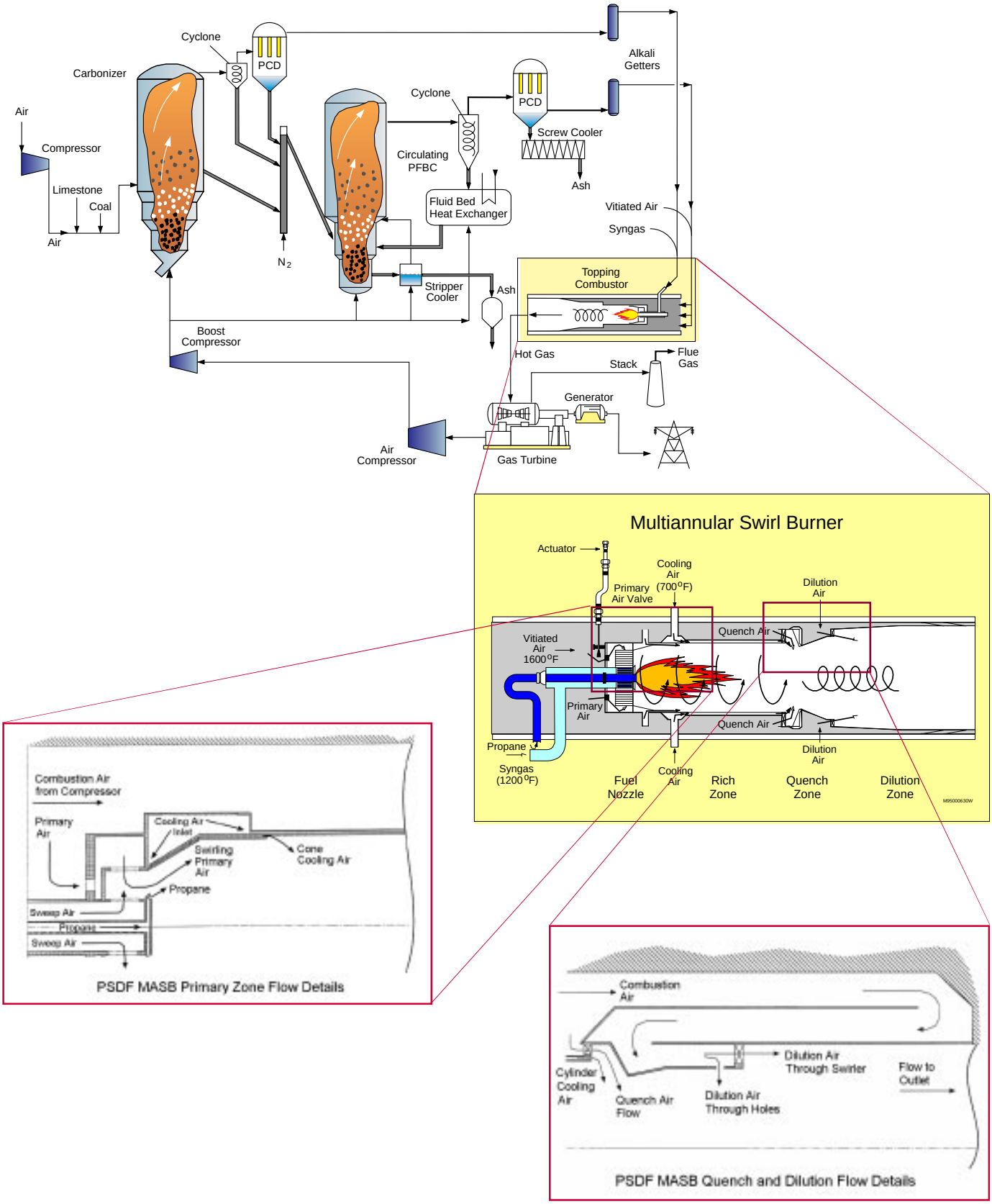

M96001585A

CRADA facts

DEPARTMENT OF ENERGY
OFFICE OF FOSSIL ENERGY

FILTRATION PROJECT

HIGH-TEMPERATURE GAS-STREAM CLEANUP TEST FACILITY

Capabilities

In support of METC's hot-gas filter development program, the high-temperature, gas-stream cleanup test facility was designed to

- investigate conventional and novel approaches to high-temperature filtration,
- conduct detailed parametric studies that characterize particulate control devices under well-controlled conditions, and
- screen new materials for other high-temperature applications, such as heat exchanger tubes.

This new facility utilizes a natural gas-fueled combustor to produce high-temperature process gas, and a screw feeder to inject ash, or other fine media, into the gas stream. The vessel that surrounds the particulate control devices has an inside diameter of roughly 0.20 meters (8 inches) and is about 3 meters (10 feet) long. Three commercial-size filter elements can be tested simultaneously, and the facility is capable of operating over a wide range of conditions. Operating temperatures can vary from 540 to 870 °C (1,000 to 1,600 °F), and the operating pressure can vary from 0 to 400 kPa (0 to 60 psig).

Opportunities

- testing and analyses of conventional high-temperature filtration devices
- testing and analyses of novel high-temperature particulate control devices
- conducting detailed parametric studies that characterize particulate control devices under well-controlled conditions
- screening materials for other high-temperature applications

CONTACT POINTS

TECHNICAL:

Doug Straub
Mechanical Engineer
Office: (304) 285-5444
E-Mail: dstrau@metc.doe.gov

Ta-Kuan Chiang
Mechanical Engineer
Office: (304) 285-4406
E-Mail: tchian@metc.doe.gov

John Shultz
Mechanical Engineer
Office: (304) 285-4861
E-Mail: jshult@metc.doe.gov

ADMINISTRATIVE:

Dr. Rodney Anderson
Technology Transfer
Program Manager
Office: (304) 285-4709
E-Mail: rander@metc.doe.gov

Ms. Lisa Jarr
Patent Advisor
Office: (304) 285-4555
E-Mail: ljarr@metc.doe.gov

MAIL ADDRESS:

U.S. Department of Energy
P.O. Box 880
3610 Collins Ferry Road
Morgantown, WV 26507-0880

FAX: (304) 285-4469

High-Temperature Gas-Stream Cleanup Test Facility

High-Temperature Gas-Stream Cleanup Test Facility Project Team

Top of filter vessel and typical filter element

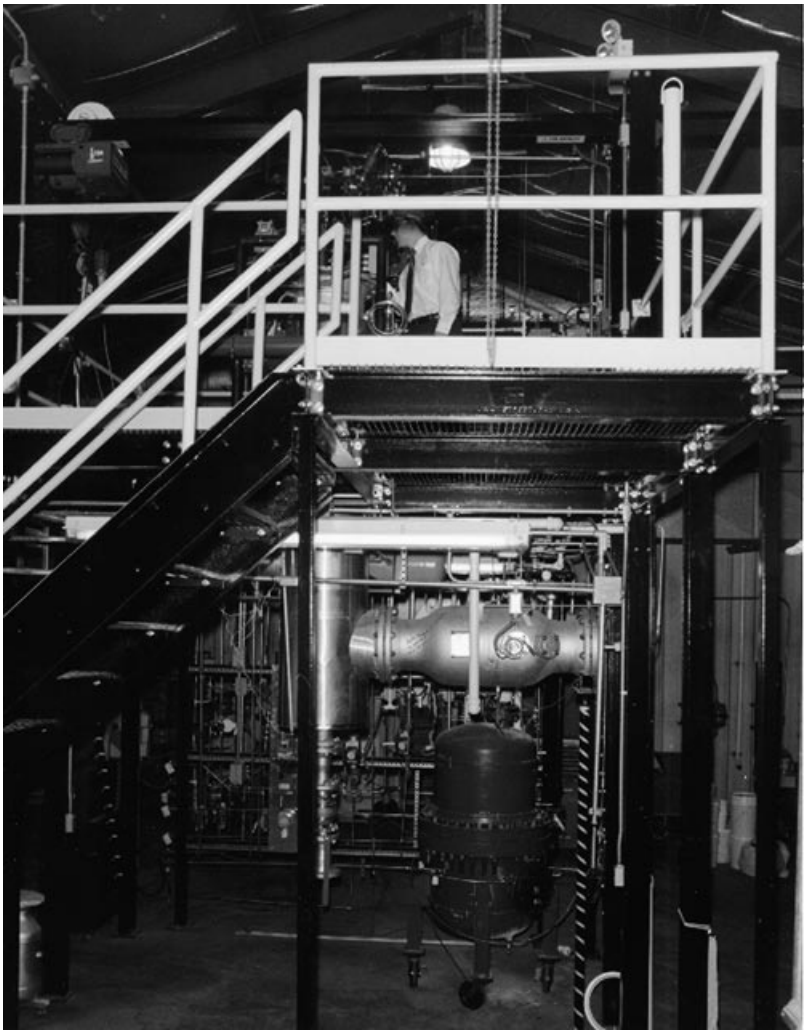

Feeder vessel (front), combustor and bottom of filter vessel (back)

M96001627A

CRADA facts

Department of Energy
Office of Fossil Energy

FILTRATION PROJECT

Granular Filtration in a Fluidized Bed

Capabilities

Successful development of advanced coal-fired power conversion systems often requires reliable and efficient cleanup devices that can remove particulate and gaseous pollutants from high-temperature, high-pressure gas streams. A novel filtration concept for particulate cleanup has been developed at the U.S. Department of Energy's Morgantown Energy Technology Center (METC).

The filtration system consists of a fine metal screen filter immersed in a fluidized bed of granular material. As the gas stream passes through the fluidized bed, a layer of the bed granular material is entrained and deposited at the screen surface. This material provides a natural granular filter to separate fine particles from the gas stream passing through the bed. Since the filtering media is the granular material supplied by the fluidized bed, the filter is not subjected to blinding like candle filters. Because only the in-flowing gas, not fine particle cohesive forces, maintains the granular layer at the screen surface, once the thickness and permeability of the granular layer are stabilized, it remains unchanged as long as the in-flowing gas flow rate remains constant. The weight of the particles and the turbulent nature of the fluidized bed limits the thickness of the granular layer on the filter leading to a self-cleaning attribute of the filter.

The granular filtration testing system consisted of a filter, a two-dimensional fluidized bed, a continuous powder feeder, a laser-based, in-line particle counting, sizing, and velocimeter (PCSV), and a continuous solid feeding/bed material withdrawal system. The two-dimensional, transparent fluidized bed allowed clear observation of the general fluidized state of the granular material and the conditions under which fines are captured by the granular layer. A series of experiments was conducted at various ranges of operating conditions with two different bed materials: a 30x270 mesh acrylic powder with a particle density of 1.1 gm/cc, and a 40x270 mesh Millwood sand with a particle density of 2.5 gm/cc. During the experiments, fine sand (less than 100 micrometers) was fed continuously to the bed through the powder feeder at a constant rate of 3.8 gm/min (0.5 lb/hr). Bed material and captured fine particles were withdrawn continuously through an overflow tube. In order to maintain a constant bed level, makeup bed material was also fed continuously through a non-mechanical valve to the bottom of the fluidized bed. Performance of this granular filtration system was measured by the PCSV downstream of the filter.

High filtration performance was measured when low-density bed material (acrylic powder) was used. Collection efficiencies over 99 percent were obtained with this bed material in a continuous flow mode. However, low filtration performance was experienced with high-density bed material (Millwood sand). The low filtration performance with heavy bed material may

CONTACT POINTS

TECHNICAL:

Dr. Joseph S. Mei
Mechanical Engineer
Office: (304) 285-4409
E-Mail: jmei@metc.doe.gov

Dr. Paul C. Yue
Physicist
Office: (304) 285-4062
E-Mail: pyue@metc.doe.gov

ADMINISTRATIVE:

Dr. Rodney Anderson
Technology Transfer
Program Manager
Office: (304) 285-4709
E-Mail: rander@metc.doe.gov

Ms. Lisa Jarr
Patent Advisor
Office: (304) 285-4555
E-Mail: ljarr@metc.doe.gov

MAIL ADDRESS:

U.S. Department of Energy
P.O. Box 880
3610 Collins Ferry Road
Morgantown, WV 26507-0880
FAX: (304) 285-4469

be attributed to the failure of maintaining a sufficiently thick granular layer at the screen filter surface. However, a modified filter was designed, fabricated, and tested in the fluidized-bed granular filtration system. Preliminary results of this modified filter showed that high filtration performance was also obtained for heavy bed material. Future activities in the program will concentrate on continuous testing of the modified filter, and adding a solid recycling and separation system to the existing two-dimensional, fluidized-bed granular filtration cold model.

Opportunities

- Apply fluidized-bed granular filtration concept to
  - Particulate cleanup/hot gas desulfurization processes
  - Combustion/flue gas desulfurization/particulate cleanup processes
  - Particulate cleanup/noise attenuation for diesel engines
- Develop concept to pilot scale through three-dimensional cold and hot model testing

The Concept

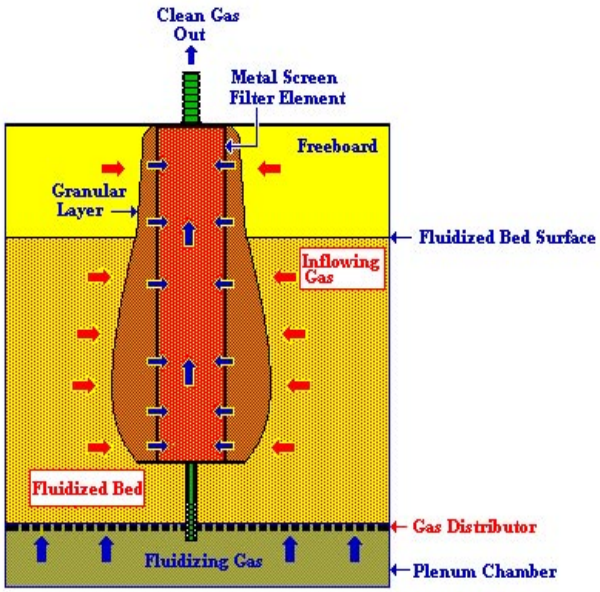

Granular Filtration in a Fluidized Bed

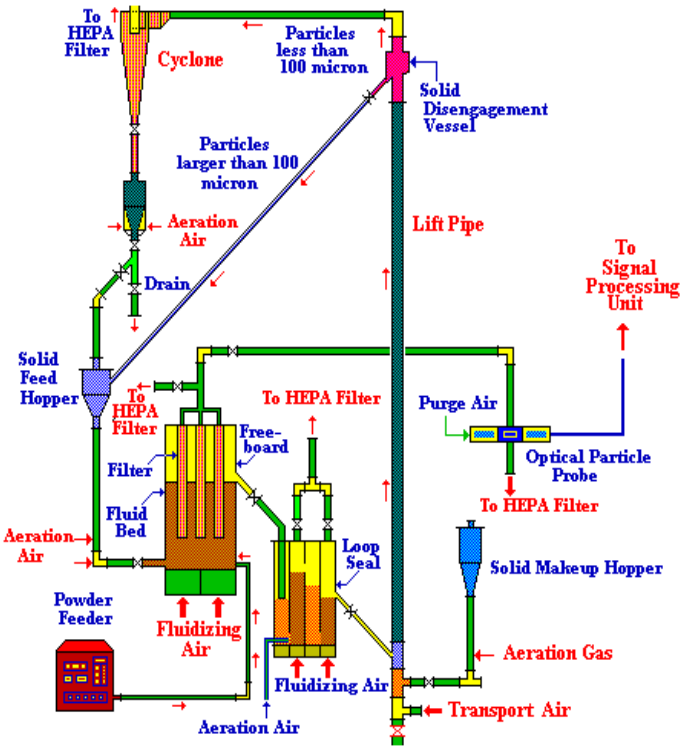

2-D Fluidized-Bed Granular Filtration Cold Model with Solid Recycling System (under construction)

CRADA facts

DEPARTMENT OF ENERGY
OFFICE OF FOSSIL ENERGY

FILTRATION PROJECT

HIGH-TEMPERATURE, HIGH-PRESSURE PROBE FOR HAZARDOUS AIR POLLUTANTS SAMPLING IN ADVANCED POWER SYSTEMS

CONTACT POINTS

TECHNICAL:

Dr. William P. Chisholm
Research Chemist
Office: (304) 285-4730
E-Mail: wchish@metc.doe.gov

ADMINISTRATIVE:

Dr. Rodney Anderson
Technology Transfer
Program Manager
Office: (304) 285-4709
E-Mail: rander@metc.doe.gov

Ms. Lisa Jarr
Patent Advisor
Office: (304) 285-4555
E-Mail: ljarr@metc.doe.gov

MAIL ADDRESS:

U.S. Department of Energy
P.O. Box 880
3610 Collins Ferry Road
Morgantown, WV 26507-0880

FAX: (304) 285-4469

Capabilities

The Morgantown Energy Technology Center (METC) has developed a number of new technologies for efficient utilization of coal in the generation of electrical power. The superior performance of these systems is currently being demonstrated in a number of locations through the Clean Coal Technology program and other programs managed by METC. However, the environmental performance of these systems has not yet been thoroughly characterized, so METC has initiated programs to address this lack of data. The first step in this regard is to measure the eleven elements identified by the U.S. Environmental Protection Agency as being air toxics.

The best way to characterize advanced systems with respect to the fate of the eleven toxic elements is to perform a mass balance as they move through the various components of the system. Irrespective of the instrumental method used to analyze a sample extracted from within an advanced system, the sampling probe will need to gather a representative sample from a high-temperature, high-pressure environment. To this end, METC tasked Radian Corporation, now known as Radian International, with the design, construction, and application of a suitable probe.

The probe was used to gather data on hazardous air pollutants (HAPs) at the Destec LGTI gasifier in Placquemine, Louisiana, in 1995. The probe performed well and provided useful particulate and gas-phase sample from the middle of the gasifier itself, prior to any cooling or pressure letdown.

The probe is a concentric tube with a ceramic filter located at the tip. A flow of nitrogen cools the probe and quenches the gas stream shortly downstream from the tip. The probe is inserted through a pair of block and bleed isolation valves, and the pressure seal around it was kept by multiple graphite gaskets. The probe is inserted and retracted by a system of hand-cranked winches, with positive action both on insertion and retraction. Two operators can readily insert the probe against a 40 bar (600 psi) pressure.

High-Temperature, High-Pressure Probe for Hazardous Air Pollutants Sampling in Advanced Power Systems

Opportunities

Hardware available for application to any pressurized system where a flange can be installed, such as:

- Gasifiers
- Pressurized combustors
- Pressurized cleanup systems

The Probe

This photo shows brass winches, rails (red), stainless steel probe and flanges, and pressurized test stand (blue).

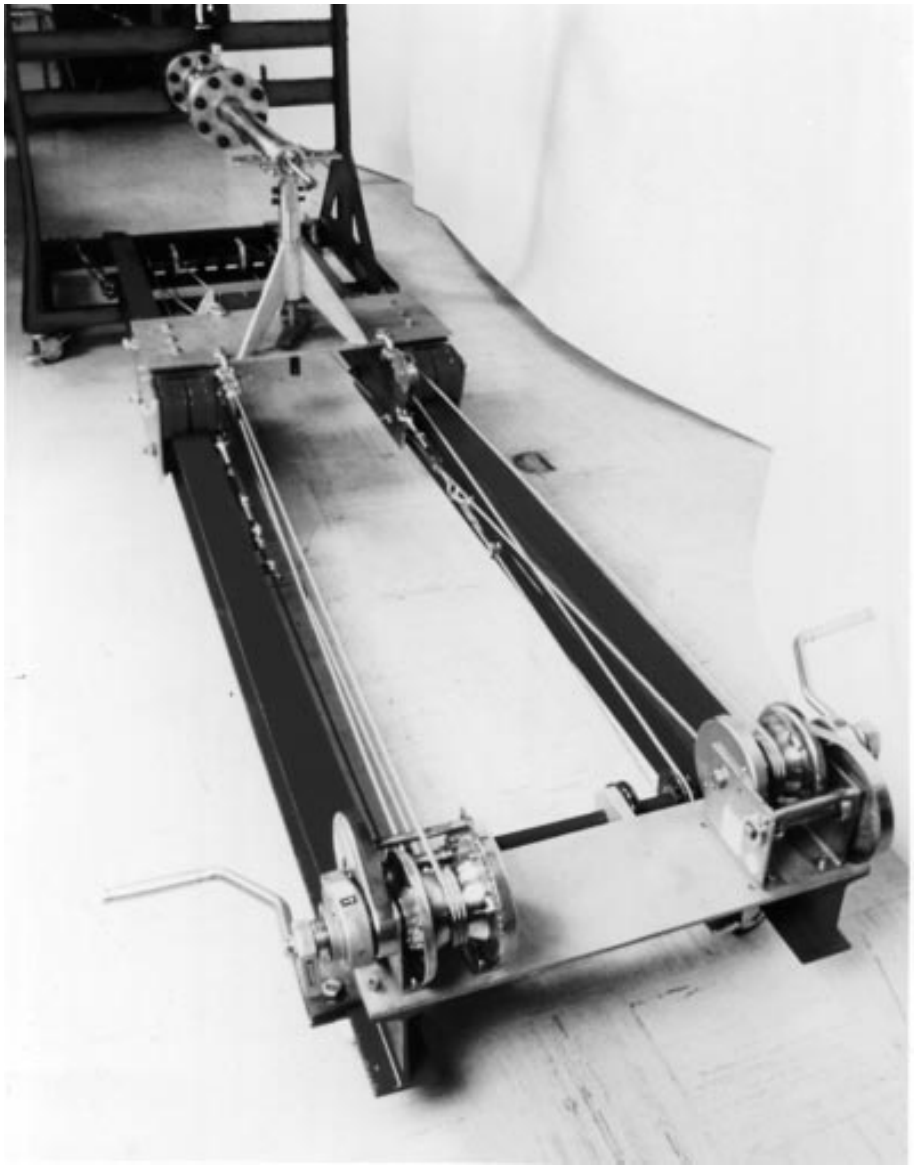

HTHP probe inserted into test stand

CRADA facts

Department of Energy
Office of Fossil Energy

FILTRATION PROJECT

Measurements of Filter-Cake Properties

Capabilities

The Pressurized Fluidized-Bed Combustion (PFBC) and Integrated Gasification Combined Cycle (IGCC) programs of the U.S. Department of Energy require filtration, at temperatures from about 600 to 900 °C, of fine particles of coal ash, char, or spent and unreacted sorbent from hot-gas streams. Achieving acceptable filter lifetimes requires solutions to, or avoidance of, such problems as incomplete filter cleaning, re-entrainment (i.e., re-filtration) of particles from filter cleaning, and bridging of filter cake between adjacent filters. These and other potential problems may arise from the materials properties of filter cakes, from the filter-bank design, and from the mechanisms of filter cleaning. Avoiding re-entrainment requires that some bonding and agglomeration of particles occur in the cakes (so that the agglomerates from filter cleaning are too large to be re-entrained), but excessive agglomeration can produce poor cleaning or bridging.

For both PFBC and IGCC applications, we can form filter cakes at process temperatures, gas compositions, and gas flow rates, and measure the gas-phase permeabilities, porosities, tensile strengths, and deformation coefficients of these filter cakes to determine their dependencies on temperature, reaction time, gas composition, particle compositions, and particle size distributions. Filter-cake shear strengths and flow factors can be measured for powders "as received," for filter cakes that we have heated to process temperatures, or for powders heated in reactive gases to simulate gas-solid reactions in process filter cakes.

In PFBC systems, the degree of agglomeration in filter cakes strongly depends on ionic diffusion, chemical reactions, and formation of necks between adjacent particles, which in turn depend on the operating temperature, gas composition, particle size distribution, and frequency of filter-cleaning. When a dolomitic sorbent is used, $CaSO_4$ and MgO are elutriated from the combustor. With a filter-vessel temperature of ~ 700 °C, capture of SO_2 by sulfation of MgO occurs in the filter cakes. Agglomeration between adjacent particles of $MgSO_4$ or of $CaSO_4$ occurs by "sintering" (ionic self-diffusion and neck formation). However, the end-product produced by sulfation in the filter cakes of the Tidd PFBC demonstration plant was not $MgSO_4$, but $Mg_2Ca(SO_4)_3$ [incorrectly identified in the literature as $Mg_3Ca(SO_4)_4$]. Necks of $Mg_2Ca(SO_4)_3$ form by chemical diffusion between adjacent particles of $MgSO_4$ and $CaSO_4$. The amounts of $Mg_2Ca(SO_4)_3$ and the rate at which it was produced also have been determined for the Tidd filter unit.

CONTACT POINTS

TECHNICAL:

Dr. Duane H. Smith
Chemist
Office: (304) 285-4069
E-Mail: dsmith@metc.doe.gov

Dr. Ulrich Grimm
Chemist
Office: (304) 285-4378
E-Mail: ugrimm@metc.doe.gov

Dr. George J. Haddad
Research Associate
National Research Council
Office: (304) 285-4246
E-Mail: ghadda@metc.doe.gov

ADMINISTRATIVE:

Dr. Rodney Anderson
Technology Transfer
Program Manager
Office: (304) 285-4709
E-Mail: rander@metc.doe.gov

Ms. Lisa Jarr
Patent Advisor
Office: (304) 285-4555
E-Mail: ljarr@metc.doe.gov

MAIL ADDRESS:

U.S. Department of Energy
P.O. Box 880
3610 Collins Ferry Road
Morgantown, WV 26507-0880

FAX: (304) 285-4469

Measurements of Filter-Cake Properties

Opportunities

- Perform advanced modeling of particle deposition patterns and filter-cleaning backpulses
- Measure porosities (as function of face velocity) for more kinds of filter cakes
- Incorporate time dependence of cake permeability
- Develop and utilize filter-cake models for re-entrainment fractions
- Diagnose performances of more filter vessels, especially Particle Control Devices at the Wilsonville PSDF

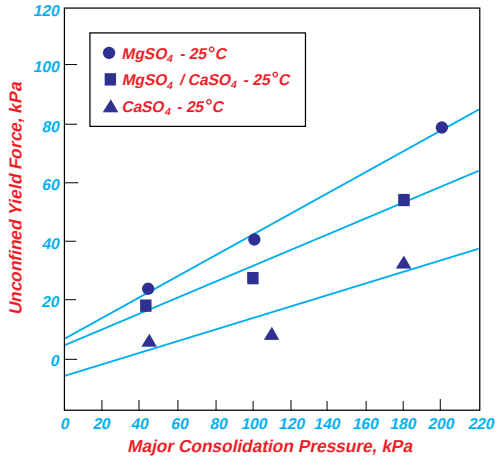

In unheated samples strength depends on $MgSO_4/CaSO_4$ ratio

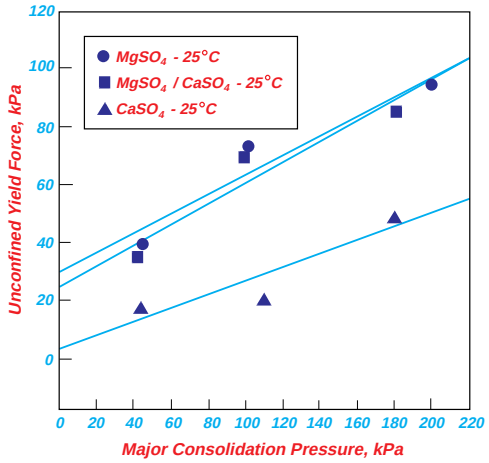

Sintering led to increased filter cake strength

$CaSO_4$ - 23kPa/750°C

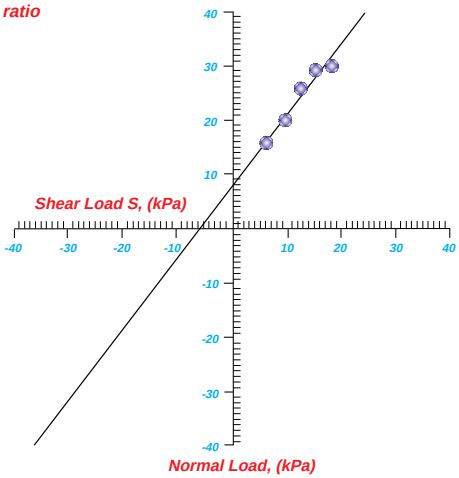

As face velocity increases cake voidage decreases (and strength increases)

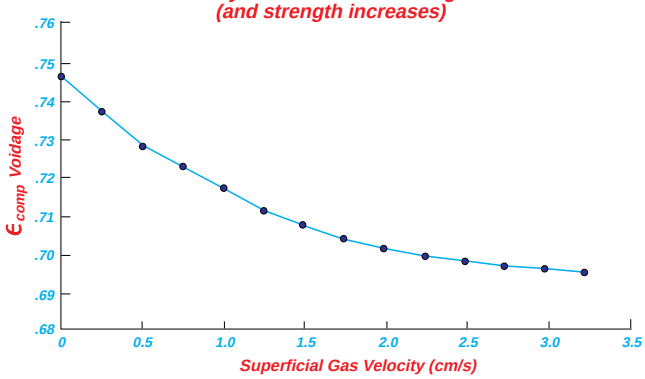

Stress Fracture vs. Voidage for Calcium Carbonate (Non hygroscopic "Model Powder")

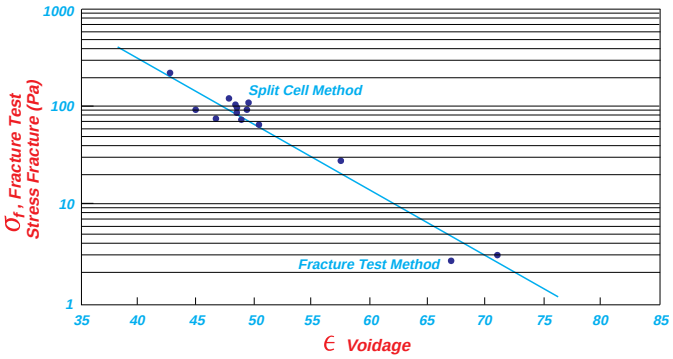

M96001625A

CRADA facts

DEPARTMENT OF ENERGY
OFFICE OF FOSSIL ENERGY

FILTRATION PROJECT

A New Hot Gas Cleanup Filter Design Methodology

Capabilities

The fluid dynamics of Hot Gas Cleanup (HGCU) systems having complex geometrical configurations are typically analyzed using computational fluid dynamics codes (CFD) or bench-scale laboratory test facilities called cold-flow models (CFM). At the present time, both CFD and CFM can be effectively used for simple flows limited to one or two characteristic length scales with well-defined boundary conditions. This is not the situation with HGCU devices. These devices have very complex geometries, low Reynolds number, multi-phase flows that operate on multiple-length scales. For this reason, both CFD and CFM analysis cannot yet be considered as a practical engineering analysis tool for modeling the entire flow field inside HGCU systems.

The thrust of this work is to provide an aerodynamic analysis methodology that can be easily applied to the complex geometries characteristic of HGCU filter vessels, but would not require the tedious numerical solution to the entire set of transport equations. The analysis methodology performs the following tasks:

- Predicts problem areas where ash deposition will most likely occur;
- Predicts residence times for particles at various locations inside the filter vessel;
- Lends itself quickly to major design changes;
- Provides a sound technical basis for more appropriate use of CFD and CFM analysis; and
- Provides CFD and CFM analysis in a more focused way where it is needed.

The technical approach taken here is to first solve for the general flow field using panel techniques. These techniques provide the exact solution to the flow field using a greatly reduced form of the transport equations and is applied only at panels that define the geometry. Thus the flow field is solved for without the need of a finite difference or finite element grids. Since the solution is exact, there are no stability or convergence problems that are typically found in other CFD solvers. This method is particularly suited for problems having complex geometries. Thus, the effect of major geometric design changes on the global flow field can be quickly assessed without major efforts in CFD or CFM analysis so that design optimization may be performed.

After a simple global solution is obtained for any particular geometry using panel methods, regions in the flow field where secondary flows develop would be revealed. These secondary flows are then analyzed in greater detail using the conventional methods of CFD and CFM analysis.

CONTACT POINTS

TECHNICAL:

Dr. John G. VanOsdol
Aerodynamicist
Office: (304) 285-5446
E-Mail: jvanos@metc.doe.gov

Richard A. Dennis
Mechanical Engineer
Office: (304) 285-4515
E-Mail: rdenni@metc.doe.gov

Franklin D. Shaffer
Office: (412) 892-5964

ADMINISTRATIVE:

Dr. Rodney Anderson
Technology Transfer
Program Manager
Office: (304) 285-4709
E-Mail: rander@metc.doe.gov

Ms. Lisa Jarr
Patent Advisor
Office: (304) 285-4555
E-Mail: ljarr@metc.doe.gov

MAIL ADDRESS:

U.S. Department of Energy
P.O. Box 880
3610 Collins Ferry Road
Morgantown, WV 26507-0880

FAX: (304) 285-4469

A New Hot Gas Cleanup Filter Design Methodology

Opportunities

- **General Fluid Dynamic Analysis Using Panel Methods and Other Global Techniques**
  - General properties of complex flow fields identified.
  - Special points of interest in the flow field identified.

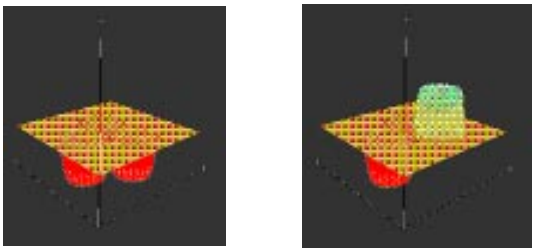

Time Sequence of Back Flush

Engineering Model

1. Solution Plane
2. Shed Roof
3. Tube Sheet
4. Candle Filter Bunch

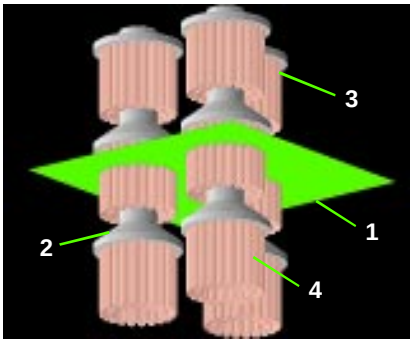

- **Computational Fluid Dynamic Analysis (CFD)**
  - Analysis performed on limited scale using the right model at the right place.
  - Different models for different situations.

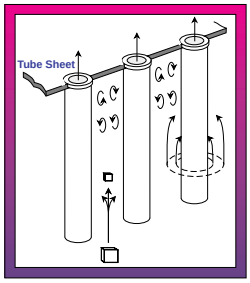

Candle Filters
(Axial Flow)

Tube Sheet Deposition:
Analysis of Small Scale Flow

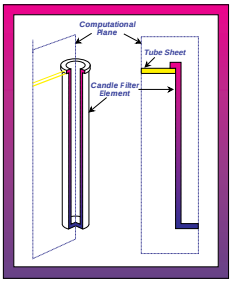

Streaklines

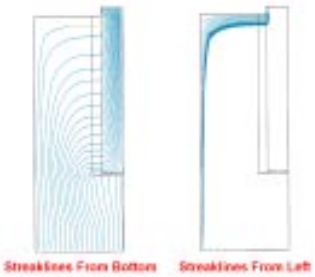

- **Bench Scale Analysis or Cold-Flow Modeling (CFM)**
  - Each analysis is set up using the laws of dynamic similarity as a basis for scaling.
  - This ensures that the results obtained in the laboratory are extendable to the prototype and can be used for engineering design calculations.

  - ***Geometrical Similarity*** (length scale matching)
  - ***Kinematic Similarity*** (flow visualization)
    - Smoke Wire Stream Line Tracing
    - Hot Wire Anemometry
    - Hot Film Anemometry
    - Schlieren
    - Focused Schlieren
    - Laser Doppler Anemometry (LDA)
    - Particle Image Velocimetry (PIV)
  - ***Dynamic Similarity*** (Newton's Laws - dimensionless group matching)
    - Reynolds Number
    - Stanton Number
    - Froude Number
    - Coefficient of Pressure
    - Pressure Gradient Matching
    - Eckert Number
    - Mach Number
    - Coefficient of Drag
    - Strouhal Number
    - Heat Transfer Coefficients
    - Euler Number
    - Coefficient of Lift
    - Rossby Number
    - Skin Coefficients
    - Prandtl Number

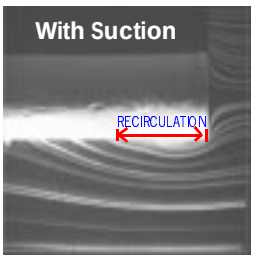

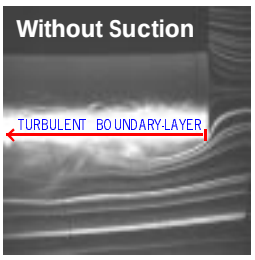

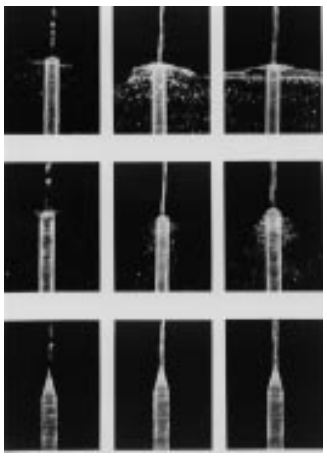

Axial Tip Flows in Water Tunnel

M96001680A

CRADA facts

DEPARTMENT OF ENERGY
OFFICE OF FOSSIL ENERGY

GAS STREAM cleanup PROJECT

HOT GAS DESULFURIZATION PDU PROJECT

CONTACT POINTS

TECHNICAL:

Larry A. Bissett
General Engineer

Office: (304) 285-4266
E-Mail: lbisse@metc.doe.gov

ADMINISTRATIVE:

Dr. Rodney Anderson
Technology Transfer
Program Manager

Office: (304) 285-4709
E-Mail: rander@metc.doe.gov

Ms. Lisa Jarr
Patent Advisor

Office: (304) 285-4555
E-Mail: ljarr@metc.doe.gov

MAIL ADDRESS:

U.S. Department of Energy
P.O. Box 880
3610 Collins Ferry Road
Morgantown, WV 26507-0880

FAX: (304) 285-4469

Capabilities

The process development unit (PDU) being constructed at METC will fill the strategic role of bridging the gap between past/current small-scale testing and future large-scale demonstrations. With the capability for both fluid-bed and transport reactor contacting, the project will provide a site for testing/proving hot gas desulfurization (HGD) process configurations and demonstrating sorbent suitability. Process conditions will be representative of anticipated commercial applications in terms of temperatures, pressures, compositions, velocities, and sorbent cycling.

The project utilizes a coupled configuration with continuous circulation of a desulfurization sorbent between the absorption (fuel gas) and regeneration (air) sides of the process. Specially fabricated high-temperature slide valves in the circulation standpipes regulate the flow (circulation) of sorbent between the absorber and regenerator. Inert gases (steam and/or nitrogen) are used to fluidize the sorbent in the standpipes above the valves and to prevent fuel gas and air intermixing. Removable spool pieces and piping along with other vessel design features (such as submerged/freeboard risers and underflow/overflow standpipes) have been incorporated to expand potential testing capabilities. Since both the absorber and regenerator sides have fluid-bed and transport reactor capabilities, four principle configurational modes of operation are possible. Sorbent is circulated by reactant gases (i.e., fuel gas and air) in transport reactor modes, and inert gases in fluidized-bed modes.

Opportunities

- Advance/leverage reactor system R&D
  - Protect/gain intellectual property
  - Eventual retrofit to applications other than HGD
- Share process technology development
  - Test planning
  - Training and observation of operations
  - Data reduction and analysis
- Qualify sorbent for commercial-scale demonstrations

Hot Gas Desulfurization PDU Project

Key Parameters

Absorption temperature	1,000 - 1,200 °F design
Regeneration temperature	1,100 - 1,400 °F design
Operating pressure	400 psia maximum
H_2S concentration	0.5 - 1 vol% typical
Sorbent circulation rate	2,000 - 5,000 lb/hr typical
Sorbent inventory	1,000 - 2,000 lb typical
Sorbent cycles per day	50 - 100 typical
Sorbent size	50 - 300 microns typical

The Project

PDU Flow Diagram

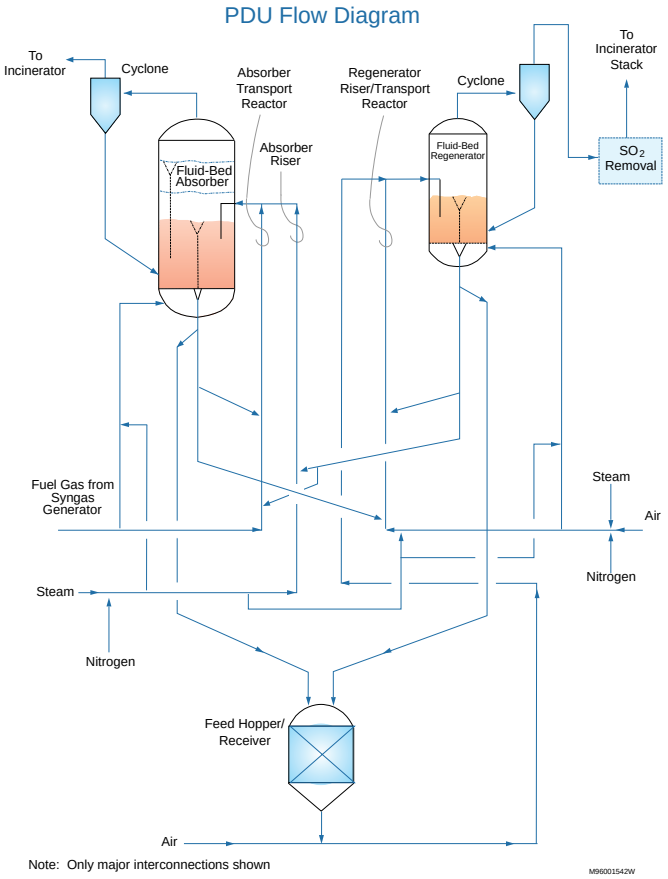

The PDU being contructed at METC

CRADA facts

DEPARTMENT OF ENERGY
OFFICE OF FOSSIL ENERGY

GAS STREAM cleanup PROJECT

FLUIDIZED-BED REACTOR AND HOT GAS CLEANUP FACILITY

CONTACT POINTS

TECHNICAL:

John M. Rockey
Chemical Engineer
Office: (304) 285-4711
E-Mail: jrocke@metc.doe.gov

ADMINISTRATIVE:

Dr. Rodney Anderson
Technology Transfer
Program Manager
Office: (304) 285-4709
E-Mail: rander@metc.doe.gov

Ms. Lisa Jarr
Patent Advisor
Office: (304) 285-4555
E-Mail: ljarr@metc.doe.gov

MAIL ADDRESS:

U.S. Department of Energy
P.O. Box 880
3610 Collins Ferry Road
Morgantown, WV 26507-0880

FAX: (304) 285-4469

Capabilities

As part of the Morgantown Energy Technology Center's (METC) Advanced Gasification and Hot Gas Cleanup Facility, a 907 kg (1 ton) coal-per-day (10-inch inside diameter) jetting fluidized-bed gasifier provides realistic fuel gas for testing and developing high-temperature, high-pressure components and processes in a reducing (gasification) and oxidizing (combustion) environment. Operated mainly as a gasifier, the 0.25-m (10-inch) diameter reactor produces up to 227 kg/hr (500 lb/hr) of coal gas at 866 K (1,100 °F) and 30 atmospheres (425 psig) for downstream testing. The raw coal gas is sampled for major and trace species and sent to a filter vessel capable of operating at 894 K (1,150 °F) and 20 atmospheres (290 psig) of pressure. After particulate removal, the gas can be independently controlled to up to five sampling or reaction vessels including fluid-bed desulfurization, transport desulfurization, chloride, alkali, or other contaminant removal or recovery processes. The fluid-bed desulfurizer is capable of being isolated, purged, and exposed to an oxidizing environment for sorbent regeneration or other oxidation reaction. Isokinetic hazardous air pollutant (HAPS) monitoring is provided at the upstream and downstream of particulate removal.

Over the past three years, 1,200 hours of operation have been completed in support of six separate Cooperative Research and Development Agreements (CRADAs). These research agreements have been in the areas of candle filters and materials testing, direct sulfur recovery from sorbent regeneration tail gases, and gasifier development.

Currently, four additional CRADAs are in development. Three of these are in further testing and development of candle filters, and the fourth is in support of the desulfurization process at the Sierra Pacific Piñon Pine, Integrated Gasification Combined Cycle (IGCC) power plant.

Opportunities

- Provide testing for advanced IGCC
  - Filtration experiments at 1,150 °F, 20 atm
  - Cyclic (reducing/oxidizing) reaction atmosphere for sorbent testing
  - Slipstreams for contaminants removal
- Provide testing for advanced PFBC
  - Filtration experiments at 1,600 °F, 30 atm
- Hardware and operational control strategy testing

Fluidized-Bed Reactor and Hot Gas Cleanup Facility

The Facility

METC's **Fluid-Bed Gasifier** and the **Modular Gas Cleanup Rig** (MGCR) combined form the **METC Gasification and Hot Gas Cleanup Facility**.

This unique facility is used to develop and test components, and to test technologies suitable for Integrated Gasification, Combined-Cycle — or IGCC — power-plant systems.

The **MGCR** is mainly used to test components, such as desulfurization sorbents, hot particulate-removal filters, and filter materials.

Testing is done at a pressure of 300 pounds per square inch and a temperature up to 1,150 °F.

The **Fluid-Bed Gasifier** is at product development unit (PDU) scale.

The 10-inch diameter reactor gasifies 80 pounds per hour of coal to produce 300 pounds per hour — or 5,000 standard cubic feet per hour — of combustible, low-Btu coal gas.

The gas is produced at high temperature — 1,700 °F — and high pressure — 425 pounds per square inch.

METC hopes to use this Gasification and Hot Gas Cleanup Facility to facilitate commercialization of advanced power systems that can significantly reduce pollutants while increasing fuel efficiency — at the lowest possible costs.

The uniqueness of the combined Modular Gas Cleanup Rig and Fluid-Bed Gasifier is that testing is done with **real coal gas** that has a realistic composition and contains the trace metals and species inherent in the feed coal.

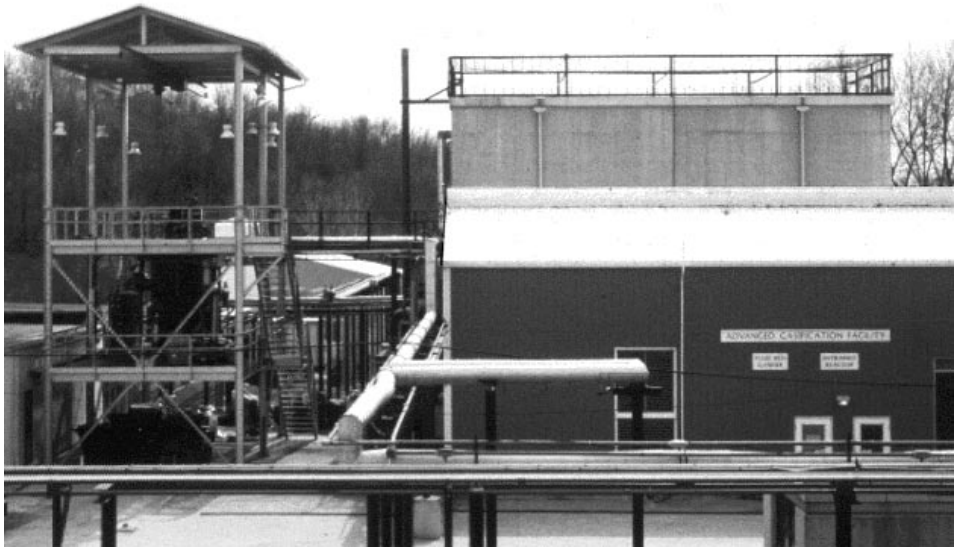

METC's **Modular Gas Cleanup Rig** (MGCR), at left, and **Fluid-Bed Gasifier**, on the right, combined form the **METC Gasification and Hot Gas Cleanup Facility**.

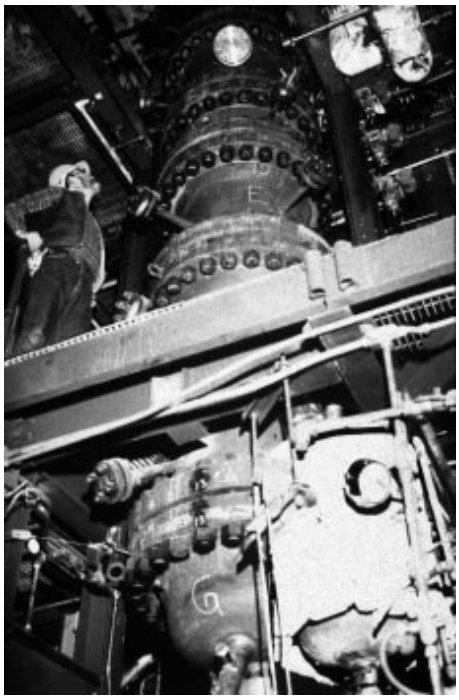

METC's Fluid-Bed Gasifier

MGCR Particulate Removal and Desulfurization Equipment

The Control Room for the Fluid-Bed Gasifier

M96001580A

CRADA facts

DEPARTMENT OF ENERGY
OFFICE OF FOSSIL ENERGY

GAS STREAM cleanup PROJECT

TRANSPORT REACTOR FACILITY

Capabilities

The Morgantown Energy Technology Center (METC) is currently evaluating hot gas desulfurization (HGD) in its on-site transport reactor facility (TRF). This facility was originally constructed in the early 1980s to explore advanced gasification processes with an entrained reactor, and has recently been modified to incorporate a transport riser reactor. The TRF supports Integrated Gasification Combined Cycle (IGCC) power systems, one of METC's advanced power generation systems. The HGD subsystem is a key developmental item in reducing the cost and increasing the efficiency of the IGCC concept.

The TRF is a unique facility with high-temperature, high-pressure, and multiple reactant gas composition capability. The TRF can be configured for reacting a single flow pass of gas and solids using a variety of gases. The gas input system allows six different gas inputs to be mixed and heated before entering the reaction zones. Current configurations allow the use of air, carbon dioxide, carbon monoxide, hydrogen, hydrogen sulfide, methane, nitrogen, oxygen, steam, or any mixture of these gases. Construction plans include the addition of a coal gas input line. This line will bring hot coal gas from the existing METC Fluidized-Bed Gasifier (FBG) via the Modular Gas Cleanup Rig (MGCR) after filtering out particulates with ceramic candle filters.

Solids can be fed either by a rotary pocket feeder or a screw feeder. Particle sizes may range from 70 to 150 micrometers. Both feeders have a hopper that can hold enough solid for fairly lengthy tests at the higher feed rates, thus eliminating the need for lockhopper transfers during operation.

If the Entrained Reactor is used alone without the Transport Riser Reactor, it can perform downflow tests under the following conditions:

Temperature: up to 2500 °F (1371 °C)
Pressure: 100 to 960 psig (0.7 to 6.6 MPa [ga])
Residence Time: 2 to 10 seconds
Solids Feed Rate: 0.5 to 10 lb/h (0.23 to 4.54 kg/h)
Gas Feed Rate: 200 to 1000 scfh (5.7 to 28.3 scmh)

If the Riser Reactor is coupled to the Entrained Reactor, upflow tests can be performed under the following conditions:

Temperature: up to 1500 °F (816 °C)
Pressure: 100 to 600 psig (0.7 to 4.1 MPa [ga])
Residence Time: 2 to 10 seconds
Solids Feed Rate: 0.5 to 10 lb/h (0.23 to 4.54 kg/h)
Gas Feed Rate: 200 to 1000 scfh (5.7 to 28.3 scmh)

CONTACT POINTS

TECHNICAL:

David A. Berry
Chemical Engineer
Office: (304) 285-4430
E-Mail: dberry@metc.doe.gov

Susan R. Shoemaker
Mechanical Engineer
Office: (304) 285-4269
E-Mail: sshoem@metc.doe.gov

ADMINISTRATIVE:

Dr. Rodney Anderson
Technology Transfer
Program Manager
Office: (304) 285-4709
E-Mail: rander@metc.doe.gov

Ms. Lisa Jarr
Patent Advisor
Office: (304) 285-4555
E-Mail: ljarr@metc.doe.gov

MAIL ADDRESS:

U.S. Department of Energy
P.O. Box 880
3610 Collins Ferry Road
Morgantown, WV 26507-0880

FAX: (304) 285-4469

Transport Reactor Facility

Currently, the TRF is conducting nonreacting gas/solid flow studies to characterize the hydrodynamics of the system. Plans call for testing of CMP-107 to characterize single pass sulfidation and regeneration of the sorbent. A synthesis gas mixture representing a KRW air-blown gasifier is planned as the reactant gas.

Opportunities

- Characterize catalytic and noncatalytic gas/solid reaction systems
- Conduct co-current entrained downflow process reactor studies for various gas/solid systems
- Conduct co-current transport upflow process reactor studies for various gas/solid systems

Transport Reactor Facility

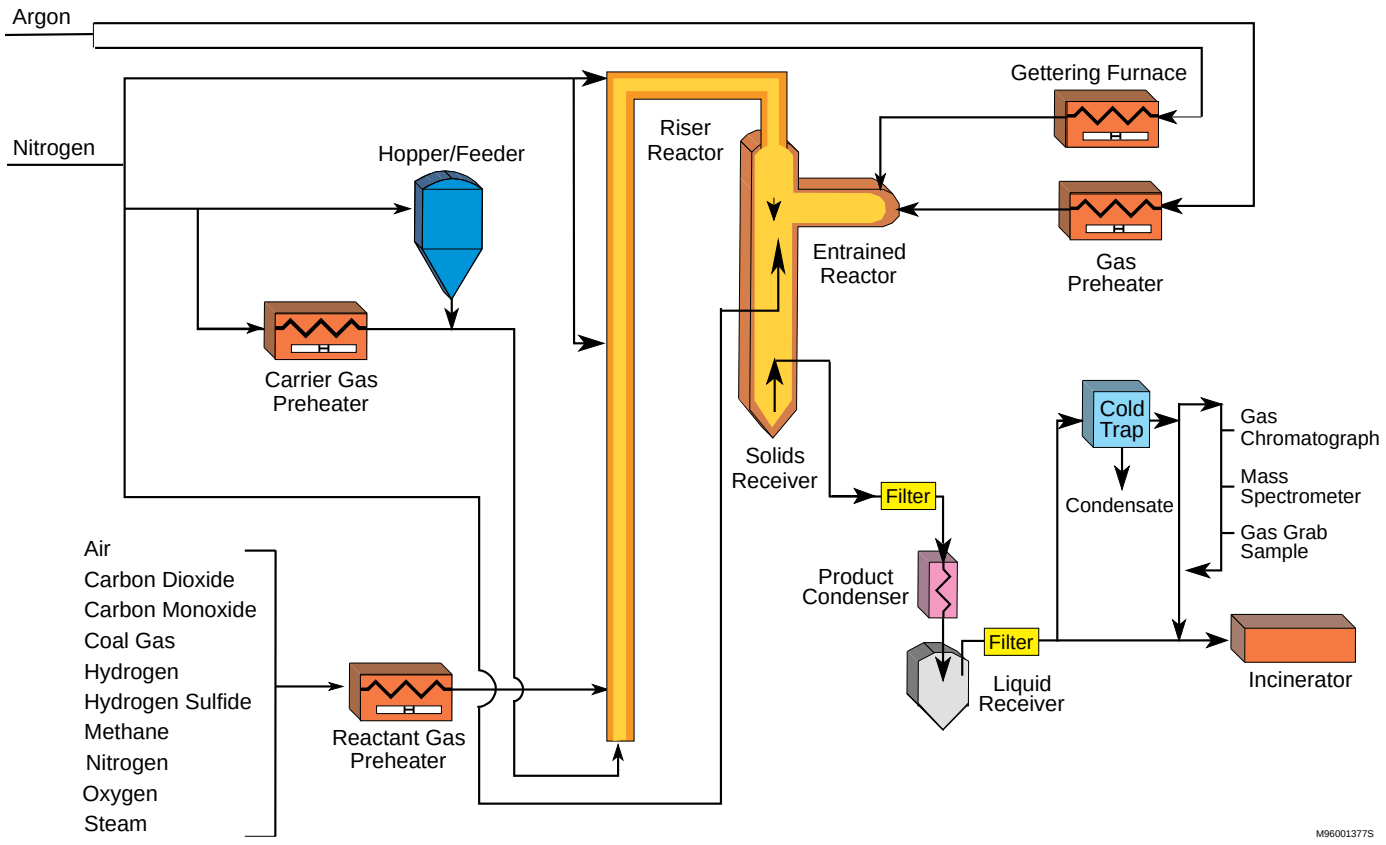

M96001581A

GAS STREAM cleanup
PROJECT

CRADA facts

DEPARTMENT OF ENERGY
OFFICE OF FOSSIL ENERGY

COLD FLOW VERIFICATION TEST FACILITY

CONTACT POINTS

TECHNICAL:

Dr. Abolghasem Shamsi
Chemist
Office: (304) 285-4360
E-Mail: ashams@metc.doe.gov

Dr. Lawrence J. Shadle
Chemist
Office: (304) 285-4647
E-Mail: lshadl@metc.doe.gov

ADMINISTRATIVE:

Dr. Rodney Anderson
Technology Transfer
Program Manager
Office: (304) 285-4709
E-Mail: rander@metc.doe.gov

Ms. Lisa Jarr
Patent Advisor
Office: (304) 285-4555
E-Mail: ljarr@metc.doe.gov

MAIL ADDRESS:

U.S. Department of Energy
P.O. Box 880
3610 Collins Ferry Road
Morgantown, WV 26507-0880
FAX: (304) 285-4469

Capabilities

The cold flow verification test facility consists of a 15-foot high, 3-foot diameter, domed vessel made of clear acrylic in two flanged sections. The unit can operate up to pressures of 14 psig. The internals include a 10-foot high jetting fluidized bed, a cylindrical baffle that hangs from the dome, and a rotating grate for control of continuous solids removal. The fluid bed is continuously fed solids (20 to 150 lb/hr) through a central nozzle made up of concentric pipes. It can either be configured as a half or full cylinder of various dimensions. The fluid bed has flow loops for separate air flow control for conveying solids (inner jet, 500 to 10000 scfh) , make-up into the jet (outer jet, 500 to 8000 scfh), spargers in the solids removal annulus (100 to 2000 scfh), and 6 air jets (20 to 200 scfh) on the sloping conical grid. Additional air (500 to 10000 scfh) can be added to the top of the dome and under the rotating grate.

The outer vessel, the hanging cylindrical baffles or skirt, and the rotating grate can be used to study issues concerning moving bed reactors. There is ample allowance for access and instrumentation in the outer shell. Furthermore, this facility is available for future Cooperative Research and Development Agreements (CRADA) to study issues and problems associated with fluid- and fixed-bed reactors. The design allows testing of different dimensions and geometries.

Opportunities

- Testing of jetting fluid bed in either half or full cylindrical configuration
- Development of rapid sensors and control systems for hydrodynamic instabilities/disturbances in jetting fluid bed
- Particulate control device visualization and testing
- Obtain data to determine operating conditions and design criteria necessary for jetting fluidized bed to avoid problems such as
  - carry over sticky coal and of tar vapor from the fluid-bed pyrolyzer
  - formation of ash-bonded clinkers around the feed jet
  - formation of coal agglomerates in the bed

Cold Flow Verification Test Facility

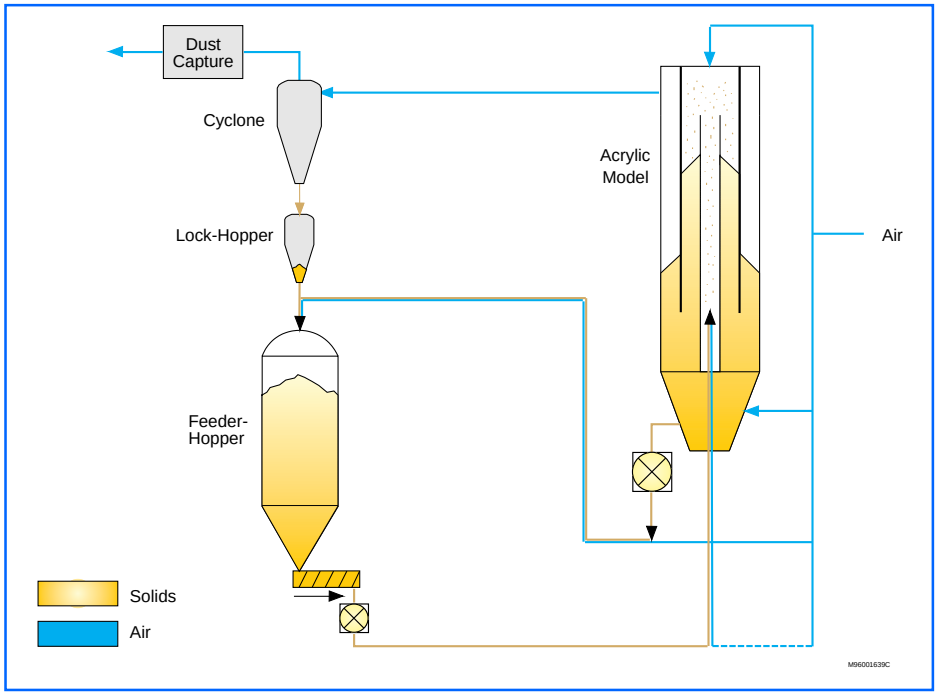

Cold Flow Model Process

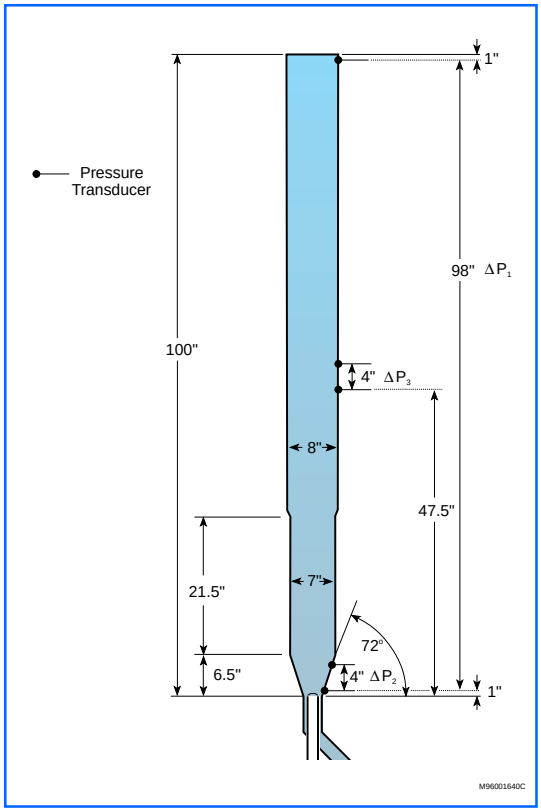

Configurations and Dimensions

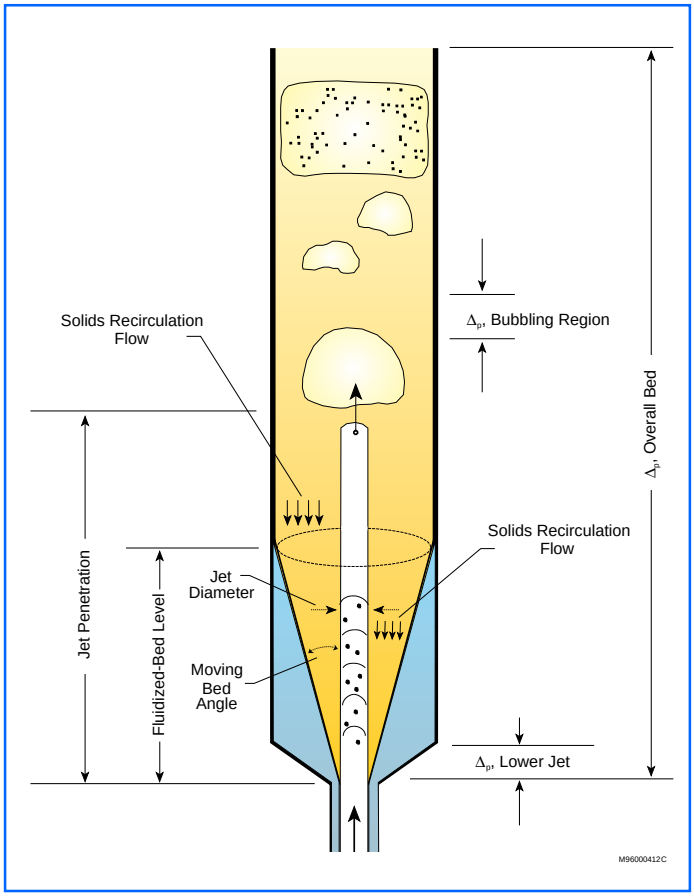

Cold Jet Fed Fluidized-Bed Measurements

M96001582A

Particulate Hot Gas Stream Cleanup Technical Issues

CONTRACT INFORMATION

Contract Number	DE-AC21-94MC31160
Contractor	Southern Research Institute 2000 Ninth Avenue South Birmingham, AL 35205 (205) 581-2000
Project Manager/Principal Investigator	Duane H. Pontius
Task Leader	Todd R. Snyder
METC Project Manager	Thomas P. Dorchak
Period of Performance	October 1994 to September 1996

The nature of the collected ash has been identified as an issue creating barriers to the commercialization of advanced particle control technologies. Since most of the emphasis and extended operation of Hot Gas Stream Cleanup (HGCU) facilities have been with ceramic candle filters, problems with ash characteristics can be understood in terms of their effects on these control devices. This project is designed to identify the ways ash characteristics affect advanced particle control technologies, to construct and maintain a data base of HGCU ashes and their measured characteristics, and to relate these characteristics to the operation and performance of these facilities.

The key characteristics of the collected ash are the morphology of the overall ash aggregate (porosity, geometry of the pores, specific surface area, etc.), and the cohesivity of the aggregate. Cohesivity is controlled in turn by the morphology of individual particles (size, shape), and the strength of the forces between particles due to sintering, chemical bonds, van der Vaals forces, adsorbed liquid layers, and salt bridges.

Our data base currently comprises 242 ash samples from 12 combustion and gasification HGCU sources. We have 116 ash samples from the Advanced Particulate Filter (APF) at the Pressurized Fluidized-Bed Combustor (PFBC) at Tidd, 51 ash samples from the Pressurized Circulating Fluid Bed (PCFB) system located at Karhula, Finland, and 17 ash samples from Foster Wheeler's Second Generation PFBC system at Livingston, New Jersey. In addition to these three operating facilities, our stock of HGCU samples includes ashes from facilities operated by Grimethorpe, Westinghouse, MW Kellogg, New York University, the University of North Dakota Energy and Environmental Research Center (UNDEERC), and KRW. We have characterized aerodynamic size distribution, specific surface area, uncompacted bulk porosity, tensile strength, true particle density, drag-equivalent diameter, specific gas flow resistance, nodule porosity, particle morphology (with Scanning Electron Micrographs), and mineral composition of selected ashes from advanced particle control devices. Ranges of values of several of these key quantities are shown in Table 1.

Table 1
Ranges of Characteristics of HGCU Samples

quantity	HGCU ashes
Stokes' MMD, µm	0.74 - 60
filter cake porosity, %	57 - 84
specific surface area, m^2/g	0.5 - 353
uncompacted bulk porosity, %	62 - 97
specific gas-flow resistance at uncompacted bulk porosity, in $H_2O/(ft/min)/(lb/ft^2)$	0.8 - 61
drag-equivalent diameter, µm	0.08 - 9.0

In general, the gasification samples we have analyzed have very high specific surface areas. Because filtering drag is accumulated as the gas being filtered passes over the surfaces of the particles in the filter cake, high specific surface areas generally correlate with small values of drag-equivalent diameter. (Drag-equivalent diameter incorporates the effects of particle morphology on filtering drag.) The effect of filter cake structure on filtering drag is determined by the cake porosity. Therefore, filtering drag is a function of the shape of the particles in the filter cake and the porosity of the cake.

Experiences at the Tidd APF

Observations of the Advanced Particulate Filter (APF) at the Tidd PFBC Demonstration Plant led to the conclusion that tenacious ash deposits had formed in the filter vessel and induced stresses that resulted in bent or broken ceramic candle filter elements. The proximity of these bent and broken candle filter elements to large, strong ash deposits emphasized the need to prevent or control the growth of these deposits, facilitate their on-line removal, and/or to develop filter design criteria to minimize their effects on individual filter elements. Similar, although less severe, problems have also been observed at the PCFB facility located in Karhula, Finland.

Tidd ash chemistry combined with the environment within the filter vessel caused ash deposits formed in the filter vessel to consolidate and strengthen. We believe the strengthening of these deposits is due to formation of eutectic compounds. These eutectics form when primary coal ash particles (containing a large percentage of aluminosilicate compounds) come into physical contact with sorbent-derived ash particles which contain relatively large amounts of magnesium and/or calcium. Aluminosilicate compounds in the coal ash particles react with alkali metals in the sorbent ash particles to form eutectics that melt at relatively low temperatures. This reduction in melting points combined with long-term exposure to the temperatures in the filter vessel tends to create relatively soft, sticky layers on the surfaces of the ash particles. The surface tension of the near-liquid layer on the particles pulls adjacent ash particles closer together, thereby eventually consolidating the structure of the entire ash agglomerate. The progress of these reactions is supported by the intimate contact of the ash particles in the agglomerate and by long-term exposure of the ash to the temperatures in the filter vessel.

The optimum solution to the problems caused by these ash aggregates is the removal of these aggregates from the filter before the eutectics have had enough time to develop. The approach that has proved most successful at Tidd for eliminating the deposits was the total bypassing of the cyclone upstream of the APF. This increased the size distribution of the particles forming the various ash deposits, thereby decreasing their inherent cohesivity. These agglomerates of lower cohesivity did not have sufficient strength to remain in the APF long enough to undergo consolidation.

Recent Analyses of HGCU Ashes

Table 2 lists three samples we have recently analyzed and that we discuss in this paper.

Table 2
Selected Samples from the HGCU Data Base

ID #	Source	Brief description
4170	DOE/METC	pilot-scale gasifier
4176	UNDEERC	TRDU P047: 4/18-20/96
4182	Karhula	middle plenum ash 1996

The first sample listed in Table 2 was obtained from the Modular Gas Cleanup Rig (MGCR) gasification facility located at DOE/METC. This sample was collected from the hopper of the pilot-scale candle filter assembly. The second sample listed in Table 2 was received from the Transport Reactor Demonstration Unit (TRDU) located at UNDEERC. This sample was identified as TRDU P047 collected from 4/18/96 to 4/20/9. Information provided by UNDEERC indicated that the TRDU operated for a total of 117 hours under gasification conditions in April. The TRDU conditions during these tests were described as not sustainable for extended use. We proceeded with a full analysis of this sample despite the limitations of the conditions under which it was produced. We also received six ash samples from the PCFB facility located in Karhula, Finland. The samples included filter cake ashes collected from the top, middle, and bottom plenum candle surfaces, as well as hopper and bottom ash samples. We selected the sample of filter cake ash from the middle plenum for detailed analysis. The results of our chemical and physical analyses of these samples are summarized in Tables 3 and 4 and discussed in the following sections.

Table 3
Chemical Analyses of Selected Samples, % wt.

constituent ID #	4170	4176	4182
Li_2O	0.02	0.01	0.01
Na_2O	0.59	0.63	0.87
K_2O	0.07	0.12	1.6
MgO	10.9	5.2	0.72
CaO	33.3	11.2	17.4
Fe_2O_3	1.17	1.9	11.0
Al_2O_3	17.4	22.9	12.6
SiO_2	31.8	54.8	34.4
TiO_2	1.49	0.8	0.6
P_2O_5	0.53	0.55	0.10
SO_3	0.32	0.96	19.8
LOI	35.9	4.3	0.22
soluble $SO_4^=$	<0.2	--	23.8
Equilibrium pH*	10.2	--	7.4

* Equilibrium pH is dimensionless.

Table 4
Physical Characteristics of Selected Samples

quantity ID #	4170	4176	4182
Stokes' MMD, µm	0.74	60	9.9
filter cake porosity, %	--	--	75
specific surface area, m^2/g	140	51	1.2
uncompacted bulk porosity, %	97	72	81
specific gas flow resistance, at uncompacted bulk porosity, in $H_2O/(ft/min)/(lb/ft^2)$	18	2.8	1.5
drag-equivalent diameter, µm	0.08	2.77	2.22
tensile strength, N/m^2	0.6	2.8	3.8
true particle density, g/cm^3	2.87	2.60	2.83

DOE/METC MGCR

Of all the gasification samples in our HGCU data base, the sample exhibiting the lowest permeability to gas flow (or the highest specific gas flow resistance) was the sample from the DOE/METC MGCR (ID # 4170). Even though this sample would be expected to initially form a

filter cake with a porosity on the order of 97 % (the uncompacted bulk porosity value measured for this sample), the morphology of the particles in this sample, specifically their small size, is the ultimate cause of its high resistance to filtering flow. Although other samples in the HGCU data base have higher values of specific surface area than this sample, it exhibited the lowest values of physical particle size and drag equivalent diameter of all the gasification samples we have tested. When the DOE/METC MGCR sample was examined with a scanning electron microscope (Figure 1), the fineness of its particle size distribution was readily apparent. Like other gasification samples, another distinctive characteristic of the DOE/METC MGCR sample was its high value (35.9 % by wt.) of loss-on-ignition (LOI).

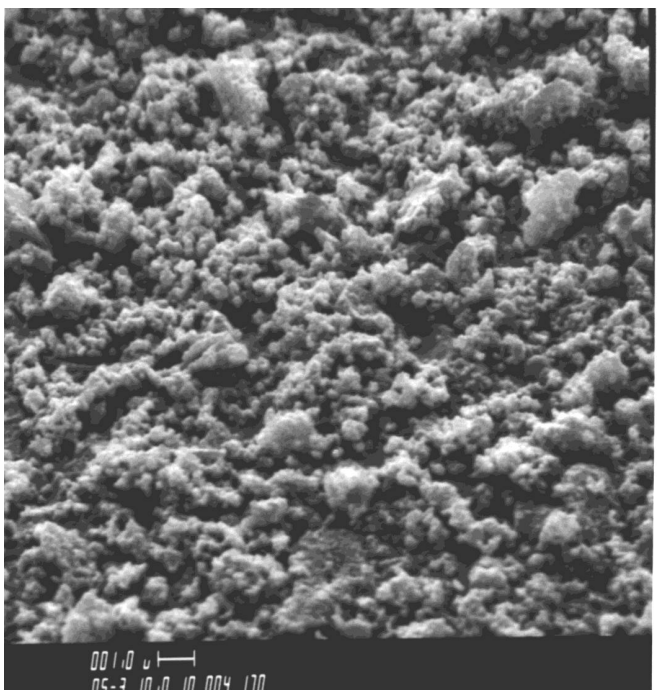

Figure 1. SEM photograph of DOE/METC MGCR gasification residue.

We also characterized the response of the DOE/METC MGCR sample to compacting forces. The compaction data, which we measured at room temperature, show that a filtering pressure drop of 3.4 psi (94 in. H_2O) may be sufficient to reduce the porosity of a filter cake formed from this sample down to about 90 %. Data from our permeability model indicate that the degree of filter cake consolidation that may be induced by normal filtering pressure drops of around 3 to 4 psi may increase filtering pressure losses by a factor of twenty or more. This is especially detrimental since the specific gas-flow resistance of this sample is quite high even when the filter cake is uncompacted. (The specific flow resistance of the MGCR sample is 18 in $H_2O/(ft/min)/(lb/ft^2)$ for a filter cake having a porosity of 97 %. If a filter cake composed of this ash is compacted to around 90 % porosity, specific gas flow resistances around 400 in $H_2O/(ft/min)/(lb/ft^2)$ could be expected.) These characteristics ultimately lead to high pressure losses and/or very frequent cleaning. Although the METC MGCR sample showed an apparent increase in strength as it was compacted, the cake compacted with a pressure of 3.4 psi still had comparatively low strength.

Overall, our observations of the DOE/METC MGCR sample and other gasification samples indicate that the filtration of gasification particulate residues can generate filter cakes that exhibit extremely low permeabilities. These low permeabilities can be traced to the presence of a high proportion of submicron particles and/or extremely high specific surface areas. In addition, filter cake compaction may exacerbate these negative characteristics. Consequently, it may be difficult to maintain a reasonable pressure drop in their filtration.

In general, the gasification samples we have tested exhibited very high uncompacted bulk porosities, which indicates that they are highly cohesive. (High uncompacted bulk porosities are generally associated with samples having fine size distributions and/or irregular particle shapes. Gasification and PFBC often generate both of these characteristics.) However, gasification samples also exhibit relatively low

tensile strengths. Normally, we would expect that highly cohesive powders would also have high tensile strengths. We are not yet certain what causes this anomaly with the gasification samples. The low tensile strengths we have measured for these samples may indicate that ash dislodged from filter elements during pulse cleaning cycles may break up into very small agglomerates. If this type of breakup occurs, reentrainment of previously collected gasification residues may pose a significant problem.

UNDEERC TRDU

The TRDU ash (ID # 4176) is very coarse, free flowing, has a high bulk density, and is medium gray. These observations agree with the quantitative evaluations we performed. SEM photographs of this ash have shown a large proportion of spherical particles, suggesting that temperatures above the fusion temperature of the ash were present in the TRDU. (We have not observed spherical particles in any of the other HGCU ashes in our data base.) This ash sample exhibited a relatively large drag-equivalent diameter and a low specific flow resistance, despite its relatively high specific surface area. These data suggest that most of the surface area is attributable to very fine pores. Because the gas flowing through a filter cake never enters extremely fine pores on the surfaces of the collected particles, the particle surface area contained in these pores does not contribute substantially to filtering pressure drop.

Karhula PCFB

Figure 2 presents an SEM photograph of a fresh fracture surface (ID # 4182) of a filter cake nodule taken from the filters at Karhula. This photograph indicates that the nodules found in the Karhula filter are concretions composed of discrete fine particles almost completely embedded in pervasive amorphous masses which apparently form in the filter vessel after the particles are initially collected. The appearance of the Karhula filter cake nodule in Figure 2 is very similar to the appearance of nodules removed from the Tidd APF. This similarity, in combination with similar ash chemistries and flue gas environments, lead us to believe that eutectic formation, as described above in the section summarizing our observations from the Tidd APF, is also responsible for nodule formation at Karhula.

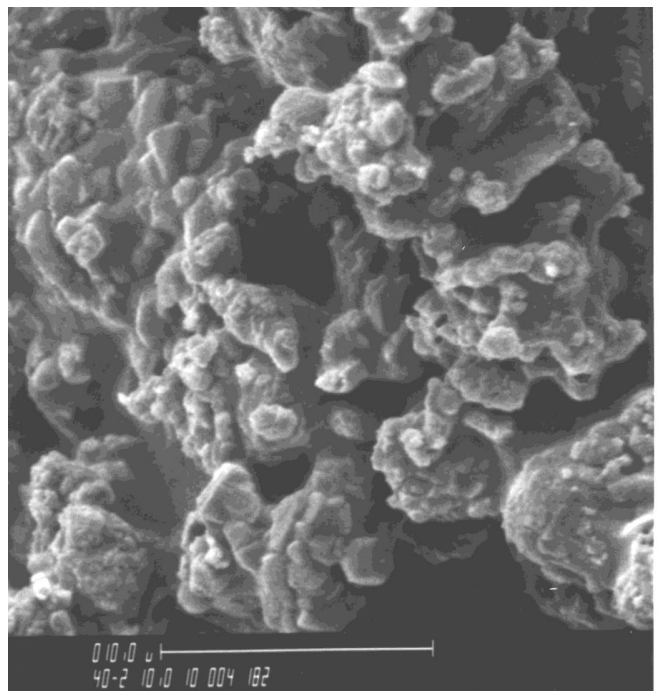

Figure 2. SEM photograph of a fresh fracture surface of a Karhula filter cake nodule.

The filter cake ash samples we received from Karhula each contained fragments of nodular filter cake. We used one of the methods we developed for measuring the overall pore volume of a nodule to characterize the nodule fragments in sample # 4182. Our on-site experience at the Tidd PFBC has shown that the porosity of the most recently deposited portions of filter cake is significantly greater than the porosity of older portions of the cake. It is very likely that during the shipment of the filter cake ash and nodule samples from Karhula to our laboratories, the fluffiest, most recently

deposited parts of the cake were shaken or rubbed off of the cake nodules. Therefore, the reported filter cake porosity value of 75 % represents a lower bound for the actual overall filter cake porosity.

HGCU Data Base Development

We have designed the primary structure of the HGCU data base that we are constructing in Microsoft Access™. Access will allow the user to compose various graphs and data presentations based on filtered and sorted groups of data. We have scanned in SEM photographs of the samples in the data base and still images taken from the videotapes we made during our four site visits to the Tidd PFBC. In addition to measured characteristics of the samples, we intend to include background information related to the various facilities such as the participating organizations, the key operating personnel, process descriptions, photographs of the facility, and literature citations. We are designing a variety of summary reports that the data base user will be able to view and print. We plan to issue the HGCU data base as a run-time version of Microsoft Access stored in CD-ROM format. This format will be required since the final data base will contain a large number of photographic images that have significant storage requirements.

High Temperature Ash Analyses

To properly assess the role of temperature and flue gas constituents on the key characteristics of the collected ash, these characteristics should be determined for samples that have been conditioned and tested in environments as much like those found in the filter vessel as possible. Therefore we plan to design, construct, and evaluate two devices that will allow measurements of the tensile strength, permeability, and uncompacted bulk porosity of samples at temperatures up to 1650 °F and in simulated flue gas environments. Our plans do not include performing these tests at elevated pressures.

The tensiometer we currently use to characterize samples at temperatures up to 300 °F operates on the principle of inducing a charge on the surface of an sample layer prepared on the grounded electrode of a parallel-plate high voltage arrangement [1]. As the electric field between the plates is increased, the attraction between the charges induced on the particles on the surface of the sample and the electrical potential of the opposite electrode eventually exceeds the force holding the charged particles to the rest of the sample. At this point the particles are ejected from the sample on the grounded electrode and travel to the opposite electrode. The electrical force required to separate these particles from the rest of the sample is equal to the tensile strength of the sample as it exists on the grounded plate. We plan to select appropriate materials and modify our design as required to construct a tensiometer that can operate at temperatures up to 1650 °F and that will be capable of conditioning and testing powder samples in simulated oxidizing or reducing flue gas environments.

We also plan to build a device to measure uncompacted bulk porosity and sample permeability at temperatures and in gases with compositions characteristic of HGCU devices. This device will consist of a vertical cylinder (approximately 20 cm in diameter) with a transparent quartz top and a porous disk (possibly a ceramic substrate like those used in the patch tester) near the bottom through which gas can flow. A small plenum on the other side of the porous disk will be connected to a heat exchanger and downstream flow measuring equipment. The device will be fitted with ceramic heaters that will maintain the device at temperatures up to 1650 °F.

Permeability measurements will be made as a function of the thickness of the sample in the isolation ring. We will measure the pressure

drop across the sample at various gas flow rates. The filtering pressure drop across the sample at a given flow rate will be used to compact the sample prior to measurement of sample permeability. Repetition of this measurement cycle will result in a series of data values relating filtering drag to sample porosity. Thus, with this device it will be possible to compare these values determined at ambient conditions with values measured at temperatures and with gas compositions typical of HGCU operation.

Acknowledgements

The authors would like to acknowledge the contributions of Thomas P. Dorchak, the METC Contracting Officer's Representative for this research. The period of performance of this contract is from October 1, 1994 through September 29, 1996.

Reference

1. Pontius, D.H. and T.R. Snyder, "Measurement of the tensile strength of uncompacted dust aggregates," Powder Technology, 68 (1991) pp. 159-162.

Hot-Gas Filter Ash Characterization Project

Bruce A. Dockter (bdockter@eerc.und.nodak.edu, 701-777-4102)
John P. Hurley (jhurley@eerc.und.nodak.edu, 701-777-5159)
Tina A. Watne (twatne@eerc.und.nodak.edu, 701-777-2233)
Karen A. Katrinak (kkatrinak@eerc.und.nodak.edu, 701-777-5283)
Catherine A. O'Keefe (cokeefe@eerc.und.nodak.edu, 701-777-5238)
Energy & Environmental Research Center
University of North Dakota
PO Box 9018
Grand Forks, ND 58202-9018

Introduction

Large-scale hot-gas testing over the past several years has revealed numerous cases of cake buildup on filter elements that have been difficult, if not impossible, to remove. At times, the cake can bridge between candle filters, leading to high filter failure rates. Physical factors, including particle-size distribution, particle shape, the aerodynamics of deposition, and system temperature contribute to difficulty in removing the cake. It is speculated that chemical as well as physical effects are playing a role in leading the ash to bond to the filter or to itself.

The Energy & Environmental Research Center (EERC) at the University of North Dakota is working with Electric Power Research Institute (EPRI) and a consortium of companies in partnership with the U. S. Department of Energy (DOE) to perform the research necessary to determine the factors that cause hot-gas cleanup filters to be blinded by ash or to develop deposits that can bridge the filters and cause them to fail. The consortium sponsors are Novem/ECN (Netherlands), PowerGen (Great Britain), Electricité de France (EDF) (France), Lurgi-Lentjes-Babcock (LLB) (Germany), Schumacher America (Germany/USA), Westinghouse (USA), ABB Carbon (Sweden), and Electric Power Development Corporation (EPDC) (Japan).

Objective

The objectives of the overall project are threefold: first, to determine the mechanisms by which difficult-to-clean ash is formed; second, to develop a method to determine the rate of blinding/bridging based on fuel and sorbent properties and operating conditions; finally, to provide suggestions for ways to prevent filter blinding by the troublesome ash.

Project Description

The research effort is composed of the following four tasks.

Task 1 – Field Sampling and Archive Sample Analyses. The American Electric Power Service Corporation (AEP) and the Ohio Power Company donated filter ash samples from several test series of the Westinghouse Advanced Particle Filter (APF) at the Tidd pressurized fluidized-bed

combustor (PFBC) demonstration plant. Residual ash samples were taken from the APF in May and October 1994. APF hopper ash (filter fines) was collected in February 1995 by AEP. The EERC also collected residual filter cake samples in May 1995 after the March 1995 shutdown of the facility.

Task 2 – Laboratory-Scale Testing. Extensive thermochemical equilibrium modeling is used to determine system, ash, and filter parameters that must be included in the experimental matrix to ensure that the experimental work reflects realistic conditions. In modeling of ash sticking, an accurate description of the chemistry of multicomponent coal ash systems implies the use of an ideal-solution model such as that derived from the FACT (Facility for the Analysis of Chemical Thermodynamics) computer code.

In other Task 2 activity, ash collected from the field and produced in the bench-scale work in Task 3 will be treated to hot-gas conditions to determine the effects of ash particle size, ash distribution, gas composition, temperature, and exposure time on ash sintering. To accomplish this portion of Task 2, laboratory methods were developed to assess tensile strength development of ash samples. First, prepared ash cakes were subjected to elevated temperatures and a simulated combustion gas environment and tested for powder tensile strength in order to identify initial levels of ash stickiness. Second, ash pellets were exposed to simulated gas conditions for extended time intervals and then tested in diametral compression mode. Finally, experiments were performed to assess ash–filter interactions after long-term exposure to gas conditions.

Task 3 – Bench-Scale Testing. The objective of Task 3 is to perform dynamic testing of ash and ash cake formation in PFBC conditions in order to help in the development of methods to predict possible filter blinding and bridging conditions. Bench-scale hot-gas filter testing is performed with the pressurized fluidized-bed reactor (PFBR), located at the EERC, under combustion conditions.

Task 4 – Model and Database Development Testing. The goal of Task 4 is to create a user-friendly computer program to predict the effects of fuel, bed material, filter type, and operating conditions on the formation of ash bridges and to create a user-friendly database for use as a research and reference tool. Potential applications of the computer program include coal selection, bed material selection, optimization of operating conditions, and design of a cleanup system. The database was designed to provide researchers with a quick and efficient tool for studying the large amounts of information generated during the course of this project.

This paper presents preliminary data from Task 2 on determining the tensile strengths of coal ash particles at elevated temperatures and simulated combustor gas conditions.

Approach

Many factors control the ultimate adhesive properties of ash deposition and the ultimate formation of cakes on rigid ceramic filters. Numerous physical properties coupled with intrinsic forces of attraction create an extremely complicated scenario for laboratory determination. Some of the

most pertinent discussions for the description of significant particle characteristics and how they interact to form adhesive properties are addressed in this paper.

The prediction of the ways in which a powder will agglomerate and form cakes is not just a matter of understanding all the ways in which particles can attract one another, but of understanding the way in which the particles fit together in the bulk. Particle shape and size are of importance in controlling the packing and caking properties of powders. Because most particles are not spherical, the first problem is the mathematical representation of the shape of the particles. The term "sphericity" has been defined as the ratio of the surface area of a sphere having the same volume as a given particle to the actual surface area of that particle (Parfitt and Sing, 1976). Particle size and shape are generally expressed as some kind of equivalent spherical diameter.

If the interparticle forces were known, the strength of the cake compact could then be calculated by specifying three-dimensional shapes with specified surface forces and then calculating the strength of the resulting cake compact. The problem is then reduced to size and shape studies on one hand and packing studies on the other. Any attempt to sum the microscopic contributions made by the particles themselves must take into account three factors, all associated with the nature of the particle surface: interparticle forces, the three-dimensional shape of the particle, and the way in which the particle interacts geometrically to form a packed structure.

Most powders are not easily characterized in terms of these microscopic quantities. If the size of a single particle is given as its equivalent spherical diameter, then the definition of particle size by a single parameter is somewhat arbitrary, and in any theoretical study, it will be necessary to use a description of the particle that will define its shape equivalencies. The situation is no less complicated with interparticle forces that are subject to changes in environment and to the effect of their previous history. In real powders, these forces can be of a variety of types (Berbner and Löffler, 1994), including the following:

- Mechanical forces caused by interlocking of irregular particles
- Surface tension forces, particularly with powder containing a variable moisture content
- Forces arising from plastic welding caused by contact points between particles coalescing under high loads
- Electrostatic forces, particularly for surfaces that easily become charged
- Solid bridge forces, where crystallization at contact points causes joining of the particles
- Molecular (or van der Waals) forces, particularly significant for particles of small diameters, say less than 10 μm

It has been stated (Christ et al., 1995) that the main cohesive forces between particles in filter cakes are van der Waals forces. This is especially true for elevated temperatures and small filtration velocities when capillary forces or sinter effects are negligible. The interparticle forces

causing hot-gas filter ashes to become "sticky" are subject to changes in a combustion environment. These forces can be of varying types including those previously identified.

Earlier results show that tensile strength, aerated porosity, and packed porosity measurements are appropriate methods to quantify the adhesive properties for coal ashes. Ash cakes with tensile strengths of less than 50 N/m^2 (0.5 g/cm^2) are likely to have significantly greater dispersement of fine particles after backpulsing than ash cakes with tensile strengths greater than 250 N/m^2 (Miller and Laudal, 1992).

In general, a filter cake detaches from the filter medium when it is subjected to a tensile stress that exceeds its strength. The cake "fails in tension" when the imposed stress exceeds either the internal cohesive strength of the cake or the strength of adhesion to the medium or to a residual dust layer. Most commonly, the cake detaches from a residual dust layer, which is finer and more strongly held by the medium. Regardless of how the cake is cleaned from the filter, the maximum stress in the cake occurs at the junction between the cake and the medium.

At present, it is not possible to predict the stresses required to detach an ash cake from a filter medium. One approach is to predict qualitively the tensile strength of a particle compact by using the classic model of Rumpf (Koch et al., 1992). He obtained the tensile forces by summing the strengths of the particle-to-particle contacts that must be broken across a surface in the compact. If the particles are spheres of diameter d_p, the tensile strength is determined by

$$\delta = \frac{f(\epsilon)}{d_p^2} F_H$$

where F_H is the interparticle force action at each contact and $f(\epsilon)$ relates the number of contacts to the void fraction. According to Rumpf:

$$F_H = \frac{(1 - \epsilon)}{\epsilon}$$

In terms of the surface energy of the particles (γ), the strength of each contact is given by:

$$F_H = \pi \gamma d_p$$

Other models of particle-to-particle contact give slightly different numerical values, but predict the same dependence on γ and d_p for F_H. Combining the three previous equations:

$$\delta = \frac{\pi (1 - \epsilon)}{\epsilon} \frac{\gamma}{d_p}$$

At present, it is necessary to measure cake detachment stresses directly, because γ depends on dust surface composition, while ϵ and the proportion of active contacts depend on the conditions under which the cake is deposited. The measurements must again be made under conditions as close as possible to those in the real application.

Accomplishments

Filter Ash Characterization. The American Electric Power Service Corporation (AEP) and Ohio Power Company have furnished ash samples from the Westinghouse advanced particle filter (APF) assembly at the Tidd pressurized fluidized-bed combustor (PFBC) demonstration plant. The APF vessel at the Tidd PFBC demonstration plant is approximately 3.0 meters in diameter and 13.4 meters in length. The vessel can contain up to 384 candle filters. The candles can be arranged in three clusters to three different levels. Each cluster contains three plenums, with 38 candles in each of the top and middle plenums and 52 candles in each of the lower plenums.

The APF experienced ash bridging and pressure drop increase during a series of test runs while firing Pittsburgh No. 8 coal and a Plum Run greenfield (PRG) dolomite. There was extensive buildup of ash on all filters. Four series of ash samples have been collected from the Tidd Station. The operation conditions are described in Table 1. During the last part of 1994, less ash buildup occurred on the filters, primarily because of the detuning of the P11 cyclone upstream of the APF. Testing at Tidd during 1995 has shown little ash buildup on filters. One reason is the complete spoiling of the P11 cyclone in 1995, but coals and sorbents were also changed during the last series of tests. Additional archived samples have been added to the characterization testing program. However, the most substantial testing to date has been on the Tidd samples. Therefore, this paper concentrates on laboratory results from the Tidd Station.

The particle sizes of Tidd ash sampled in May 1994 were much smaller than the February 1995 ash samples. The finer-particle sizes resulted in the "stickier" 1994 ash sample. The upset condition in 1995 resulted in more coarse-grained ash particles getting into the APF vessel, causing the agglomerated ash deposits to be less adhesive than previously observed.

Tensile Testing. A measurement of the tensile strength of powder deposits is useful for determining the magnitude of the cohesive forces that cause the powder to agglomerate. Key cohesive characteristics that are well defined and can be quantitatively measured are tensile strength and porosity (Miller and Laudal, 1993). A direct correlation exists between the porosity of a powder bed and the tensile forces required to fracture the bed. At ambient-temperature testing conditions, as porosity decreases, the tensile strength increases. Meanwhile, porosity is a function of bed compaction and particle-size distribution.

Several procedures and methods exist for determining tensile strengths of powder beds. One such method in use at the EERC is a commercially available instrument called a Cohetester, from Hosokawa Micron International Inc. This instrument directly measures the tensile strength of bulk powders as a function of compaction pressure. It consists of a horizontal split cell, 5 cm in diameter, with one-half of the cell movable and the other half fixed. The cell is suspended so

TABLE 1

Operating Conditions at the Tidd PFBC

Parameter	May 1994	October 1994	February 1995	May 1995
Coal	Pittsburgh No. 8	Pittsburgh No. 8	Pittsburgh No. 8	Consol and Pittsburgh No. 8
Sorbent	PRG dolomite	PRG dolomite and Bucyrus limestone	Mulzer dolomite	PRG dolomite
Bed Temp., °C (°F)	818 (1504)	855 (1571)	861 (1581)	856 (1572)
Cyclone Inlet Temp., °C (°F)	748 (1378)	793 (1385)	799 (1471)	787 (1449)
APF Inlet Temp., °C (°F)	727 (1340)	760 (1400)	802 (1475)	NA
APF Pressure, kPa (psig)	890 (129)	890 (129)	945 (137)	NA
Upstream P11 Cyclone	Partially spoiled	Partially spoiled	Completely spoiled	Completely spoiled
Filter Cakes	Difficult to clean	Difficult to clean	Easy to clean	Easy to clean

that it can be pulled apart with minimal force when no sample is in the cell, minimizing error from external friction forces. The Cohetester, like all other tensile-testing apparatuses, is designed to evaluate powder beds under ambient temperatures. However, for the hot-gas filter ash characterization project, tensile strength testing needs to be performed at elevated temperatures (700°–900°C) and in atmospheres similar to PFBC conditions.

To evaluate tensile strengths of powders in elevated-temperature testing environments, a modification to the Cohetester is used. A schematic of the high-temperature powder tensile strength tester is shown in Figure 1. As in the design of the Cohetester, alleviation of friction problems is accomplished by using a movable split cylinder suspended and free to move with minimal resistance. The oven is split in half, with the top portion retractable to allow the

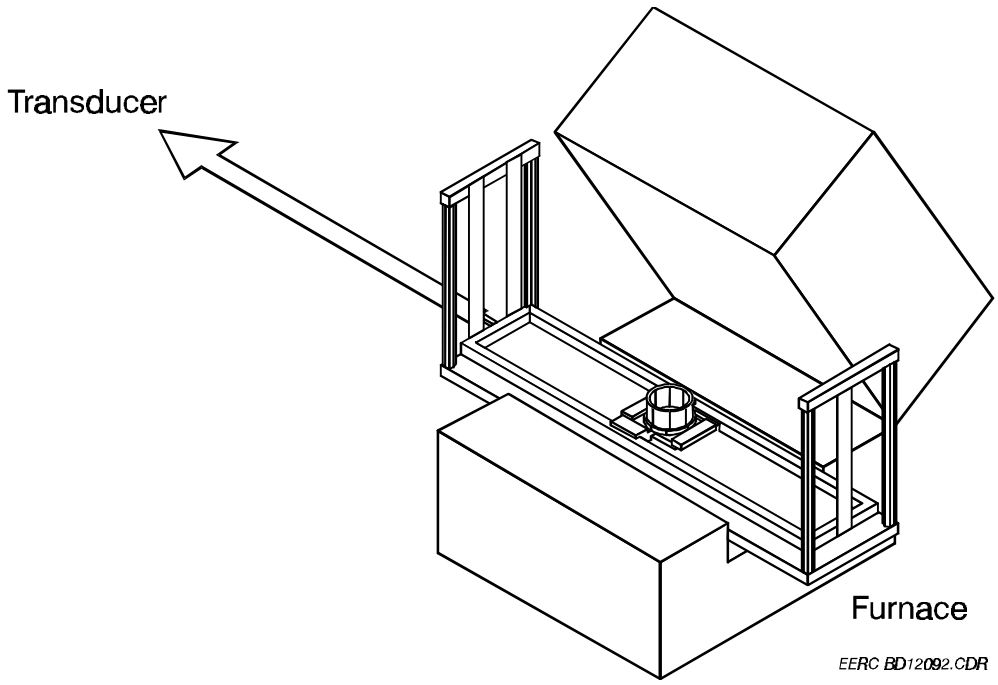

Figure 1. Schematic of the high-temperature powder tensile strength tester.

specimen chamber to be prepared for sample testing. The suspended split-cylinder half is pulled away from the stationary cylinder half, and the load is measured with a transducer or load cell. Several blank loads, i.e., cylinder chamber containing no ash cake sample, have been measured at a range of temperatures. The blank loads are highly consistent regardless of testing temperature, generally 10–12 grams of force.

The ash samples were prepared for testing by first baking them in a 200°C oven. They were then placed directly into the sample holder in the high-temperature tensile tester and allowed to cool for ambient tests. The results of the Tidd ash evaluation from February 1995, at elevated temperatures, is given in Figure 2. In general, strength increases considerably as the ash cakes are compressed and porosity decreases. The blank-load testing (using no ash) showed that the increases in strength were not due to the effects of the higher temperature of the sample cell on the instruments.

There is a noticeable trend in tensile strength increase with increasing temperature and decreasing void fraction. In addition, the prepared ash cakes have exhibited substantial sintering action at the higher levels of compaction (lower porosity). This indicates that at higher levels of particle packing, which is a function of size distribution, the ash cakes will sinter and gain strength at a higher rate. The cake porosity, which seems to correlate to sintering action, can be correlated to pressure drop as well.

The bulk ash from the Tidd Station (February 1995) is also being classified into size fractions for evaluating the effects of size distribution on tensile strength. The size distribution bands are of a

caliper diameter greater than 10 µm, 3–10 µm, 1–3 µm, and less than 1.0 µm. It is a general understanding that the finer size particles, particularly submicron, have a significant impact on the stickiness behavior of problematic ash. However, introducing larger-size ash particles is not necessarily the solution because of the increased potential for candle filter damage and subsequent corrosion of the gas turbine. A specific particle-size range is necessary to allow an ash cake to form on a candle with sufficient adhesive strength to allow the cake bed to be detached without redistributing the residual ash particles elsewhere in the system. All of these properties need to be understood at atmospheres similar to those in the actual system.

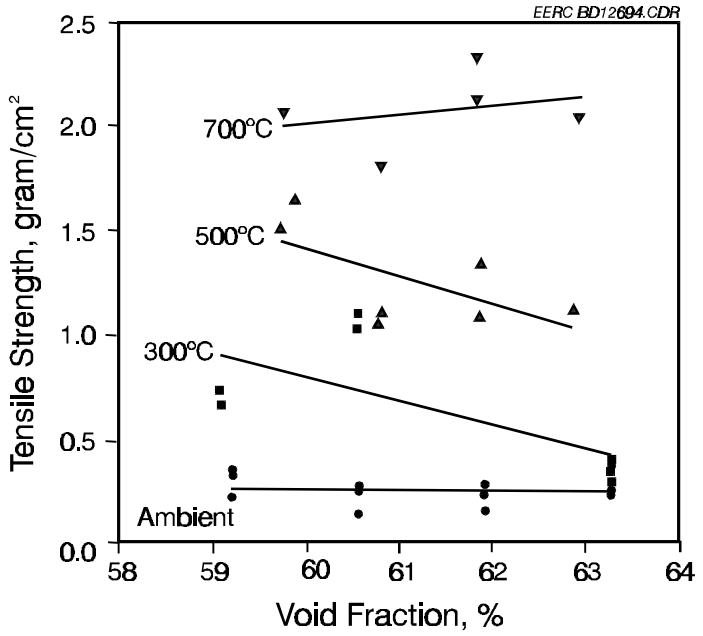

Figure 2. Tensile strength of February 1995 Tidd ash at elevated temperatures.

The high-temperature tensile tester is designed to evaluate powder cake tensile strength while exposed to elevated temperatures and simulated gas environments for short periods of time (less than 1 hour), as for the active cake on a filter. However, passive ash deposits such as residual cake or shroud deposits may be present for much longer times, possibly sintering to greater strength than can be measured by the high-temperature tensile tester. To test ash strength development over long periods, the long-duration sintering test was developed. A schematic of the sintering chamber is shown in Figure 3. This apparatus allows the preparation of multiple samples simultaneously. The specimens measure 1.0 cm in diameter by approximately 1.5 cm in length. The sintered specimens are tested in diametral compression (Figure 4). This method is commonly used for predicting tensile forces while testing is performed in a compressive mode.

Two tests have been completed thus far for long-term pellet sintering. The first test, using February 1995 Tidd ash, was run at 900°C for 50 hours in an air atmosphere. The second test, using May 1994 Tidd ash, was also run at 900°C, but lasted 120 hours and was in an atmosphere of 30% O_2, 15% H_2O, 3300 ppmv SO_2, 1100 ppmv HCl, 10 ppmv NaCl, and a N_2 balance. In the air atmosphere, little or no

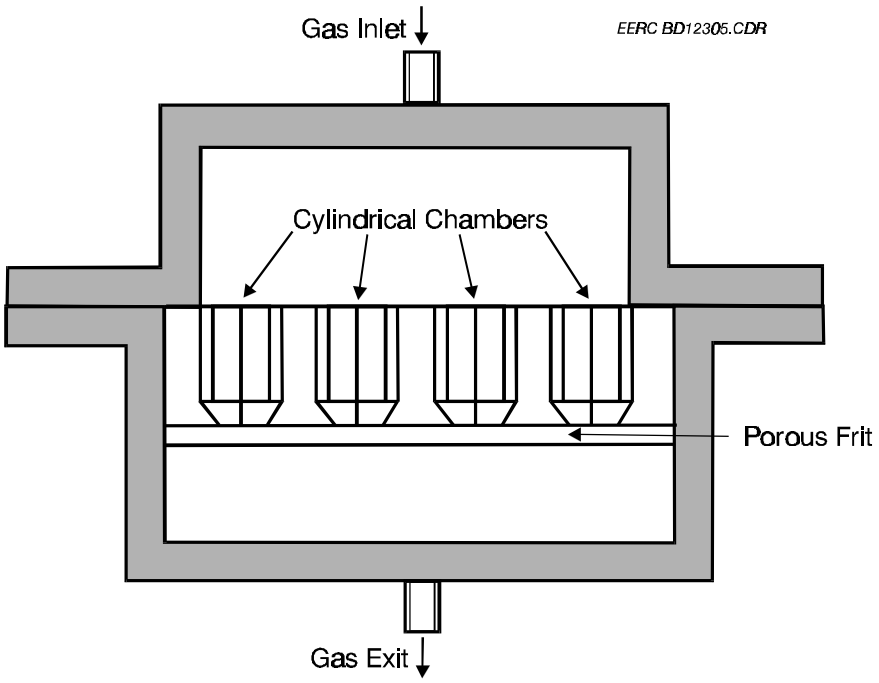

Figure 3. The long-duration ash-sintering chamber.

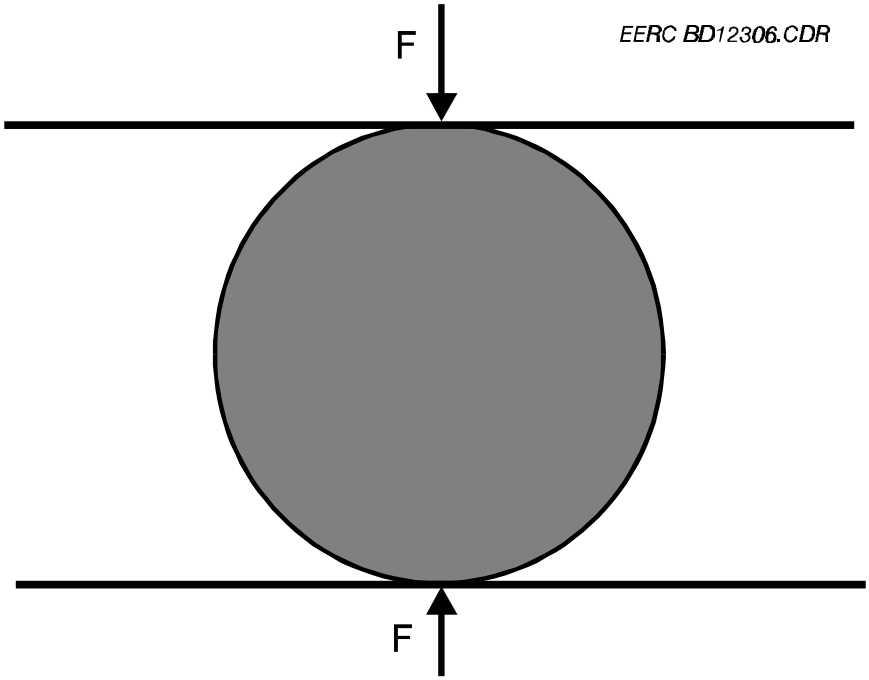

Figure 4. Schematic of the diametral compression test: the stress state is tensile (directed perpendicularly) along the diameter joining the loading points.

sintering occurred. In the simulated PFBC atmosphere, slight sintering does appear to occur, but the resulting strength is still very small. Work on thermochemical equilibrium modeling has indicated that eutectic temperatures present in hot-gas cleaning environments might be causing softening of particle surfaces and, consequently, causing the surface stickiness. However, this assessment is made at the very early stages of the thermochemical equilibrium task and needs further development. Now that sintering has been correlated to cake porosity and particle packing, pellet sintering can be performed on variable compaction levels and particle-size distributions. More tests will be run at 900°C under the corrosive environment previously mentioned, but for longer periods of time.

Contract Information and Acknowledgments

The METC Contracting Officer's Representative is Dr. Hubert Veringa. The DOE contract number is RP 3910-01, and the period of performance is from July 1, 1994, to March 31, 1997. The Electric Power Research Institute (EPRI) is the prime project contractor. All research is carried out by the Energy & Environmental Research Center (EERC). The EERC, through its Cooperative Agreement with the U.S. Department of Energy (DOE) Morgantown Energy Technology Center (METC), is able to approximately match funds contributed by the commercial sponsors.

References

Berbner, S.; Löffler, F. "Influence of High Temperatures on Particle Adhesion," Powder Technology 1994, 78, 273–280.

Christ, A.; Giercth, B.; Renz, U. "Possible Improvements to the Back-Pulse Cleaning of Ceramic Candle Filters," In Proceedings of the 13th International Conference on Fluidized Bed Combustion; ASME, 1995, Vol. 1.

Koch, D.; Cheung, W.; Seville, J. P.K.; Clift, R. "Effects of Dust Properties on Gas Cleaning Using Rigid Ceramic Filters," Filtration & Separation 1992, 29 (4).

Miller, S.J.; Laudal, D.L. "Pulse-Jet Baghouse Performance Improvement with Flue Gas Conditioning," EERC publication; Oct. 1992.

Miller, S.J.; Laudal, D.L.; Heidt, M.K. "Cohesive Properties of Fly Ash and How They Affect Particle Control Optimization," Presented at 10th Particle Control Symposium, Washington, DC April 5–8, 1993.

Parfitt, G.D.; Sing, K.S.W. Characterization of Powder Surfaces; Academic Press: London, 1976.

Nondestructive Degradation Evaluation of Ceramic Candle Filters using Vibration Signatures[1]

Roger H, L, Chen, Associate Professor (hlchen@wvnvm.wvnet.edu; 304-293-3031 x.63 1)
Balaji Parthasarathy, Research Assistant (balaji@coe.wvu.edu; 304-293-3031 x.644)
Department of Civil and Environmental Engineering
West Virginia University
Morgantown, WV 26506-6103

Introduction

The structural integrity of ceramic candle filters is a key element for hot gas cleanup systems, They protect the heat exchanger and gas turbine components from getting clogged and also prevent erosion. Ceramic candle filters used in the recent demonstration plant have experienced degradation and fracturing. Preliminary examination of these ceramic filters indicated that damage of the filters may have resulted from strength degradation at consistent high temperature operation, thermal transient events, excessive ash accumulation and bridging and pulse cleaning (Alvin et al. 1994 and Spain et al. 1994). The ceramic candle filter is a slender structure made of layers of porous materials. The structure has high acoustic attenuation which has greatly limited the conventional ultrasonic detection capability. In general, stiffness reduction of a structure will cause the change of the modal parameters of the structure (Chen et al., 1995). In this study, the stiffness degradation of the ceramic candle filters will be evaluated by using the dynamic response of the filters.

One Refraction filter and twelve Schumacher Dia Schumalith filters were tested. All these ceramic filters are clay bonded Silicon Carbide (SiC) candle filters. The Refraction filter is of 59 inch (1.5 m) length, and 2.36 inch (60 mm) outer diameter and 1.57 inch (40 mm) inner diameter, while all the Schumacher filters are of 59 inch (1.5 m) length, and 2.36 inch (60 mm) outer diameter and 1.18 inch (30 mm) inner diameter. The Refraction filter is an unused filter. In the case of the Schumacher filters, 7 of them were used for 1705 hours (group A specimens) and 5 of them were used for 460 hours (group B specimens). So a difference in period of usage of 1245 hours exists between the two groups of Schumacher specimens. A comparison was made between the dynamic response obtained from group A and group B specimens.

Project Description

This study proposes a nondestructive approach for evaluating the structural properties of the ceramic filters using dynamic characterization method. The vibration signatures of the ceramic filters at different degradation levels are established using transient impact-response technique.

---

[1]Research sponsored by the U.S. Department of Energy's Morgantown Energy Technology Center, under contract DE-AP21 -95MC05 134 with Department of Civil and Environmental Engineering, West Virginia University, Morgantown, WV 26506-6103; telefax: 304-293-7109

A tripod shaped wooden framework was constructed from which the filter was suspended freely using elastic strings to simulate a free-free boundary condition (Figure 1), The filter was subjected to an excitation using an impact hammer and the response was picked by an accelerometer, Two sensor locations L/4 and 0.55L were selected and impact was given at L/S, L/4, L/3, L/2, 0.55L, 2L/3, 3L/4, and 7L/8 where L is the length of the filter and all distances were measured from the open end, Both the input and output waveforms were stored in a digital oscilloscope. Fast Fourier Transform (FFT) was performed on both the input and output waveforms to get the Frequency Response Function (FRF). The FRF shows a plot with various peaks each of which correspond to the natural frequency of vibration of the filter in different modes. The first 8 vibration modes, covering a frequency range of 0-4000 Hz were studied for the filters. A typical FRF plot is shown in Figure 2.

From the FRF plots the frequency and amplitude values were noted for all the impact locations and sensor locations. The frequency obtained in each mode from all impacts were averaged. This was done to minimize experimental errors arising from improper impacts. Also this averaging was done for both sensor locations. Finally, the frequency obtained in each mode for all the group A and group B specimens were compared and the average shifts in frequency response which occurs between the two groups of specimens were calculated. The amplitude values obtained from the FRF plots were used to plot the mode shapes,

Analysis using dynamic finite element method (FEM) was also conducted to compare with the experimental results. Linear elastic modal analysis was performed. To study the effect of local damages in the filter on its frequency response, FEM modal analysis was conducted on models with different damage zone sizes. Damage zones of 4.8%, 10.6%, and 100% of the total length of the filter were modeled and located at the mid-span of the filter. For 4.8'% and 10.6% damage zone, the stiffness of the darnage zone was taken as 50% of the original stiffness while for the 100°/0 damage zone the stiffness of the damage zone was taken as 90°/0 of the original stiffness.

Results

After noting these frequency values for both the A and B specimens in different vibration modes, the percentage frequency shift between the two groups of specimens was calculated. Figure 3 shows the comparison of the Coefficient of Variation (COV) of group A and group B filters with the percentage difference in frequency between the two groups of filters in different vibration modes. A maximum frequency shift was observed in the first mode, of about 6. 19%, and a minimum shift was observed in the fourth mode, of about 4.94°/0, with an average frequency shift of about 5.42°/0. This is equivalent to a stiffness change of about 8.16%. Also, the average coefficient of variation (COV) for the group A and group B specimens was found to be 2.40 and 1.12 respectively. In addition, the COV for both group A and group B specimens was found to be almost the same in all the 8 modes. This indicates that the dynamic characterization method can be used for degradation evaluation of filters for difference in period of usage of 1245 hours and above, The Schumacher specimens were studied using FEM analysis (Figure 4). The FEM simulations were in good agreement with the experimental results with a maximum percentage difference in frequency results of 0.8% and 1.11 % in the case of group A and group B filters respectively, The FEM results show that

there is a uniform 8.16 % stiffness degradation of the filters corresponding to the frequency reduction between group A and B filters.

Figure 4 shows the comparison of the undamaged and damaged frequency results in terms of percentage difference in different modes using FEM analysis. Results of FEM models indicated that for a darnage zone of 4.8°/0 of length the deviation from undamaged frequency results was high in the odd modes with a gradual reduction in deviation at the higher modes. For a damage zone of 10,6% of length, the deviation in frequency is high in the odd modes and low in the even modes upto the fourth mode and then attains a constant deviation of about 5%. For a damage zone throughout the length (100Y0) and a stiffness reduction of 10%, there is a constant deviation of about 5 ,5°/0 in all the modes.

Application

Results from this study indicate that the vibration signatures of the filters can be used as an index to quantify the darnage condition of the filters. The results also indicate the feasibility of using the vibration mode shapes to predict the damage location. The application of this study can be implemented to develop a nondestructive evaluation method for future in-situ inspection of the ceramic filters,

Acknowledgements

The authors acknowledge the support provided by Department of Energy, Morgantown Energy Technology Center for conducting this study. Special thanks are extended to Dr. T.K. Chiang and Dr. Paul Yue of DOE/METC for their valuable comments and encouragement. The authors also acknowledge Ms. Mary Anne Alvin of Westinghouse Electric Corporation, Science and Technology Center and Mr. Richard Dennis of DOE/METC for their help in providing the used Schumacher filter specimens,

References

Alvin, M. A., R.E. Tressler, T.E. Lippert, E.S. Diaz, and E.E. Smeltzer. June 1994. "Durability of Ceramic Filters," Paper Presented at the Coal-Fired Power Systems 94-- Advances In IGCC and PFBC Review Meeting, 545-571. DOE/METC-94/1008. NTIS/DE94012253. Morgantown, WV.

Chen, H.L., Spyrakos, C. C., Venkatesh, G. 1995. "Evaluating Structural Deterioration by Dynamic Response," Journal of Structural Engineering, Vol. 121, No.8, 1197-1204.

Spain, J. D., Starrett, H. S., Southern Research Institute. April 1994. "Physical, Mechanical, and Thermal Properties of Schumacher SiC filter material ," Report to U.S. Department of Energy, Morgantown Energy Technology Center.

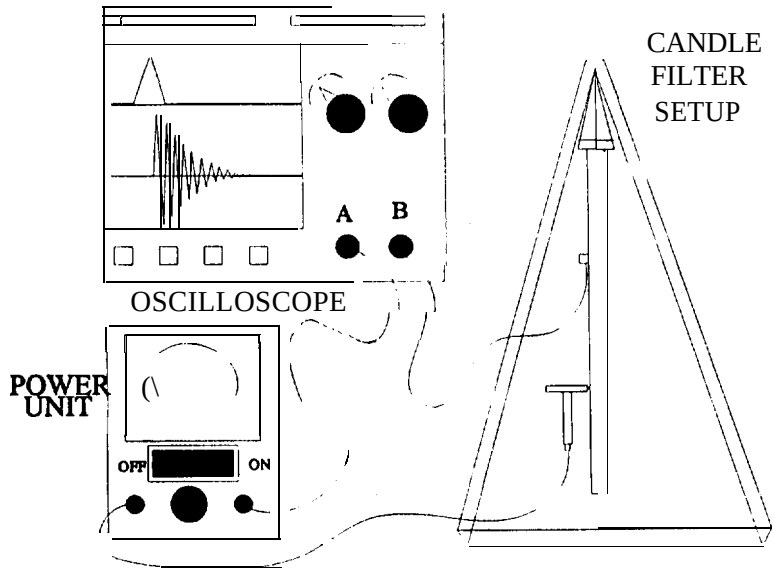

Figure 1 Schematic Drawing of Experimental Setup

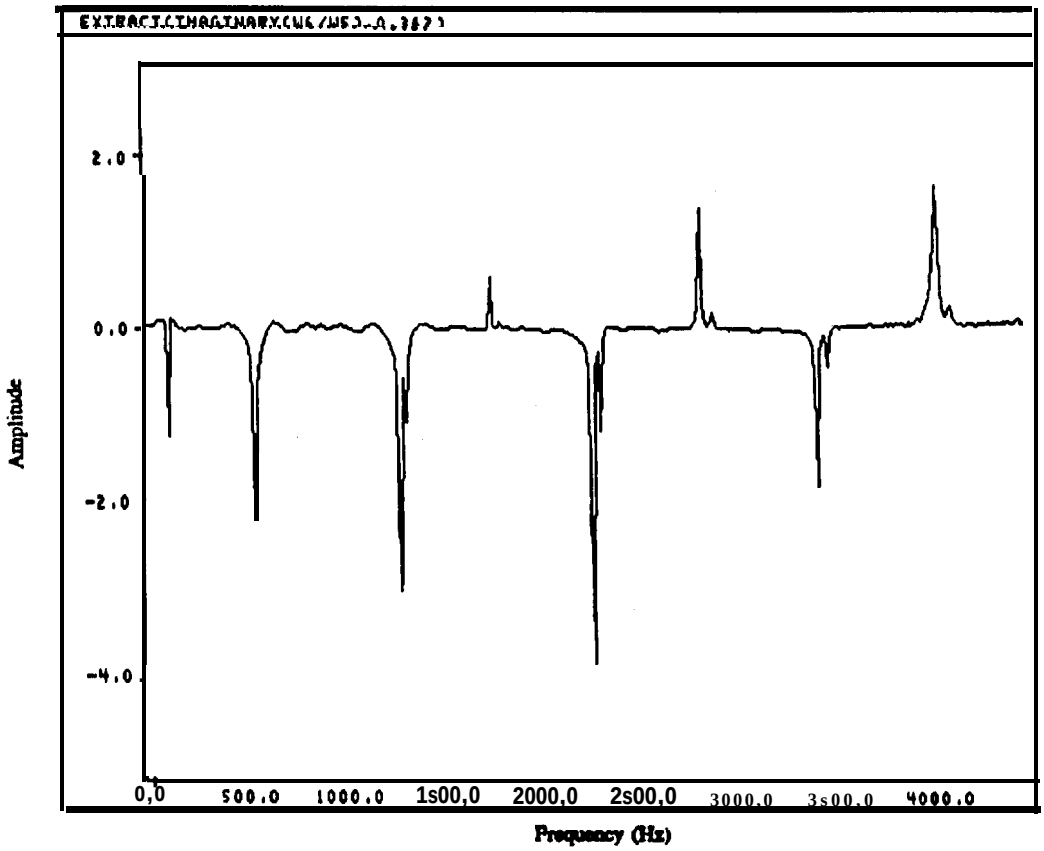

Figure 2 A Typical Frequency Response Function for a Ceramic Filter (Schumacher A Filter)

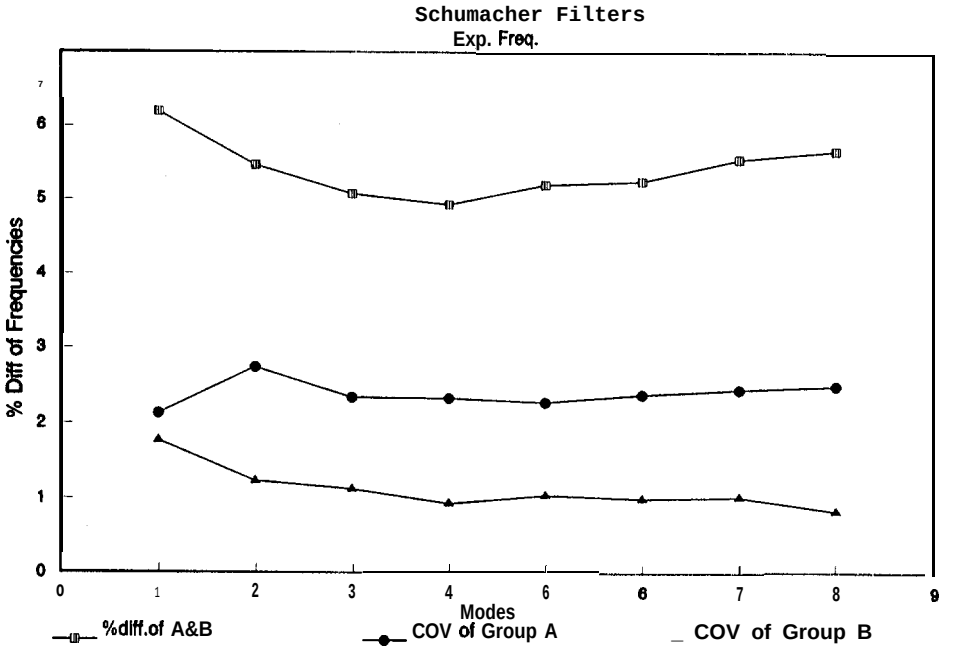

Figure 3 Comparison of COV's of Group A and Group B with Percentage Difference in Frequency between the Two Groups

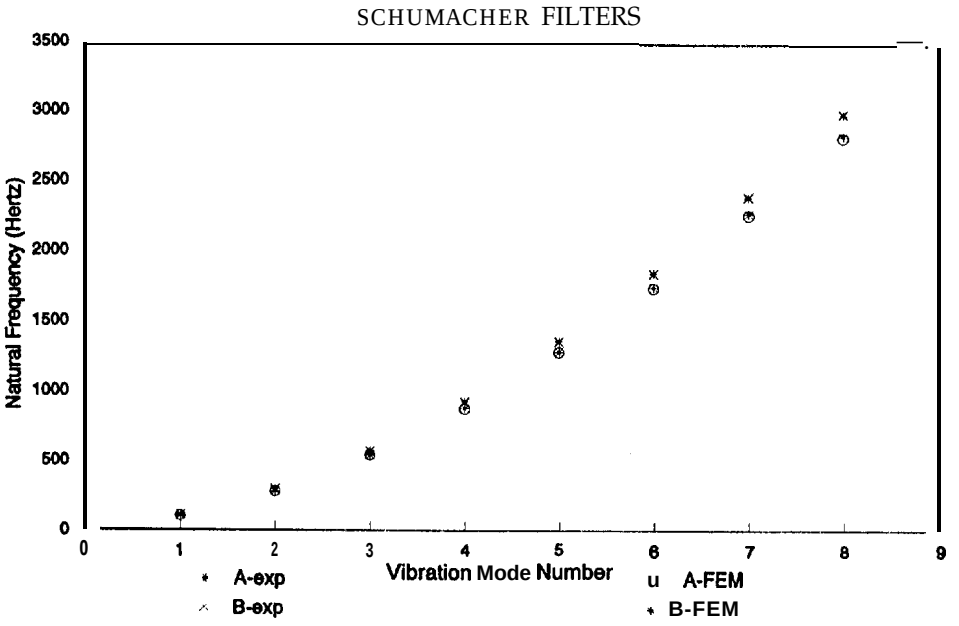

Figure 4 Comparison of Frequencies of Experimental and FEM Results for Schumacher Filters

Determination of Filter-Cake Thicknesses from On-Line Flow Measurements and Gas/Particle Transport Modeling

Duane H. Smith, (DSMITH@metc.doe.gov; 304-285-4069), U. S. Department of Energy, Morgantown Energy Technology Center, Morgantown, WV 26507-0880,

Victor Powell, (powell@stat.duke.edu) ORISE Faculty participant at U. S. Department of Energy, Morgantown Energy Technology Center, Morgantown, WV 26507-0880,

Martin Ferer, (FERER@wvums.wvnet.edu, 304-293-3422), Department of Physics, West Virginia University, Morgantown, WV 26506,

Goodarz Ahmadi, (AHMADI@sun.soe.clarkson.edu, 315-268-2322), National Research Council Senior Associate at U. S. Department of Energy, Morgantown Energy Technology Center, Morgantown, WV 26507-0880, and

Essam Ibrahim (emeei@acd.tusk.edu, 334-727-8974), ORISE Faculty participant at U. S. Department of Energy, Morgantown Energy Technology Center, Morgantown, WV 26507-0880

INTRODUCTION

The use of cylindrical candle filters to remove fine (~0.005 mm) particles from hot (~500-900 ^{o}C) gas streams currently is being developed for applications in advanced pressurized fluidized bed combustion (PFBC) and integrated gasification combined cycle (IGCC) technologies. Successfully deployed with hot-gas filtration, PFBC and IGCC technologies will allow the conversion of coal to electrical energy by direct passage of the filtered gases into non-ruggedized turbines and thus provide substantially greater conversion efficiencies with reduced environmental impacts [1].

In the usual approach, one or more clusters of candle filters are suspended from a tubesheet in a pressurized (P ~< 1 MPa) vessel into which hot gases and suspended particles enter, the gases pass through the walls of the cylindrical filters, and the filtered particles form a cake on the outside of each filter ([2-4]). The cake is then removed periodically (typically, two or three times per hour), by a backpulse of compressed air from inside the filter, which passes through the filter wall and filter cake.

In various development or demonstration systems the thickness of the filter cake has proved to be an important, but unknown, process parameter. For example, the distance between adjacent filters typically is on the order of 5 cm. If the filter-cake thickness should reach 2.5 cm, "bridging" of cake between adjacent filters would occur, leaving little space between the filters into which the incoming gases and particles could flow. Bridging might eventually occur if the

removal of cake at each cleaning were not quite complete, or if a fraction of the particles removed were re-entrained and refiltered after each cleaning backpulse.

The accumulation of particulates around and among filters is not just a hypothetical concern. Operating experience with the Tidd PFBC Demonstration Plant revealed that under some conditions the buildup of large masses of particulates among the filters can, indeed, be an important problem, producing excessive pressure drops within the filter vessel and even filter breakage [5].

Because of the high temperatures and pressures, the geometries of the filter clusters and mechanical supports, and the presence of fine particles to scatter any light, on-line measurement of cake thicknesses during filter-system operation has not been feasible in most systems. However, when the pressure drop across the filter tubesheet, the gas flow rate, and the particle concentration in the incoming gases are measured, these data can be used to calculate the mass of filter cake on each filter. If filter-cake samples can be obtained (e.g., from the filter-vessel hopper or during shut-down) so that the filter cake porosity can be measured, then the filter-cake thickness can be estimated during plant operation, as well. In a typical filter system, the needed flow data are logged and the cake thickness can be estimated several times per minute, so that the filter system need not be operated "blindly," without knowledge of the extent of cake buildup.

The following section describes a physical model for cake and pressure buildups between cleaning backpulses, and for longer term buildups of the "baseline" pressure drop, as caused by incomplete filter cleaning and/or re-entrainment. When combined with operating data and laboratory measurements of the cake porosity, the model may be used to calculate the (average) filter permeability, the filter-cake thickness and permeability, and the fraction of filter-cake left on the filter by the cleaning backpulse or re-entrained after the backpulse.

When used for a variety of operating conditions (e.g., different coals, sorbents, temperatures, etc.), the model eventually may provide useful information on how the filter-cake properties depend on the various operating parameters.

MODELS

Consider a filter vessel with n candle filters. For each filter, the gas flows through the filter cake, then through the filter wall, so that the *i*th filter and the corresponding filter cake constitute two resistances in series:

$$ {}^{i}R_p = {}^{i}R_f + {}^{i}R_c. \qquad (1) $$

All *n* filters (and their cakes) operate in parallel and are subjected to the same pressure drop. Thus their effective resistance R is given as:

$$ 1/R = \Sigma(1/{}^{i}R_p). \qquad (2) $$

The net, measured pressure drop is the sum of the pressure drop across filters and filter cakes and the pressure drop through other flow paths in the filtration system. Therefore, the net vessel resistance R_n is:

$$R_n = R + R_o, \tag{3}$$

where R_o is the passage resistance. It should be noted here that the passage resistance is, in general, a function of flow rate.

The model used here makes the following assumptions: (1) all *n* filters have the same permeability; (2) essentially all particles that enter the filter vessel are deposited on the filters; (3) the particles are distributed uniformly among the filters and on each filter surface; and (4) the filter cakes (as well as the filters) obey Darcy's law,

$$\mathbf{v} = (k/\mu)\nabla P, \tag{4}$$

where **v** is the velocity vector, P is the pressure and k is the permeability.

To simplify the model, the small area at the bottom of the filter (about 1% of the total filter surface), for which the gas flow rate differs significantly from the rest of the filter, is ignored in the subsequent analysis. Under assumptions (1)-(3), ${}^iR_f$ and ${}^iR_c$ are the same for all *n* filters, and eq (3) reduces to

$$R_n = (1/n)(R_f + R_c) + R_o. \tag{5}$$

Because of the cylindrical geometry of the filters and filter cakes, Darcy's law is solved in polar coordinates. Assuming that the pressure varies only radially, the resulting pressure drop across each clean candle filter (in the absence of filter cake) is (Yang et al.[4]):

$$\Delta P_f = (1/2\pi k_f)\mu(Q/nh)\ln(b/a), \tag{6}$$

where Q is the vessel (volumetric) gas flow rate, k_f is the filter permeability, *h* is the filter length, and *a* and *b* are the inside and outside radii of the filter wall, respectively.

At constant gas flow rate into the filter vessel, *Q*, and constant volume fraction of particles in the incoming gas, *F*, the volume of filtered particles per filter that arrives in the filter vessel during time interval *t* is

$$V = FQt/n. \tag{7}$$

The corresponding volume of each filter cake is

$$V(t) = FQt/n(1-\phi) \tag{8}$$

where ϕ is porosity of the cake. The outer radius of the filter cake , B(t), at time t then is given by

$$B(t) = b[1 + FQt/\pi nh(1- \phi)b^2]^{1/2}. \quad (9)$$

The increase in the pressure drop across the filter cakes over the time interval from $t = 0$ to time t is

$$\Delta P_c(t) = (1/4\pi k_c)\mu(Q/nh) \ln [1 + FQt/nh\pi(1- \phi)b^2], \quad (10)$$

where k_c is the filter-cake permeability. Typically the filters are cleaned periodically after interval t' (t' ~ 20 to 60 min) with a backpulse of compressed air of about 0.2 s duration. In equation (10), t is the time measured after the backpulse.

Ideal operation

In the simplest case, cleaning of the filters by the backpulse is complete and no "re-entrainment" (i.e., refiltration) of any of the cake occurs. At time $t = 0$ the filter cake thickness is zero, and the pressure drop $\Delta P - \Delta P_o$ arises only from the clean filters:

$$\Delta P - \Delta P_o = (1/2\pi k_f)\mu(Q/nh) \ln(b/a). \quad (11)$$

Over the time interval $t = 0$ to $t = t'$ filtration occurs, and

$$\Delta P - \Delta P_o = \mu(Q/2\pi nh)\{(1/k_f) \ln(b/a) + (1/2k_c) \ln [1 + FQt/nh\pi(1- \phi)b^2]\}. \quad (12)$$

At $t = t'$ the backpulse occurs, and $\Delta P - \Delta P_o$ becomes negative. Because cake removal is complete and no re-entrainment occurs, after the backpulse the pressure drop returns to the initial value for the clean filters:

$$\Delta P(t = t') - \Delta P_o = \Delta P(t = 0) - \Delta P_{o,} \quad (13)$$

[where $\Delta P(t = 0) - \Delta P_o$ is given by eq (11)]. During the second cycle and all subsequent cycles, the cake buildup, pressure buildup, and cleaning of the first cycle are simply repeated.

For typical systems, the flow that produces ΔP_o in various passages is turbulent and

$$\Delta P_o = cQ^2, \quad (14)$$

so that the value of c can be obtained from pressure drops measured at different flow rates. Then, from on-line measurements of F and Q (and of the temperature, to get μ), and from laboratory measurements of the filter dimensions (a, b, h) and cake porosity (ϕ), fits of eq (12) to the experimental data yield the filter permeability (k_f), the filter-cake permeability (k_c), and the thickness of the filter cake

$$\delta = B(t) - b = b\{[1 + Fqt/\pi nh(1-\phi)b^2]^{1/2} - 1\} \quad (15)$$

at any time.

Incomplete cleaning

If the performance of filter systems always conformed to the ideal case, there would be little need to determine filter-cake permeabilities and thicknesses during system operation. However, all too often, filter systems do not exhibit ideal behavior. It seems unavoidable that, after each cleaning, some portion of the cake will remain on the filter and/or some of the fragments of filter cake removed by the backpulse will be recollected on the filter surface. Intuitively, it also may appear inevitable that the thickness of the "residual" cake from incomplete cleaning and re-entrainment must increase without limit, until all of space between adjacent filters is filled and bridging occurs.

Imagine that an outer cylinder of cake of uniform thickness is removed by the *j*th backpulse, leaving a uniform cake of outer radius B_j on the filter at the beginning of the *j*th + 1 cycle. Hence, at the start of the *j*th + 1 cycle the pressure drop is no longer $\Delta P - \Delta P_o = \Delta P_f = (1/2\pi k_f)\mu(Q/nh)\ \ln(b/a)$ [eq (11)], but

$$\Delta P - \Delta P_o = (1/2\pi)\mu(Q/nh)\ [\ln(b/a)/k_f + \ln(B_j/b)/k_c]. \quad (16)$$

If the incremental thickness of cake left on the filter after each cleaning is a constant fraction, $^r f$, of the cake deposited *during that cycle*, then

$$\Delta B_j = \Delta B = {}^r f\ (B' - b), \quad (17)$$

where $B' = B(t=t')$ is the radius of the cake at the end of the first cycle. Assuming that the deposited cake thickness for different cycle is essentially constant, at the beginning of the *j*th+1 cycle the cake thickness is

$$B - b = j\ {}^r f\ (B' - b), \quad (18)$$

and

$$\Delta P - \Delta P_o = (1/2\pi)\mu(Q/nh)\{(1/k_f)\ \ln(b/a) + (1/k_c)\ \ln[j\ {}^r f\ (B' - b)/b + 1]\}. \quad (19)$$

After $j = 1/{}^r f$ cycles the thickness of the residual cake left after the filter cleaning is equal to the thickness of the cake deposited just before the first cleaning backpulse. Thus, unless $^r f$ is very small, the cake thickness quickly becomes many times as large as the thickest cake ever encountered in the ideal case. In normal operation $B_{max} - b >> B' - b$, where B_{max} is the maximum possible filter-cake thickness (less than half the nearest neighbor distance between filters). Hence, if $^r f$ = constant, satisfactory operation requires

$$T_s < (t'/{}^{r}f)\ (B_{max} - b\ )/(B' - b) \qquad (20)$$

where T_s is the time of operation before the filter vessel must be opened and manually cleaned.

Re-entrainment.

In refiltration, or re-entrainment, the removal of filter cake by the cleaning backpulse is complete, but some fraction of the resulting filter-cake fragments return to the filter surface. The fraction of re-entrained particles is a function of the size distribution of the cake fragments: fragments that are sufficiently large move downward under the force of gravity and tend to escape; fragments that are not much larger than the largest particles entering the vessel have a high probability of being re-entrained. The new locations of these fragments on the filters may be different from their location before the backpulse, but these fragments will be refiltered within a short time after the backpulse occurs.

The mass (or volume) of particles and filter cake re-filtered during the *j*th filtration cycle will be some fraction, f_j, of the total mass of cake removed by the *j*th - 1 backpulse. By the end of the first cycle a mass of cake ${}^{e}m_1 = m' = \rho FQt/n$ (and volume ${}^{e}V_1 = V' = FQt'/n(1-\phi)$ [eq (8)]) forms on each filter, which causes a pressure increase

$${}^{e}(\Delta P)_1 = \Delta P' = \Delta P(t'), \qquad (21)$$

as given by eq (10). Within a short while after the first cleaning backpulse an amount

$${}^{i}m_2 = f_2 m' \qquad (22a)$$

of blown-off cake fragments is recaptured on each filter, which causes an increased pressure drop

$${}^{i}(\Delta P)_2 = f_2\ \Delta P'. \qquad (22b)$$

Here f_2 is the fraction recaptured; and it is assumed that, for small f's, the increase in pressure drop is proportional to the increase in cake radius. During the second cycle an amount m' of freshly filtered particles is added to the cake already present from re-entrainment, so that at the end of the second cycle (just before the cleaning backpulse) the mass of filter cake is

$${}^{e}m_2 = m' + f_2 m' = (1 + f_2)\ m' \qquad (22c)$$

and the pressure drop is

$${}^{e}(\Delta P)_2 = (1 + f_2)\ \Delta P' \qquad (22d)$$

After the second backpulse and the re-entrainment at the beginning of cycle 3, the cake-

mass is

$$^{i}m_{3} = f_{3}(1 + f_{2})\, m' \tag{23a}$$

and the pressure drop is

$$^{i}(\Delta P)_{3} = f_{3}(1 + f_{2})\, \Delta P'. \tag{23b}$$

At the end of cycle 3 the filter-cake mass and the pressure drop are, respectively,

$$^{e}m_{3} = [1 + f_{3}(1 + f_{2})]m' \tag{23c}$$

and

$$^{e}(\Delta P)_{3} = [1 + f_{3}(1 + f_{2})]\Delta P'. \tag{23d}$$

For the *j*th cycle the recaptured cake-mass is

$$^{i}m_{j} = (f_{j} + f_{j}f_{j-1} + f_{j}f_{j-1}f_{j-2} + \ldots + f_{j}f_{j-1} \ldots f_{3}f_{2})m' \tag{24a}$$

and the increase in pressure drop is

$$^{i}(\Delta P)_{j} = (f_{j} + f_{j}f_{j-1} + f_{j}f_{j-1}f_{j-2} + \ldots + f_{j}f_{j-1} \ldots f_{3}f_{2})\Delta P' \tag{24b}$$

At the end of the *j*th cycle the filter-cake mass and the pressure drop are, respectively,

$$^{e}m_{j} = (1 + f_{j} + f_{j}f_{j-1} + f_{j}f_{j-1}f_{j-2} + \ldots + f_{j}f_{j-1} \ldots f_{3}f_{2})m' \tag{24c}$$

and

$$^{e}(\Delta P)_{j} = (1 + f_{j} + f_{j}f_{j-1} + f_{j}f_{j-1}f_{j-2} + \ldots + f_{j}f_{j-1} \ldots f_{3}f_{2})\Delta P'. \tag{24d}$$

These quantities define the "baseline" and "topline" of the pressure drop versus time. Thus, eqs (22b) and (22d) may be used with the pressure drops measured at the beginning and end, respectively, of the second cycle to give "duplicate" measurements of f_2; the "best" value of f_2, along with eqs (23b) and (23d) and the pressure drops measured at the beginning and end of the third cycle give "duplicate" measurements of f_3; etc.

A plausible hypothesis is that the fraction of filter cake re-entrained during each cycle should be constant for all cycles. With this hypothesis eq (24d) reduces to

$$^{e}(\Delta P)_{j} = (1 + f + f^{2} + \ldots + f^{j-1})\Delta P' \tag{25}$$

As the number of cycles becomes very large ($j \Rightarrow$ infinity), the maximum pressure drop encountered at the beginning of each cycle is

$$^{e}(\Delta P) = \Delta P'/(1-f), \tag{26}$$

where $0 \leq f < 1$ is assumed.

RESULTS

Figure 1 shows the variation of the ratio of pressure drop to flow rate versus time for fifteen one-hour cycles of operation of the "MGCR" filter vessel. The corresponding time variation of the flow rate through the vessel is shown in Figure 2. (The units are pressure drop [ΔP] = lb/in^2, flow rate [Q] = scfh, and time [t] = s.) The roughly linear buildup of pressure drop after each backpulse is clearly observed from Figure 1. The flow rate appears to be steady with some random variations. At about 15,000 s, there is a step change of about 10 percent in the mean flow rate. For t < 15,000 s, a portion of the gas from the gasification unit was sampled for particle concentration measurements, while for larger times, the entire flow was passed through the filter vessel. During the transition, some adjustment of the operation was also required. As a result, the pressure variation in the fifth cycle shows an abnormal behavior.

Ideal operation

If only a few filtration/cleaning cycles are monitored, the operation of the filter system may appear ideal upon casual inspection. To clearly illustrate the details of the pressure drop buildup and its sharp reduction during the backpulse, a set of operational data, $\Delta P/Q$ versus t, for three cycles of the filter vessel of the MGCR (gasification) unit are shown in in Figure 3. The apparent constancy of the baseline values seems to indicate that no incomplete cleaning or re-entrainment occurred (unless an asymptotic limit for re-entrainment had been nearly reached).

Laboratory measurements showed that the filter cake had high porosity. Here a porosity of $\phi = 0.6$ for the filter cake is assumed, and a least-square error fit of the ideal operation model [eq (12)] to the data for the fifteen cycles (of 54,000 s duration) is evaluated. The resulting expression is given as

$$\Delta P_j/Q = 0.00135 + 0.003097 \ln [1 + 3.67 \times 10^{-8} Qt], \tag{27}$$

where the operation condition units are used.

The predictions of equation (27) for the three and the fifteen cycles are plotted in Figures 4 and 5, respectively. Comparing Figures 1 and 3 with 4 and 5, it is readily apparent that the ideal operation model provides a reasonable fit to the data. By including the time variations of the flow rate, it was even possible to predict some of the "noise" in the operating pressure drop data. Here the statistical R^2-value is 0.78 (which indicates that roughly 78 percent of the data are explained by the ideal model).

A more detailed check on the statistical fit of the model is provided by Figure 6. This figure illustrates the statistical residual [measured value minus value calculated from the fit] for each of the individual measured values. The observed low level of residual indicates that the statistical fit is quite good. The very largest residuals correspond to the sporadic fluctuations in the detectors and/or other system "noise." It also appears from Figure 6 that the residuals for first 15,000 s with lower flow rate are positive, while those for the larger times are negative. There is also a high level of residual for the fifth cycle, which is as expected from the operational changes made at that time.

The coefficient of the logarithm term in equation (12) is related to the cake permeability. The correlation given by equation (27) may then be used to estimate k_c. Accordingly, the estimated cake permeability is 8.8×10^{-13} m^2 which is in the expected range. The cake thickness may also be evaluated from equation (9) as a function of time, under the idealized cleaning assumption. For a gas flow rate of 2,000 scfh, the corresponding peak cake thickness at the end of an ideal cycle (with compete cleaning after each backpulse) becomes $B(t') - b \approx 4$ mm.

In spite of the reasonable agreement, one feature of the ideal model prediction is noticeably different from the experimental data. Figures 4 and 5 show that the model lead to an identical pressure drop level after each backpulse, while Figure 1 indicates a random deviation in the baseline pressure drop due to incomplete cleaning, re-entrainment and/or removal of some additional residual filter cake deposited in the earlier cycles. The ideal model was extended to account for the effect of initial variation of the pressure drop after each backpulse. The resulting best statistical fit to the data then is given as

$$\Delta P_j/Q = 0.001526 + 0.003172 \ln [1 + 3.67 \times 10^{-8} Qt] - \Theta_j, \qquad (28)$$

where $\Theta_j = [{}^i(\Delta P_j) - {}^i(\Delta P_{j-1})]/Q$ is the change in the base pressure drop (divided by the flow rate) just after the backpulse for the *jth* cycle. With an average of $\Theta_{ave} = -1.06 \times 10^{-5}$, the values of Θ vary from -1.32×10^{-4} to 9.4×10^{-5} with the extreme values appearing at the beginning and the end of the fifth cycle . (The operating system unit used for Θ is $lb/in^2/scfh$.)

Figures 7 and 8 show the predictions of equation (28) for the fifteen and the three cycles of operation, respectively. Comparison of these figures with Figures 1 and 3 indicates good agreement with the data. The statistical R^2-value is now 0.93, which shows a significant improvement over that for equation (27). Figure 9 shows the corresponding time variation of the residuals of the fit. Comparing with Figure 6, it appears that the amplitude of the residuals are reduced and the residuals now fluctuate around zero. However, a systematic and roughly periodic variations in the residuals is observable in both Figures 6 and 9. These periodic deviations appear to be associated with the statistical effect of operational changes made at the time of cycle five on the fitted correlation.

Use of the correlation given by (28) leads to an estimated cake permeability of $k_c = 8.6$

$\times 10^{-13}$ m^2 which is comparable with the earlier value for the idealized case. The value of filter permeability, k_f, could not be estimated because the pressure drop of the system , ΔP_o, was not measured.

Incomplete cleaning

The volume of "residual" cake remaining on the filter immediately after cleaning and the baseline pressure drop caused by this residual cake, as calculated from the incomplete filter-cleaning model [eq (19)], are illustrated in Figure 10. Results are included for 1%, 5%, or 10% of the cake left on the filter after each cleaning. For $^r f = 0.01$, after 70 cleaning cycles (i.e., 35 hr, if t' = 1/2 hr) the cake volume after cleaning is about 1/2 the volume of cake deposited during one filtration cycle. For $^r f = 0.05$, after 70 cleaning cycles the cake volume after cleaning is almost 4 times the volume of cake deposited during one filtration cycle. And if $^r f = 0.10$, the volume of cake left after cleaning is about 10 times the volume of cake deposited during one filtration cycle. To a first approximation, more-frequent cleaning will extend the time-to-shutdown only if it reduces $^r f$ (e.g., by reducing the cake sintering time and cake strength).

Re-entrainment

Counter-intuitive insights into the effects of re-entrainment on filter-cake thickness and tubesheet pressure drops can be obtained by examining the effects of different fractions of re-entrainment in the constant-fraction re-entrainment model [eq (26)]. Figure 6 illustrates the behavior of $(\Delta P - \Delta P_o)/\Delta P'$ versus *t*, as predicted for 25%, 50%, 75%, and 90% re-entrainment fractions. Although re-entrainment of 25% of the removed cake may seem substantial, its effects on the pressure drop and cake thickness are not large; this degree of re-entrainment increases the baseline pressure drop by slightly less than half of $\Delta P'$ (i.e., the maximum cake-induced pressure drop, if no re-entrainment occurs). Likewise, the additional cake thickness caused by the re-entrainment is less than 1/2 the thickness of the cake just before cleaning, if no re-entrainment occurred. For 25% re-entrainment, the approach to these asymptotic limits is very rapid, being almost complete after two cycles. As the re-entrainment fraction increases, both the asymptotic limit and the time required to approach this limit increase. For 50% re-entrainment, the maximum pressure drop (and cake thickness) are doubled by the re-entrainment. For 75% re-entrainment the maximum cake thickness is quadrupled, and for 90% re-entrainment the cake thickness and pressure drop increase nine-fold. Even for this extreme degree of re-entrainment, the approach to steady-state operation is very rapid compared to the required operating time of the filter system.

Evaluation of f's

The Θ_i term was introduced in the model equation given by (28) to account for the changes in the baseline differential pressure after each backpulse. These are equal to the differences between the initial pressure drops in consecutive cycles normalized by the volumetric gas flow rate. Thus, for the jth cycle,

$$\Theta_{j+1} = [{}^{i}(\Delta P_{j+1}) - {}^{i}(\Delta P_{j})]/Q, \tag{29}$$

where ${}^{i}(\Delta P)_j$ is the baseline pressure drop in the jth cycle given by (22b). It then follows that

$$\Theta_{j+1} = [f_{j+1}\ {}^{e}(\Delta P_{j}) - f_{j}\ {}^{e}(\Delta P_{j-1})]/Q. \tag{30}$$

Here ${}^{e}(\Delta P)_j$ is the pressure drop at the end of the jth cycle before the backpulse. Assuming that equation (21) holds, we find

$$\Theta_j = (f_j - f_{j-1})\ (\Delta P')/Q, \tag{31}$$

from which f_j may be evaluated as

$$f_j = f_{j-1} + \Theta_j\ Q/\Delta P'. \tag{32}$$

Equation (32) provides an iterative expression for determining the values of *f*. As was noted before, the values of Θ could be positive or negative. The positive values of Θ indicates an increase in the cake thickness due to re-entrainment and/or incomplete cleaning. The negative values of Θ corresponds to the cases that the backpulse causes part of the residual cake buildup from the earlier cycles together with the one of the current cycle to be removed.

CONCLUSION

The presented results indicate that the simple filter model together with appropriate statistical fits may be used to capture the main features of the MGCR filter vessel pressure drop variations. The results may also be used to estimate the filter cake permeability. Such information could provide a semi-empirical procedure for estimating the filter cake thickness during the operation of the filter vessel.

The analyses of MGCR data indicate the importance of simultaneously measuring particle concentrations as well as gas-flow rates and tubesheet pressure drops. The analyses also suggest that computer control of cleaning backpulses may be important to maintain accurate reproducibility and measurement of the length of the filtration cycle.

It might seem that re-entrainment should cause the tubesheet pressure drop and filter-cake thickness to increase without limit, but the results presented here indicate that this is not necessarily so. So long as no more than about 25% of the cake fragments are re-entrained, the pressure-drop increases caused be re-entrainment should be acceptable. The calculations indicate that for re-entrainment the approach to "stable" (i.e., asymptotic-limit) operation occurs relatively rapidly. Re-entrainment should be a problem only if more than 1/2 of the cake removed by each backpulse is re-entrained. For the incomplete filter-cleaning model presented, however, the pressure drop and cake thickness do increase without limit, and stable operation never is achieved.

The difference between stable and unstable operation is this: In unstable operation the amount of cake permanently removed by the filter-cleaning step was a constant fraction of the cake deposited *during that cycle*; in stable operation, the amount of cake permanently removed by each backpulse was a constant fraction of the *total cake present* just before cleaning. The crucial difference is, that in the latter case, as the total amount of accumulated cake increases, the amount of cake removed by cleaning also increases; hence, an asymptotic limit exists. If the absolute amount of cake removed by each cleaning stays constant (or decreases) as filter cake accumulates over multiple cycles, stable filter-system performance cannot be achieved.

NOMENCLATURE

a	=	inside filter radius
b	=	outside filter radius
c	=	proportionality constant between ΔP_o and Q^2
f	=	fraction of filter-cake fragments re-entrained (in constant re-entrainment fraction model)
${}^{r}f$	=	fraction of filter-cake not removed by a cleaning backpulse
f_j	=	fraction of filter-cake fragments re-entrained during jth cycle
h	=	filter length
k_c	=	filter-cake permeability
k_f	=	filter permeability
n	=	number of filters
t	=	time (measured from the time of backpulse)
T_s	=	limiting operation time
B	=	outside filter-cake radius
B_{max}	=	filter-cake radius at which bridging occurs
F	=	volume fraction of particulates in incoming gas/particle stream
N	=	number of filtration cycles
ΔP	=	total pressure drop across tubesheet
$\Delta P'$	=	increase of pressure drop across cake during one cycle
ΔP_f	=	pressure drop across (clean) filter
ΔP_o	=	total pressure drop minus pressure drop across filters and filter cakes
Q	=	(volumetric) gas flow rate
R	=	resistance
μ	=	gas viscosity
ϕ	=	filter-cake porosity
ρ	=	volume average particle density

ACKNOWLEDGEMENTS

V. Powell and E. Ibrahim were Faculty Participants under the Oak Ridge Institute for Science and Education (ORISE) program; G. Ahmadi was a Senior Associate under the National Research Council (NRC) program. This work was funded by the Office of Fossil Energy, U.S. Department of Energy.

REFERENCES

1. Mudd, M. J. and & Bauer, D. A., (1987) Proceedings 1987 International Conference on Fluidized Bed Combustion, ASME, Ed. Mustonen, J.P., pp. 256-260.

2. Clift, R. and Seville, J.P.K., (1993) Gas Cleaning at High Temperatures, Blackie Academic & Professional, New York.

3. Thambimuthu, K.V., (1993) Gas Cleaning for Advanced Coal-Based Power Generation, IEACR/53, IEA Coal Research, London.

4. Yang, W.C., Newby, R.A., Lippert, T.E. and Cicerco, D.C., (1995) "Westinghouse Advanced Particle Filter System," in Proceedings of Advanced Coal-Fired Power System '95, U.S. Department of Energy, Morgantown Energy Technology Center, Morgantown, WV, June 27-29.

5. Lippert, T.E., Bruck, G.J. Sanjana, Z.N. and Newby, R.A. (1995) "Westinghouse Advanced Particle Filter System," in Proceedings of Advanced Coal-Fired Power System '95, U.S. Department of Energy, Morgantown Energy Technology Center, Morgantown, WV, June 27-29.

FIGURES

Figure 1. Variation of operational data, $\Delta P/Q$ versus t , for the filter vessel of the MGCR (gasification) unit.

Figure 2. Variation of operational data, Q versus t , for the filter vessel of the MGCR (gasification) unit.

Figure 3. Variation of operational data, $\Delta P/Q$ versus t , for the filter vessel of the MGCR (gasification) unit.

Figure 4. Variation of $\Delta P/Q$ with time as calculated from equation (27).

Figure 5. Variation of $\Delta P/Q$ with time as calculated from equation (27).

Figure 6. Residuals from the fit of equation (27) to the operation data of Figure 1.

Figure 7. Variation of $\Delta P/Q$ with time as calculated from equation (28).

Figure 8. Variation of $\Delta P/Q$ with time as calculated from equation (28).

Figure 9. Residuals from the fit of equation (28) to the operation data of Figure 1.

Figure 10. Filter-cake thickness and pressure drop, $\Delta P - P_o$, versus t for the case of constant-fraction incomplete filter cleaning and no re-entrainment.

Figure 11. $(\Delta P - \Delta P_o)/\Delta P'$ versus t , as predicted by the constant-fraction re-entrainment model [eq (26)], for different fractions of re-entrainment.

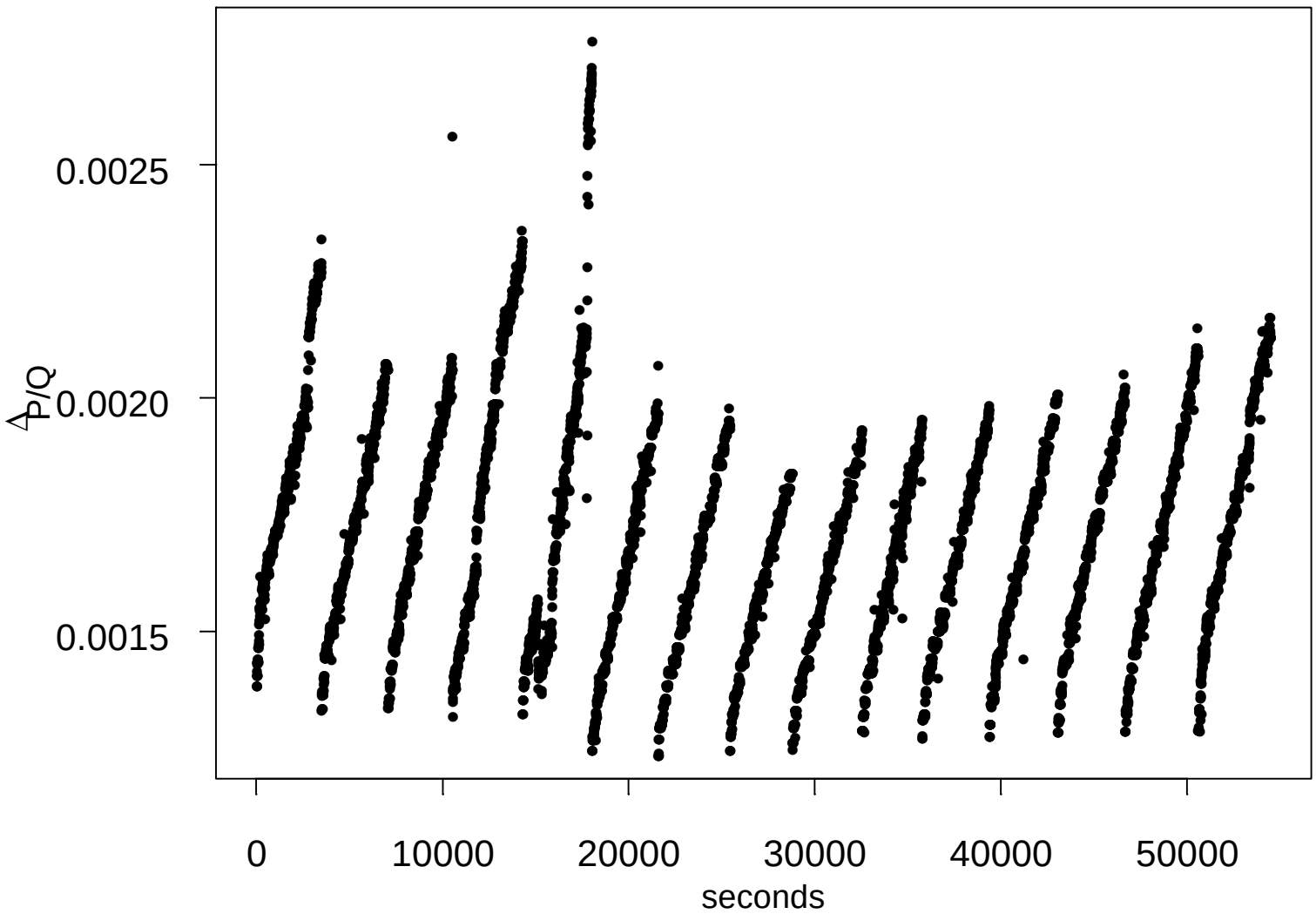

Figure 1. Variation of operational data, ΔP/Q versus t, for the filter vessel of the MGCR (gasification) unit.

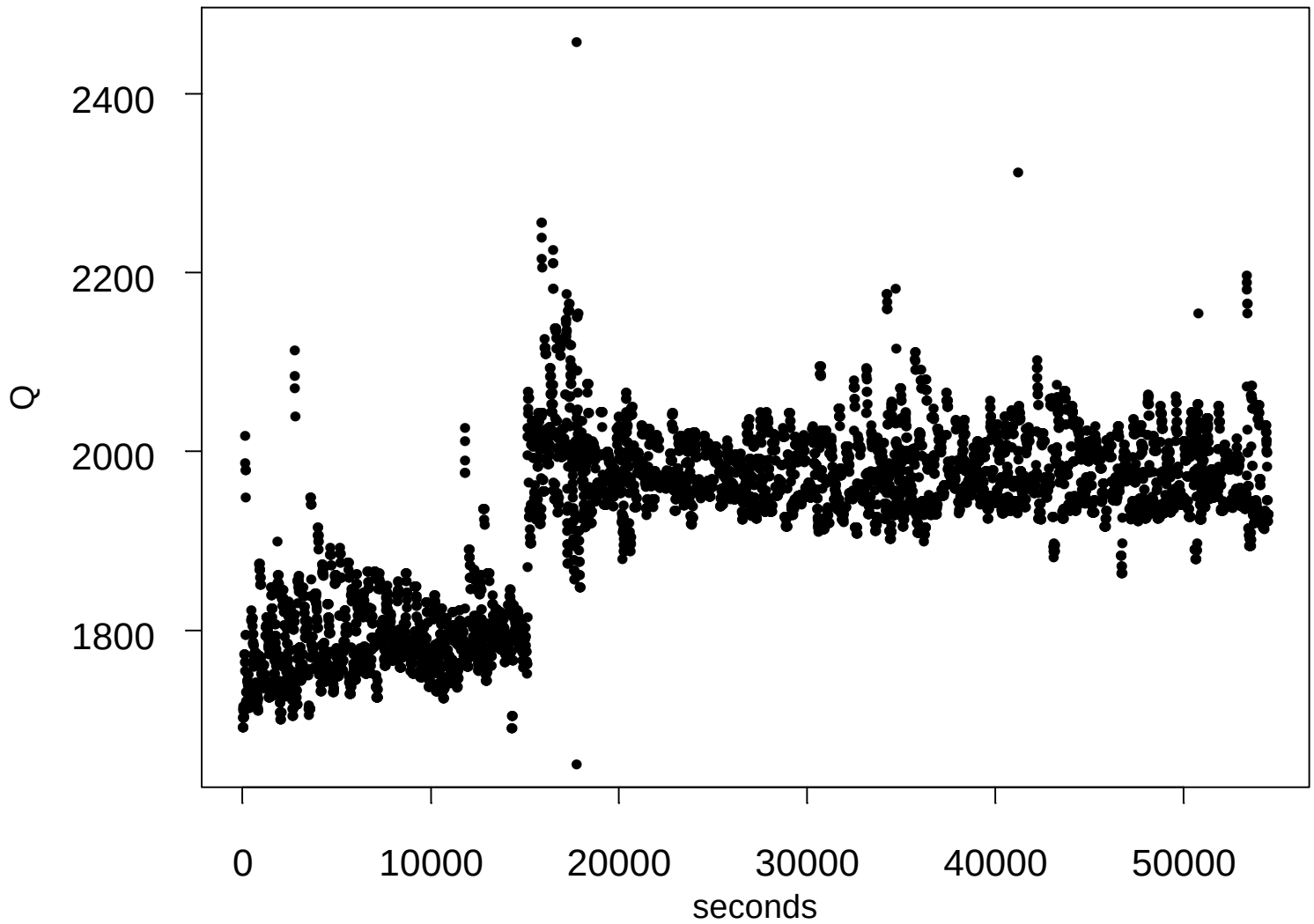

Figure 2. Variation of operational data, Q versus t, for the filter vessel of the MGCR (gasification) unit.

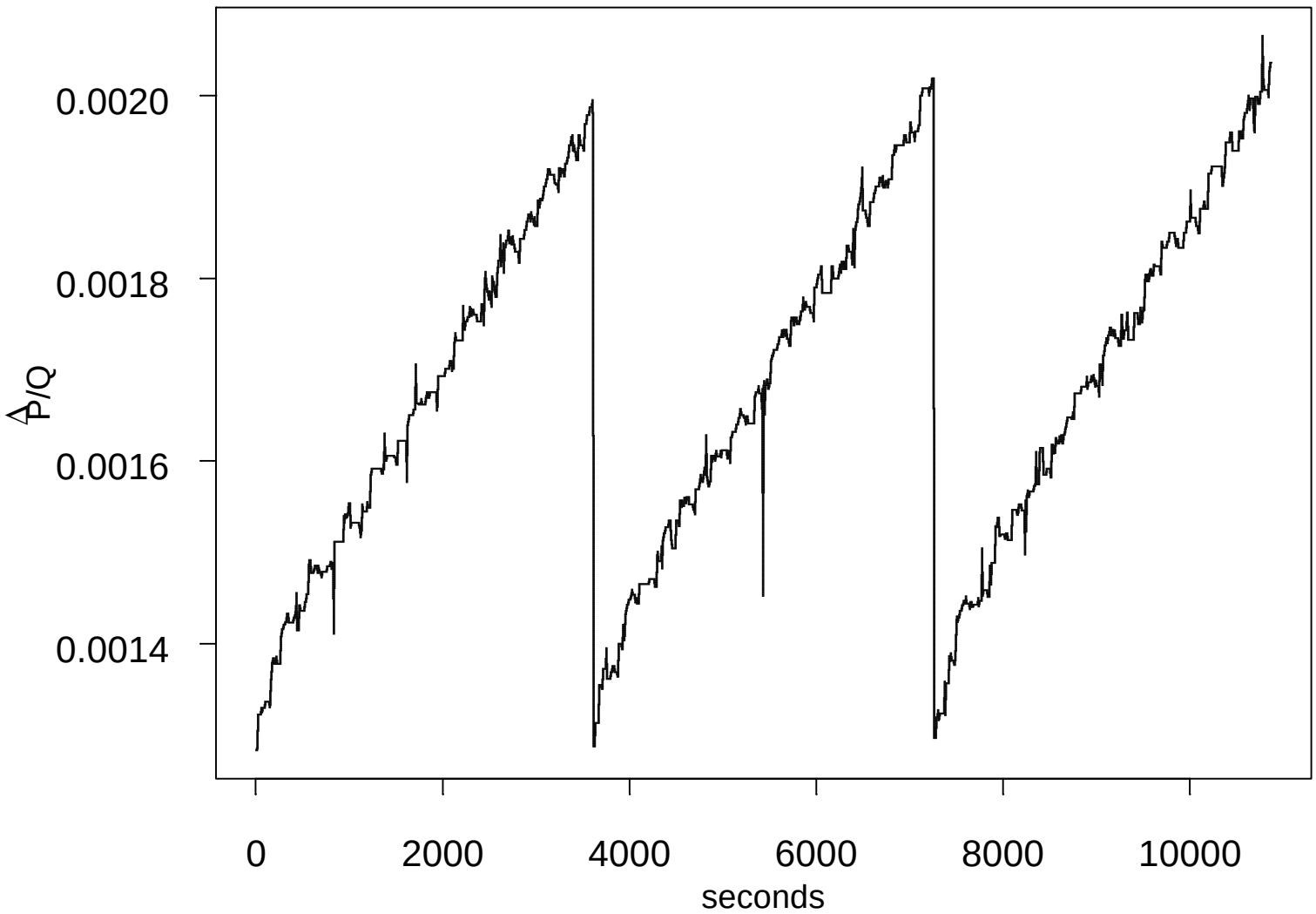

Figure 3. Variation of operational data, ΔP/Q versus t, for the filter vessel of the MGCR (gasification) unit.

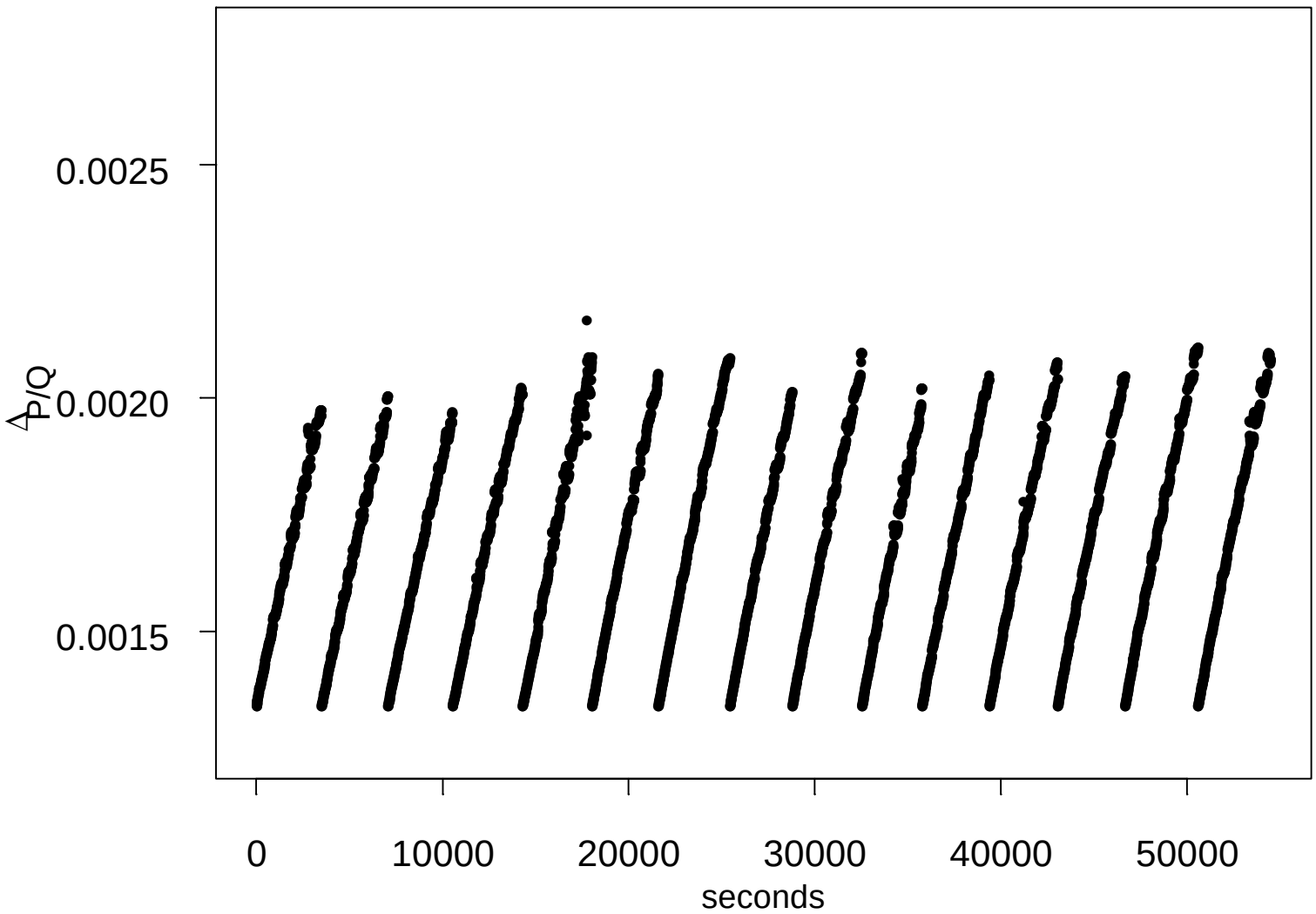

Figure 4. Variation of $\Delta P/Q$ with time as calculated from equation (27).

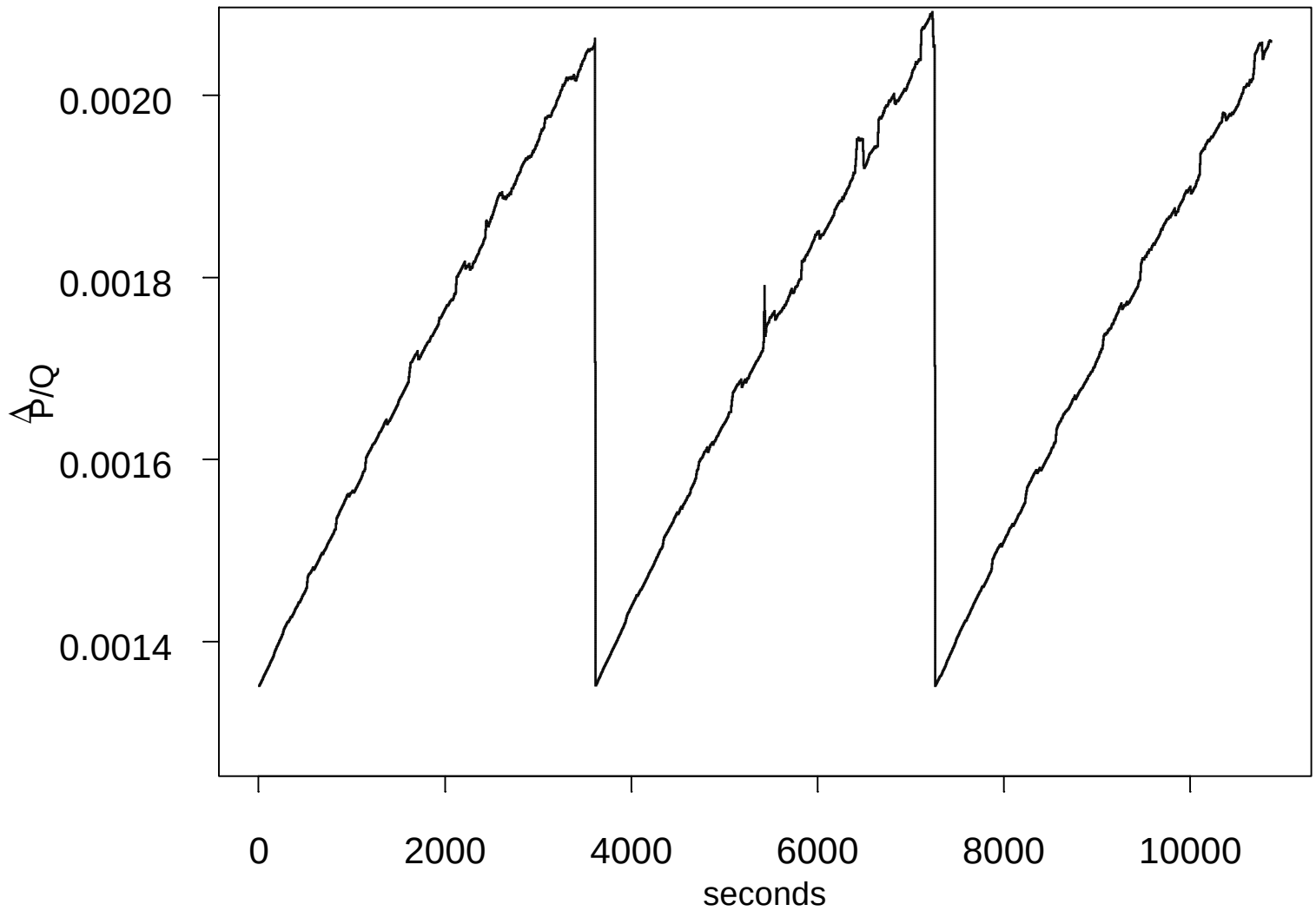

Figure 5. Variation of $\Delta P/Q$ with time as calculated from equation (27).

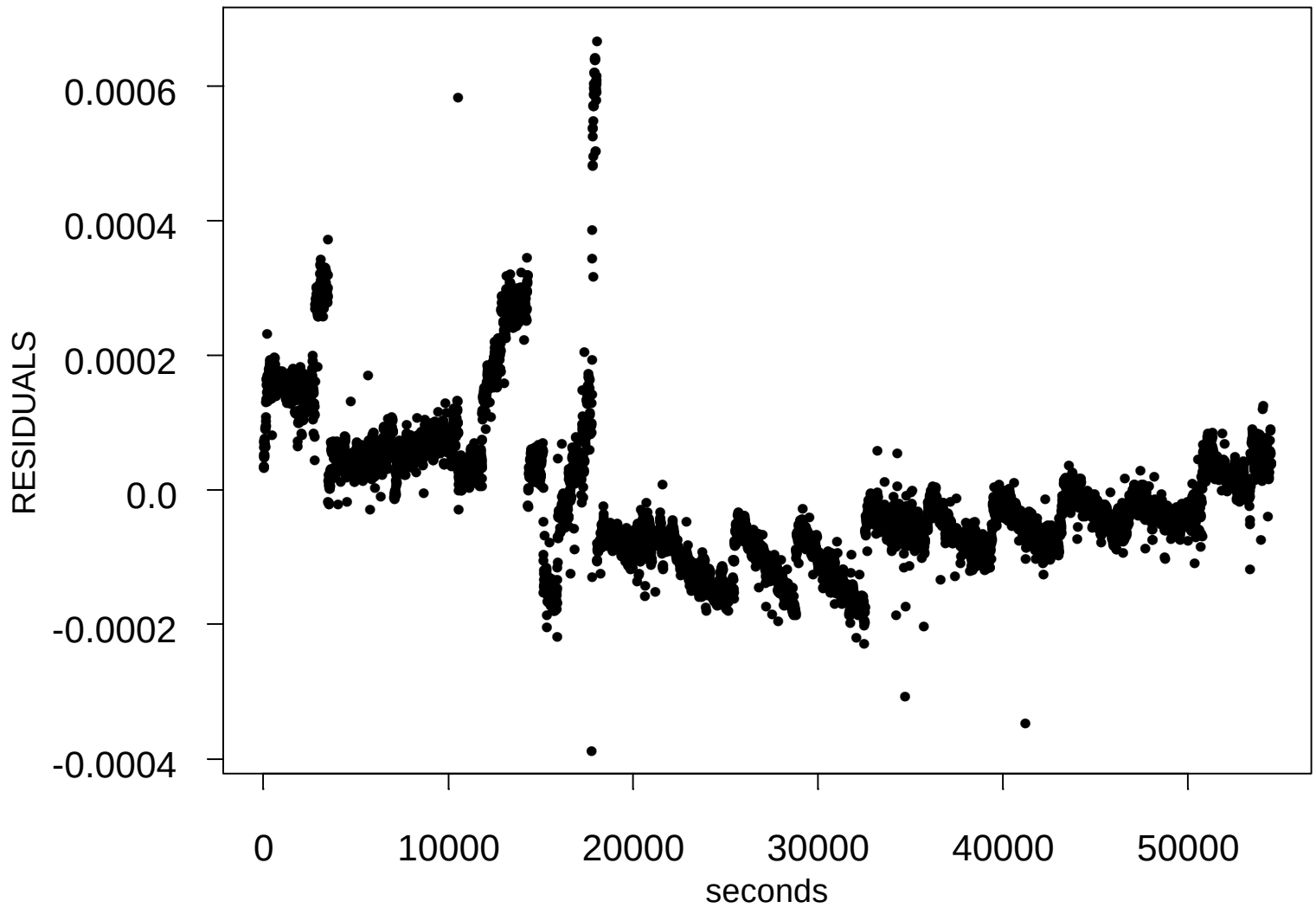

Figure 6. Residuals from the fit of equation (27) to the operation data of Figure 1.

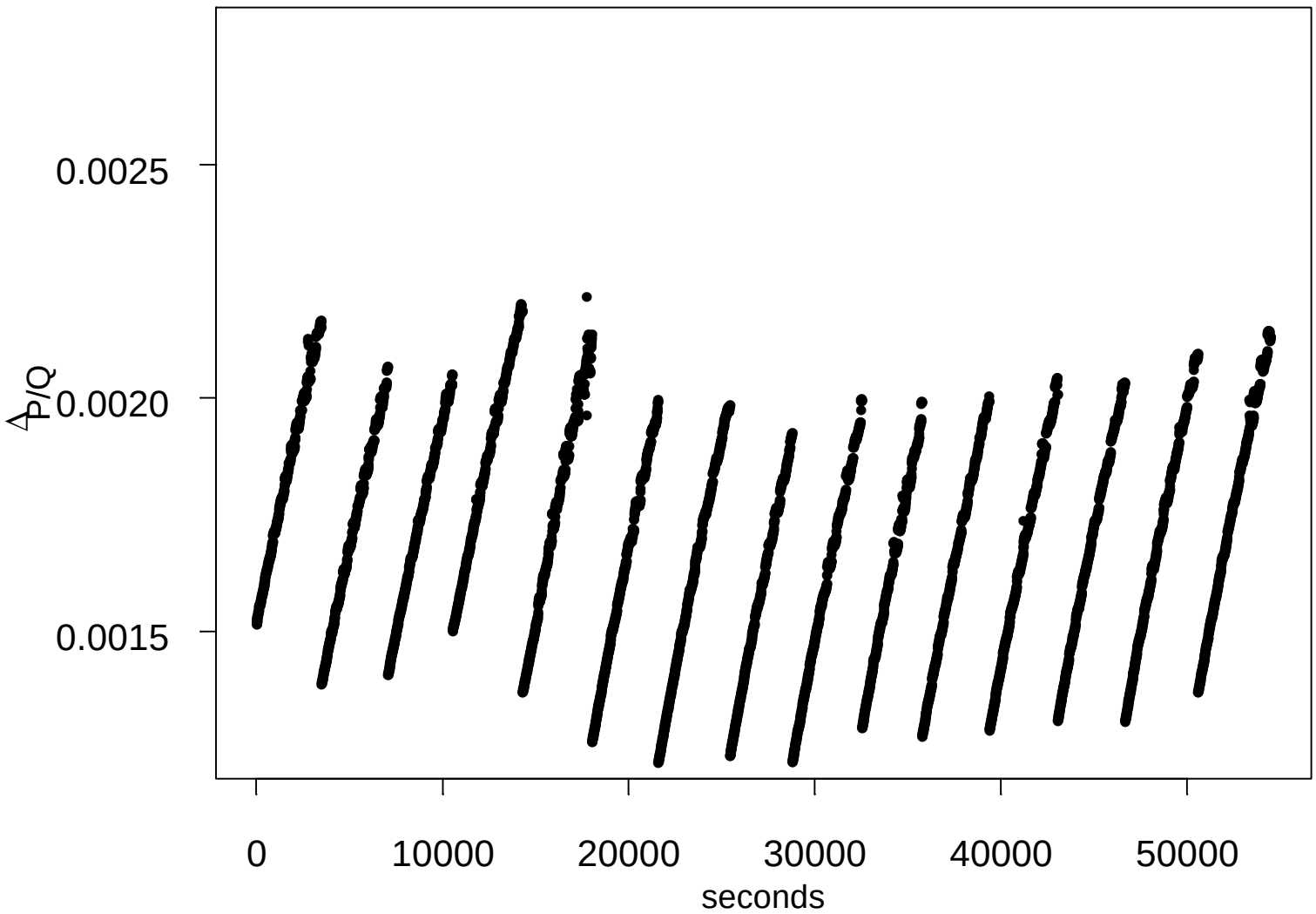

Figure 7. Variation of ΔP/Q with time as calculated from equation (28).

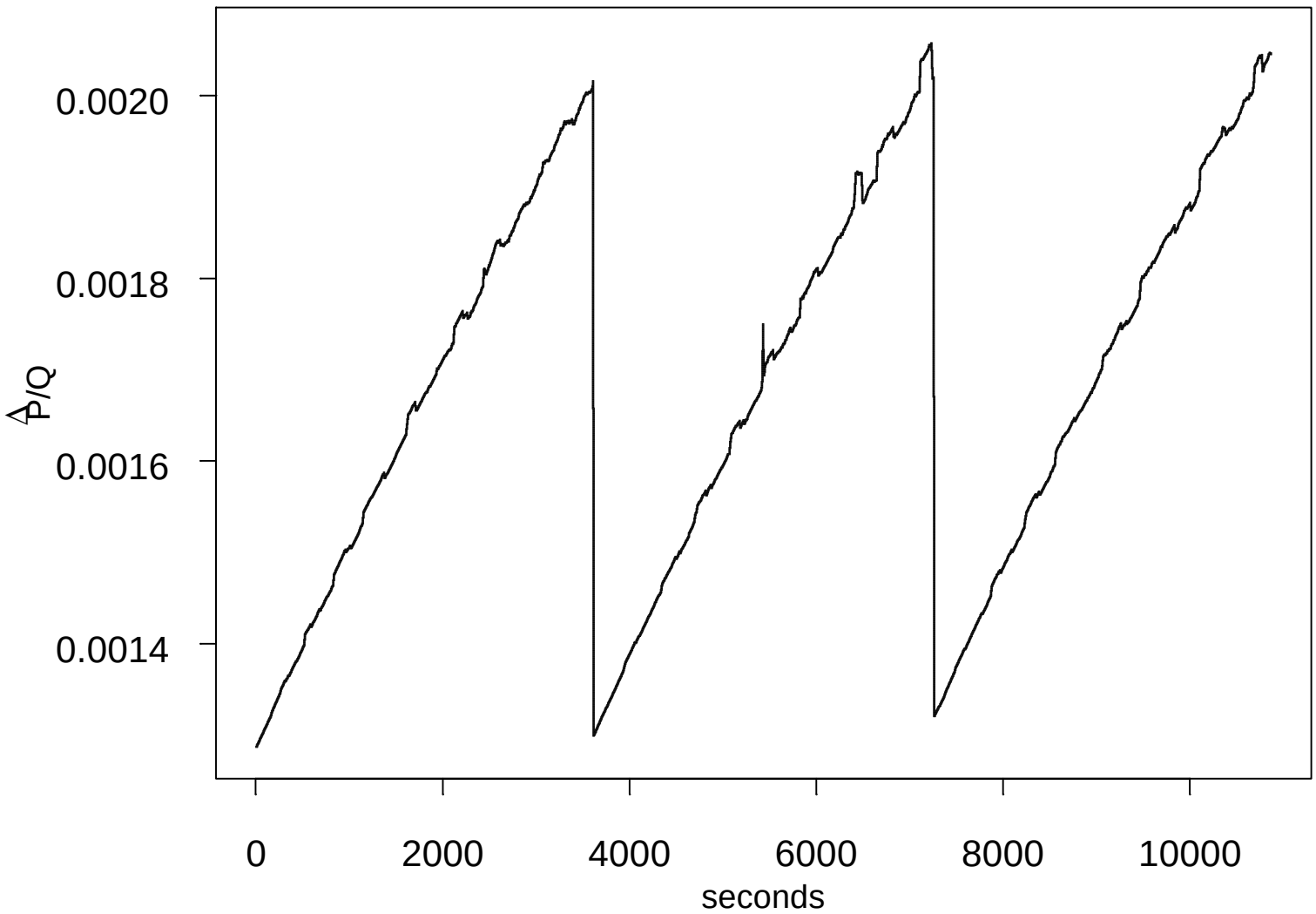

Figure 8. Variation of $\Delta P/Q$ with time as calculated from equation (28).

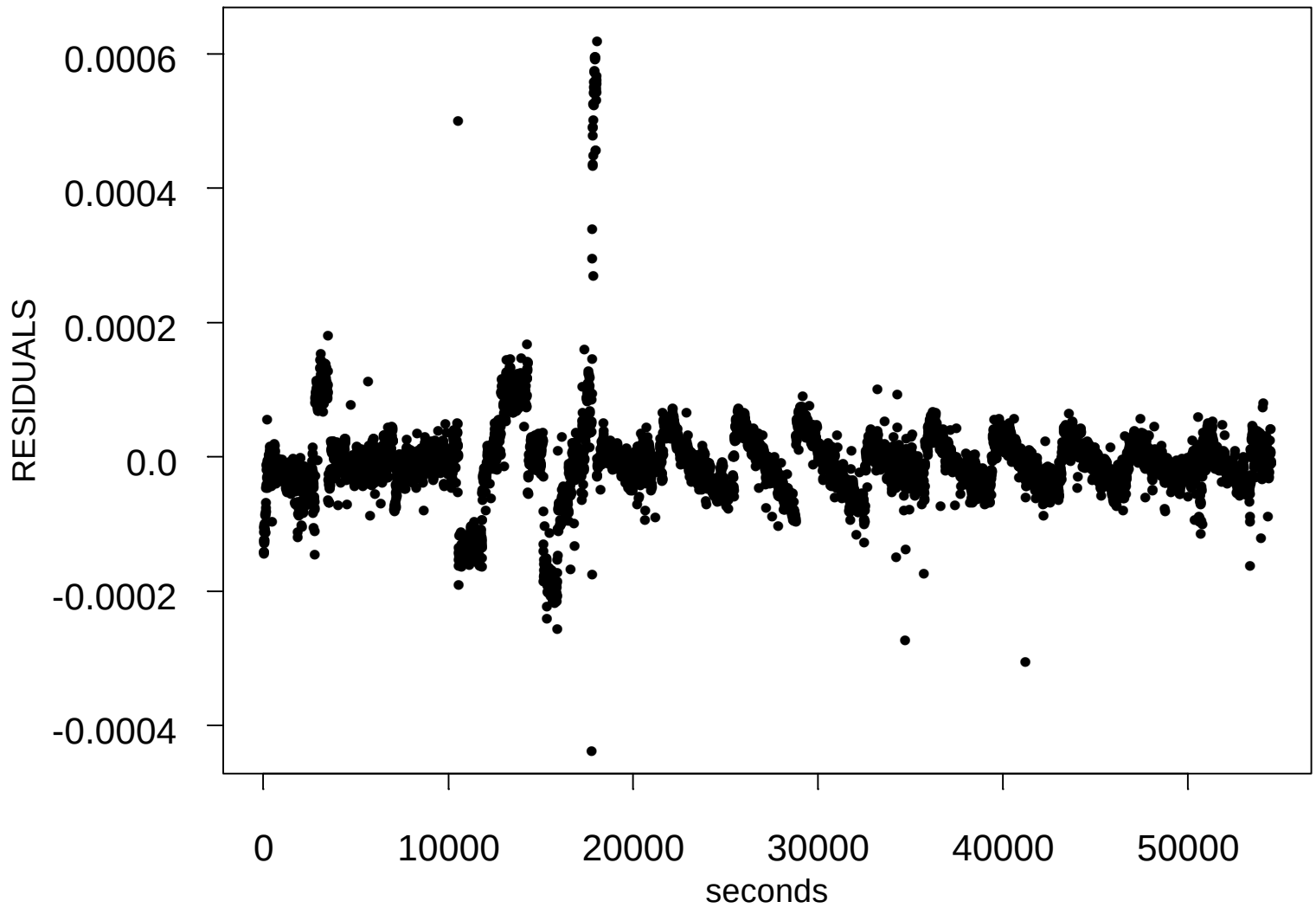

Figure 9. Residuals from the fit of equation (28) to the operation data of Figure 1.

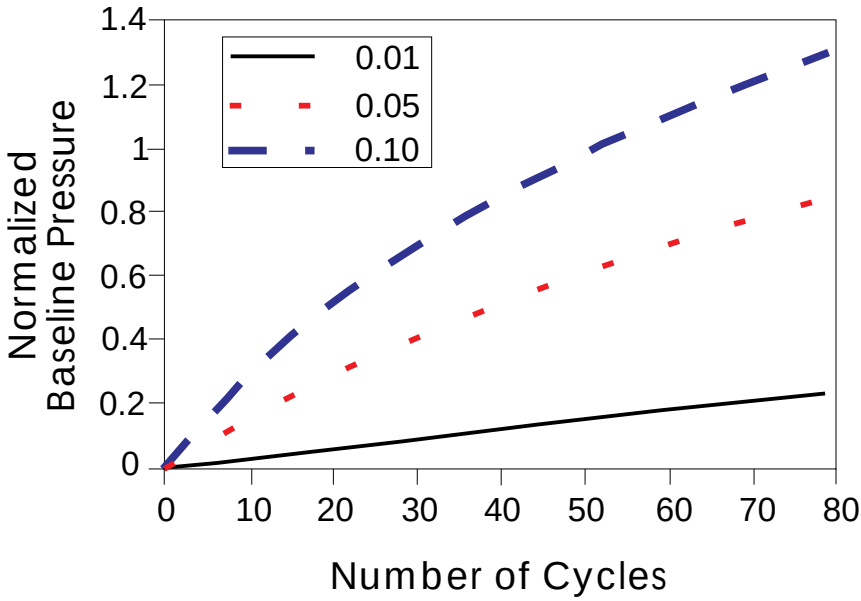
Normalized
Baseline Pressure
1.4
1.2
1
0.8
0.6
0.4
0.2
0
0.01
0.05
0.10
0
10
20
30
40
50
60
70
80
Number of Cycles

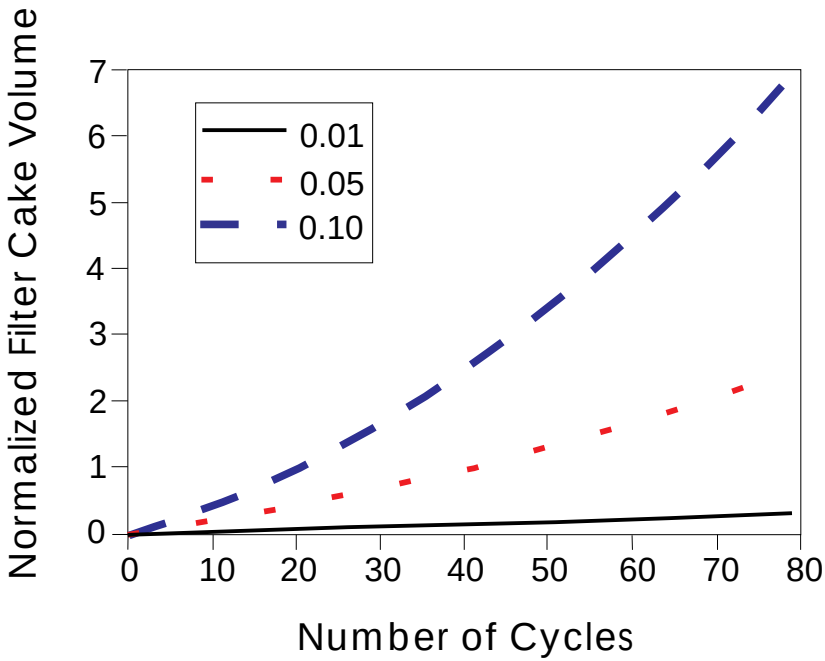
Normalized Filter Cake Volume
7
6
5
4
3
2
1
0
0.01
0.05
0.10
0
10
20
30
40
50
60
70
80
Number of Cycles

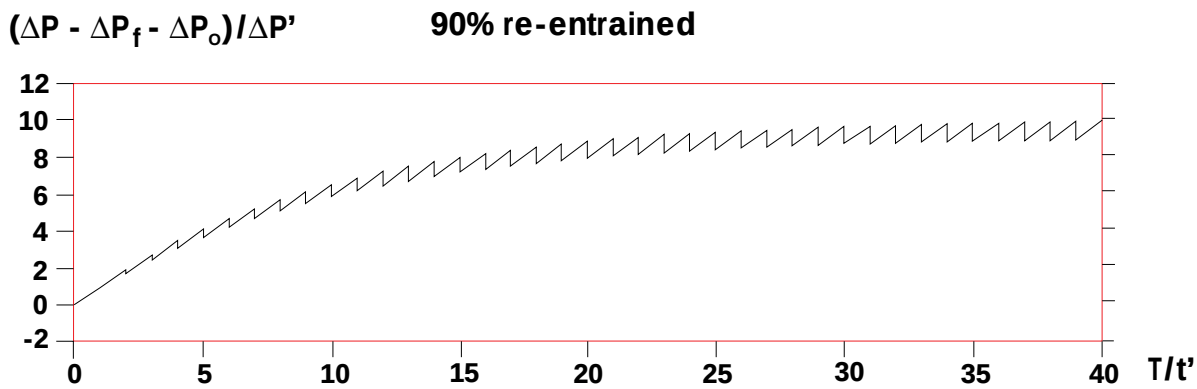
(ΔP - ΔPf - ΔPo)/ΔP'
90% re-entrained
12
10
8
6
4
2
0
-2
0
5
10
15
20
25
30
35
40
T/t'

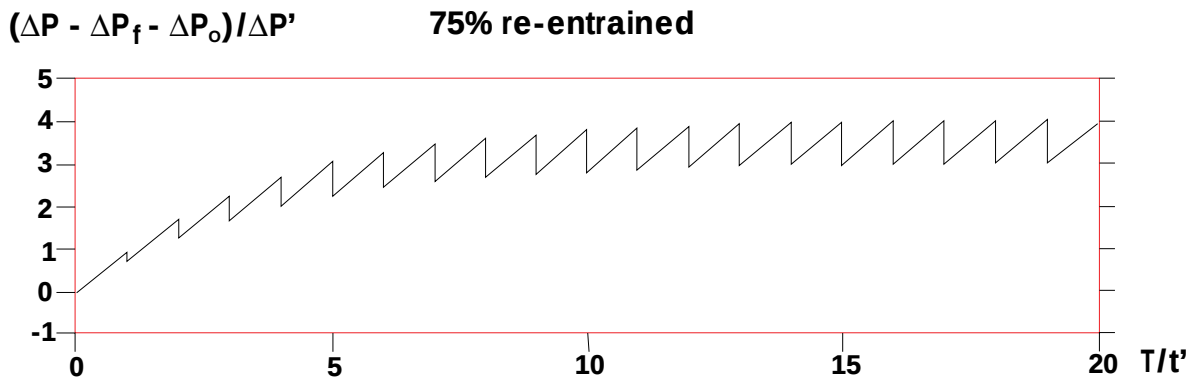
(ΔP - ΔPf - ΔPo)/ΔP'
75% re-entrained
5
4
3
2
1
0
-1
0
5
10
15
20
T/t'

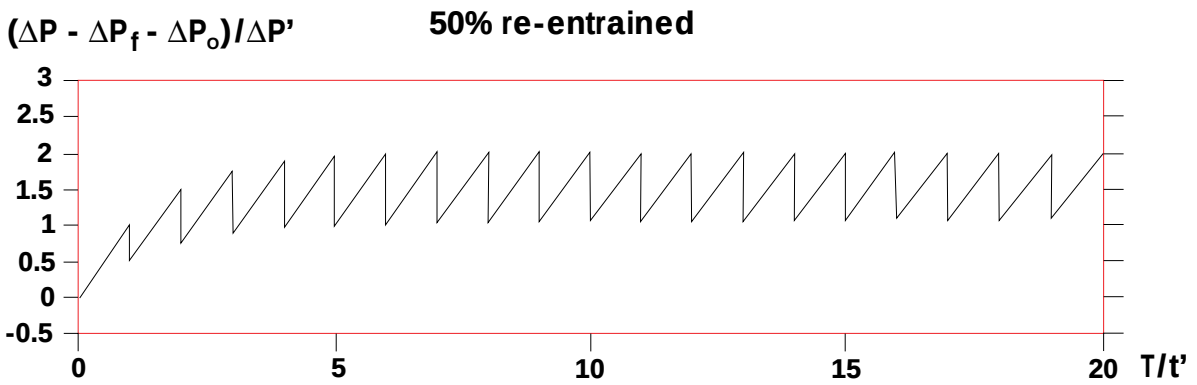
(ΔP - ΔPf - ΔPo)/ΔP'
50% re-entrained
3
2.5
2
1.5
1
0.5
0
-0.5
0
5
10
15
20
T/t'

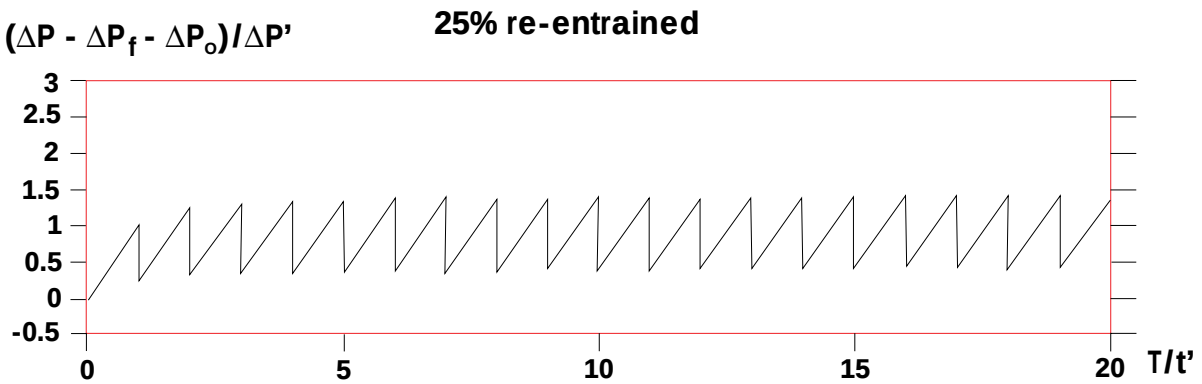
(ΔP - ΔPf - ΔPo)/ΔP'
25% re-entrained
3
2.5
2
1.5
1
0.5
0
-0.5
0
5
10
15
20
T/t'

M96001970C

Development of a Monolithic Ceramic Cross-Flow Filter: Part 2

David A. Larsen (518-436-1263)
Blasch Precision Ceramics, Inc.
580 Broadway
Albany, New York 12204

Introduction

Ceramic cross-flow filters were designed to provide high temperature, high pressure removal of particulates from hot gas streams in coal fueled power systems, with the benefit of high surface area per unit volume. An important need has been identified as a one-piece monolithic ceramic cross-flow filter, rather than the most recent segmented filter that has been known to delaminate/separate in service. Current ceramic technology has proved incapable of forming a complex one-piece shape such as this, with an acceptable permeable, porous ceramic material. Blasch's unique and proprietary injection mold ceramic forming process has commercially produced complex shapes of this nature for many years, but of a non-permeable ceramic. In the earlier SBIR Phase I work, permeable, porous ceramic compositions were developed, targeted to meet the filtration and other requirements of cross-flow filters. In this SBIR Phase II effort, the ceramic composition data and lab scale process techniques established in Phase I are being used as the basis for prototype production of full-size monolithic ceramic cross-flow filters. After production, these prototypes will be subjected to filtration testing, followed by post-test characterization.

Progress thus far in Phase II (through the first half of the project) includes design of a prototype full size monolithic ceramic cross-flow filter, acceptable material screening tests including room temperature permeability and particulate collection efficiency, design and fabrication of a mold, development of a larger scale process to produce prototypes, and production of some initial prototype filters.

Objectives

The overall primary objective of this Phase II project is to use the ceramic composition data and lab scale process techniques established in Phase I for prototype full scale production and filtration testing/ characterization of monolithic ceramic cross-flow filters. The specific project objectives for the duration of this project, simply stated, are:

Research sponsored by the U.S. Department of Energy's Morgantown Energy Technology Center, under contract DE-FG02-94ER18718 with Blasch Precision Ceramics, Inc., 580 Broadway, Albany, NY 12204; fax 518-436-0098; phone 518-436-1263.

1. Design a prototype full size one-piece monolithic cross-flow filter ceramic shape to be produced using the Blasch process and permeable ceramic compositions developed in Phase I.

2. Design and fabricate a mold system capable of forming this prototype full size monolithic ceramic cross-flow filter.

3. Characterize permeable ceramic compositions to be used for this prototype filter, to include room temperature permeability, particulate collection efficiency, and corrosion testing.

4. Produce prototype full size monolithic ceramic cross-flow filters by upscaling the lab scale process developed in Phase I.

5. Evaluate performance of these prototype filters in filtration testing and characterize after testing.

Approach

The detailed design of a prototype full size monolithic ceramic cross-flow filter was first determined before a mold system could be designed for a complex shape of this nature. This design had to include consideration of fulfilling the application requirements, as well as manufacturability. Knowledgeable people from Westinghouse and DOE-METC provided input to Blasch regarding design criteria for this prototype filter. Dimensional tolerances for the filter part were also determined as part of this design. Various clean-gas and dirty-gas channel layouts and sizes were considered, to yield a monolithic cross-flow filter that has beneficial filtration surface area, is manufacturable, and is not likely to plug during hot gas filtration application.

This monolithic cross-flow filter design was used as the basis for the design of the mold system required to form this filter prototype shape. This mold system was designed to be useable in Blasch's process and to yield the tight dimensional tolerance requirements of the filter design. Once this mold system was designed, fabrication was performed.

A fairly simple mold was also designed and fabricated to form the different sized ceramic disk specimens needed for room temperature permeability testing, particulate collection efficiency testing, and corrosion testing, all by Westinghouse. These specimens were made using the technique and composition(s) developed during Phase I..

It was realized that the production of prototype monolithic ceramic cross-flow filters would require some equipment of a larger size than the lab scale equipment used in Phase I. Blasch already possessed most of the necessary equipment, but needed a larger mixing apparatus for hi-speed mixing of the constituents of the permeable compositions developed in Phase I, including organic additives.

Engineering was performed to determine appropriate type, size, and speed of mixer needed for this process step. Subsequently, this mixing apparatus was procured. After installation of this equipment, mixing parameters were determined (such as time, speed, and batch size) by trials, and microscopic comparison of the same slurry composition mixed on a much smaller, lab scale.

Ceramic raw materials were and are being prepared, including sieving, to obtain particles of the proper size. Kiln furniture setter plates, on which to set the ceramic cross-flow filters during firing were specified and procured. These plates must handle the specified firing conditions of the filters, and also be very flat and resist hot load deformation to assure that the prototype filters are made with flat surfaces.

The lab scale process used in Phase I to make small test specimens was upscaled in this Phase II effort to produce monolithic ceramic cross-flow filters. Specific batching, mixing, and forming method details were planned based upon past upscaling experience, including the Phase I work. This upscaled method was and is subject to modification based upon the experience gained while trying to produce these ceramic cross-flow filters. Drying and firing cycles were also determined, to assure that the filter prototypes do not deform, crack, or explode during drying or firing. Several prototype filters are likely to be produced while streamlining the process, in attempt to make filters that meet the permeability, surface quality, dimensional, and other requirements.

Finally, three prototype full sized monolithic cross-flow filters each of two different permeable ceramic compositions will be submitted to Westinghouse. Filtration testing of two filters each of two compositions (the remaining one filter of each composition will be retained by Westinghouse as a reference for later comparison) will be performed by Westinghouse, followed by full characterization of the filters **after** this testing (post-test characterization). The filtration testing will occur in Westinghouse's HTHP PFBC simulated test vessel, at "typical conditions". These conditions include the following: 845þC temperature, 10 atm pressure, combusted natural gas atmosphere, with gas velocity of 10 fpm. The filters will be operated for a period when ash is delivered to form the dust cake along the filter surface. The cake will then be removed by pulse cleaning. Various measurements will be taken during the test.

Project Description

Blasch's unique and proprietary injection mold ceramic forming process has commercially produced complex shapes for many years, but of a non-permeable nature. In the earlier SBIR Phase I work, permeable, porous ceramic compositions were developed, targeted to meet the filtration and other requirements of cross-flow filters. In this Phase II effort, the Blasch forming process is being used as the basis along with the ceramic composition data and lab scale process techniques established in Phase I, for prototype production of full size monolithic ceramic cross-flow filters.

Generally speaking, the proprietary Blasch forming process includes the following steps: batching/weighing, wet batch mixing, injection of ceramic slurry into molds, solidification by freezing,

removal of mold, drying, and firing. This same general process is being used to make these prototype monolithic ceramic cross-flow filters, but with modification based upon Phase I experience. This modification includes a more intensive mixing procedure, to assure the organic additives are well dispersed and mixed. Also, drying and firing cycles are different to accomodate the slow burn-out of these organics; otherwise the filter prototype could crack, deform, or even explode.

Permeable ceramic material compositions developed in Phase I are being used for these prototype filters. The alumina-mullite permeable ceramic compositions identified as #4-270 and #4-300 were selected based upon these Phase I results. These two are actually the same raw material composition, but are fired at different temperatures, resulting in different mullite contents. Composition #4-300 is the higher fired body, with the higher % mullite.

In accordance with the earlier stated "Approach", the following has been performed during the first half of this project:

1. A prototype full size monolithic cross-flow filter was designed that seems to be manufacturable. This design also seems to fulfill the stated criteria for the application with regards to high surface area of filtering walls (about 8.4 square feet), and large enough dirty gas channels to reduce plugging (0.30 inches high x 0.9 inches wide, and 0.30 inches high x 2.0 inches wide). Figure 1 in the results depicts a three-dimensional cut-away view of this monolithic cross-flow filter design.

2. A mold system for the filter prototype was designed and fabricated. The mold system was made with smooth surfaces and tight dimensional tolerances to accomodate the dimensional and surface finish requirements incorporated into the filter design.

3. A mold was designed and fabricated for the different sized ceramic disk specimens required for Westinghouse's room temperature permeability testing, particulate collection efficiency testing, and corrosion testing. Ceramic disk specimens of compositions #4-270 and #4-300 were formed, dried, fired and sent to Westinghouse for testing.

4. Westinghouse performed room temperature permeability and particulate collection efficiency testing on compositions #4-270 and #4-300. Results are discussed later in this paper. Corrosion testing on composition #4-300 is in process as this report is being written.

5. Mixing apparatus was investigated, engineering was performed, and a larger scale hi-speed mixer was procured. After installation, mixing parameters were determined, including speed and mixing time. This was done by microscopic comparison of permeable ceramic composition raw wet mix specimens mixed in this new mixer, compared to samples of the same composition mixed in the lab scale mixer used earlier in Phase I.

6. In effort to determine optimum processing techniques and parameters, several (ten at the time of this paper) prototype monolithic ceramic cross-flow filters were produced. All were dried and fired based on cycles that were determined earlier. Various ceramic forming technique

modifications were and are being tried to eliminate the voids on interior filter walls. These include use of different vibration techniques and composition moisture contents.

Results

Many of the results are obvious based upon earlier discussion of the project descripition. The prototype monolithic ceramic cross-flow filter was designed, and has approximate overall outside dimensions of 12 inches x 12 inches x 4 inches (not including the flange at the bottom). The intake "dirty gas" channels are 0.30 inches high x 2.0 (or 0.9) inches wide x 3.8 inches long. The exhaust "clean gas" channels run perpendicular to the dirty gas channels, and measure 0.14 inches high x 1.5 inches wide x 11.6 inches long. This design yielded filter surface area of about 8.4 square feet. Figure 1 is a three dimensional view of this filter design. Also, it is specified in this design that all internal filtering walls, which are nominally 0.11 inches thick, are to be free of voids larger than 0.025 inches diameter, such that the chance for a "blow-through" is minimized.

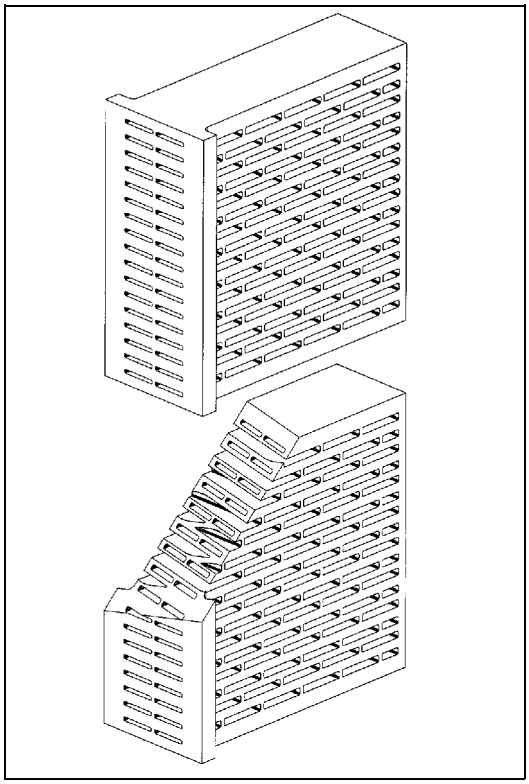

Figure 1. 3-D Depiction of Prototype Full Size Monolithic Ceramic Cross-Flow Filter

Westinghouse performed room temperature gas permeability and particulate collection efficicncy testing on disk specimens of compositions #4-270 and #4-300. Westinghouse indicated that the room temperature gas permeability results for both composition specimens was acceptable with regards to their target of 1 in-wg/fpm, as is shown in the following table.

Disk ID No.	Room Temperature Gas Flow Resistance, in-wg/fpm
BPC 4-270	1.06 - 1.13
BPC 4-300	0.93 - 1.01

In the particulate collection efficiency test, 75 grams of dust were fed to each of the two disk specimens (compositions #4-270 and #4-300). No observable dust was detected in the outlet gas during testing. Similarly, an approximate 1mm thick dust cake was formed along one surface of each disk, and when the disks were fractured, limited penetration of fines was detected in each matrix. From these qualitative observations, the dust cake layer formation and extent of penetration was considered to be acceptable by Westinghouse, in terms of particulate infiltration into the first pore layers of these porous ceramic bodies. Further, Westinghouse indicated that their gas flow resistance and particulate collection efficiency data imply that the Blasch oxide-based matrix was reproducibly manufactured for use in this effort. As this paper is being written, results from Westinghouse on corrosion resistance testing of disk specimen of composition #4-300 are not yet available.

Ten prototype full size monolithic ceramic cross-flow filters have been made thus far in this project. Some were made of composition #4-270 and others of #4-300. These met the prescribed dimensional tolerance criteria, had no sign of firing warpage or deformation, and had in general, had very good exterior appearance, but had minor voids (unacceptable) in the filtering walls. One filter did however have a deformed top area and another cracked badly: in both cases, the fault occurred because of identified specific variations in forming and mold-use techniques. Of the prototypes produced by Blasch thus far, the design criteria has been met as shown in the following table.

Filter No.	Compos-ition	Warp/ Deform	Meet Dimensional Tolerances?	Meet Void Specs?	Overall Appearance
4-A	4-270	none	yes	no	v. good
4-B	4-300	broke	yes	no	poor
4-C	4-270	none	yes	no	v. good
4-D	4-270	none	yes	no	v. good
4-E	4-300	none	yes	no	v. good
4-F	4-300	none	yes	no	v. good
4-GW	4-300-W*	some	yes	no	poor
4-HW	4-270-W*	none	yes	no	v. good
4-IW	4-270-W*	none	yes	no	v. good
4-JW	4-300-W*	none	yes	no	v. good

* "-W" denotes additional moisture added to wet mix.

Figure 2 is a photograph of one of the prototype monolithic ceramic cross-flow filters made in this project using the Blasch process. This filter is typical of those produced so far.

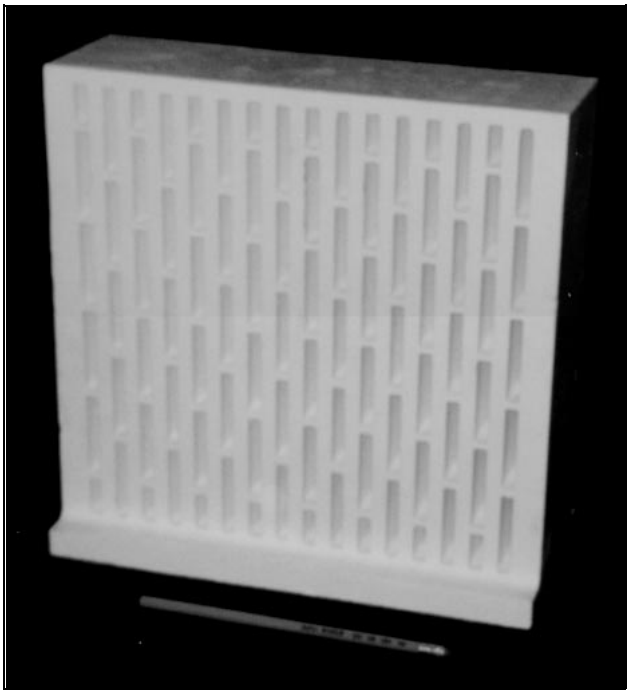

Figure 2. Photograph of Prototype Full Size Monolithic Ceramic Cross-Flow Filter Made With Blasch Process

Application

The application for this monolithic ceramic cross-flow filter product is to provide high temperature, high pressure removal of particulates from hot gas streams in coal fueled power systems. These power systems include IGCC (Integrated Gasification Combined Cycle) and PFBC (Pressurized Fluid Bed Combustor) types. The major benefit of the cross-flow filter design compared to the currently used candle filters is much higher filtration surface area. The monolithic cross-flow filter designed in this project has a filtration surface area of about 8.4 square feet vs. less than 3 square feet for a candle filter. This additional filter surface area is expected to yield significantly better filter efficiency.

In comparison to competitive box-shaped filters, there are two that are known. One is the "dead-end" ceramic membrane filter. This filter has high filtration surface area, but has so far been limited to dead-end dirty gas channels of relatively small cross-sectional size, that may be prone to plugging in application and also may be more difficult to clean via reverse pulse method. Although this project is not yet finished, the Blasch technology is already producing prototype monolithic ceramic cross-flow filters with dirty gas channels that are open on both ends and are approximately 8mm high. With a new mold, this same technology could be used to make channels of even larger size, if deemed beneficial. The other known ceramic cross-flow filter design is segmented, where grooved plates are stacked and adhered together to form the filter. The disadvantage of this filter design is that it has been known to delaminate/ separate in service. It is anticipated that the monolithic, one-piece design of the Blasch cross-flow filter will eliminate this delamination problem.

Future Activities

This Phase II SBIR project is approximately half finished. Future activities include further streamlining of processing techniques to produce ceramic cross-flow filters that are improved with regards to minimizing voids on internal filtering walls. Corrosion testing of composition #4-300 by Westinghouse will be completed. It also is planned that three prototype filters each of two compositions will be submitted to subcontractor Westinghouse for simulated filtration testing in their HTHP PFBC test vessel, followed by post-test characterization. Further specifics of this testing are included in the "Approach" section of this paper.

Acknowledgements

This work was performed with the guidance of METC Contracting Officer Representative, Mr. Ted McMahon. The period of performance for this DOE SBIR Phase II Grant is June 21,1995, through June 20, 1997. This paper provides progress report through the first half of this project. Also, the author would like to acknowledge Ms. Mary Anne Alvin and Dr. Thomas Lippert of Westinghouse Electric Corporation for their support as a subcontractor to Blasch throughout this project.

References

1. Discussions/meetings with Mr. Ted McMahon and others of DOE METC, from 1993 through June, 1996.

2. Discussions with Ms. Mary Anne Alvin and Dr. Tom Lippert of Westinghouse Electric Corporation, Science and Technology Center, Pittsburgh.

3. McDaniel, H.M., Mollot, D.J., Venkataraman, V.K., Proceedings of the Advanced Coal-Fired Power Systems '95 Review Meeting, Volumes I and II: DOE/METC-95/1018. June, 1995.

4. Lippert, T.E., Alvin, M.A., Smeltzer, E.E., Bachovchin, D.M., and Meyer, J.H., Subpilot Scale Gasifier Evaluation of Ceramic Cross Flow Filter, Final Report-February 1, 1988-December 31, 1992: DOE/MC/24021-3544. August, 1993.

5. Lippert, T.E., Smeltzer, E.E., Alvin, M.A., and Bachovchin, D.M., Long-Term Durability Testing of Ceramic Cross-Flow Filter: Final Report-September 29, 1987-December 31, 1992: DOE/MC/24022-3654. August, 1993.

6. Alvin, M.A., Lippert, T.E., and Lane, J.E., "Assessment of Porous Ceramic Materials for Hot Gas Filtration Applications", Ceramic Bulletin, Vol 70, No. 9, 1991.

7. Bosart, S.J., Cicero, D.C., Zeh, C.M., and Bedick, R.C., Gas Stream Cleanup Technology Status Report: DOE/METC--91/0273. August, 1990.

8. Ventkataraman, V.L., Rath, L.K., Martin, J.W., Bedick, R.C., Proceedings of the Eleventh Annual Gasification and Gas Stream Cleanup Systems Contractors Review Meeting, Volumes I and II: DOE/METC--91/6123. August, 1991.

9. Webb, H.A., Bedick, R.C., Geiling, D.W., Cicero, D.C., Proceedings of the Eighth Annual Coal Fueled Heat Engines and Gas Stream Cleanup Systems Contractors Review Meeting: DOE/METC--91/6122. July, 1991.

Initial Failure Analysis of Ceramic Filters

Ziaul Huque (zhuque@pvcea.pvamu.edu; 409-857-4023)
Daniel Mei (dmei@pvcea.pvamu.edu; 409-857-4023)
Jianren Zhou (jzhou@pvcea.pvamu.edu; 409-857-4023)
Mechanical Engineering/Prniric View A&M University
College of Engineering and Architecture
Post Office 130X 397
Prairie View, Tx 77446-0397

Abstract

Effective high temperature ceramic filters are indispensable in the advanced, coal based power systems (IGCC and PFBC). To meet the environmental particulate emission requirements and improve thermal efficiency, ceramic filters are utilized to cleanup the hot gas particulate to protect downstream heat exchanger and gas turbine components from fouling and corrosion. The mechanical integrity of ceramic filters and an efficient dust cake removal system are the key issues for hot gas cleanup systems. The filters must survive combined stresses due to mechanical, thermal, chemical and steam attack throughout normal operations (cold back pulse cleaning jets), unexpected excessive ash accumulation, and the start up and shut down conditions.

To evaluate the design and performance of ceramic filters, different long term filter testing programs were conducted. To fullfill this purpose, two Advanced Particle Filter (APF) systems were complete at Tidd PFBC Demonstration Plant in Brilliant, Ohio in late 1990 as part of the Department of Energy's (DOE) Clean Coal Technology Program. However, many filter failures were reported prior to its desired life time. In Tidd APF vessel, 28 filters failed one time,

The objectives of this program were to provide an understanding of the factors pertinent to the failures of ceramic filters by characterizing filter properties and the dust cake removal mechanism, Researches were emphasized on understanding of changes of filter properties and back pulse cleaning mechanism to resolve the issues relating to filter permeability variations, ash bridging and micro-thermal cracks induced during cold back pulse cleaning.

To perform failure analysis of ceramic filters, thermal numerical simulation, material laboratory analysis on filter materials and dust cake, and measurements on filter properties and back pulse intensity along filter axis within a bench scale filter chamber were conducted.

The initial failure analysis of ceramic filters program consisted of five phases:

Phase I - Literature survey, filter chamber design and test plan generation
Phase II - Test chamber fabrication, assembly and filter property testing
Phase 111- Thermal numerical simulation on candle filter during back pulse cleaning
Phase IV - Material laboratory analysis on filters, dust cake and microscopic study by means of X-ray diffractometer, SEM and X-ray photoelectron spectroscope
Phase V - Measurement on pulse intensity and optimization on back pulse system design

Material laboratory analysis indicates that the outer layer of used filters have different phase structure than its inner layers due to filtration of foreign materials, The permeability y of used filters varies randomly compared with the unused ones. Back pulse induced micro-cracks can be reduced by providing heated back pulse stream to reduce the temperature gradient within the filter. Back pulse cleanup efficiency can be improved by optimizing the back pulse system design.

Even dust layer deposition on filter is particle size and cohesive force dependent, an efficient dust cake removal system can help prevent excessive dust cake deposit on filter surface and eliminate ash bridging problems contributing to the failures of ceramic filters, Thermal induced load which damaged candle filters could be eliminated as ash bridging disappears. Test data collected by this research program can help filter researchers verify the accuracy of their numerical simulation results prior to extensive simulation on filter system design and analysis.

More measurements and analysis will be performed on filter clusters within a bench scale filter chamber to help optimize the back pulse plenum system design.

Acknowledgements

We would like to thank our Contracting Ofl-leer's Representative, Dr. Norman Holcombe, filter cluster leaders, Dr. T. K, Chiang and Dr. Duane Smith, and Mr. Charlie Komar as well as the management at DOE/METC for their extensive support on this research program and made our visits to other research institutes and filter industries possible for helpful technical discussions, Special thanks to Mr. Komar for all of his efforts in helping establish Hot Gas Cleanup (HGCU) research program at Prairie View A&M University.

Research sponsored by the U.S. Department of Energy's Morgantown Energy Technology Center, under contract DJ3-FG21 -94MC3 1203 with Mechanical Engineering/Prairie View A&M University, College of Engineering and Architecture, P.O. Box 397, Prairie View Tx 77446-0397; 'l'cl: (409) 857-4023 Fax: (409) 857-4395

Introduction

Electricity demand has been closely tied to economic growth, The need for electrical power is estimated to double for every twenty years. Coal gasification is an critical process in advanced energy conversion systems for power generation, because it can improve the efficiency of electricity generation with less cost along with the Integrated Gasification Combined Cycle system, To protect high temperature gas turbine system, heat exchange components from corrosion and damages caused by gasified particulate, and meet the environmental protection measures, hot gas cleanup is one of the most critical technologies required to ensure the success of low-cost methods of electric power generation. Ceramic filters are indispensable in removing the particulate in coal gasification applications, Among the current hot gas cleanup technologies, the most economical one is the use of rigid ceramic candle filters to remove particulate from gas streams being introduced into hot gas turbine. The mechanical integrity of ceramic filters and an efficient dust cake removal system are the key issues to be resolved for hot gas cleanup systems. The filters must survive combined stresses due to mechanical, thermal, chemical and steam attack throughout cold back pulse cleaning jets and system start up and shut down conditions.

Problems

To evaluate the design and performance of ceramic filters, different long term filter testing programs were conducted. To fulfill this purpose, two Advanced Particle Filter (APF) systems were complete at Tidd PFBC Demonstration Plant, in Brilliant, Ohio in late 1990 as part of the Department of Energy's (DOE) Clean Coal Technology Program. But the most undesirable thing ever happened was the sudden fictional and physical failures of filters prior to its designed life time, In Tidd APF filter vessel, twenty eight (28) filters failed one time. Significant research effort has been carried out to find out the exact cause of early failure of filters, In this work, the studies are emphasized on the possible failure cause analysis of rigid ceramic candle filters.

Objectives

The objectives of this program were to provide an understanding of the factors pertinent to the failures of ceramic filters by characterizing filter properties and the dust cake removal mechanism, Researches were emphasized on understanding of changes of filter properties and back pulse cleaning mechanism to resolve the issues relating to filter permeability variations, ash bridging and micro-thermal cracks induced during cold back pulse cleaning.

Approach

To perform failure analysis of ceramic filters, thermal numerical simulation, material laboratory analysis on filter materials and measurements on filter properties and gas stream pressure field along filter axis within a bench scale filter chamber were conducted,

Project Description

The initial failure analysis of ceramic filters program consisted of five phases:

Phase I - Literature survey, filter chamber design and test plan generation

Extensive literature survey was performed on research work conducted by academic and industrial researchers. Most of work was concentrated on the microstructural or material aspect (mechanical, thermal and chemical properties) of filters, Westinghouse and South Research Institute has performed significant amount of testing on the thermo-mechanical properties of various filters provided by filter industry. But little work had been conducted on the variations of filter permeability and the pressure distribution field of the gas stream during dust cake cleaning process, Therefore, a filter chamber and a testing plan for candle filter were designed to study the variations of filter permeability y and gas flow pressure field in the filter chamber.

After a thorough discussion, the samples for this analysis program are silicon carbide ceramic filters supplied by IF&P, Chicago, Illinois, U.S.A. with 154.83 cm long, 3,81 cm I.D. and an O. Il. of 6.35 cm.

Phase 11- Test chamber fabrication, assembly and filter property testing

The schematic of the room ambient temperature filter test chamber is shown in Figure 1. To facilitate the testing, this test chamber vessel was made from a transparent plastic pipe with a 15,24 cm O. D., 198.12 cm long and 0,71 cm wall thickness. This test chamber vessel passed a 150.0 psig static pressure testing, compatible with Tidd APF pressure level, prior to its final assembly. Ten 1/2 -20 threaded holes are evenly spaced along the chamber axis to mount fast response pressure transducers and the pressure calibrator, A filter sealing plug base (15.33 cm diameter by 8.90 cm long) and a pressure inlet plug (1 5.33 cm diameter and 8.9 cm long) are placed at the top and bottom end of the test chamber respectively. All the test chamber components were carefully machined with a tight tolerance control within +/- 0,001 inches.

The candle filter is installed in the pressure sealing assembly to ensure the hermeticity of pressure sealing and the filter is located along the center of the vessel axis to provide a cylindrical symmetric system, Rubber pads are placed in between the filter and the sealing plug to reduce shock and mechanical stress on the filter flange during pressure testing, A pressure sealing diaphragm is installed on the top of the filter sealing assembly. The technique of perforating the diaphragm was utilized to seal and release filter test chamber pressure. The sealing diaphragm was perforated by a special designed perforating device to establish the chamber pressure pcr the ambient pressure test plan. Figure 2 shows the schematic of the diaphragm perforating arrangement.

An advanced microprocessor based hand held pressure calibrator and micro-machined silicon pressure transducers for each pressure range were installed along the axis of the filter test chamber to characterize candle filter permeability variations and the gas flow pressure distribution field in the test chamber. All of the pressure transducers were carefully calibrated prior to the use

of pressure in the testing work, A data acquisition system is utilized to collect test data.

The total leak time required for preset positive chamber pressure to reduce to room ambient pressure was recorded as a relative measure to correlate the permeability variations of the filters to be evaluated. Positive pressure was provided by nitrogen bottle. Vacuum chamber environment is support by a vacuum system,

To character IF&P filter performance, permeability changes of unused and used filters were first evaluated within an innovative test setup assembled in the mechanical engineering laboratory at Prairie View A&MU. To ensure the validity of the test results, the test setup and controls had been modified and improved until repeatable test environment and controls were available, The permeability distribution of IF&P filters was then carefully measured and characterized along the axis of the filters with different exposure percentage of filter surfaces to the gas flow.

A technique has been successfully developed to seal the filter surface. This technique was applied on partial filter surface areas to characterize the variations of filter permeability along filter axis and along filter perimeter. To facilitate the characterization of filter permeability variations, it was decided that only 25°/0 of the filter surface area, along filter axis and its perimeter, was evaluated each time after a few test iterations. Each filter was tested four times with the same test environment under one pressure range. Four to five tests wereperformed for each pressure range and test data were reviewed and ensured it were consistent and repeatable. Therefore, the averaged data represents the characteristics of filter performance with good confidence.

Every test was repeatedly performed five times. After technical discussion and evaluation, the test results were found to be repeatable and representative as planned. This testing philosophy was applied on all testings. These measurements did identify the variations of filter permeability can be randomly distributed only along the used filter axis and its perimeter; and the variations could be filter operation history dependent.

Phase 111- Thermal numerical simulation on candle filter during back pulse cleaning

A finite element analysis was initiated using the commercial finite element code ANSYS (Version 5.0), The initial analysis was focused on temperature distribution within filter during dust cake cleanup process. Half of a filter cut along the vertical plane of symmetry was used as the calculation domain.

The module was developed by dividing the computation zone into five volumes. This multizone approach was used in order to overcome the difficulties in meshing due to high slenderness ratio (length to diameter) of the filter.Discretization of the computational zone was done using two types of 3-D elements from the ANSYS element library, The bottom closed end of the filter was meshed with 3-D 10-node tetrahedral thermal solid, The rest of the cylinder was meshed with 20-node Thermal Solid Brick, In total for the entire computation domain 3598 elements were used. Connective boundary conditions were used for both outside and inside surface, The inside environmental temperature was assumed to be 40 degree C and the outside environment temperature was taken as 800 degree C, selected because it is close to the working

temperature. 40 degree C at the inside was used to be close to the back pulse temperature.

The convective heat transfer coefficients were obtained using correlation for forced flow. the thermal conductivity for the filter was taken as 87-86 W/mK, a value for silicon carbide. The convective heat transfer coefficients used were 1105W/mK and 992 W/mK for inside and outside surface respectively. Figure 3 shows the model of the entire half filter with exact scale factor. Figure 4 shows a blow-up of the filter near the flange neck. The figure also depicts the meshing of the elements. Figure 5 shows the temperature contour plots. The highest temperatures were on the outside surface close to the middle of the filter. The lowest temperature was on the inner surface close to the neck, The temperature variation ranges from about 567 degree C to about 405 degree C.

The initial analysis was done using solid wall for the filter and using steady state boundary conditions. Subsequent analysis will focus on unsteady state boundary conditions with solid wall and porous wall with unsteady state conditions. This will require coupling of heat transfer and fluid flow equations. The fluid solver that will be used is FLOTRAN which is a stand alone version of fluid flow solver in ANSYS. The analysis will include flow and pressure boundary conditions as are obtained from experiments in our laboratory.

Phase IV - Material laboratory analysis on filters and microscopic study by means of X-ray diffractometer, SEM and X-ray photoelectron spectroscope

Ceramic candle filters have been extensively used in the filtration of coal derived gases at high temperature and pressure. However, due to severe working condition and environment, some filters deteriorated prior to the desired life time. It is very important to identify and investigate the filter degradation mechanisms,

Figure 6, 7, 8 and 9 show some results of related investigation. It shows that the unused ceramic filter is a double-layer porous candle with gray color. The broken used filter samples were in dark yellow color. The yellow color surface layer is the product of emission particle deposition and the chemical reactions between emission gases and filter material. The composition of this layer are mainly Si02, Al2O3 and Al2Si4O10 according to the XRD analysis (Figure 7). This layer would reduce the efficiency of ceramic filters.

The observation and analysis also indicates that there is no significant difference in morphological characteristics between used and unused ceramic filters. it seems to indicate that no obvious change in microstructure occurred after usage. But, the XRD spectrashowed that after usage the crystal structure of the main composition SiC has been changed. The crystal plan spaces of the SiC in the outer layer were increased, For the inner layer, not only has SiC changed the crystal plane spaces, but also its grain orientation, The preferred orientation along (1034) of SiC in the inner layer of the used ceramic filter can be seen clearly in Figure 9. The growing and change in microstructure of the grain caused by thermal cycle may result in great stress inside the filter, The thermal induced stresses may promote the nucleation and the propagation of microcracks leading to the final fatigue fracture failure of the ceramic filters,

Phase V - Measurement on pulse intensity and optimization on back pulse system design

The negative pressure is generated within the filter test chamber with the use of the diaphragm sealing technique. Therefore, the back pulse pressure can be created at various pressure ranges, sealed by the diaphragm per the vacuum pressure level maintained in the filter chamber. The testing for the measurement of the pressure distribution of the back pulse is under way. Parameters for back pulse jet optimization has complete planning.

Results

Material laboratory analysis indicates that the outer layer of used filters have different phase structure than its inner layers due to filtration of foreign materials at very high temperature gradient. The main thermal attack tied to the back pulse cleaning did change the grain orientation and spacing of microstructure of the filters. The permeability of used filters varies randomly compared with the unused ones. These variations is also responsible for the nonuniform gas flow pressure field found in the filter test chamber.

Back pulse induced micro-cracks can be reduced by providing heated back pulse stream to reduce the temperature gradient within the filter. Back pulse cleanup efficiency can be improved by optimizing the back pulse system design, Figure 3,4 and 5 display the finite element simulation of thermal analysis, Figure 6, 7, 8 and 9 display the material study results. Filter permeability test data are attached in Appendix A.

The test data indicated that the unused filter is characterized with a fairly uniform permeability distribution along its axis. The permeability distributions of the four sections along the filter axis are almost the same, However, the used filter displayed a random and nonuniform permeability distribution along filter axis and its perimeter, when both type of filters were tested under the same environment with the same test setup. The used filter displays the same or better permeability in section 111 area. But the filter permeability at area section IV area is much less than that of the unused filter as shown in figure 10. Along the filter chamber wall, area section 111 always display a lower pressure field and that of area IV displayed a higher pressure field. Reverse gas flows were also monitored during the gas stream flowing process at a range of pressure level close to filter section area 111, These observations were consistent with different chamber pressure levels. This indicates that the pressure field in the filter chamber can not be assumed with a laminar flow or a steady state flow for flow process simulation.

Pressure fluctuations also were observed within the candle filter along the axis of the filter as the gas stream filtered through the filter wall. The pressure fluctuations are also consistent with the permeability variations of the filter under tested. A small scale reverse flow were also observed within the filter cavity with a flow pattern resemble outside flow pressure field.

These findings provide insights into the different pressure field distributions can happen both outside and inside the filter. These changes agrees with the variations of the permeability changes of the filter after its operation in the field. The changes of the permeability y indicate a random pattern and the induced pressure distribution will affect the efficiency of particulate filtration and

the back pulse cleanup. The pressure variation is also filter chamber pressure related. At much higher filter chamber operation pressure, the pressure field fluctuations could be worse. More severe adverse pressure field distributions may appear in both the filter chamber and the filter cavity. Blind cleanup spots or dust patches may have better chances to deposit along the filter surface to generate a vicious circulation.

Thermal cycles, chemical attacks did generate microcracks along the inner surface wall of the filter. The changes of the filter permeability after its field operation make the filter assembly a function of time, Without a optimized dust cake removal system, nonuniform dust cake removal is inevitable, which will definitely contribute to the patching of dust cake along filter surface. The randomly distributed filter permeability and the defects of filter integrity maybe the primary causes of the failure of ceramic filters. Piled dust cake, dust pileup induced thermal and mechanical stress applied on filter clusters may be the secondary causes that caused filter failures.

At Prairie View A&M University, we decide that we can not afford keep testing filters at a very high operation cost without knowing the fundamental variation and mechanism of dust cake cleaning,

These test data can be served as a filter performance data base to support numerical simulation analysis, back pulse cleanup optimization and filter failure analysis, As more test data are collected at PV A&MU, it can be utilized to support researchers, including professor M. Jhon of Carnegie Mellon Universit y and professor G. Ahmadi of Clarkson University on the verification of their numerical simulation analysis for back pulse flow and particulate flow pattern per PV A&MU research setup configuration.

In the future, PV A&MU will also report all of the test data to D.O.E. to support filter research institutes and filter industry for as required.

The research efforts planned at PV A&MU in the future will include the following areas:

- Measurement of filter permeability and flow rate under controlled environments on various filters.

- Measurement of back pulse pressure distribution in filter chamber for candle filters with and without dust cake

- Back pulse pressure distribution studies for unused and used filters for back pulse cleaning design optimization.

- Pressure field measurement for filter cluster during back pulse cleaning process.

- The optimization on back pulse system design.

Application and Benefits

Even dust layer deposition on filter is particle size and cohesive force dependent, an efficient dust cake removal system can help prevent excessive dust cake deposit on filter surface and eliminate ash bridging problems contributing to the failures of ceramic filters, Thermal induced load which damaged candle filters could be eliminated as ash bridging disappears. Test data collected by this research program can help filter researchers verify the accuracy of their numerical simulation results prior to extensive simulation on filter system design and analysis.

Future Activities

More measurements and analysis will be performed on filter clusters within a bench scale filter chamber to help optimize the back pulse plenum system design,

Acknowledgements

We would like to thank our Contracting Officer's Representative, Dr. Norman Holcombe, filter cluster leaders, Dr. T. K. Chiang and Dr. Duane Smith, and Mr. Charlie Komar as well as the management at DOE/METC for their extensive support on this research program and made our visits to other research institutes and filter industries possible for helpful technical discussions. Special thanks to Mr. Komar for all of his efforts in helping establish Hot Gas Cleanup (HGCU) research program at Prairie View A&M University.

References

Alvin, M. A., Tressler, R. E., Lippert, T. E., Diaz, E.S. and Smeltzer, E. E., 1994, “Durability of ceramic filter” Proceedings of the Coal Fired Power System 93- Adavances in IGCC and PFBC Review Meeting, U.S. Department of Energy

Bruck, G.J. and Isaksson Juhani, 1994, "Karhula Hot Gas Cleanup Test Results” Proceedings of the Coal Fired Power System 93- Advances in IGCC and PFBC Review Meeting, U.S. Department of Energy

Goldsmith, R. L., September, 1992, "Ceramic Filters for Removal of Particulate from Hot Gas Streams”, Proceedings of the Twelfth Annual Gasification and Gas Stream Systems Contractors Review Meeting, Volume 1

Heather M. McDaniel, Ronald K Staubly, Venkat K, Venkataraman, June, 1994, “Proceedings of the Coal Fired Power System 94- Advances in IGCC and PFBC Review Meeting” Volume 1, U.S. Department of Energy

Smoot, L.D. and Smith, P. J., 1985, “Coal Combustion and Gasification” Plenum Press, New York, NY

Klignspor, J.C. and Cope, D., FGD Handbook, May, 1987, “Flue Gas Desulfurization Systems” ICEAS/B5, International Energy Agency Coal Research, London, United Kingdom

Mei, D., 1995, “Characterization and Testing of Ceramic Filter and Dust Cake for Hot Gas Cleanup Program”, Summer Research Study report presented at METC, United States Department of Energy

Pontitus, D.H. and Starrett, H. S., 1994 “Properties of Ceramic Candle Filters” Proceedings of the Coal Fired Power Systems 93- Advances in IGCC and PFBC Review Meeting, U.S. Department of Energy

Zievers, J. F., Eggerstedt, P. M., Aguilar, P.C. and Zievers, E, C., 1993, “Some Ceramic Options” Proceedings of the Coal Fired Power Systems 93- Advances in IGCC and PFBC Review Meeting, U.S. Department of Energy

APPENDIX A

PERMEABILITY TEST DATA OF UNUSED AND USED FILTERS

UNUSED FILTER

SECTION I EXPOSED		SECTION 2EXPOSED		SECTION 3EXPOSED		SECTION 4 EXPOSED	
Time(min)	Press(psi)	Time(min)	Press(psi)	Time(min)	Press(psi)	Time(min)	Press(psi)
0.00	10.72	0.00	10.79	0.00	10.65	0.00	10.37
0,50	5.08	0.50	5.12	0.50	5.01	0.50	4.96
1.00	2.43	1.00	2.48	1.00	2.37	1.00	2.35
1.50	0.69	1,50	0.75	1.50	0.70	1.50	0.63
1.68	0.00	1.75	0.00	1,71	0.00	1.69	0.00

SECTION 1 EXPOSED		SECTION 2 EXPOSED		SECTION 3 EXPOSED		SECTION 4 EXPOSED	
Time(min)	Press(psi)	Time(min)	Press(psi)	Time(min)	Press(psi)	Time(min)	Press(psi)
0.00	15.40	0.00	15,13	0.00	15,34	0,00	15.63
0.50	10.85	0.50	10.59	0.50	10,88	0.50	10.92
1.00	4.95	1.00	4.78	1.00	485	1,00	5.02
1,50	2.10	1.50	2.15	1.50	1.98	1,50	2.05
2.00	0.48	2.00	0.33	2,00	0.36	2.00	0.44
2,11	0.00	2.08	0.00	2.10	0.00	2,18	0.00

UNUSED FILTER

SECTION 1 EXPOSED		SECTION 2 EXPOSED		SECTION 3 EXPOSED		SECTION 4 EXPOSED	
Time(min)	Press(psi)	Time(min)	Press(psi)	Time(min)	Press(psi)	Time(min)	Press(psi)
0.00	20.27	0.00	20.39	0.00	20.22	0.00	20.37
0.50	16.14	0.50	16.09	0.50	16.17	0.50	16,10
1.00	11.29	1.00	11,33	1.00	11.23	1.00	11,29
1.50	6.59	1,50	6.61	1,50	6.58	1.50	6.77
2.00	2.98	2.00	2.93	2.00	2.88	2.00	3,02
2.50	0.82	2.50	0.84	2,50	0.78	2.50	0.85
2.72	0.00	2.75	0.00	2,68	0.00	2,70	0.00

USED FILTER

SECTION 1 EXPOSED		SECTION 2 EXPOSED		SECTION 3 EXPOSED		SECTION 4 EXPOSED	
Time(min)	Press(psi)	Time(min)	Press(psi)	Time(min)	Press(psi)	Time(min)	Press(psi)
0.00	10,79	0.00	10.75	0,00	10.75	0.00	10,63
0.50	7.57	0.50	5.98	0.50	4.55	0.50	8.44
1.00	5.66	1.00	2.94	1.00	2.89	1.00	7.31
1.50	4.08	1,50	1.83	1.50	1,53	1.50	6.05
2.00	2.84	2,00	0,29	1.85	0.00	2.00	4.78
2.50	0,87	2.13	0.00			2.50	3.28
2.86	0.00					3.00	1.11
						3,50	0.12
						3.70	0.00

SECTION 1 EXPOSED		SECTION 2 EXPOSED		SECTION 3 EXPOSED		SECTION 4 EXPOSED	
Time(min)	Press(psi)	Time(min)	Press(psi)	Time(min)	Press(psi)	Time(min)	Press(psi)
0,00	15,86	0.00	15,38	0.00	15.82	0.00	15.80
0,50	10.66	0.50	12.82	0.50	12.23	0.50	12.13
1,00	6.85	1.00	7.81	1.00	7.37	1.00	9.14
1,50	3.72	1.50	4.37	1.50	3.01	1.50	6.58
2.00	1.62	2,00	1,86	2.00	0.87	2.00	4.49
2.50	0.41	2.50	0.49	2.40	0,00	2.50	2.78
3.00	0.00	2.61	0.00			3.00	1.48
						3.50	0,60
						4.00	0.12
						4.25	0.00

USED FILTER

SECTION I EXPOSED		SECTION 2EXPOSED		SECTION 3EXPOSED		SECTION 4EXPOSED	
Time(min)	Press(psi)	Time(min)	Press(psi)	Time(min)	Press(psi)	Time(min)	Press(psi)
0,00	20.57	0.00	20.15	0.00	20.60	0.00	20.42
0.50	15,16	0.50	14,78	0.50	13,64	0.50	18.01
1.00	12,75	1.00	10.64	1.00	9,04	1,00	16.19
1.50	8,17	1,50	7.01	1.50	3,96	1.50	14.64
2.00	5.27	2.00	4.03	2.00	1.88	2.00	13,03
2.50	2.61	2.50	1.22	2.50	0.35	2.50	11.06
3.00	1.02	3.00	0.25	2.79	0,00	3.00	9.92
3.50	0.00	3,09	0.00			3.50	7.04
						4.00	4.55
						4.50	2.07
						5.00	0.31
						5.12	0.00

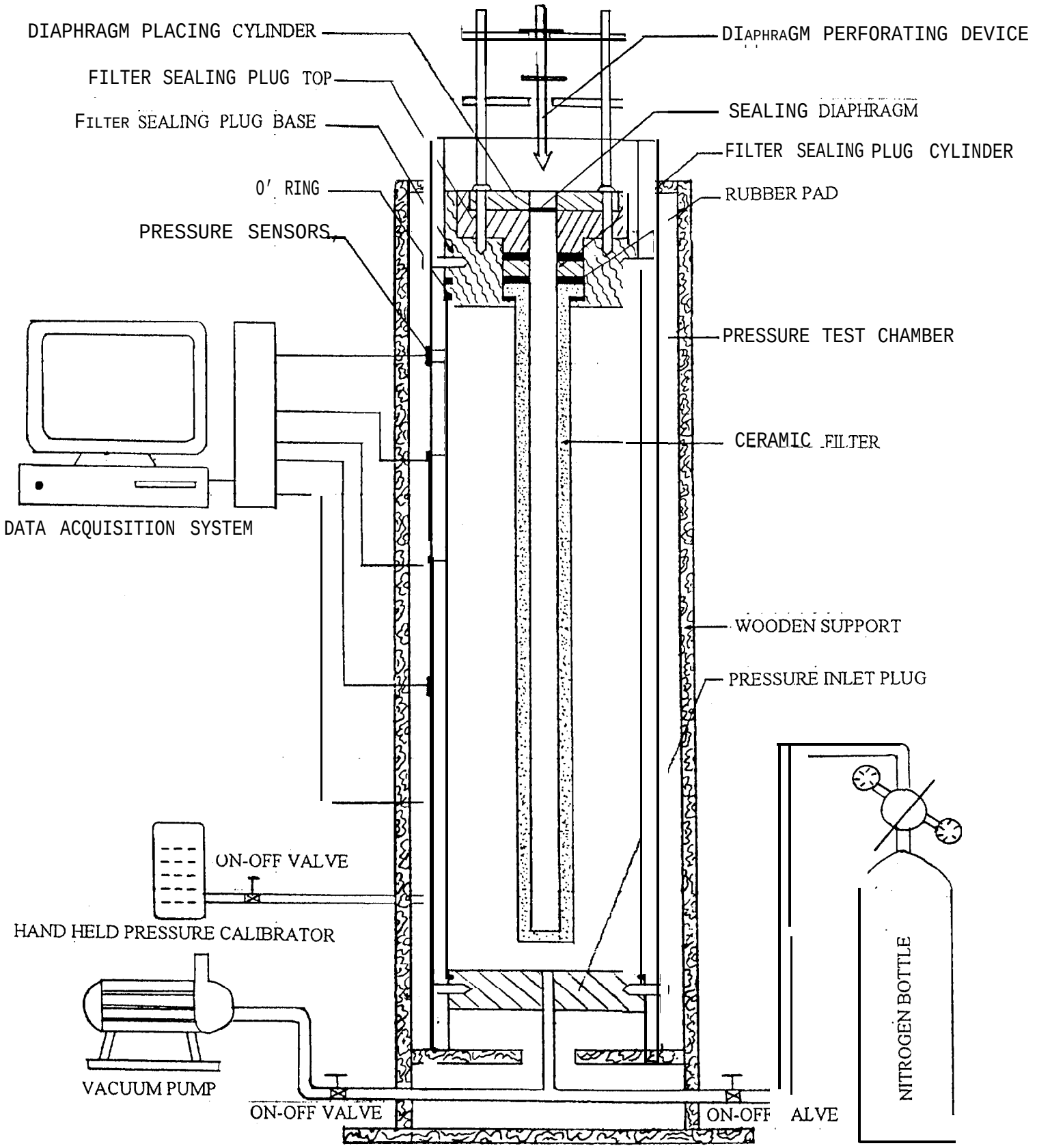

Fig. 1 SCHEMATIC DIAGRAM FOR UNUSED AND USED CERAMIC FILTER TEST

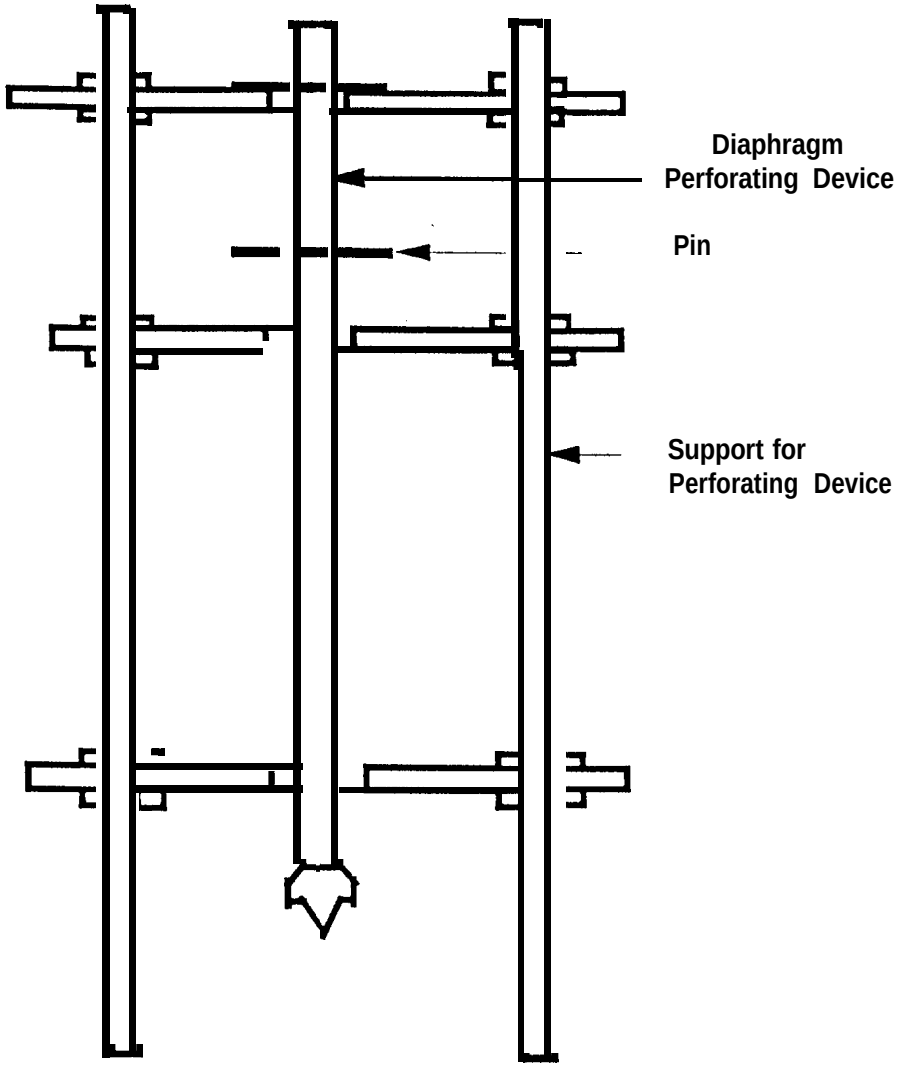

Figure 2 : Pressure Sealing Diaphragm Perforating Device

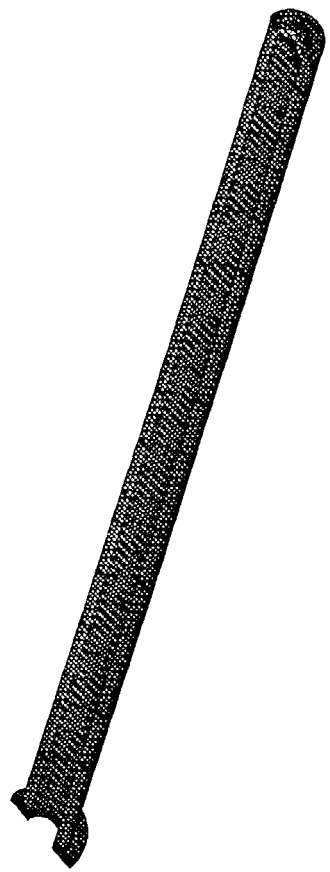

ANSYS 5.0 A 2o
JUN 25 1996
13:14:11
PLOT NO. 1
ELEMENTS
TYPE NUM

XV =-0.298836
YV =-0.429547
ZV =-0.852166
*DIST=0.738934
*XF =0.046958
*YF =0.055429
*ZF =0.728796
A-ZS=-56.38
CENTROID HIDEN

Fig. 3 Model of the filter

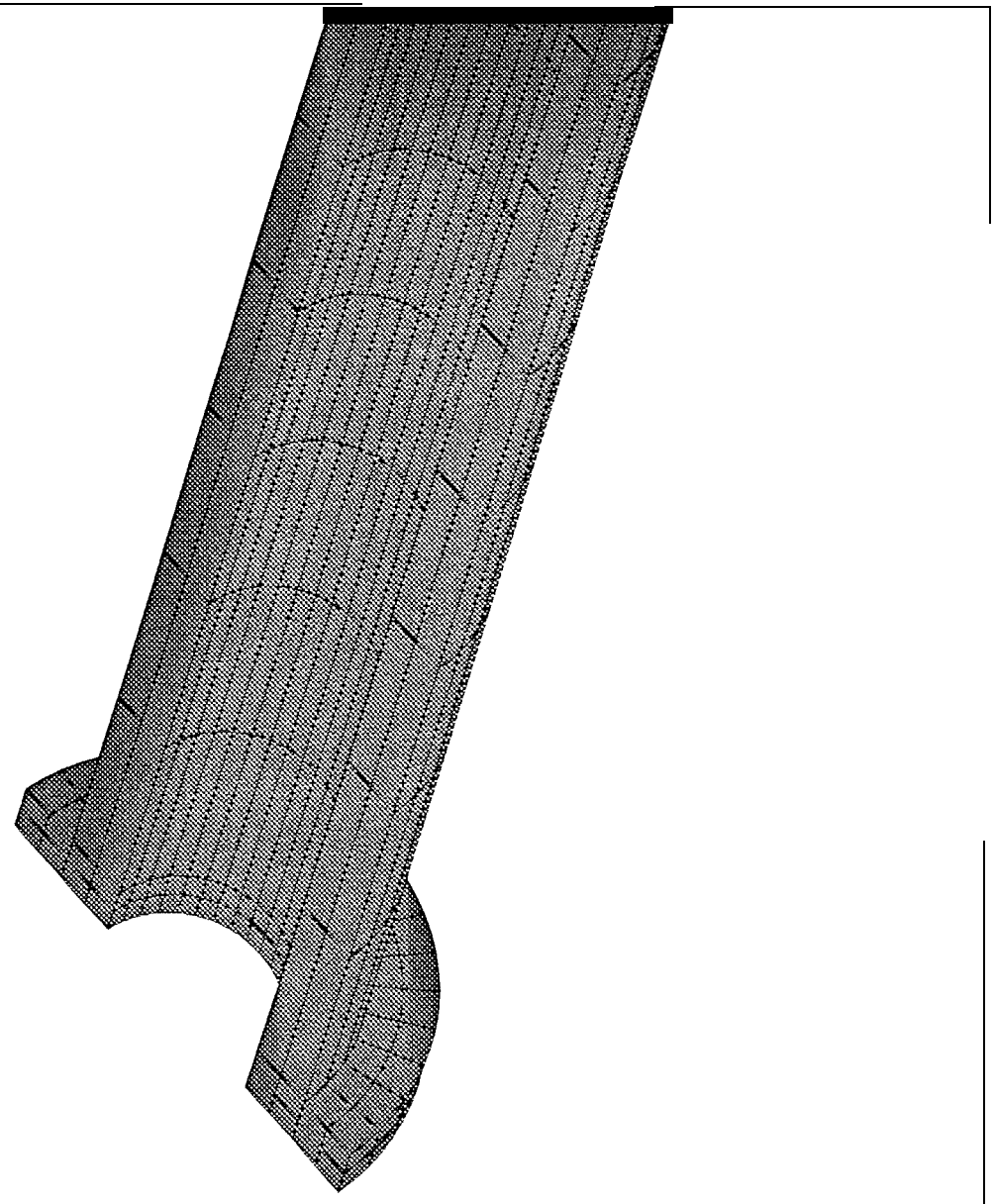

Fig. 4 Blow up of the model (Filter) near the neck with element meshing

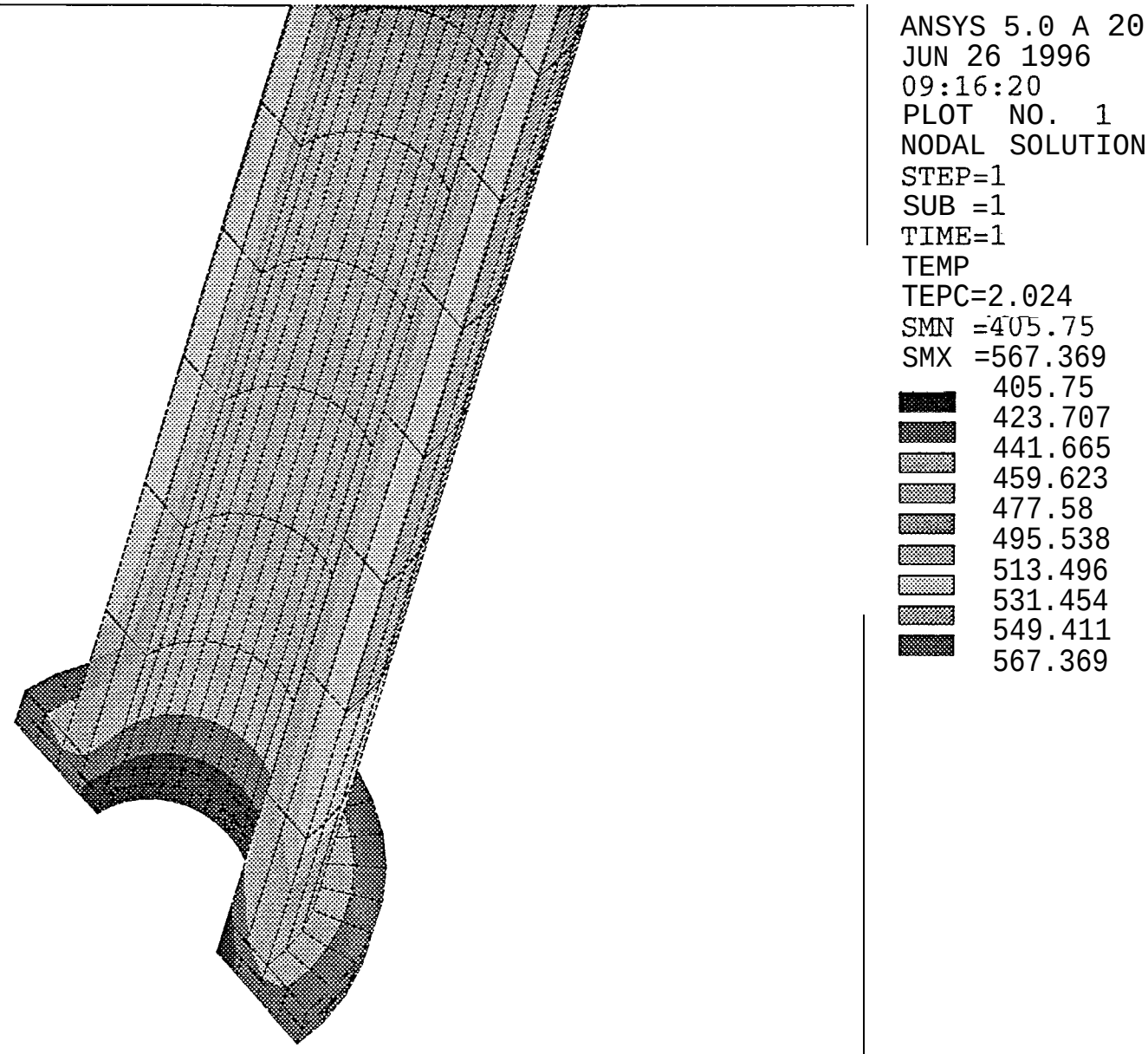

Fig. 5 Temperature contour from FEM ANALYSIS

(a)

(b)

(c)

Figure 6 (a) Metallographic photo of the unused ceramic filter showing the double layer structure, x80, (b) Microstructure of the inner layer of unused and (c) used ceramic filters, x200.

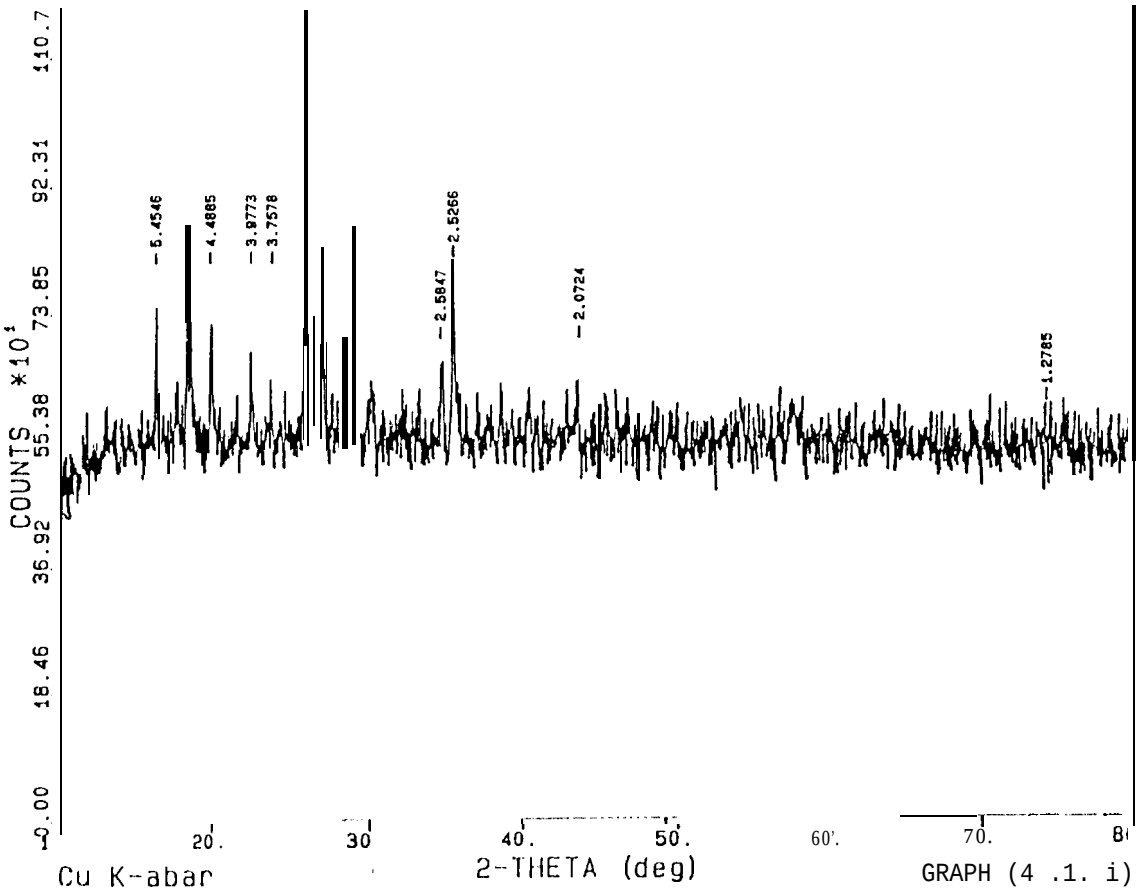

Figure 7 XRD spectrum of the deposition and reaction layer on the surface of the used ceramic filter,

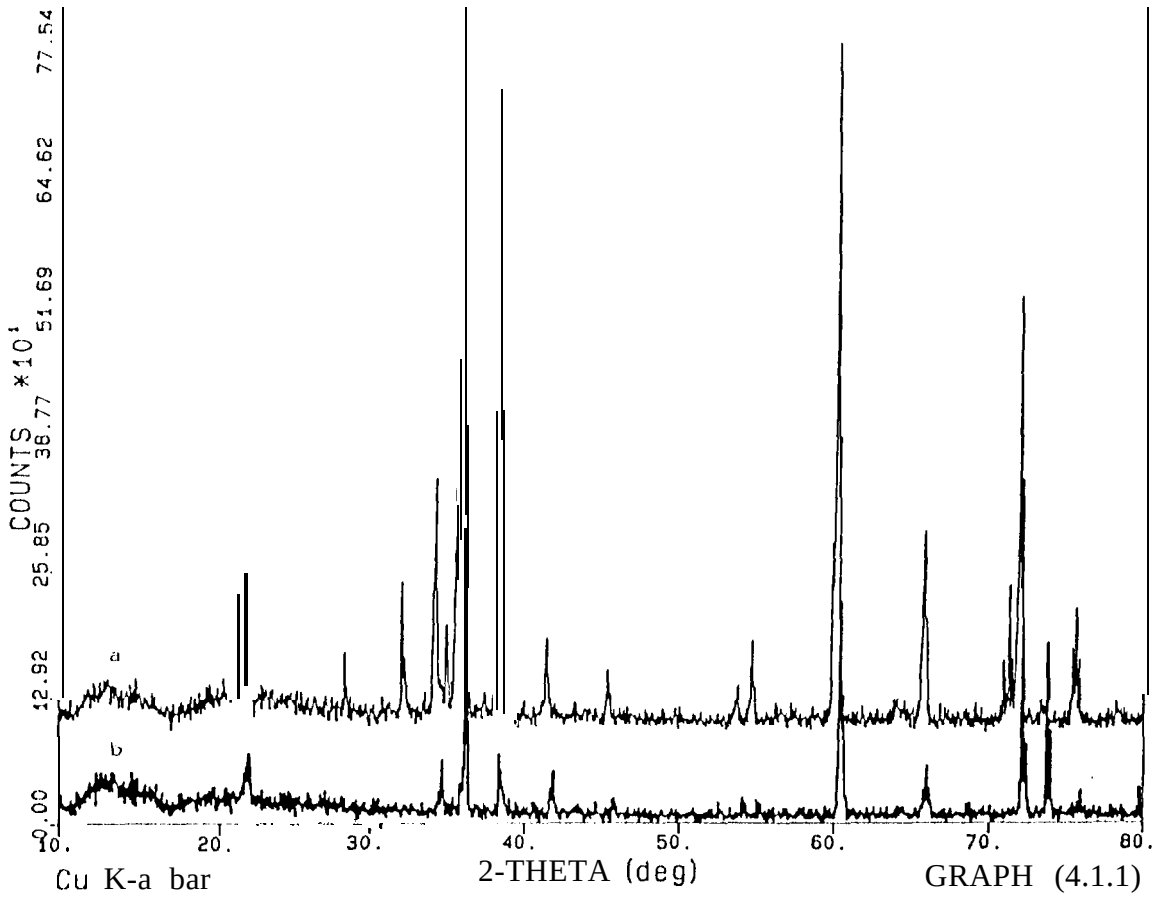

Figure 8 XRD spectra of the outer layers of (a) the used and (b) the unused ceramic filters, showing changes in crystal plane spaces after usage.

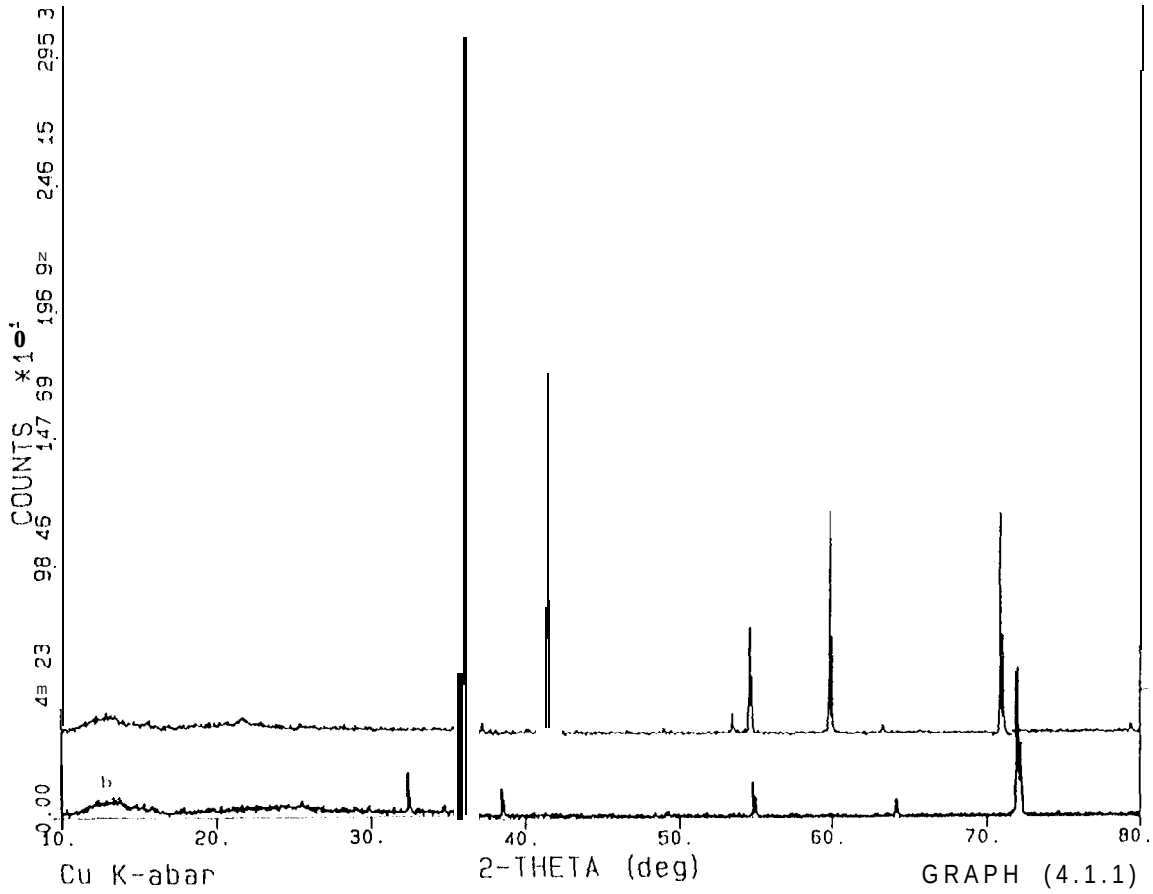

Figure 9 XRD spectra of the inner layers of (a) the used and (b) the unused ceramic filters, showing changes in crystal plane spaces and orientation after usage.

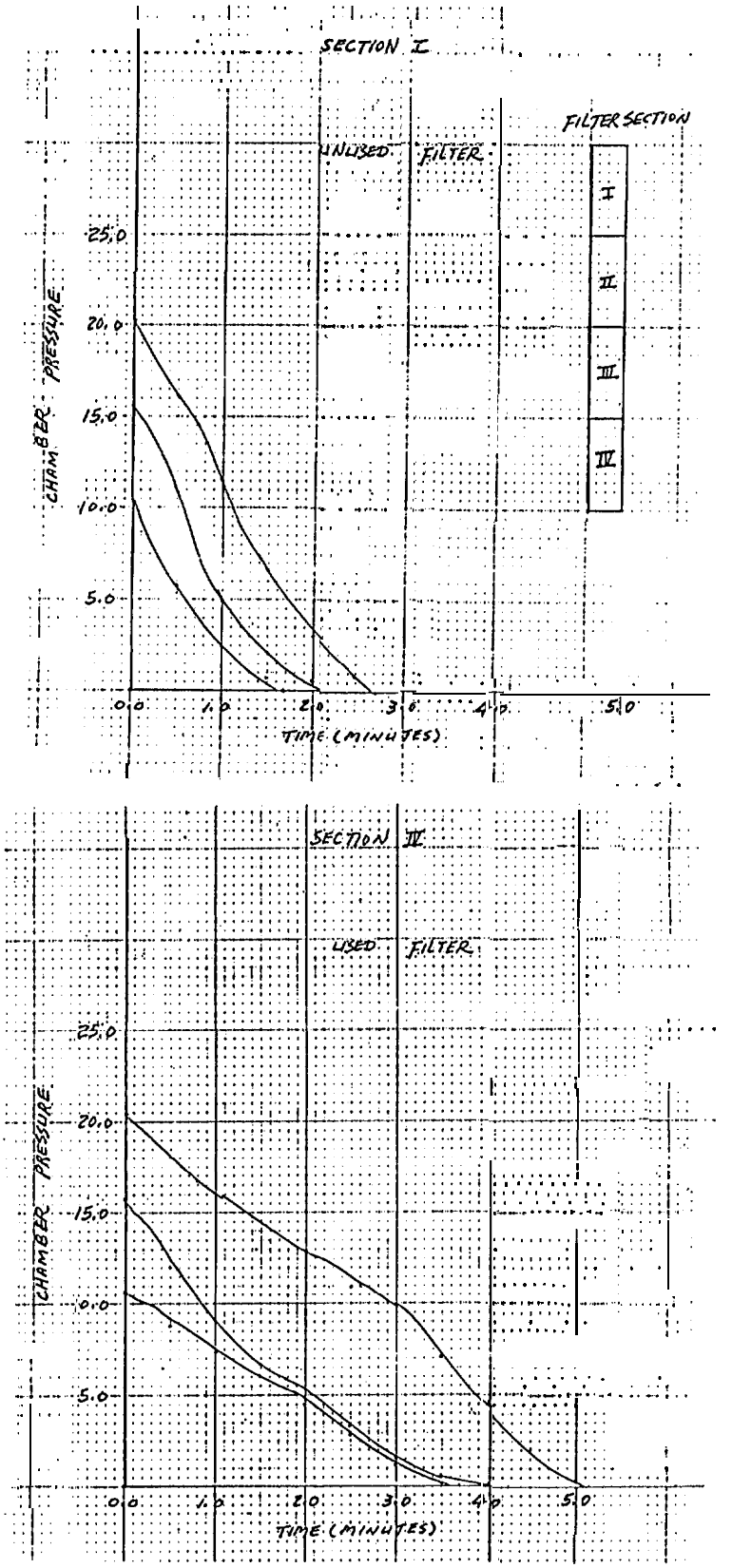

Figure 10: Filter permeability variations of used filter compared to unused filter

Ceramic Component Development Process Analysis

D. Boss (dboss@nwu.edu; 847-491-3373)
S. Sambasivan (ssambasivan@nwu.edu; 847-491-4619)
C. Kuehmann (ckuehmann@nwu.edu; 847-491-2439)
BIRL/Northwestern University
1801 Maple Ave.
Evanston, IL 60201

K. Faber (k_faber@nwu.edu; 847-491-2444)
Northwestern University
MEAS Materials Science & Engineering
2225 N. Campus Drive
Evanston, IL 60201

Abstract

The development of ceramic components and coatings is critical to the demonstration of advanced fossil energy systems. Ceramic components and coatings will play critical roles in hot-gas filtration, high-temperature heat exchangers, thermal barrier coatings, and the hot-section of turbines. Continuous-fiber ceramic composites (CFCC) are expected to play an increasing role in these applications. This program encompassed five technical areas related to ceramic component development for fossil energy systems.

Filter Process Evaluation

The development of reliable and efficient hot-gas filters is critical to the acceptance of fluidized-bed combustion, coal gasification, direct coal-fired turbines, and fuel cells. This effort focused on reviewing the status of the processes for five filter developers in terms of process monitoring/control, process repeatability, identification of critical operations, and the path to process scale-up. The status of the selected programs were reviewed in a one-day site visit, which was performed under the auspices of a non-disclosure agreement to protect the process information of each manufacturer. To date, site visits have been done with Techniweave (oxide/oxide CFCC), B&W (oxide/oxide CFCC), and Pall Corporation (Fe_xAl) have been performed, negotiations to visit DuPont Lanxide Composites (PRD-66 oxide composite) are continuing, and preliminary discussions with a fifth organization have been initiated. A topical report presenting the status of each of the programs, and including recommendations for future needs will be delivered at the conclusion of this task.

Interface Coatings

The use of CFCC components is currently limited by the environmental and thermal

Research sponsored by the U. S. Department of Energy's Morgantown Energy Technology Center, under contract DE-AC21-95MC32085 with Northwestern University, 633 Clark Street, Evanston, IL 60208, telefax 847-491-4486

stability of both the fiber reinforcement and the fiber-interface coating, A state-of-the-art review for fiber-interface coatings is being prepared. The report will review current production materials, the status of fiber-interface development work at NASA, USAF, AFOSR, DARPA, and other leading organizations, provide insight into which interface materials may be suitable for a variety of CFCC systems and application environments, and discuss the future direction of fiber-interface materials development.

Protective Coatings for SiC Heat Exchanger

Several advanced power systems (EFCC and HITAF) will rely upon SiC heat exchangers, which should withstand exposure to coal combustion by-products at temperatures over 1200°C for thousands of hours, A Protective coating is needed to meet this performance need. The coating should protect the SiC from the environment, resist erosion by the hot-gas stream and particles, and withstand thermal cycling/shocks without spalling. A review of efforts underway by other researchers, existing literature and phase diagrams, and simple thermodynamic modeling was used to identify 10 candidate materials for testing and evaluation, A topical report summarizing the results of this effort is being prepared,

Materials Screening

The materials identified in the previous task are being exposed to a Illinois #6 slag sample (provided by John Hurley at UND-EERC) from the Baldwin Plant. Bulk samples of each material are being partially immersed in this slag at 13500C for 100 hours with 100 seem of moistened air flowing through the retort. After exposure, the samples undergo microanalysis to determine the extent of reaction and x-ray diffraction for phase identification. The hot hardness of the candidate materials will also be determined as a measure of their erosion resistance at temperature. A topical report summarizing this effort will be prepared.

Data Analysis

A number of test methods are being used to assess the mechanical and physical properties of hot-gas filters. The test methods used by filter manufacturers during development, independent evaluation efforts, and post-exposure evaluation all provide insight to the materials properties, but the results are not directly comparable. This effort focuses on reviewing the current filter test methods, identifying means for data comparison, and suggesting preferred test methods for future activities.

Acknowledgment

A special thanks to Ted McMahon, for his support and input to the program as the COR, and to Lee Paulson for his input for the protective coatings task, This contract has a period of performance from 9/29/95 to 9/28/96

Performance of Ceramic Membrane Filters

Rajesh K. Ahluwalia (walia@td.anl.gov; 708-252-5979)
Kwan H. Im (im@td.anl.gov; 708-252-5985)
Howard K. Geyer (geyer@td.anl.gov; 708-252-5995)
Argonne National Laboratory
9700 South Cass Avenue, Building 207
Argonne, IL 60439-4841

David L. Shelleman (814-865-0634)
Richard E. Tressler (814-865-7961)
The Pennsylvania State University
101 Steidle Building
University Park, PA 16802

Introduction

CeraMem Corporation's ceramic-membrane coated, dead-end ceramic filters offer a promising alternative to ceramic candle filters provided long-term operational and reliability issues are resolved. One outstanding operational issue pertains to regenerability of filter passages by the simple back pulse technique in a repeatable manner over a time span of thousands of hours. For commercial acceptance, the tolerance of the CeraMem cordierite material to exposure to alkali-containing combustion gas, being able to absorb Na_2O without serious degradation of the mechanical properties at use temperatures, must be demonstrated. The performance must be correlated to the phase composition and microstructure after exposure.

The thermal and chemical aging at use temperature may significantly alter the thermophysical and mechanical properties of these materials in ways which must be documented. In fact, the values of thermal expansion coefficient, thermal conductivity, and elastic moduli as a function of temperature must be measured for the as-fired or as-received materials in addition to the thermally and chemically aged materials. These parameters determine the thermal gradients in the components during transient and steady state operating conditions, and the thermoelastic stresses which develop in the components as a result of these thermal gradients. The thermoelastic stresses can be accurately mapped in a given component if the temperature distributions are known (assumed and/or calculated) and the thermomechanical properties are known as a function of temperature and aging history. In conjunction with a knowledge of the strength distribution of the material as a function of temperature and aging exposure, these thermoelastic stress calculations can be used to predict survival of the components in actual or simulated use.

Research sponsored by the U.S. Department of Energy's Morgantown Energy Technology Center, FTPA Number ANL-49966, B&R Code AC-15.

In addition, when the details of the microstructural changes are established as a function of temperature and thermochemical aging and the properties are related in a cause-effect relationship, the microstructure (phase composition, grain size, pore size and shape) can be tailored to resist the deleterious changes.

Objectives

1. Develop a fluid mechanics and particle transport model for analyzing filtration and back pulse cleaning of dead-end ceramic membrane filters.

2. Develop a data base on the effects of thermal and chemical aging on flow behavior and thermophysical and mechanical properties of ceramic filters.

3. Develop the capability of predicting the probability of survival of commercial filters under anticipated service conditions from calculated thermoelastic stresses and measured material properties.

Approach

This program utilizes combined experience, skills and facilities at three organizations: Argonne National Laboratory (ANL), Penn State University (PSU) under subcontract to ANL, and CeraMem Corp. (not funded under this initiative). ANL is responsible for analytical modeling of filtration and pulse-cleaning operations, flow-through testing, and prediction of filter response to thermal cycling under realistic service conditions. PSU is responsible for measuring properties and microstructural changes of exposed filter specimens. CeraMem is charged with the responsibility of fabricating and supplying the filters, advising ANL on its experience with pulse cleaning, and conducting exploratory or confirmatory laboratory tests as needed.

Project Description

We previously reported on the analysis of forward and reverse flows in dead-end filters, based on models for jet entrainment and mixing, fluid flow in filter passages, and venturi nozzle and diffuser [Ahluwalia and Geyer, 1996]. A test apparatus, shown schematically in Fig. 1, was assembled to expose ceramic filter specimens to chemical environments simulating operation of pressurized fluidized bed (PFB) and integrated gasification combined cycle (IGCC) plants [Ahluwalia et al, 1995]. An air-blast elutriator was fabricated to feed ash at 0.5-2 g/h. It is particularly suitable for low feed rates and highly agglomerating ash such as the ash from Tidd plant. The feed rate in this device is controlled by the transport gas throughput and the speed of the chain conveying ash from the hopper to the suspension chamber. An ultrasonic nebulizer is used to feed alkaline water containing dissolved sodium chloride or sodium hydroxide. The gas-phase alkali concentration is controlled by the alkali content of water solution, vibration frequency of the nebulizer diaphragm and the flow rate of purge gas used to

entrain the mist produced by the ultrasonic action. A concentric tube arrangement is employed to

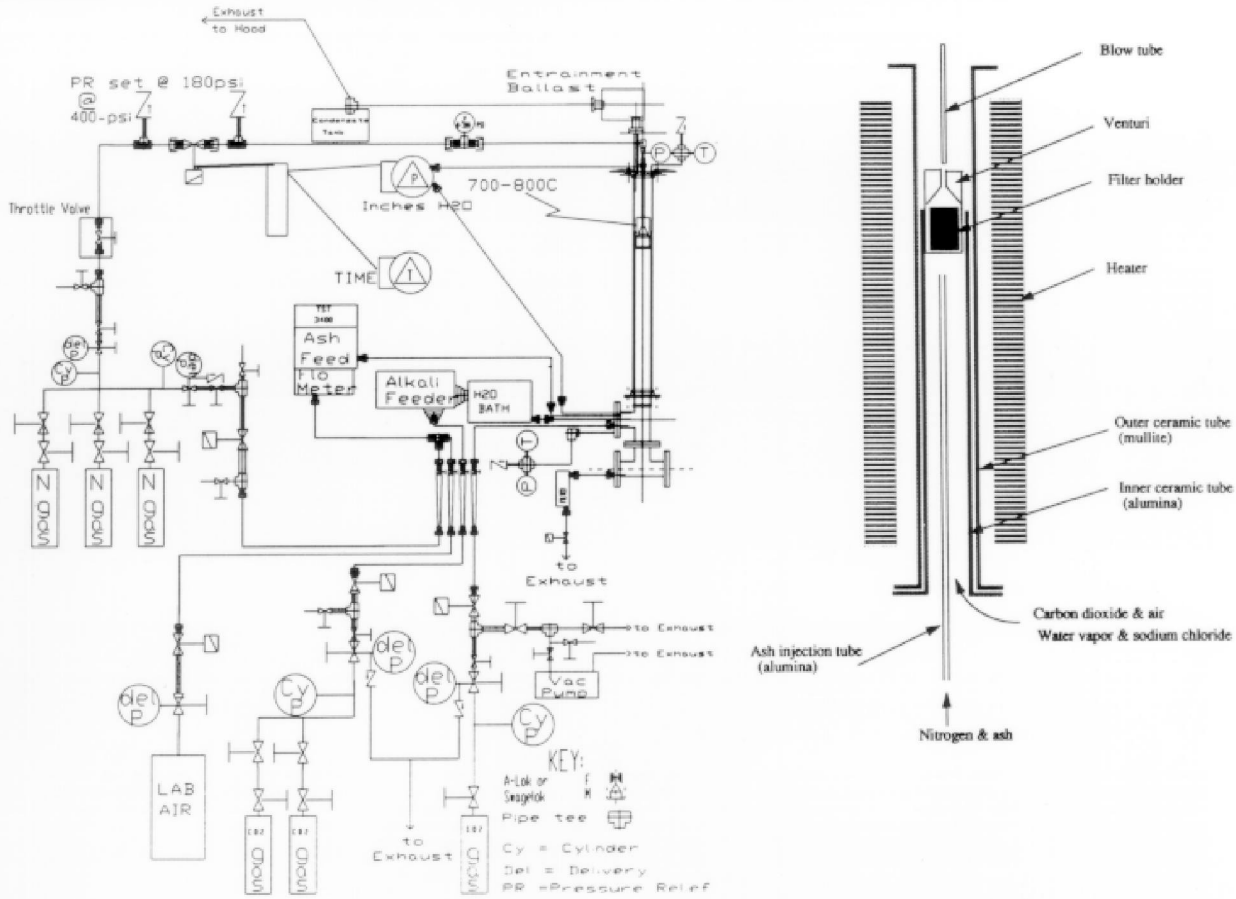

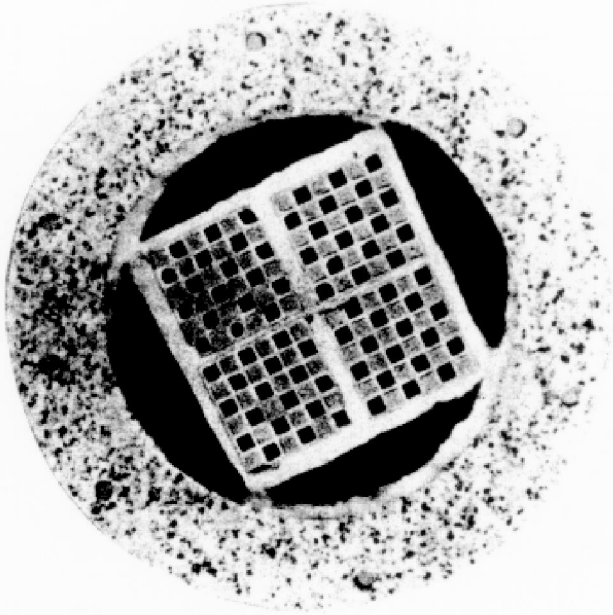

Figure 1. Schematics of the filter exposure apparatus, concentric tube arrangement and filter holder.

contain and heat the gases and position the filter holder which is machined from Inconel 625 and alonized for added corrosion resistance. The holder accommodates four 6 cell x 6 cell specimens (100 cells per square inch, 5.08-cm long) surrounded by dense ceramic fillers and held together with a steel clamp. For leak-tightedness, a compressible ceramic mat is placed between the filters and between the filters and the fillers. The clearance between the filters and the filter holder is also packed with the ceramic mat.

The pulse gas from a high-pressure nitrogen reservoir is directed into a blow pipe and issues from a small blow hole of 1.25-mm diameter. It discharges into the plenum region and entrains some of the clean hot gas. The resulting mixed jet enters the venturi atop the filter holder. It is estimated that a differential pressure of about 22 kPa can be generated in the venturi at a reservoir pressure of 10 bar and a trigger pressure of 40-cm H_2O. Pulse duration and frequency are adjustable by means of a computer-controlled solenoid valve.

A number of tests were conducted to ensure leak tightness and optimize the method of assembling the filter specimens inside the holder. Extensive data was obtained to characterize the flow behavior of the clean filter. Figure 2 summarizes the selected data on filtration pressure drop (ΔP) vs flow rate at different gas temperatures and on ΔP vs temperature at different flow rates. The available data is consistent with an effective permeability of 5.9×10^{-10} m for the Ex-80 membrane-coated cordierite monolith having 48% porosity, 0.4 cc/g pore volume and 12.5 μm mean pore size.

Results

Four long-duration tests have been conducted in which 100-cpsi channel filters were exposed to ash collected downstream of the cyclone separator at the PFBC plant at Tidd. The median diameter of ash is 2.8 μm and the top size is less than 10 μm. The pressure drop across the filters was monitored during the test. A data base has been established on the microstructure and the mechanical properties of the as-received filter material. Effect of thermal aging on the mechanical properties has been determined. Measurements are continuing to determine the changes in the microstructure and the mechanical properties after exposure in the four tests.

System Checkout. A long duration test (Run 1) lasting twenty-five days, was run to study the behavior of system components under different operating conditions. The apparatus was operated in an attended mode in which ash and alkali were fed during the day time only. There was no SO_2 injection and the pulse valve was operated manually. Figure 3 shows the pressure trace for different gas temperatures (800-950°C furnace temperature), gas flow rates (6.4-10 slm), pulse gas reservoir pressures (7.8-11.2 bars), time between pulses (0.5-5 h), and number of pulses (1-4). The tests confirmed the existence of a conditioning time during which the baseline filtration pressure drop (ΔP after pulsing) increased steadily. Over the limited time

span, the filters could be regenerated at 900 °C by using pulse gas at 11.2 bar reservoir pressure.

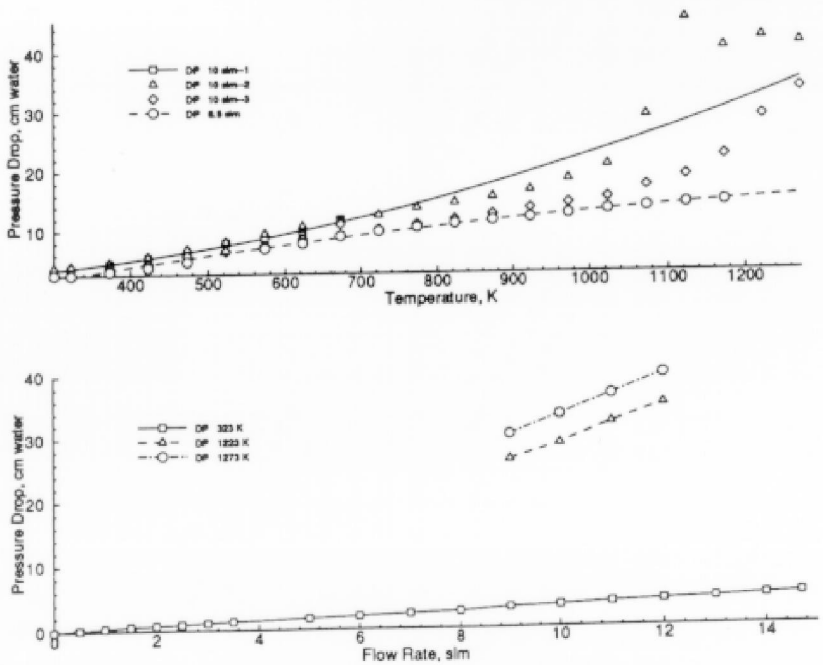

Figure 2. Pressure drop behavior of clean filter.

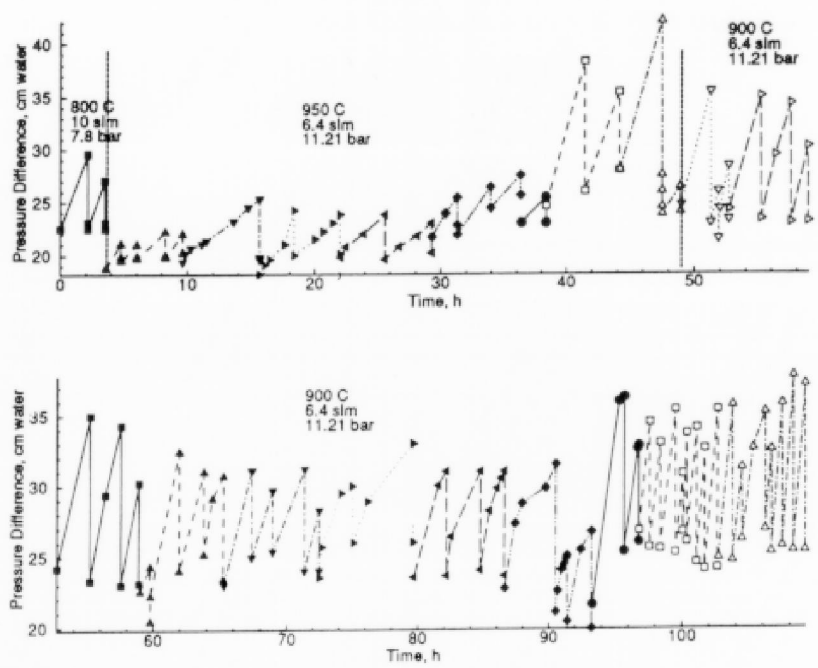

Figure 3. Filtration pressure drop and back pulse cleaning during system checkout (Run 1).

Filter regenerability was not affected by time interval between pulses. A single pulse was generally sufficient to recover to the baseline ΔP. Incremental recovery in ΔP with multiple pulses was small. Various subsystems for gas handling, gas heating, pulse gas, filtration and ash feed operated reliably although leakage problems were experienced with the alkali feed system and corrected. Post test inspection of the filter specimens revealed no visual deterioration in integrity or ash penetration across the membrane walls.

Performance at 900 °C. A long duration test (Run 2) was conducted to expose filter specimens at 900 °C furnace temperature. Mean gas composition was 75.2% N_2, 13.9% CO_2, 3.3% O_2 and 7.6% H_2O. The contaminant loading was 900 ppmw ash, 70 ppmv alkali and 250 ppmv SO_2. The operation of the solenoid valve was computer controlled. A single pulse of nominal 1 s duration was used. The pulse frequency was 3/h at start of the test (0-18 h), once every hour during much of the test (18-1008 h), and increased to 2/h near the end. The reservoir gas pressure was 7.8 bar at start of the test (0-268 h), raised to and maintained at 9.8-11.3 bar during the middle portion (268-1015 h), and raised further to 14.6 bar near the end. Figure 4 depicts the pressure drop behavior at 2.4 cm/s face velocity. The data indicates a filter conditioning time of about 100 h during which the baseline ΔP increased from 15-cm H_2O (clean filter ΔP) to about 30-cm H_2O. Between 200-900 h, a steady saw-tooth ΔP profile was established with a pressure swing of about 7-10 cm H_2O between the pulses. Some ΔP excursions were observed due to an unresolved bug in the control software which unpredictably missed 1-5 pulse cycles at a time. Some excursions were caused by the heated line between the nebulizer and the inlet plenum developing a blockage due to NaCl deposits. In the steady-state mode of operation, the system was able to recover from these excursions. At about 980 h, both baseline ΔP and the pressure swing between the pulses started to climb gradually. At 1008 h, the pulse frequency was doubled after the pressure swing had reached 20-cm H_2O. This had the favorable effect of controlling the pressure swing although the baseline ΔP continued to climb slowly. At 1015 h, the reservoir pressure was raised to 14.6 bar in an attempt to control the baseline ΔP. Although temporarily successful, baseline ΔP resumed its climb. The situation was exasperated by the control software missing three consecutive pulses. At this point, the filter specimens could not be regenerated resulting in termination of the test.

Figure 4 also presents the fine details of pressure recovery following a pulse operation. It shows ability to regenerate the filter passages after pressure excursions as at 50 h, 385 h and 1000 h. It indicates limited incremental benefit in going to double (225 h, 275 h and 315 h) and triple (275 h and 1000 h) pulses spaced 200 to 400 s apart. For the filter specimens used in these tests, the characteristic time for pressure recovery appears to be less than 50 s.

Post test inspection revealed that the ceramic ash transport tube was clean. There were mounds of ash built up on the cement plugs at filter inlet. All channels were accessible to gas flow. There was no visual evidence of ash penetration across to the clean channels or of ash sintering. There were metal corrosion products on top of the venturi which came from the ballast tank. There was minimal deterioration of the

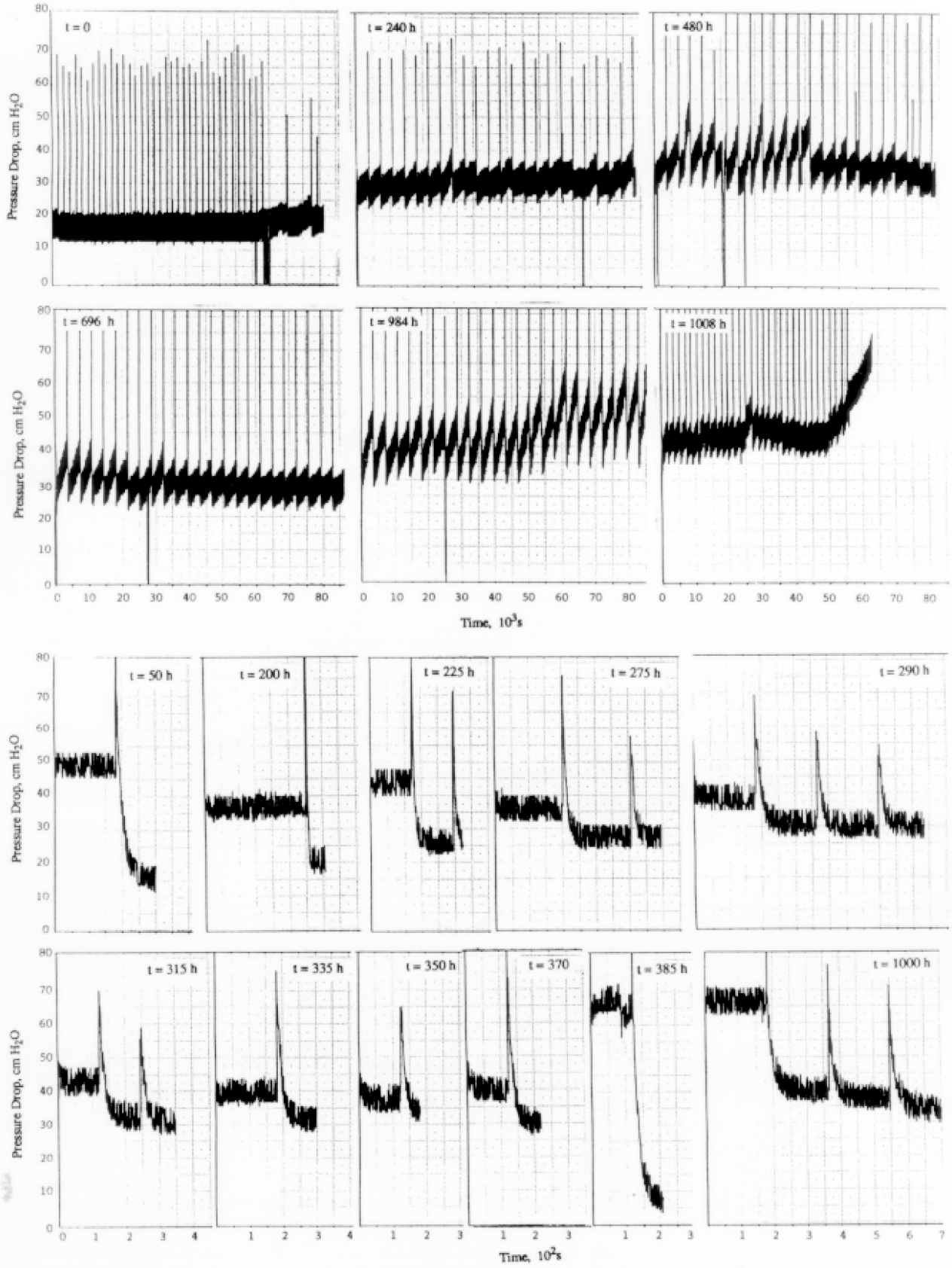

Figure 4. Pressure traces from 1050-h test at 900°C (Run 2).

alonized filter holder and venturi but the metal screws joining the holder and venturi were severely corroded and easily broken (as designed). Ash at various locations had different coloration. In order to analyze the pattern of residual ash filling up the passages, the channels were probed with a thin wire. From the resistance felt while inserting the wire, it was concluded that there was considerable variation of the residual ash content in the channels and along the passage length. To confirm these observations, one of the filter specimens was cracked near mid length. Optical macrographs of the fractured filter surface indicate that the channels are severely filled with ash.

Three of the four exposed filter specimens contained several transverse cracks which were clearly visible on the outer surfaces. The cracks are believed to have been caused by overtightening of the steel clamp used to hold the filter specimens together.

As stated earlier, several operational problems were encountered in Run 2 due primarily to the control software skipping several pulse cycles. This resulted in overpressurization of the inlet plenum and flow leakage from the glass tank housing the nebulizer. The leakage problem was solved with a redesign leading to the elimination of the glass tank. In order to resolve the effect of pressure excursions on the observed flow behavior, it was decided to repeat the test (Run 3) with a new control software employing a pulse schedule closer to the field practice. The schedule consisted of a double pulse, each of 100-ms duration and 100-ms apart. To minimize possible ash-membrane interaction, the pulse frequency was changed to 3/h regardless of ΔP. The test ran smoothly without experiencing any problems with ash feed, alkali injection or pulse gas system. The system was shut down for Christmas break after 364-h. Upon restart, the filters could not be regenerated with back pulsing and the test was terminated after 388-h exposure. The post test observations revealed no visual signs of filter deterioration. There were no surface transverse cracks since care was taken to not overtighten the steel clamp. Much later during Run 4, it was realized that the failure to regenerate the filter was related to the nozzle (blow hole) being nearly blocked by a small quantity of metal corrosion products. The blockage was easily relieved with water washing.

Performance at 800 °C. A 2000-h test (Run 4) was conducted in which the filter specimens were exposed to simulated combustion gas (3.3% excess oxygen) containing 7.6% H_2O, 11.2 ppmv NaCl and 1011 ppmw entrained ash. The filters were maintained at 800 °C. A single pulse of 1-s duration was used to regenerate the filter passages. Initially, the time interval between the pulses was set at 30 min which was reduced to 15-20 min as the ΔP swing became larger. Right at the start of the test, difficulty was experienced in regenerating the filter passages and was traced to the blow hole being blocked by the blow-tube corrosion products. The blockage problem was alleviated by continuously purging the blow tube with a small quantity of N_2 (less than 0.5 slm) and isolating it from the alkali rich gas. The reservoir pressure for pulse gas varied between 11.2 and 14.6 bars. As indicated in Fig. 5, the baseline ΔP was stable at 30-32 cm H_2O for exposure time less than about 1000 h. Over a longer time

period, it gradually crept up to above 50-cm H_2O. Consistent with the earlier experience, ΔP swing increased with exposure time from 1-cm H_2O to 10-cm H_2O. At various times attempts were made to investigate if the residual ash could be dislodged by allowing the filters to cool down to a lower temperature, back pulsing and raising the temperature back to 800 °C. The results were not encouraging although some success was gained early in the test. The observed variation of ΔP with temperature was quite remarkable (Fig. 6). For a clean filter, a single value of effective permeability (K_{eff}) can explain the measured ΔP as a function of temperature and flow rate. An exposed filter, after cold pulsing, has K_{eff} which is a strong function of temperature. After 1000-2000 h exposure, K_{eff} has even stronger temperature dependence.

Strength. Table I summarizes the average strength and standard deviation of the flexure specimens machined from as-received, thermally aged, and exposed filters. No significant changes in strength were observed as a function of temperature or membrane coating for the as-received 25 cpsi filters. Even after thermal aging at 800°C for 1000 hours, only a slight increase in strength was observed at 870 °C.

Flexure specimens machined from filters exposed at 1600 °F for 300 hours at the Ahlstrom Pyropower combustor in San Diego exhibited no significant changes in strength with the possible exception of the 870 °C data which showed a slight strength increase (depending on lot-to-lot variations).

As for the 100 cpsi filters, strengths that were independent of test temperature were again observed at 800 °C and 870°C. However, flexure specimens from filters exposed in Runs 3 and 4 exhibited approximately 44% and 33% reductions in strength, respectively. Even with the limited number of specimens tested (5 for Run 3 and 7 for Run 4) a relatively large amount of scatter was observed in the strength measurements, which suggests that hot corrosion of these filters may not be uniform. Additional strength testing and detailed characterization are needed to quantify the effects of hot corrosion on these filters.

The observed reductions in strength may be associated with the alkaline content used in the exposure runs. Flexure specimens from filters exposed in Run 3 exhibited a 44% reduction in strength and were exposed to ~70 ppm of sodium, while flexure specimens from filters used in Run 4 exhibited a 33% reduction in strength and were exposed to ~11 ppm of sodium. Powders from filters used in Runs 3 and 4 were analyzed by x-ray diffraction. While definite peaks for the nepheline [$(Na, K) Al SiO_4$] are present in the pattern obtained from filters exposed in Run 3, nepheline peaks are not as evident in the pattern for filters from Run 4. Peaks corresponding to nepheline may be present in pattern from Run 4 but are on the order of the background noise level.

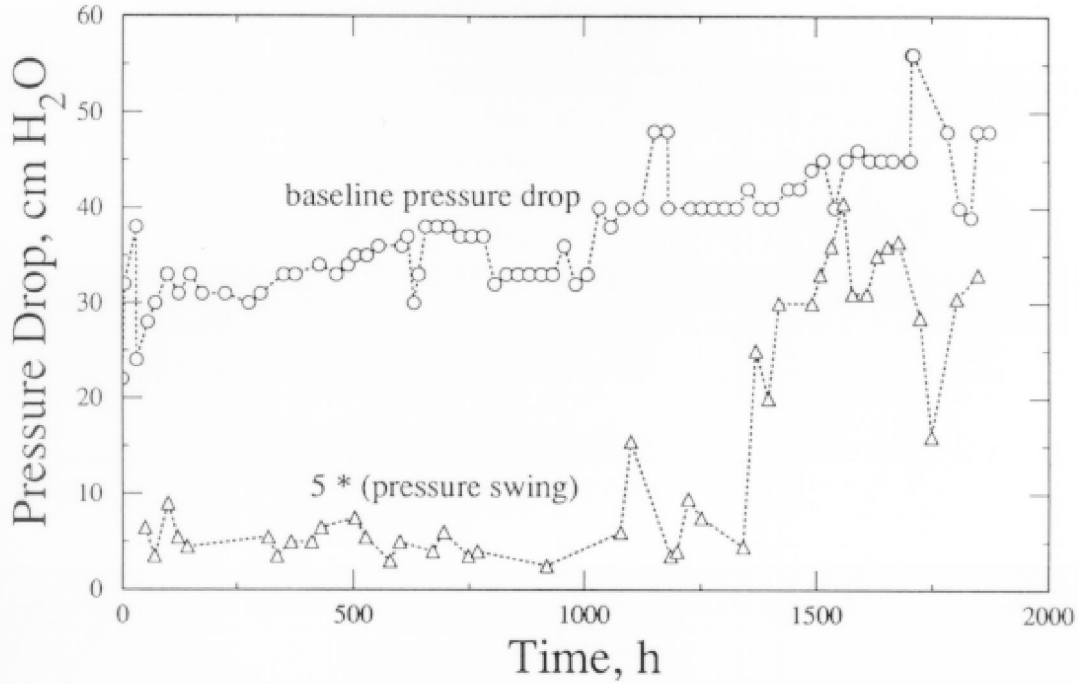

Figure 5. Variation of baseline pressure drop and pressure swing during the 2000-h test at 800°C (Run 4).

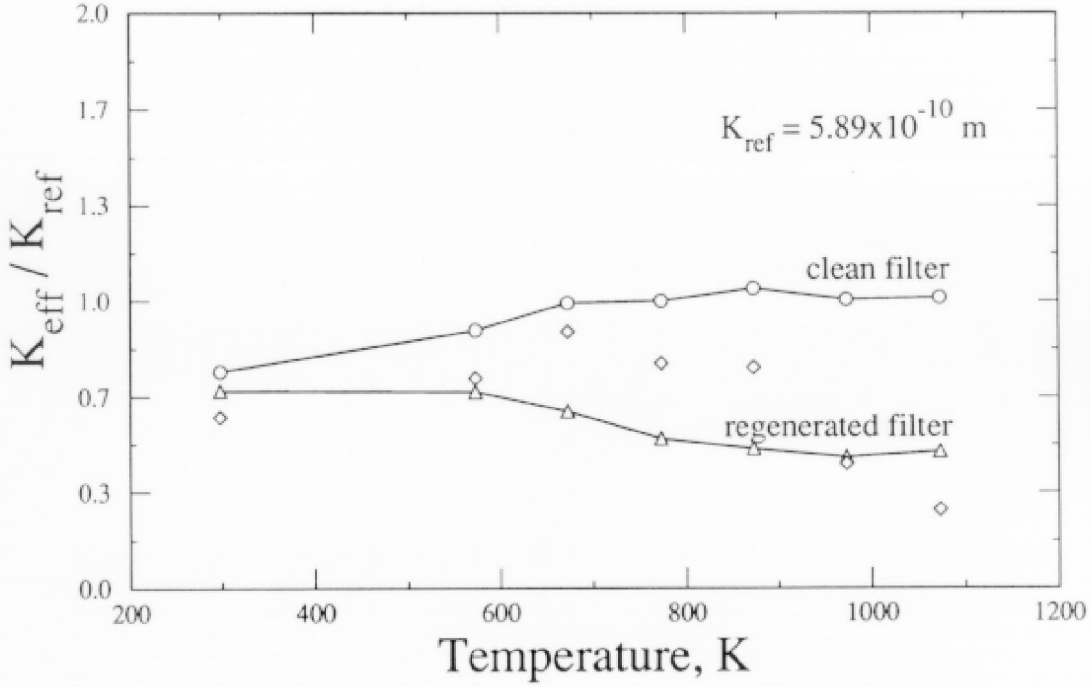

Figure 6. Temperature dependence of filtration pressure drop for clean (○) and regenerated (Δ, ◊) filters.

Table I. MOR (Modulus of Rupture) strength data from four-point bend tests

Size	Condition	Strength, MPa		
		25 °C	800 °C	870 °C
25 cpsi	As-received, Uncoated	9.5±0.6	9.7±1.5	10.8±1.3
	As-received, Coated	10.1±0.4	10.2±1.3	10.4±0.9
	As-received, Coated 1000 hrs @ 800 °C	9.1±0.8	11.4±0.9	11.0±0.8
	Ahlstrom 300 h [a]	10.4±0.7	12.3±2.2	12.5±1.0
	Ahlstrom 300 h [b]	10.9±0.7	11.3±1.8	10.7±1.5
100 cpsi	As-received, Coated	8.8±0.8	8.4±0.9	8.6±1.5
	Run 3: 388 h @ 900 °C		4.7±2.0	
	Run 4: 2000 h @ 800 °C		6.5±2.6	

a - Tensile surface of flexure specimen was from clean side of filter channel.
b - Tensile surface of flexure specimen was from filtering side of filter channel.

The reaction of cordierite with alkalis (Na and K) to form nepheline may be a possible hot corrosion mechanism that could lead to a reduction in the strength of these filters. Nepheline has a thermal expansion coefficient that is at least 10 times greater that of cordierite. Such thermal expansion difference could lead to the formation of microcracks which can weaken the filters. The formation of microcracks will decrease the elastic modulus of the material (as discussed in the following section). Due to the size and geometry of the 100 cpsi filters, we were not able to measure the elastic modulus of the exposed filters to determine if the modulus of the exposed filters is significantly lower than that of the unexposed filters. Exposure testing of the 25 cpsi filters would enable us to measure the elastic modulus of the exposed filters. Additional strength testing and characterization are needed to verify that nepheline is the source of the strength degradation in these exposed filters.

Elastic Modulus. The elastic modulus of the 25 cpsi filters were measured as a function of temperature using the acoustic resonance technique. Samples six cells wide by two cells thick by two inches in length were machined from the as-received uncoated, coated, and exposed filters from Ahlstrom Pyropower to measure the structural stiffness (E_S) of the filters as a function of temperature (both heating to 950 °C and cooling to room temperature). The structural stiffness of the filters was then multiplied by the ratio of the cell length to the thickness of the cell walls (l_S/w_S) to calculate the elastic modulus (E^*) of the material.

Table II. Elastic modulus data for 25-cpsi filter specimens

	Structural Stiffness, E_S (GPa)				Elastic Modulus of Material, E* (GPa)			
	Uncoated	Coated	A300[1]	T1000[2]	Uncoated	Coated	A300[1]	T1000[2]
Heating (°C)								
22	2.6	2.4	2.2	2.2	13.2	9.9	10.2	9.2
400	2.7	2.5	2.4	2.3	13.3	10.1	11.0	9.4
800	3.1	3.2	2.6	3.0	15.5	13.4	12.0	12.4
870	3.3	3.4	2.7	3.2	16.6	14.4	12.5	13.2
950	3.5		2.7	3.5	17.5	12.6		14.6
Cooling (°C)								
870	3.6	3.8	2.8	3.6	17.8	15.8	13.1	14.9
800	3.6	3.7	2.9	3.6	17.9	15.5	13.5	14.9
400	3.0	2.9	2.8	2.9	15.2	11.9	12.8	11.8
22	2.6	2.4	2.2	2.2	13.2	9.9	10.6	9.1

* Based on the following equation: $E^* = E_S$ (Strut length/Strut thickness).
[1] CeraMem filters exposed for 300 h at 1600 °F in a combustor at Ahlstrom Pyropower.
[2] CeraMem filters (25 cpsi) thermally aged for 1000 h at 800 °C.

As was observed for the strength of these filters, the elastic modulus of the material was not significantly affected by the coating or thermal aging (see Table II). The elastic modulus does exhibit a hytere tic behavior upon heating and cooling which is presumably caused by closing and opening of microcracks. As the material is heated, microcracks that formed during cooling from processing temperature, begin to close and continue to close up to 1000 °C. The closure of microcracks results in an increase in the elastic modulus of the material. Upon cooling, the microcracks begin to open around 650 °C and the modulus decreases with temperature.

Microstructural Characterization. Scanning electron microscopy and energy dispersive x-ray spectroscopy were used to investigate possible ash/membrane interaction on the exposed filters. Three out of four 100 cpsi filters exposed in Run 2 (~1050 hours at ~850 °C) contained transverse cracks, which resulted from excessive clamping forces used to mount the filters in the exposure rig. Filter #2, which possessed

some cracks, was deliberately fractured in half across its width to analyze the microstructure of the filter walls, membrane, and ash for possible interactions. There was some evidence of necking between ash particles near the membrane suggesting that ash-membrane interactions may have occurred. The necking of the ash particles, while not necessarily resulting in densification of the ash, does indicate that liquid phase sintering may have occurred. The particles of ash located towards the center of the filtering cell did not show evidence of necking, but resemble agglomerates of individual ash particles.

Optical microscopy was used to examine fractured flexure specimens machined from a filter used in Run 4 (2000 hours at 800 °C) and tested at 800 °C. The ash in one of the two filtering cells was seen to have pulled out of the opposing cell when fractured. This suggests that there was no significant bonding between the ash and the membrane coating. A higher magnification micrograph of the ash adjacent to the membrane and near the center of the cell revealed no evidence of ash/membrane interactions or necking between ash particles.

Energy dispersion spectroscopy was used to identify elements present in the ash. A series of EDS patterns were obtained starting from the cell wall on the clean side of the cell through to the ash in the center of the filtering cell. With the exception of detecting Mg, Al, and Si from the cordierite of the cell wall as well as elements associated with the proprietary membrane coating, high concentrations of calcium, iron and sulfur were detected in the regions of the ash, but the sodium level did not vary much from one region of the filter to the other.

Discussion

A bench-scale, flow-through apparatus has been assembled for continuous, unattended exposure of ceramic filter specimens to oxidizing and reducing environments of PFBC and IGCC plants. Feed systems are provided for introducing ash, alkali and sulfur impurities into the gas stream. The apparatus includes an on-line pulse gas system to dislodge the ash deposits from the ceramic filters after accumulation for a defined interval of time or to a defined pressure drop.

Four long-duration tests have been completed to characterize the filtration and pulse cleaning behavior of CeraMem's ceramic filters with 2-mm square channels. The tests were conducted under oxidizing conditions. The test data indicates a conditioning time during which the pressure drop increases to a steady-state value. A repetitive saw-tooth ΔP profile is maintained for 200-900 h at 900 °C and for more than 1000 h at 800 °C. Beyond this time, the baseline ΔP and the pressure swing between consecutive pulses begin to climb gradually. A stage is asymptotically approached where the filters cannot be regenerated online by the simple back pulse technique. For exposure times exceeding 1000 h, attempts to pulse-clean the filters at lower than the working temperature proved unsuccessful. It remains to show whether a fouled filter can be taken off line and regenerated with a water rinse.

For the test conditions investigated, filter cleanability is not affected by the pulse schedule, i.e., a single pulse performed as well as a multiple pulse. The filters display a remarkable ability to recover after severe ΔP excursions due to system upsets (missed pulses). At 900 °C and 70 ppmv NaCl concentration SEM micrographs exhibit some membrane-ash interaction and necking between the ash particles deposited on the membrane. No such interactions were observed at 800 °C and 11 ppmv NaCl concentration when the pulse schedule was more frequent (15-30 min pulse interval vs. up to 1 h at 900 °C). Post test examinations revealed that the filter passages were quite filled with residual ash. Thus, the reason for measured creep in baseline ΔP at long exposure time is not related to ash sintering to the filter membrane but is of fluid mechanic origin. The phenomenon of residual ash filling up the passages from the back has also been observed in other tests with 4-mm channels. Based on the measured temperature dependence of ΔP, it appears inappropriate to describe the pressure drop by porous media equations when the filter passages are filled with ash.

A data base has been established on the mechanical properties of as received membrane-coated cordierite material, properties after thermal aging, and after chemical exposure. Four-point flexure tests on 4-mm cell size coated and uncoated as-received specimens exhibit only a small increase in strength with temperature in the range 20-870 °C (mean strength about 10 MPa). Little change in strength was measured (±10%) after thermal aging the specimens for 1000 h in a furnace at 800 °C. The measured strength decreased by more than 60%, to 4.7±2 MPa at 800 °C, after the filters were exposed to contaminants (70 ppmv NaCl concentration) at 900 °C for 388 h (Run 3). The strength data for the exposed filters was averaged over six test specimens. The data had a large variation, from 2.6 to 7.9 MPa. The reduction in strength was somewhat smaller (35% to 6.5±2.6 MPa at 800 °C) for the filters exposed to simulated combustion gas containing 11 ppmv NaCl at 800 °C for 2000 h (Run 4).

A possible hot corrosion mechanism has been identified which involves the reaction between the cordierite and alkalis to form nepheline. During pulse cleaning, the filter is subjected to thermal cycling which may produce microcracks because of the large differential in the thermal expansion coefficients for nepheline and cordierite. It is proposed that the microcracks are responsible for the observed degradation in strength.

Future Activities

The immediate focus of this project has now shifted to exposing the advanced candle filter specimens to reducing gas environments containing NaCl, H_2S, H_2O and gasification ash. The fibrosic candle (15.2 cm long, 5.6 mm outer diameter) manufactured by Industrial Filter and Pump Manufacturing Company (IFPM) will be the first to be tested. In the meantime, work is continuing on characterizing the microstructure and measuring the mechanical properties of the CeraMem filter specimens exposed in Runs 1-4. In a parallel effort, modeling work is being initiated to

use the material property database being generated in this project and predict the probability of survival of commercial filters under anticipated service conditions.

References

Ahluwalia, R.K. and Geyer, H.K., “Fluid Mechanics of Membrane-Coated Ceramic Filters,” To appear in ASME Journal of Engineering for Gas Turbines and Power, Vol, 118, July 1996.

Ahluwalia, R.K., Geyer, H.K. et al, “Assessment of Ceramic Membrane Filters,” Proceedings of the Advanced Coal-Fired Power Systems’ 95 Review Meeting, 279-291. DOE/METC-95/1018. NTIS/DE 95009732. Springfield, VA: National Technical Information Service.

Acknowledgement

This research is sponsored by DOE-METC with Dr. Norman Holcombe as the project manager. Dr. Chao Zhu of ANL assisted in assembling the apparatus and conducting Runs 1 and 2. Dr. Vince Novick is a consultant to this project. Jim Nasiatka is responsible for maintenance of the test apparatus.

Preliminary Strength Measurements of High Temperature Ash Filter Deposits

B.S.Kang (Kang@cemr.wvu.edu; (304)293-3111)
E.K.Johnson (Johnson@cemr.wvu.edu; (304)293-3111)
R. Mallela
J.F.Barberio
Mechanical and Aerospace Engineering Department
West Virginia University
Morgantown, WV 26506, U.S.A.

Introduction

The objective of this study is to develop and evaluate preliminary strength measurement techniques for high temperature candle filter ash deposits. The efficient performance of a high temperature gas filtering system is essential for many of the new thermal cycles being proposed for power plants of the future. These new cycles hold the promise of higher thermal efficiency and lower emissions of pollutants. Many of these cycles involve the combustion or gasification of coal to produce high temperature gases to eventually be used in gas turbines. These high temperature gases must be relatively free of particulates. Today, the candle filter appears to be the leading candidate for high temperature particulate removal.

The performance of a candle filter depends on the ash deposits shattering into relatively large particles during the pulse cleaning (back flushing) of the filters. These relatively large particles fall into the ash hopper and are removed from the system. Therefore, these particles must be sufficiently large so that they will not be re-entrained by the gas flow. The shattering process is dictated by the strength characteristics of the ash deposits. Consequently, the objective of this research is to develop measurements for the desired strength characteristics of the ash deposits.

The strength characteristics of an ash deposit is a function of it's environment. Experimentally, it has been found that the deposit layer next to the filter surface has been extremely difficult to remove. This inner layer is referred to as a hard deposit. The outer layer of the deposit, which is much easier to remove, is referred to as soft deposit. Obviously, the notation comes from handling the two types of deposits. The deposits employed in this study were obtained from an operating power plant. Both soft and hard deposits were readily identified. To date, the strength measurements have concentrated on the normal strain and the Young's modulus of the deposits.

Background

The basic geometry of an ideal ash deposit on a candle filter is schematically shown in Figure 1. The ash deposit is of uniform thickness over the entire surface of the filter. A simple stress model is shown in Figure 2 for the ash deposit during the pulse cleaning, just prior to the shattering of the deposit. With the assumed symmetry, the dominant stresses are 1) the normal (hoop) stresses for the soft and hard deposits ($\sigma_{\theta\theta}^{S}$ and $\sigma_{\theta\theta}^{H}$), and the adhesive stress (σ_A) between the hard deposit and the filter surface. The pressure due to pulse cleaning is shown as P_2. The adhesive stress is due to particles becoming wedged into the pores of the filter and forming a rather hard, ridged, structure. Additional particles impacting this layer will stick to the layer and will be wedged tighter into the structure as the continuing stream particles impact the structure. The particles arriving later do not undergo the continuing impacts and subsequently do not form as rigid a structure. In addition, at the high temperatures encountered in these systems, the potential for a chemical reaction forming bonds is significant. With pulse cleaning, the reversed flow of gases only remove particles in the weaker portion of the structure.

The formation of the ash deposits depend on: 1) the particle size distribution of the dust, 2) the face velocity, 3) ash chemistry, and 4) the pressure and temperature of the gases. Ash samples from an operating power plant were obtained from DOE/METC for this study so that these measurements might proceed in an expeditious manner.

Experimental Approach and Results

Room Temperature Tests

The approach developed in this research to measure the strength characteristics of ash deposits at room temperature is to glue a filter cake (ash deposit) specimen to a flexural beam. An aluminum beam was used in the room temperature tests. A load is then applied to the beam to produce a known bending moment in the beam as shown in Figure 3. The attached specimens were obtained by cutting the as-received large "chunks" of ash deposits into flat slabs to fit onto the beam. This procedure was rather tedious due to the softness of the ash deposits and relatively large particles in the ash sample which made it difficult to obtain a smooth surface. The cutting process was continued until smooth parallel surfaces were obtained on the specimen. The specimen was then glued to the beam using epoxy. The experiment consisted of loading the beam incrementally and recording the strain gage readings. A long distance microscope fitted with a color CCD camera and monitor was used to inspect the surface of the specimen for crack initiation site and an analog video printer was used to print out the images, as shown in Figure 3. The loading was continued until the formation of an initial crack was detected.

The analysis of the data for the room temperature tests were based on the model shown in Figure 4. As shown, the strain distribution was assumed to vary linearly in the beam and the cake specimen. The unknowns to be determined are the maximum cake strain $(\varepsilon_{cake})_{max}$ and modulus of elasticity (E_1) of the filter cake. The dimensions, a and b, and the modulus of elasticity of the aluminum beam (E_2) are known. The strain (ε_0) along the underside of the beam can be determined based on linear interpolation of the two strain gage readings. The equations for calculating the unknowns are

$$(\epsilon_{cake})_{\max} = \frac{\epsilon_0(c+a)}{(c-b)}$$

$$E_1 = \frac{-B+\sqrt{(B^2-4a^4C)}}{2a^4}$$

Where

$$B = 2ab(3ab+2a^2+2b^2)E_2+6a(a+2b)\frac{M}{\epsilon_o}$$

$$C = b^2E_2(\frac{6M}{\epsilon_0}+b^2E_2).$$

A total of four tests (two hard deposits and two soft deposits) were conducted. Figures 5 to 8 show the test results also shown in the figures are the dimensions of the ash samples. Figures 9 to 12 show load versus ash deposit strain plots. Tables 1 to 4 show the tabulated results for each test. Finally, Table 5 shows the summary results. These results show quite consistent failure tensile strain values for the hard deposit as well as the soft deposit. However, Test No. 2 of the hard deposit showed substantially higher Young's modulus value comparing to Test No.1. This may due to the fact that SuperGlue was used in Test No. 2 to bond the ash cake to the beam. The SuperGlue may have penetrated into the ash deposit creating an artificial stiffness of the filter cake. For the rest of the room temperature tests, a high viscosity epoxy was used and no glue penetration was observed.

Elevated Temperature Test Results

Two types of elevated temperature tests were conducted. The first type of test consisted of using a bending beam (BB) apparatus, as shown in Figures 13 and 14. The second type of test involved employing a thermal expansion mismatch (TEM) measurement procedure to obtain the failure tensile strain of ash deposit. Both the beam and the bending apparatus are made of IN718 superalloy. All the elevated temperature tests were conducted on soft ash deposits. The BB tests were performed at 1200^0F and the TEM tests were performed at a much lower elevated temperature.

The BB tests consisted of placing a thin (0.06 inch) specimen on the IN718 beam, and the whole bending beam apparatus was then put inside a furnace. The furnace was heated to 1200^0F. At this temperature, the furnace was opened and both ends of the specimen were glued to the beam. Alumina cement was used as the glue. This approach avoided introducing the effect of thermal expansion mismatch during heating up the furnace. The beam was now loaded incrementally until a crack in the specimen was observed through the long distance microscope. Figure 15 shows the results of one high temperature test. The tensile strain was calculated for the surface of the beam at each contact (glue) point using the simple bending beam formula. The

tensile strain in the specimen was then calculated as the average of the two beam surface strains. Two tests were conducted and both showed that the failure cake strain at 1200 ^{o}F is approximately 450 μ. In order to verify this approach, this test procedure was repeated at room temperature. The failure tensile strain was determined to be 1200μ, which is in good agreement with the data in Table 5.

The TEM method consisted of attaching a thin specimen to a beam. Both end of the specimen were glued to the beam using alumina cement. The test system was then placed in a furnace and the temperature was slowly increased until a crack in the specimen was observed. The initiation of a crack was again detected using a long distance microscope. Four tests were performed, each showed a crack appeared at a temperature of 190^{0}F. A typical test result is shown in Figure 16. From the equation

$$\varepsilon_{cake} = (\alpha_{718} - \alpha_{cake})\ \Delta T = (7.2*10^{-6} - 4.0*10^{-6})*(190°F - 80°F) = 352\ \mu$$

The failure tensile strain of the ash deposit at 190^{0}F is then determined.

Figure 17 shows the failure tensile strain as a function of temperature for a soft ash deposit. The rapid decrease of the failure tensile strain with temperature is probably due to the removal of moisture in the ash deposit specimen.

Conclusion

Experimental procedures were developed to measure Young's modulus of the ash deposit at room temperature and the failure tensile strain of ash deposits from room temperature to elevated temperatures. Preliminary data has been obtained for both soft and hard ash deposits. The qualifier "preliminary" is used to indicate that these measurements are a first for this material, and consequently, the measurement techniques are not perfected. In addition, the ash deposits tested are not necessarily uniform and further tests are needed in order to obtain meaningful average data.

Acknowledgment

This research was jointly supported by METC and WVU NRCCE. We would like to express our appreciation to R. Dennis and T.K.Chiang at METC for their support and encouragement of this exploratory research effort.

Table 1 Experiment No. 1 Hard Deposit

Load (N)	ϵ_0 (10^{-6} m/m)	$(\epsilon_{cake})_{max}$ (10^{-6} m/m)	Young's Modulus (GPa)
9.86	-192.64	401.11	8.93
19.72	-385.84	803.39	8.76
41.95	-827.52	1723.05	8.54
63.93	-1209.80	2519.03	9.70
81.77 *	-1585.00	3300.27	9.01

* Crack initiation.

Table 2 Experiment No. 2 Hard Deposit

Load (N)	ϵ_0 (10^{-6} m/m)	$(\epsilon_{cake})_{max}$ (10^{-6} m/m)	Young's Modulus (GPa)
22.36	-405.60	764.40	35.62
41.10	-779.70	1469.43	30.36
59.83	-1161.70	2189.35	28.03
80.36	-1571.00	2960.70	27.34
91.56 *	-1834.90	3458.08	25.03

* Crack initiation.

Table 3 Experiment No. 1 Soft Deposit

Load (N)	ϵ_0 (10^{-6} m/m)	$(\epsilon_{cake})_{max}$ (10^{-6} m/m)	Young's Modulus (GPa)
2.24	-51.20	173.18	0.27
4.48	-102.10	345.35	0.31
8.96	-204.10	690.36	0.32
13.44	-306.40	1036.39	0.31
17.92 *	-401.10	1380.39	0.32

* Crack initiation.

Table 4 Experiment No. 2 Soft deposit

Load (N)	ϵ_0 (10^{-6} m/m)	$(\epsilon_{cake})_{max}$ (10^{-6} m/m)	Young's Modulus (GPa)
2.24	-98.50	301.97	0.35
4.48	-197.20	604.55	0.33
6.72	-291.60	893.95	0.31
8.96 *	-393.80	1207.26	0.36

* Crack initiation.

Table 5 Room Temperature Tests

Test	Filter Cake	Thickness (10^{-3} m)	Temperature	Filter Cake Tensile Strain (10^{-6} m/m)	Young's Modulus (GPa)
1	Hard	5.08	Room	3300.27	8.988
2	Hard	3.048	Room	3456.38	29.276
3	Soft	3.81	Room	1380.39	0.306
4	Soft	3.302	Room	1207.26	0.3375

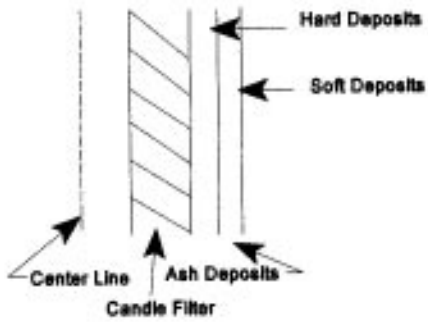

Figure 1 Schematic drawing of ideal ash deposit on a candle filter.

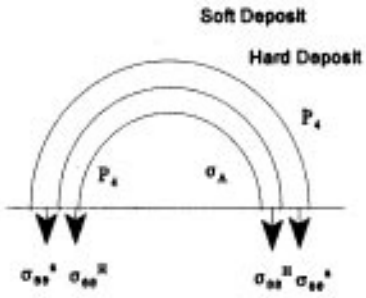

Figure 2 Stress model for ash deposit during pulse cleaning.

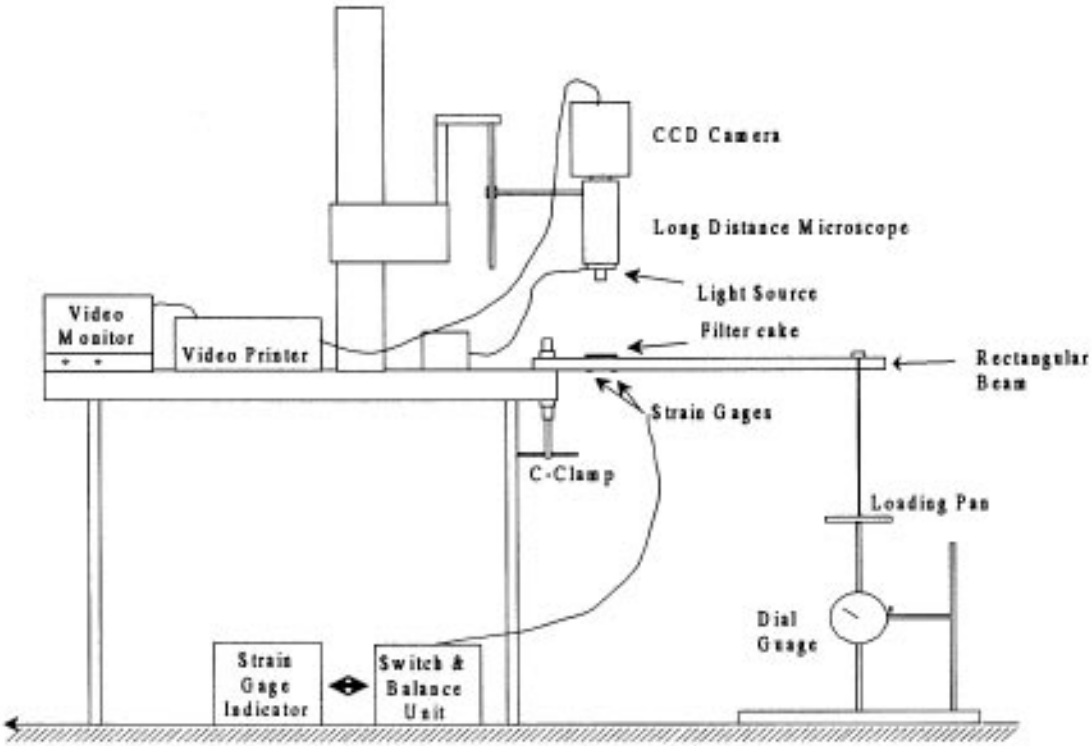

Figure 3 Room temperature filter cake strength test setup.

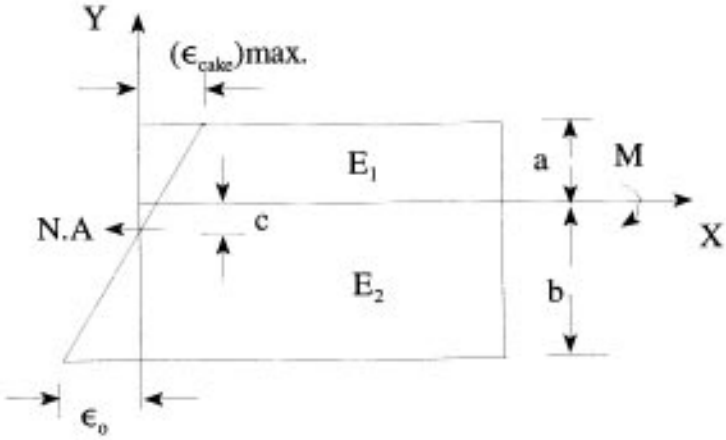

E_1 = Young's modulus of the ash deposit

E_2 = Young's modulus of the beam material
M = Applied bending moment
ϵ_0 = Strain gage reading

N.A = Neutral axis

a = Ash deposit thicknes
b = Beam thicknes

Figure 4 Analytical model for filter cake strain and Young's modulus determination.

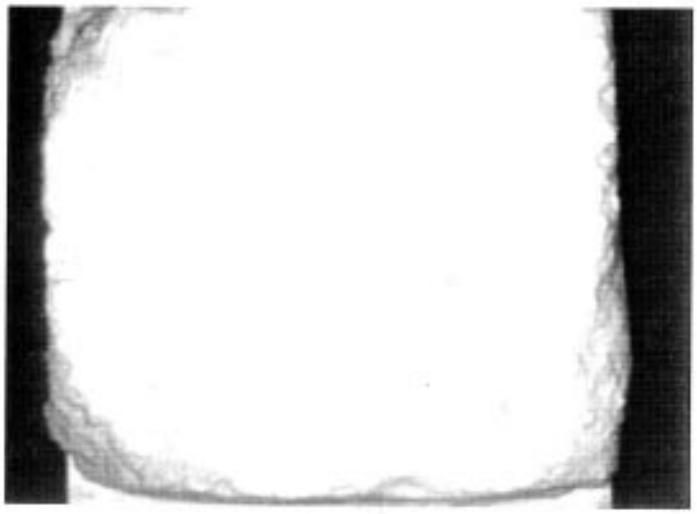

BEFORE LOADING

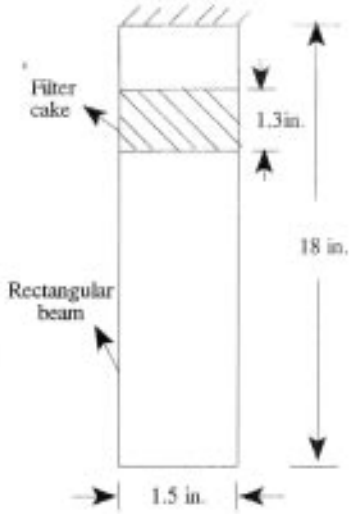

Crack initiation

CRACK INITIATION

Figure 5 Hard ash deposit test no. 1.

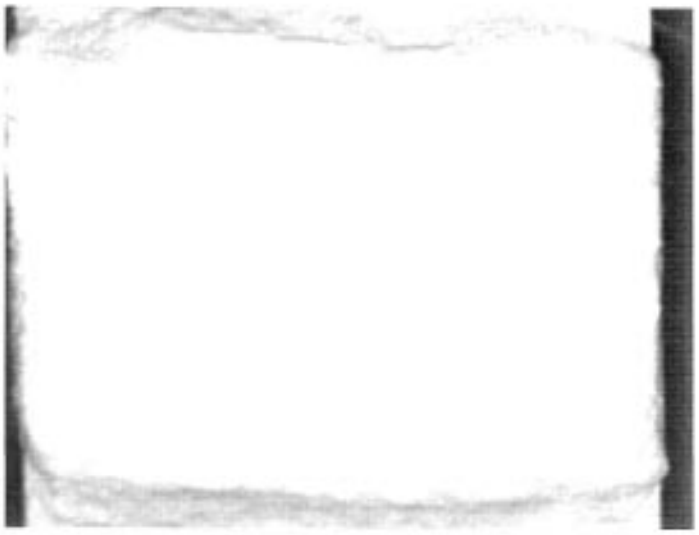

BEFORE LOADING

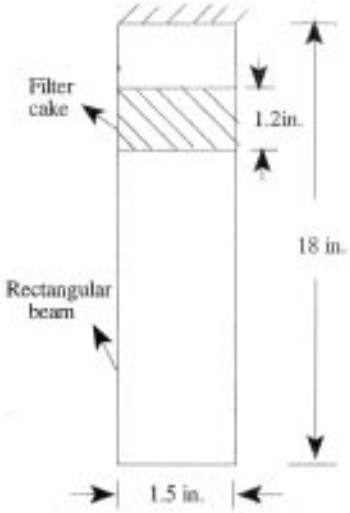

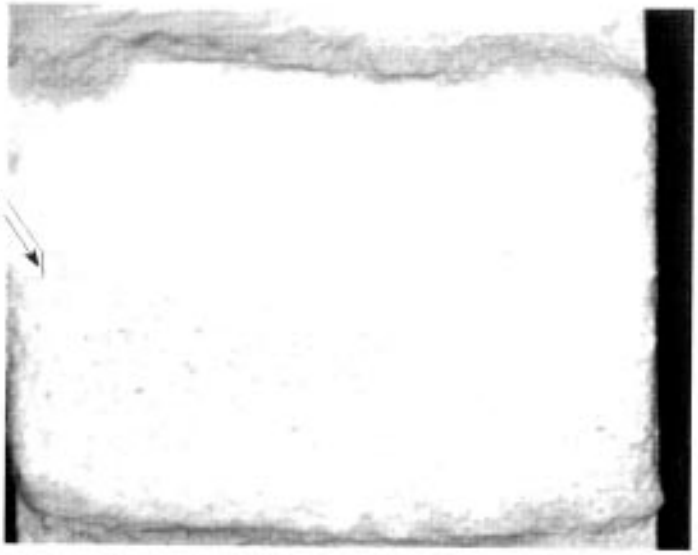

CRACK INITIATION

Figure 6 Hard ash deposit test no. 2.

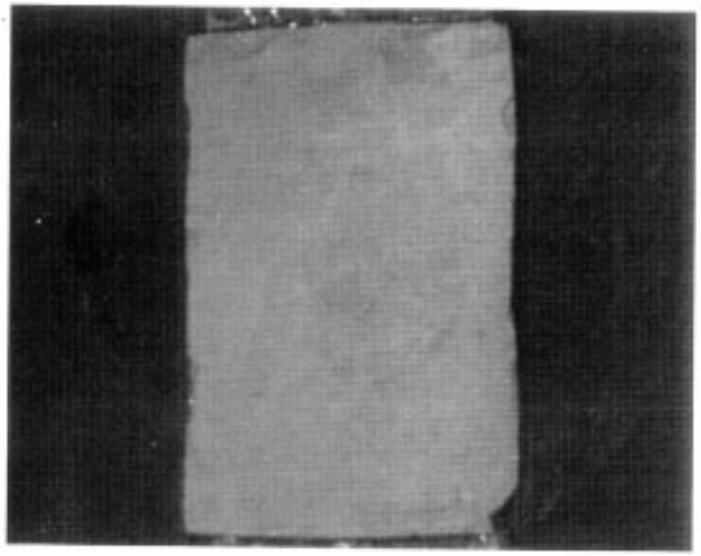

BEFORE LOADING

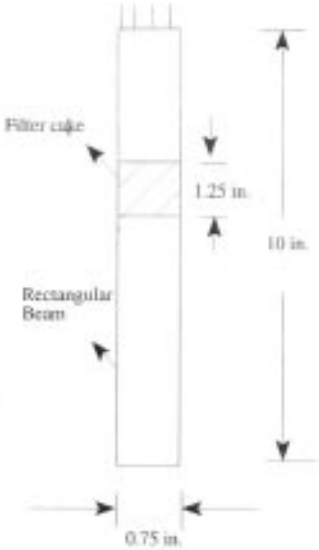

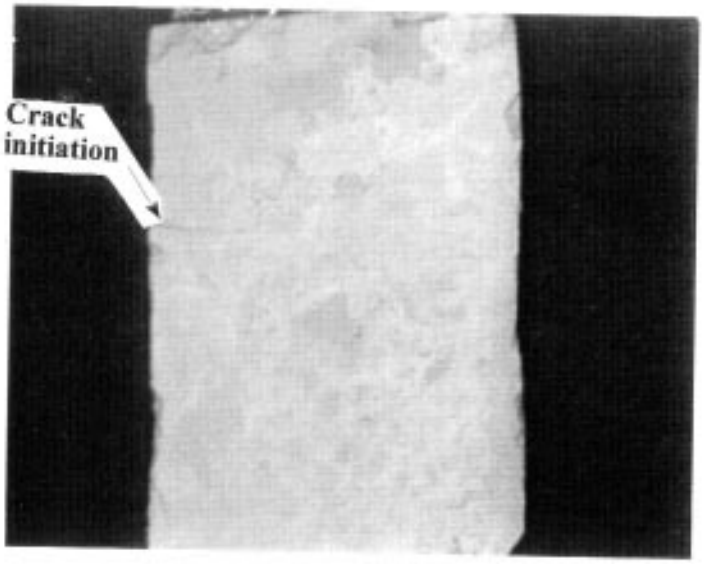

CRACK INITIATION

Figure 7 Soft ash deposit test no. 1.

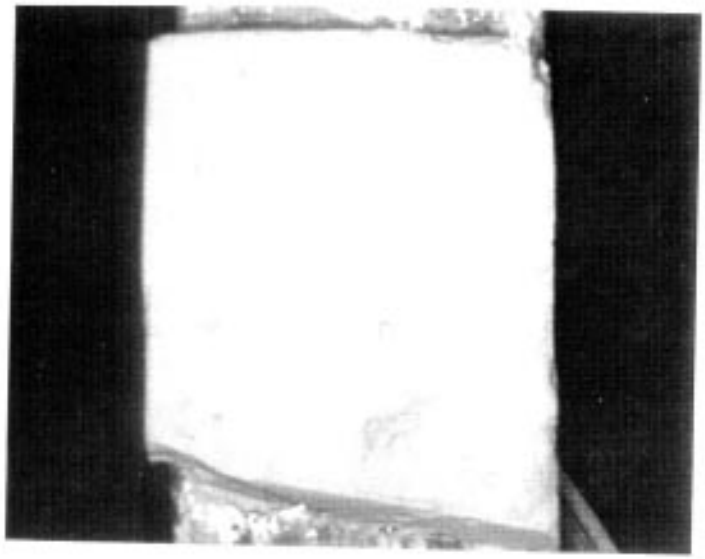

BEFORE LOADING

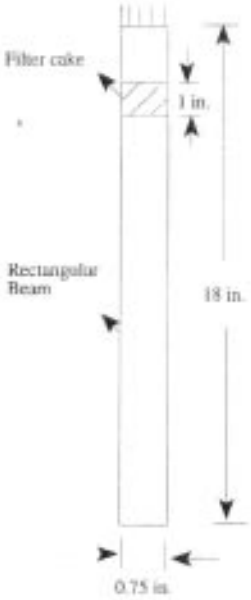

CRACK INITIATION

Figure 8 Soft ash deposit test no. 2.

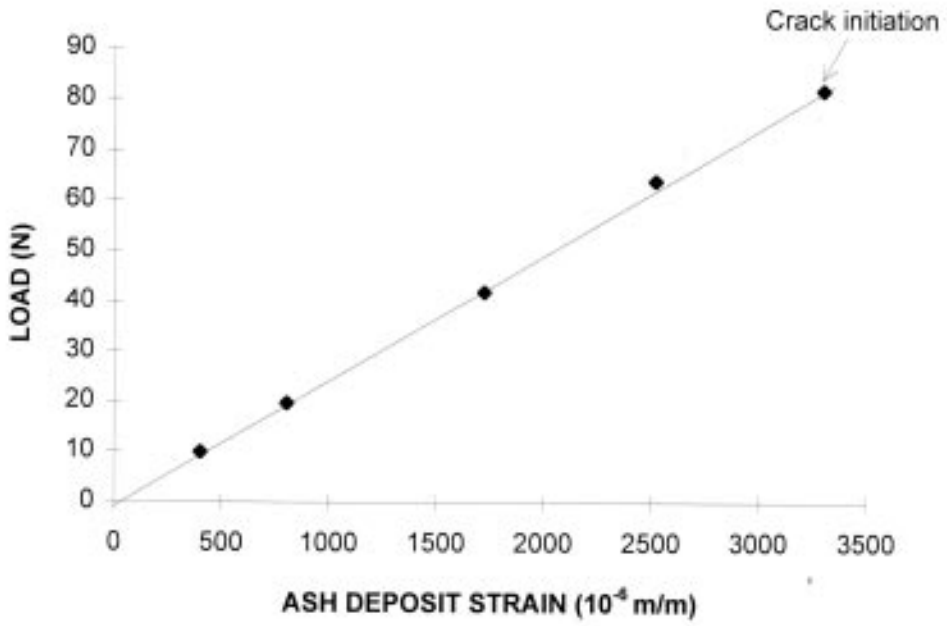

Figure 9 Load versus ash deposit strain plot.
(Hard ash deposit, test no. 1)

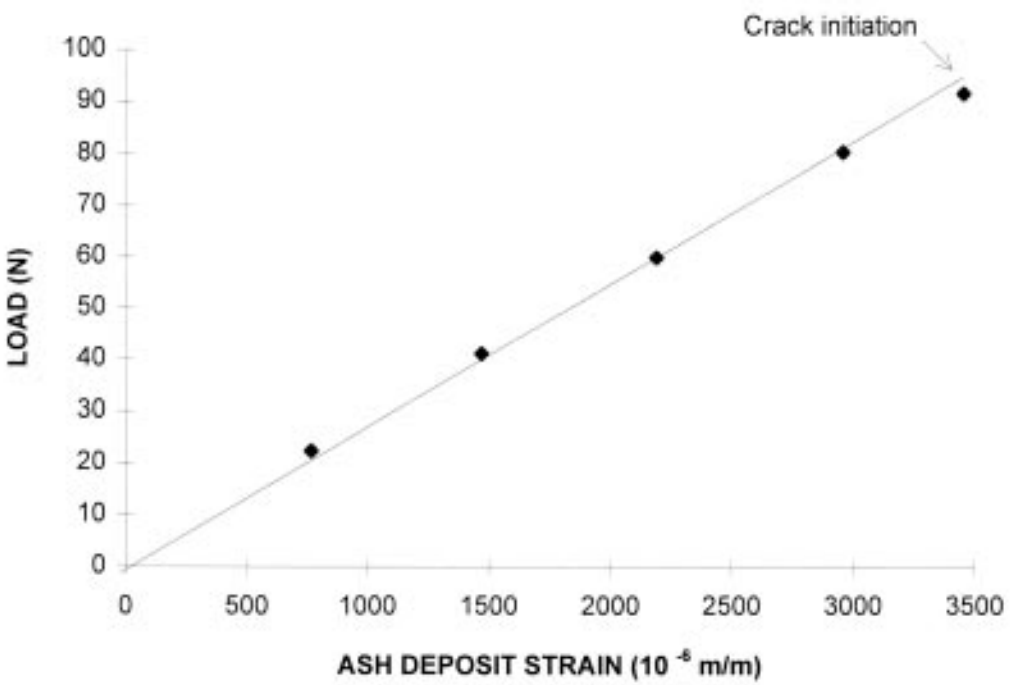

Figure 10 Load versus ash deposit strain plot.
(Hard ash deposit, test no. 2)

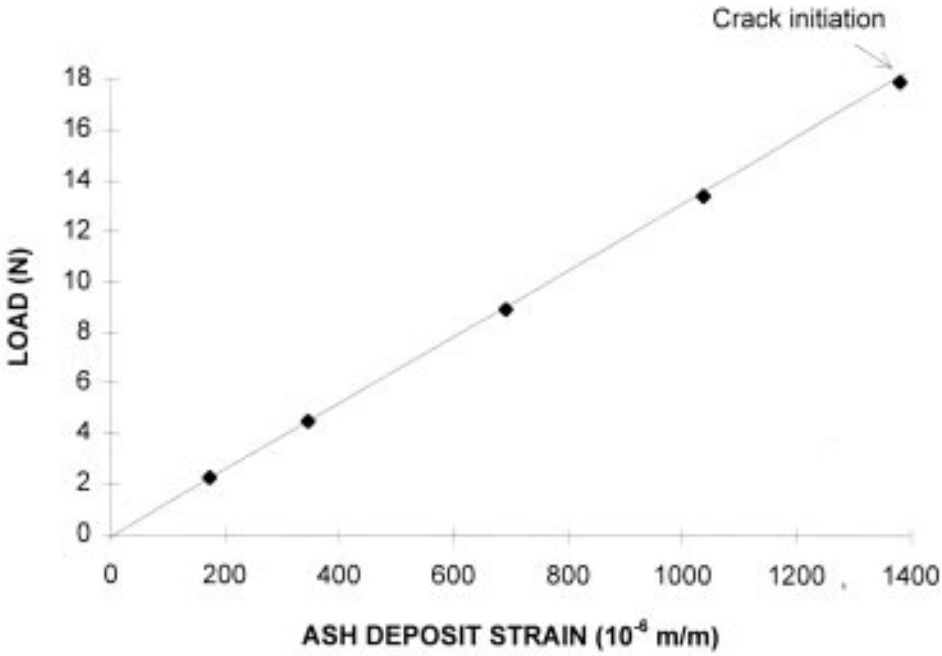

Figure 11 Load versus ash deposit strain plot.
(Soft ash deposit, test no. 1)

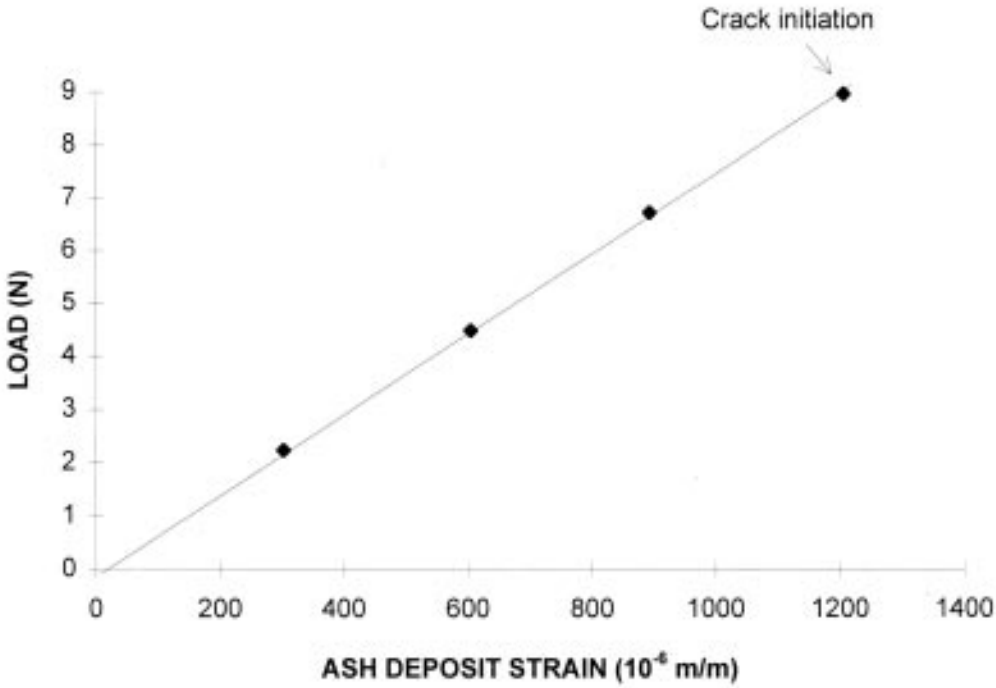

Figure 12 Load versus ash deposit strain plot.
(Soft ash deposit, test no. 2)

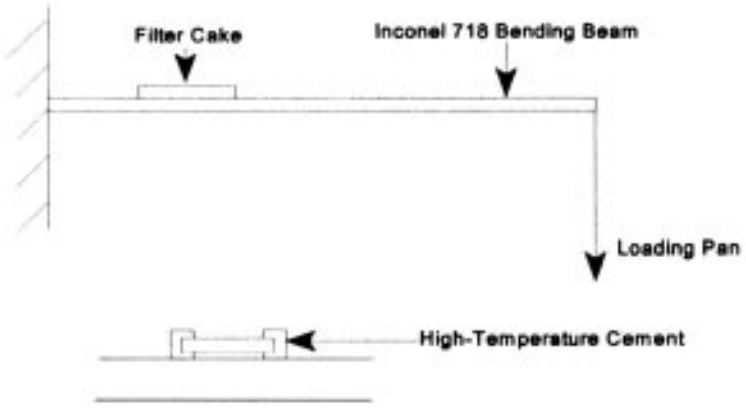

Figure 13 Schematic drawing of ash specimen layout for high temperature test or thermal expansion mismatch measurement.

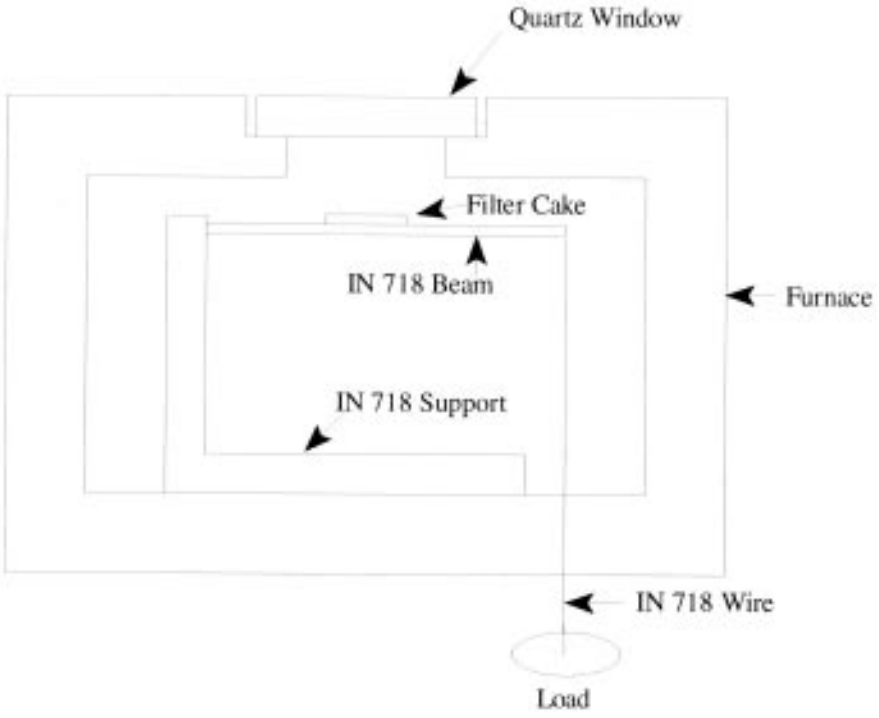

Figure 14 Schematic drawing of high temperature ash strain measurement test setup.

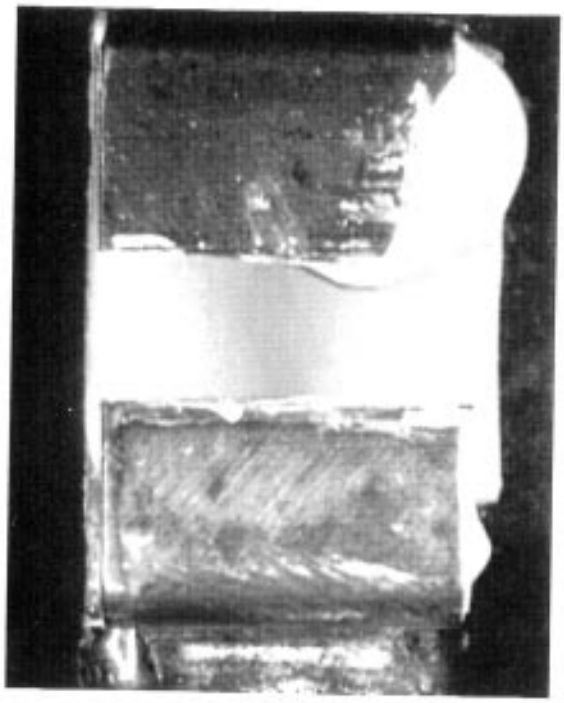

T = 80 °F
(NO LOAD)

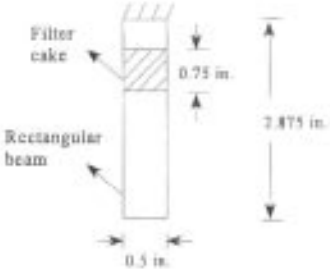

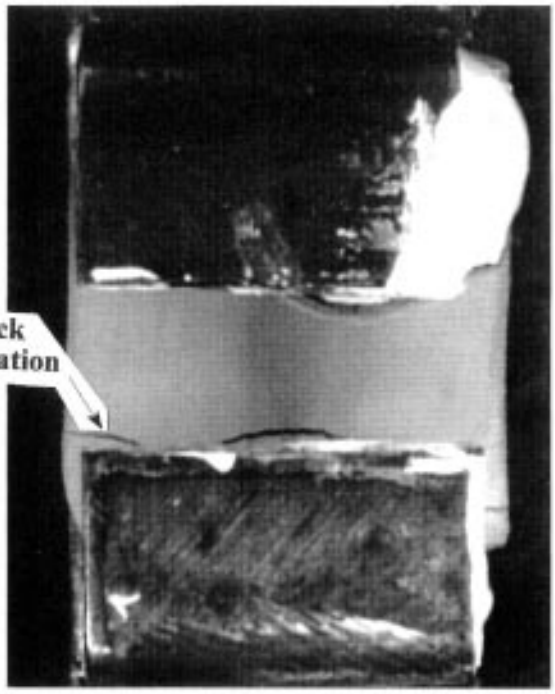

T = 1200 °F
(WITH APPLIED LOAD)

Figure 15 Typical high temperature test result.

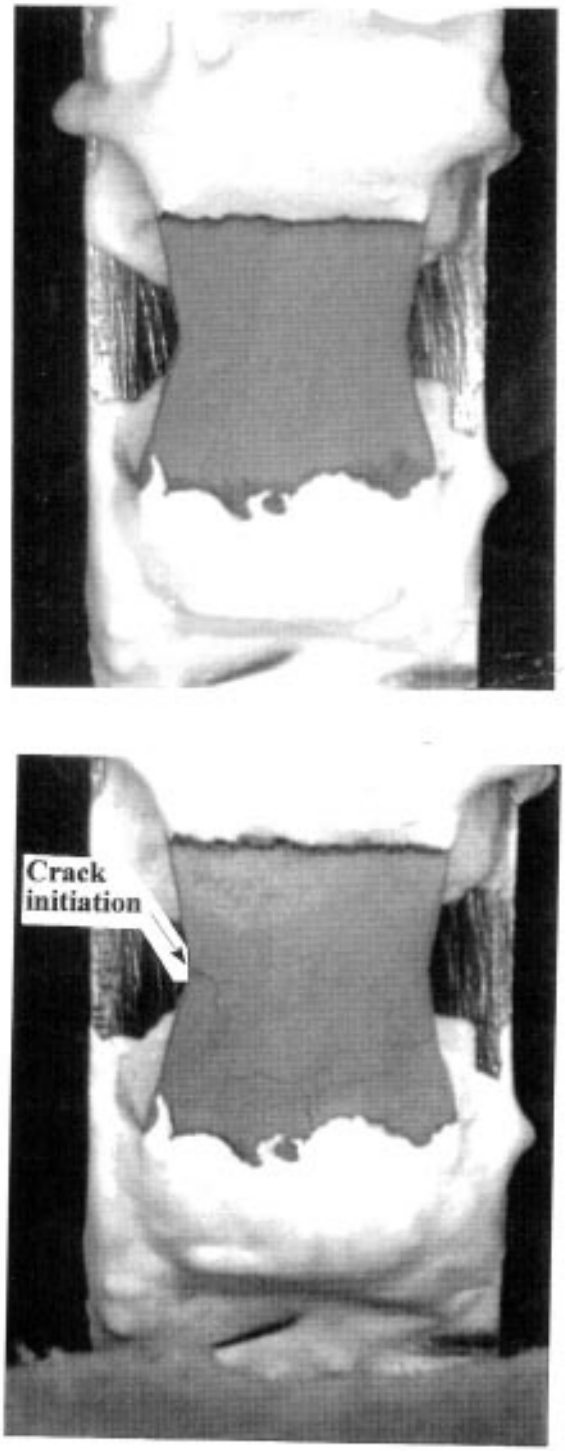

, T = 80 °F

T = 190 °F

Figure 16 Typical thermal expansion mismatch test result.

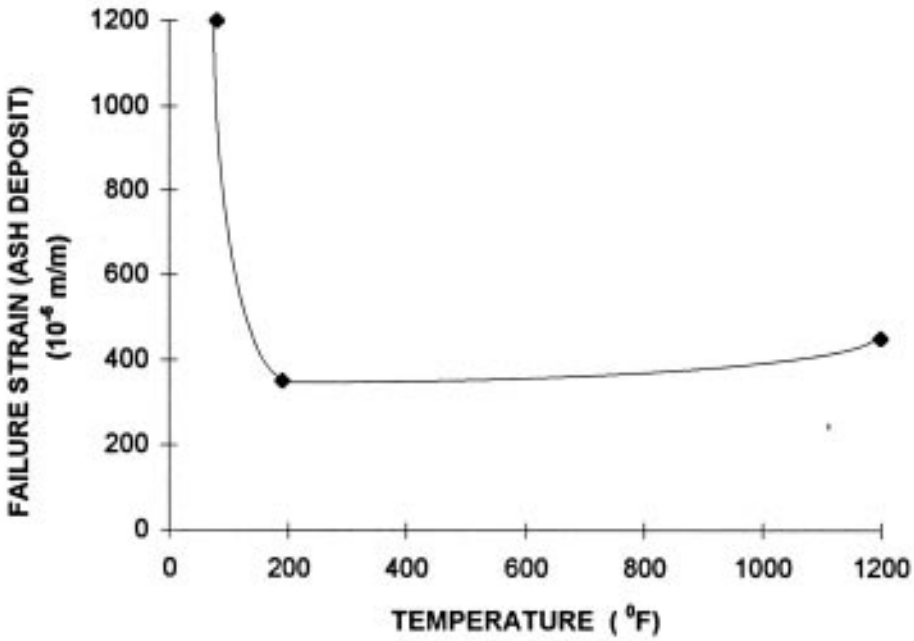

Figure 17 Ash deposit strain versus temperature plot.

Long Life $ZnO-TiO_2$ and Novel Sorbents

Robert J. Copeland (copeland@tda.com; 303-940-2323)
Mike Cesario (czar@tda.com; 303-940-2336)
Dan Feinberg (daf@tda.com; 303-940-2311)
Dr. Brent MacQueen (dbmacque@tda.com; 303-940-2343)
Jack Sibold (siboldj@tda.com; 303-940-2319)
Brian Windecker (mech@tda.com; 303-940-2306)
Jing Yang (yangj@tda.com; 303-940-2328))
TDA Research, Inc.
12345 West 52nd Avenue
Wheat Ridge, Colorado 80033

Introduction

Combined cycles (combinations of a gas turbine and a steam bottoming cycle) are the most efficient power generation technology, while coal is the lowest cost fuel. Therefore, the combination of Coal Gasifiers and Combined Cycles is predicted to be the lowest cost source of baseload electric power in the next decade. In a GCC, the sulfur and particulates are removed from the gasifier gases before they enter the turbine combuster. While H_2S (and COS/CS_2) can be removed effectively by cooling hot gases down to near room temperature and scrubbing them with an aqueous amine solution, removing the H_2S without cooling the gases (*i.e.*, hot gas cleanup) is more advantageous.

The leading hot gas sulfur absorbent uses a regenerable zinc oxide (ZnO) based sorbent, zinc titanate (Zn_2TiO_4 and/or $ZnTiO_3$), to remove the H_2S and other sulfur compounds from the hot coal gases. The zinc absorbs H_2S, forming zinc sulfide (ZnS); ZnS is then regenerated with oxygen (air), releasing the sulfur as a concentrated stream of SO_2. The SO_2 can be converted into sulfuric acid, sulfur, or reacted with calcium carbonate to form calcium sulfate (gypsum). The sorbent may be operated in a fluidized bed reactor, transport reactor, or moving bed reactor.

Both the fluidized-bed and the transport reactor use two separate reactors; one absorbs H_2S COS and CS_2 and converts the ZnO to ZnS; the second bed regenerates the sorbent with air converting the ZnS back to ZnO and producing SO_2 (Figure 1); the sorbent moves between the two reactors to carry sulfur out of the absorber and return regenerated sorbent. Fluidized bed and transport reactors circulate very small particles at high gas velocity. The high gas-solid contact area of very small particles rapidly transfers both heat and mass within the reactor.

The fluidized bed and transport reactor hot gas cleanup desulfurization systems are very similar and the sorbent particles are also of the same size (*i.e.*, 50 to 400 micron). While there are several differences between the two reactors, the one which most affects the sorbent is the operation of the regenerator: fluidized bed reactors operate with diluted air while transport reactors operate with undiluted air.

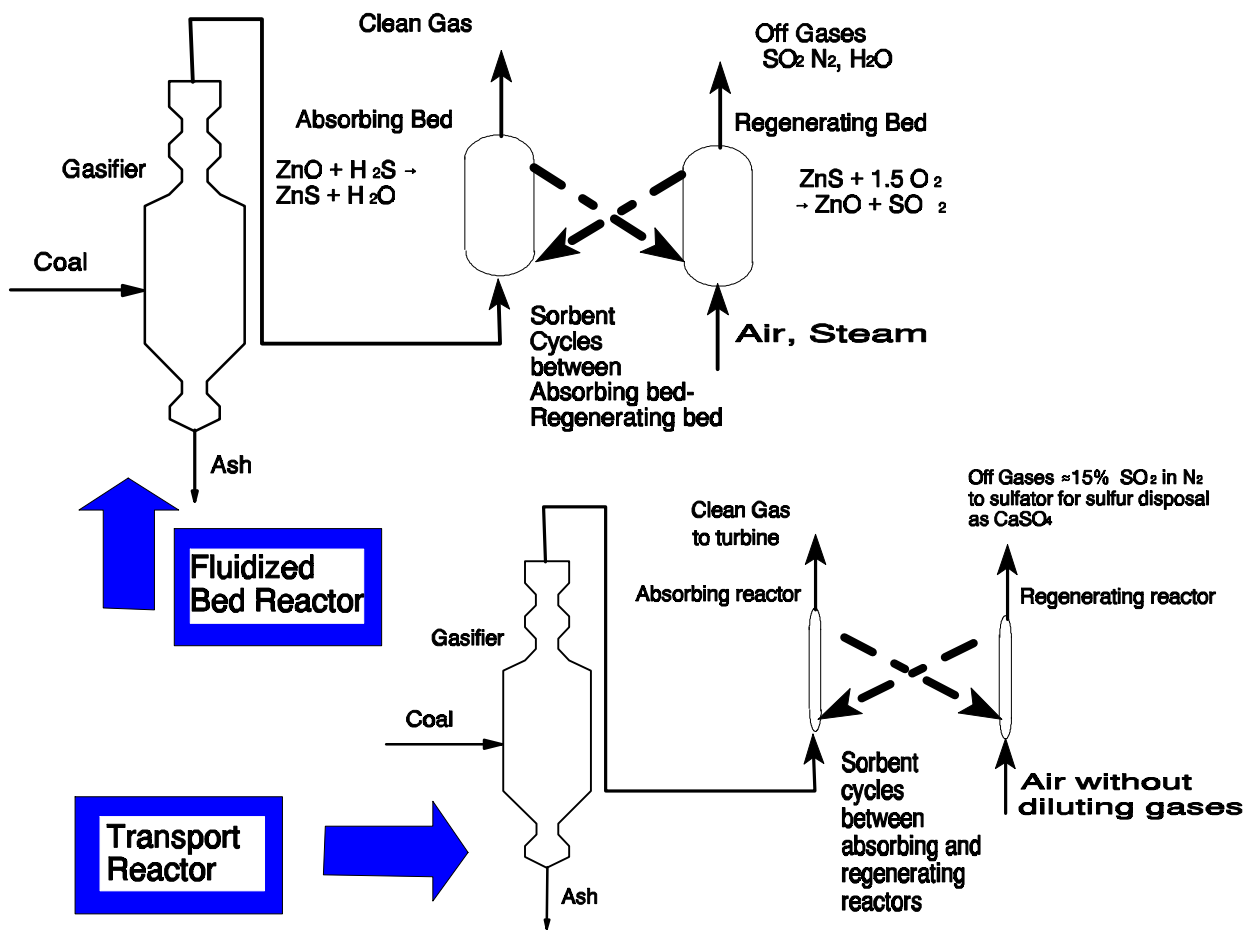

Figure 1 Hot gas desulfurization with fluidized bed and transport reactors.

A schematic of a moving bed system with the production of sulfuric acid from the SO_2 is shown in Figure 2. Again, two reactors are utilized with the sorbent moving between the two. The particle size is large (*i.e.*, 3 to 5 mm = 3000 to 5000 micron). Due to the particle size difference and other factors the reactions occur in a relatively short time in a fluidized or transport reactor, the dwell time in a moving reactor typically being on the order of 6 hours resulting in a different sorbent formulation for the different types of reactors.

ZnO has a high affinity for H_2S and produces a very clean gas stream. Unfortunately, the life of many ZnO based sorbents is very limited, especially in fixed and moving bed reactors. The molar volume of the ZnS is 50% greater than that of ZnO. During regeneration some zinc sulfate can form, which can occupy more than 250% of the original ZnO volume of the original ZnO. Prior to returning to the absorber, the zinc sulfate is decomposed and returns the sorbent to its original oxide form. Thus, the zinc atoms move substantially during absorption (to ZnS), to regeneration (to ZnO and some $ZnO*2ZnSO_4$), and finally back to the oxide (ZnO). This repeated expansion and contraction of the sorbent as it is cycled causes many sorbents to spall (*i.e.*, break into small pieces), which eventually destroys the sorbent (Jung *et al.* 1992)(Mei *et al.* 1993). Because of the high sorbent loss rate, fresh sorbent must be continually added to the process which in turn increases the cost of sulfur removal; substantial cost reductions could be achieved by making a more durable sorbent.

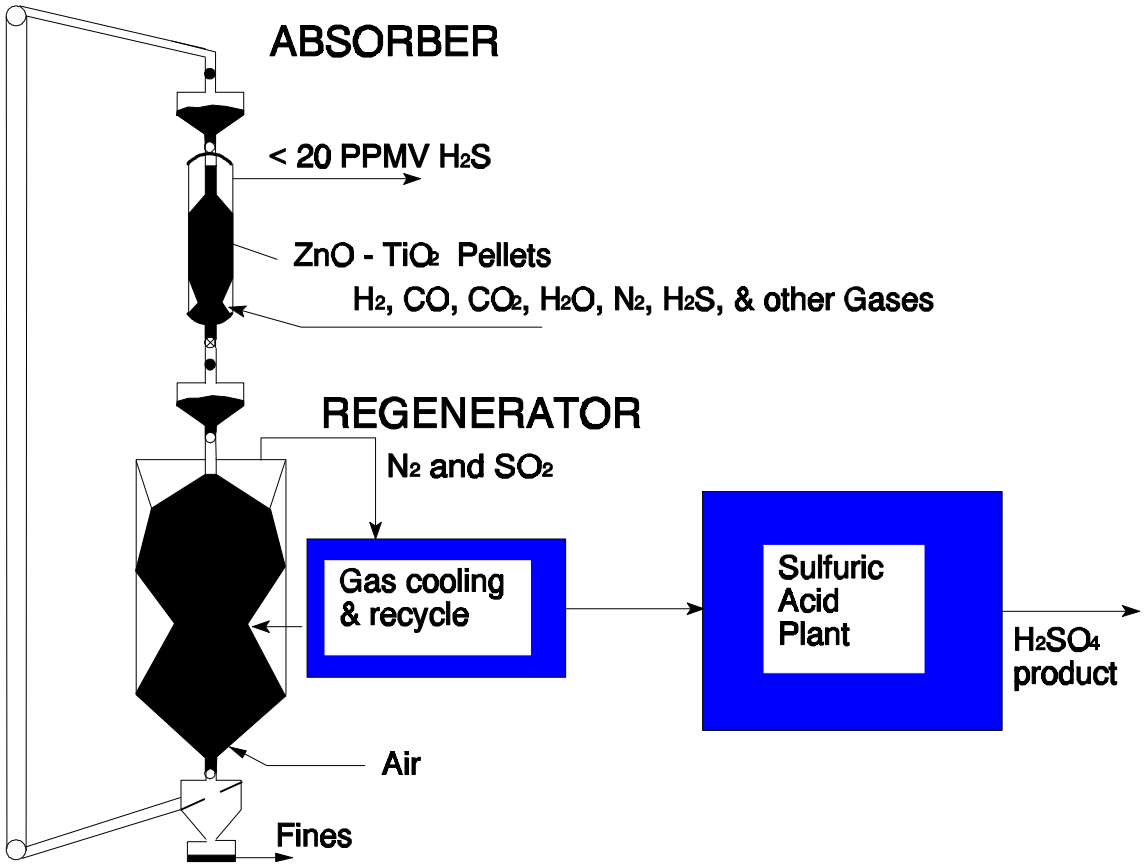

Figure 2. Moving Bed Reactor System

Recent developments in hot gas cleanup sorbents have reduced the spalling of the sorbent. Ayala *et al.* (1994) present data on both Z-Sorb and an improved zinc titanate. Z-Sorb, a product of Phillips Petroleum Company, performs well but is currently expensive. Similarly the zinc titanates are also expensive. These high costs are in part due to the high costs associated with small scale production but there may be factors in their production that require high costs. For example, several of Phillips' patents (*e.g.,* Khare 1994, Khare 1993, and Kidd *et al.* 1993) require the use of an aqueous acid solution (*e.g.,* nitric acid or acetic acid), which is later decomposed. Since the acids are lost in manufacture and the production equipment to handle acidic mixtures may be inherently expensive, Z-Sorb may be unavoidably expensive. A low cost sorbent that contains a large amount of active and accessible chemical sorbent and maintains a long life is necessary.

TDA Research, Inc. (TDA) is developing sorbents suitable for all three types of reactors. Under one contract, TDA is evaluating 3 to 5 mm sized sorbents for moving bed reactors ("A Long Life ZnO-TiO_2 Sorbent"); under a second contract ("A Novel Desulfurization Sorbent") we are evaluating 50 to 400 micron sized sorbents suitable for fluidized bed or transport reactors.

Objectives

The objective of this work was to develop and test long life sorbents for hot gas cleanup. Specifically, we measured the sulfur loading at space velocities typically used for absorption of H_2S and regenerated the sorbent with diluted air for multiple cycles. Based on the experimental results, we prepare a conceptual design of the sorbent fabrication system, and estimated the cost of sorbent production and of sulfur removal.

Technology

In order to make a sorbent pellet capable of holding large amounts of sorbent without being destroyed by the absorption-regeneration process, TDA has developed a new sorbent structure with the following characteristics: 1) is very strong, 2) allows the sorbent to expand and contract freely without disrupting the pellet structure, 3) allows the H_2S to diffuse quickly into the interior of the pellet, and 4) can contain very large amounts of sorbent without spalling.

TDA's process to produce the sorbent is also inherently low in cost and can achieve high loadings of the chemically active material. The sorbent is formed by mixed metal oxide techniques (*i.e.*, all of the ingredients are mixed at ambient temperature and fired only once), yet the sorbent has the high strength and long life typical of a catalyst support. In addition, the sorbent fabrication process does not require the use of an expensive decomposable salt.

Approach

TDA assembled a team to evaluate, produce and test sorbents for moving bed and fluidized bed reactors. The team members are TDA, Norton Chemical Process Products Corporation (Norton), and the Institute of Gas Technology (IGT). TDA defines the sorbents to be evaluated and conducts multiple cycle tests in our fixed bed reactors. Norton produces the sorbent by techniques representative of commercial production. IGT tested our sorbents for fluidized bed and/or transport reactor systems. General Electric will also be a subcontractor to evaluate our sorbents for moving bed applications.

TDA prepared small quantities of sorbents with many different compositions in order to identify the preferred firing conditions and starting materials. First we screened our raw materials by producing small batches of either chemical sorbent only or inert support only. Several sources of ZnO and titania were evaluated and tested to determine their crush strength, porosity, and surface area. From this matrix, we selected one source of zinc oxide and one of titania. To minimize the loss of surface area in the sorbent, we required that the sorbent be fired at a temperatures of 900°C (1652°F) or less.

We then produced sorbents with varying ZnO contents. We exposed these samples to 1% H_2S using simulated gasifier gases. We measured the sulfur content by chemical analysis after the first absorption and eliminated those compositions that had low sulfur loadings. We prepared a larger quantity of different sorbents and cycled them through several absorption and regeneration

cycles. We measured the sulfur content, pore volume, and crush strength of the initial material, and then remeasured these properties after absorptions after regenerations.

Norton Chemical Process Products Corporation (Norton) Based upon the test results we selected formulations for further evaluation. We then described the sorbent preparation methods to Norton. Norton is one of the world's leading producers of ceramic products and catalyst supports. Once under contract with TDA, Norton prepared larger batches of sorbents. Norton prepared >1 kg samples of the most promising formulations using techniques that are representative of commercial practice. After analysis of the Norton materials, we then tested formulations for multiple cycles measuring the breakthrough with the sorbent.

IGT Measurement of Attrition Resistance for Fluidized Bed Reactors A total of three zinc-oxide based sorbents were provided by TDA for testing in the attrition test unit to determine the relative attrition resistance of the sorbents. The attrition test unit at IGT was used to measure the relative resistance of the sorbents to attrition. In a unit of this type, the sorbent is exposed to a high velocity air jet for a specified period of time and the change in particle size distribution is measured. The unit consists of a 2.54-cm ID by 152-cm tall glass tube with a single 0.38-mm orifice gas inlet. During an attrition test the air flow is set to generate sonic velocity through the orifice, thus creating turbulence and a strong shearing effect to provide measurable attrition between the particles. These effects simulate attrition in commercial fluid-bed reactors over a much longer period of time.

To compare the attrition resistance of TDA's sorbents with that of other known material, IGT also conducted attrition tests with a sample of UCI 4169 zinc titanate sorbent as well as a limestone and a dolomite. This UCI sorbent was tested at Enviropower's pilot unit and was shown to have acceptable resistance to attrition during the pilot test. Therefore, it was decided to use this sorbent as the benchmark to evaluate the attrition resistance of other sorbents.

The results of the attrition tests are shown in Figure 3, indicating that all three TDA sorbents are more attrition resistant than the UCI's 4169 zinc titanate sorbent, which was tested by the Enviropower in the pilot scale unit. Furthermore, the attrition resistance of the sorbent 40ZN appears to be better than the limestone and the dolomite samples tested at the same operating condition. Based on the results of the attrition tests, the sorbent 40ZN was selected by TDA for sulfur reactivity test in a fluidized bed reactor and the same sorbent was tested at TDA in their fixed bed reactor.

Results

Moving Bed Reactor

TDA prepared sorbents and evaluated them for moving bed applications. Last year (Copeland *et al.* 1995) we reported on a spalling resistant sorbent tested for 20 cycles. This year we have improved our sorbent formulation. Over 60 formulations have been screened, non-promising sorbents (defined as having low reactivity, strength or attrition resistance) being eliminated. We have improved our attrition resistance to better than 98.5% while retaining high chemical activity

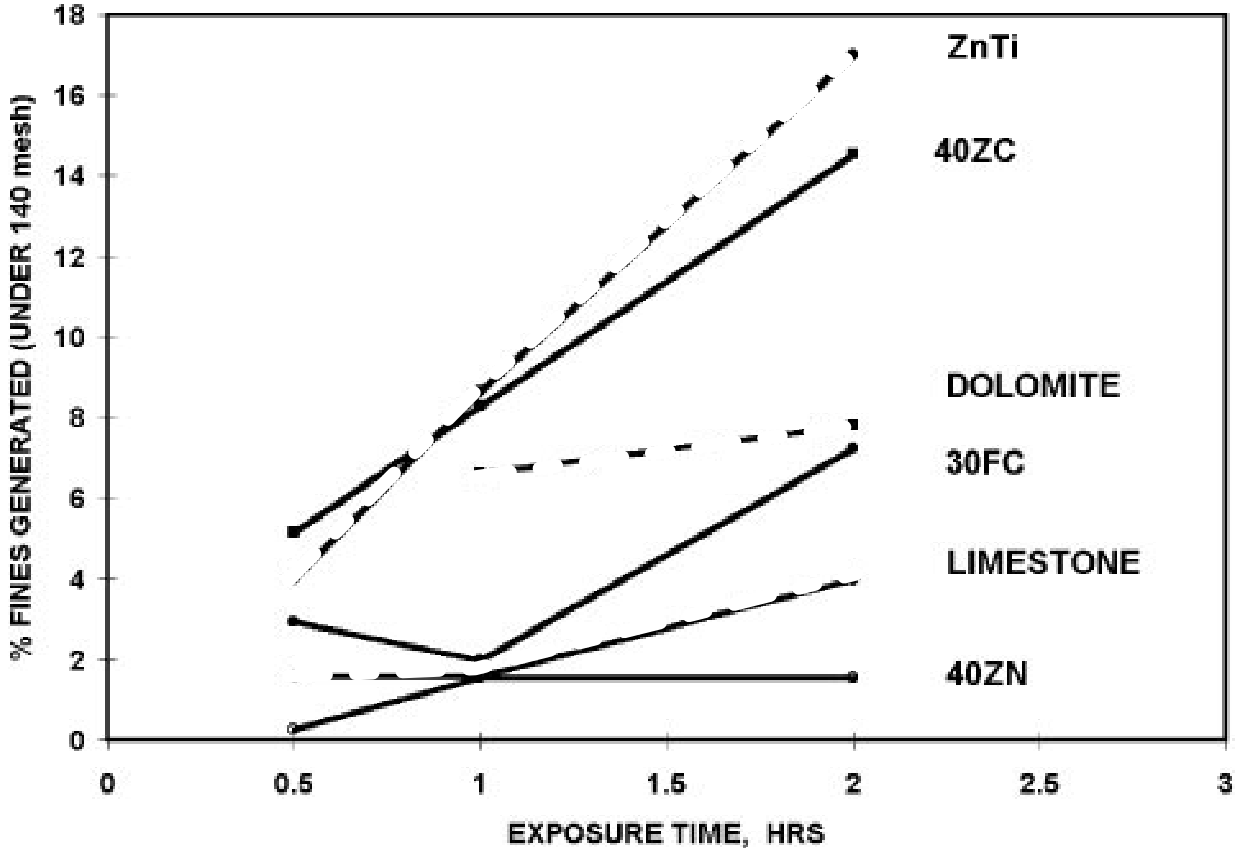

Figure 3 Attrition resistance of various sorbents.

and sulfur loadings.

Figure 4 presents the breakthrough of one of our latest sorbents with the addition of an improved (quartz liner) reactor. In this case, the sorbent removes the H_2S to less than 10 ppmv for several hours before breakthrough occurs. Since we are in the early stages of testing, additional cycles are currently being conducted.

The breakthrough in Figure 4 was conducted at 490°C and 11 atm in 1% H_2S and simulated Texaco gasifier gases. This sorbent, identified as ZVT12LN, has an initial crush strength of 14.8 lb/mm, porosity of 38% void, surface area of 1.3 m^2/g, an attrition resistance of >98.8% and a bulk density of 1.75 g/cc (109 lb/ft^3).

Table I presents the crush strength and sulfur capacity of several other sorbents currently being evaluated by TDA. Several different formulations were prepared and fired at different temperatures. Some of the series (*e.g.*, the ZZVTs) had high strength but relatively low sulfur capacities. Others high sulfur but relatively low strength. The ZZVS2 and ZAF11 had both high sulfur and high strengths. TDA is conducting additional cycling tests on these materials and will select one sorbent for 50 complete absorption/regeneration cycles.

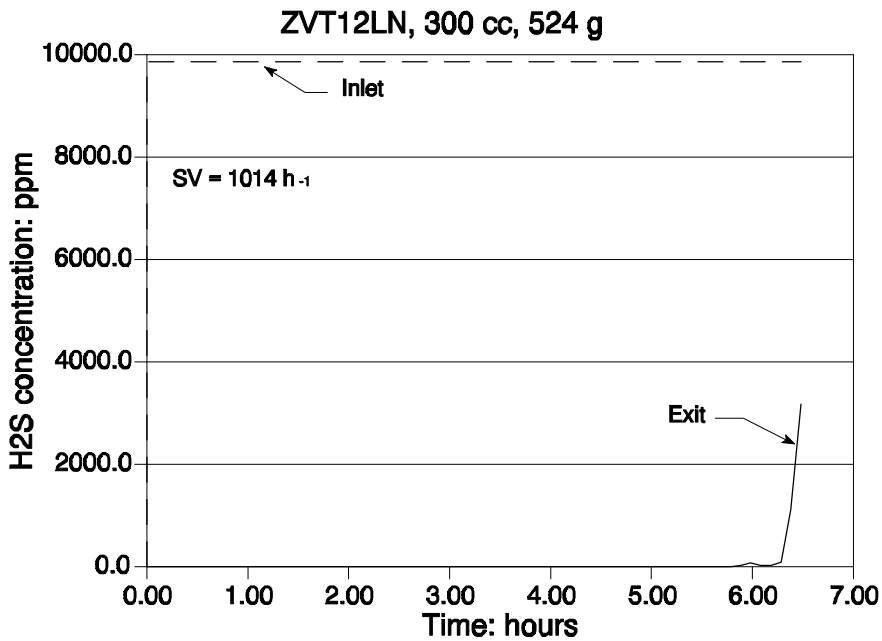

Figure 4. Cycling Of high strength/high capacity sorbent.

Table I Sulfur capacity sorbents for moving bed reactors at 482˚C (900˚F).

Sorbent	Crush strength fresh	Crush strength after regeneration	Sulfur loading lb/100 lb sorbent
ZZVT5	8.3	8.0	6.3
ZZVT6	10.6	8.4	4.5
ZZVS2	6.5	5.4	10.8
ZZVS3	6.2	5.5	8.5
ZZVS5	6.8	5.9	8.8
ZAF9	3.5	3.5	11.7
ZAF10	3.5	3.3	12.4
ZAF11	6.1	6.3	10.7

Fluidized Bed and Transport Reactors

Breakthrough Test Results Each of the absorption half cycles was conducted with simulated fluidized bed gasifier gases containing 1% H_2S entering the reactor at 538°C (1,000°F). The breakthrough data were measured until the exit gas stream exceeded 500 ppmv H_2S. Breakthrough cycles were carried out as follows:

- 40ZN 20 cycles in a fixed bed at TDA
- 40ZN 5 cycles in a fluidized bed at IGT

During the regenerations we raised the sorbent bed to 600°C and flowed diluted air for about 8 hours to oxidize the ZnS to ZnO. We then increased the O_2 concentration in stages, finally flowing only air through the reactor at 600°C to 650°C (all 40ZN tests). SO_2 was never added to the inlet air throughout any of these regenerations, which simulates the operating conditions of fluidized bed and transport reactors.

Table II presents the measured properties of the 40ZN sorbent before and after a 20 cycle test in a fixed bed reactor. There is very little change in the characteristics of the sorbent over the 20 cycles. The crush strength increased slightly but the porosity and surface area decreased. The bulk density was increased and some sulfur remained at the end of the 20th regeneration, probably in the form of zinc sulfate. Perhaps most importantly, we measured the mass of the sorbent added to and removed from the reactor after the tests.

Table II Properties of fresh and cycled 40ZN.

Property	Fresh	20 cycles *
Crush Strength	9.6 lb/mm	10.4 lb/mm
Pore Volume	0.22 ml/g	0.20 ml/g
Bulk Density	1.35 g/cc 84.2 lb/ft^3	1.47 g/cc 91.8 lb/ft^3
Surface Area	2.0 m^2/g	1.26 m^2/g
Sulfur (wt.)	0.00%	1.69% **

* After 20th Regeneration

** Equivalent to a 3.9% weight gain, if all sulfur is sulfate, indicating a net 2.2% loss in 20 cycles or 0.11%/cycle.

Figure 5 presents the breakthrough characteristics for 40ZN through 20 cycles. The sorbent removes H_2S effectively, a level less than 10 ppm(v) H_2S measured in our tests prior to breakthrough. The breakthrough data also show that the sorbent remained active throughout the 20 cycles. Unfortunately, the data for the first five cycles were lost which was due to experimental difficulties including problems with the mass flow controllers, which showed some times registered high and at others low. IGT also measured the breakthrough for the first five cycles on the same sorbent (see Figure 7) and showed no significant change in reactivity for the first cycles.

Figure 6 shows the sulfur capacity of the 40ZN, cycles 6-20. The data show some scatter in the breakthrough time. Another problem was found after we received data on the sulfur content of the regenerated sorbent after cycle 10. Those data showed that the sorbent was not being completely regenerated. Thus, some of the loss in the sulfur capacity may be due to incomplete regeneration in the fixed bed reactor (flowing gases for a fluidized bed reactor).

Figure 6 also presents data on the sulfur capacity of Z-SORB as a function of cycling. These data were measured by Gangwal *et al.* (1994) in a fluidized bed reactor and show a continuing loss of capacity for more than 20 cycles. Gangwal *et al.* measured the data for 50 cycles and the

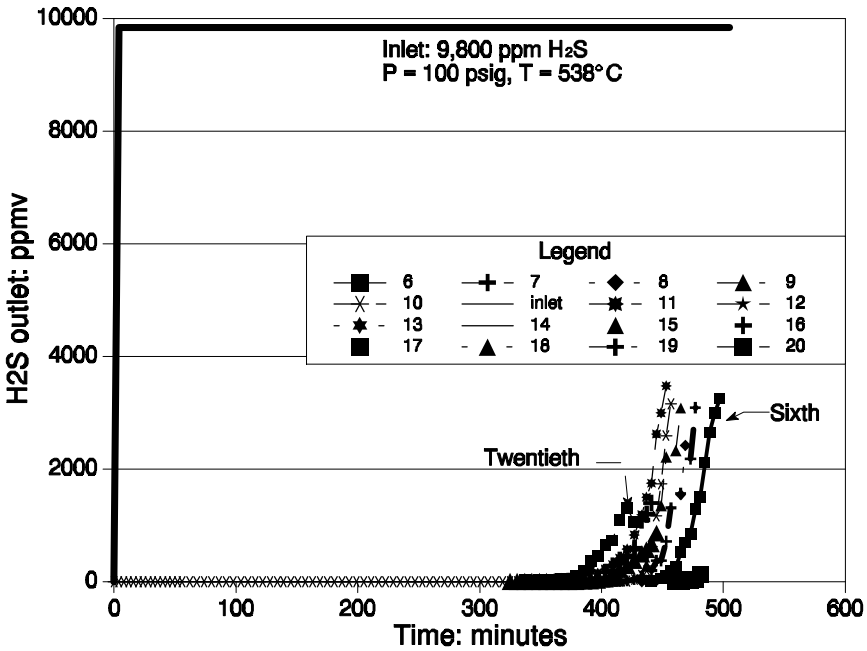

Figure 5 Cycling of 40ZN.

Z-SORB sorbent had been reduced to about half of its initial capacity at the end of their testing.

Sulfur Reactivity Tests at IGT The cyclic sulfidation/regeneration tests were conducted with the 40ZN sorbent over five cycles in the high-pressure/high-temperature reactor (HPTR) unit in the fluidized-bed mode of operation. This unit includes simulated hot coal-derived gas feed systems, an absorption/regeneration reactor, and associated process instrumentation and control devices. This bench-scale unit at IGT has been used for over hundreds of tests with excellent reproducibility and reliability. The gas feed system is capable of delivering simulated gas mixtures with different compositions representing various gasifiers containing CO, CO_2, H_2, H_2O, H_2S, N_2 and CH_4.

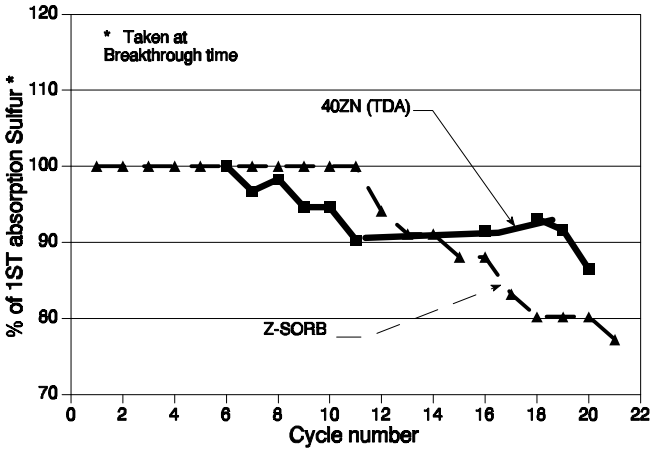

Figure 6 Sulfur capacity of 40ZN and Z-Sorb with cycling.

The H_2S breakthrough concentrations as a function of sulfur loading for the five sulfidation cycles are shown in Figure 7. The results indicate that the reactivity of the 40ZN sorbent did not decrease during the course of the five-cycle test. It should be emphasized that in order to test the sorbent and determine the effect of cycling on the sorbent reactivity, the experiments were conducted in a very short fluidized bed (and gas residence time), making the H_2S breakthrough concentration very sensitive to the reactivity of the sorbent. Therefore, in actual process, where

the gas residence time is expected to be several seconds (compared to about 0.5 seconds in these experiments), the H_2S breakthrough concentration will be very low.

In an earlier work performed by IGT for Enviropower Inc., the zinc titanate sorbent (ZnTi) selected for the pilot-scale testing was evaluated under similar operating conditions. Comparison of the results indicate that the initial reactivity of TDA's 40ZN is slightly lower than UCI's 4169. Although the reactivity of the latter has been shown to decrease gradually by about 50% in 30 cycles, mathematical simulation at IGT and pilot plant testing at Enviropower have shown that the reactivity of the UCI's 4169, after 30 cycles, is sufficient to reduce the H_2S content of the coal gas to below 20 ppmv.

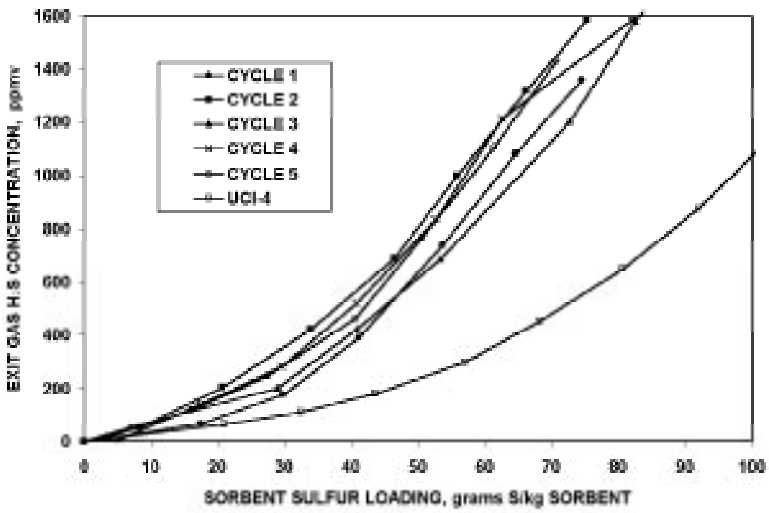

Figure 7 Reactivity of the 40ZN sorbent in successive cycles.

Given the excellent attrition resistance of the 40ZN, it is logical to assume that the rate of deterioration of this sorbent (if any), should be lower than that of other zinc titanate sorbents tested. Therefore, after a large number of cycles, the reactivity of the 40ZN is expected to be higher than the other zinc titanate sorbents, making it suitable for hot gas desulfurization in the IGCC process.

Application

We compared our sorbent to other sorbents currently under development for hot gas cleanup. The results for the moving bed application were presented last year (Copeland *et. al.* 1995) and showed significant advantages for our sorbents.

We compared our fluidized bed/transport reactor sorbents to other sorbents currently under development for hot gas cleanup. Table III presents a comparison between the 40ZN and Z-Sorb B, produced by the Phillips Petroleum Corporation. Our sorbents are more dense and have a similar, though lower, sulfur capacity.

The attrition resistance of 40ZN is very good. The data from IGT show loss rates of only 1% per hour under test conditions where zinc titanate lost 8% per hour. Z-Sorb, when tested under fluidized bed conditions (Gangwall *et al.* 1994), lost only 0.5% in 50 cycles, which is similar to zinc titanate (less than 2% in 100 cycles with a measured attrition resistance of 8%/h) (Gangwal *et al.* 1995). Thus, we can anticipate that our higher attrition resistance will lead to a sorbent with a longer life. Although an improvement factor of 8 is indicated by the available attrition

data, we conservatively estimate an improvement factor of 3 in the life of the sorbent.

Table III Comparison of ZnO based sorbents.

	40ZN TDA	Z-SORB B Phillips
Sulfur Capacity (lb S/100 lb fresh)	12	10.6-16.2
lb sorbent/ft^3 of Bed	84	60

Although the sulfur loadings of both TDA's sorbent and Z-Sorb are similar, only a fraction of the sulfur capacity is utilized in a transport reactor. The transport reactor at Piñon Pine is designed to never fully regenerate the sorbent and a significant fraction of the sorbent remains in the sulfided form when it leaves the regenerator. This design eliminates any formation of sulfate, due to the very low equilibrium oxygen pressure. The reactor design also limits the quantity of sulfur that is removed per cycle to about 3 lbs of sulfur per 100 lbs of fresh sorbent, regardless of the total sulfur loading in the sorbent. Although TDA's sorbents have lower sulfur loading, the greatly higher attrition resistance improves our economic potential substantially, since Sierra Pacific reports that attrition loss is one of the major concerns with Z-Sorb in their plant.

The improvement in sorbent replacement costs, calculated from the available data, is shown in Table IV. The data on Z-Sorb was taken from the letter from Sierra Pacific; *i.e.*, a cost of $8/lb for Z-Sorb and 10 lbs of sulfur removed per lb of sulfur loss (although we have other information from Kellogg that indicates that Z-Sorb will not meet this goal). As can be seen by our estimates, the cost/performance for 40ZN is significantly less than other systems developed to date, and can meet or exceed the cost goals set for hot gas cleanup systems. As we are still in the early stages of our development, we anticipate the cost/performance of our sorbents to further improved with future work.

Future Activities

TDA produced several different sorbent formulations with different zinc oxide contents, and different strengths and pore volumes. One sorbent formulation was selected for multiple cycle tests, and the measured properties of the sorbent improved slightly over the 20 cycle test. The initial selection was a sorbent that has a high sulfur loading capacity. The sorbent is resistant to spalling and retained its reactivity, porosity, and crush strength with cycling.

TDA compared the performance of our sorbents to that of other sorbents. We found that our sorbents have a higher sulfur content per unit volume and similar costs to other hot gas cleanup sorbents. However, additional work will be needed to develop and demonstrate that these improvements can be achieved on a larger scale and for more cycles.

We will be improving the properties of our sorbent. A number of multiple cycle breakthrough tests will be conducted to determine the impact of cycling on different methods of forming the sorbent. Finally, after an improved sorbent formulation has been developed and proven, a revised

Table IV Sorbent replacement costs for zinc oxide based sorbents.

Cost Element	40ZN	Z-Sorb
Sulfur removal rate	3 lbs sulfur removed per 100 lbs of fresh sorbent per cycle	3 lbs sulfur removed per 100 lbs of fresh sorbent per cycle
Loss Rate:	1% per hour of fluidization (about 30 lbs sulfur/lb sorbent consumed)	10 lbs sulfur/lb sorbent (goal, currently less than this value)
Cost: $/ton sorbent	≈ 16,000*	16,000**
Cost of Sorbent Replacement	≈ $600 per ton sulfur	> $1,800 per ton sulfur

* at $8/lb, estimated by Norton for small production lots.
** Cost data from Sierra Pacific.

production cost analysis will be conducted and the economics of hot gas cleanup calculated and compared to that of other sorbents.

References

Ayala, R.E., T. Chuck, E. Gal, and R.P. Gupta (1994). Development of Sorbents for High Temperature Desulfurization in Moving-Bed Systems," in *Proceedings of the Coal-Fired Power Systems 94 -- Advances in IGCC and PFBC Review Meeting*, Bonk, sponsored by U.S., Department of Energy, Morgantown Energy Technology Center: Morgantown, West Virginia, Report No. DOE/METC-94/1008, (CONF-9406131). Springfield, VA: National Technical Information Service.

Copeland, R.J., M. Cesario, M. Dubovik, D. Feinberg, and B. Windecker (1995). "A Long Life ZnO-TiO_2 Sorbent," in *Proceedings of the Advanced Coal-Fired Power Systems 95 Review Meeting*, sponsored by U.S., Department of Energy, Morgantown Energy Technology Center: Morgantown, West Virginia, Report No. DOE/METC-95/1018, (NTIS/DE95009733). Springfield, VA: National Technical Information Service.

Gangwal, S.K. and R.P. Gupta (1994). "Fluidized-Bed Sorbents," in *Proceedings of the Coal-Fired Power Systems 94 -- Advances in IGCC and PFBC Review Meeting*, editor H.M. McDaniel, R.K. Staubly, and V.K. Venkataraman, sponsored by U.S., Department of Energy, Morgantown Energy Technology Center: Morgantown, West Virginia, Report No. DOE/METC-94/1008 (CONF-9406131). Springfield, VA: National Technical Information Service.

Jung, D.Y., J.S. Kassman, T.F. Leininger, J.K. Wolfenbarger, and P.P. Yang (1992). "Integration and Testing of Hot Desulfurization and Entrained Flow Gasification for Power Generation

Systems," presented at the *Twelfth Annual Gasification and Gas Stream Cleanup Systems Contractors Review Meeting*, Morgantown, West Virginia: Morgantown Energy Technology Center, U.S. Department of Energy, September 15-17. Springfield, VA: National Technical Information Service.

Khare, G.P. (1993). *Absorption of Hydrogen Sulfide and Absorbent Composition therefor*, United States patent Number 5,244,641.

Khare, G.P. (1994). *Absorption of Hydrogen Sulfide and Absorbent Composition therefor*, United States patent Number 5,306,685.

Kidd, D.R., G.A. Delzere, D.H. Kubicek, and P.F. Schubert (1993). *Selective Removal of Hydrogen Sulfide over a Zinc Oxide and Silica Absorbing Composition*, United States patent Number 5,248,489.

Mei, J.S., L. Gasper-Galvin, C.E. Everitit, and S. Katta (1993). "Fixed-Bed Testing of a Molybdenum-Promoted Zinc Titanate Sorbent for Hot Gas Desulfurization," in *Proceedings of the Coal-Fired Power Systems 93 -- Advances in IGCC and PFBC Review Meeting*, editor D.L. Bonk, sponsored by U.S., Department of Energy, Morgantown Energy Technology Center: Morgantown, West Virginia, Report No. DOE/METC-93/6131 (CONF-9306148). Springfield, VA: National Technical Information Service.

Contract Information

Contract Number: Research sponsored by the U.S. Department of Energy, SBIR program, under contracts DE-FG03-94ER84881 and DE-FG03-95ER82090; **Contractor**: TDA Research, Inc., 12345 West 52nd Avenue; Wheat Ridge, Colorado 80033; (303) 422-7819; FAX (303) 422-7763. TDA Research, Inc. Contractor Project Manager: Michael E. Karpuk.

Acknowledgements

TDA gratefully acknowledges the technical guidance of Ronald Staubly, our METC Project Manager, the work of our two subcontractors: Norton Chemical Process Products Corporation, who fabricated sorbents for our tests and the Institute of Gas Technology who conducted the fluidized bed reactor tests, and the technical latest data on moving bed reactors from Raul Ayala of General Electric. Period of Performance: August 1994 - June 1997.

Manganese-Based Sorbents for Coal Gas Desulfurization

Lee D. Gasper-Galvin (LGASPE@METC.DOE.GOV; 304-285-4832)
Edward P. Fisher (EFISHE@METC.DOE.GOV; 304-285-4011)
Morgantown Energy Technology Center

William J. Goyette (410-789-8800, x167)
Chemetals

Introduction

Manganese-based sorbents have previously been investigated for sulfur removal from coal gases at high temperatures, e.g., 800 °C (1,472 °F) and above, and with simulated low-Btu fuel gas or mixtures of H_2S and H_2 in N_2 (Turkdogan and Olsson, 1978; Hepworth and Slimane, 1994). The special emphasis on higher temperatures was because manganese oxide is one of the few metal oxides that have stability and coal gas desulfurization potential at such temperatures.

Some studies have been performed at lower temperatures, e.g., 400 to 800 °C (752 to 1,472 °F) (Wakker and Gerritsen, 1990a, 1990b); these researchers showed that increasing H_2 and CO increases the sulfur capacity of a sorbent containing Mn oxide and alumina, while increasing H_2O decreases the sulfur capacity. Thermodynamic studies (Westmoreland, et al. 1976) suggest that Mn-based sorbents may perform much better in the range of 400 to 800 °C (752 to 1,472 °F) than at higher temperatures. Hepworth and Slimane (1994) also showed a graph of calculated equilibrium levels of H_2S in the presence of temperatures from 700 to 1,200 °C (1,292 to 2,192 °F) for different types of coal gas. The graph indicated that the lowest equilibrium H_2S levels were obtained in the presence of oxygen-blown Shell gas at the lowest temperatures. Thermogravimetric analysis studies by Westmoreland, et al. (1977) showed that among sorbents consisting of the oxides of Mn, V, Ca, and Zn, the Mn oxide showed the highest reaction rate over the temperature range 300 to 800 °C (572 to 1,472 °F).

Since overall sorbent performance is a combination of the effects of thermodynamics, kinetics, and gas-solid mass transfer resistance, it seems reasonable from the information cited above that an Mn-based sorbent would perform very well in a highly reducing Shell gas at lower temperatures. The present study shows the effect of temperature, inlet H_2S concentration, and type of coal gas (air-blown KRW gas versus oxygen-blown Shell gas) on the performance of Mn-based sorbent. The sorbent used for these studies was CST-939 from Chemetals (Baltimore, Maryland). The CST-939 is a proprietary sorbent containing essentially 96 percent MnO, and has previously been marketed as guard bed material for use downstream from hydrodesulfurization units and upstream from reformers in petrochemical refining.

Objectives

The intent of this study is to perform a preliminary screening on a particular Mn-based sorbent, CST-939 (from Chemetals), for hot gas desulfurization. The purpose of the preliminary screening is to determine which temperature and type of coal gas this sorbent demonstrates the greatest capacity and efficiency for sulfur removal.

Approach

The first two sets of experiments, tests CST1 and CST2, were conducted with simulated KRW gas containing 2,000 ppmv H_2S and 871 and 343 °C (1,600 and 650 °F), respectively. Due to the tremendous capacity of the sorbent, these experiments required as long as 75 hours to achieve breakthrough (breakthrough is defined as 200 ppmv H_2S in the outlet gas). Therefore, the later experiments were conducted with simulated KRW gas (or Shell gas) containing 30,000 ppmv H_2S to decrease the time required for breakthrough. A set of six experiments, three with KRW gas and three with Shall gas, were conducted for 1.5 cycles each at temperatures of 343, 538, and 871 °C (650, 1,000, and 1,600 °F). A fresh sample of the sorbent was used for each set of experiments.

During one of the early experiments (test CST2) using 2,000 ppmv H_2S, the regeneration temperature was ramped from 343 °C (650 °F) to 871 °C (1,600 °F) to determine the lowest temperature that may be sufficient for regeneration with 50 mol percent air/50 mol percent steam. The extent of regeneration was indicated by the amount of SO_2 given off at each temperature. Sulfur dioxide as high as 3.0 volume percent was given off after 1/2 hour on-stream at 343 °C (650 °F), as shown by gas chromatographic analysis, but the concentration then dropped off rapidly and regeneration was not sustained at this temperature. A relatively small amount of SO_2 was released at 538 °C (1,000 °F). The rate of regeneration finally increased at 649 °C (1,200 °F), at which temperature concentrations as high as 23.8 percent by volume SO_2 were measured. The additional SO_2 that was released at 760 °C (1,400 °F) was minimal. Finally, when the sorbent bed was raised to a temperature of 871 °C (1,600 °F), significant quantities of SO_2 were released, giving a concentration as high as 2.2 percent by volume. Since $MnSO_4$ decomposes in air at an atmospheric pressure of 850 °C (1,562 °F), it is not surprising that additional sulfur was released after heating the sorbent to 871 °C (1,600 °F). It was concluded that 871 °C (1,600 °F) would be the best temperature for air-steam regeneration of the sorbent.

During the second sulfidation of the CST2 series of experiments described above, it was noted that a significant amount of SO_2 was released during the first hour on-stream. This indicated that regeneration was not complete, even after using the air-steam mixture at 871 °C (1,600 °F). Another set of experiments (CST3) was conducted in which the first regeneration was conducted with air-steam at 871 °C (1,600 °F) and the second regeneration was performed in the same manner, except the oxidative regeneration step was followed by a reductive regeneration step. Reductive regeneration was carried out with simulated KRW gas without H_2S for 11 hours. The result of the reductive regeneration was that no SO_2 was detected during the first 2-1/2 hours on-stream and no higher than 3.0 ppmv was detected afterward.

Thus, it could be seen that a reductive regeneration step was helpful. For the remaining experiments, a simplified reductive regeneration was used, as described in the Experimental Methods section.

Experimental Methods

A schematic diagram of the experimental apparatus is shown in Figure 1. The apparatus consisted of a gas-mixing system, a fixed-bed reactor, a water-cooled condenser with a water knock-out pot, an ice water-cooled condenser with a water knock-out pot, a gas sampling system, and a tail-gas cleanup system. The gas mixture feed to the reactor simulated the partially quenched exit gas of an air-blown KRW fluidized-bed coal gasifier or an oxygen-blown Shell entrained-bed coal gasifier, with the molar compositions given in Table 1. Gases were supplied from gas cylinders and the flow rates were controlled and monitored through MKS Model 1159B mass flow controllers with two MKS Model 247C four-channel digital readouts, except for the nitrogen purge gas, which was metered through a Matheson Model FM-1050-VIA, 603 tube rotameter. After the gases were mixed in a manifold, they were fed into the fixed-bed reactor. Steam was introduced by feeding a predetermined amount of water into the gas stream via an ISCO Model 100D metering pump.

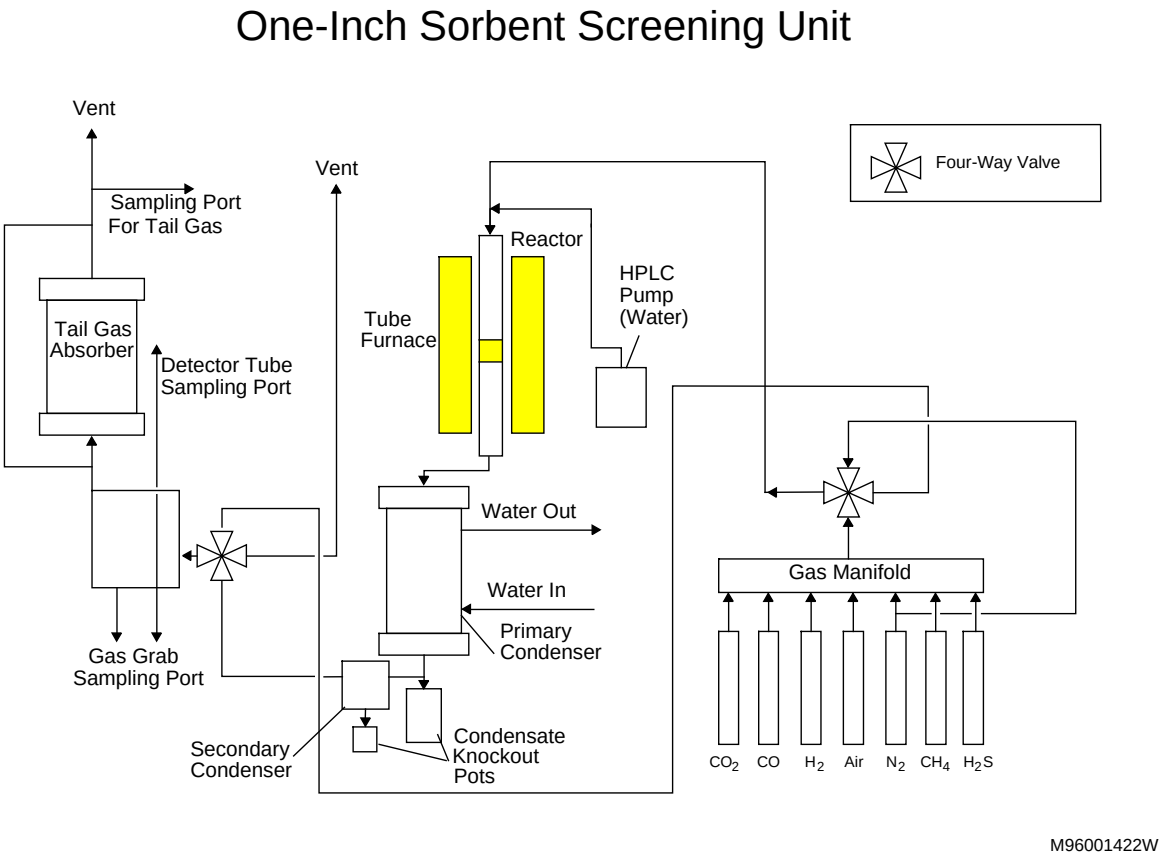

Figure 1

Table 1. Simulated Gas Composition

Shell Gas Percent		KRW Gas Percent	
Carbon Dioxide	2.0	Carbon Dioxide	11.0
Carbon Monoxide	64.1	Carbon Monoxide	12.5
Hydrogen Sulfide	3.0	Hydrogen Sulfide	3.0
Methane	0.0	Methane	1.0
Hydrogen	27.3	Hydrogen	13.8
Steam	2.0	Steam	19.0
Nitrogen	Balance	Nitrogen	Balance

The reactor consisted of an alonized 316-stainless steel (SS) tube, with a 2.54-cm (1-inch) outside diameter (OD), a 0.165-cm (0.065-inch) wall thickness, and 114.3-cm (45-inch) length. Alonization of the reactor was necessary to minimize the corrosion of the stainless steel by H_2S, particularly in the presence of high-temperature steam. The reactor was placed vertically in a Lindberg tubular electric furnace.

The gas mixture was preheated as it passed through the top half of the reactor tube. The temperatures of the gas at the inlet and the center of the reactor bed were measured by Omega K-type quick-connect thermocouples located along the central axis. The thermocouples were connected to an Omega Model 199A digital readout via an Omega Model OSW3-20-PG rotary selector switch. The reactor inlet and outlet pressures were measured with Matheson Model 63-5651 308 kPa (30 psig) test gauges. The reactor was designed to withstand a pressure of 308 kPa (30 psig) and a temperature of 982 °C (1,800 °F). The over-temperature circuit on the tube furnace was set for 927 °C (1,700 °F).

The sorbent sample was placed in the center of the reactor and the bed height was 7.6 cm (3 inches). The sorbent bed was supported on an alonized, 316 SS perforated plate with a layer of glass wool to catch any fines that might be produced from the bed. The gas lines between the reactor outlet and the condenser inlet were heated via Thermolyne heavy Samox-insulated heating tapes regulated with Omega 6200 temperature controllers and were insulated with a Fiberfax blanket to prevent steam condensation in the gas lines. The exit gas from the reactor was filtered with a Balston Model B49 filter unit containing a Balston Model 050-11-BQ filter tube, cooled in two condensers (a primary condenser that was water-cooled, followed by a secondary condenser that was ice water-cooled), and sampled for gas analysis. The tail gas was sent through an absorber (316 SS, 8.9-cm [3.5-inch] OD, schedule 40 pipe, 41.9 cm [16.5 inches] long) containing a zinc-based sorbent to remove the sulfurous gases before discharge to the atmosphere. The condensates from the two condensers were caught in their respective water knock-out pots located below the condensers. The water knock-out pots consisted of 1.3-cm (0.5-inch) OD, 0.089-cm (0.035-inch) wall, 25.4-cm (10-inch) long 316 SS tubes.

The conditions for oxidative regeneration and reductive regeneration are shown in Table 2. The test matrix, with actual run numbers, sulfidation conditions, and the number of sulfidation/regeneration cycles, is given in Table 3. Gastec precision gas detector tubes were used to determine the H_2S and SO_2 concentrations in the inlet and outlet gas streams to plus or minus 25 percent. All gaseous components (other than water vapor) were analyzed by gas chromatography of gas grab samples and/or via an on-line VG Prima 600 mass spectrometer. Sulfidation was stopped when the hydrogen sulfide concentration of the effluent gas reached 1,000 ppmv for sulfidations run with KRW gas and 400 ppmv for sulfidations run with Shell gas. Following sulfidation, the reactor was purged with nitrogen to flush out the reducing gas. The oxidative regeneration with air-steam was stopped when the SO_2 concentration of the effluent gas was below 50 ppmv. Reductive regeneration was conducted for 4 hours unless the combination of ppmv H_2S plus ppmv SO_2 dropped below 50 ppmv prior to 4 hours on-stream, at which time the regeneration was stopped. A fresh load of sorbent was subjected to each set of sulfidation/regeneration conditions to establish its sulfur sorption capacity and efficiency. Some experiments were repeated to verify the results, particularly for cases in which any operating difficulties were encountered.

Table 2. Regeneration Conditions

Oxidative		Reductive	
Temperature	1,600 °F	Temperature	1,600 °F
Pressure	15 psig	Pressure	15 psig
Composition:		Composition:	
Air	50%	Hydrogen	25%
Steam	50%	Nitrogen	75%

Table 3. Sorbent Test Matrix

Test Number	Coal Gas/H_2S Concentration	Temperature/Cycles
CST1	KRW/0.2%	871 °C/1.5
CST2	KRW/0.2%	343 °C/1.5
CST3	KRW/3.0%	871 °C/2.5
CST4	KRW/3.0%	871 °C/1.5
CST5	KRW/3.0%	538 °C/1.5
CST6	Shell/3.0%	343 °C/~1.0
CST7	Shell/3.0%	538 °C/1.5
CST8	Shell/3.0%	871 °C/1.5
CST9	Shell/3.0%	343 °C/1.5
CST10	KRW/3.0%	343 °C/1.5
CST11	Shell/3.0%	871 °C/1.5

Sorbent samples were analyzed for total sulfur content and crush strength. Sulfur content was determined using a LECO analyzer. Crush strengths were obtained by compressing the

sorbent extrudates between the two flat surfaces of a Chatillon crush strength tester until the point of breakage.

Results and Discussion

Selected H_2S breakthrough curves are shown in Figures 2 through 5. These graphs show the effect of temperature in simulated KRW gas, inlet H_2S concentration in simulated KRW gas, type of simulated gas mixture (i.e., KRW or Shell gas), and the effect of temperature in simulated Shell gas, respectively. Each of these graphs will be discussed in more detail below. The data shown are the result of detector tube or mass spectrometer analysis of the outlet H_2S concentration.

The H_2S breakthrough curves from test series CST1 and CST2, shown in Figure 2, illustrates the dramatic effect of temperature on sulfur removal efficiency and capacity. These tests were conducted with simulated KRW gas containing 2,000 ppmv of H_2S, at 871 °C (1,600 °F), and 343 °C (650 °F), respectively. The final letter of each test number indicates whether it was a first or second sulfidation, e.g., CST1A was the first sulfidation of test series CST1, while CST1C was the second sulfidation of the same test series (CST1B, which is not shown, was the first regeneration). It is apparent from Figure 2 that the CST-939 sorbent performed poorly at 871 °C (1,600 °F) in the presence of simulated KRW gas. However, at 343 °C (650 °F), it performed quite satisfactory during the first sulfidation, yielding a pre-breakthrough H_2S concentration of approximately 40 to 60 ppmv for nearly 60 hours on-stream. With breakthrough defined as the point at which the outlet concentration of H_2S reaches 200 ppmv, then breakthrough occurred at approximately 75 hours on-stream. The second sulfidation, however, broke through at 41 hours on-stream and significant quantities of SO_2 (usually > 100 ppmv) were released during the first 30 hours on-stream. This early breakthrough and SO_2 release suggests there may have been a problem with regenerability. However, many sorbents do not show stable performance until the third or fourth cycle and, therefore, a multicycle test would be required to establish the extent of regenerability of the sorbent under these conditions.

Figure 3 shows the comparison of series CST1, with an inlet concentration of 2,000 ppmv H_2S, and series CST4, with 30,000 ppmv H_2S, conducted with simulated KRW gas at 871 °C (1,600 °F). As expected, the higher concentration shows more rapid breakthrough.

The dependence of sorbent performance on the type of simulated coal gas is shown in Figure 4. These experiments were conducted at 538 °C (1,000 °F) with 30,000 ppmv H_2S inlet concentration. The CST5 series was run with simulated KRW gas, and the CST7 series was run with simulated Shell gas. It is clearly seen that both the efficiency and the capacity of the sorbent are considerably better in the presence of Shell gas. This is in agreement with what had been (1) predicted by the equilibrium calculations of Hepworth and Slimane (1994), and (2) implicated by experiments on the effect of increasing H_2 and CO, while decreasing H_2O, by Wakker and Gerritsen (1990). While the sorbent performance in Shell gas, showing a pre-breakthrough concentration of 50 ppmv or less of H_2S, would be acceptable for most

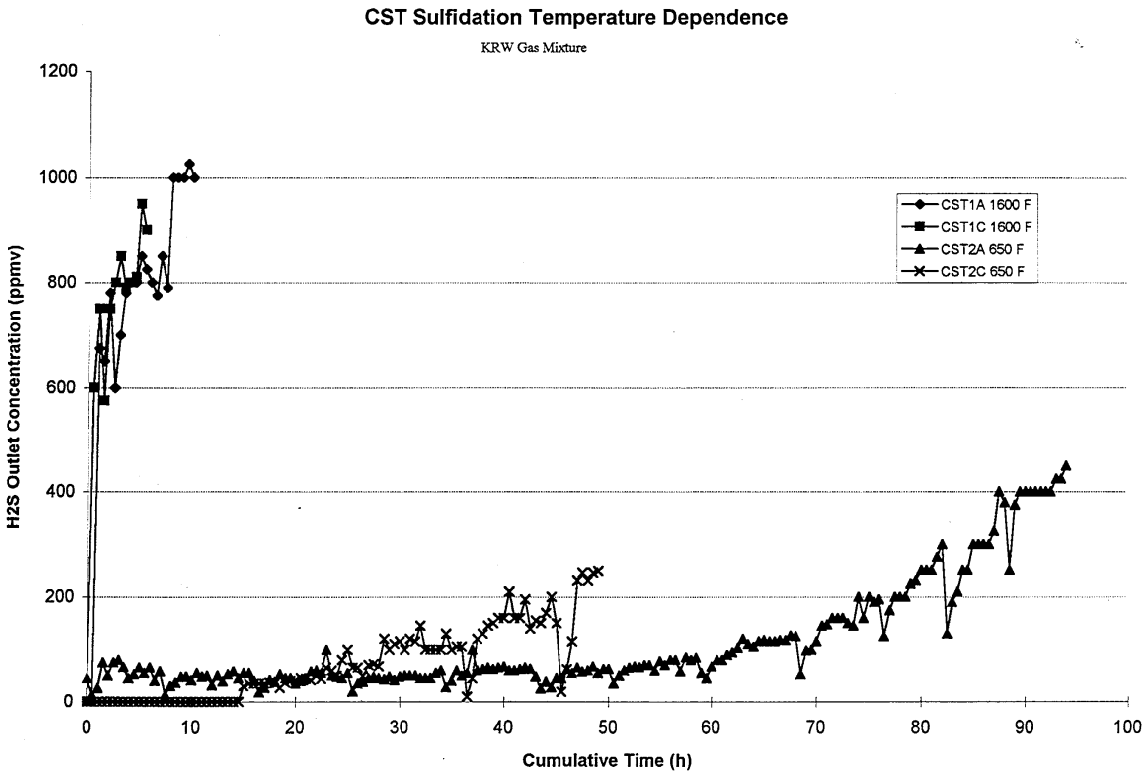

Figure 2

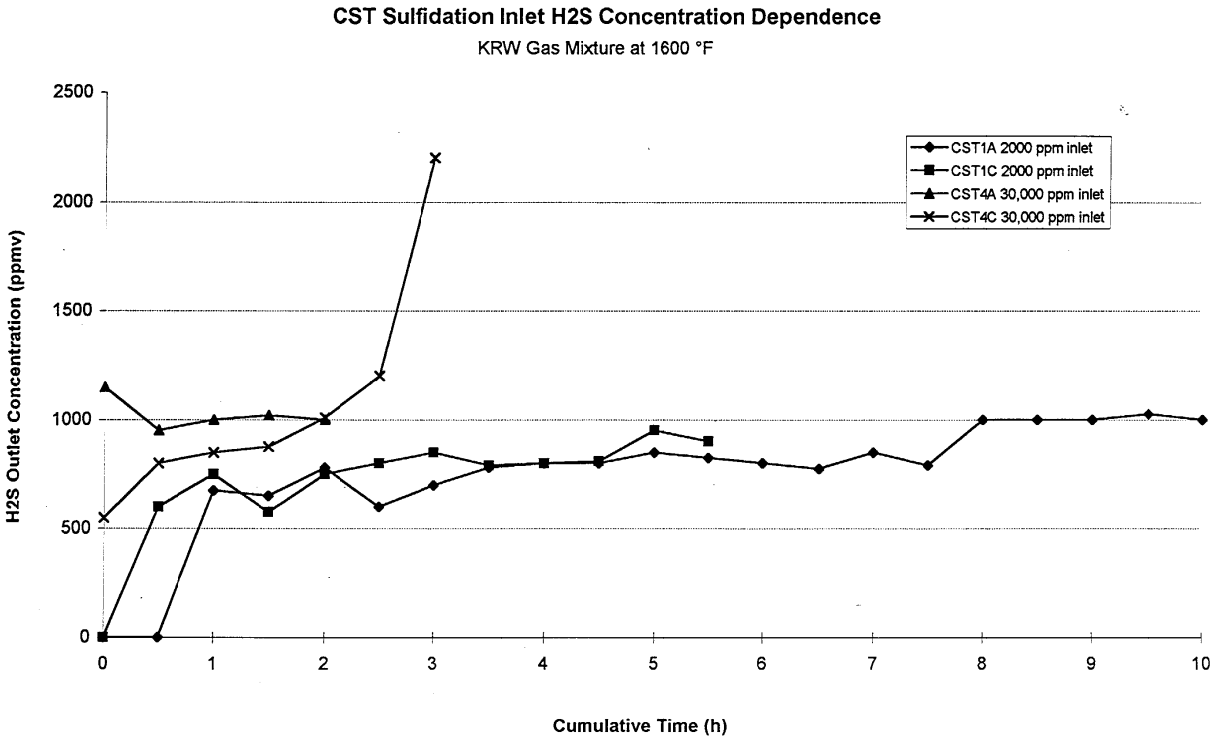

Figure 3

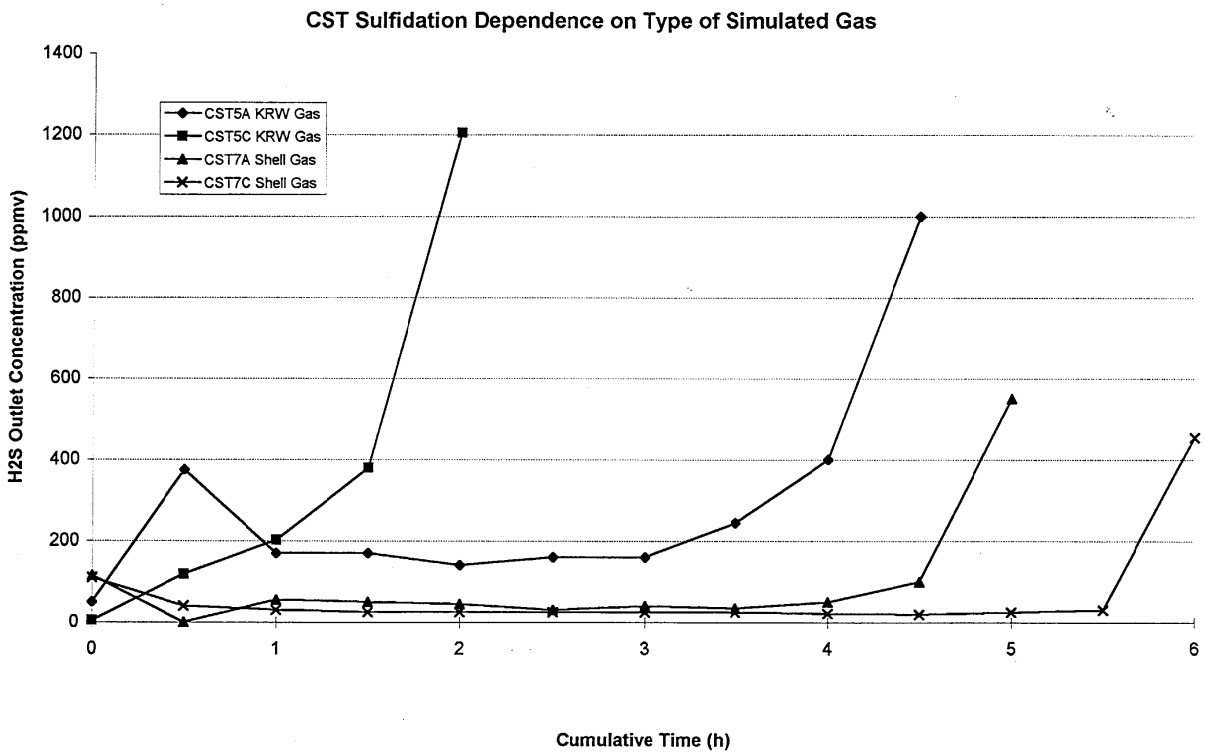

Figure 4

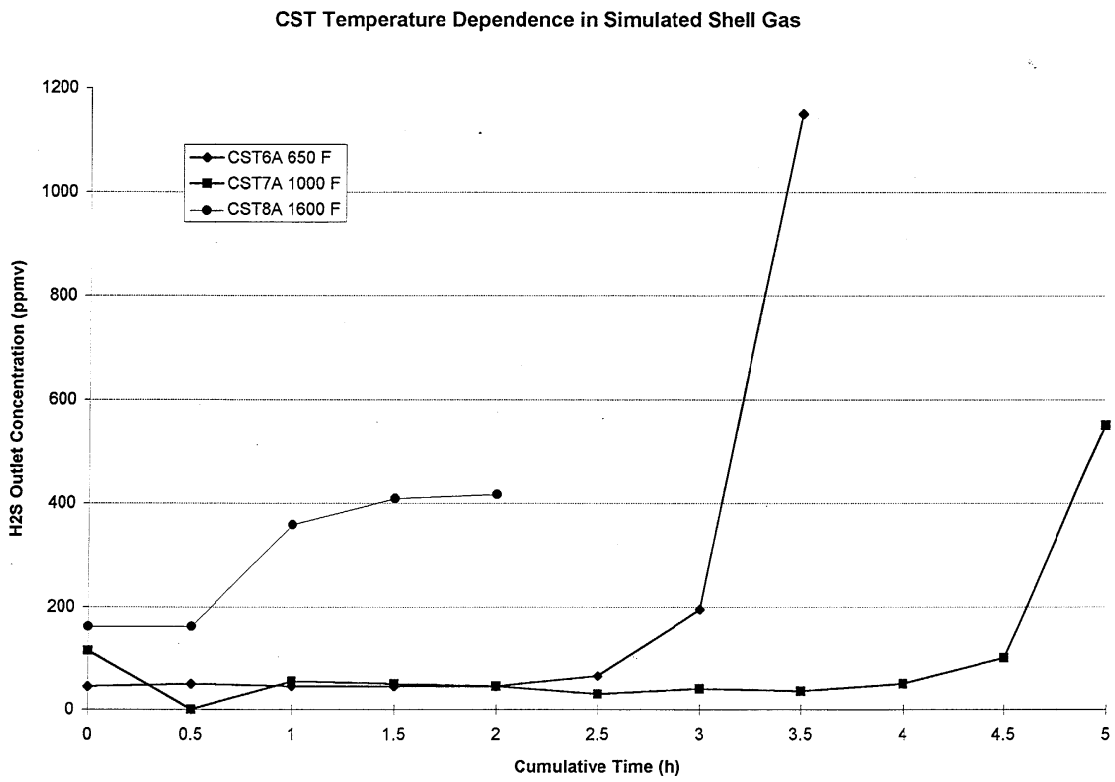

Figure 5

IGCC applications, the performance in KRW gas, with approximately 180 ppmv H_2S in the outlet gas, would be unacceptable.

Figure 5 shows the temperature dependence of sorbent performance in simulated Shell gas during the first sulfidation at 343, 538, and 871 °C (650, 1,000, and 1,600 °F). All measured concentrations of H_2S during the experiment at 871 °C (1,600 °F) were unacceptably high. However, the sorbent performed quite well at the lower temperatures of 343 and 538 °C (650 and 1,000 °F), with pre-breakthrough H_2S concentrations of approximately 50 ppmv. These data suggest that 538 °C (1,000 °F) may be the best operating temperature, since the breakthrough time at this temperature was 50 percent longer. Caution should be used in this interpretation, however, because many sorbents do not show their stable performance until the third cycle of sulfidation/regeneration.

Table 4 shows the sulfur loading of each sorbent after being removed from the reactor, through test CST8. The loading was determined by LECO analysis for total sulfur content. Note that the sulfur loadings for CST7 and CST8, which were conducted with simulated Shell gas, were significantly higher than those for CST4 and CST5, which were run with simulated KRW gas under otherwise similar conditions. This is consistent with the related breakthrough curve results.

Table 4. Sorbent Sulfur Loading

Sorbent Type	Sulfur Loading (%)
CST1A-C	0.76
CST2A-C	10.75
CST3A-E	9.39
CST4A-C	6.76
CST5A-C	7.02
CST6A-B	1.78
CST7A-C	21.27
CST8A-C	14.85

by Leco analysis

The crush strength (in lb/pellet) for the fresh sorbent and reacted samples through test CST8 are shown in Table 5. The values given are the average from testing 15 pellets, with the standard deviation given in square brackets. It is important to note that in spite of the substantial amounts of sulfur loaded, the crush strength was not significantly less than that of the fresh sorbent, and in many cases was significantly greater.

Table 5. Crush Strength

Sorbent Type	Crush Strength [std. dev.]
CST-939 (fresh)	10.4 [3.0]
CST1A-C	17.7 [7.0]
CST2A-C	9.4 [5.1]
CST3A-E	13.6 [6.8]
CST4A-C	16.2 [7.0]
CST5A-C	12.4 [4.6]
CST6A-B	11.8 [5.2]
CST7A-C	33.5 [10.4]
CST8A-C	16.7 [7.9]

Conclusions

The following conclusions were made from the data collected on the CST-939 sorbent:

- The sorbent efficiency and capacity are much greater at 343 °C (650 °F) than at 871 °C (1,600 °F).
- The sorbent efficiency and capacity are much greater in the presence of the more highly-reducing Shell gas than with the less-reducing KRW gas.
- The sorbent showed tremendous capacity for sulfur pickup, with actual loadings as high as 21 weight percent.
- Oxidative regeneration at 871 °C (1,600 °F) appeared to decompose sulfate; however, unusually high SO_2 release during the second sulfidations and/or reductive regenerations indicated incomplete regeneration.
- The average crush strength of the reacted sorbent did not indicate any loss of strength as compared to the fresh sorbent.
- Superior sorbent performance was obtained in the presence of simulated Shell gas at 538 °C (1,000 °F).

Future Work

Future work will include a 10-cycle test of the CST-939 sorbent with simulated Shell gas at 538 °C (1,000 °F) to test for sorbent regenerability and longer term durability.

References

Hepworth, M.T. and R.B. Slimane. *Hot Coal Gas Desulfurization With Manganese-Based Sorbents*. University of Minnesota, DOE/MC/29246-3941, NTIS/DE95000034, 1994.

Turkdogan, E.T. and R.G. Olsson. Desulfurization of Hot Reducing Gases With Manganese Oxide Pellets. *Proceedings of the Third International Iron and Steel Congress*, American Society for Metals: Chicago, Illinois, April 16-20, 1978, pp. 277-288.

Wakker, J.P. and A.W. Gerritsen. Coal Gasification: Higher Temperature H_2S Removal in a Steam Regenerative Process Under Realistic Conditions. *American Chemical Society Preprints*, 1990a, 35(1), 179.

Wakker, J.P. and A.W. Gerritsen. High Temperature H_2S Removal From Process Gases in a Steam Regenerative Process Using MnO or FeO on Gamma-Alumina Acceptors. *American Chemical Society Preprints*, 1990b, 35(1), 170.

Westmoreland, P.R., J.B. Gibson, and D.P. Harrison. Comparative Kinetics of High Temperature Reaction Between H_2S and Selected Metal Oxides. *Environ. Sci. Technol.*, 1977, 11, 488.

Westmoreland, P.R. and D.P. Harrison. Evaluation of Candidate Solids for High-Temperature Desulfurization of Low Btu Gases. *Environ. Sci. Technol.*, 1976, 10, 659.

LGASPE\1:961282

Reactivity of Metal Oxide Sorbents for Removal of H_2S

Kyung C. Kwon (kwonk@acd.tusk.edu; (334)-727-8976)
Edward R. Crowe (ecrowe@acd.tusk.edu; (334) -727-8975)
Chemical Engineering Department, School of Engineering and Architecture,
Tuskegee University, Tuskegee, Alabama 36088

Research sponsored by the U.S. Department of Energy's Morgantown Energy Technology Center, under Contract DE-FG21-94MC31206 with Tuskegee University, Tuskegee, AL 36088; telephone: (334) 727-8976/(334) 724-4528; fax: (334) 727-8976/ (334) 724-4188

Introduction

Removal of hydrogen sulfide contained in hot coal gases produced from integrated gasification combined cycle power generation systems is required to protect downstream combustion turbines from being corroded with sulfur compounds. Removal of sulfur compounds from hot coal gas products is investigated by using various metal oxide sorbents and membrane separation methods. The main requirements of these metal oxide sorbents are durability and high sulfur-loading capacity during absorption-regeneration cycles. In this research, durable metal oxide sorbents were formulated. Reactivity of the formulated metal oxide sorbents with simulated coal gas mixtures was examined to search for an ideal sorbent formulation with a high-sulfur-loading capacity suitable for removal of hydrogen sulfide from coal gases.

Objectives

The main objectives of this research are to formulate durable metal oxide sorbents with high-sulfur-loading capacity by a physical mixing method, to investigate reaction kinetics on the removal of sulfur compounds from coal gases at high temperature and pressure, to study reaction kinetics on the regeneration of sulfided sorbents, to identify effects of hydrogen partial pressures and moisture on equilibrium/dynamic absorption of hydrogen sulfide into formulated metal oxide sorbents as well as initial reaction rates of H_2S with formulated metal oxide sorbents, and to evaluate intraparticular diffusivity of H_2S into formulated sorbents at various reaction conditions.

Experimental Approach

Fresh metal oxide sorbent particles with promising formulas and simulated coal gases containing hydrogen sulfide are introduced in a 35 cm^3 316 stainless steel batch reactor (see FIGURE 1). The batch reactor, loaded with a fresh sorbent and a simulated coal gas mixture, is submerged in a fluidized sand bath to maintain the chosen heterogeneous reaction system at a desired reaction temperature [1]. Fine metal oxide sorbents are used to minimize effects of

intraparticle diffusion of hydrogen sulfide through sulfided sorbent particles for the evaluation of initial reaction rates of H_2S with formulated metal oxide sorbents. The batch reactor, loaded with a mixture of the fresh sorbent and the simulated coal gas mixture, is shaken in a constant-temperature fluidized sand bath to reduce effects of mass transfer of hydrogen sulfide to the sorbent particles. The sulfidation reaction is terminated at a desired reaction duration. Conversions of the sorbent are analyzed with a gas chromatograph.

The metal oxide sorbents such as TU-1, TU-19, TU-24, TU-25 and TU-28 were formulated with zinc oxide powder as an active sorbent ingredient, bentonite as a binding material and titanium oxide as a supporting metal oxide. This pasty mixture was extrudated 1-mm cylindrical rods. The viscosity of the pasty mixture appeared to be sensitive to the amount of water as well as the amount of bentonite added to the powder mixture at room temperature. Homogeneous mixing of these pasty slurry mixtures seemed to be very important in producing duplicate formulations of sorbents. The formulated metal oxide sorbents were calcined for 2 hours at 800 - 900 °C. The ingredients and some physical properties of the formulated sorbents were presented in TABLE 1.

FIGURE1. Batch Reactor Assembly

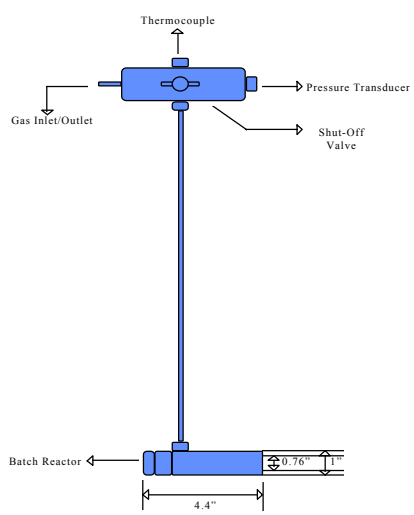

The fresh formulated metal oxide sorbents in the form of 1-mm cylindrical rod were crushed to obtain 100- 200 mesh particles and minus 200-mesh particles to evaluate initial intrinsic sulfidation kinetics as well as dynamic absorption of H_2S into sorbents. Metal oxide sorbents with 100-200 mesh particles were reacted with simulated coal gases containing hydrogen sulfide in the 35 cm^3 316 stainless steel batch reactor for 30-150 seconds at 500 °C (see Table 2).

The formulated metal oxide sorbents in the form of 1-mm cylindrical rod were used in evaluating intraparticular diffusivity of H_2S into the metal oxide matrices. Concentrations of hydrogen sulfide were analyzed with a gas chromatograph at various reaction durations to evaluate reaction rates of H_2S as well as equilibrium/dynamic absorption of H_2S into the sorbents.

TABLE 1. Formulation of metal oxide sorbents .

	TU-1	TU-19	TU-24	TU-25	TU-28
ZnO, g	1	1	1.8	0.5	1
TiO_2, g	2	2	1.2	2.5	2
Bentonite, g	0.1	0.15	0.15	0.15	0.1
Calcination Temperature, °C	850	800	800	830	830
Calcination Duration, min	120	100	100	100	100
Density of Sorbent, g/cm^3	1.73	1.73	1.73		
Specific Pore Volume, cm^3/g	0.36	0.36	0.36		

TABLE 2. Experimental conditions for the reaction of H_2S with sorbents .

Reactor Volume, cm^3	35
Temperature, °C	350 - 550
Reaction Time, min	0.5 - 60
Particle Size	100 - 200 mesh, <200 mesh, 200 µm, 1 mm cylindrical rod
Amount of Sorbent, g	0.015 - 0.4
Initial Partial Pressure of Hydrogen at 25 °C, psia	14.7 -24.7
Initial Amount of Water, g	0.085 - 0.120
Initial Concentration of H_2S, ppm	8000 - 8700
Initial Partial Pressure of Nitrogen at 25 °C, psia	140 -150
Initial Total Pressure of Reaction Mixture at 25°C, psia	164.7

Results

Experimental data of H_2S concentrations at various reaction durations were obtained by reacting H_2S with the sorbents formulated at our laboratory as well as the ZT-4 sorbent formulated at the Research Triangle Institute. Several blank experimental runs were made to evaluate absorption of H_2S into the 316 stainless steel reactor wall at various temperatures. These experimental data were used in evaluating equilibrium/dynamic absorption of H_2S into metal oxide sorbents as well as reaction rates of H_2S with metal oxide sorbents. Experiments on reactivity of hydrogen sulfide contained in a simulated coal gas mixture with the 316 SS batch reactor wall were performed at various reaction temperatures to evaluate effects of reaction temperatures on its reactivity with the wall. The simulated coal gas mixture consists of 9107-ppm hydrogen sulfide (0.005 g; 1 w%), 0.085-g water (15.84 -17.08 w%), 0.0029-g hydrogen (0.58 w%), and 0.4046-g nitrogen (81.34 w%). Absorption of hydrogen sulfide on the reactor wall increases with absorption temperatures. Absorption of H_2S into the 316 SS wall increases with absorption durations above 400 ^oC. However, absorption of H_2S into the 316 SS wall does not take place at 350 ^oC and previously-absorbed H_2S appears to be released from the 316 SS wall at 350 ^oC[2,3] (see FIGURE 2).

A series of experiments on effects of ZT-4 sorbent quantities on removal of H_2S were carried out in the presence of initial 8700-ppm H_2S and 0.085-g moisture for 10 min at 500 ^oC (see FIGURE 3). Removal of H_2S increases with amounts of the sorbent, but appears to level off above 0.1-g sorbent. These data may suggest that equilibrium concentration of H_2S in the reaction with the sorbent is reachable within 10-min reaction duration. A series of experiments were carried out in the presence of initial 8700-ppm H_2S and 0.085-g moisture for 60 min at 500 ^oC to investigate effects of varying the amount of TU-19 sorbent in the form of 1-mm cylindrical rod on the removal of H_2S (see FIGURE 4). The removal of H_2S

FIGURE 2. Reactivity of 316 stainless steel with H_2S .

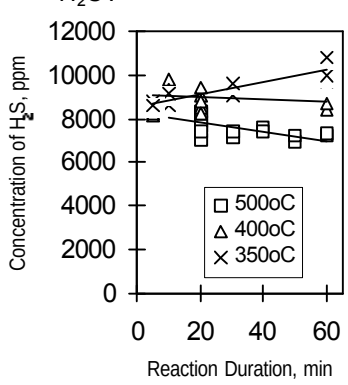

FIGURE 3. Effects of ZT-4 sorbent amounts on removal of H_2S with for 10 min at 500°C.

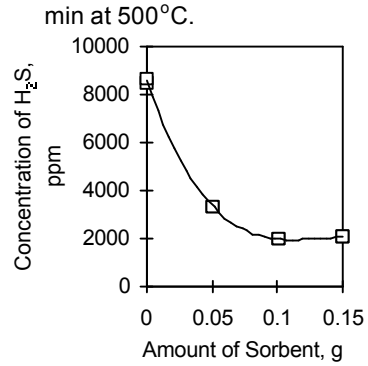

FIGURE 4. Effects of TU-19 sorbent amounts on removal of H_2S for 1 hour at 500°C.

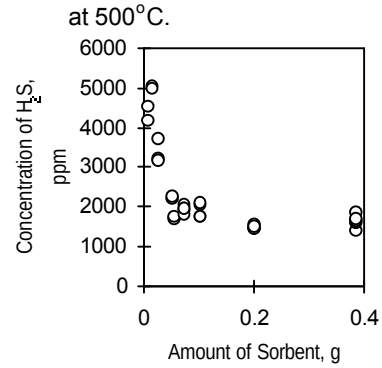

increases with amounts of the sorbent, but appears to level off above 0.05-g sorbent. These observations may suggest that equilibrium concentrations of H_2S are independent of sorbent quantities above 0.05-g sorbent.

Effects of moisture on reactivity of 200- μm ZT-4 sorbent with initial 9107-ppm H_2S were investigated at 350 °C (see FIGURE 5). Increased moisture increases removal of H_2S below equilibrium absorption. This observation may suggest that dynamic absorption of H_2S into the sorbent is dependent on moisture quantities at 350 °C. Equilibrium absorption of H_2S appears to be independent of moisture amounts. This fact may indicate that moisture does not affect equilibrium absorption of H_2S into the sorbent at 350 °C.

Reactivity of 200- μm ZT-4 sorbent with initial 9107-ppm H_2S was examined in the presence of 0.085-g moisture at various reaction temperatures (FIGURE 6). Reactivity of the sorbent with H_2S increases with reaction temperatures. Equilibrium removal of H_2S increases with reaction temperature and requires longer reaction durations with lower reaction temperatures. Absorption of H_2S into the sorbent increases with absorption durations below equilibrium absorption.

Reactivity of TU-1 sorbent in the form of 1-mm cylindrical-rod with initial 9107-ppm H_2S, the first sorbent formulated at our laboratory, was examined in the presence of 0.085-g moisture at 350 °C (see FIGURE 7). Absorption of H_2S into the sorbent also increases with absorption durations below equilibrium absorption, as observed from the experimental data of the ZT-4 sorbent.

FIGURE 5. Effects of moisture on reactivity of 0.1-g ZT-4 sorbent with H_2S at 350°C.

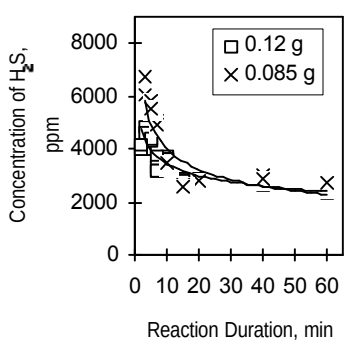

FIGURE 6. Reactivity of 0.1-g ZT-4 sorbent with H_2S

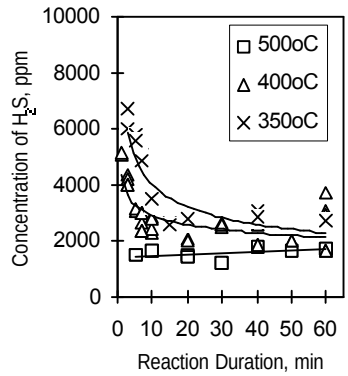

FIGURE 7. Reactivity of 0.1-g TU-1 sorbent with H_2S at 350°C

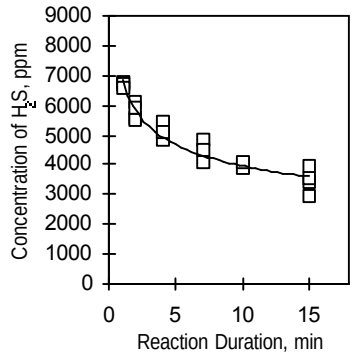

Effects of particle sizes of the ZT-4 sorbent on the removal of H_2S were examined in the presence of initial 9107-ppm H_2S and 0.085-g moisture at 350 °C as shown in FIGURE 8. The minus-127-μm (micron) ZT-4 sorbent removes more H_2S than the 200-μm (micron) sorbent below equilibrium absorption. Equilibrium absorption of H_2S is not affected by particle sizes. These observations may suggest that the intraparticular mass transfer of H_2S into pores of the sorbent is a limiting step for absorption of H_2S into the sorbent at 350 °C. These experimental data may indicate that reaction rates of H_2S with the sorbent increases with decreased particle sizes.

Reactivity of TU-19 sorbent in the form of 0.1-g 1-mm cylindrical rod was investigated in the presence of the initial concentration 8700-ppm H_2S and 0.085-g moisture at 500 ^oC and various reaction durations (see FIGURE 9). These experimental data showed that most absorption of H_2S into the sorbent occurs during the first 5-min reaction duration. These experimental data were utilized in evaluating intraparticular diffusivity of H_2S through the TU-19 sorbent matrix, using a developed cylindrical rod model.

FIGURE 8. Effects of particle sizes on reactivity of 0.1-g ZT-4 sorbent at 350°C.

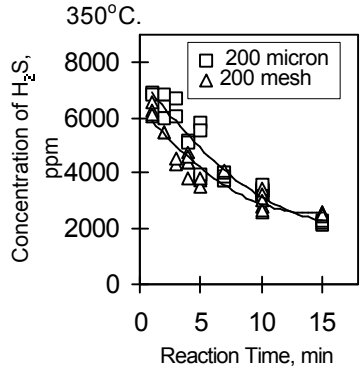

FIGURE 9. Reactivity of 0.1-g TU-19 sorbent with H_2S at 500°C.

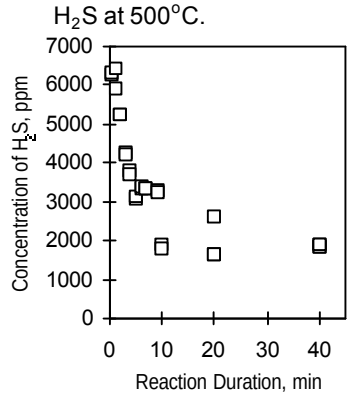

FIGURE 10. Left-side values vs. right-side values of the cylindrical rod model

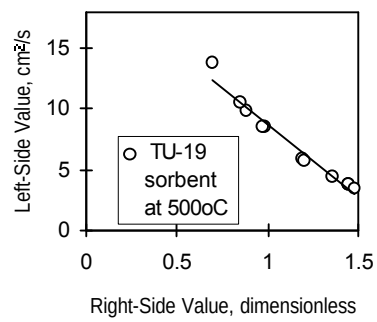

Intraparticular diffusivity of H_2S through the TU-19 sorbent in the form of 1-mm cylindrical rods was evaluated at 500 ^oC, using the following cylindrical rod model. The model[4,5] was developed with the unreacted core assumption and the quasi steady state assumption. Left-side values of Equation (1) were plotted against the right-side values (see FIGURE 10). Intraparticle diffusivity was determined from the slope of this plot. The intraparticle diffusivity of H_2S into the TU-19 sorbent was found to be 2.018×10^{-3} cm^2/s at 500°C.

$$\ln\left(\frac{r}{R}\right) r \frac{dr}{dt} = D_e \left(\frac{B}{b}\right)(1 + Ar^2) + \text{constant} \qquad (1)$$

$$r = \left(R^2 - \left(\frac{C_{AO} - C_A}{b\rho L r_B}\right)V\right)^{0.5} \qquad (2)$$

$$B = \frac{C_{Ao}}{r_B} - \frac{bV_B}{V} \qquad (3)$$

$$A = \frac{b\rho L}{BV} \qquad (4)$$

where
- r: radius of an unreacted core
- R: radius of a cylindrical-rod sorbent
- t: reaction time
- V_B: volume of a cylindrical-rod sorbent
- L: Length of a cylindrical-rod sorbent
- ρ_B: density of a cylindrical-rod sorbent
- D_e: intraparticle diffusivity

V: reactor volume
b: equilibrium absorption
C_{AO}: initial concentration of H_2S
C_A: concentration of H_2S

Equilibrium absorption of the TU-19 sorbent in the presence of the initial 24.7-psia H_2 is compared with that in the presence of the initial 14.7-psia H_2. Equilibrium absorption of the TU-19 sorbent in the presence of the initial 24.7-psia H_2 is higher than that in the presence of the initial 14.7-psia H_2 (see FIGURE 11). This observation may indicate that partial pressure of hydrogen appears to affect significantly equilibrium absorption of H_2S into the sorbent. Effects of hydrogen partial pressures on reactivity of the 100-200 mesh TU-25 sorbent as well as dynamic absorption of H_2S into the 100-200 mesh TU-25 sorbent were investigated in the presence of 0.085-g moisture for 1 min at 500 °C, as shown in FIGURE 12. Reactivity of H_2S with the TU-25 sorbent in the presence of the initial 14.7-psia hydrogen is higher than that in the presence of the initial 24.7-psia hydrogen, and reaction rates of H_2S with the sorbent increases with quantities of the sorbent (see FIGURE 12). Dynamic absorption of H_2S into the TU-25 sorbent in the presence of the initial 14.7-psia hydrogen is higher than that in the presence of the initial 24.7-psia hydrogen, and dynamic absorption of H_2S into the TU-25 sorbent decreases with increased quantities of the sorbent (see FIGURE 13).

FIGURE 11. Effects of H_2 pressure on equilibrium absorption of H_2S into TU-19 sorbent at 500 °C.

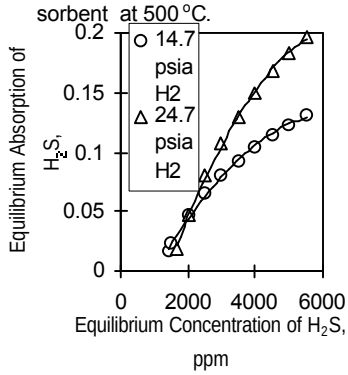

FIGURE 12. Effects of hydrogen on reactivity of TU-25 sorbent with H_2S for 1 min at 500°C.

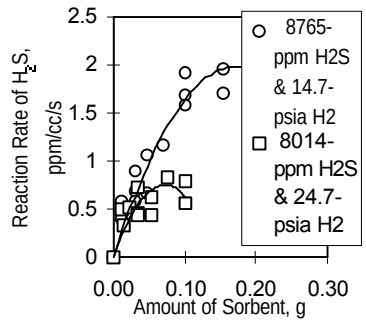

FIGURE 13. Effects of hydrogen on dynamic absorption of H_2S intoTU-25 sorbent for 1 min at 500°C

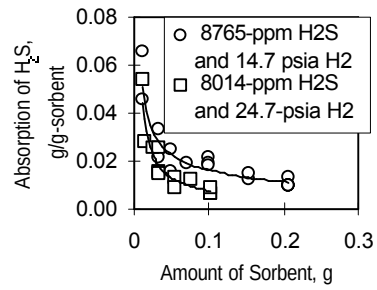

The TU-24 sorbent was reacted with the 8700-ppm initial concentration H_2S in the presence of initial 14.7-psia H_2 and 0.085-g moisture for 30 -150 seconds at 500 °C, as shown in FIGURE 14. Concentrations of H_2S decrease with increased reaction durations as well as increased amounts of the sorbent. These experimental data of H_2S concentrations at various reaction durations were used in evaluating reaction rates of H_2S with the TU-24 sorbent as well as dynamic absorption of H_2S into the sorbent at 500 °C. FIGURE 15 shows that reaction rates of H_2S with the TU-24 sorbent increase with increased quantities of the sorbent and decreased reaction durations. FIGURE 16 shows that reaction rates of H_2S with the TU-24 sorbent increase with increased quantities of the sorbent as well as increased concentrations of H_2S. Dynamic absorption of H_2S into the TU-24 sorbent at 500 °C increases with increased reaction durations and decreased quantities of the sorbent, as shown in FIGURE 17. FIGURE

18 shows that reaction rates of H_2S with the TU-24 sorbent decrease drastically with reaction durations for the short reaction duration of 30 - 150 seconds.

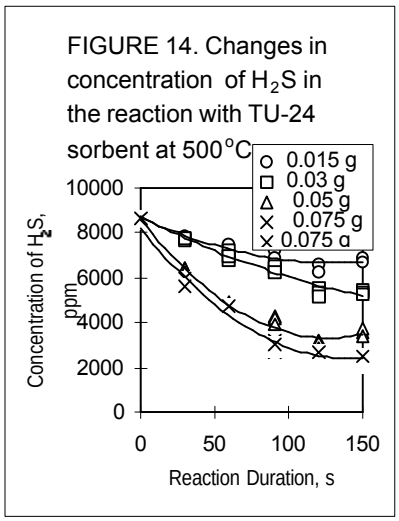

FIGURE 14. Changes in concentration of H_2S in the reaction with TU-24 sorbent at 500°C.

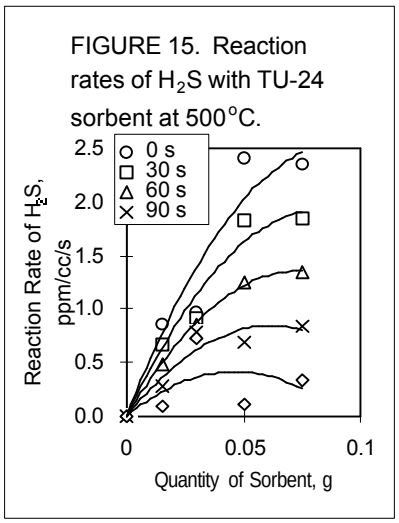

FIGURE 15. Reaction rates of H_2S with TU-24 sorbent at 500°C.

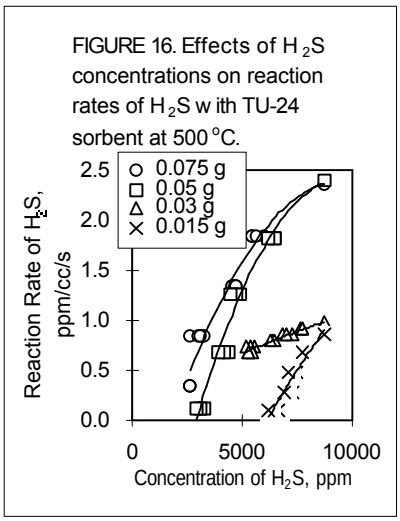

FIGURE 16. Effects of H_2S concentrations on reaction rates of H_2S with TU-24 sorbent at 500°C.

The following reaction rate equation may be proposed, since reaction rates of H_2S with TU-24 sorbent are dependent on concentrations of H_2S and quantities of the sorbent, as shown in Figures 15 and 16.

$$-r_A = k_A C_A^{\alpha} M_S^{\beta} \qquad (5)$$

where
- $-r_A$: reaction rates of H_2S, g-mole/cm^3/s
- C_A: concentrations of H_2S, g-mole/cm^3
- M_S: quantities of sorbents, g/cm^3
- k_A: reaction rate constant in terms of disappearance of H_2S, cc$^{(\alpha+\beta-1)}$/g$^{\beta}$/g-mole$^{(\alpha-1)}$/s
- α: reaction order with respect to concentrations of H_2S
- β: reaction order with respect to quantities of sorbents
- cc: cm^3

The equation (5) is linearized by applying a logarithm to the both sides of the proposed reaction rate equation [4,5]. The following linearized equation is obtained to evaluate k_A, α and β.

$$\ln(-r_A) = \ln(k_A) + \alpha\ln(C_A) + \beta\ln(M_S) \qquad (6)$$

The experimental data of H_2S concentrations at various reaction durations (see FIGURE 14) are applied to equation (6), and then the reaction rate constant k_A and the reaction orders such as α and β are obtained using the multiple linear regression method [6] as well as the Gauss-Seidel method [7], as shown in equation 7.

$$-r_A = 9908 C_A^{1.5165} M_S^{1.1397} \qquad (7)$$

The reaction rate constant k_A in terms of disappearance of H_2S was found to be 9908 $cm^{4.9686}/g^{1.1397}/g\text{-}mole^{0.5165}/s$ at the reaction temperature 500 °C. The reaction order α with respect to concentrations of H_2S was found to be 1.5165, while the reaction order β with respect to quantities of the TU-24 sorbent was found to be 1.1397. Reaction rates of H_2S obtained from the experimental data points were compared with reaction rates of H_2S predicted from the developed reaction rate equation (see equation 7), as shown in FIGURE 19.

FIGURE 17. Effects of sorbent amounts on dynamic absorption of H_2S into TU-24 at 500°C.

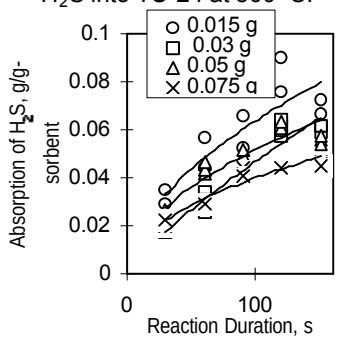

FIGURE 18. Reactivity of TU-24 sorbent with initial 8702-ppm H_2S at 500°C.

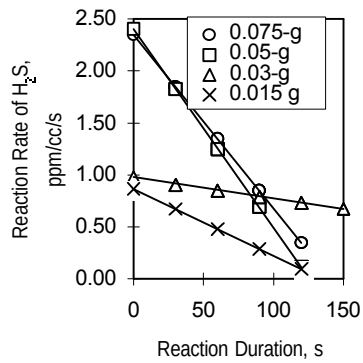

FIGURE 19. A comparison of experimental reaction rates of H_2S with predicted reaction rates of H_2S with TU-24 sorbent for 0-150 s at 500°C.

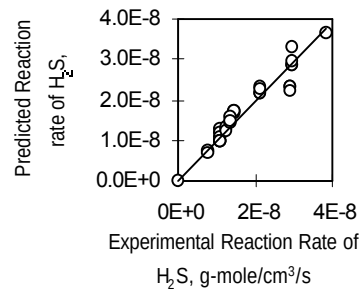

ACCOMPLISHMENTS

The cylindrical rod model was developed to determine intraparticle diffusivity of hydrogen sulfide into metal oxide sorbents. The intraparticle diffusivity of H_2S into the TU-28 sorbent was found to be 2.018×10^{-3} cm^2/s at 500°C. Dynamic absorption of H_2S into the 100-200 mesh TU-25 sorbent decreases with increased sorbent quantities and decreased reaction temperatures.

The reaction rate equation in terms of disappearance of H_2S with the TU-24 sorbent for short reaction durations of 30 -150 seconds at 500 °C was developed with the experimental data in order to determine a reaction rate constant in terms of disappearance of H_2S, a reaction order with respect to concentrations of H_2S, and a reaction order with respect to quantities of the solid TU-24 sorbent. The reaction rate constant in terms of disappearance of H_2S was found to be 9908 $cm^{4.9686}/g^{1.1397}/g\text{-}mole^{0.5165}/s$ at the reaction temperature 500 °C. The reaction order with respect to concentrations of H_2S was found to be 1.5165, while the reaction order with respect to quantities of the TU-24 sorbent was found to be 1.1397.

Effects of hydrogen partial pressures on reactivity of the 100-200 mesh TU-25 sorbent were investigated in the presence of 0.085-g moisture for 1 min at 500 °C. Reactivity of the TU-25 sorbent with H_2S was found to be significantly affected by partial pressures of hydrogen. Equilibrium absorption as well as dynamic absorption of H_2S into metal oxide sorbents also was found to be significantly influenced by compositions of hydrogen

contained in simulated coal gas mixtures. Compositions of moisture contained in simulated coal gas mixtures were identified to affect equilibrium absorption of hydrogen sulfide into formulated metal oxide sorbents.

Application

The developed reaction rate equation will be useful in designing a bench-scale or commercial reactor for removal of surfur compounds from hot coal gas mixtures. Effects of hydrogen partial pressures and moisture on equilibrium absorption as well as dynamic absorption of H_2S into formulated metal oxide sorbents should be incorporated into evaluating relatively capacities and reactivities of metal oxide sorbents. Effects of moisture and hydrogen partial pressures on reaction kinetics should be considered in designing a fluidized-bed reactor or a transport reactor for removal of hydrogen sulfide from hot coal gas mixtures.

Future Activities

A durable and reactive metal oxide sorbent with a high-sulfur-loading capacity will be formulated, and its reactivity, durability, and surfur-loading capacity will be evaluated. A reaction rate equation in terms of disappearance of H_2S at various reaction temperatures will be developed to evaluate effects of reaction temperatures on reaction rate constants in terms of disappearance of H_2S. Effects of moisture as well as hydrogen partial pressures on reactivity of formulated sorbents will be delineated. Experiments on effects of hydrogen partial pressures and moisture on equilibrium absorption as well as dynamic absorption of H_2S into formulated metal oxide sorbents will be conducted at various reaction conditions. Reaction kinetics on regeneration of sulfided metal oxide sorbents will be investigated at various regeneration conditions.

ACKNOWLEDGMENT

Financial support for this work was provided by the U.S. Department of Energy's Morgantown Energy Technology Center, Grant DE-FG21-94MC31206. The authors appreciate guidance and comments on this paper given by Mrs. Susan. K. Joines, METC Contracting Officer's Representative and Mr. Charles A. Komar. Valuable guidance, advice and comments on this research project were provided by Dr. Santosh K. Gangwal, Research Triangle Institute, the subcontractor of this research project.

References

1. Kwon, N. Vahdat and W. Ayers, "Chemical Reaction Experiment for the Undergraduate Laboratory", Chemical Engineering Education, Vol. 21, No. 1, p. 30, 1987.

2. Kwon, E. R. Crowe, and S. K. Gangwal, “Reaction Kinetics on Removal of Hydrogen Sulfide with Metal Oxide Sorbents at High Temperature and Pressure, was accepted for publication in Separation Science and Technology.

3. Kwon, E. R. Crowe, and S. K. Gangwal, “Removal of Hydrogen Sulfide from Simulated Coal Gases, Using Metal Oxide Sorbents at High Temperature and High Pressure “, Pages 123 - 128, The Proceedings for The Fourth Annual HBCU/Private Sector-Energy Research and Development Technology Transfer Symposium, Greensboro, North Carolina, April 2-4, 1996.

4. Elements of Chemical Reaction Engineering, H. Scott Fogler, 2nd Ed., Prentice-Hall, 1992

5. Octave Levenspiel, Chemical Reaction Engineering, 2nd Edition, John Wiley & Sons, 1972.

6. Heat Transfer, J. P. Holman, 7th Ed., McGraw-Hill, 1990.

7. Schaum's Outline Series Statistics, 2nd Edition, McGraw-Hill, New York.

Development of Disposable Sorbents for Chloride Removal from High-Temperature Coal-Derived Gases

Gopala N. Krishnan (gopala_krishnan@qm.sri.com; 415-859-2627)
Anastasia Canizales (canizal@qm.sri.com; 415-859-2715)
SRI International
333 Ravenswood Avenue
Menlo Park, CA 94025

Raghubir Gupta (gupta@rti.org; 919-541-8023)
Research Triangle Institute
3040 Cornwallis Road
Research Triangle Park, NC 27709

Raul Ayala (ayala@crd.ge.com; 518-387-5850)
GE Corporate Research and Development
Building K-1, P. O. Box 8
Schenectady, NY 12301

Introduction

The integrated coal-gasification combined-cycle approach is an efficient process for producing electric power from coal by gasification, followed by high-temperature removal of gaseous impurities, then electricity generation by gas turbines. Alternatively, molten carbonate fuel cells (MCFC) may be used instead of gas turbine generators. The coal gas must be treated to remove impurities such as hydrogen chloride (HCl), a reactive, corrosive, and toxic gas, which is produced during gasification from chloride species in the coal. HCl vapor must be removed to meet environmental regulations, to protect power generation equipment such as fuel cells or gas turbines, and to minimize deterioration of hot coal gas desulfurization sorbents.

Concentrations of HCl in coal gas have not been determined precisely, but they are estimated to be in the range 1 to 500 ppm (TRW, 1981). Bakker and Perkins (1991) point out that concentrations of HCl in coal gas can be about five times higher than those in coal-fired boiler combustion gas streams because of the lower volume of the coal gas. The actual concentration of HCl vapor in a coal gas stream will depend on the chlorine content of the coal, the gasification temperature, and the type of gasifier. Recently, (Bevan et al., 1994, 1995) measured the concentration of HCl to be about 300 to 600 ppm in a fixed-bed gasifier operating at 30 atm using Illinois #6 or a blend of Illinois #6 and Crown II coals.

The role of HCl as an impurity in coal gas used to fuel a gas turbine is not well defined and currently no concentration limit standards exist. In spite of the absence of specified limits, the removal of HCl vapor from the fuel can only be beneficial for IGCC systems, because the presence of HCl vapor is generally deleterious to the metal components of the IGCC systems. Perkins et al. (1990) report that the chloride deposits found on syngas coolers accelerate the corrosion of the heat exchanger material. HCl reacts with the deposited slags forming low-melting iron chlorides, and thereby accelerates the corrosion rate. For sustained and efficient operation of the MCFC, the feedgas must be free of chloride species. Halogen compounds are deleterious to MCFCs because they can lead to severe corrosion of cathode hardware (Kinoshita et al., 1988). HCl also can react

This research was sponsored by the U.S. Department of Energy's Morgantown Energy Technology Center, under contract DE-AC21-93MC3005 with SRI International, 333 Ravenswood Avenue, Menlo Park, CA 94025. Telephone: 415-326-6200; fax: 415-326-5512

with the molten carbonate electrolyte to form halides such as LiCl and KCl. The high vapor pressures of these compounds enhance electrolyte loss. An increase in the cell resistance and a corresponding decrease in the cell voltage were observed in feed gas containing 1 ppmv HCl vapor (Pigeaud and Wilemski, 1992). Hence, the allowable HCl concentration in a MCFC feedgas is estimated to be less than 0.1 ppmv.

A number of processes are available for removing HCl vapor from industrial and incinerator waste gases. These processes scavenge HCl by adsorption onto activated carbon or alumina or by reaction with alkali or alkaline earth carbonates or oxides. In chemical plants where HCl must be removed from process feedstocks, commercial sorbents called chloride guards are marketed by catalyst manufacturers and these sorbents are relatively expensive. These sorbents reduce chloride contaminant levels to <l ppm, but they must operate at temperatures <450°C. Furthermore, none of them are economically regenerable. Hence, inexpensive and disposable sorbents are needed for the chloride removal in hot coal-derived gas streams.

Objectives

The objectives of this study are to: (1) investigate methods to fabricate reactive sorbent pellets or granules that are capable of reducing HCl vapor in high-temperature coal gas streams to less than 1 ppm in the temperature range 400° to 650°C and the pressure range 1 to 20 atm; (2) testing their suitability in bench-scale fixed- or fluidized-bed reactors; (3) testing a superior sorbent in a circulating fluidized-bed reactor using a gas stream from an operating coal gasifier; and (4) updating the economics of high temperature HCl removal.

Approach

Equilibrium thermodynamic calculations showed that only sodium and potassium compounds are capable of reducing HCl vapor levels to less than 1 ppm level at 527°C. Potassium compounds are capable of achieving the lowest HCl vapor levels, but the vapor pressure of KCl(g) exceeds that of NaCl(g). If potassium compounds are to be used for HCl removal, then the release of alkali vapor in the hot coal gas could be higher than the case in which sodium compounds are used. The sodium minerals are more abundant than potassium minerals in nature. Hence, the use of sodium minerals are preferable as disposable sorbents for HCl removal.

Of the major sodium minerals in the U.S., nahcolite ($NaHCO_3$) mineral is suitable for the HCl removal applications. Approximately 30 billion tons of nahcolite minerals occur in the Piceance Creek Basin of northwestern Colorado and of these, 17.5 billion tons could be recovered economically (Farris and Mains, 1978). Nahcolite is converted to soda ash on heating to a temperature above 150°C:

$$2NaHCO_3 = Na_2CO_3 + H_2O\ (g) + CO_2\ (g)$$

The release of steam and CO_2 results in a porous and reactive sorbent. At the temperature of interest, HCl reacts with Na_2CO_3 to form NaCl:

$$Na_2CO_3 + 2\ HCl\ (g) = 2\ NaCl + H_2O\ (g) + CO_2\ (g)$$

Previous studies demonstrated that nahcolite is capable of high HCl reactivity and high chloride capture capacity (Krishnan et al., 1986). Bench-scale experiments showed that the HCl vapor level were reduced to less than 1 ppm in the temperature range 400° to 550°C and chloride loading levels in the spent sorbent could be as high as 50 wt%.

The sorbents can be used in fixed-, fluidized, or moving-bed reactors. In fluidized-bed reactor applications, the fresh sorbent can be introduced pneumatically at the outlet of the gasifier and the spent sorbent can be collected along with the coal ash in a cyclone (Bevan et al., 1994). This simple reactor concept is adequate for applications in which HCl level should be low. However, for MCFC applications where the residual level of HCl level must be less than 1 ppm, fixed- or moving-bed reactors are needed to provide sufficient contact time. In a guard-bed mode, the fixed-bed reactors could be relatively compact or the sorbent pellets need to be changed only after a relatively long period of time. An economic evaluation using fixed-bed reactors for HCl cleanup indicated that the use of nahcolite to remove HCl vapor would add only about $0.002/kWh (2 mills/kWh) to the cost of the generated electric power (Krishnan et al., 1986).

Project Description

Bench-scale, cylindrical stainless steel pressure vessels, capable of operating at temperatures up to 923 K (1202°F) and pressures up to 20 atm, were used for both fixed-bed (at SRI) and fluidized-bed (at RTI) tests. The sorbent beds were contained in 5-cm ID quartz tubes mounted inside the pressure vessels. To minimize corrosion, only the non-corrosive components of the simulated coal gas mixtures could come into contact with the stainless steel walls. HCl and H_2S were introduced directly into the quartz tube, upstream of the sorbent bed. Pressure was controlled by a Hastelloy servocontrolled valve at the outlet of the pressure vessel. The reactor effluent was cooled in a heat exchanger made of glass, wherein residual HCl vapor dissolved in the steam condensate. The chloride level in the condensate, determined by ion chromatography, provided a measure of the residual HCl vapor concentration. This procedure is capable of measuring sub-ppm levels of HCl vapor.

Several sorbent pellets made by extrusion using nahcolite powder (obtained from NaTec Resources, Inc., Houston, Texas) and bentonite or sodium silicate binders. These pellets, in the size range 1.5 to 4 mm, were used for fixed-bed reactor testing. For the fluidized-bed reactor studies, nahcolite sorbent granules (40 to 150 µm in size) with kaolinite and bentonite binders were made using a spray dryer. A simulated coal gas composition representative of Texaco oxygen-blown gasifier was used in the bench scale studies. The HCl level was set arbitarily at a high level of 1750 ppm. The H_2S and H_2O levels were typically 3000 ppm and 25 vol%, respectively.

In addition to the bench-scale tests with simulated gas, a small batch of the spray-dried sorbent was also tested at the pilot-scale fixed-bed gasifier facility located at the General Electric Corporate Research and Development site.

Results

Experimental tests were conducted during the previous years in this program (Krishnan et al., 1994; 1995) provided the following results:

- No significant differences in the HCl reactivity were observed between sodium silicate and bentonite binders. At a space velocity of 3000 h^{-1}, the HCl level was reduced from 1750 ppm to less than 1 ppm and the maximum chloride content of the spent pellets was about 55 wt%. The maximum chloride capacity of the pellets with sodium silicate binder was 10% higher than that of the pellets with bentonite binder, but the rate of initial reaction did not depend strongly on the nature of the binder.

- Pellets containing sodium silicate binder agglomerated when the reaction temperature was higher than 500°C. No such agglomeration was observed when bentonite was used as the binder.

- The crush strength of the pellets made with nahcolite was comparable to that of zinc titanate desulfurization sorbents and it did not change significantly with the extent of chlorination.

- The sorbents prepared by spray-drying have a superior reactivity and chloride capacity than the raw nahcolite powder. The attrition resistance of the spray-dried sorbent was comparable to that of a commercial FCC catalyst.

- Experiments in a 2.5-cm diameter fluidized-bed reactor showed that the spray-dried sorbent also has a high reactivity for HCl and a high chloride capture capacity. The residual HCl level was less than 1 ppm at 550°C with spent sorbents containing as high as 50 wt% chloride indicating nearly complete capacity utilization.

- The presence of H_2S did not affect the HCl reactivity or the chloride capacity of the sorbent under atmospheric pressure conditions.

Recent experiments focussed on experiments at elevated pressures. Fixed-bed reactor experiments with simulated coal gas containing both HCl and H_2S vapor showed similar results as with atmospheric pressure runs. As shown in Figures 1 and 2, the residual HCl level remained below 1 ppm and the HCl breakthrough occurred at periods longer than 20 h.

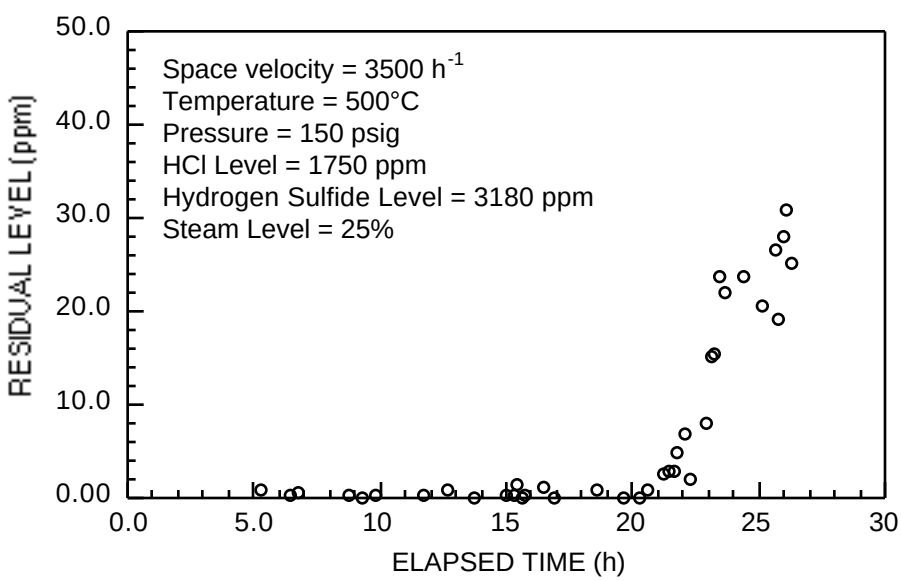

Figure 1. The residual HCl level as a function of reaction time.

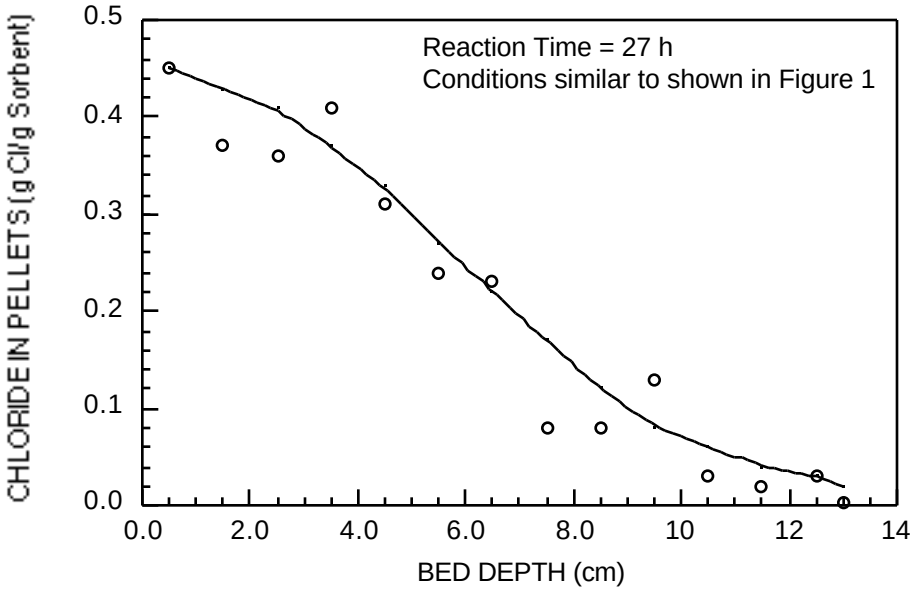

Figure 2. The chloride content of the pellets as a function of bed depth.

Experiments were also conducted with pellets made from trona ore ($Na_2CO_3 \cdot NaHCO_3$) at 1 atm. However, the reactivity and chloride capacity of trona pellets were significantly inferior than those of nahcolite pellets (Figure 3). Similar results were also found in tests with fluidized-bed reactors.

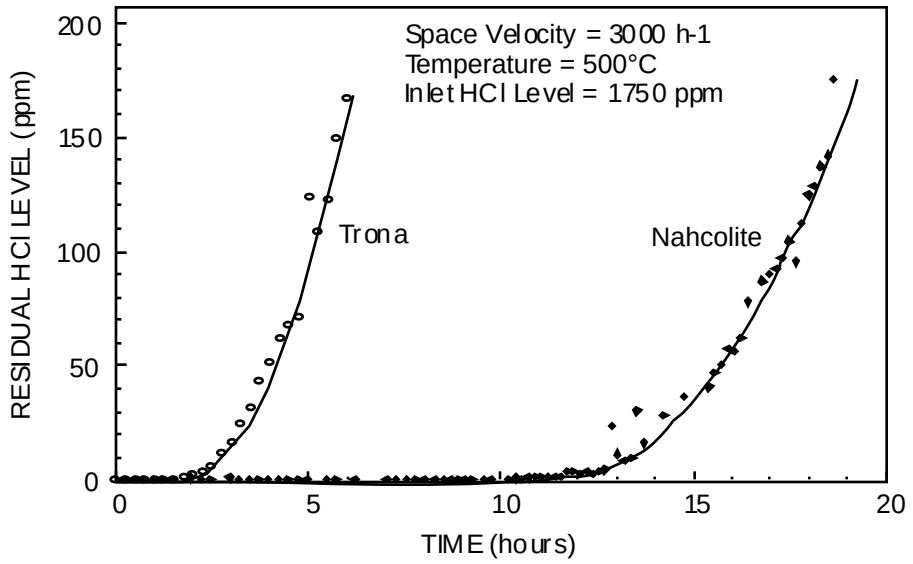

Figure 3. Comparison of HCl removal by trona and nahcolite pellets at 1 atm.

A fluidized-bed reactor test was also conducted with a commercial sorbent made by United Catalyst, Inc. The UCI sorbent also reduced HCl level to less than 1 ppm, but its chloride capacity was significantly less than that nahcolite pellets (Figure 4). This result is expected, because the UCI sorbent is made for guard bed applications rather than for bulk removal of HCl vapor.

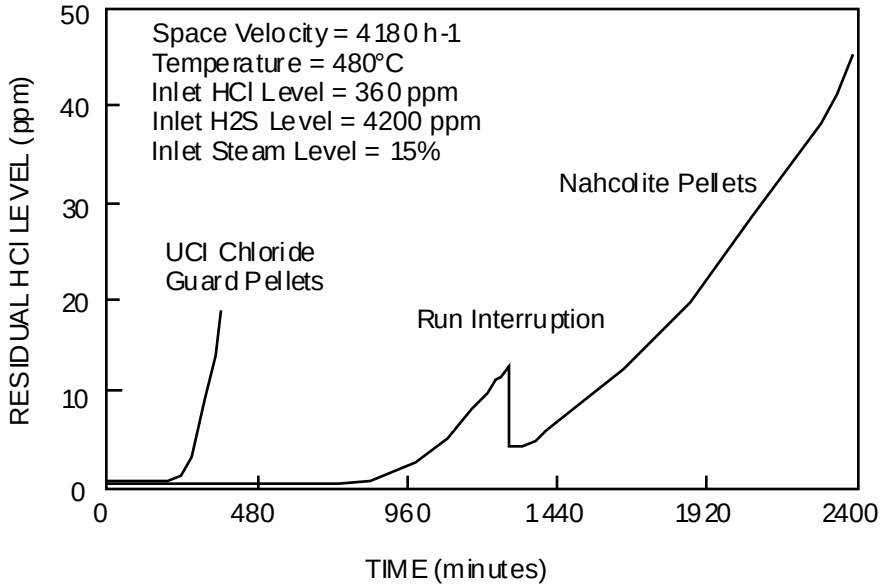

Figure 4. Comparison of HCl removal by a commercial chloride guard and nahcolite pellets.

A preliminary pilot-run at the GE fixed-bed gasifier facility using their circulating fluidized-bed facility showed that both sodium carbonate and spray-dried sorbent could reduce the HCl level in the hot coal gas stream from about 580 ppm to less than 15 ppm (Figure 5). Grade #2 sodium bicarbonate powder was used as the HCl removal sorbent during the initial 110 h. The sorbent was injected into the reactor pneumatically using a nitrogen carrier gas. The initial residual HCl level was somewhat high due to low sorbent level in the reactor. As the bed inventory was increased, the HCl removal efficiency increased. During the last 5 h of the test, the Grade #2 sodium carbonate was replaced with 100 lbs of spray-dried nahcolite granules supplied by RTI. The calculated HCl removal efficiency was greater than 97% with both sorbents. The spent spray-dried sorbent contained as much as 38 wt% chloride, corresponding to a sorbent utilization of 71%.

The spray-dried sorbents before and after coal gas exposure were analyzed to determine whether any trace element species present in the hot coal gas stream would be retained. As shown in Table 1, B, Pb, and Zn species were significantly higher in the spent sorbent than in the the original sorbent. The data is insufficient to conclude that the observed increase in the levels of Cd, Mo, and Cu is significant. The trace metal species accumulated on the spent sorbent could be either from the trace metal vapors adosrbed or reacted with the sorbent or fine ash particles retained in the sorbent bed. Additional tests are needed to determine the origin and extent of trace element species that accumulate on the sorbents.

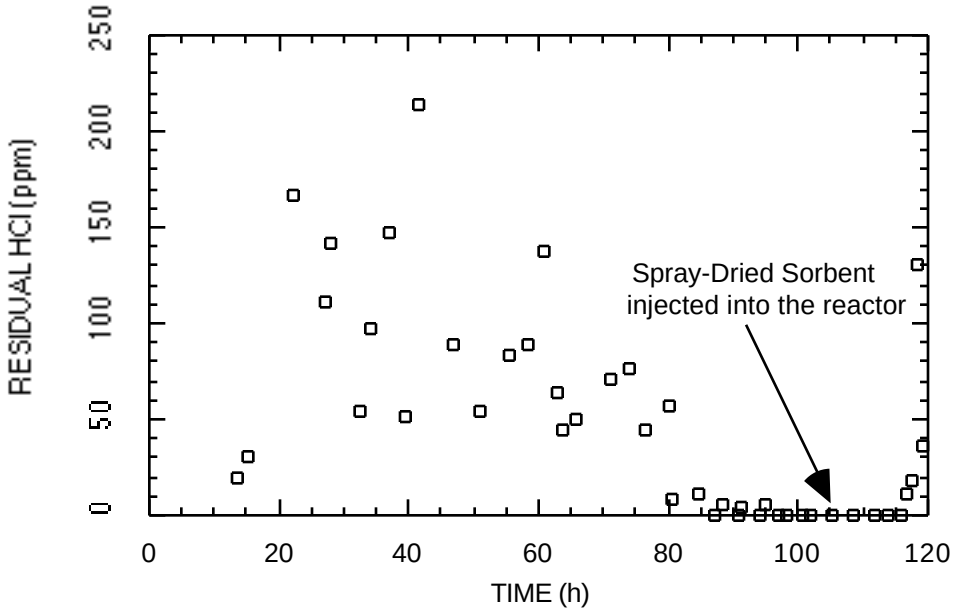

Figure 5. The residual HCl vapor level in the pilot-scale test with sodium bicarbonate powder and spray-dried sorbent.

Table 1. Concentrations of Trace Elements in the Original and Coal-Gas Exposed Spray-Dried Sorbent

Element	Concentration in Original Sorbent (ppm)	Concentration in Spent Sorbent (ppm)
B	<15	1425
Ba	41	42
Be	<1	<1
Cd	<3	5
Cr	15	<10
Cu	<10	22
Pb	<15	1065
Mn	<10	<10
Mo	<15	<30
Ni	<15	<15
Sr	31	30
V	30	30
Zn	65	145

A second gasifier gas stream test using a 400 kg of spray-dried sorbent was scheduled in March 1996. An improved sorbent was prepared for this test. However, difficulties were encountered in feeding the sorbent because of bridging in the feed hopper.

Applications

The results of the current program have demonstrated that HCl vapor can be removed from coal gas streams at elevated temperatures using disposable, inexpensive, naturally occurring minerals. The HCl vapor in the gas could be reduced to levels required to meet environmental regulations and MCFC applications. This technology results in a dry process with minimal amount of a solid waste to be disposed of. The alternative technology, which is the current practice, is to quench the coal gas with water and remove the HCl vapor in the aqueous solution. The waste solution is more difficult to dispose than the solid waste.

Future Activities

Future activities in the program include preparation of about 400 kg of spray-dried sorbent for another pilot-plant test, parametric testing of the sorbents in a bench-scale fluidized-bed reactor, and a preliminary economic assessment of the chloride removal process.

Acknowledgments

The authors gratefully acknowledge the guidance and assistance of Mr. Ron K. Staubly, the METC Contracting Officer's Representative. Subcontract support is support is provided by Research Triangle Institute and GE-Corporate Research and Development. The contract period of performance is from September 1, 1993 to February 28, 1997.

References

Bakker, W.T., and R.A. Perkins (1991). "The Effect of Coal Bound Chlorine on Corrosion of Coal Gasification Plant." In *Proceedings of International Conference on Chlorine in Coal*, J. Stringer and D.D. Banerjee, Eds., Elsevier.

Bevan, , S., E. Gal, A. Najewicz, A. H. Furman, R. Ayala, and A. Feitelberg (1994). Integrated Operation of a Pressurized Gasifier, Hot Gas Desulfurization System and Turbine Simulator, *In Proceedings of the Coal-fired Power Systems 94 - Advances in IGCC and PFBC Review Meeting*, H. McDaniel, R. K. Staubly, and V. Venkataraman, Eds., Report No.: DOE/METC-94/1008, Morgantown Energy Technology Center, U.S. Department of Energy, Morgantown, WV.

Bevan, , S., E. Gal, A. Najewicz, A. H. Furman, R. Ayala, and A. Feitelberg (1995). Integrated Operation of a Pressurized Gasifier, Hot Gas Desulfurization System and Turbine Simulator, *In Proceedings of the Coal-fired Power Systems 94 - Advances in Coal-Fired Power Systems '95 Review Meeting*, H. McDaniel, D. J. Mollot, and V. Venkataraman, Eds., Report No.: DOE/METC-95/1018, Morgantown Energy Technology Center, U.S. Department of Energy, Morgantown, WV.

Farris, C. B. and C. J. Mannis (1978). "Dawsonite and Nahcolite Survey, Vol 1: Reserves, Technology, and Market Assessment," Colorado School of Mines Research Institute, Report to U. S. Department of Energy, Report IDO-183-1.

Kinoshita, K., F. R. McLarnon and E. J. Cairns (1988). *Fuel Cells: A Handbook*, Report No. DOE/METC-88/6096, Morgantown Energy Technology Center, U.S. Department of Energy, Morgantown, WV.

Krishnan, G. N., B. J. Wood, A. Canizales, R. Gupta, S. D. Sheluker, and R. Ayala (1994). "Development of Disposable Sorbents for Chloride Removal from High-Temperature Coal-Derived

Gases." *In Proceedings of the Coal-fired Power Systems 94 - Advances in IGCC and PFBC Review Meeting*, H. McDaniel, R. K. Staubly, and V. Venkataraman, Eds., Report No.: DOE/METC-94/1008, Morgantown Energy Technology Center, U.S. Department of Energy, Morgantown, WV.

Krishnan, G. N., B. J. Wood, A. Canizales, R. Gupta, S. D. Sheluker, and R. Ayala (1995). "Development of Disposable Sorbents for Chloride Removal from High-Temperature Coal-Derived Gases." *In Proceedings of the Coal-fired Power Systems 94 - Advances in Coal-Fired Power Systems '95 Review Meeting*, H. McDaniel, D. J. Mollot, and V. Venkataraman, Eds., Report No.: DOE/METC-95/1018, Morgantown Energy Technology Center, U.S. Department of Energy, Morgantown, WV.

Krishnan, G.N., G.T. Tong, B.J. Wood, and N. Korens (1986). "High-Temperature Coal-Gas Chloride Cleanup for MCFC Applications." Report No. DOE/MC/21167-2080, Morgantown Energy Technology Center, U.S. Department of Energy, Morgantown, WV.

Perkins, R.A., D.L. Marsh, and P.R. Clark (1990). "Corrosion in Syngas Coolers of Entrained Slagging Gasifiers." Report No. EPRI GS-6971, Electric Power Research Institute, Palo Alto, CA.

Pigeaud, A. and G. Wilemski (1992). "Effects of Coal-Derived Trace Species on the Performance of Carbonate Fuel Cells." *In Proceedings of the Fourth Annual Fuel Cells Contractors Review Meeting*, W. J. Huber, Ed., Report No.: DOE/METC-92/6127, Morgantown Energy Technology Center, U.S. Department of Energy, Morgantown, WV.

TRW (1981). "Monitoring Contaminants in Coal Derived Gas for Molten Carbonate Fuel Cells," Final Report to Argonne National Laboratory under contract No. 31-109-38-6108.

A Membrane Reactor for H_2S Decomposition*

D. Edlund (Bendresearch@bendres.com; 541-382-4100)
Bend Research, Inc.
64550 Research Road
Bend, OR 97701-8599

Introduction

Hydrogen sulfide (H_2S) is a common contaminant produced during gasification of coal and refining petroleum and is often present in natural gas. Federal and state regulations limit the discharge of H_2S to the atmosphere, and commercial methods exist for removal of H_2S, but they have drawbacks. Generally, these methods produce other pollutants (e.g., sulfur oxides) or hazardous wastes (e.g., metal sulfides). Clearly, new methods are needed for the disposal of H_2S in an environmentally benign fashion.

It has long been recognized that H_2S can be thermally decomposed, yielding hydrogen and elemental sulfur (S_2) as the primary byproducts (Raymont, 1975). However, the equilibrium constant for this thermolysis reaction is unfavorable. The reaction must be conducted at about 700°C to achieve even 10% conversion to hydrogen and sulfur, and complete decomposition of H_2S is achieved only at temperatures above 1500°C.

Given the high reaction temperatures and unfavorable equilibrium constant, it is not practical to achieve complete decomposition of H_2S by condensing or otherwise removing the byproduct sulfur and, to date, selective removal of the byproduct hydrogen has not been a practical alternative. Ceramic membranes, which can tolerate the high reaction temperatures, are not sufficiently selective for hydrogen. Metallic membranes do have high selectivity for hydrogen and tolerate high operating temperatures but, to date, have not been compatible with H_2S. In this paper, we describe our research to develop a practical metal-membrane-based system for the direct thermolysis of H_2S.

Objectives

The objectives of this work were to develop practical and economical solutions to key technical problems that have limited the suitability of metal-membrane reactors for direct thermolysis of H_2S. Specifically, the objectives of this work were to

1. demonstrate high hydrogen flux through a sulfidation-resistant metal membrane;

* Research sponsored by the U.S. Department of Energy's Morgantown Energy Technology Center, under Contract DE-FG03-92ER81419, with Venkat K. Venkataraman, P.O. Box 880, Morgantown, WV 25606; telefax: 304-211-4469.

2. identify structural alloys or coatings for use in fabricating membrane modules that are resistant to corrosion by hot H_2S;
3. develop membrane-module designs that are efficient and economical; and
4. achieve these objectives within the overall economic constraints (e.g., capital costs, membrane lifetimes) dictated by the specific application.

Technical Approach

Our technical approach is to use a metal-membrane reactor to achieve direct thermolysis of H_2S at high temperatures. In this new process, hot gas from the coal gasifier, rich in H_2S but depleted of H_2, is fed to the metal-membrane reactor at $\geq$500°C (see Figure 1). At these high temperatures, the thermal decomposition of H_2S over a catalyst is a very fast reaction (Edlund and Pledger, 1993). However, as noted above, at equilibrium, the reaction proceeds to only 10% to 20% completion (producing H_2 and S_2 predominantly) due to limitations imposed by the thermodynamic equilibrium. In our process, as H_2 is produced within the metal-membrane reactor (Figure 2), it is selectively and rapidly separated from the hot feed gases by an H_2-permeable metal membrane, causing the H_2S decomposition reaction to be driven toward completion. The membrane reactor, then, decomposes H_2S almost completely, producing only H_2 and S_2 as byproducts. Unlike conventional H_2S-removal technologies (e.g., the Claus process), the process does not produce sulfur oxides or other environmentally objectionable byproducts.

The H_2 that permeates the metal membrane is catalytically reacted with oxygen to form water or is removed by a sweep stream. (If the sweep gas is condensable [e.g., steam], then pure H_2 may be recovered at moderate pressures.) However, burning the permeate H_2 is probably preferred for applications in which H_2S is a minor component of the feed stream (as in coal gasification), because

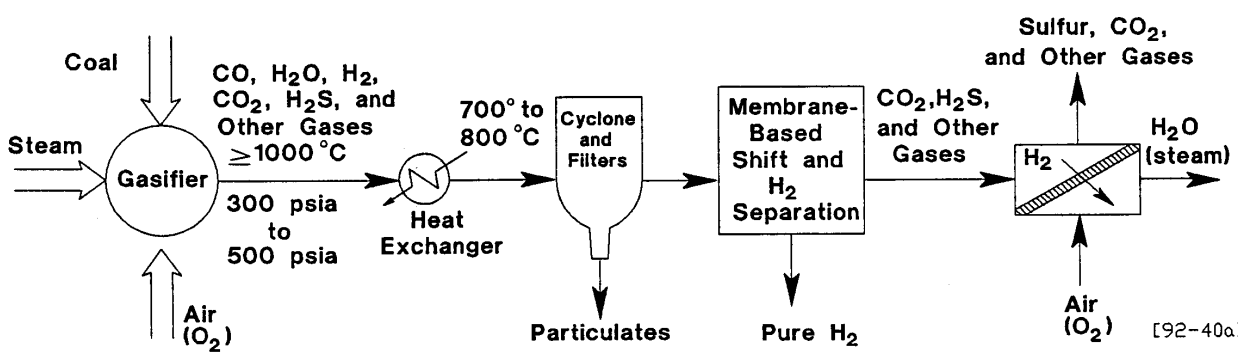

Figure 1. Membrane-Reactor Process for Efficiently Separating and Decomposing H_2S From a Hot Coal-Gas Stream. (The membrane-based shift and H_2-separation process has been developed under a separate DOE program [Grant No. DE-FG03-91ER81229].)

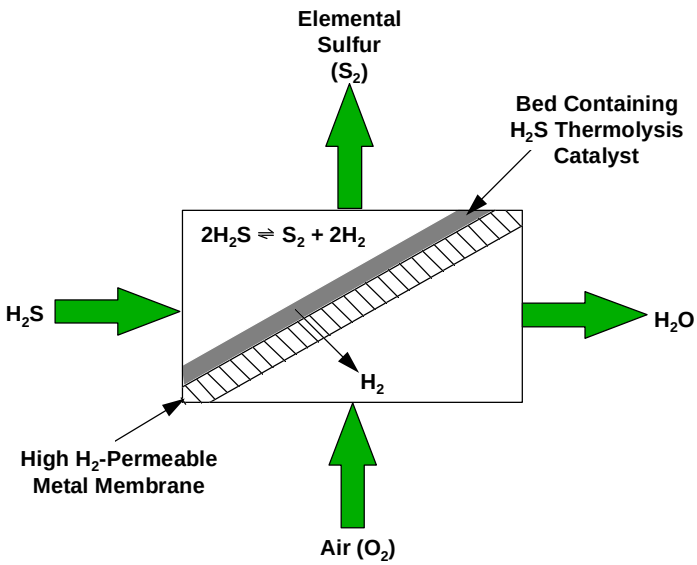

Figure 2. Membrane-Reactor Process to Drive the Thermal Decomposition of H_2S Toward Completion

- the energy produced by burning the permeate H_2 more than compensates for the energy consumed by the endothermic H_2S decomposition reaction; and
- a low partial pressure of H_2 is maintained at the permeate side of the membrane as a result of the reaction, thereby providing a high driving force for H_2 permeation.

The process is based on the use of a composite-metal membrane that we have developed. As shown in Figure 3, the membrane consists of three distinct layers: (1) a base-metal/mechanical support layer, (2) an intermediate layer, and (3) a coating-metal layer, as shown in Figure 3. If the total sulfur concentration of the feed stream is high ($\geq$5 ppm), the coating-metal layer must be an H_2-permeable metal that is resistant to chemical corrosion by H_2S (e.g., Pd alloyed with about 40% Cu—see below).

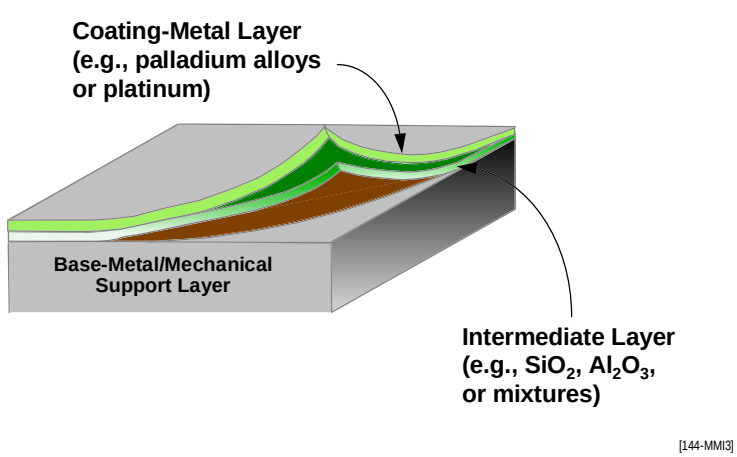

Figure 3. Key Features of Bend Research Composite-Metal Membrane

In a parallel DOE program, we demonstrated that this composite-metal membrane effectively drives the water-gas shift (WGS) reaction ($CO + H_2O \rightleftharpoons H_2 + CO_2$) toward complete conversion at high temperature by removing H_2 as it is produced (Edlund et al., 1995). This result shows the promise of the composite-metal membrane for use in a multi-stage membrane-reactor process to maximize the production of pure H_2 during coal gasification, as well as to decompose the H_2S present in the feed stream.

Project Description

This program consisted of experimental evaluation of new metal-membrane compositions, experimental evaluation of the corrosion resistance of structural alloys and coatings for use in fabricating membrane reactors, development and evaluation of new membrane reactor designs, and economic analysis of the membrane reactor-based process for H_2S thermolysis and membrane-reactor fabrication. Our results are described below.

Results

Evaluation Of New Metal Membrane Compositions

Alloys of Au with Pd are known to exhibit H_2 permeability in the presence of low concentrations (<20 ppm) of H_2S at about 300°C (McKinley, 1967). Surprisingly, McKinley also reports that Pd-Cu alloys are more resistant than Pd-Ag alloys or pure Pd to H_2S (McKinley, 1967). Reasoning that the H_2 permeability of these sulfur-resistant alloys should increase with increasing operating temperature and that they should exhibit even greater tolerance to H_2S at elevated operating temperatures, we evaluated Au-coated Pd and Pd-Cu alloys for H_2 flux in the presence of 50 ppm to 10% at 500°C (the minimum temperature that is practical for H_2S thermolysis). Because the Pd-Au alloys did not perform as well as the Pd-Cu alloy, the remainder of this paper is focused on Pd-Cu membranes.

We purchased an alloy of Pd with 40 wt% Cu (Pd-40Cu) as foil of two different thicknesses (nominally 25 μm and 50 μm thick) and tested it for resistance to H_2S. Figure 4 shows data for long-term stability tests of the 50-μm-thick Pd-40Cu membrane. As the figure shows, the Pd-40Cu membrane retained relatively high flux in the presence of high H_2S concentrations.

Furthermore, the Pd-40Cu alloy is not permanently poisoned by exposure to 10% H_2S and the membrane exhibited stable flux over 350 hours (14 days) of continuous operation (the duration of the experiment, see Figure 4). In addition to demonstrating exceptional resistance to H_2S at operating temperatures $\geq$500°C in the laboratory, the Pd-40Cu composite-metal membranes have demonstrated exceptional durability in laboratory and field tests, exhibiting more than 150 days of continuous operation without flux decline or a decrease in the purity of the permeate H_2.

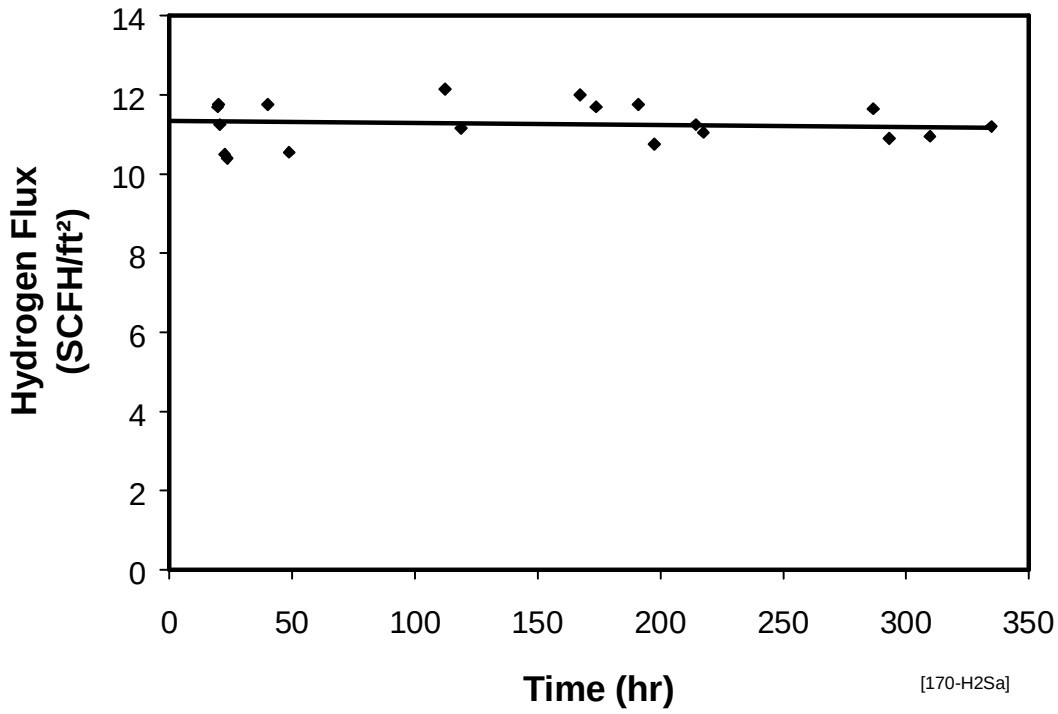

Figure 4. Long-Term Stability of H_2 Flux Through a 50-µm-Thick Pd-40Cu Membrane
Conditions: 500°C; feed is 1000 ppm H_2S in H_2 at 100-psig total pressure; permeate is at ambient pressure

The durability and permeability of the Pd-40Cu membrane has been verified by independent tests conducted on a coal-gasifier slipstream by the University of North Dakota Energy and Environmental Research Center at Grand Forks, North Dakota (Swanson et al., 1996).

Evaluation Of Corrosion-Resistant Alloys And Coatings For Reactor Construction

An important step in developing a practical and economical membrane for use in with feed streams containing H_2S and other sulfur compounds is to identify suitable structural alloys for making the module components that will be in contact with the feed stream.
Acceptable materials for this purpose must satisfy two requirements:

- the alloy must exhibit a low rate of corrosion by hot H_2S; and
- the alloy must have sufficient strength at high temperature to serve as a load-bearing component of the module.

We evaluated two classes of materials: (1) corrosion-resistant alloys with low iron content, and (2) aluminum-oxide-coated stainless steel prepared by a commercial process.

Corrosion-Resistant Alloys

A search for alloys resistant to high-temperature corrosion by H_2S revealed two promising candidates: (1) HR-160, a high chromium, low-iron stainless steel made by Haynes International, Inc. (Kokomo, Indiana); and (2) C103, an alloy containing primarily niobium and titanium made by Teledyne Wah Chang (Albany, Oregon).

These two alloys and a control sample of 316 stainless steel were tested for corrosion resistance with H_2S at 700°C. These tests suggest that HR-60 will be unsuitable for use with hot H_2S-bearing feed streams, but that C103 should exhibit adequate corrosions resistance and provide long operating lifetimes. C103 also has adequate strength at high temperatures for this application.

Aluminum-Oxide-Coated Stainless Steel

The ALON Company (Tarrytown, New York) offers a commercial vapor-diffusion process for applying aluminum-oxide coatings to steel. This process, called Alonizing, initially produces an aluminum-rich coating on the steel that rapidly oxidizes in air, yielding a tenacious coating of aluminum oxide. Aluminum oxide has excellent chemical resistance to hot H_2S, so we expected Alonized stainless steel to exhibit good stability to high concentrations of H_2S at high temperatures. Samples of Alonized stainless-steel tubing were tested in 10% H_2S in N_2 at 500°C to 700°C. These tests show that Alonized stainless steel exhibits good corrosion resistance to hot H_2S. Structurally, alonized stainless steel is equivalent to the alloy from which it is prepared—these alloys have adequate strength at high temperature for this application.

Development Of New Reactor Designs

We developed a plate-and-frame module that was successfully demonstrated as a membrane reactor for conducting equilibrium-limited reactions. Figure 5 shows the key elements of this reactor design. The various reactor components (end plates, feed plates, and ports for allowing sulfur-bearing gas streams to flow into and out of the reactor) can be fabricated from a corrosion-resistant alloy, such as C103, or fabricated from stainless steel and then coated with aluminum oxide using a process such as Alonizing.

We have focused our efforts on the plate-and-frame design due to its simplicity and durability. We have demonstrated that a catalyst bed can be incorporated into the membrane reactor at the feed side of the membrane (as shown in Figure 6). In another program, a prototype membrane reactor of this configuration has been used to drive an equilibrium-limited reaction toward complete conversion (Edlund et al., 1995)

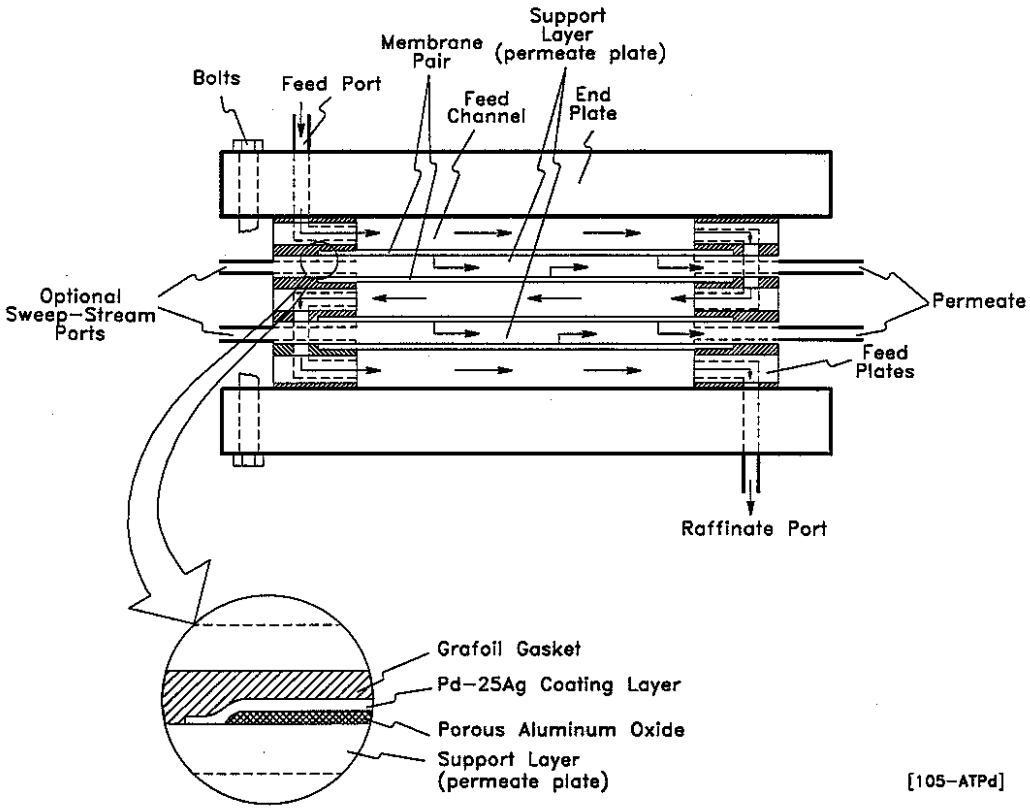

Figure 5. Cross Section of Plate-and-Frame Membrane Reactor

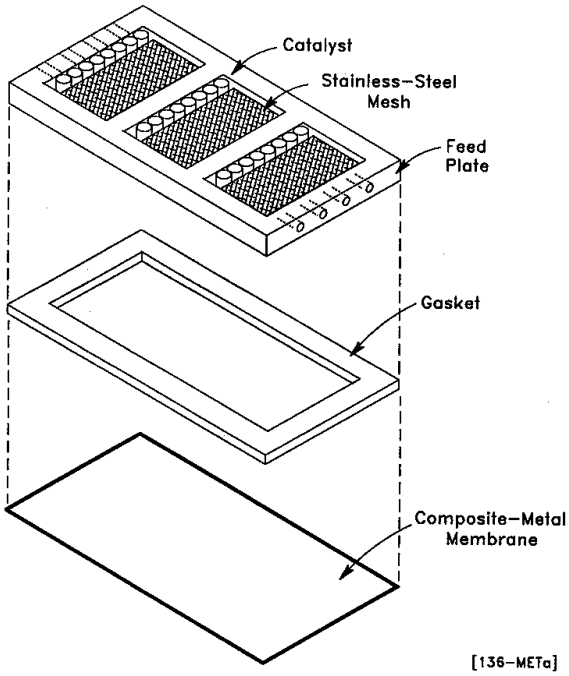

Figure 6. Location of Catalyst Bed in Prototype Membrane Reactor

Evaluation Of Process Economics

Preliminary economic analyses indicate that the membrane-reactor process will ultimately be a cost-effective, energy-efficient, and environmentally acceptable means for the separation and treatment of H_2S from hot coal-gasifier streams. We estimate that the proposed process will separate and decompose H_2S at a cost that is one-half to one-fifth that of conventional technology for this application—amine scrubbers coupled with the Claus process.

Potential Applications

The membrane-reactor process promises to offer an improved technology for H_2S separation and treatment from hot coal-gas streams. By replacing expensive, complex conventional technology with a single, simpler technology, the proposed process would reduce the overall cost of coal gasification. This technology will help enable coal to become economically competitive with petroleum and natural-gas feedstocks for the manufacture of H_2 and syngas.

Two primary benefits would be realized through development of this technology:

- the efficient and economical separation and decomposition of H_2S to environmentally benign products (hydrogen and sulfur) without the formation of sulfur oxides; and
- the reduction or elimination of Claus plants, a major source of sulfur oxide production and contributor to “acid rain.”

Successful development of the technology would also yield important secondary benefits, through increased use of coal as a feedstock. These benefits should include a decrease in reliance on foreign oil and an increase in the fraction of domestic oil and gas made available for transportation uses and production of clean-burning fuels.

In addition to the cleanup of hot coal gas, potential uses of the proposed membrane-reactor process include

- separation and recovery of H_2 from refinery gas streams that contain H_2S; and
- decomposition of H_2S to elemental sulfur and H_2 at refineries and natural-gas wells (in many cases replacing Claus plants and wet-oxidation processes for the treatment of H_2S).

Future Activities

Current development efforts are aimed at (1) improving the design of the membrane module to further reduce costs, and (2) continuing slipstream tests of the membrane module in feed streams that contain sulfur.

Acknowledgements

This work was supported by the U.S. Department of Energy through Grant Nos.:

DE-FG03-91ER81228, titled "A Membrane Process for Hot-Gas Cleanup and Decomposition of H_2S to Elemental Sulfur," METC Contracting Officer's Representative (COR): Thomas Dorchak; Period of Performance: 7/92 - 7/95 with extension; Subcontract Information: N/A.

DE-FG03-92ER81419, titled "A Process for Sweetening Sour Gas By Direct Thermolysis of Hydrogen Sulfide," METC Contracting Officer's Representative (COR): Venkat K. Venkataraman; Period of Performance: 5/93 - 5/95; Subcontract Information: N/A.

DE-FG03-91ER81229, titled "A Catalytic Membrane Reactor for Facilitating Water-Gas Shift Reaction at High Temperatures," METC Contracting Officer's Representative (COR): Venkat K. Venkataraman; Period of Performance: 3/92 to 3/95 with exteision; Subcontract Information: N/A.

References

Edlund, D.J., and W.A. Pledger, "Thermolysis of Hydrogen Sulfide in a Metal-Membrane Reactor," *J. Membrane Sci.*, 77(1993)255.

Edlund, D.J., C.B. Frost, J.R. Pledger, W.A. Pledger, T.A. Reynolds, and W.C. Babcock, A Catalytic Membrane Reactor for Facilitating the Water-Gas-Shift Reaction at High Temperatures--Phase II. Final Report to the U.S. Department of Energy on Contract No. DE-FG03-91-ER81229, from Bend Research, Inc., Bend, Oregon (1995).

McKinley, D.L., "Metal Alloy for Hydrogen Separation and Purification," U.S. Patent No. 3,350,845 (1967).

Raymont, M.E.D., "The Thermal Decomposition of Hydrogen Sulfide", Ph.D. Thesis, The University of Calgary, Department of Chemistry (1974).

Swanson, M.L., R.O. Ness, Jr., and J.P. Hurley. Semiannual report for the period January 1 to June 30, 1996, for Cooperative Agreement No. DE-FC21-93MC30097, to the U.S. Department of Energy, Morgantown Energy Technology Center, from the University of North Dakota Energy and Environmental Research Center, Grand Forks, North Dakota (1996).

DJE/rmf/jac
f:\data\admin\inbox\becky\H2S-METC

Separation of Hydrogen Using Electroless Deposited Thin-Film Palladium-Ceramic Composite Membrane

Shamsuddin Ilias (ilias@ncat.edu; 910-334-7564)
Franklin G. King (king@ncat.edu; 910-334-7564)
Ting-Fang Fan (tingfang@ncat.edu; 910-334-7564)
Sabita Roy (sabita@ncat.edu; 910-334-7564)
Department of Chemical Engineering
North Carolina A&T State University
Greensboro, NC 27411

INTRODUCTION

The development of high temperature membranes to recover hydrogen is a topic of considerable scientific interest. Since coal gasification and several high-temperature industrial processes generate hydrogen as a byproduct, the recovery of hydrogen is of significant commercial importance. Many heterogeneous catalytic reactions can not achieve high conversion because of the limit imposed by the reaction equilibrium. For example, the dehydrogenation reaction of cyclohexane, catalyzed with platinum/alumina at 215ºC in a conventional reactor, is limited to 33% conversion [1]. If, however, hydrogen is continuously removed from the reaction mixture through an inorganic membrane, the equilibrium is displaced towards the product side and the conversion is increased to nearly 80%. Since, this reaction is also favored by an increase in temperature, the temperature needed for desired conversion can be lowered. These principles can be applied to several other industrially significant reactions where the efficiency of the process depends on the effectiveness of hydrogen removal. Hence, the conversion of reactants can be enhanced dramatically if a method can be developed for recovering hydrogen at higher temperatures.

Recently, there has been increased interest in developing inorganic and composite membranes for in-situ separation of hydrogen to achieve equilibrium shift in a catalytic reactor [2]. However, the productivity of these membrane reactors is severely limited by the poor permeability of currently available membranes. Commercially available non-porous membranes are either thick film or thick walled tubes. Since permeability is inversely proportional to film thickness, a thick film membrane acts as a poor perm-separator. Thus, the major challenge lies in developing a perm-selective thin film, without compromising the integrity of the film.

To develop a new class of perm-selective inorganic membranes, we identified electroless plating to deposit a thin metal film on microporous substrate. Electroless plating is the controlled autocatalytic deposition of a continuous film on the surface of a substrate by the interaction of a metal salt and a chemical reducing agent. This method can be used to make thin films of metals, alloys and composites on both conducting and nonconducting surfaces.

OBJECTIVES

The primary objective of this project was to prepare and characterize a hydrogen permselective palladium-ceramic composite membrane for high temperature gas separations and catalytic membrane reactors. Electroless plating method was used to deposit a thin palladium film on microporous ceramic substrate. The objective of this paper is to discuss the preparation and characterization of a thin-film palladium-ceramic composite membrane for selective separation of hydrogen at elevated temperatures and pressures. In this paper, we also present a model to describe the hydrogen transport through the palladium-ceramic composite membrane in a cocurrent flow configuration.

PROJECT DESCRIPTION

Membrane Preparation and Characterization

The major tasks involved in the development of a thin-film palladium-ceramic composite membrane are (a) electroless plating of palladium on ceramic substrate, (b) characterization of palladium-ceramic composite membrane formed, © measurement and evaluation of perm-selectivity of the composite membrane for hydrogen separation. Microporous ceramic alumina membranes (α-alumina, ⌀ 39 mm × 2 mm thickness, nominal pore size 150 nm and open porosity ≈ 42% obtained from Velterop Ceramic Membrane Company of the Netherlands) were coated with a thin palladium film by electroless plating. Electroless plating is a three step process involving pretreatment of the substrate, sensitization and activation of the substrate surface, and electroless plating. The details of the plating procedures and formulations of the plating solutions are reported elsewhere [3]. The palladium-ceramic membranes were studied by taking SEM (scanning electron microscope) micrographs, EDX (energy-dispersive X-ray) analysis and measuring the thickness of the coated film by a weight-gain method.

Permeability Measurements

A steady state counter diffusion method, using gas chromatographic analysis, was used to evaluate the permeability and selectivity of the composite palladium membrane for hydrogen separation. The membranes were evaluated for hydrogen separation by conducting permeability measurements with hydrogen and argon at various temperatures and transmembrane pressure differentials. The permeability testing assembly consisted of gas sources, a diffusion cell, a tubular furnace, rotameters and a gas chromatograph. Experimental details are reported elsewhere [3].

Modeling of Gas Separation Module

The permeation of hydrogen through a palladium film is a complex process. The process begins with sorption of hydrogen molecules on the film surface and ends with hydrogen desorption from the ceramic substrate. It is believed that the hydrogen molecule dissociates into hydrogen atoms on one side of the film. The hydrogen atoms then diffuse through the film and reassociate on the other

side. Since the reaction kinetics of formation of hydrogen atoms from molecules and the reverse reaction are assumed to be very fast, the permeation of the hydrogen atoms through the film is the rate limiting step. The permeability can be considered as product of solubility and diffusivity. The permeation rate of hydrogen can be given by [4]:

$$J_a = \frac{Q_a}{h}\left[(Px_a)^n - (py_a)^n\right] \qquad \textbf{(1)}$$

If diffusion through the bulk metal is the rate limiting step and hydrogen atoms form an ideal solution in the metal, then Sievert's law hydrogen solubility dependence holds and n is equal to 0.5. The hydrogen flux is inversely proportional to the palladium film thickness (h) when the bulk diffusion is the rate limiting step. In case of polymeric membrane where selective transport of a gas is by a solution-diffusion process, the index n in Eqn. (1) has always been taken as 1. For thin-film palladium-ceramic composite membrane, since n lies between 0.5 to 1.0, the designs of membrane modules require detailed analysis of flow patterns for gas separations using Eqn. (1). In this paper, we present a generalized mathematical model for a cocurrent flow pattern in a membrane separator with n varying from 0.5 to 1.0 which depend on the type of membrane used.

Figure 1 illustrates a single permeation stage of gas separation by permeation with cocurrent plug flow on both sides of the membrane. In this flow pattern, the concentrations and flow rates of the feed and sweep gases are fixed. The design problem is to determine the states of the product and residue gas streams and membrane area requirement for a desired residue or product concentration.

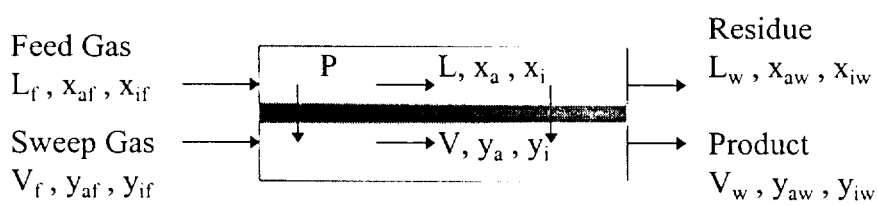

Figure 1. Schematic of Co-Current Flow Patterns of Gas Separation Module

The material and component balances between the inlet and at any point along the membrane, under certain simplifying assumptions, may be given as:

$$\begin{aligned} L + V &= L_f + V_f \,; & Lx_a + Vy_a &= L_f x_{af} + V_f y_{af} \\ Lx_i &= L_f x_{if} = constant \,; & Vy_i &= V_f y_{if} = constant \\ x_a + x_b + x_i &= 1 \,; & y_a + y_b + y_i &= 1 \end{aligned} \qquad \textbf{(2a,b,c)}$$

The rates of permeation of the permeable components per unit membrane area are given by:

$$\frac{d(Vy_a)}{dS} = \left(\frac{Q_a}{h}\right)\left[(Px_a)^n - (py_a)^n\right]$$
$$\frac{d(Vy_b)}{dS} = \left(\frac{Q_b}{h}\right)\left[(Px_b)^n - (py_b)^n\right] \qquad \textbf{(3a,b)}$$

Equations (3a,b) along with the material balance Eqns. (2a,b,c) are solved subject to initial conditions:

$$At \quad S = 0, \quad L = L_f \; ; \quad x_a = x_{af} \; ; \quad x_i = x_{if} \quad and \quad V = V_f \; ; \quad y_a = y_{af} \; ; \quad y_I = y_{if}$$

The equations were solved numerically to evaluate the performance of the membrane module. The details of the model developments and solution methodology is given elsewhere [5].

RESULTS AND DISCUSSIONS

Thin-film, Pd-ceramic composite membrane was developed by electroless deposition of palladium on planar ceramic substrate. Two sample Pd-ceramic composite membranes were fabricated and tested for hydrogen separation at high temperatures. The membranes were characterized by SEM and EDX analysis. The EDX analysis of the membrane specimen showed that the palladium film was essentially pure. SEM micrographs of the composite membrane specimen showed that the substrate pores were fully covered by solid palladium film. No pin holes were detected. The membrane specimens were fabricated by electroless deposition method as discussed. The palladium film thicknesses were estimated to be 8.5 µm and 12 µm by a weight-gain method. The permeability experiments were conducted in a diffusion cell at temperatures of 373K, 473K and 573K. The pressures on the high-pressure side ranged from 170 kPa to 240 kPa and the low pressure side was maintained at about 136 kPa. Based on Eqn. (1), the hydrogen flux data were analyzed to estimate the value of n by using the Marquardt-Levenberg non-linear least squares method. For the 8.5 µm and 12 µm films, the average values of n were estimated as 0.778 and 0.501, respectively. From this analysis, it appears that a palladium film of 12 µm thickness approaches the limiting definition of dense Pd-film according to Sievert's law.

Table 1 shows measured hydrogen permeability data at specific temperatures along with that reported by Collins and Way [6]. In their work, Collins & Way used ceramic substrate with 200 nm pore and hydrogen permeability measurements were performed at temperatures in the range of 773K to 873K. In our work, we used ceramic substrate with 150 nm pore and hydrogen permeabilities were measured at temperatures in the range of 373K to 573K. Although the palladium thicknesses were not same, one can use Arrhenius type equation to extrapolate the

TABLE 1. Summary of Hydrogen Permeability Data at Specific Temperatures for Palladium-Ceramic Composite Membranes

Membrane Description	Temperature (K)	Permeability (P_H)[#]
8.5 µm Pd-film on ceramic membrane with 150 nm pore (n=0.778)[*]	373 473 573	7.62×10^{-10} 1.16×10^{-9} 1.46×10^{-9}
12 µm Pd-film on ceramic membrane with 150 nm pore (n=0.501)[*]	373 473 573	8.84×10^{-9} 2.47×10^{-8} 3.87×10^{-8}
17 µm Pd-film on ceramic membrane with 200 nm pore (n=0.573)[**]	723 773 823	2.34×10^{-9} 4.04×10^{-9} 6.82×10^{-9}
11.4 µm Pd-film on ceramic membrane with 200 nm pore (n=0.580)[**]	823 873	3.23×10^{-9} 5.84×10^{-9}

[*] This work [3] [**] Collins & Way [6]
[#] Permeability, P_H (mol·m/m^2·s·Pa^n)

TABLE 2. Computed Hydrogen Permeability Using $P_H = P_{HO} \exp(-E_H/RT)$ at Indicated Temperatures for New Palladium-Ceramic Composite Membranes:
$P_{HO} = 4.99\times10^{-9}$ mol-m/m^2-s-Pa^n; E_H = 5,684 J/mol for 8.5 µm Pd-film
$P_{HO} = 6.63\times10^{-7}$ mol-m/m^2-s-Pa^n; E_H = 12,995 J/mol for 12 µm Pd-film

Membrane Description	Temperature (K)	Permeability (P_H)
8.5 µm Pd-film on ceramic membrane with 150 nm pore (n=0.778)	773 823 873	2.02×10^{-9} 2.14×10^{-9} 2.24×10^{-9}
12 µm Pd-film on ceramic membrane with 150 nm pore (n=0.501)	773 823 873	8.39×10^{-8} 9.52×10^{-8} 1.06×10^{-7}

hydrogen permeabilities at different temperatures. Table 2 presents computed hydrogen permeabilities of our membranes at temperatures similar to that of Collins & Way [6]. The results clearly shows that the electroless plated palladium-ceramic composite membranes developed in this work provides significantly higher hydrogen permeability.

For a cocurrent permeation cell, we conducted a parametric study of the effects of various operating parameters on the separation process. The factors considered were stage-cut, selectivity, pressure ratio, membrane area and membrane specific characteristic index, n. Figure 2 shows the variation of enrichment factor as a function of membrane selectivity with pressure ratio as a parameter. The example shown here is for cocurrent permeation with n=0.501, and the feed composition (more permeable component, hydrogen) changing from 0.71 at the inlet to 0.40 mole fraction as residue. The results show that with decreasing pressure ratio (increasing pressure on the feed side), nearly pure permeate may be obtained at relatively high membrane selectivity. However, at high pressure ratio the membrane selectivity has marginal effect on permeate purity.

The effect membrane surface area on residue concentration is shown in Figure 3 for various pressure ratio. In this example, membrane selectivity is taken as 650 with n=0.501, feed flow rate 1 mol/s and the low pressure side pressure as 1 bar. The results indicate that with increasing pressure, a larger membrane area would be required for the same residue concentration. In other words, for a given membrane module area higher separation (low residue concentration) is achieved if the module is operated at low pressure ratios.

CONCLUSIONS

A thin-film palladium-ceramic composite membrane was developed by depositing palladium on ceramic substrate by electroless plating. Permeability measurements at elevated temperatures and pressures showed that the composite membrane has a very high permeability and selectivity for hydrogen. The thickness of Pd-film dictate the hydrogen flux through the composite membrane. As the film thickness increases, one may approach the case of thick dense metallic film. Based on this work, it appears that a film thickness of 12 µm approaches the limit of dense film (with index n estimated as 0.501). A mathematical model is presented to describe the performance of a cocurrent permeation cell. The model includes the effect of membrane specific characteristic index n which varies from 0.5 to 1.0. We believe that the new Pd-ceramic composite membrane has great potential in high temperature hydrogen separations and membrane reactors if the fabrication process can be perfected.

CONTRACT INFORMATION

Research sponsored by the U.S. DOE - METC, under contract DE-FG22-93MT93008 with North Carolina A&T State University, Greensboro, NC 27411; (910) 334-7995. Drs. S. Ilias and F.G. King are the PIs of the project and Dr. V.K. Venkataraman is the METC Project Manager.

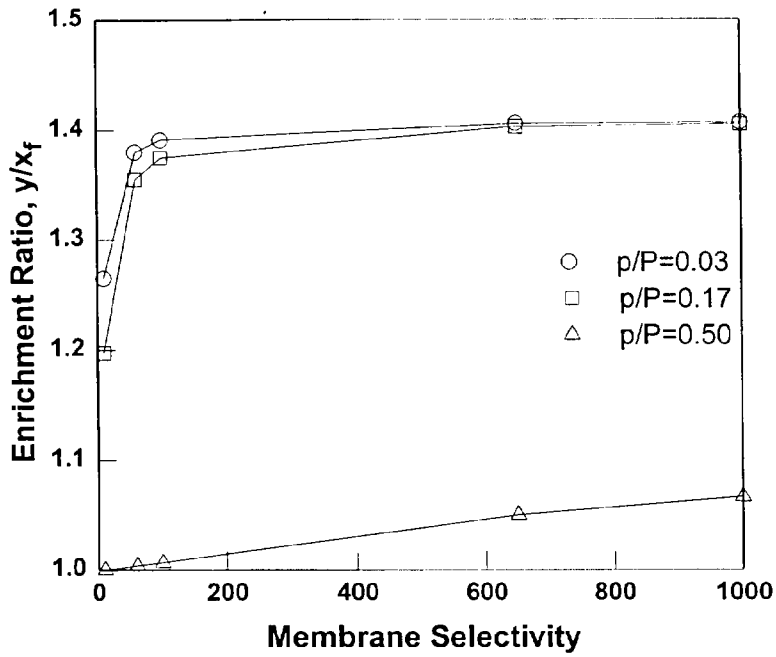

Figure 2. Effect of pressure ratio on enrichment factor as a function of membrane selectivity in a cocurrent permeation cell (n=0.501, mole fraction of hydrogen in feed, x_f=0.71 and residue x_w=0.4)

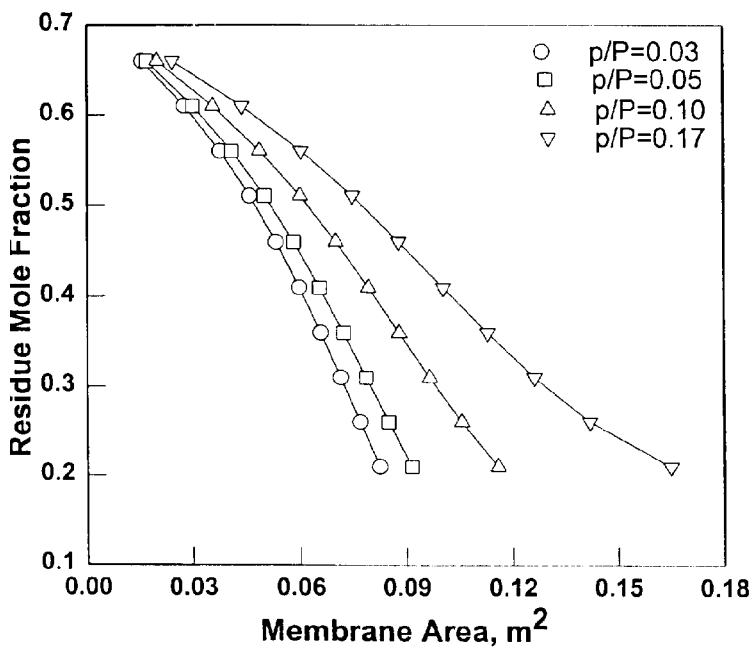

Figure 3. Effect of pressure ratio on residue concentration as a function of membrane area (n=0.501, x_f=0.71, α=650, p=1 bar, L_f=1 mol/s).

ACKNOWLEDGEMENTS

This research was sponsored by the Morgantown Energy Technology Center, U.S. DOE under grant DE-FG22-93MT93008. The authors wish to thank Drs. Carl Udovich, Gary P. Hagen and Vasu Kulkarni, Amoco Chemical Company - R&D Center, Naperville, for their invaluable suggestions and discussions.

NOMENCLATURE

h	Membrane thickness, m
L	Feed-side flow rate, mol/hr
L_f	Inlet feed flow rate, mol/hr
P	Feed-side pressure, Pa
p	Permeate-side pressure, Pa
Q_a	Membrane permeability of more permeable component A, mol-m/m^2-hr-Pa^n
Q_b	Membrane permeability of less permeable component B, mol-m/m^2-hr-Pa^n
S	Membrane area, m^2
V	Permeate-side flow rate, mol/hr
V_f	Sweep gas flow rate, mol/hr
x_s	mole fractions in feed side (a=more permeable, b=less permeable, af=feed gas, aw=residue, I=inert, if=inert in feed gas, iw=inert in residue)
y_s	mole fractions in permeate side (a=more permeable, b=less permeable, af=feed inlet end, aw=residue end, I=inert, if=inert in feed inlet end, iw=inert at residue end)
α	Membrane selectivity, Q_a/Q_b
γ	p/P, permeate to feed pressure ratio

REFERENCES

1. Itoh, N., and Govind, R., **AIChE Symp. Series 268**, **85**, 168 (1989).
2. Shu, J., Grandjean, B.P.A., Neste, A.V., and Kallagune, S., **CJChE.**, **69**, 1036 (1991).
3. Ilias, S., Su, N., Udo-Aka, U.I., and King, F.G., **Sep. Sci. Tech.**, 1996 (In Press).
4. Uemiya, S., Sato, N., Ando, H., and Kikuchi, E., **App. Cat.**, **67**, 223 (1991).
5. Tan, T-F., **Perm-Selectivity of Hydrogen Through Electroless Deposited Thin-Film Palladium Composite Membrane**, MS Thesis, North Carolina A&T State University, Greensboro, NC, 1996.
6. Collins, J.P., and Way, J.D., **Ind. Eng. Che. Res.**, **32**, 3006 (1993).

Advances in Ammonia Removal from Hot Coal Gas

K. Jothimurugesan (jothi@et.hamptonu.edu; 804-727-5817)
Department of Chemical Engineering
Hampton University, Hampton, VA 23668.

Santosh K. Gangwal (skg@rti.org; 919-541-8033)
Research Triangle Institute
3040 Cornwallis Road
Research Triangle Park, NC 27709.

Introduction

Nitrogen occurs in coal in the form of tightly bound organic ring compounds, typically at levels of 1 to 2 wt%. During coal gasification, this fuel bound nitrogen is released principally as ammonia (NH_3). When hot coal gas is used to generate electricity in integrated gasification combined cycle (IGCC) power plants, NH_3 is converted to nitrogen oxides (NO_x) which are difficult to remove and are highly undesirable as atmospheric pollutants. Similarly, while the efficiency of integrated gasification molten carbonate fuel cell (IGFC) power plants is not affected by NH_3, NO_x is generated during combustion of the anode exhaust gas. Thus NH_3 must be removed from hot coal gas before it can be burned in a turbine or fuel cell.

The product stream from a high-temperature, oxygen-blown gasifier, such as Texaco, contains about 2,000 ppmv of NH_3, where as higher concentrations (about 5,000 ppmv) occur when the gasification is conducted at lower temperatures, such as in the Lurgi or GE air-blown gasifier. A range of 1,500 to 3,000 ppmv is considered for this study.

Removal of H_2S using zinc-based mixed-metal oxide sorbents, particularly zinc titanate, to <20 ppmv levels has been well established (Lew et al., 1989; Jothimurugesan and Harrison, 1990; Woods et al., 1990; Gupta and Gangwal, 1993; Jothimurugesan et al., 1995). A previous study indicated that nickel-based catalysts have high activities for NH_3 decomposition (Krishnan et al., 1988). If desulfurization sorbents such as zinc titanate could be used along with the NH_3 decomposition catalysts to decompose ammonia present in hot coal gas, then the number of unit processes necessary to clean hot coal gas could be reduced by one. Simultaneous removal of both H_2S and NH_3 in one process unit would reduce the capital and operating costs of electric power generation from coal.

Research sponsored by the U.S. Department of Energy's Pittsburgh Energy Technology Center, under contract No. DE-FG22-93MT93005 with Hampton University. Telefax: 804-727-5189

Objectives

The objective of this study is to develop a successful combination of an NH_3 decomposition catalyst with a zinc-based mixed-metal oxide sorbent so that the sorbent-catalyst activity remains stable for NH_3 decomposition in addition to H_2S removal under cyclic sulfidation-regeneration conditions in the temperature range of 500 to 750 °C.

Approach

A number of zinc-based sorbents will be prepared in combination with NH_3 decomposition catalysts. The catalyst candidates include Ni, Co, Mo, and W. Sorbent-catalyst formulations will be screened for NH_3 decomposition activity and H_2S adsorption reactivity in a fixed-bed reactor using simulated coal gas at 1 to 20 atm and 500 to 750 °C. One of the superior formulations will be tested for long-term durability over at least 30 cycles.

Project Description

Experimental

Sorbent-Catalyst Preparation . A highly promising method was recently developed in cooperation with a commercial catalyst vendor under this project to prepare suitable sorbent-catalysts. The catalyst vendor provided the required input to keep the preparation procedure on a commercial track by making sure that the techniques used were scalable. Several sorbent-catalysts were prepared using this proprietary technique. The following analytical techniques were used to characterize sorbent-catalysts: (1) X-ray Diffraction (XRD) for the crystalline phase; (2) the standard BET method for surface area measurement; (3) Hg-porosimetry for pore volume, bulk density, average pore diameter and pore size distribution determination; and (4) Atomic Absorption (AA) Spectrometry for elemental composition analysis.

Experimental Setup . The materials prepared were tested in a laboratory-scale, high-pressure and high-temperature fixed-bed reactor. Briefly, the experimental setup consisted of a gas delivery system, a fixed-bed reactor, and a gas analysis system. Using the gas delivery system, a simulated fuel gas of any desired composition could be generated with the help of bottled gases, a set of mass flow controllers, and a high-pressure syringe pump. Steam was added to the mixed dry gas by vaporizing liquid water injected into the gas stream at a controlled rate by a high-pressure syringe pump. NH_3 was added to the gas mixture downstream of the generator where the temperature was high enough to avoid the formation of ammonium carbonates or sulfides. The reactor was constructed of a 316 stainless steel pipe. Inside the pipe there was a removable 316 stainless steel 1.0 cm I.D. tube with a porous alumina plate at the bottom that acted as a gas distributor. The inside of the tube was Alon-processed to prevent corrosion of stainless steel by sulfurous gases in the presence of steam. The pressure inside the reactor was controlled by a back pressure regulator and measured by an electronic pressure sensor. The thermocouples were positioned to measure the temperatures of the preheated feed gas, the reactor bed, and the product gas. The tests with sorbent-catalyst were conducted with a simulated gas containing 10% H_2, 15% CO, 5 mol% CO_2, 1 mol% H_2S, 15 mol% H_2O, 0.18% NH_3, and balance N_2. The outlet

H_2S and SO_2 concentrations were monitored using detector tubes and gas chromatography. The outlet NH_3 concentration was measured using ion selective electrodes and ion chromatography.

A typical run consisted of loading about 1.0 g of the sorbent in a particle size range of -32+ 64 mesh and heating the reactor to a desired temperature of 500 to 750 °C with continuous flow of nitrogen. Once the desired temperature was attained, the flow of fuel gas to the reactor was started and the concentration of H_2S and NH_3 were measured intermittently in the effluent gas. When the H_2S concentration reached 300 ppmv, indicating breakthrough, the sulfidation was stopped and the system was prepared for regeneration. The regeneration of sulfided material was carried out at the desired temperature ranging between 500 to 750 °C with 2 to 4 % oxygen in nitrogen. In all runs, the space velocity used was in the range of 2,000-3,000 h^{-1}. The regeneration of the sulfided material was carried out until the SO_2 concentration in the reactor effluent dropped below 50 ppm. These sulfidation-regeneration cycles were repeated as many times as desired. Typically each material was tested for 5 to 10 cycles to obtain meaningful data on material durability. At the end of the 5- to 10-cycle run, the material was removed from the reactor and physical and chemical characterizations were carried out on the reacted material to determine changes due to reaction.

Results

The extent of NH_3 decomposition in a simulated coal gas was determined for several proprietary sorbent-catalyst formulations. The following simulated gas was used in this study, to test the sorbent-catalyst: 10% H_2, 15% CO, 5% CO_2, 1% H_2S, 15% H_2O, 0.18% NH_3, and balance N_2 (mol%). The gas hourly space velocity was about 2500 h^{-1} in both sulfidation and regeneration. Regeneration between cycles was conducted with 10 mol% air-90 mol% N_2 at 700 °C.

Nickel-containing zinc-based sorbent-catalysts were the initial sorbent-catalysts tested. Figure 1 shows the ammonia decomposition activity of various sorbent-catalysts tested. As seen in Figure 1, HART-38 sorbent-catalyst showed a very high activity (>90%) for about 40 min. After that, the decline in activity was mainly due to the poisoning of the catalyst by H_2S. In order to increase this 90% decomposition time window, various catalyst additives were tested. Catalysts containing Ni, Co, Mo, and W compounds were candidates for this study. As seen from Figure 1, the window increased from 40 min for HART-38 to about 150 min for HART-49 sorbent-catalyst. The ammonia decomposition activity increased as the temperature was increased from 500 to 700 °C. As shown in Figure 2, however, even at 500 °C, >90% decomposition activity was maintained for nearly 70 minutes.

Life-cycle testing, consisting of 30 cycles of sulfidation, ammonia decomposition, and regeneration was successfully performed on the HART-49 sorbent-catalyst to demonstrate its long-term durability and reactivity. As shown in Figure 3, up to 180 min the sorbent-catalyst showed a very high activity (>90%). The decline in activity after 180 min is mainly due to the poisoning of the catalyst by H_2S. The pre-breakthrough H_2S level was below 20 ppm (not shown in figure). Nearly complete sorbent conversion (100%) was observed at breakthrough.

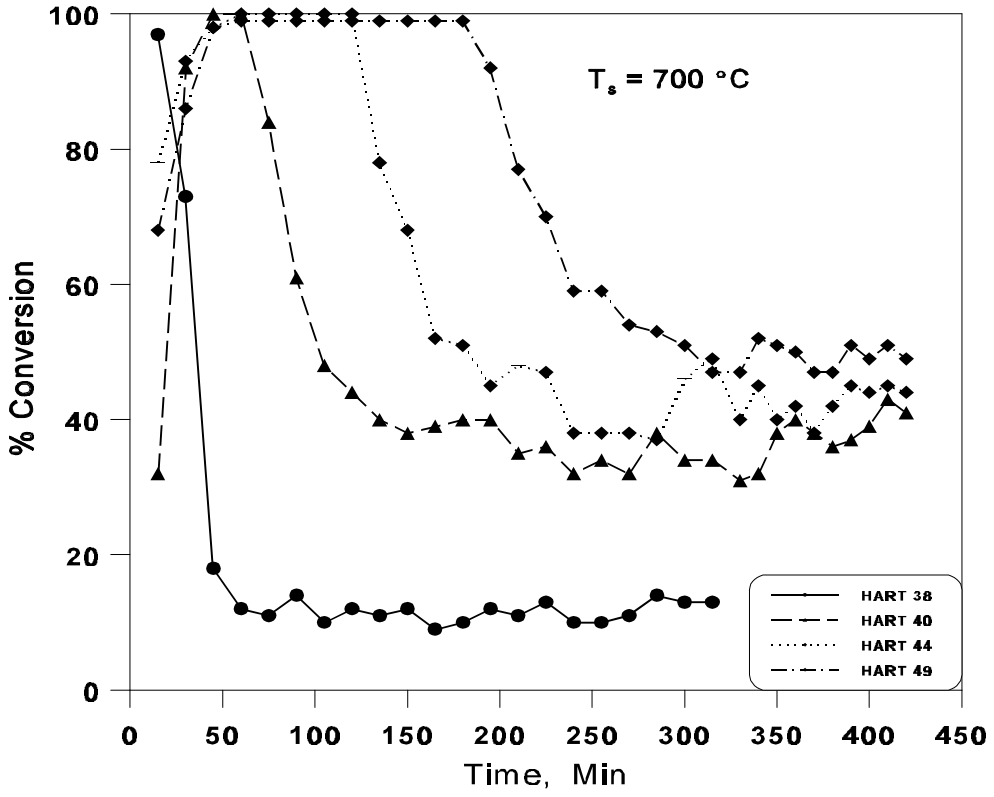

Figure 1. Conversion of Ammonia on HART Sorbent-Catalysts

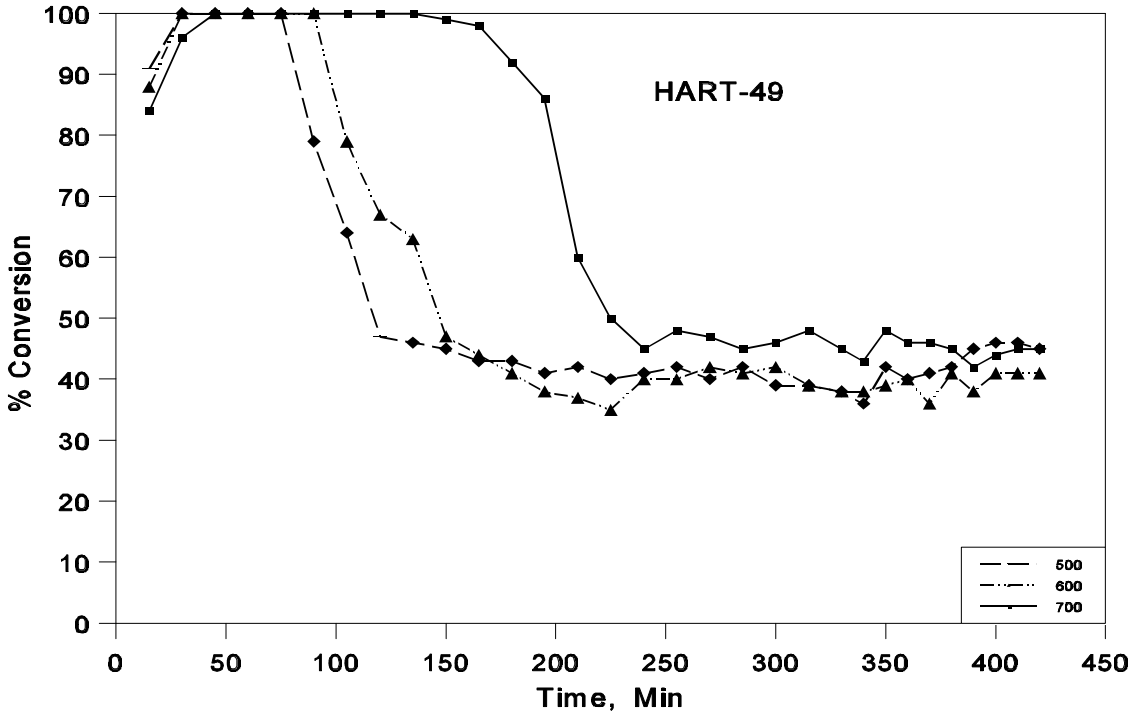

Figure 2. Effect of Temperature on the Activity of HART-49 Sorbent-Catalysts

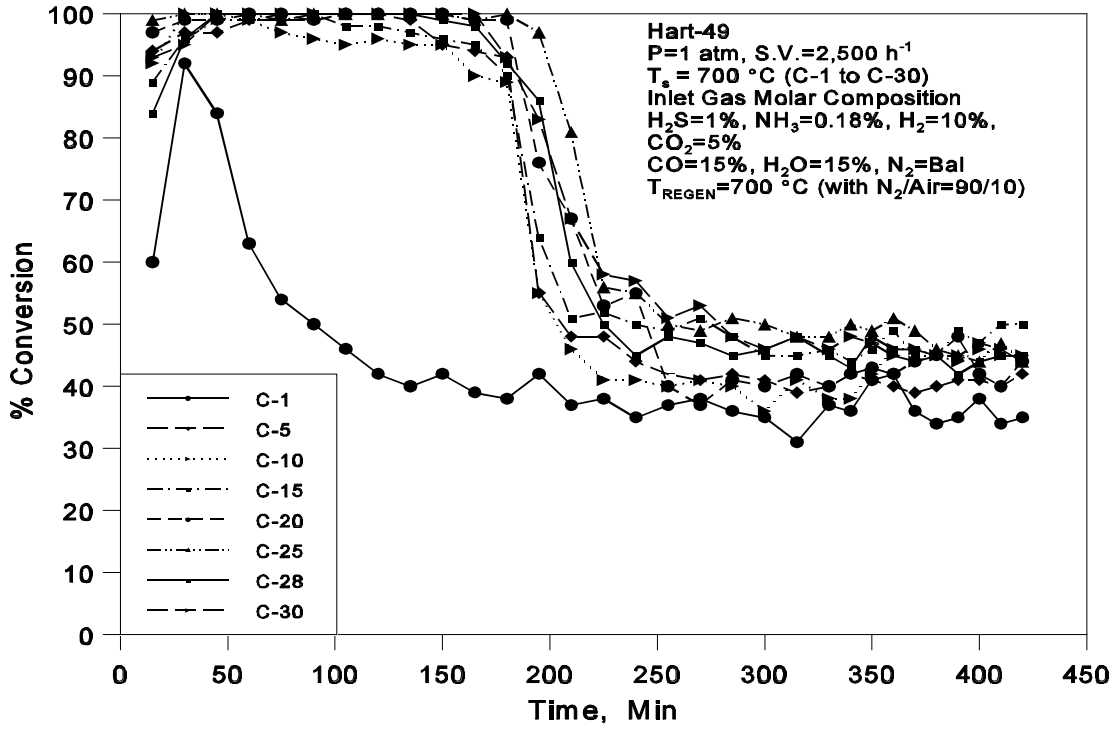

Figure 3. Conversion of NH_3 on HART-49 Sorbent-Catalyst at 700 °C

The 30-cycle test showed that HART-49 sorbent-catalyst developed under this project exhibited superior NH_3 decomposition activity, sulfur adsorption reactivity, and regenerability.

Application

Nickel-based-catalysts containing zinc-based sorbents have a moderate activity for NH_3 decomposition at 500 to 700 °C in simulated coal gas streams. The sorbent-catalysts prepared to date consistently removed 99% or more of the H_2S from a simulated coal gas containing 1% H_2S and were regenerable for multicycle operation. A superior HART-49 formulation demonstrated quite reasonable NH_3 decomposition activity in presence of 1% H_2S even at temperatures as low as 500 °C. By using the HART-49 formulation, simultaneous H_2S removal and NH_3 decomposition may become viable at practical IGCC temperatures as low as 500 °C (932 °F). Carrying out these steps simultaneously could result in reduced operating and capital costs of the IGCC plant.

Acknowledgments

The authors would like to gratefully acknowledge the guidance and assistance of Dr. Kamalendu Das, the Morgantown Energy Technology Center Contracting Officer's Representative. Research Triangle Institute provided subcontract support to the project. The period of performance is from September 2, 1993 to September 1, 1996.

References

Gupta, R. and S.K. Gangwal, "Fludizable Zinc Titanate Materials with High Chemical Reactivity and Attrition Resistance," U.S. Patent 5,254,516, 1993.

Jothimurugesan, K, A.A. Adeyiga, and S.K. Gangwal, "Simultaneous Removal of H_2S and NH_3 from Hot Coal Gas," Twelfth Annual International Pittsburgh Coal Conference Proceedings, pp. 1201-1206, September 11-15, 1995.

Jothimurugesan, K. and D.P. Harrison, "The Reaction Between H_2S and Zinc Oxide-Titanium Oxide Sorbents: II. Single Pellet Sulfidation Modeling," Ind. Eng. Chem. Res , 29,1167(1990).

Krishnan, G.N., B.J. Wood, G.T. Tong, and J.G. McCarty, "Study of Ammonia Removal in Coal Gasification Processes," Final Report to U.S. DOE/METC. Contract Number DE-AC21-86MC23087, 1988.

Lew, S., K. Jothimurugesan, and M. Flytzani-Stephanopoulos, "High-Temperature H_2S Removal from Fuel Gases by Regenerable Zinc Oxide -Titanium Dioxide Sorbents," Ind. Eng. Chem. Res. , 28,535(1989).

Woods, M.C., S.K. Gangwal, K. Jothimurugesan, and D.P. Harrison, "The Reaction Between H_2S and Zinc oxide-Titanium Oxide Sorbents: I. Single Pellet Kinetic Studies," Ind. Eng. Chem. Res, 29,1160(1990).

Market Assessment and Technical Feasibility Study of Pressurized Fluidized Bed Combustion Ash Use

Alan E. Bland (307-721-2443)
Terry H. Brown (307-721-2241)
Western Research Institute
365 No. 9th Street
Laramie, WY 82071

CONTRACT INFORMATION

Contract Number:	DE-FC21-93MC30127
Contractor:	Western Research Institute 365 No. 9th Street Laramie, WY 82071
Industrial Co-Sponsors:	Electric Power Research Institute Foster Wheeler Energy International, Inc.
Contractor Program Manager:	Alan E. Bland
METC COR	Dr. Madhav Ghate

INTRODUCTION

The commercial introduction of pressurized fluidized bed combustion (PFBC) has spurred evaluation of ash management options for this technology. The unique operating characteristics of PFBC compared to atmospheric fluidized bed combustion (AFBC) units indicate that PFBC ash will exhibit unique chemical and physical characteristics, and hence, unique ash use opportunities.

The utilization of ash from fluidized bed combustion (FBC) units is a promising ash management option. The chemical characteristics of pressurized fluidized bed combustion (PFBC) ash compared to other FBC ashes have generated interest in the use of PFBC ash for various construction and agricultural applications. However, before commercial entities and financial institutions are ready to commit to the concept of PFBC, ash management options must be documented and the costs determined.

Western Research Institute (WRI), in conjunction with the Electric Power Research Institute, Foster Wheeler Energy International, Inc. and the U.S. Department of Energy (DOE) Morgantown Energy Technology Center (METC), has undertaken a research and demonstration

program designed to examine the market potential and the technical feasibility of ash use options for PFBC ashes. The assessment is designed to address six applications, including: (1) structural fill, (2) road base construction, (3) supplementary cementing materials in portland cement, (4) synthetic aggregate, and (5) agricultural/soil amendment applications. Ash from low-sulfur subbituminous coal-fired Foster Wheeler Energia Oy pilot circulating PFBC tests in Karhula, Finland, and ash from the high-sulfur bituminous coal-fired American Electric Power (AEP) bubbling PFBC in Brilliant, Ohio, were evaluated in laboratory and pilot-scale ash use testing.

This paper addresses the technical feasibility of ash use options for PFBC units using low-sulfur coal and limestone sorbent (Karhula ash) and high-sulfur coal and dolomite sorbents (AEP Tidd ash).

OBJECTIVES

Western Research Institute (WRI), has initiated a project under sponsorship of the Electric Power Research Institute (EPRI), Foster Wheeler Energy International, Inc., and the U.S. Department of Energy (DOE), Morgantown Energy Technology Center (METC) that addresses ash use markets and options for PFBC technologies. The overall objectives of this study are to determine the market potential and the technical feasibility of using PFBC ash in high-volume use applications. The study is of direct use to the utility industry in assessing the economics of PFBC power generation, particularly in light of ash disposal avoidance achieved through ash use. Additional benefits can be realized to a utility through CO_2 offset credits resulting from ash penetration into certain markets that generate high levels of greenhouse gases during manufacturing (e.g., cement production).

The specific objectives of the program are:

- to define present and future market potential of PFBC ash for a range of applications;
- to assess the technical feasibility of PFBC ash use in construction and soil/spoil amendment applications; and
- to demonstrate the most promising of the ash use options in full-scale field demonstrations.

RESULTS

A laboratory and pilot-scale testing program was conducted to address the use of PFBC ash in both construction-related applications as well as agricultural and soil remediation applications. The study has focused to date on two ash sources: (1) ash from the Foster Wheeler Energia Oy Karhula circulating PFBC pilot plant and (2) ash from the AEP Tidd bubbling PFBC demonstration plant. Ashes from the Foster Wheeler Energia Oy R and D Laboratory CPFBC pilot unit in Karhula, Finland, represent the combustion of low-sulfur Powder River Basin subbituminous coal (Black Thunder) with limestone sorbent. Fly ash and bed ash from the AEP Tidd bubbling PFBC facility in Brilliant, Ohio represented ash from the combustion of high-sulfur Ohio No. 8 (Illinois Basin) coal and Plum Run dolomite.

Ash Characteristics

With the exception of relatively high mineral carbon, the chemistry of the PFBC ashes is typical of ashes from FBC of low-sulfur and high-sulfur coals using limestone and dolomite sorbents. The chemical compositions of the Karhula and AEP Tidd ashes have been presented in Bland et al., (1995a). The Karhula ashes are composed principally of anhydrite ($CaSO_4$), calcite ($CaCO_3$), coal ash oxides, and dehydroxylated clays. In addition to these phases, the Tidd ashes contain dolomite ($(Ca,Mg)_2CO_3$) and periclase (MgO), reflecting the use of a dolomite sorbent. These results are similar to those reported by Bigham et al.(1993). It should be noted that the dolomite is principally in the fly ash, while periclase is principally in the bed ash. The dolomite in the fly ash is probably the result of fine dolomite sorbent blow-through. The lack of lime (CaO) in the PFBC ashes is distinctly different from AFBC ashes, which contain large amounts of lime. In PFBC systems, the partial pressure of CO_2 favors the equilibrium conditions of both calcination and recarbonization. This results in low lime and high carbonates (calcite or dolomite) in pressurized FBC ash as compared to high lime and low carbonates in the atmospheric FBC ash.

The general physical properties of the ashes were also determined, including particle size distribution, specific gravity, and bulk densities. The size distribution is similar to that of other FBC ashes reported in the literature (Georgiou, et al., 1993; Bland, et al., 1993b; Bigham, et al., 1993). The bulk densities of the Karhula and the AEP Tidd fly ashes and bed ashes were determined according to ASTM procedures. The bulk densities for the Karhula ashes were 59.2 pcf (poured) and 72.5 pcf (packed) for the fly ash and 85.4 pcf (poured) and 95.4 pcf (packed) for the bed ash, while those for the Tidd ash were 53.3 pcf (poured) and 74.3 pcf (packed) for the fly ash and 80.2 pcf (poured) and 90.1 pcf (packed) for the bed ash. Specific gravities for the Karhula fly ash and bed ash materials were determined to be 2.8 and 2.7 g/cc, respectively, while the specific gravities of the Tidd fly ash and bed ash were 2.8 g/cc and 3.0 g/cc, respectively.

Ash Use Applications

Laboratory and pilot-scale tests were conducted to address the use of Karhula and Tidd PFBC ash in a number of construction-related applications, including (1) cement replacement and cement manufacturing, (2) fills and embankment construction, (3) soil stabilization applications, and (4) synthetic aggregate production. In addition, greenhouse and soils amelioration studies were conducted to addresss ash use in agricultural and soils remediation aplications.

<u>PFBC Ash Use in Concrete and Cement Production</u> The use of PFBC ash appears to be technically feasible in the cement industry. PFBC ash use in concrete and in cement production, including (1) the replacement of cement in portland cement concrete; or (2) the use as pozzolanic material in the production of pozzolanic cements (e.g., Type IP); and (3) the use as set retardant interground with cement as a replacement for gypsum.

The concrete and cement markets for PFBC ash are very large. Over 6 million tons of fly ash are used annually as a replacement for portland cement in

ready-mix concrete and concrete products. Approximately 42% of all ready-mix concrete contains fly ash at an average of 20% replacement of the cement. In addition, over 80 million tons of portland cement were produced in the United States, consuming approximately 1 million tons of fly ash in the production of pozzolanic cement.

Cement Replacement - The use of PFBC ash in concrete and concrete products relies on the pozzolanic property of the ash. Fly ash, including FBC ash, is known to be a pozzolan and therefore is used as a cement replacement in portland cement concrete. The use of PFBC ash as a pozzolan for portland cement and concrete products is dependent on a number of characteristics that are tested according to methods of ASTM C-311 and must comply with the specifications of ASTM C-618. The fly ashes from Karhula and AEP Tidd were analyzed for chemical and physical properties as related to their use as pozzolans for cement replacement in portland cement and concrete products. The results are presented in Table 2. The data indicate that the ashes do not qualify as pozzolans according to ASTM C-311 because the sulfate levels exceed the ASTM C-618 specification of 5% maximum SO_3 content. This will restrict the use of certain PFBC ashes as pozzolans for portland cement applications.

Portland Cement Production - PFBC ash can be incorporated into the cement manufacturing process as an ingredient in the clinker production and secondly as an interground material in the production of Type IP pozzolanic cements. The characteristics of the ash for these applications are defined under ASTM C-595 and C-593.

Table 2. Results of ASTM C-311 Testing of Karhula and AEP Tidd Fly Ashes as Pozzolans for Cement Replacement

	Karhula Fly Ash	AEP Tidd Fly Ash	ASTM C-618 Specifications	
			Class F	Class C
Chemical Properties				
$SiO_2+Al_2O_3+Fe_2O_3$ (wt.%)	57.57	49.39	70 min	50 min
Sulfur Trioxide (wt.%)	12.17	10.55	5 max	5 max
Moisture Content (wt. %)	0.09	0.11	3 max	3 max
Loss on Ignition (wt. %)	0.81	11.08	6 max	6 max
Available Alkalis (wt.%)	0.70	0.68	1.5 max	1.5 max
Physical Properties				
Fineness (% retained 325 mesh)	25.58	21.97	34 max	34 max
Pozzolanic Activity Index				
With PC* (% of control @ 28 days)	83.4	89.8	75 min	75 min
Water Requirement (% of control)	97.7	98.3	105 max	105 max
Soundness - Autoclave Expansion (%)	-0.040	0.000	0.8 max	0.8 max
Drying Shrinkage Increase @ 28 days (%)	0.016	0.011	0.03 max	0.03 max

*PC - portland cement

Table 3. Summary of PFBC Ash Use in Type IP Blended Hydraulic Cement – Chemical Specifications

Chemical Requirements	Karhula Fly Ash [1]	AEP Tidd Fly Ash [2]	ASTM C-595 Specifications
MgO (%)	2.9	4.0	5.0 Max.
SO3	2.9	2.9	4.0 Max.
LOI	1.0	1.8	5.0 Max.
Fly Ash Addition (%)	23.8	18.0	-
Gypsum Required (%)	-	2.15	-

1. Calculations are based on fly ash interground with Type I portland cement to achieve (1) equivalent of 5% gypsum addition or (2) a maximum of 4% MgO content in cement.

The use of ash as a pozzolan in blended cement according to ASTM C-595 does not rely on the chemical properties of the pozzolan and instead is based on performance specifications for the resultant blended cement. Calculations were made related to the potential use of the PFBC ashes in the manufacturing of blended Type IP cement and are presented in Table 3. It is clear that PFBC ash could be used in substantial amounts in Type IP portland cement.

PFBC Ash Use as Structural Fill and Embankment Materials The application of PFBC residue as an engineered material for structural fills and embankments represents a large-scale use option. Structural fills and embankments are numerous in the road construction, mining and industrial construction industries.

In addition to these compacted fill applications, PFBC ash is potentially applicable for use in controlled density low-strength flowable fill (CDLSFF) applications. This material is not really concrete and is highly flowable (slump 9-10 inches). CDLSFF is usually mixed in a ready-mix concrete truck, with mixing continuing during transport to prevent segregation. The CDLSFF is discharged and placed using chutes or can be pumped using standard concrete or grout equipment. A number of applications have been documented for CDLSFF, including excavatable backfills and trench/pipe bedding, structural fills, road bases, caisson and pile fills, and mine void filling. PFBC ash is expected to be marketable in both of the compacted fill and flowable fill applications.

Geotechnical tests using the ashes from Karhula and AEP Tidd were conducted to determine the possible use of the ashes as compacted structural fill or embankment material, as well as flowable fill material for excavatable trench grade and structural fill applications. A description of the results of testing for each of these engineered fill materials is provided below.

Compacted Fills and Embankments - The geotechnical tests related to compacted structural fills and embankments focused on the moisture-density relationship (Proctors), unconfined compressive strength, expansion and swell, and permeability.

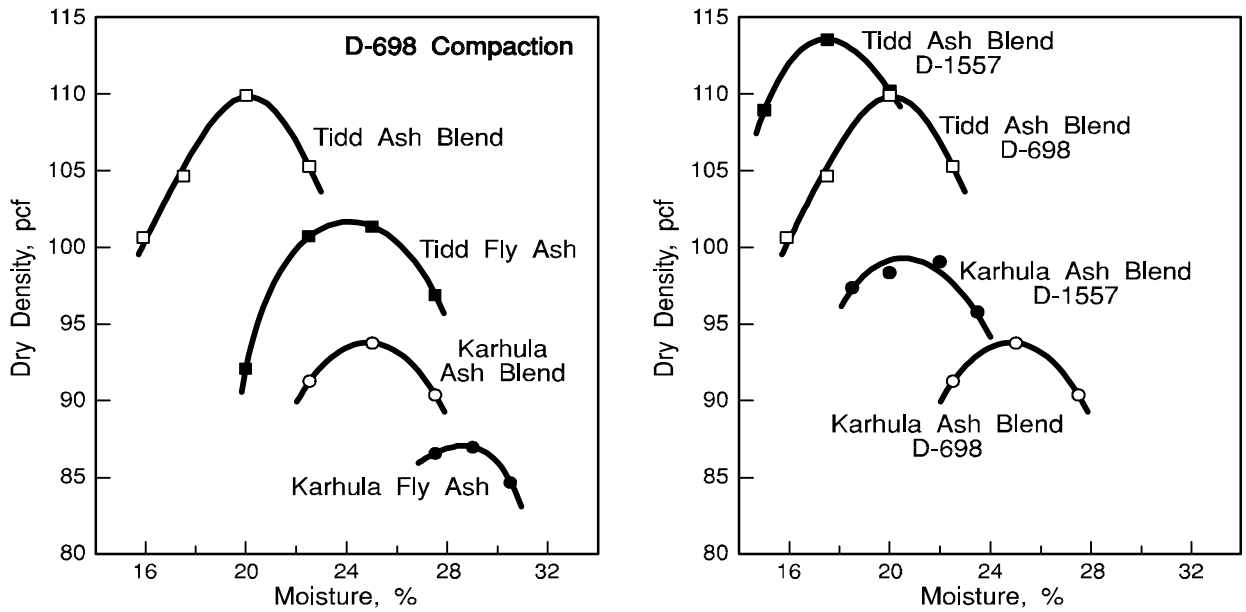

Figure 1 . Moisture-Density Relationships of Karhula and AEP Tidd PFBC Ashes

Moisture-density relationships were determined using ASTM D-698 and ASTM D-1557 compactive efforts. The compactive effort employed in the ASTM D-1557 tests is twice that for ASTM D-698. These compactive efforts typically cover the range of compaction achievable with standard construction equipment. The results are presented in Figure 1. The lower optimum moisture and higher maximum dry density observed for the ash blend is consistent with the larger particle size and specific gravity of the bed ash relative to the fly ash. The ASTM D-698 and D-1557 modified Proctor data are consistent with the expected behavior of different compactive efforts (i.e., lower optimum moisture and higher maximum dry density for increased compactive effort).

Testing also addressed the strength development of the Karhula and AEP Tidd ash blends as related to their use in compacted structural fills and embankments. The ash blends are a composite of the fly ash and the bed ash in approximate proportions to that produced in the combustor. Specimens were prepared at the optimum moisture and densities represented by ASTM D-698 and D-1557 and cured under sealed and saturated (100% relative humidity) conditions at 23°C.

Strength development for the Karhula and AEP Tidd ash blends under sealed conditions for different compactive efforts is presented in Figure 2. Both of the PFBC ashes showed strengths in excess of the needs of fills and embankments. The strength development of the Karhula PFBC ash is a factor of 4 to 10 times higher than that for other soils and fill materials, while the strength of the AEP Tidd ash was even higher. The ASTM D-1557 compacted specimens were stronger than the ASTM D-698 compacted specimens, as expected. The differences in strength between the Karhula and AEP

Tidd ashes are related to differences in the hydration reaction chemistry of the two ashes (Bland, 1995a). These differences appear to be more related to fuel sulfur content and hence sorbent requirement and the type of sorbent used than to whether the ash was produced in a circulating or bubbling PFBC unit.

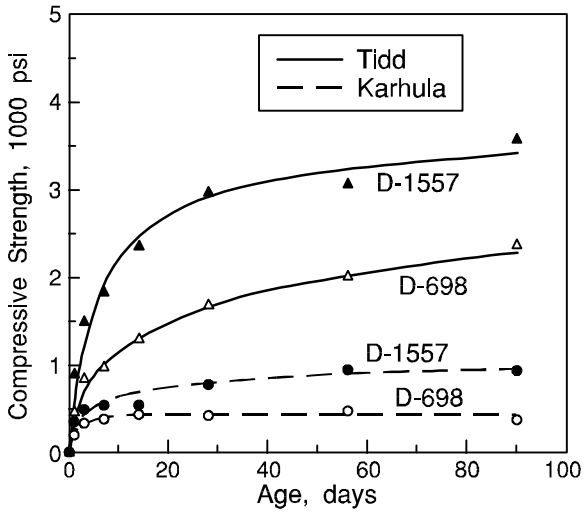

Figure 2. Strength Development of Karhula and AEP Tidd Ash Blends, Sealed Curing Condition at 23°C

The expansion properties of the conditioned and compacted Karhula and AEP Tidd ashes were determined according to modified ASTM C-157 procedures in which the expansion is essentially unrestricted. The results for the Karhula and AEP Tidd ash blend for ASTM D-698 and D-1557 compactive efforts are essentially identical, with expansion of near zero percent. In addition, the ASTM D-698 and D-1557 compacted ash blend specimens cured under both sealed and saturated conditions showed essentially no expansion. The Karhula and AEP Tidd ash blends appear to be dimensionally stable and thereby suited for compacted fill and embankment applications.

The permeability of the Karhula and AEP Tidd ash blends were determined according to ASTM procedures. The ashes were compacted at ASTM D-698 optimum moisture. As expected, the permeability of the ash blends continued to decrease with curing. Hydraulic conductivities in the range of 9×10^{-6} cm/sec were determined at early ages and continued to decrease to values of 2 x E-6 cm/sec, after which the values appeared to stabilize. These values are typical of those reported for CFBC ashes (Georgiou, et al., 1993).

Controlled Density Low-Strength Flowable Fills - The second application involves controlled density low-strength flowable fill, which has been used in construction applications for a number of years. Controlled density low-strength flowable fill material is a mixture of cement, fly ash, sand and water that has a specific strength dependent upon the end use. CDLSFF offers favorable economics compared to other fill materials because it requires less excavation and compaction during construction.

The results of tests using Karhula and AEP Tidd PFBC ashes in CDLSFF are represented in Table 4. Structural fill grade CDLSFF requiring in excess of 1200 psi strength and excavatable trench fill grade, requiring strengths in the range of 100 to 200 psi, were tested. The data clearly show that both the Karhula and the AEP Tidd fly ashes can be used as CDLSFF.

PFBC Ash Use for Soil Stabilization The use of PFBC ash and other FBC residues for stabilization of soils is a potentially

Table 4. Summary of Properties of Flowable Fill Materials Made with Karhula and AEP Tidd PFBC Ash

	Structural Fill Grade		Excavatable Trench Fill Grade	
	Karhula	AEP Tidd	Karhula	AEP Tidd
Mix Components (lbs/yd ^{3})				
Portland Cement	190	190	80	80
PFBC Fly Ash	450	450	450	450
Penetration Resistance (psi)				
4 hours	58	5	4	0
8 hours	314	109	28	16
24 hours	384	786	128	192
Compressive Strength (psi)				
2 days	131	88	46	6
7 days	298	398	84	143
28 days	1031	1199	203	234

large ash use market. This ash use application is similar to the cement stabilization of soils commonly applied in the construction industry. Soil stabilization is based on the treatment of clay soils with a material to provide strength and stability. Cement, fly ash and lime-ash materials are commonly employed at levels of 10 to 20% of the soil. FBC ashes exhibit self-cementing characteristics and, as such, have been proposed as a viable stabilizing agent.

For a material to be considered as a cementing agent for soil stabilization applications, the material must show strength development, freeze/thaw durability, and wet/dry durability in compliance with ASTM D-1632, D-560, and D-559, respectively. A viable cementing material needs to exhibit sufficient strength in the range of 4000 psi and durability of 12 cycles of freeze/thaw and wet/dry for the cementing material only. These requirements result from stabilized soil specifications of 400 psi and durability to 12 cycles of wet/dry and freeze/thaw when soils are treated at 10 to 0% cementing levels.

Unconfined Compressive Strength Relationship - Testing was conducted using the Karhula and AEP Tidd ash blends with and without hydrated lime addition, in order to determine their potential as a cementing agent for soil stabilization applications. The test specimens were cured under sealed and saturated conditions (23°C). Typical results of the testing are displayed in Figure 3. The strength development of both of the PFBC ashes was more than sufficient for soil stabilization applications. The results showed 5% hydrated lime increased the strength development dramatically (over 6,000 psi at 90 days for Karhula ash and over 9,000 psi at 90 days for AEP Tidd ash). The ash blend without hydrated lime enhancement showed strengths of less than 1000 psi for the Karhula ash and less than 3,500 psi for the AEP Tidd ash. As mentioned earlier, these differences in strength are due to differences in the hydration chemistry of the two ashes (Bland, 1995a). Once

again, these differences appear to be more related to fuel sulfur content and hence sorbent requirement and the type of sorbent used than to whether the ash was produced in a circulating or bubbling PFBC unit. The low strengths of the ash blends without lime are sufficient for many applications, such as fills and embankments. However, for other applications, such as soil stabilization, lime enhancement will be required at some level (e.g., 5% or less).

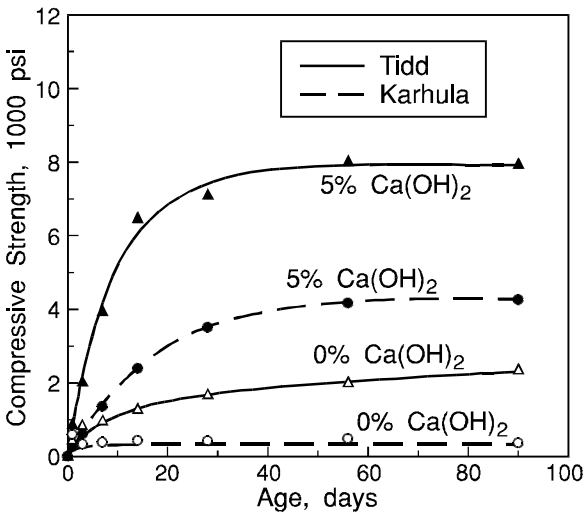

Figure 3. Strength Development of Karhula and AEP Tidd Ash Blends with and without Lime Enhancement

Expansion Properties - The expansion properties of the conditioned and compacted Karhula and AEP Tidd ashes with and without hydrated lime addition were tested for soil stabilization applications, according to a modified ASTM C-157 procedure. The Karhula and AEP Tidd ashes with and without hydrated lime addition were conditioned and compacted at the ASTM D-698 optimum moisture and proctor density. The results for the Karhula ash are shown in Figure 4.

The lime-enhanced Karhula ash blend showed expansion in the range of 1.5%, while the ash blend without lime enhancement showed essentially no expansion. The expansion noted for the lime-enhanced ash appears to occur early, within the first 20 to 30 days. Although the expansion is significant, it appears controllable and manageable, and it should be possible to balance the strength and swelling properties in certain applications. For example, in certain grouting applications, such as subsidence control in underground construction operations, controlled expansion of the magnitude reported is desirable.

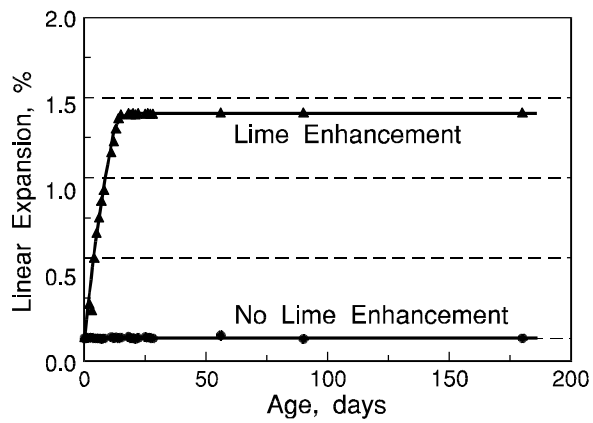

Figure 4. Expansion of Karhula Ash Blend with and without Lime Enhancement

Freeze/Thaw and Wet/Dry Cycles - Conditioned and compacted Karhula and AEP Tidd ash blend specimens were subjected to 12 cycles of freeze/thaw (ASTM D-560) and wet/dry (ASTM D-559) conditions. The results indicated that the PFBC ashes with 5% lime addition survived the entire 12 cycles with losses less than the 15% maximum limit. In fact, losses in the range of 1% were determined for these PFBC ashes.

PFBC Ash Use in Synthetic Aggregate Production The aggregate market in the United States is enormous. In 1992, approximately 1.2 billion tons of crushed stone and approximately 0.8 billion tons of sand and gravel were produced for a market valued in excess of $8 billion. The aggregate market encompasses conventional aggregate products, such as masonry units and ready-mix concrete. Also, with crushing, aggregates can be produced for use in asphalt paving, road base construction and even roller compacted concrete. Lightweight aggregate can also be used in many structural building products.

Synthetic aggregate has been manufactured from power plant ash that can meet the requirements for conventional aggregate products, such as masonry units and ready-mix concrete, and with crushing can be produced for use in asphalt paving, road base construction and even roller-compacted concrete. As such, synthetic aggregate for construction applications appears to be a major market for PFBC ashes, as well as a method for storage of ash in the construction off-season.

Pelletizing Trials - Pelletizing trials were conducted simulating the AET process for the pelletization of FBC ashes, as described in the literature (Bland et al., 1992, 1993). A schematic of the AET pelletizing process for PFBC ash is presented in Figure 5.

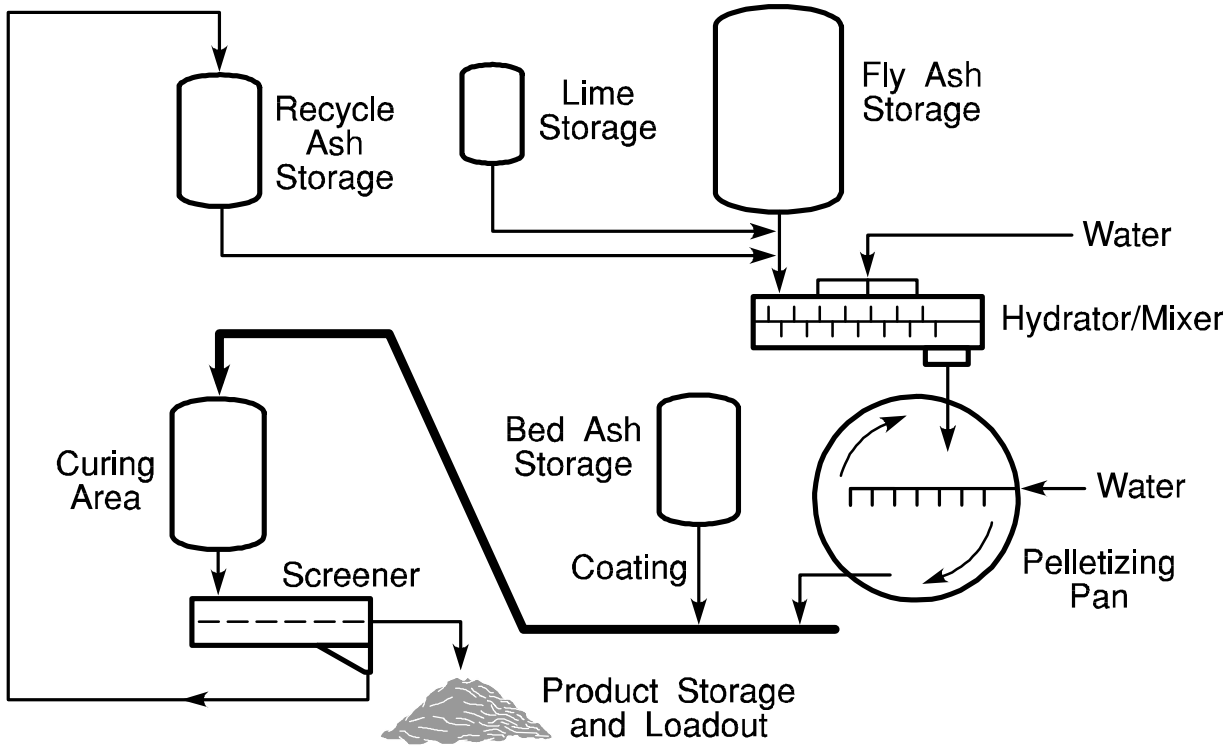

Figure 5. Schematic of the AET Synthetic Aggregate Process for PFBC Ashes

Table 5. Summary of the Properties of PFBC Ash-Based Synthetic Aggregate

Aggregate Properties*	No Lime Enhancement		Lime Enhancement	
	Karhula Ash	AEP Tidd Ash	Karhula Ash	AEP Tidd Ash
Crush Strength (lbs)				
24 hours	23	75	323	240
48 hours	24	81	306	226
7 days	31	104	340	276
28 days	52	164	289	282
LA Abrasion Resistance				
Grade	B	C	B	C
Loss @ 28 days (%)	75.29	42.1	26.07	11.1
Resistance				
Loss after 5 cycles**	27.97	15.08	-4.23	2.35

* Curing Conditions - 180 °F Sealed for 24 hours.
** Magnesium Sulfate Solution.

Pelletizing trials were conducted at the WRI Waste Management Laboratory, employing a high-speed pin mixer for conditioning of the ash and a 3-foot diameter pelletizing pan for the agglomeration of the conditioned ash into a pelletized form.

Pelletizing trials have been conducted employing Karhula and AEP Tidd ash blends with and without lime enhancement. The pelletizing trials were conducted to address the water requirement and other processing parameters pertinent to defining the technical feasibility and relative economics of aggregate production from PFBC ashes.

Pelletized Ash Testing - The pelletized aggregate produced from Karhula and AEP Tidd PFBC ash was tested according to ASTM procedures as they relate to its use in various construction applications. Pelletized ash from each of the pelletizing trials was tested for crush strength, Los Angeles abrasion resistance (ASTM C-131) and soundness (ASTM C-88). The results of testing are presented in Table 5. The results indicate that without hydrated lime addition, the pelletized PFBC ash does not meet the ASTM or AASHTO construction aggregate requirements of a maximum of 40% weight loss. However, the addition of 5% hydrated lime results in compliance with ASTM and AASHTO requirement for construction aggregate. The soundness of the aggregate using magnesium sulfate solutions were well below the AASHTO specifications of less than 18% loss after 5 cycles. In fact, the Karhula aggregate actually gained weight due to continued hydration during the five cycles.

Ash Use in Soil/Mine Spoil Amendment Applications

PFBC ash use as a soil amendment for agricultural and reclamation activities represents a potentially large market. A number of benefits can result from the application of PFBC residue to agricultural soils or mine spoils, including the modification of soil pH, supply of essential plant micro-nutrients for crop production, increasing water infiltration, and

modification of soil structure promoting root growth. The availability of nutrients, such as sulfur, potassium, and phosphorous, along with micronutrients is also expected to benefit plant growth. In addition, the neutralization potential of the ash materials can alleviate acid conditions found in many soils. Also, PFBC ash contains anhydrite or gypsum, often used to reclaim sodic materials (i.e., materials influenced by high levels of sodium).

PFBC ashes generated at the Karhula and AEP Tidd plants were evaluated as soil amendments to ameliorate acid and sodic conditions on problem soils. As mentioned earlier, this material was thought to be useful because of its high neutralization potential, high $CaSO_4$ content, and nutritional potential. A very important consideration for the use of this material for ameliorating problem soils was the potential for negative impact of other constituents on the environment. Saturated paste extracts have shown that the ash materials do not contain any elements at concentrations deemed harmful to the environment.

Acidic Soils and Mine Spoils Amelioration Study - Laboratory equilibration studies were conducted to address the use of PFBC ashes as amendments to ameliorate acidic spoil and soil conditions. The laboratory equilibration study was designed to determine the potential of the ash materials to neutralize the available acid and the potential acidity associated with oxidation of reduced materials present in the spoil. An acid spoil material from Texas was used for the study. Humidity cells were used to simulate the oxidation of acid-forming soils under amended and non-treated conditions. Ag-lime ($CaCO_3$) and Karhula fly ash were used as the soil neutralization amendment materials in the equilibrium humidity cell studies. The acid spoil material was treated with three levels of ag-lime and three levels of Karhula fly ash:

- Level 1 = 30.4 g ag-lime or 89.1 g Karhula fly ash/1000 g of spoil
- Level 2 = 26.2 g ag-lime or 77.4 g Karhula fly ash/1000 g of spoil
- Level 3 = 17.6 g ag-lime or 51.6 g Karhula fly ash/1000 g of spoil

The amount of ag-lime used was based on the calcium carbonate equivalent (CCE) of the material and the acid/base accounting values of the acid spoil. The PFBC fly ash application rates were equivalent to the acid neutralization potential used for the ag-lime tests. Treatment of acid soils usually employs an application rate of 1.2 times that calculated from the neutralization potential. The humidity cell equilibration study showed the Karhula fly ash to be an effective acid neutralization amendment (Figure 6).

The acid present in the treated materials was neutralized and the formation of acid from acid-forming minerals present in the spoil material was significantly reduced due to treatment with PFBC ashes. It is apparent that the neutralization reaction rate of the Karhula fly ash in raising pH of the acid spoil is slower than that of the ag-lime. While the Karhula fly ash shows a delayed response, the ag-lime reacted immediately with the spoil material, increasing the pH and maintaining it with time. Although the Karhula fly ash is an effective long-term amendment for acid soils and spoils, the lower early pH levels of approximately 4

for the Karhula fly ash-treated spoils may cause some problems with germination and early plant growth with sensitive plant species.

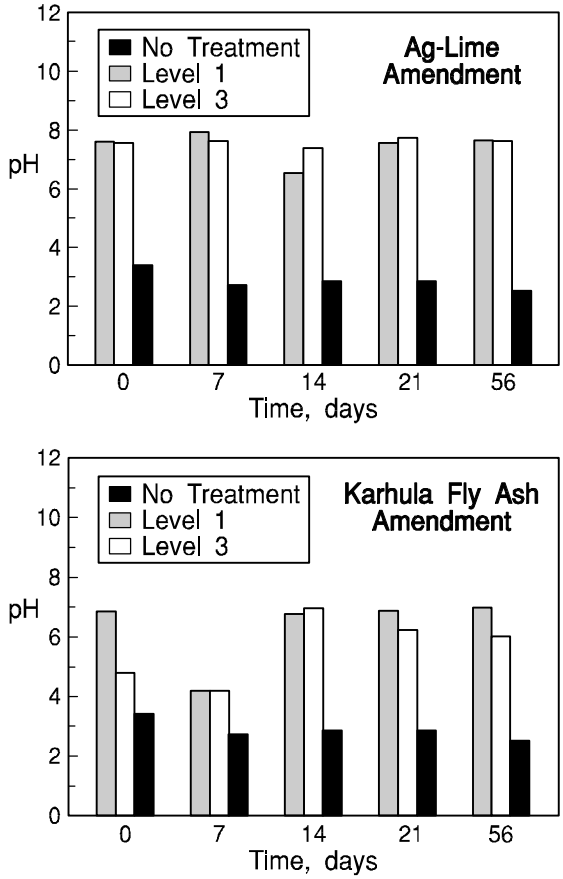

Figure 6. Influence of Ag-Lime and Karhula Fly Ash on Acidic Mine Spoil pH

Greenhouse Productivity Study - A greenhouse study was conducted to show the influence of PFBC ashes on the productivity of acidic mine spoil containing very high potential acidity. The study compared the production of Garrison Meadow foxtail grass (*Alopecuras protensis* cult. Garrison) on acid spoil materials amended with ash from the Karhula and AEP Tidd operations and with ag-lime ($CaCO_3$). The greenhouse study was conducted under controlled conditions of light, temperature, fertilizer levels, and soil moisture requirements to maximize plant growth conditions. Fertilizer additions were based on nitrogen, phosphorous, and potassium levels and did not include concerns for nutrient ratios and micronutrient deficiencies.

The results of the study are shown in Figure 7. The results clearly indicate that extremely poor quality soils can be successfully treated with PFBC ashes, resulting in good plant productivity. The results show PFBC ashes to be as effective as ag-lime in seed germination and more effective than ag-lime in plant production and root penetration. Total plant production was about 25% higher for the Tidd and Karhula ash treatments compared to the ag-lime treatment at the high level (Level 1) of application (Figure 7).

At the low amendment application rate the Karhula treatment resulted in plant production about 30 % higher compared to the Tidd and ag-lime treatments, which were comparable. An obvious factor responsible for the differences in the plant production between the PFBC ash-amended spoils and the ag-lime amended spoil was the root penetration. The PFBC ash treated soils contained root matter throughout the potted soil, while much of the root mass in the ag-lime treated soil was associated with the sides of the pots. No problems with the early low pH were found.

Sodic Soils Amelioration Study - Permeability testing of sodic spoil materials collected from a mine site located in North Dakota indicated that PFBC ash was an effective treatment resulting in the potential for enhanced root

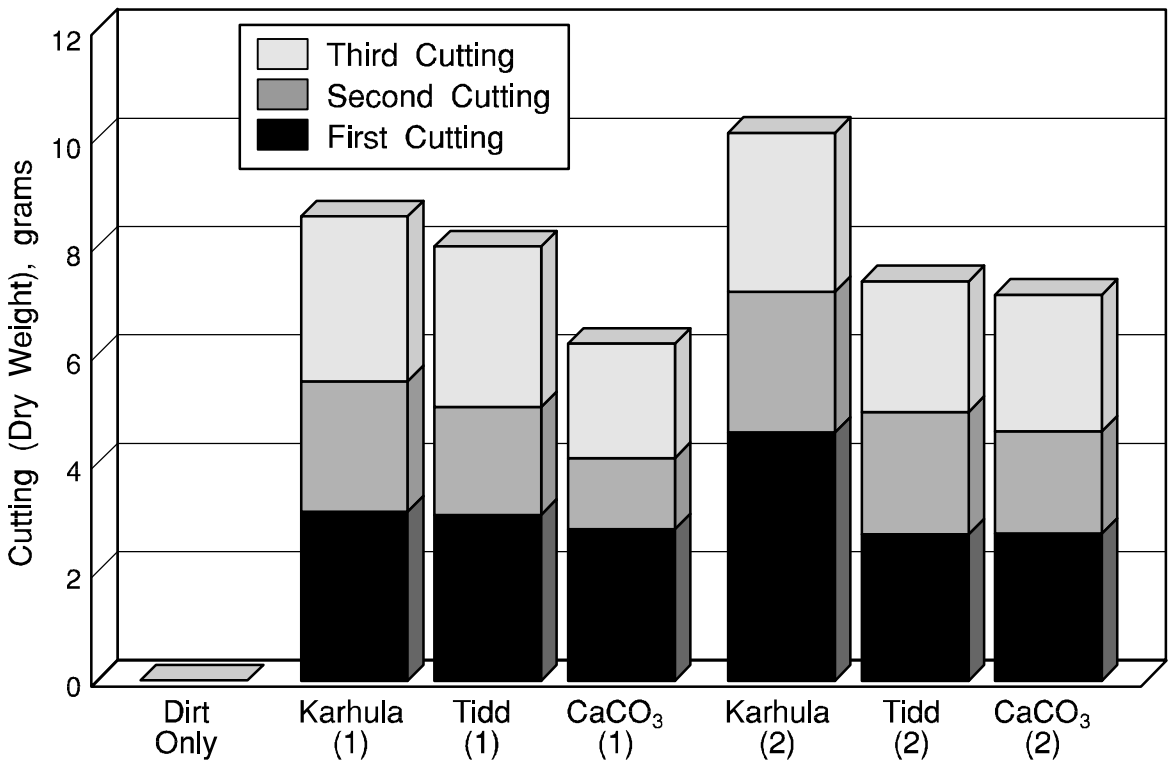

Figure 7. Dry Weight Production of Meadow Foxtail Grass Grown on Karhula Fly Ash, AEP Tidd Fly Ash and Ag-Lime Amended Acidic Mine Spoil (Level 1 –High Application Rate; Level 2 –Low Application Rate)

penetration and gas and liquid movement within the spoil material. The untreated spoil material allowed no water penetration into the material or movement through the material during the permeability tests. Treated material allowed water penetration and movement through the material at a relatively high rate.

FUTURE ACTIVITIES

Activities for FY '96 includes the acquisition and testing of an additional ash from the Foster Wheeler Energia Oy R and D center in Karhula Finland. This ash was produced in the 10 MW_e PCFBC pilot plant employing high sulfur bituminous coal and limestone sorbent from Illinois. As such, this ash expands the range of composition of ashes evaluated in this project. The testing will evaluate construction related applications including cement and concrete use, fills and embankment construction, soil stabilization; and synthetic aggregate production. In addition, a greenhouse study will be conducted related to its use in agricultural and soils remediation applications.

ACCOMPLISHMENTS

In summary, Western Research Institute, in conjunction with the Electric Power Research Institute, Foster Wheeler International, Inc., and the U.S. Department of Energy (METC), has undertaken a research and demonstration program designed to examine the market potential and the technical feasibility of ash

use options for PFBC ashes. Ash from low-sulfur subbituminous coal-fired Ahlstrom pilot circulating PFBC tests in Karhula, Finland, and ash from the AEP's high-sulfur bituminous coal-fired bubbling PFBC in Brilliant, Ohio, were evaluated in laboratory and pilot-scale ash use testing at WRI.

The technical feasibility study examined the use of PFBC ash in construction-related applications, including its use as a cementing material in concrete and use in cement manufacturing, fill and embankment materials, soil stabilization agent, and use in synthetic aggregate production. Testing was also conducted to determine the technical feasibility of PFBC ash as a soil amendment for acidic and sodic problem soils and spoils encountered in agricultural and reclamation applications.

The results of the technical feasibility testing indicated the following:

- PFBC ash does not meet the chemical requirements as a pozzolan for cement replacement. However, it does appear that potential may exist for its use in cement production as a pozzolan and/or as a set retardant.

- PFBC ash shows relatively high strength development, low expansion and low permeability properties that make its use in fills and embankments promising.

- Testing has also indicated that PFBC ash, when mixed with low amounts of lime, develops high strengths, suitable for soil stabilization applications and synthetic aggregate production. Synthetic aggregate produced from PFBC ash is capable of meeting ASTM/AASHTO specifications for many construction applications.

- The residual calcium carbonate and calcium sulfate in the PFBC ash has been shown to be of value in making PFBC ash a suitable soil amendment for acidic and sodic problem soils and mine spoils.

In conclusion, PFBC ash represents a viable material for use in currently established applications for conventional coal combustion ashes. As such, PFBC ash should be viewed as a valuable resource, and commercial opportunities for these materials should be explored for planned PFBC installations.

REFERENCES

Bigham, J., W. Dick, L. Forster, F. Hitzhusen, E. McCoy, R. Stehouwer, S.W. Traina, W. Wolfe, and R. Haefner, 1993, "Land Application Uses for Dry FGD By-Products; Phase I Report." U.S. Department of Energy, Morgantown Energy Technology Center.

Bland, A. E., C. E. Jones, J. G. Rose, and M. N. Jarrett, 1987. "Production of No-Cement Concretes Utilizing Fluidized Bed Combustion Waste and Power Plant Flyash", In Proceedings of 9th International Conference on Fluidized Bed Combustion, Boston, May 3-7, 1987 pp 947-953.

Bland, A.E., C.E. Jones, J.G. Rose, and J.L. Harness, 1989a, "Ash Management Options for Bubbling FBC Technologies". In Proceedings of

ASME Joint Power Generation Conference, Dallas, Oct. 22-26, FACT Vol. 6, pp 9-19.

Bland, A.E., C.E. Jones, J.G. Rose, and J.L. Harness, 1989b, "Ash Management Options for AFBC." Proc., 10th International Conference on Fluidized Bed Combustion, San Francisco, April 30 - May 3, 1989, pp 323-333.

Bland, A.E., S.M. Burwell, and R.K. Kissel, 1991a, "Commercialization Potential of AFBC Concretes: Part 1. Mix Design and Engineering Properties." EPRI Project No. 2708-4, 1991., EPRI Report GS-7122.

Bland, A.E., R.K. Kissel, and G.G. Ross, 1991b, "Utilization of CFBC Ashes in Roller Compacted Concrete Applications." Proc., 11th International Conference on Fluidized Bed Combustion, Montreal, Canada, April, 1991, pp 857-863.

Bland, A.E., R. Cox, A. Rowen, E.R. Lichty, and R.A. Schumann, 1992, Pelletizing Ash, United States Patent Number 5,137.753, August 11, 1992.

Bland, A.E., R. Cox, A. Rowen, and E.R. Lichty, 1993, "Pelletization as an Ash Management Option for CFBC Ash Handling and Utilization." Proc., 12th International Conference on Fluidized Bed Combustion, La Jolla, CA, May, 1993, pp. 1341-1350.

Bland, A.E., 1994, "Overview of Management Options for Residues from FBC Technologies." Proc., EPRI 1994 Fluidized Bed Combustion Symposium, Atlanta, May, 1994.

Bland, A.E., 1995a, "Hydration Reaction Chemistry Associated with Management of Pressurized Fluidized Bed Combustion Ash." Proc., 1995 Ash Utilization Symposium, University of Kentucky and ACAA, Lexington, KY.

Bland, A.E., T.H. Brown, L.-J. Young, M.B. Ashbaugh and J.M. Wheeldon, 1995b, "Use Potential of Ash From Circulating Pressurized Fluidized Bed Combustion Using Low-Sulfur Subbituminous Coal." Proc., 13th International Conference on Fluidized Bed Combustion, ASME, Orlando, FL, pp 1229-1242.

Burwell, S.M., R.K. Kissel, A.E. Bland, and D.M. Golden, 1993, "Fluidized Bed Combustion Ash Concrete." Proc., 12th International Conference on Fluidized Bed Combustion, La Jolla, CA, May, 1993, pp. 847-858.

Georgiou, D.N., A.E. Bland, and D. Sundstrom, 1993, "Laboratory Evaluation of a Low Sulfur Coal CFBC Residue as a Structural Fill." Proc., 12th International Conference on Fluidized Bed Combustion, La Jolla, CA, May, 1993, pp 629-639.

ACKNOWLEDGMENTS

The authors acknowledge the support of the Electric Power Research Institute, Foster Wheeler Energy International, Inc., and the U.S. Department of Energy (DOE), Morgantown Energy Technology Center (METC), under Cooperative Agreement Number DE-FC21-93MC30127. The

support of Dr. Madhav Ghate, METC COR is appreciated.

The authors also wish to acknowledge the technical assistance of Kumar M. Sellakumar of Foster Wheeler Energy International, Inc.; John M. Wheeldon and Richard Brown of EPRI; American Electric Power Services for contributing the ashes from AEP Tidd and Kamalendu Das of METC for his project support and assistance.

Conference Proceedings - Power Systems '96
U.S. DOE (METC) July 16-18, 1996

The Impact of Leachate From Clean Coal Technology Waste on the Stability of Clay and Synthetic Liners

Terry H. Brown (307-721-2241)
Western Research Institute
365 N. 9th Street
Laramie, WY 82071

CONTRACT INFORMATION

Contract Number:	*DE-FC21-93MC30127*
Contractor:	*Western Research Institute* *365 N. 9th Street* *Laramie, WY 82071*
Industrial Co-Sponsors:	*Public Service Company of Colorado*
Contractor Project Manager:	*Terry H. Brown*
METC - COR:	*Dr. Madhav Ghate*

ABSTRACT

This project was developed to provide design criteria for landfill disposal sites used for sludges such as those generated using the Clean Coal Technologies (CCT) tested at the Public Service Company of Colorado's Arapahoe Power Plant. The CCT wastes used were produced at the Arapahoe Plant Unit No.4 that was equipped with the integrated dry NO_x/SO_2 emissions control system installed under the Clean Coal Technology (CCT) Program. The investigation emphasized the potential impact of clean coal technology materials (sodium and calcium injection systems, and urea injection) on the permeability and stability characteristics of clay liner materials and the stability of synthetic liner materials.

Flexible-wall permeameters were used to determine the hydraulic conductivities (HC) of the clay liner materials impacted by various compactive conditions. Tests were conducted using the waste materials overlying the clay liner materials under wet/dry cycles, freeze/thaw cycles, and over 120-day periods.

The impact of CCT materials on the characteristics of the clay liner materials studied in this project was minimal. The HC measurements of the waste/clay liner systems were similar to the water/clay liner systems. HC decreased for clay liners compacted at moisture levels slightly higher than optimum (standard Procter) and increased for liners compacted at moisture levels lower than optimum (standard Procter). Although some

swelling was evident in the sodium materials, the sludge materials did not have a negative impact on the integrity of the liners over 120-day tests. Wet/dry cycles tended to result in lower HC, while freeze/thaw cycles substantially increased HC for the liners tested.

Tests were also conducted to assess the compatibility of synthetic liner materials with the CCT by-products. The test program was conducted using methods specified and/or referenced in EPA, SW 846-Method 9090 with some modifications. Compatibility evaluations were made using high-density polyethylene (HDPE), very low-density polyethylene (VDPE), and polyvinyl chloride (PVC) synthetic liner materials treated with baseline fly ash materials (no CCT used), sodium injection materials, calcium injection materials, and materials generated from the sodium injection/urea injection/low NO_x burner control system. The synthetic liner materials were subjected to a 50:50 ratio of sludge to water for periods to 120 days at room temperature (23°C). At the end of each equilibration period, the liner materials were tested using mechanical engineering techniques and weight losses due to volatiles and extractables.

Sustained increment changes in the measured physical properties of the materials over time were not observed. Some abrupt changes in strength were found at several times during the testing period. However, these aberrations seemed more indicative of isolated changes in the conditioning methods or test procedures and could be related to flaws or changes in the materials related to manufacturing conditions. After 120 days of conditioning, none of the measured physical properties varied significantly from those for the untreated liner materials. This was true for all samples regardless of the conditioning solution used.

The volatiles and extractables tests for the HDPE and VDPE materials indicated that the waste materials had little influence on their overall structure. However, the extractables data suggest that PVC liner material might decompose in the waste environments evaluated. The PVC liner material reacted similarly for all treatments with about a 30% weight loss.

Introduction

Landfills commonly used for disposal of solid wastes pose a potential threat to surface and groundwater quality. The major concern is that the leachates form the waste may contain elements that are detrimental to the quality of the waters for their designated uses. Clay liners are usually used in landfills often in combination with synthetic liner materials to help assure the prevention of the movement of leachate from the disposal site. It is important to determine the compatibility of both the clay liner material and the synthetic liner material to the specific waste prior to prescribing a suitable liner system for a specific application.

Clay liners are often used in landfills to contain and attenuate the leachate from solid waste materials. The suitability of soil materials for liner use is usually based on permeability criteria (Brown and Anderson, 1980). However, other considerations relative to chemical-physical relationships often determine whether a clay liner is compatible to a specific type of waste. These relationships must be evaluated in detail before an appropriate liner can be prescribed for a specific landfill.

Problems often found with clay liners are related to volume shrinkage's (Hettiaratchi et al., 1988). Shrinkage's in compacted liners often result from increases in salt concentrations in the solutions within the clay liner (Green et al., 1983). Also, the impact of acidic and alkaline solutions on the dissolution of the clay minerals present in the clay liner materials results in increased permeability's for similar reasons (Peterson and Krupka, 1981). The presence of certain organic compounds in the leachates are sometimes associated with increased permeability's (Green, et al., 1983).

There are a number of variables that determine the effect of waste leachate on the long-term stability of a clay liner material. The primary variables include clay mineralogy, texture, surface chemistry considerations, the physical nature of the materials, and the chemistry of the waste leachate. Increased in salt concentrations can result in double layer collapse or less interaction between clay particles and resulting decreases in repulsive forces (Bohn et al., 1985). A decrease in repulsive forces causes the materials to flocculate reducing the effective stress in the liner which results in a volume shrinkage (Hettiaratchi et al., 1988). The mineralogy of the clay and the specific elements present in the solution associated with the clay will determine the amount of shrinkage that will result from double layer collapse. The 2:1 layer clay minerals such as montmorillinite have a much greater tendency for swelling and shrinking than the 1:1 clay types such as kaolinite. In addition, monovalent elements like sodium that have a very large hydrated radius have the potential to cause swelling, while divalent elements such as calcium have a tendency to reduce double layer expansion. Therefore, materials that have high-swelling montmorillonite clay minerals with sodium as the dominant element should be avoided. Elements such as calcium can displace the sodium and cause the double layers to collapse. this type of reaction resulted in a large amount of shrinkage in studies done by Hettiaratchi et al. (1988) with permeant solutions containing calcium. These authors suggested that clay liner materials should be conditioned with calcium solutions during the compaction stage to prevent shrinkage and cracking due to double layer collapse. However, it should be noted that if the salt concentration is increased to high levels (high electrical conductivity or EC) due to leachate migrating into the clay liner, no matter which cation is present, double layer collapse could occur resulting in the formation of cracks.

Shrinkage of clay liners can also be caused by the influence of organic compounds on the electrical double layer. The low dielectric constant of organic compounds relative to water reduces the influence of the surface charge, promoting flocculation of clay particles causing cracking of clay liners (Green et al., 1983). However, the amount of organic compounds seems to determine the degree of impact that the clay liners experience. Daniel et al. (1988) found that solutions containing low levels of organic compound did not cause shrinkage of clay liner materials. Therefore, it is apparent that most situations will require testing for compatibility between the specific wastes and the clay liner material to be used at the disposal site.

The load on the clay liner associated with the waste will also impact the effective stress experienced by the clay liner. Changes in effective stress with time may be an important factor relative to the long-term stability of a clay liner.

SPECIFIC PROBLEM

Wastes generated from CCT's have much different physical and chemical characteristics than the wastes generated from conventional power plants. As noted previously, the various wastes generated from implementation of CCT have significantly different impacts on the permeability of clay liners (Koegler et al., 1991). Also, the active lifetime of a compacted clay liner is generally assessed through permeability or saturated hydraulic conductivity and effective porosity measurements. Such assessments, however, do not take into account the influence of waste leachate chemical composition or the effects of alternating wetting and drying, and freezing and thawing cycles on leachate transport through clay liners. These "weathering" cycles need to be considered in the compatibility of a certain type of clay liner material with the waste being generated. Without good compatibility information, serious mistakes might be made that impact the environment and the consumer through environmental clean-up costs.

Flexible membrane liner compatibility studies have been conducted using clean coal technology (CCT) wastes by Koegler et al. (1991). These tests were done using fly ash/sludge materials that were generated from a number of power plants that represented desulfurization technologies such as spray dryer, atmospheric fluidized bed combustors (AFBC), limestone injection and sodium injection. These researchers looked at 20 synthetic membrane liners of various types from different venders. The findings indicated that water slurries of the wastes tested are chemically incompatible with some of the synthetic membrane liners tested. They also found that variations between synthetic liners of the same type, but obtained from different vendors, were significant. Therefore, it is recommended that before a liner is selected for a specific installation, compatibility tests using the actual waste material and liner samples form specific vendors should be completed.

OBJECTIVES

The purpose of this research was to investigate the potential impact of clean coal technology solid wastes on the permeability and attenuation characteristics of clay liner materials and on the integrity of synthetic membranes.

EXPERIMENTAL PLAN

The test program included three clay liner materials representing different overall characteristics. The liner materials represent two landfill sites located in Colorado and one site currently being used in California. Four waste materials generated at the Arapahoe Power Plant during the Clean Coal Technology testing program were used in the testing. The CCT materials used in this study include: materials collected during baseline operations without the applications of the CCT; the sodium injection materials; the calcium injection materials; and the materials generated from the sodium/urea injection/low NO_X control system. This paper will address the general aspects of the research findings.

Flexible-wall permeameters were used to determine the hydraulic conductivities (HC) of the clay liner materials impacted by various compactive conditions, confining pressures,

gradients, effective stresses and solution chemistry conditions. In addition, tests were conducted using the waste materials overlying the clay liner materials under wet/dry cycles, freeze/thaw cycles, and over long time periods. Dry cycles were conducted by allowing the liner materials to air dry to a point near field capacity (-1/3 bar matric potential), and did not represent an oven-dry condition.

Clay liner and fly ash materials were tested using compacted cyclinders, 6-inches long and 4-inches in diameter. The tests were conducted at densities based on moisture/density relationships as described in ASTM D698. Clay liner material/fly ash simulations were done using 2 inches of clay liner material overlain by 2 inches of fly ash materials. The hydraulic conductivities of the various materials were determined using ASTM D5084-90.

The test program included compatibility evaluations for 3 types of synthetic liner materials including: (1) high-density polyethylene (HDPE); (3) very low density polyethylene (VDPE); and (3) polyvinyl chloride (PVC);. The synthetic liners were immersed in the leachate environment associated with 4 waste materials generated at the Arapahoe Power Plant during the CCT testing program as noted previously. The synthetic liners were subjected to the fly ash materials for periods of 30, 60, 90, and 120 days. The 50:50 ratio of sludge to water used in this study deviates from the EPA Method 9090 which requires a 5 to 15% solids solution. This procedure was modified because the pH values associated with the dilute system specified in Method 9090 were 2 pH units lower than the pH of the 50% solids solution. In addition, the pH of the 50% solution compared well to the pH of the saturated pastes of the sludge materials used in the study. The studies were done at room temperature (23° C). Comparisons of measurements of the synthetic material's physical properties, taken before and after contact with the leachates from the fly ash materials, were used to evaluate the compatibility of the liner with the waste over time. Testing included physical tests, tensile strength properties, and changes in volatile and extractable components of the materials.

The mechanical testing was performed using the guidelines of EPA Method 9090 with the exception of the puncture test which was done using ASTM D4833. As directed by EPA Method 9090, the tensile properties method was specified as ASTM D638. The modulus of elasticity was measured for the HDPE and VDPE materials per ASTM D882, Method A. Tear strength was measured per ASTM D1004. The punch strength test method used was specified in ASTM D4833. The change in volatile and extractable weights presented on a percentage basis was done using methods specified in SW 870 Appendix III-D and Appendix III-E. Volatile losses provide indications of the amount of water absorbed into the liner. Large amounts of absorption show a degradation of the liner. A decrease in liner extractions as compared to the material before testing, provides an indication of the components leached from the liner during exposure to a waste.

RESULTS

Clay Liner Material Evaluations

In general, the impact of CCT wastes on the characteristics of the clay liner materials studied in this project was minimal. As shown in Table 1, the HC measurements decreased for clay liners compacted at moisture levels slightly higher than optimum (standard Procter) and increased for liners compacted at moisture levels lower than optimum (standard Procter). The HC measurements of the waste/clay liner system reacted very similar to the water/clay liner systems. Although some swelling was evident in the sodium waste materials, the sludge materials did not have a negative impact on the integrity of the liners over the 120-day tests (Figure 1). The column did not show any signs of cracking and the hydraulic conductivity decreased with time. Some initial dispersion of clays resulting in plugging of pores maybe responsible for the gradual reduction in HC. The potential swelling and shrinkage due to the high sodium or sodic condition followed by the impact of high salt concentrations on the electronic double layer, did not occur. This clay chemistry phenomena was expected to have a negative impact on the integrity of the clay liner materials.

Table 1. Hydraulic Conductivity Evaluations for the Clay Liner Material at Various Water Content/Density Conditions.

	cm/s
H.C. at Std Dry	2.0E-05
H.C. at Std Opt.	4.0E-09
H.C. at Std Wet	2.0E-09
H.C. at Mod Dry	2.0E-08
H.C. at Mod Opt.	7.5E-09
H.C. at Mod Wet	1.3E-09

The HC values for the 120-day test of the clay liner materials contacted with calcium injection waste are presented in Figure 2. Shrinkage of the clay liner materials due to high electrical conductivity levels was expected to potentially cause cracking of the clay liner. However, cracking was not apparent and the HC values stabilized within several weeks indicating that the clay liner remained stable.

Wet/dry cycles did not have a major impact on the HC of the clay liner materials with time. The impact of wet/dry cycles on the system with sodium-injection fly ash overlaying a clay liner is shown in Figure 3. The decline of HC values with time resemble closely the trend shown in Figure 1 for a liner not impacted with wet/dry cycles.

The influence of freeze/thaw cycles on the HC values of a clay liner impacted with a calcium injection fly ash is shown in Figure 4. The initial HC values resemble those shown in Figure 2 for the calcium fly ash overlaying the clay liner. However, each freeze/thaw cycle substantially increases HC values for the system above the previous equilibration HC level. These results suggest that during the initial development and use of a disposal site, freezing conditions could result in the failure of the clay liner system.

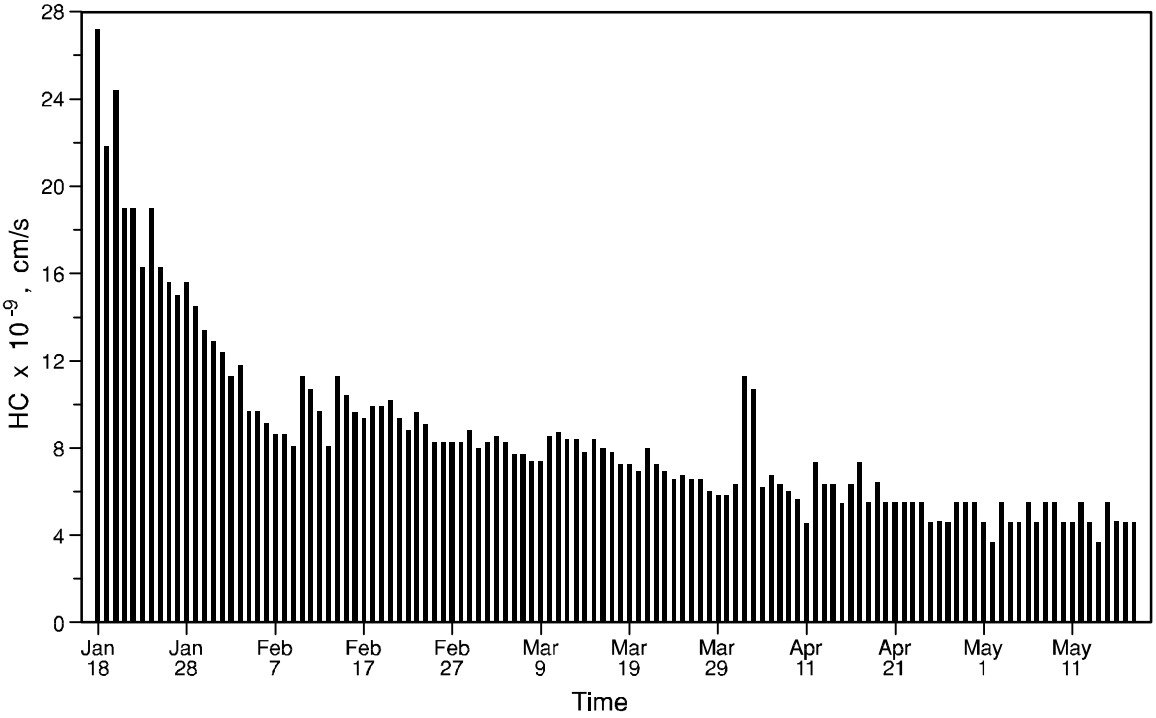

Figure 1. Long-term hydraulic conductivity values for a clay liner impacted by sodium injection fly ash leachate.

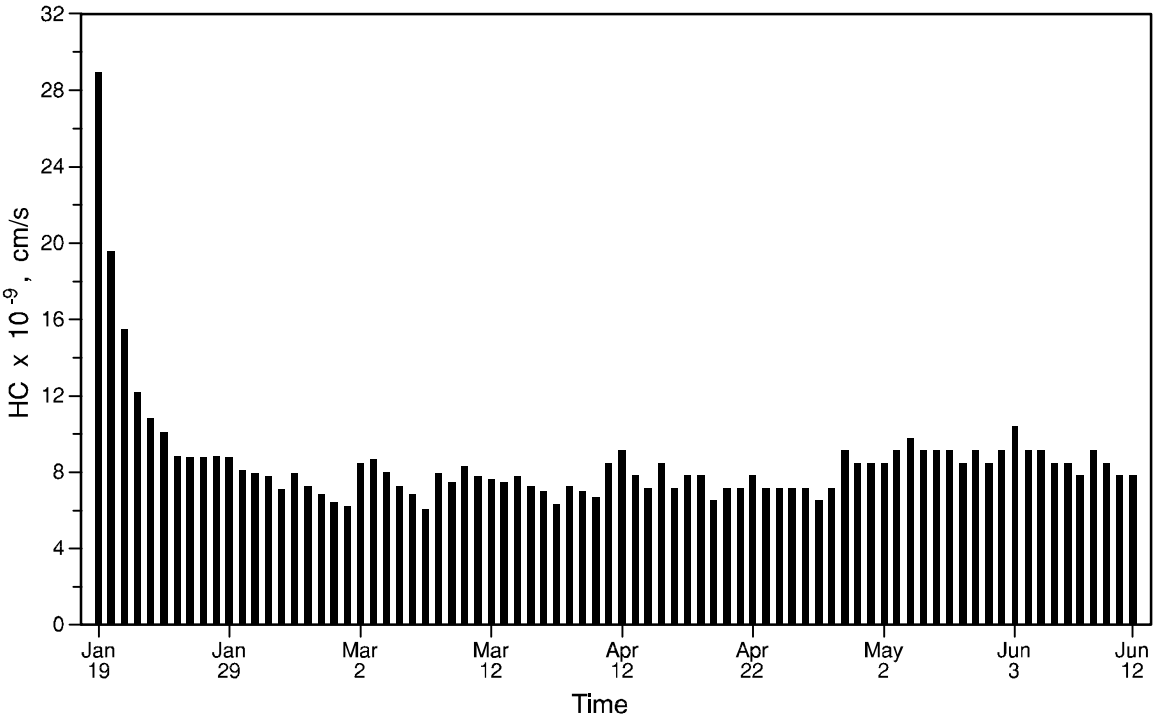

Figure 2. Long-term hydraulic conductivity values for a clay liner material overlain by calcium injection fly ash.

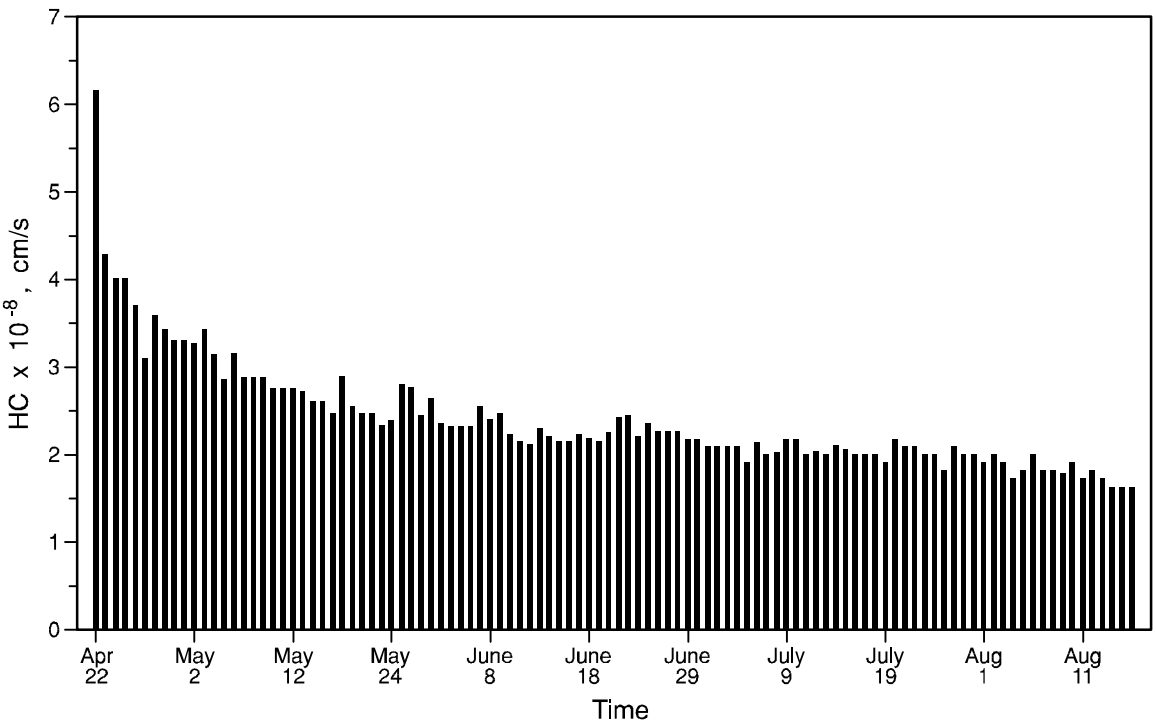

Figure 3. Hydraulic conductivity values for a clay liner material impacted by leachate from sodium injection fly ash under-going wet/dry cycles.

Synthetic Liner Evaluations

Mechanical Testing

The punch strength test data for the HDPE, VDPE and PVC materials are shown in Figure 5. This is the only property that permits direct comparison across the three materials tested, since the test was performed identically for each material type and at the same crosshead speed as required by the testing methods. The information demonstrates that the materials have much different capabilities to resist puncture. The heavy, thicker HDPE has the strongest punch strength as compared to the VDPE and the PVC materials. The PVC material which is slightly thicker and stiffer has more strength than the VDPE which is a very low density polyethylene material. However, it is apparent that the influence of the various wastes on the integrity of the synthetic liner materials is not significant. This was also found to be true for the tear strength with grain and stress at 100% elongation with grain (Figures 6 and 7). The HDPE had high tear strength as compared to the VDPE and the PVC which have comparable tear strength. However, the stress at 100% elongation with grain for the PVC material (untreated and treated) was the same as the HDPE material, and both had higher stress strength than the VDPE material. This information provides an indication that the HDPE, VDPE and PVC materials have the overall strength capabilities after 120 days of treatment with the various wastes as the untreated liner materials have. The HDPE material has higher strength as compared to the VDPE and PVC materials. However, the strength characteristics of the VDPE and PVC materials are not compromised by the waste materials.

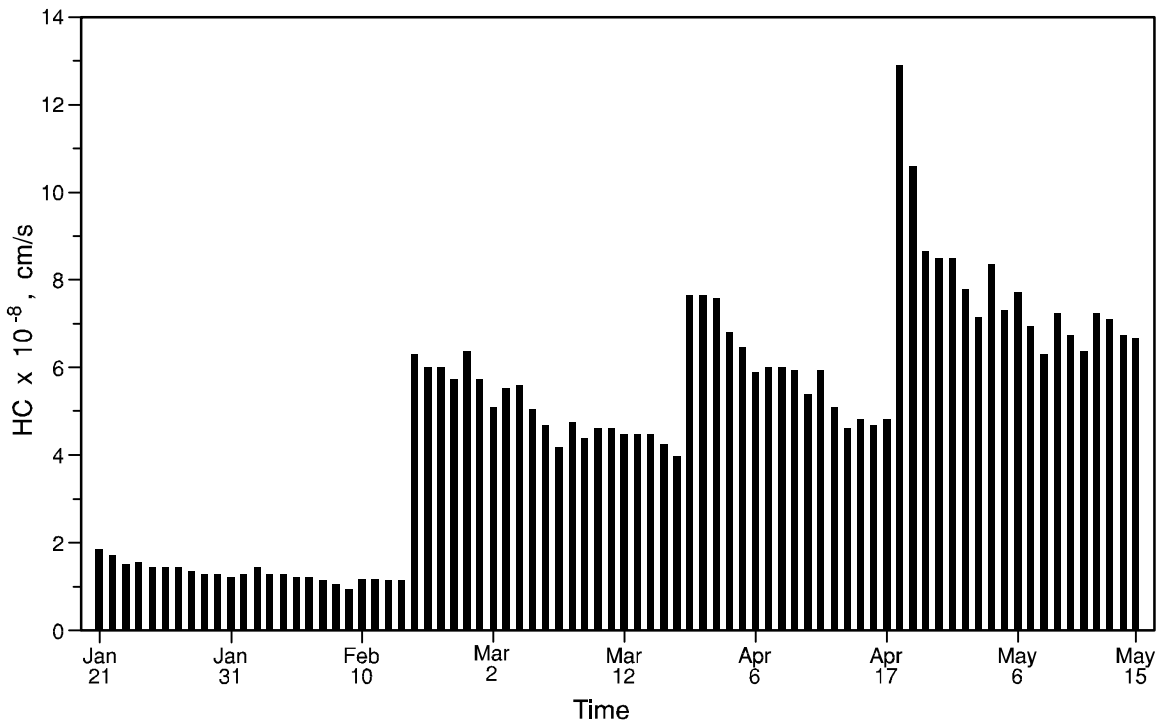

Figure 4. The influence of freeze/thaw cycles on the HC values of a clay liner impacted by solution extracted from calcium injection fly ash.

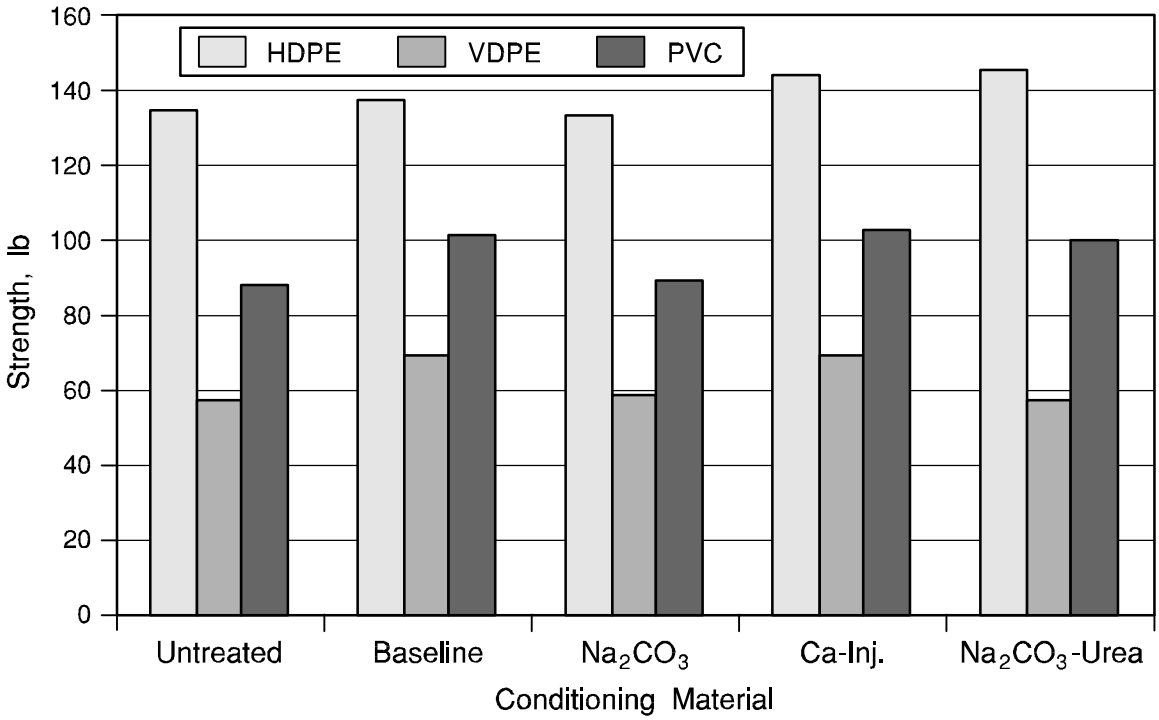

Figure 5. Punch Strength after 120 days of Conditioning

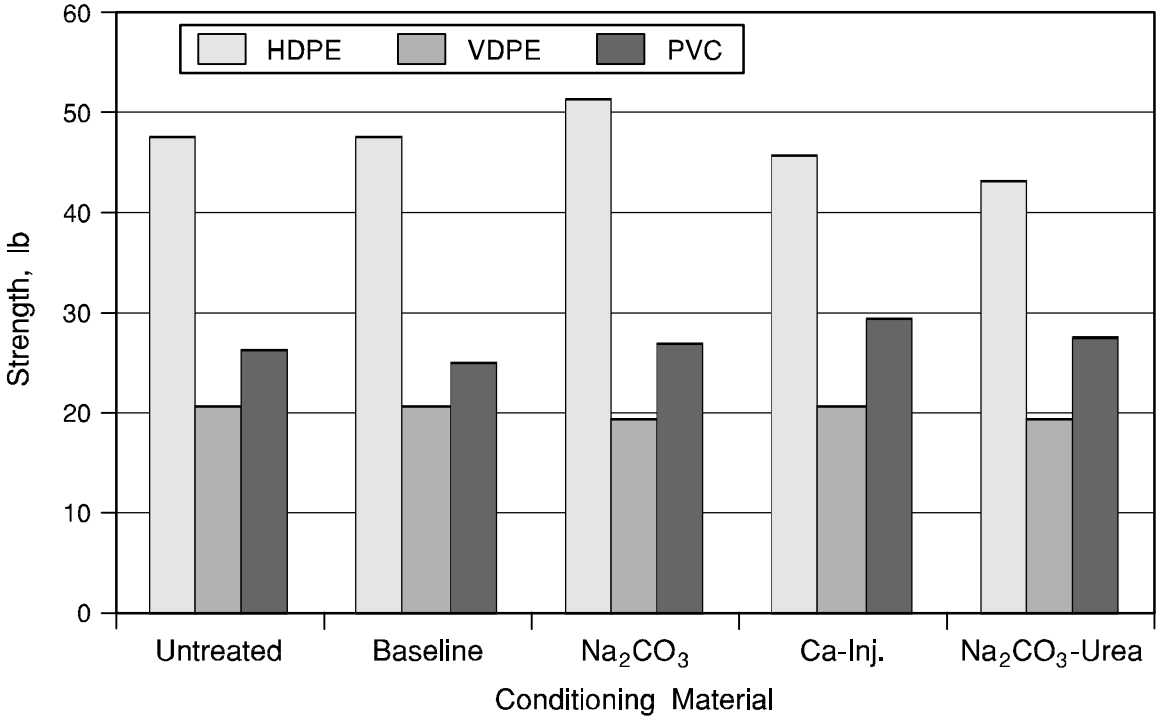

Figure 6. Tear Strength with Grain after 120 days of Conditioning

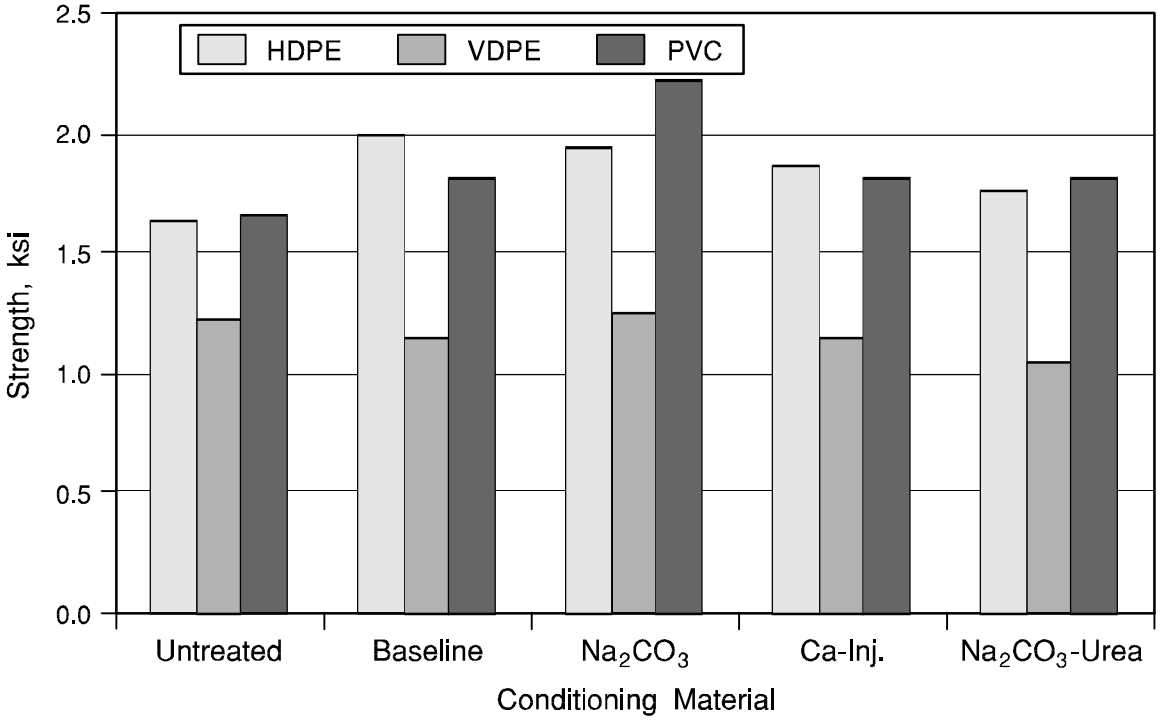

Figure 7. Stress at 100% Elongation with Grain after 120 days of Conditioning

Volatiles and Extractables Tests

Volatiles

An increase in volatile losses is an indication of water absorption into the liner materials. The percentage volatiles present in the liner samples after exposure to the sludge materials are presented in Table 2. The volatile loses associated with the PVC material are similar after a 120 day period of conditioning in the baseline, Na_2CO_3, and the Na_2CO_3-Urea sludge materials. The volatile loses associated with the Ca injection waste treatment appear to be higher. However, volatile loses for all the treated materials were rather small with the largest loss found to be about 0.25%.

Table 2. Weight Losses Due to Volatiles andExtractables

Membrane/Treatment	Volatiles, % Wt. Loss	Extractables, % Wt. Loss
PVC-Baseline	0.19	30.76
PVC-Na_2CO_3 Inj.	0.20	30.19
PVC-Na_2CO_3 Inj.	0.20	30.33
PVC-Na_2CO_3-Urea Inj.	0.20	30.21
PVC-Ca Inj.	0.26	30.36
HDPE-Baseline	0.14	0.34
HDPE-Na_2CO_3 Inj.	0.08	0.53
HDPE-Na_2CO_3 Inj.	0.10	0.61
HDPE-Na_2CO_3-Urea Inj.	0.08	0.53
HDPE-Ca Inj.	-0.01	0.60
VDPE-Baseline	0.07	1.31
VDPE-Na_2CO_3 Inj.	0.07	1.23
VDPE-Na_2CO_3-Urea Inj.	0.16	1.12
VDPE-Na_2CO_3-Urea Inj.	0.13	1.06
VDPE-Ca Inj.	0.05	1.38

For the HDPE liner materials, the influence of the sludge generated under baseline conditions had a weight loss of 0.14% which was higher than the CCT sludge treatments. The treatments using Na_2CO_3 and Na_2CO_3-Urea sludges resulted in volatile loses of about 0.1% and 0.08%, respectively, and the Ca injection material gained 0.01% weight after 120 days of treatment. This data demonstrate that the water absorption into the HDPE liner materials is very limited.

The VDPE liner material also tended not to absorb much water. The liner treated with Ca-injection, Na_2CO_3, and baseline materials lost about equal amounts of weight at about 0.06%. The liner treated with Na_2CO_3 had a volatile loss of about 0.16% which is significantly higher than the loses resulting from treatment with the other wastes used.

Extractables

A decrease in weight loss due to liner extractables is an indication that liner components are leached from the liner due to exposure to a waste. The weight loss associated with liner materials is presented in Table 2. The PVC liner material reacted similarly for all treatments with about a 30% weight loss due to extractables. The HDPE and VDPE liner materials reacted much differently as the extractable loses for the HDPE were about 0.5% for each treatment and the loses for the VDPE materials varied from about 1.06% for the Na_2CO_3-Urea material to about 1.38% for the Ca injection fly ash. These data suggest that PVC liner material might decompose relatively rapid in the waste environments evaluated.

CONCLUSIONS

The impact of CCT materials on the characteristics of the clay liner materials studied in this project was minimal. The HC measurements of the waste/clay liner systems were similar to the water/clay liner systems. HC decreased for clay liners compacted at moisture levels slightly higher than optimum (standard Procter) and increased for liners compacted at moisture levels lower than optimum (standard Procter). Although some swelling was evident in the sodium materials, the sludge materials did not have a negative impact on the integrity of the liners over 120-day tests. Wet/dry cycles tended to result in lower HC, while freeze/thaw cycles substantially increased HC for the liners tested.

Sustained increment changes in the measured physical properties of the materials over time were not observed. Some abrupt changes in strength were found at several times during the testing period. However, these aberrations seemed more indicative of isolated changes in the conditioning methods or test procedures and could be related to flaws or changes in the materials related to manufacturing conditions. After 120 days of conditioning, none of the measured physical properties varied significantly form those for the untreated liner materials. This was true for all samples regardless of the conditioning solution used. It is apparent from the results of this study, that the HDPE liner material would be expected to perform better than the VDPE and PVC liner materials due to its higher strength characteristics.

The volatiles and extractables tests for the HDPE and VDPE materials indicated that the waste materials had little influence on their overall structure. However, the extractables data suggest that PVC liner material might decompose in the waste environments evaluated. The PVC liner material reacted similarly for all treatments with about a 30% weight loss.

ACKNOWLEDGMENTS

This paper was prepared with the support of the U.S. Department of Energy, Morgantown Energy Technology Center, Cooperative Agreement No. DE-FC21-93MC30127 and the Public Service Company of Colorado. However, any opinions, findings, conclusions, or recommendations expressed herein are those of the author(s) and do not necessarily reflect the views of the DOE or the Public Service Company of Colorado.

REFERENCES

American Society for Testing and Materials. 1991. D638-91, Standard Test Method for Tensile Properties of Plastics. Annual Book of ASTM Standards.

American Society for Testing and Materials. 1991. D698-91, Standard Test Method for Laboratory Compaction Characteristics of Soil Using Standard Effort. Annual Book of ASTM Standards.

American Society for Testing and Materials. 1991. D882-91 (Method A), Standard Test Method for Tensile Properties of Thin Plastic Sheeting. Annual Book of ASTM Standards.

American Society for Testing and Materials. 1990. D1004-90, Standard Test Method for Initial Tear Resistance of Plastic Film and Sheeting. Annual Book of ASTM Standards.

American Society for Testing and Materials. 1988. D4833-88, Standard Test Method for Index Puncture Resistance of Geotextiles, Geomembranes, and Related Products. Annual Book of ASTM Standards.

American Society for Testing and Materials. 1990. D5084-90, Standard Test Method for Measurement of Hydraulic Conductivity of Saturated Porous Materials Using a Flexible Wall Permeameter. Annual Book of ASTM Standards.

Bohn, H.L., B.L. McNeal, and G.A. O'Connor. 1985. Soil Chemistry. John Wiley and Sons, New York, New York.

Brown, K.W., and D. Anderson. 1980. Effect of Organic Chemicals on Clay Liner Permeability: A Review of the Literature. In Proceedings of the Sixth Annual Research Symposium, Chicago, Illinois. March 17-20, 1980.

Daniel, D.E., H.M. Liljestrand, G.P. Broderick, and J.J. Bowders, Jr.. 1988. Interaction of Earthen Liner Materials with Industrial Waste Leachate. Haz. Waste & Haz. Mat. 5(2):93-108.

Green, W.J., G.F. Lee, R.A. Jones, and T. Palit. 1983. Interaction of Clay Soils with Water and Organic Solvents: Implications for the Disposal of Hazardous Wastes. Environ. Sci., Tech. 17:278-282.

Hettiaratchi, J.P., S.E. Hrudey, D.W. Smith, and D.C. Sego. 1988. Shrinkage Behavior of Clay Liner Material Exposed to Simulated Municipal Solid Waste Landfill Leachate. Can. J. Civ. Eng. 15:500-508.

Koegler, S.S., J.R. Divine and B.E. Opitz. 1991. Compatibility of Admix and Synthetic Liner Materials with Clean Coal Technology By-Products. Final Report: Report No. EPRI GS-7226, Electric Power Research Institute.

Peterson, S.R., and K.M. Krupka. 1981. Contact of Clay-Liner Materials with Acidic Tailings: II. Chemical Modeling. In Proceedings of the Fourth Symposium of Uranium Mill Tailings Management Seminar, Fort Collins, Colorado. October 26-27, 1981.

U.S. Environmental Protection Agency. 1986. EPA-SW846, Method 9090.

U.S. Environmental Protection Agency. EPA-SW870.

PB.19 Utilization of Lightweight Materials Made from Coal Gasification Slags

Vas Choudhry (70402.3 150@compuserve.tom; 408-945-4282)
Steve Hadley (70402.3 150@?,compuserve.tom; 408-945-4282)

Praxis Engineers, Inc.
852 North Hillview Drive
Milpitas, CA 95035

Abstract

The integrated gasification combined-cycle (IGCC) coal conversion process has been demonstrated to be a clean, efficient, and environmentally acceptable method of generating power; however, it generates solid waste materials in relatively large quantities. For example, a 400-MW power plant using 4000 tons of 10% ash coal per day may generate over 440 tons/day of solid waste or slag, consisting of vitrified mineral matter and unburned carbon. The disposal of these wastes represents significant costs, Regulatory trends with respect to solid waste disposal, landfill development costs, and public concern make utilization of solid wastes a high-priority issue. As coal gasification technologies find increasing commercial applications for power generation or production of chemical feed stocks, it becomes imperative that slag utilization methods be developed, tested, and commercialized in order to offset disposal costs.

Praxis is working on a DOE/METC funded project to demonstrate the technical and economic feasibility of making lightweight and ultra-lightweight aggregates from slags left as solid by-products from the coal gasification process. These aggregates are produced by controlled heating of the slags to temperatures ranging between 1600 and 1900°F. Over 10 tons of expanded slag lightweight aggregates (SLA) were produced using a direct-fired rotary kiln and a fluidized bed calciner with unit weights varying between 20 and 50 lb/ft^3. The slag-based aggregates are being evaluated at the laboratory scale as substitutes for conventional lightweight aggregates in making lightweight structural concrete, roof tiles, blocks, insulating concrete, and a number of other applications. Based on the laboratory data, large-scale testing will be performed and the durability of the finished products evaluated. Conventional lightweight aggregates are made from pyroprocessing of expansible shale or clay and sell at $30-40/ton. The net production costs of SLA are in the range of $22 to $24/ton. Thus, the technology provides a good opportunity for economic use of gasification slags.

Research sponsored by the U.S. Department of Energy's Morgantown Energy Technology Center, under contract DE-FC21-94MC30056 with Praxis Engineers, Inc, 852 North Hillview Drive, Milpitas, CA 95035.

Utilization of Lightweight Materials Made from Coal Gasification Slags

Praxis Engineers, Inc.
Milpitas, California 95035

Funding Sources: METC, EPRI, and ICCI

Project Objectives

- Develop and demonstrate the technology for producing slag-based lightweight aggregates (SLA)
- Produce 10 tons of SLA Products with different unit weights from two slags
- Collect operational and emissions data from pilot-scale operations
- Laboratory- and commercial-scale evaluation of SLA with conventional lightweight and ultra-lightweight aggregates (LWA and ULWA)

Project Objectives (contd)

Characterize SLA products for leachability and conduct applications testing

Evaluate recovered char for recycle to the gasifier, and for use as a fuel during slag expansion or in the boiler

Conduct preliminary economics of SLA production

Slag, LWA, ULWA, & SLA: Definitions

- Slag is a solid residue by-product of coal gasification combined-cycle process

- Gasification slag is vitrified ash containing some unconverted carbon

- Conventional LWA:
  - Produced by pyroprocessing clays and shales at 2 100”F
  - Unit weight is 50 lb/ft^3
  - Used to make lightweight structural concrete, blocks, and roof tiles
    Market price is $20-30/ton

Definitions (contd)

- Conventional ULWA:
  - Produced by pyroprocessing perlite ores at 2000ºF
  - Unit weight is 4-12 lb/ft^3
  - Used for horticultural and insulation applications
  - Market price is over $200/ton

- Slag can be expanded under controlled conditions to produce lightweight materials, termed slag-based LWA or SLA:
  - Produced by pyroprocessing at 1600-1800”F
  - Unit weight is 12-50 lb/ft3
  - Blendable with existing raw materials
  - Can be substituted for all or part of the ingredients of some LWA and ULWA applications

MUFFLE BURN TESTS - EXTRUDED MIXTURES

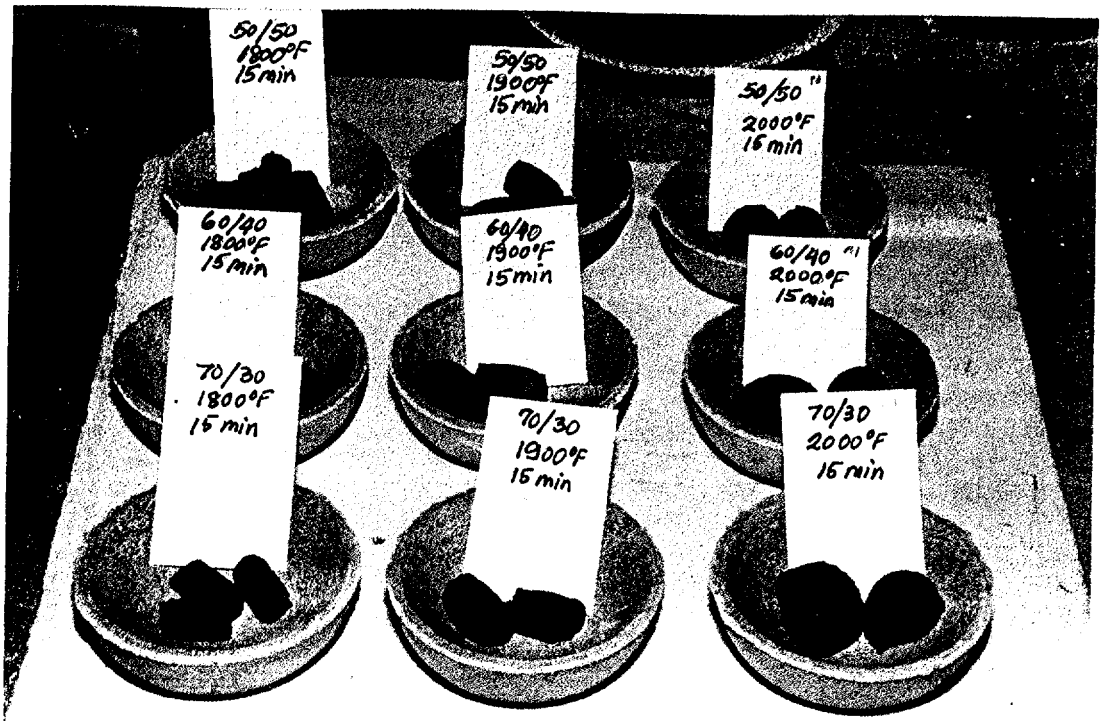

BURN TESTS ALL THREE BLENDS

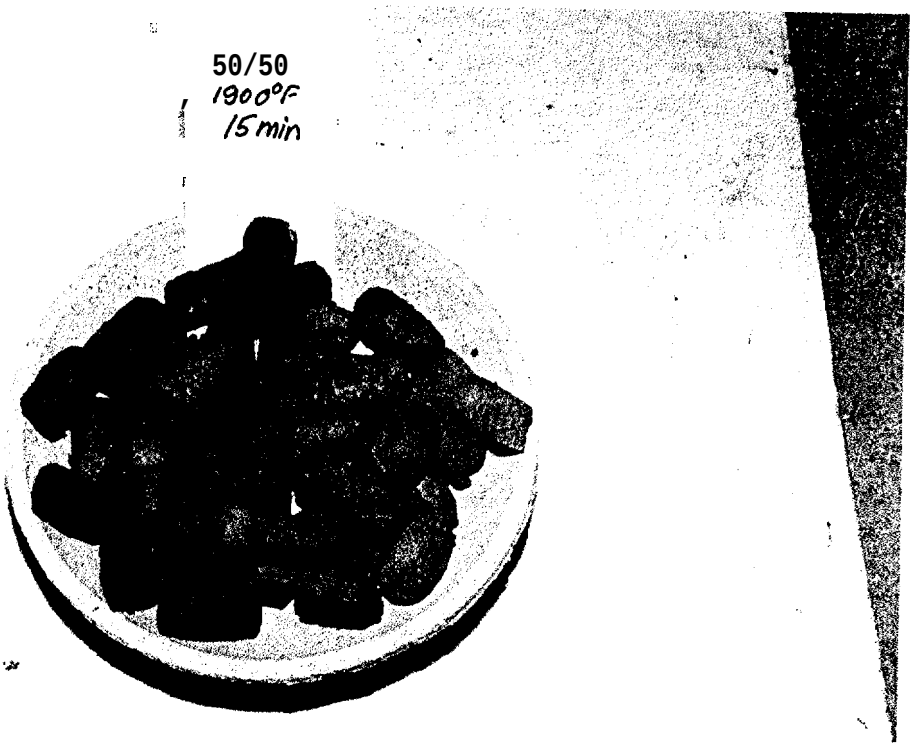

50/50 MIX-COMPLETE CUP BURN - 1900°F

6" Diameter Bench-Scale Fluid Bed Reactor

Specifications

Bed Height:	3 ft
Feed Height (Above Grid):	2 ft
Inside Diameter:	0.5 ft
Temperature:	+1420°C
Fuel:	Gas/Oil

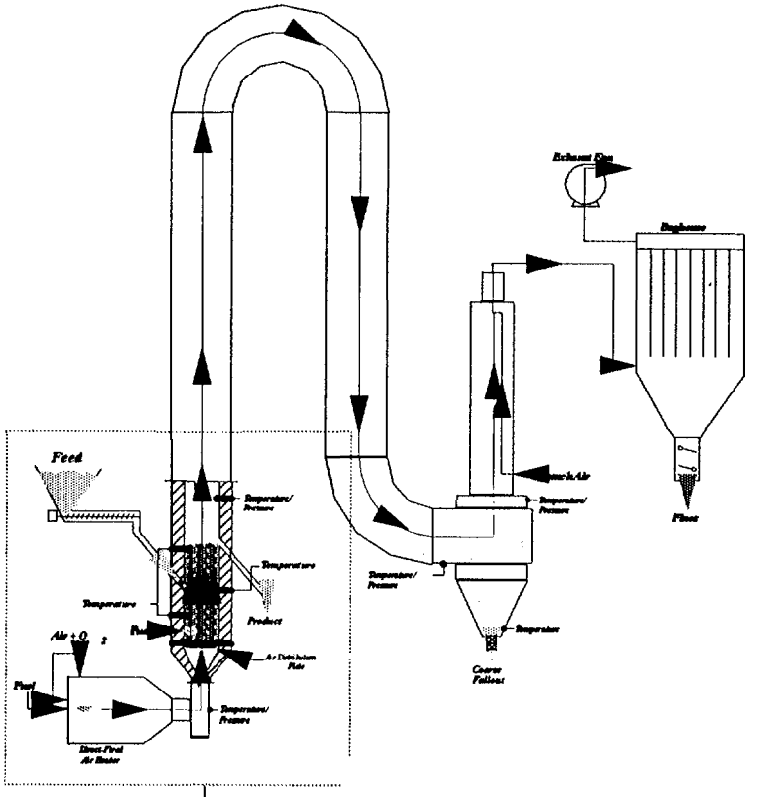

Reactor Section Detail

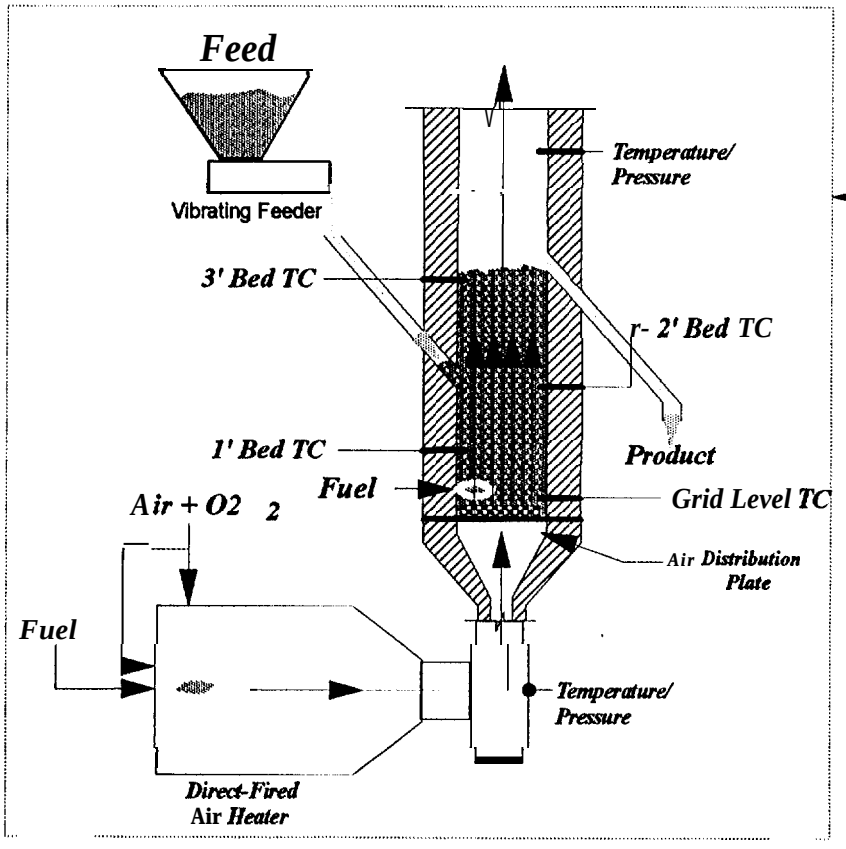

Material Flow

Gas Flow

3'x30' Rotary Kiln Schematic

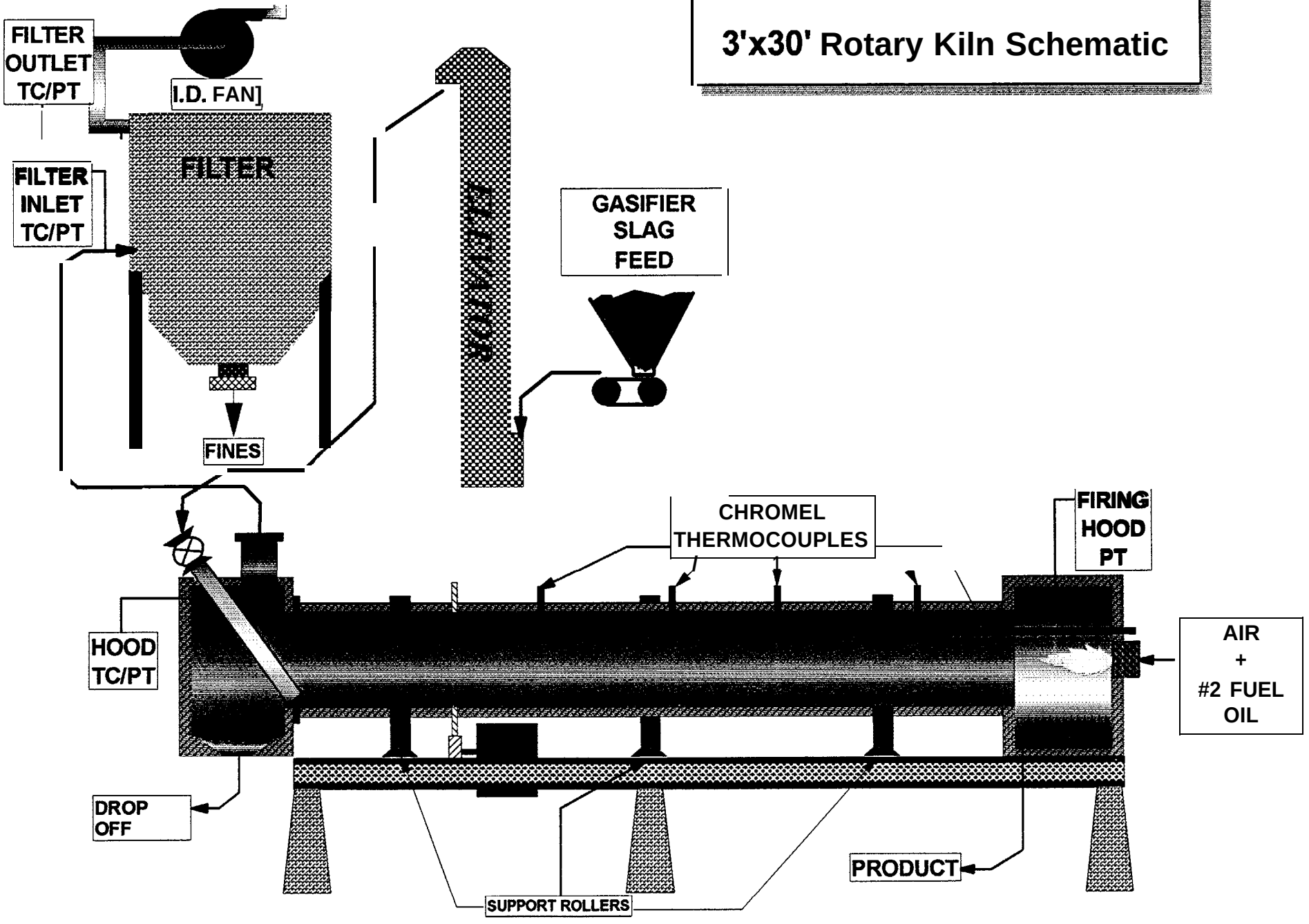

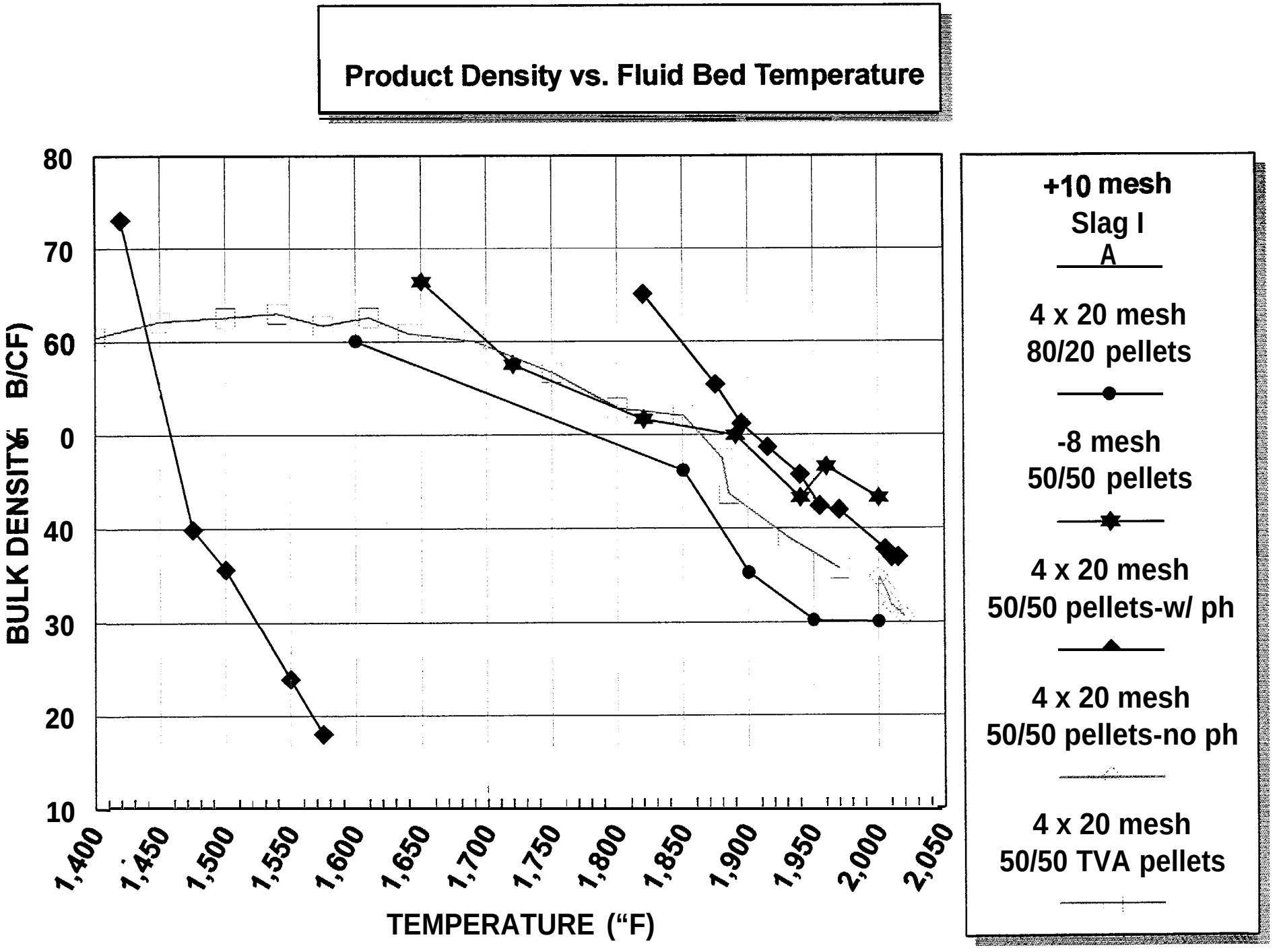
Product Density vs. Fluid Bed Temperature
BULK DENSITY (LB/CF)
80
70
60
50
40
30
20
10
1,400
1,450
1,500
1,550
1,600
1,650
1,700
1,750
1,800
1,850
1,900
1,950
2,000
2,050
TEMPERATURE ("F)
+10 mesh
Slag I
A
4 x 20 mesh
80/20 pellets
-8 mesh
50/50 pellets
4 x 20 mesh
50/50 pellets-w/ ph
4 x 20 mesh
50/50 pellets-no ph
4 x 20 mesh
50/50 TVA pellets

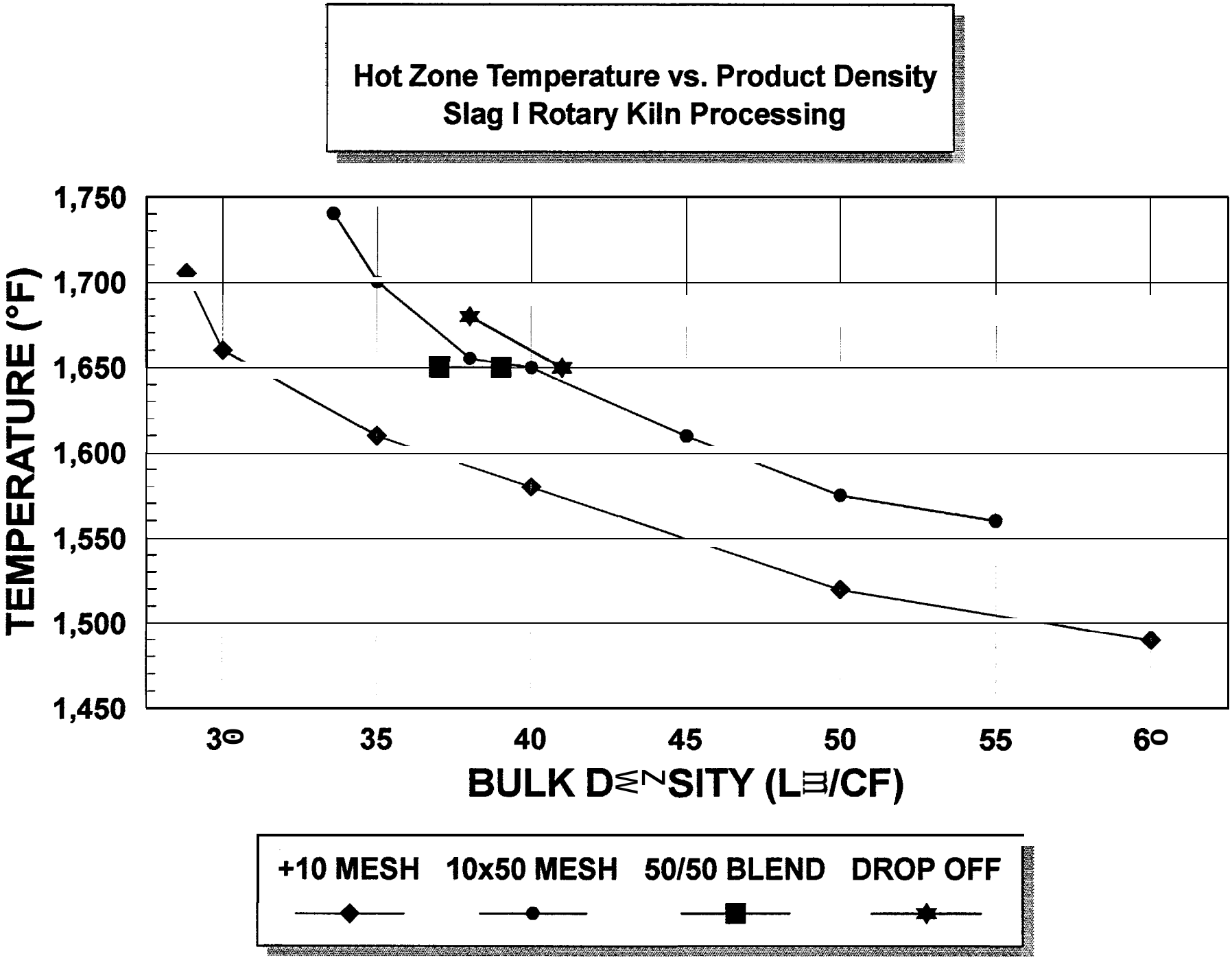
Hot Zone Temperature vs. Product Density
Slag I Rotary Kiln Processing
TEMPERATURE (°F)
1,750
1,700
1,650
1,600
1,550
1,500
1,450
30
35
40
45
50
55
60
BULK DENSITY (LB/CF)
+10 MESH
10x50 MESH
50/50 BLEND
DROP OFF

Stack Gas Analysis from Rotary Kiln Testing
14 November 1995

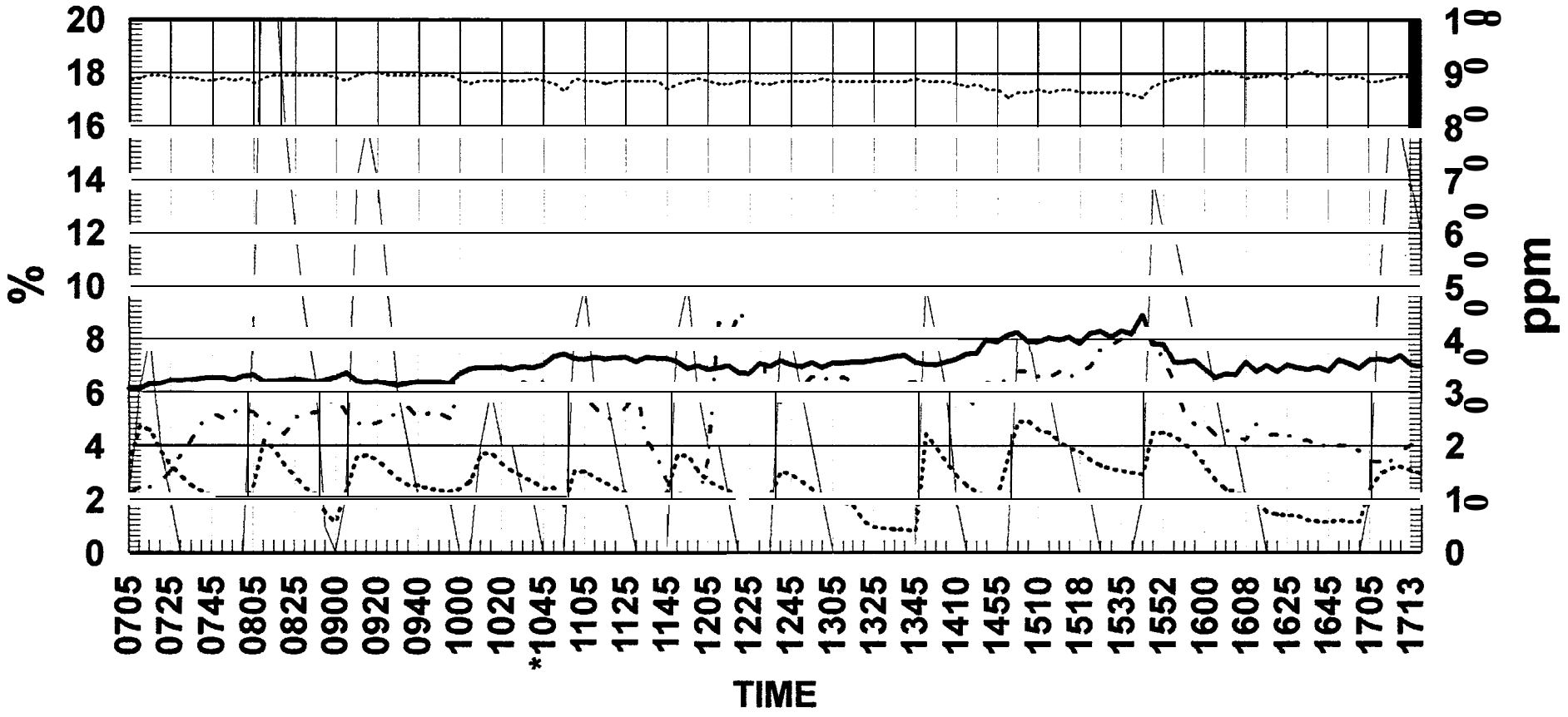

NOx ppm	SO2 ppm	O2 %	CO ppm	CO2 %

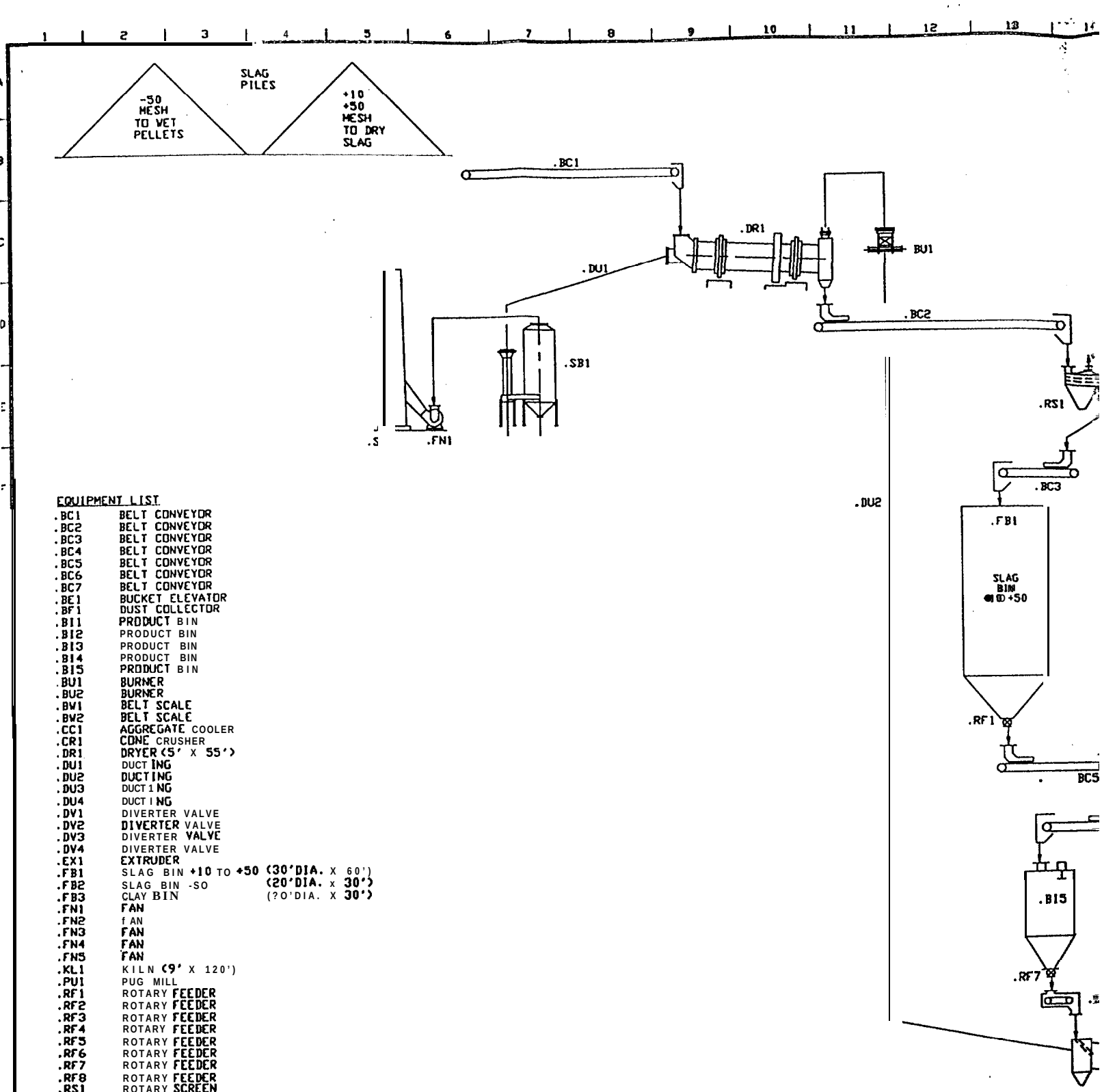

EQUIPMENT LIST

.BC1	BELT CONVEYOR
.BC2	BELT CONVEYOR
.BC3	BELT CONVEYOR
.BC4	BELT CONVEYOR
.BC5	BELT CONVEYOR
.BC6	BELT CONVEYOR
.BC7	BELT CONVEYOR
.BE1	BUCKET ELEVATOR
.BF1	DUST COLLECTOR
.BI1	PRODUCT BIN
.BI2	PRODUCT BIN
.BI3	PRODUCT BIN
.BI4	PRODUCT BIN
.BI5	PRODUCT BIN
.BU1	BURNER
.BU2	BURNER
.BW1	BELT SCALE
.BW2	BELT SCALE
.CC1	AGGREGATE COOLER
.CR1	CONE CRUSHER
.DR1	DRYER (5' X 55')
.DU1	DUCTING
.DU2	DUCTING
.DU3	DUCTING
.DU4	DUCTING
.DV1	DIVERTER VALVE
.DV2	DIVERTER VALVE
.DV3	DIVERTER VALVE
.DV4	DIVERTER VALVE
.EX1	EXTRUDER
.FB1	SLAG BIN +10 TO +50 (30'DIA. X 60')
.FB2	SLAG BIN -SO (20'DIA. x 30')
.FB3	CLAY BIN (?O'DIA. X 30')
.FN1	FAN
.FN2	fAN
.FN3	FAN
.FN4	FAN
.FN5	FAN
.KL1	KILN (9' X 120')
.PU1	PUG MILL
.RF1	ROTARY FEEDER
.RF2	ROTARY FEEDER
.RF3	ROTARY FEEDER
.RF4	ROTARY FEEDER
.RF5	ROTARY FEEDER
.RF6	ROTARY FEEDER
.RF7	ROTARY FEEDER
.RF8	ROTARY FEEDER
.RS1	ROTARY SCREEN
.SB1	SCRUBBER
.SC1	SCREW CONVEYOR
.SF1	CLAY FEEDER
.SK1	STACK
.SK2	STACK

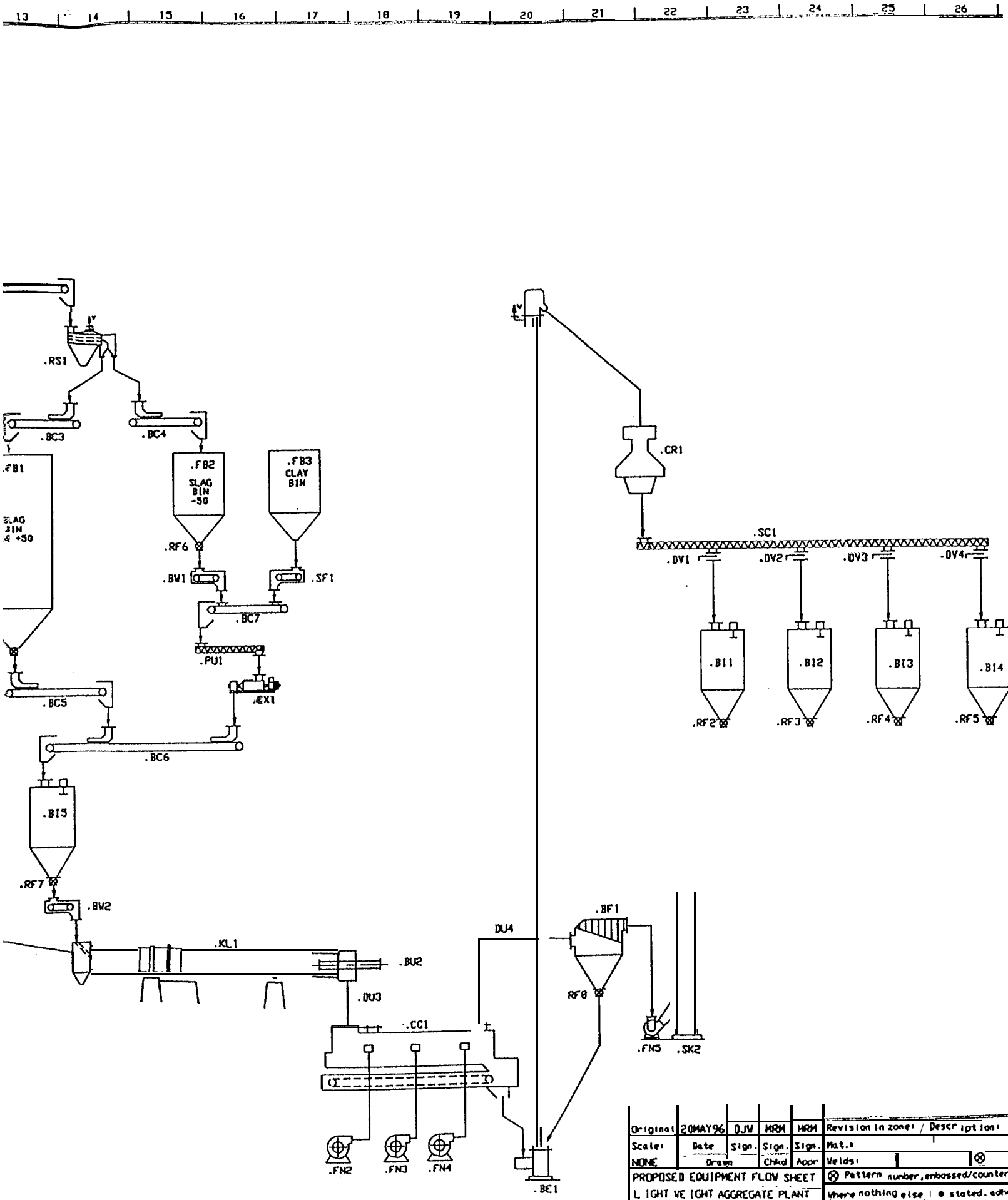
13 14 15 16 17 18 19 20 21 22 23 24 25 26
.RS1
.BC3
.BC4
.FB1
SLAG BIN +50
.FB2
SLAG BIN -50
.FB3
CLAY BIN
.RF6
.BW1
.SF1
.BC7
.PU1
.EX1
.BC5
.BC6
.BI5
.RF7
.BV2
.KL1
.BU2
.DU3
.CC1
.FN2
.FN3
.FN4
.BE1
DU4
.BF1
RF8
.FN5
.SK2
.CR1
.SC1
.DV1
.DV2
.DV3
.DV4
.BI1
.BI2
.BI3
.BI4
.RF2
.RF3
.RF4
.RF5
Original 20MAY96 DJV MRM MRM
Scale: NONE
Date Sign. Sign. Sign.
Drawn Chkd Appr
Revision in zone: / Description:
Mat.:
Welds:
Pattern number, embossed/counter
Where nothing else is stated, adhe to general instructions No. 52053
PROPOSED EQUIPMENT FLOW SHEET
LIGHTWEIGHT AGGREGATE PLANT
235 TPD WET PELETS
200 TPD DRY SLAG
PC: 143
FULLER
PROPOSAL
Drawing Number
1.725762

SLA Products Made at Pilot Scale

Slag/Size/ Mix Type	Direct-Fired Kiln lb/ft^3	Fluidized Bed Expander lb/ft^3
Slag I: +1OM	28-67	24-73
Char injection	--	16-26
Slag I: 10x 50M	34-58	--
Slag I: +50M	38	16-58
Extruded Slag I/Clay		
80/20	27-62	--
50/50	21-42	--
0/100	18-41	--
Slag I/Clay Granules		
80/20 4 x 20M	.-	30-60
80/20 4 x 30M	--	37-42
50/50 4 x 20M	--	31-65
50/50 -8M	--	43-66
Slag II: +1OM	**22-82**	--
Slag 11/Clay Granules		
50/50 4 x 20M	--	33-63

Production Costs of SLA vs. LWA and ULWA ($/Ton)

Cost Item	Shale/Clay LWA[1]	Perlite ULWA[2]	SLA[3]
System	Rotary Kiln	Vert.Shaft Furnace	Rotary Kiln
Fuel	011	Natl gas	Coal/char
Mining/prep	6.00	40.00	-
Transport	0.50	40.00	
Clay binder			1.45
Labor	6.23	12.00	6.25
Fuel	5.09	8.00	1.64
Power	1.37	4.50	1.35
M&S	1.85	3.00	1.48
Other	1.11	2.00	1.10
Overhead	2.24	10.00	-
Depreciate	5.71	4.75	4.28
Interest	excluded	excluded	6.85
Total	30.10	124.25	24.40

Estimated by(1) Fuller Co., (2) Silbrico, (3) Praxis/Fuller

Conclusions: Slag Processing

- Slag I was expanded to unit weights of 30-50 lb/ft^3 and Slag II to 20-50 lb/ft^3 by means of temperature control. Attempts to lower these further resulted in fusion which is a function of slag chemistry.

- The entire 1/4" x 50M fraction can be processed in the kiln as a single feed.

- Minus 50M fines must be extruded prior to kiln processing. Extruded pellets using 20-50% expansive clay binder yielded product unit weights of 27-33 lb/ft^3 at 1800 -1900ºF.

Conclusions: Char Utilization

- Char can be recovered from slag easily and used as a fuel

- A char product containing 45-54% ash was upgraded successfully to 70!% carbon

- Char can be utilized as a substitute for 50% of the fuel in a rotary kiln and 80°/0 of the fuel in a fluidized bed system

Conclusions: SLA Economics

- Expansion temperature for slag is 300-400 “F lower than that typically required for expansible clays and shales and represents significant energy savings

- SLA production costs from a large (440 t/d) facility were estimated at $24.40/ton using rotary kiln and $21.87/ton using fluidized bed vs. $30. 10/ton for conventional LWA plant

- Preliminary analyses also indicate that small SLA plants can be economically attractive if the avoided costs of slag disposal ($10-$20/ton) are factored in.

Planned Product Evaluation (Phase II)

Commercial-scale testing of SLA as a substitute for LWA and ULWA in the following applications:

- Structural concrete using 3/4″ coarse and 3/8″ LWA
- Lightweight blocks (2-3 blends)
- Insulating concrete (ASTM C 332 Group II concrete, 45-90 lb/ft^3)
- Lightweight roof tile aggregate
- Loose fill insulation (ASTM C 549)
- Horticultural applications

Continuous Mercury and Chloride Monitors for Coal Gasifiers

G. Norton (norton@ameslab.gov; 515-294-1035)
D. Eckels (eckels@ameslab.gov; 515-294-7943)
C. Chriswell (chriswell@ameslab.gov; 515-294-6776)
Ames Laboratory
Iowa State University
Ames, Iowa 50011

Introduction

The capability to continuously monitor and effectively control critical effluents must be developed in order to implement new clean coal technologies. Although mercury (Hg) and hydrogen chloride (HCl) concentrations in hot, high-pressure gases from power producing systems are of environmental and technological concern, instruments suitable for determining Hg and HCl in those environments have not yet been sufficiently developed and tested. On-line analysis is more complex for such systems than for more conventional coal-based power producing systems because of the high temperatures (up to 500°C) and pressures (up to 300 psi) involved. In addition, the different gas compositions in emerging coal-based power producing systems relative to those present in conventional combustors can pose special analytical problems. Concentrations of Hg are anticipated to be in the range of 2 - 200 ppb_w in the raw gas. Concentrations of HCl are anticipated to be in the range of 50 - 500 ppm in the raw gas and less than 1 ppm after the flue gas is treated (1-3).

Objectives

Ames Laboratory will develop an integrated sampling and analysis system suitable for on-line monitoring of Hg and HCl in advanced coal-based gasifiers. The objectives of this project are to 1) summarize current technology for monitoring Hg and HCl in gaseous effluents, 2) identify analytical techniques for such determinations in high-temperature, high-pressure gases from coal-based systems for producing electrical power, 3) evaluate promising analytical approaches, and 4) produce reliable on-line monitors which are adaptable to plant-scale diagnostics and process control.

Project Description

Commercially available instruments which were potentially suitable for monitoring Hg and HCl in coal gasifiers were screened and the most promising techniques were selected for laboratory evaluation. For Hg, the techniques selected for further consideration were atomic absorption (AA) and atomic fluorescence (AF). For HCl, gas-filter-correlation infrared spectroscopy (GFCIR), a dry colorimetric procedure, and ion mobility spectroscopy (IMS) were selected for testing in the laboratory. The analytical systems selected for use in on-line Hg and HCl

analyzers will be adapted for application to monitoring hot pressurized gases from coal gasifiers. Additional work will involve developing suitable gas conditioning and sample introduction systems. That work may be as important as the development of the analytical detectors themselves. After the laboratory studies have been completed, prototype instruments will be tested and evaluated in the field.

Results

Mercury Studies. In previous work (4), we performed a laboratory evaluation of two Hg detectors (one each based on AA and AF). After carefully considering the pros and cons of each approach, AA was selected as the method of choice for monitoring Hg in coal gasifier streams. The decision was based largely on the fact that sample gases could not be passed directly into the AF detection cell because of severe quenching of the fluorescence signal by gases present in coal gasification streams. The quenching effects would result in inadequate detection limits for the anticipated Hg levels if the sample gases were passed directly into the detection cell.

In recent work, recoveries of Hg injected into simulated gasifier streams were studied. Injections of Hg were initially made into stainless steel lines containing the simulated gasifier streams as the gases were slowly heated to 200°C. When the gas stream contained a mixture of CO, CO_2, CH_4, COS, H_2, and H_2S, no Hg was recovered in the temperature range studied. In follow-up tests, Hg injections were made into Teflon sample lines containing various gas mixtures. Full recoveries were obtained when the carrier gas contained mixtures of only H_2, CO, CO_2, and CH_4, while recoveries decreased to about 75% when the carrier gas also contained either 1% (v/v) H_2S or 0.5% COS. Because the majority of the Hg was recovered using the simulated gasifier streams in Teflon lines, even in the presence of sulfur-containing gases, chemical interactions between Hg and the other gases present are not believed to be the primary cause of poor Hg recoveries observed using the same gas mixtures in stainless steel sample lines. Rather, the low recoveries in steel appear to be from wall losses. Although these problems may be alleviated by the use of continuous Hg streams (as opposed to injections), which allow for conditioning of the walls of the sample lines, the results from the Hg injections are being used to identify potential areas of concern regarding sampling of Hg in coal gasifiers.

Potential spectral interferences were studied with our AA detector (Thermo Separation Products, Model 3200) for confirmation of published absorbance values, as a check on equipment calibration, and to provide useful information related to the deuterium ($D_{2)}$ lamp background correction approach that is being investigated. Tests were performed by using injections of various gas species and by using continuous streams of the gases of interest directly into the AA detector. For the injections, 100 μL of a given gas were injected into an air or nitrogen stream flowing at a rate of 170 cc/min into the detector. For the continuous flows of potentially interfering gases, diluted streams of each gas were examined. By blending 10 cc/min of a given gas with the carrier gas stream flowing at 1000 cc/min, a 1% concentration for each gas of interest was obtained. Gases tested include CH_4, CO_2, CO, COS, H_2S, SO_2, O_2, and H_2. The SO_2 and O_2 were included since some of the gas conditioning approaches being considered involve oxidation of the gas stream.

For the injections, comparable results were obtained for both air and nitrogen carrier gases. Relative absorbance values based on the injections of individual gases were in agreement with those obtained using the continuous flows of potentially interfering gases. For the tests using continuous flows of the gases of interest, experimental absorbance readings were in good agreement with published values. Not surprisingly, results from the injections and continuous gas streams indicated that the strongest interferences were for the sulfur-containing gases. The absorbance produced by COS was comparable to that produced by H_2S, although H_2S is of much greater concern because it will be present in gasifier streams at much higher concentrations than COS. By using published absorbtivity values and our own experimental data, we determined that about 500 ppm_v H_2S will produce a signal equivalent in magnitude to the signal from a 1 ppb_w Hg stream. Based on the anticipated H_2S levels in coal gasification effluents, the interference from H_2S could produce an absorption value equivalent to that observed for a 10 ppb_w Hg stream. This interference is severe enough that either background corrections must be made or else the H_2S must be eliminated before the sample gas enters the detection cell. Although the H_2S could be oxidized, this would produce SO_2, which interferes 30 times more strongly than H_2S.

In addition to the interferences from COS, H_2S and SO_2, a substantial absorbance was noted when CO was introduced to the AA cell. This is of concern since gasifier streams contain large concentrations of CO. From our review of published work thus far, it is somewhat surprising that CO would be an interfering gas. Also, injections of "pure" CO obtained from two different manufacturers gave absorbance values that differed by more than a factor of two. Therefore, additional work will be performed to determine whether the interference is actually from CO or whether it is from some impurity in the CO gas stream.

The possibility of using a commercially available AA instrument with a D_2 lamp background correction was investigated. Based on data provided by several major manufacturers of those instruments, blank readings had too much base line variability for determining Hg in gasifier streams at the anticipated Hg concentrations. However, due to the high stability of our AA detector, we explored the possibility of adding a D_2 lamp to our AA detection system. As a step in investigating the potential for using a D_2 lamp background correction approach, the AA base line variation was observed by directing the detector towards an external D_2 lamp while the AA cell in our instrument was removed. The magnitude of base line noise using the D_2 lamp was typically about 10 times greater than when using the Hg lamp built into the unit. By using the base line variabilities observed with our Hg lamp and with a D_2 lamp in our laboratories, relative errors of about 10% and 80% at Hg concentrations of 10 and 1 ppb_w, respectively, are anticipated. The magnitude of these errors resulting from the use of a D_2 lamp is acceptable at the levels of Hg involved. It should also be emphasized that these measured base line variabilities pertain to a specific D_2 lamp, and it may be possible to purchase a D_2 lamp that is even more stable than the one we currently have. Dual photodiodes were also purchased and subsequently tested to determine whether they would be suitable for use in conjunction with a D_2 lamp for background correction of the Hg signal. Experimental results indicate that the use of the photodiodes should not add significant analytical uncertainties in the determination of Hg at the ppb level.

In addition to using a D_2 lamp for a background correction, we also considered the possibility of using a D_2 lamp for both the background correction and source lamp for the Hg determination. However, after performing a variety of tests, it appears that the resolution necessary for the determination would be too large for the sensitivity required.

One manufacturer of AA systems performed some tests to observe the base line stability obtained using an electrodeless discharge lamp (EDL) in their attempt to reduce base line noise levels from that observed using a Hg hollow cathode lamp. Although the base line using an EDL was less noisy than that obtained with a Hg hollow cathode lamp, there was still too much base line variability for our monitoring application. Our AA detector has about an order of magnitude less base line variability than the commercially available AA unit using an EDL.

Hydrogen Chloride Studies. In previous work (4), a Thermo Environmental Instruments Model 15 Gas Filter Correlation IR (GFCIR) HCl analyzer was evaluated in our laboratories. When using compressed gases for the HCl standard, instrument readings were very stable, baseline fluctuations were minimal, and the calibration curve was linear in the range of about 25 to 3000 ppm_v HCl. Erratic responses were noted at lower concentrations, which could be from uncertainties in blending the calibration gases. When HCl permeation tubes were used to provide gas stream concentrations of HCl from 0.2 to 2 ppm_v, the instrument response showed good linearity from about 0.5 to 2 ppm_v. Long equilibration times and pronounced memory effects were noted when passing low concentrations of HCl through the sample lines and flow meters. Other tests indicated that 300-400 ppm CH_4 (a known interference) gives a response equivalent to 1 ppm HCl. Depending on the relative concentrations of CH_4 and HCl in the gasifier effluents, 75% to nearly 100% of the CH_4 will need to be removed prior to HCl determinations. Results of recent work are discussed below.

Colorimetric Method. Testing and evaluation of an MDA Scientific Model 7100 Continuous Gas Analyzer was performed. That instrument is based on exposing a strip of color-indicating paper to a metered sample stream. Any HCl present in the sample gas reacts with the paper to form a colored, circular (i.e., "dot") stain. The intensity of the stain is proportional to the HCl concentration and is quantified by using a photocell to detect the amount of reflected light from the portion of the paper exposed to the sample gas. The color-indicating paper is in the form of a continuous strip and is mounted in a cassette cartridge, which is referred to as a chemcassette. This allows the monitor to provide "continuous" analysis of a gas stream. The standard chemcassette determines HCl in the range of about 0.2 - 50 ppm_v. In addition, a low-level chemcassette is available for determining HCl down to about 50 ppb_v. The low-level chemcassette employs different reaction chemistry than the standard chemcassette and requires different instrument software. Our tests were performed using both the standard and low-level tapes.

The manufacturer recommends humidifying the sample stream to 25-75% relative humidity (RH) at ambient temperature. Significant errors can result if the RH is outside of this range. If dry gases are to be used, a special low-RH calibration should be performed. The instrument

manufacturer reports that HCN and HF are possible interferences, but little information was available on the magnitude of those interferences. Both of those gases are expected to be present in coal gasifier streams. We investigated the HF interference by using anhydrous HF from a permeation tube with room air as the carrier gas. The HCN interference was studied by using a compressed gas cylinder containing 1% HCN in a nitrogen balance. Compressed gas cylinders containing HCl in a nitrogen balance were used for the tests with the standard chemcassette, while permeation tubes containing aqueous HCl were used for the tests with the low-level chemcassette. Results obtained with the standard and low-level HCl chemcassettes are discussed separately below. Relative standard deviations (RSDs) for all tests were typically $\pm$ 5% or less.

Standard Chemcassettes. A calibration curve was obtained by blending 100 ppm HCl (in a nitrogen balance) with air and passing the blended gases into the analyzer. These results are shown in Figure 1. The measured detection limit was on the order of several tenths of a ppm and the calibration curve was generally linear down to several ppm. At lower concentrations, the nonlinearity may be a result of instrument inaccuracies or dilution errors in the gas stream. When 25 ppm HCl in nitrogen was sent to the detector, results were about 50% higher when the gas stream was humidified. Although it was known that results could be affected by the relative humidity of the gas, these results demonstrate that the errors incurred can be substantial.

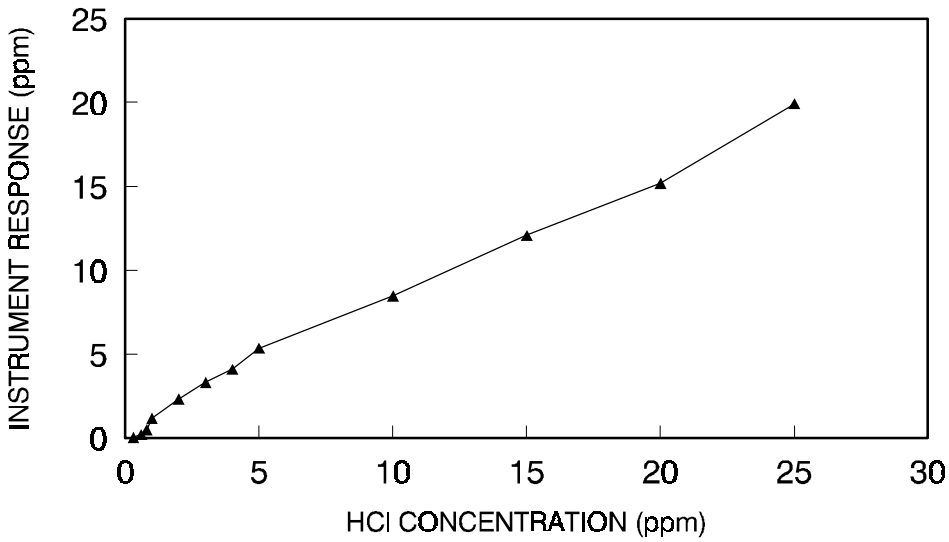

Figure 1. Calibration Curve Obtained with the Colorimetric Analyzer Using Blended Gases.

When 15 ppm dry HF in air was sent to the HCl analyzer in the absence of HCl, a reading corresponding to about 0.5 ppm HCl was obtained. When those gases were humidified by passing the diluent air over a pool of water prior to blending with the HF stream, the reading on the HCl analyzer dropped to zero. The signal quickly returned to 0.5 ppm once the source of added humidity was removed. The elevated humidity appeared to suppress the signal due to HF

and is probably related to the chemcassette tape chemistry. For tests with HF in the presence of HCl, 15 ppm HF (the anticipated maximum concentration in gasifier effluents) in a 1 ppm HCl stream had a negligible effect on the reported HCl concentration, regardless of whether the gas stream entering the analyzer was humidified.

When 100 to 2000 ppm HCN was sent to the analyzer in the absence of HCl, a small positive response on the analyzer was noted. The ratio of the HCN concentration to the instrument response was generally constant, with 1000 ppm HCN giving a reading corresponding to about 1 ppm HCl. As was the case with HF, the signal went to zero when humidity was added by humidifying the diluent air prior to blending it with the HCN stream. In gas streams containing 10 ppm HCl, the HCl signal was not significantly affected by the presence of 150 ppm HCN.

Low-Level Chemcassettes. With the low-level chemcassette, the measured detection limit was on the order of 50 ppb HCl. As the HCl concentration was decreased from 400 to 75 ppb, good linearity in the calibration curve was obtained. However, as the HCl concentration decreased further, some anomalous readings indicative of desorption wall effects were observed. The permeation tube was removed from the chamber, but significant HCl concentrations were still reported by the analyzer for more than two days when air passing through the chamber was sent to the calibrator. When the calibrator was set to send zero air to the analyzer, the HCl analyzer consistently reported "0 ppb". Since the gases from the calibrator passed through common sample lines in each case, and since the gas flow rate through the sample line was the same for each set of tests, the memory effects are likely to be within the calibrator itself rather than in the analyzer or sample transport lines. After ensuring that no HCl was being emitted from the calibrator, a calibration curve was obtained by increasing the HCl concentration (HCl concentration was decreased in the initial tests). Because of pronounced adsorption/desorption effects, the slopes and intercepts of the two calibration curves (one each from increasing and decreasing the HCl concentration) were much different. This has important implications regarding field monitoring and calibration of analytical instruments, since wall effects can result in lengthy equilibration times (e.g., 24 hours or more).

Humidification of the nitrogen stream containing HCl had a more pronounced effect on the HCl reading when using the low-level chemcassette as opposed to the standard chemcassette. However, this is not necessarily due to differences in tape chemistry between the standard and low-level chemcassettes. The humidity may have provided a "flushing" effect which removed adsorbed HCl in the sample lines. Such a flushing effect could be much more prominent (greater percent change in concentration reading) at the relatively low HCl concentrations used with the low-level chemcassettes.

HF was a major interference when using the low-level chemcassette. When the gas stream entering the analyzer contained 1000 ppb of HF only (i.e., no HCl), an HCl reading of 130 ppb was obtained. In contrast to the standard chemcassette where humidifying the gas stream eliminated the signal observed when using HF only, the opposite effect was observed with the low-level tape. For example, when the gases were humidified, the reading increased from 130 ppb to nearly 200 ppb. These results demonstrate the potential magnitude of the HF interference and also indicate that HF from the permeation tube was getting to the analyzer after

humidifying the gas stream. Thus, 15 ppm HF (the anticipated maximum concentration in gasifier streams) could cause a signal equivalent to that produced from several ppm HCl. Therefore, the HF interference should be negligible if the HCl concentration is significantly greater than the HF concentration. If the HCl concentrations are 1 ppm or greater, if would be preferable to use the standard chemcassette since HF interferences with that chemcassette are less prominent.

When 2800 ppm HCN was introduced to the analyzer in the absence of HCl, a signal equivalent to only 100 ppb HCl was obtained, indicating that HCN is not a significant interference with the low-level chemcassette in low-humidity gases. When the tests were repeated in the presence of 150 ppb HCl, the HCN again had little effect on the HCl reading. Results on the effects of humidity and on the effects of HCN in humidified gases were inconclusive in view of data uncertainties. Those uncertainties may be related to severe adsorption/desorption effects, "flushing" of the walls in the presence of humidity, or chemical interactions occurring on the detection tape or sample transport lines.

Discussion. Unlike other monitors being considered, the colorimetric analyzer provides visual confirmation of results through the use of colored dots. This is useful at low HCl readings where, for other instruments, it can be difficult to distinguish between a small HCl reading from a baseline variation. Also, by simply replacing a chemcassette, the colorimetric monitor (with the appropriate internal calibrations and software) can be used to monitor other individual gas species of interest. Another potential advantage to the colorimetric monitor is the smaller amount of internal surface area, where adsorption/desorption phenomena can lead to memory effects.

Disadvantages of the colorimetric monitor include the sensitivity of the technique to relative humidity of the sample gases, the need for different chemcassettes employing different chemistry for different ranges of HCl concentrations, and possible complications regarding color formation in the complex gas matrices of a coal gasifier. If methane can be effectively removed from sample gases without affecting HCl concentrations, using the colorimetric monitor with the standard chemcassette does not appear to offer any significant advantages over the gas-filter-correlation infrared (GFCIR) unit we investigated previously. Although the low-level chemcassette can detect lower levels of HCl than GFCIR, our results suggest that data should be viewed with extreme caution when using that chemcassette in complex gas matrices. In view of these considerations, the dry colorimetric analyzer will not be employed for on-line analysis of coal gasifier streams.

Ion Mobility Spectroscopy. Ion mobility spectroscopy (IMS) was evaluated in our laboratories using an IMS unit manufactured by ETG. As with the colorimetric method, IMS has a narrow dynamic range (about 200). For our initial tests, a concentration range of 0.1 to 20 ppm_v was used. Gases with higher concentrations of HCl can still be analyzed by diluting the gas stream. Compressed gases were used to examine instrument response and the linearity of calibration curves. Air was blended with a 100 ppm HCl gas stream (in a nitrogen balance) to give the desired HCl concentrations. When the HCl flow was first sent to the detector, it took about 20 minutes to reach 90% of its final response to the HCl stream. However, after this initial period

in which HCl was equilibrating with the walls of the sample transport lines and portions of the IMS system, the unit responded rapidly to changes in HCl concentration. The detector gave a linear response to HCl concentrations ranging from 1 to 25 ppm, as shown in Figure 2. The discrepancy between the HCl reading on the instrument and our nominal HCl concentrations may reflect gas metering uncertainties or insufficient conditioning periods in our work. Those possibilities will be explored further. Additional tests with the IMS system are in progress to examine potential interferences and to examine instrument response to HCl concentrations in the ppb range.

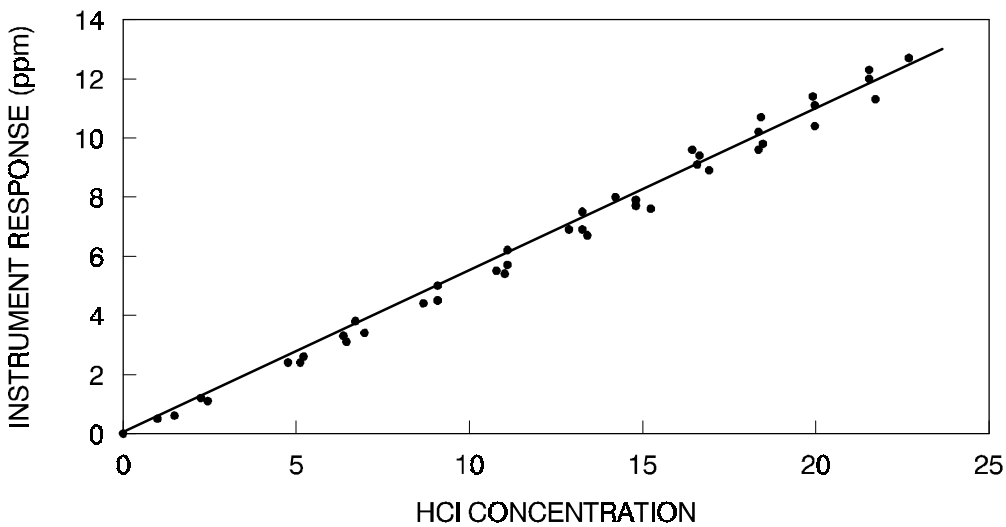

Figure 2. Calibration Curve Obtained for IMS Unit Using Blended Gases.

Ammonia Removal. In the presence of ammonia (NH_3), chloride losses can occur during sample transport due to formation and deposition of solid NH_4Cl. This compound can be kept in the vapor phase during sample transport by heating the sample lines. However, since most of the HCl monitors being considered operate at relatively low temperatures (less than 100ºC) and require the chloride to be present as HCl rather than NH_4Cl, the presence of NH_3 gases in the sample stream presents a problem. Consequently, it is desirable to remove the NH_3 from the gasifier stream in order to avoid the formation of NH_4Cl prior to determining HCl.

Tests were performed with a beaded (1/8-inch) platinum catalyst (United Catalysts, Louisville, KY) on an alumina substrate to determine how effectively it removes NH_3 gases. For these tests 3% (v/v) NH_3 in a given carrier gas stream was passed through about 100 cc of catalyst with a total gas flow of about 1 liter/minute. The temperature of the catalyst was varied from ambient to 400ºC, and a given temperature was maintained to within 5ºC for 30 minutes before obtaining semiquantitative measurements of the NH_3 concentration exiting the catalyst tube using color-indicating paper sensitive to NH_3. In base line tests using blends of nitrogen and NH_3, little or no NH_3 was removed as the temperature was increased to 400ºC. When the NH_3

was blended with air rather than nitrogen, virtually no NH_3 was removed at temperatures below about 250°C. As the temperature was increased to about 250°C, exothermic reactions began occurring, which made it more difficult to maintain the desired temperature. Also, the formation of water was evident (condensation was observed after exiting the catalyst tube) and no NH_3 was detected with the color-indicating paper. After heating the catalyst tube outlet to avoid condensed water, a Sensidyne pump and color-indicating tubes (accurate to within 25%) were used to help quantify the NH_3 concentration exiting the catalyst tube at 300°C. Results indicated that the NH_3 concentration was less than 1 ppm_v, which equates to a NH_3 removal efficiency of 100%.

The water formed during the catalytic oxidation of NH_3 was very acidic (pH < 1) and is believed to be nitric acid. When the catalyst tube was at 300°C and the outlet of the tube was heated to avoid condensation, gases exiting the tube were bubbled into deionized water for several minutes. Analysis of this water sample by ion chromatography indicated that it had a lot of nitrate and a considerable amount of an unidentified compound, which is believed to be a nitric acid precursor. Nitric acid is often commercially made by the catalytic oxidation of NH_3 using the Ostwald process. In that process, NH_3 is oxidized to produce NO and H_2O. The NO is subsequently oxidized to NO_2, which then dissolves in water to form HNO_3 and NO. Attempts were made to maintain the oxidation of NH_3 without promoting the subsequent formation of nitric acid by initially activating the catalyst at about 250°C and then subsequently decreasing the temperature. As the temperature was gradually decreased, it was held at each desired temperature for periods ranging from 2 to 12 hours. The NH_3 was completely removed and acidic water was noted regardless of temperature. This was true even after 12 hours at 60°C, which was the minimum temperature attained with no external heat supplied to the catalyst. The catalytic oxidation reactions were disrupted only after terminating the NH_3 flow and purging the catalyst tube with either air or nitrogen. After doing so, the catalyst tube was heated to 200°C and the NH_3 flow was resumed. No NH_3 removal was observed and no moisture was formed even after 7 hours at that temperature. Apparently, a minimum activation energy is required in order to initiate the catalytic oxidation of NH_3. Also, these results indicate that lowering the reaction temperature after initial activation of the catalyst is not a viable approach for preventing acid formation when 3% NH_3 is in an air stream. Attempts are currently being made to destroy the NH_3 without forming nitric acid by using air/nitrogen blends to decrease the oxygen content of the gas stream. In doing so, it may be possible to have sufficient oxygen for oxidizing the NH_3, but not for subsequent oxidation of the NO byproduct to NO_2.

Hydrocarbon Removal. Because methane is a severe interference in the determination of HCl by the IR method, tests were performed to determine whether a platinum/palladium catalytic converter can effectively remove hydrocarbon gases at reasonably low temperatures. Preliminary tests were performed by passing an air stream containing approximately 10% propane by volume through an automotive catalytic converter. At the time of these tests, the commercially available platinum catalyst used for the NH_3 studies was not yet available. Semiquantitative results indicated that hydrocarbon gases could largely be destroyed by the converter at temperatures of less than 500°C. Tests were also performed to see whether the converter could pass low concentrations of HCl. For those tests, HCl from a compressed gas

cylinder was diluted to 25 ppm and then passed through the catalytic converter at various temperatures. The gases exiting the converter were analyzed using a dry colorimetric analyzer. Little or no HCl was detected at the converter outlet until the temperature reached 450°C or more, where substantial amounts of HCl were emitted. This suggests that it may be possible to use platinum catalysts to destroy hydrocarbons without affecting the HCl content. Additional tests are being performed using the platinum catalyst from United Catalysts.

Future Activities

For Hg, problems associated with the use of AA will be investigated. The primary problem anticipated is the presence of interfering compounds (e.g., aromatic hydrocarbons and sulfur compounds) in actual gasifier streams. Future work will focus on studying approaches for either removing interfering compounds through gas conditioning or for performing suitable spectral background corrections during analysis of the gasifier streams. The best approach for use in an on-line analyzer for coal gasifiers will then be selected. Because of the possibility that oxidized Hg species (e.g., dimethyl Hg) may be present in gasifier streams, work will be performed with a pyrolyzer intended for use in the on-line monitor to ensure that it is pyrolyzing oxidized Hg species to elemental Hg (required for detection) with essentially 100% conversion efficiencies.

For HCl, the analytical method to be used for the on-line monitor will be selected. Studies on the delivery of known amounts of HCl will continue. The use and accuracy of permeation tubes and permeation tube calibration systems will continue to be investigated. Methods for removing or destroying NH_3 and hydrocarbons in the sample gas prior to HCl analysis will continue to be tested.

For both Hg and HCl, subsequent testing will include determining the effects of gas composition (including moisture content) on detection limits, precision, and accuracy. The effects of sample line material will also be considered. Modifications to existing commercial instruments will be made in order to adapt those systems for use with gasifier streams.

Suitable sample handling systems will be developed. Gas conditioning steps which will be required include temperature and pressure adjustments, filtering particulate matter, and removing interfering gases. The removal of moisture from gas streams without affecting the analyte will also be studied. The amount and type of gas conditioning will be largely dependent on the analytical methodology employed. The effects of any necessary sample conditioning steps (e.g., moisture removal) on analyte concentrations will be examined. Ultimately, prototype integrated analytical systems which appear to be acceptable based on results of laboratory studies will be tested in the field.

Contract Information

This work was performed with funds provided by the U.S. Department of Energy through the Morgantown Energy Technology Center under Contract 93MC30024.000(METC) with Ames Laboratory, Iowa State University, Ames, Iowa 50011; telefax:515-294-3091. Ames

Laboratory is operated for the U.S. D.O.E. by Iowa State University under Contract No. W-7405-Eng-82.

Acknowledgements

We thank Zellweger Analytics for the loan of an MDA Model 7100 Gas Monitor. We also thank Amy Gensch and Josh O'Donnell for their help in evaluating the colorimetric monitor. Susan Joines served as the METC Contracting Officer's Representative for this continuing project.

References

1. G. N. Krishnan, G. T. Tong, B. J. Wood, and N. Korens, "High Temperature Coal Gas Chloride Cleanup for Molten Carbonate Fuel Cell Applications," Final Report, DOE/MC/21167-2080 (DE87001041), November 1986, pp. 57-60.

2. G. L. Anderson, F. O. Berry, B. D. Harmon, R. M. Laurens, and R. Biljetina, "Development of a Hot Gas Cleanup System for Integrated Coal Gasification/Molten Carbonate Fuel Cell Power Plants," Final Report, DOE/MC/19403-1816 (DE86001589), October 1985, p. A-4.

3. T. Grindley and T. H. Gardner, "Trace Contaminants in Fixed-Bed Gasifier Gas," in Proc. Twelfth Annual Gasification and Gas Stream Cleanup Systems Contractors Review Meeting, Volume II, DOE/METC-92/6128, Vol. 2 (DE93000229), September 1992, pp. 479-497.

4. G. A. Norton, C. D. Chriswell, D. E. Eckels, and R. E. Peters, and W. H. Buttermore, "Development of Mercury and Chloride Monitors for Coal Gasifiers," in Proc. Advanced Coal-Fired Power Systems '95 Review Meeting, Vol. II, Morgantown, WV, June 27-29, 1995, 574-586.

Dynamic Analysis of Process Reactors

by
Lawrence J. Shadle
Larry O. Lawson
Stephen D. Noel
Morgantown Energy Technology Center

ABSTRACT

The process design for integration of advanced gasifiers for combined-cycle facilities requires a dynamic analysis tool for predicting the gasifier performance and stability. Such a tool provides an understanding of both process reactions and the interaction of process components. To illustrate the utility of the process dynamic tool, a Gasifier Dynamic Model (GDM) was developed at the Morgantown Energy Technology Center (METC) to investigate alternative designs and operational scenarios during process design development.

Empirical data and first principles were combined into steady-state process models to develop sensitivity parameters around a nominal process design condition. These gain factors were then coupled with time-dependent functions for process mass and energy inventories to develop the dynamic model (GDM). Engineering calculations performed in the GDM were used to predict process responses such as gas make, flow, pressure, and temperature.

Small research facilities were constructed and operated to validate both the steady-state process and dynamic models. GDM predictions provided engineers insights into the design integrity and operational safety of the reactions, components, and control elements.

INTRODUCTION

METC is involved in the design of an advanced, hybrid coal gasifier based on the PyGas™ process (Carson et al., 1994). This process incorporates a centrally located, jetting, fluid-bed pyrolyzer to mitigate the caking of bituminous coals and a concentric, counterflow, moving-bed section to gasify the remaining carbon (Figure 1). The complexities involved in integrating these reaction components into a single vessel demand an advanced analysis method for process design, operation, and control. This method combined steady-state parameter estimation and process dynamic modeling. The resulting model was a gasifier process simulator for control strategy evaluation.

In the first step of the control analysis, steady-state process models were used to calculate lumped parameter, input-output gain factors. Sensitivity analysis on these models yielded qualitative insights into the dominant reactions as well as mass and energy transfer mechanisms at nominal gasifier operating conditions. The steady-state process models work by converging solutions of the non-linear, mechanistic equations for reactions and dynamics of the jetting fluidized-bed pyrolyzer and the moving-bed gasifier sections of the PyGas™ concept. The localized gain coefficients, attained from exercising the process models, were the key inputs as gain parameters to the GDM.

Simplified Schematic and Hybrid Pressure Balance Resistance Network

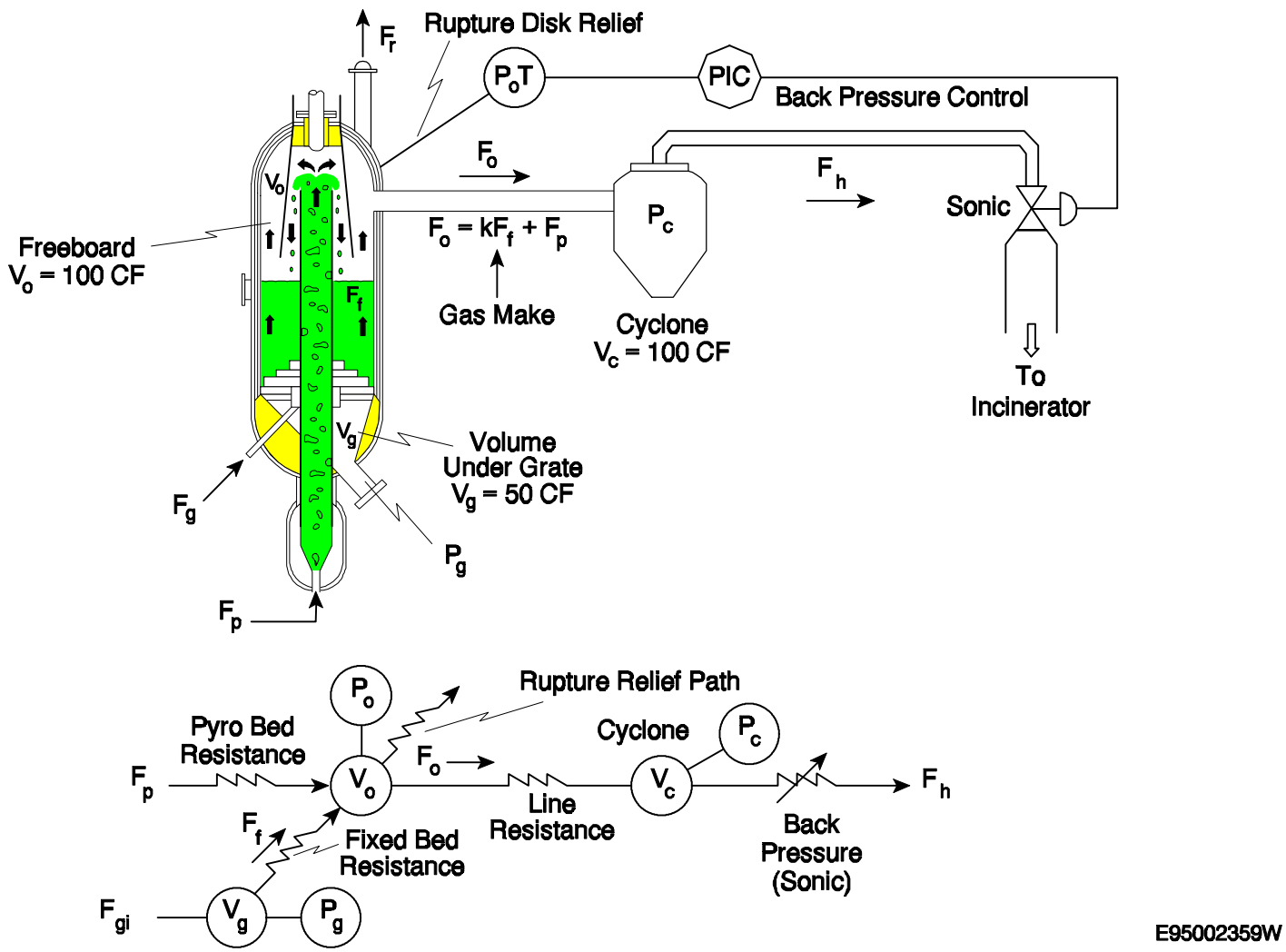

Figure 1. Simplified Schematic and Hybrid Pressure Balance Resistance Network

The integrated dynamic model was developed from the global process phenomena of the integrated design. The equations for the chemical, physical, or thermodynamic mechanisms were defined for interactions between the process variables. The previously identified gain factors were combined with the heat and material inventory capacitances to define a differential equation. Solution of this system of equations would be difficult in closed form, but a computational simulation of each term of the equations enabled the analysis. The GDM, thus simulating process dynamics, was coupled with control strategies to test operational scenarios.

To gain confidence in the predictive capability of both the steady-state and the dynamic models, validation data are being obtained from reactor facility tests at METC. These research facilities include: (1) a one-half scale, plastic, cold-flow model of the PyGas™ gasifier; (2) a 10-inch jetting, fluid-bed coal gasifier; and (3) a pressurized, fixed-bed, char gasification pot which is currently under design.

There is timely utility in performing the dynamic analysis of operational scenarios, instrument placement, and process design prior to construction and operation. The results of simulation yield a measure of control effectiveness. The objective of the dynamic analyses was to test transients in measured or controlled parameters against design constraints and thresholds during operational disturbances. These disturbances may include internal reaction upsets, changes in load variables, and changes in inlet conditions. The dynamic engineering model has also been adapted to the form of a process simulator for off-line training of operators to recognize process disturbances.

PREDICTIVE PROCESS MODELS

Consider first the process models which predict the steady-state performance of the gasifier and from which gain coefficients were derived for the dynamic model. The pyrolyzer model was developed by METC specifically for this application because no commercial software met all the requirements (e.g. hydrodynamics and chemical kinetics) needed for this process. Modeling requirements included reactions that do not achieve equilibrium, spatial voidage, jet height, carbon conversion, thermal equilibrium, pressure profile, and superficial velocities.

The model of the complete, integrated process is called the PyGas™ Heuristic Automatic Modeling Executive model or PHAME (Trapp 1994). PHAME executes three models that represent the three zones in the gasifier where streams are introduced. The three zones are the pyrolyzer, the top and co-flow, and the fixed bed. Although they are separate, these zones depend upon and interact with each other. As would be anticipated, these models do not converge to state-space balance in real-time nor do they compute time-dependent functions.

The first model, JET, was used to simulate the jetting, fluid-bed pyrolyzer (Noel et al., 1995). A mass and energy balance was calculated for the given coal composition considering, volatile matter and tar compositions. All major gasification and combustion reactions that apply were considered; however, only the water-gas shift reaction was allowed to reach equi-

librium. To better represent a gasifier, some empirical functions were introduced into the model. Empirical functions were developed based on Foster Wheeler carbonizer test data to determine the amount of volatile matter that reacts with inlet air and the amount of char gasification in the jet (Archer and LaNeve, 1994).

The JET model also includes empirical hydrodynamic parameters. These parameters include jet penetration (Yang and Keairns 1982), char recirculation into the jet, superficial velocities of solids and gases, and fluidization regime (Yang et al., 1986). The model's results were favorably matched with Foster Wheeler carbonizer (Katta, et al. 1988), KRW gasifier (Froehlich et al., 1994), and METC fluid-bed gasifier data (Rockey et al., 1995). Conversion, gas heating value, and process temperatures were readily matched based on experimental, nominal operating inlet flows by adjusting several indirect parameters, but agreement between model and experimental gas compositions as constrained by the water-gas shift equilibrium was only fair. Since the operating conditions for the pyrolyzer most closely approximate those of the Foster Wheeler carbonizer, it was decided to fix the adjustable indirect parameters based on the best match with that data.

The outputs from the pyrolyzer model and any air introduced into the top combustor were used as inputs into the top and co-flow model in PHAME. This model was developed using the METC Gasifier Advanced Simulation (MGAS) (Syamlal and Bissett 1992). MGAS describes a gasifier in terms of a gas phase and a solids (coal or char) phase and considers coal combustion, steam and CO_2 gasification, methanation, water-gas shift, volatile evolution, tar cracking, and gas phase combustion reactions. The kinetic rate expressions for the gasification reactions were taken from Wen et al.(1982). In MGAS, a set of mass balance equations and energy balance equations are solved for the gas and the solids phases. The solution of these equations gives the time-dependent, one-dimensional distribution of species mass fractions, and temperatures.

Simulations of METC, Wellman-Galusha, General Electric, and Lurgi/Westfield gasifiers (Thimsen and Maurer, 1990) were done using MGAS for code validation purposes. The steady-state values of the product gas flow rates, composition, and temperature calculated by MGAS were found to be in reasonable agreement with the experimental data.

The outputs from the top and co-flow zones of the gasifier, and any air or steam introduced into the grate were input to a second MGAS model set up to simulate the countercurrent fixed-bed configuration. This second MGAS model was configured to accurately simulate the geometric entrance of streams into the gasifier. The solid material coming out of the co-flow zones was the only stream considered to enter into the top of the fixed-bed model. The gases exiting from the co-flow zone were mixed with the exit gases from the counterflow fixed-bed by PHAME to best represent the total gasifier outlet gas.

STEADY-STATE PROCESS GAIN FACTORS

Process control development first requires characterization of the process sensitivities to inputs. Since this gasifier design is an experimental process, prediction of gasifier behavior is speculative. Computer simulations gave computational insight into the reactor's perfor-

mance and behavior. Multiple sensitivity studies were conducted using output from steady-state predictive models to provide key transfer-function gains (input/output). Obviously, the extensive, spatially distributed calculations in the models described above do not execute to converge in real time. Thus, a macro-process model was formulated from the sensitivity analysis of these models to achieve a real-time simulation. The transfer functions resulting from the parametric sensitivities served to reduce the spatially dependent factors to lumped parameters in the macro. See Figure 1 of illustrated components and an analogous network representation of lumped parameters.

The approach taken was to assume that the complex process functions can be linearized as lumped parameters once the relative effects were quantified through parametric sensitivities. Sensitivities were performed over a narrow range around the expected operating point in order to choose several possible control schemes. Where nonlinear functions were known over a wider operating range, they were included in the dynamic model and tested in the steady state for validation. Only by the use of a dynamic model, can a final control scheme be chosen.

For this analysis, only measurable output parameters such as temperatures, gas flow, and gas compositions were considered around a nominal operating condition. All flows were taken from nominal design heat and material balance calculations. Gas-make was calculated as a lumped parameter from the ratio of output to input stoichiometric mass flow balances. The benefit to experimenters and operators of models' integration is in understanding the scale of these process parameters.

Localized linearization was done by using the steady-state predictive model results observed from runs with a 5 percent change of each manipulated variable around (localized to) the operating point. The gains were calculated by the ratio of measured variable change to the manipulated variable change.

TIME-DEPENDENT DYNAMIC TERMS

The steady-state process model does not represent time-dependent functions inherent in the process and so cannot simulate transient characteristics. The dominant time-dependent functions were derived from the dynamic driving and convergence mechanisms in the GDM. Capacitance for heat and material in the process are time rate parameters that determine inventory as a function of time. Capacitances were determined for the process reactor geometric dimensions and material properties (specific heat and density). The equations which balance time-dependent inventory building with inventory removal were expressed in terms of the time functions. The parameters of inventory gain or loss due to the process variables (pressure, flow, gas make, and temperature) were taken as those determined from the steady-state process models.

Each coefficient in a set of differential equations represents a process parameter. These systems of equations, once solved in closed form, would yield a characteristic process state. But this mathematical complexity makes an alternative, simulation method more attractive. Simulation in the time domain reveals more of the response than would a single process

state. The time domain simulation engages the process engineer. The system of equations that describes gasifier dynamics simulates transient responses to changes in input conditions (flows and pressures) as well as changes in internal process parameters (bed resistance and control valve position) as these parameters change through time.

MEANS OF SIMULATION

The representational structure of the commercial TUTSIM model used in this study allowed additional mathematical expressions to be added as modules of computational blocks shown in Figure 2. In each block the individual terms in the system of equations described above were computed. As the computation proceeds, the time-dependent functions in the model drive the system of interconnected computational blocks to simulate difference equations of mass and energy balance equations. Each connecting line represents a time-dependent process variable. Chains of model function blocks and connecting lines form loops which couple processes on themselves.

REAL-TIME SIMULATION

If the speed of the computer is sufficient to execute simulation time steps on an actual time scale, the model then becomes capable of real-time simulation of the process. Obviously, if rapid dynamics are inherent, a slower than real-time simulation has the advantage of expanding time for observation. Conversely, if slow dynamics are prevalent, compression of time helps to observe long time responses. If an objective is to test interaction between the simulated process, control systems and operators, a real-time simulation is needed. Simulations of the gasifier have shown utility for all three treatments of time.

PRESSURE PROFILE DYNAMICS

A gas pressure profile dynamic originates from a dependence between the stored volume of gas in the gasifier, the rate of gas production, and the pressure dependence of the exiting flow rate function. Capacitance terms in the dynamic model provide the time-dependent functions needed to simulate the pressure balance coupling between cyclone volume, back pressure valve, fixed-bed gas production, and pyrolyzer gas production (Figure 1).

The model was centered around the common freeboard volume of the gasifier. The product gas from the fluidized-bed pyrolyzer and the fixed bed contribute gas flow in response to input air flows. It was assumed that each bed acts as a readily available supply of solid fuel, and that changes from the nominal inlet air flows have an immediate, proportional deviation on the gas production rates. This assumption is valid due to the small time constant of gas production relative to pressure deviations of gas inventory in the freeboard.

The air flow to the fixed bed was found to be a function of the pressure drop across the flow resistance of the fixed bed. The driving pressure is a time-dependent function of the inventory of gas above the bed, in the freeboard, and below the grate. Further, an under grate volume present between the inlet streams and the fixed bed resulted in a time lag between manipulation of input air flow and actual air flow within the fixed bed.

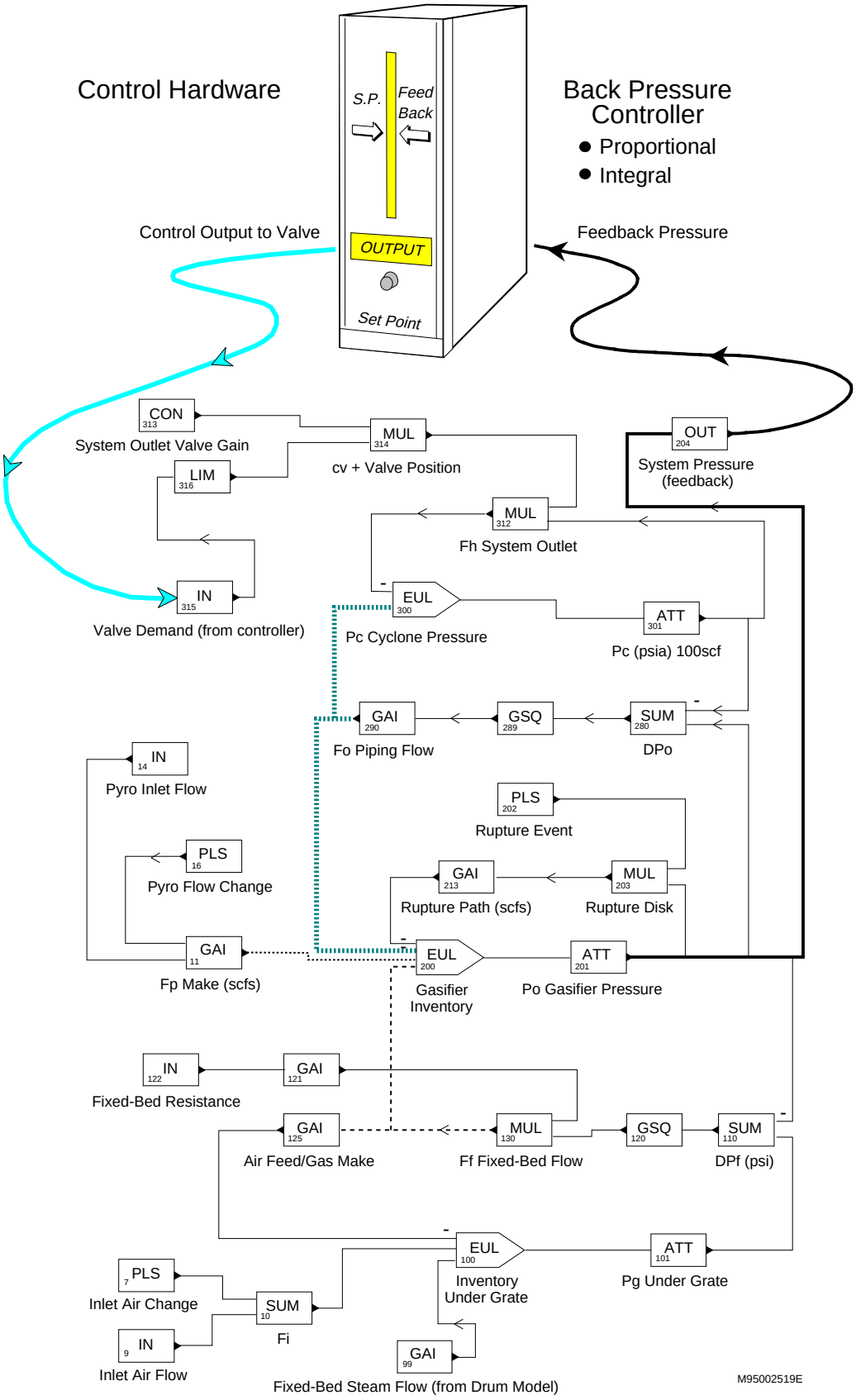

Figure 2. Dynamic Model Simulator

Likewise for the fluidized bed, a resistance function of pressure drop with flow through the bed was incorporated but assumes no inventory volume under the bed. It is important to understand that the increase in flow through a fluid bed results in **decreased** pressure drop across the bed due to increased void fraction. This effectively represented a negative dynamic bed resistance. Complex, mixed-phase dynamics were expected to take place as spatially distributed functions within the fluid bed, but the resulting pressure and flow functions were generally considered rapid compared to gasifier inventory derived terms. The fluid-bed resistance was reduced to a single, lumped parameter in the Gasifier Dynamic Simulation.

RESULTING PRESSURE AND FLOW RESPONSES

The under grate pressure, Pg of Figure 3, responded smoothly to an imposed 2 scfs increase of the air flow under the grate, Fi. The freeboard outlet flow, Fo, similarly responded with a rise to the eventual, new flow balance seen in Figure 4. This appeared to be a first-order response, but was, in fact, a coupled response of the under grate inventory and freeboard inventory.

The effect of imposing 2 scfs increase in pyrolyzer inlet air flow, Fp, resulted in an abrupt freeboard outlet flow, Fo, of Figure 5. The magnitude of deviation in the freeboard outlet flow, Fo, in Figure 5 was similar to the response to the previous change in the fixed-bed, Fg. The response, however, was more immediate due to the small relative volume and gas residence time in the pyrolyzer. In response to the same increased pyrolyzer flow, a negative going, transient decrease in fixed-bed flow, Fg, was observed (Figure 6). This inverse response of fixed-bed flow was due to an increase in system back pressure due, in turn, leading to increased total outlet flow across the outlet resistance. It is interesting to note that the eventual recovery of original fixed-bed flow, Fg, corresponded to the eventual new pressure and flow balances.

It would be difficult to calculate the effect chages in flow rates on the time-dependent balance in system pressure. But the dynamic model allowed simulation to attain the computational balance and frees the observer to understand the resulting effects.

THERMAL MODEL DYNAMICS

With a gas inventory model established, the next dominant mechanism anticipated was the evolution and removal of heat from the fixed bed. The thermodynamic control volume to be modeled was that of the entire bed mass as a constant. The inventory of solids was assumed to be readily available for reaction with air to produce heat. Thus, the incremental amount of heat produced was proportional to the deviation in air flow from the nominal. The thermal model became an additional module of difference equations that utilize the existing flow balancing structure. The resulting temperature variable became a compensating term to the gas density computation. In this way the model quickly begins to capture and represent the coupled dynamics of both gas and thermal inventories. The relative time constant of the thermal model was found to be long (hundreds of seconds) compared to the volumetric time constant of the gas inventory (tens of seconds).

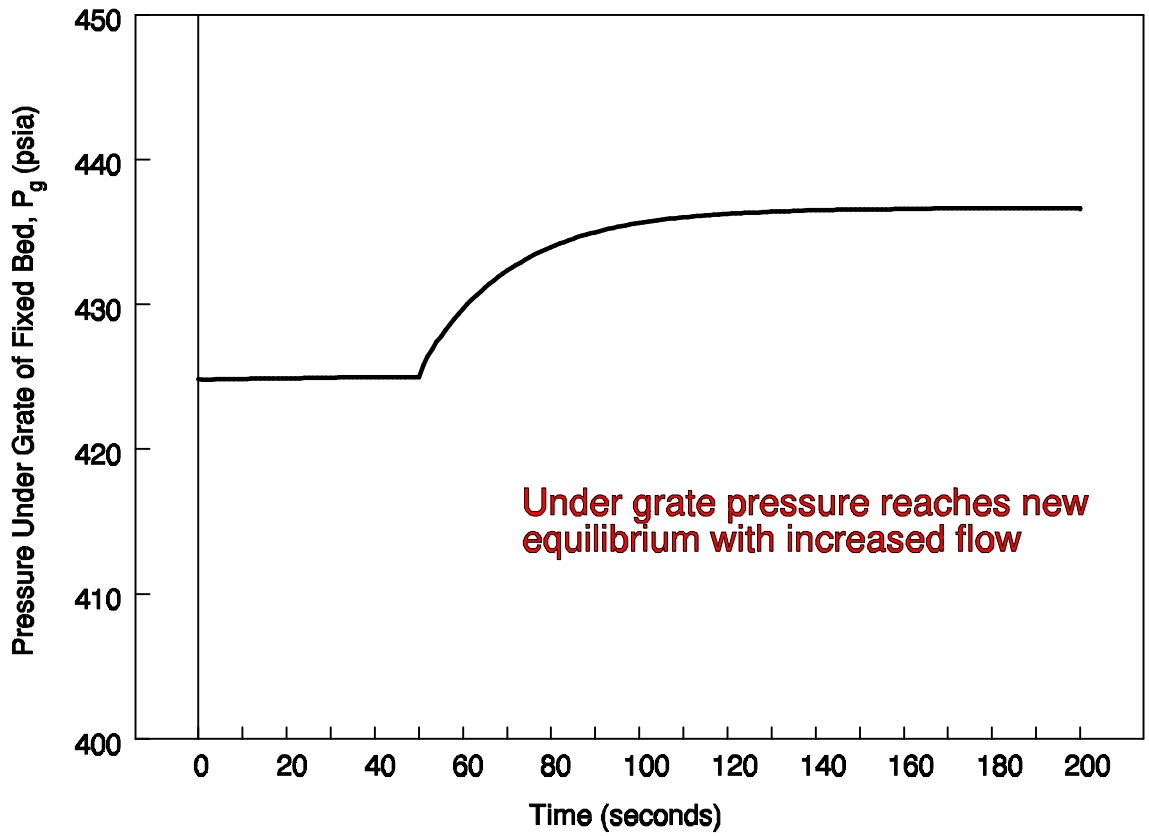

E95002799W

Figure 3. P_g Response to Step Increase of F_i at Time t = 50 sec

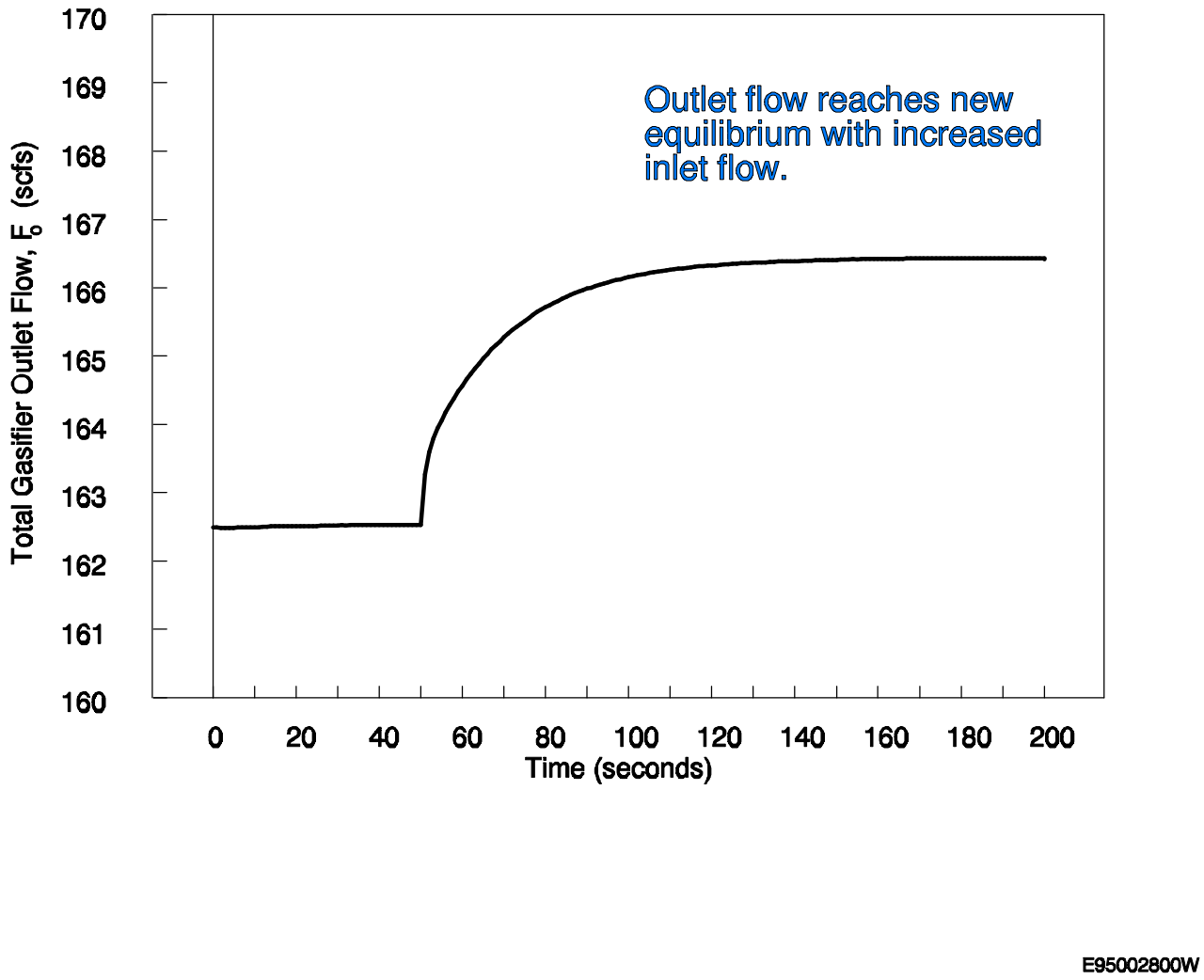

Figure 4. F_o Response to Step Increase of F_i at Time t = 50 sec

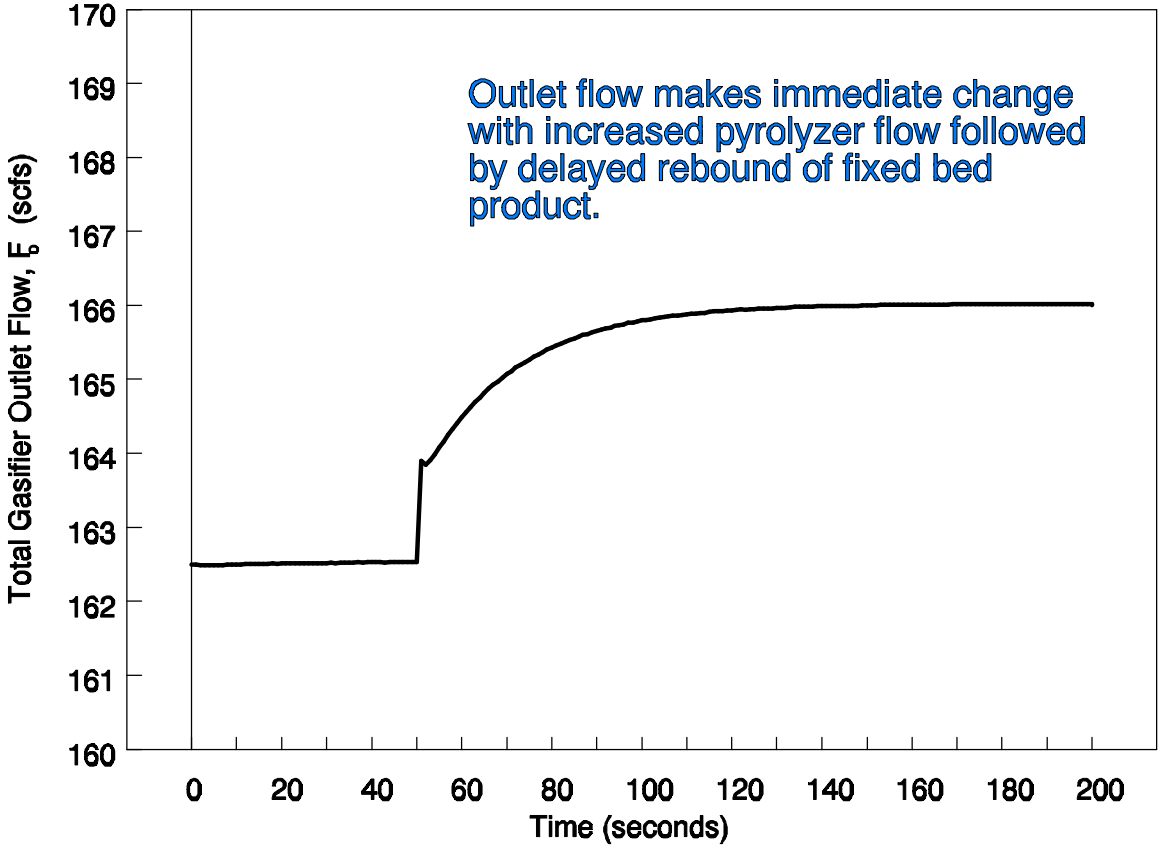

E95002801W

Figure 5. F_o Response to Step Increase of F_p at Time t = 50 sec

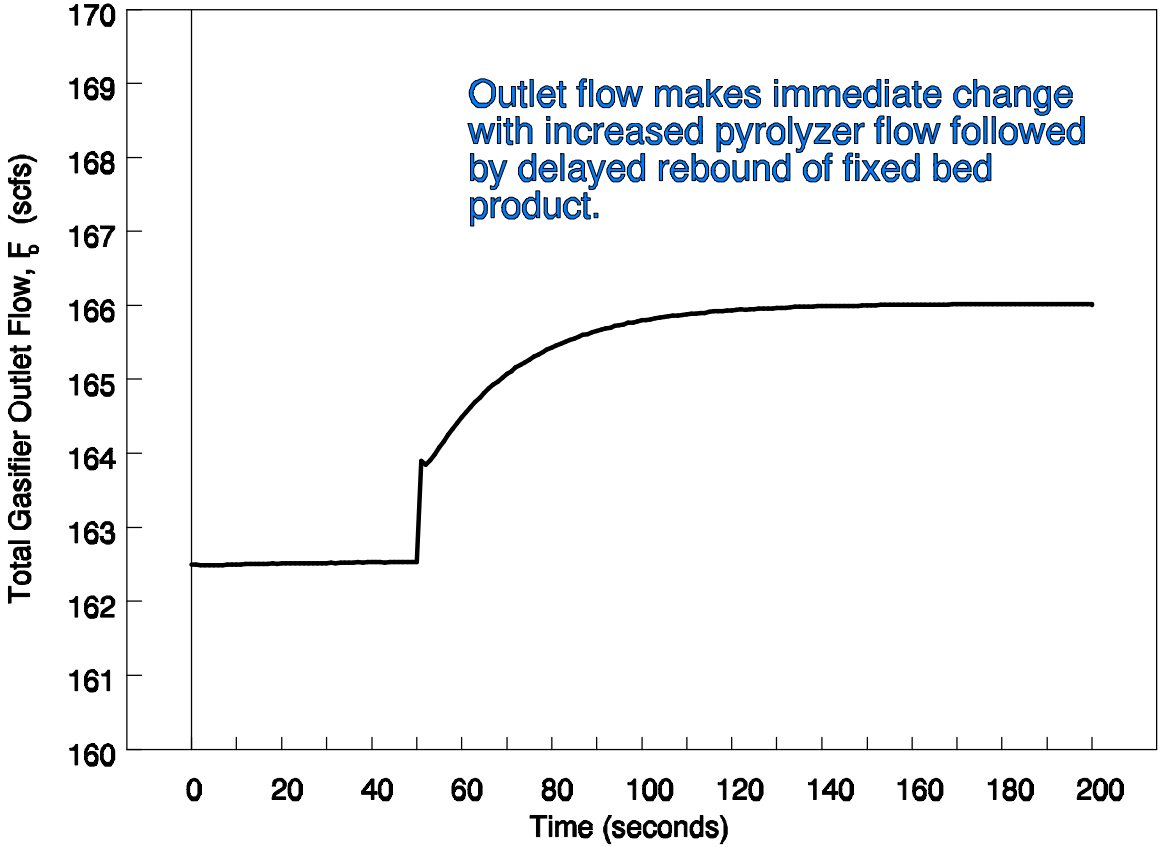

E95002801W

Figure 6. F_g Response to Step Increase of F_p at Time t = 50 sec

STEAM DRUM DYNAMIC MODEL

An important dynamic aspect of a water-cooled gasifier was the interaction of the gasifier pressure with the cooling water jacket circuits and steam drum pressure. An adaptive extension of the dynamic model tested the stability of the mechanisms of steam production in the steam drum as they couple to pressure transients in the gasifier. A self-passivization shutdown scenario would rely on stable pressure balance between the gasifier pressure and water jacket steam drum.

Time-dependent terms arose from the inventory of water, steam, and heat energy in the jacket and drum as a function of steam conditions. Steam conditions were, in turn, a function of temperature and pressure. The drum system was represented as a system of coupled mass and energy balance equations and simulated by a additional dynamic module to the GDM.

Two mechanisms couple the gasifier with the water jacket system. First, heat transfer through the wall to the water jacket coupled to steam generation in the steam drum. Second, the steam generated in the jacket drum flowed (through a suitably sized fixed orifice) to the pyrolyzer and grate zones of the gasifier for inerting the reactions and sustaining a small pressure differential between the water jacket and the gasifier during shutdown depressurization cases.

The modular structure of the GDM allowed the addition of suitable steam drum dynamics to identify the worst case scenario by testing for violation of thermal shock and mechanical stress constraints.

FUTURE INTEGRATION OF MODULES

Variations of the dynamic model currently under development at METC were needed to validate single-loop and multi-loop control schemes. As a result, the product gas temperature emerging from the pyrolyzer and fixed-bed regions, presently constant parameters, can be modeled as coupled variables between the thermal model and the pressure profile model. As a tool for process design, the objective was to test design parameters that were not yet cast in concrete and steel.

There is a great likelihood that as positive coupling mechanisms are added, second-order dynamics will result in instabilities. Care must be taken to rank the relative coupling gains of various modules so as to recognize when one mechanism dominates or "swamps" the effects of others.

The resulting dynamic process simulation of transients can show breeches in mechanical or physical constraints, system instabilities leading to divergence from steady-state, undesired side effects, and excessively long thermal time constants relative to shorter, desired balancing mechanisms. The process of testing and discovery allows thorough design and testing of the process control scheme before the process parameters (due to geometric dimensions) are cast into a fabrication design.

The model helps one to understand which process variables are important but not directly measurable, thus helping to define process instrumentation needs. The exercises of the model help to define the operational test matrix to validate process performance. For process variables that are not directly measurable, on-line dynamic computations can infer process data that is not directly observable.

EXPERIMENTAL VALIDATION

A one-half scale, plastic, cold flow model was fabricated and is being operated to demonstrate the fluid dynamics of the PyGas™ concept. This model includes components including the pyrolyzer tube, a rotating grate used to support and distribute air through a counterflow fixed bed, and a freeboard annular gas exit region. The cold flow unit has a 30-inch inner diameter, a 10-foot external shell, and a hemispherical dome on top. The model is capable of being operated with continuous solids and gas flow at conditions scaled from the process design. This unit is being operated to provide data to validate the process model estimates of fluid dynamic behavior in the hot unit.

A second research facility being used to validate the models is the METC 10-inch fluid-bed gasifier system which consists of a pressurized (425 psig) gasifier and several subsystems, e.g., coal storage conveying system, air preheater, particulate removal system, and an incinerator. The gasifier is a 20-foot high, nominal 80 lb/hr, air-blown and refractory-lined vessel. Coal is fed into the gasifier by ambient (convey) air through the center core of a concentric nozzle located at the bottom of the bed. Preheated (reactor) air and steam are premixed and introduced into the bed through the annular core of the nozzle. This system produces about 300 lb/hr of flue gas with a heating value of 120 Btu/scf. This gasifier has provided operational data to verify predictive process models, and it is being used to test and verify advanced control schemes.

A third research reactor for model validation is the Pressurized Gasification Pot (PGP). The PGP will be 2 feet in diameter and 5 feet in height, with an inner diameter of 1 foot for the fixed-bed reactor and refractory surrounding it. The unit will be operated up to 600 psi, 1,600 °F, gasifying coke and char generated from the above described, fluidized-bed gasifier. The offgas of the gasification pot will flow to a gas chromatograph for gas analysis. Data collected on char conversion rate, gas production, and other performance factors will be used to validate the fixed-bed process models.

CONCLUSIONS

The models described have a primary benefit of providing the process control engineer the means of understanding the critical process interactions. They have already enabled testing of alternative control strategies for the PyGas™ gasifier. Although modeling codes were initially developed to optimize a control scheme, they will have utility throughout the operational life of the process for model based process control.

Longer term modeling applications involve optimization of the gasification process. Operations will be simplified by uncoupling the hybrid reactor components' responses to inlet

changes through control scheme development. Operational surprises will be minimized by anticipating the process response to inlet changes.

The model has become a suitable simulator for testing and tuning the control loops prior to plant start-up. As an off-line simulator, the model may act as a training simulator for operators. As an on-line simulator, once validated, the model may prove useful as an operational tool in diagnosing operational problems such as bed channeling, clinker agglomeration, and bed slugging.

REFERENCES

Archer, D., and M. LaNeve, 1994, "Foster Wheeler Carbonizer Data: Material/Energy Balance Analysis Pyrolysis/Combustion/Gasification Balance", Private Communication.

Branham, R. L., 1990, "Scientific Data Analysis: An Introduction to Overdetermined Systems," pp. 199-232.

Carson R.D., V.B.Dixit, R.S.Sadowski, W.H.Skinner, R.A.Lisauskas, and S.A.Johnson, 1994, "Gasification Product Improvement Facility Status", Proceedings of the Coal Fired Power Systems -- Advances in IGCC and PFBC Review Meeting, Volume I. pp. 83-92.

Froehlich, R., A. Robertson, and J. VanHook, 1994, "Second-Generation Pressurized Fluidized-Bed Combustion Research and Development; Phase 2-Task 4 Carbonizer Testing Volume 1," DE-AC21-86MC21023, November 1994.

Katta, S., D. M. Ettehadieh, B. Haldipur, G. B. Haldipur, R. A. Newby, and W. C. Yang, 1988, "A 32-Month Gasifier Mechanistic Study and Downstream Unit Process Development Program for the Pressurized Ash-Agglomerating Fluidized-Bed Gasification System," DE-AC21-84MC21063, May 1988.

Luyben, W. L., "Process Modeling, Simulation, and Control for Chemical Engineers," 1990, pp. 572-573.

Moore, C., 1986, "Application of Singular Value Decomposition to the Design, Analysis, and Control of Industrial Processes," Proc. Am. Control Conf., Seattle, p. 643.

Noel, S., G. Q. Zhang, and L. J. Shadle, 1995, "Modeling of a Jetting Fluid-Bed Gasifier," to be submitted for publication.

Pillai, K. K., 1981, "Influence of Coal on Devolatilization and Combustion in Fluidized Beds," J. of Inst. of Energy, 54, pp. 142-150.

Seborg, D. E., T. F. Edgar, and D. A. Mellichamp, 1989, "Process Dynamics and Control," p. 461.

Syamlal, M., 1991, "MGAS Validation Results," Unpublished EG&G Report No. 93AA-R91-003, March 1991.

Syamlal, M., and L. A. Bissett, "METC Gasifier Advanced Simulation (MGAS) Model," Technical Note, DOE/METC-92/4108, NTIS/DE92001111, National Technical Information Service, Springfield, Virginia, 1992.

Thimsen, D. P., and R. E. Maurer, 1990, "Coal Devolatilization in a Moving-Bed Gasifier," EPRI GS-6797, Project 2525-14, October 1990.

Trapp, G., 1995, "PyGas Modeling Effort: The PHAME System," Research Report DE-AP21-93MC54845, June 1995.

Wen, C. Y., H. Chen, and M. Onozaki, 1992, "User's Manual for Computer Simulation and Design of the Moving-Bed Coal Gasifier," NTIS Report DOE/MC/16474-1390 (DE83009533), January 1982.

Yang, W. C., B. Ettehadieh, and G. B. Haldipur, 1986, "Solids Circulation Pattern and Particles Mixing in a Large Jetting Fluidized Bed," AIChE. J., Vol. 32, 12, pp. 1994-2001.

Yang, W. C., and D. L. Keairns, 1982, "Solids Entrainment Rate into Gas and Gas-Solid, Two-Phase Jets in a Fluidized Bed," Powder Technology, 33 (1982), pp. 89-94.

Proceedings of the
Advanced Coal-Fired Power Systems '96
Review Meeting

Meeting Participants

Javad Abbasian
Manager, Hot Gas Cleanup, Institute of Gas Technology
1700 S. Mt. Prospect Road, Des Plaines, IL 60018
847-768-0611m Fax: 847-768-0600, ABBASIAN@IGT.ORG

Pankaj Agarwal
Environmental Engineer, North Carolina Air Quality Division
P.O. Box 29580, Raleigh, NC 27626-0580
919-733-1468, Fax: 919-715-7476, PANKAJ_AGARWAL@AQ.EHNR.STATE.NC

G. Ahmadi
Morgantown Energy Technology Center
U.S. Department of Energy, P.O. Box 880, MS L08, Morgantown, WV 26507-0880
304-285-4799, Fax: 304-285-4403, GAHMAD@METC.DOE.GOV

Rajesh Ahluwalia
Mechanical Engineer, Argonne National Labs
9700 South Cass Avenue, Argonne, IL 60439-4841
708-252-5979, Fax: 708-252-1774, WALIA@TD.ANL.GOV

Mary Anne Alvin
Fellow Scientist, Westinghouse STC
1310 Beulah Road, Pittsburgh, PA 15235-5098
412-256-2066, Fax: 412-256-2121, ALVIN.M.A@WEC.COM

David H. Archer
Adjunct Professor, Carnegie Mellon University
114 Kentzel Road, Pittsburgh, PA 15237-2816
412-268-6808, Fax: 412-268-3348, ARCHERDH@ANDREW.CMU.EDU

Raul E. Ayala
Chemical Engineer, GE Corporate R&D
One Research Circle, Schenectady, NY 12309
518-387-5850, Fax: 518-387-7258, AYALA@CRD.GE.COM

William Ayers
Division Director, Project Engineering, Morgantown Energy Technology Center
U.S. Department of Energy, P.O. Box 880, MS C03, Morgantown, WV 26507-0880
304-285-4125, Fax: 304-285-4403, WAYERS@METC.DOE.GOV

E. Wayne Bahr
Manager, Coal R&D, Illinois Office of Coal Development
325 W. Adams Street, Springfield, IL 62704
217-785-2017, Fax: 217-785-2618,

Richard A. Bajura
Director, NRCCE, West Virginia University
P.O. Box 6064, Morgantown, WV 26506
304-293-2867, Fax: 304-293-3749

Rita A. Bajura
Deputy Director, Morgantown Energy Technology Center
U.S. Department of Energy, P.O. Box 880, MS B06, Morgantown, WV 26507-0880
304-285-4109, Fax: 304-285-4403, RBAJUR@METC.DOE.GOV

Tim Banfield
Engineer, R&D, Allegheny Power
800 Cabin Hill Drive, Greensburg, PA 15601
412-830-5688, Fax: 412-838-6888, TBANFIE@ALLEGHENYPOWER.COM

James Barberio
1416 North 14th Street, Clarksburg, WV 26301
304-622-3337

Joe Berns
University of Minnesota
7500 20th Avenue, South, Minneapolis, MN 55417
612-729-8136

David A. Berry
Chemical Engineer, Morgantown Energy Technology Center
U.S. Department of Energy
P.O. Box 880, MS N04, Morgantown, WV 26507-0880
304-285-4430, Fax: 304-285-4403, DBERRY@METC.DOE.GOV

Steve Bevan
Program Manager, GE Environmental Systems
280 N. 7th Street, Lebanon, PA 17046
717-274-7077, Fax: 717-274-7060

Bruce Bishop
Vice President and Director of Operations, Ceramem Separations, Inc.
12 Clematis Avenue, Waltham, MA 02154
617-899-0467, Fax: 617-899-1227

Larry A. Bissett
General Engineer, Morgantown Energy Technology Center
U.S. Department of Energy, P.O. Box 880, MS N04, Morgantown, WV 26507-0880
304-285-4266, Fax: 304-285-4403, LBISSE@METC.DOE.GOV

Alan E. Bland
Program Manager, Western Research Institute
365 N. 9th Street, Laramie, WY 82071
307-721-2443, Fax: 307-721-2345

Morton Blinn
Task Manager, Burns & Roe Services Corporation
P.O. Box 18288, Pittsburgh, PA 15236
412-892-4716, Fax: 412-892-4604, BLINN@PETC.DOE.GOV

Jeff Bolebruch
Market Manager, Blasch Precision Ceramics
580 Broadway, Albany, NY 12204
518-436-1263, Fax: 518-436-0098

George Booras
Manager, Technology Assessment, Electric Power Research Institute
P.O. Box 10412, Palo Alto, CA 94303-0813
415-855-2471, Fax: 415-855-2950, GBOORAS@EPRINET.EPRI.COM

Daniel E. Boss
Research Scientist, Northwestern University
1801 Maple Avenue, Evanston, IL 60201-3140
847-491-3373, Fax: 847-467-1022, DBOSS@NWU.EDU

Peter E. Botros
Project Manager, Morgantown Energy Technology Center
U.S. Department of Energy, P.O. Box 880, MS C04, Morgantown, WV 26507-0880
304-285-4162, Fax: 304-285-4403, PBOTRO@METC.DOE.GOV

Dan Brdar
Product Manager, IGCC, Morgantown Energy Technology Center
U.S. Department of Energy, P.O. Box 880, MS E01, Morgantown, WV 26507-0880
304-285-4666, Fax: 304-285-4403, RBRDAR@METC.DOE.GOV

Sandra L. Brosious
Senior Product Development Manager, Pall Corporation
3669 State Route 281, Cortland, NY 13045
607-753-6041, Fax: 607-753-1220

Terry H. Brown
Program Manager, Western Research Institute
365 N. 9th Street, Laramie, WY 82070-3380
307-721-2241, Fax: 307-721-2345

John W. Byam, Jr.
President, JB International
228 Grand Street, Morgantown, WV 26505-7509
304-296-0598, Fax: 304-296-0838, JBINTL@ACCESS.MOUNTAIN.NET

Kent H. Casleton
Research Chemist, Morgantown Energy Technology Center
U.S. Department of Energy, P.O. Box 880, MS N05, Morgantown, WV 26507-0880
304-285-4573, Fax: 304-285-4403, KCASLE@METC.DOE.GOV

Carlo Castaldini
Engineer, Acurex Environmental Corporation
555 Clyde Avenue, Mountain View, CA 94043
415-961-5700, Fax: 415-254-2497

John Chen
Assistant Professor, North Carolina A&T State University
1601 East Market Street, Greensboro, NC 27411
910-334-7620, Fax: 910-334-7417, JCHEN@NCAT.EDU

Roger H. L. Chen
Associate Professor, West Virginia University
Dept. of Civil & Environmental Engineering, P.O. Box 6103, Morgantown, WV 26506-6103
304-293-3031, Fax: 304-293-7109, HLCHEN@WVNVM.WVNET.EDU

Ta-Kuan Chiang
Mechanical Engineer, Morgantown Energy Technology Center
U.S. Department of Energy, P.O. Box 880, MS N05, Morgantown, WV 26507-0880
304-285-4406, Fax: 304-285-4403, TCHIAN@METC.DOE.GOV

William P. Chisholm
Cluster Leader, Morgantown Energy Technology Center
U.S. Department of Energy, P.O. Box 880, MS A04, Morgantown, WV 26507-0880
304-285-4730, Fax: 304-285-4403, WCHISH@METC.DOE.GOV

Vas Choudhry
Engineering Manager, Praxis Engineers, Inc.
852 N. Hillview Drive, Milpitas, CA 95035
408-945-4282, Fax: 408-263-2821, 70402.3150@COMPUSERVE.COM

Jin-Do Chung
Senior Researcher, KEPRI
103-16 Moonji-Dong, Yusumg-Ku, Taejon 305-380, Korea
JDCHUNG@HAMBIT.KEPRI.RG.KR

Daniel C. Cicero
Project Manager, Morgantown Energy Technology Center
U.S. Department of Energy, P.O. Box 880, MS C04, Morgantown, WV 26507-0880
304-285-4826, Fax: 304-285-4403, DCICER@METC.DOE.GOV

Robert J. Copeland
Principal Engineer, TDA Research, Inc.
12345 W. 52nd Avenue, Wheat Ridge, CO 80033
303-940-2323, Fax: 303-422-7763, COPELAND@TDA.COM

Kevin Craig
Senior Chemical Process Engineer, National Renewable Energy Lab
1617 Cole Boulevard, Golden, CO 80401
303-275-2931, Fax: 303-275-2905, CRAIGK@TCPLINK.NREL.GOV

Ashok S. Damle
Senior Research Engineer, Technochem Company
203-A Creek Ridge Road, Greensboro, NC 27406
910-370-9440, Fax: 910-370-9448

Ran K. Datta
Visiting Professor, Virginia Polytechnic Institute
301 Holden Hall, Blacksburg, VA 24061-0256
540-231-3577, Fax: 540-231-3028

Mark De Cock
Energy Projects
Regentlaan 8, Brussel 1000, Belgium
02-518-6053, Fax: 02-518-6412

Michael R. Delallo
Manager, Federal Programs, Parsons Power Group, Inc.
2675 Morgantown Road, Reading, PA 19607
610-855-2675, Fax: 610-855-2384, GC!GHMAIL02!AL569@GILCOM.

Tim Demoss
Associate Editor, Power Engineering
1421 S. Sheridan Road, Tulsa, OK 74112
918-831-9866, Fax: 918-831-9834, TIMD@PENNWELL.COM

Richard A. Dennis
Project Manager, Morgantown Energy Technology Center
U.S. Department of Energy, P.O. Box 880, MS C04, Morgantown, WV 26507-0880
304-285-4515, Fax: 304-285-4403, RDENNI@METC.DOE.GOV

Stephen Dipietro
Team Leader, CMC Products, Textron Specialty Materials
2 Industrial Avenue, Lowell, MA 01851
508-454-5488, Fax: 508-454-5632, SPUTBOY@AOL.COM

Urmila M. Diwekar
Senior Research Scientist, Carnegie Mellon University
Baker Hall 129, Pittsburgh, PA 15213
412-268-3003, Fax: 412-268-3757

Bruce A. Dockter
Research Engineer, Energy & Environmental Research Center
P.O. Box 9018, Grand Forks, ND 58202-9018
701-777-4102, Fax: 701-777-5181, BDOCKTER@EERC.UND.NODAK.EDU

Egon L. Doering
Engineering Consultant
2611 Williamsburg, Pasadena, TX 77502
713-944-9815, Fax: 713-241-0842

George J. Dooley
Research Director, U.S. Department of Energy
1450 Queen Avenue, S.W., Albany, OR 97321
541-967-5893, Fax: 541-967-5936, DOOLEY@ALRC.USBM.GOV

Thomas P. Dorchak
Project Manager, Morgantown Energy Technology Center
U.S. Department of Energy, P.O. Box 880, MS C04, Morgantown, WV 26507-0880
304-285-4305, Fax: 304-285-4403, TDORCH@METC.DOE.GOV

Chris Ebel
Consultant, Selee Corporation
137 Old Comers Road, Chatham, MA 02633
508-945-9812, Fax: 508-945-9812

David J. Edlund
Consultant, Bend Research, Inc.
64550 Research Road, Bend, OR 97701
541-382-4100, Fax: 541-382-2713, BENDRESEARCH@BENDRES.COM

Paul M. Eggerstedt
Executive Vice President, Industrial Filter & Pump
5900 Ogden Avenue, Cicero, IL 60650
708-656-7800, Fax: 708-656-7806, IFPCO@INTERACCESS.COM

Thomas Erickson
Senior Research Manager, Energy & Environmental Research Center
P.O. Box 9018, Grand Forks, ND 58202-9018
701-777-5153, Fax: 701-777-5181, TERICKSON@EERC.UND.NODAK.EDU

Maydi A. Essawy
Postdoctoral Research Assistant, Tennessee State University
Centennial Boulevard, Nashville, TN 37209
615-963-5385

Tingfang Fan
Graduate Student, North Carolina A&T State University
1601 East Market Street, Chemical Engineering Department, Greensboro, NC 27411
910-334-7564, Fax: 910-334-7904, TINGFANG@NCAT.EDU

Martin Fankhanel
Project Manager, The M.W. Kellogg Company
601 Jefferson Avenue, Houston, TX 77002-7990
713-753-2938, Fax: 713-753-3800

Jack R. Farmer
Research Director, Research Triangle Institute
3040 Cornwallis Road, Research Triangle Park, NC 27709
919-541-6909, Fax: 919-541-6936, JRF@RTI.ORG

Marty Ferer
Professor, West Virginia University
Department of Physics, P.O. Box 6315, Morgantown, WV 26506
304-293-3422, Fax: 304-293-5732

Ed Fischer
Specialist, 3M Ceramic Fiber Products
3M Center, 207-1W-11, St. Paul, MN 55144
612-736-1005, Fax: 612-733-0221

R. W. Foster-Pegg
P.E., Consultant
1224 Princeton Lane, West Chester, PA 19380
610-429-4880, Fax: 610-429-4880

Gregory C. Franzen
Vice President, Operations, Gold & Manganese Resources Company
P.O. Box 70, Emily, MN 56447
218-763-3880, Fax: 218-763-3881

H. Christopher Frey
Assistant Professor, North Carolina State University
Department of Civil Engineering, Raleigh, NC 27695-7908
919-515-1155, Fax: 919-515-7908, FREY@EOS.NCSU.EDU

Eli Gal
Manager, Technology Development, GE Environmental Systems
200 North 7th Street, Lebanon, PA 17046
717-274-7049, Fax: 717-274-7103

David Gallaspy
Vice President, Asia & Pacific Rim, Southern Electric International
900 Ashwood Parkway, Atlanta, GA 30338
770-379-7137, Fax: 770-379-7726

Santosh K. Gangwal
Senior Program Director, Research Triangle Institute
3040 Cornwallis Road, Research Triangle Park, NC 27709
919-541-8033, Fax: 919-541-8000, SKG@RTI.ORG

John E. Garnier
Account Manager, Dupont Lanxide Composites
1300 Marrows Road, P.O. Box 6077, Newark, DE 19714-6077
302-456-6578, Fax: 302-456-6480

Lee Gasper-Galvin
General Engineer, Morgantown Energy Technology Center
U.S. Department of Energy, P.O. Box 880, MS N04, Morgantown, WV 26507-0880
304-285-4832. Fax: 304-285-4403, LGASPE@METC.DOE.GOV

John G. Gaydos
President, JGG Services
559 Reverse Road, West Chester, PA 19382
610-430-6624, Fax: 610-565-9384

Harvey N. Goldstein
Senior Engineering Consultant, Parsons Power Group, Inc.
2675 Morgantown Road, Reading, PA 19607
610-855-3281, Fax: 610-855-2384

Leonard E. Graham
Associate Director, Product Technology, Morgantown Energy Technology Center
U.S. Department of Energy, P.O. Box 880, MS B06, Morgantown, WV 26507-0880
304-285-4714, Fax: 304-285-4403, LGRAHA@METC.DOE.GOV

Kenneth M. Gray
GPU/GENCO
1001 Broad Street, Johnstown, PA 15907
814-533-8044, Fax: 814-533-8108, KMGRAY@GPU.COM

Thomas Grindley
Chemical Engineer, Morgantown Energy Technology Center
U.S. Department of Energy, P.O. Box 880, MS A04, Morgantown, WV 26507-0880
304-285-4286, Fax: 304-285-4403, TGRIND@METC.DOE.GOV

Raghubir P. Gupta
Research Chemical Engineer, Research Triangle Institute
3040 Cornwallis Road, Research Triangle Park, NC 27709
919-541-8023, Fax: 919-541-8000, GUPTA@RTI.ORG

John C. Haas
Manager, R&D, Combustion Power Company
150 West 20th Avenue, San Mateo, CA 94403
415-372-1155, Fax: 415-372-1165

George Haddad
NRC Research Associate, Morgantown Energy Technology Center
U.S. Department of Energy, P.O. Box 880, MS A04, Morgantown, WV 26507-0880
304-285-4246, Fax: 304-285-4403, GHADDA@METC.DOE.GOV

Gary J. Hanus
Vice President, Phoenix Solutions Company
5900 Olson Memorial Highway, Minneapolis, MN 55422
612-544-2721, Fax: 612-546-5617, 76424.1606@COMPUSERVE.COM

Douglas P. Harrison
Alumni Professor, Louisiana State University
Department of Chemical Engineering, Baton Rouge, LA 70803-7303
504-388-3066, Fax: 504-388-1476, CMHARR@LSUVM.SNCC.LSU.EDU

John M. Hasman
Technical Sales Representative, United Catalysts, Inc.
1227 South 12th Street, Louisville, KY 40210
502-634-7288, Fax: 502-637-3732

Malcolm T. Hepworth
Professor, University of Minnesota
Civil Engineering Department, 500 Pillsbury Drive, S.E., Minneapolis, MN 55455-0220
612-625-6357, Fax: 612-626-7750, HEPWO001@MAROON.TC.UMN.EDU

Steven Hodges
Senior Research Scientist, HRL Technology PTY Ltd.
677 Springvale Road, Mulgrave, Victoria 3170, Australia
HODGS@HRL.COM.AU

Norman Holcombe
Project Manager, Morgantown Energy Technology Center
U.S. Department of Energy, P.O. Box 880, MS C05, Morgantown, WV 26507-0880
304-285-4829, Fax: 304-285-4403, NHOLCO@METC.DOE.GOV

Ziaul Huque
Assistant Professor, Prairie View A&M University
Mechanical Engineering Department, Prairie View, TX 77446
409-857-4023, Fax: 409-857-4395

John Hurley
Senior Product Development Manager, Pall Corporation
3669 West Road, Cortland, NY 14045
607-753-6041, Fax: 607-753-1220, JOHN-HURLEY@PALL.COM

Shelley Martha Hutson
Student Researcher, Hampton University
Engineering Department, Hampton, VA 23668
804-838-6849

Essam A. Ibrahim
Associate Professor, Morgantown Energy Technology Center
U.S. Department of Energy, P.O. Box 880, MS K02, Morgantown, WV 26507-0880
304-285-4076, Fax: 304-285-4403

Suresh C. Jain
Program Manager, U.S. Department of Energy
19901 Germantown Road, Germantown, MD 20876
301-903-0508, Fax: 301-903-2406, SURESH.JAIN@HQ.DOE.GOV

Michael Janus
Mechanical Engineer, Morgantown Energy Technology Center
U.S. Department of Energy, P.O. Box 880, MS N05, Morgantown, WV 26507-0880
304-285-4912, Fax: 304-285-4403, MJANUS@METC.DOE.GOV

Andrew J. Jarabak
Manager, Program Development, Westinghouse STC
1310 Beulah Road 501-3B28, Pittsburgh, PA 15235
412-256-2881, Fax: 412-256-1948, JARABAK.A.J@WEC.COM

Andrew B. Jeffery
President, Specific Surface Corporation
One Apple Hill, Suite 316, Natick, MA 01760
508-647-9270, Fax: 508-647-9279, SURFACES@AOL.COM

Doug Jewell
Project Manager, Morgantown Energy Technology Center
U.S. Department of Energy, P.O. Box 880, MS D04, Morgantown, WV 26507-0880
304-285-4720, Fax: 304-285-4403, DJEWEL@METC.DOE.GOV

Eric Johnson
Professor, West Virginia University
P.O. Box 6106, Morgantown, WV 26506-6106
304-293-3111, Fax: 304-293-6689

Kandaswamy Jothimurugesan
Assistant Professor, Hampton University
Department of Engineering, Hampton, VA 23668
804-727-5817, Fax: 804-727-5189, JOTHI@ET.HAMTONU.EDU

Roddie R. Judkins
Manager, Oak Ridge National Laboratory
P.O. Box 2008, Oak Ridge, TN 37831-6084
423-574-4572, Fax: 423-574-5812, JUDKINSRR@ORNL.GOV

Bruce S. Kang
Associate Professor, West Virginia University
Mechanical & Aerospace Engineering, Morgantown, WV 26506-6106
304-293-3111, Fax: 304-293-6689, KANG@CEMR.WVU.EDU

Frank Kelleher
Vice President, Foster Wheeler Energy Corporation
P.O. Box 8026, McLean, VA 22106
703-848-8300, Fax: 703-848-8301

Kent W. Keys
Regional Business Unit Manager, United Catalysts, Inc.
1227 South 12th Street, Louisville, KY 40210
502-634-7245, Fax: 502-637-3732

Gyanesh P. Khare
Senior Research Specialist, Phillips Petroleum Company
Corporate Technology, 92-E, PRC, Bartlesville, OK 74004
918-661-9435, Fax: 918-662-1115, GPKHARE@BVEMX.PPCO.COM

Seoung Mo Kim
Director, Korea Institute of Energy Research
40-81 Daehwa-Dong, Daeduck-Gu, Taejon 306020, Korea
40-81 DAEHWA-DONC, DAEDUCK-CU

David Kinsinger
Licensing Specialist, Phillips Petroleum Company
212 PLB, Bartlesville, OK 74004
918-661-1244, Fax: 918-662-2007

Julie Klara
Chemical Engineer, Pittsburgh Energy Technology Center
P.O. Box 10940, Pittsburgh, PA 15236-6289
412-892-6289, Fax: 412-892-4818, JKLARA@PETC.DOE.GOV

Michael G. Klett
Senior Engineer, Parsons Power Group, Inc.
2675 Morgantown Road, Reading, PA 19607
610-855-2854, Fax: 610-855-2384

Chuck Komar
Staff Engineer, Morgantown Energy Technology Center
U.S. Department of Energy, P.O. Box 880, MS B05, Morgantown, WV 26507-0880
304-285-4107, Fax: 304-285-4403, CKOMAR@METC.DOE.GOV

Hisashi O. Kono
Professor, West Virginia University
P.O. Box 6102, Morgantown, WV 26506-6102
304-293-2111, Fax: 304-293-4139, KONO@FACULTY.COE.WVU.EDU

Gopala Krishnan
Program Manager, SRI International
333 Ravenswood Avenue, Menlo Park, CA 94025
415-859-2627, Fax: 415-859-2111, GOPALA-KRISHNAN@QM.SRI.COM

Kyung C. Kwon
Professor, Tuskegee University
Chemical Engineering Department, Tuskegee, AL 36088
334-727-8976, Fax: 334-727-8976, KWONK@ACD.TUSK.EDU

Michael A. Lacey
Mechanical Engineer, GE Corporate R&D
Bldg. K-1, Room 103, P.O. Box 8, Schenectady, NY 12301
518-387-7989, Fax: 518-387-7258, LACEY@CRD.GE.COM

Wu K. Lan
Project Manager, Morgantown Energy Technology Center
U.S. Department of Energy, P.O. Box 880, MS C05, Morgantown, WV 26507-0880
304-285-4044, Fax: 304-285-4403, WLAN@METC.DOE.GOV

Jay E. Lane
Program Manager, Westinghouse STC
1310 Beulah Road, Pittsburgh, PA 15235-5098
412-256-2195, Fax: 412-256-1267, LANE.J.E.@WEC.COM

Leonard N. Lapatnick
Project Engineer, Air Toxics, Public Services Electric & Gas Company
80 Park Plaza, T16 G, Newark, NJ 07101
201-430-8129, Fax: 201-733-9281, LLAPATNI@PSEG.COM

David A. Larsen
Manager of Product Development, Blasch Precision Ceramics, Inc.
580 Broadway, Albany, NY 12204
518-436-1263, Fax: 518-436-0098

Bill Lawson
Division Director, Technology Base Program, Morgantown Energy Technology Center
U.S. Department of Energy, P.O. Box 880, MS B05, Morgantown, WV 26507-0880
304-285-4173, Fax: 304-285-4403, WLAWSO@METC.DOE.GOV

Jean-Francois Le Costaouec
Senior Engineer, Techniweave, Inc.
109 Chestnut Hill Road, P.O. Box 6314, Rochester, NH 03868
603-335-2115, Fax: 503-335-3200

Seong W. Lee
Associate Professor, Morgan State University
Cold Spring Lane & Hillen Road, Baltimore, MD 21239
410-319-3137, Fax: 410-319-3843, SLEE@MOE.MORGAN.EDU

Yinzhong Li
Engineer, Central Coal Mining Research Institute
Hepingli, Beijing, 100013, China

Thomas E. Lippert
Manager, Westinghouse STC
1310 Beulah Road, Pittsburgh, PA 15235-5098
412-256-2440, Fax: 412-256-2121, LIPPERT.T.E@WEC.COM

James Longanbach
Project Manager, Morgantown Energy Technology Center
U.S. Department of Energy, P.O. Box 880, MS C04, Morgantown, WV 26507-0880
304-285-4659, Fax: 304-285-4403, JLONGA@METC.DOE.GOV

Chris Ludlow
General Engineer, Morgantown Energy Technology Center
U.S. Department of Energy, P.O. Box 880, MS B05, Morgantown, WV 26507-0880
304-285-4608, Fax: 304-285-4403, JLUDLO@METC.DOE.GOV

Rajeev Mallela
Graduate Research Assistant, West Virginia University
445 Oakland Street, No. 503, Morgantown, WV 26505
304-599-3025

P. Roa Mandava
Engineering Manager, Westinghouse Electric Corporation
806 Fairview Road, Pittsburgh, PA 15238
412-967-9023, Fax: 412-374-5535

James D. McClung
Program Manager, Foster Wheeler Development
12 Peach Tree Hill Road, Livingston, NJ 07039
201-535-2309, 201-535-2242

Nicole McGee
Student Researcher, Hampton University
Chemical Engineering Department, Hampton, VA 23669
804-720-6647

Theodore J. McMahon
Project Manager, Morgantown Energy Technology Center
U.S. Department of Energy, P.O. Box 880, MS C04, Morgantown, WV 26507-0880
304-285-4865, Fax: 304-285-4403, TMCMAH@METC.DOE.GOV

Terence J. McManus
Project Scientist, Advanced Technology Systems
3000 Tech Center Drive, Monroeville, PA 15146
412-829-2208, Fax: 412-829-2415

Michael H. McMillian
Mechanical Engineer, Morgantown Energy Technology Center
U.S. Department of Energy, P.O. Box 880, MS N04, Morgantown, WV 26507-0880
304-285-4669, Fax: 304-285-4403, MMCMIL@METC.DOE.GOV

Daniel Mei
Associate Professor, Prairie View A&M University
Mechanical Engineering Department, P.O. Box 397, Prairie View, TX 77446
409-857-4023, Fax: 409-857-4395

Joseph S. Mei
Mechanical Engineer, Morgantown Energy Technology Center
U.S. Department of Energy, P.O. Box 880, MS N05, Morgantown, WV 26507-0880
304-285-4409, Fax: 304-285-4403, JMEI@METC.DOE.GOV

Xiande Meng
Project Manager, Central Coal Mining Research Institute
Hepingli, Beijing, 100013, China

Eric L. Moorehead
Vice President, Technology Development, M.W. Kellogg Technology Company
16200 Park Row, Houston, TX 77084
713-492-5713, Fax: 713-492-5832, MOOREHEAD@MWK.COM

Atsushi Morihara
Senior Researcher, Hitachi, Ltd.
832-2 Horiguchi, Hitachi-Naka 312, Japan
MORIHARA@HRL.HITACHI.CO.JP

John W. Motter
Executive Project Director, Sierra Pacific Power Company
P.O. Box 10100, Reno, NV 89520
702-343-0602, fax: 702-343-0407, JACK@SPP07.SPPCO.COM

Harvey M. Ness
Division Director, Gasification, Morgantown Energy Technology Center
U.S. Department of Energy, P.O. Box 880, MS C04, Morgantown, WV 26507-0880
304-285-4172, Fax: 304-285-4403, HNESS@METC.DOE.GOV

Robert Ness
Research Manager, Energy & Environmental Research Center
P.O. Box 9018, Grand Forks, ND 58202
701-777-5209, Fax: 701-777-5181, BNESS@EERC.UND.NODAK.EDU

Grady B. Nichols
Principal Engineer, Southern Research Institute
P.O. Box 55305, Birmingham, AL 35255-5305
205-581-2361, Fax: 205-581-2448

Glenn Norton
Associate Chemist, Ames National Lab
Iowa State University, 281 Metals Development Building, Ames, IA 50011
515-294-1035, Fax: 515-294-3091, NORTON@AMESLAB.GOV

Thomas S. Norton
Mechanical Engineer, Morgantown Energy Technology Center
U.S. Department of Energy, , P.O. Box 880, MS N05, Morgantown, WV 26507-0880
304-285-4617, Fax: 304-285-4403, TNORTO@METC.DOE.GOV

John Notestein
Chief Engineer, Morgantown Energy Technology Center
U.S. Department of Energy, P.O. Box 880, MS A05, Morgantown, WV 26507-0880
304-285-4232, Fax: 304-285-4403, JNOTES@METC.DOE.GOV

Masahide Okamoto
Manager, R&D Section, Sasakura Engineering Company, Ltd.
7-32 Takeshima-4-Chome, Nishivodogawa-Lu, Osaka 555, Japan
816-473-2138, Fax: 816-473-4290

William Owens
Senior Program Manager, Parsons Power Group, Inc.
19644 Club House Road, Suite 820, Gaithersburg, MD 20879
301-869-9191, Fax: 301-977-7507

Balaji Parthasarathy
West Virginia University, Department of Civil Engineering
6th Floor, Engineering Sciences Bldg., Morgantown, WV 26506
304-293-3031

Henry Phillips
Consultant
22 Beacon Hill Drive, Metuchen, NJ 08840
908-549-0332

Timothy E. Pinkston
Technical Manager, Southern Company Services
P.O. Box 1069, Wilsonville, AL 35186
205-669-5860, Fax: 205-669-5843, TIM.E.PINKSTON@SCSNET.COM

Michael Pjetraj
Environmental Engineer, North Carolina Air Quality Division
P.O. Box 29580, Raleigh, NC 27626-0580
919-733-1469, Fax: 919-733-1812, MICHAEL_PJETRAJ@AQ.EHNR.STATE.N

John E. Plunkett
Manager, Scientific & Engineering, EG&G/TSWV
P.O. Box 880, MS M02, Morgantown, WV 26507-0880
304-285-4605, Fax: 304-285-4403, JPLUNK@METC.DOE.GOV

Duane H. Pontius
Director, Particulate Sciences, Southern Research Institute
2000 9th Avenue, South, Birmingham, AL 35205
205-581-2268, Fax: 205-581-2448, DHPSRI@AOL.COM

Jeffrey W. Portzer
Research Chemical Engineer, Research Triangle Institute
3040 Cornwallis Road, Research Triangle Park, NC 27709
919-541-8025, Fax: 919-541-8000, JWP@RTI.ORG

Charles A. Powell
Maintenance Supervisor, Southern Company Services
P.O. Box 1069, Wilsonville, AL 35186
205-669-5869, Fax: 205-669-5843, CHARLES.A.POWELL@SCSNET.COM

Tyra B. Powell
ORISE Faculty, Morgantown Energy Technology Center
U.S. Department of Energy, P.O. Box 880, MS A04, Morgantown, WV 26507-0880
304-285-4827, Fax: 304-285-4403

Victor Powell
Researcher, Morgantown Energy Technology Center
U.S. Department of Energy, P.O. Box 880, MS A04, Morgantown, WV 26507-0880
304-285-4076, Fax: 304-285-4403

Shaik A. Qader
President, Energy & Environmental Tech. Corp.
11609 Treviso Avenue, Rancho Cucamonga, CA 91701
909-466-6266, Fax: 909-466-6246

Junjie Qin
Senior Engineer, Central Coal Mining Research Institute
Hepingli, Beijing, 100013, China

Massood Ramezan
Principal Engineer, Pittsburgh Energy Technology Center
P.O. Box 10940, Pittsburgh, PA 15236-6289
412-892-5916

Neil Raskin
General Manager, Cerafilter Systems, Inc.
8925 Rehco Road, San Diego, CA 92121
619-452-3301, Fax: 619-458-3190, NRASKIN@CTO.COM

Maria Reidpath
Engineer, EG&G/TSWV
P.O. Box 880, MS L02, Morgantown, WV 26507-0880
304-285-4140, Fax: 304-285-4403, MREIDP@METC.DOE.GOV

Robert B. Reuther
Product Manager, PFBC, Morgantown Energy Technology Center
U.S. Department of Energy, P.O. Box 880, MS D01, Morgantown, WV 26507-0880
304-285-4578, Fax: 304-285-4403, RREUTH@METC.DOE.GOV

George A. Richards
General Engineer, Morgantown Energy Technology Center
U.S. Department of Energy, P.O. Box 880, MS N05, Morgantown, WV 26507-0880
304-285-4458, Fax: 304-285-4403, GRICHA@METC.DOE.GOV

Larry Matthew Richman
West Virginia University
Chemical Engineering Department, Morgantown, WV 26505
304-293-2111

John M. Rockey
Chemical Engineer, Morgantown Energy Technology Center
U.S. Department of Energy, P.O. Box 880, MS N04, Morgantown, WV 26507-0880
304-285-4711, Fax: 304-285-4403, JROCKE@METC.DOE.GOV

Paul D. Rodebaugh
Supervising Engineer, Florida Power & Light
P.O. Box 14000, Juno Beach, FL 33408-0420
407-691-2620, Fax: 407-691-2695

Robert Romanosky
Division Director, Technical Support, Morgantown Energy Technology Center
U.S. Department of Energy, P.O. Box 880, MS A04, Morgantown, WV 26507-0880
304-285-4721, Fax: 304-285-4403, RROMAN@METC.DOE.GOV

David E. Romans
Process Engineer, Southern Company Services
P.O. Box 1069, Wilsonville, AL 35186
205-669-5862, Fax: 205-669-5843, DAVID.E.ROMANS@SCSNET.COM;205-6

Giulio Rossi
Senior Research Scientist, Selee Corporation
700 Shepherd Street, Hendersonville, NC 28792
704-697-2411, Fax: 704-697-7960

Edward S. Rubin
Professor, Carnegie Mellon University
Baker Hall 128-A, Pittsburgh, PA 15213
412-268-5897, Fax: 412-268-3757, RUBIN@CMU.EDU

Michael D. Rutkowski
Project Manager, Parsons Power Group, Inc.
2675 Morgantown Road, Reading, PA 19607
610-855-2698, Fax: 610-855-2384, GC!GHMAIL02!A6575@GILCOM.ATTMAI

Ramanathan Sampath
Research Scientist, Clark Atlanta University
Department of Engineering, 223 James P. Brawley Drive, S.W., Atlanta, GA 30314
404-880-6733, Fax: 404-880-6890, RSAMPATH@CAU.EDU

John Sawyer
Manager, High Temperature Filtration, Pall Corporation
309 Second Street, Suite 8, Las Altos, CA 94022
415-917-9103, Fax: 415-917-9105, JOHN_SAWYER@PALL.COM

Karsten Schulz
Manager of Research, Schumacher
P.O. Box 1562, Crailsheim, D-74555, Belgium

Kal Seshadri
Systems Analyst, EG&G/TSWV
P.O. Box 880, MS M02, Morgantown, WV 26507-0880
304-285-4680, Fax: 204-285-4403, KSESHA@METC.DOE.GOV

Philip T. Seymour
President, Schumacher Filters America
P.O. Box 8040, Asheville, NC 28814
704-252-9000, Fax: 704-253-7773

Larry Shadle
Cluster Leader, Morgantown Energy Technology Center
U.S. Department of Energy, P.O. Box 880, MS N04, Morgantown, WV 26507-0880
304-285-4647, Fax: 304-285-4403, LSHADL@METC.DOE.GOV

Abolghasem Shamsi
Research Chemist, Morgantown Energy Technology Center
U.S. Department of Energy, P.O. Box 880, MS N04, Morgantown, WV 26507-0880
304-285-4360, Fax: 304-285-4403, ASHAMS@METC.DOE.GOV

Jerry Shang
Program Manager, U.S. Department of Energy
Fossil Energy, FE-232, Washington, DC 20585
301-903-2795, Fax: 301-903-2406

Susan R. Shoemaker
Mechanical Engineer, Morgantown Energy Technology Center
U.S. Department of Energy, P.O. Box 880, MS N04, Morgantown, WV 26507-0880
304-285-4269, Fax: 304-285-4403, SSHOEM@METC.DOE.GOV

Jack Sibold
Senior Engineer, TDA Research, Inc.
12345 W. 52nd Avenue, Wheat Ridge, CO 80033
303-940-2319, Fax: 303-422-7763, SIBOLDS@TDA.COM

Ranjani V. Siriwardane
Research Chemist, Morgantown Energy Technology Center
U.S. Department of Energy, P.O. Box 880, MS N04, Morgantown, WV 26507-0880
304-285-4513, Fax: 304-285-4403, RSIRIW@METC.DOE.GOV

Duane H. Smith
Cluster Leader, Morgantown Energy Technology Center
U.S. Department of Energy, P.O. Box 880, MS A04, Morgantown, WV 26507-0880
304-285-4069, Fax: 304-285-4403, DSMITH@METC.DOE.GOV

Merrill A. Smith
Program Manager, U.S. Department of Energy
1000 Independence Avenue, S.W., Washington, DC 20585-0121
202-586-3646, Fax: 202-586-3237, MERRILL.SMITH@HQ.DOE.GOV

Robert G. Smith
Senior Research Specialist, 3M General Offices
3M Center, Building 203-1-01, St. Paul, MN 55144-1000
612-733-2564, Fax: 612-737-5484, RGSMITH@MMM.COM

Karl Smith-Berntson
Vice President R&D, Donlee Technologies, Inc.
693 North Hills Road, York, PA 17402-2211
717-755-1081, Fax: 717-755-0020, 71370.146@COMPUSERVE.COM

Todd R. Snyder
Research Environmental Engineer, Southern Research Institute
2000 9th Avenue, South, Birmingham, AL 35205
205-581-2606, Fax: 205-581-2448

Jack D. Spain
Research Engineer, Southern Research Institute
P.O. Box 55305, Birmingham, AL 35225-5305
205-581-2323, Fax: 205-581-2414

Ron Staubly
Project Manager, Morgantown Energy Technology Center
U.S. Department of Energy, P.O. Box 880, MS C04, Morgantown, WV 26507-0880
304-285-4991, Fax: 304-285-4403, RSTAUB@METC.DOE.GOV

Douglas L. Straub
Mechanical Engineer, Morgantown Energy Technology Center
U.S. Department of Energy, P.O. Box 880, MS N05, Morgantown, WV 26507-0880
304-285-5444, Fax: 304-285-4403, DSTRAU@METC.DOE.GOV

Larry D. Strickland
Division Director, Gas Cleanup, Morgantown Energy Technology Center
U.S. Department of Energy, P.O. Box 880, MS N04, Morgantown, WV 26507-0880
304-285-4494, Fax: 304-285-4403, LSTRIC@METC.DOE.GOV

Michael L. Swanson
Research Engineer, Energy & Environmental Research Center
P.O. Box 9018, Grand Forks, ND 58202
701-777-5000, Fax: 701-777-5181, MSWANSON@EERC.UND.NODAK.EDU

James H. Swisher
Partner, E&A Associates
126 Misty Lake Drive, Murphysboro, IL 62966
618-529-5958, Fax: 618-985-2919, JIMS@SIU.EDU

Robert Travers
Program Manager, U.S. Department of Energy
19901 Germantown Road, FE 232, Germantown, MD 20874
301-903-6166

Brian S. Turk
Research Chemical Engineer, Research Triangle Institute
3040 Cornwallis Road, Research Triangle Park, NC 27709
919-541-8024, Fax: 919-541-8000, BST@RTI.ORG

Lawrence E. Van Bibber
Project Manager, Parsons Power Group, Inc.
P.O. Box 10940, MS 922-204, Pittsburgh, PA 15236-0940
412-892-4194, Fax: 412-892-4818, VANBIBB@PETC.DOE.GOV

John Vanosdol
Engineer, Morgantown Energy Technology Center
U.S. Department of Energy, P.O. Box 880, MS A04, Morgantown, WV 26507-0880
304-285-5446, Fax: 304-285-4403, JVANOS@METC.DOE.GOV

Venkat Venkataraman
Project Manager, Morgantown Energy Technology Center
U.S. Department of Energy, P.O. Box 880, MS M02, Morgantown, WV 26507-0880
304-285-4962, Fax: 304-285-4403, VVENKA@METC.DOE.GOV

Albert A. Vierheilig
Manager, New Product Development, Intercat, Inc.
115 Eli Whitney Boulevard, Savannah, GA 31408
912-748-0630, Fax: 912-748-8663, AL1@MSN.COM

Joe Voelker
Engineer Test Manager, Micro Composite Materials Corp.
4608-D Industry Lane, Durham, NC 27713
919-361-3535, Fax: 919-361-3535

Richard A. Wagner
Principal Engineer, Babcock & Wilcox
P.O. Box 11165, Lynchburg, VA 24502-1165
804-522-5697, Fax: 804-522-6980, RICH.A.WAGNER@MCDERMOTT.COM

Grace Wang
Scientist, EG&G/TSWV
P.O. Box 880, MS M02, Morgantown, WV 26507-0880
304-285-5453, Fax: 304-285-4403, GWANG@METC.DOE.GOV

Paul S. Weitzel
Technical Consultant, Babcock & Wilcox
20 S. Van Buren, Barberton, OH 44614
330-860-1655, Fax: 330-860-2348

Harvey Wen
Principal Engineer, Bechtel
9801 Washington Boulevard, Gaithersburg, MD 20878-5356
301-417-4507, Fax: 301-869-4078

Ronald A. Westmoreland
Chemical Engineer, Tennessee Valley Authority
P.O. Box 1010 (CEB4C), Muscle Shoals, AL 35662-1010
205-386-2038, Fax: 205-386-3799

Gerald Wheeler
Lead Program Manager, U.S. Department of Energy
19901 Germantown Road, FE-231, Germantown, MD 20545
301-903-3511, Fax: 301-903-2406, GERALD.WHEELER@HQ.DOE.GOV

Jay White
Process Engineer, Parsons Power Group
1498 Morgantown Road, Reading, PA 19106
610-855-2693

Young-Ho Wi
Senior Researcher, KEPRI
103-16 Mumji-Dong, Yusung-Ku, Taejon 305-380, Korea
YHWI@HAMBIT.KEPRI.RE.KR

James T. Wilbur
Manager, Technical Projects, Burns & Roe Services Corp.
P.O. Box 18288, Pittsburgh, PA 15236
412-892-5916, Fax: 412-892-4604, WILBUR@PETC.DOE.GOV

Mark Williams
Product Manager, Fuel Cells, Morgantown Energy Technology Center
U.S. Department of Energy, P.O. Box 880, MS D01, Morgantown, WV 26507-0880
304-285-4747, Fax: 304-285-4403, MWILLI@METC.DOE.GOV

William G. Wilson
President, Gas Desulfurization Corporation
820 Harden Drive, Pittsburgh, PA 15229
412-364-1822, Fax: 412-367-1254

M. Wise
Sales Manager, Chemetals, Inc.
610 Pittman Road, Baltimore, MD 21226
410-636-7107, Fax: 410-636-7113

David C. Wolfe
R&D Manager, United Catalysts, Inc.
1227 South 12th Street, Louisville, KY 40210
502-634-7349, Fax: 502-637-3732

John C. Wolfmeyer
R&D Engineer, Duke Power Company
P.O. Box 1006, EC04J, Charlotte, NC 28201-1006
704-382-4017, Fax: 704-382-9849, JCW7122@DUKEPOWER.COM

Steven D. Woodruff
Research Chemist, Morgantown Energy Technology Center
U.S. Department of Energy, P.O. Box 880, MS A04, Morgantown, WV 26507-0880
304-285-4175, Fax: 304-285-4403, SWOODR@METC.DOE.GOV

Robert Wright
U.S. Department of Energy
Office of Fossil Energy, FE-22, Washington, DC 20585-0002
301-903-5471, Fax: 301-903-2713, ROBERT.WRIGHT@HG.DOE.GOV

Keyu Xie
Deputy Director, Central Coal Mining Research Institute
Hepingli, Beijing 100013, China

Anthony S. Yagiela
Senior Marketing Specialist, Babcock & Wilcox
1562 Beeson Street, Alliance, OH 44601
330-829-7403, Fax: 330-829-7801, ANTHONY.S.YAGIELA@MCDERMOTT.COM

Wang Yang
Research Professor, Institute of Coal Chemistry
27 Taoyuan South Road, Taiyuan, Shanxi 030001, China

Chang-Keun Yi
Research Engineer, Korea Institute of Energy Research
71-2 Jang-Dong, Taejon 305-343, Korea
CKYI@SUN330.KIER.RE.KR

Guojun Yuan
Engineer, Central Coal Mining Research Institute
Hepingli, Beijing, 100013, China

Paul Yue
Physicist, Morgantown Energy Technology Center
U.S. Department of Energy, P.O. Box 880, MS A04, Morgantown, WV 26507-0880
304-285-4062, Fax: 304-285-4403, PYUE@METC.DOE.GOV

Kenneth B. Zella
Marketing Manager, Pall Aerospace Company
6301 49th Street, North, Pinellas Park, FL 34647
813-522-3111, Fax: 813-528-0516, KEN_ZELLA@PALL.CO

Claudio Zeppi
ENEL, Italian National Electric Board
Aia A. Pisano, 120, Pisa 56122, Italy
50-53-5644, Fax: 50-53-5651

Jianren Zhou
Assistant Professor, Prairie View A&M University
Mechanical Engineering Department, Prarie View, TX 77446
409-857-4023, Fax: 409-857-4395, JZHOU@MC.PRAIRIE.EDU

To return to the Proceedings *Contents* page or the *Cover*, click the **Go Back** button (the double left-pointing arrow) from the tool bar at the top of the screen, or choose **Go Back** from the view menu.